

Near-vertical multiple ScS phases and vertically averaged mantle properties

Hiroo Kanamori, Seismological Laboratory, California Institute of Technology, Pasadena, CA 91125. E-mail: hiroo@gps.caltech.edu

and

Luis Rivera, Institut de Physique du Globe de Strasbourg, Université de Strasbourg CNRS, Strasbourg, France. E-mail: luis.rivera@unistra.fr, and

Seismological Laboratory, California Institute of Technology, Pasadena, CA 91125.

ABSTRACT

Near-vertical multiple ScS phases are among the cleanest seismic phases traveling over several thousand km in the Earth's mantle and are useful for constraining the average attenuation and shear wave speed in the whole mantle. However, the available multiple ScS pairs are limited. We took advantage of the recent dramatic increase in the number of global broad-band stations, and made a thorough computer-assisted search for high-quality data of multiple ScS pairs. We could find 220 station-event pairs which provided us with robust local estimates of average Q and 2-way shear wave travel times. With the assumption that geometric focusing caused by lateral velocity heterogeneity does not seriously affect the amplitude measurements, the Q values exhibit strong short-range lateral variations, with very high and low Q regions closely adjacent to each other. The mantle beneath KIP, Hawaii, has normal Q and shear wave speed, which supports the result of earlier studies. The mantle beneath AFI, Samoa Islands, has a very high Q , possibly larger than 1400, and the slowest shear wave speed. The stations on the upper plate of the Tonga and Japan subduction zones yield average to low Q values. In contrast, the stations on the trenchward side of the upper plate of some subduction zones, e.g., LVC, Chile, and PET, Kamchatka, indicate high Q values, larger than 1000. We found no obvious correlation between Q and shear wave speed, which suggests that different factors like temperature, composition, anisotropy, etc are controlling these properties in the mantle of different tectonic environments.

Keywords: ScS, mantle Q , mantle shear wave speed, hot spot, Samoa, Hawaii

INTRODUCTION

The multiple ScS phase, shear wave reflected at the Earth's surface and the core-mantle boundary, is among the most distinct seismic phases. Press (1956) and Anderson and Kovach (1964) used clear near-vertical ScS phases from South American deep earthquakes to determine an upper bound of the core rigidity and Q (quality factor) averaged vertically for the whole mantle. The average Q was estimated to be approximately 500 at periods from 10 to 25 sec. Because of the simplicity of the ray geometry, very few assumptions are required for the analysis, and the method provides spatially local estimates of Q and shear wave speed.

Press (1956) and Anderson and Kovach (1964) used the peak amplitude of the observed seismograms. These studies were followed by Kovach and Anderson (1964) and Yoshida and Tsujiura (1975) who used spectral ratios. The method was then extended to wide-angle ScS analyses using multiple ScS pairs observed at large distances by many investigators, such as Okal and Anderson (1975), Sipkin and Jordan (1975, 1976, 1979), Nakanishi (1979), Lay and Wallace (1983, 1988), and Chan and Der (1988). Romanowicz and Mitchell (2007) contains the most recent summary on multiple ScS studies.

A distinct advantage of using near-vertical observations is simplicity. In wide-angle observations, complexities in the earthquake mechanism and the near-surface structural heterogeneities can complicate amplitude measurements. Unfortunately, the number of available near-vertical pairs was very limited compared with that of wide-angle observations. For the last 30 years, the number of high-quality broadband stations has increased dramatically, and now we can find many more pairs of near-vertical ScS

than in the 1980's and earlier. We took advantage of the expansion of global broad-band networks, and made an extensive search for high-quality near-vertical pairs to improve the spatial coverage. Although we have succeeded in expanding the data base significantly, spatial coverage is still limited compared with that provided by wide-angle ScS and other paired phase (e.g., S and SS etc) observations. Nevertheless, because of the simplicity of the ray geometry, our results provide robust local (over an area of approximately 1,000 km in diameter (Julian, 2005) estimates of Q and the vertical 2-way (between the surface and the core-mantle boundary) travel-times of shear waves that can be used to compare with global tomographic models and to constrain interpretation of 3-dimensional mantle structure.

With the use of broadband records, our measurements are at longer period than in most previous studies.

DATA SELECTION METHOD

Since the quality of our measurements critically depends on the quality of the records, we chose our records following the 3 steps described below. First, we manually examined about 20 records from the stations such as KIP (Hawaii), AFI (Samoa Is.), LVC (Chile), MAJO (Japan), and PET(Kamchatka) to establish the criteria for selection, regarding the event mechanism, frequency band, magnitude, waveform similarity, and signal-to-noise ratios (S/N) of the ScS phases. In this study, we use only ScS₁ and ScS₂ phases to maximize S/N. After having established a set of criteria, we made automated search as follows.

We used the GCMT (Global Centroid Moment Tensor) catalog for the period from January 1976 to April 2014, and selected events with $M_w \geq 6.2$ with primarily a dip-slip mechanism with a steeply dipping nodal plane. Specifically, we chose events with

$$\sqrt{M_{r\phi}^2 + M_{r\theta}^2} / M_0 \geq 0.5 \quad (1)$$

where $M_{r\phi}$ and $M_{r\theta}$ are the vertical-east and vertical-south components of the moment tensor, and M_0 is the scalar moment. This condition ensures that the corresponding ground motion records are mainly shear waves. We then searched through the IRIS (Incorporated Research Institutions for Seismology) database for stations within 5° of the epicenter. This search resulted in more than 3,000 event-station pairs. We converted each record to ground displacement and filtered it between 0.008 and 0.0275 Hz with a 4th order causal Butterworth filter. For each record we defined three time windows (Figure 1): $W_1 = (t_1-80s, t_1+160s)$, $W_2 = (t_2-80s, t_2+160s)$ and $W_n = (t_1+600s, t_1+900s)$ where t_1 and t_2 are the predicted arrival times of ScS₁ and ScS₂, respectively. W_1 and W_2 contain ScS₁ and ScS₂, respectively, and W_n contains a sample of the noise. We used these data segments for two purposes. First, we performed amplitude measurements: maximum peak-to-peak on W_1 (PP1) and W_2 (PP2) and RMS (root-mean-square) on W_n and used them to define ScS₁ and ScS₂ signal-to-noise ratios: $sn_1 = PP1 / (2\sqrt{2}RMS)$, $sn_2 = PP2 / (2\sqrt{2}RMS)$. Second, we measured the waveform similarity between ScS₁ and ScS₂ by cross-correlation, i.e.,

$$C_r = \max \int_{-\infty}^{+\infty} ScS_1(t)ScS_2(t+\tau)dt / \sqrt{\int_{-\infty}^{+\infty} ScS_1^2(t)dt \int_{-\infty}^{+\infty} ScS_2^2(t)dt} \quad (2)$$

where $ScS_1(t)$ and $ScS_2(t)$ are assumed to be 0 outside the window, and “max” mean the maximum value of the integral as the lag τ is varied. Using these quantities, we chose the records which satisfy the following 3 conditions:

$$sn_1 > 7, \quad sn_2 > 3 \quad \text{and} \quad C_r > 0.8.$$

These conditions have been determined by the visual examination of the sample records. The distinction between SH and SV is negligible for near vertical incidence. More important is the total shear wave motion regardless of SH and SV. Thus, when several records are available for the same event-station pair, we selected the record with the largest ScS_1 peak-to-peak amplitude. In a few cases where the 2 components have about the same amplitude, we rotated them to produce a component with the largest S wave amplitude. We did not always want to rotate because the S/N of the smaller amplitude component is often large, and rotation can decrease the S/N ratio of the rotated trace.

As the last step of screening, we manually examined almost every single record to remove those contaminated by unexpected glitches, overlapping aftershocks, interfering phases etc. At the end, we were left with 220 event-station pairs, each one being represented by a single record. We added the KIP record of the April 26, 1973 event in Hawaii, which was used by Best et al. (1974).

We first show several representative records thus selected to illustrate the quality and the first-order conclusions we can derive from these records. All the records we used are displacement records band-pass filtered at 0.008 to 0.0275 Hz. For some stations, we

compared the observed seismograms with the synthetics computed for PREM (Preliminary Reference Earth Model, Dziewonski and Anderson, 1981) and a 3-dimensional (3-D) structure. The 3-D synthetics are taken from the IRIS database (Tromp et al., 2010) and are based upon the 3-D velocity models of Kustowski et al. (2008) and Bassin et al. (2000). The Q model used for the 3-D synthetics is the 1-D model, QL6, obtained by Durek and Ekström (1996).

KIP

Figure 2A shows the seismogram of the 6/26/1989 earthquake ($M_w=6.4$, $h(\text{depth})=15$ km) recorded at KIP, Hawaii. Also shown is a synthetic seismogram computed using PREM. The whole mantle average Q is 294 for PREM. (Here, the average is the harmonic average weighted by the travel time as defined later by equation 5.) The peak-to-peak amplitude ratio ScS_2/ScS_1 , r , and the cross correlation C_r are indicated on the figure. The observed ratio, r , is approximately the same as that of the synthetic, indicating that the whole mantle Q beneath KIP at a period of about 40 sec is approximately the same as that of PREM.

The record of another event on 10/15/2006 ($M_w=6.7$, $h=48$ km) yields (Figure 2B) $r=0.41$ which translates to $Q=330$. These values are consistent with the value, $Q=300$ estimated by Best et al. (1974) from a High-Gain-Long-Period seismogram observed for the 4/26/1973 event. For this event, 1-D and 3-D synthetic seismograms are shown for comparison. We also analyzed the 1973 event and obtained $r=0.40$ and $Q=272$. Sipkin and Jordan (1980b) assessed the effect of noise and obtained, $Q=188$. Although this value is somewhat lower than the values we obtained, the difference could be due to the

presence of relatively large noise of this record, with a low correlation coefficient, $Cr=0.874$, compared with the other two records, $Cr=0.910$, and $Cr=0.940$ (see Table 1.)

AFI

Figure 2C shows a similar plot for the 4/7/1995 event ($M_w=7.3$, $h=88$ km) recorded at AFI. The observed ratio, $r=0.51$ is much larger than that for the synthetic, $r=0.38$. We note that, in the context of our model given by equation 3, the ratio should be at most 0.5, which corresponds to $Q=\infty$. Thus, the observed ratio 0.51 suggests that the ratio is affected by either noise or geometrical focusing of the ray, but even if we allow for these effects, this result indicates that overall attenuation of shear waves in the mantle below AFI is very low. Considering the noise, we set the upper bound of Q at 1400, the value estimated by Anderson and Kovach (1964) for the lower mantle, when the ratio is larger than about 0.49. Although this large ratio, i.e., high Q , is somewhat surprising, we have 6 determinations with $r \geq 0.48$ for AFI, as shown later, and we believe that the high- Q mantle beneath AFI is a real feature. The synthetic seismogram computed for PREM shows significantly smaller ratios of ScS_2/ScS_1 and ScS_3/ScS_1 .

LVC

Figure 2D shows a seismogram of the 1/23/1997 event ($M_w=7.1$, $h=282$ km) recorded at LVC, Chile; this example also indicates a large ratio, $r=0.50$. The PREM synthetic shows, $r=0.39$. This is not an isolated observation; 8 observations at LVC show $r \geq 0.4$

ADK

Figure 2E shows an example of low Q observations. The seismogram shown is from ADK for the 6/24/2011 earthquake ($M_w=7.3$, $h=74$ km). The observed ratio, $r=0.30$, is much smaller than that, $r=0.39$, of the synthetic for PREM, and, $r=0.34$, for the 3-D synthetic. The estimated Q value is 117.

PET

Figure 2F compares the observed seismogram of the 5/24/2013 Okhotsk deep earthquake ($M_w=8.3$, $h=611$ km) recorded at PET and the synthetic seismograms computed for PREM (1-D) and the 3-D model. The observed ratio is larger than those of the synthetics suggesting that the whole mantle Q beneath the station PET is higher than that of PREM.

Figure 2 demonstrates that the quality and the noise level of our records are sufficient for distinguishing the high Q , low Q , and intermediate Q cases. In the following sections we will estimate Q and give their nominal values for all the records we selected, but our main concern in this paper is the characterization of the records in these 3 categories. The 3 categories we use are: $Q > 800$ (high Q , blue box), $180 < Q \leq 800$ (intermediate Q , green box), and $Q \leq 180$ (low Q , red box).

ANALYSIS

We follow the method of Press (1956) and Anderson and Kovach (1964), and estimate Q from the peak-to-peak amplitude of ScS_1 and ScS_2 phases. However, we include the effect of waveform distortion by attenuation, examine the spectral ratios, and

determine the ScS₂ - ScS₁ travel times by waveform cross correlation. We use the following iterative method for this analysis

The ratio of the frequency spectrum of ScS₂, $ScS_2(f)$, to that of ScS₁, $ScS_1(f)$ can be written as

$$\left| \frac{ScS_2(f)}{ScS_1(f)} \right| = g \cdot \exp\left(-\frac{\pi f t_r}{Q}\right) \quad (3)$$

$$g = \left(\frac{2 - h/H}{4 - h/H} \right) \quad (4)$$

where g is the ratio of geometrical spreading of ScS₂ to ScS₁ phases, h is the source depth, H is the depth to the core-mantle boundary, t_r is the ScS₂ - ScS₁ travel time (i.e., 2-way vertical shear wave travel time in the mantle), and Q is the average Q defined by

$$Q = \frac{t_r}{\int_0^H \left(\frac{2}{Q_s(s)\beta} \right) ds} \quad (5)$$

where s is the distance along the near-vertical ray and $Q_s(s)$ is the quality factor of the medium along the path. The integral on the right-hand side is usually called t^* .

To obtain first approximations for Q and t^* , we use the maximum time-domain amplitude of ScS₁ and ScS₂ phases, as was done by Press (1956) and Anderson and Kovach (1964). In this case the frequency f in (3) is understood as a dominant

frequency. We determine the dominant period, $\tau = 1/f$, with the method described in Kanamori (2005).

From the amplitude ratio, the dominant period τ , and the travel time t_r , we compute the first approximation of Q and t^* using (3), (4), and (5). The corrections for ellipticity and station elevation are included in these computations. Although these estimates are fairly accurate, the waveform distortion due to attenuation is ignored at this step. This distortion is small, but it does affect the estimates slightly. Thus, in the next step, we compute the attenuation operator $F(t; t^*)$ with the t^* computed in the first stage. using the expression

$$F(t; t^*) = \int_{-\infty}^{+\infty} \exp(-\pi f t^*) \exp \left\{ 2\pi i f \left[t + \frac{t^*}{\pi} \ln \left(\frac{f}{s_2} \right) \right] \right\} df$$

which is derived from an absorption-band model (Kanamori and Anderson, 1977). Here, s_2 is the frequency of the upper bound of the absorption band, here taken at 0.5 Hz. As far as the waveform is concerned, this parameter is not relevant as long as it is higher than our pass-band. Implicit with the attenuation operator is that Q is approximately constant over our frequency band, 0.008 to 0.0275 Hz. Then we compute

$$ScS_2^c(t; t^*) = g \cdot ScS_1(t) \otimes F(t; t^*) \quad (6)$$

where \otimes means convolution. This is to correct for the small difference in the frequency spectrum of ScS_1 and ScS_2 . A similar method was used by Chan and Der (1988) and Lay and Wallace (1988). Then we update t^* and Q such that the peak-to-peak amplitudes of $ScS_2^c(t; t^*)$ and $ScS_2(t)$ are matched.

In the course of iteration we compute the spectral ratio, $\left| \frac{ScS_2(f)}{ScS_1(f)} \right|$. Although we do not use it directly to estimate the Q values, we use it to check the consistency between our results and the time-domain method and the spectral ratios.

Our procedure described above is illustrated for several events in Figure 3. Having updated t^* , we compute $g \cdot \exp\left(-\frac{\pi ft_r}{Q}\right)$ in equation 3, and compare it with the observed spectral ratio, as shown in Figure 3. The computed trend is generally consistent with the spectral ratio, indicating that our time-domain approach is compatible with the frequency domain approach.

The results are listed in Table 1. Figures 4a, 4b, and 4c show the waveforms of $ScS_1(t)$, $ScS_2(t)$ and $ScS_2^c(t)$ at the end of iteration for many station-event pairs together with the updated Q and the cross correlation coefficient. We note that the records with $Cr \geq 0.93$ are almost noise free and the results are reliable. Since the amplitude differences between $ScS_2(t)$ and $ScS_2^c(t)$ for the records with $Q \geq 500$ are small, the result is considered marginal if the final correlation $Cr \leq 0.9$. The results for these cases will be shown with smaller symbols in the later figures.

As pointed out by Butler (1977), inclusion of attenuation causes a time shift of a few second for low Q records, but exact amounts of correction depend on the attenuation model, reference frequency, and the period of the waves used. Thus, we did not include this correction in Table 1, but since we include both uncorrected travel time and Q , the time shift can be computed if desired.

Figures like Figures 3 and 4 for all the events are included in the Appendices.

RESULTS

Figure 5 shows the results for all the station-event pairs on a global map (Figure 5a) and regional maps (Figures 5b and 5c). The bars are drawn in the direction of a line segment connecting the station and the event, with the center at the mid-point between the station and the epicenter. Although the spatial coverage is limited, we believe that these results are robust, especially for the cases with $Cr \geq 0.93$. In what follows we summarize a few key observations.

- 1) The Q values for KIP, Hawaii, are in the intermediate range. The Q values we obtained from the 2 high-quality records are consistent with the earlier result by Best et al. (1974) reinforcing the earlier conclusion that the depth-average structure beneath KIP is not drastically different from the average.
- 2) The results from AFI, Samoa Is., consistently indicate very high Q values, indicating that the attenuation in the entire mantle beneath AFI is very low. It is interesting that the travel time result indicates that the mantle beneath AFI is close to the slowest with $t_r = 944$ sec (*cf.* t_r for PREM is 933 sec).
- 3) For subduction zones, we can see two distinct patterns. If the station is on the trenchward side of the upper plate, the Q values are very high (e.g., LVC, Chile) indicating low attenuation in the mantle beneath the subducting oceanic plate. However, as the station location moves close to the volcanic axis and beyond, the attenuation rapidly increases (e.g., MAJO, Japan, LPAZ, Bolivia).
- 4) The stations on the volcanic islands of the subduction zones (e.g., ADK, GUMO, OGS) exhibit very low Q values.

- 5) A deep Spanish earthquake ($M_w=6.3$, $h=617$ km) exhibits an interesting pattern. The station to the south (RTC, Morocco) indicates a very high Q , while the Q values at stations in Spain are considerably lower. This pattern is similar to that at the subduction zone along South America.
- 6) The stations on the continents indicate relatively high Q . However, our spatial coverage is so limited that this should not be regarded as the general feature.

Our Q values tend to be higher than those obtained in earlier studies. There are at least two reasons for this. First, our estimate is at a period of about 50 sec which is generally greater than the period used in some of the earlier studies. We will show later that there is an indication that Q at a shorter period, around 20 sec, is considerably lower. Second, the difference may be due to very rapid spatial variations of Q . Our near-vertical measurements provide local measurements, and can resolve such short-range variations. Because of the way Q is measured (harmonic average weighted by the travel time, see equation 5), if we have adjacent high and low Q regions, the average for the two regions tends to be closer to the low value. For example, if we have adjacent regions with $Q=1000$ and 100 with equal travel times, the average Q is 182. We believe that the very high Q value we obtained represents a real local feature.

A possibility remains that the observed large amplitude ratio is a result of focusing caused by lateral heterogeneities in the mantle. However, the overall consistency between the amplitude ratio and the frequency spectral ratio, as shown in Figures 3a, 3b, and 3c, suggests that the focusing effect, even if it exists, is not dominant. The high spectral ratio over the entire frequency band for AFI shown in Figure 3a would

be difficult to explain without very high Q in the whole mantle. Here, we proceed with the assumption that focusing would not seriously affect our amplitude measurements, until some specific structures are proposed. However, considering our limited knowledge about lateral heterogeneities of the mantle structure, we cannot rule out the possibility of energy focusing.

Given the effects of upper-mantle layering discussed by Revenaugh and Jordan (1991), and of complex core-mantle boundary structures, all of which would tend to reduce the amplitude ratio, we consider the observed high ratio close to 0.5 remarkable. Although finite-wavelength effects, as discussed by Julian (2005) specifically for multiple ScS phases may need to be considered in some cases, the observed high amplitude ratios over the entire frequency band shown in Figure 3a appears to preclude a large volume of high attenuation.

Figure 6 shows a plot of Q vs. t_r (ScS₂ – ScS₁ travel time) for all the records used in this study. Although our spatial coverage is limited, Q seems to be uncorrelated with t_r . The mantle beneath AFI has a very high Q but t_r is the largest, $t_r=944$ sec. In contrast, the mantle beneath ADK is very attenuating, but t_r is the smallest ($t_r=930$ sec). This observation suggests that different factors, such as temperature, composition, anisotropy etc control mantle properties in a different way in different tectonic environments. For example, variations in Fe/Mg ratio may affect the shear wave speed but not necessarily Q .

Since our measurements are local while many of the earlier results are on a regional scale, it is not straightforward to compare our results with the previously

published results, especially if the short-range heterogeneity is strong, as suggested by this study. Nevertheless, we can make a few comparisons of Q measurements.

Press (1956), Anderson and Kovach (1964), and Kovach and Anderson (1964) obtained a relatively high whole-mantle Q around 500 for South American paths. This value is significantly larger than the values obtained in the later studies. Our result for station LVC, close to the events studied by Press (1956), Anderson and Kovach (1964), and Kovach and Anderson (1964), shows high Q values on the average and are generally consistent with these early studies.

The average of our 3 measurements at KIP is $Q=276$, which is close to the value obtained by Best et al. (1974) from the KIP record of the 1973 earthquake. Sipkin and Jordan (1979) obtained $Q=188$ from the same record. The difference between this value and ours can be attributed to noise. However, for our present discussion, all these values suggest that the attenuation beneath KIP, Hawaii, is intermediate.

Lay and Wallace (1983) used an event in El Salvador and estimated $Q=145$ near Mexico. This value is compatible with the Q values, 157 and 423, we obtained from the station UNM. Lay and Wallace (1983) obtained $Q=232$ for the paths from El Salvador to South America which can be compared with the values we obtained from OTAV ($Q=138, 115, 353$). Their result for the paths beneath northern South America ($Q=93$) can be compared with the relatively low Q values we obtained from LAPZ ($Q=135, 114, 143$). Lay and Wallace (1988) obtained a relatively high value ($Q=344$) for the Pacific Northwest, which can be compared with our values from OCWA ($Q=313$) and LLLB (225). They obtained a relatively high value, $Q=257$, for the Pacific. We do not have

many observations in this area, but we also obtained a fairly high value ($Q=466$) from the record at COR.

For most subduction zones, our Q values range from 125 to 500, which is compatible with $Q=290$ obtained by Yoshida and Tsujiura (1975) beneath Japan, and with $Q=187$ to 233 estimated by Chan and Der (1988) near Japan. Sipkin and Jordan (1980b) obtained $Q=197$ and 266 for the Kuril-Japan subduction zone and the western South America subduction zones, respectively. Our range of Q is from 140 to 300 for Japan (Figure 6). This range is comparable to that for Japan obtained by Kato et al. (2001)

The Q values we obtained for the South America subduction zone exhibit large variations from 114 to 143 for LPAZ, and 204 to 1400 for LVC, but if averaged, this range is compatible with the somewhat high value, 266, reported by Sipkin and Jordan (1980b). Chan and Der (1988) reported a relatively small $t^*=2.5$ (i.e., high $Q=380$) for an event on 11/17/1984 recorded at AFI ($\Delta=7.7^\circ$). Although the distance is slightly larger than the threshold distance we used, $\Delta = 5.0^\circ$, this value appears to be lower than our values at AFI. We examined the record of this event used by Chan and Der (1988), and found that the difference is mainly due to the difference in the frequency band. If we use our frequency band, 0.008 to 0.0275 Hz, we obtained a large Q , at least 1000, but over the higher frequency band used by Chan and Der (1988), we obtained a lower value compatible with that obtained by them. This frequency dependence is opposite to what is suggested by laboratory data (e.g., Jackson and Faul, 2010; Jackson et al., 2009), but the lower value of Q measured by Chan and Der (1988) could be due to scattering of energy caused by structural heterogeneity rather than the intrinsic effect. Souriau et al.

(2012) (figure 6 and table 1) lists Q_{670} (average Q above the depth of 670 km with PREM's lower mantle Q)=148 for the Tonga-Kermadec subduction zone. This value corresponds to a whole mantle Q =235 which falls in the middle of the range of Q we obtained for the Tonga-Kermadec subduction zone (Figure 6).

Figures 5b and 5c show scattered high Q spots indicating that the mantle can have a very high Q value locally. In fact, Gomer and Okal (2003) found an unusually high Q =366 beneath the Ontong-Java Plateau.

To compare the ScS_2 - ScS_1 travel times we measured with those for a tomographic model, we measured t_r for the 3-D synthetics computed for the Kustowski et al.'s (2008) tomographic model (Figure 2). We added a result obtained from the 3-D synthetic computed for station AFI (9/29/2009, Samoa Is. earthquake, M_w =8.1). We obtained, t_r =938 sec (KIP), 931 sec (ADK), 933 sec (PET), and 939 sec (AFI) which are generally consistent with our measurements, except that the observed t_r for AFI is about 5 sec larger than predicted by the tomographic model.

TEST WITH SYNTHETIC SEISMOGRAMS

Since we have not explored the effect of 3-D structures on amplitude measurements, strictly speaking, our Q values presented above should be interpreted as apparent Q rather than intrinsic Q . Without specific 3-D structures for each region we cannot address this question at present, but it is instructive to test our method using the 1-D and 3-D synthetic seismograms available at the IRIS data center. We have already made some comparisons in Figure 2. Using the same screening criteria as that we used

for the observed seismograms (Figure 1), we have extracted 699 1-D seismograms and 703 3-D seismograms.

Test with 1-D Synthetic Seismograms.

We measured Q and the travel time t_r using the 1-D (PREM) synthetics. Since the structure is laterally homogeneous, the result is expected to be essentially independent of the station location. We found that the measured Q and t_r values are tightly clustered around the averages of Q and t_r for PREM, 294 and 933 sec, respectively. This is not surprising but the result confirms that our assumption that the small difference in the radiation pattern of ScS₁ and ScS₂ does not affect the result. Also, the small deviation from the vertical incidence at the surface and the mantle-core boundary does not affect our measurements. The PREM model has a simple 24 km thick 2-layered crust, but we did not see any obvious effects of its frequency-dependent response; we did not see any systematic differences between shallow and deep events.

Thus, the PREM synthetics are useful as reference synthetic seismograms for interpretation of 3-D synthetics as discussed below.

Test with 3-D Synthetic Seismograms.

We used the 3-D synthetics in the IRIS data base. We found that the result of t_r measurements using the 3-D synthetics is consistent with those obtained for selected station as shown in the previous section. In contrast, the result of Q measurements is far more complex, and suggests significant influence of 3-D structures on Q measurements. Thus, we focus on the result of Q measurements in the following.

First, we compare the result for the event-station pairs we used in this study. Since the IRIS synthetic seismograms are not available for the earlier events, we found 3-D synthetics for only 32 pairs. Figure 7 compares the Q values determined from these pairs. The observed Q values for these pairs are shown for comparison. Since the Q model, QL6, used for the 3-D synthetics is a 1-D model, the Q values computed from the 3-D synthetics, Q_{3-D} must be approximately constant. Thus, the variation of Q values for different event-station pairs must be due to either the 3-D effect or measurement errors caused by noise. Although the scatter of Q_{3-D} is considerably larger than that from the 1-D synthetics, we did not find particularly anomalous values. The harmonic average of Q_{3-D} is 212, which is slightly smaller than the average for PREM, 294. The observed Q values for the stations LVC and RTC are very large, but the Q_{3-D} values are 365, and 384 for LVC and RTC, respectively.

We did not have any 3-D synthetics for the events recorded at AFI for which we obtained very high $Q=1400$. We examined the synthetic AFI records for the events we did not study. Figures 8A and 8B compare the 3-D and 1-D synthetics for AFI for the 2 events we extracted from the IRIS data base. One event (2009.272) is shallow (12 km) and the other (2009.272) is at an intermediate depth (242 km). For both records, the amplitude ratio on the 3-D synthetic is essentially the same as that on the 1-D synthetic. The measured Q_{3-D} are 295 and 291 for the first and the second event. Thus, the 3-D structure used for the synthetics does not significantly affect the amplitude measurements, and the observed high Q values must be due to something else, either high intrinsic Q , or more complex 3-D structures than that used for the IRIS 3-D synthetics.

We found that the 3-D synthetics for many events which occurred in a shallow continental crust are extremely complex due to the scattered energy over the entire time window containing ScS₁ and ScS₂. Figures 8C and 8D show two examples. The amplitude of the scattered wave is so large that we cannot measure the amplitude ratio, ScS₂/ScS₁, accurately. We have practically no records of this kind (i.e., shallow continental event) in our observed data set. Probably, the noise on those records is so large that they must have been screened out. The noise on the 1-D synthetics for these events is low enough to show clear isolated ScS₁ and ScS₂ phases. Since the thickness of the oceanic crust is much thinner than that of PREM (24 km), we would not have this difficulty for the events in shallow oceanic events. The AFI record of a shallow event shown in Figure 8A does show some scattered energy, but it is not nearly as bad as that for the events in a continental crust.

We found 21 event-station pairs (out of 703 total pairs) that show a very high $Q_{3-D} = 1400$. These 21 pairs include the very noisy records shown in Figures 8C and 8D. Many other records have similar noise characteristics. Although not every shallow event is as bad as those shown in Figures 8C and 8D, the amplitude measurements from these seismograms are likely affected by the scattered energy and unreliable. Since most of these events are shallow, we remove the events shallower than 30 km. Then, we are left with only 4 records with $Q_{3-D} = 1400$. Three of these 4 records are from LPAZ shown in Figures 8E, 8F and 8G. Figure 8E, in particular, clearly shows that the ratio ScS₂/ScS₁ is significantly larger than that on the reference 1-D record. We do not have a definitive explanation for this, but the 3-D structure around the station LPAZ is most likely the cause of this large ratio. One possibility is that the extremely high elevation (4,817 m)

and the corresponding thick crust may have different responses to ScS₁ and ScS₂, resulting in the anomalous amplitude ratio. This example indicates that some 3-D structures can cause significant errors in the amplitude measurements, and we need to exercise caution in interpreting our observations. If the high elevation and the thick crust are indeed responsible for this, we may have to worry about the significance of the observed high- Q values at stations LVC (2,960 m) too. To further investigate this question, it would be necessary to consider the effect of detailed crustal velocity and Q structures beneath the individual stations.

The character of the noise on the 3-D synthetics for shallow events (e.g., Figures 8C, 8D, 8G, and 8H) is somewhat different from that of the record we used to determine the screening criteria (Figure 1). On the 3-D synthetics, the most problematic noises are the ones immediately after ScS₁ and ScS₂ (Figures 8C, 8D, 8G, and 8H), while we use a window in the mid section between ScS₁ and ScS₂ to define the noise level. We are not sure what causes the large reverberations before ScS₂ and even after ScS₂ on the 3-D synthetics, but this question needs to be investigated with more detailed studies of synthetic seismograms.

We can summarize the result of this test as follows. Except for shallow events in the continental crust, the effect of the particular 3-D structure we used is not very serious in general. The only exception seems to be the case for the stations with high altitude possibly with a thick crust. The results for the oceanic event are not significantly affected. We believe that the effect we see in this test is primarily due to the crust. Since the mantle tomographic model used for the 3-D synthetics is primarily based on global studies, it should be regarded as representing only long wavelength

heterogeneities. Thus, our test cannot address the effect of short wavelength structural heterogeneities, and further studies are obviously required before we can make more definitive interpretations of our results in terms of intrinsic Q in the mantle.

DISCUSSION

As shown above, our results are in general qualitatively compatible with those reported in the many previous studies, given the difference in the averaging scheme. However, the very high Q values we obtained for the paths near AFI and those at LVC and PET appear different from those obtained in the previous studies.

The results from AFI are robust. If we include ScS₃ and ScS₄ in the analysis, the Q values may decrease slightly, but they are still in our high Q category. At face value, this result is in contradiction with the generally held view that the Samoa Is. is an active hotspot of deep origin (e.g., Koppers et al., 2008). The upper and lower mantles in this region have been tomographically imaged to be anomalously slow (e.g., French et al., 2013). Our result with a large $t_r = 944$ sec is consistent with this. However, Gung and Romanowicz's (2004, figure 9) result indicates that the mantle near the Samoa island has a very low Q at all depths in the upper mantle. One way to reconcile this apparent contradiction is to introduce a strongly laterally heterogeneous structure which can enhance the amplitude of ScS by focusing energy. If the mantle beneath the Samoa Is. has a low velocity core surrounded by a high velocity sheath, it can enhance the ScS amplitude by focusing. It must also explain the relatively constant amplitude ratio of ScS₂/ScS₁ over the frequency band of 0.008 to 0.0275 Hz as observed (Figure 3a). If

such a structure can be constructed, it would be a viable structure that might explain all the observations, and provides a strong constraint on the type of structures beneath the Samoa Is. Construction of such a model would be an interesting project.

The very high Q values observed at stations LVC and PET indicate that the mantle beneath the oceanic plate near the trench is not attenuating. Sipkin and Jordan (1980b) found higher Q values at Kuril-Japan and western South American subduction zones than those beneath the ocean basins. Our observations of very high Q values may be a manifestation of this trend. The pattern of Q value distribution found for a deep Spanish earthquake shows a similar trend (Figure 5c). However, in case of LVC, the high elevation and the thick crust beneath the station may have affected our measurements.

ACKNOWLEDGMENTS

We benefited a great deal from Yoko Tono's careful independent examinations of some of the records we used. We thank Yoshio Fukao, Hitoshi Kawakatsu, and Thorne Lay for careful reviews of the early version of the manuscript. We thank three anonymous reviewers for providing us with helpful suggestions. We extensively used the continuous broadband seismograms orderly archived at the Data Management Center of IRIS without which this study would not have been possible. We acknowledge the contributions of many global seismic networks which provided their data to the IRIS database.

REFERENCES SITED

- Anderson, D. L., and R. L. Kovach (1964), Attenuation in the mantle and rigidity of the core from multiply reflected core phases, *Proc. N. A. S.*, 51, 168172.
- Bassin, C., G. Laski, and G. Masters (2000), The Current Limits of resolution for surface wave tomography in North America, *EOS Trans. AGU*, 81, 2000.
- Best, W. J., L. R. Johnson, and T. V. McEvilly (1974), ScS and the mantle beneath Hawaii, *EOS (transactions, American Geophysical Union)*, 55, 1147.
- Butler, R. (1977), A source of bias in multiple ScS differential travel times determined by waveform correlation, *Geophysical Research Letters*, 4(12), 593-595, doi:10.1029/GL004i012p00593.
- Chan, W. W., and Z. A. Der (1988), Attenuation of multiple ScS in various parts of the world, *Geophysical Journal International*, 92(2), 303-314, doi:10.1111/j.1365-246X.1988.tb01141.x.
- Dziewonski, A. M., and D. L. Anderson (1981), Preliminary reference Earth model, *Physics of the Earth and Planetary Interiors*, 25(4), 297-356, doi:http://dx.doi.org/10.1016/0031-9201(81)90046-7.
- Durek, J. J., and G. Ekström (1996), A radial model of anelasticity consistent with long-period surface-wave attenuation, *Bulletin of the Seismological Society of America*, 86(1A), 144-158.
- French, S., V. Lekic, and B. Romanowicz (2013), Waveform Tomography Reveals Channeled Flow at the Base of the Oceanic Asthenosphere, *Science*, 342(6155), 227-230, doi:10.1126/science.1241514.
- Gomer, B. M., and E. A. Okal (2003), Multiple-ScS probing of the Ontong-Java Plateau, *Physics of the Earth and Planetary Interiors*, 138(3-4), 317-331, doi:http://dx.doi.org/10.1016/S0031-9201(03)00114-6.

Gung, Y., and B. Romanowicz (2004), Q tomography of the upper mantle using three-component long-period waveforms, *Geophysical Journal International*, 157(2), 813-830, doi:10.1111/j.1365-246X.2004.02265.x.

Jackson, I., A. Barnhoorn, Y. Aizawa, and C. Saint (2009), Improved procedures for the laboratory study of high-temperature viscoelastic relaxation, *Physics of the Earth and Planetary Interiors*, 172(1–2), 104-115, doi:http://dx.doi.org/10.1016/j.pepi.2008.03.010.

Jackson, I., and U. H. Faul (2010), Grainsize-sensitive viscoelastic relaxation in olivine: Towards a robust laboratory-based model for seismological application, *Physics of the Earth and Planetary Interiors*, 183(1–2), 151-163, doi:http://dx.doi.org/10.1016/j.pepi.2010.09.005.

Julian, B. R. (2005), What can seismology say about hotspots?, in *Plates, plumes, and paradises: Geological Society of America Special Paper 388*, edited by G. R. Foulger, Natland, J. H., Presnall, D. C., and Anderson, D. L., pp. 155-169, Geological Society of America.

Kanamori, H., and D. L. Anderson (1977), Importance of physical dispersion in surface wave and free oscillation problems: Review, *Reviews of Geophysics*, 15(1), 105-112, doi:10.1029/RG015i001p00105.

Kanamori, H. (2005), Real-time seismology and earthquake damage mitigation *Annual Review of Earth and Planetary Sciences*, 33, 195-214, DOI: 110.1146/annurev.earth.1133.092203.122626.

Kato, M., Misawa, M., and Kawakatsu, H., 2001, Small subsidence of the 660-km discontinuity beneath Japan probed by ScS reverberations: *Geophysical Research Letters*, v. 28, no. 3, p. 447-450.

Koppers, A. A. P., J. A. Russell, M. G. Jackson, J. Konter, H. Staudigel, and S. R. Hart (2008), Samoa reinstated as a primary hotspot trail, *Geology*, 36(6), 435-438, doi:10.1130/g24630a.1.

Kovach, R. L., and D. L. Anderson (1964), Attenuation of shear waves in the upper and lower mantle, *Bulletin of the Seismological Society of America*, 54(6A), 1855-1864.

Kustowski, B., G. Ekström, and A. M. Dziewoński (2008), Anisotropic shear-wave velocity structure of the Earth's mantle: A global model, *Journal of Geophysical Research: Solid Earth*, 113(B6), B06306, doi:10.1029/2007JB005169.

Lay, T., and T. C. Wallace (1983), Multiple SCS travel times and attenuation beneath Mexico and Central America, *Geophysical Research Letters*, 10(4), 301-304, doi:10.1029/GL010i004p00301.

Lay, T., and T. C. Wallace (1988), Multiple ScS attenuation and travel times beneath western North America, *Bulletin of the Seismological Society of America*, 78(6), 2041-2061.

Nakanishi, I. (1979), Attenuation of multiple ScS waves beneath the Japanese Arc, *Physics of the Earth and Planetary Interiors*, 19(4), 337-347, doi:http://dx.doi.org/10.1016/0031-9201(79)90006-2.

Okal, E. A., and D. L. Anderson (1975), A study of lateral inhomogeneities in the upper mantle by multiple ScS travel-time residuals, *Geophysical Research Letters*, 2(8), 313-316, doi:10.1029/GL002i008p00313.

Press, F. (1956), Rigidity of the Earth's core, *Science*, 124, 1204.

Revenaugh, J., and T. H. Jordan (1991), Mantle layering from ScS reverberations: 1. Waveform inversion of zeroth-order reverberations, *Journal of Geophysical Research: Solid Earth*, 96(B12), 19749-19762, doi:10.1029/91JB01659.

Romanowicz, B., and B. J. Mitchell (2007), Deep earth structure - Q of the Earth from crust to core, in *Treatise on Geophysics*, edited by B. Romanowicz, and Dziewonsli, A. , pp. 731-774, Elsevier, Amsterdam.

Sipkin, S. A., and T. H. Jordan (1975), Lateral heterogeneity of the upper mantle determined from the travel times of ScS, *Journal of Geophysical Research*, 80(11), 1474-1484, doi:10.1029/JB080i011p01474.

Sipkin, S. A., and T. H. Jordan (1976), Lateral heterogeneity of the upper mantle determined from the travel times of multiple ScS, *Journal of Geophysical Research*, 81(35), 6307-6320, doi:10.1029/JB081i035p06307.

Sipkin, S. A., and T. H. Jordan (1979), Frequency dependence of QScS, *Bulletin of the Seismological Society of America*, 69(4), 1055-1079.

Sipkin, S. A., and T. H. Jordan (1980a), Multiple ScS travel times in the western Pacific: Implications for mantle heterogeneity, *Journal of Geophysical Research: Solid Earth*, 85(B2), 853-861, doi:10.1029/JB085iB02p00853.

Sipkin, S. A., and T. H. Jordan (1980b), Regional variation of QScS, *Bulletin of the Seismological Society of America*, 70(4), 1071-1102

Souriau, A., L. Rivera, A. Maggi, and J.-J. L  v  que (2012), Seismic attenuation in the eastern Australian and Antarctic plates, from multiple ScS waves, *Geophysical Journal International*, 190(1), 569-579, doi:10.1111/j.1365-246X.2012.05501.x.

Tromp, J., et al. (2010), Near real-time simulations of global CMT earthquakes, *Geophysical Journal International*, 183(1), 381-389, doi:10.1111/j.1365-246X.2010.04734.x.

Yoshida, M., and M. Tsujiura (1975), Spectrum and attenuation of multiply reflected core phases, *J. Physics Earth*, 23, 31-42.

Figure Caption

Figure 1. Illustration of data selection method. Green dots indicate the theoretical arrival times of ScS₁ and ScS₂ phases. Vertical dashed lines with arrow-heads indicate the peak-to-peak amplitude of ScS₁ and ScS₂ phases. Horizontal red dashed lines indicate the approximate RMS amplitude of the noise. Time windows W₁, and W₂ are used for ScS₁ and ScS₂ to compute the cross correlation C_r , and W_n indicates the window used for determination of the noise level.

Figure 2. Examples of the displacement records (band-passed at 0.008 to 0.0275 Hz) used in this study. For some records, synthetic records computed for PREM and a 3-D earth model are shown for comparison. r is the ScS₂/ScS₁ amplitude ratio and C_r is the correlation coefficient between ScS₁ and ScS₂.

Figure 3a. Illustration of the analysis method for an AFI seismogram, which represents a high Q case. A). The original broad-band record. B). Band-passed (0.008 to 0.0275 Hz) displacement record showing ScS₁ and ScS₂ phases. C) Comparison of $(g \cdot ScS_1)$ (thin black trace), ScS₂ (blue trace), and $ScS_2^c (= g \cdot ScS_1 \otimes F(t; t^*))$ (red trace). In this figure, the red trace is on top of black trace because of the very high $Q=1400$. The peak-to-peak amplitudes of red and blue traces are matched to determine t^* . D). The Fourier spectrum of ScS₁ and ScS₂ phases and the spectral ratio (green). Shaded parts of the spectrum are not used. The dashed green line indicates the trend given by the t^* determined by amplitude matching shown in C). The left ordinate is \log_{10} (displacement amplitude spectral density) in arbitrary unit, common to both ScS₁ and ScS₂. E) Information on the event and stations, and details of the parameters determined.

Figure 3b. Illustration of the analysis method for an ADK seismogram which represents a low Q case. (see caption for Figure 3a.)

Figure 3c. Illustration of the analysis method for a KIP seismogram which represents an intermediate case. (see caption for Figure 3a.)

Figure 4a. Comparison of the peak-to-peak amplitudes of ScS₁, ScS₂, and ScS₂^c (the same as C) of Figure 3a,) for several records which show high Q . Red and blue traces are almost on top of each other.

Figure 4b. Comparison of the peak-to-peak amplitudes of ScS₁, ScS₂, and ScS₂^c (the same as C) of Figure 3a,) for several records which show low Q .

Figure 4c. Comparison of the peak-to-peak amplitudes of ScS₁, ScS₂, and ScS₂^c (the same as C) of Figure 3a,) for several records which show intermediate Q .

Figure 5. a) Global and b), c) regional maps showing the distribution of Q and t_r . The color code is given for the 3 categories: high Q (blue, 800 to 1400), intermediate Q (green, 180 to 800), and low Q (red, <180), and is the same for global and regional maps. The color code for the t_r maps is: Red, $t_r > 940$ sec; Green ($935 \text{ sec} < t_r \leq 940 \text{ sec}$); Blue ($t_r < 935 \text{ sec}$).

Figure 6. Q vs. 2-way travel time of ScS for the records used in this study. The ellipses indicate approximate grouping of the stations. The circle for LVC is only for the high Q group. Small symbols indicate less reliable data. Heavy black circle indicates the point for PREM. The Q values in the parentheses on the right ordinate indicate the average Q

values for the top 670 km of the mantle with the assumption that the lower mantle Q is 1400.

Figure 7. Comparison of observed Q values, Q_{obs} (red), with those measured from the 3-D synthetic seismograms, Q_{3-D} (blue), for the station-event pairs studied.

Figure 8. Comparison of 3-D synthetics (black trace) with 1-D synthetics (red trace).

Table 1. Seismograms used for the analysis and Q , t^* , τ (period), t_r (ScS₂ – ScS₁ travel time), s/n_1 (S/N of ScS₁), s/n_2 (S/N of ScS₂), C_r , S_{rp} , lat (event latitude), lon (event longitude), depth, Mw, and the epicentral distance in degree. The record with .LHX is the rotated record with shear wave amplitude maximized.

Appendix 1.

Details of the analysis and results for the complete set of records used in this study.

A). The original broad-band record. B). Band-passed (0.008 to 0.0275 Hz) displacement record showing ScS₁ and ScS₂ phases. C) Comparison of ($g \cdot ScS_1$) (thin black trace), ScS₂ (blue trace), and $ScS_2^c (= g \cdot ScS_1 \otimes F(t; t^*))$ (red trace). The peak-to-peak amplitudes of red and blue traces are matched to determine t^* . D). The Fourier spectrum of ScS₁ and ScS₂ phases and the spectral ratio (green). Shaded parts of the spectrum are not used. The dashed green line indicates the trend given by the t^* determined by amplitude matching shown in C). The left ordinate is \log_{10} (displacement amplitude

spectral density) in arbitrary unit, common to both ScS_1 and ScS_2 . E) Information on the event and stations, and details of the parameters determined.

Appendix 2.

Comparison of the peak-to-peak amplitudes of ScS_1 , ScS_2 , and ScS_2^c for all the records used in this study.

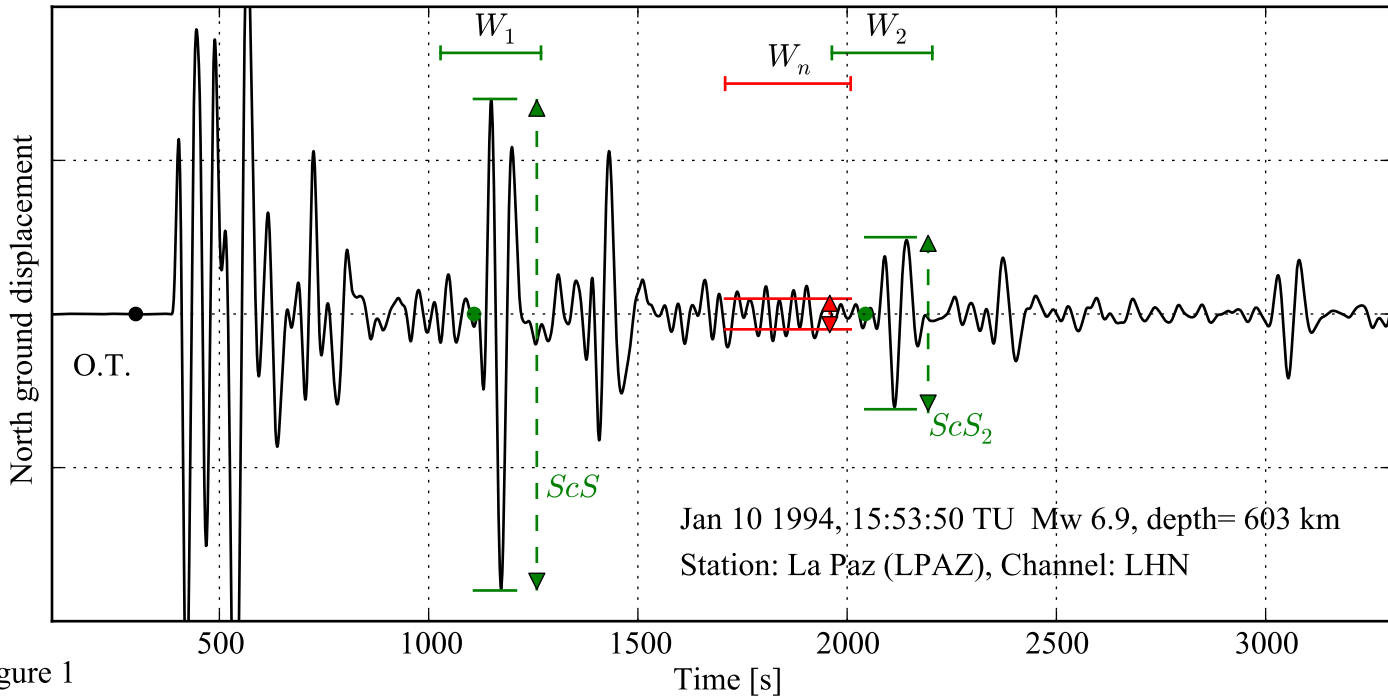


Figure 1

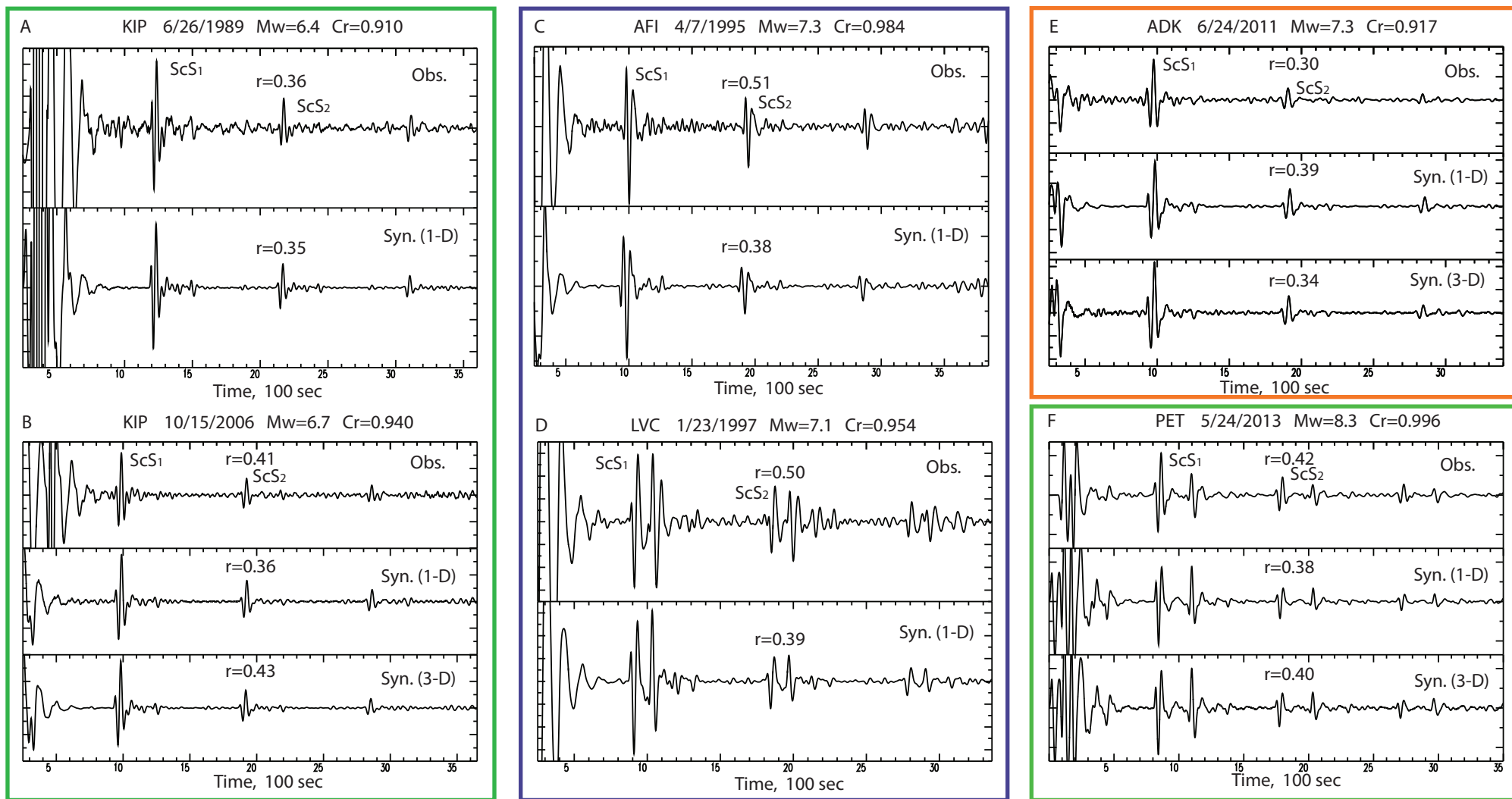


Figure 2

1995.097.22.01.58.718.IU.AFI..LHN.SAC

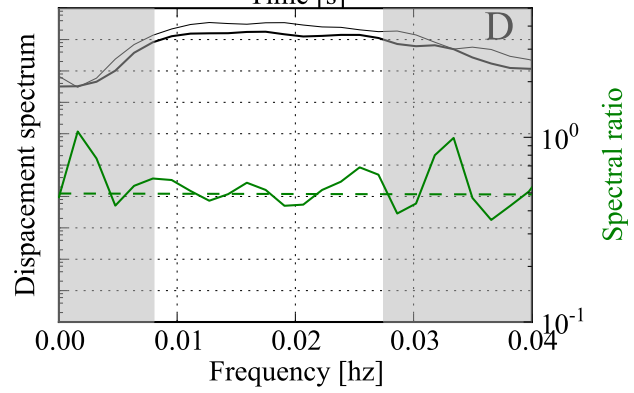
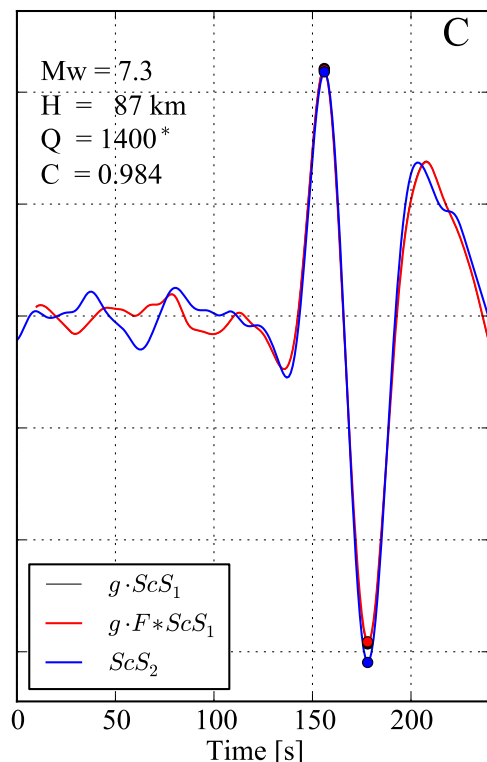
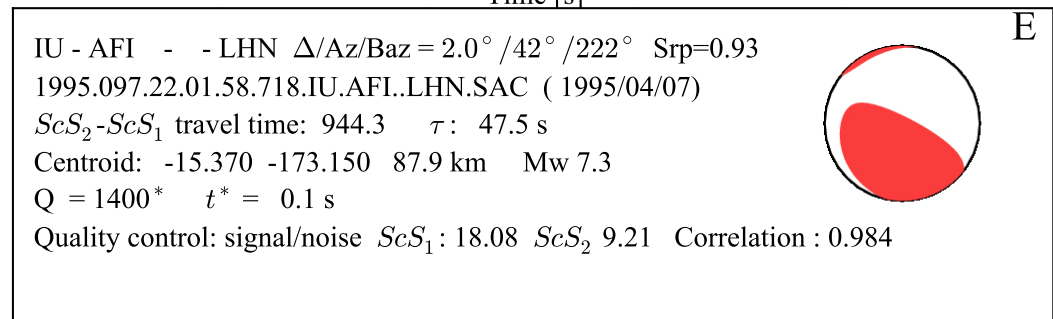
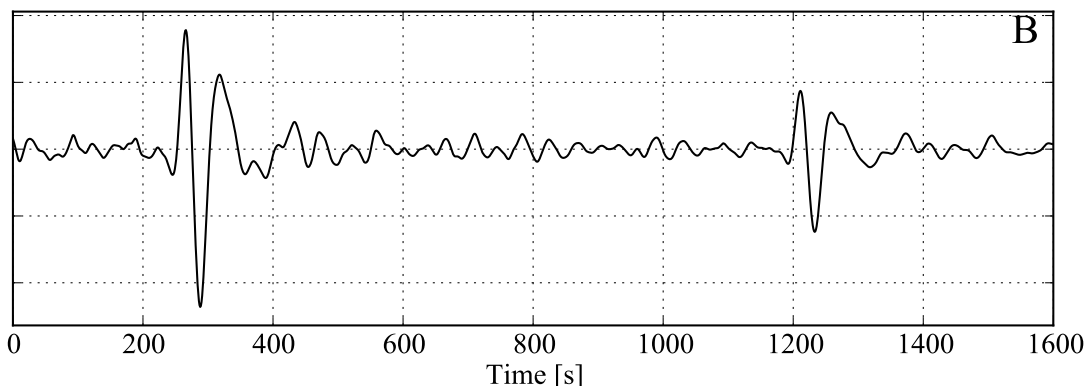
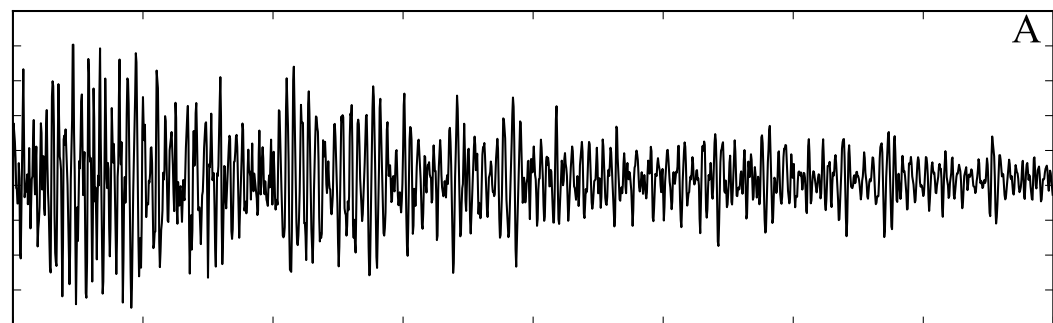


Figure 3a

2011.175.03.04.39.069.IU.ADK.00.LH1.SAC

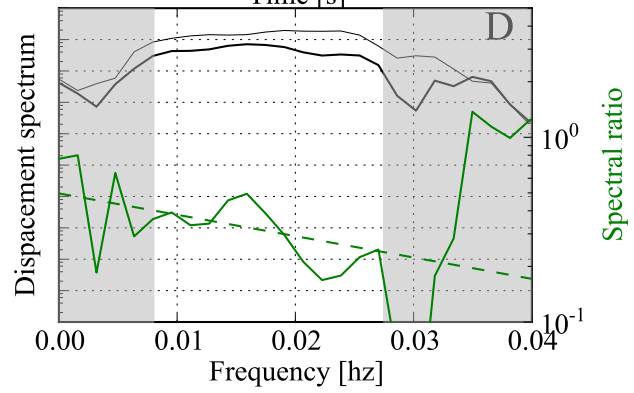
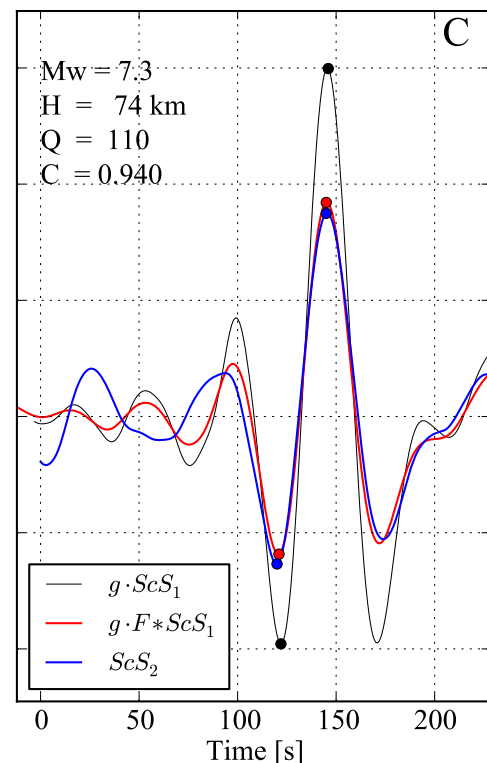
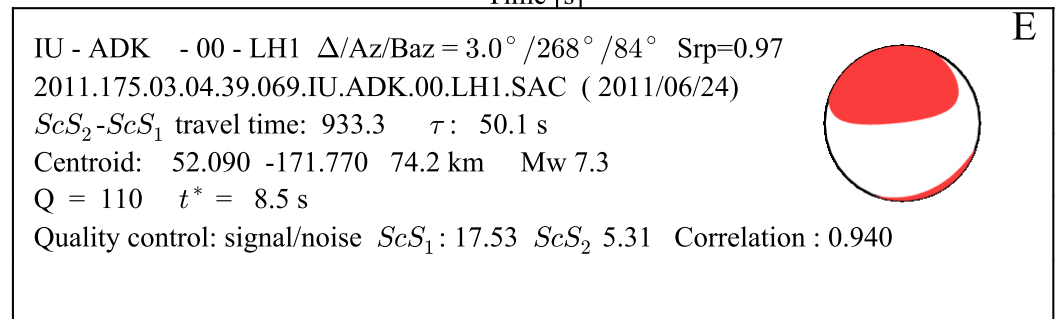
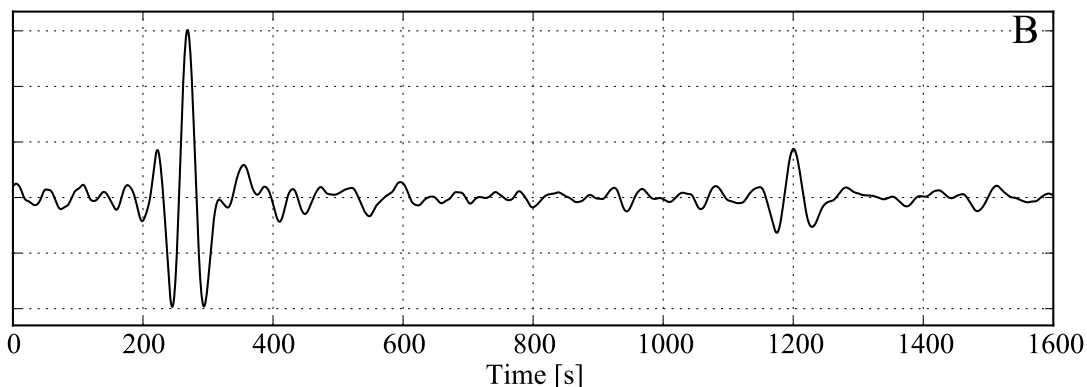
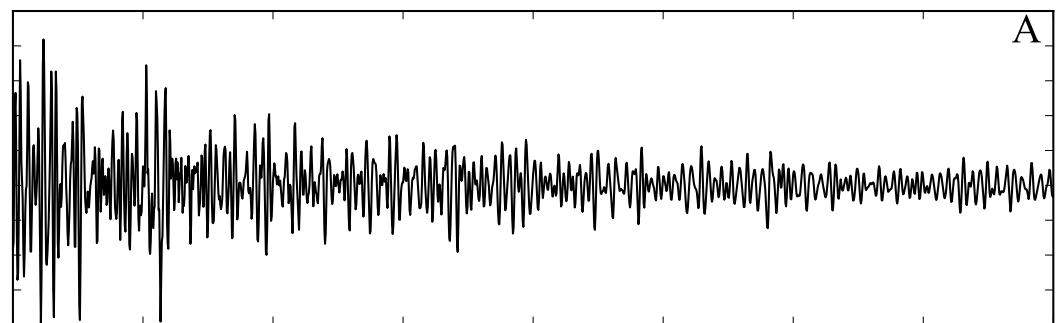


Figure 3b

1989.177.03.22.03.157.G.KIP..LHN.SAC

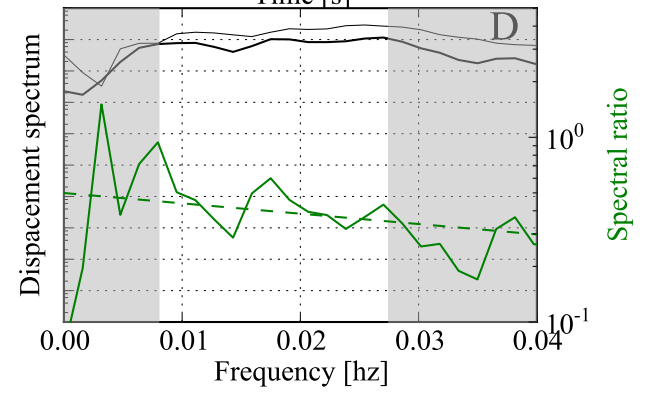
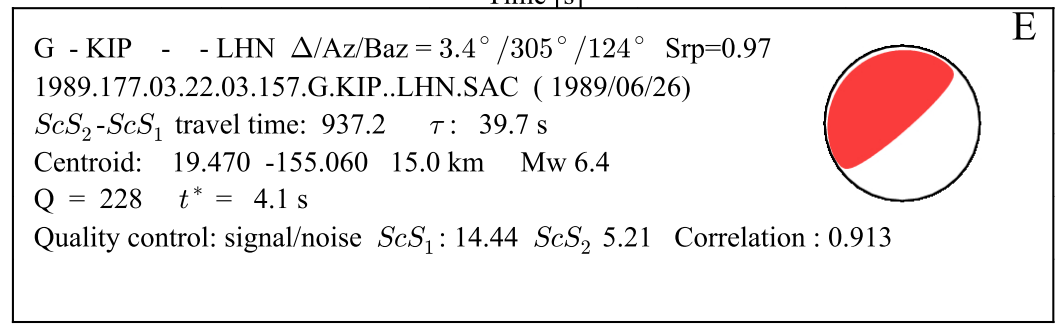
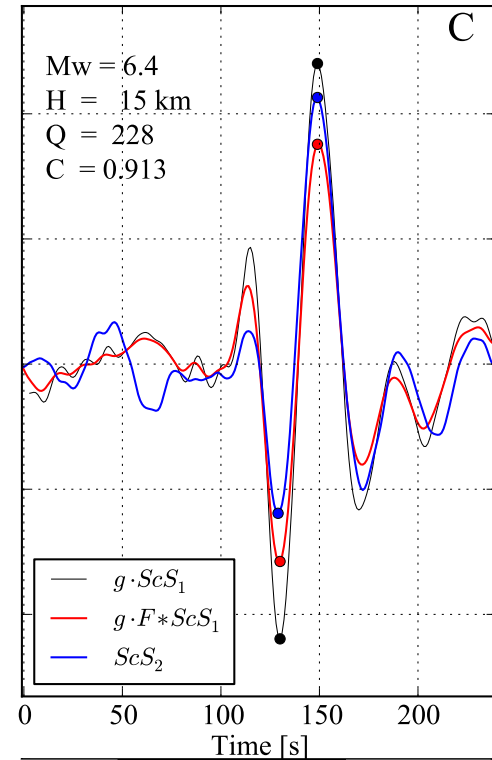
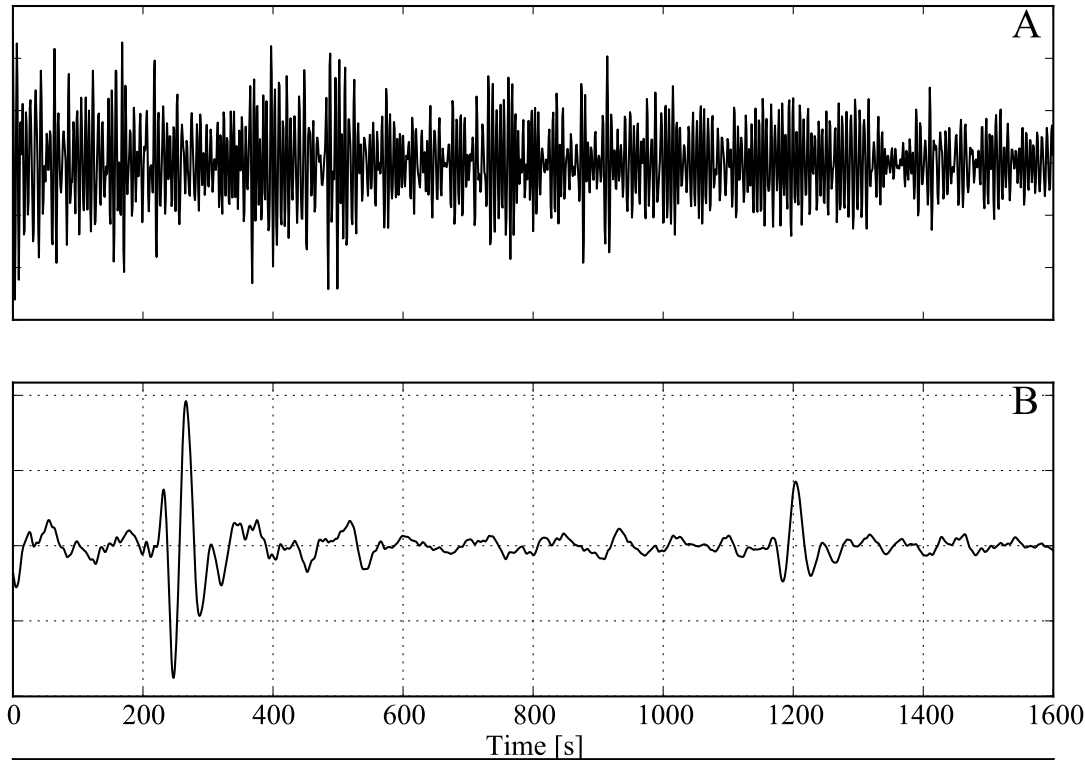


Figure 3c

High Q

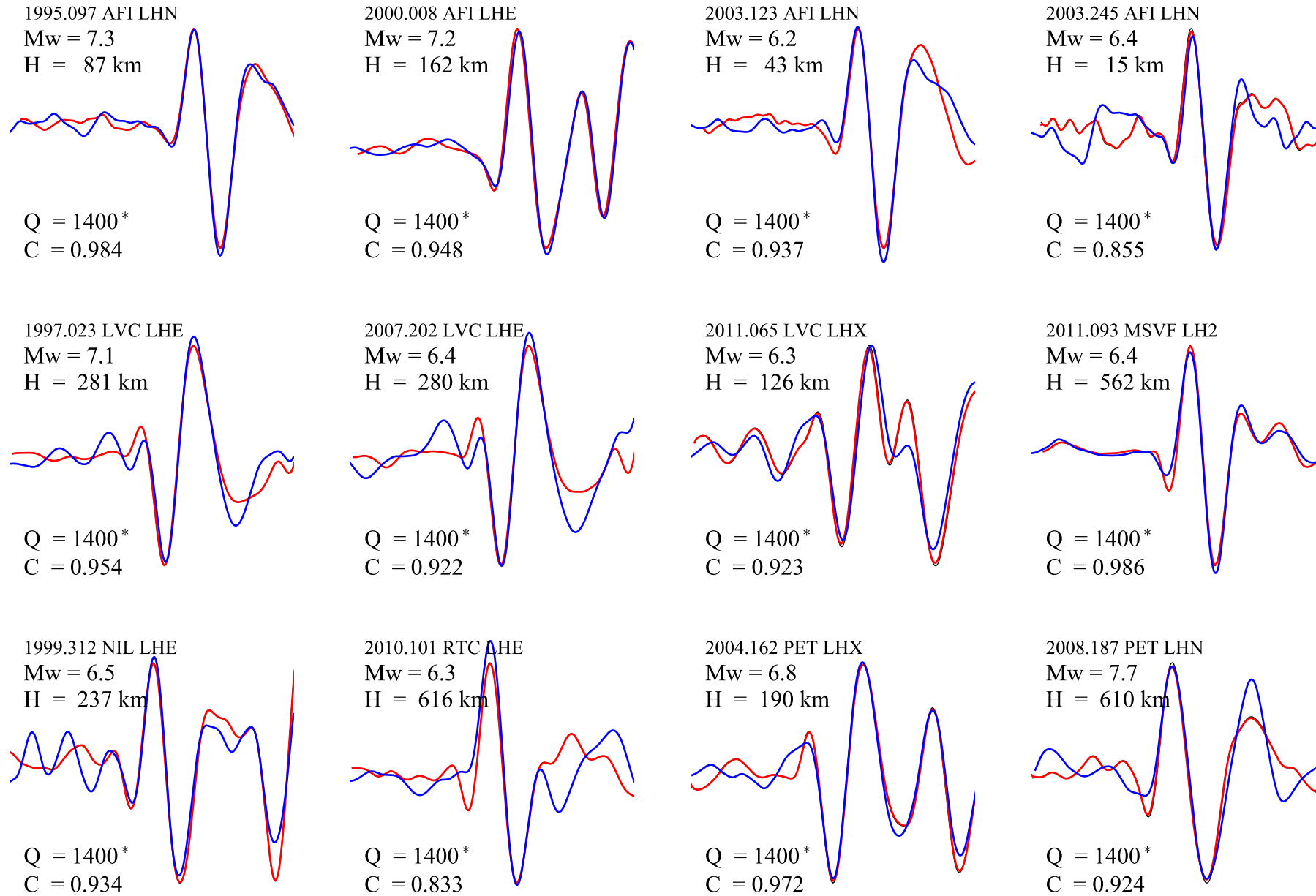


Figure 4a

Low Q

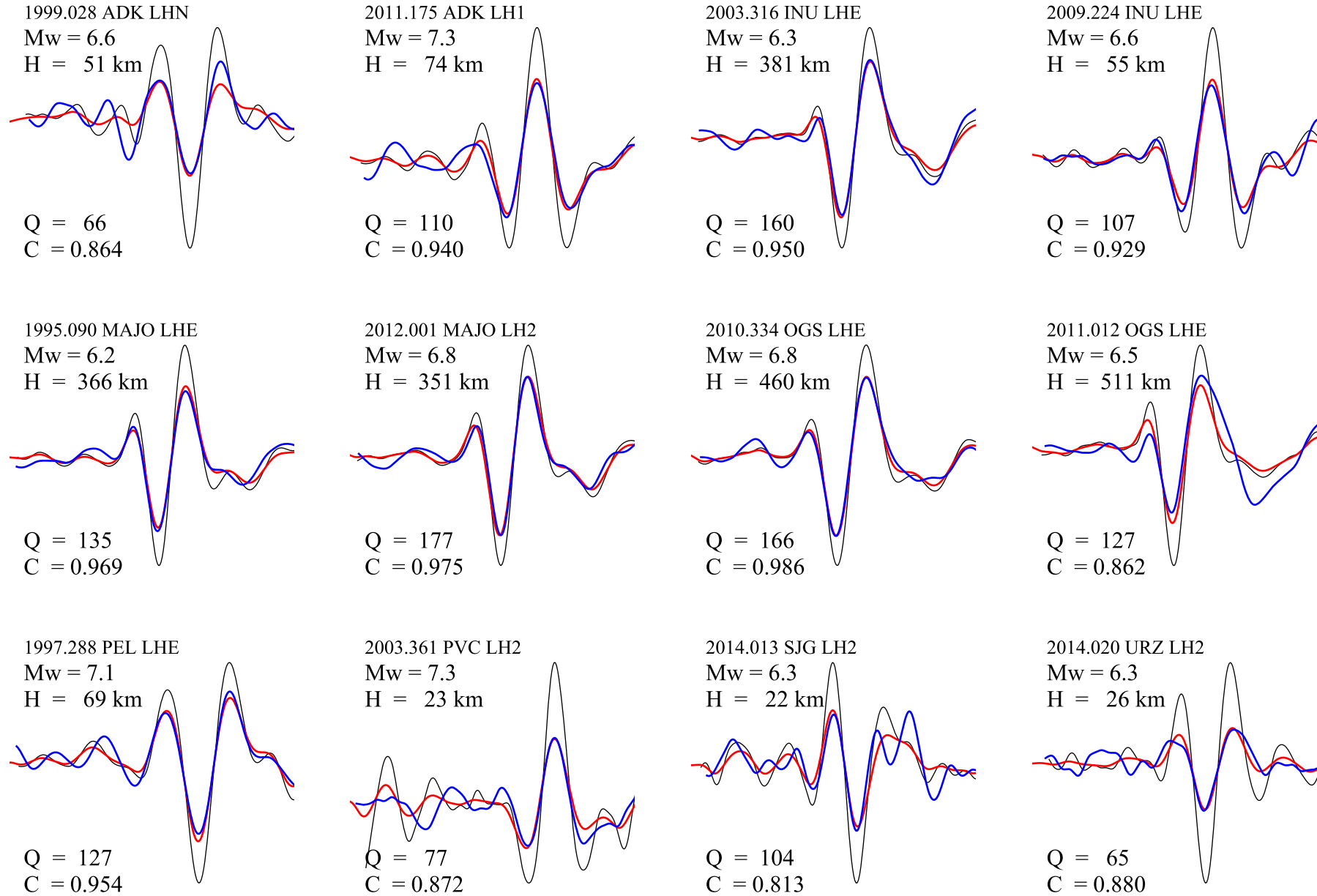


Figure 4b

Intermediate Q

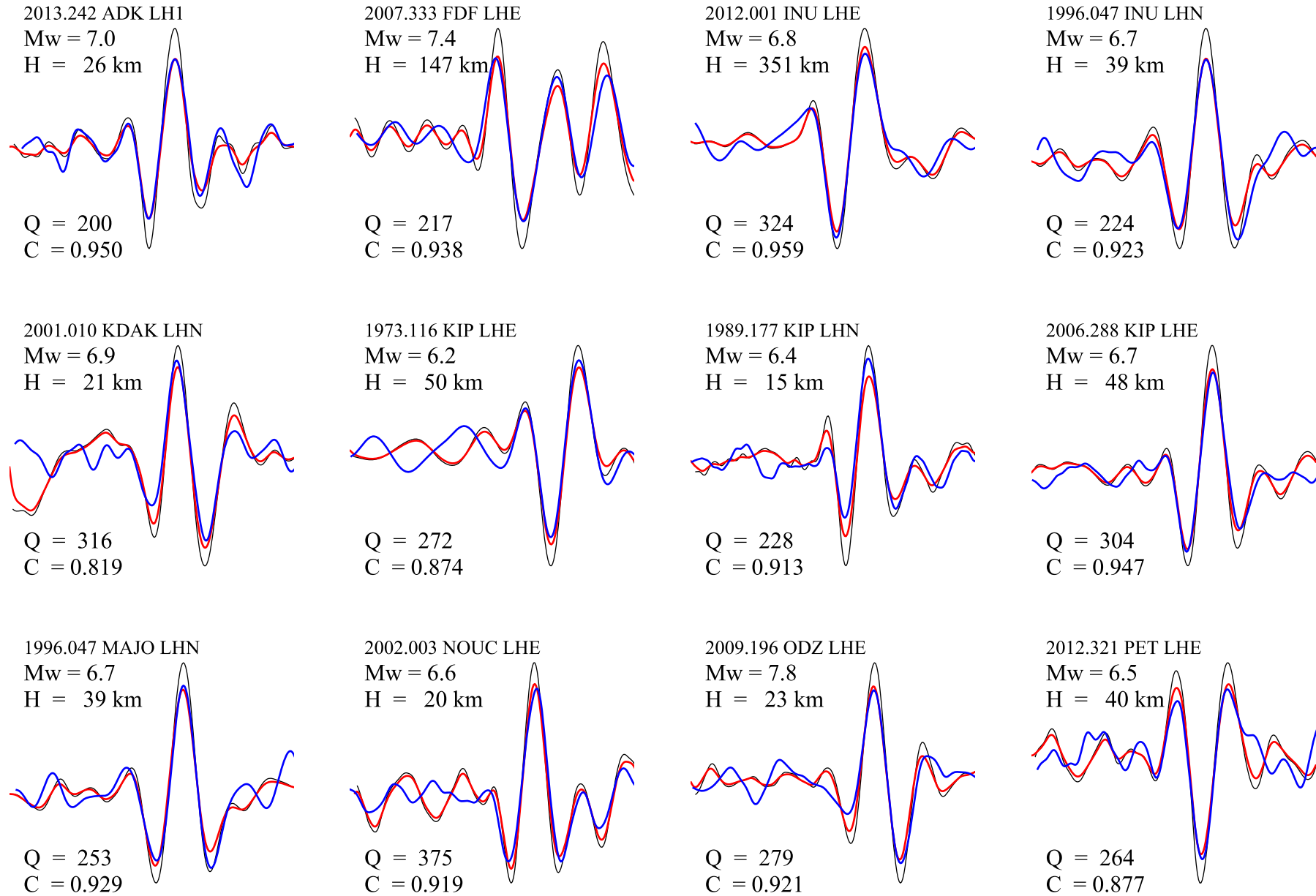
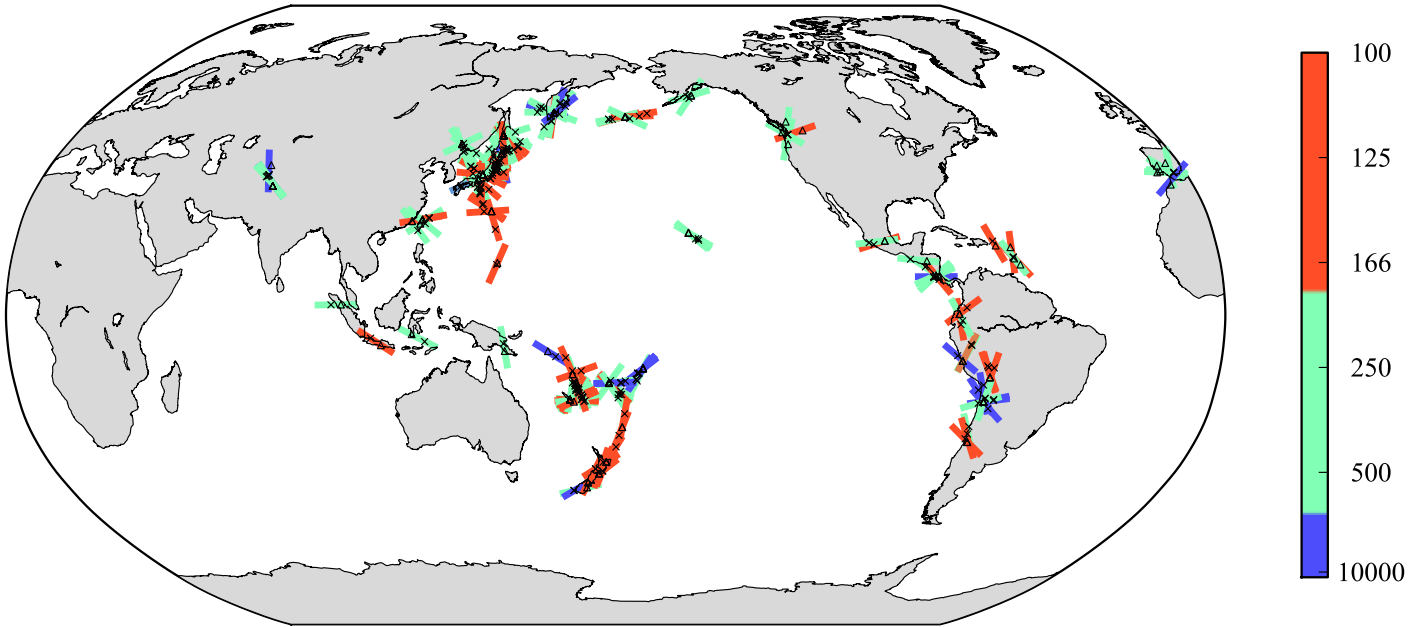


Figure 4c

Quality factor



$ScS_2 - ScS_1$ travel time

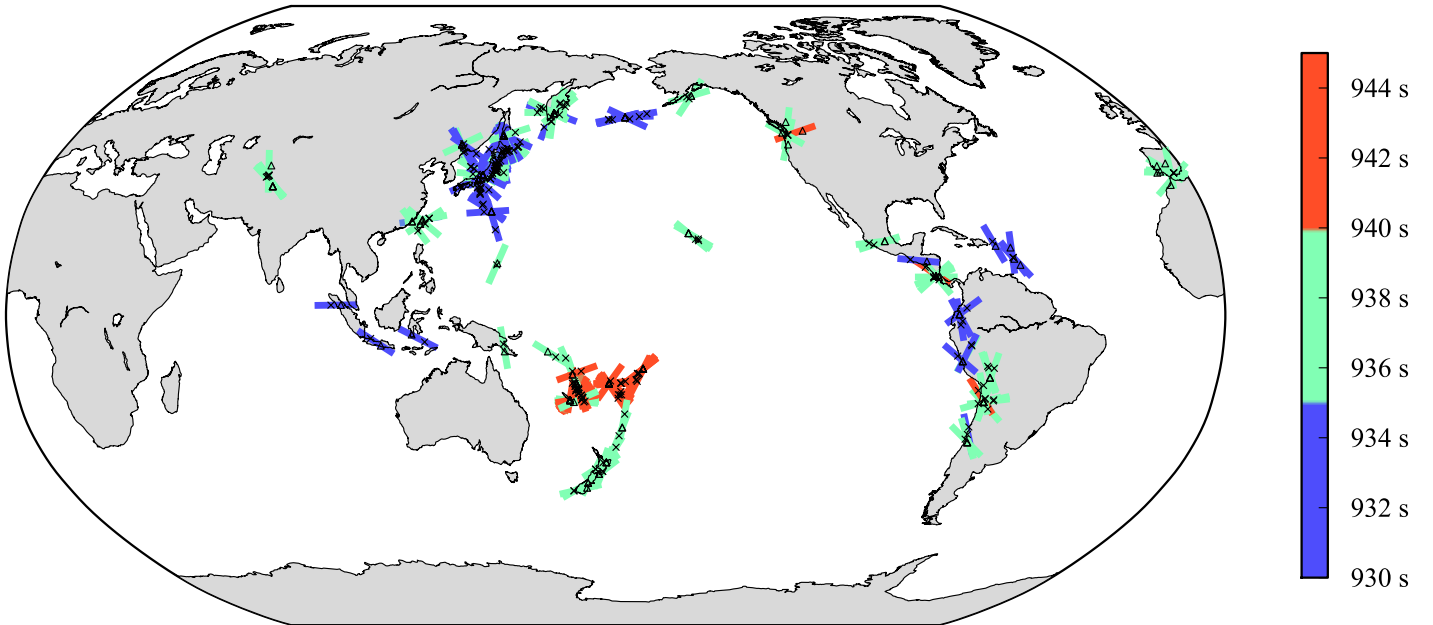


Figure 5a

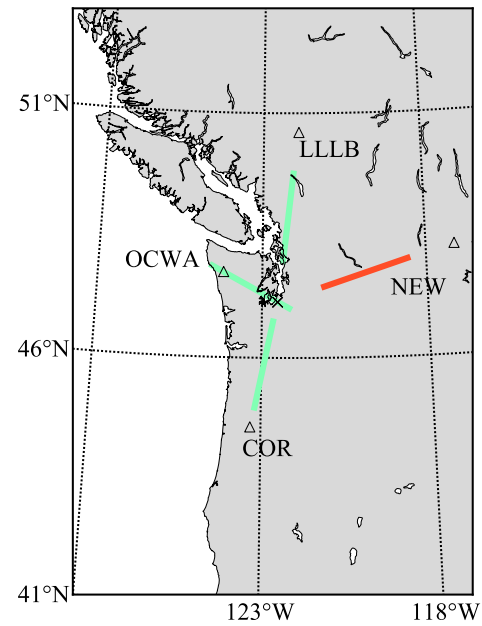
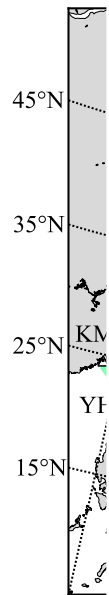
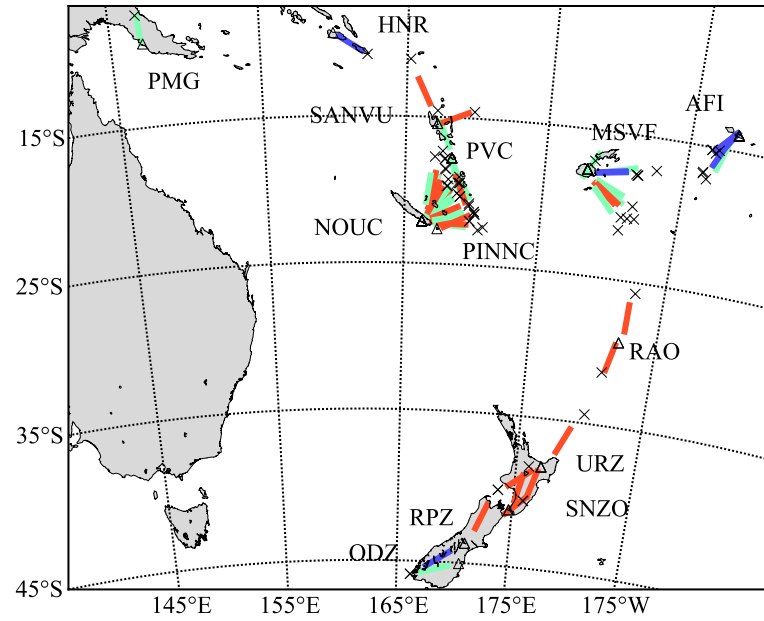
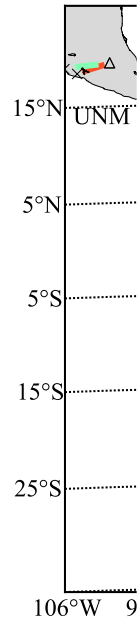


Figure 5b

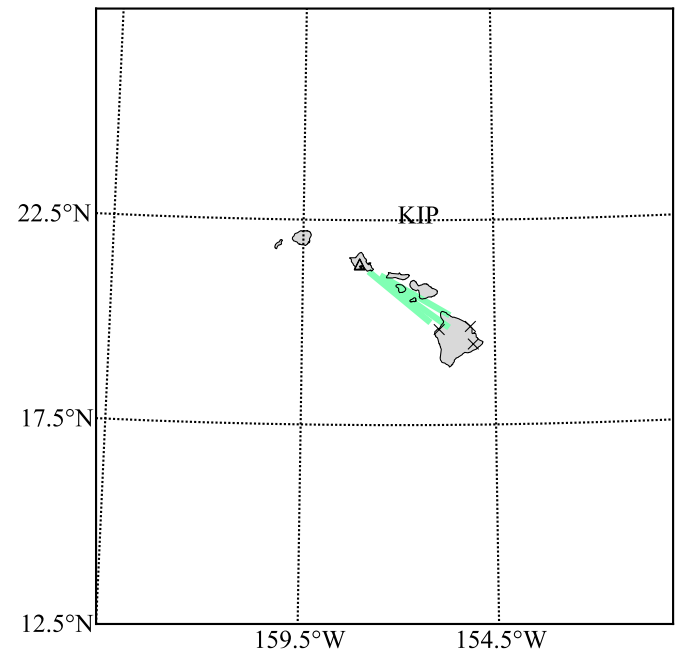
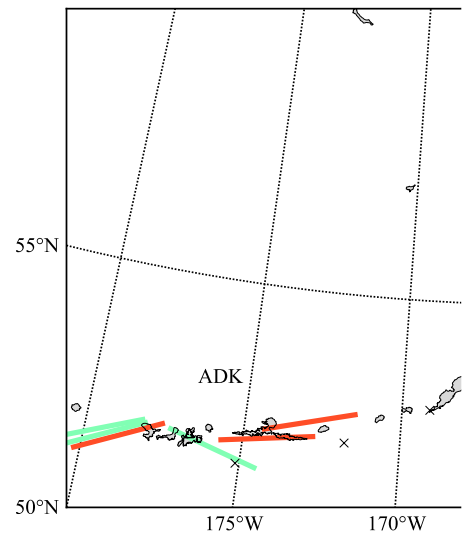
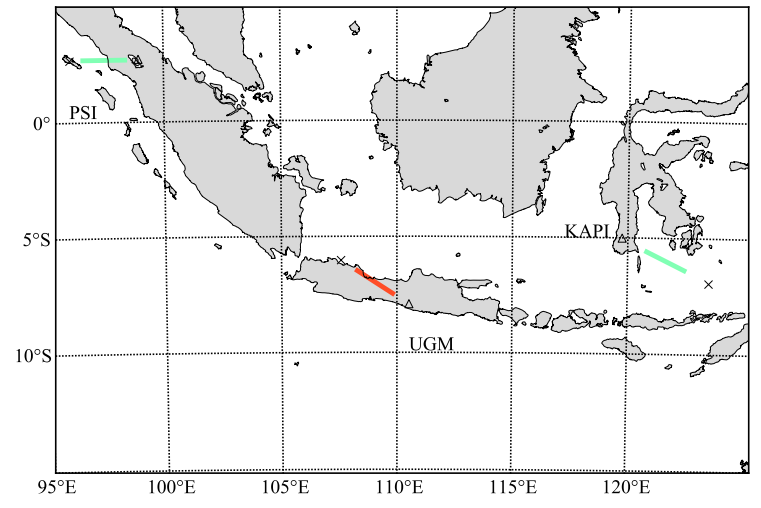
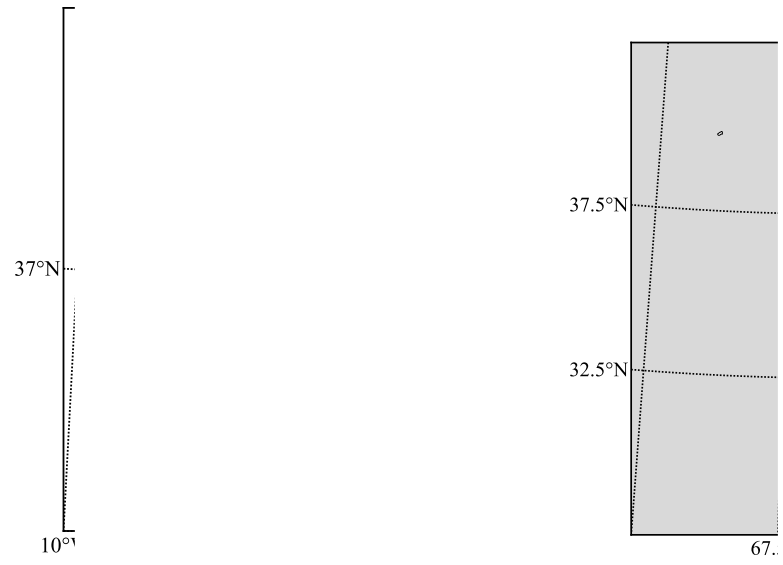


Figure 5c

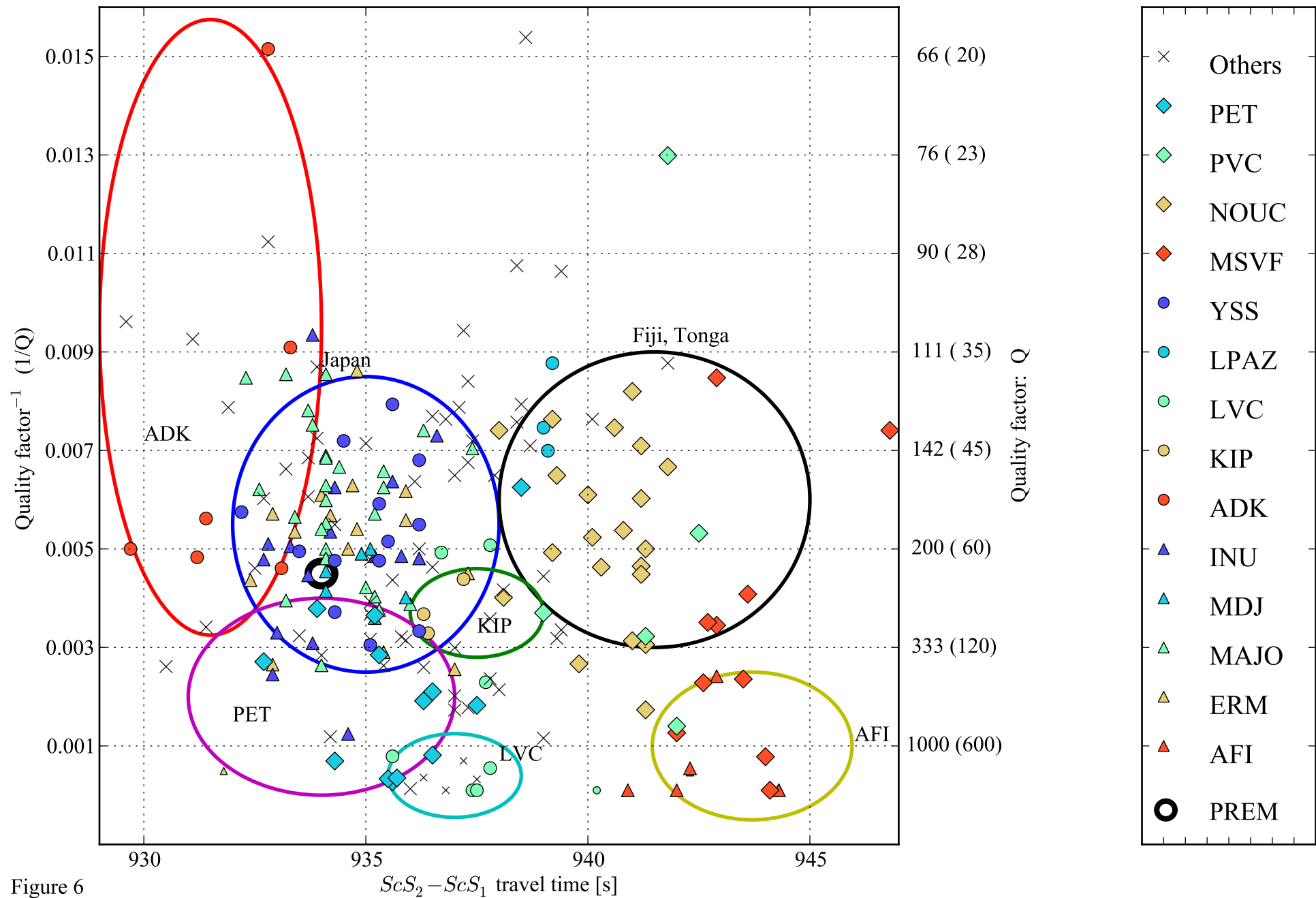


Figure 6

Observed and 3-D model Quality factor

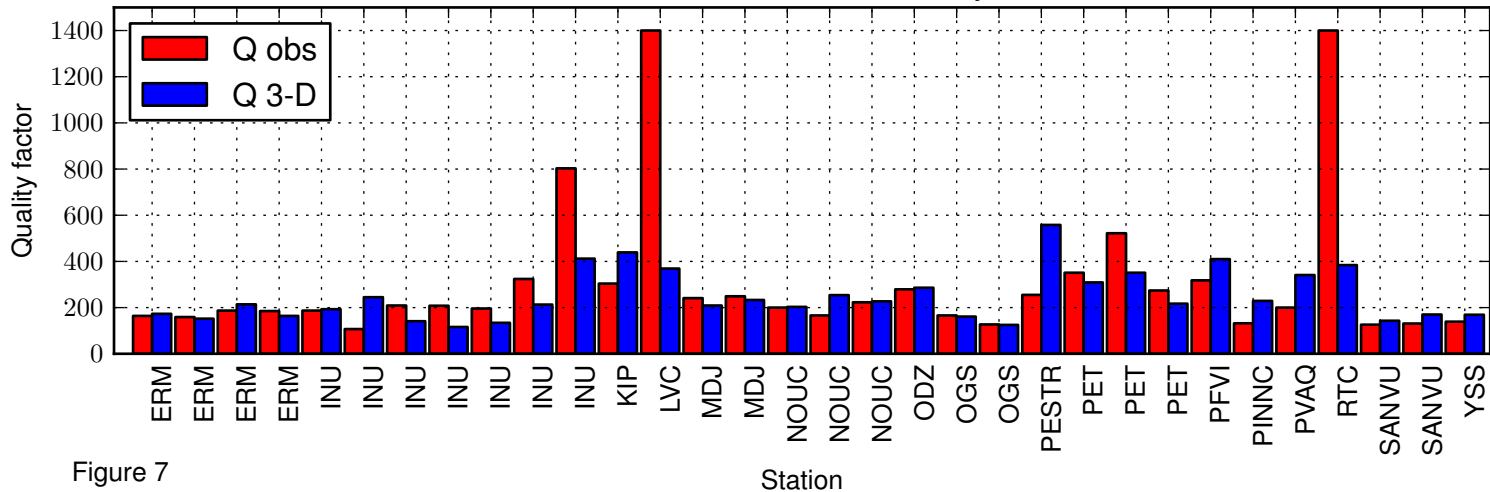


Figure 7

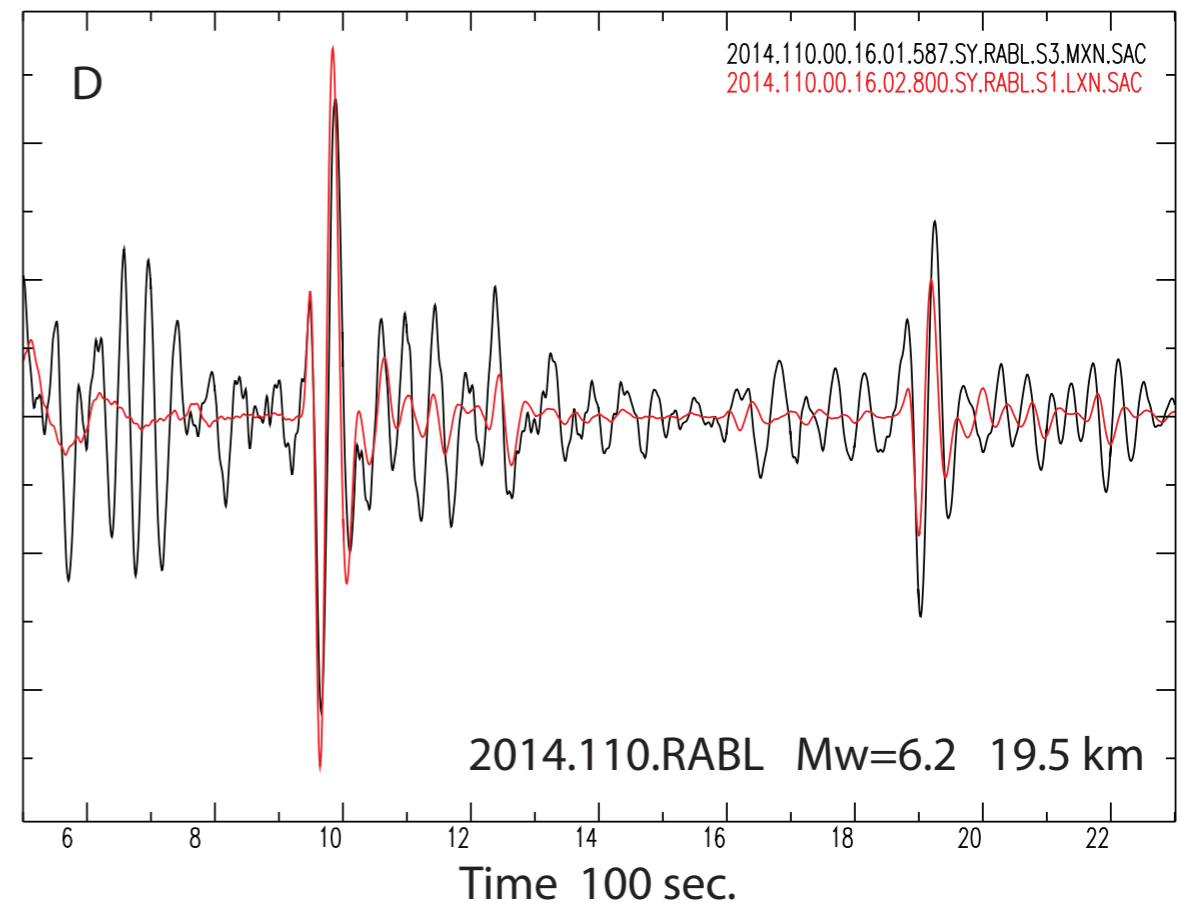
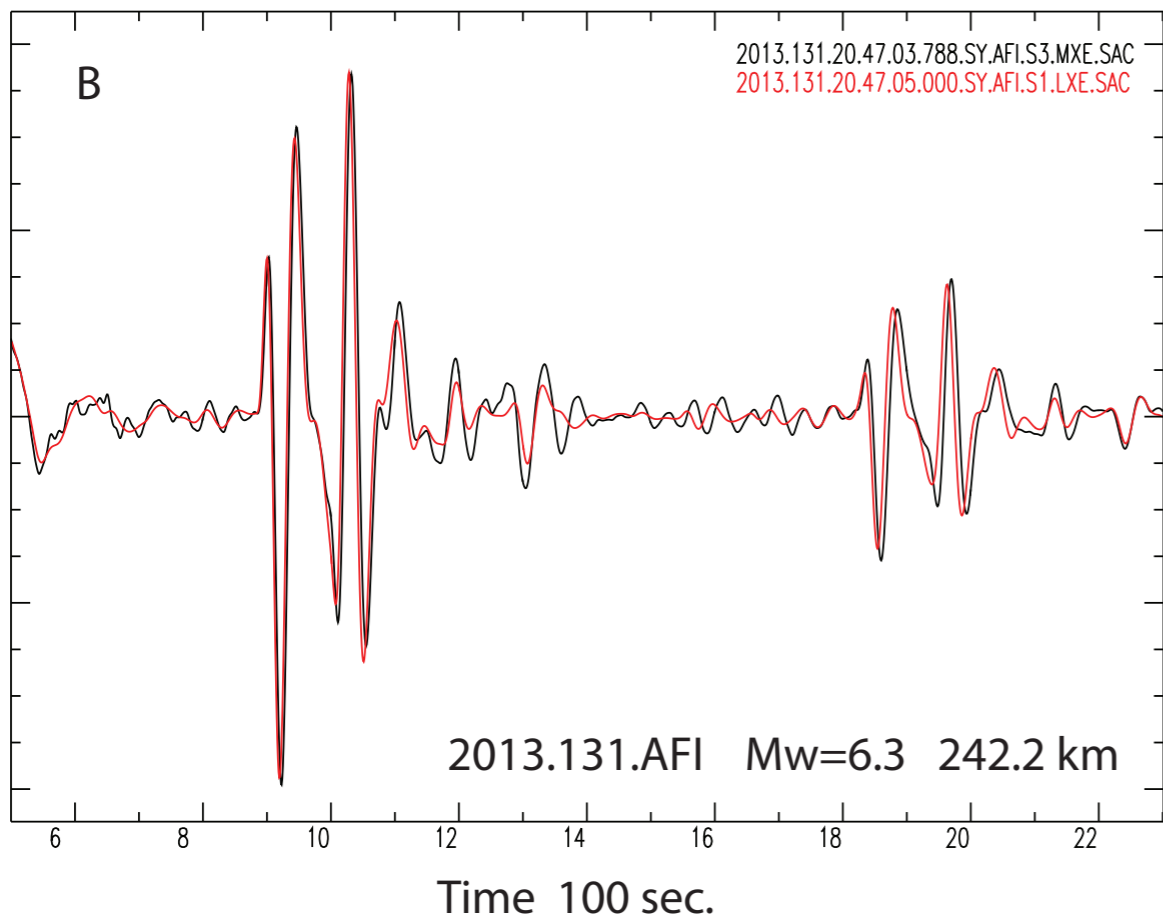
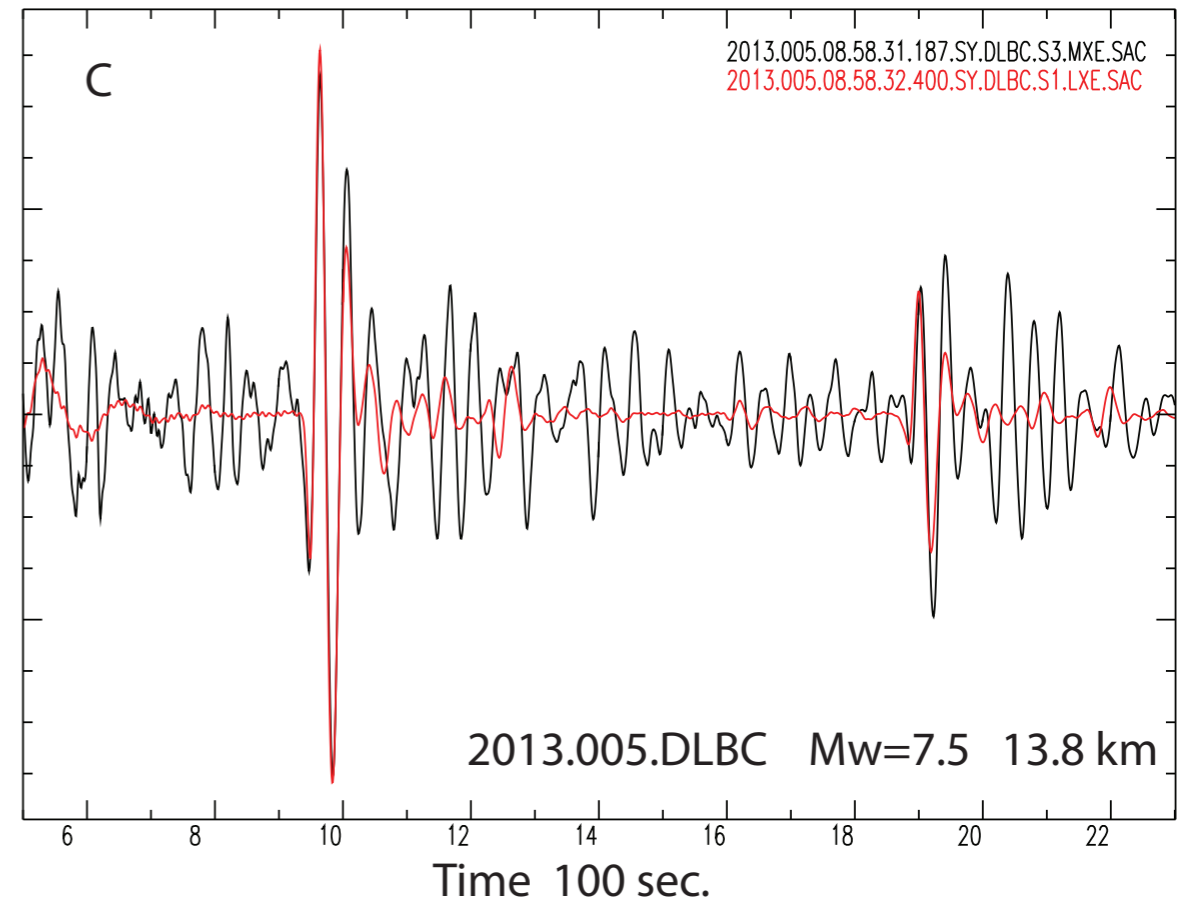
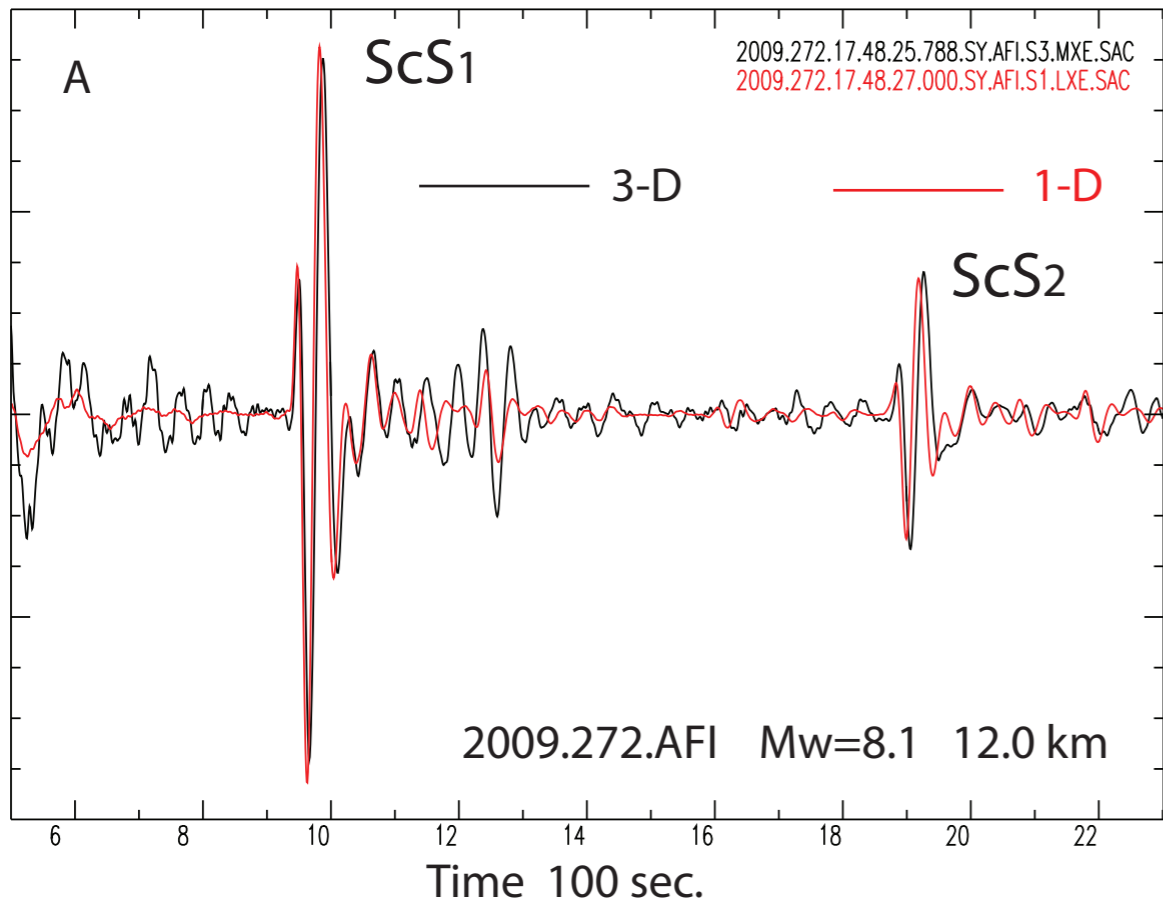


Figure 8 (to be continued)

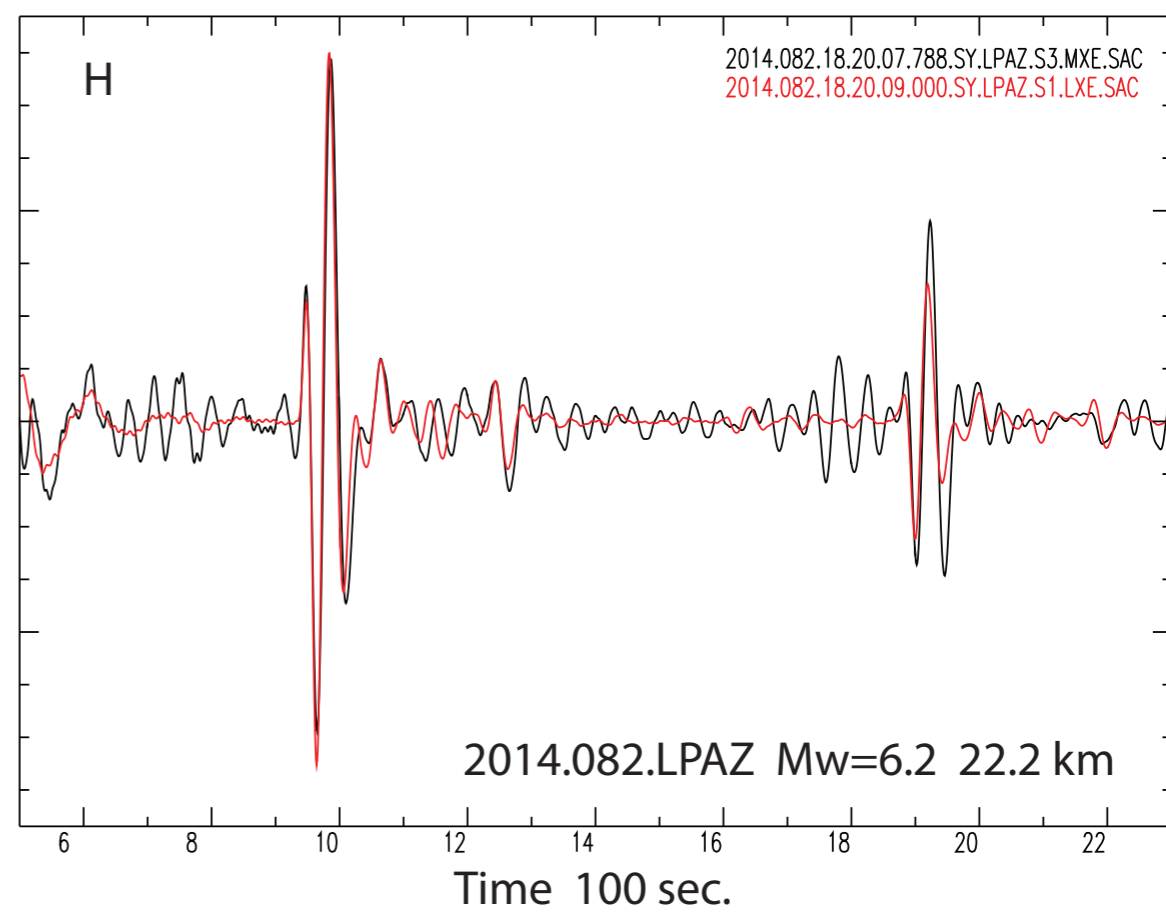
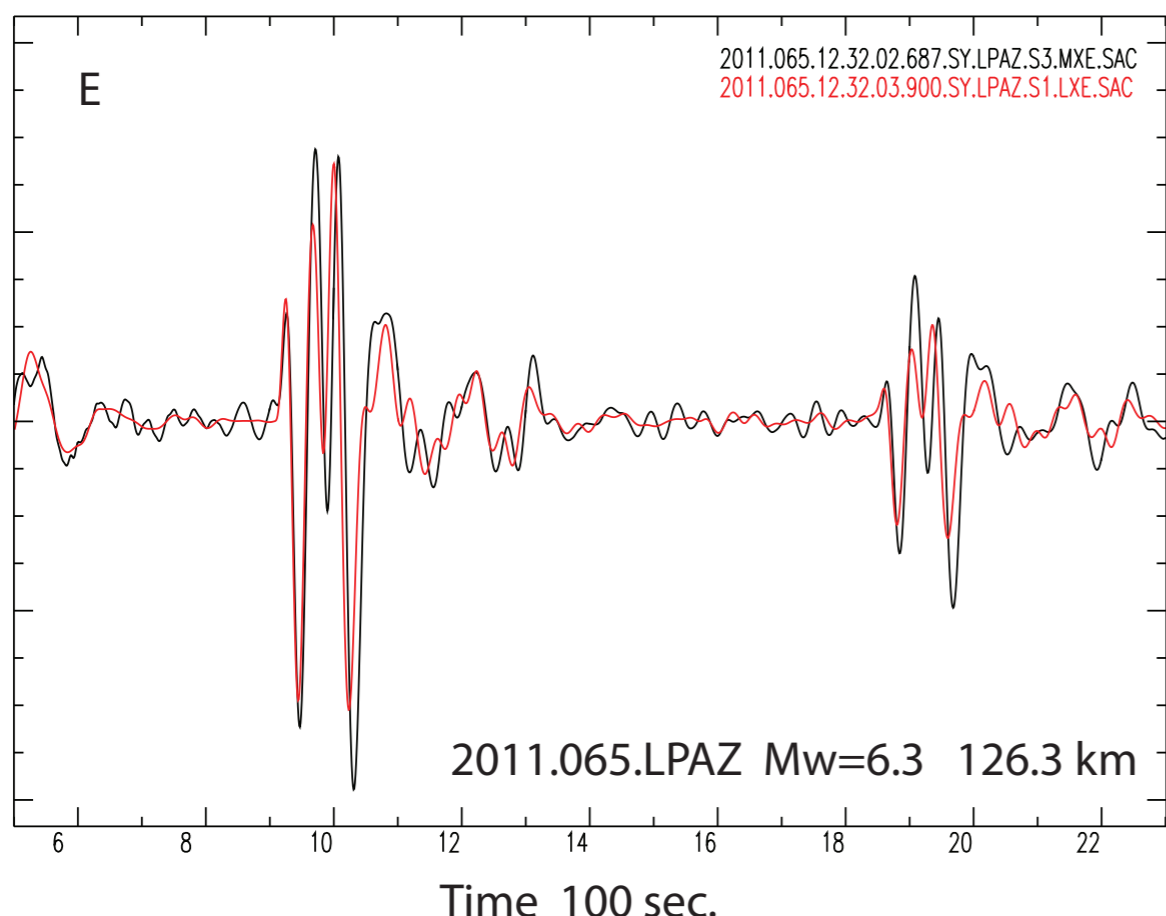
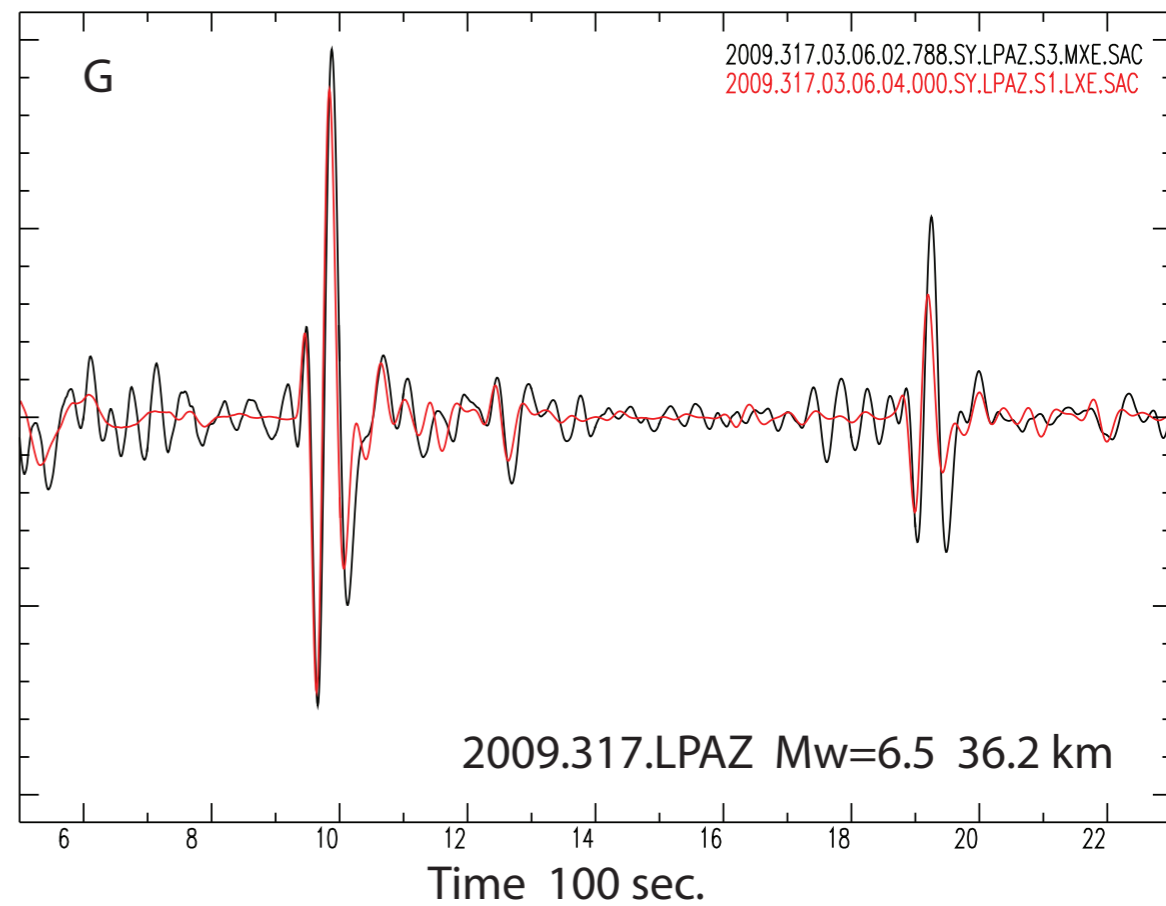
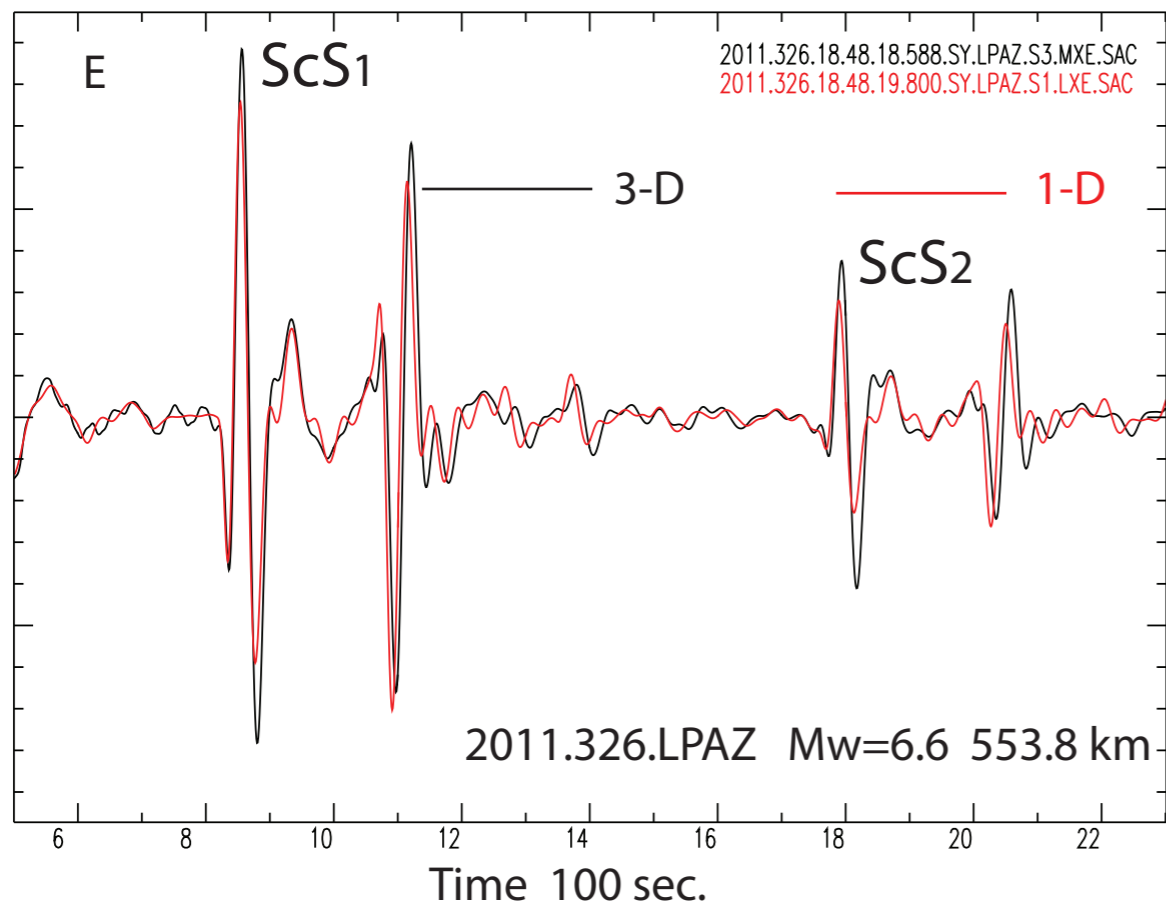


Figure 8 (continued)

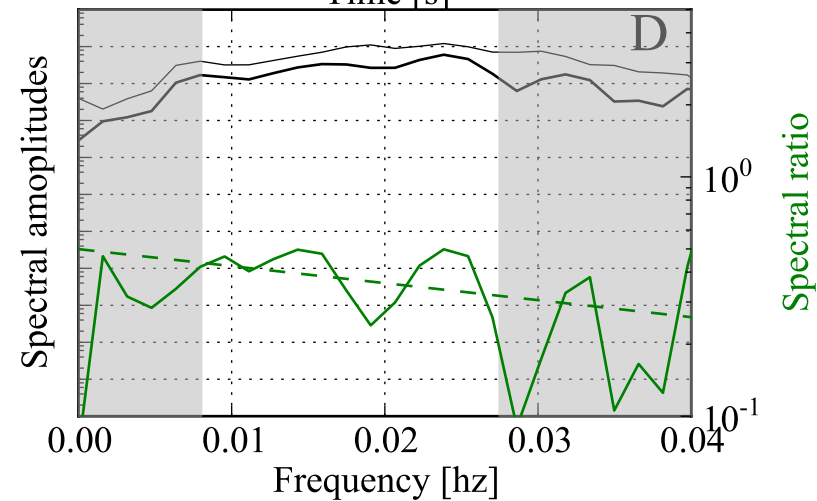
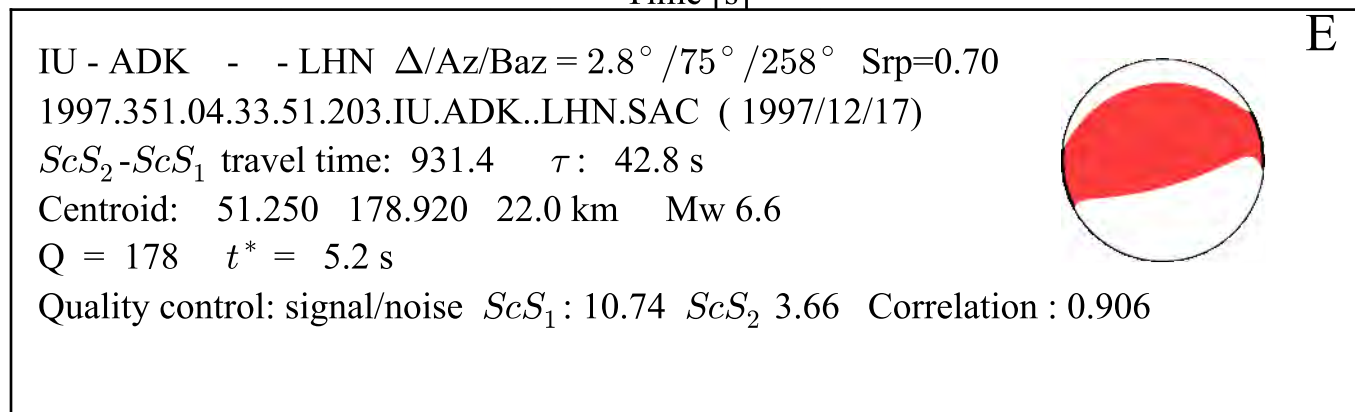
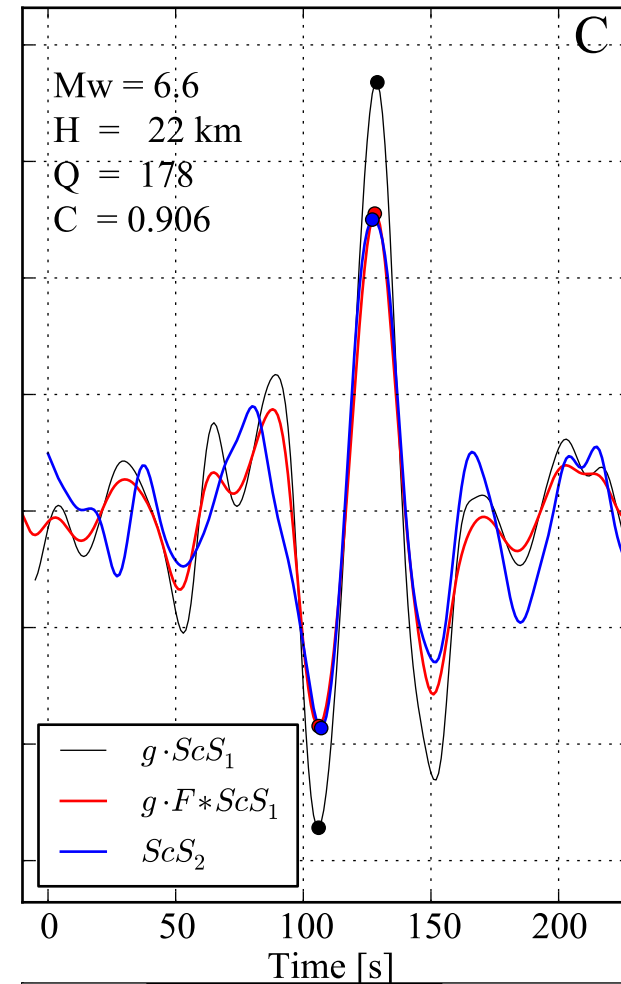
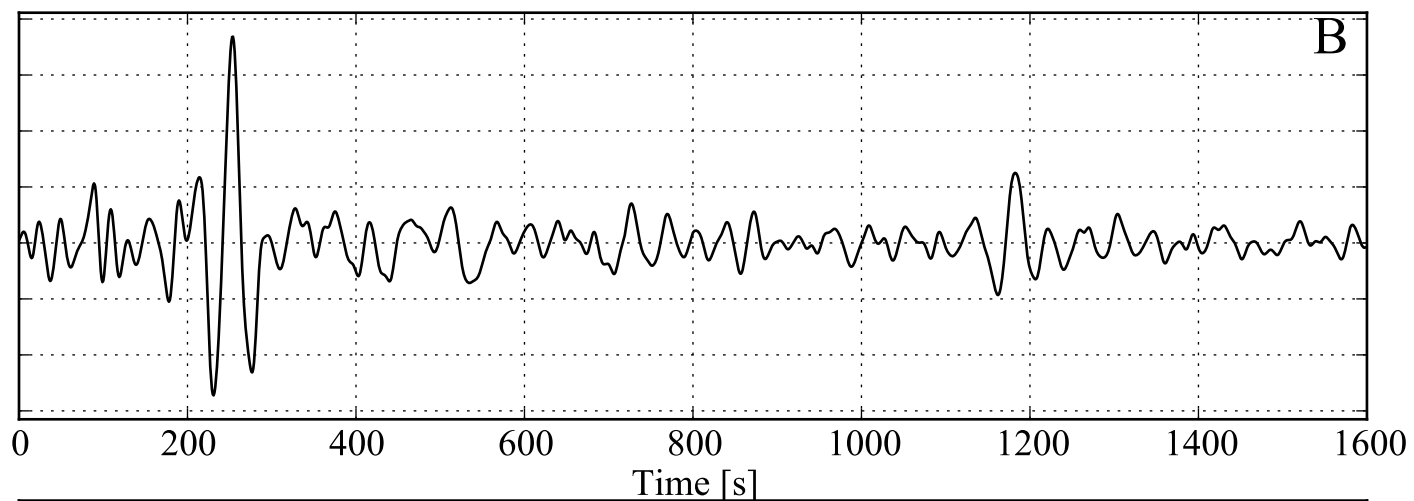
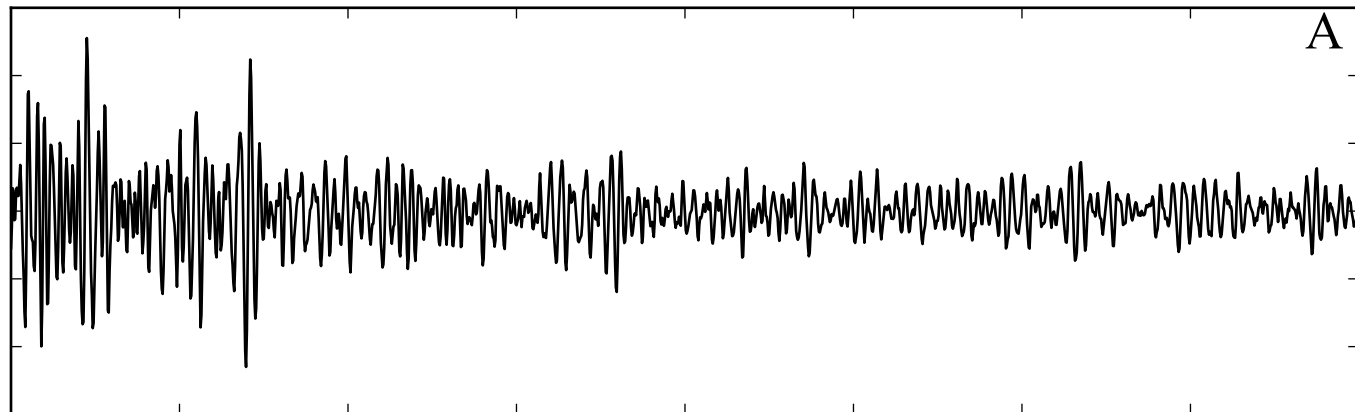
43	1996.047.15.17.57.495.G.INU..LHN	224	4.2	48.5	933.7	11.3	4.3	0.923	0.950	37.32	142.31	39	6.7	4.7
44	2003.316.08.21.43.500.G.INU..LHE	160	5.8	52.1	934.3	18.1	6.2	0.950	0.768	33.31	137.09	381	6.3	2.0
45	2005.228.02.41.28.603.G.INU..LHE	137	6.8	50.6	936.6	15.5	5.2	0.971	0.848	38.24	142.05	37	7.2	5.0
46	2008.201.02.34.28.511.G.INU.00.LHE	157	5.9	46.6	935.6	9.6	3.3	0.903	0.851	37.47	142.42	21	6.9	4.8
47	2009.221.10.50.55.511.G.INU.00.LHE	187	5.0	50.2	934.2	14.7	5.2	0.935	0.943	33.05	138.19	301	7.1	2.5
48	2009.224.22.43.51.511.G.INU.00.LHE	107	8.7	50.2	933.8	22.1	6.4	0.929	0.871	32.74	140.68	55	6.6	4.0
49	2010.073.08.03.04.511.G.INU.00.LHE	209	4.4	47.7	932.7	9.8	3.6	0.858	0.674	37.70	141.98	45	6.5	4.6
50	2011.111.13.32.03.511.G.INU.00.LHE	208	4.5	48.5	936.2	10.9	4.0	0.920	0.606	35.56	140.78	42	6.2	3.1
51	2011.205.18.46.24.511.G.INU.00.LHE	196	4.8	47.0	932.8	11.0	4.0	0.894	0.696	37.70	141.66	47	6.3	4.4
52	2011.211.18.48.49.511.G.INU.00.LHE	303	3.1	47.2	933.0	9.3	3.8	0.865	0.372	37.00	141.16	52	6.4	3.7
53	2012.001.05.22.56.511.G.INU.00.LHE	324	2.9	50.3	933.8	16.1	6.5	0.959	0.935	31.61	138.17	352	6.8	3.9
54	2014.072.17.01.51.511.G.INU.00.LHE	803	1.2	58.8	934.6	8.8	4.1	0.911	0.866	33.60	131.85	87	6.3	4.6
55	1999.232.09.57.21.049.II.JTS.00.LHN	148	6.3	38.2	937.3	14.1	4.3	0.902	0.614	9.28	-84.10	24	6.9	1.3
56	2012.249.14.37.07.069.II.JTS.00.LH2	385	2.4	42.7	936.3	9.3	3.9	0.932	0.836	10.00	-85.64	29	7.6	0.7
57	2012.298.00.40.33.069.II.JTS.00.LH2	563	1.7	39.6	937.3	8.9	3.9	0.877	0.677	9.71	-85.60	22	6.4	0.9
58	2000.220.14.28.55.075.II.KAPI.00.LHN	293	3.2	45.7	931.4	11.8	4.5	0.916	0.609	-6.95	123.53	648	6.5	4.2
59	2000.193.01.27.28.052.II.KDAK.00.LHN	209	4.5	49.5	935.1	10.8	4.1	0.804	0.599	57.54	-154.22	52	6.5	0.9
60	2001.010.15.57.44.086.II.KDAK.00.LHN	316	3.0	46.0	935.1	13.7	5.6	0.819	0.962	56.99	-153.56	21	6.9	0.9
61	1973.116.19.50.24.100.HG.KIP..LHE	272	3.4	46.9	936.3	16.6	6.6	0.874	0.069	19.90	-155.13	50	6.2	3.1
62	1989.177.03.22.03.157.G.KIP..LHN	228	4.1	39.7	937.2	14.4	5.2	0.913	0.967	19.47	-155.06	15	6.4	3.4
63	2006.288.17.02.49.048.G.KIP..LHE	304	3.1	43.9	936.4	24.1	9.8	0.947	0.564	19.83	-155.94	48	6.7	2.5
64	2005.288.15.46.07.518.TW.KMNB..LHN	140	6.7	48.9	935.0	14.8	4.7	0.917	0.897	25.29	123.43	194	6.4	4.7
65	2006.360.12.29.13.490.TW.KMNB..LHN	298	3.1	41.5	939.4	7.9	3.1	0.848	0.693	22.02	120.40	32	6.9	3.1
66	2001.059.18.49.32.000.CN.LLLB..LHE	225	4.2	47.1	939.0	11.2	4.3	0.850	0.827	47.14	-122.53	46	6.8	3.5
67	1994.010.15.48.49.450.GT.LPAZ..LHN	134	7.0	49.2	939.0	11.6	3.6	0.937	0.878	-13.28	-69.27	603	6.9	3.2
68	1994.160.00.28.16.449.GT.LPAZ..LHN	114	8.2	53.4	939.2	16.9	5.0	0.939	0.952	-13.82	-67.25	647	8.2	2.6
69	1997.332.22.48.41.035.GT.LPAZ..LHN	143	6.5	48.0	939.1	17.6	5.5	0.950	0.982	-13.70	-68.90	600	6.6	2.7
70	1997.023.02.10.22.365.GE.LVC..LHE	1400*	0.1	54.4	937.4	16.9	8.4	0.954	0.998	-22.04	-65.92	281	7.1	2.8
71	2002.087.04.51.22.610.IU.LVC.00.LHE	203	4.6	50.0	936.7	11.1	4.2	0.941	0.971	-21.69	-68.57	137	6.4	1.0
72	2006.237.00.39.46.910.IU.LVC.00.LHX	1266	0.7	54.3	935.6	8.4	4.0	0.935	0.576	-24.44	-67.18	185	6.6	2.4
73	2007.202.15.22.52.298.IU.LVC.00.LHE	1400*	0.1	52.0	937.5	8.4	4.3	0.922	0.998	-22.31	-66.00	280	6.4	2.7
74	2007.350.08.04.17.298.IU.LVC.00.LHE	436	2.1	48.3	937.7	12.9	5.6	0.938	0.992	-23.02	-70.41	30	6.7	1.4
75	2009.317.03.00.57.069.IU.LVC.00.LH2	1400*	0.1	43.9	940.2	7.2	4.2	0.897	0.677	-19.60	-71.01	36	6.5	3.6
76	2011.065.12.26.59.069.IU.LVC.00.LHX	1400*	0.5	46.8	937.8	13.7	6.5	0.923	0.809	-18.28	-69.73	126	6.3	4.4
77	2011.171.16.31.01.069.IU.LVC.00.LH2	197	4.8	50.7	937.8	11.3	4.2	0.938	0.978	-21.89	-68.63	131	6.5	0.8
78	1992.242.19.14.07.425.IU.MAJO..LHE	159	5.9	48.6	934.1	31.2	10.4	0.982	0.953	33.40	138.09	309	6.2	3.1
79	1993.019.14.34.26.705.IU.MAJO..LHE	258	3.6	47.5	936.0	11.0	4.2	0.969	0.529	38.70	133.96	461	6.5	4.0
80	1993.284.15.49.22.040.IU.MAJO..LHE	161	5.8	49.7	932.6	24.6	8.3	0.980	0.987	32.12	138.02	364	6.9	4.4
81	1995.090.13.56.40.573.IU.MAJO..LHE	135	6.9	47.7	936.3	31.3	9.6	0.969	0.969	38.16	135.11	366	6.2	3.0
82	1996.047.15.17.57.400.IU.MAJO..LHN	253	3.7	48.2	933.2	11.6	4.6	0.929	0.950	37.32	142.31	39	6.7	3.4
83	2002.307.03.32.42.698.IU.MAJO.00.LHE	181	5.1	45.1	934.1	14.0	4.9	0.956	0.796	38.84	142.14	44	6.4	3.9
84	2003.146.09.19.33.248.IU.MAJO.00.LHE	248	3.8	53.5	935.2	16.8	6.7	0.978	0.798	38.94	141.57	61	7.0	3.6
85	2003.304.01.01.28.898.IU.MAJO.00.LHE	145	6.4	44.9	934.1	14.1	4.7	0.953	0.952	37.89	142.68	15	7.0	3.8
86	2003.316.08.21.43.898.IU.MAJO.00.LHE	379	2.5	49.4	934.0	18.3	7.6	0.962	0.768	33.31	137.09	381	6.3	3.4
87	2005.228.02.41.28.266.IU.MAJO.00.LHE	175	5.3	48.6	935.2	13.4	4.7	0.952	0.848	38.24	142.05	37	7.2	3.5

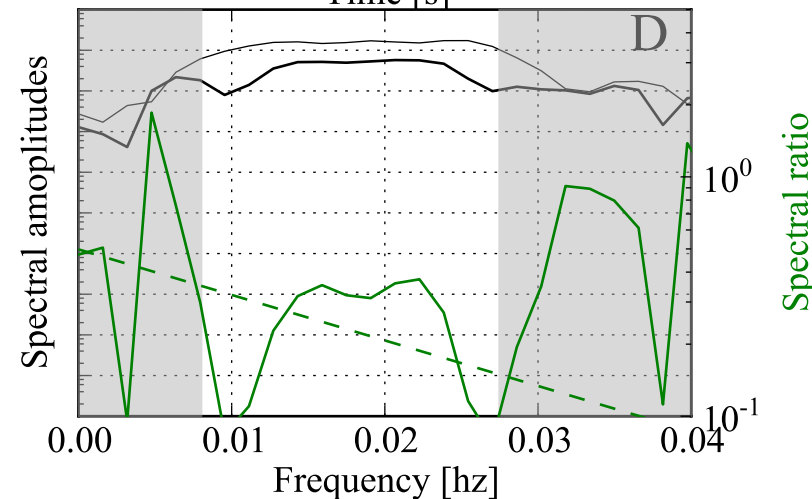
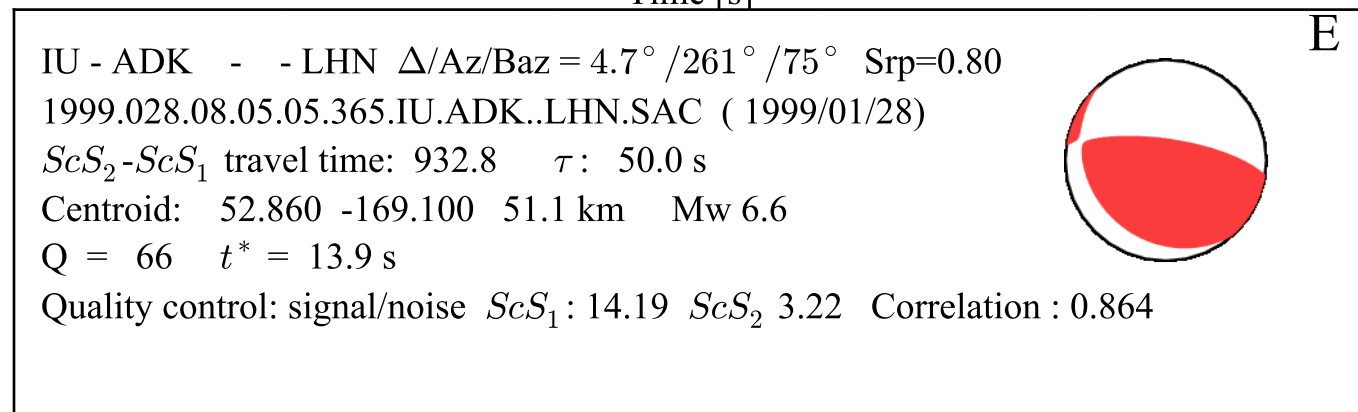
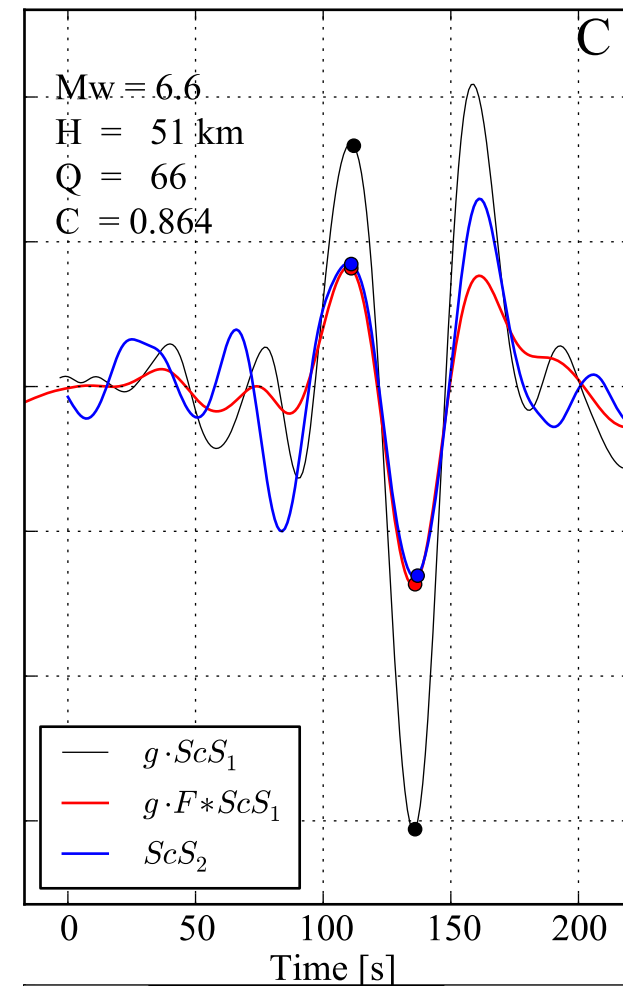
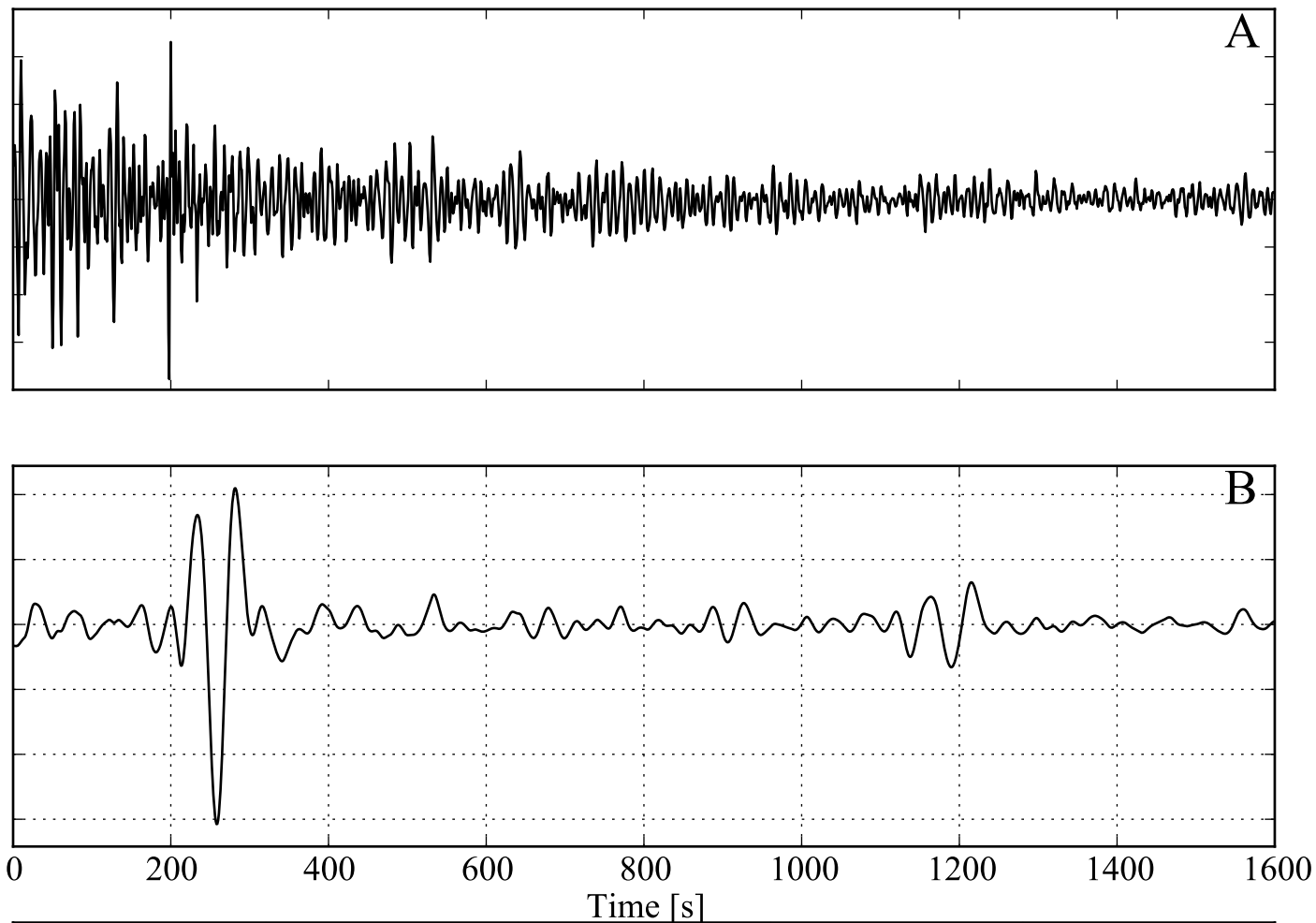
88	2005.292.11.39.42.923.IU.MAJO.00.LHE	142	6.6	48.1	937.4	9.7	3.2	0.915	0.718	36.33	141.18	37	6.3	2.4
89	2005.336.13.08.09.923.IU.MAJO.00.LHE	167	5.6	46.0	934.1	11.7	4.0	0.904	0.764	38.11	142.38	34	6.5	3.7
90	2007.197.14.12.37.648.IU.MAJO.00.LHE	152	6.1	48.9	935.4	15.0	4.9	0.948	0.692	36.84	135.03	374	6.8	2.6
91	2008.201.02.34.28.348.IU.MAJO.00.LHE	117	8.0	44.7	934.1	13.1	3.8	0.938	0.851	37.47	142.42	21	6.9	3.5
92	2008.205.15.21.20.348.IU.MAJO.00.LHE	237	3.9	48.4	935.0	14.5	5.6	0.965	0.799	39.73	141.51	98	6.8	4.1
93	2010.073.08.03.04.069.IU.MAJO.00.LH2	117	7.9	46.3	933.2	12.5	3.8	0.936	0.674	37.70	141.98	45	6.5	3.2
94	2010.185.21.50.52.069.IU.MAJO.00.LH2	133	7.0	45.3	933.8	16.2	5.1	0.955	0.724	39.68	142.77	35	6.3	4.8
95	2011.084.11.31.24.069.IU.MAJO.00.LH2	200	4.7	45.3	934.1	11.9	4.3	0.938	0.683	38.78	142.17	45	6.2	3.9
96	2011.086.22.18.58.069.IU.MAJO.10.LH1	146	6.4	43.2	934.1	12.2	3.8	0.911	0.648	38.40	142.09	21	6.2	3.6
97	2011.111.13.32.03.069.IU.MAJO.00.LH2	150	6.2	47.2	934.4	13.9	4.6	0.902	0.606	35.56	140.78	42	6.2	2.3
98	2011.173.21.45.52.069.IU.MAJO.00.LH2	128	7.2	47.3	933.7	15.3	4.8	0.936	0.725	39.99	142.51	41	6.7	4.8
99	2011.204.04.29.24.069.IU.MAJO.00.LH2	208	4.5	45.8	934.1	10.3	3.8	0.942	0.697	38.96	142.10	47	6.3	3.9
100	2011.205.18.46.24.069.IU.MAJO.00.LH2	118	7.9	46.4	932.3	12.6	3.8	0.933	0.696	37.70	141.66	47	6.3	3.0
101	2011.211.18.48.49.069.IU.MAJO.10.LH2	160	5.8	45.4	935.4	8.8	3.0	0.852	0.372	37.00	141.16	52	6.4	2.4
102	2011.231.05.31.33.069.IU.MAJO.10.LH2	266	3.5	48.0	935.3	8.1	3.2	0.871	0.350	37.69	141.71	48	6.3	3.0
103	2012.001.05.22.56.069.IU.MAJO.00.LH2	177	5.3	50.1	933.4	19.6	6.8	0.975	0.935	31.61	138.17	352	6.8	4.9
104	2012.169.20.27.20.069.IU.MAJO.00.LH2	185	5.0	45.4	934.0	14.2	5.0	0.950	0.686	38.92	142.15	47	6.3	3.9
105	1999.098.13.05.34.528.IC.MDJ..LHE	200	4.7	48.4	935.1	24.8	8.7	0.967	0.890	43.66	130.47	575	7.1	1.1
106	2002.179.17.14.30.098.IC.MDJ.00.LHE	220	4.2	48.7	934.1	23.3	8.4	0.959	0.891	43.74	130.45	581	7.3	1.1
107	2002.258.08.34.32.273.IC.MDJ.00.LHE	278	3.4	48.7	935.2	26.0	9.9	0.986	0.935	44.77	130.04	589	6.4	0.4
108	2009.358.00.18.33.823.IC.MDJ.00.LHE	241	3.9	48.7	934.1	27.4	10.3	0.960	0.904	42.12	134.93	390	6.3	4.6
109	2010.049.01.08.19.260.IC.MDJ.00.LHE	249	3.8	48.6	935.9	28.5	10.6	0.972	0.962	42.48	130.66	578	6.9	2.3
110	2013.095.12.55.02.322.IC.MDJ.00.LHE	204	4.6	48.7	934.9	27.9	9.8	0.971	0.973	42.77	131.02	571	6.3	2.1
111	1995.017.16.49.12.998.II.MSVF.00.LH2	118	8.0	44.3	942.9	17.0	4.7	0.832	0.874	-20.71	-179.13	649	6.3	4.0
112	1996.218.22.33.22.044.II.MSVF.00.LH1	245	3.8	47.2	943.6	25.6	9.4	0.978	0.771	-20.72	-178.16	555	7.4	4.6
113	2000.125.20.31.32.053.II.MSVF.00.LHX	790	1.2	44.1	942.0	17.6	7.7	0.931	0.421	-17.72	-178.31	539	6.4	3.5
114	2004.322.21.04.13.911.II.MSVF.00.LH1	290	3.2	46.9	942.9	19.2	7.3	0.986	0.968	-19.87	-178.40	629	6.5	4.0
115	2008.201.22.34.52.000.II.MSVF.00.LH2	438	2.1	43.4	942.6	25.3	10.5	0.983	0.409	-17.22	-177.05	395	6.4	4.7
116	2009.313.10.39.54.000.II.MSVF.00.LH1	424	2.2	48.6	943.5	16.0	6.5	0.979	0.547	-17.11	178.53	603	7.3	0.8
117	2009.326.07.43.20.000.II.MSVF.00.LHX	1281	0.7	45.0	944.0	29.3	13.2	0.982	0.831	-17.72	-178.36	546	6.3	3.4
118	2010.228.19.30.49.000.II.MSVF.00.LH2	135	7.0	45.8	946.8	12.5	3.7	0.950	0.668	-20.74	-178.67	604	6.2	4.3
119	2011.093.14.02.09.184.II.MSVF.00.LH2	1400*	0.1	44.3	944.1	27.0	12.9	0.986	0.993	-17.65	-178.45	562	6.4	3.3
120	2011.258.19.26.04.000.II.MSVF.00.LH1	285	3.3	50.3	942.7	16.7	6.4	0.964	0.791	-21.61	-179.21	624	7.3	4.6
121	2001.059.18.49.32.755.US.NEW..LHE	114	8.2	50.0	941.8	12.7	3.9	0.883	0.827	47.14	-122.53	46	6.8	3.8
122	1995.291.09.25.38.023.II.NIL.00.LHN	578	1.6	46.8	937.0	9.9	4.4	0.912	0.631	36.18	70.45	238	6.2	3.4
123	1998.051.12.13.06.035.II.NIL.00.LHE	496	1.9	47.9	937.0	11.2	4.8	0.943	0.860	36.50	70.88	243	6.3	3.5
124	1999.312.16.40.43.093.II.NIL.00.LHE	1400*	0.1	47.6	936.0	9.1	4.4	0.934	0.605	36.48	70.81	237	6.5	3.5
125	2000.199.22.48.47.285.II.NIL.00.LHN	272	3.4	43.4	935.1	8.6	3.2	0.814	0.845	36.24	70.82	145	6.3	3.3
126	2004.096.21.19.04.402.II.NIL.00.LHE	334	2.8	50.8	937.0	7.7	3.2	0.928	0.769	36.52	70.84	183	6.5	3.5
127	1995.266.22.26.58.009.II.NNA.00.LHE	843	1.1	51.5	934.2	14.8	6.9	0.941	0.762	-10.62	-78.47	73	6.4	2.1
128	1998.093.21.56.48.069.II.NNA.00.LHE	380	2.5	53.6	935.4	11.1	4.8	0.916	0.969	-7.96	-74.48	153	6.6	4.6
129	2011.236.17.41.11.069.II.NNA.10.LH1	182	5.1	52.1	934.3	9.4	3.4	0.897	0.398	-7.68	-74.66	144	7.0	4.8
130	1995.180.12.19.03.212.G.NOUC..LHE	191	4.9	46.2	940.1	15.8	5.7	0.981	0.958	-19.42	168.95	142	6.6	3.6
131	1995.282.13.38.42.183.G.NOUC..LHN	215	4.4	42.6	941.2	12.3	4.5	0.964	0.641	-21.35	170.10	115	6.3	3.6
132	1997.141.14.05.26.584.G.NOUC..LHE	327	2.9	47.9	941.3	15.5	6.4	0.945	0.679	-20.34	169.03	64	6.7	3.1

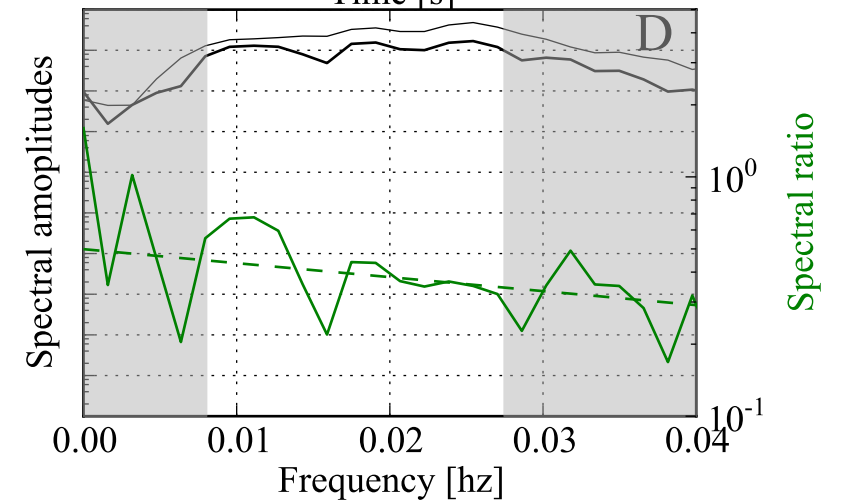
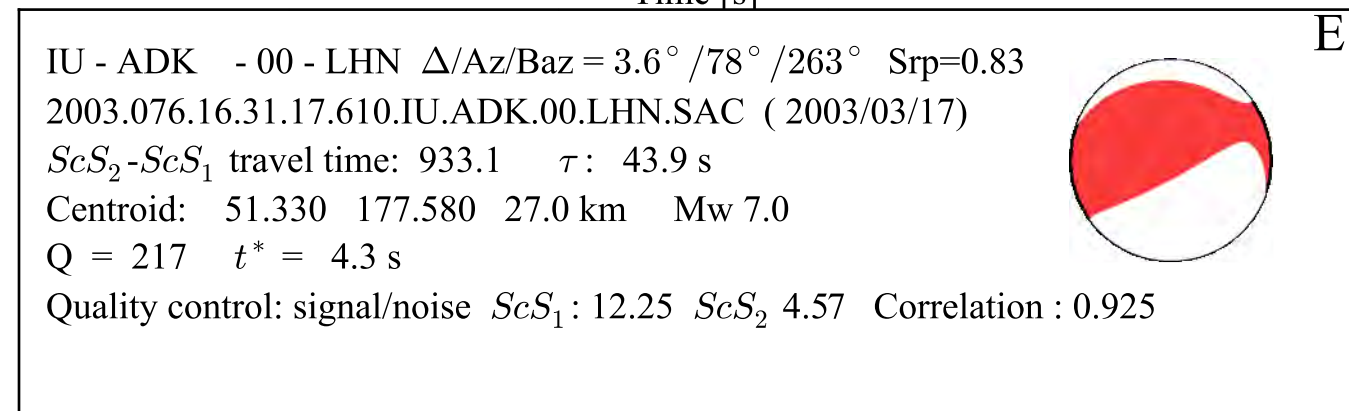
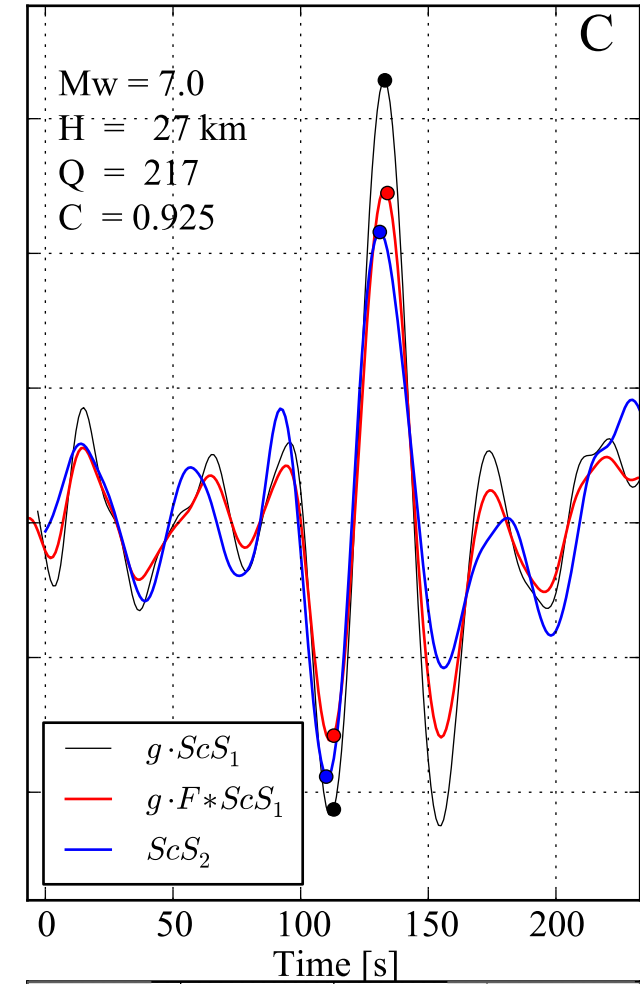
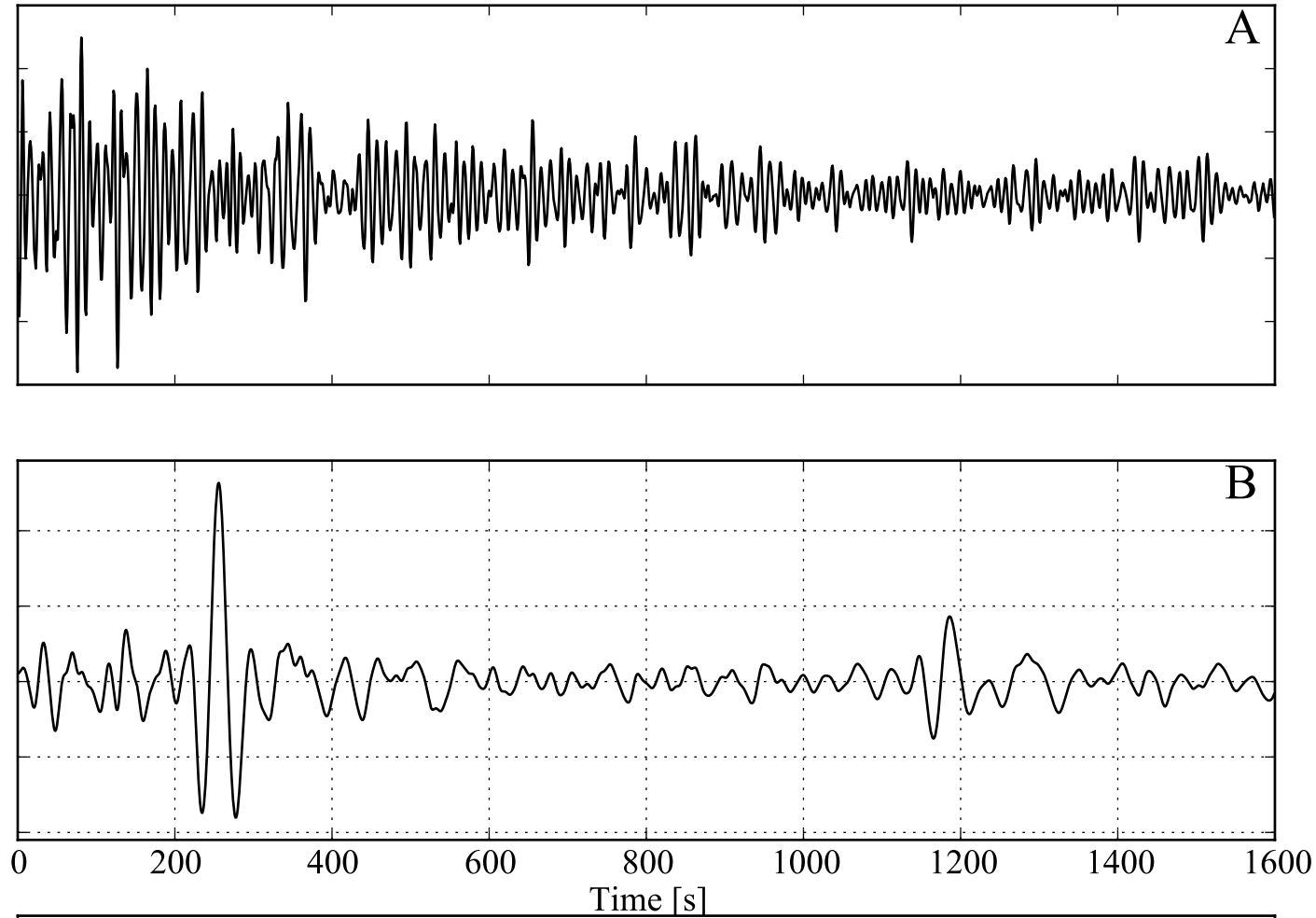
133	2001.272.02.35.07.758.G.NOUC..LHE	122	7.7	41.4	941.0	14.9	4.2	0.806	0.743	-18.48	167.87	16	6.3	3.9
134	2002.002.17.17.48.783.G.NOUC..LHE	150	6.2	43.5	941.8	29.4	9.6	0.972	0.931	-17.78	167.85	40	7.2	4.5
135	2002.003.10.12.36.751.G.NOUC..LHE	375	2.5	42.2	939.8	19.5	8.1	0.919	0.495	-17.84	167.82	20	6.6	4.5
136	2003.117.15.58.40.065.G.NOUC..LHE	203	4.6	50.5	939.2	8.4	3.2	0.880	0.514	-20.94	169.71	83	6.3	3.4
137	2003.310.10.33.04.584.G.NOUC..LHE	131	7.1	49.1	939.2	12.8	3.9	0.936	0.713	-19.41	168.82	114	6.6	3.6
138	2003.361.15.55.59.986.G.NOUC..LHE	154	6.1	46.2	939.3	13.4	4.5	0.876	0.542	-21.99	169.81	23	7.3	3.2
139	2006.023.05.57.59.110.G.NOUC..LHE	134	7.0	42.6	940.6	14.6	4.4	0.824	0.511	-17.29	167.65	30	6.4	5.0
140	2006.276.17.58.14.166.G.NOUC..LHE	319	2.9	48.0	941.0	15.9	6.5	0.977	0.755	-19.01	168.91	166	6.3	3.9
141	2008.100.12.41.12.116.G.NOUC..LHE	216	4.3	45.0	940.3	13.9	5.2	0.865	0.527	-20.12	168.80	35	7.3	3.0
142	2009.015.07.22.20.003.G.NOUC..LHN	249	3.8	42.5	938.1	13.4	5.0	0.855	0.535	-22.58	170.46	27	6.6	3.9
143	2009.343.09.41.03.708.G.NOUC..LHN	135	6.9	45.6	938.0	10.8	3.3	0.876	0.484	-22.36	170.82	58	6.4	4.2
144	2010.359.13.11.37.175.G.NOUC..LHE	577	1.6	40.1	941.3	10.7	4.7	0.839	0.382	-19.67	168.04	16	7.3	2.9
145	2010.363.06.49.19.753.G.NOUC..LHE	200	4.7	38.9	941.3	20.3	6.9	0.885	0.587	-19.65	168.10	12	6.3	3.0
146	2011.009.09.58.44.752.G.NOUC..LHE	141	6.6	39.7	941.2	10.5	3.2	0.785	0.357	-19.20	168.13	12	6.5	3.4
147	2011.232.16.50.02.391.G.NOUC..LHE	164	5.7	42.0	940.0	13.8	4.6	0.941	0.525	-18.52	167.94	33	7.1	3.9
148	2011.246.22.50.40.403.G.NOUC..LHN	166	5.6	48.7	941.2	22.1	7.8	0.961	0.838	-20.79	169.72	151	7.0	3.4
149	2012.033.13.29.40.013.G.NOUC..LHN	186	5.0	46.4	940.8	8.6	3.1	0.866	0.282	-17.69	167.11	20	7.0	4.5
150	2014.121.06.31.35.000.G.NOUC.00.LHN	223	4.2	42.3	941.2	13.4	5.0	0.948	0.783	-21.51	170.15	119	6.6	3.6
151	2001.059.18.49.32.389.US.OCWA..LHE	314	3.0	47.3	939.3	9.2	3.8	0.874	0.827	47.14	-122.53	46	6.8	1.3
152	2009.196.09.17.29.069.NZ.ODZ.10.LHE	279	3.4	43.5	937.8	14.9	5.8	0.921	0.786	-45.85	166.26	23	7.8	3.2
153	1998.232.06.35.55.000.PS.OGS..LHE	146	6.4	61.0	933.7	21.6	7.6	0.968	0.880	28.99	139.47	425	7.1	3.1
154	2000.088.10.55.22.000.PS.OGS..LHN	89	10.4	72.2	932.8	8.9	3.0	0.885	0.950	22.32	143.76	99	7.6	4.9
155	2010.334.03.19.41.511.PS.OGS..LHE	166	5.6	53.1	932.7	19.4	6.7	0.986	0.816	28.69	139.26	460	6.8	3.1
156	2011.012.21.27.55.511.PS.OGS..LHE	127	7.3	48.3	931.9	12.6	3.7	0.862	0.773	26.94	139.94	511	6.5	2.0
157	2007.320.03.08.00.835.IU.OTAV.00.LHN	115	8.1	47.8	933.9	13.3	4.0	0.921	0.721	-2.50	-78.00	114	6.8	2.8
158	2010.224.11.49.15.069.IU.OTAV.00.LH1	352	2.6	53.3	934.0	12.6	5.3	0.890	0.770	-1.51	-77.51	197	7.1	2.0
159	2012.274.16.26.36.069.IU.OTAV.00.LH1	138	6.8	52.3	933.9	10.9	3.6	0.805	0.312	1.89	-76.22	159	7.2	2.8
160	2010.101.22.03.12.069.IU.PAB.00.LH2	216	4.3	47.2	936.5	28.3	10.0	0.943	0.777	37.10	-3.69	616	6.3	2.5
161	1995.305.00.30.32.138.G.PEL..LHE	383	2.4	45.8	930.5	8.3	3.5	0.893	0.679	-29.11	-71.68	22	6.6	4.1
162	1997.288.00.58.33.131.G.PEL..LHE	127	7.4	52.9	937.1	14.8	4.7	0.954	0.938	-31.06	-71.42	69	7.1	2.2
163	1998.210.07.09.24.150.G.PEL..LHN	119	7.8	48.2	937.3	10.9	3.3	0.794	0.378	-32.30	-71.67	58	6.4	1.2
164	2010.101.22.03.12.150.PM.PESTR..LHE	255	3.7	46.7	935.1	17.0	6.3	0.959	0.777	37.10	-3.69	616	6.3	3.5
165	2001.281.18.09.26.386.IU.PET.00.LHE	369	2.5	42.2	932.7	10.5	4.3	0.880	0.747	52.59	160.56	28	6.4	1.2
166	2003.167.22.03.02.235.IU.PET.00.LHX	1400*	0.2	51.8	935.6	25.7	12.4	0.971	0.845	55.48	160.25	180	6.9	2.6
167	2004.162.15.14.57.235.IU.PET.00.LHX	1400*	0.3	52.5	935.5	30.5	14.7	0.972	0.946	55.79	160.32	190	6.8	2.9
168	2007.150.20.17.12.085.IU.PET.00.LHE	1400*	0.3	46.1	935.7	7.4	3.6	0.974	0.979	52.01	157.78	123	6.4	1.1
169	2008.187.02.07.04.035.IU.PET.00.LHN	1400*	0.7	55.8	934.3	11.8	5.4	0.924	0.534	54.12	153.37	610	7.7	3.3
170	2008.206.01.38.16.035.IU.PET.00.LHN	160	5.8	47.8	938.5	9.7	3.3	0.809	0.403	50.71	158.15	42	6.2	2.3
171	2008.329.08.57.58.397.IU.PET.00.LHE	476	2.0	50.9	936.5	25.3	10.7	0.987	0.914	54.27	154.71	502	7.3	2.7
172	2011.051.21.38.24.385.IU.PET.00.LHE	351	2.7	44.4	935.3	18.5	7.6	0.907	0.995	55.80	162.60	25	6.2	3.6
173	2012.321.18.07.39.810.IU.PET.00.LHE	264	3.5	44.5	933.9	10.8	4.1	0.877	0.441	49.22	155.87	40	6.5	4.2
174	2013.059.14.00.50.692.IU.PET.00.LHE	548	1.7	47.9	937.5	9.2	4.1	0.807	0.446	50.83	157.93	45	6.8	2.2
175	2013.144.05.39.49.635.IU.PET.00.LHE	522	1.8	51.8	936.3	22.0	9.3	0.996	0.923	54.61	153.77	611	8.3	3.3
176	2013.274.03.33.21.635.IU.PET.00.LHE	274	3.4	46.4	935.2	20.8	7.9	0.972	0.639	53.20	152.81	585	6.7	3.5
177	2013.316.06.58.51.635.IU.PET.00.LHE	1229	0.8	47.4	936.5	12.3	5.8	0.924	0.993	54.79	162.29	29	6.5	2.8

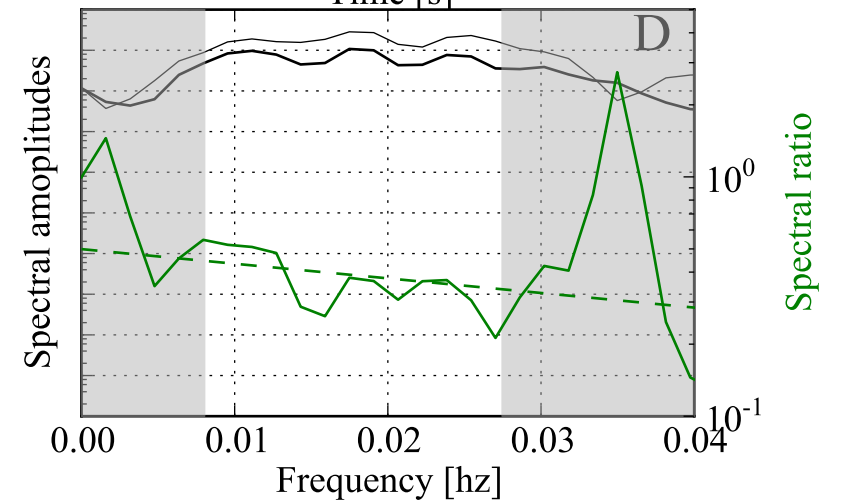
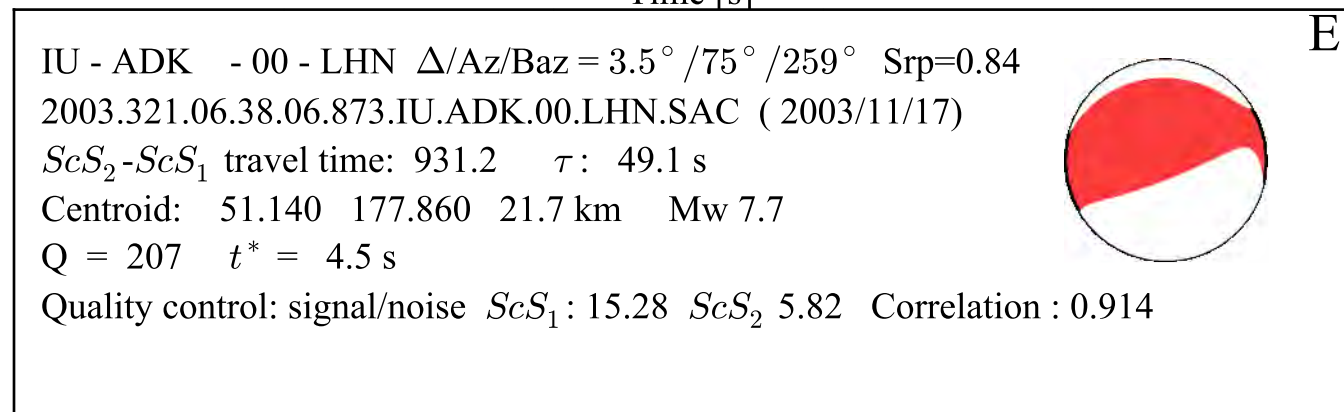
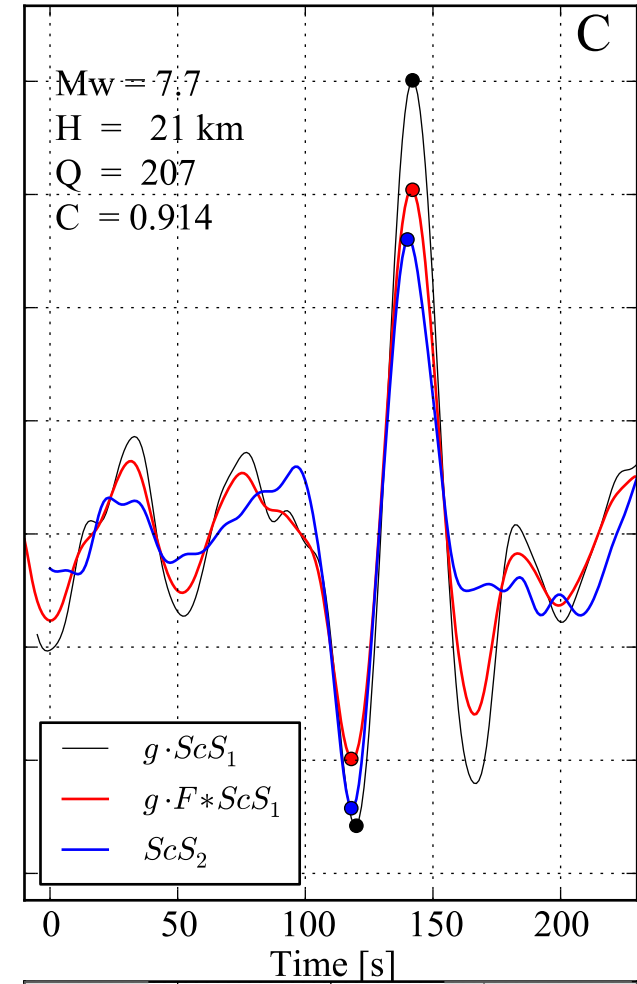
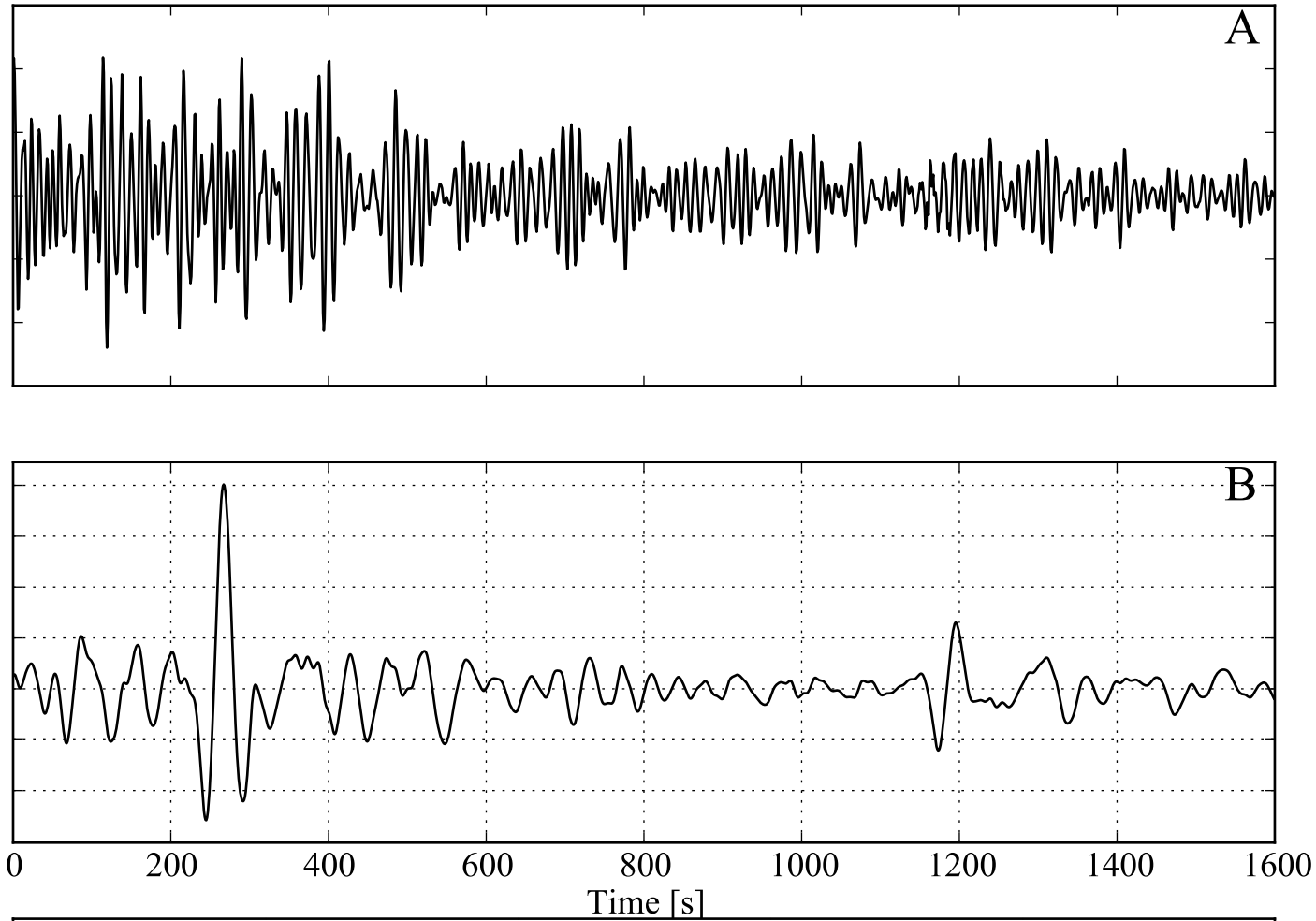
178	2010.101.22.03.12.120.PM.PFVI..LHE	318	2.9	48.3	935.9	12.4	4.8	0.850	0.777	37.10	-3.69	616	6.3	4.1
179	2014.121.06.31.35.956.ND.PINNC.00.LHN	132	7.1	42.9	938.4	12.0	3.5	0.920	0.783	-21.51	170.15	119	6.6	2.7
180	2011.348.04.59.59.069.IU.PMG.00.LH2	240	3.9	47.4	938.1	11.4	4.4	0.948	0.907	-7.49	146.83	132	7.1	1.9
181	2002.306.01.21.10.000.PS.PSI..LHE	469	2.0	50.8	927.8	8.1	3.6	0.842	0.862	2.65	95.99	23	7.2	2.9
182	2010.101.22.03.12.200.PM.PVAQ..LHE	200	4.7	48.3	936.2	17.1	5.9	0.935	0.777	37.10	-3.69	616	6.3	3.2
183	1995.180.12.19.03.345.G.PVC..LH2	188	5.0	49.7	942.5	21.7	7.9	0.986	0.958	-19.42	168.95	142	6.6	1.8
184	1995.282.13.38.42.521.G.PVC..LH1	713	1.3	56.7	942.0	8.3	3.8	0.956	0.641	-21.35	170.10	115	6.3	4.0
185	1996.077.14.43.56.905.G.PVC..LH1	270	3.5	49.2	939.0	11.0	4.3	0.807	0.414	-14.57	167.19	171	6.7	3.3
186	1997.141.14.05.26.603.G.PVC..LH2	310	3.0	48.7	941.3	13.7	5.7	0.926	0.679	-20.34	169.03	64	6.7	2.7
187	2003.361.15.55.59.022.G.PVC..LH2	77	12.2	48.4	941.8	13.8	3.4	0.872	0.542	-21.99	169.81	23	7.3	4.5
188	2006.136.10.34.23.398.IU.RAO.10.LHE	154	6.1	50.5	937.0	8.7	3.1	0.840	0.831	-31.41	-178.91	151	7.4	2.3
189	2007.343.07.23.20.473.IU.RAO.10.LHN	130	7.2	52.1	936.5	17.8	5.8	0.936	0.776	-25.75	-177.22	149	7.8	3.5
190	2009.196.09.17.29.812.NZ.RPZ.10.LH2	1400*	0.3	47.3	937.5	8.4	4.1	0.895	0.786	-45.85	166.26	23	7.8	4.0
191	2012.185.10.31.15.528.NZ.RPZ.10.LH1	106	8.8	48.8	937.2	12.4	3.5	0.887	0.949	-40.05	173.63	230	6.3	4.1
192	2010.101.22.03.12.607.MN.RTC..LHE	1400*	0.1	48.5	936.8	11.1	5.8	0.833	0.777	37.10	-3.69	616	6.3	4.0
193	2013.032.22.11.34.000.G.SANVU.00.LHE	126	7.4	40.1	938.5	13.5	3.8	0.873	0.835	-11.15	165.23	13	6.4	4.7
194	2014.064.09.51.58.000.G.SANVU.00.LHE	131	7.2	45.8	940.1	24.2	7.1	0.907	0.892	-14.56	169.77	660	6.3	2.6
195	2014.013.03.56.04.069.IU.SJG.00.LH2	104	8.9	43.4	929.6	13.0	3.4	0.813	0.872	19.24	-66.85	22	6.3	1.3
196	2012.342.18.14.06.069.IU.SNZO.00.LH2	94	9.9	50.6	939.4	13.2	3.6	0.918	0.860	-38.31	176.08	165	6.3	3.2
197	2014.020.02.47.45.069.IU.SNZO.00.LH1	154	6.1	41.5	937.9	12.9	4.0	0.811	0.846	-40.63	175.88	26	6.3	1.1
198	2005.288.15.46.07.548.TW.SSLB..LHX	229	4.1	46.9	935.6	13.1	4.9	0.876	0.897	25.29	123.43	194	6.4	2.7
199	2005.288.15.46.07.673.IU.TATO.00.LH1	131	7.1	48.5	936.8	16.9	5.3	0.944	0.897	25.29	123.43	194	6.4	1.8
200	2013.250.00.08.29.000.CU.TGUH.00.LH2	309	3.0	50.4	933.5	10.7	4.5	0.901	0.968	14.54	-92.11	79	6.4	4.7
201	2007.220.16.59.57.069.GE.UGM..LHN	165	5.7	48.7	933.7	10.1	3.4	0.951	0.822	-6.03	107.58	304	7.5	3.5
202	1997.011.20.23.26.581.G.UNM..LHN	157	5.9	49.0	936.1	13.3	4.6	0.885	0.913	18.34	-102.58	40	7.1	3.4
203	2003.022.02.01.34.643.G.UNM..LHX	423	2.2	44.4	937.8	11.8	5.0	0.899	0.921	18.86	-103.90	26	7.5	4.5
204	2011.108.12.58.02.646.NZ.URZ.10.LH2	141	6.7	51.1	938.7	13.5	4.4	0.962	0.865	-34.40	-179.83	99	6.5	4.6
205	2012.185.10.31.15.646.NZ.URZ.10.LH1	93	10.1	54.1	938.4	17.7	4.9	0.955	0.949	-40.05	173.63	230	6.3	3.2
206	2014.020.02.47.45.646.NZ.URZ.10.LH2	65	14.3	44.1	938.6	18.6	3.4	0.880	0.846	-40.63	175.88	26	6.3	2.5
207	2004.313.15.50.01.069.TW.YHNB..LHN	311	3.0	39.9	935.8	8.7	3.4	0.892	0.842	23.86	122.43	33	6.3	1.3
208	1993.015.11.01.05.802.IU.YSS..LHN	194	4.8	56.2	935.5	15.5	5.8	0.970	0.983	43.06	144.29	100	7.6	4.0
209	1994.282.07.50.38.528.IU.YSS..LHE	169	5.5	43.7	935.3	14.4	4.8	0.945	0.799	43.87	147.96	33	7.2	4.8
210	1995.118.16.25.00.329.IU.YSS..LHE	147	6.3	42.3	936.2	15.3	4.9	0.929	0.742	43.98	148.25	33	6.9	4.9
211	1996.053.14.54.09.178.IU.YSS..LHN	202	4.6	44.1	933.5	9.2	3.3	0.951	0.968	45.29	148.56	130	6.3	4.4
212	1996.357.14.48.27.128.IU.YSS..LHN	210	4.4	48.2	934.3	11.9	4.4	0.888	0.794	43.29	138.78	244	6.5	4.6
213	1999.132.17.54.22.298.IU.YSS.00.LHN	126	7.4	48.1	935.6	9.5	2.8	0.933	0.711	43.12	143.70	96	6.2	3.9
214	2000.028.14.16.07.948.IU.YSS.00.LHN	174	5.3	46.0	932.2	11.2	4.0	0.899	0.747	43.08	146.81	50	6.8	4.8
215	2002.321.04.48.53.110.IU.YSS.00.LHE	328	2.8	48.0	935.1	23.9	9.5	0.944	0.975	47.81	146.45	479	7.3	2.6
216	2003.268.19.45.06.297.IU.YSS.00.LHE	182	5.1	49.6	936.2	16.5	6.0	0.953	0.951	42.21	143.84	28	8.3	4.8
217	2003.281.09.01.55.298.IU.YSS.00.LHE	300	3.1	43.3	936.2	16.7	6.6	0.919	0.834	42.48	144.82	36	6.6	4.7
218	2004.333.18.27.14.785.IU.YSS.00.LHE	210	4.4	45.7	935.3	14.5	5.4	0.943	0.703	42.88	145.36	47	7.0	4.5
219	2005.018.14.04.06.785.IU.YSS.00.LHE	269	3.5	46.1	934.3	9.7	3.8	0.913	0.579	42.80	145.06	53	6.2	4.5
220	2013.033.14.12.35.898.IU.YSS.00.LHN	139	6.7	46.4	934.5	20.7	6.6	0.958	0.980	42.85	143.24	105	6.9	4.1

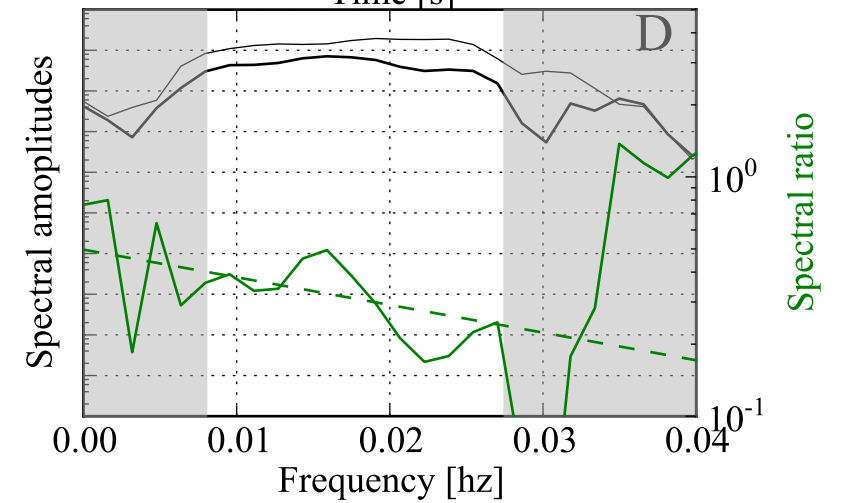
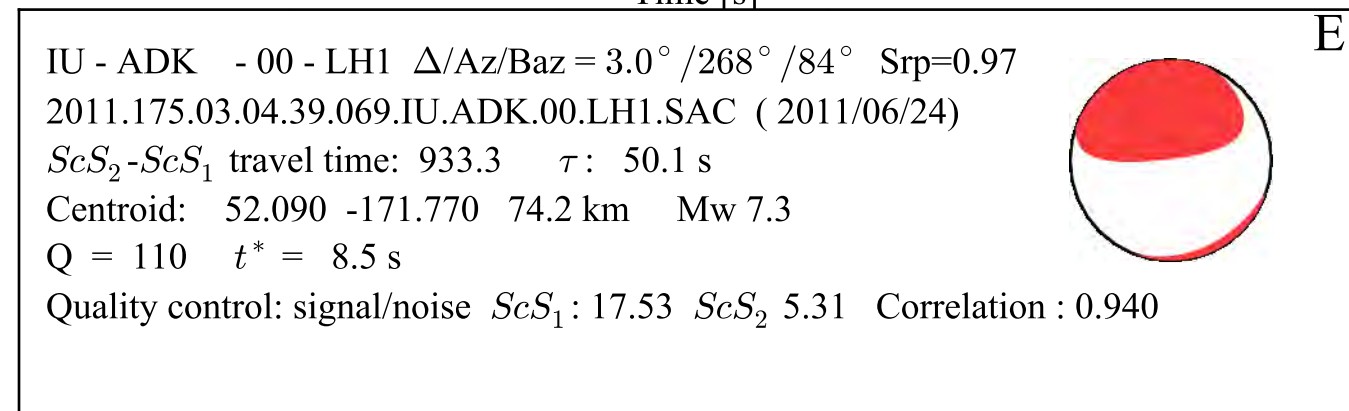
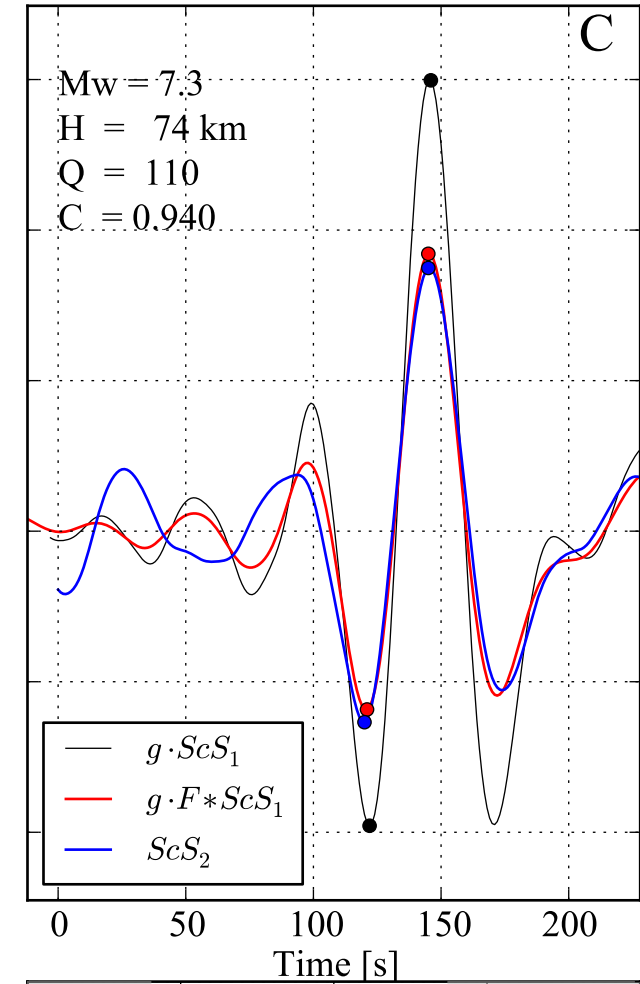
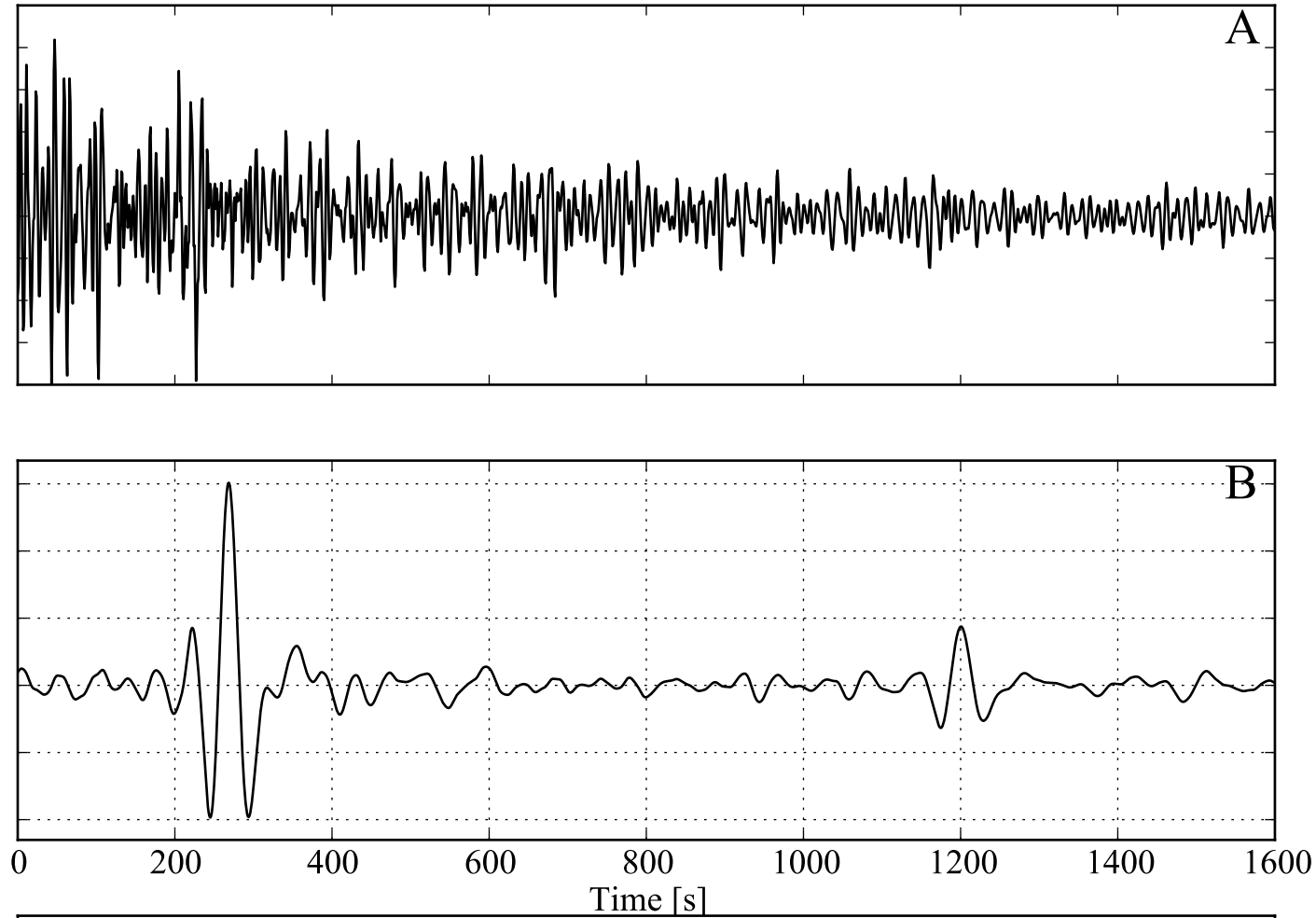
Appendices

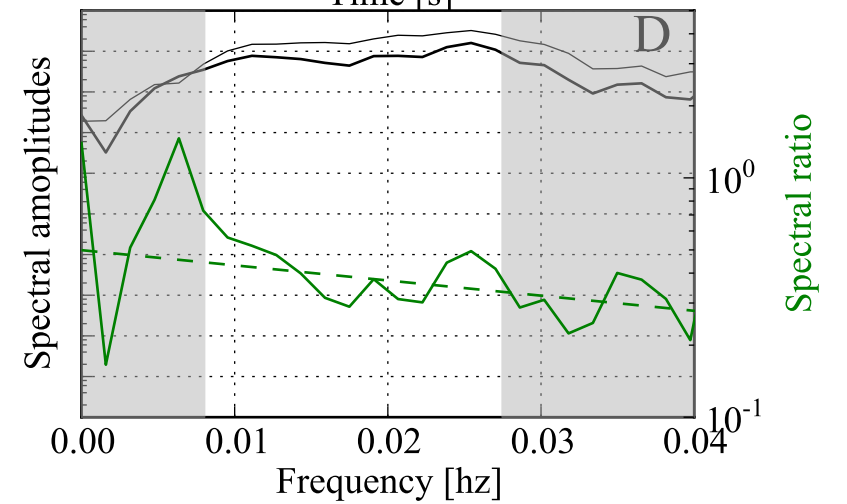
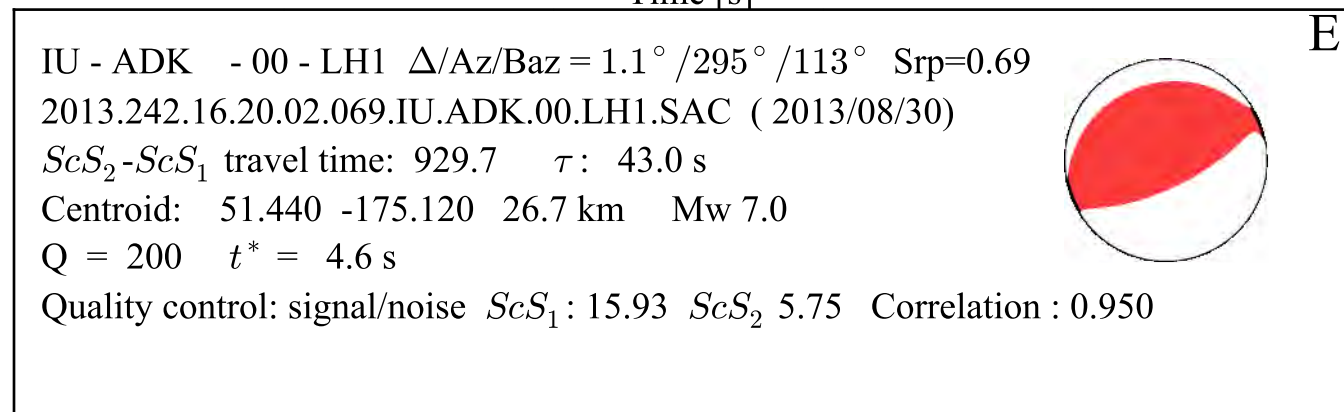
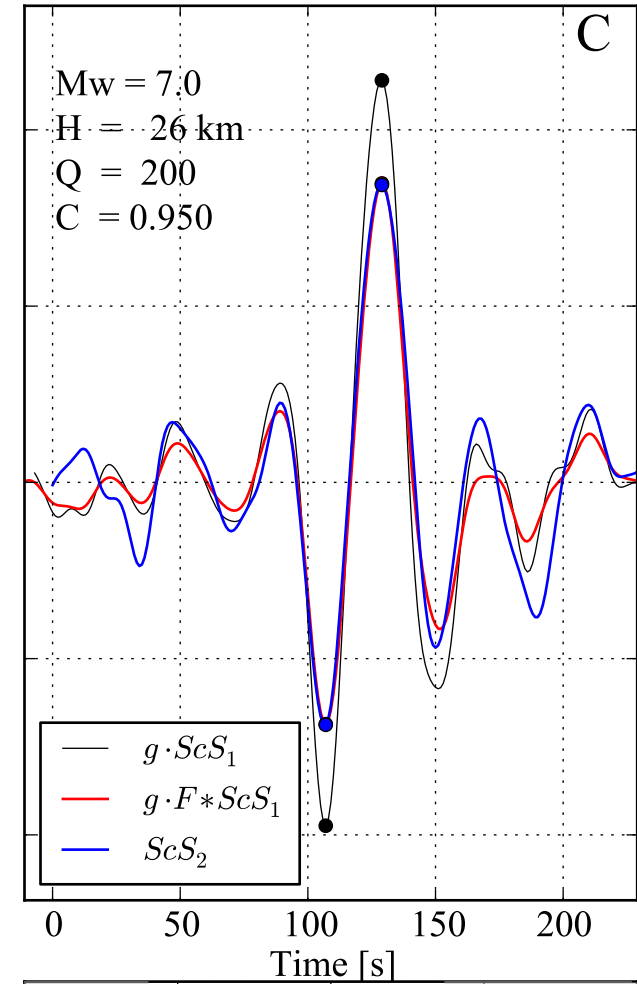
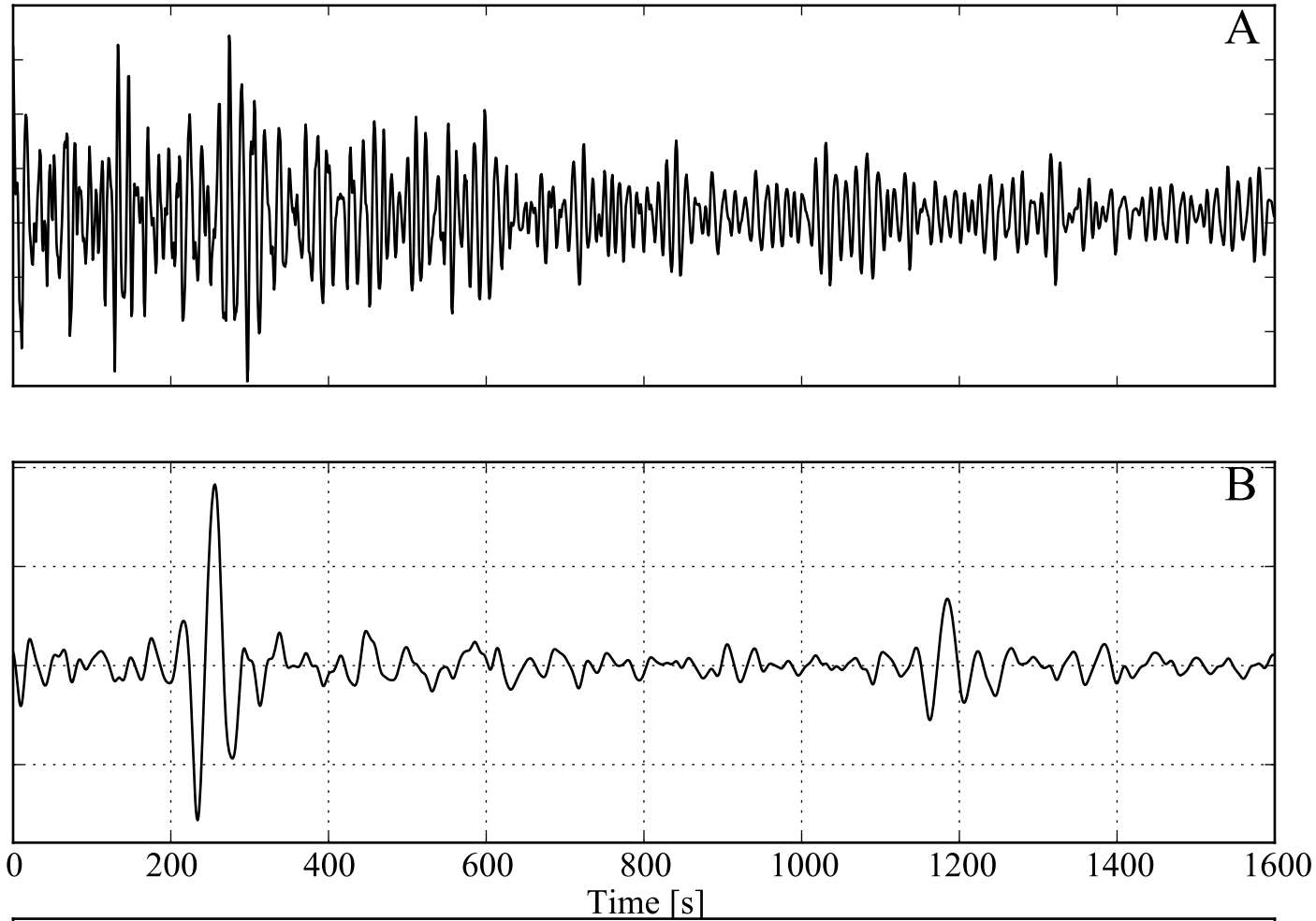


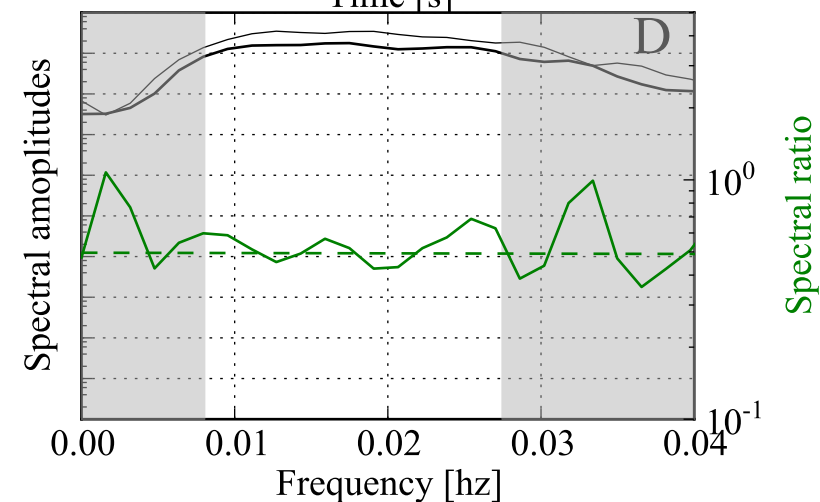
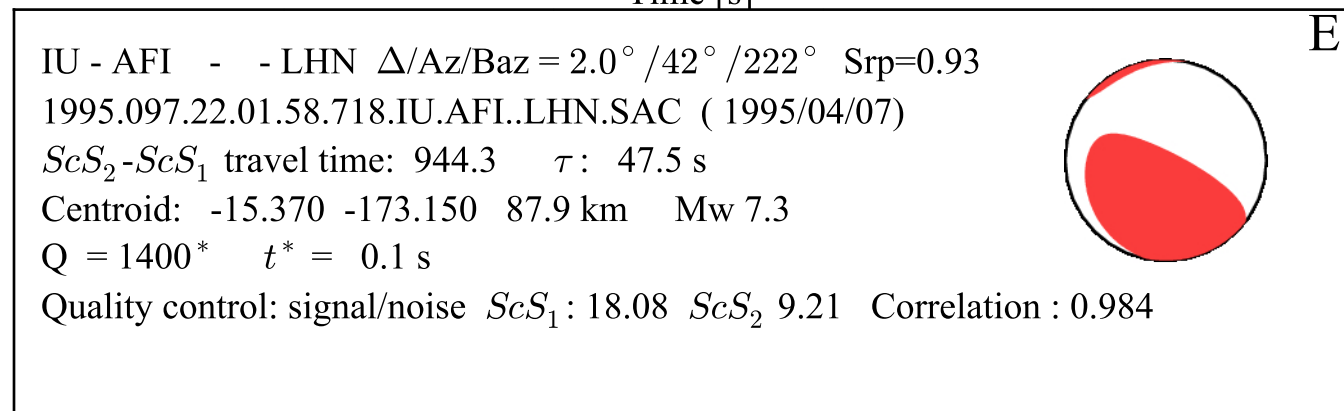
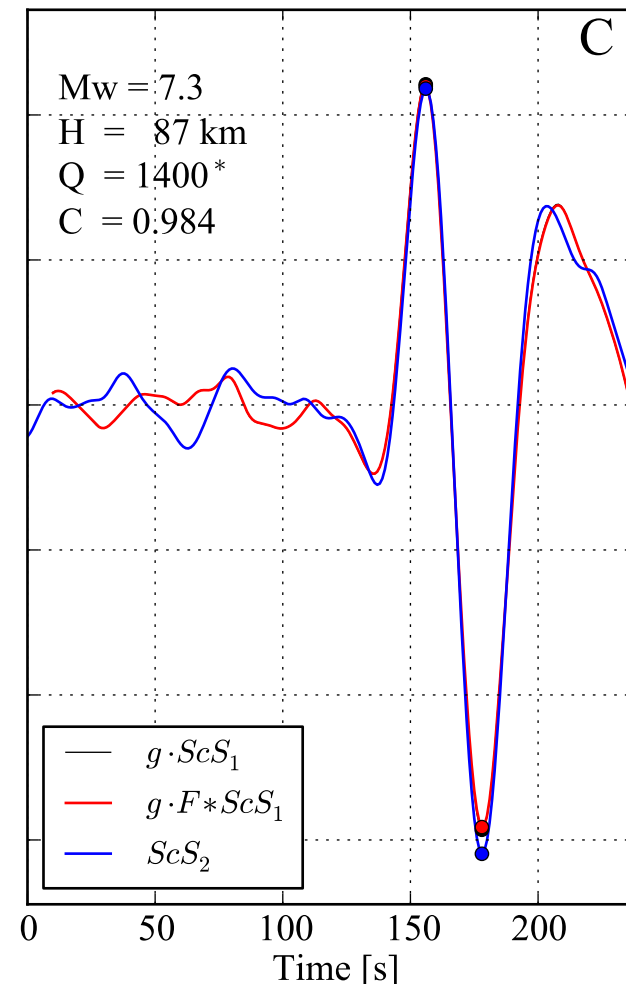
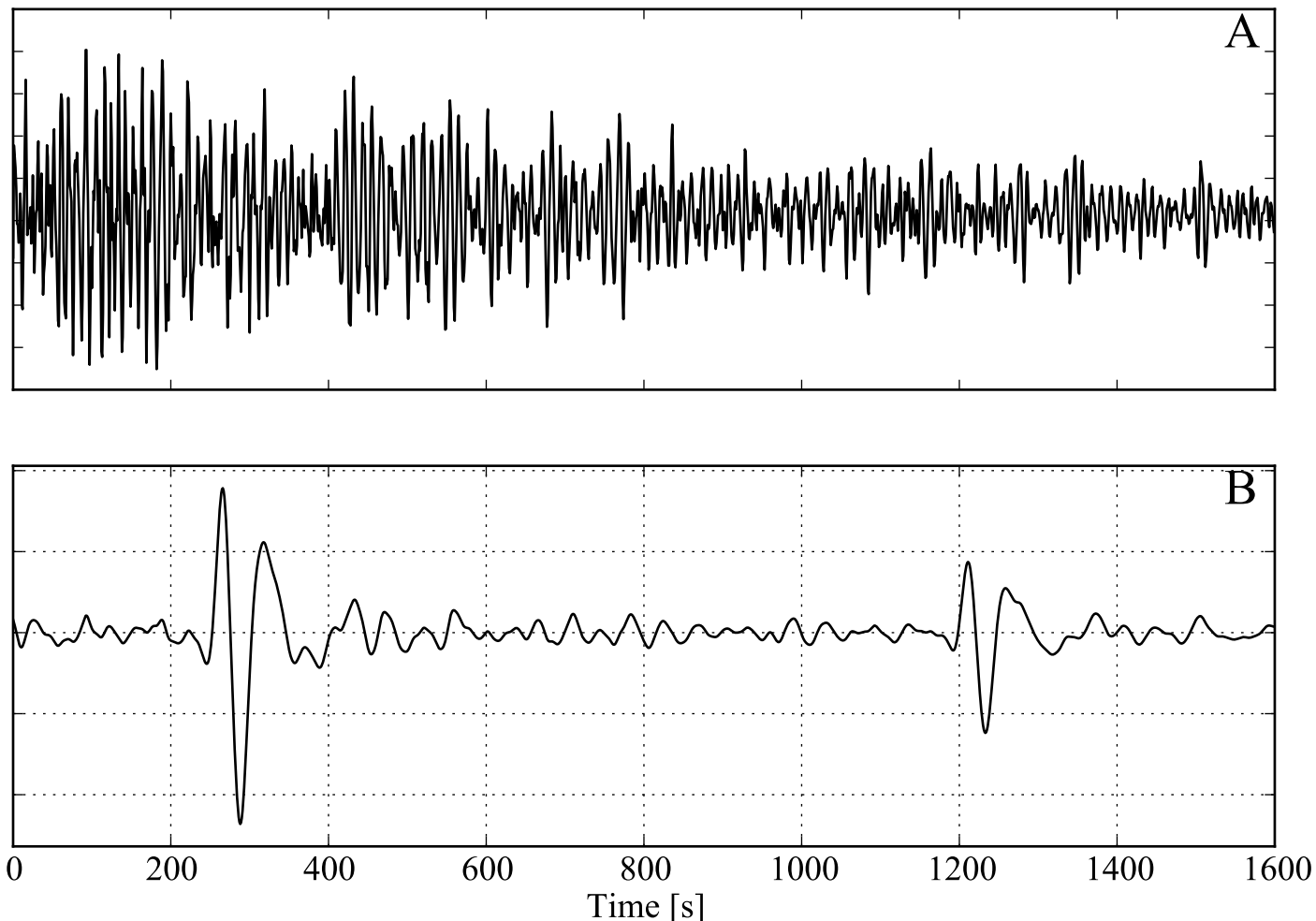


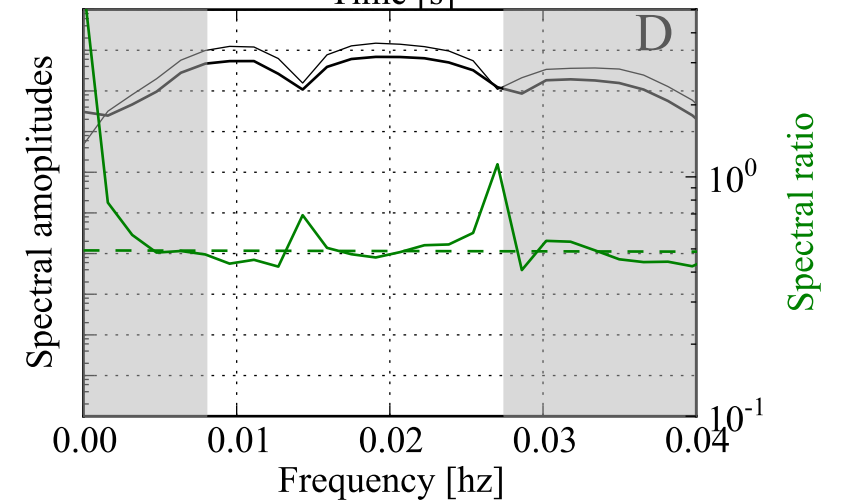
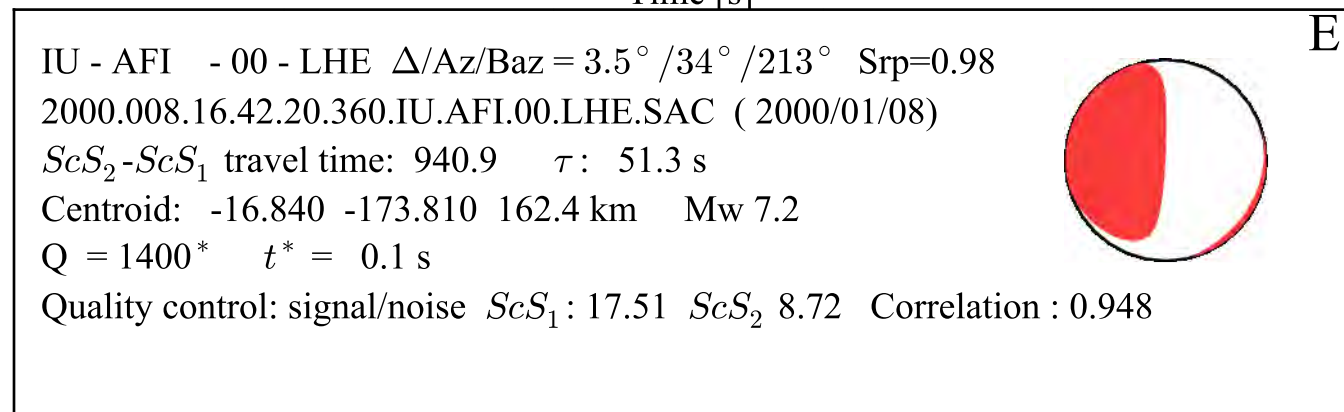
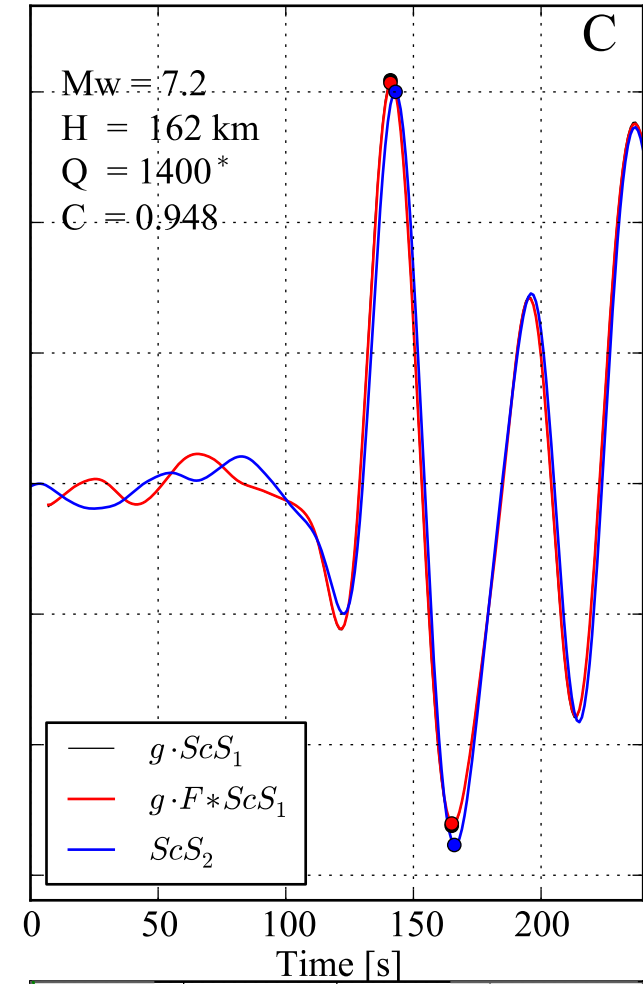
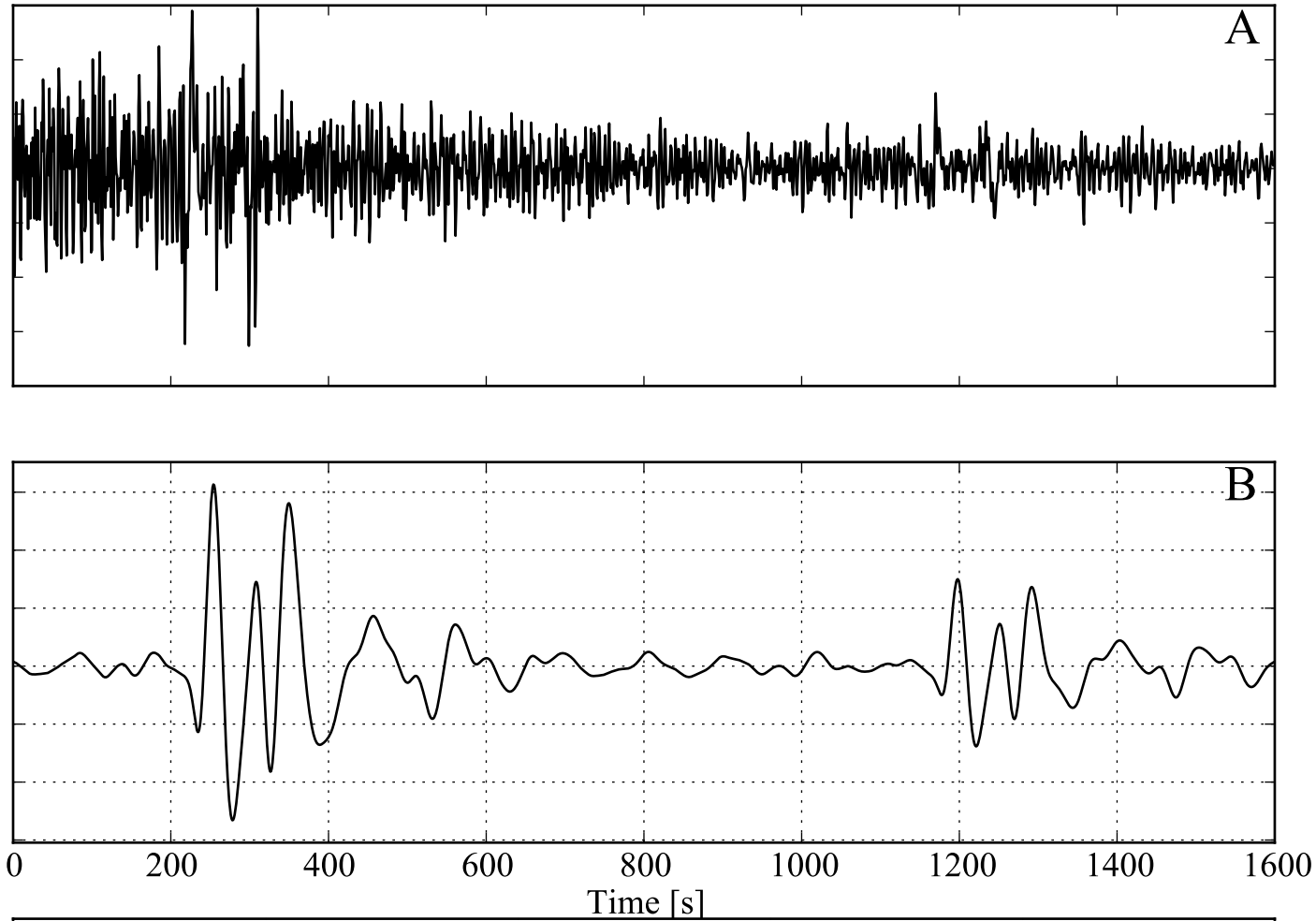


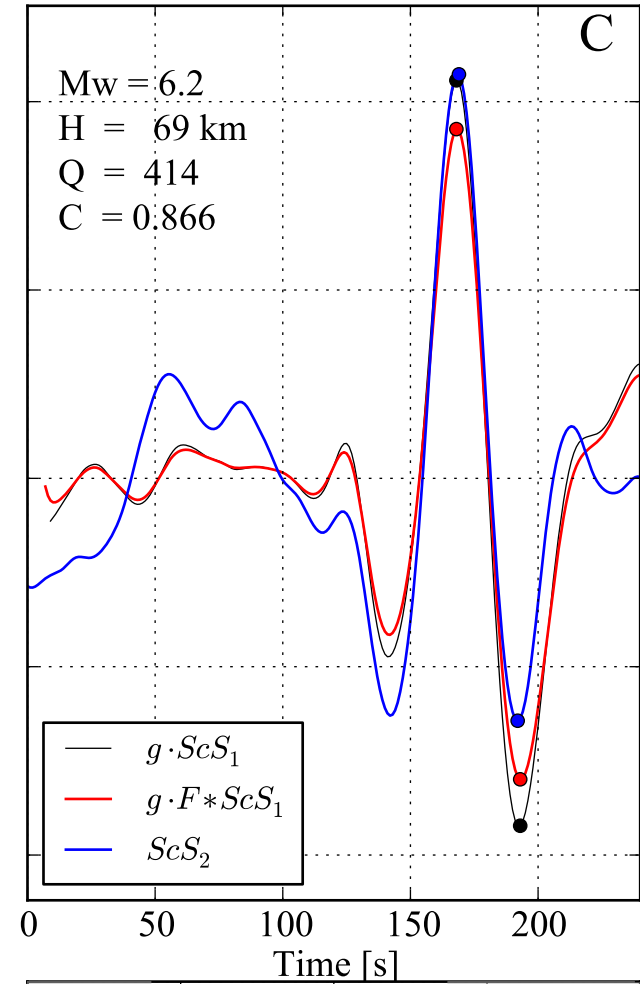
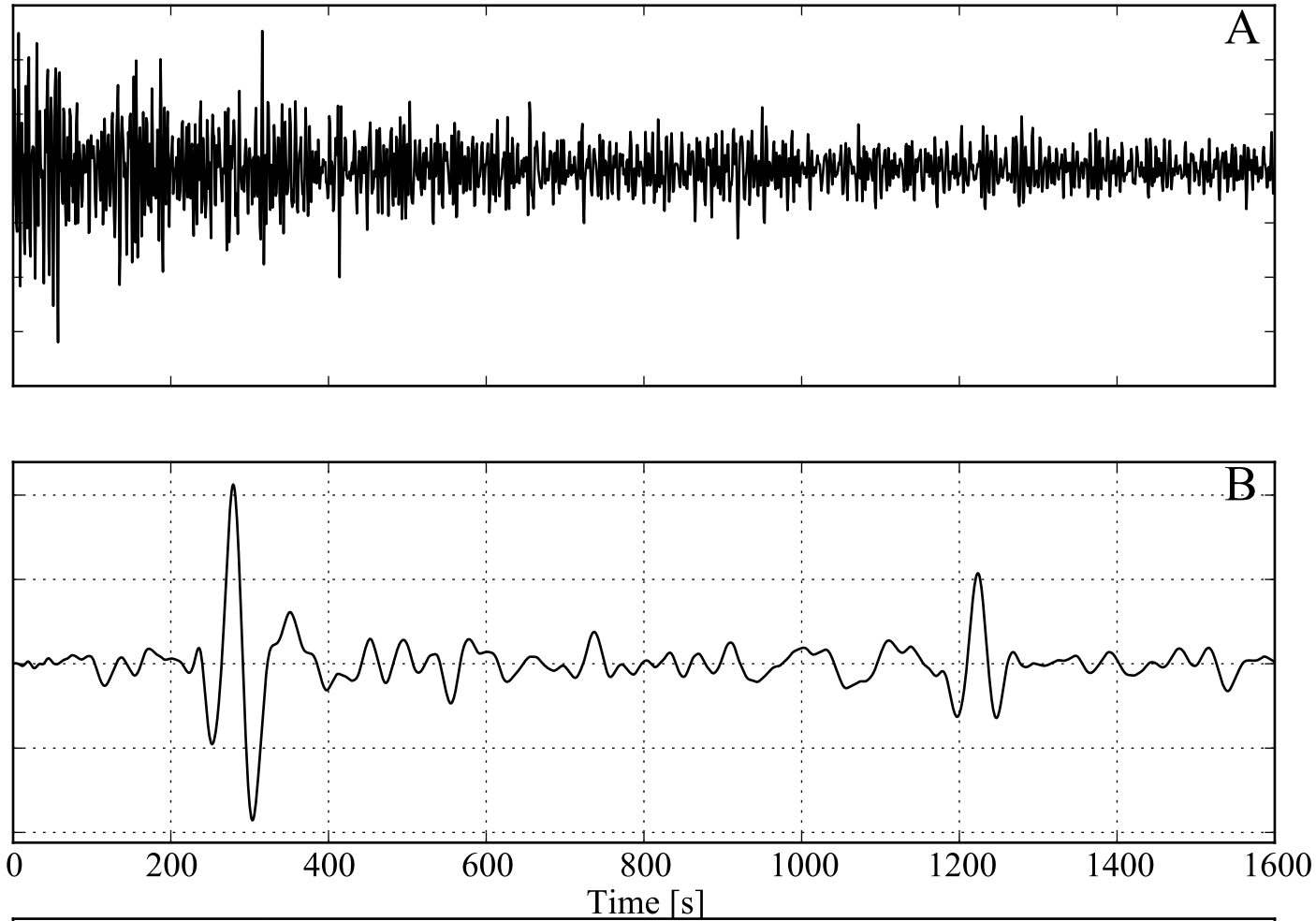





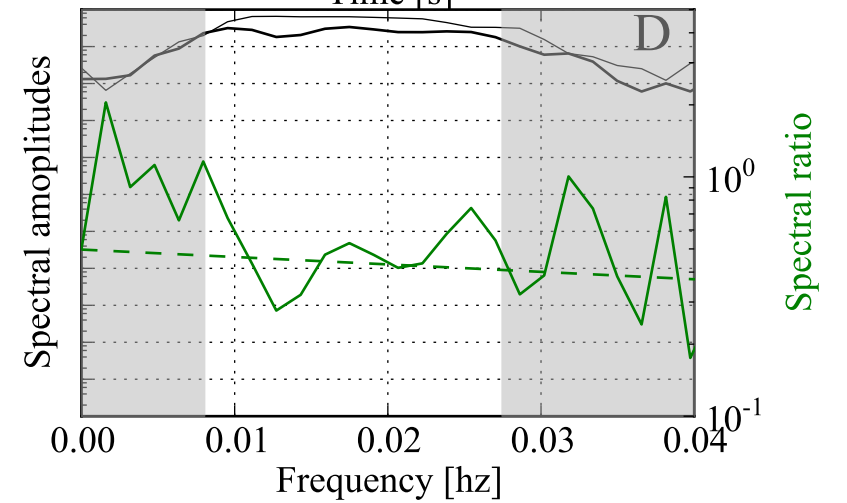


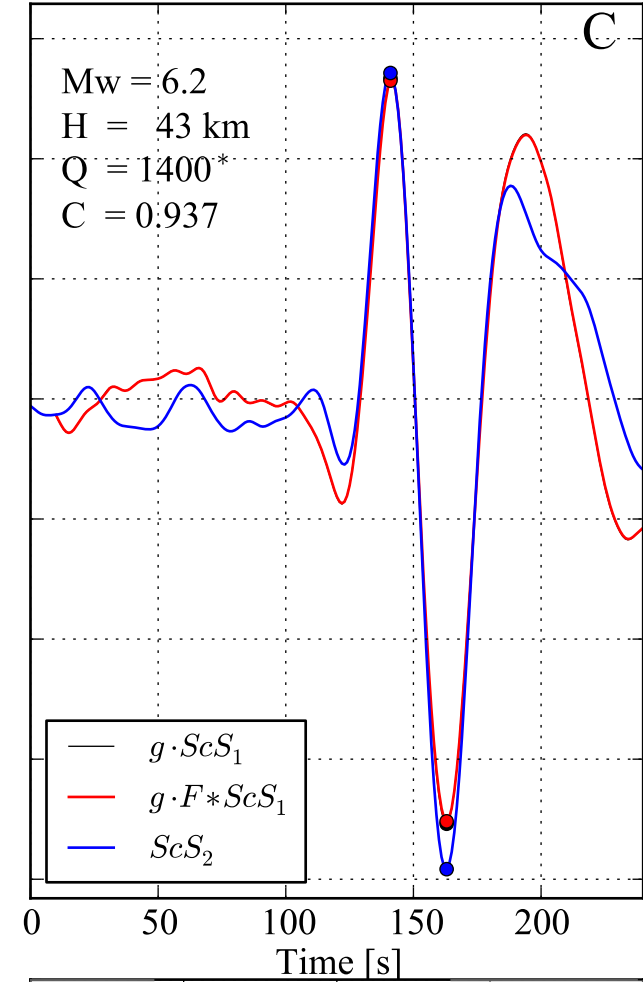
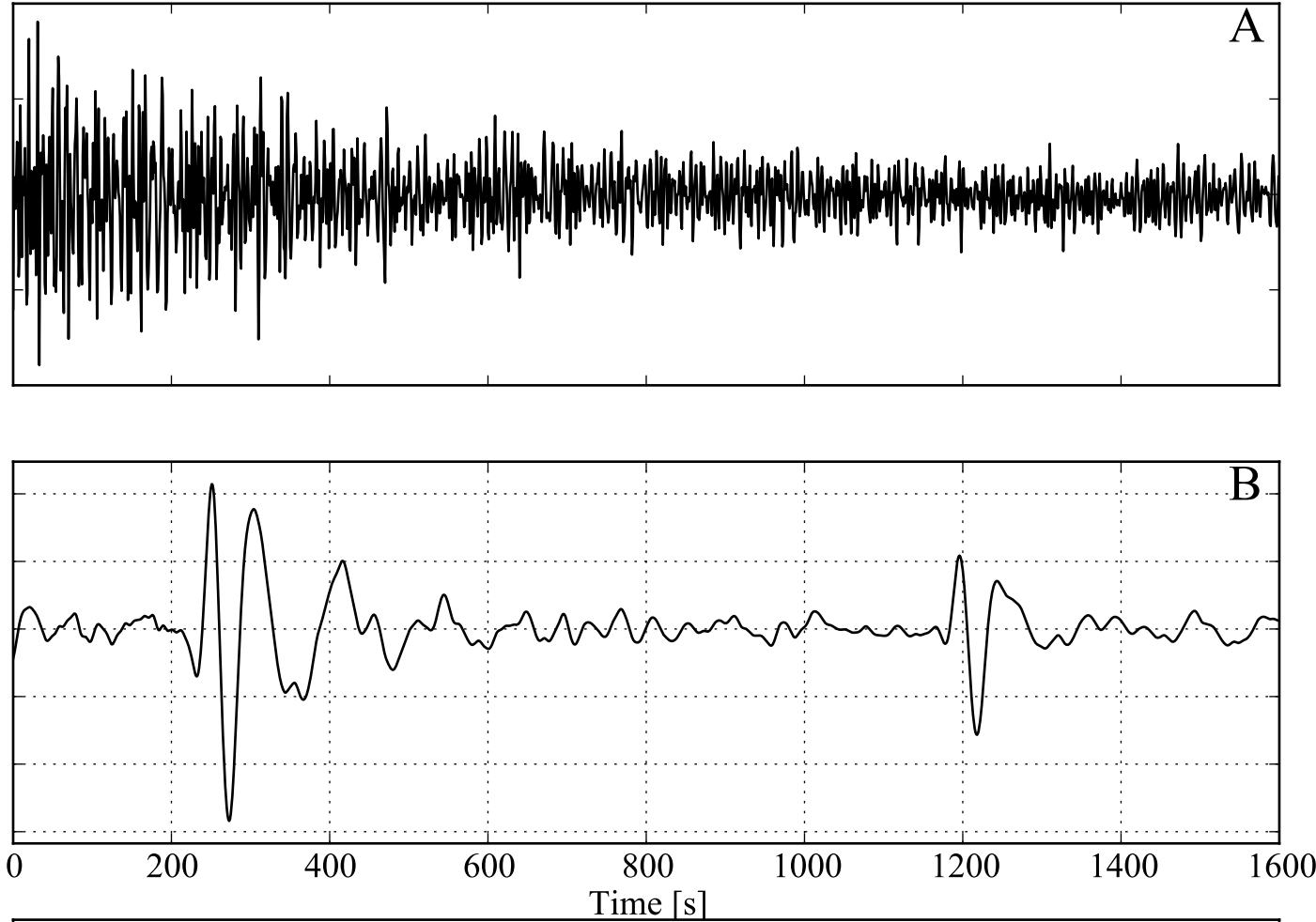







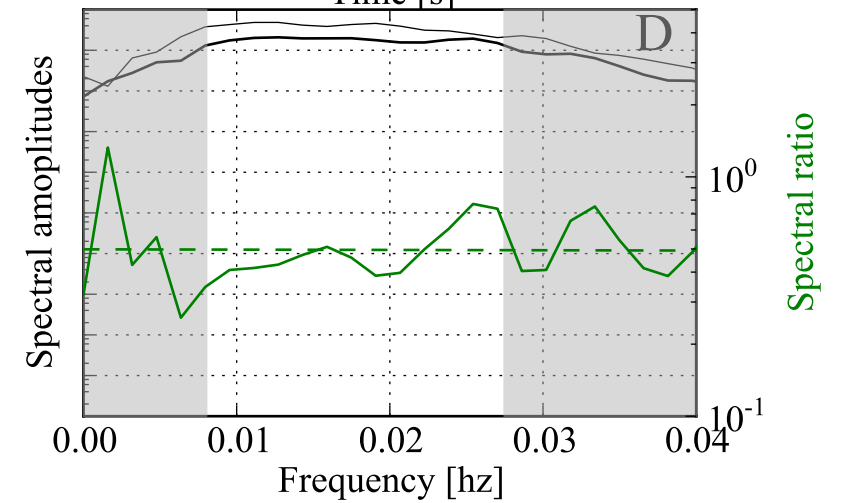
IU - AFI - 10 - LHE $\Delta/Az/Baz = 3.7^\circ / 27^\circ / 206^\circ$ $Srp=0.86$
 2000.026.13.21.50.360.IU.AFI.10.LHE.SAC (2000/01/26)
 $ScS_2 - ScS_1$ travel time: 942.9 τ : 50.1 s
 Centroid: -17.210 -173.510 69.2 km M_w 6.2
 $Q = 414$ $t^* = 2.3$ s
 Quality control: signal/noise ScS_1 : 9.92 ScS_2 4.27 Correlation : 0.866

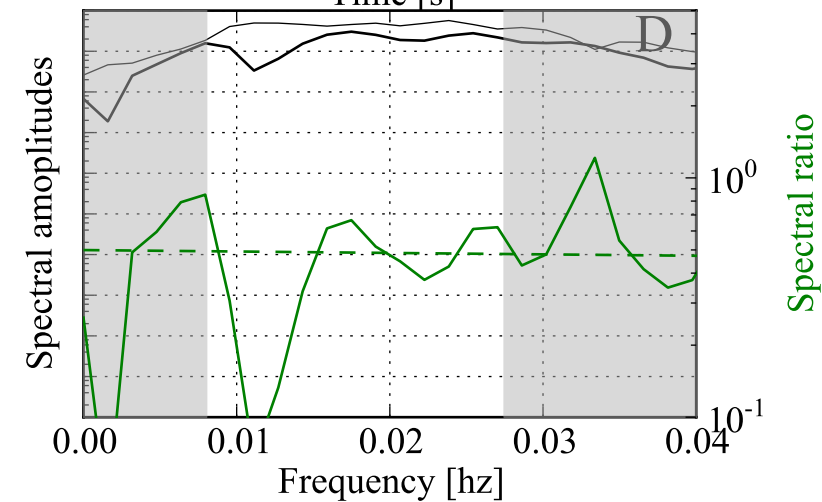
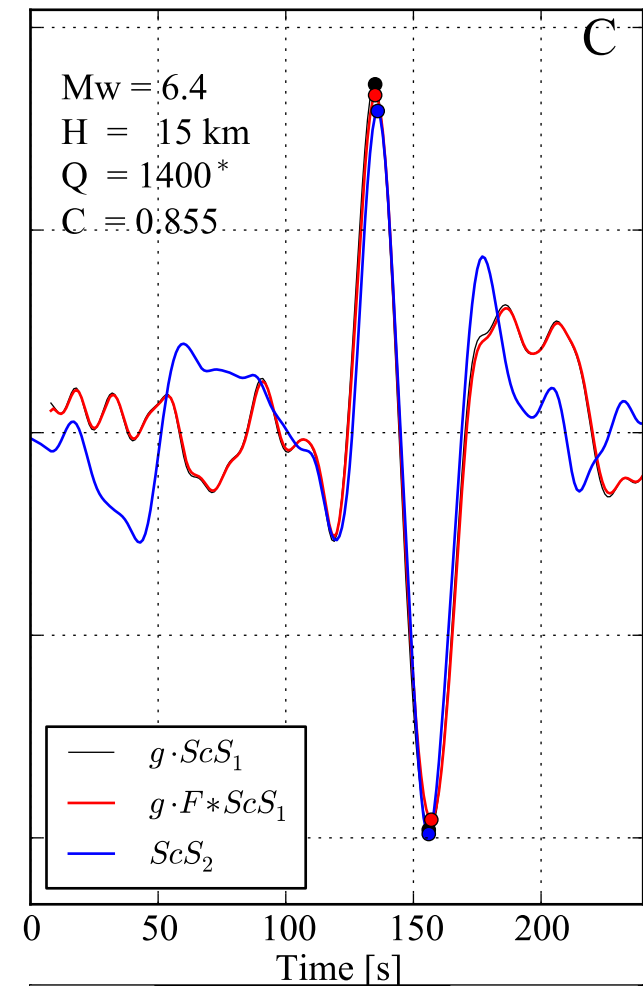
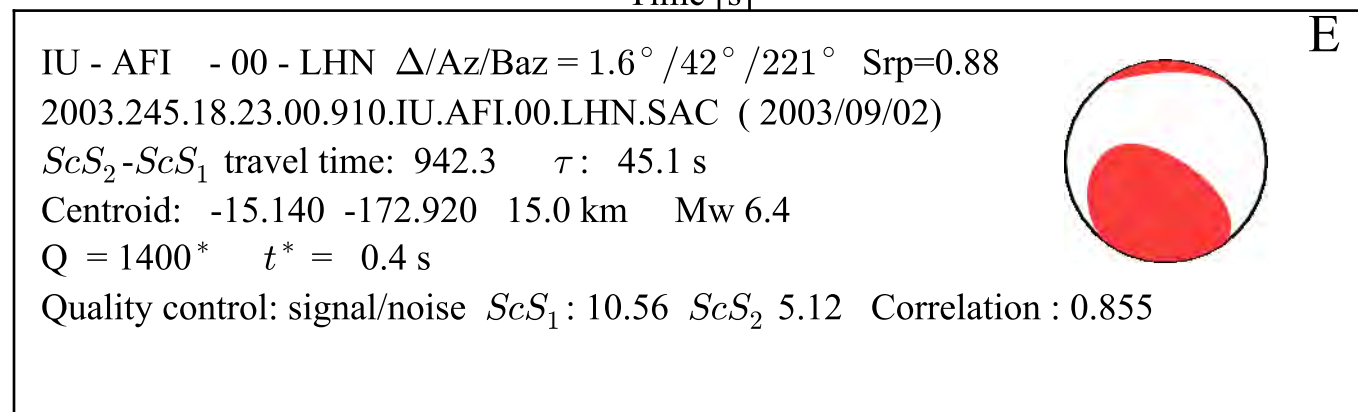
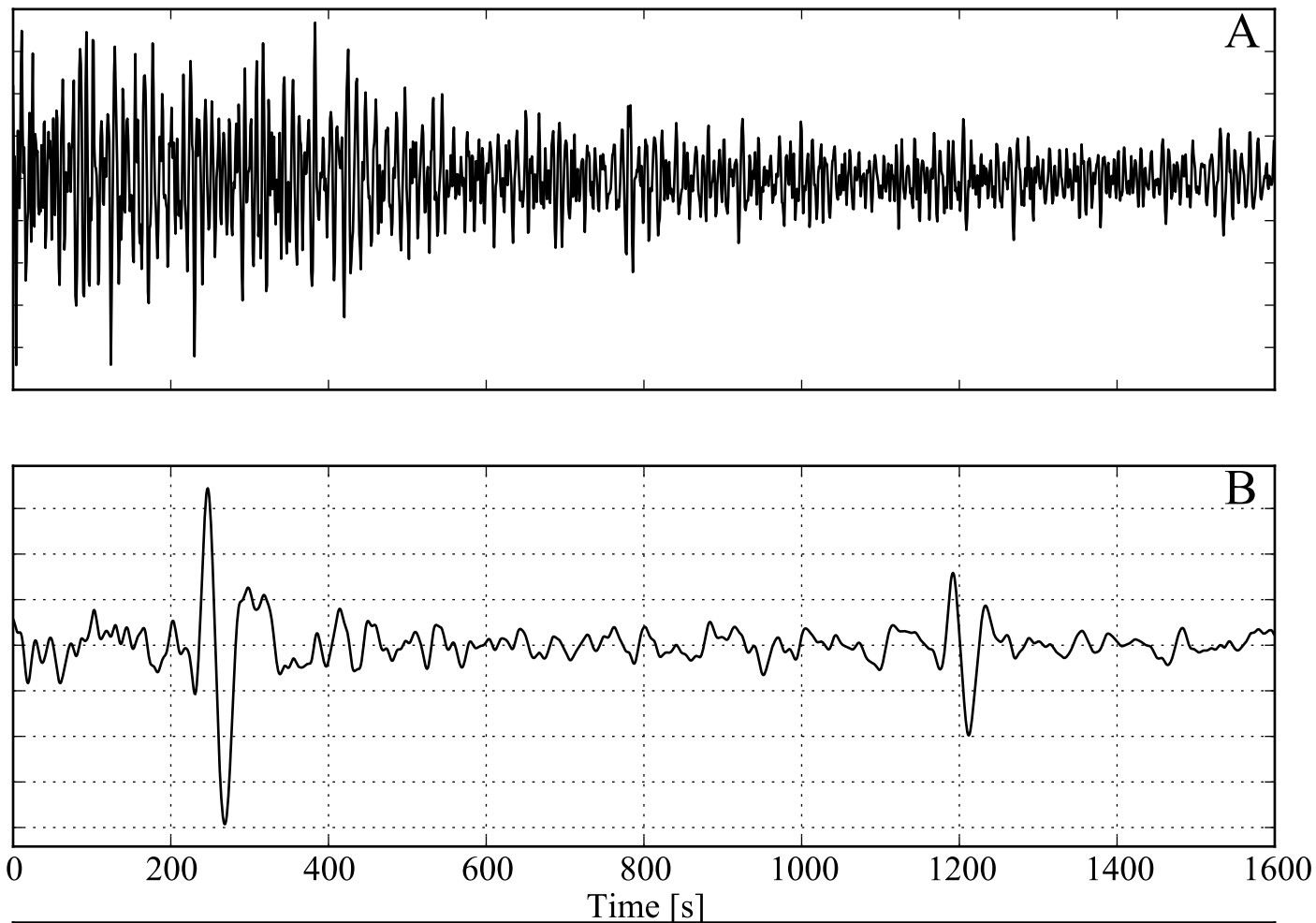



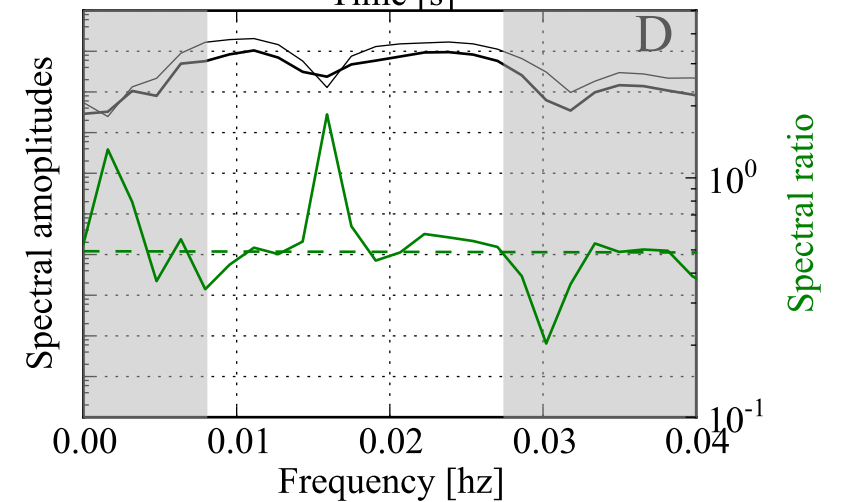
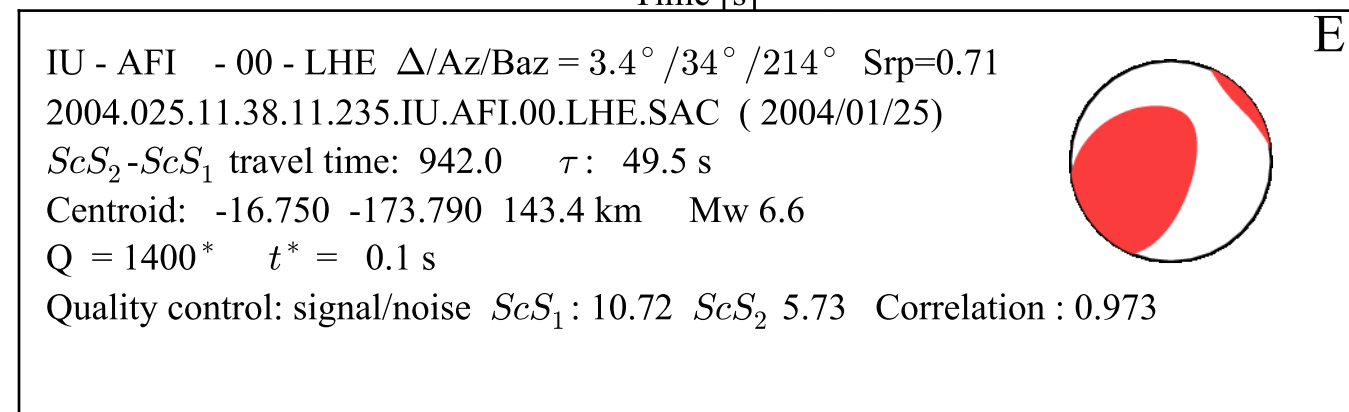
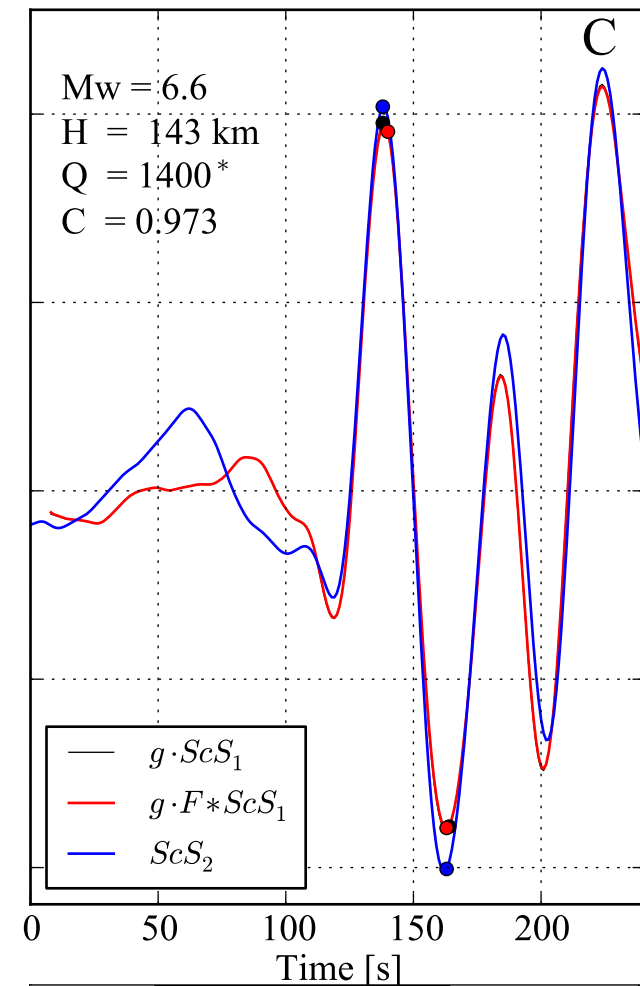
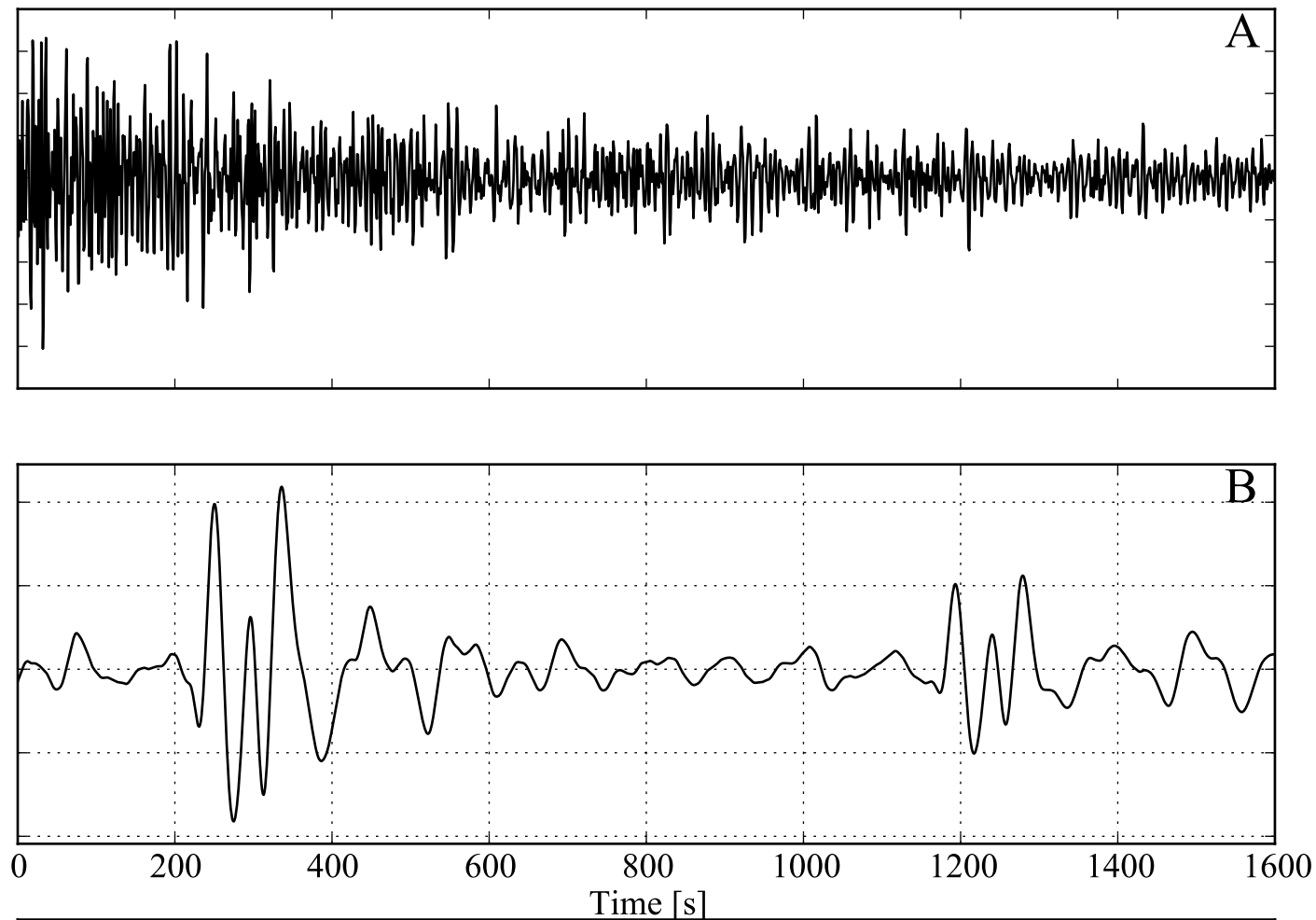


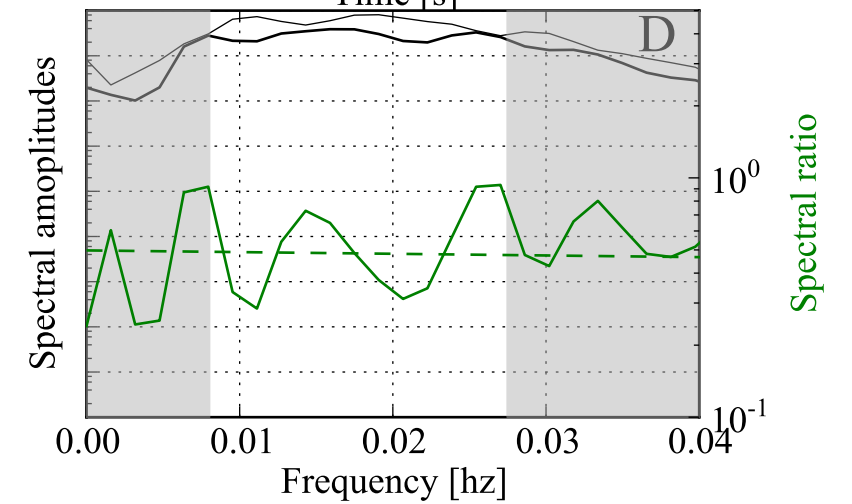
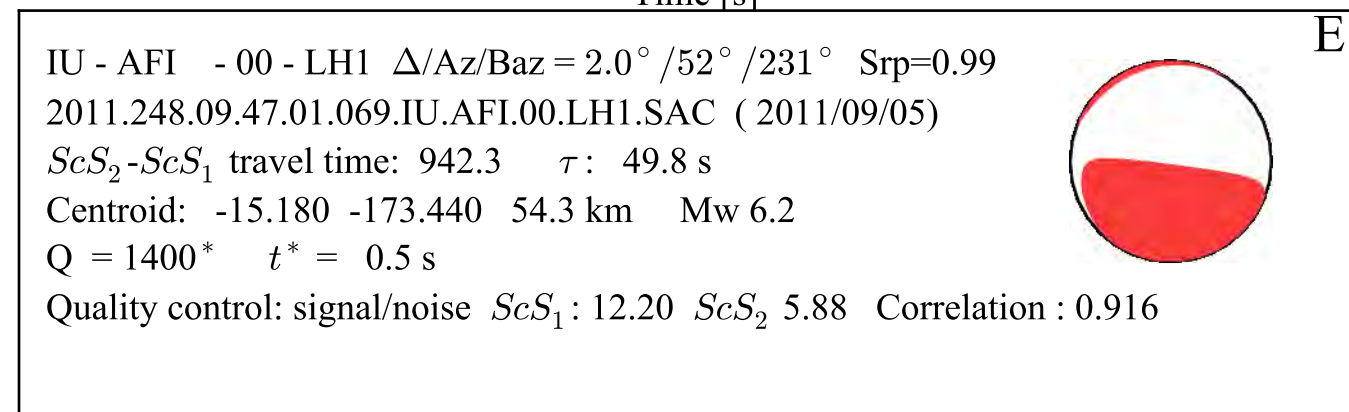
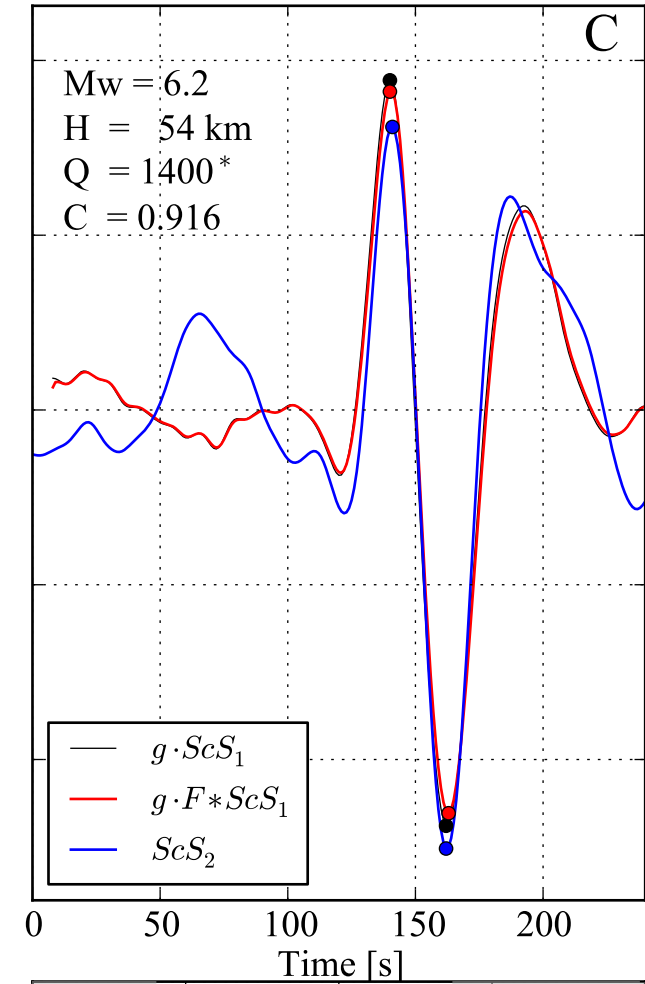
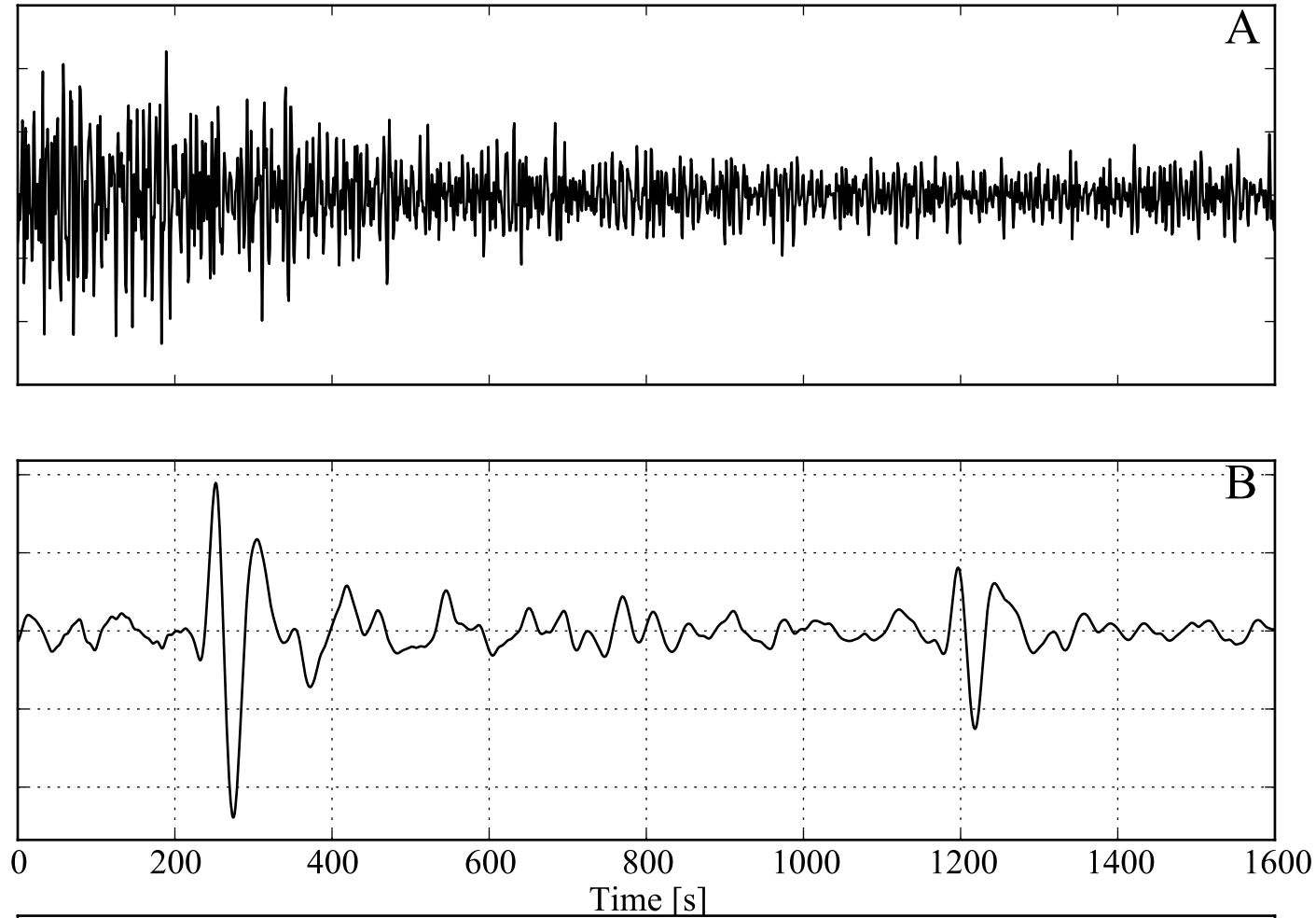
E

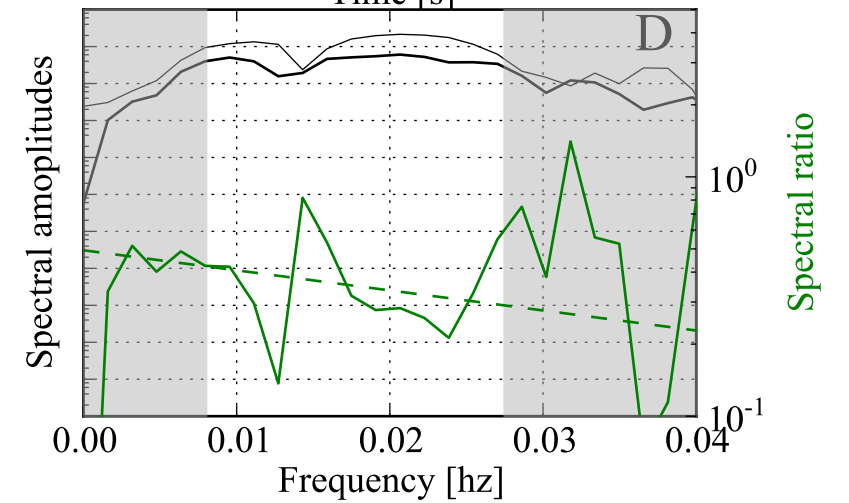
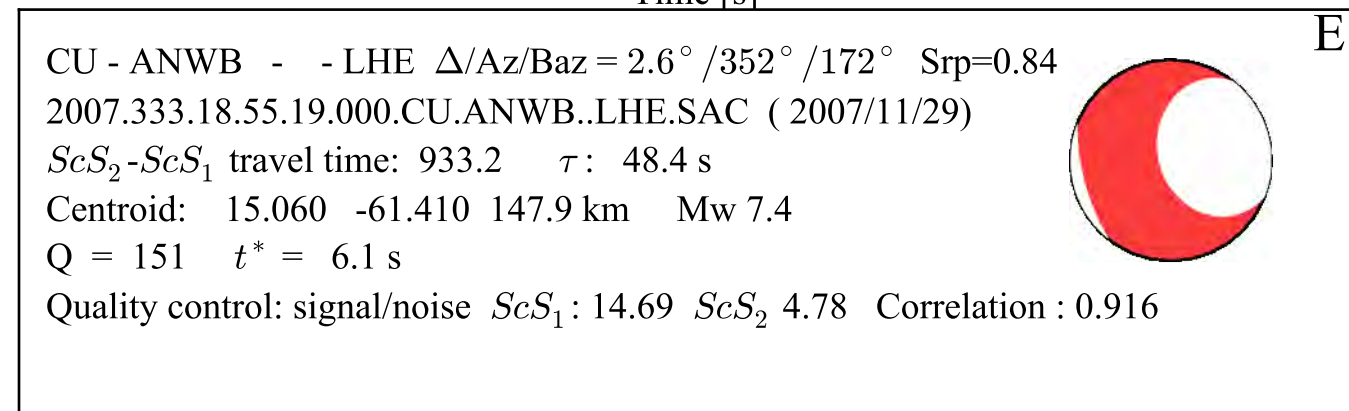
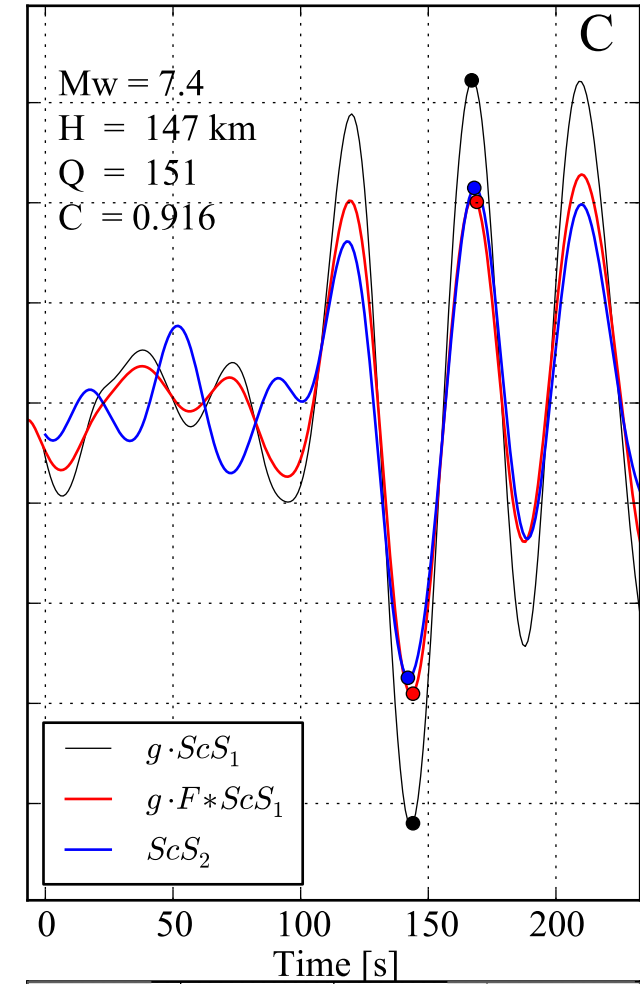
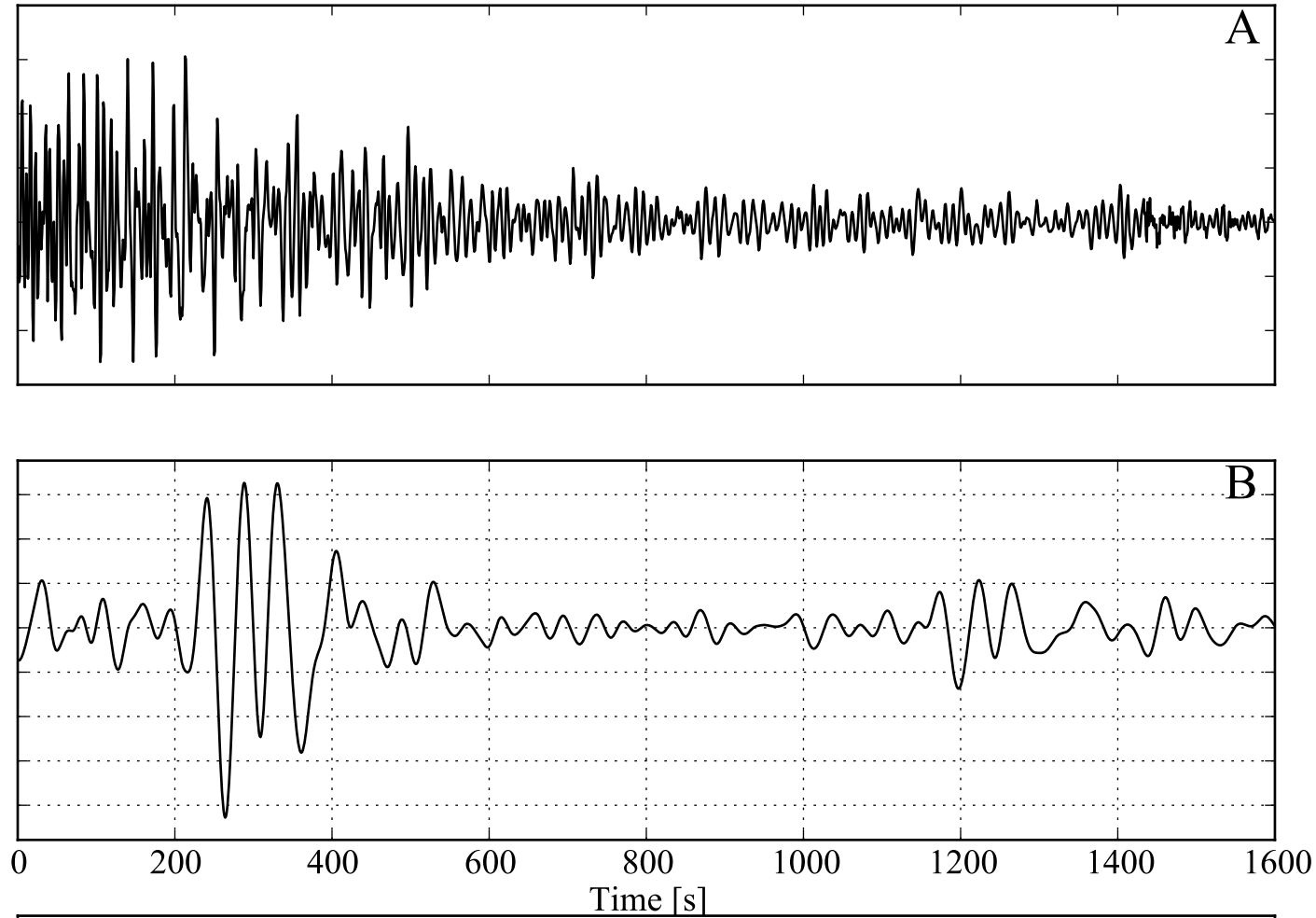
IU - AFI - 00 - LHN $\Delta/Az/Baz = 2.0^\circ / 52^\circ / 231^\circ$ Srp=0.98
 2003.123.04.58.03.935.IU.AFI.00.LHN.SAC (2003/05/03)
 $ScS_2 - ScS_1$ travel time: 944.3 τ : 47.8 s
 Centroid: -15.160 -173.410 43.0 km Mw 6.2
 Q = 1400* $t^* = 0.1$ s
 Quality control: signal/noise ScS_1 : 16.33 ScS_2 8.69 Correlation : 0.937

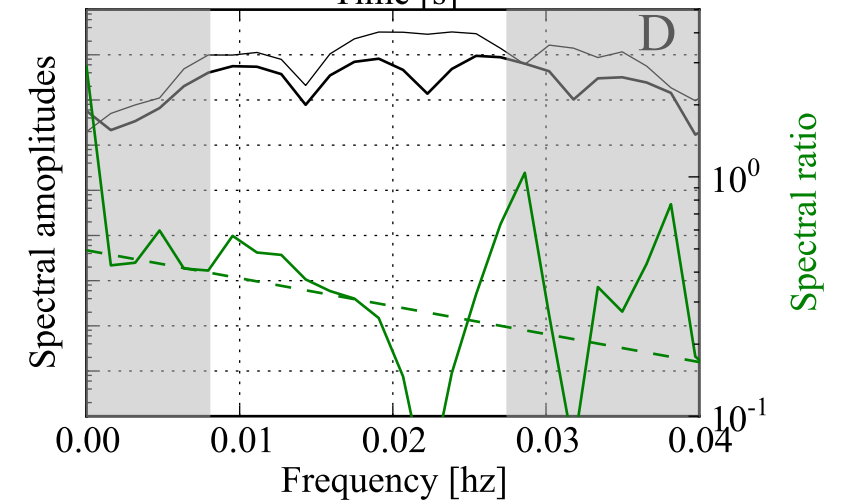
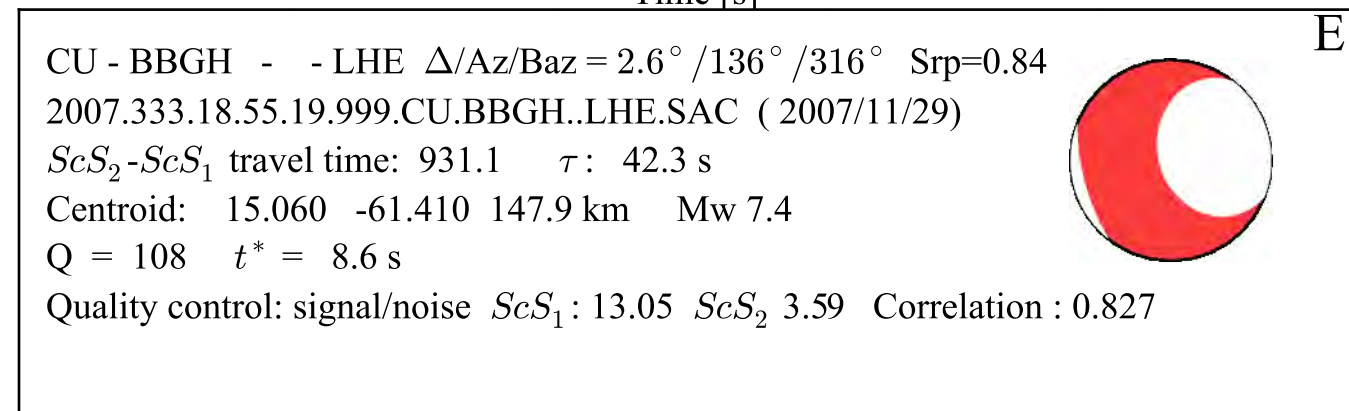
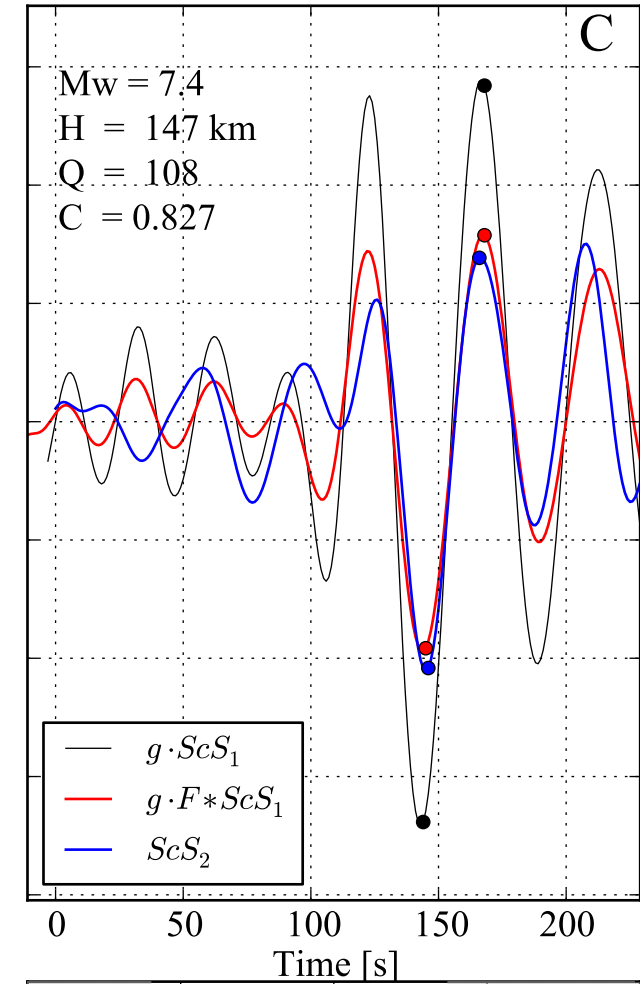
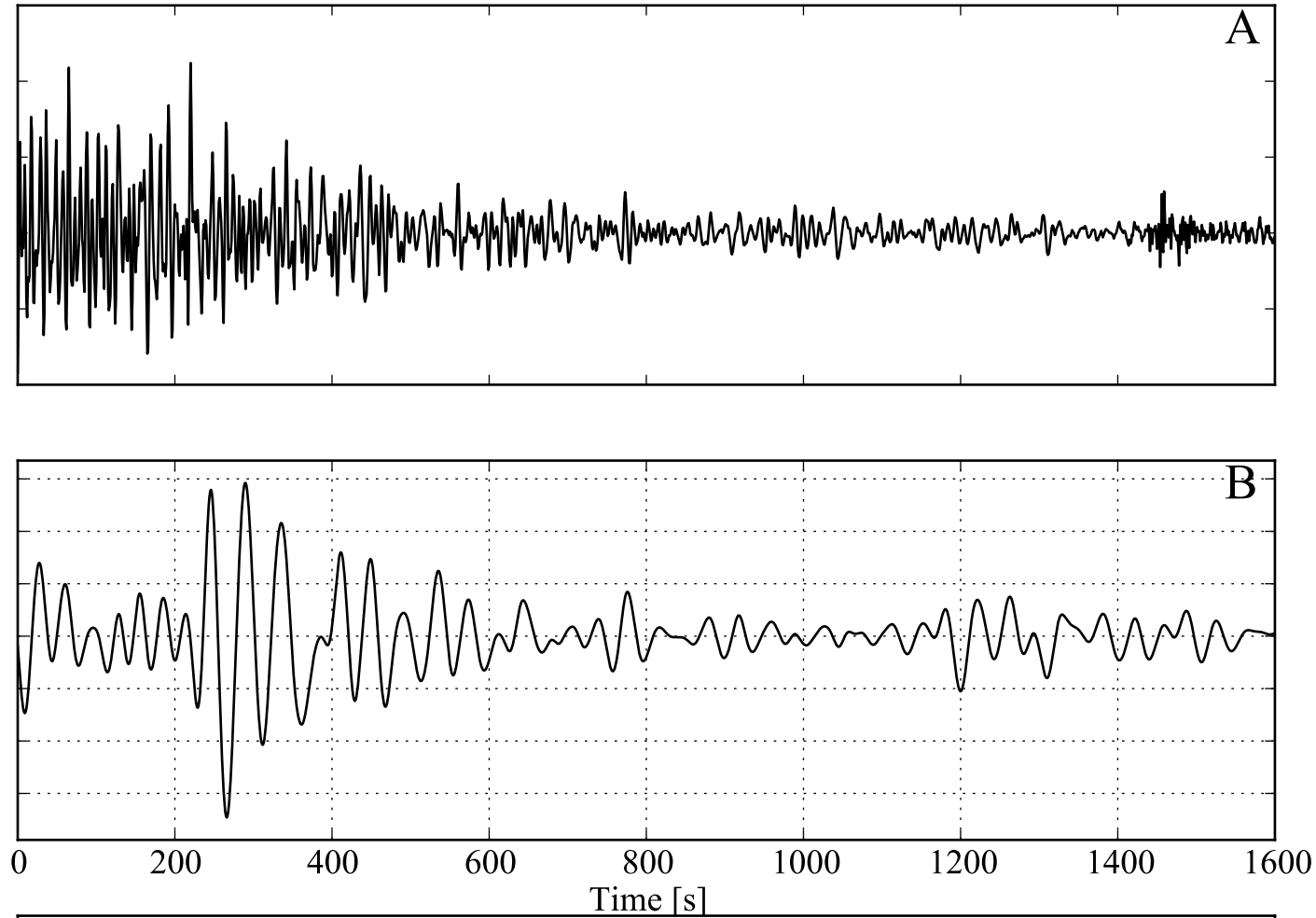



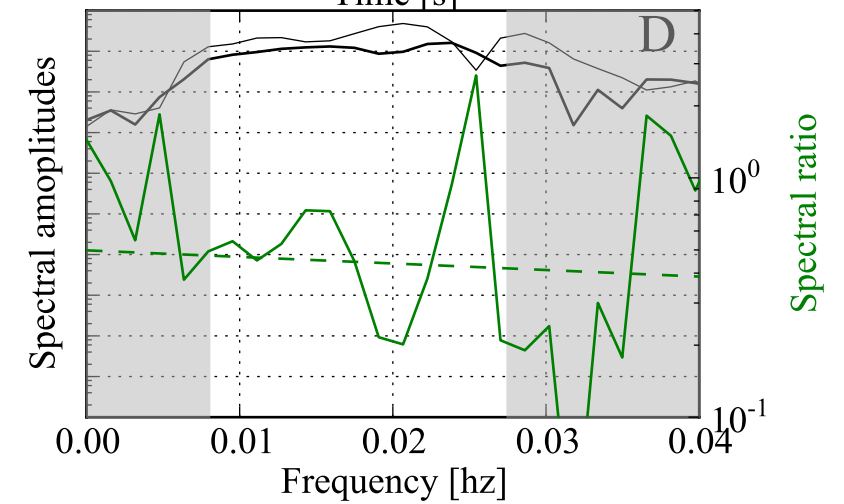
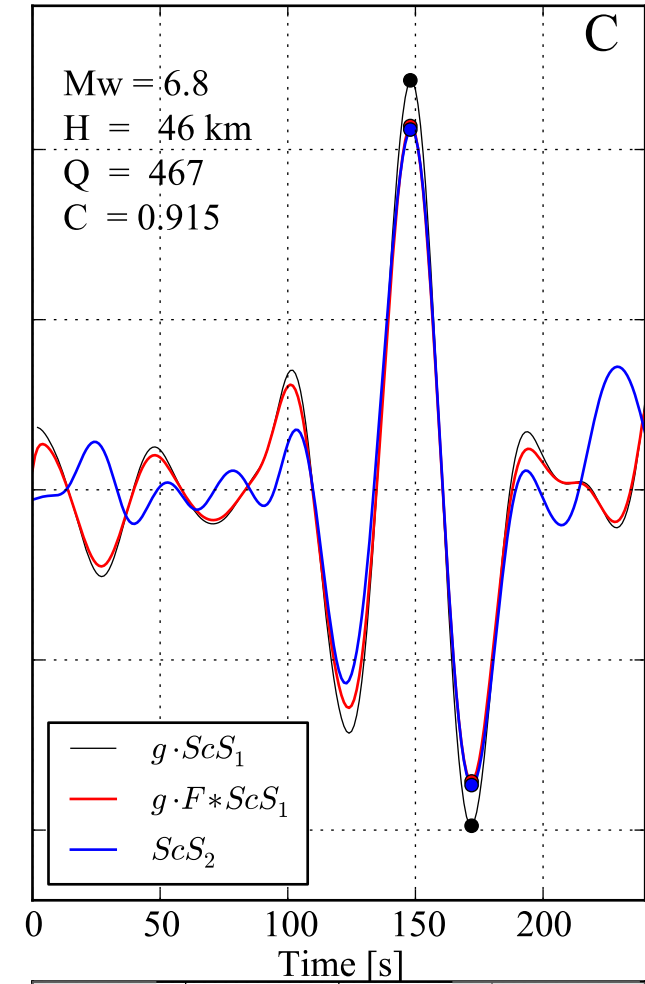
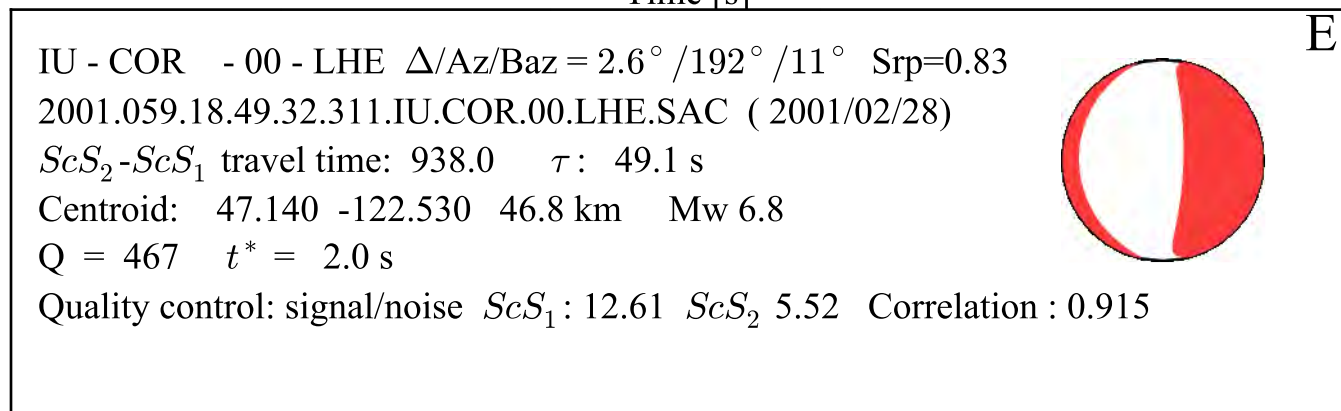
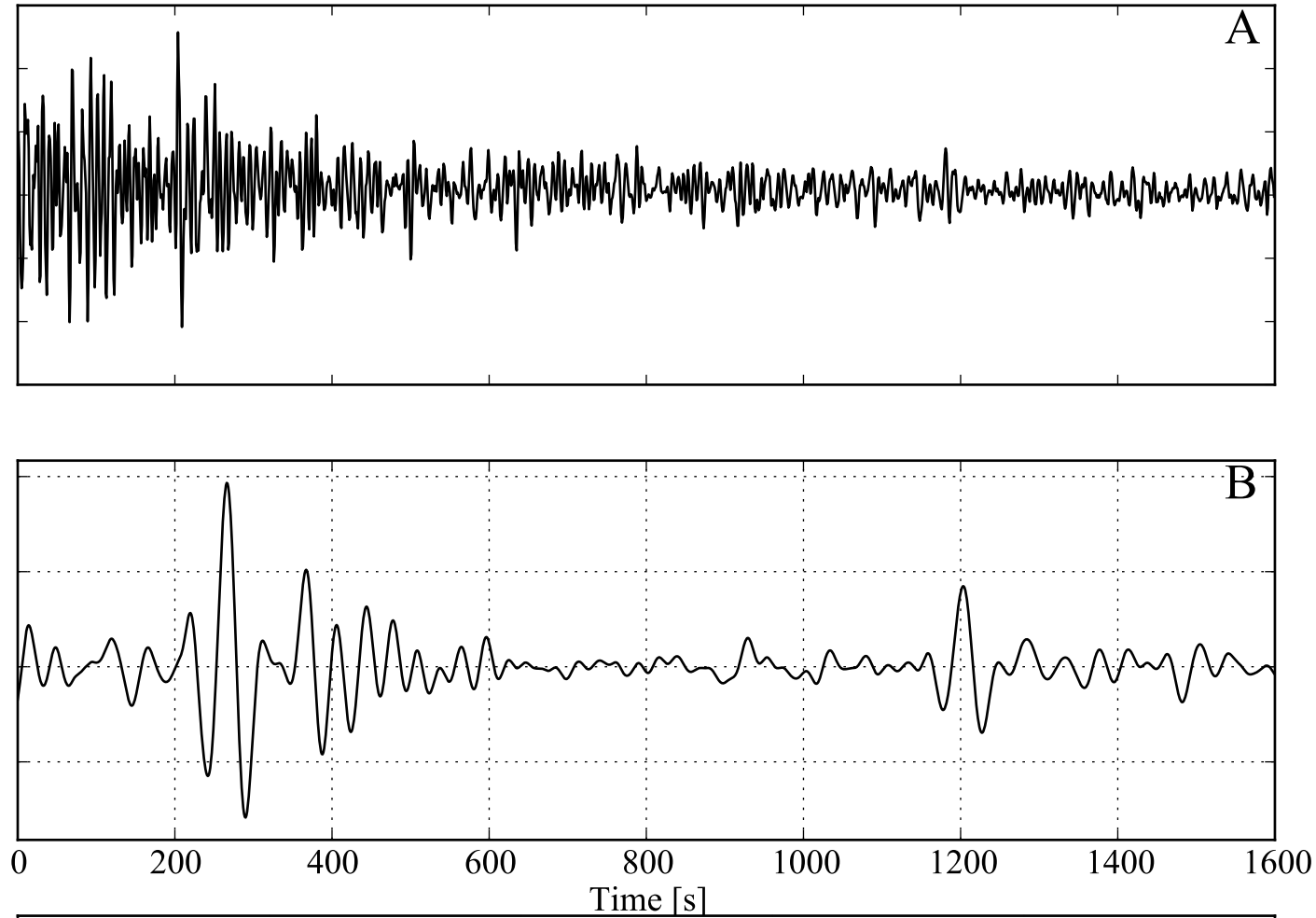


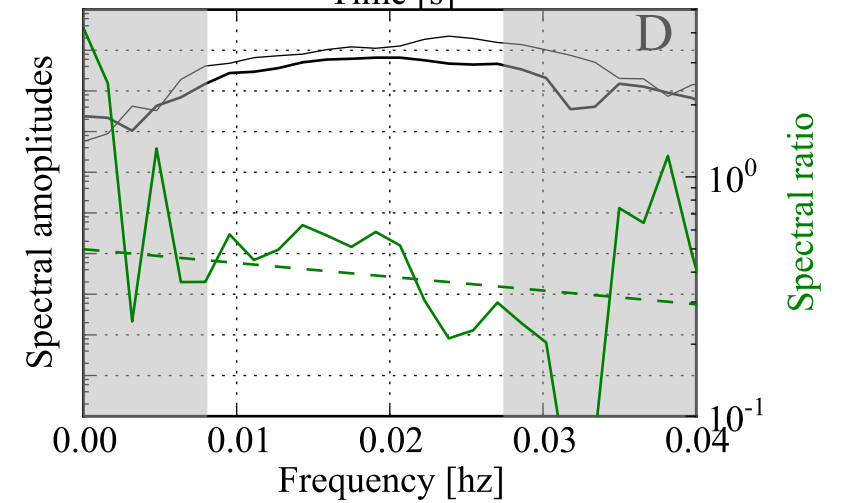
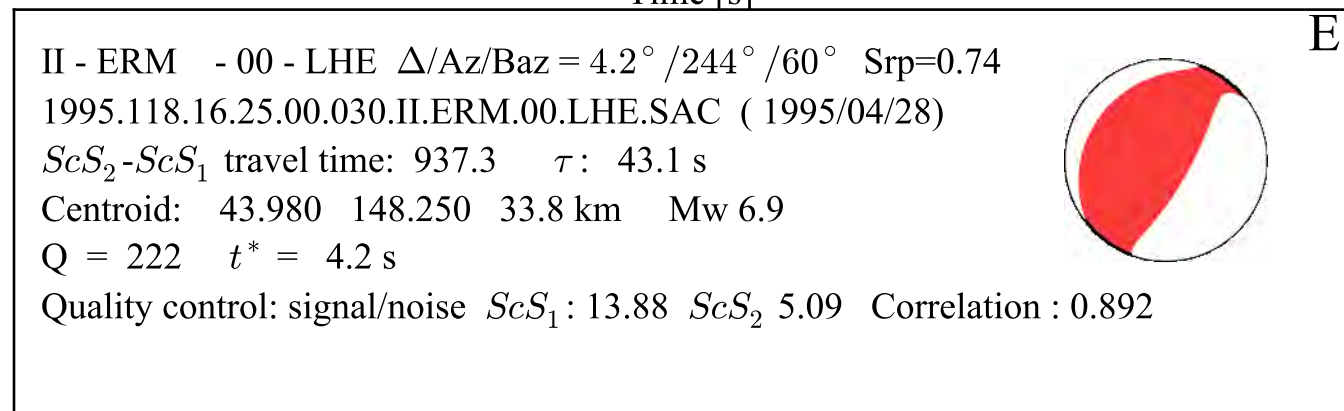
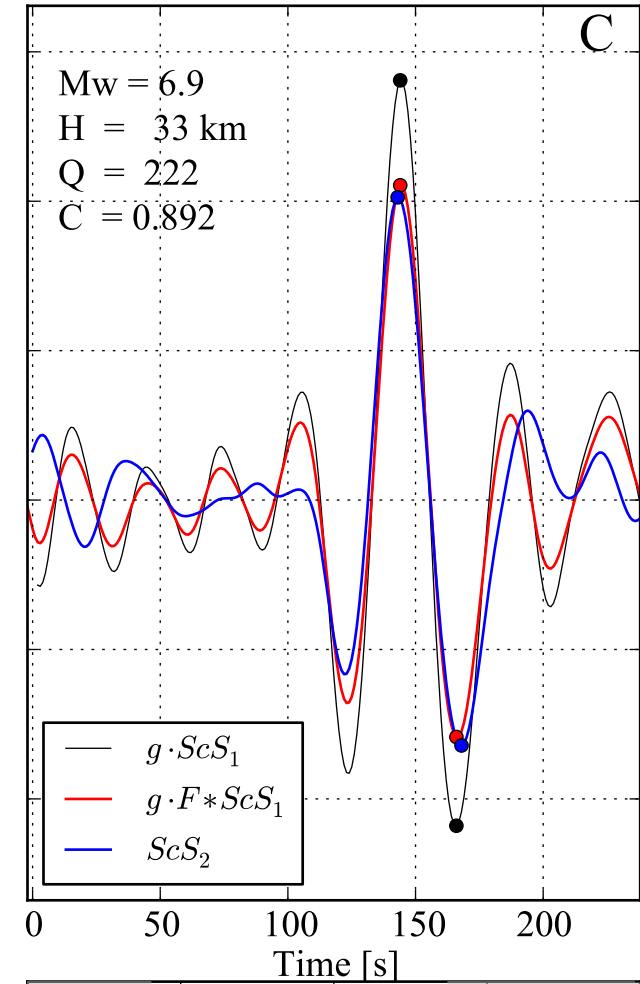
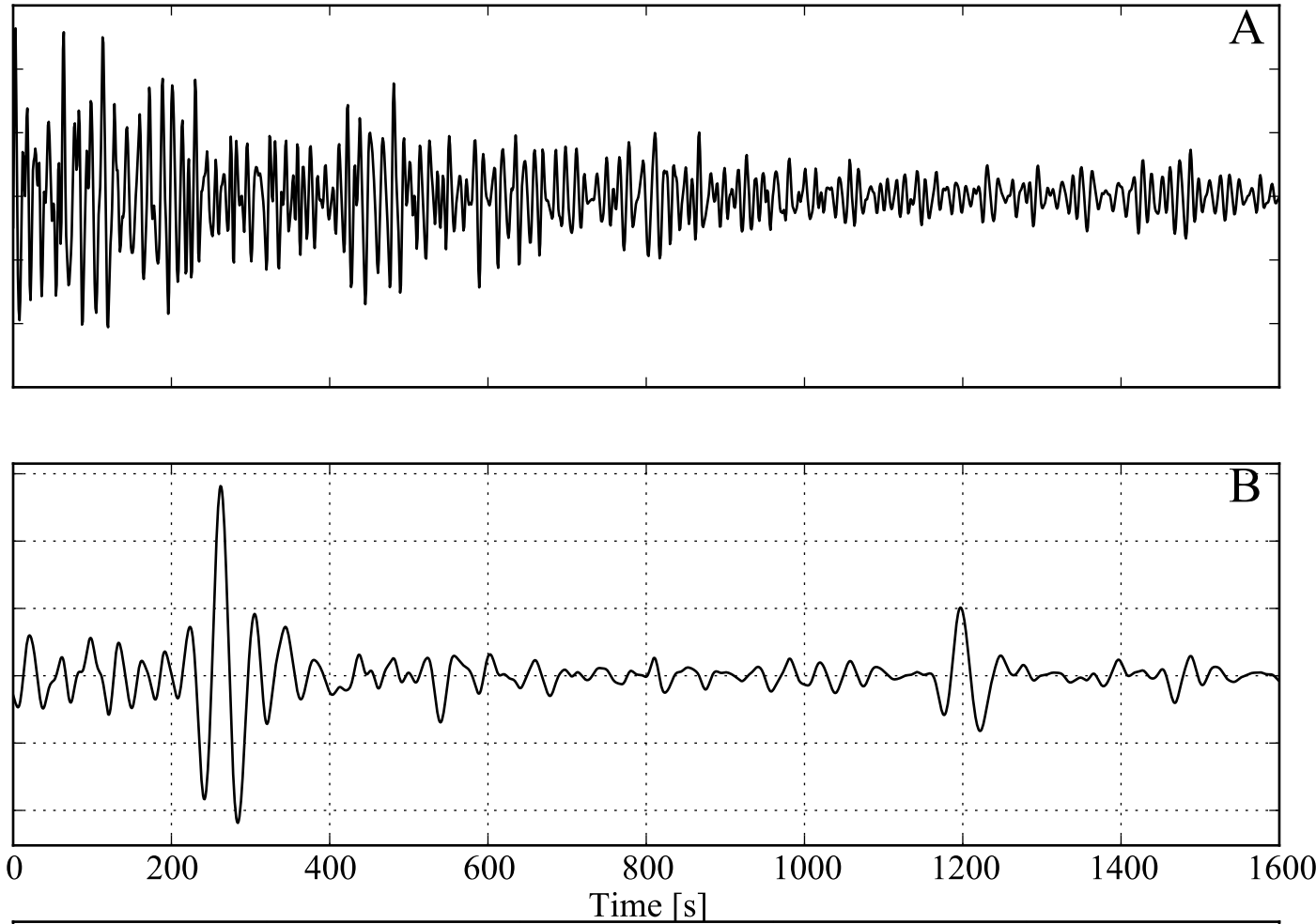


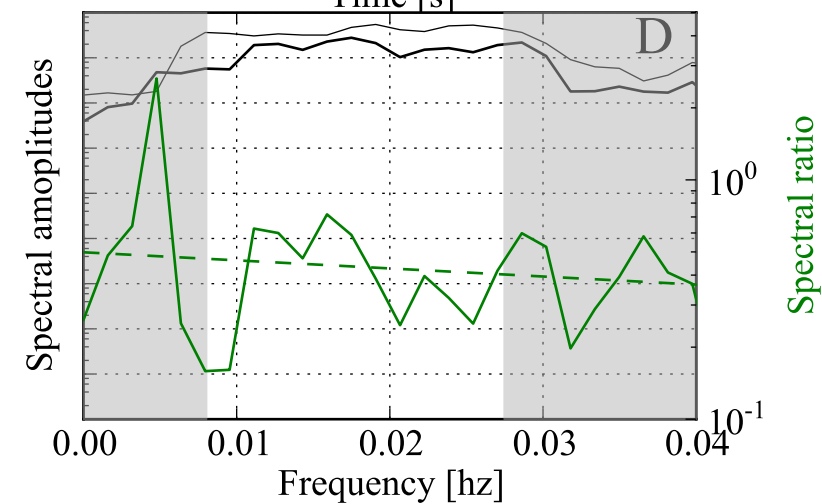
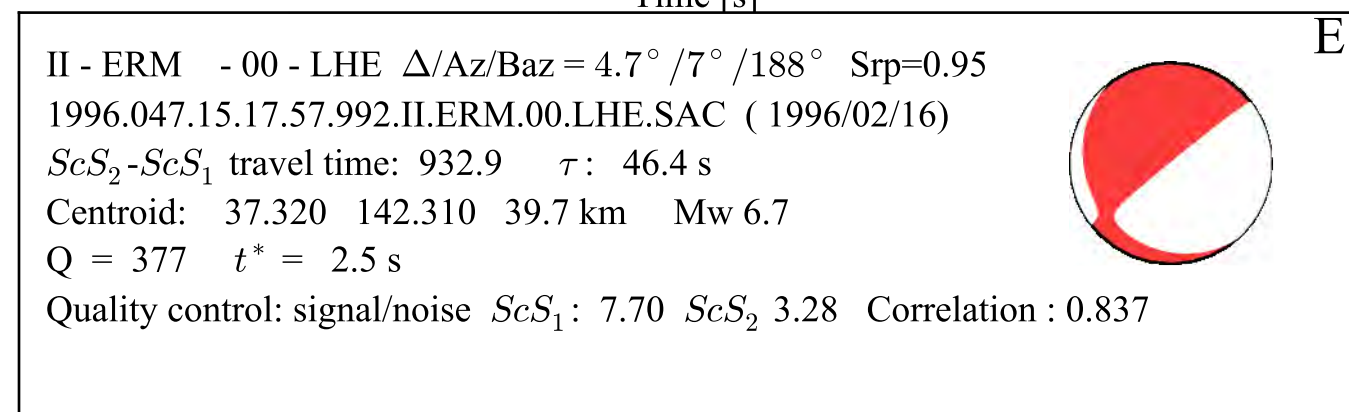
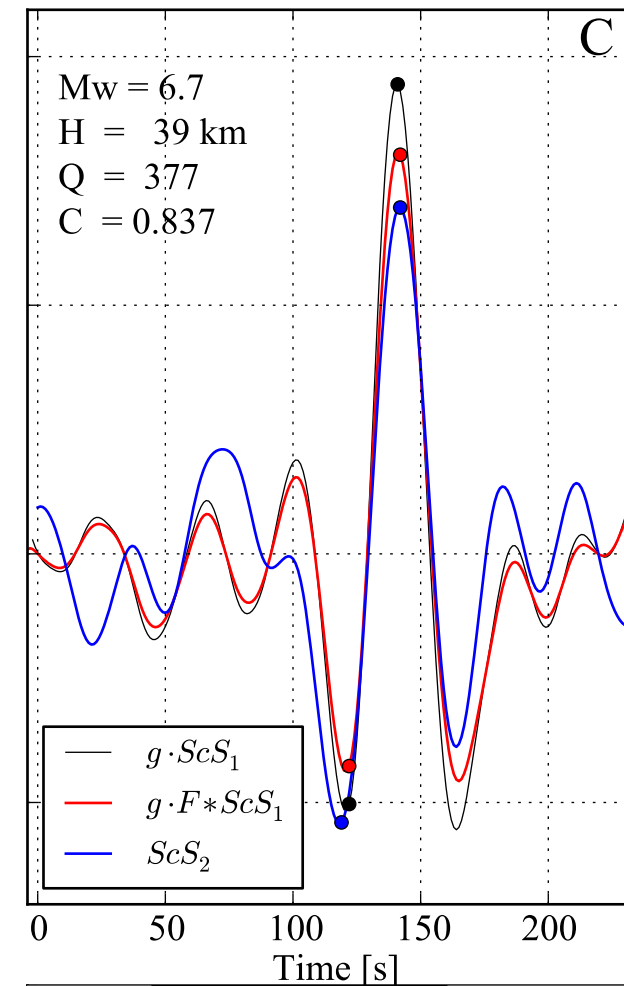
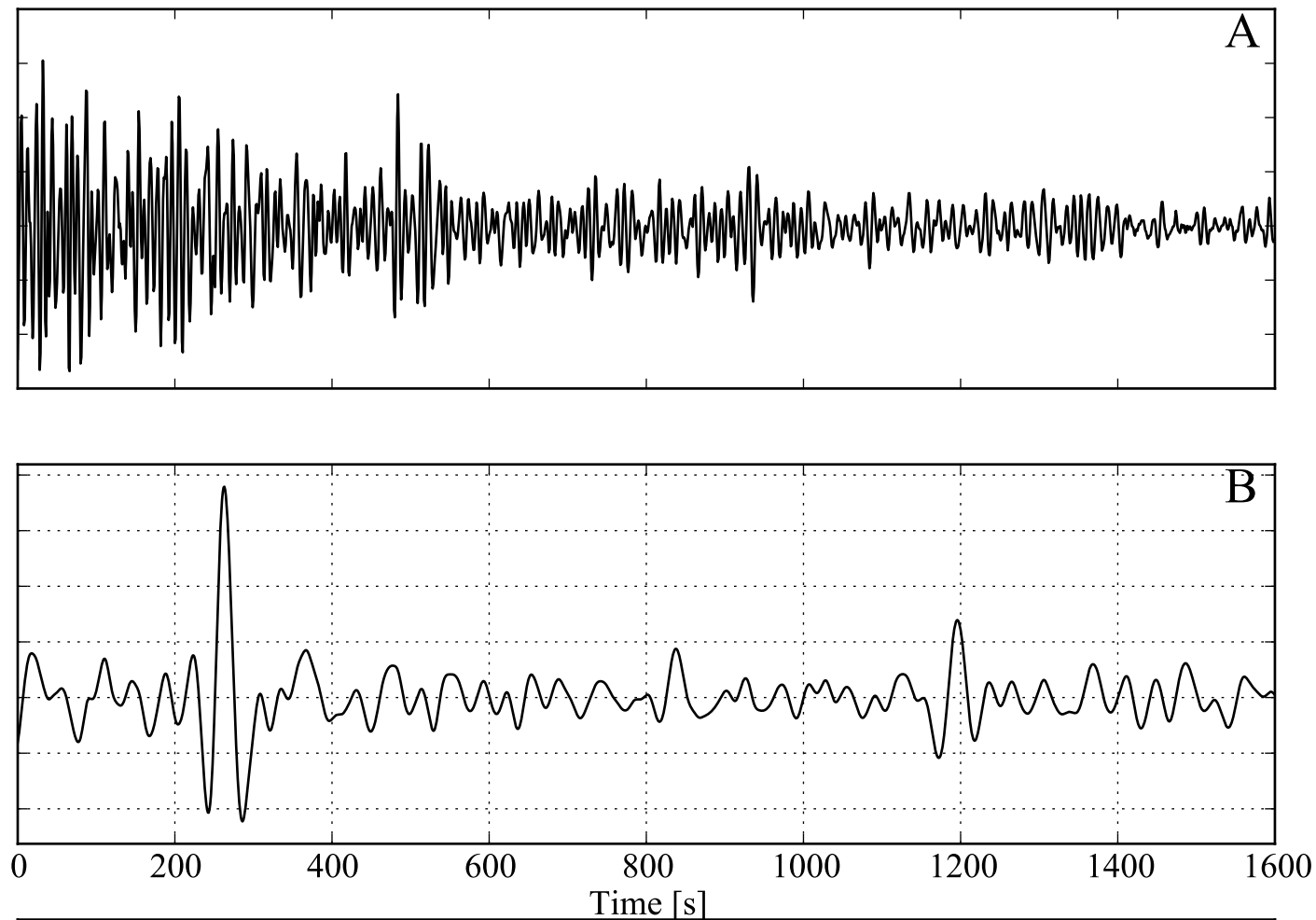


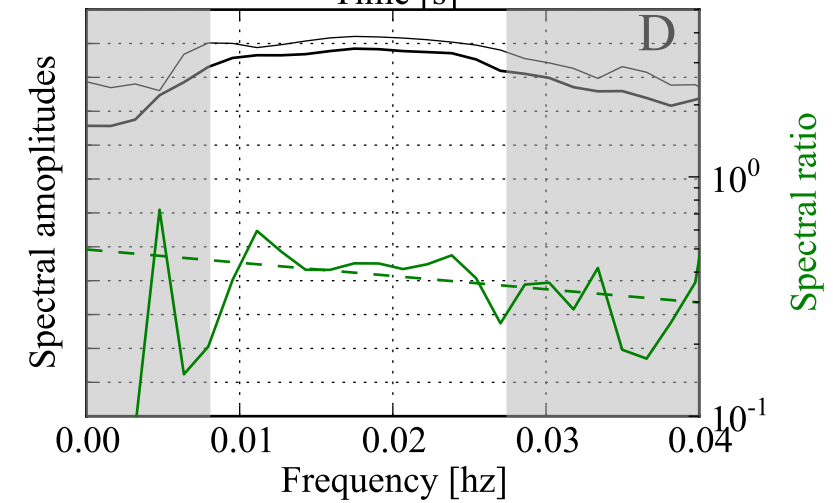
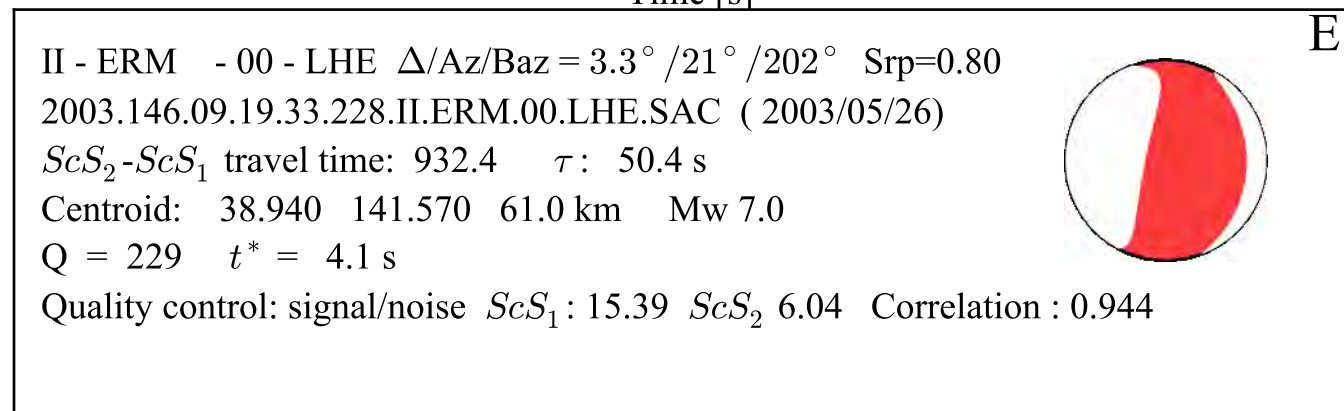
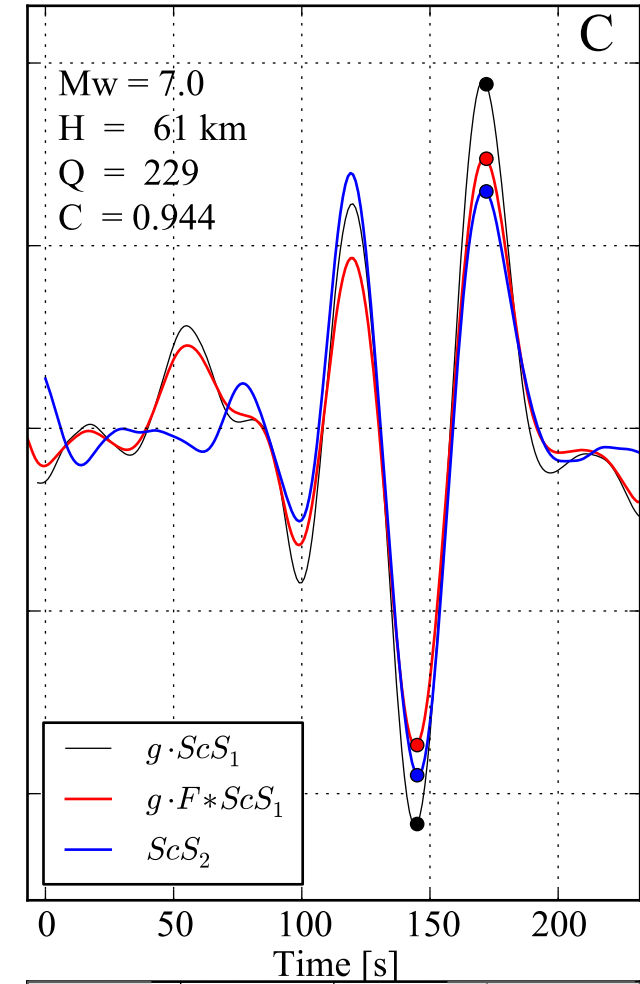
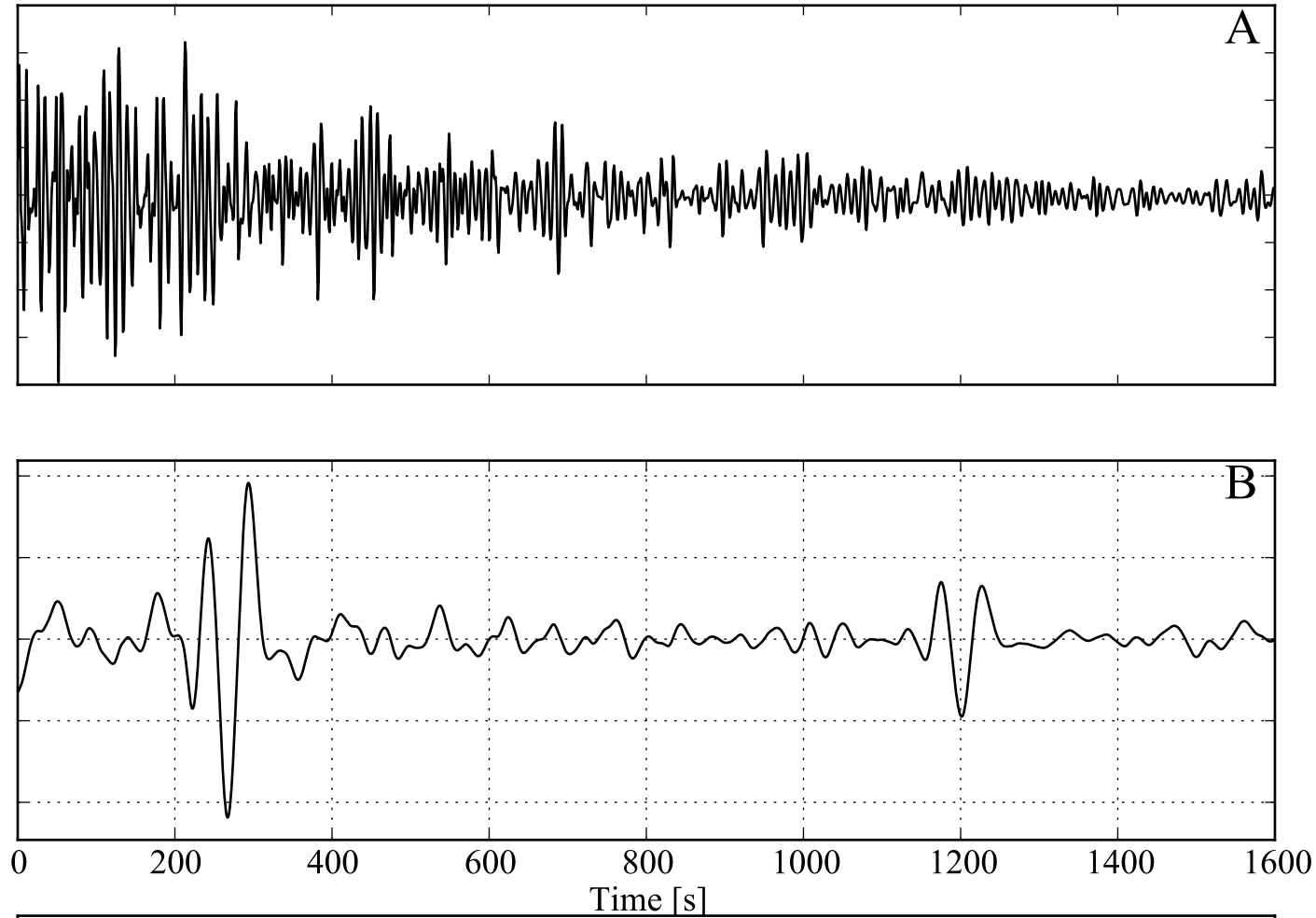


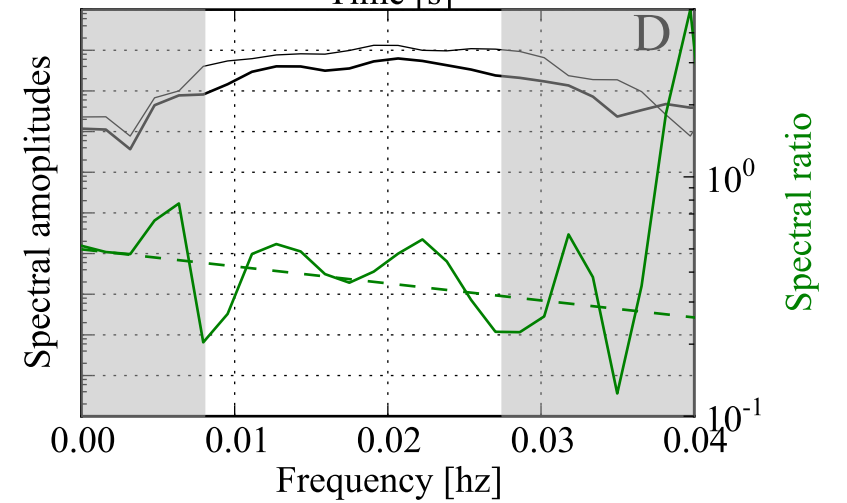
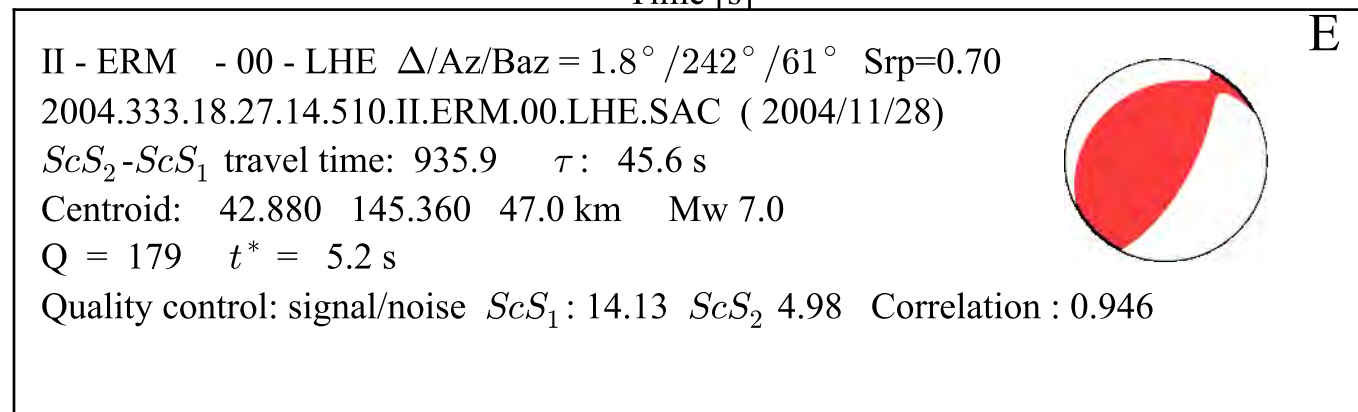
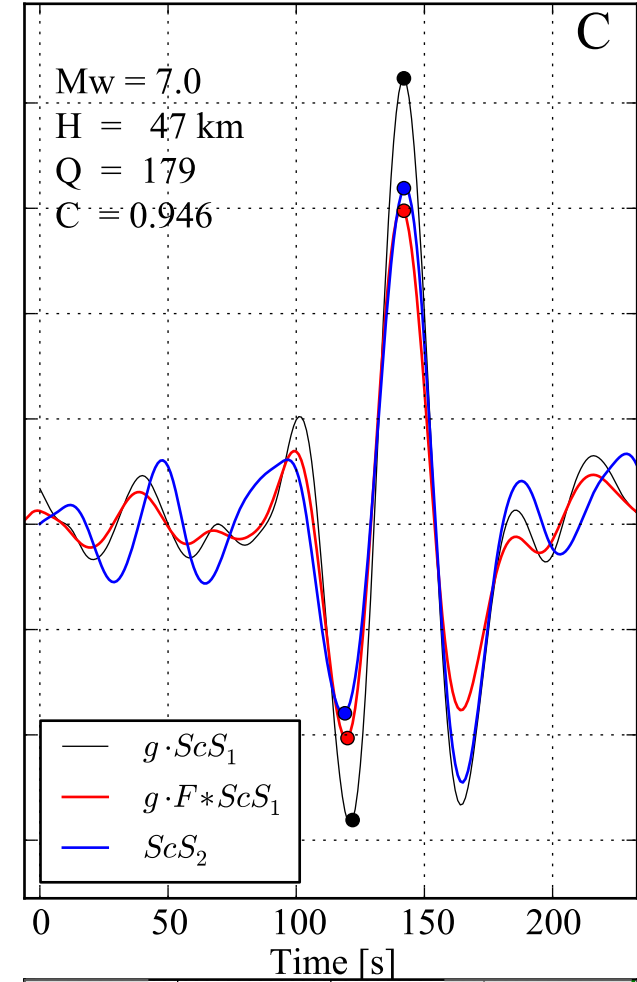
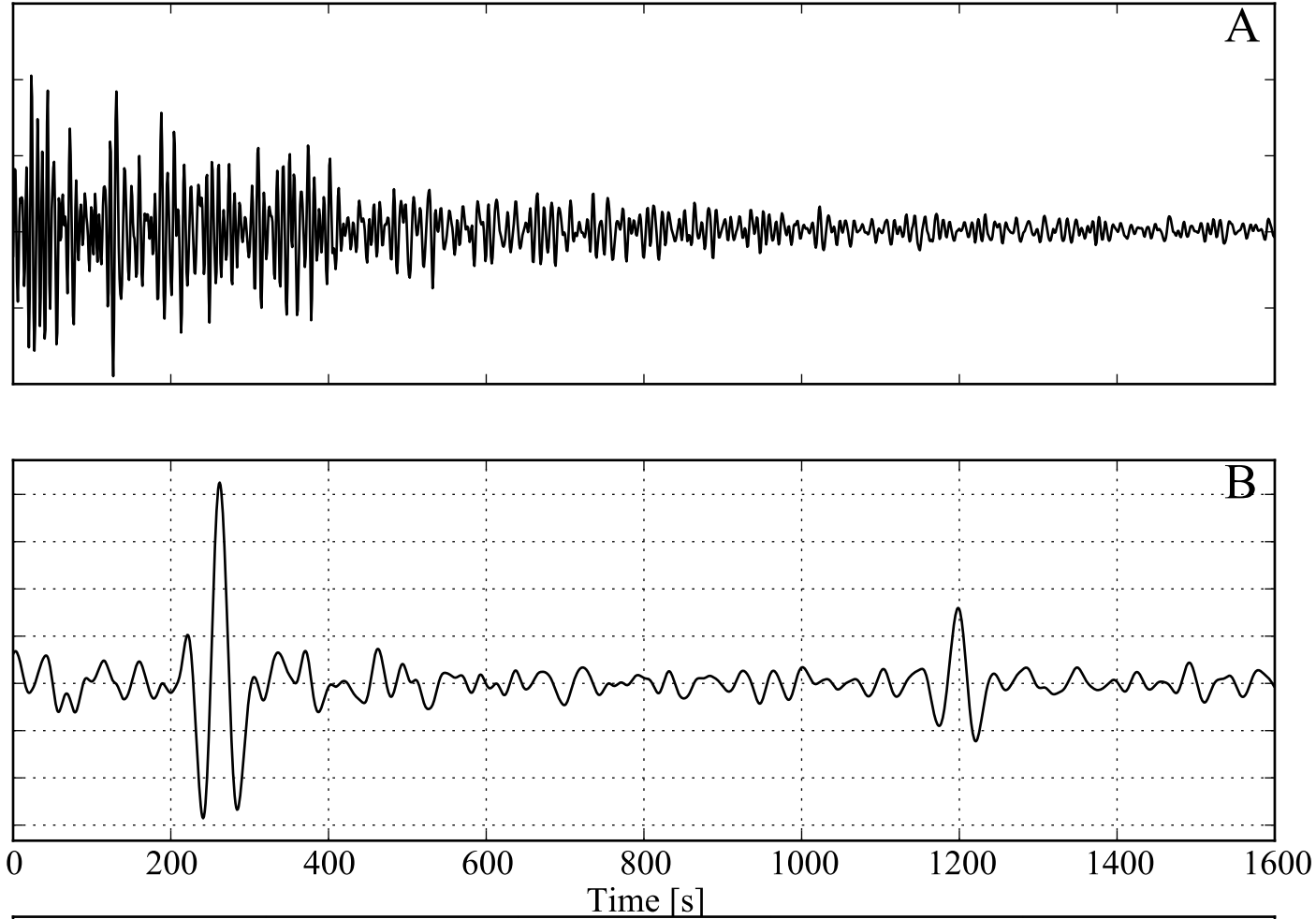


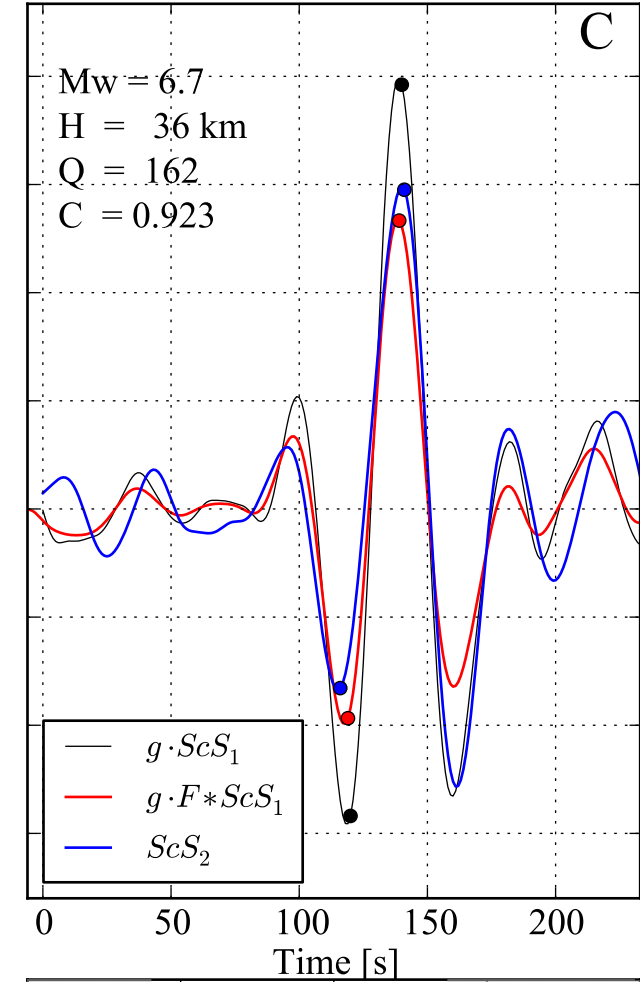
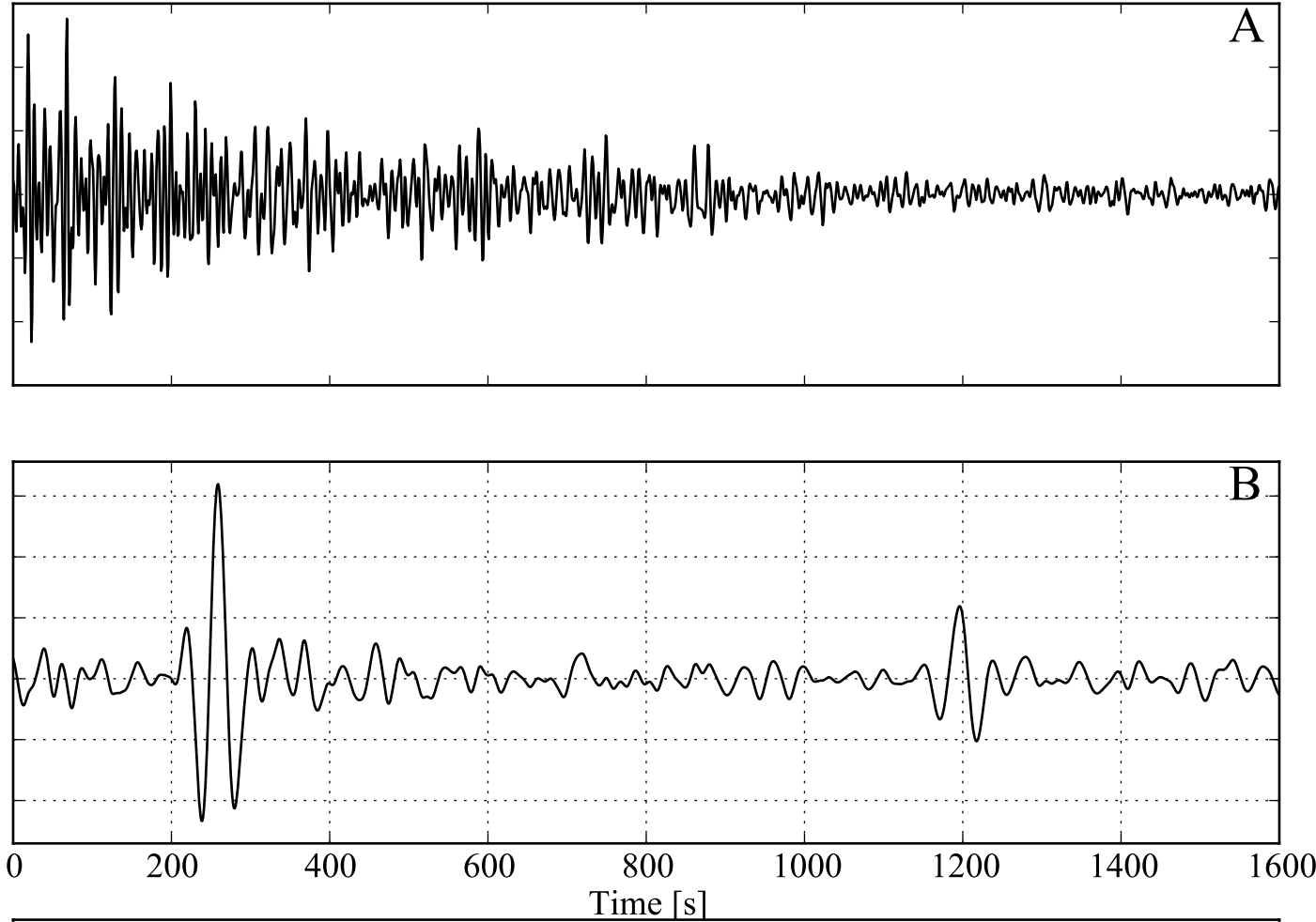






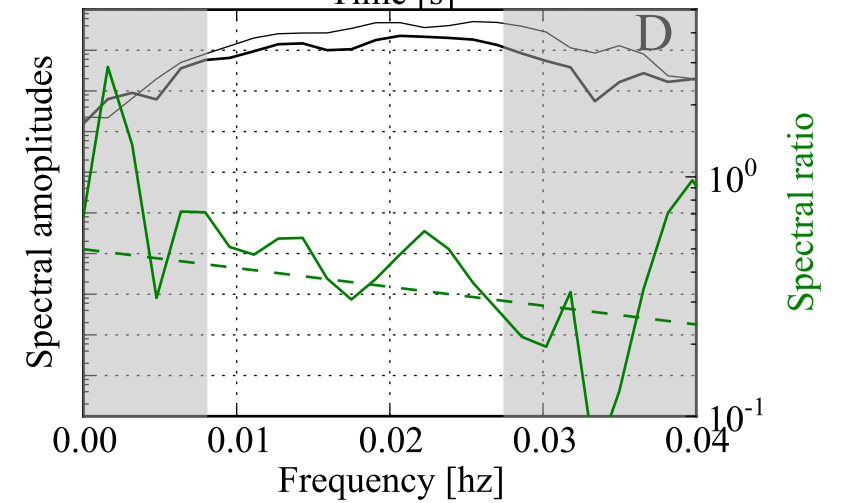


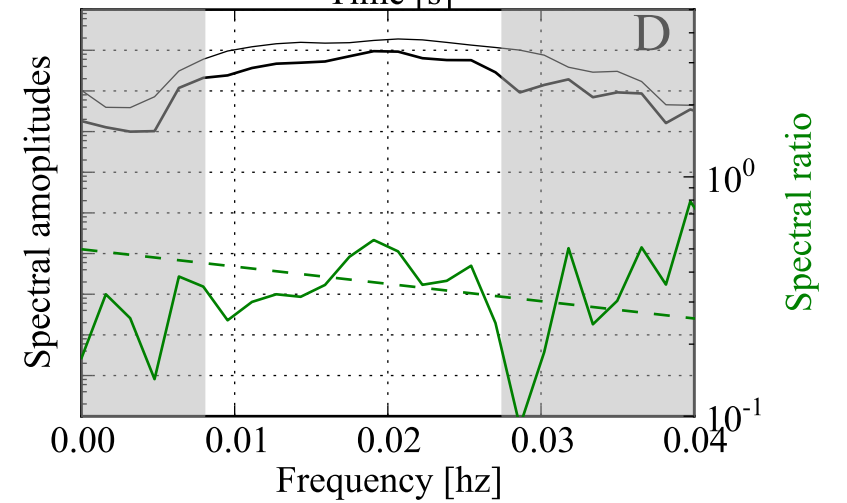
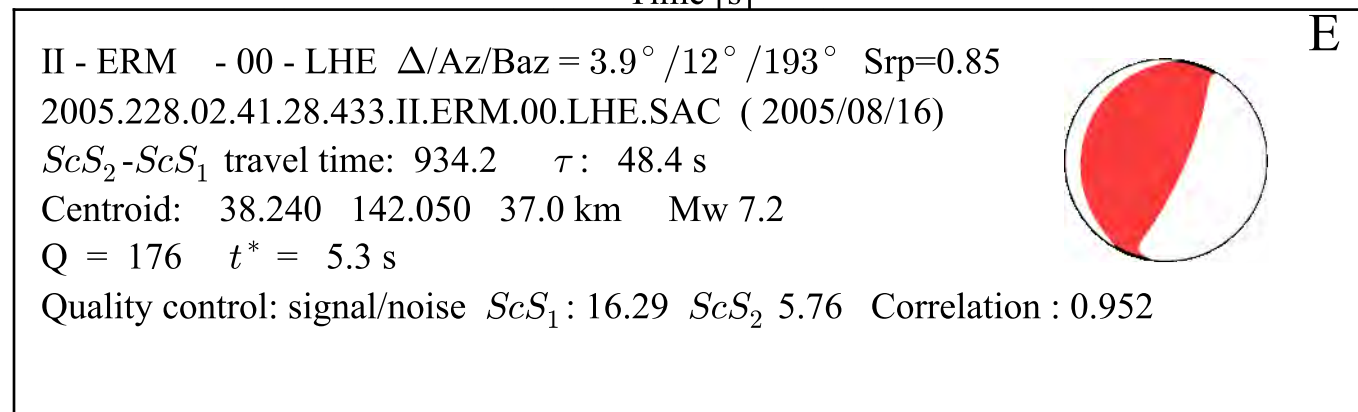
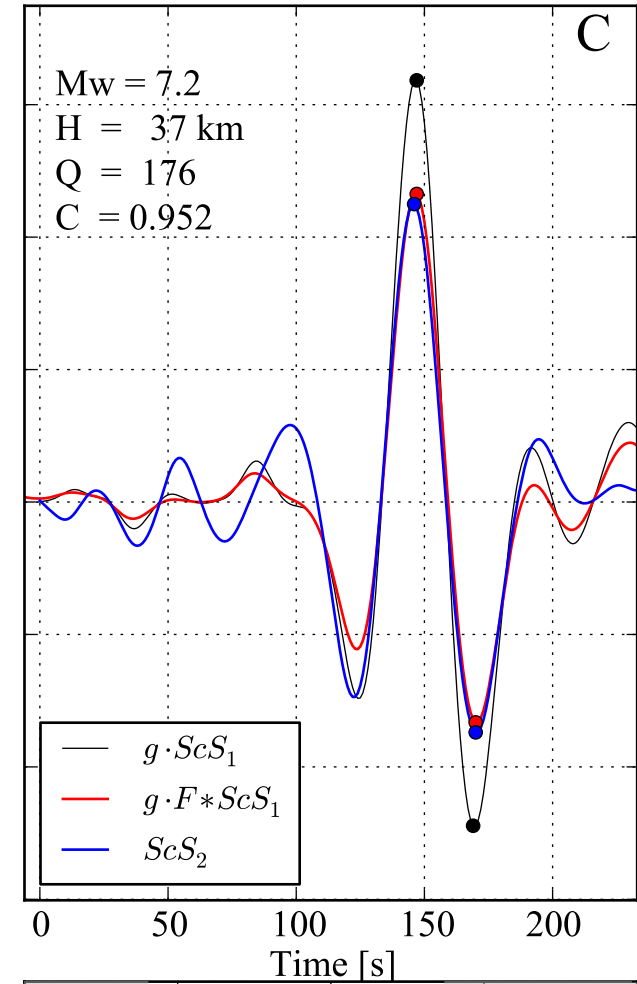
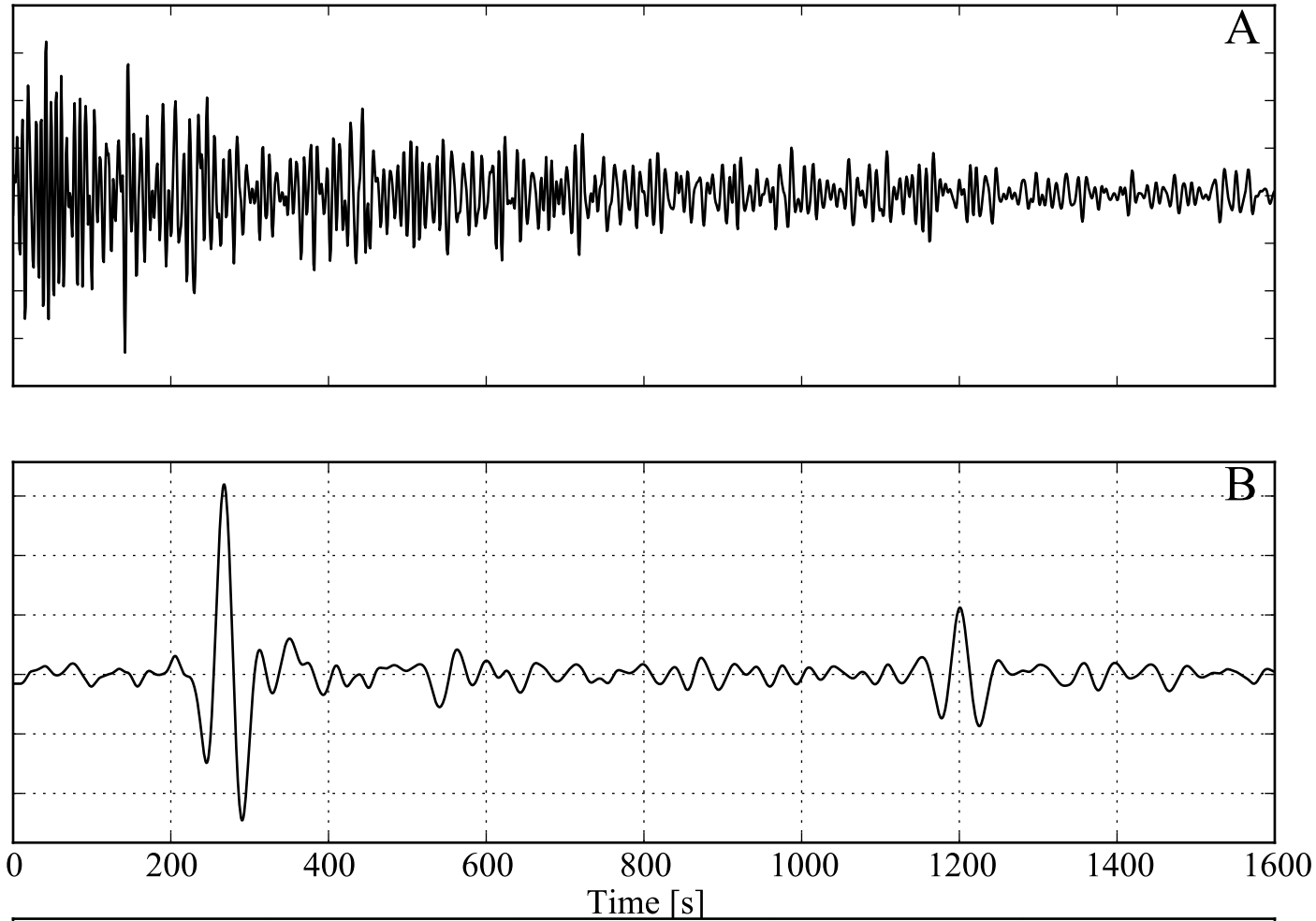


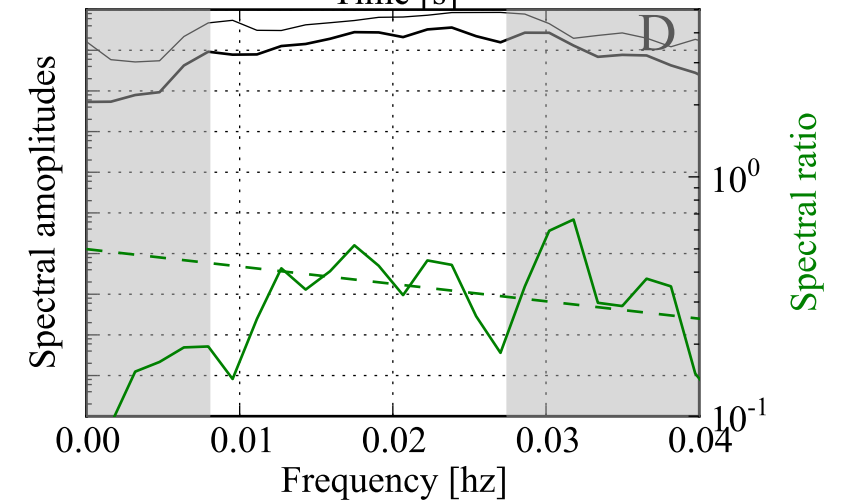
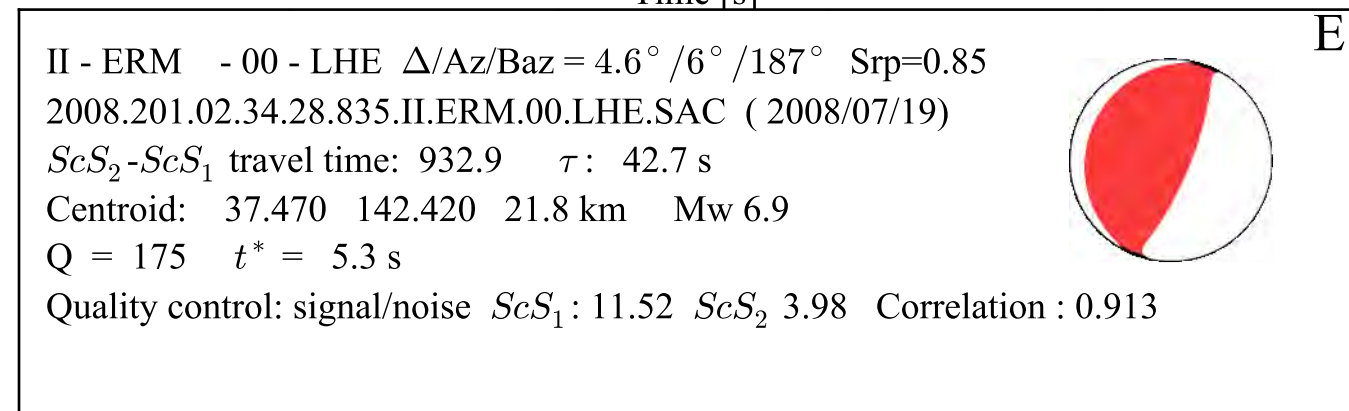
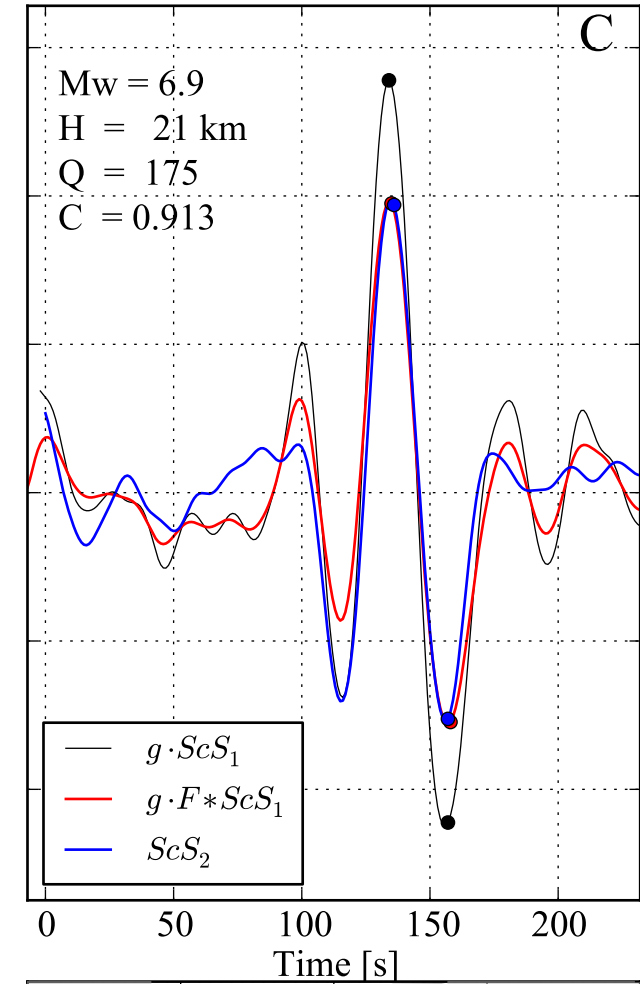
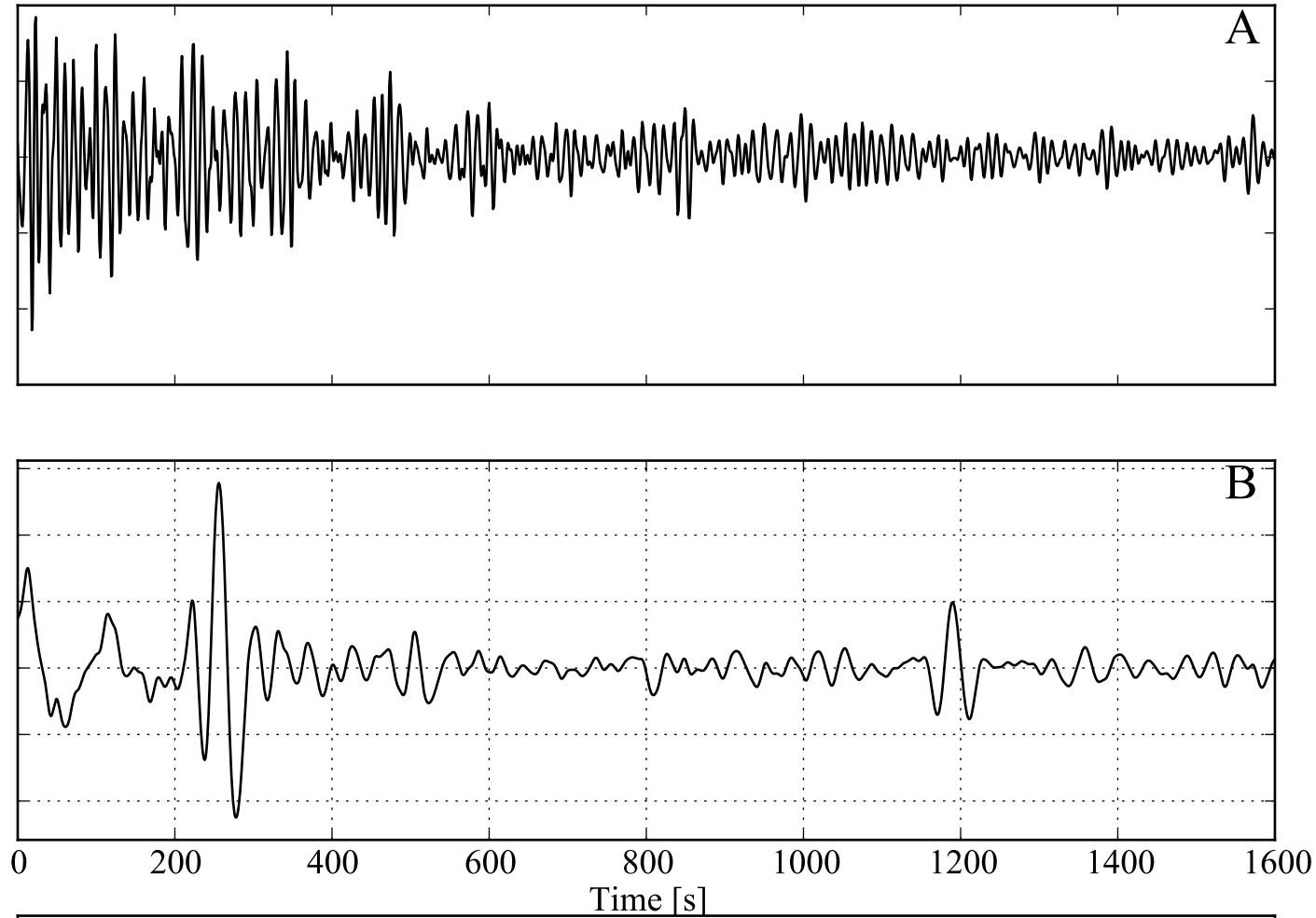


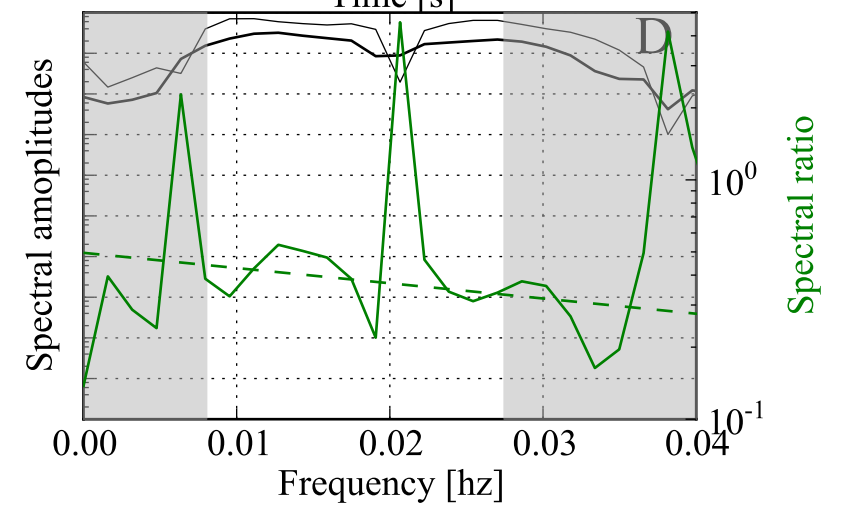
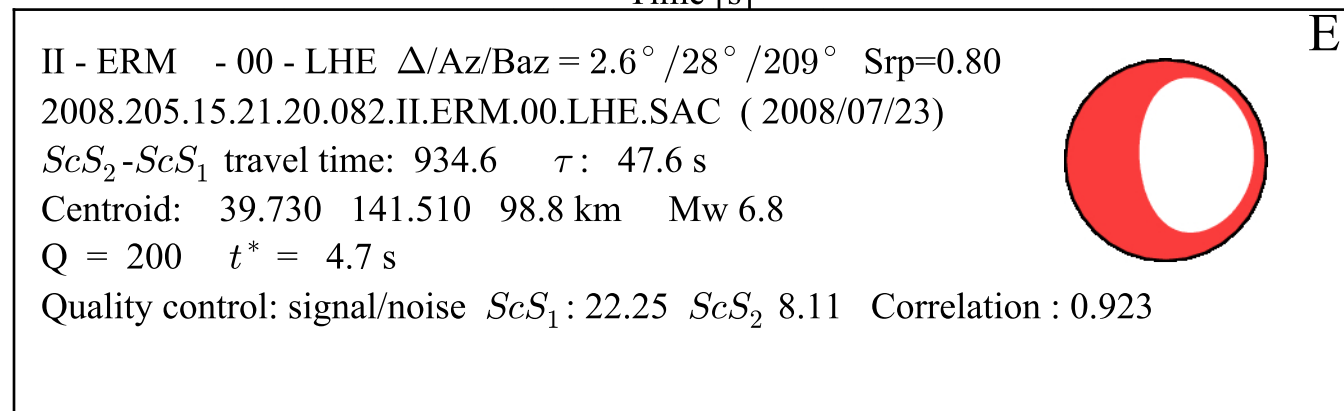
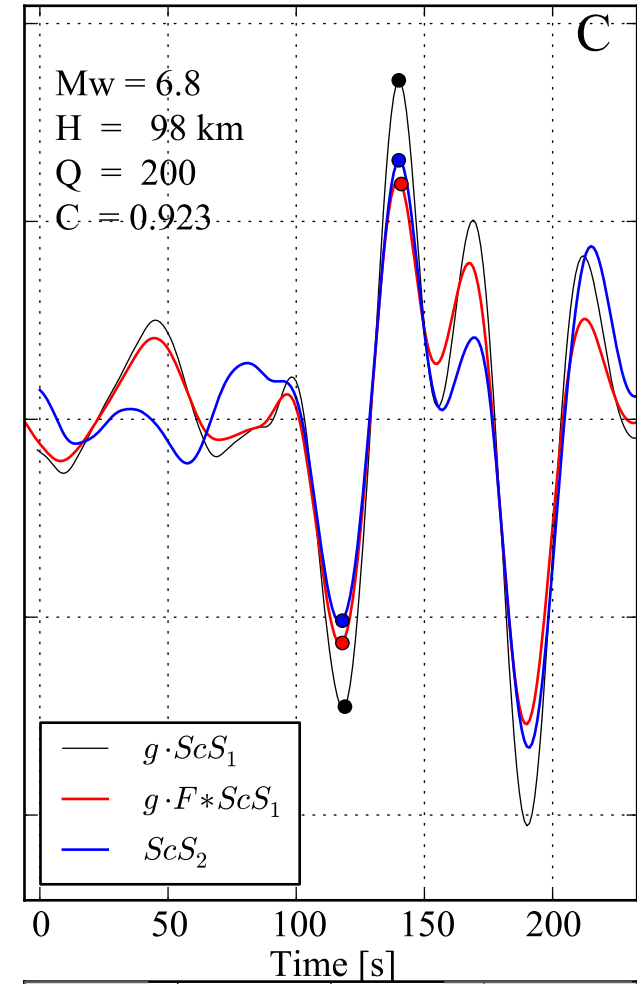
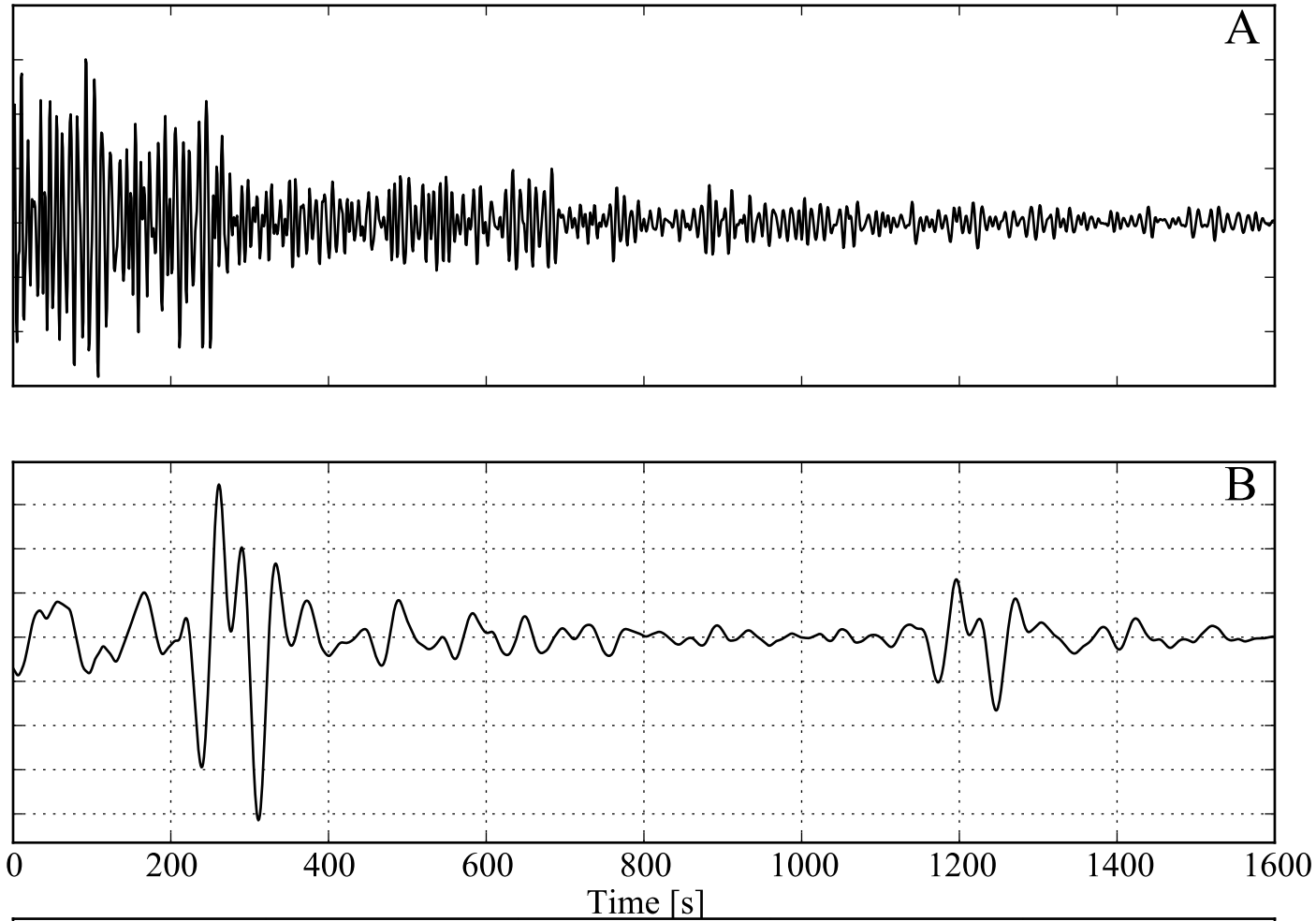
E

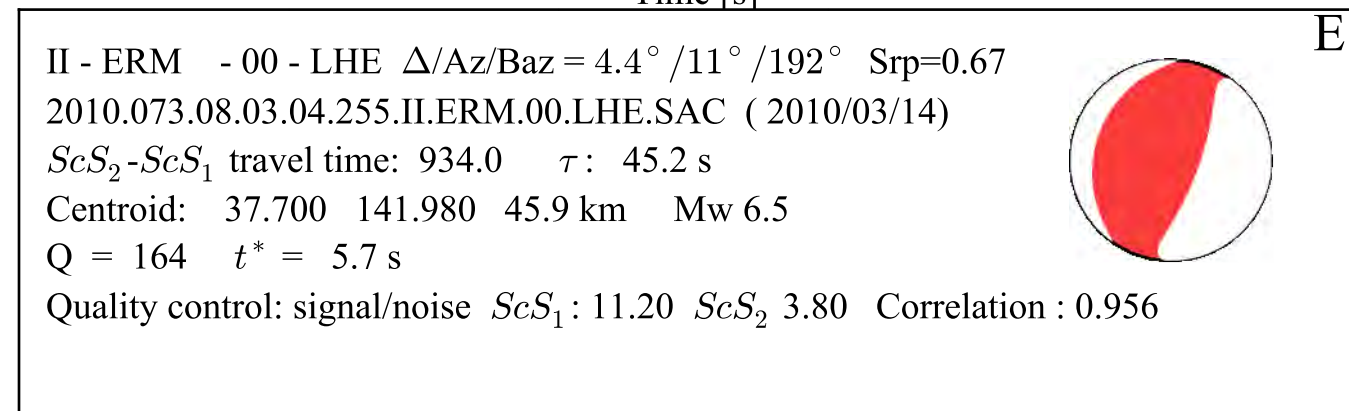
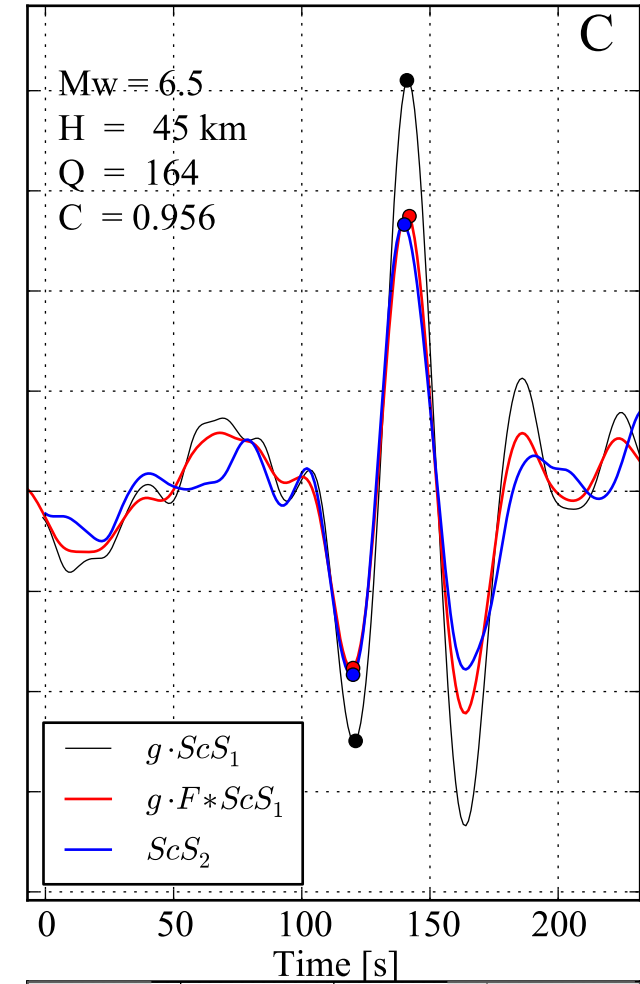
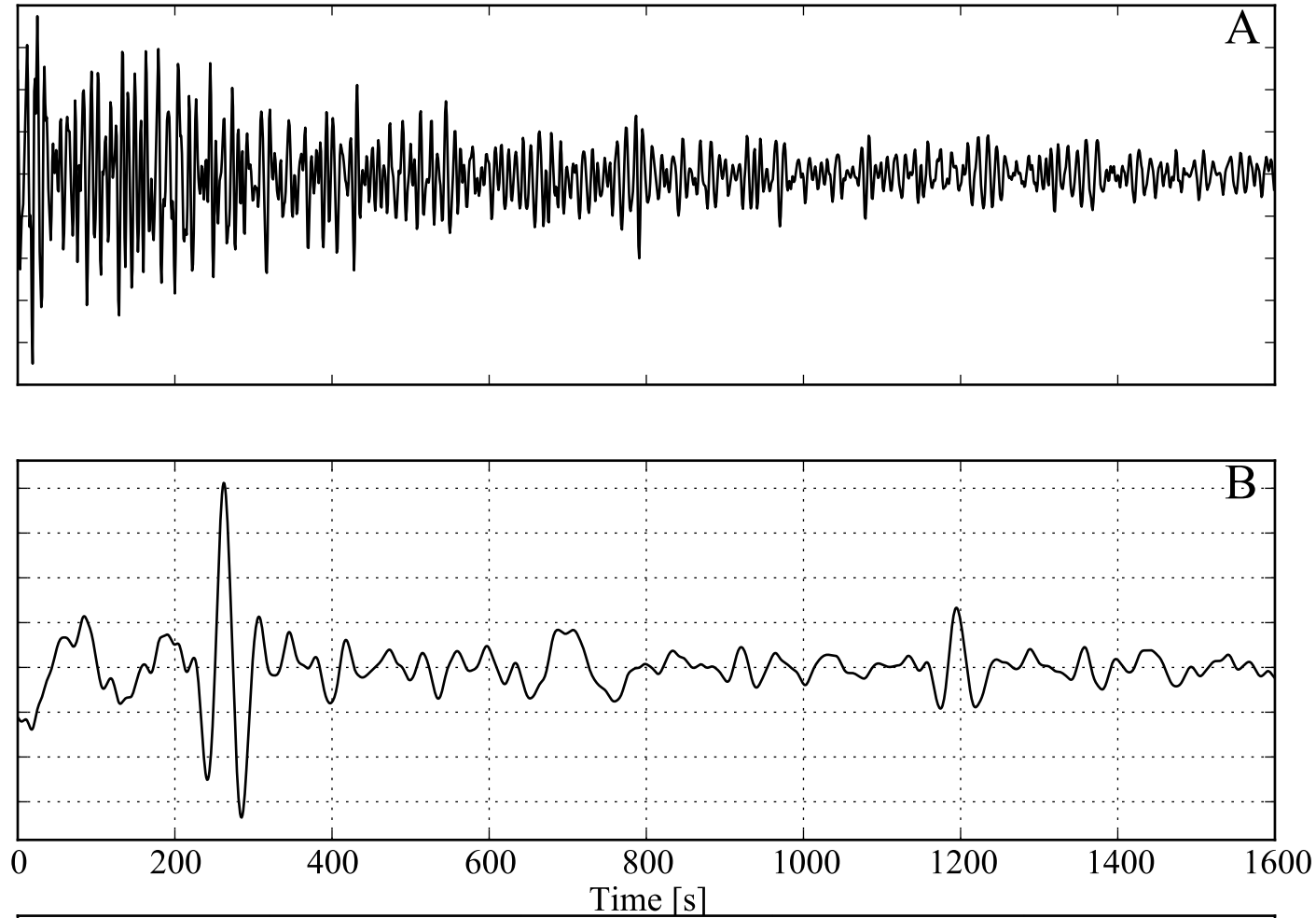
II - ERM - 00 - LHE $\Delta/Az/Baz = 1.9^\circ / 245^\circ / 63^\circ$ Srp=0.76
 2004.341.14.10.11.829.II.ERM.00.LHE.SAC (2004/12/06)
 $ScS_2 - ScS_1$ travel time: 935.9 τ : 43.6 s
 Centroid: 42.820 145.410 36.0 km Mw 6.7
 Q = 162 $t^* = 5.8$ s
 Quality control: signal/noise ScS_1 : 12.85 ScS_2 4.36 Correlation : 0.923

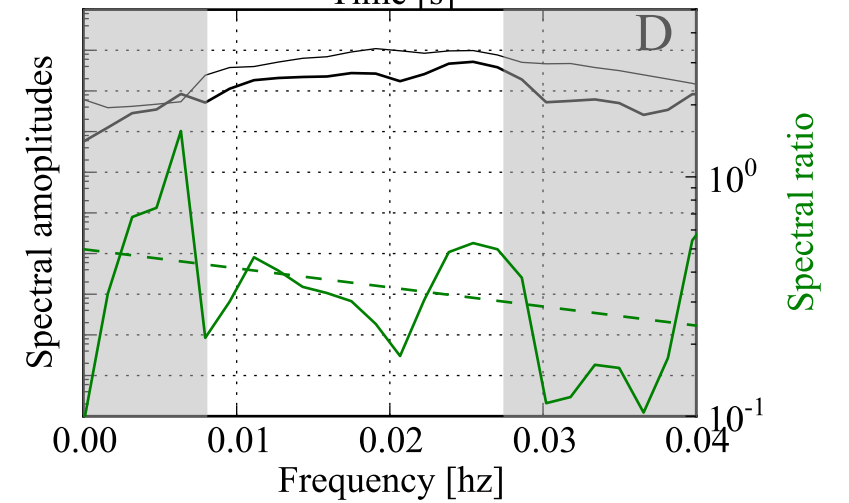
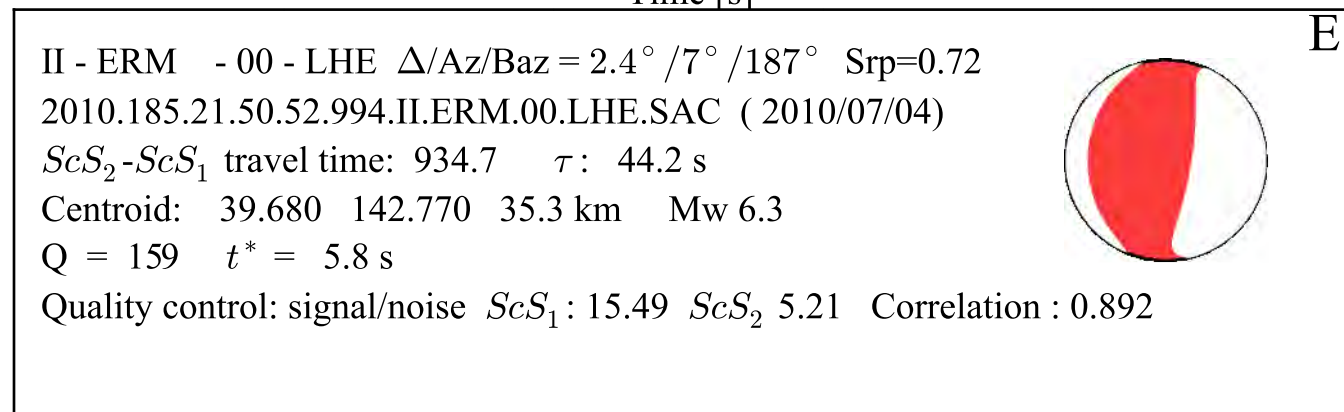
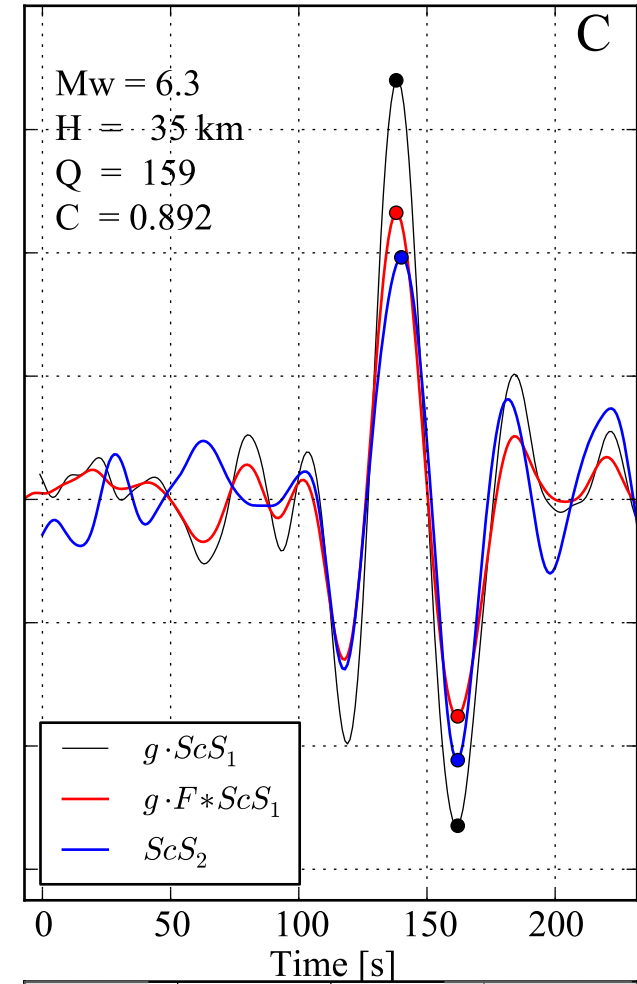
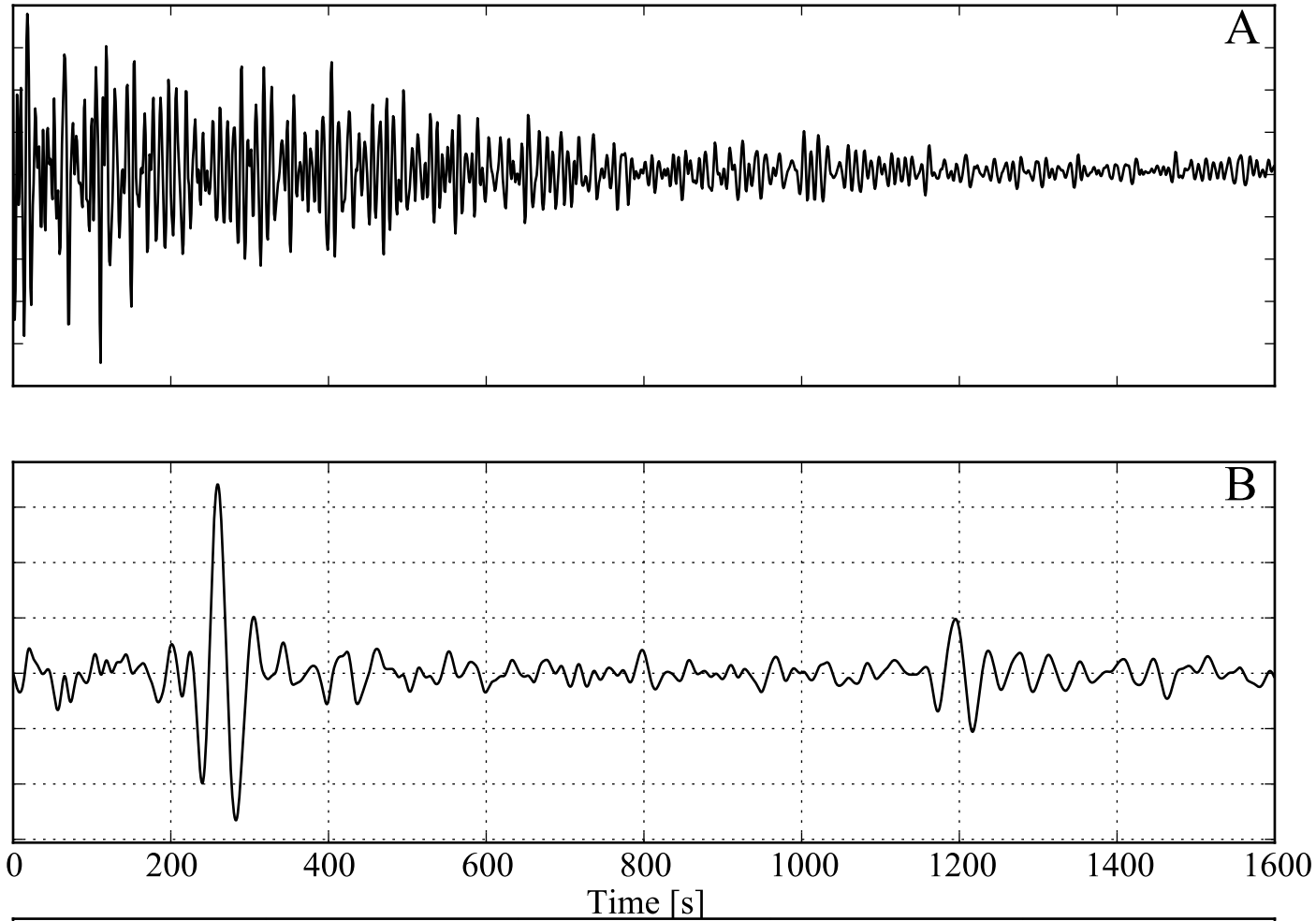


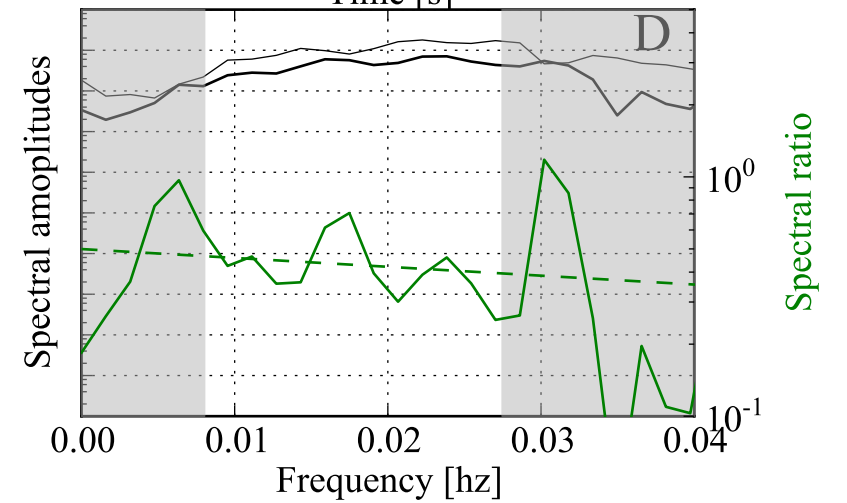
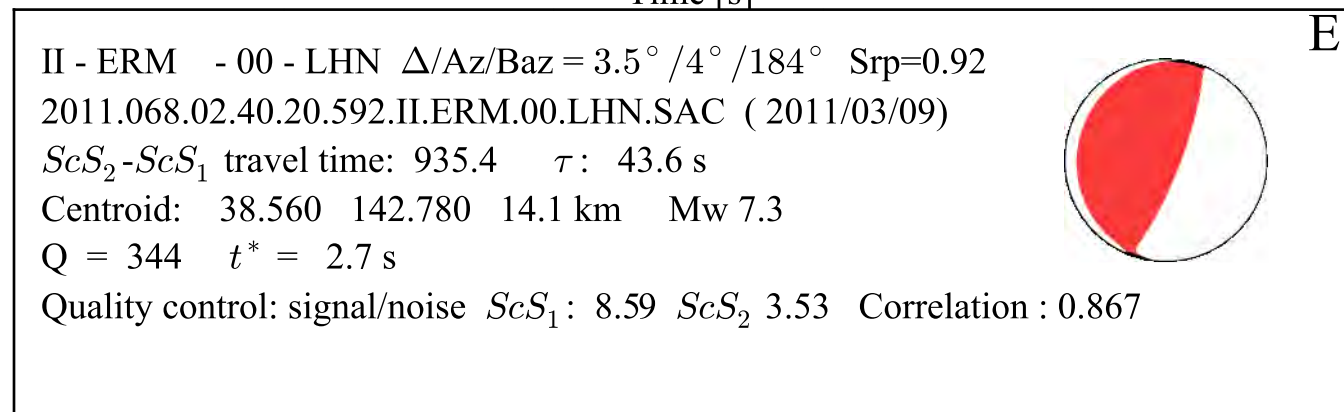
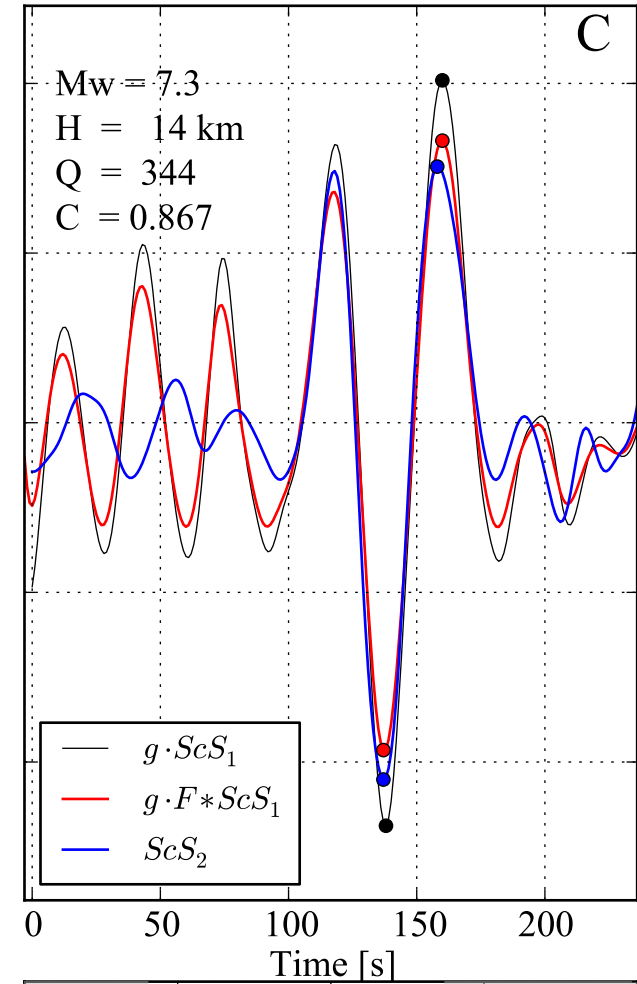
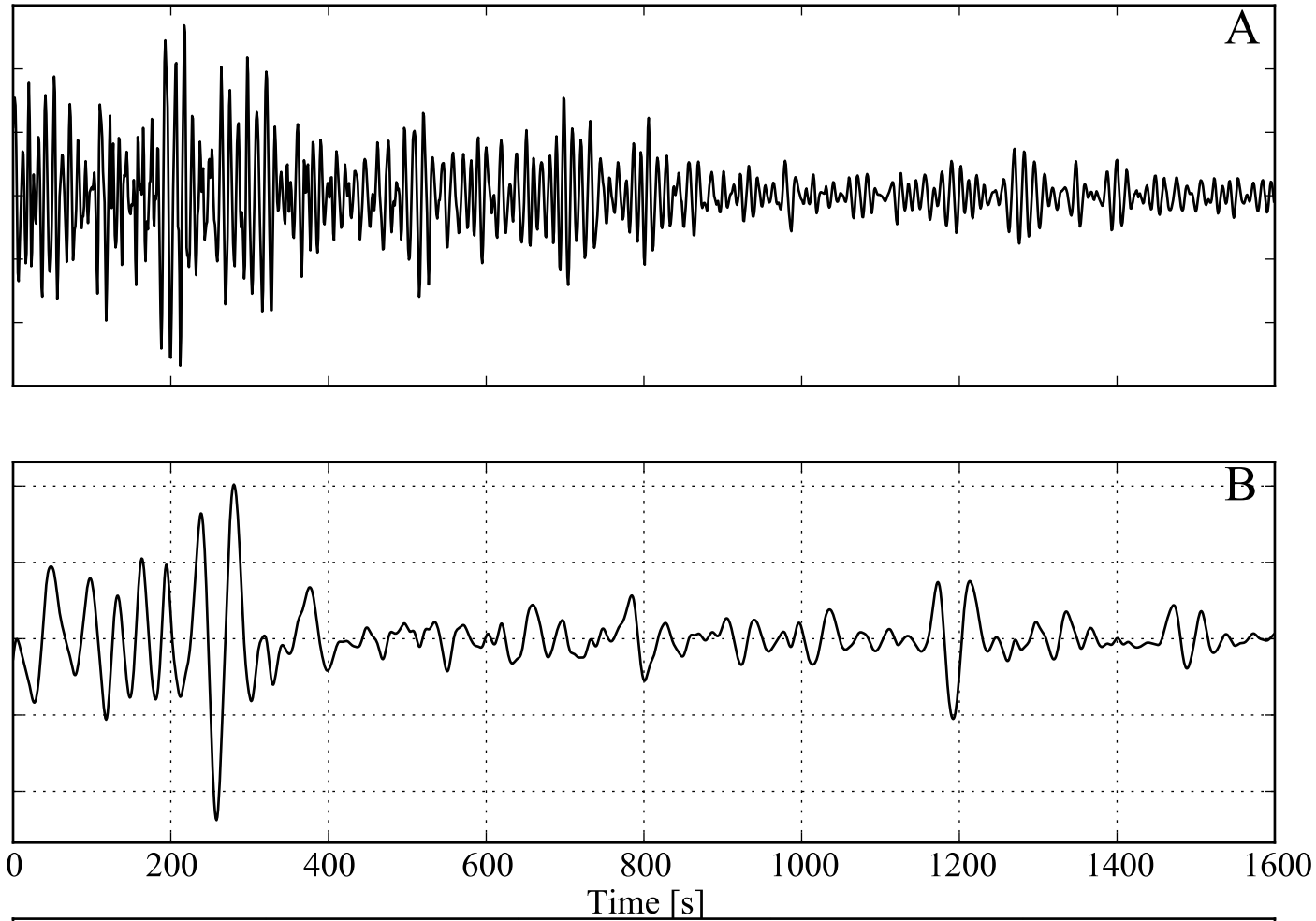


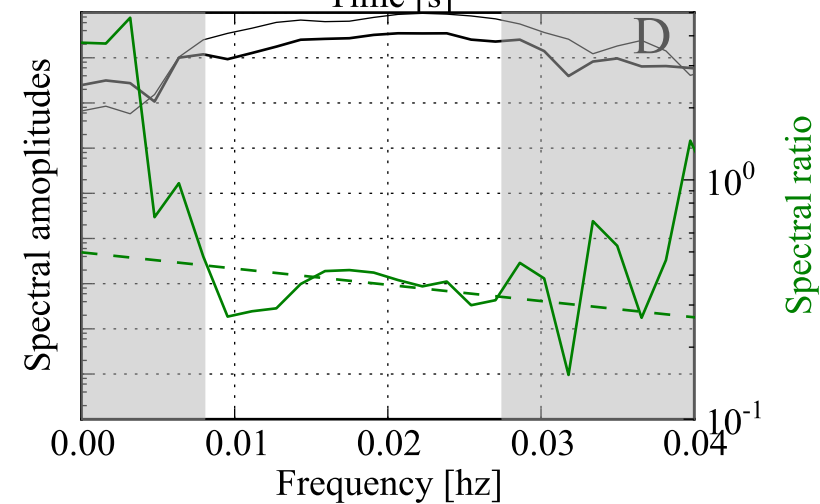
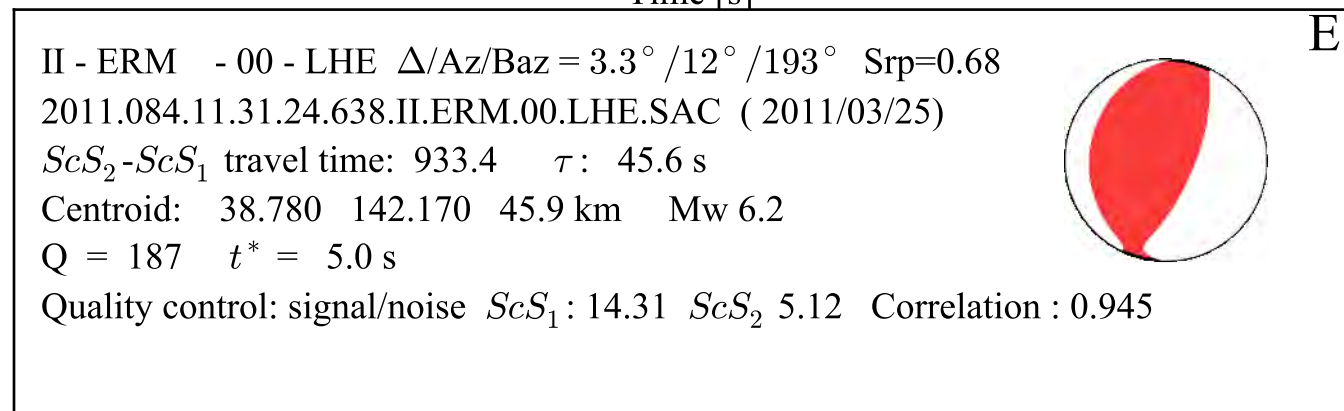
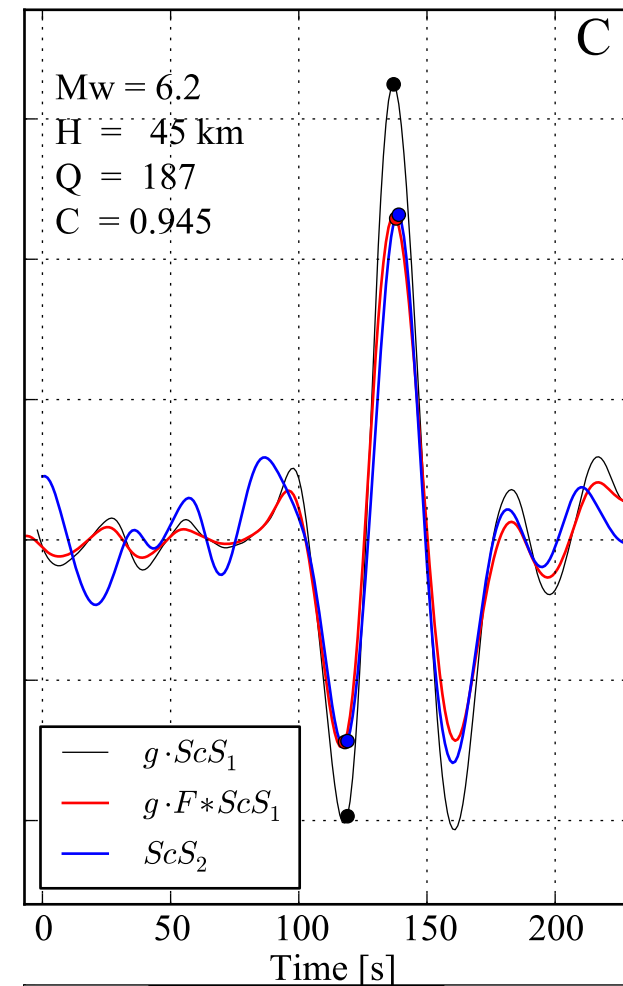
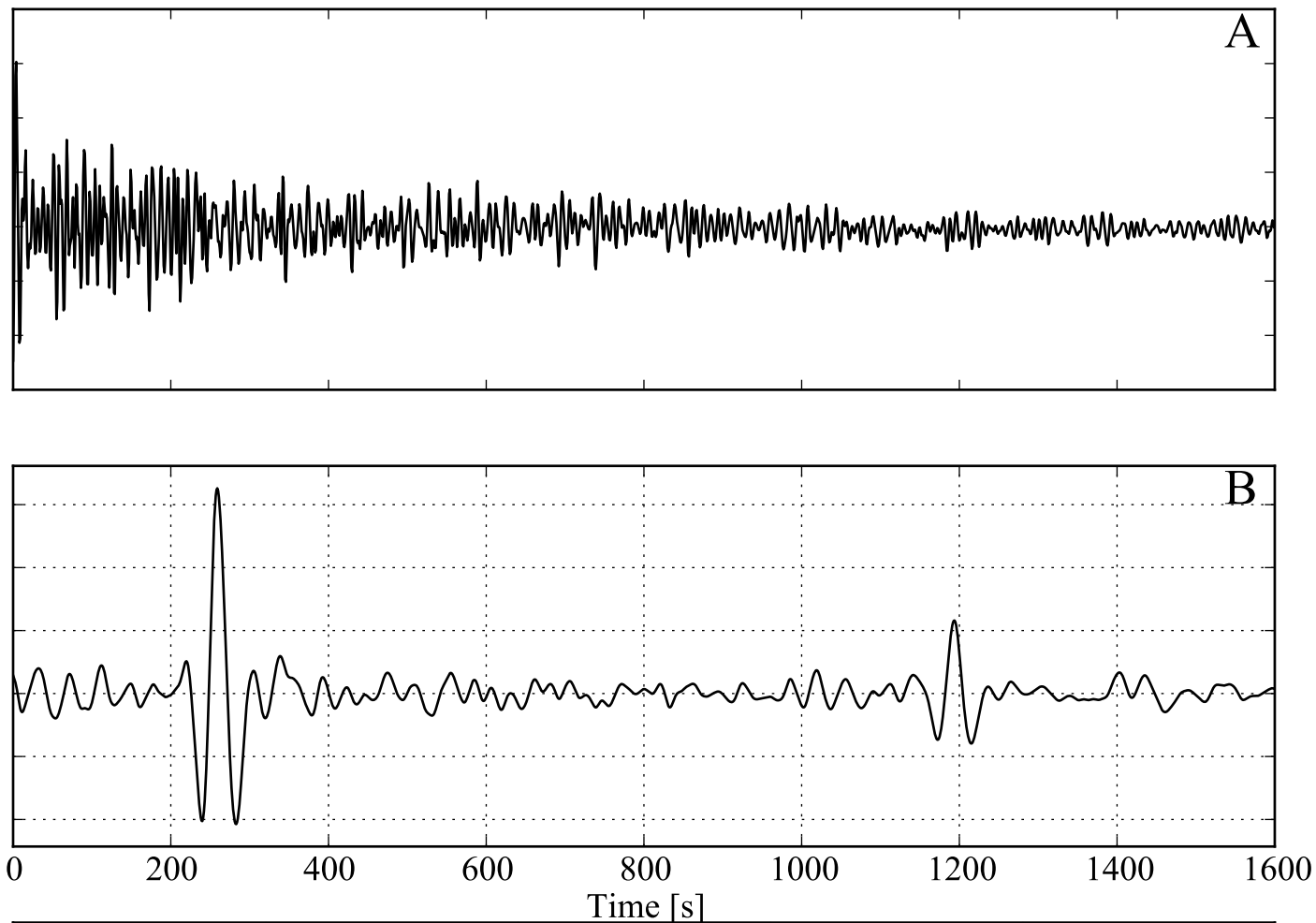


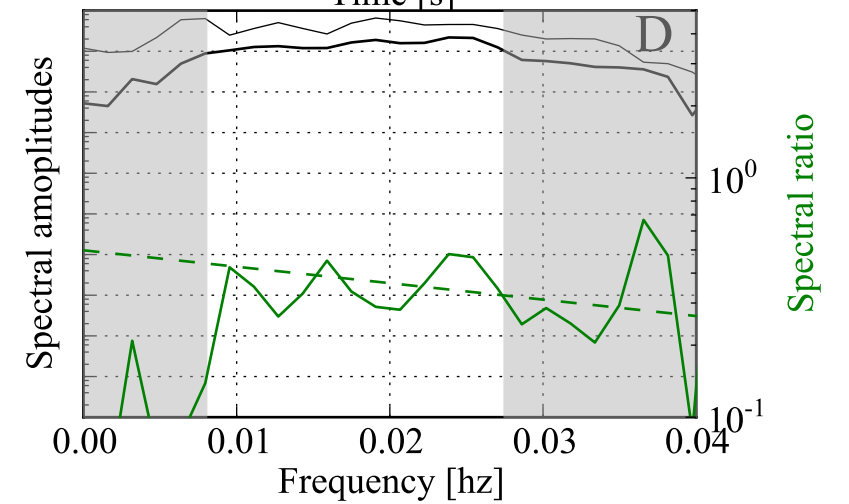
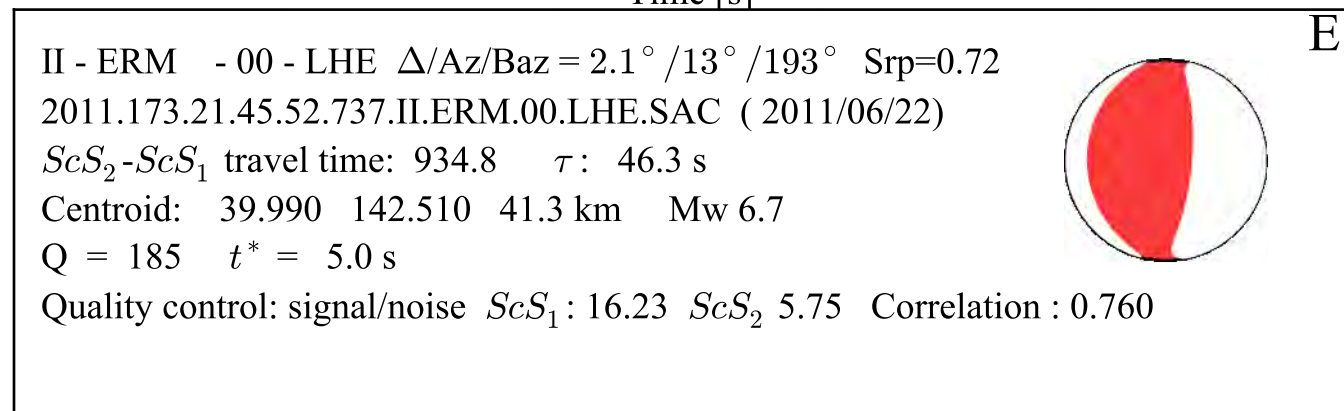
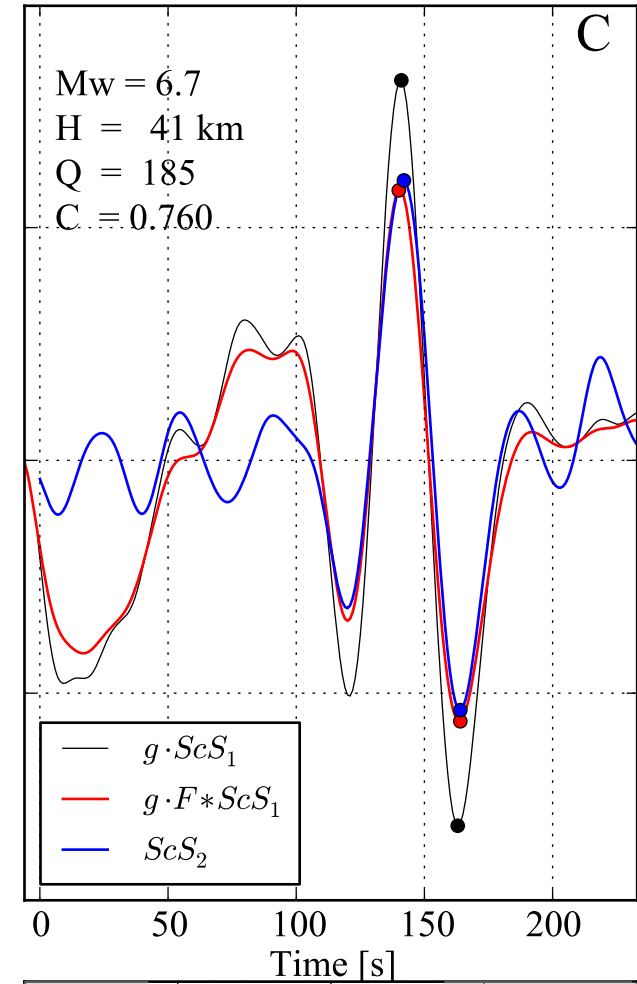
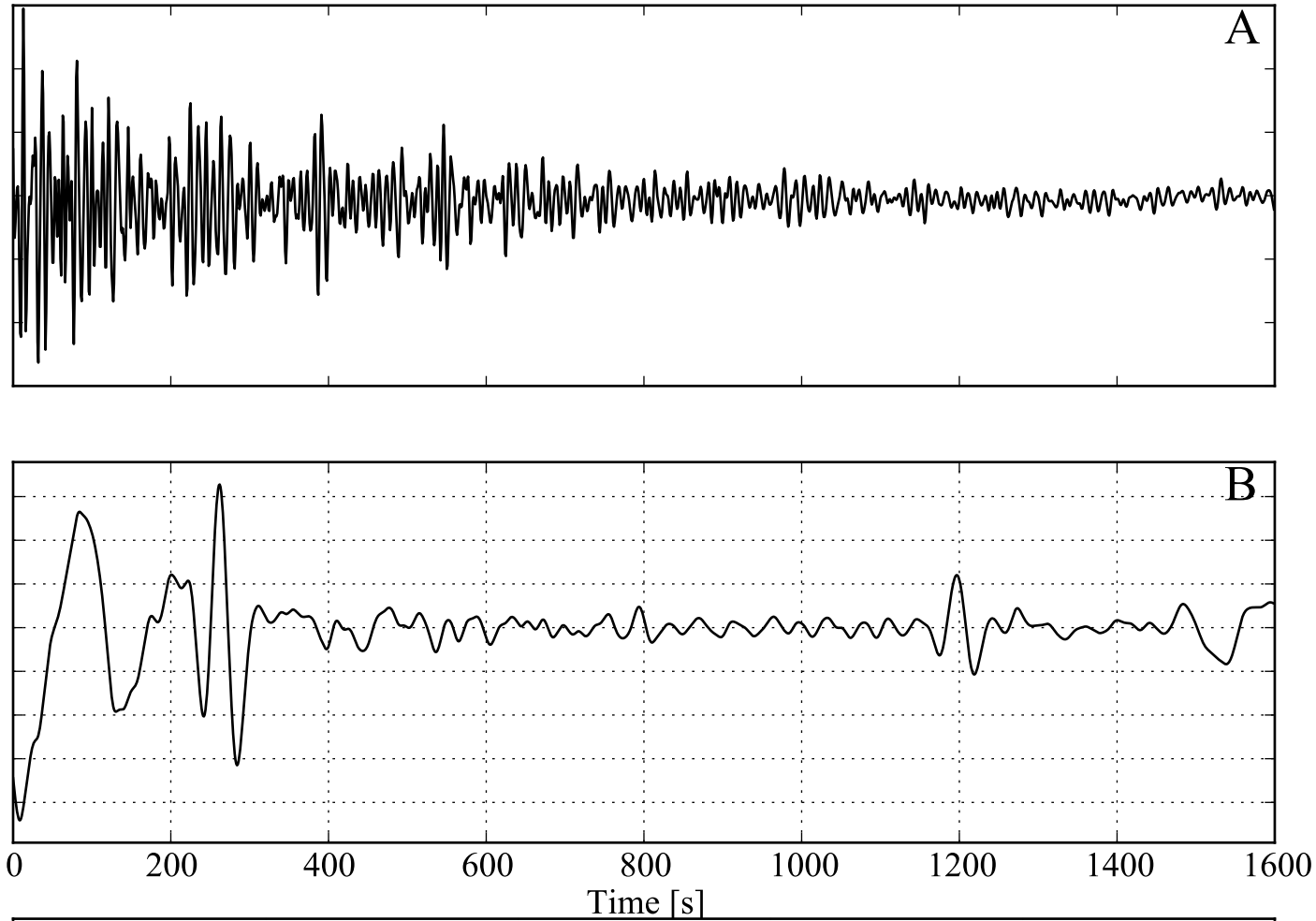


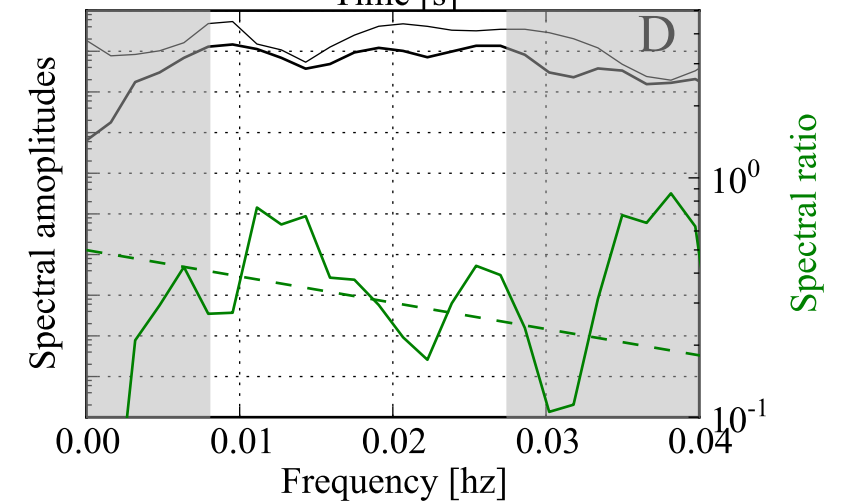
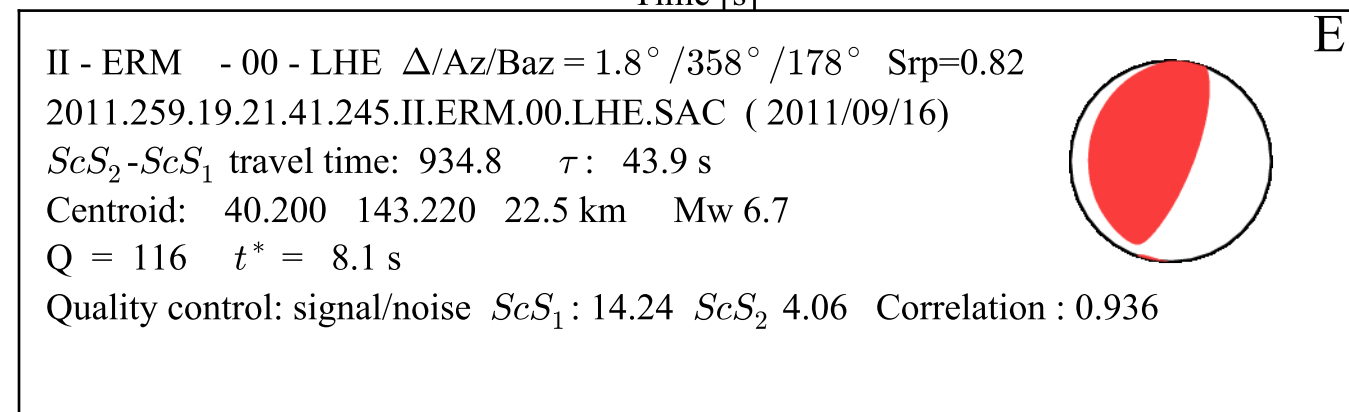
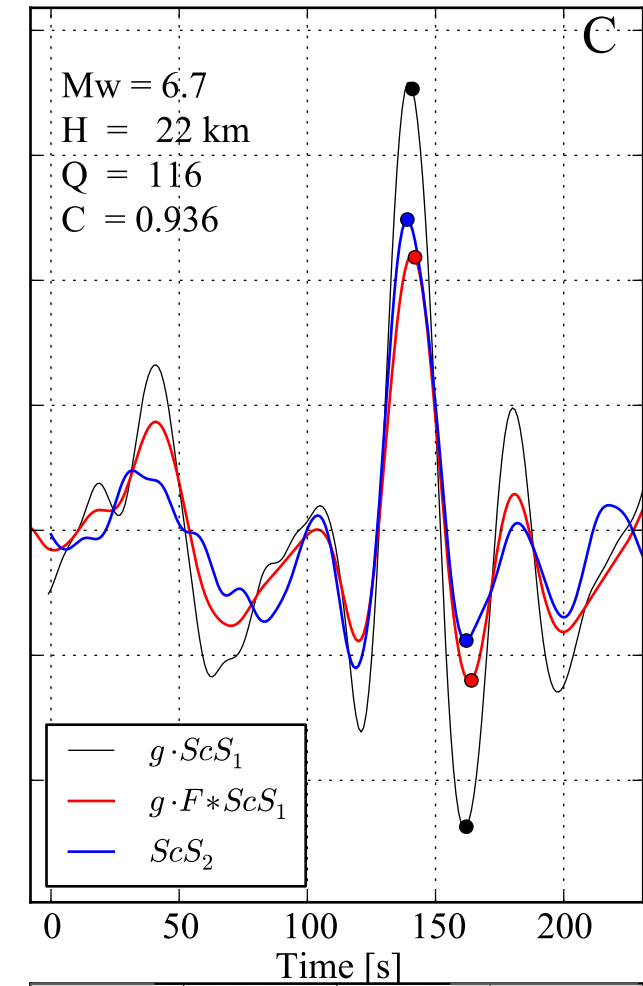
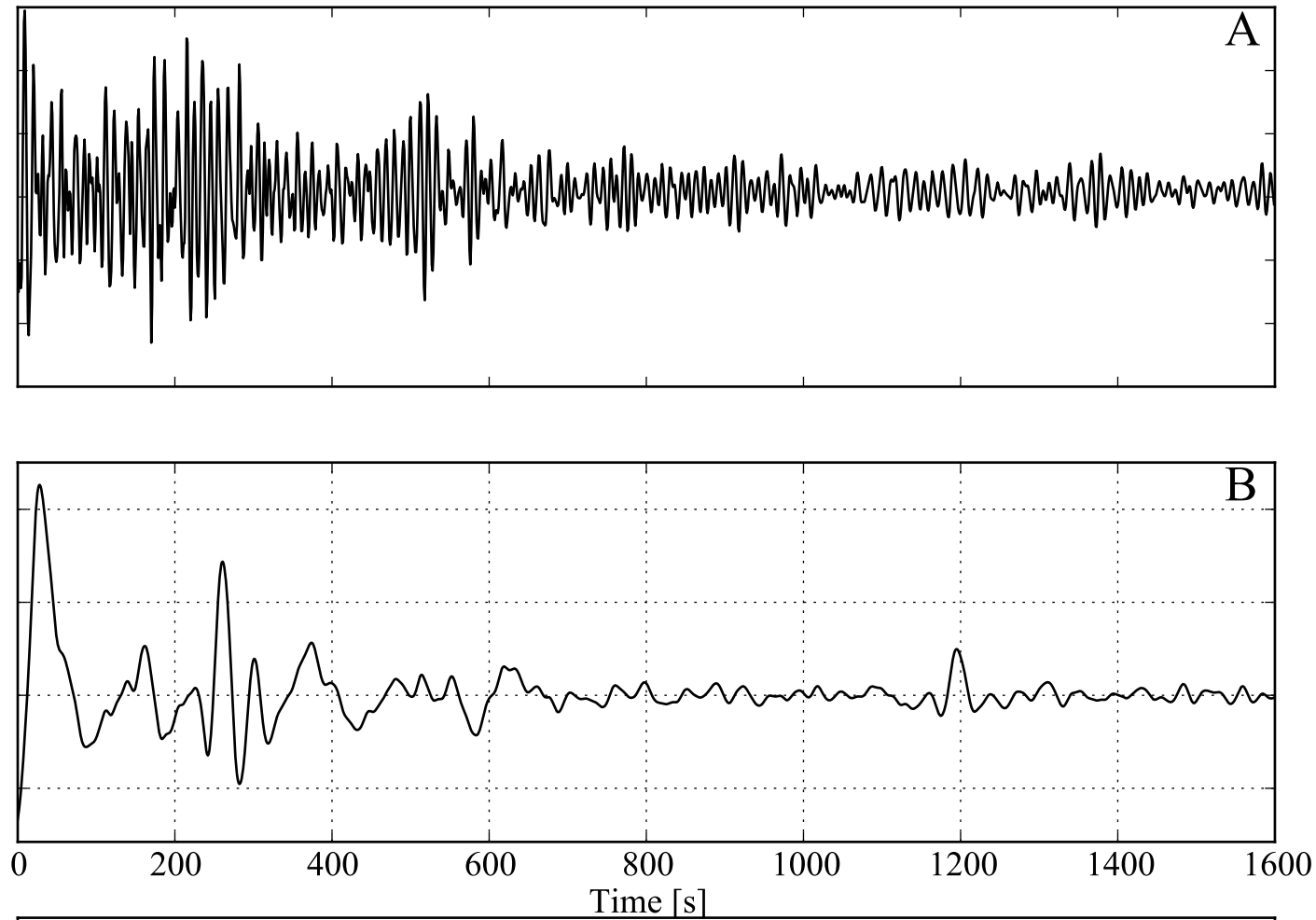


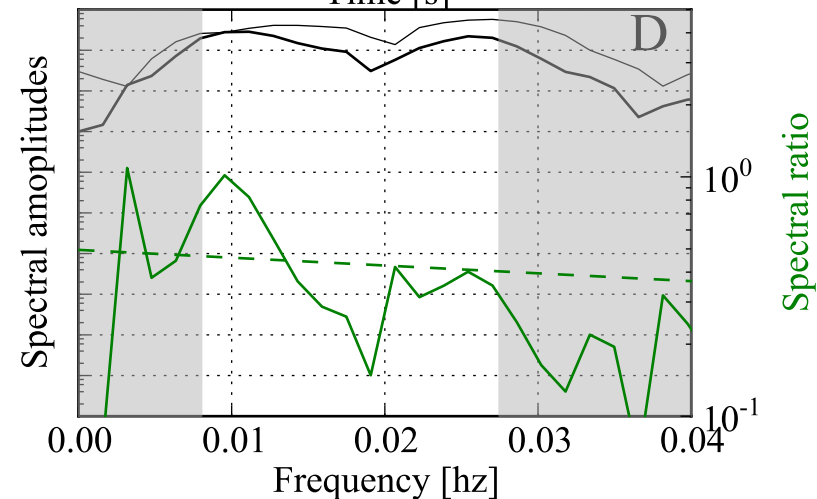
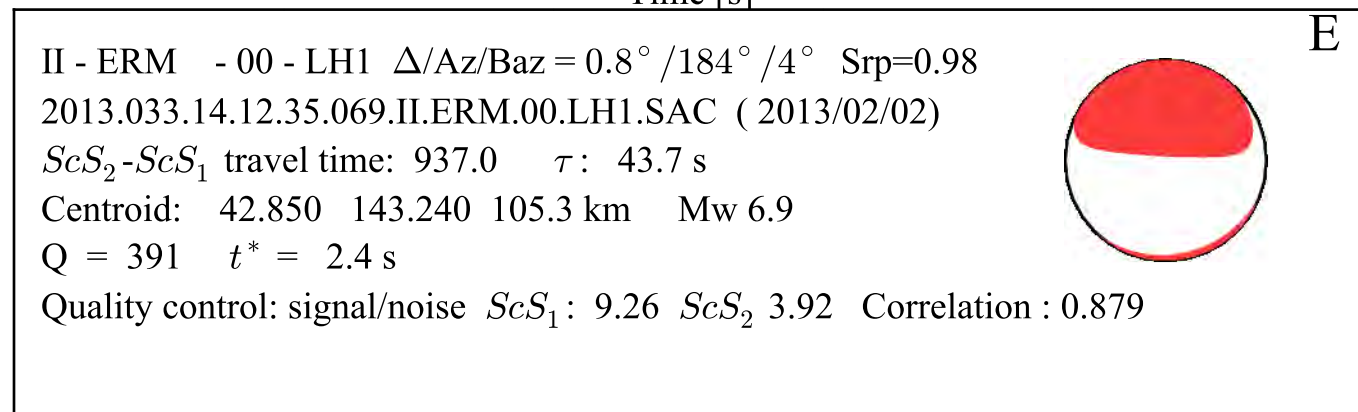
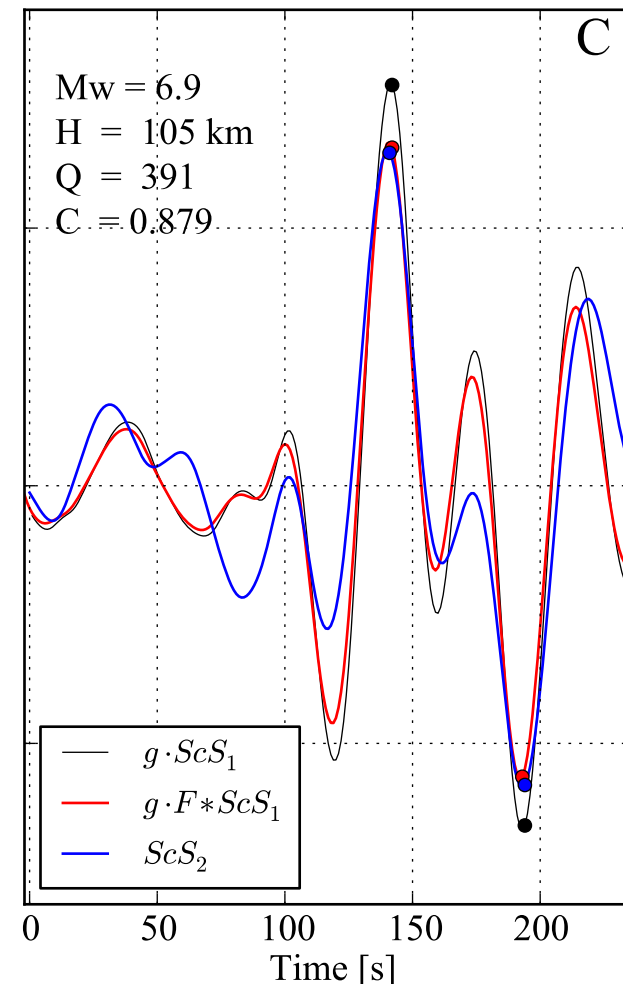
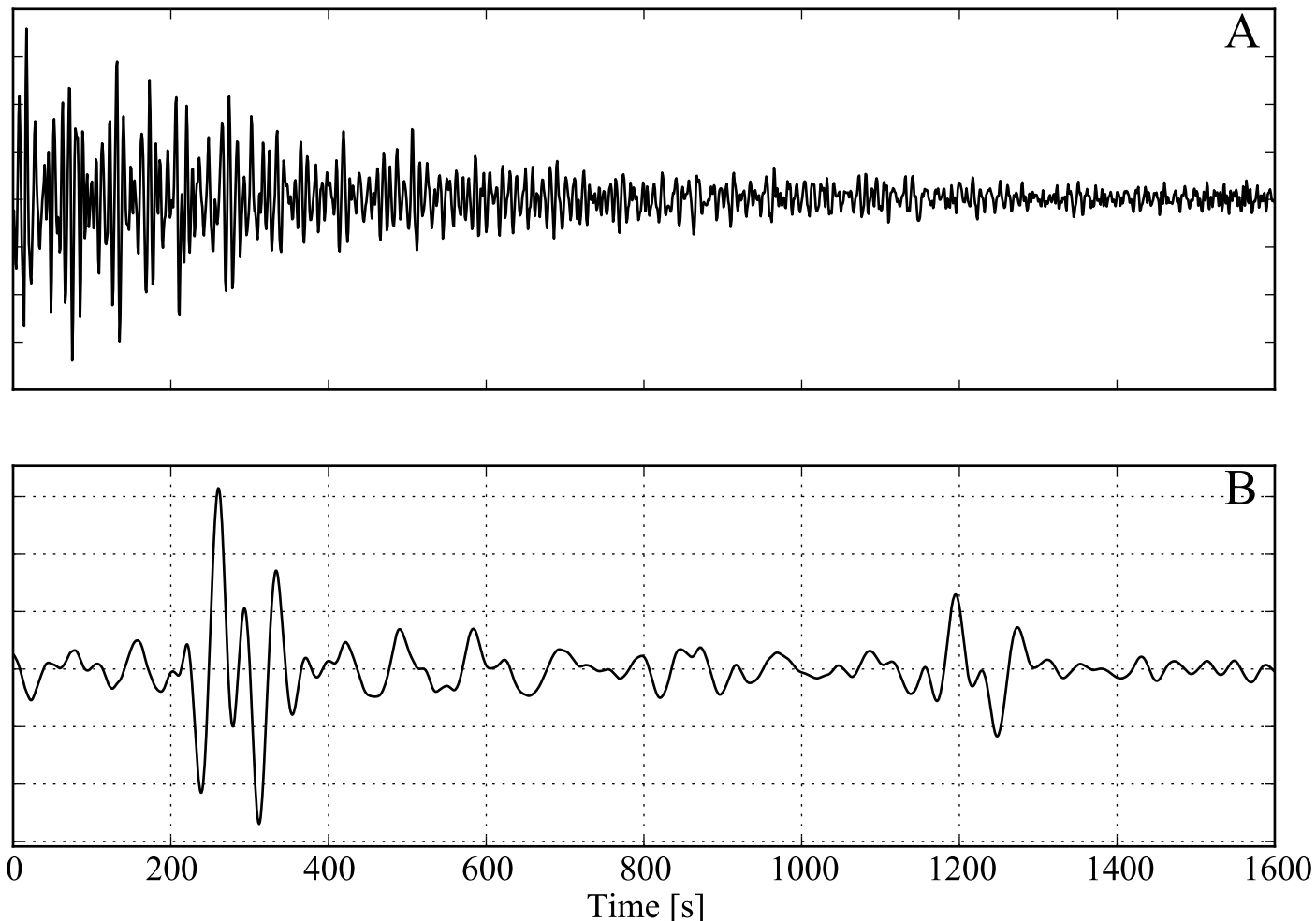


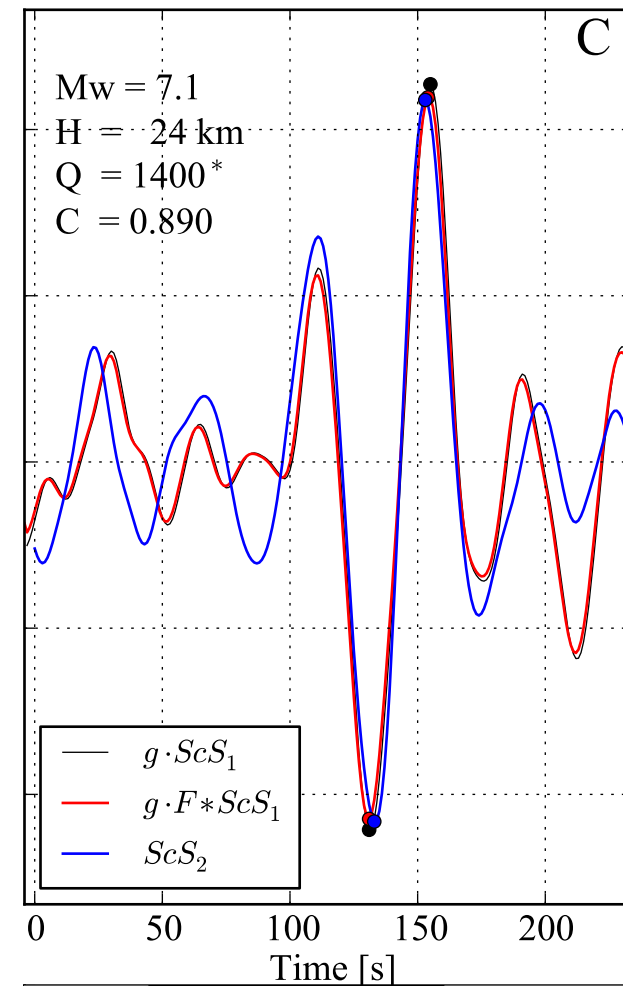
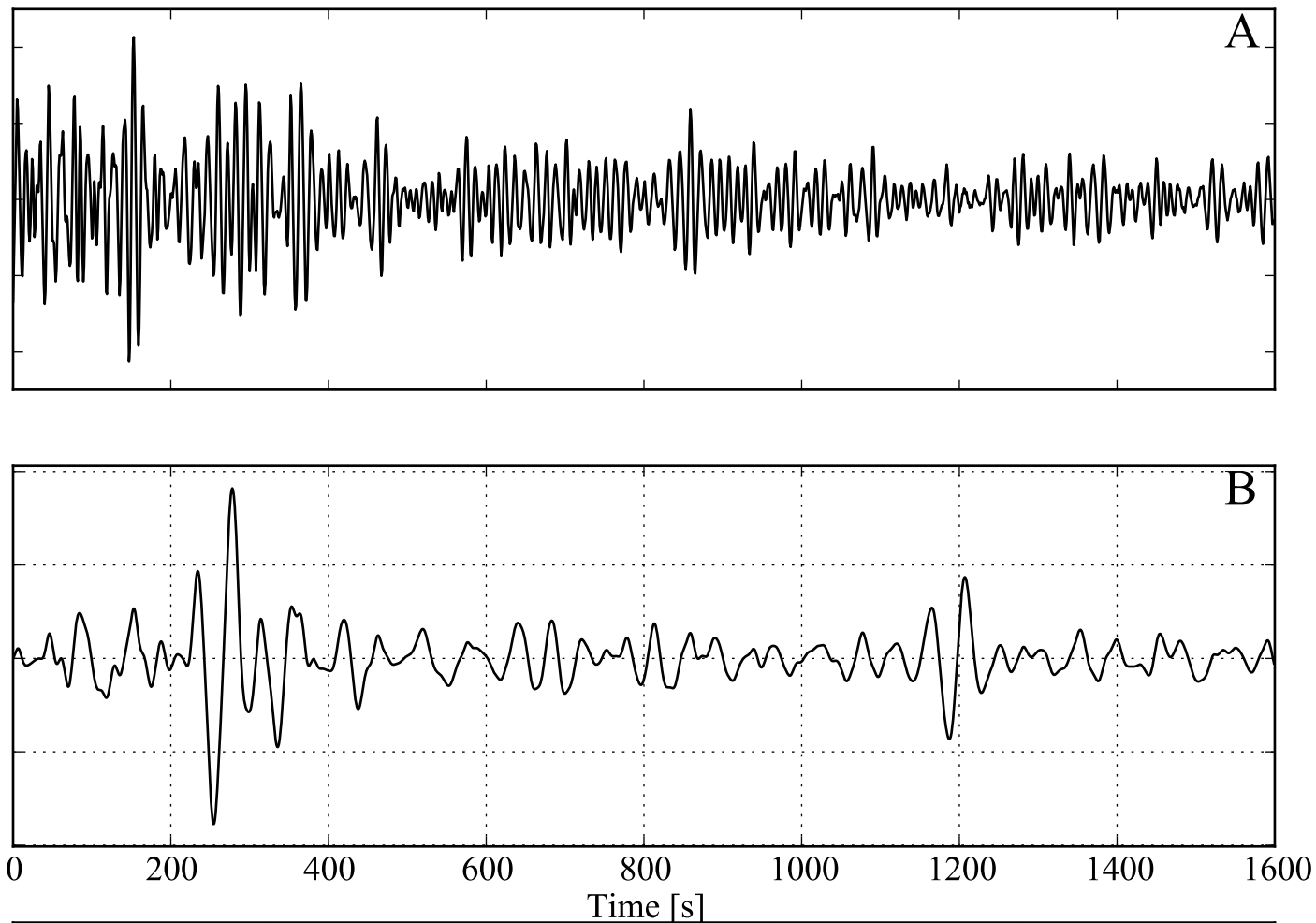






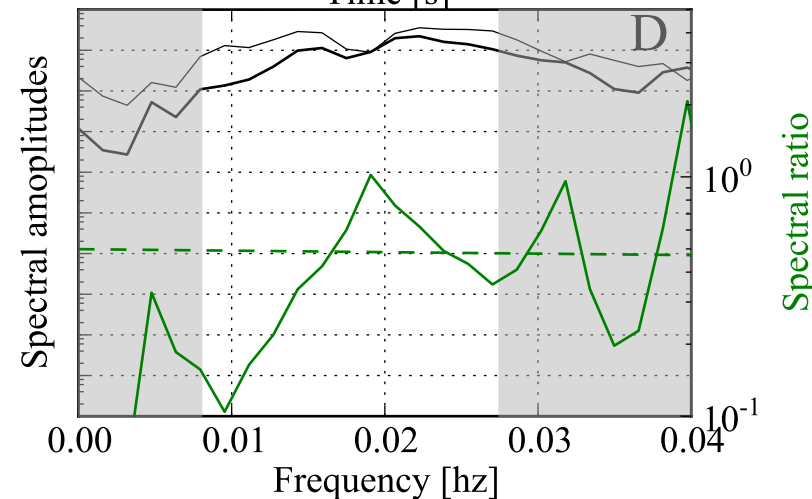


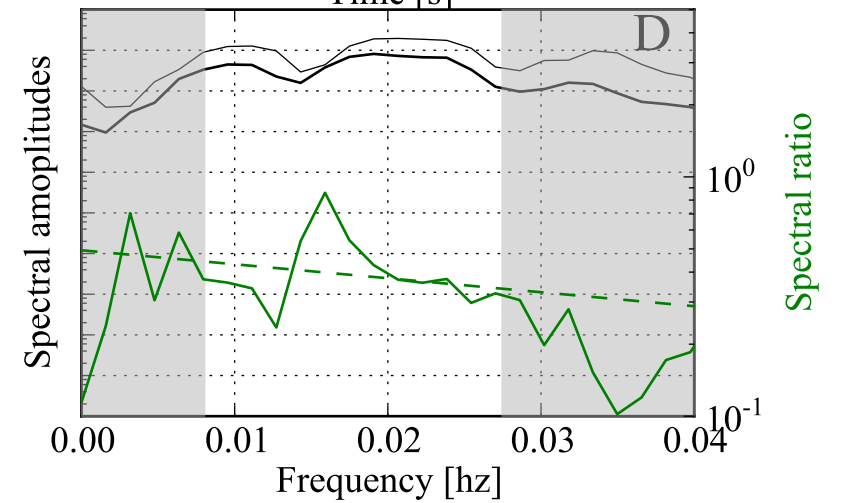
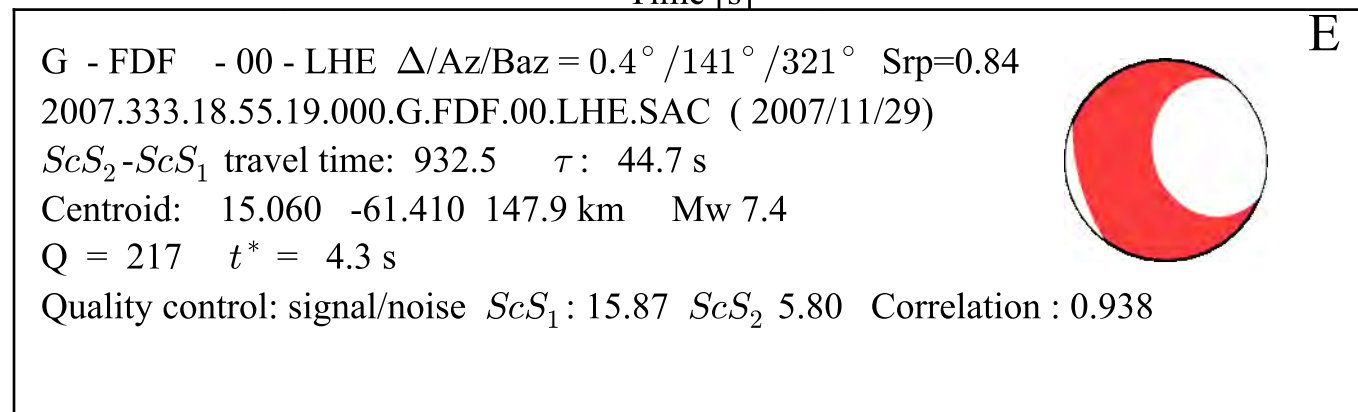
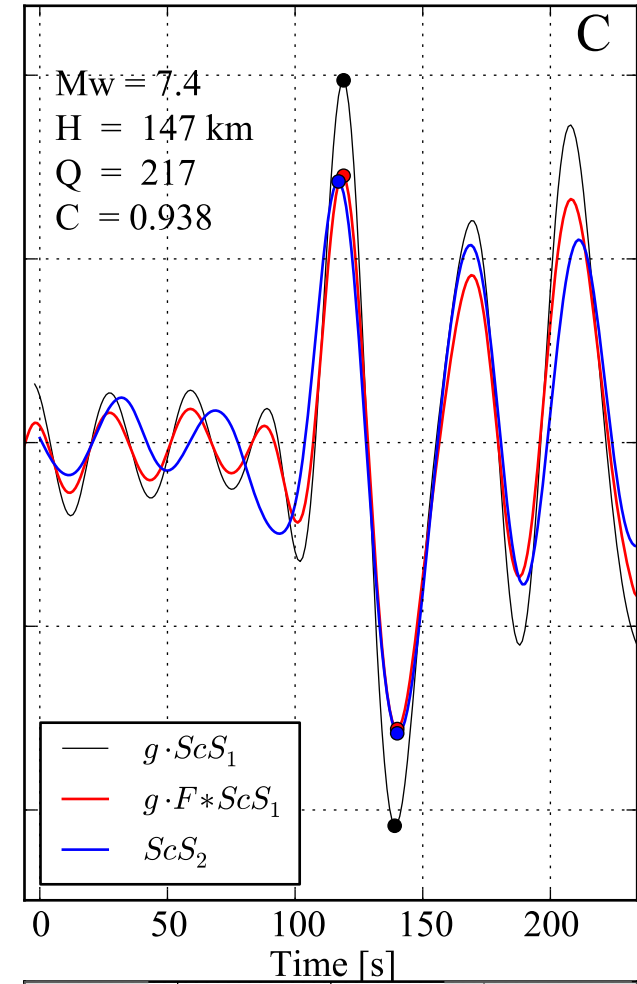
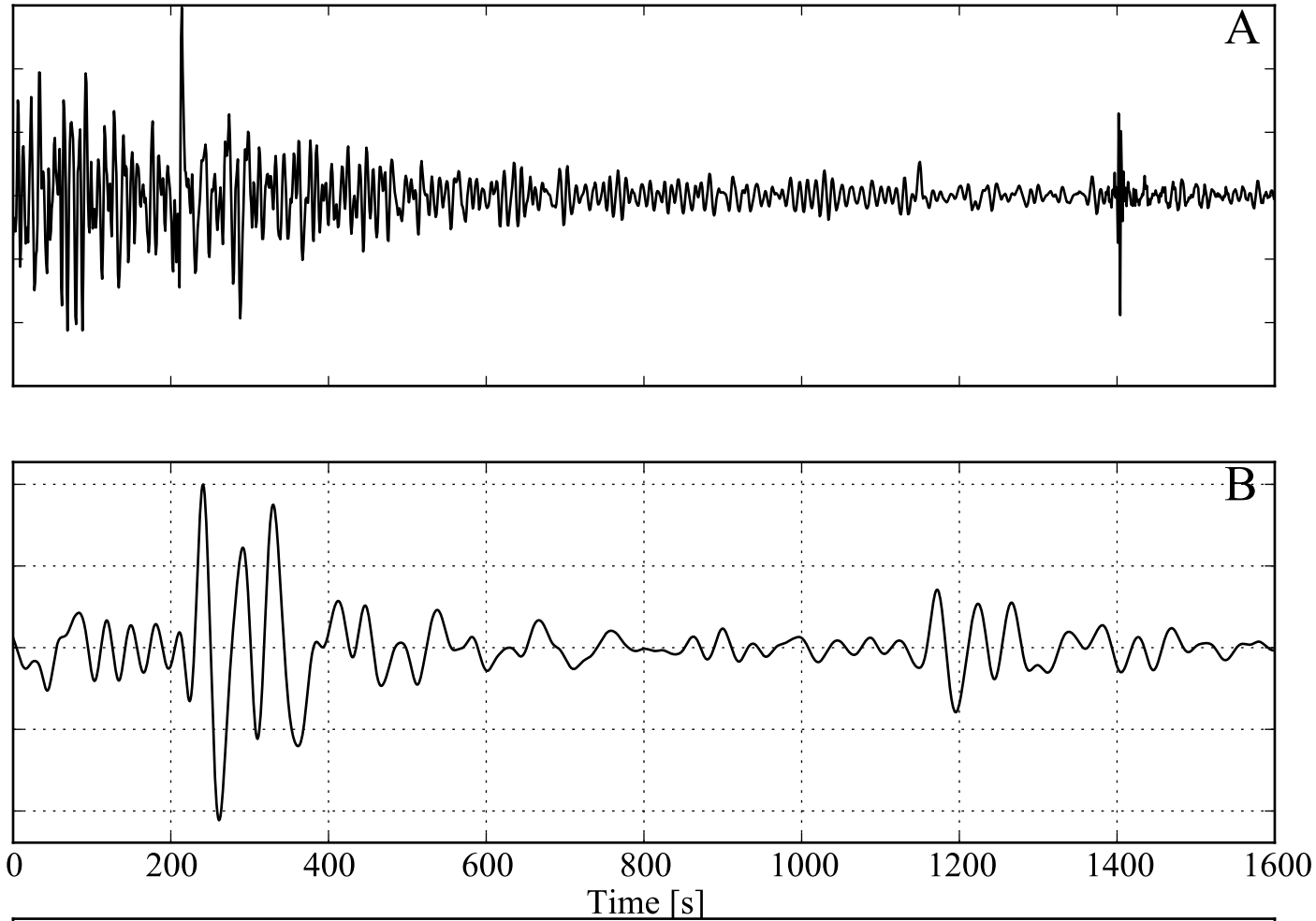


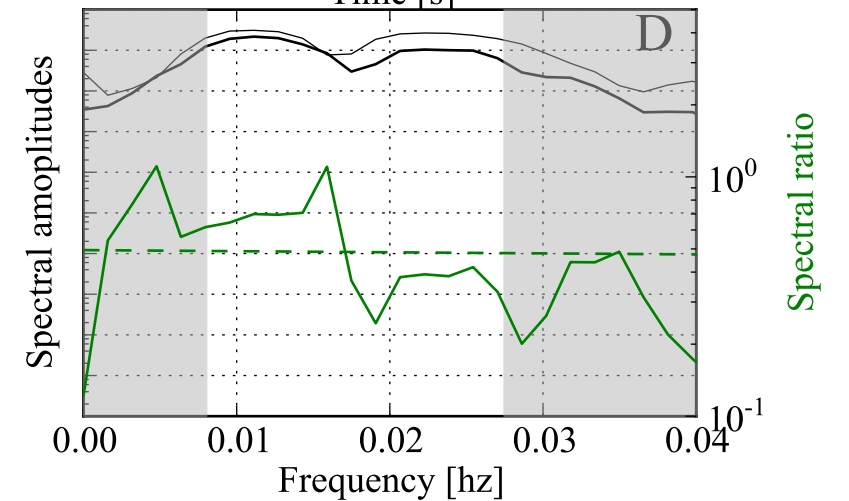
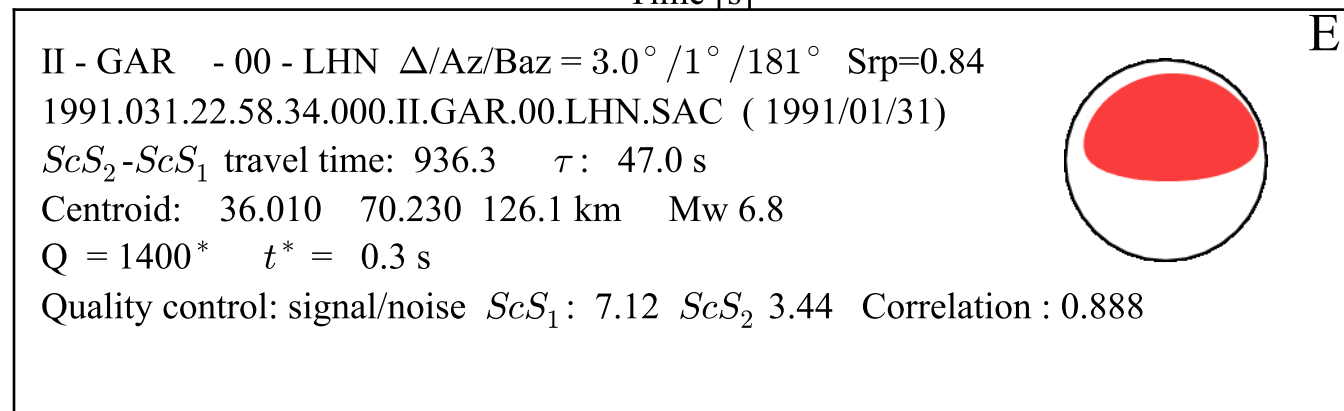
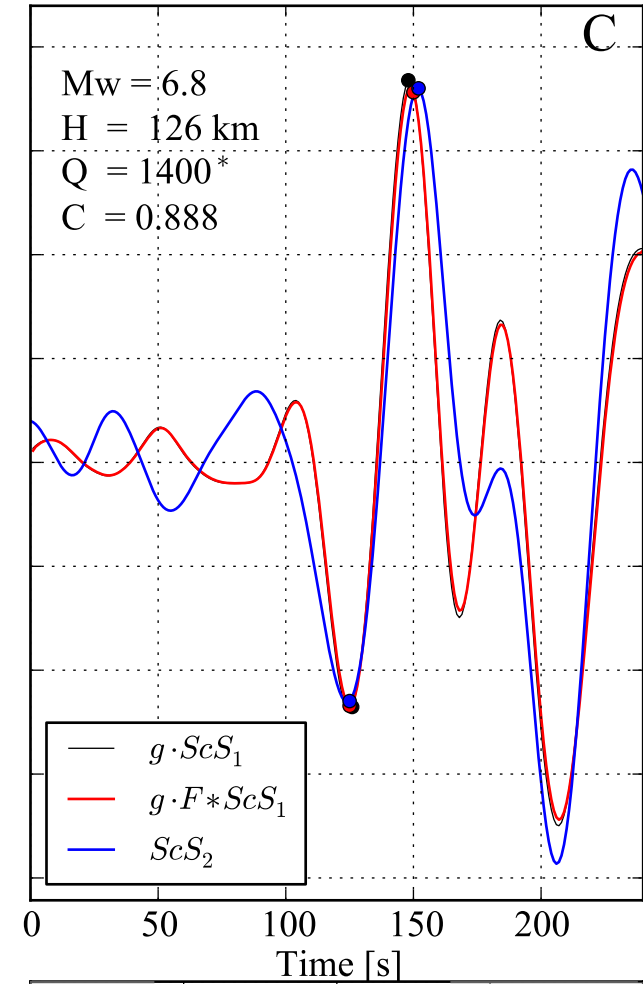
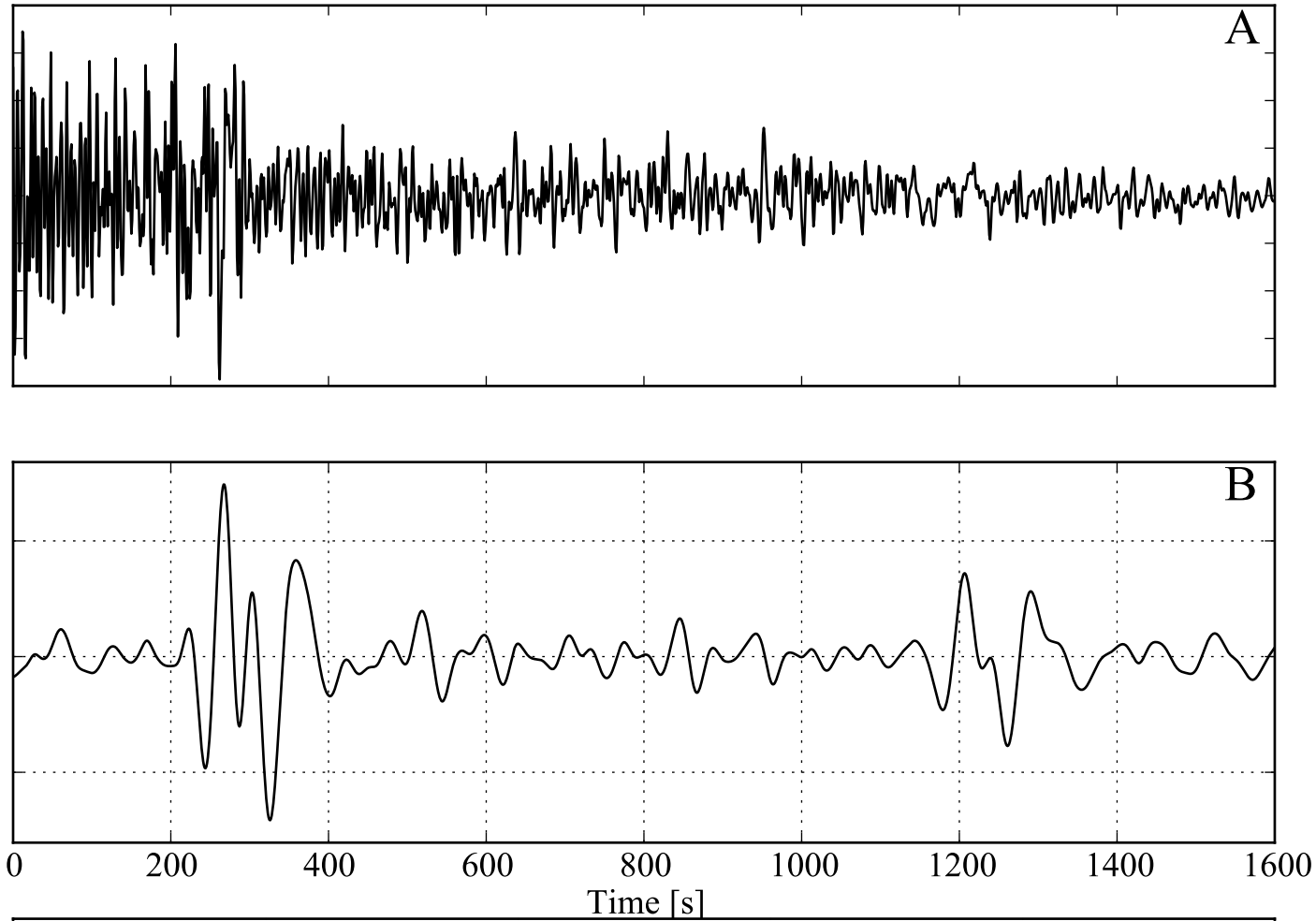


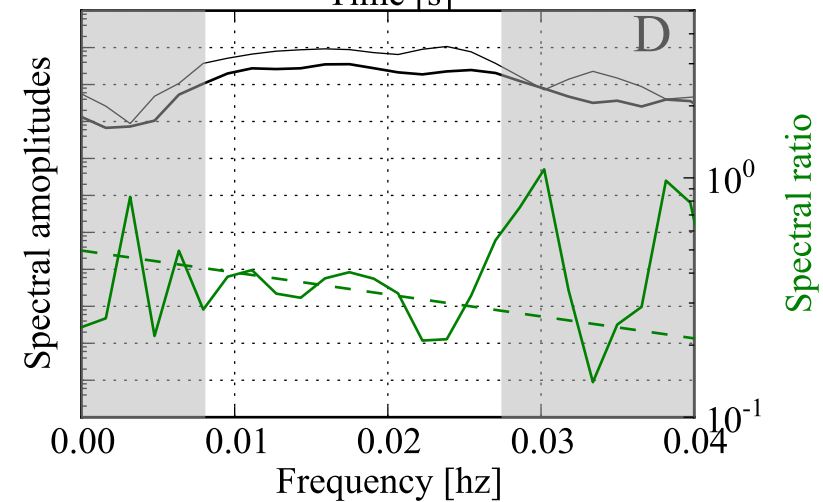
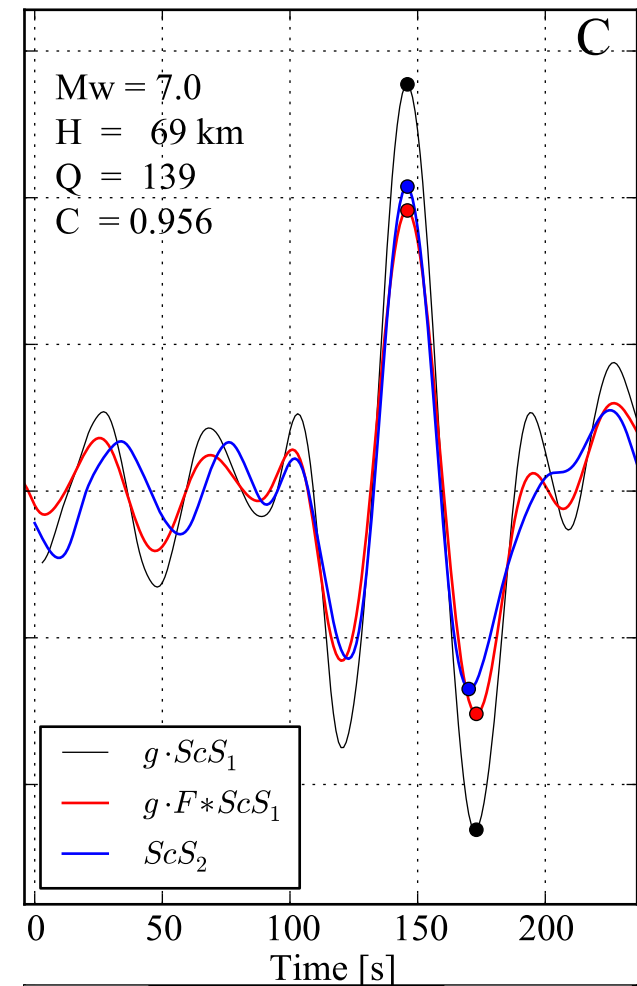
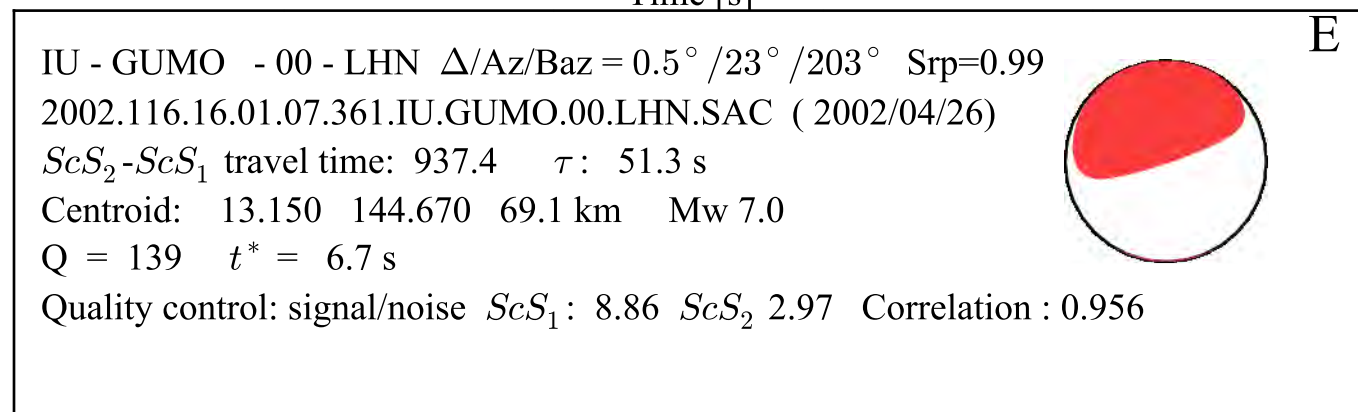
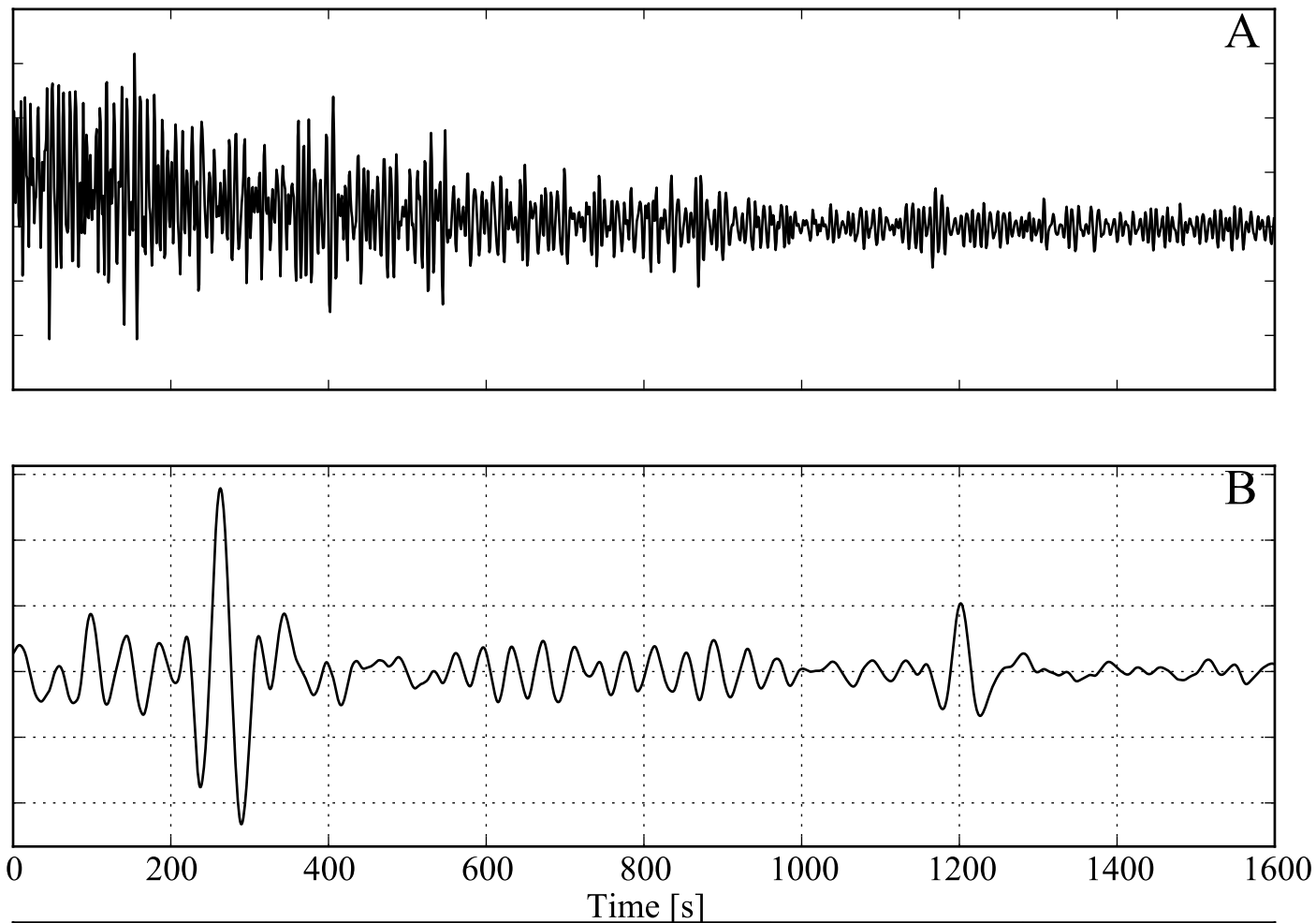
E

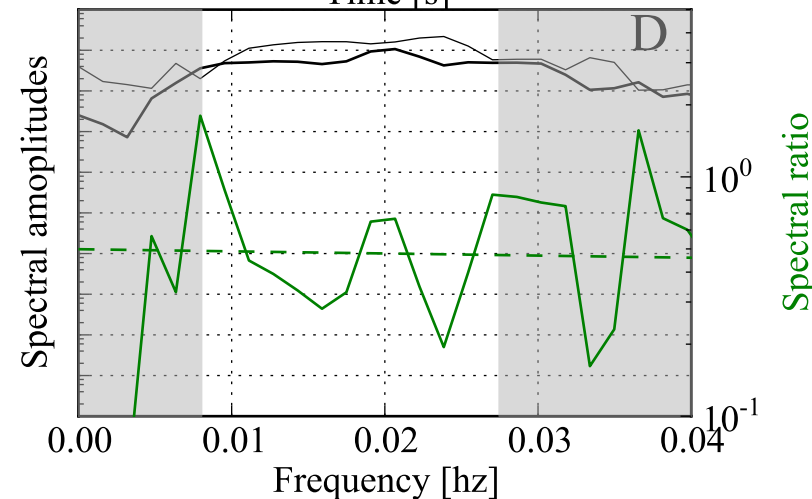
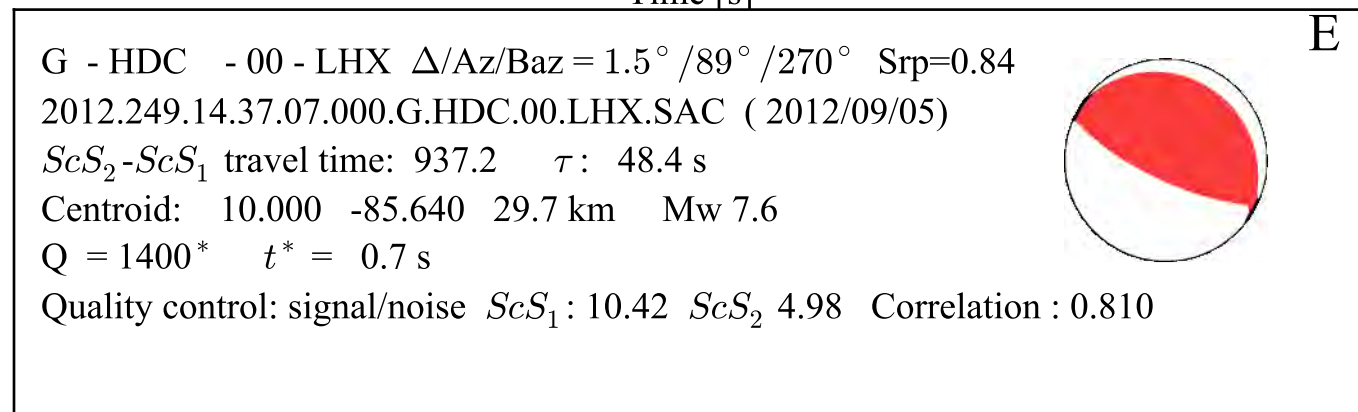
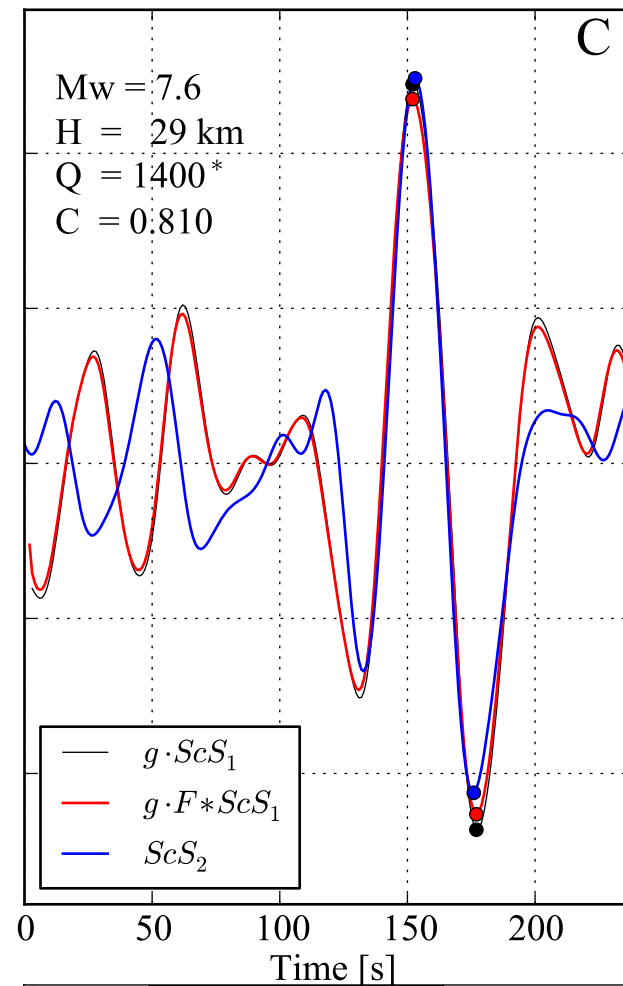
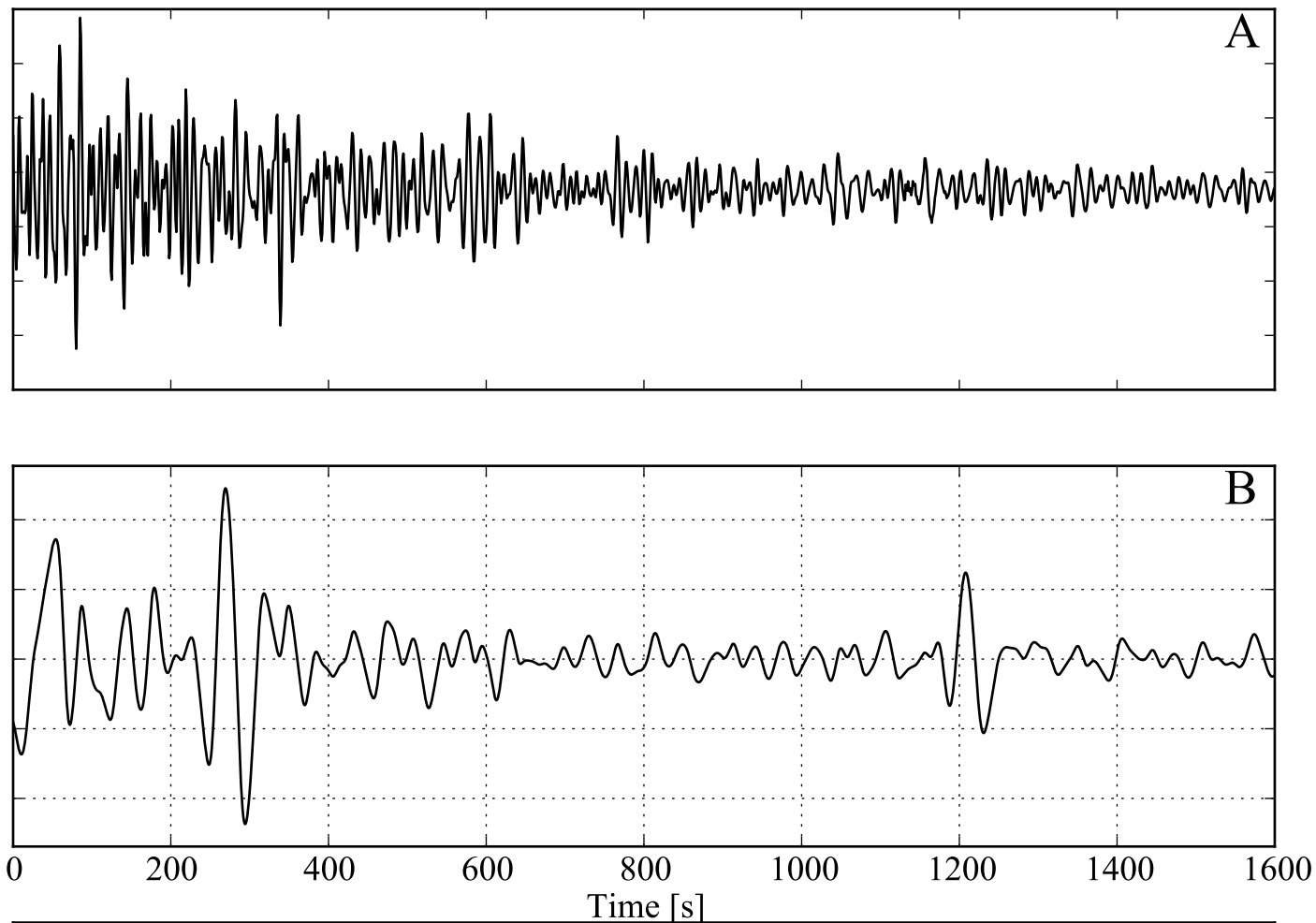
II - ERM - 10 - LH2 $\Delta/Az/Baz = 5.0^\circ / 346^\circ / 166^\circ$ Srp=0.24
 2013.298.17.05.19.069.II.ERM.10.LH2.SAC (2013/10/25)
 $ScS_2 - ScS_1$ travel time: 931.8 τ : 44.3 s
 Centroid: 37.170 144.660 24.9 km Mw 7.1
 Q = 1400* $t^* = 0.5$ s
 Quality control: signal/noise ScS_1 : 8.26 ScS_2 3.99 Correlation : 0.890

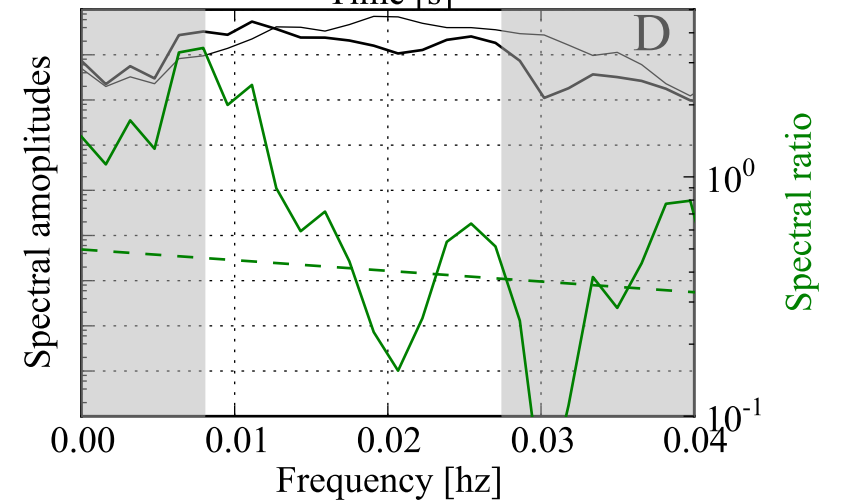
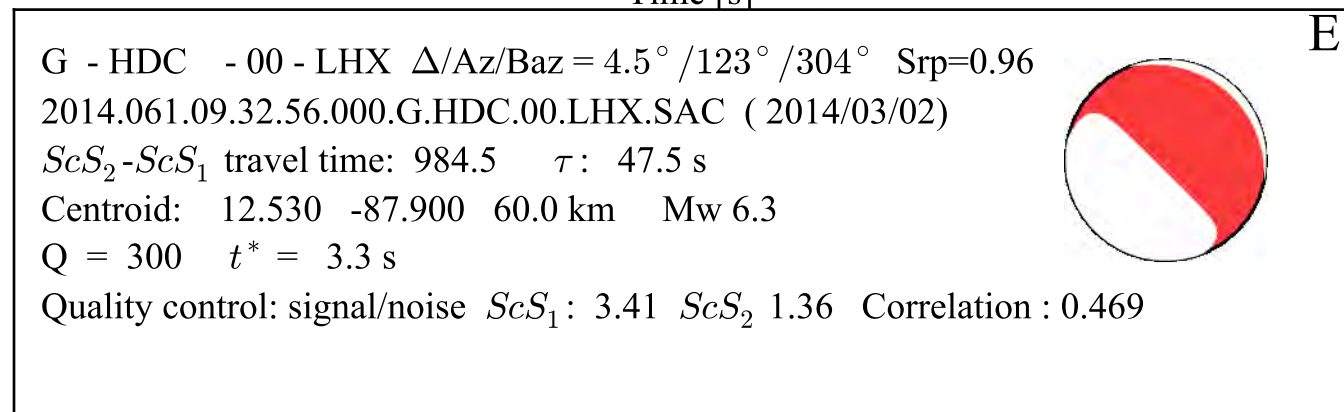
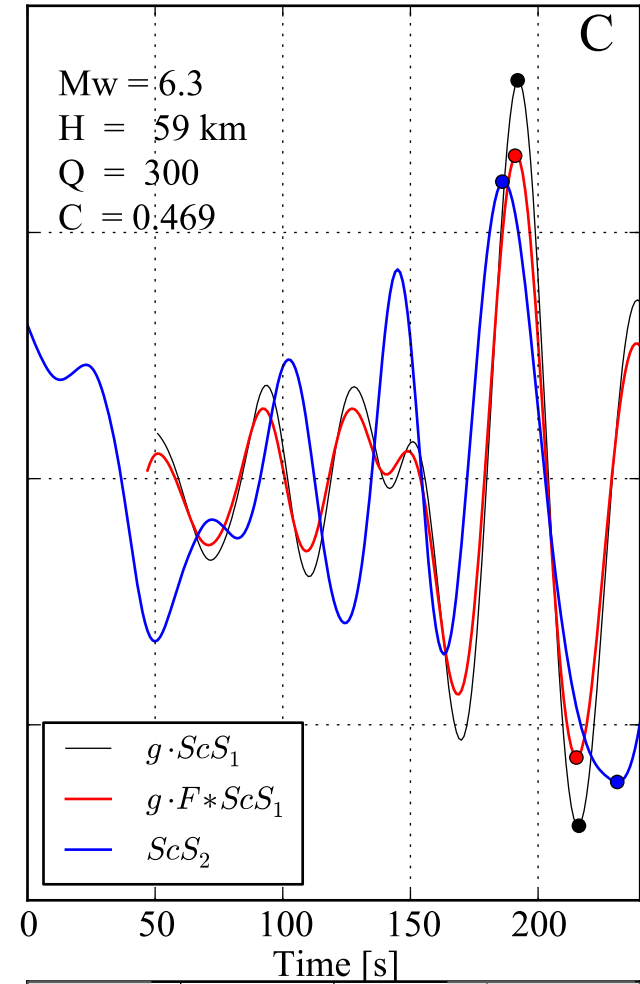
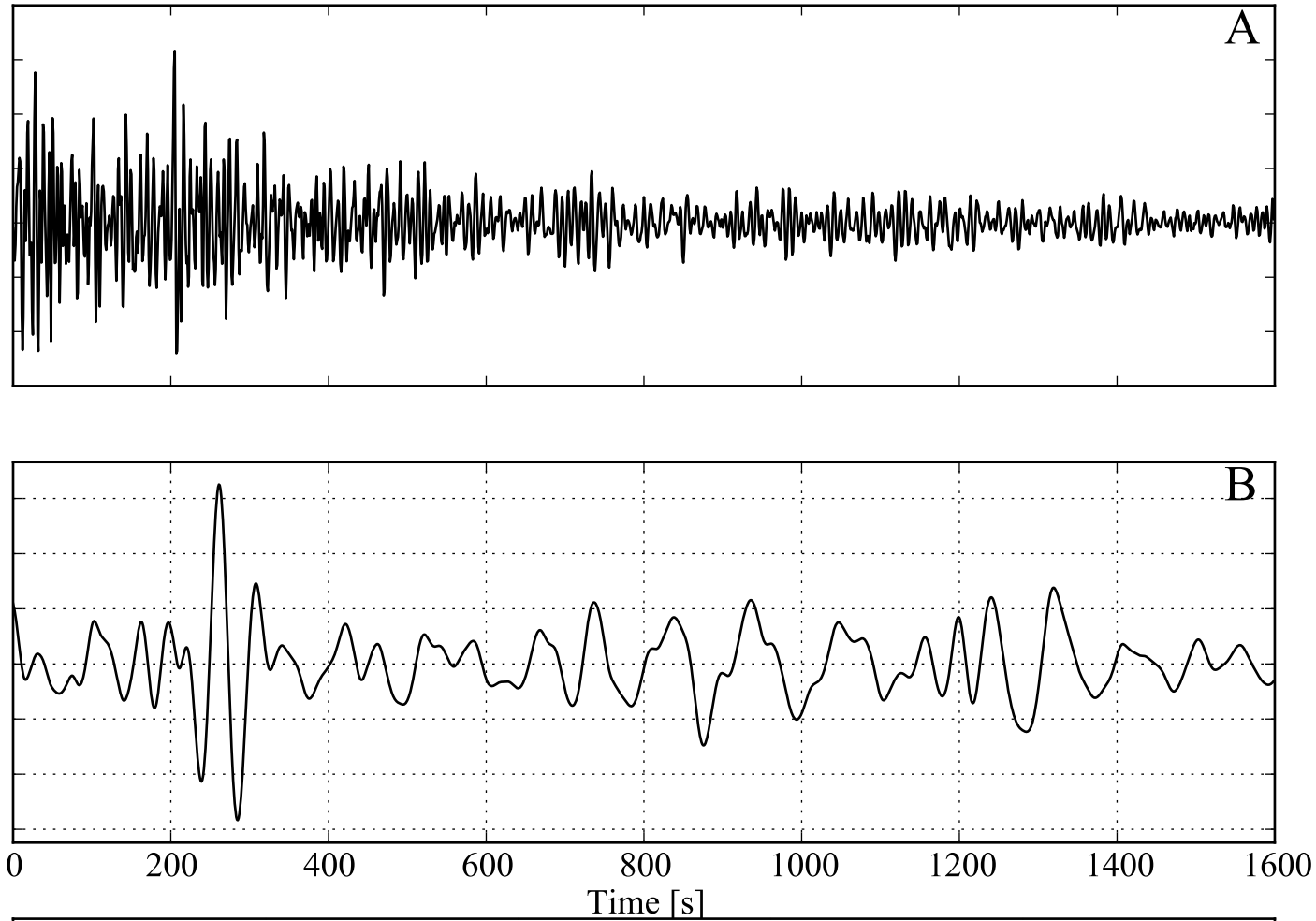


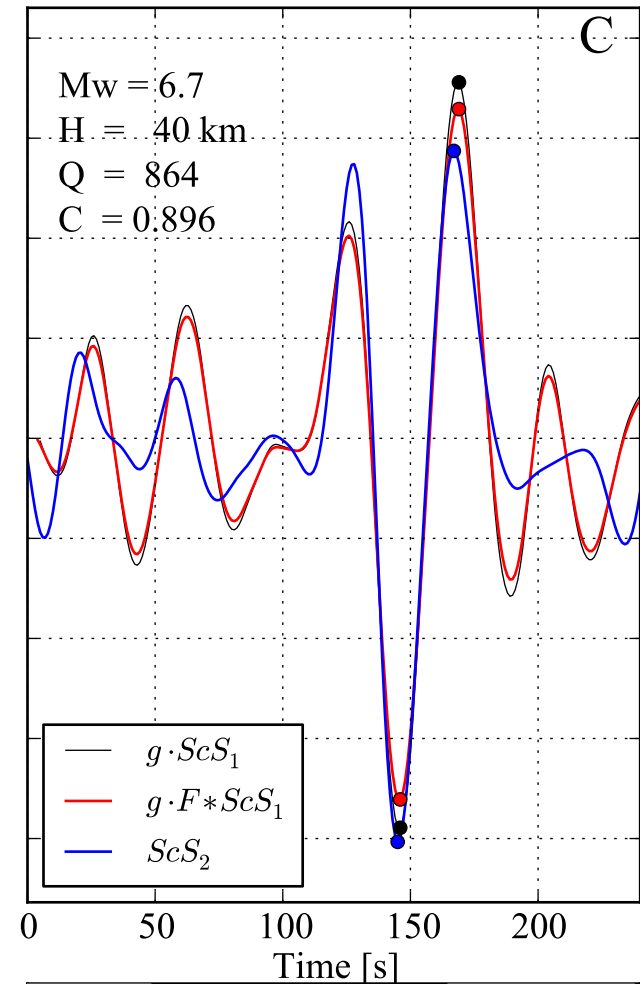
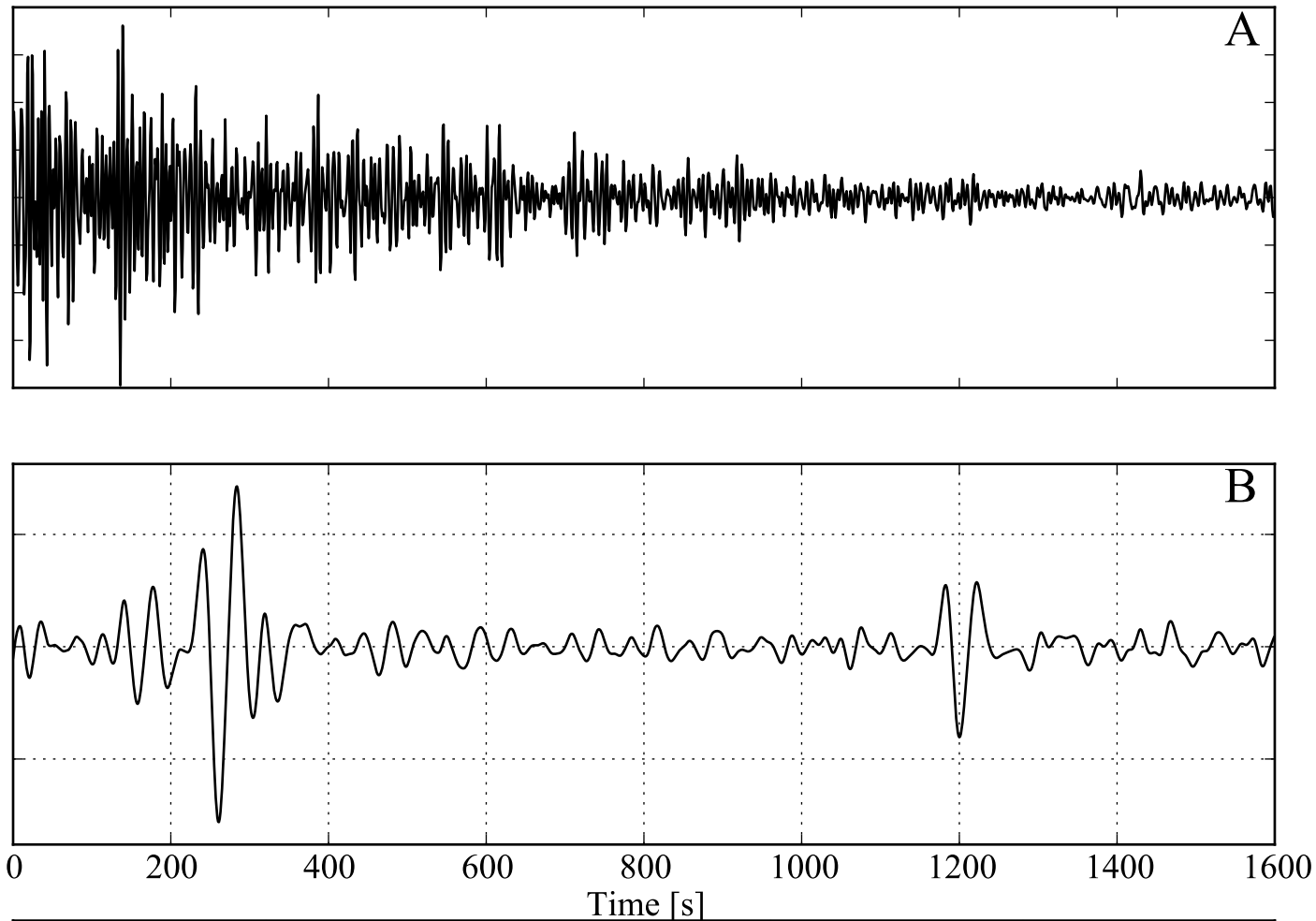






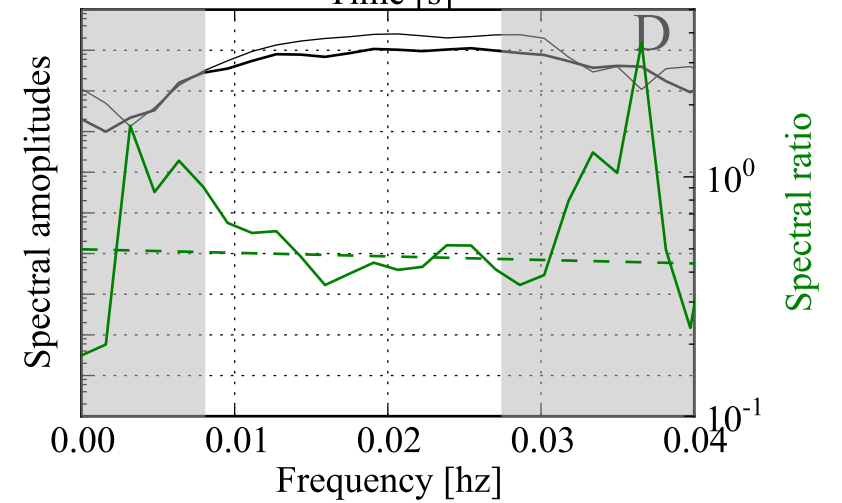


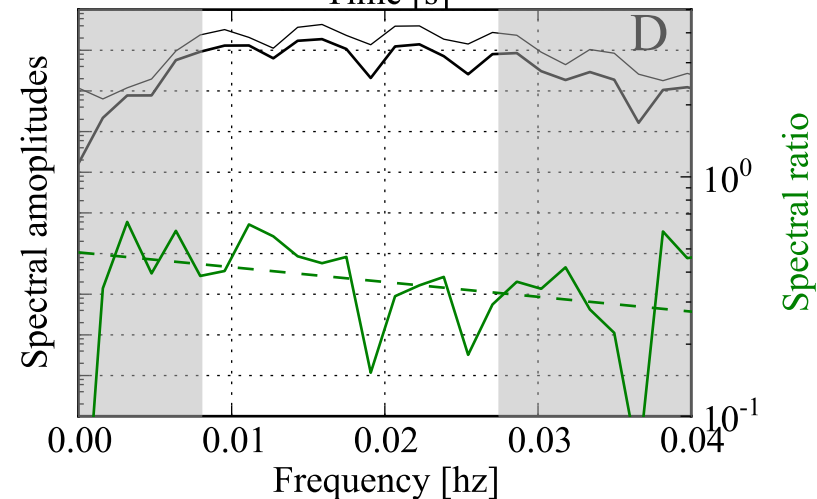
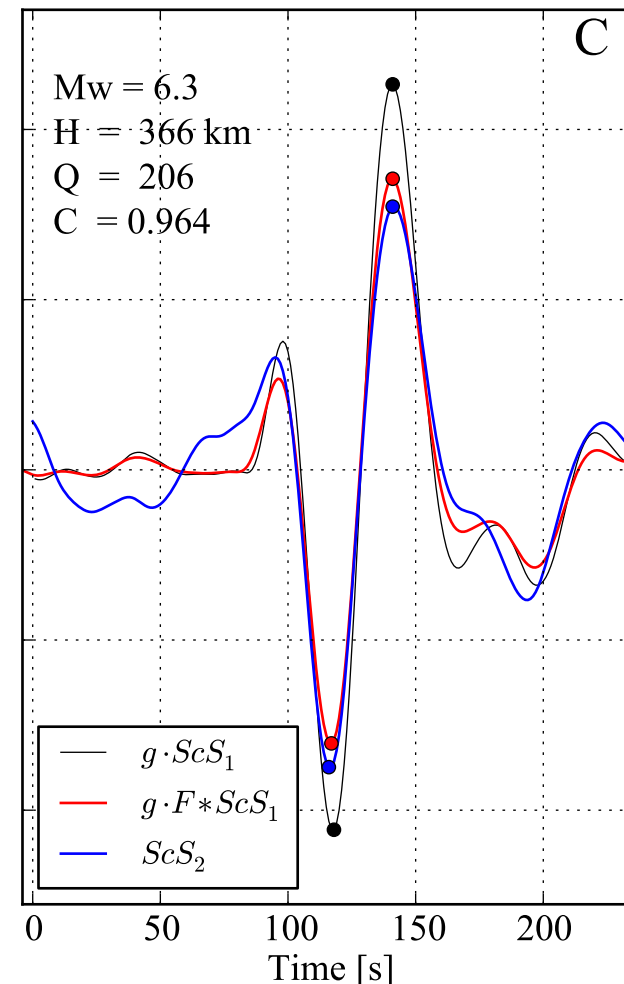
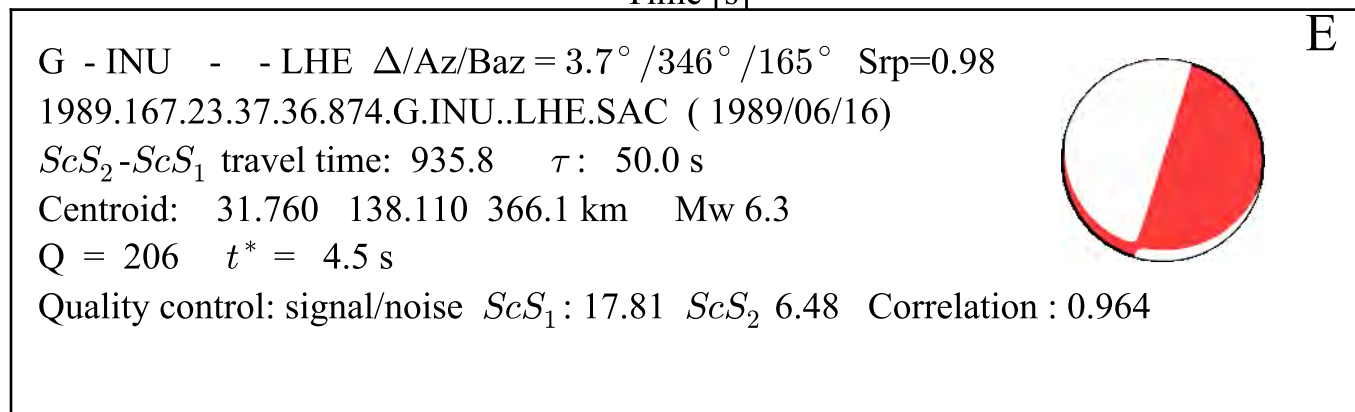
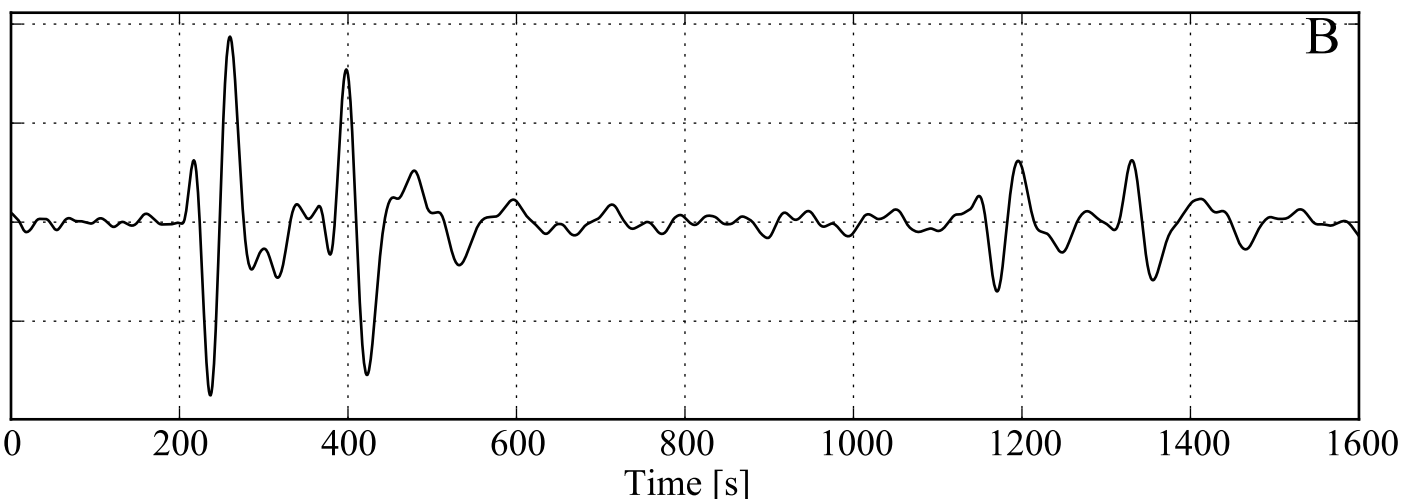
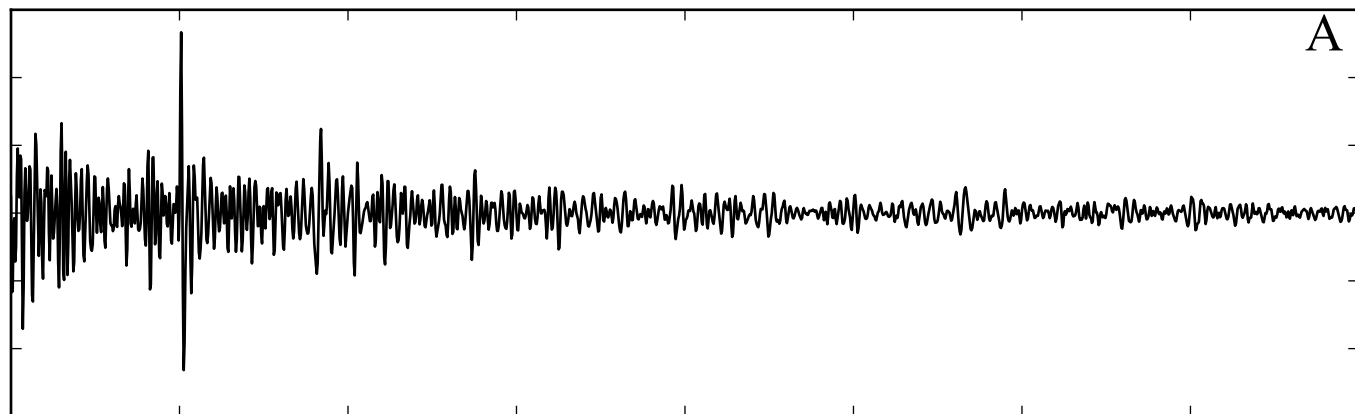


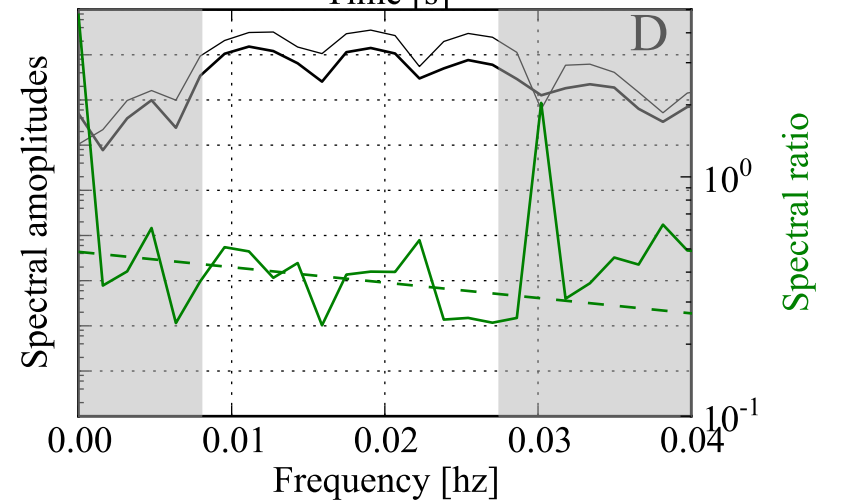
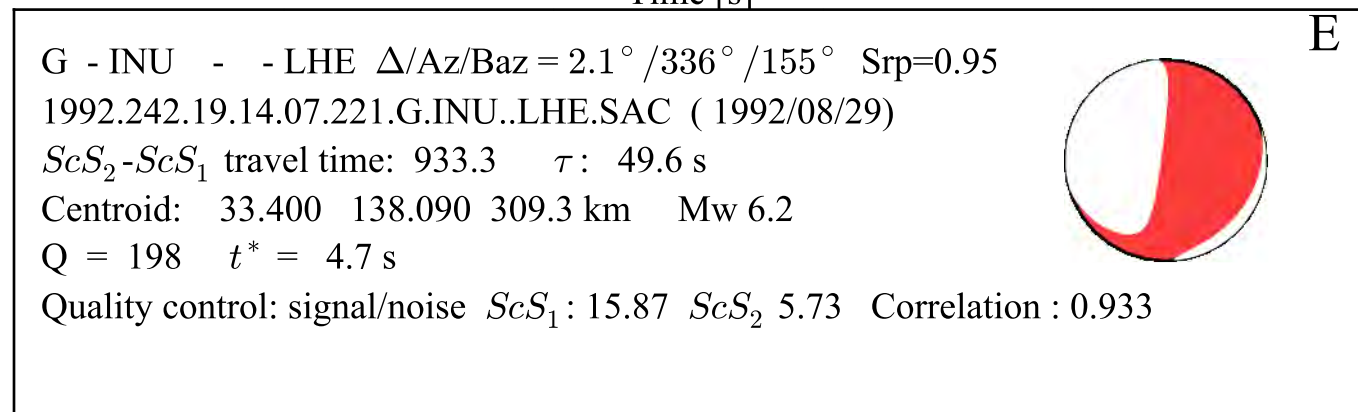
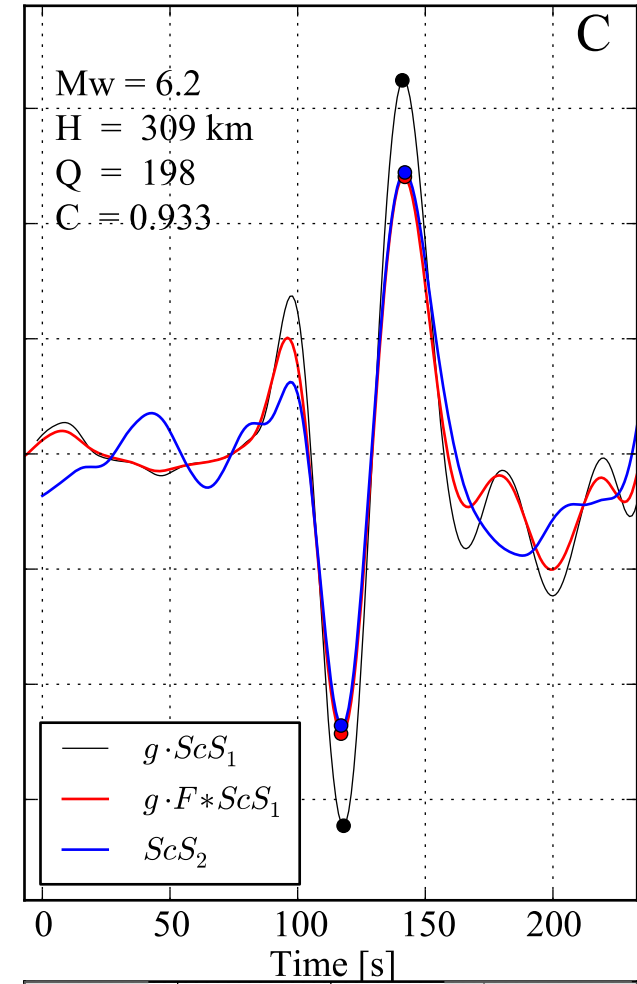
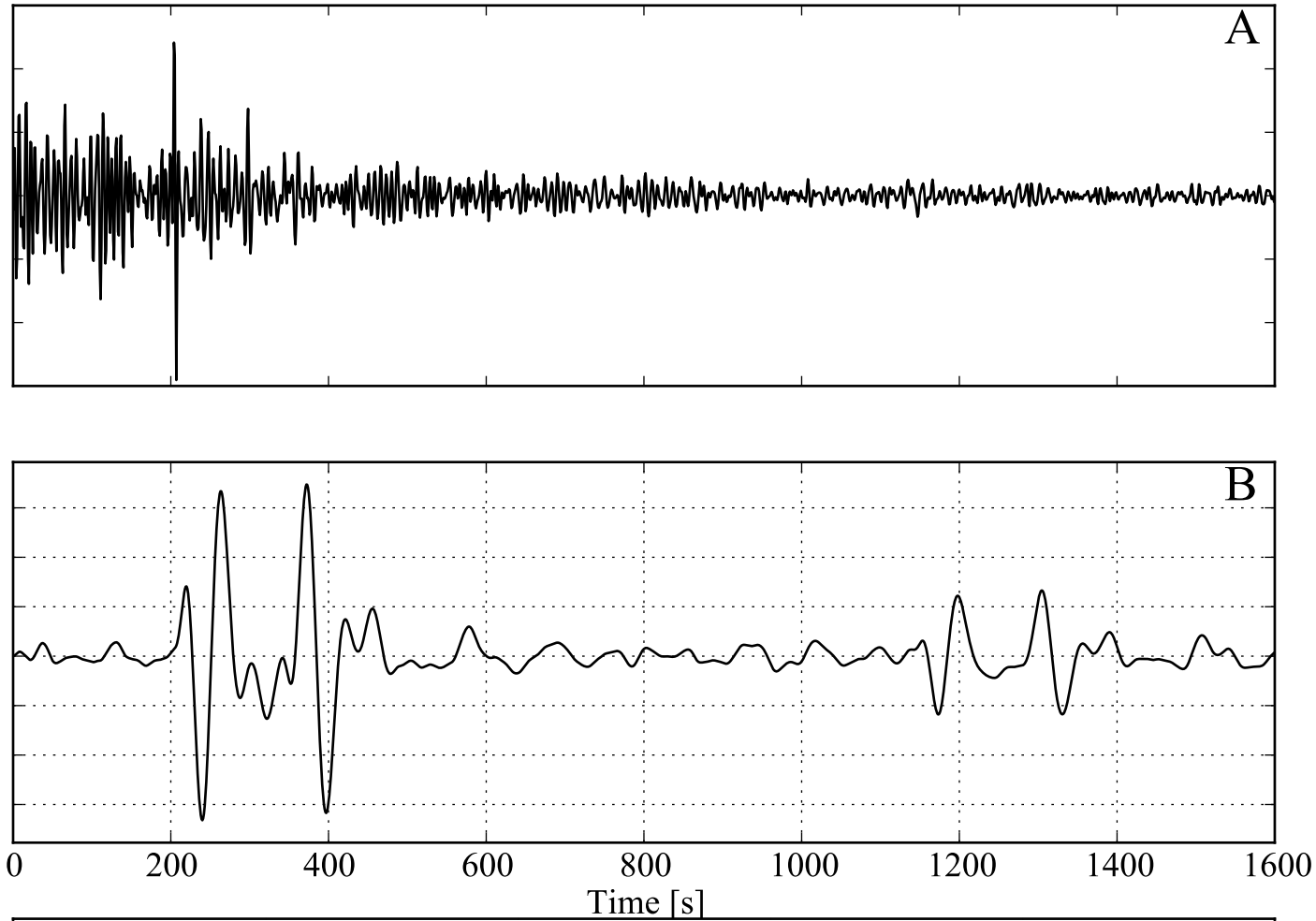


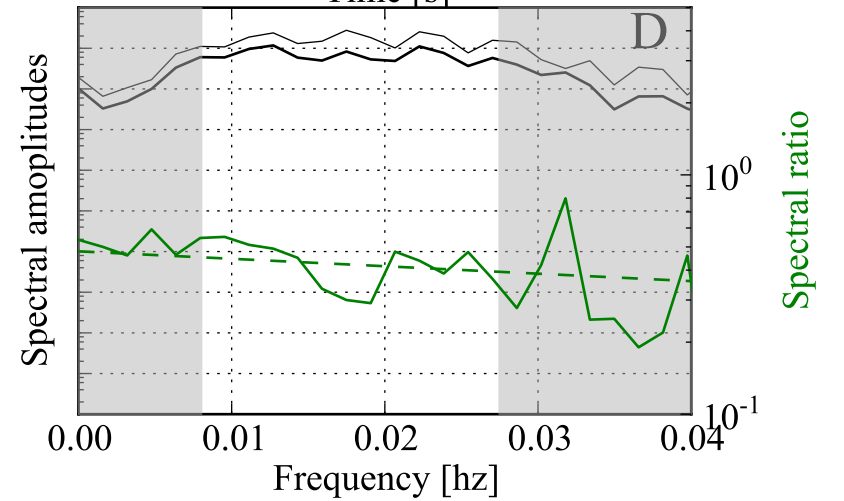
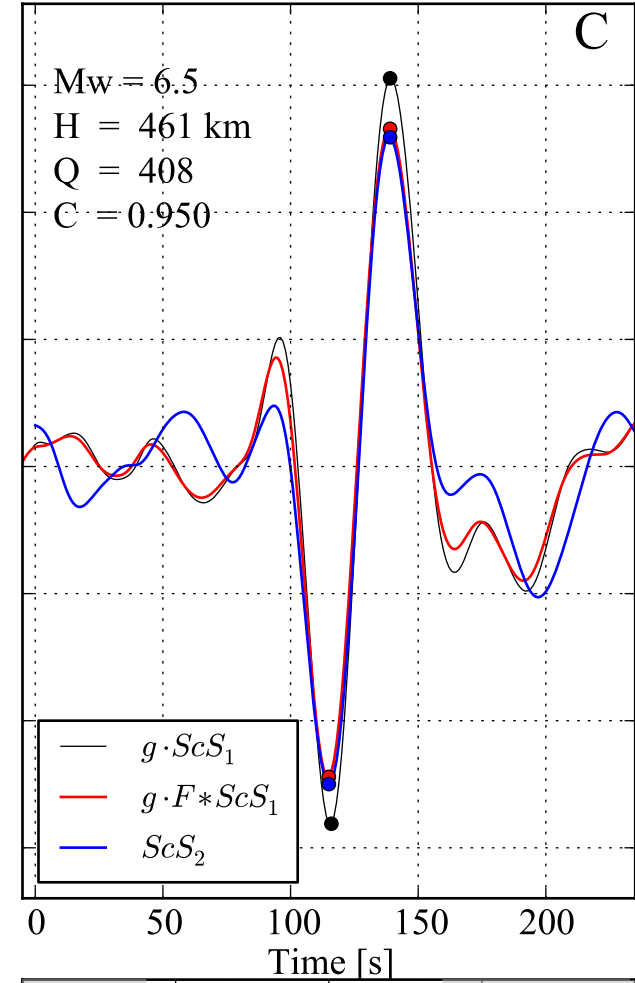
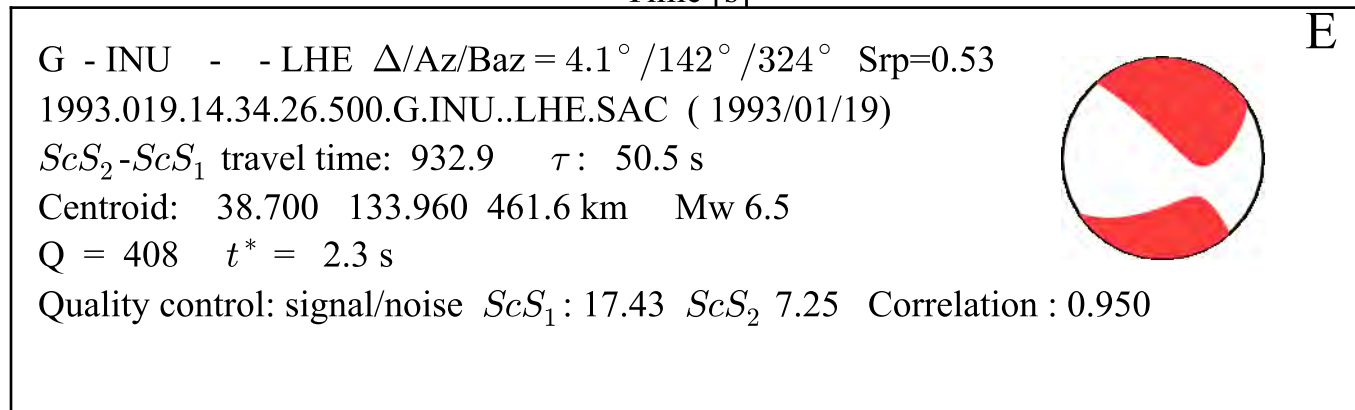
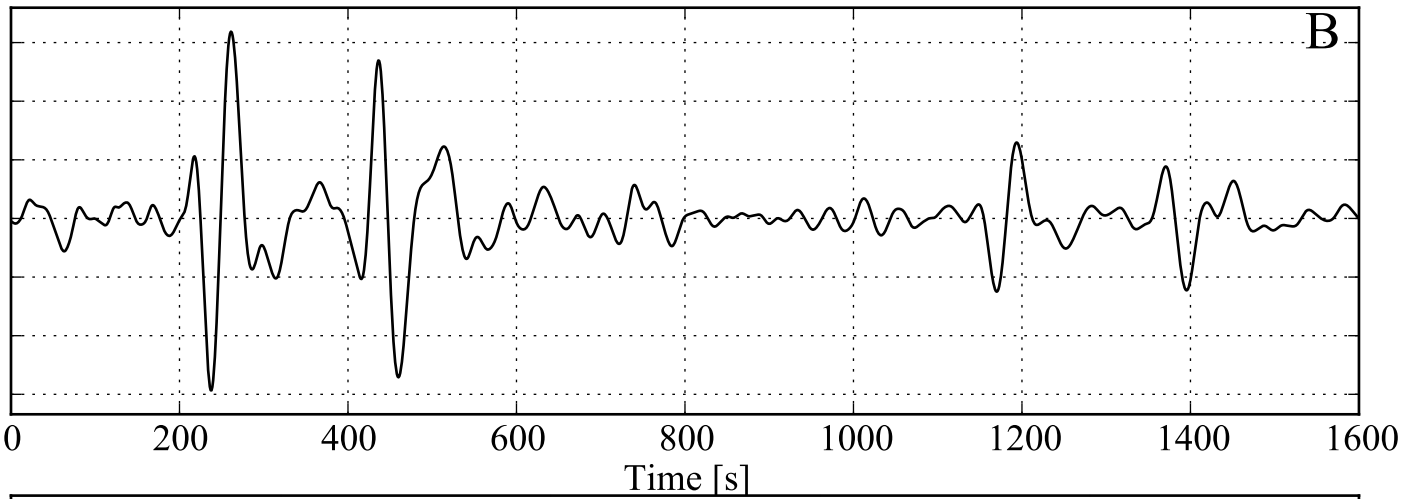
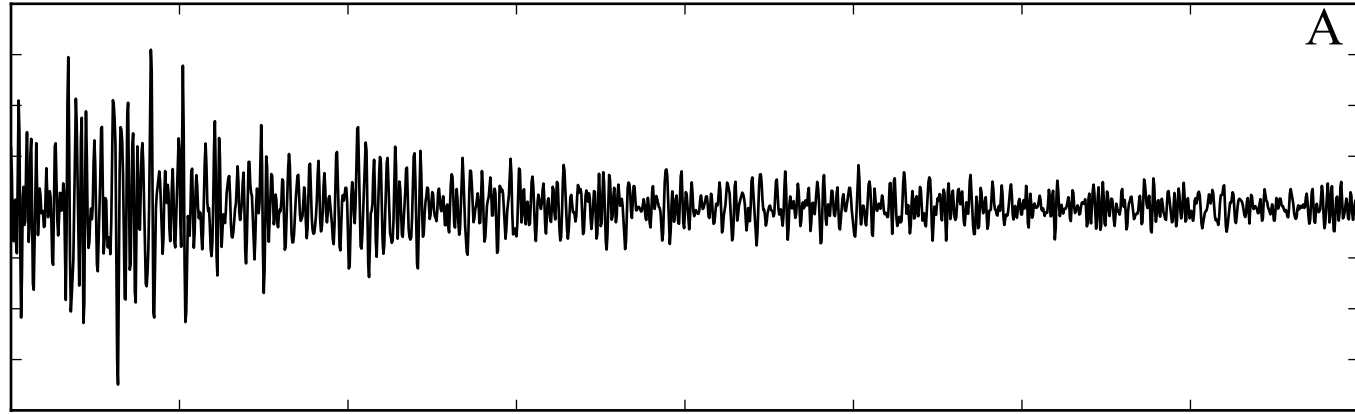
E

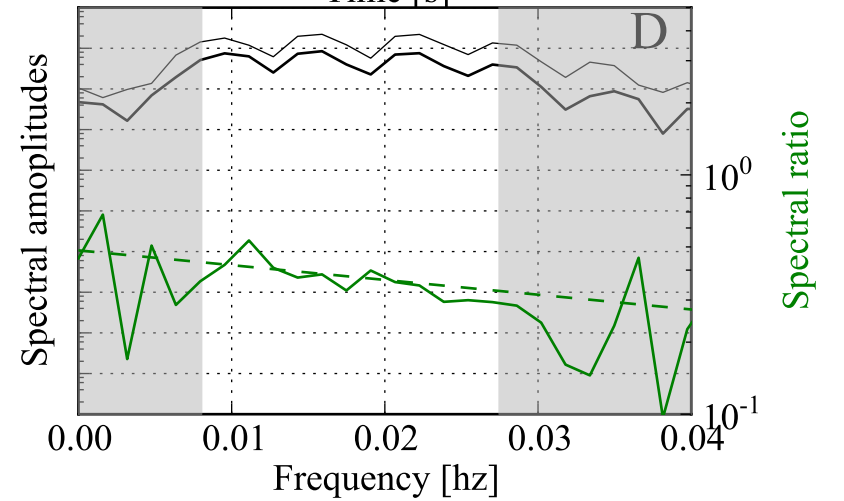
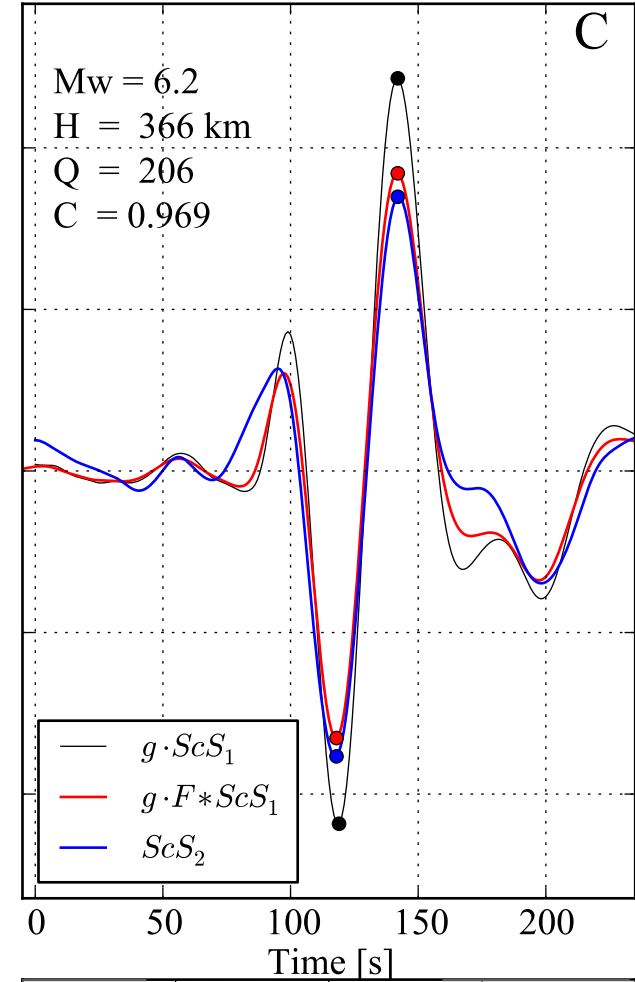
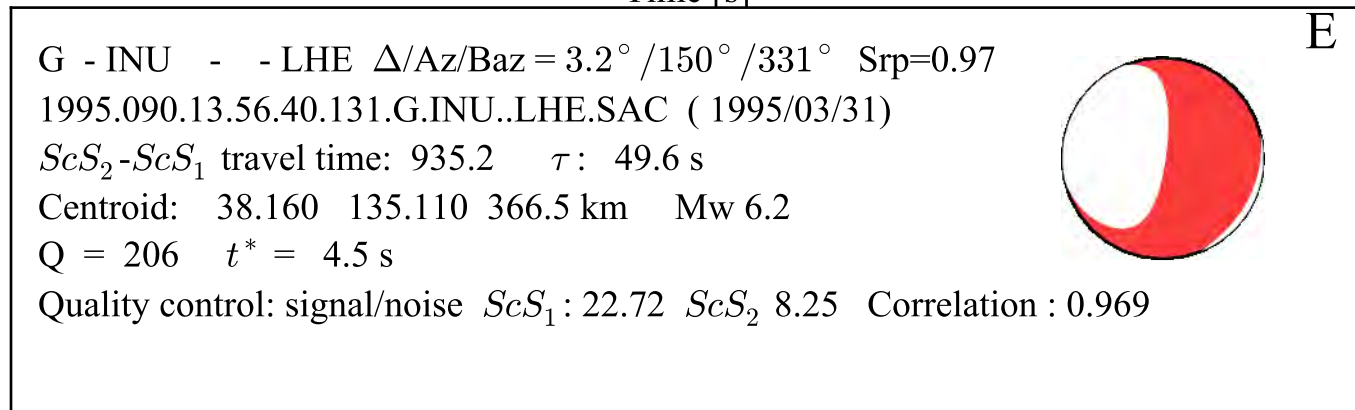
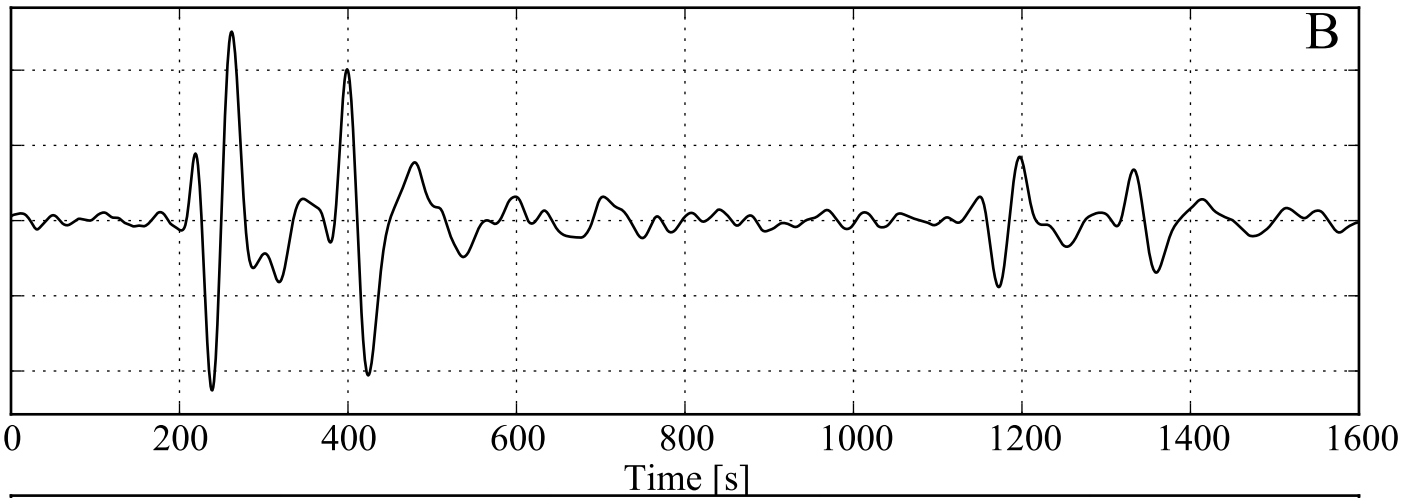
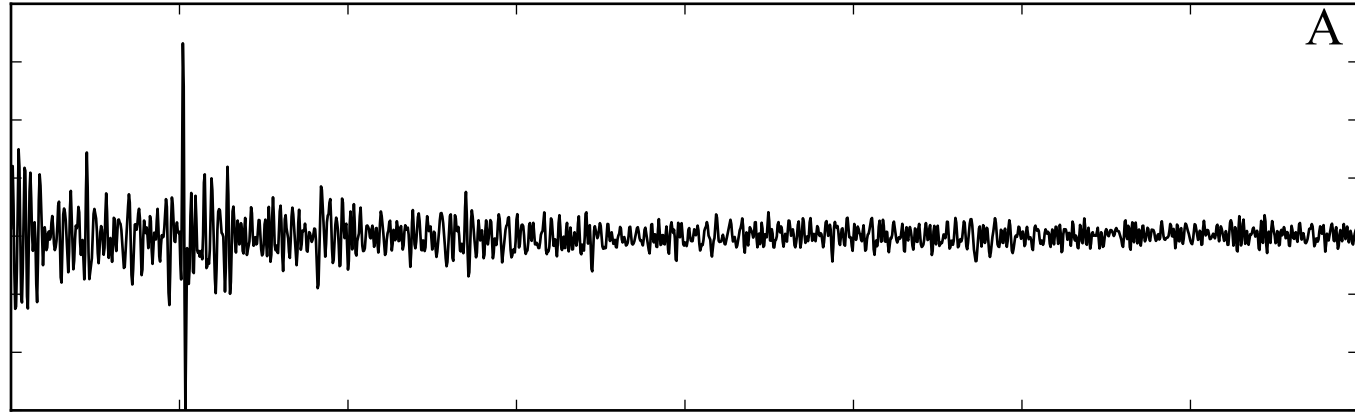
IU - HNR - 10 - LHX $\Delta/Az/Baz = 2.7^\circ / 301^\circ / 122^\circ$ Srp=0.68
 2004.282.08.22.53.296.IU.HNR.10.LHX.SAC (2004/10/08)
 $ScS_2 - ScS_1$ travel time: 939.0 τ : 45.0 s
 Centroid: -10.870 162.270 40.0 km Mw 6.7
 Q = 864 $t^* = 1.1$ s
 Quality control: signal/noise ScS_1 : 12.93 ScS_2 5.97 Correlation : 0.896

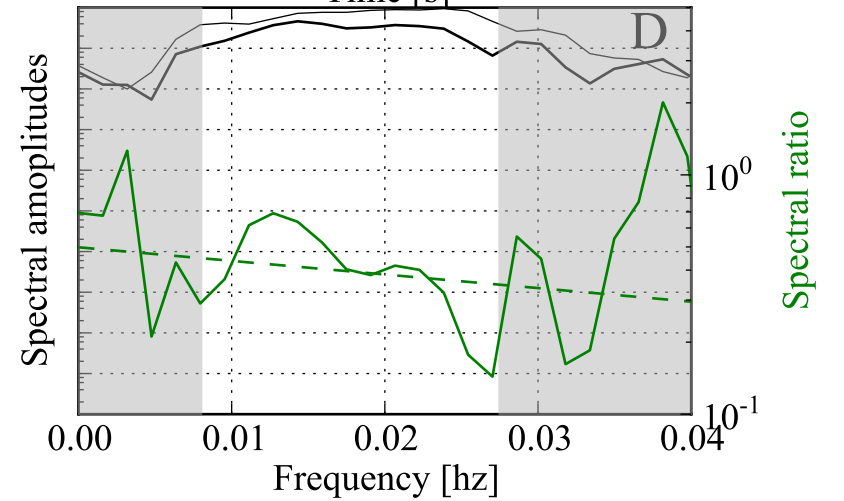
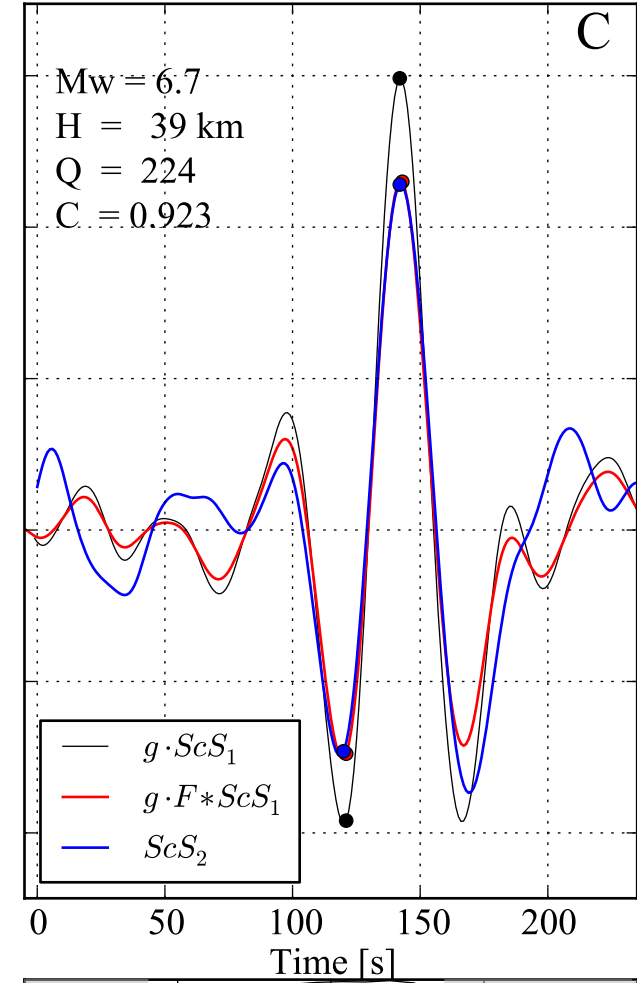
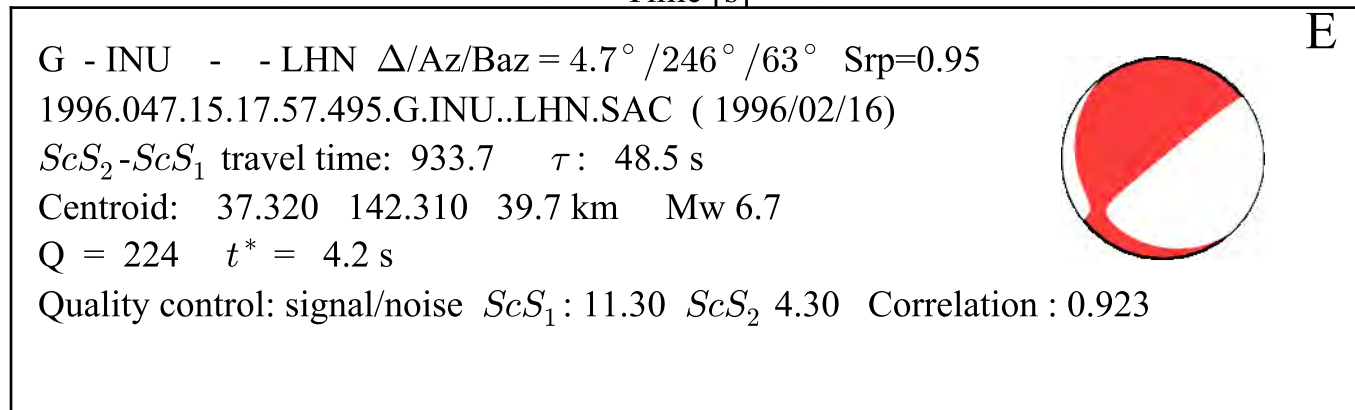
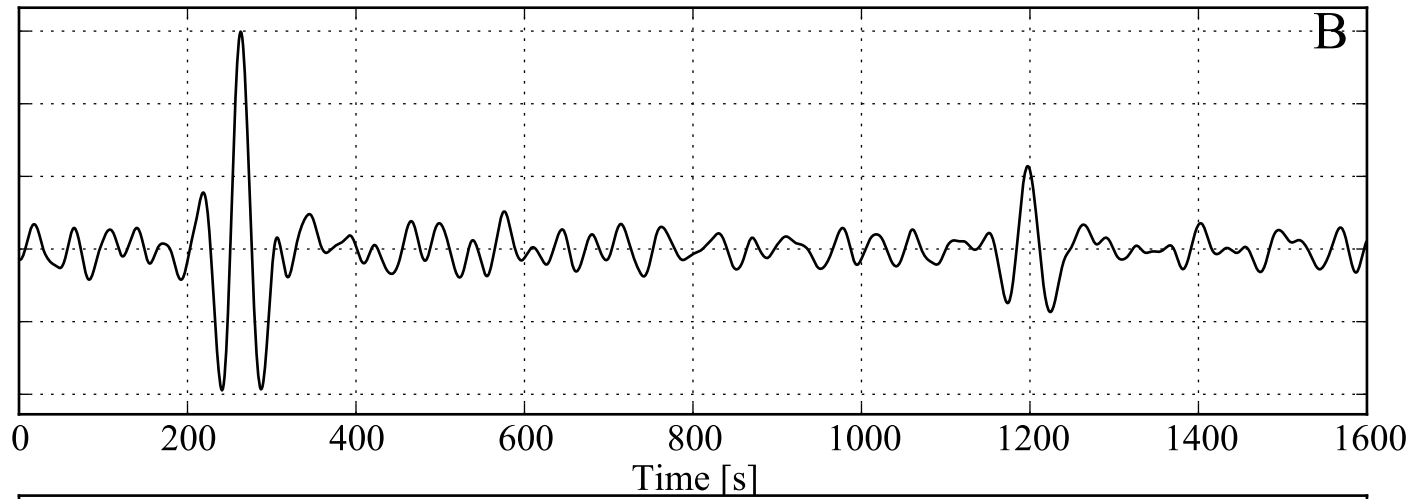
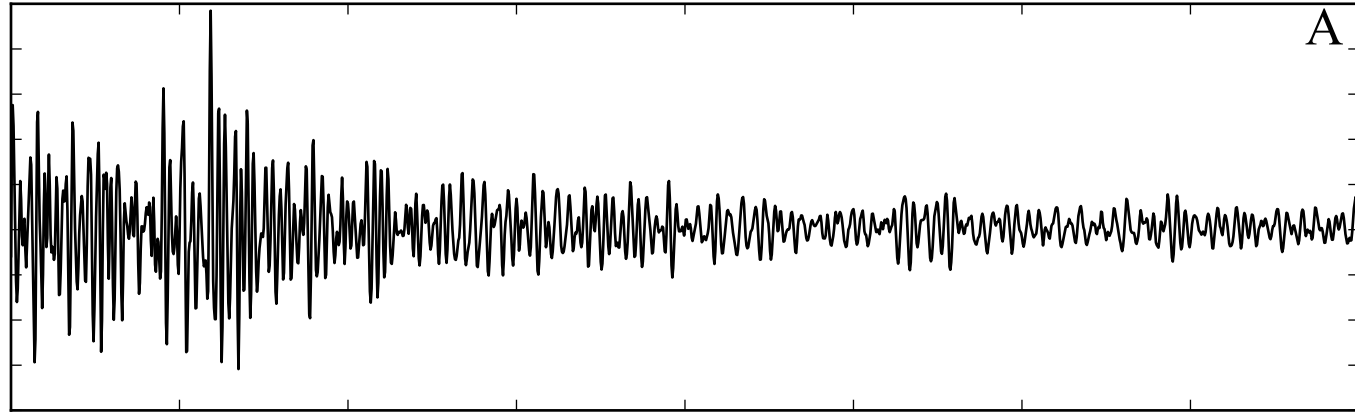


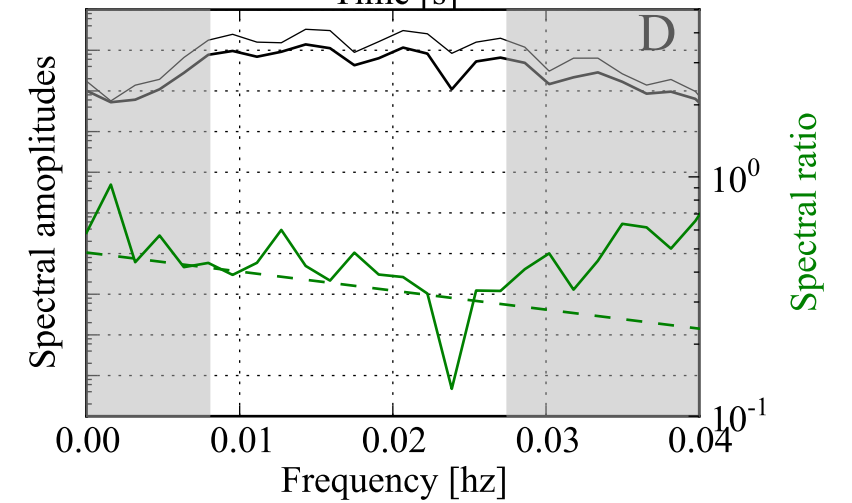
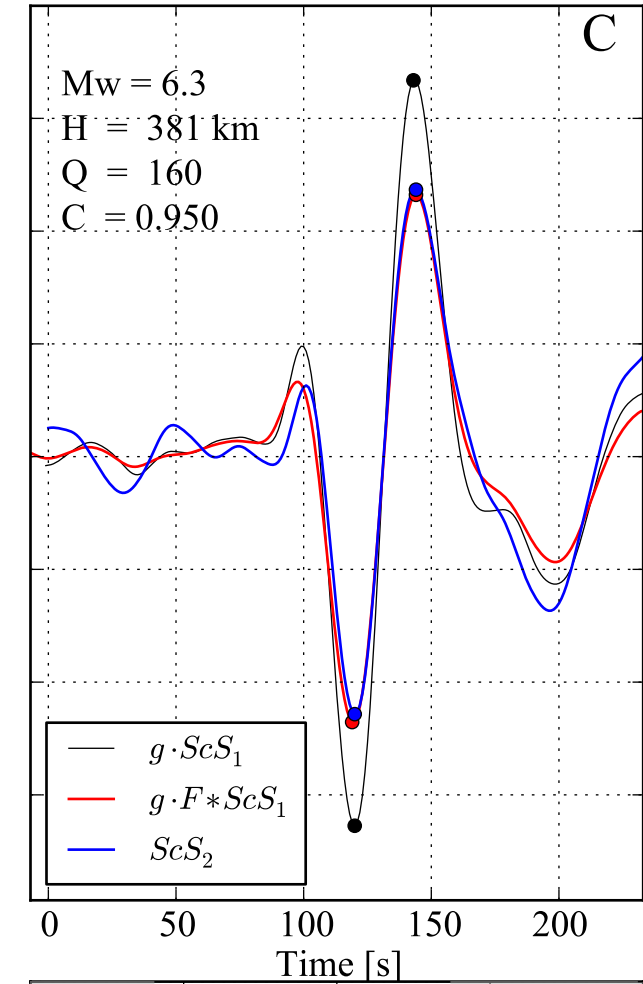
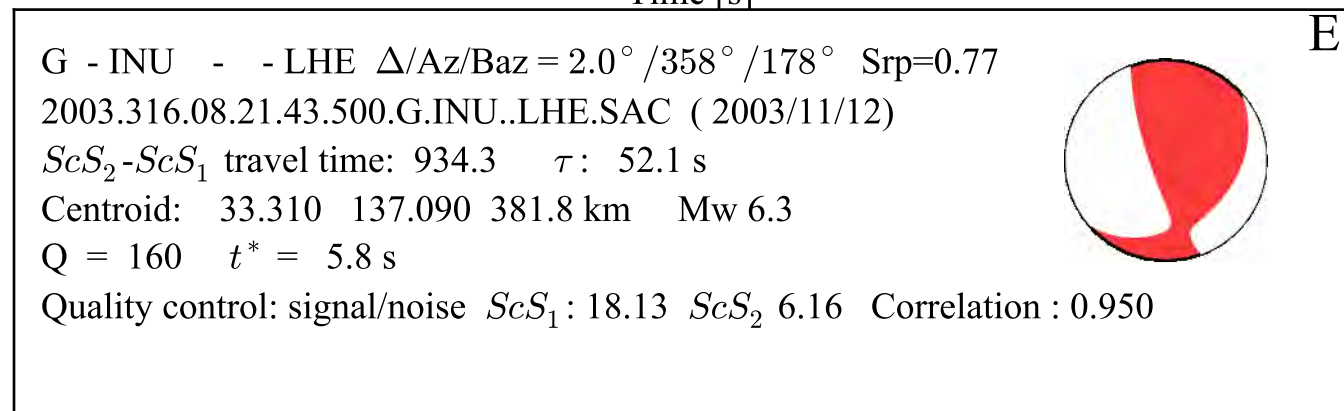
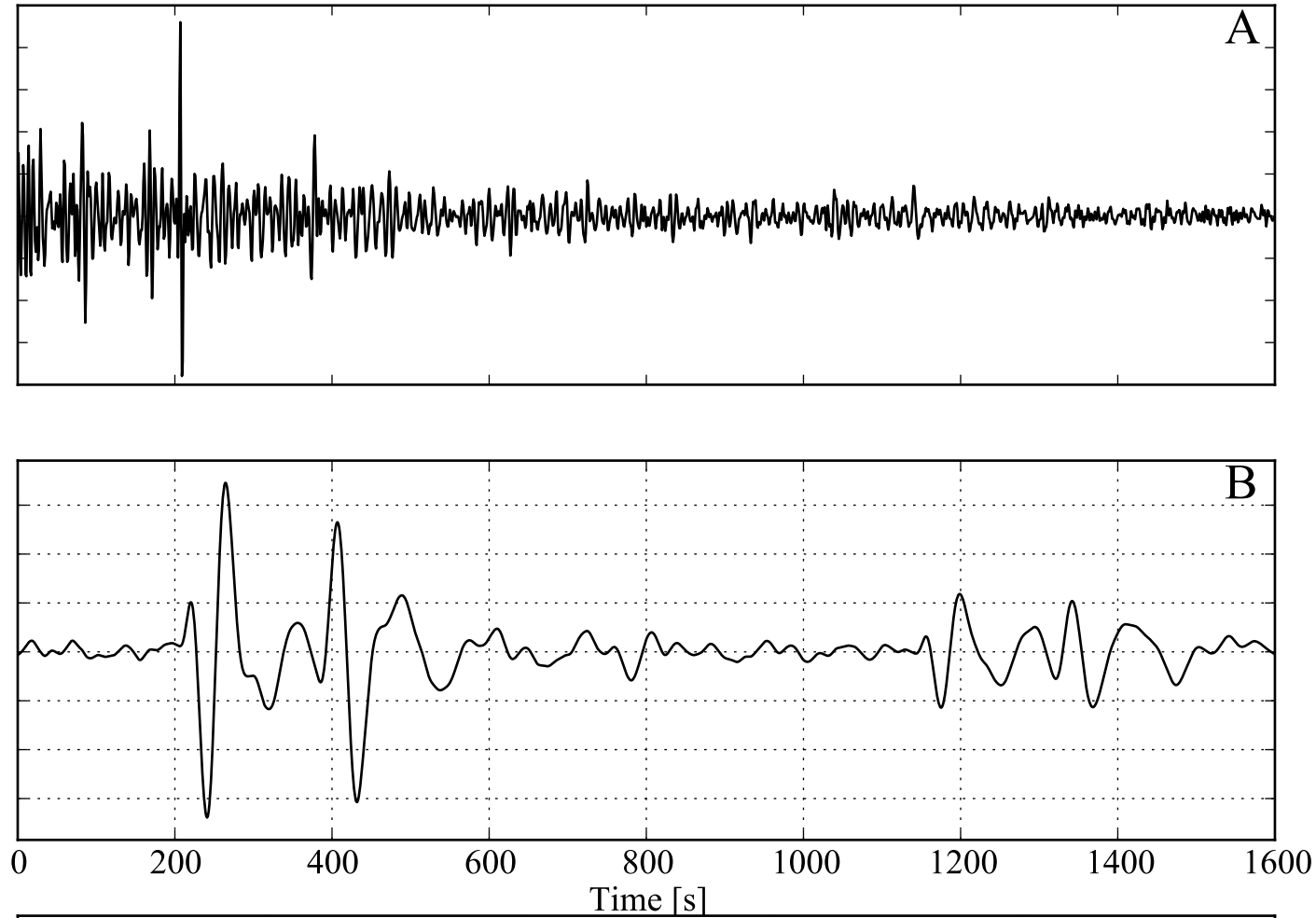


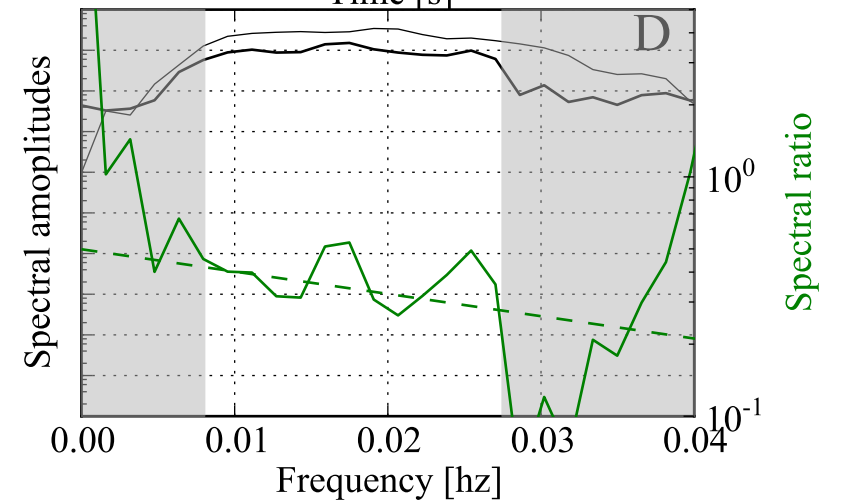
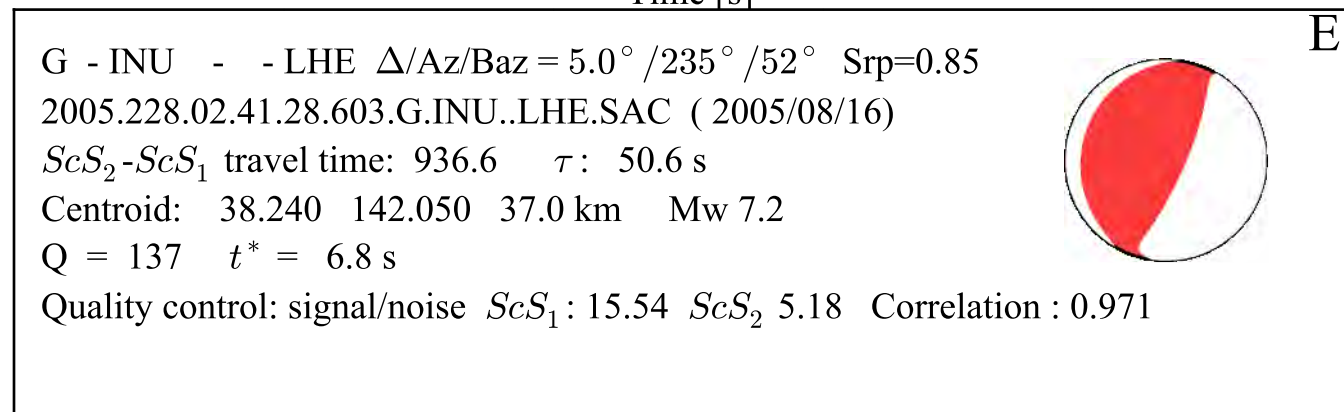
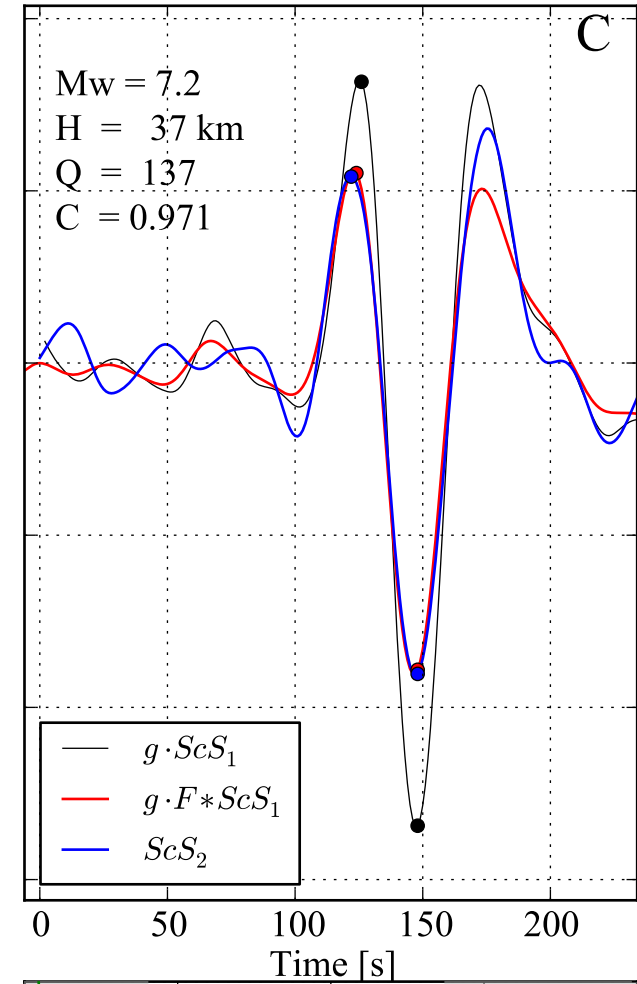
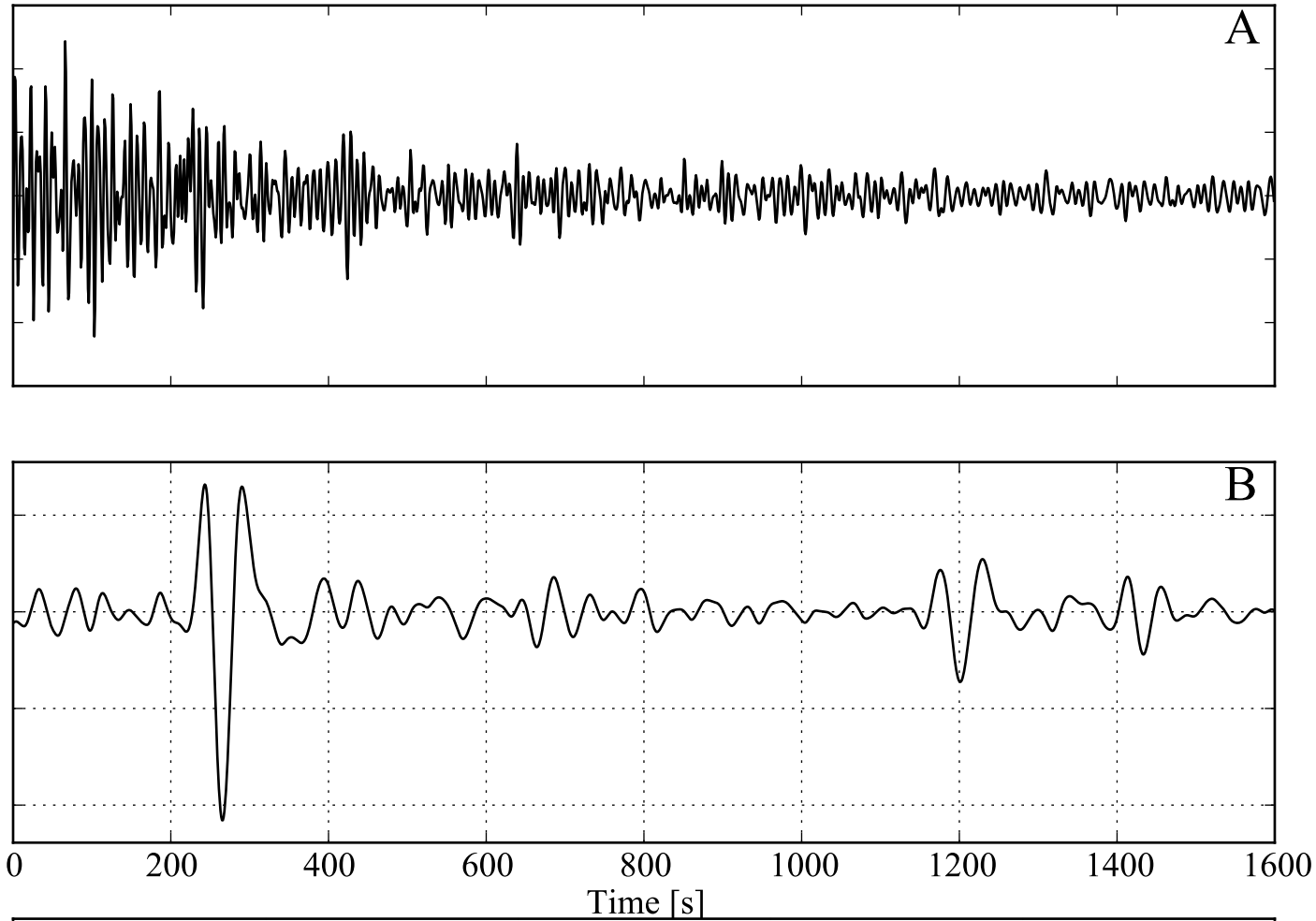


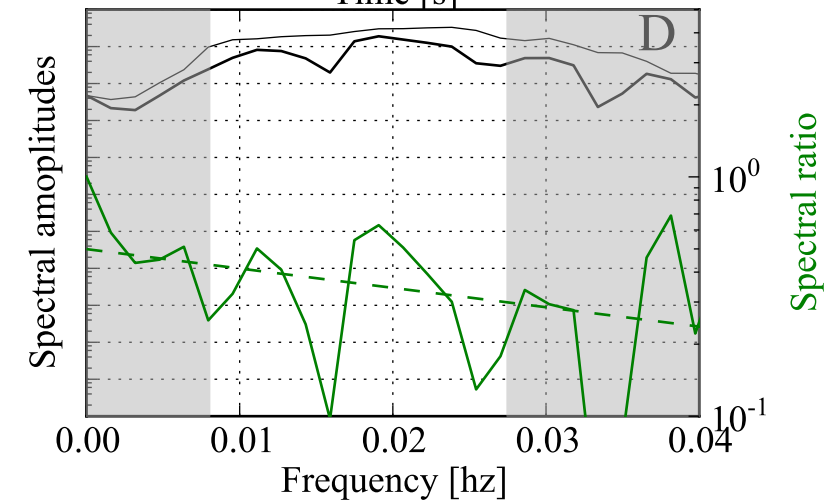
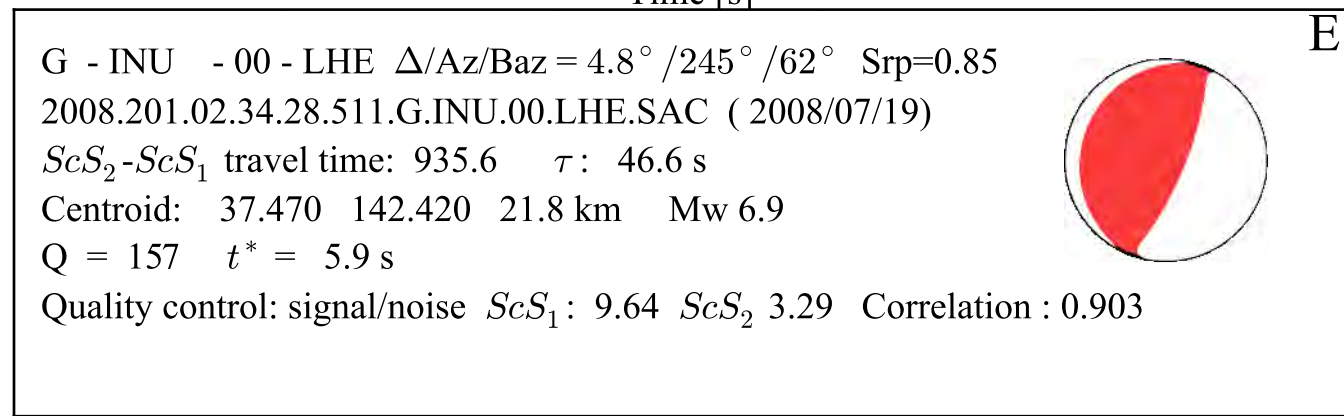
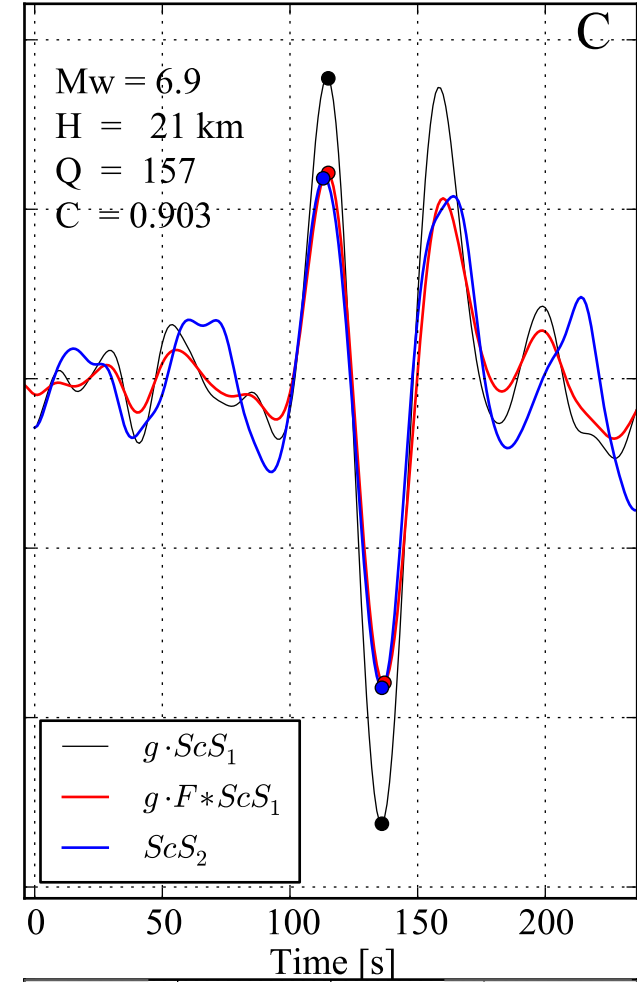
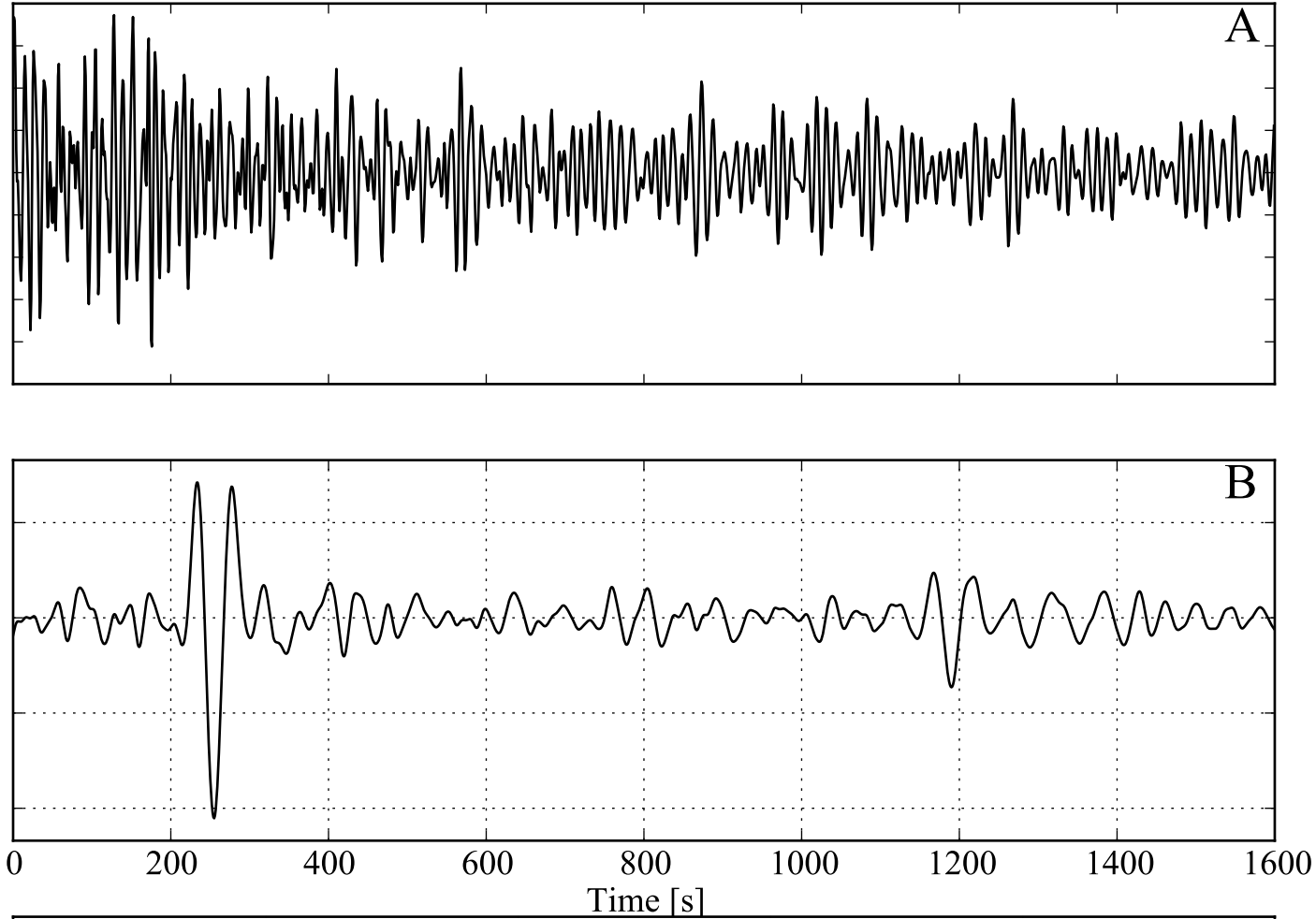


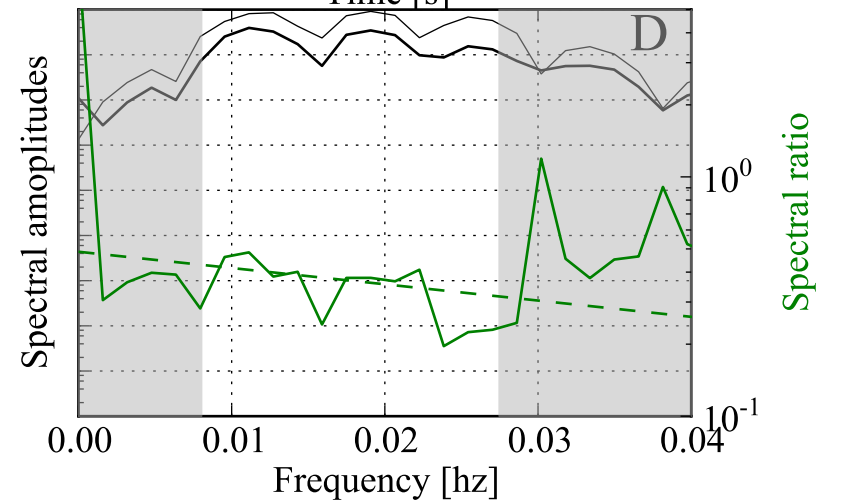
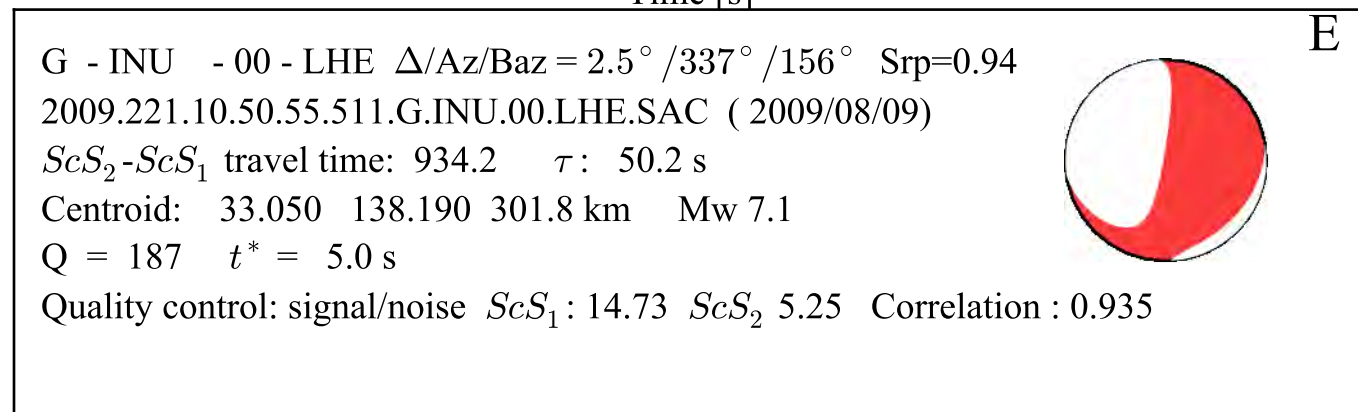
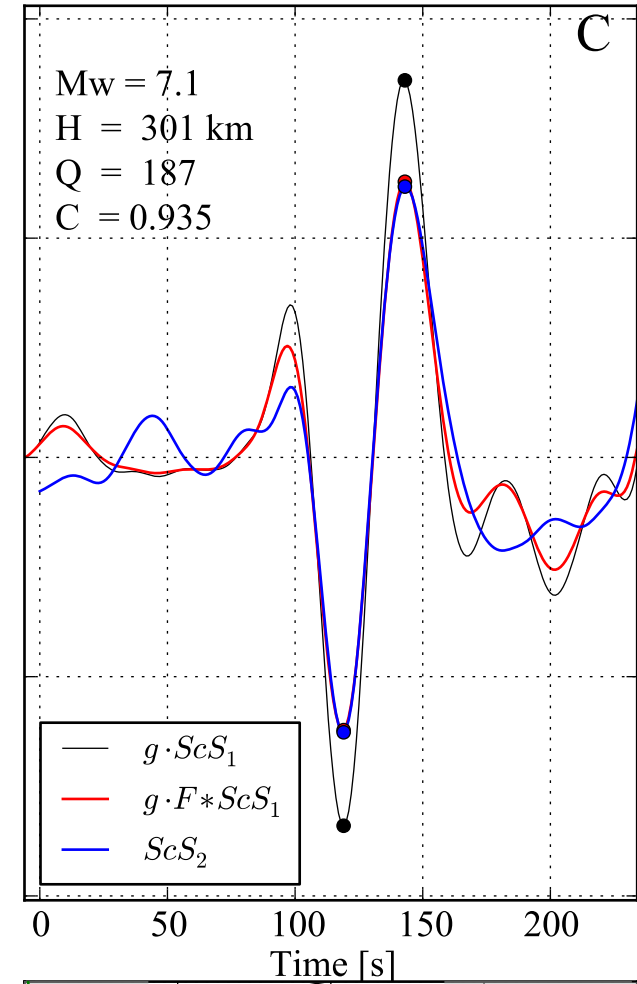
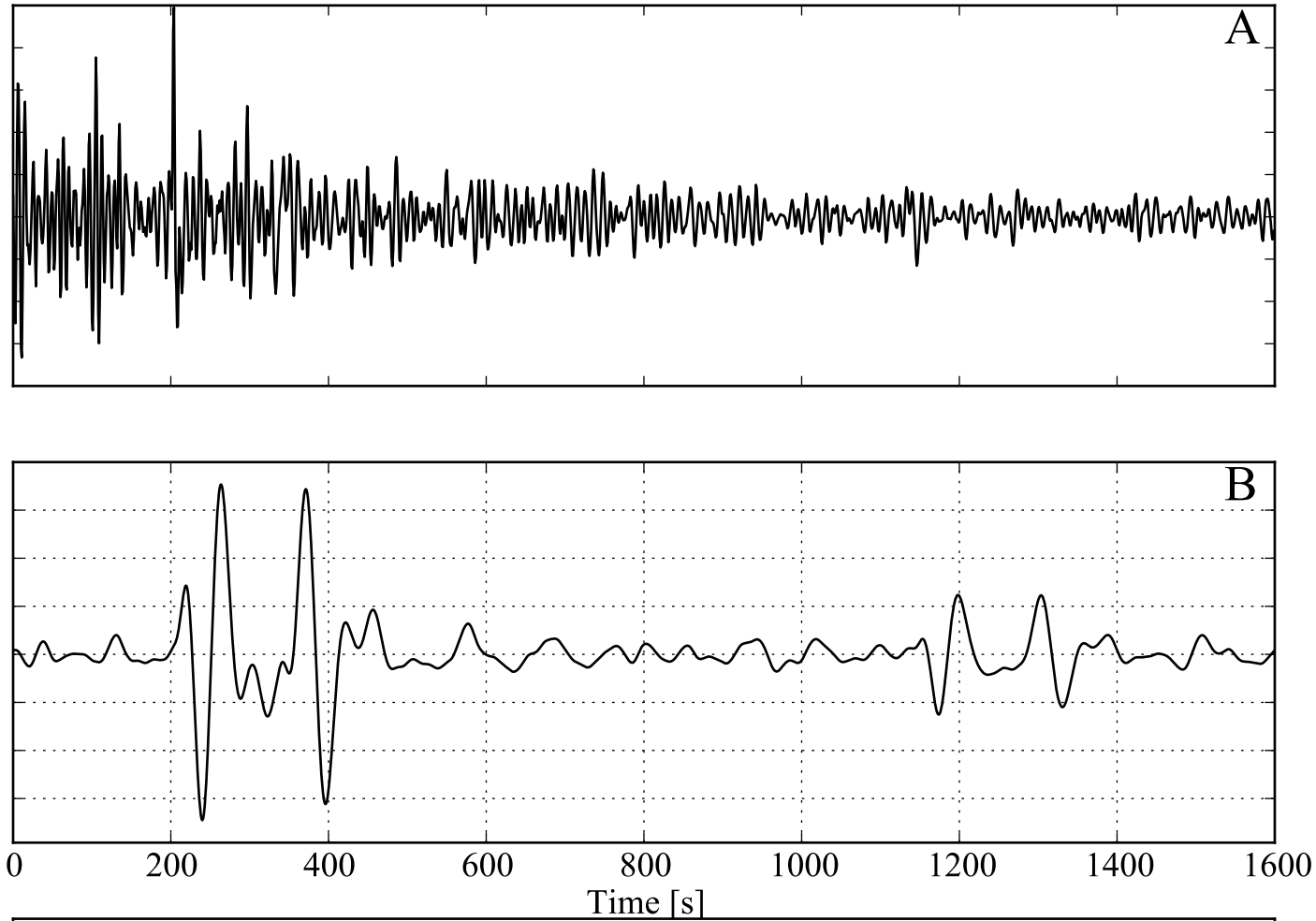


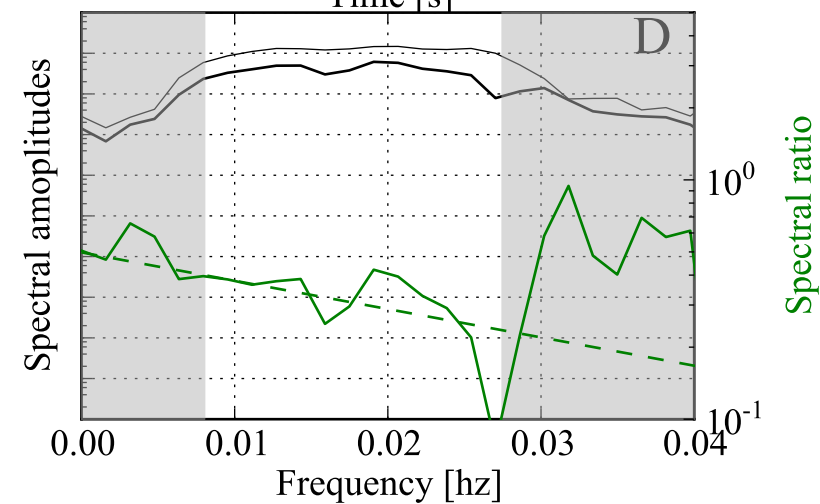
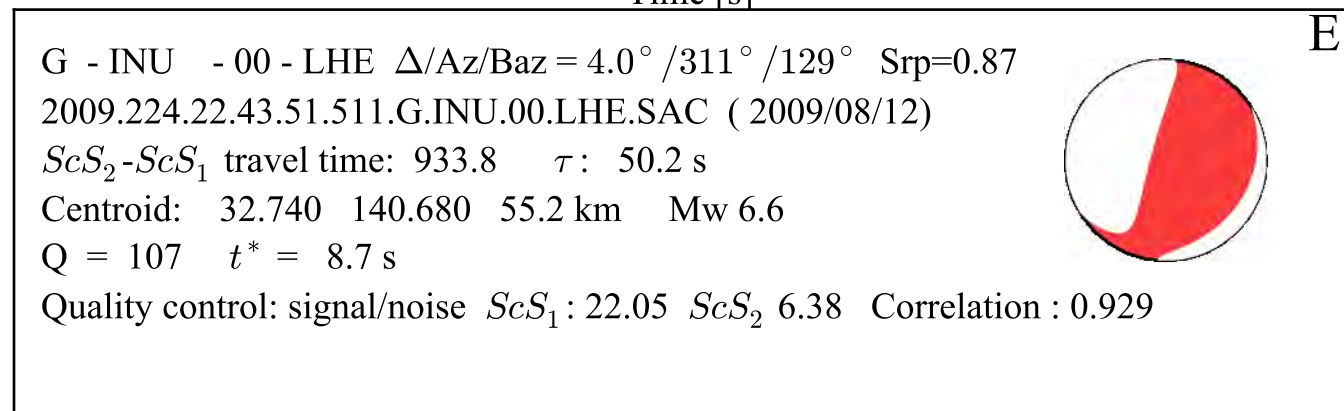
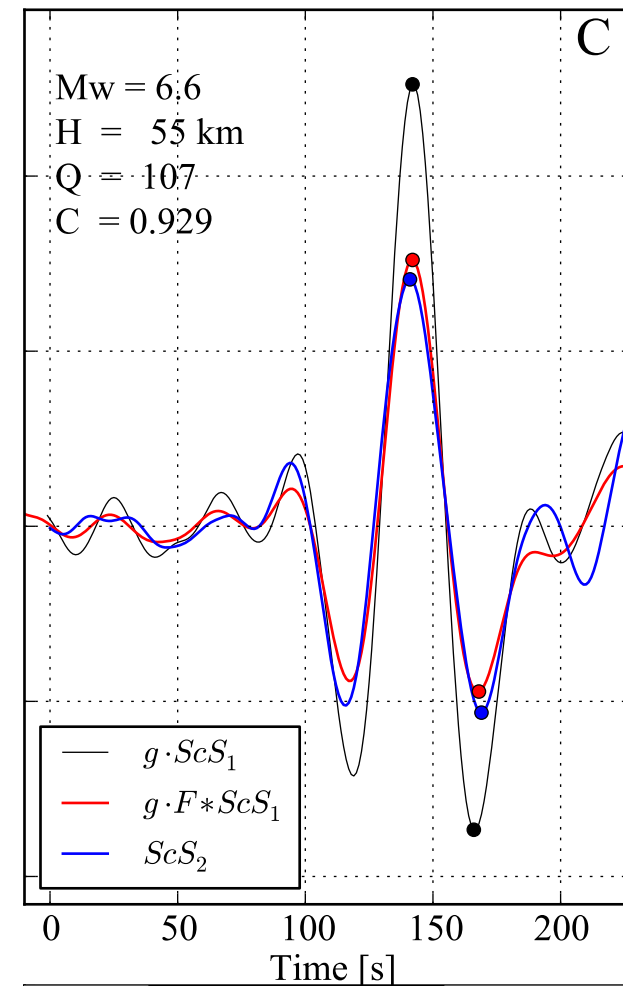
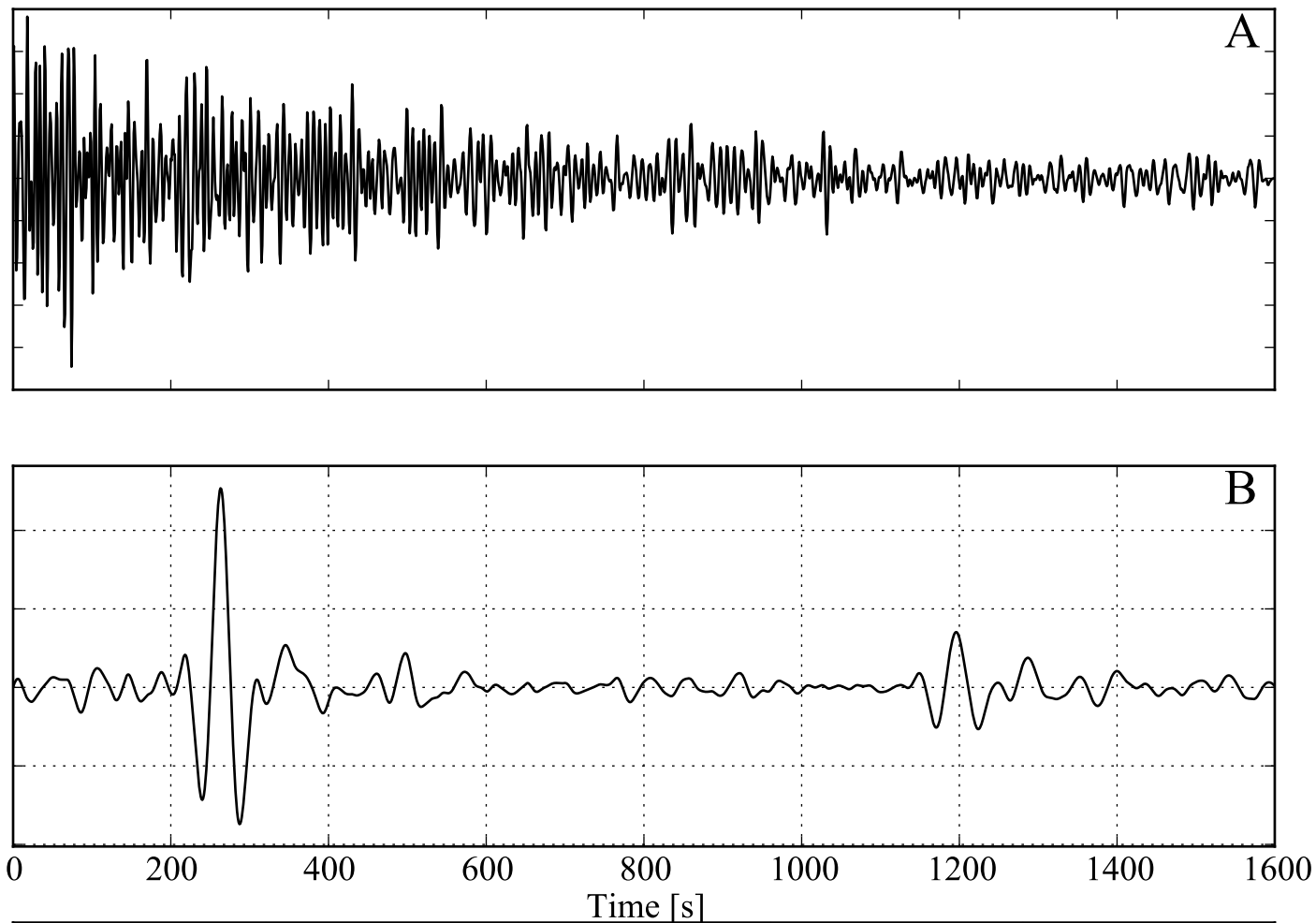


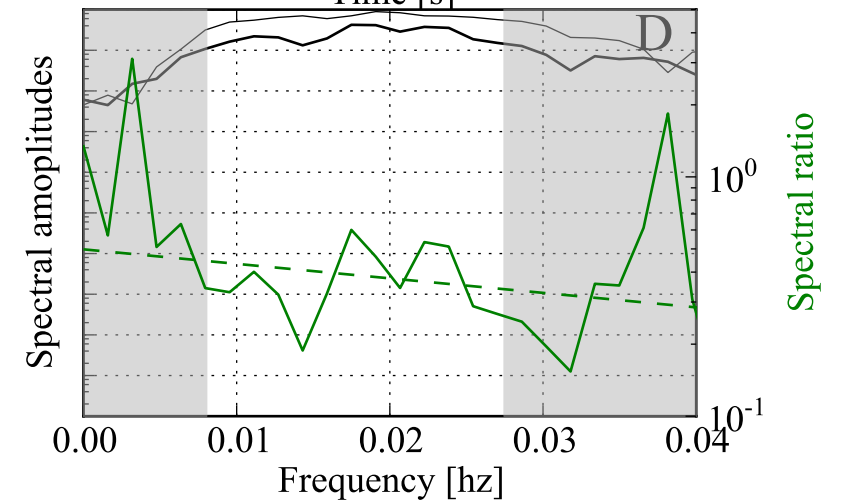
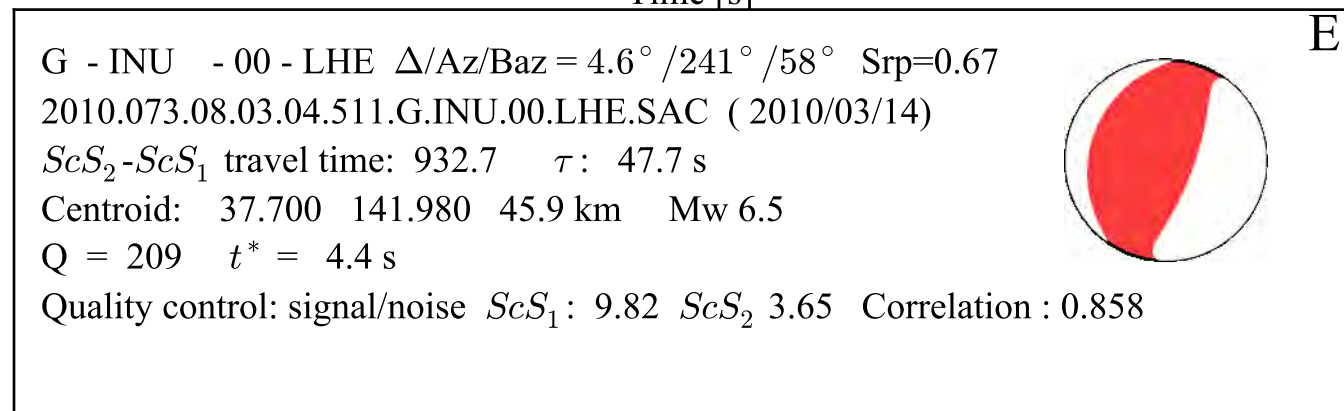
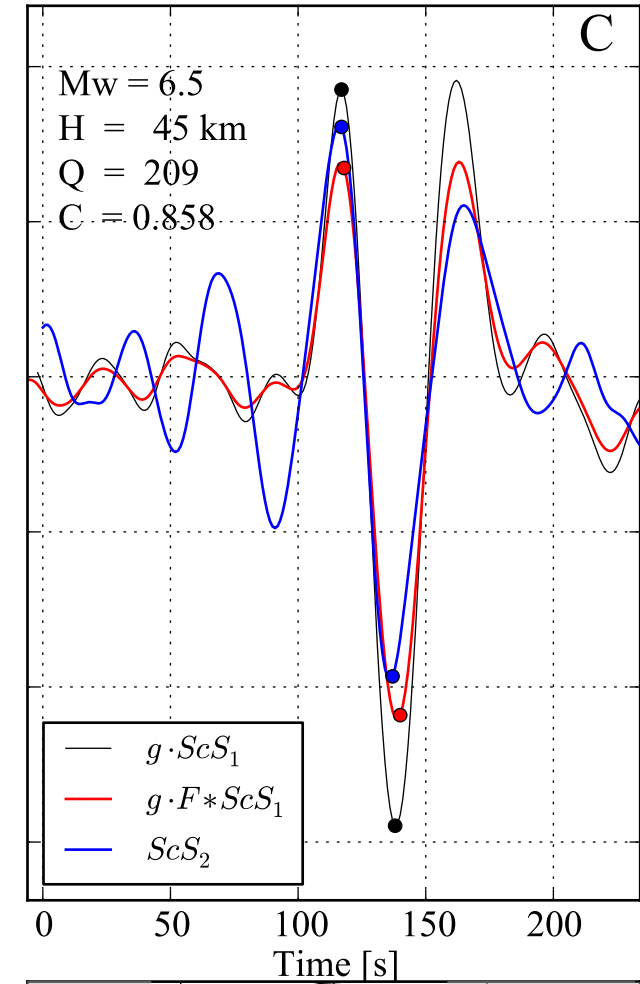
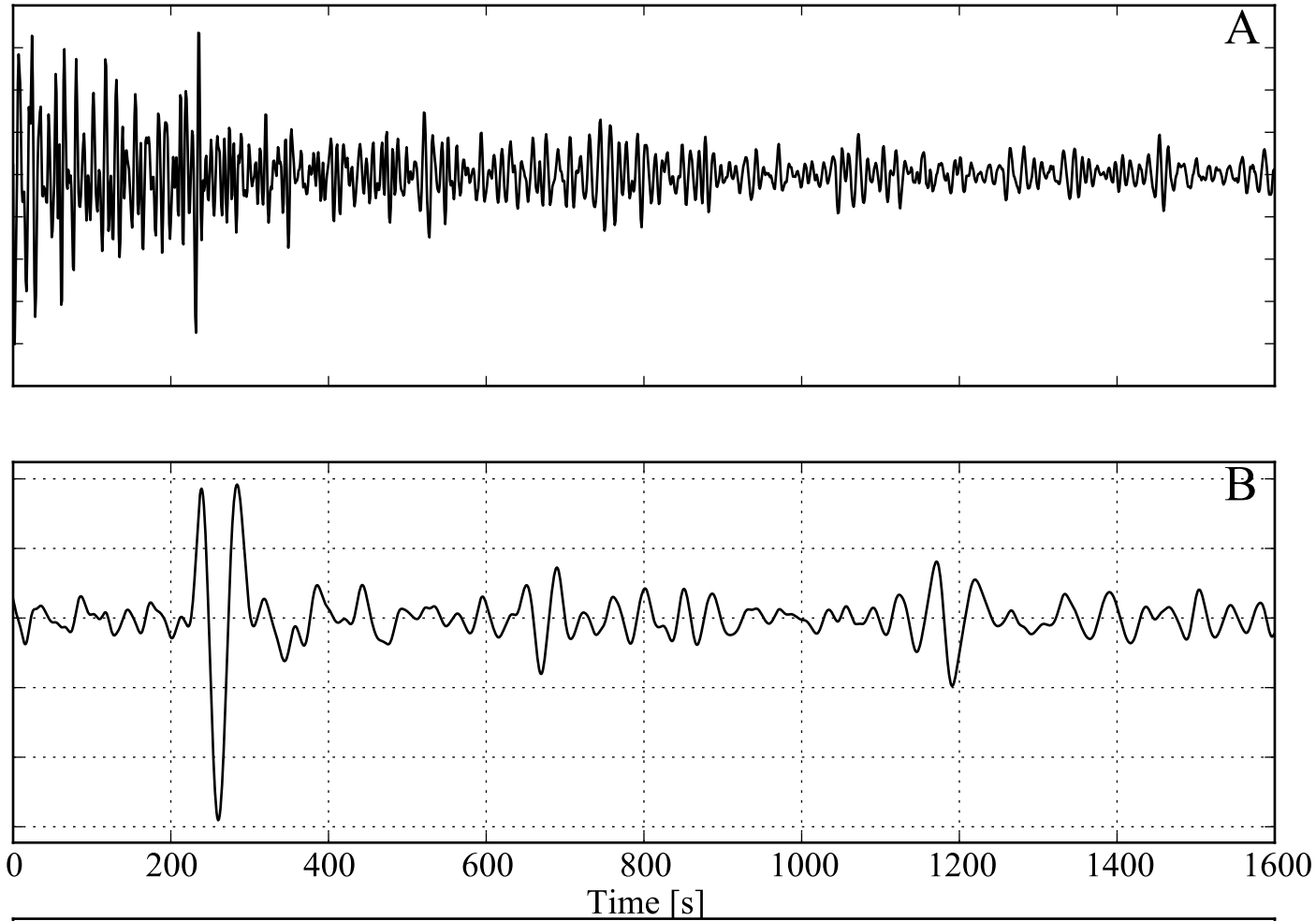


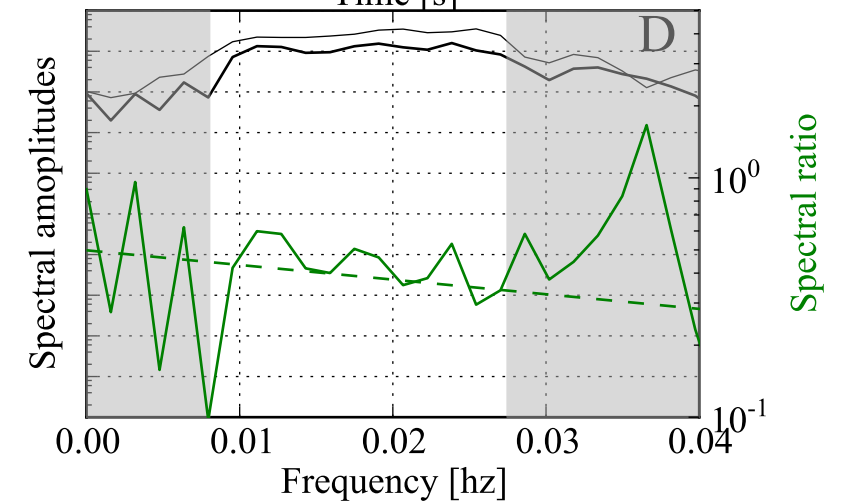
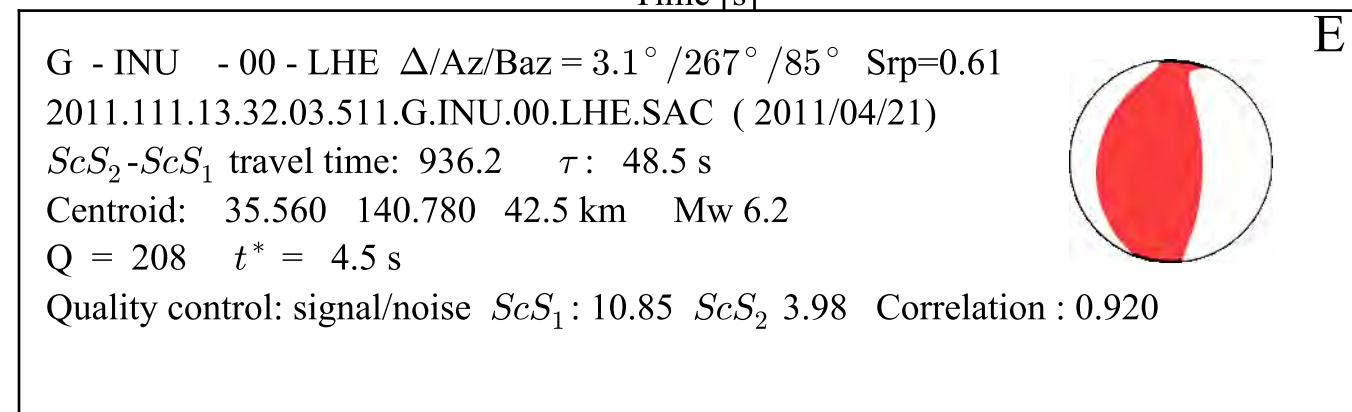
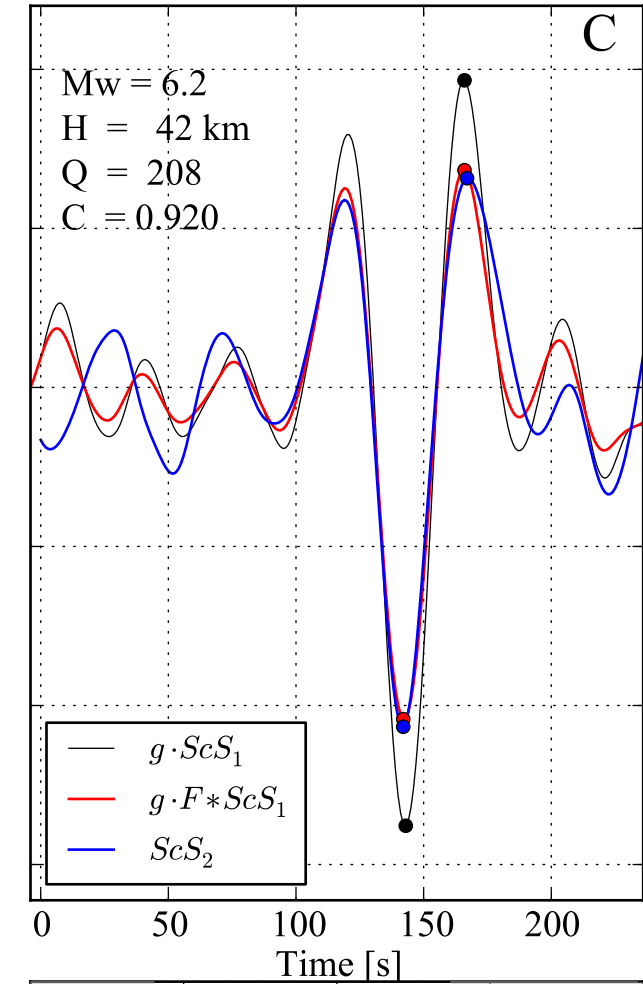
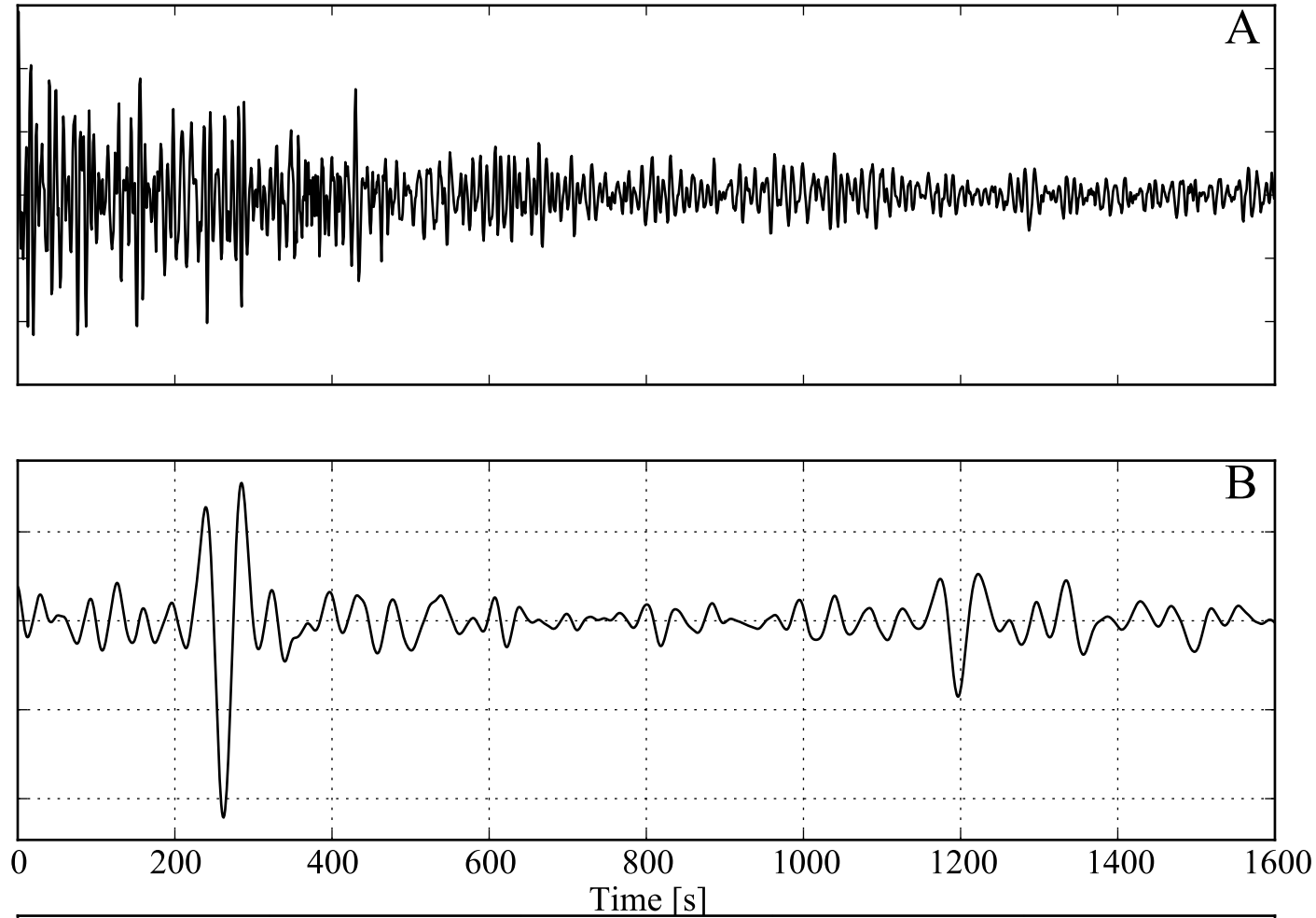


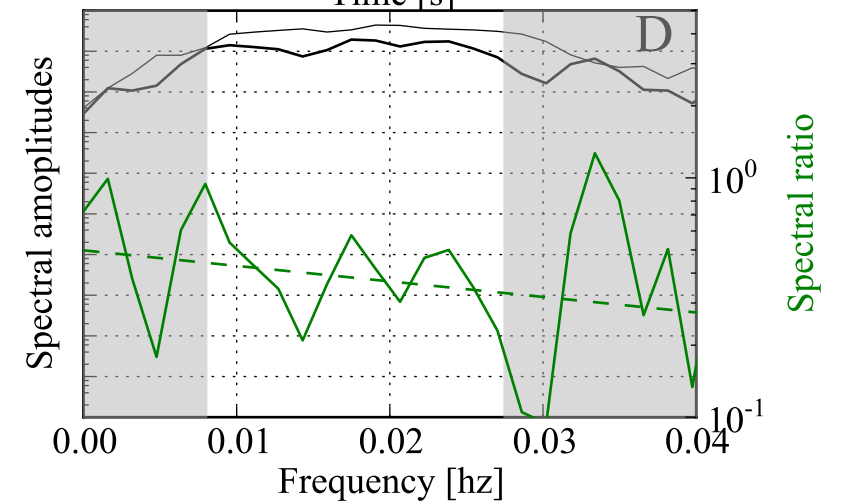
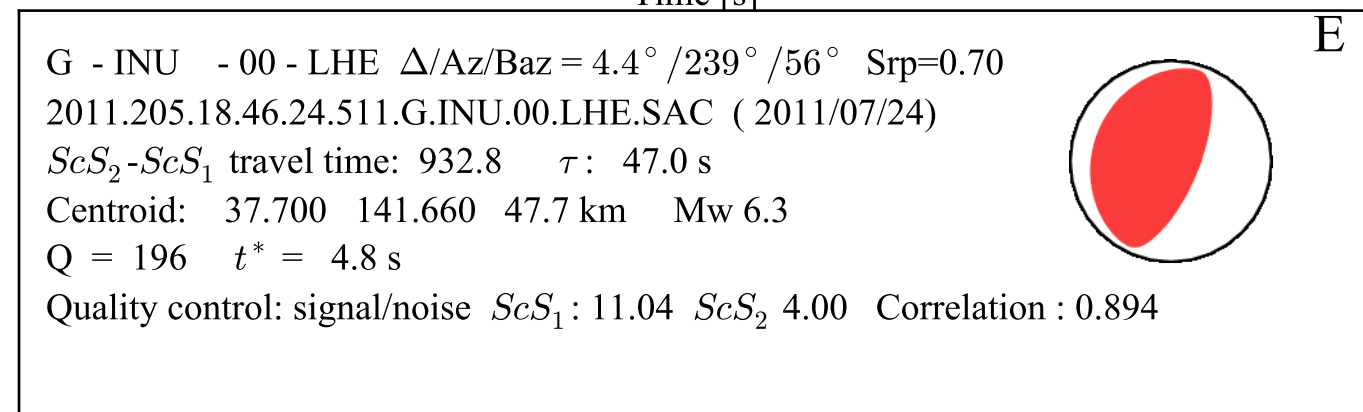
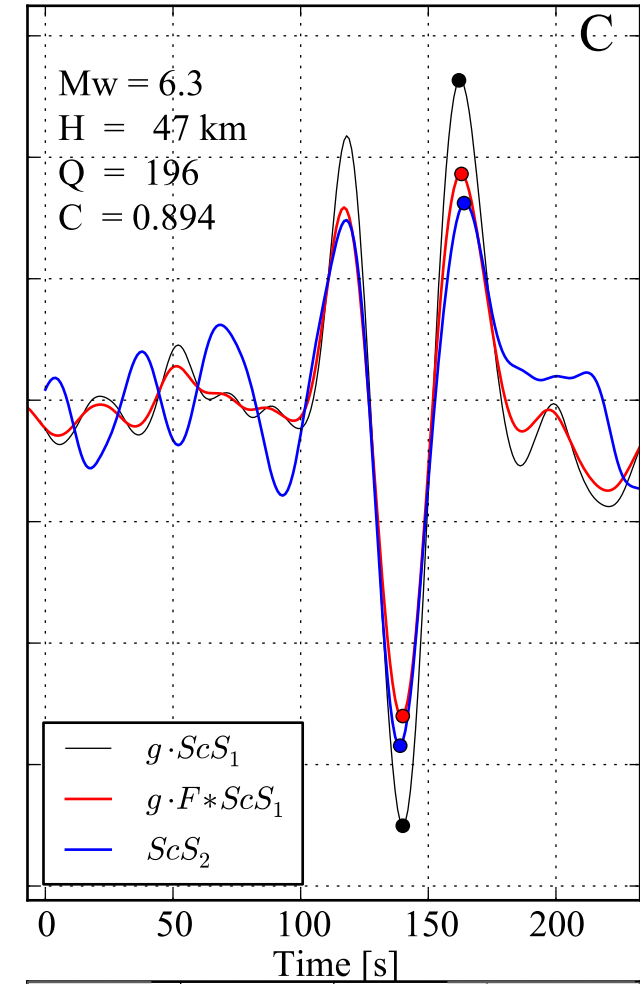
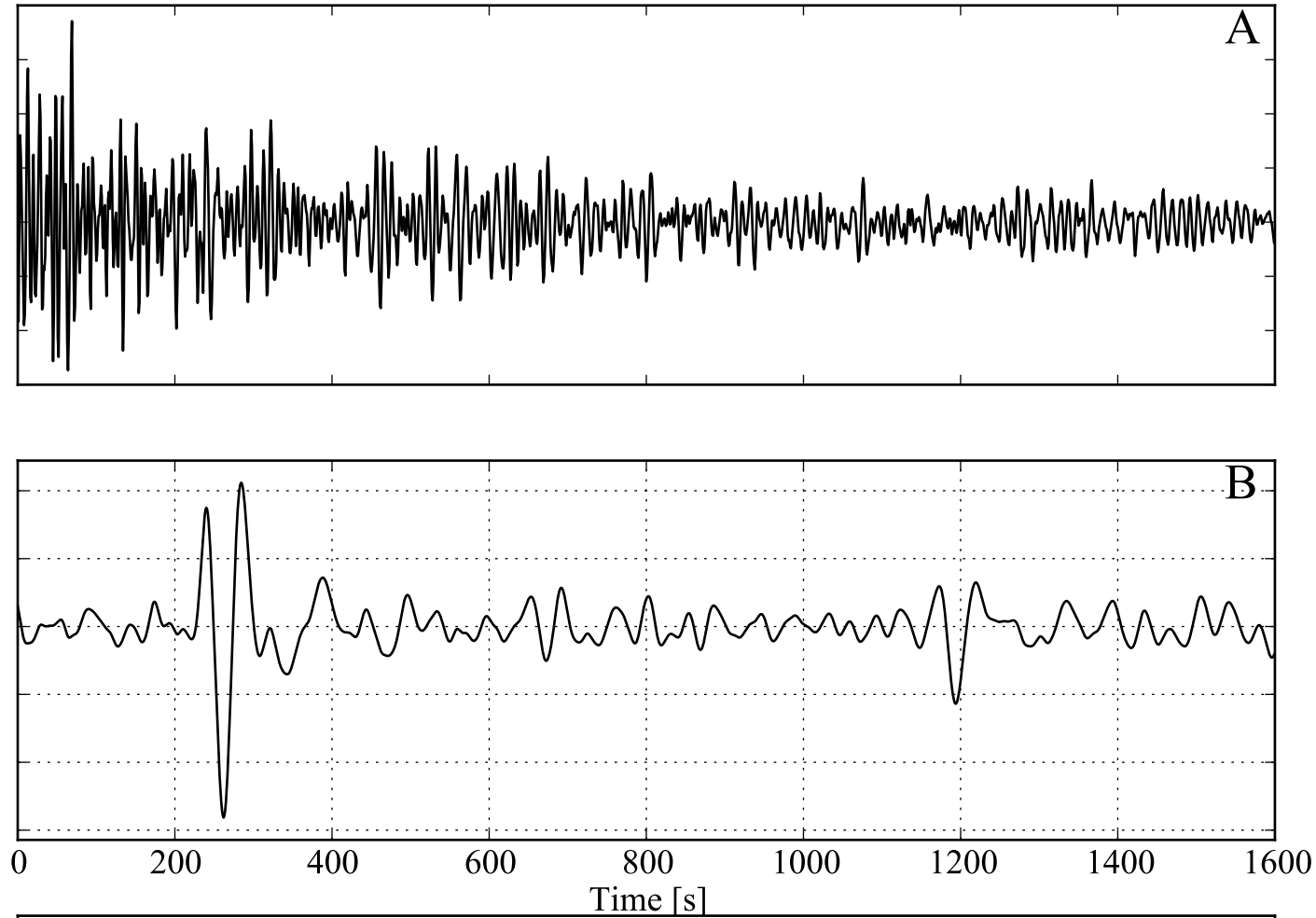


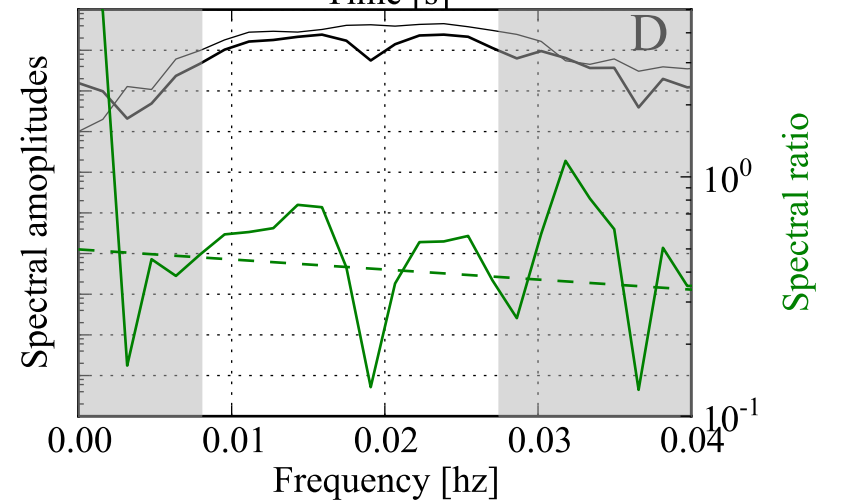
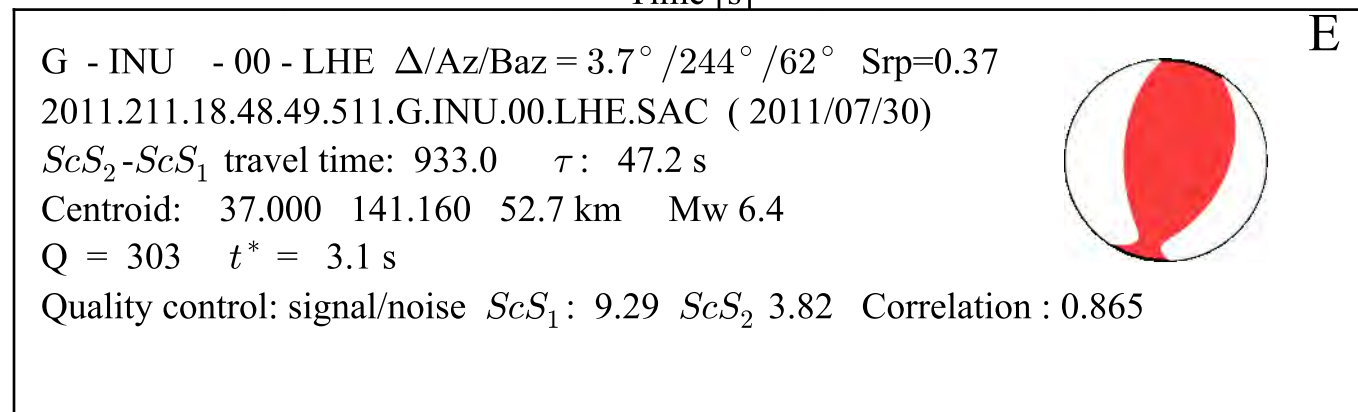
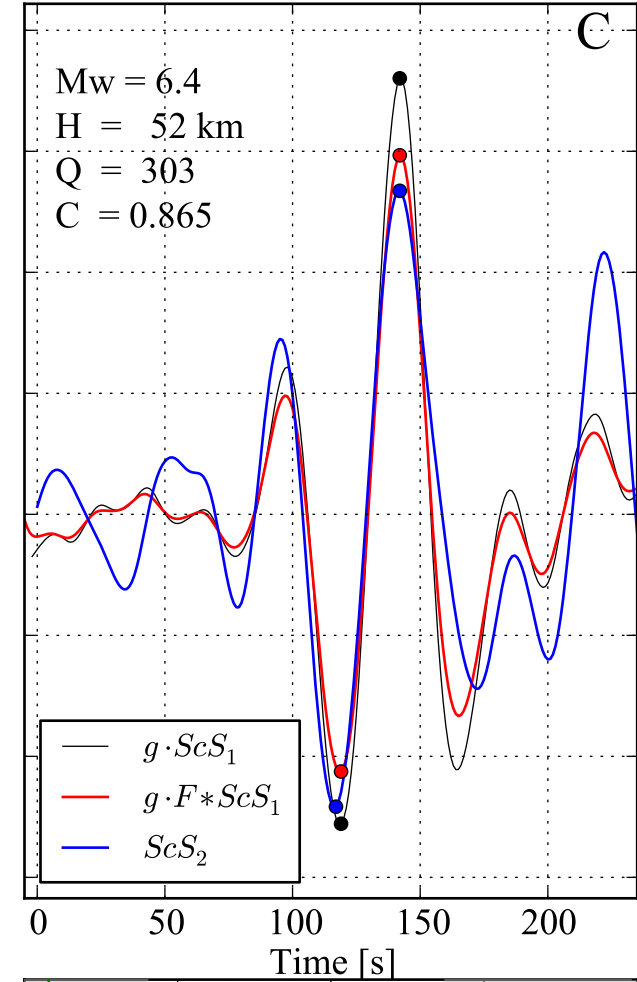
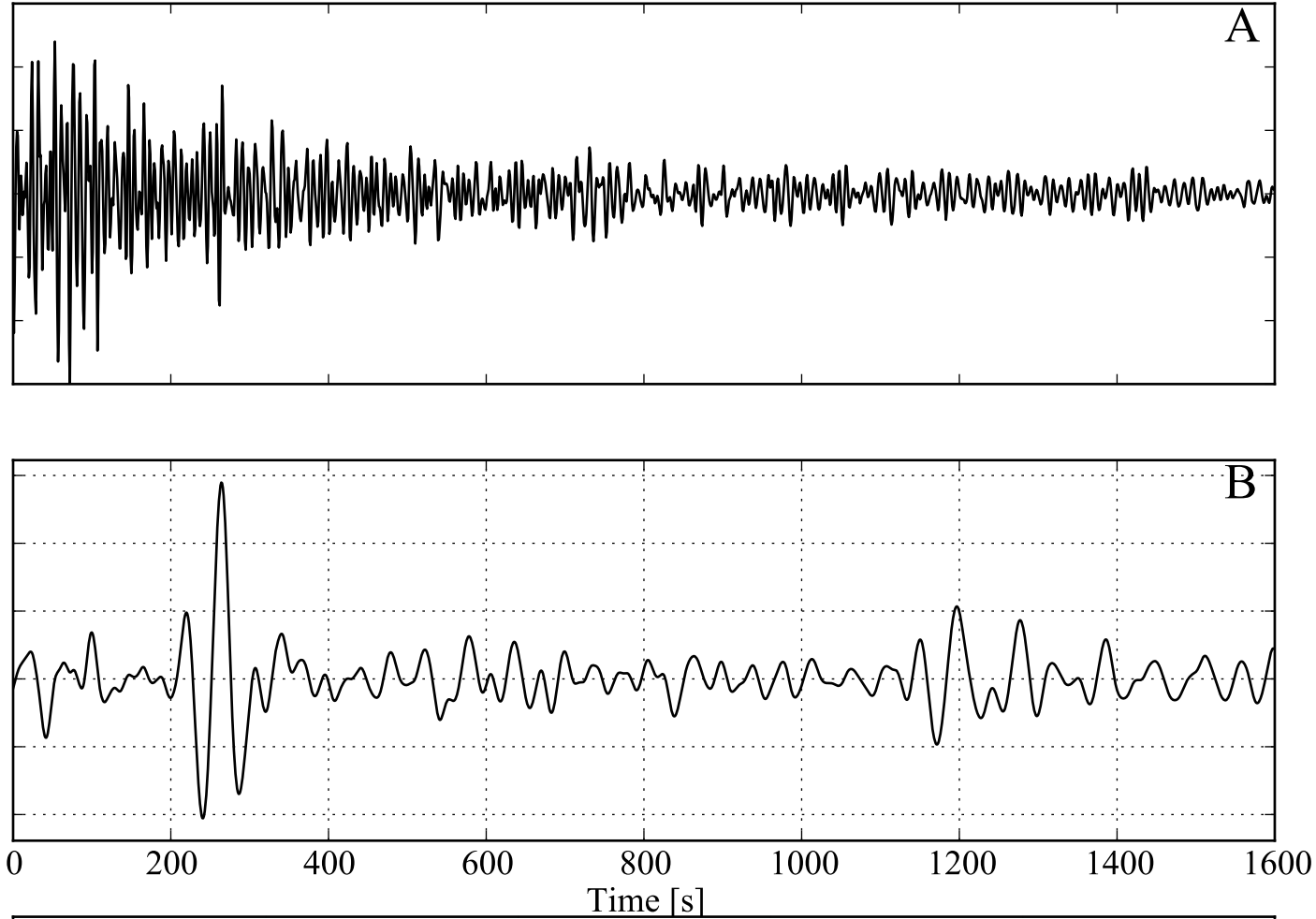


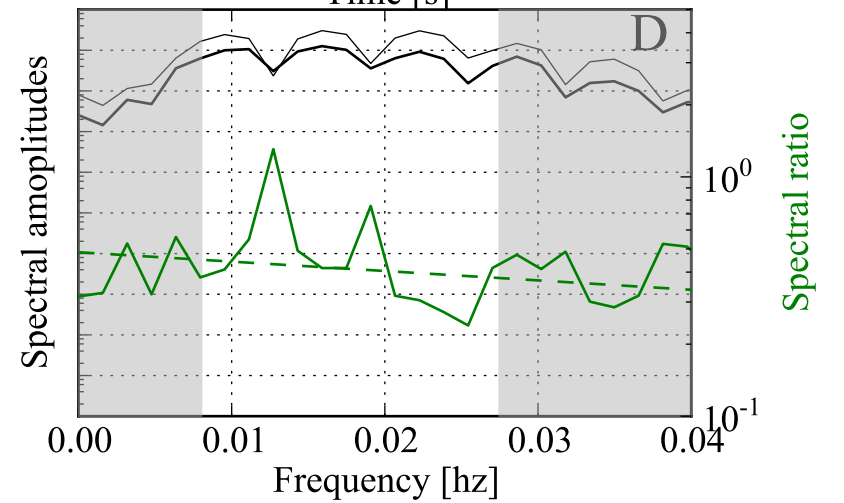
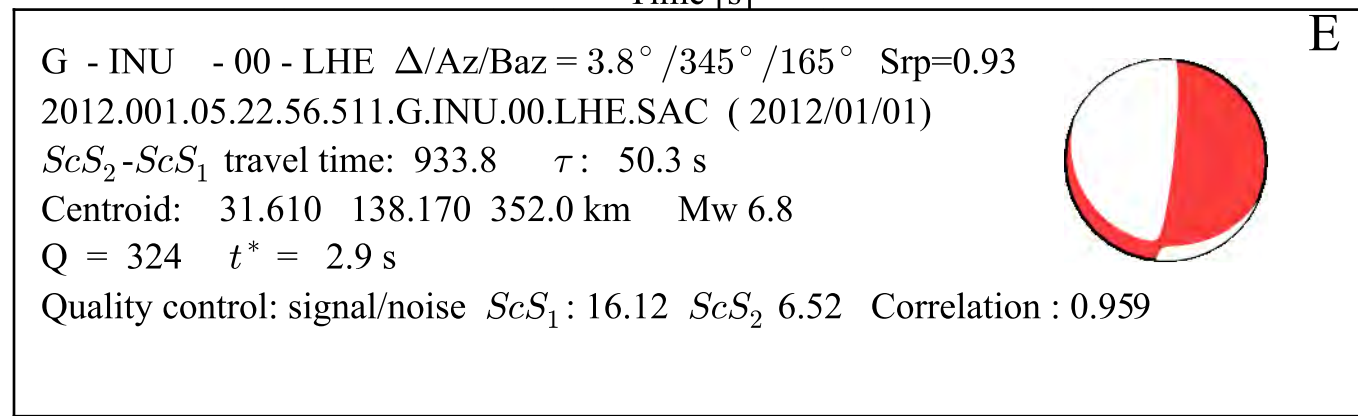
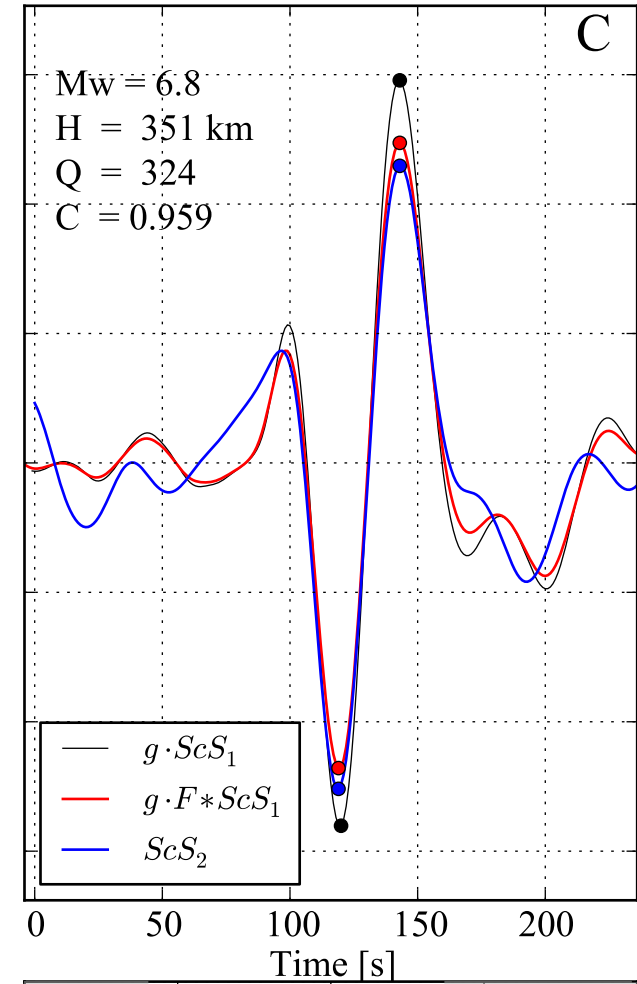
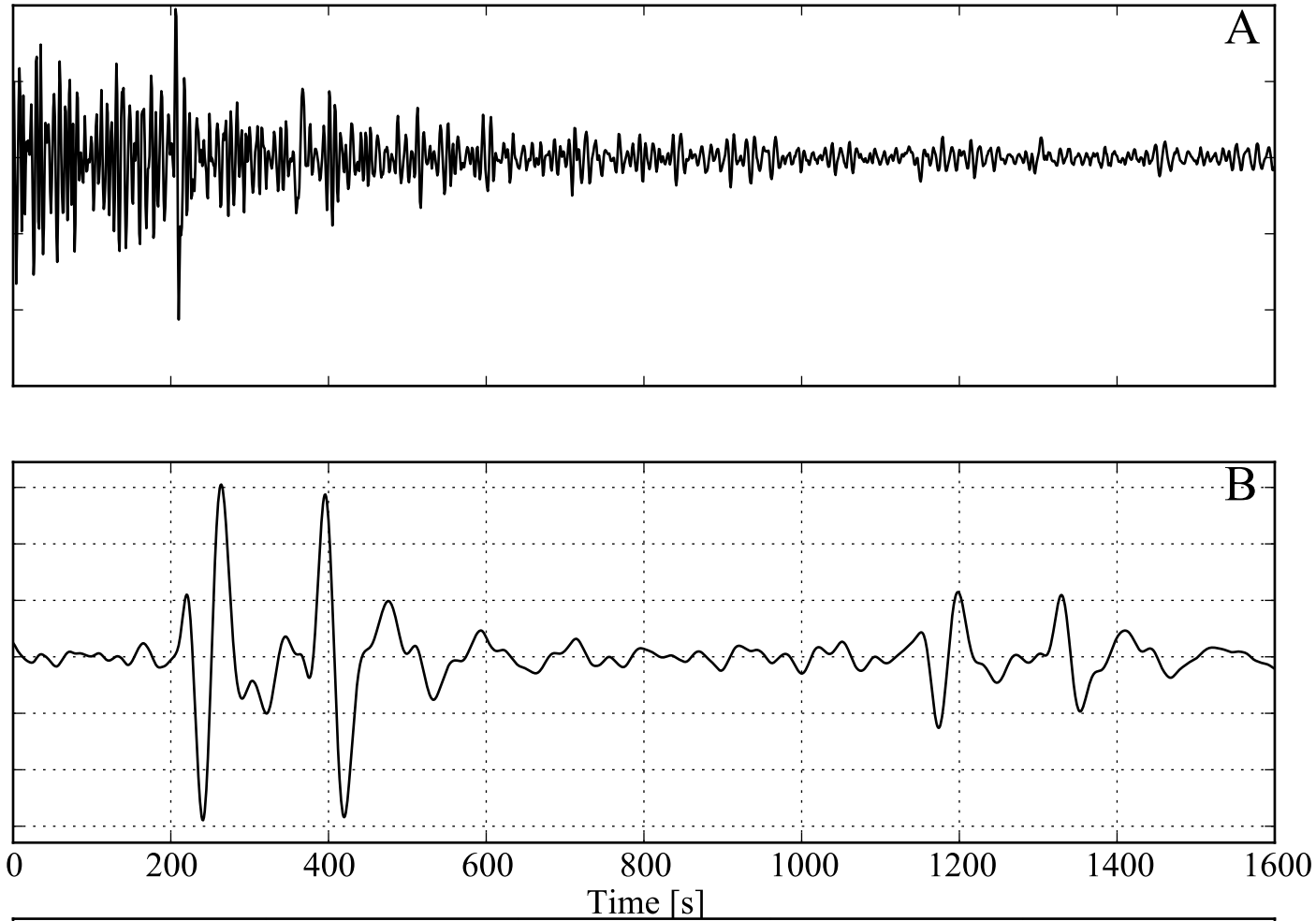


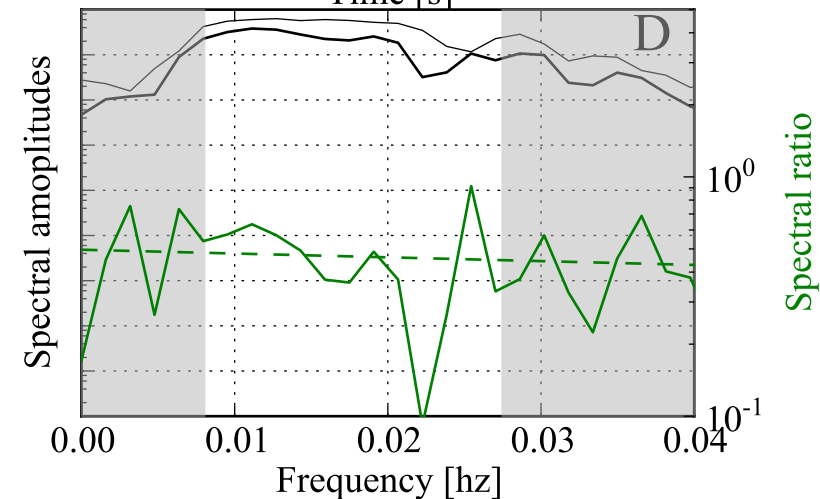
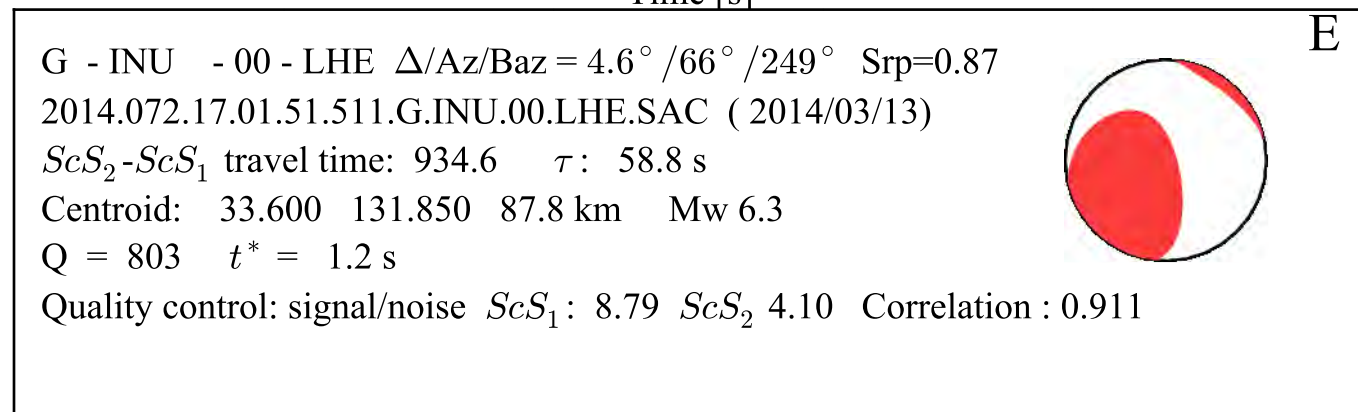
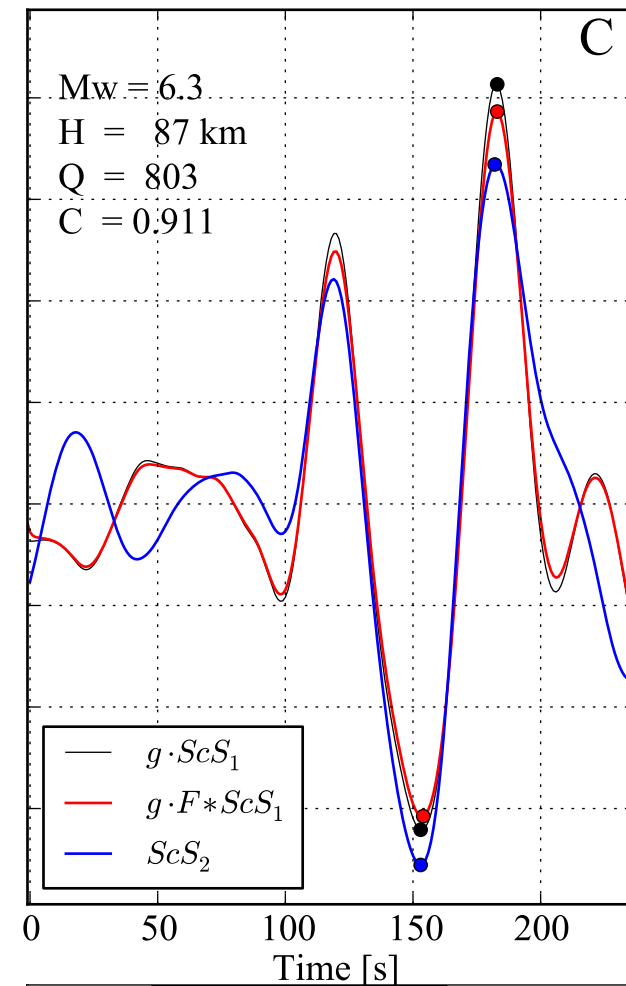
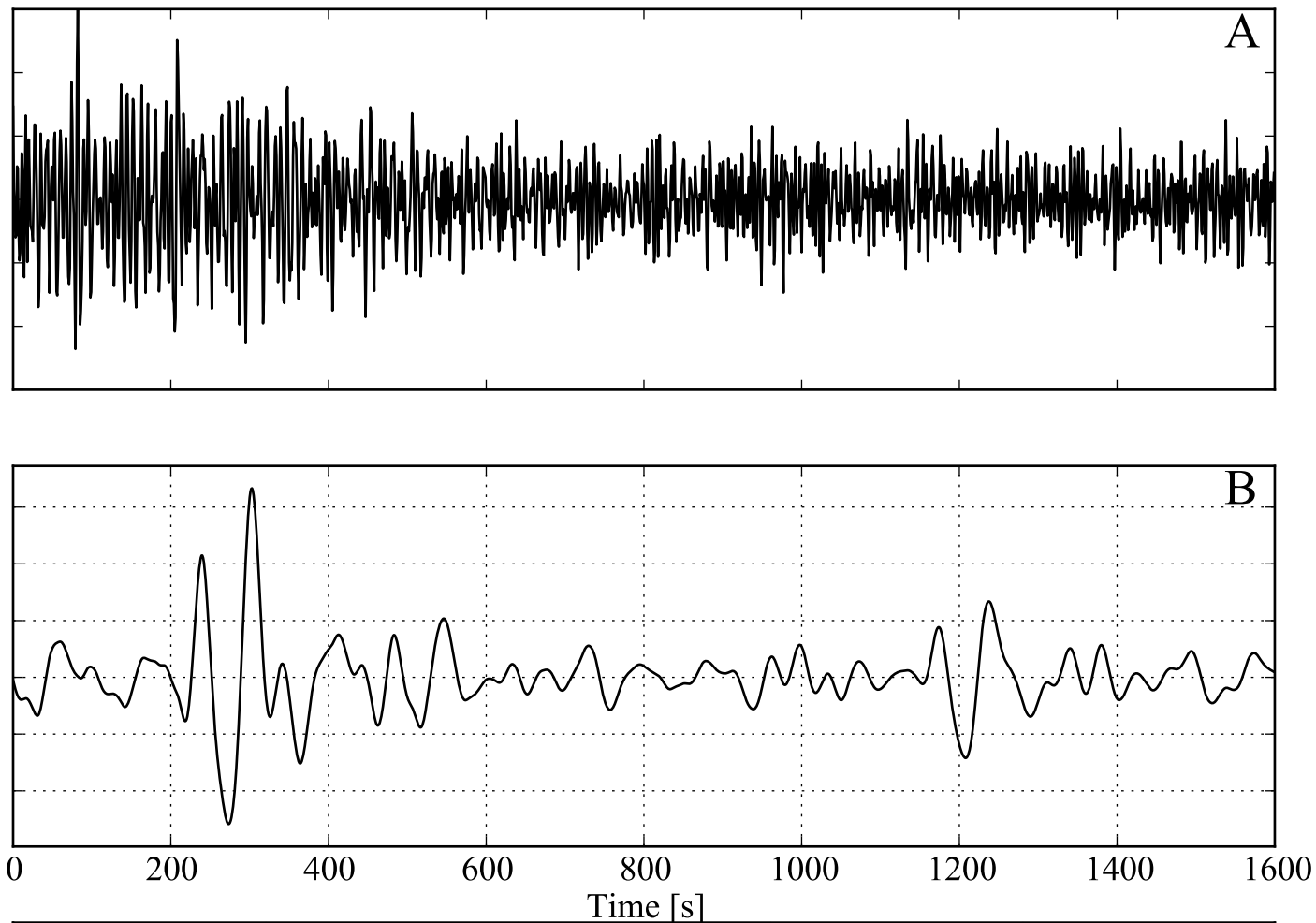


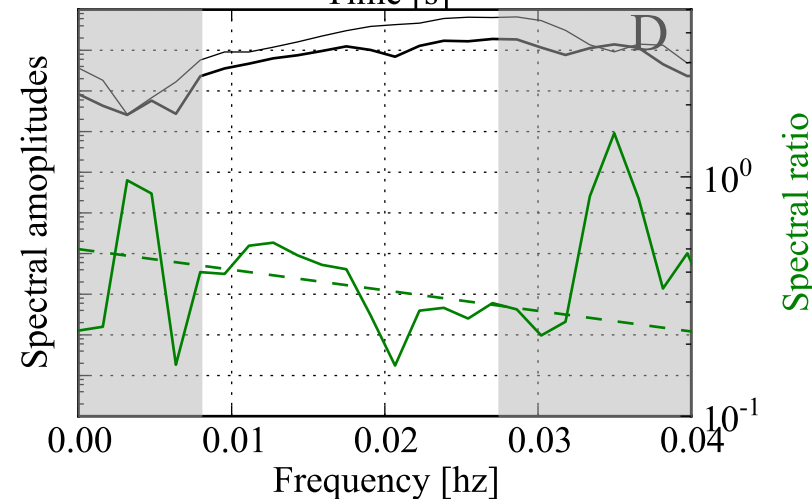
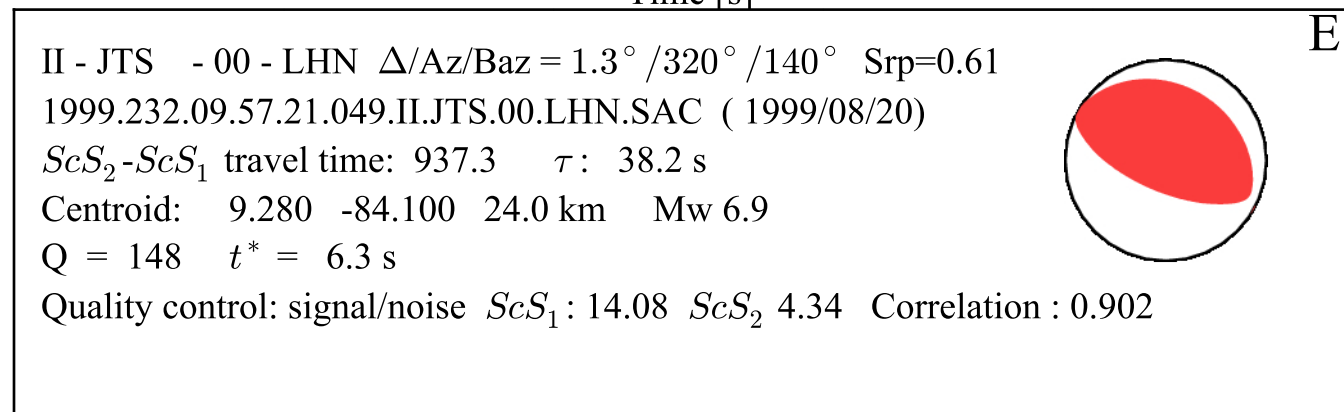
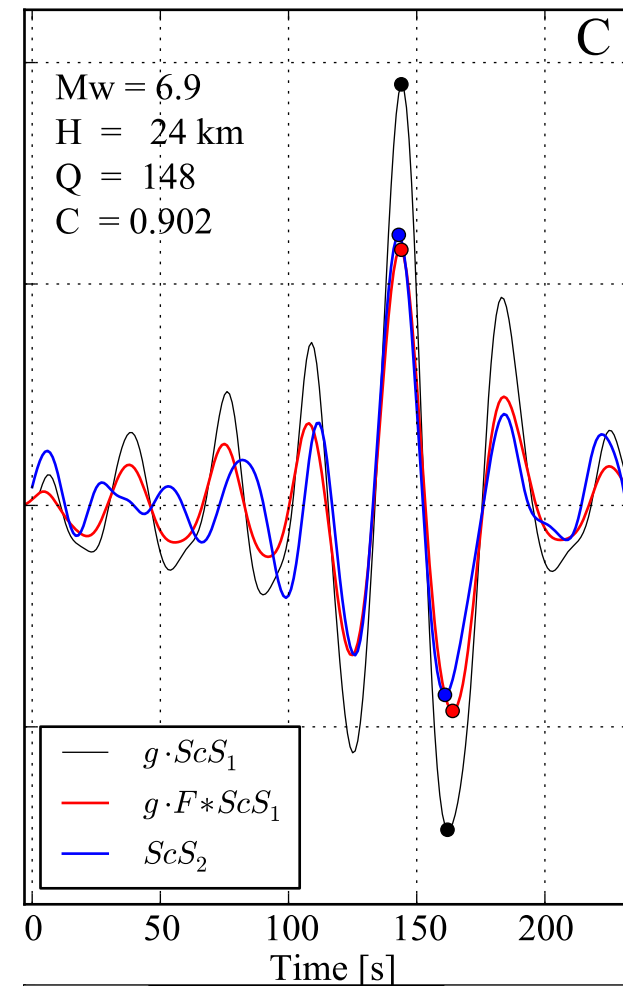
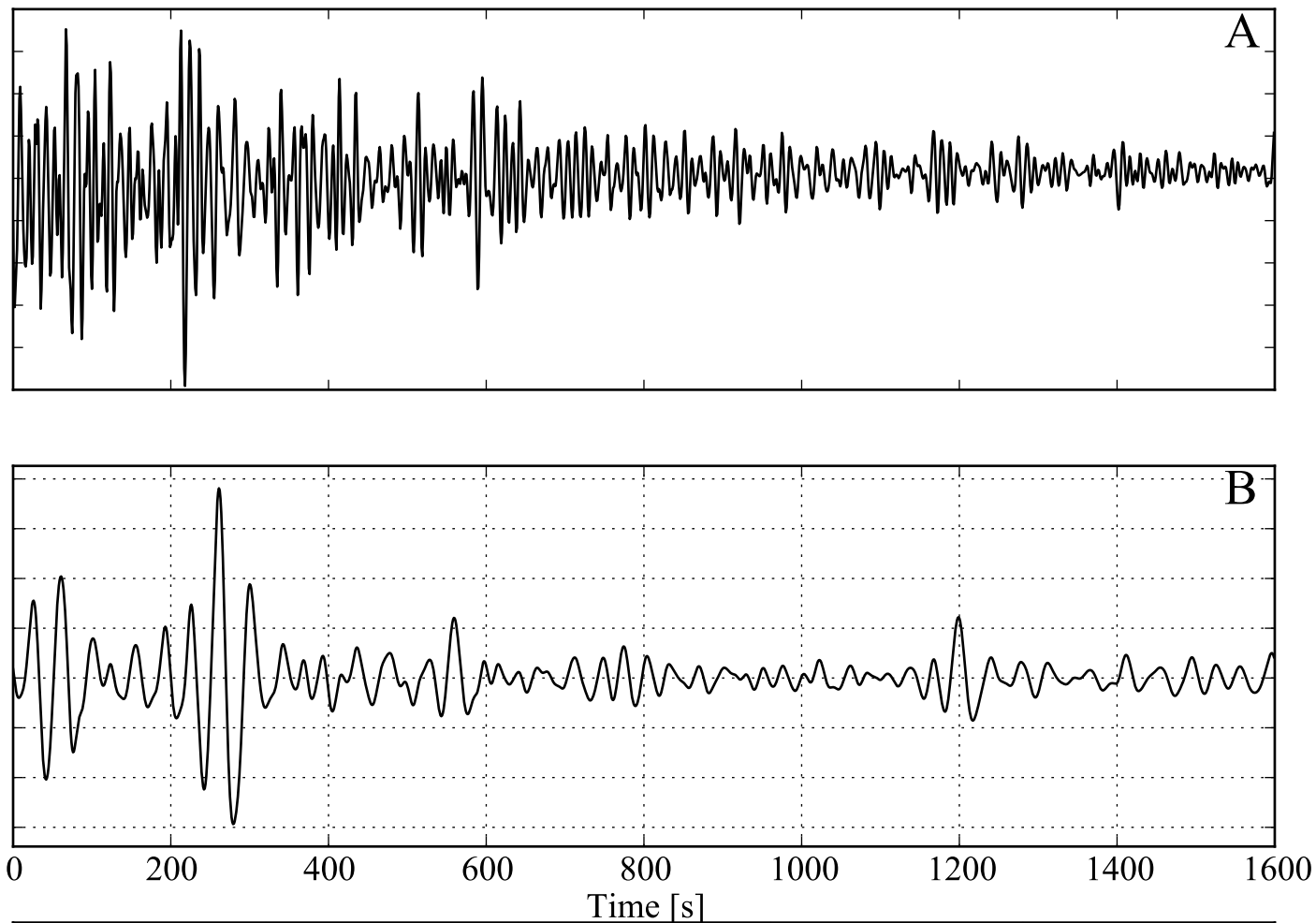


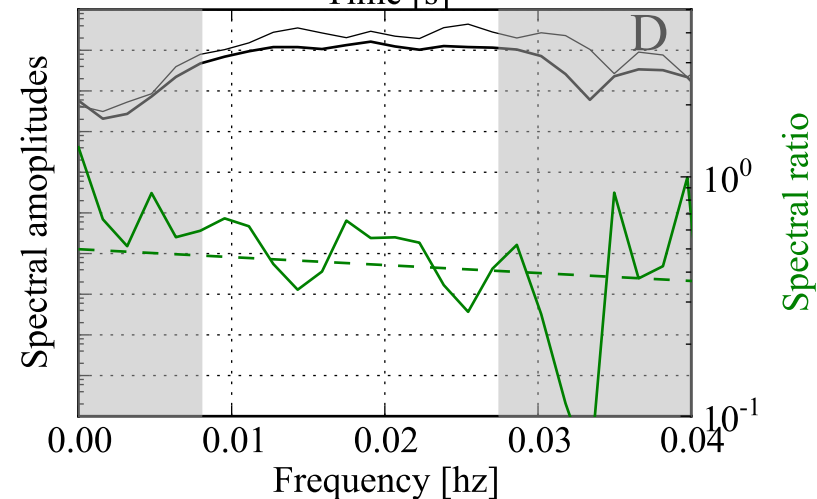
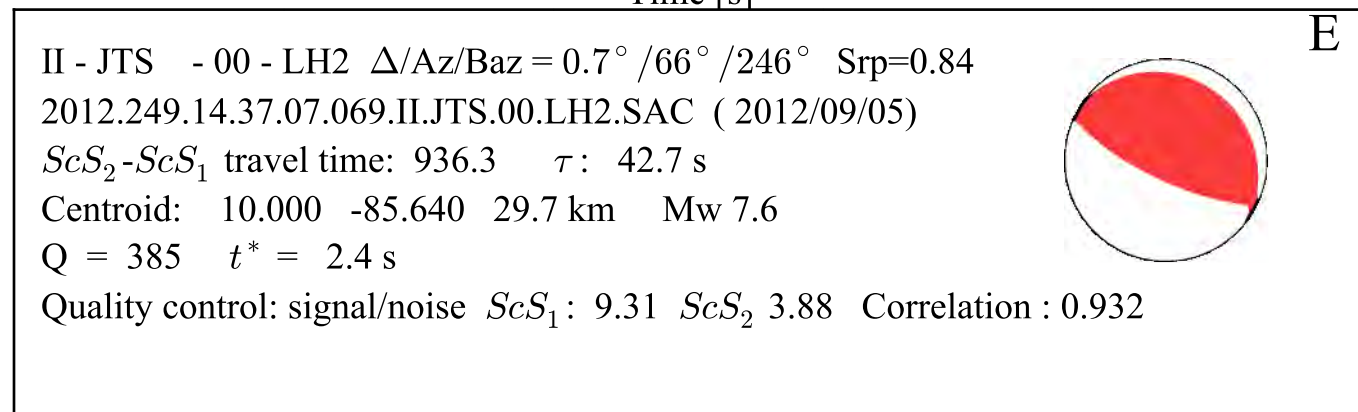
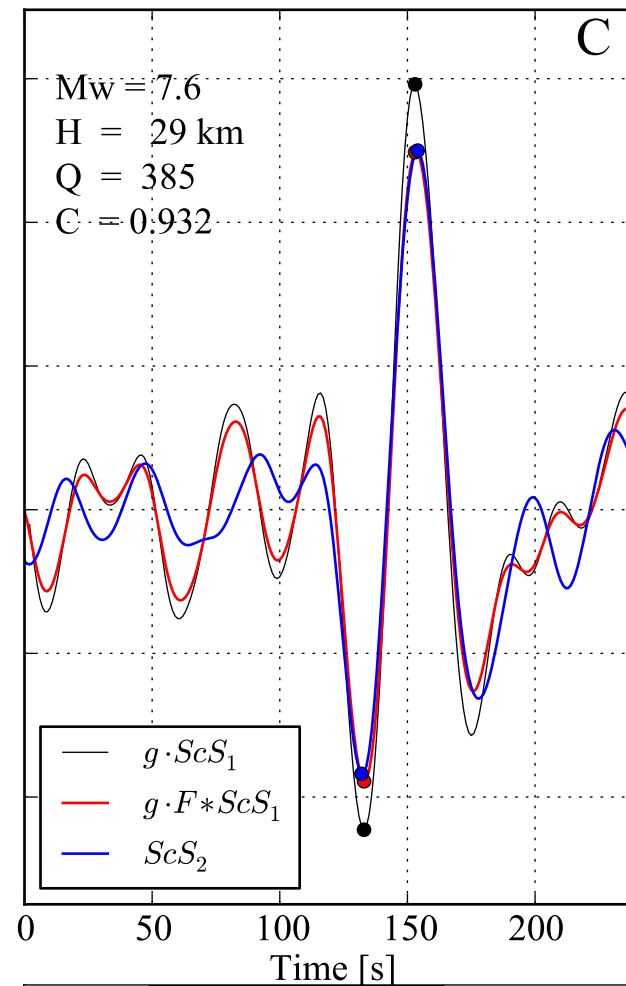
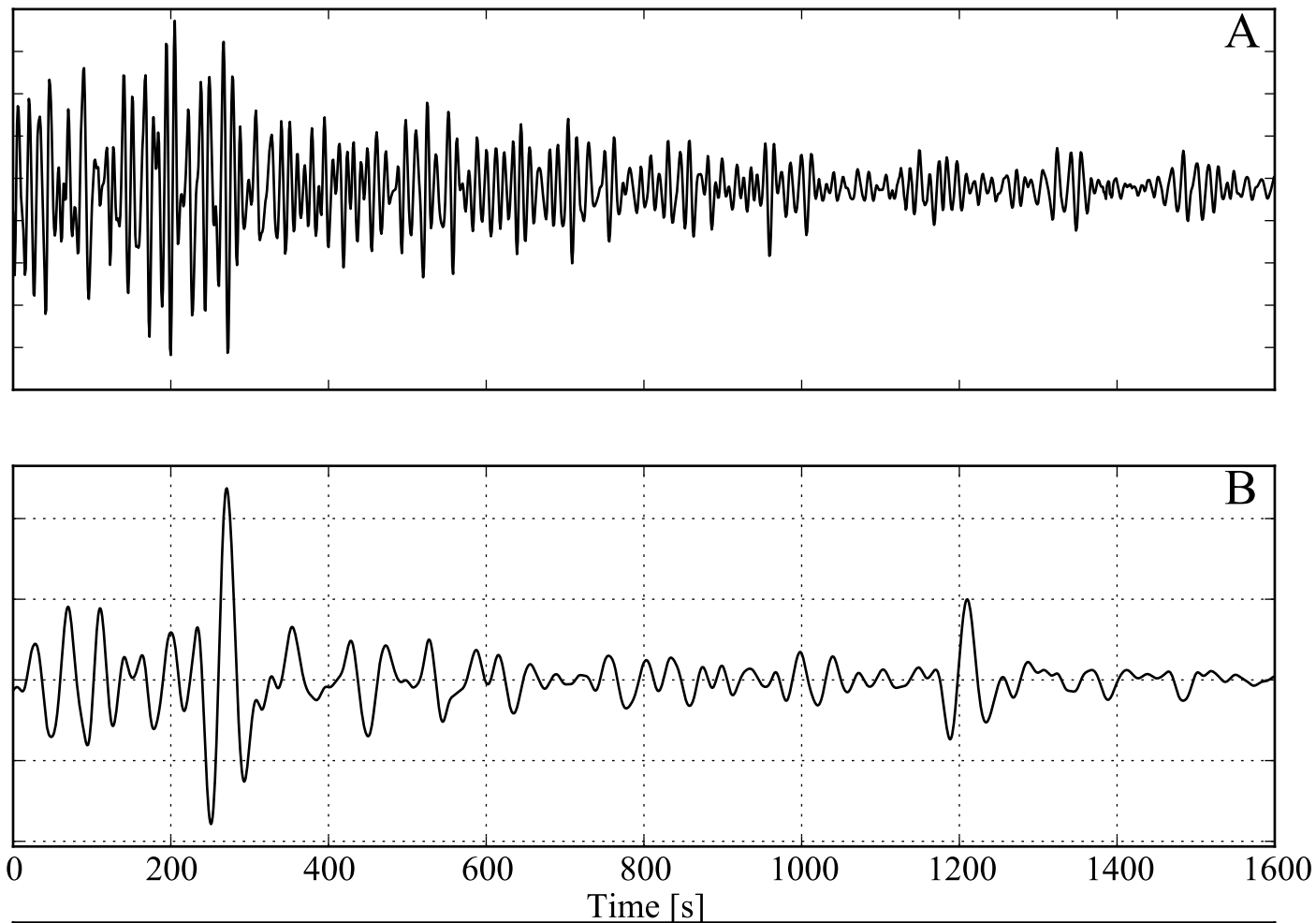


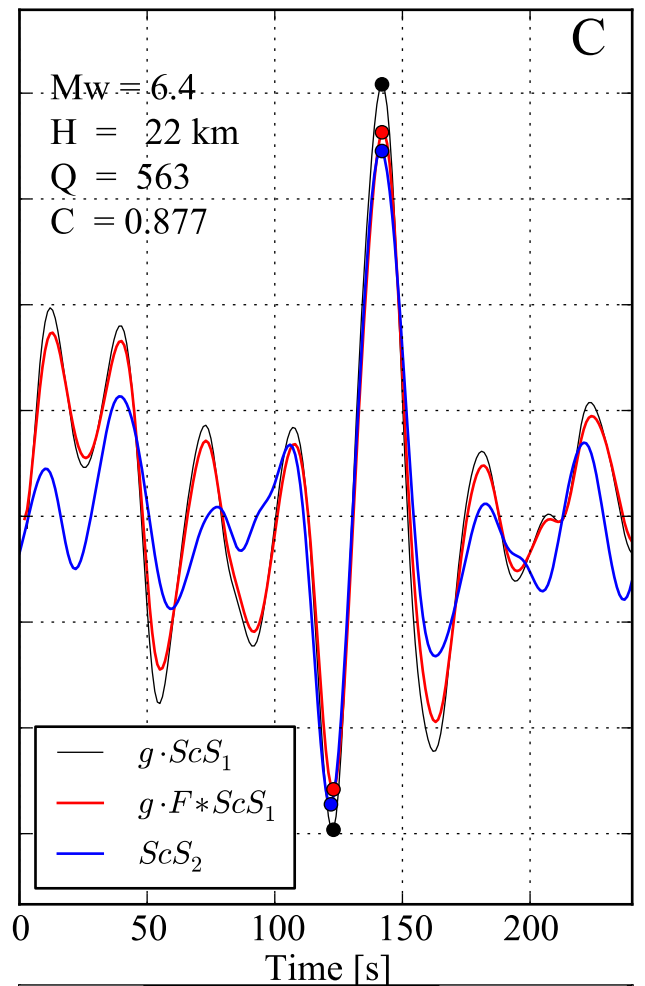
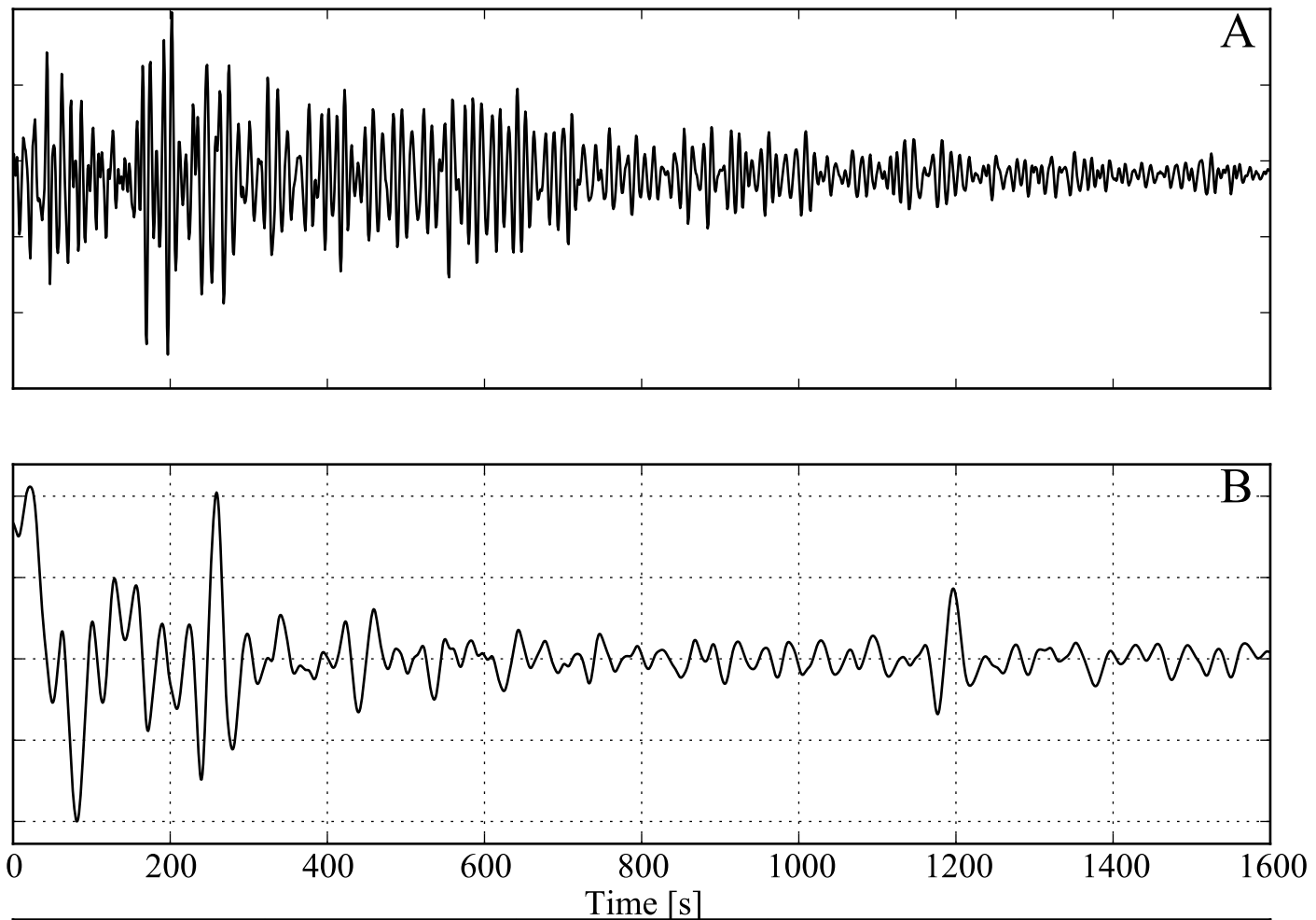







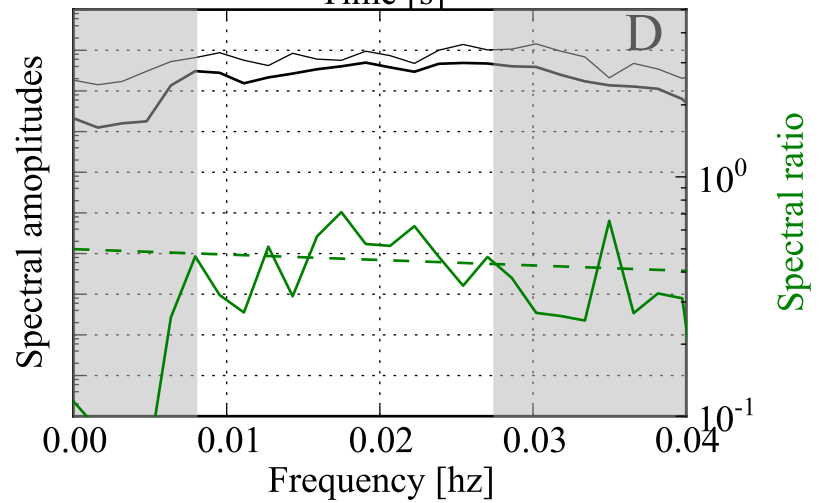


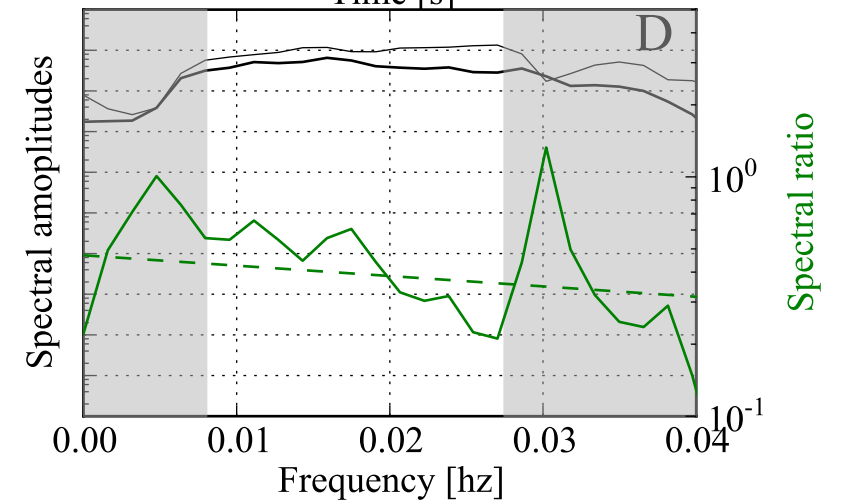
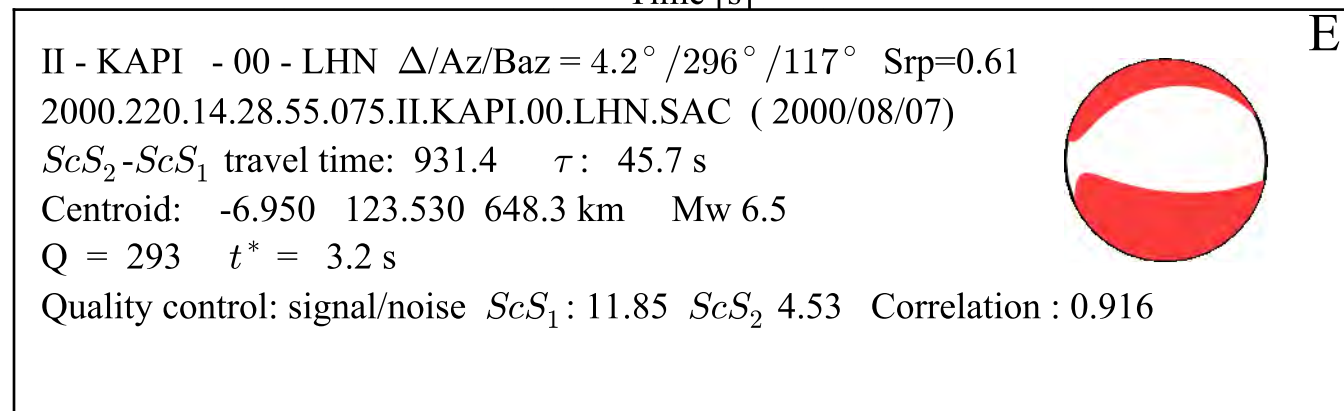
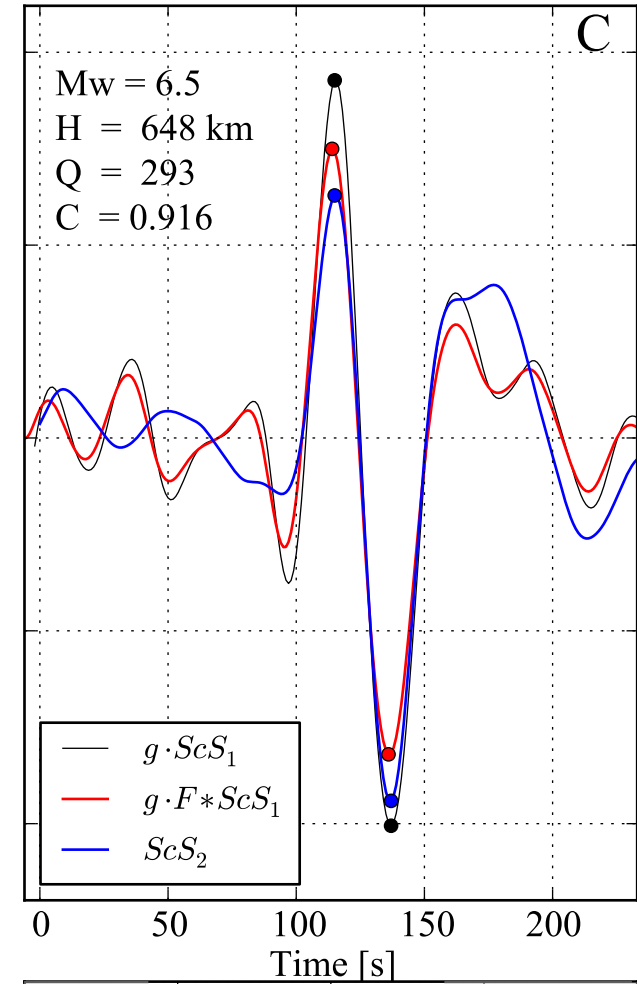
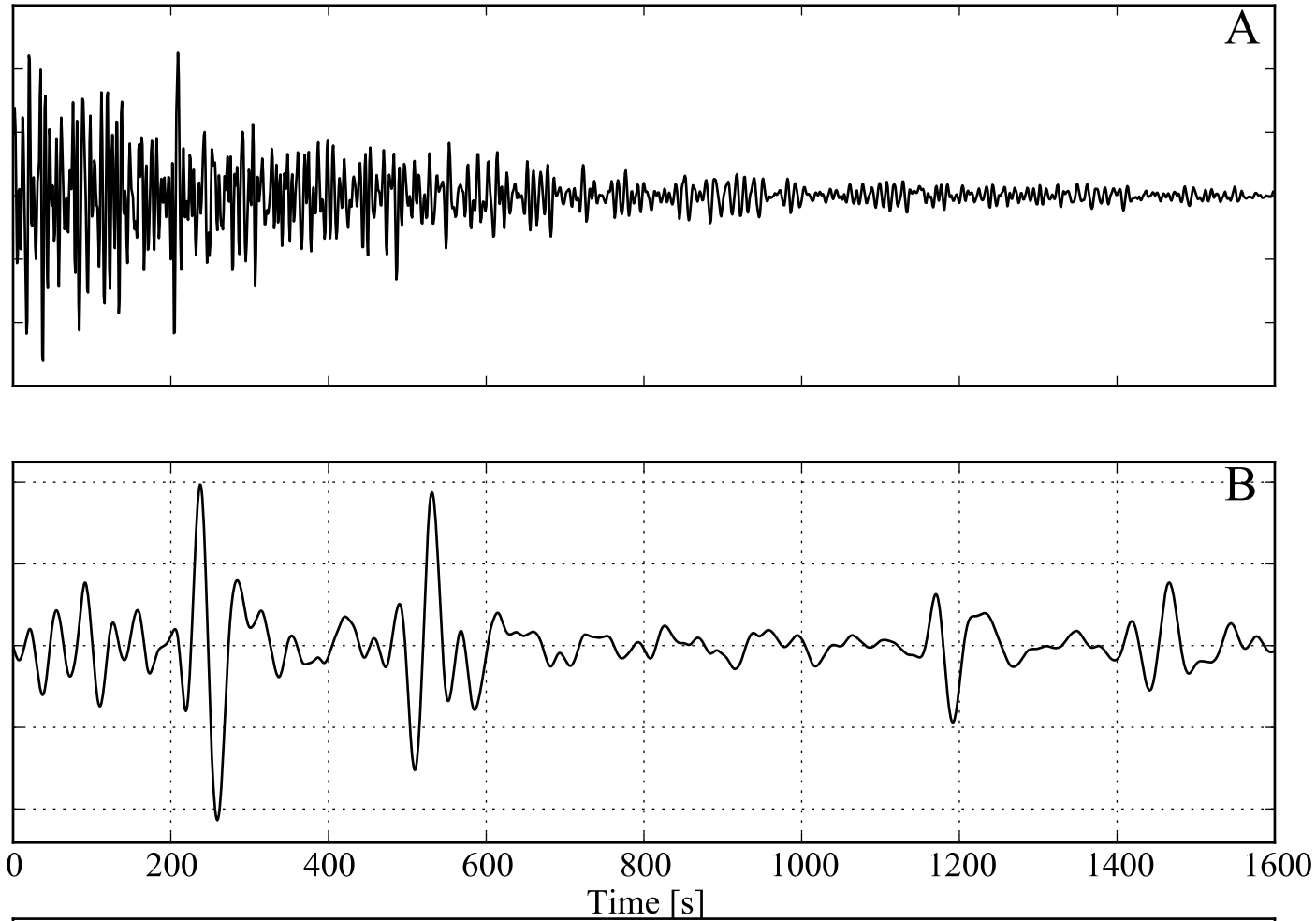


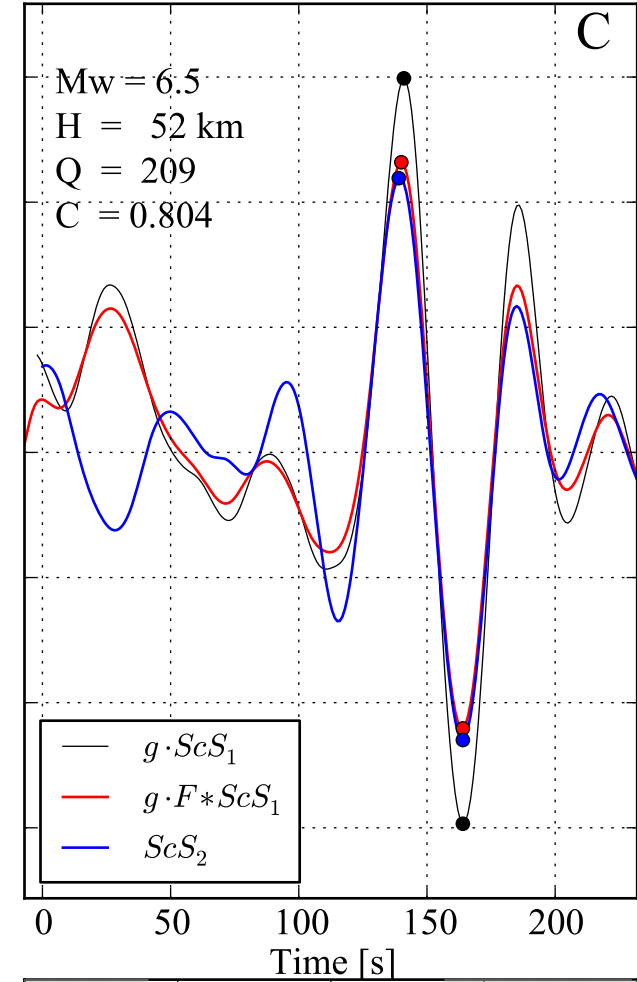
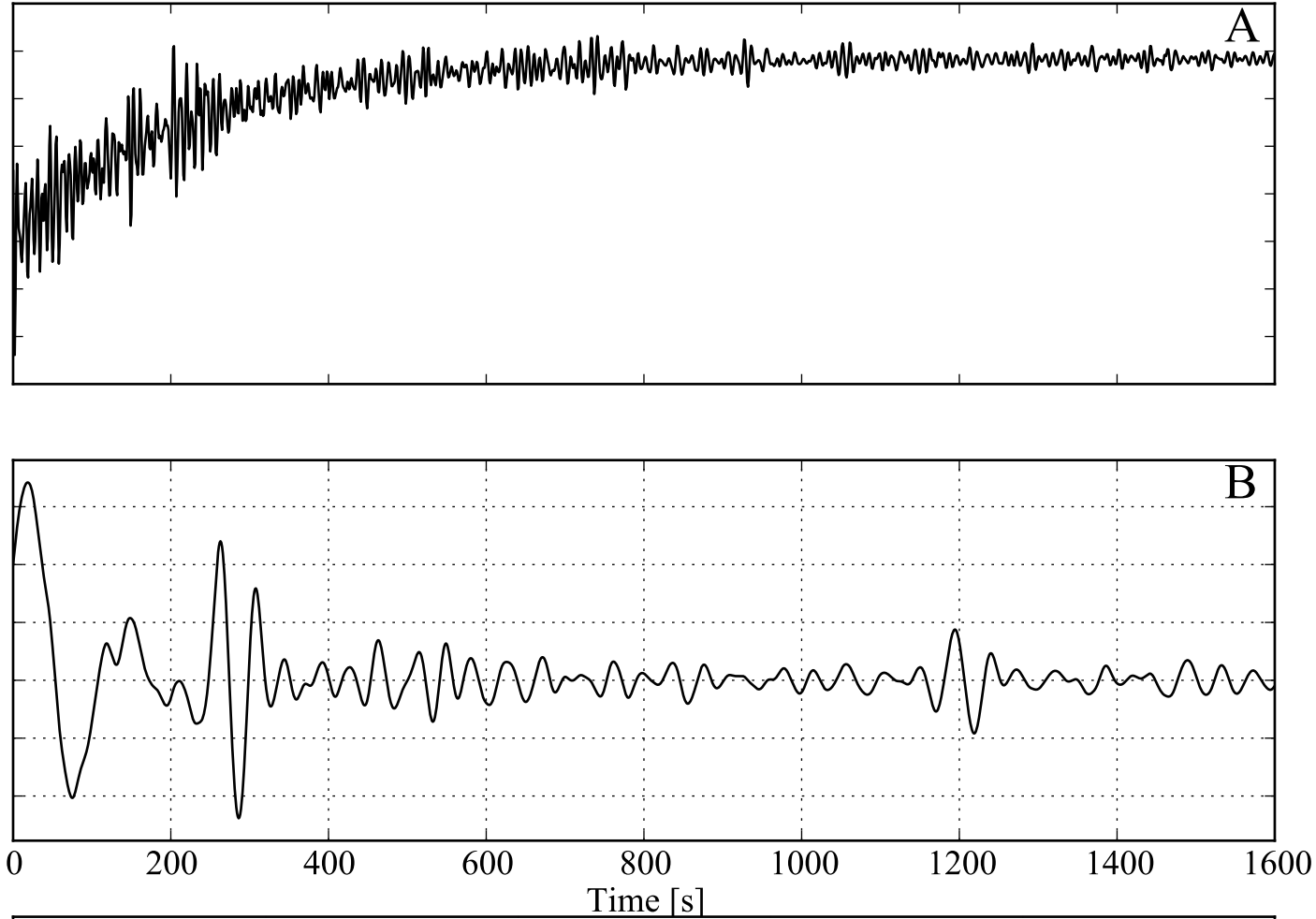


E

II - JTS - 00 - LH2 $\Delta/Az/Baz = 0.9^\circ / 47^\circ / 227^\circ$ $Srp=0.68$
 2012.298.00.40.33.069.II.JTS.00.LH2.SAC (2012/10/24)
 $ScS_2 - ScS_1$ travel time: 937.3 τ : 39.6 s
 Centroid: 9.710 -85.600 22.1 km M_w 6.4
 $Q = 563$ $t^* = 1.7$ s
 Quality control: signal/noise ScS_1 : 8.85 ScS_2 3.87 Correlation : 0.877

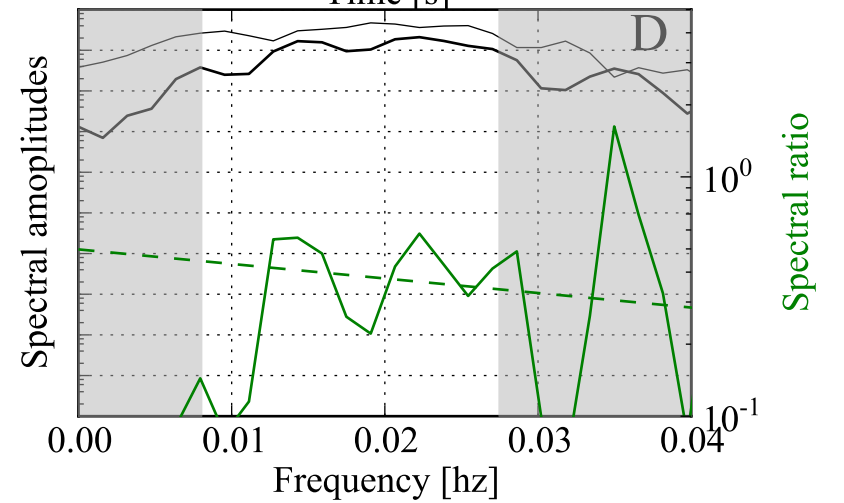



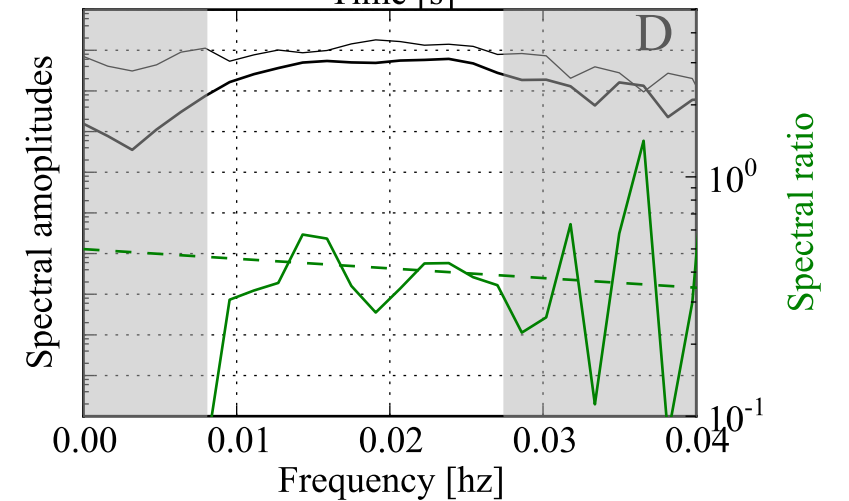
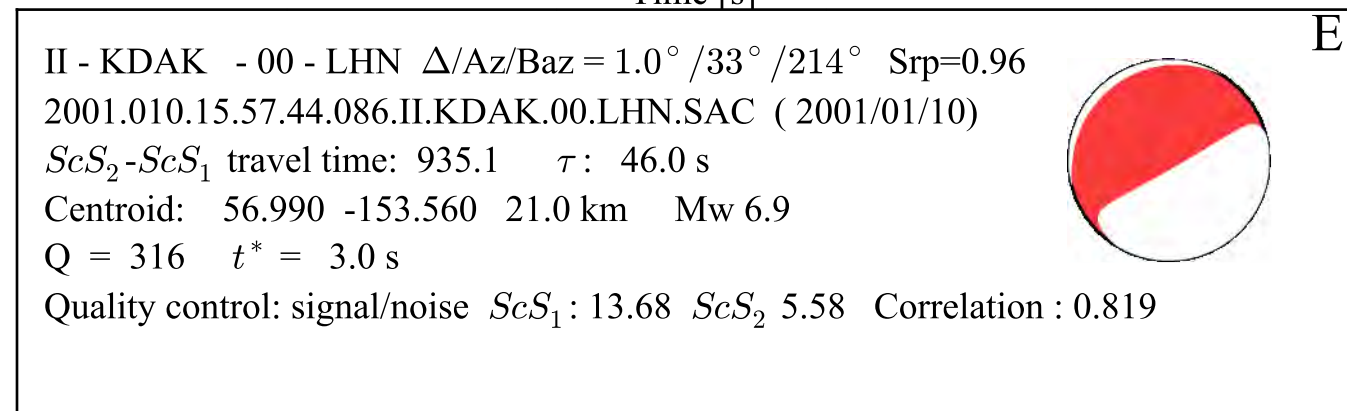
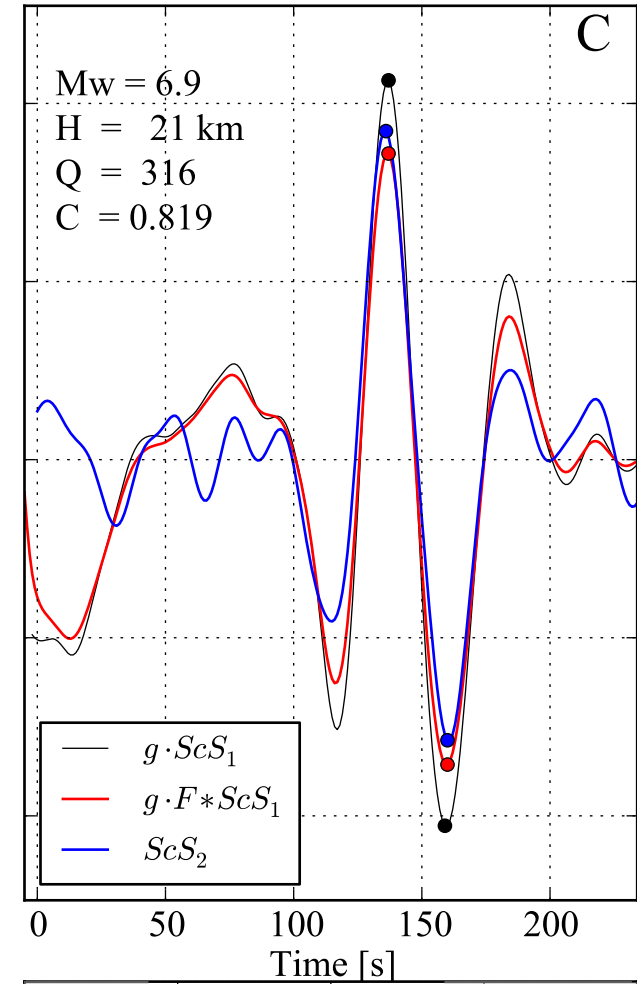
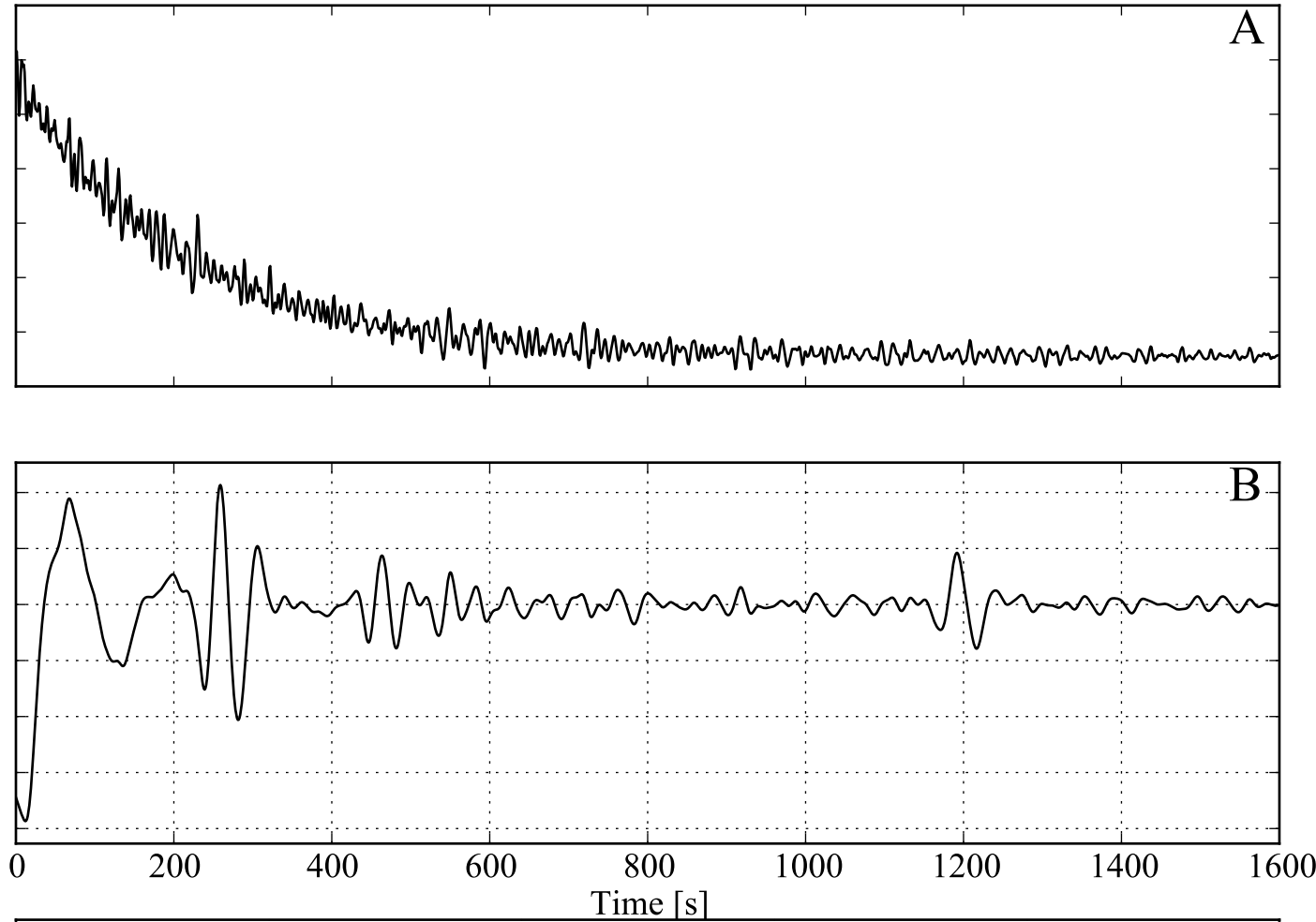


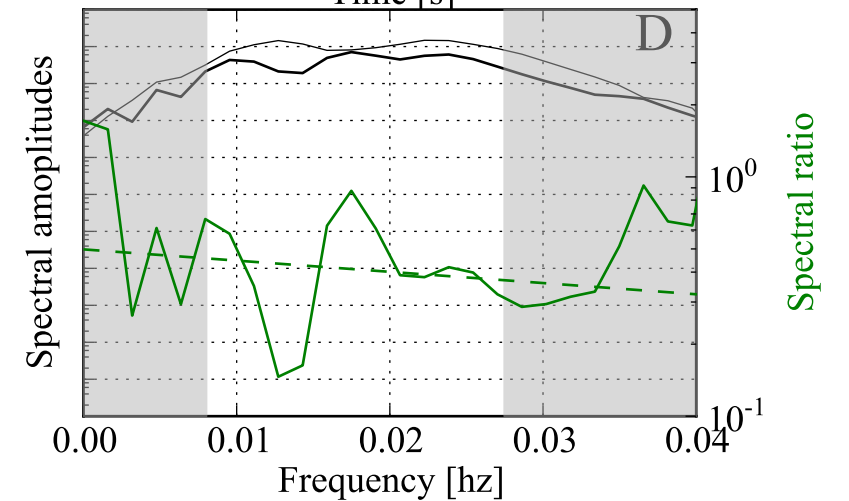
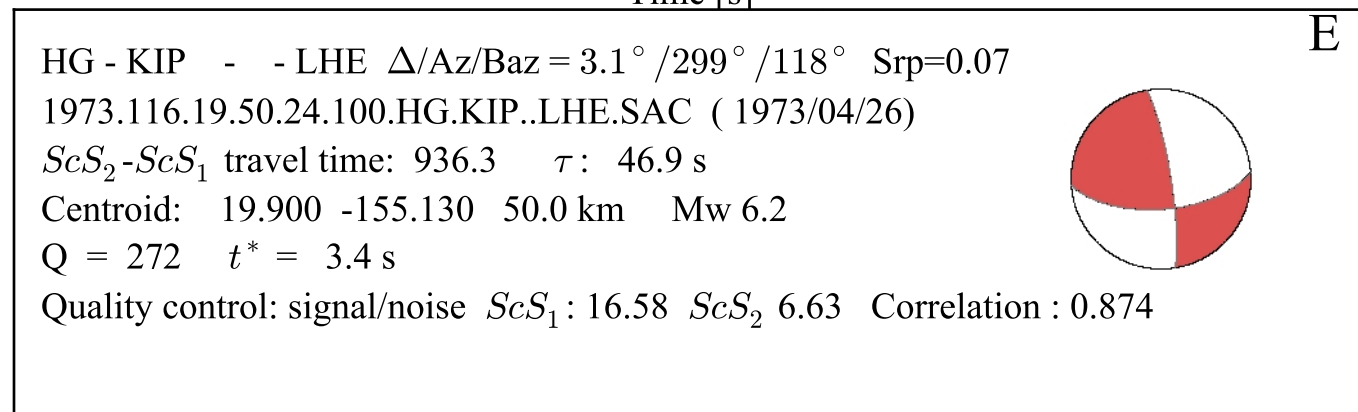
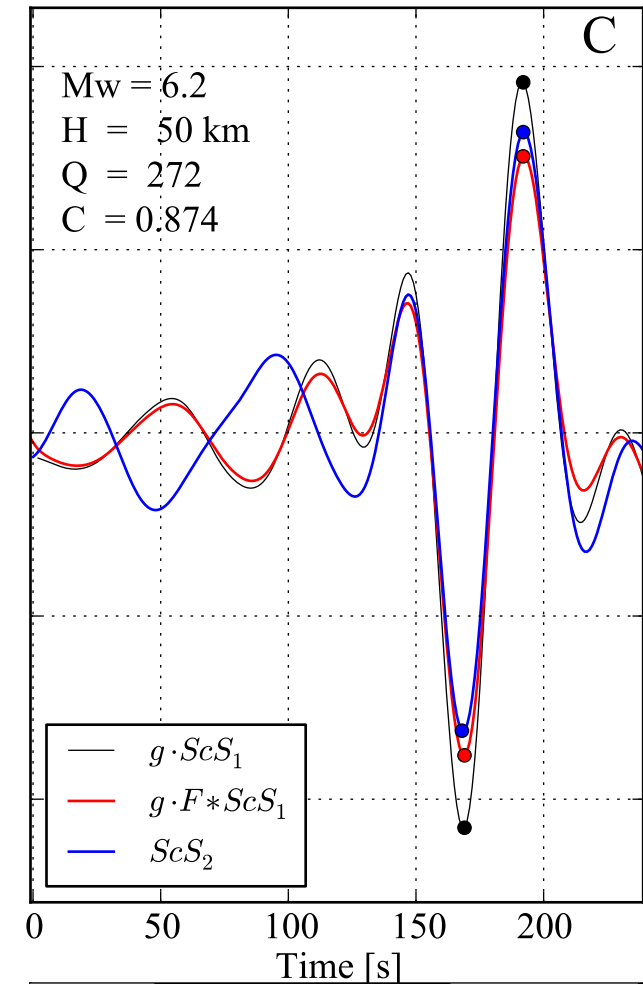
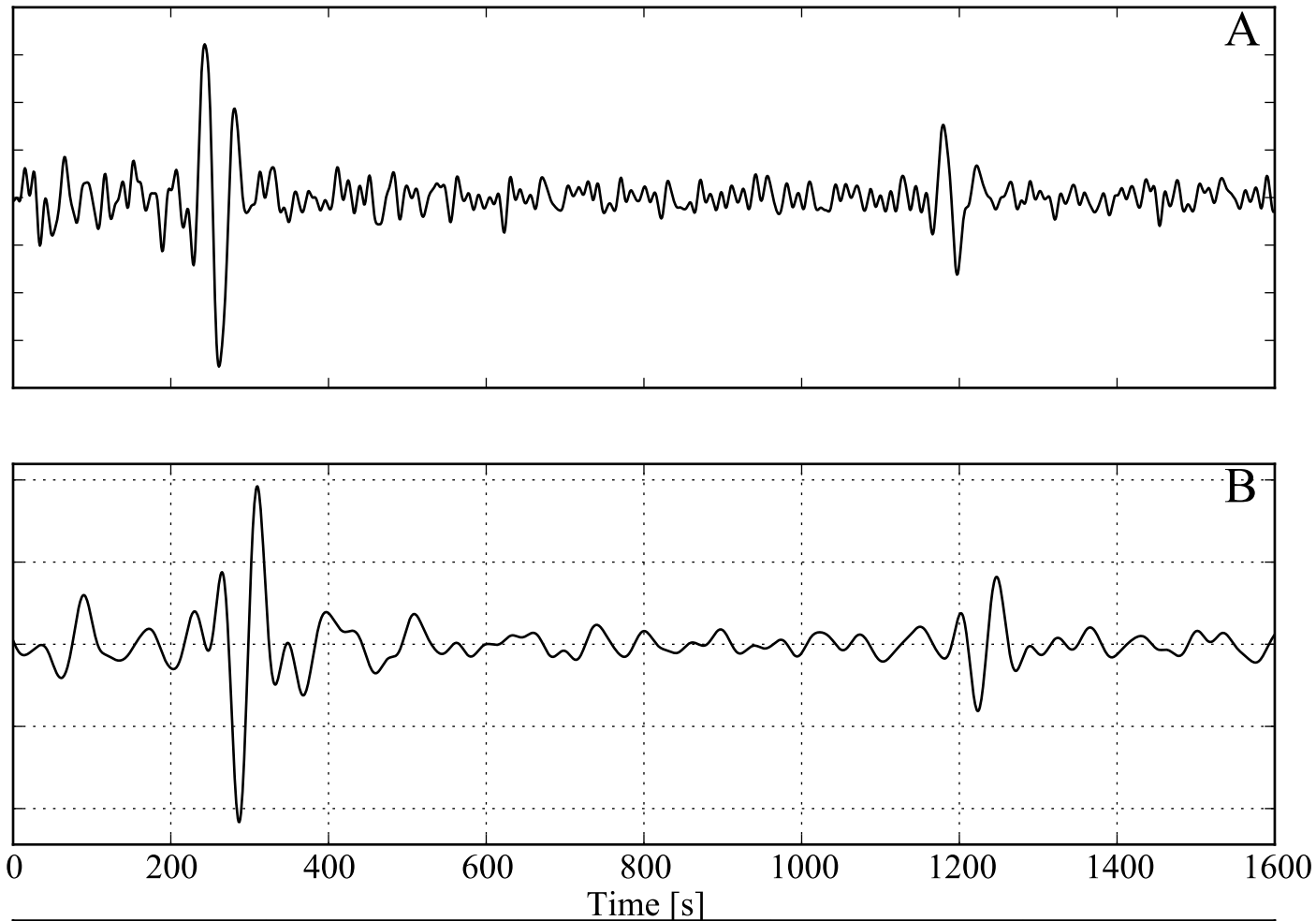


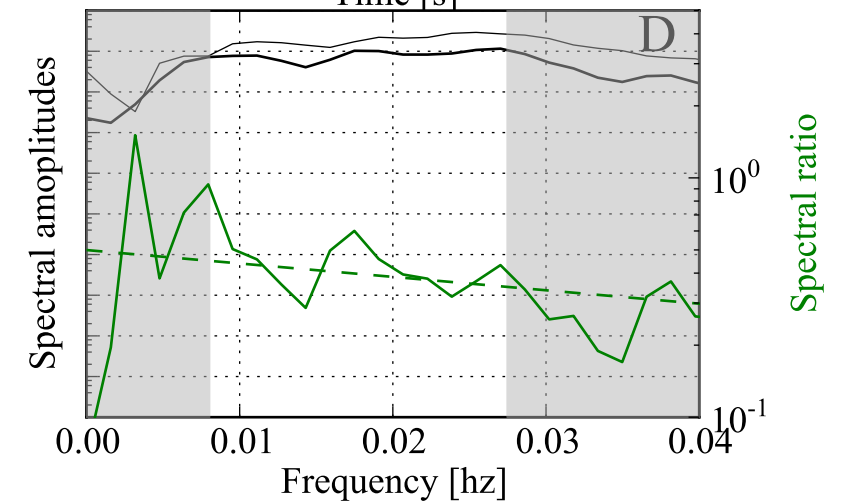
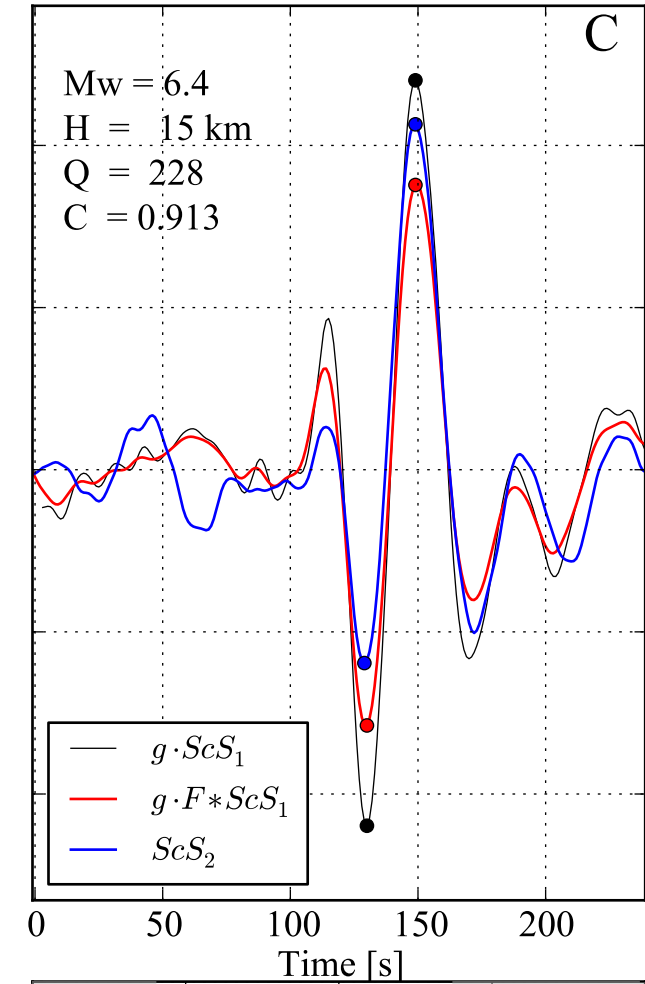
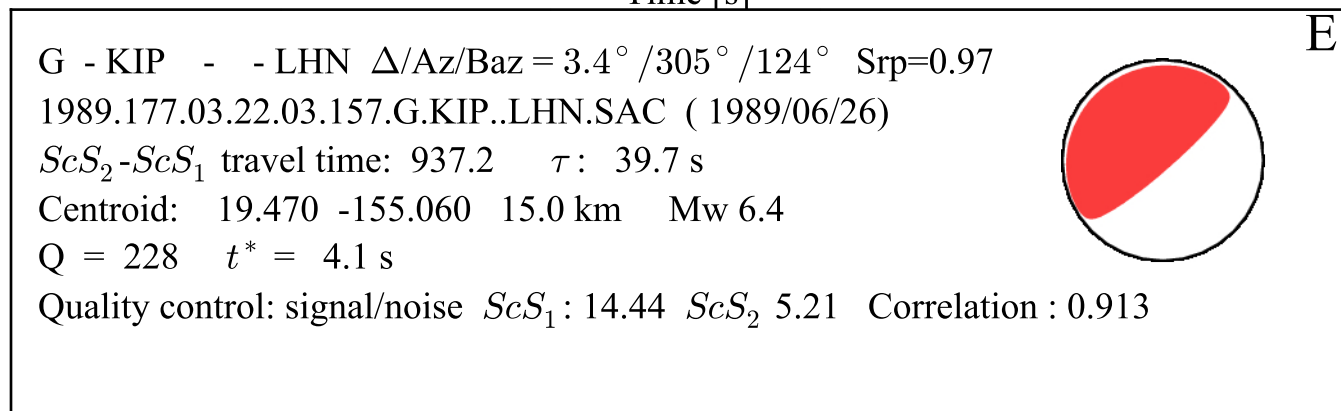
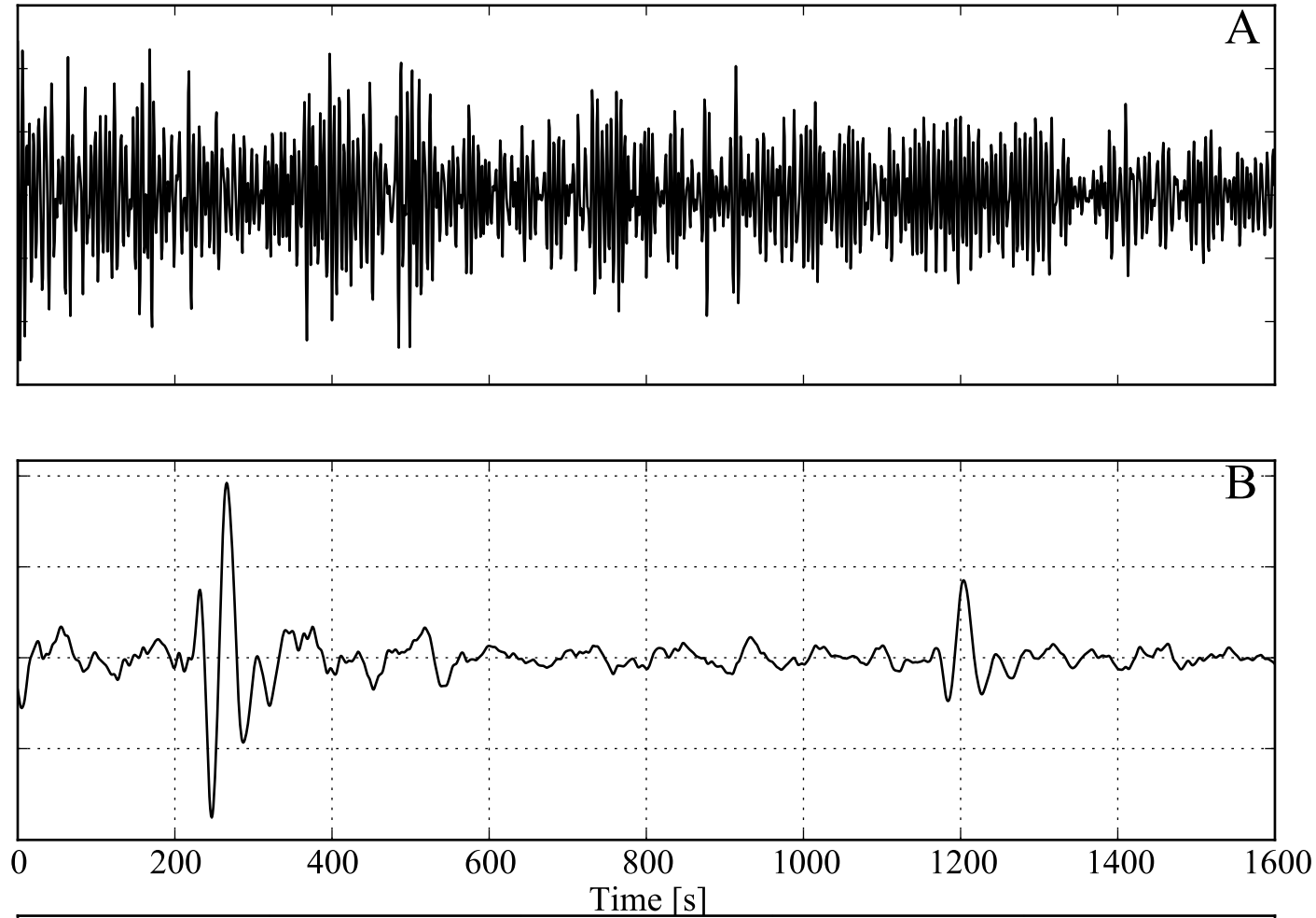
E

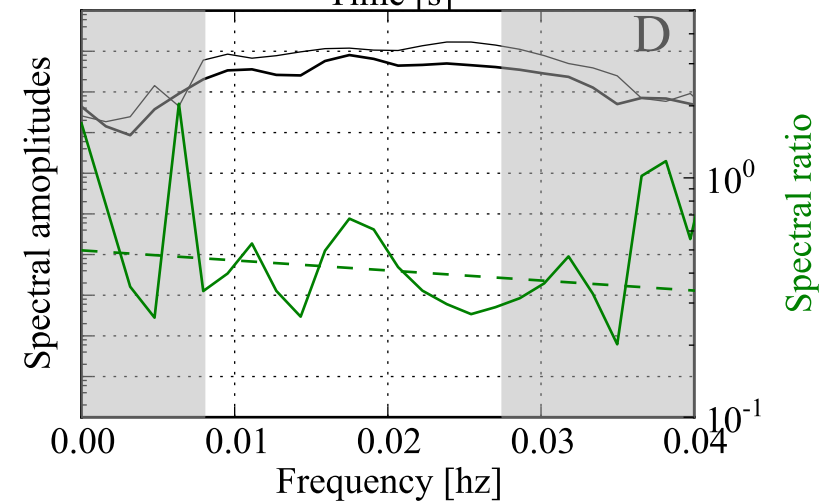
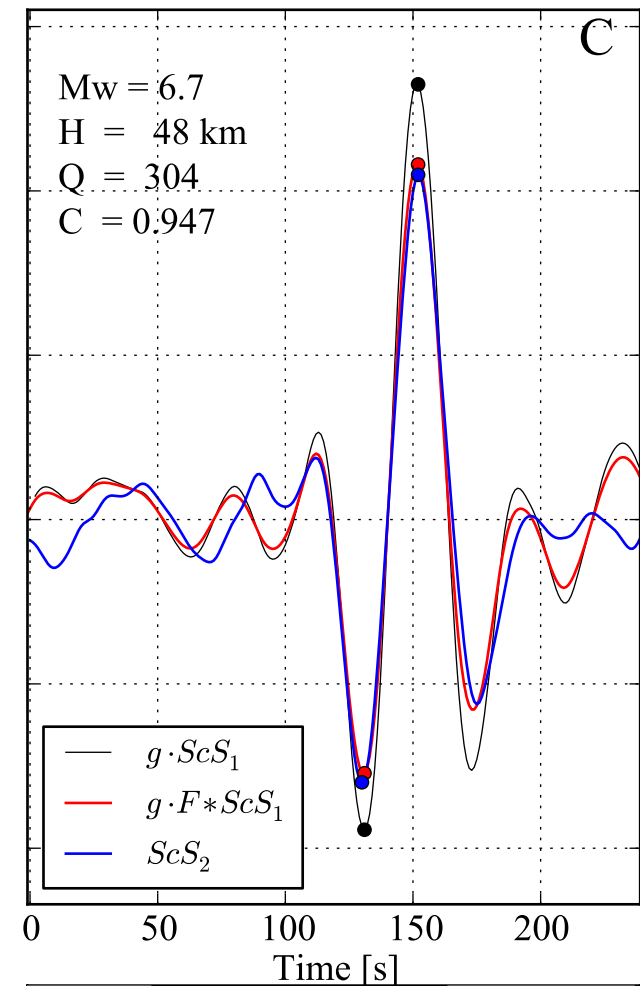
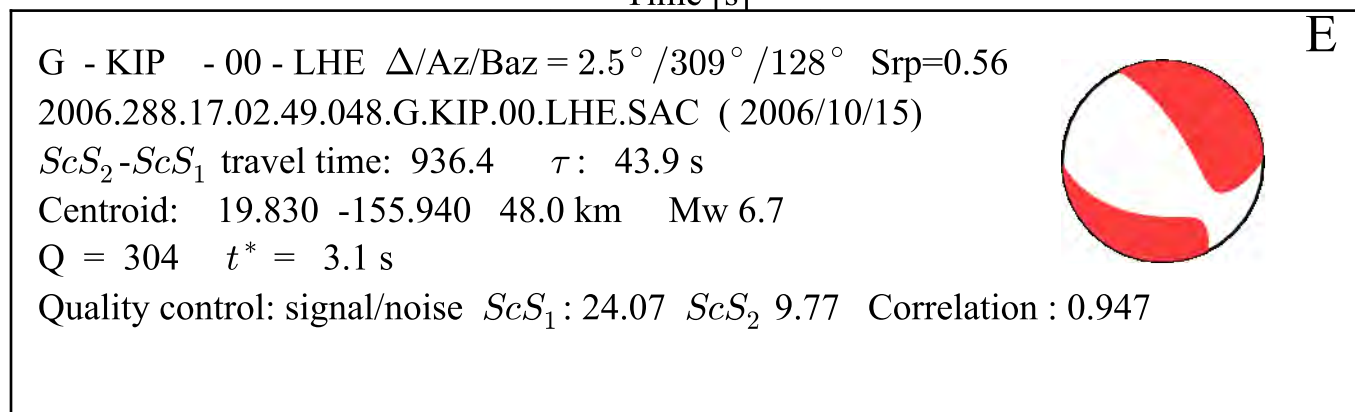
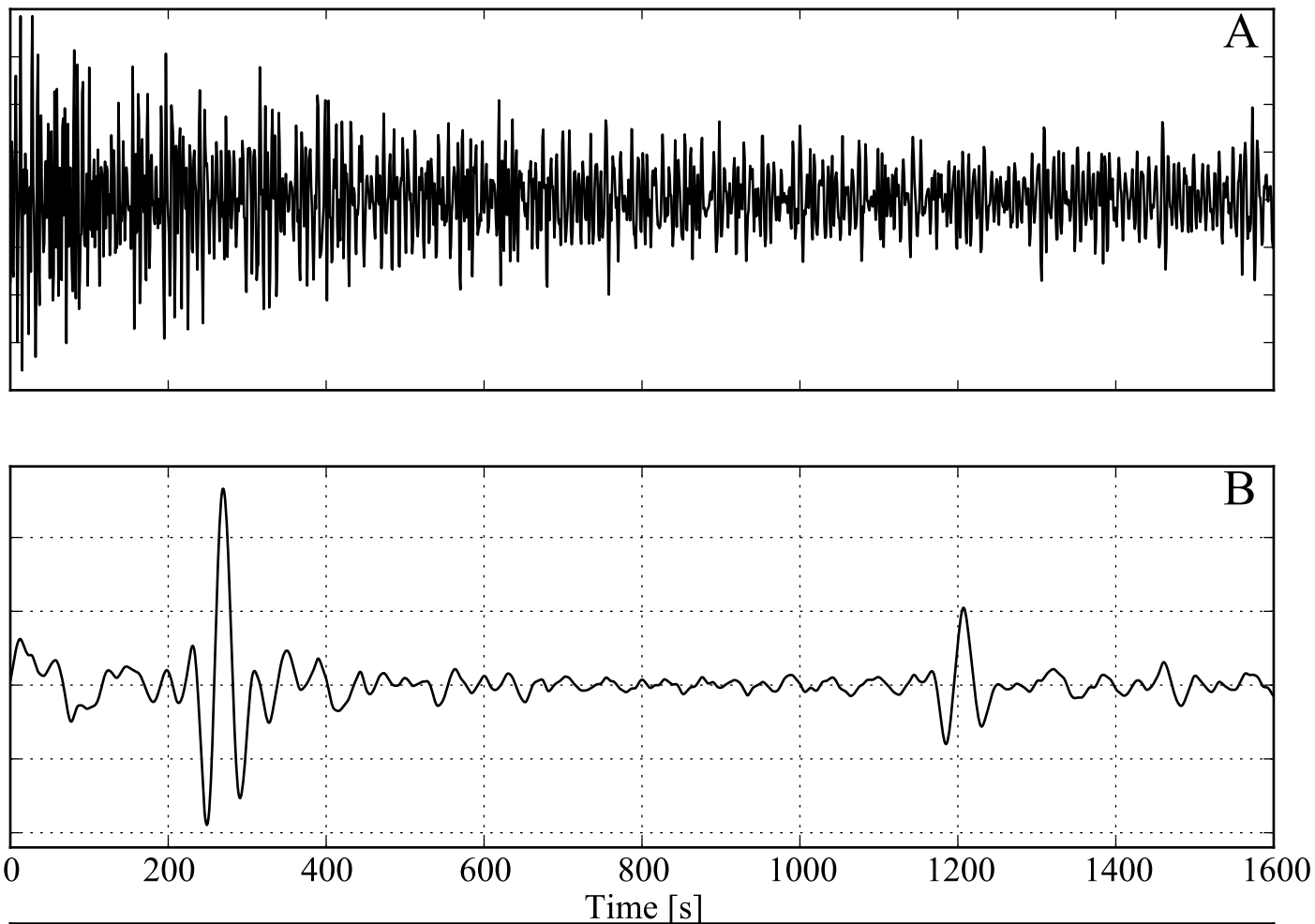
II - KDAK - 00 - LHN $\Delta/Az/Baz = 0.9^\circ / 73^\circ / 255^\circ$ $Srp=0.60$
 2000.193.01.27.28.052.II.KDAK.00.LHN.SAC (2000/07/11)
 ScS_2-ScS_1 travel time: 935.1 τ : 49.5 s
 Centroid: 57.540 -154.220 52.0 km Mw 6.5
 Q = 209 $t^* = 4.5$ s
 Quality control: signal/noise ScS_1 : 10.83 ScS_2 4.06 Correlation : 0.804

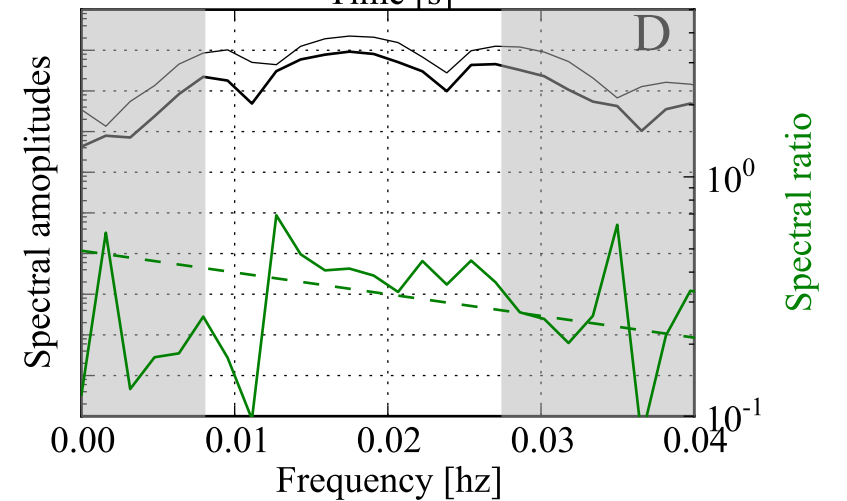
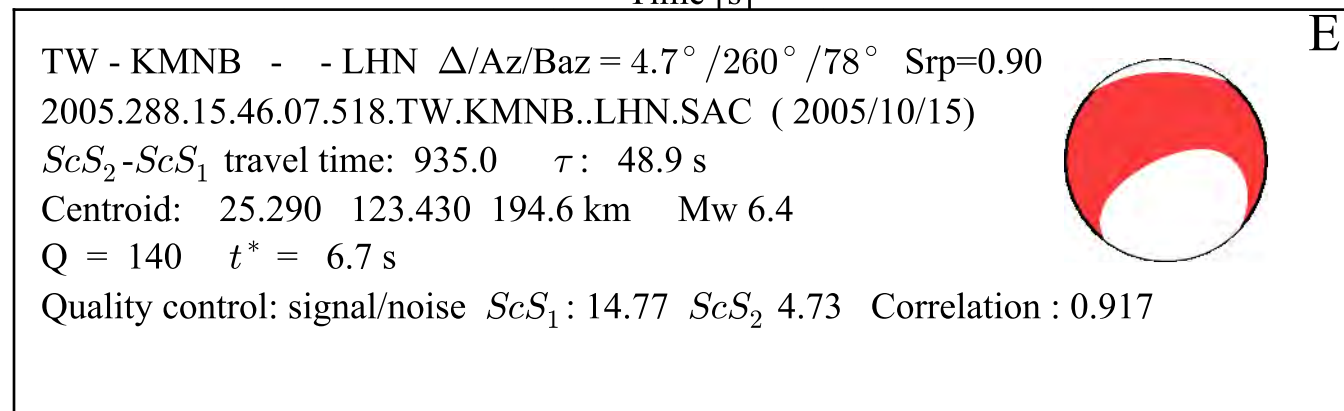
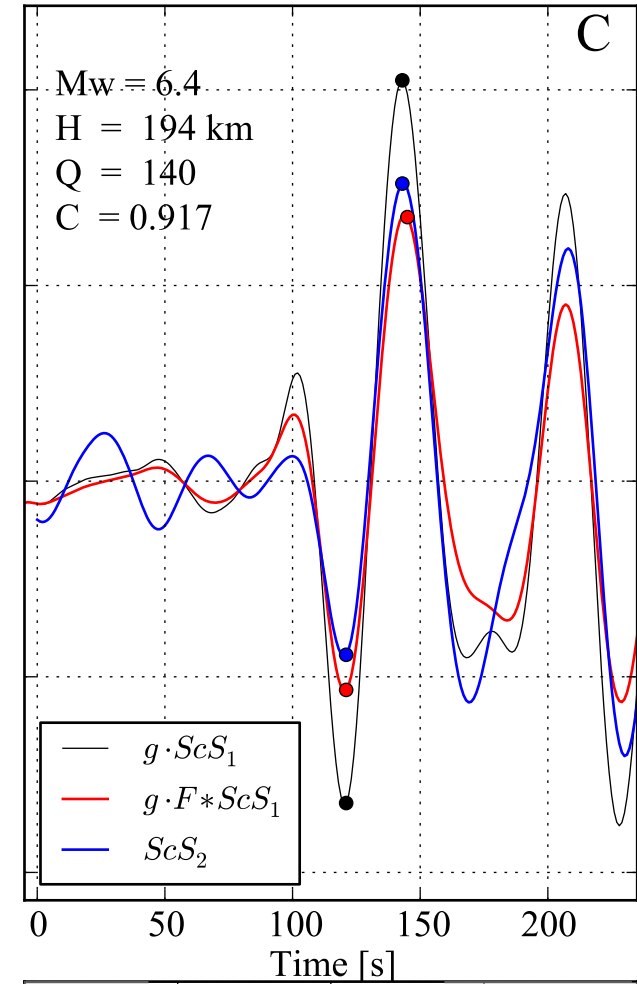
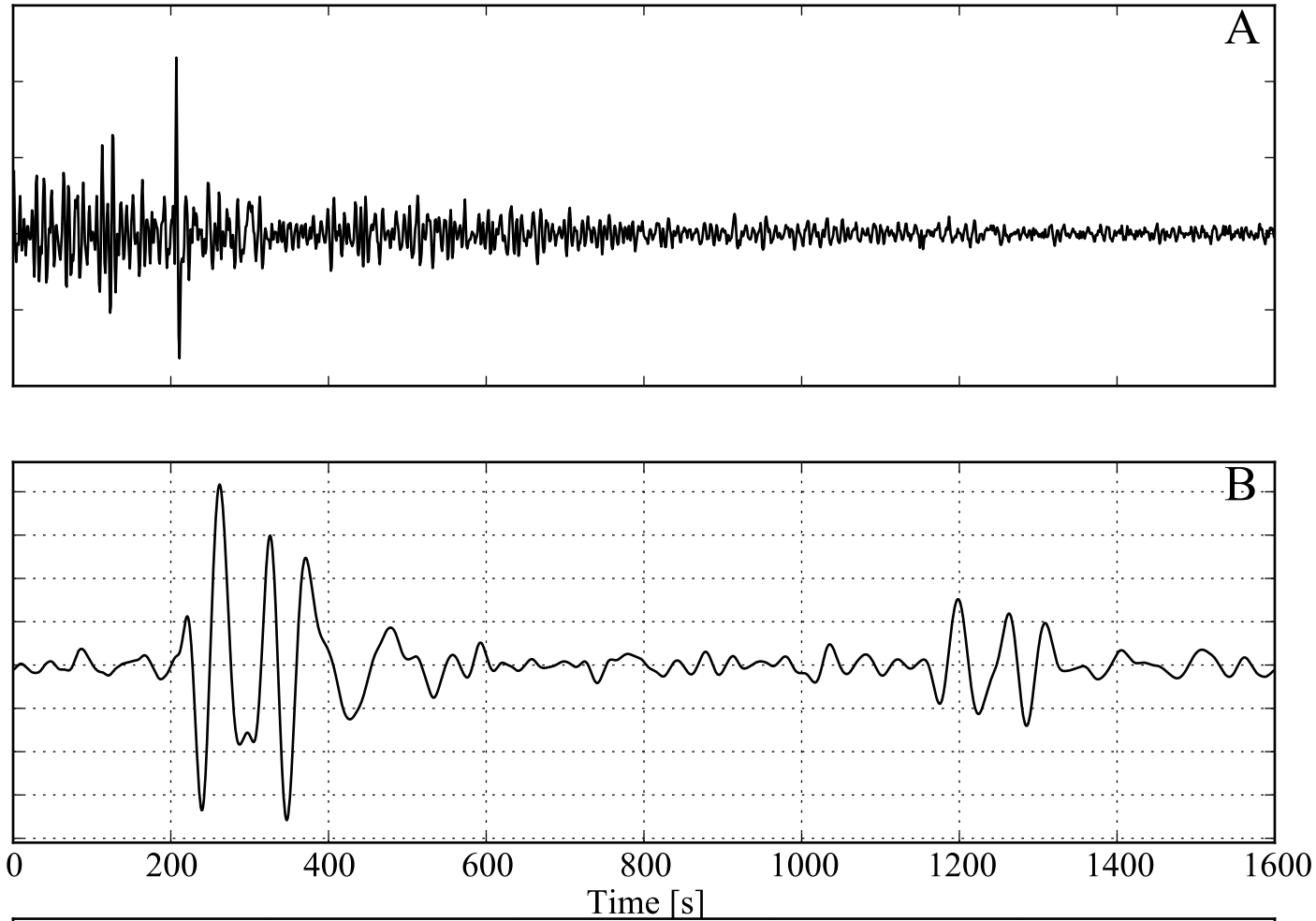


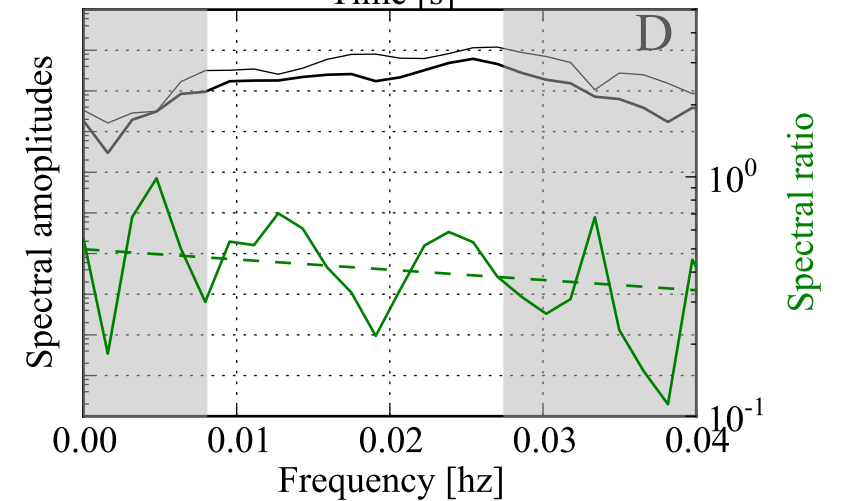
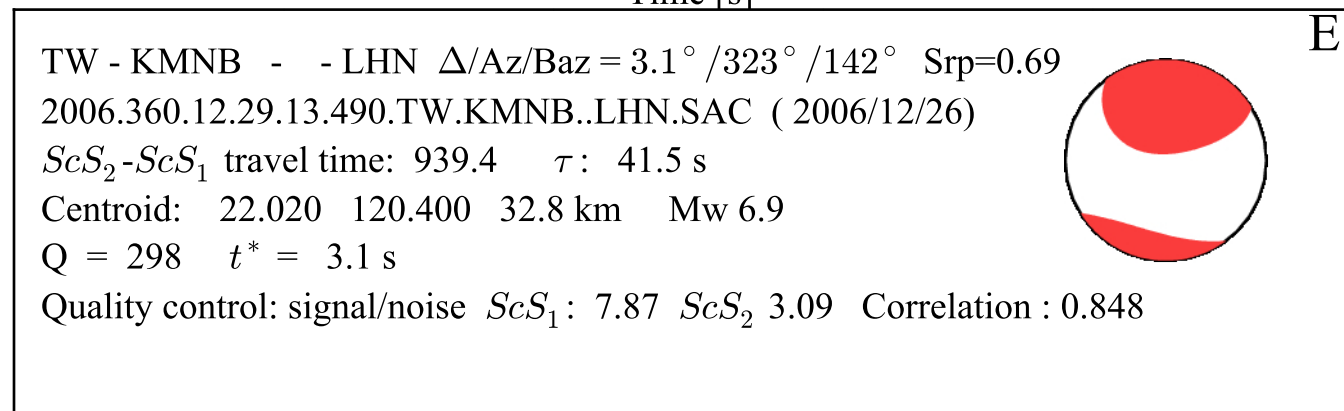
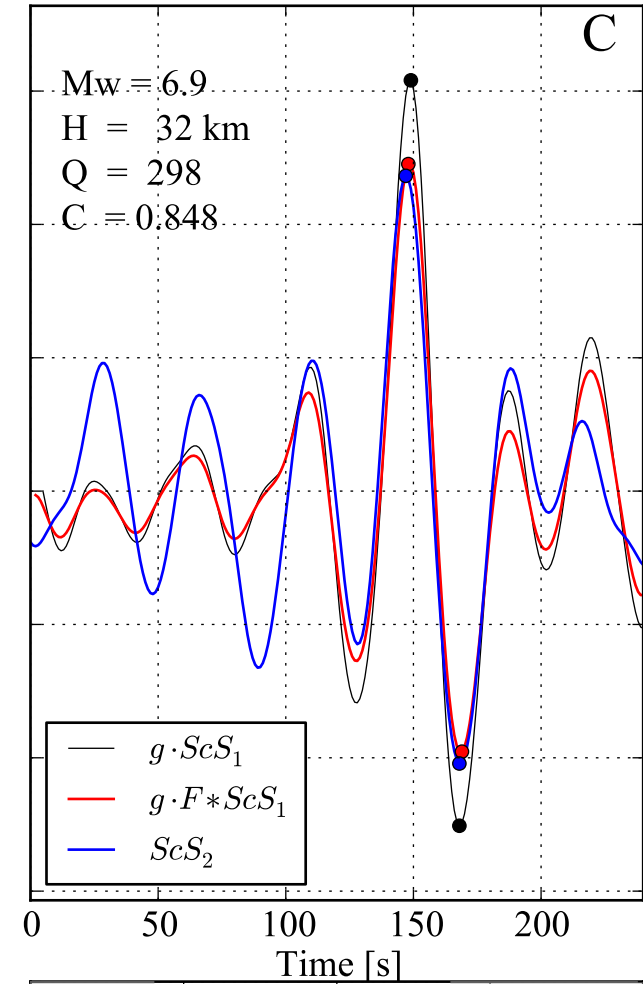
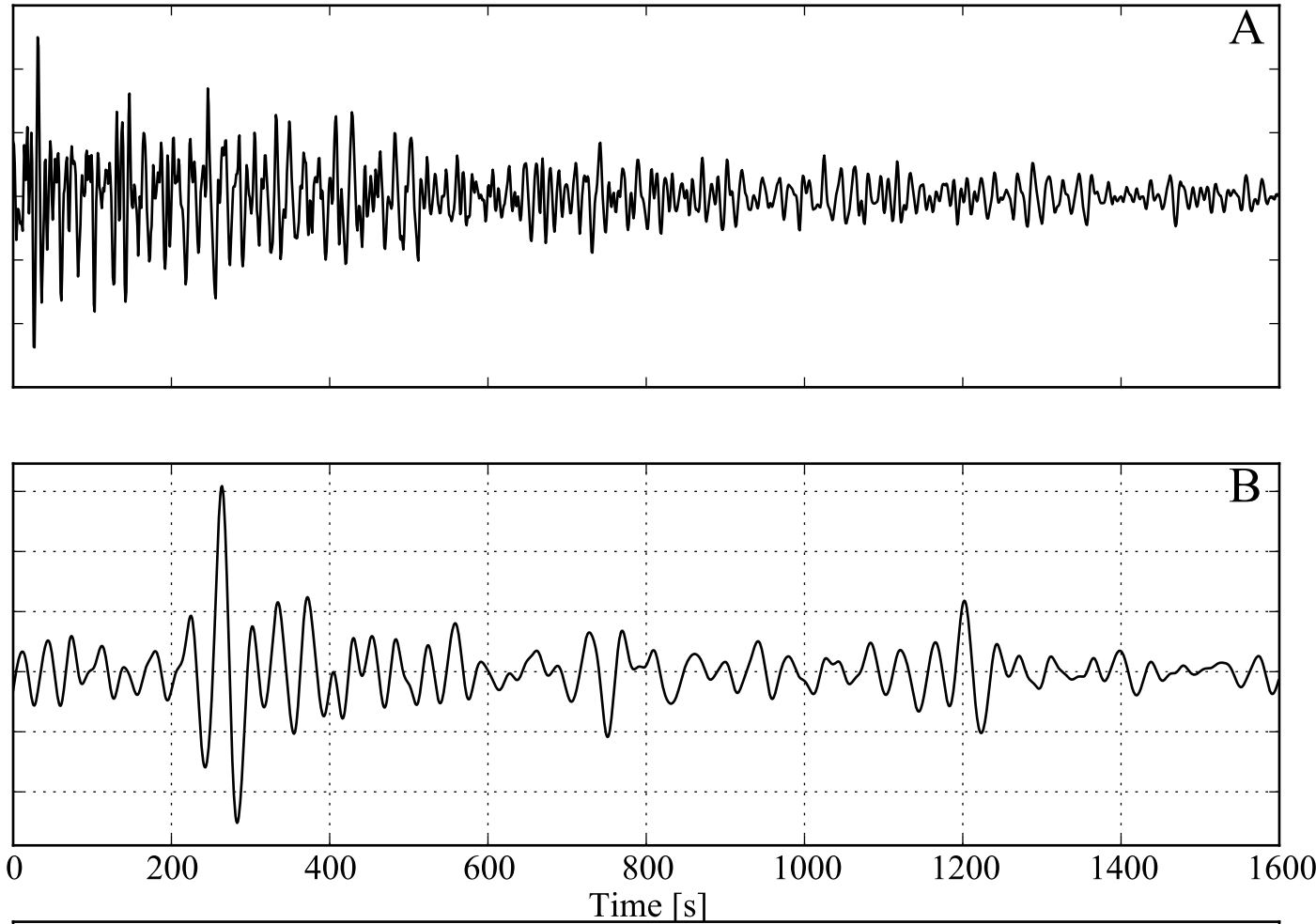


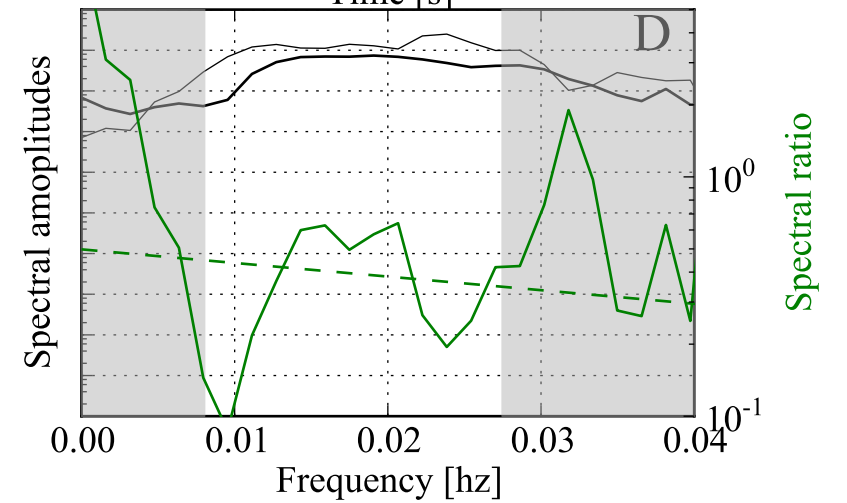
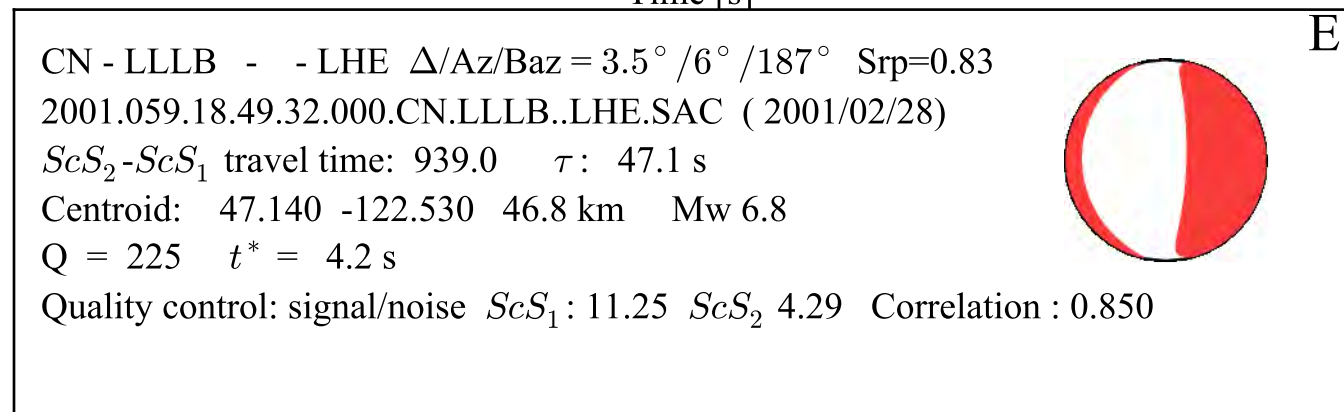
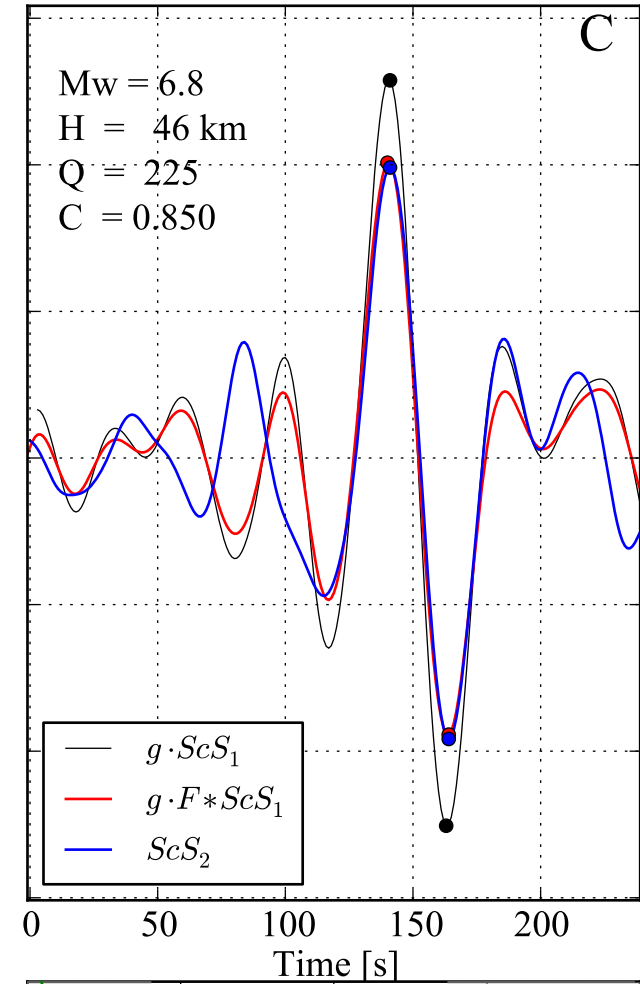
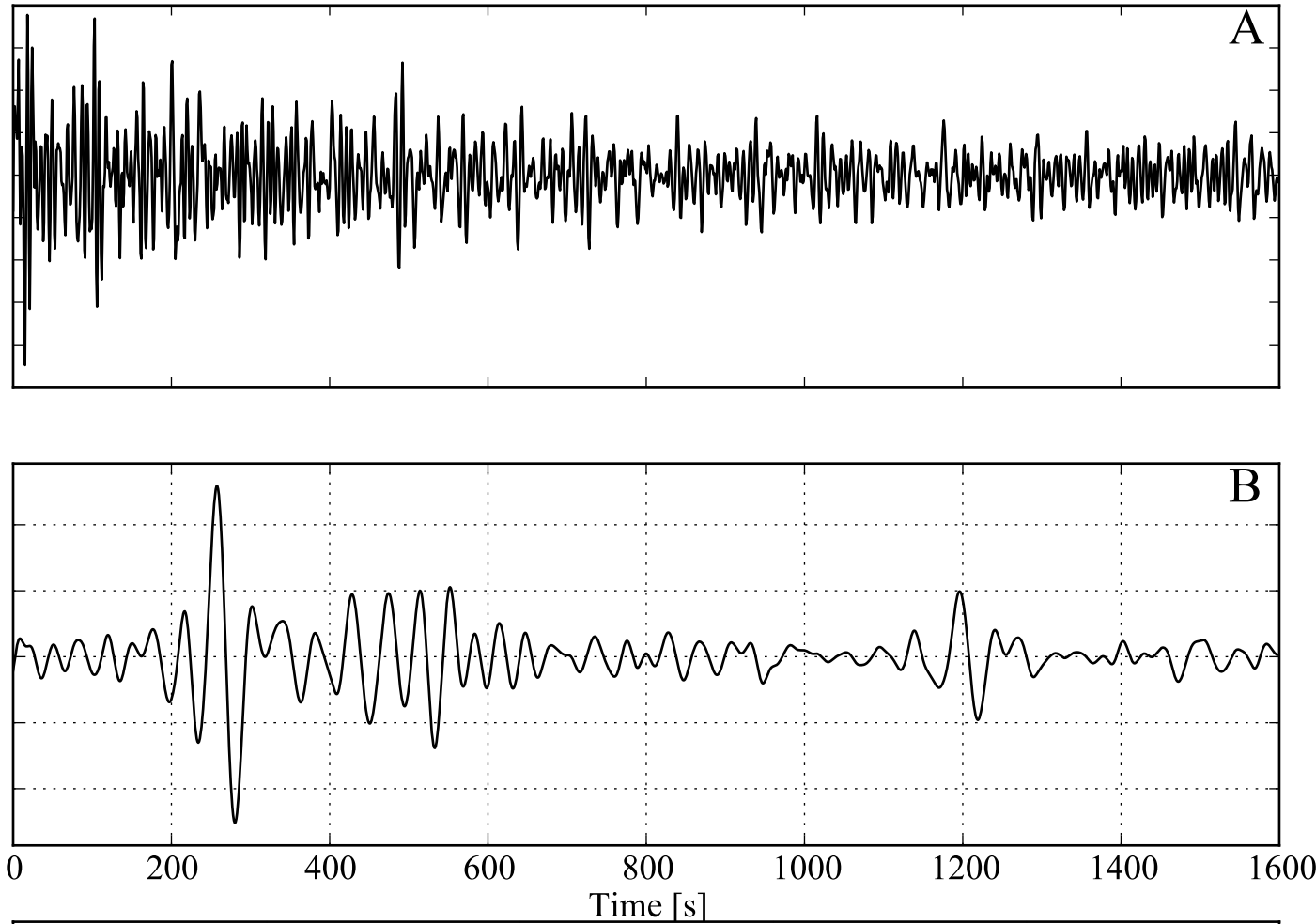


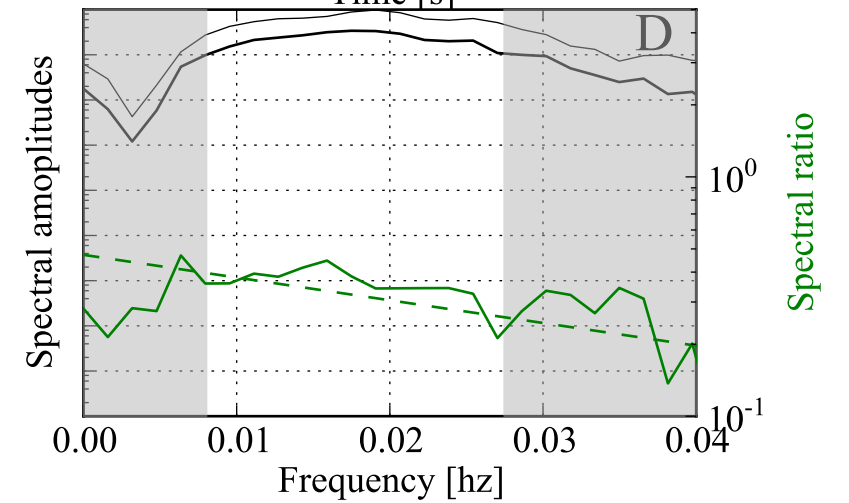
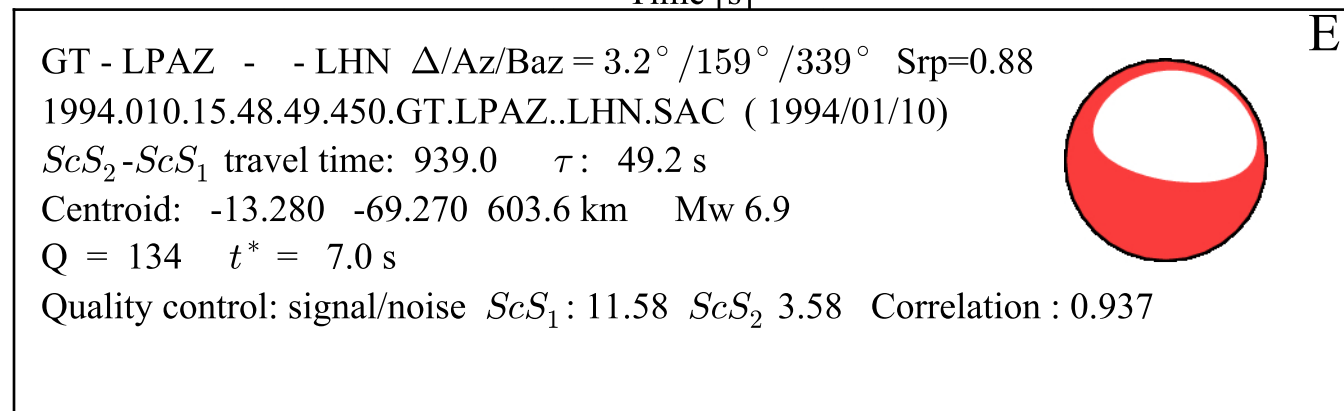
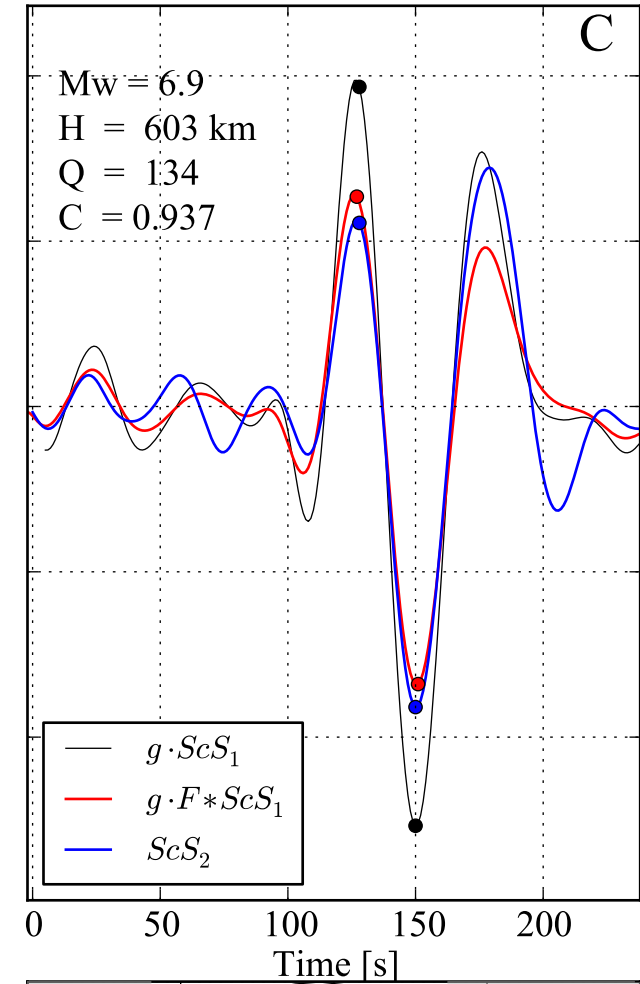
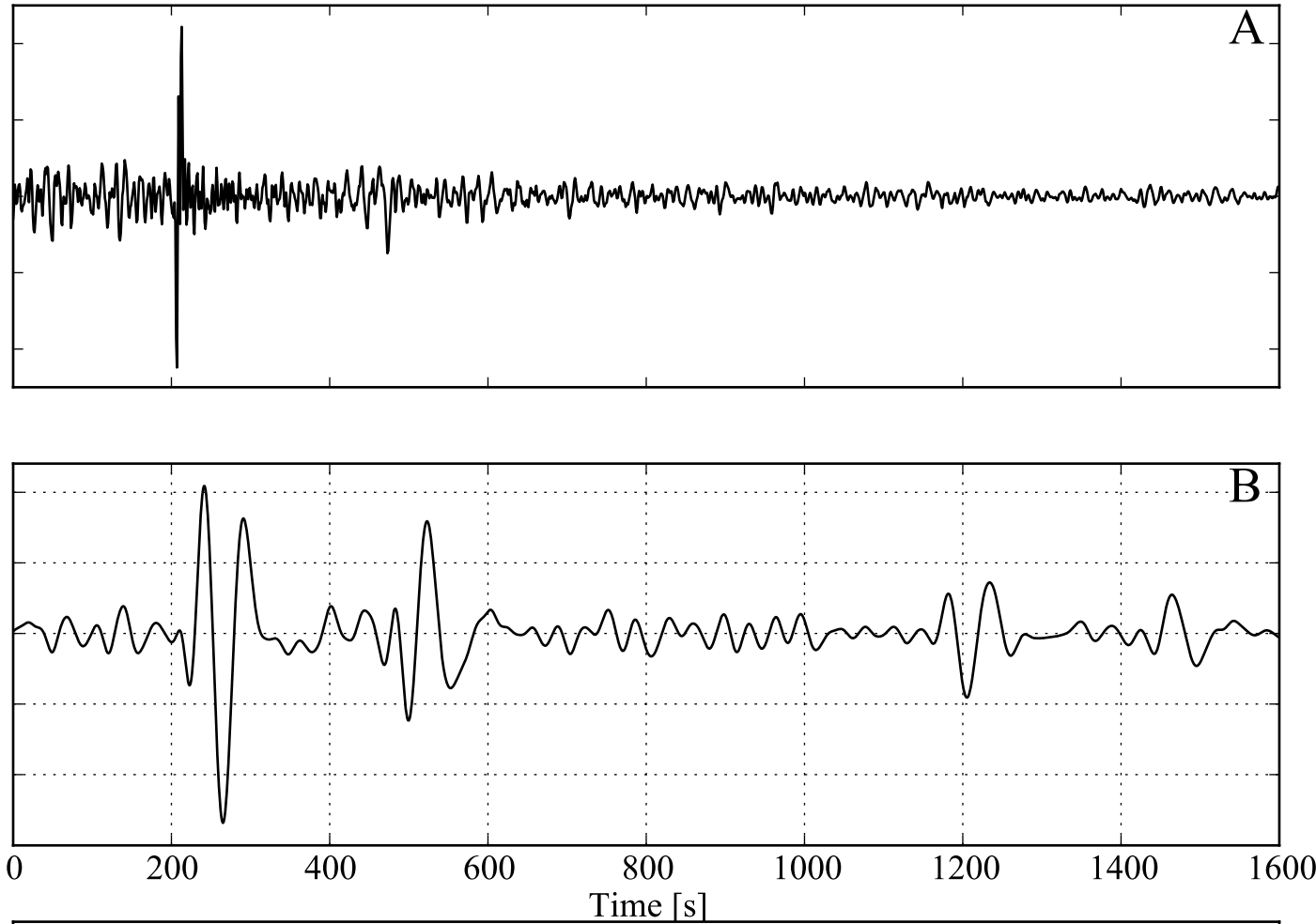


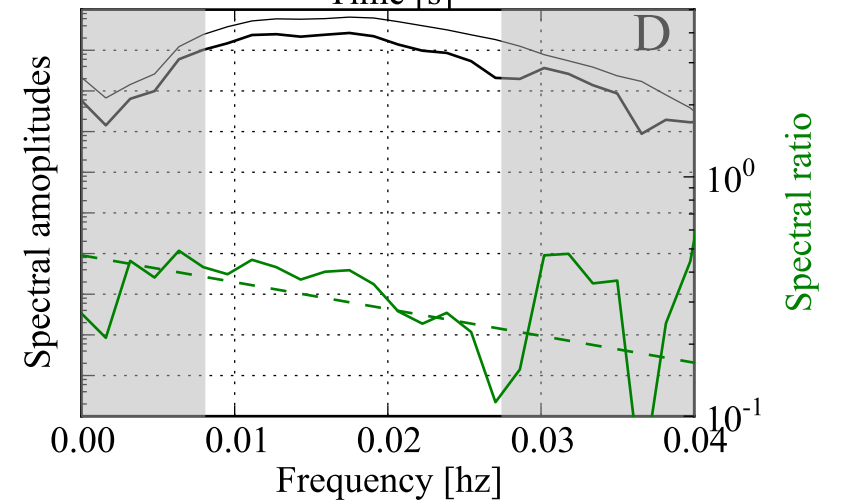
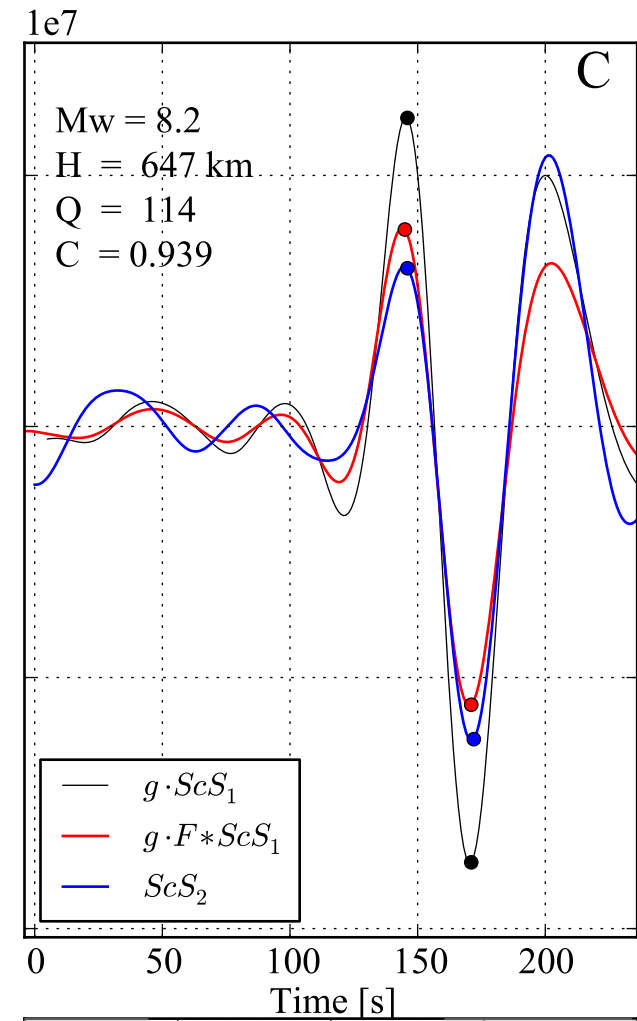
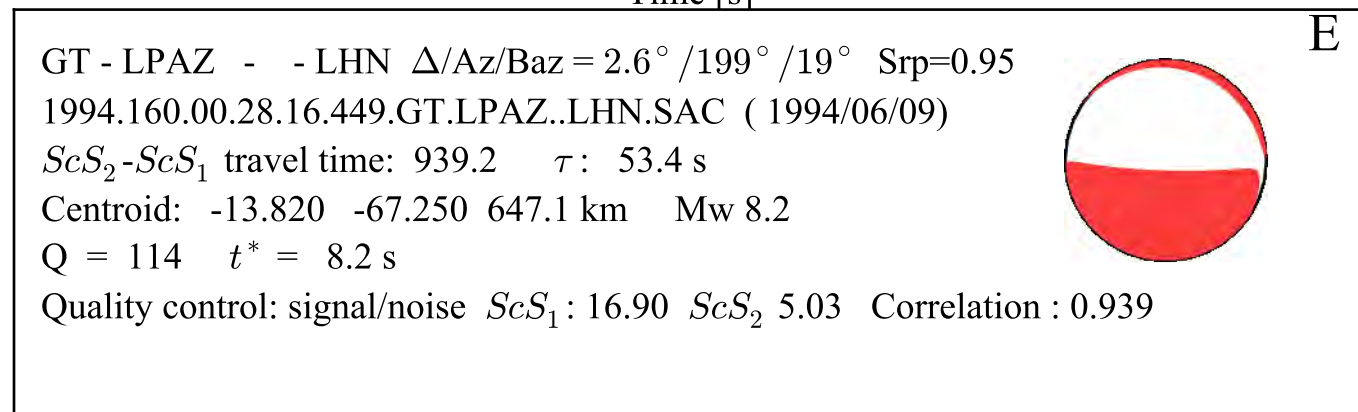
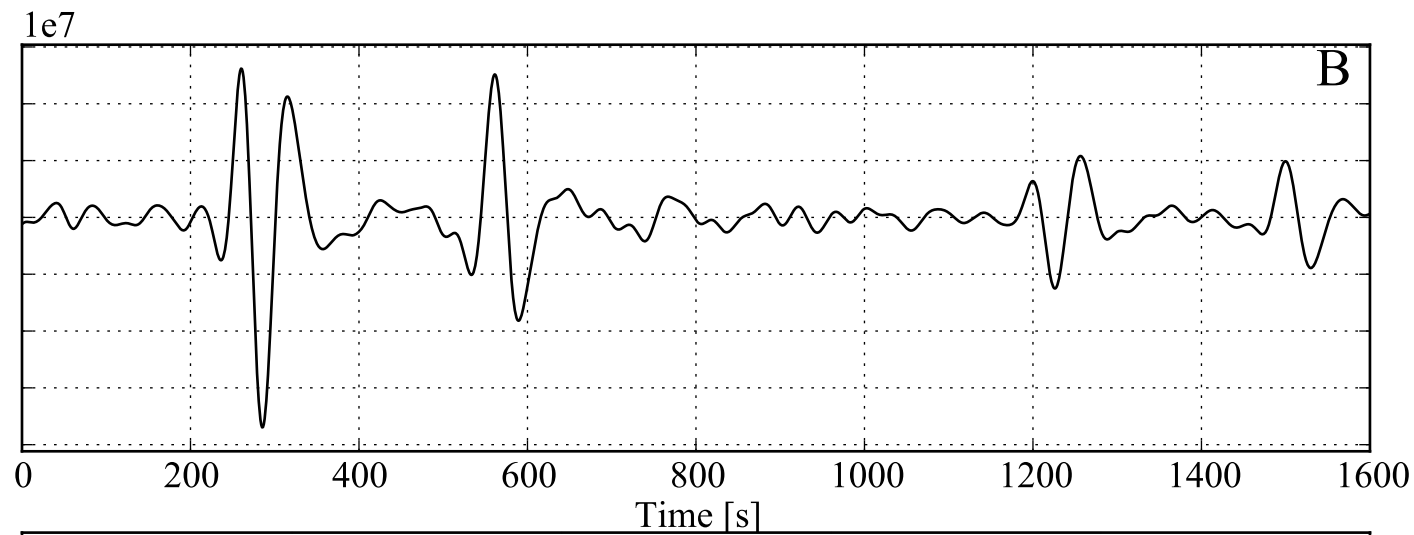
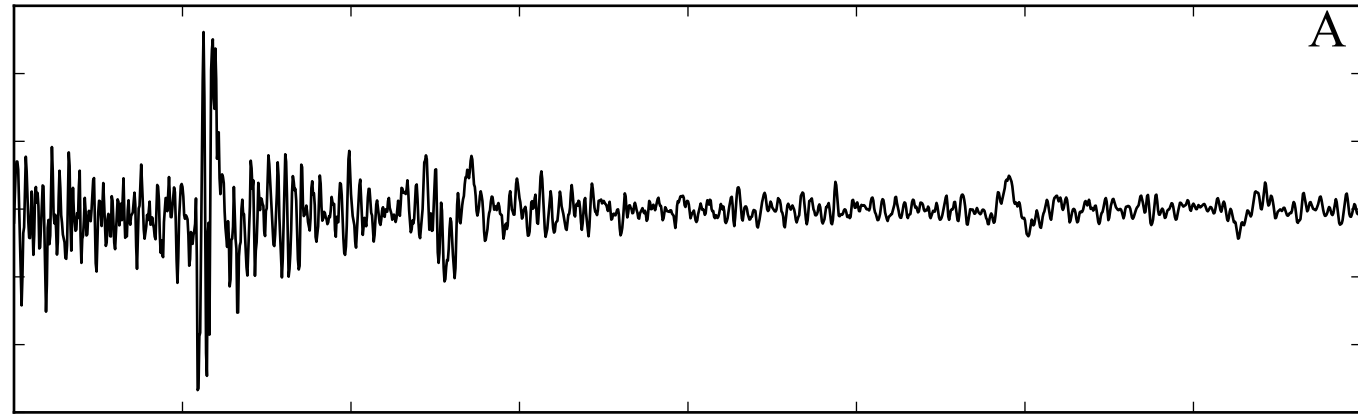


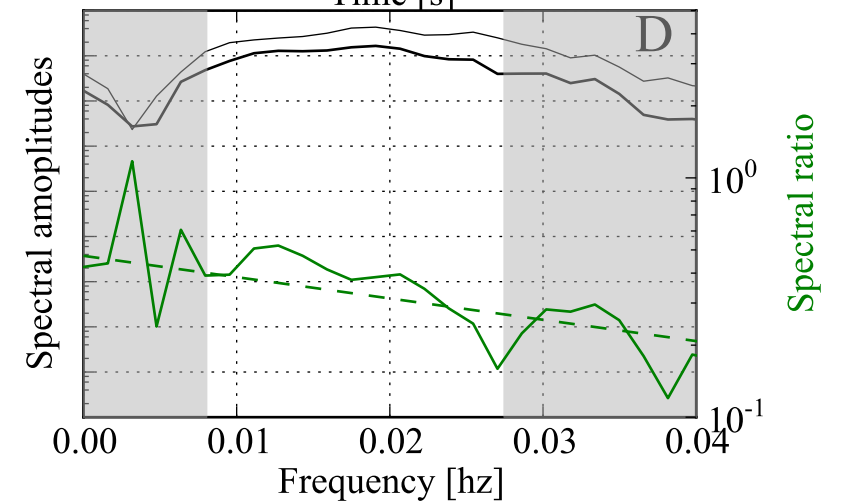
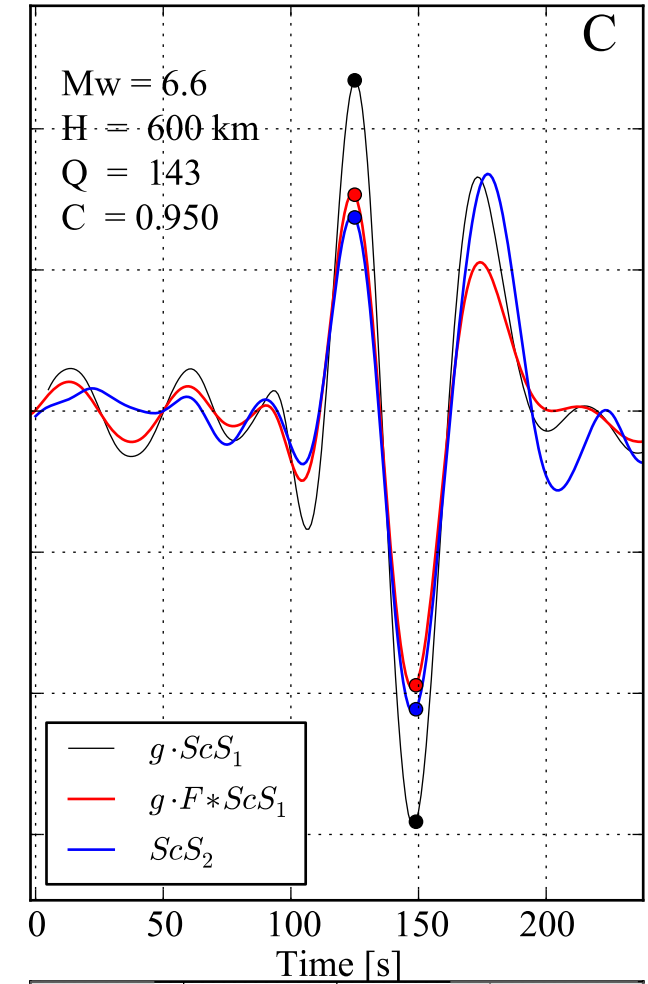
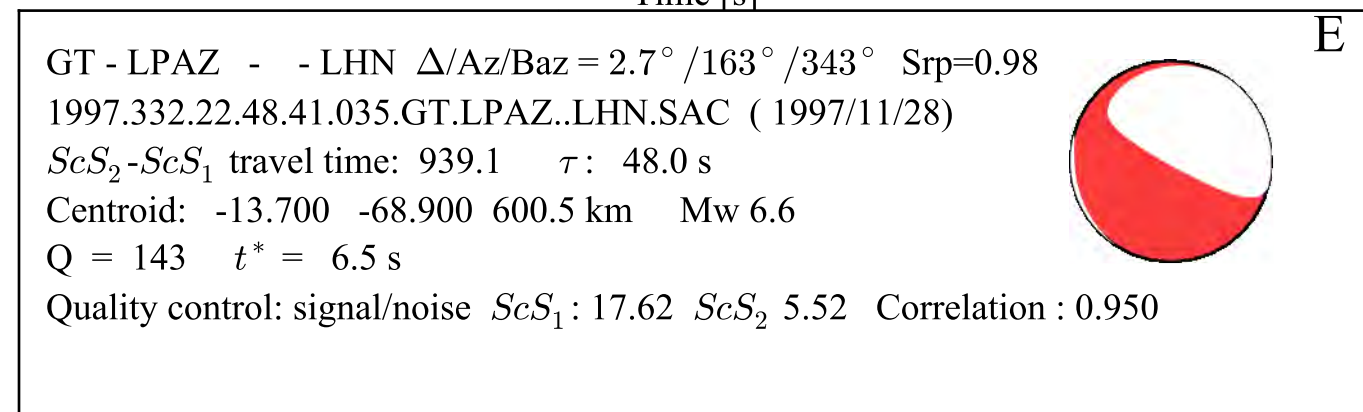
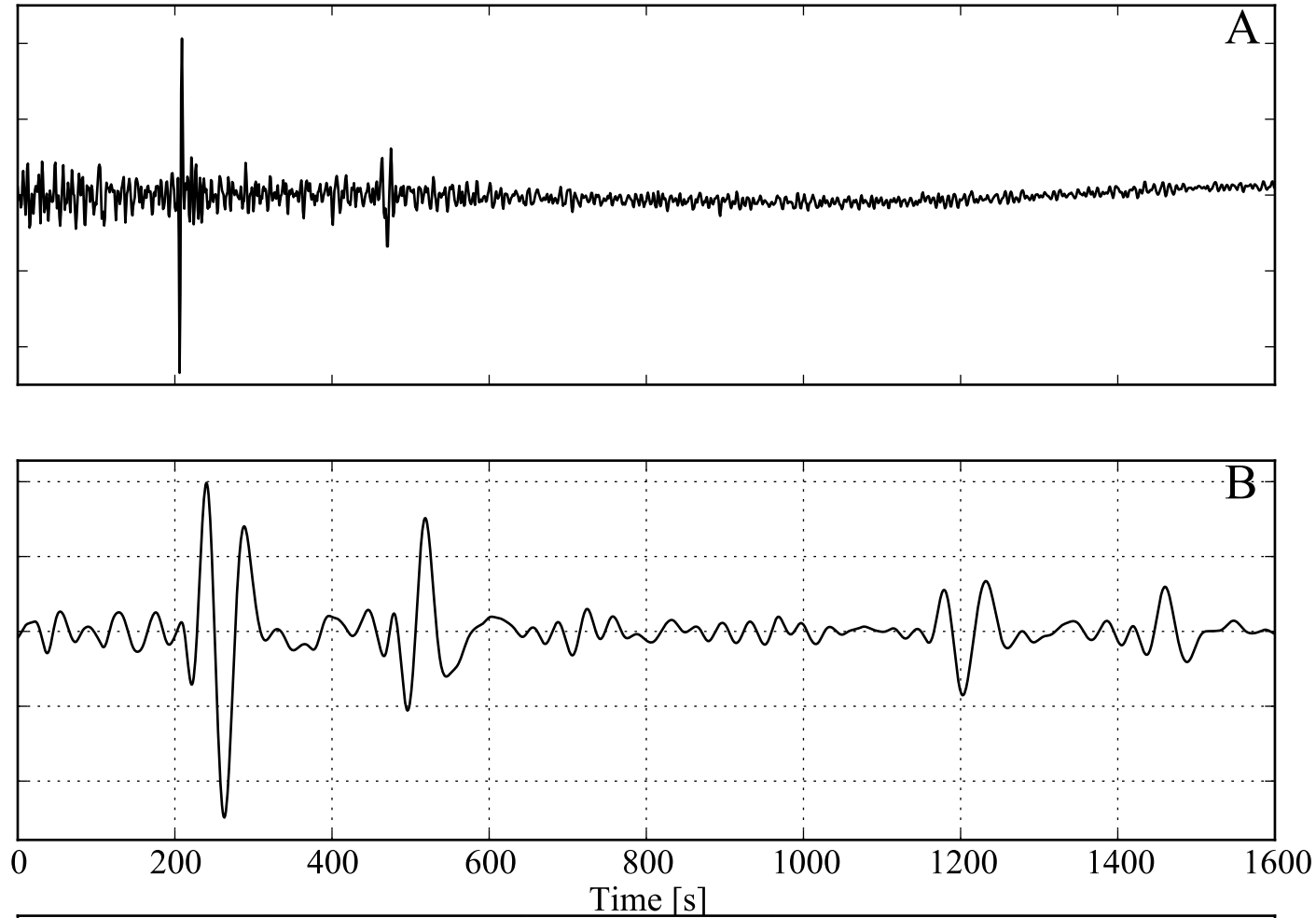


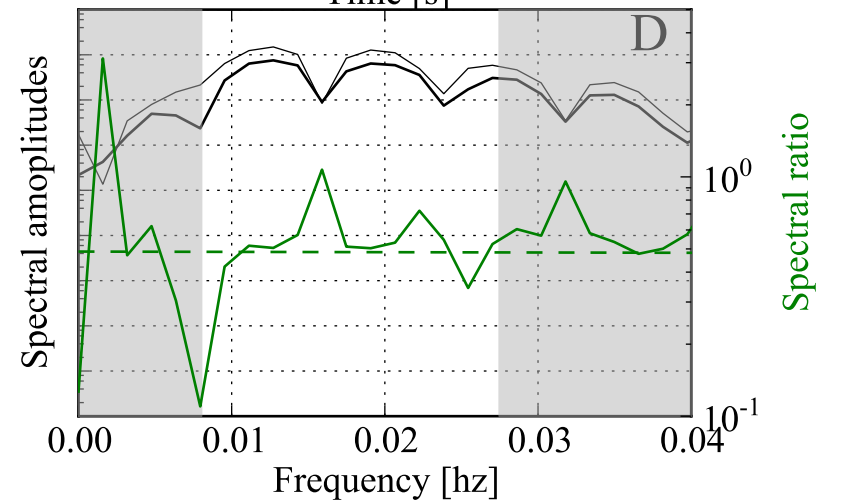
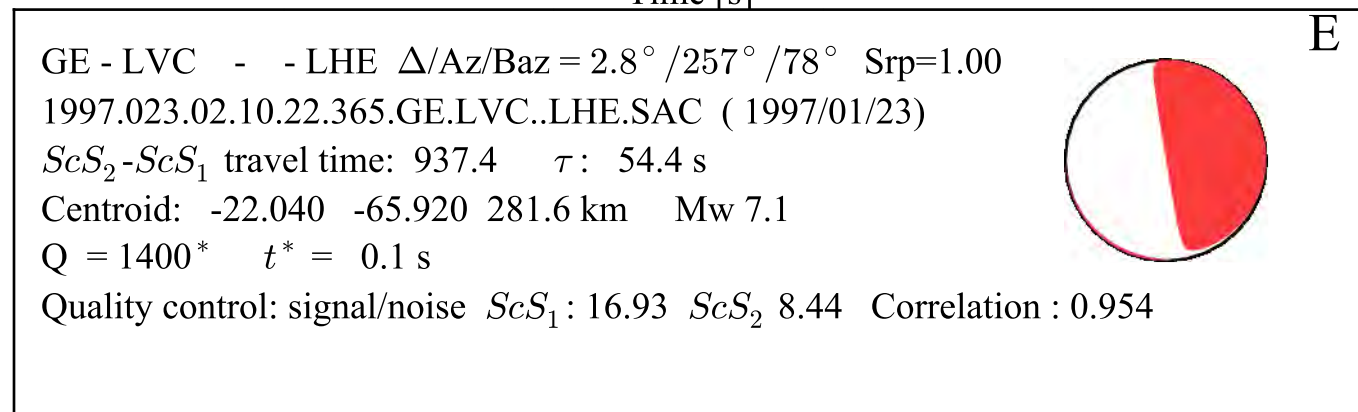
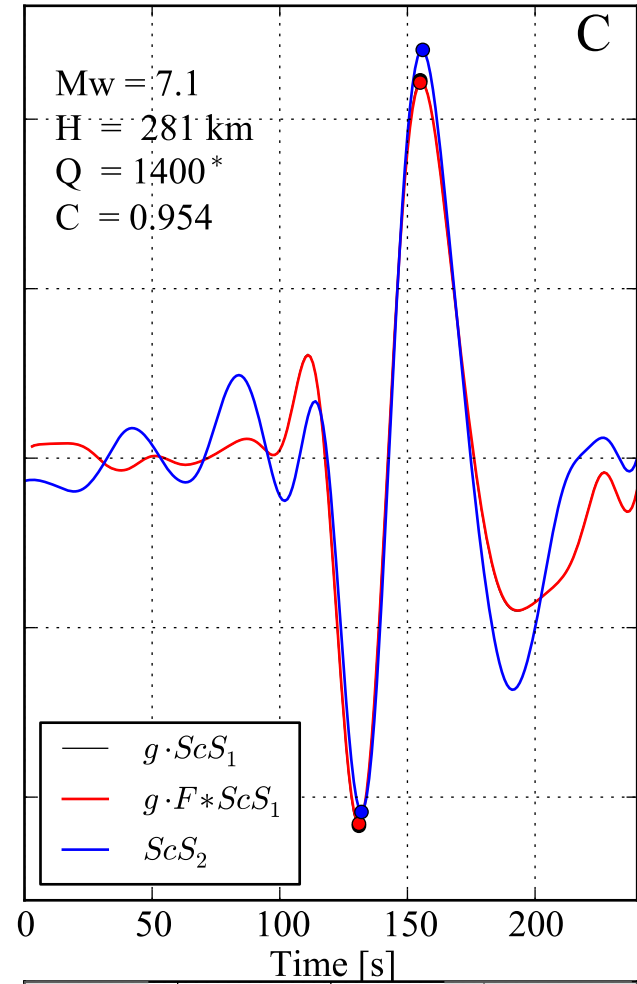
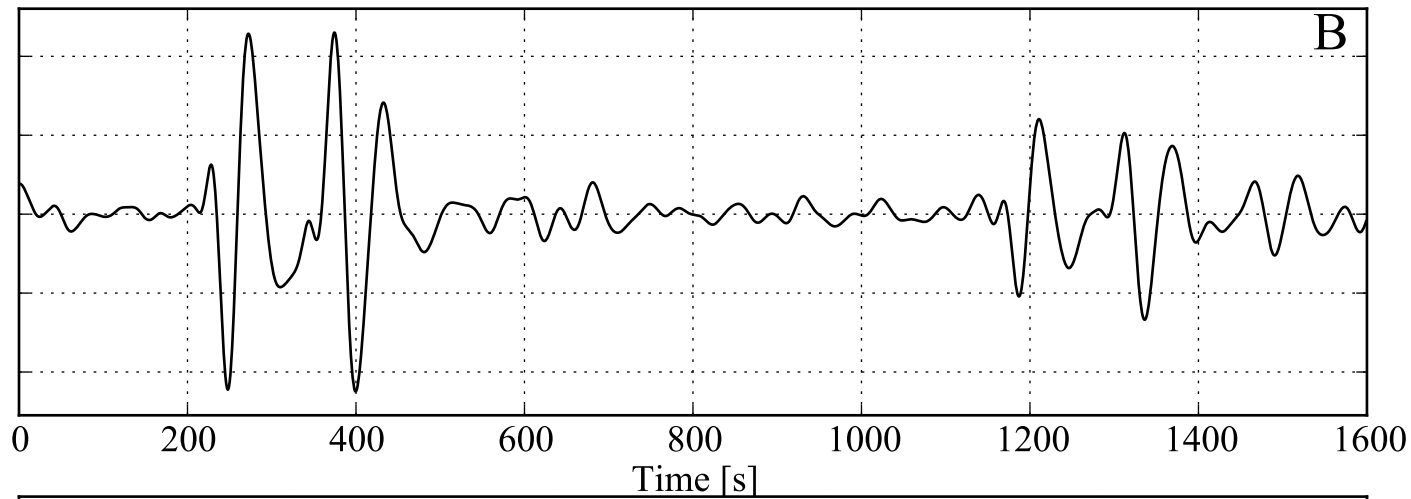
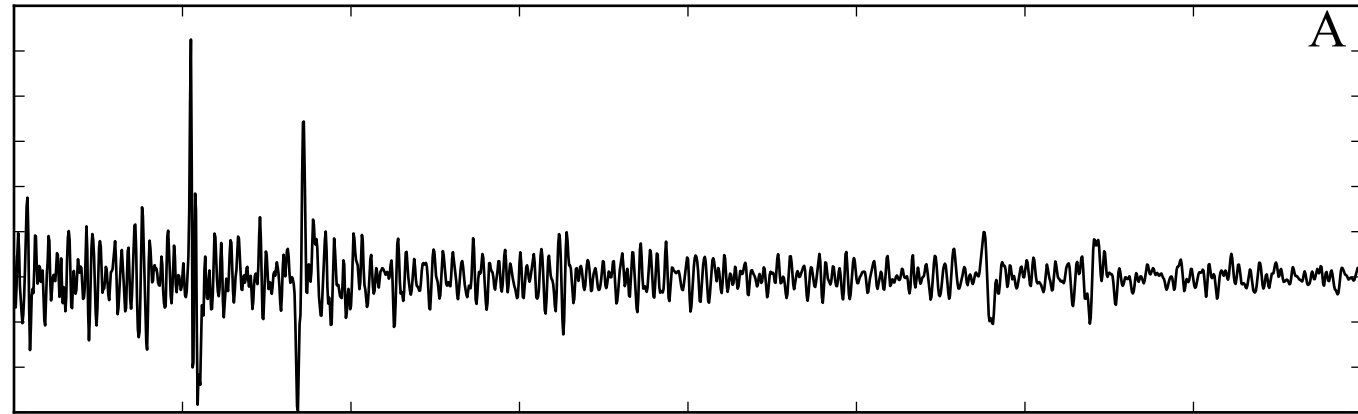


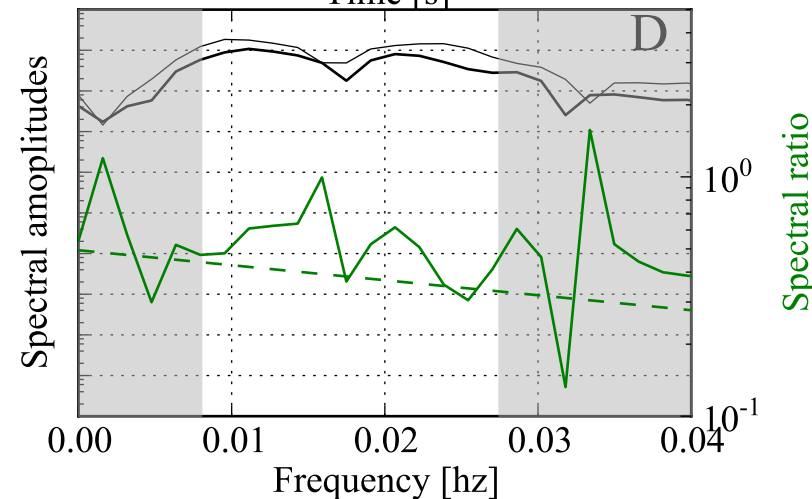
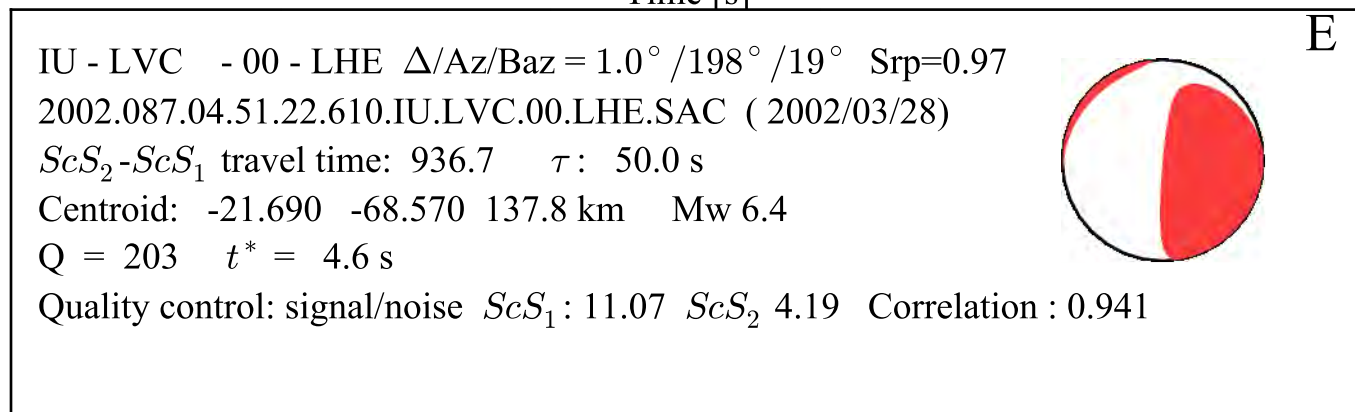
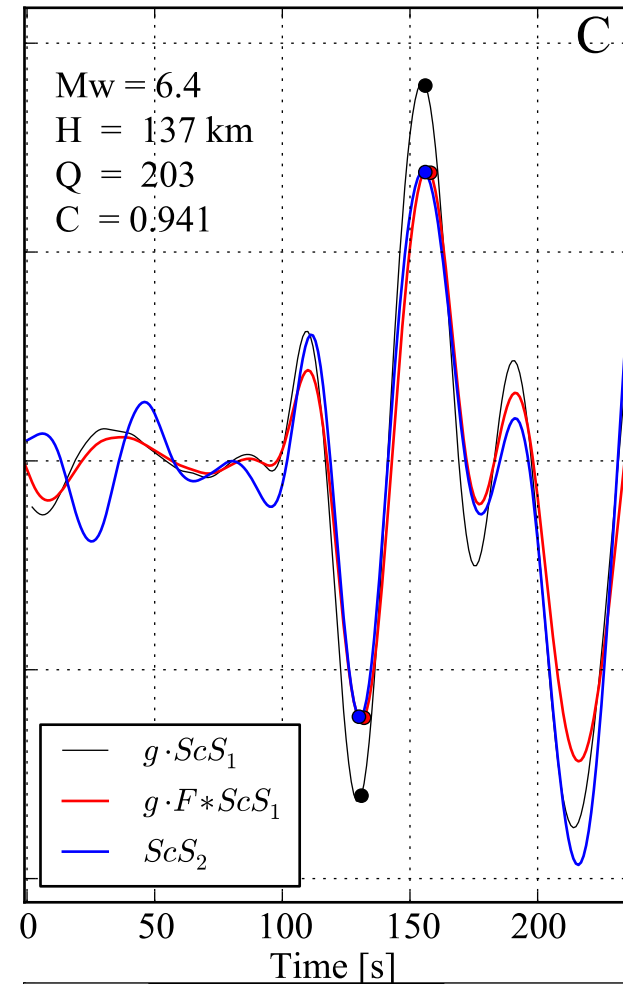
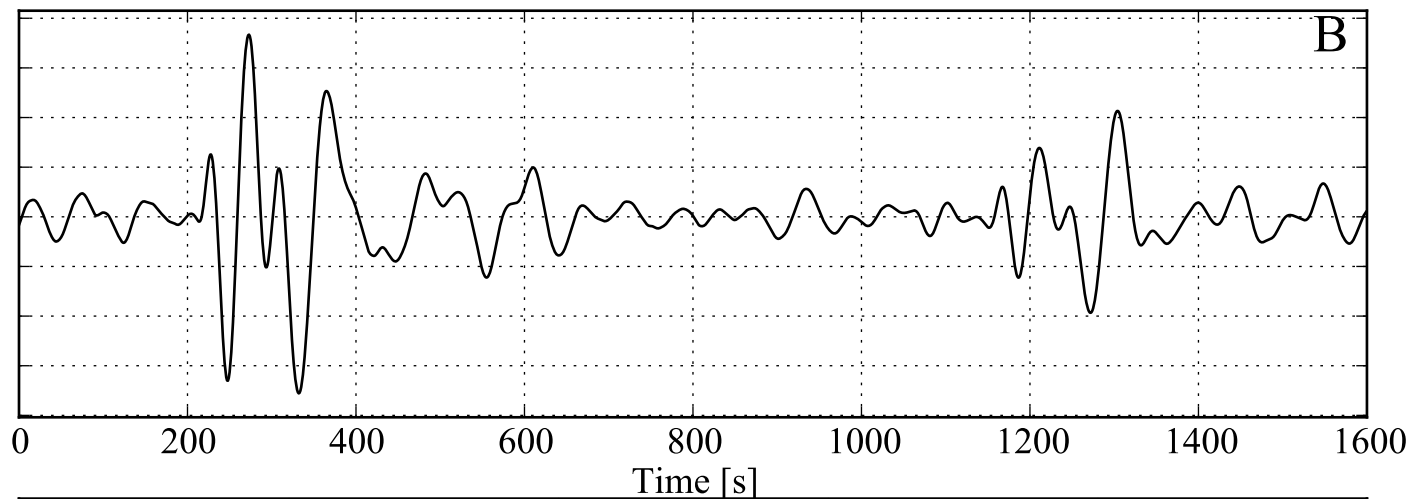
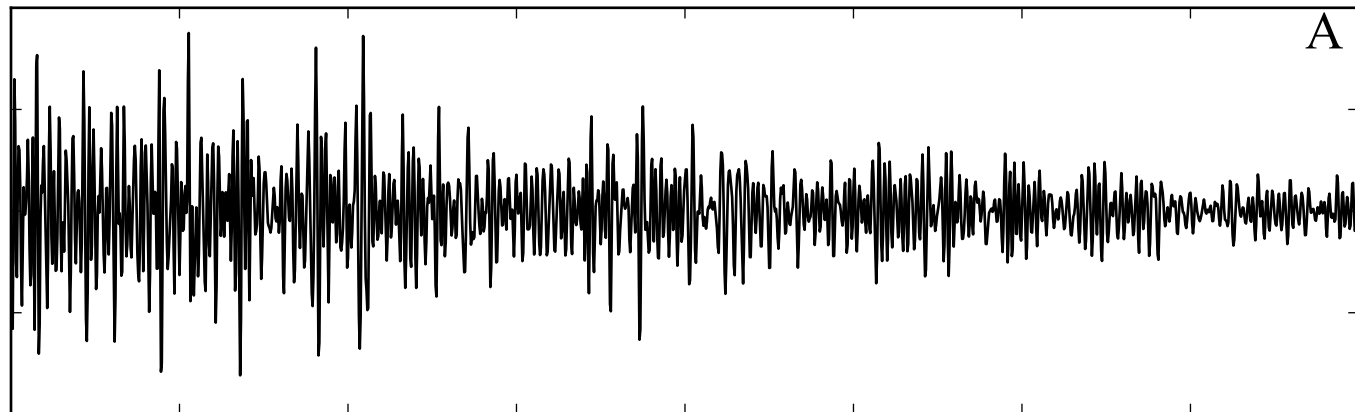


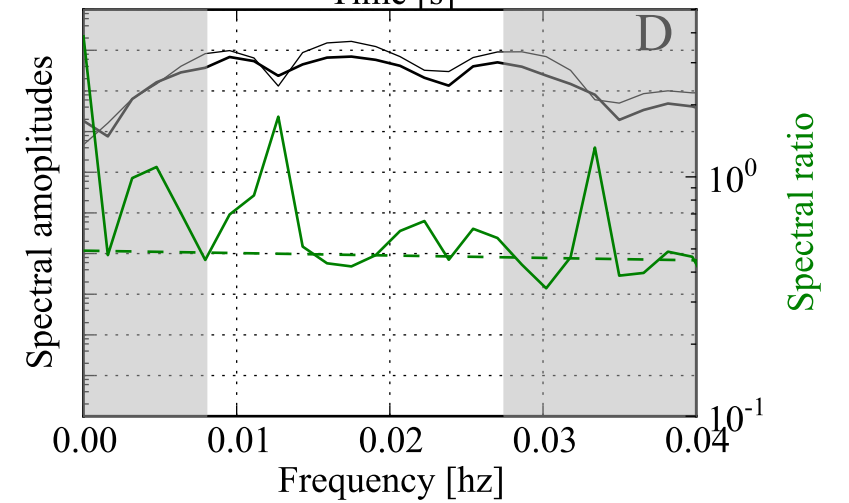
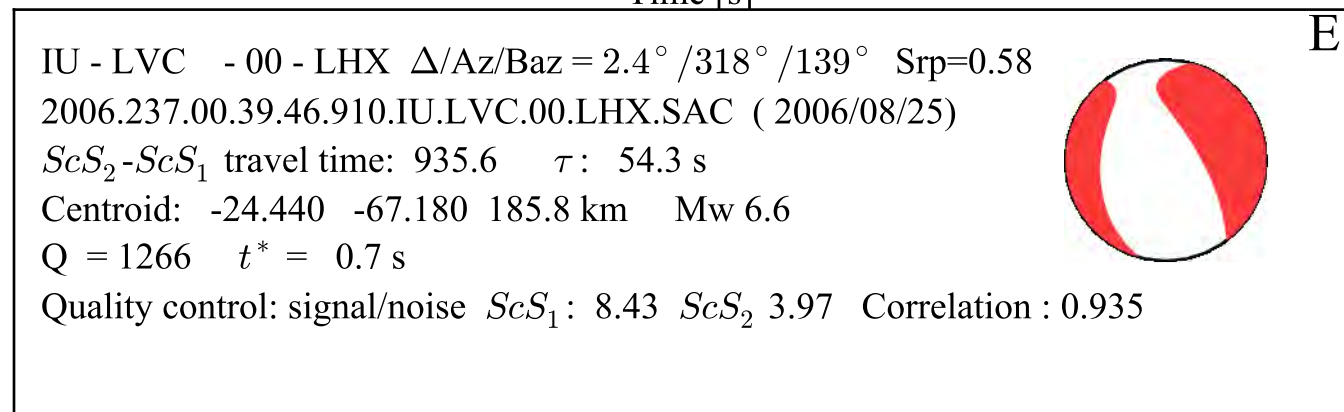
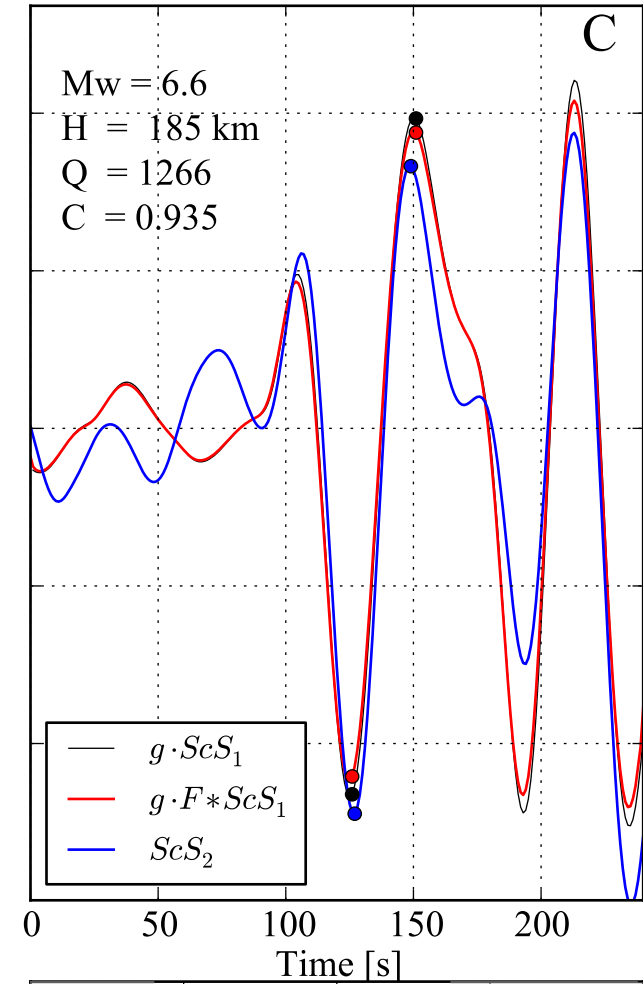
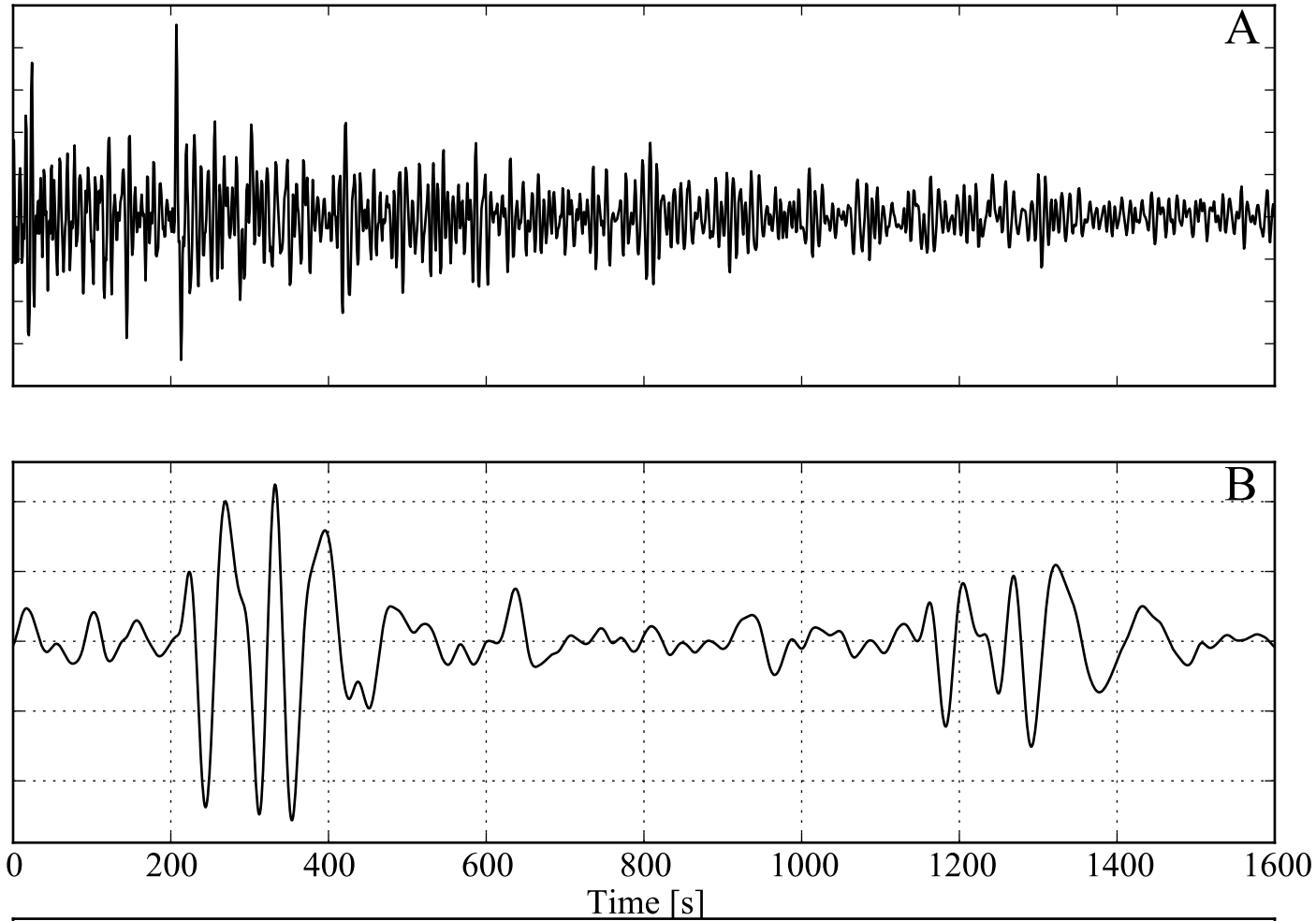


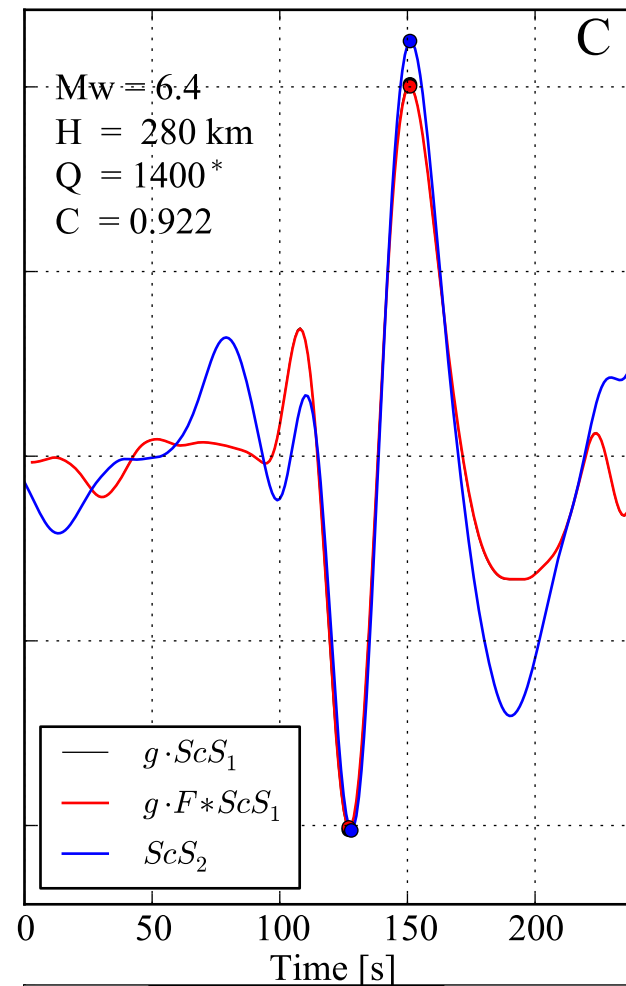
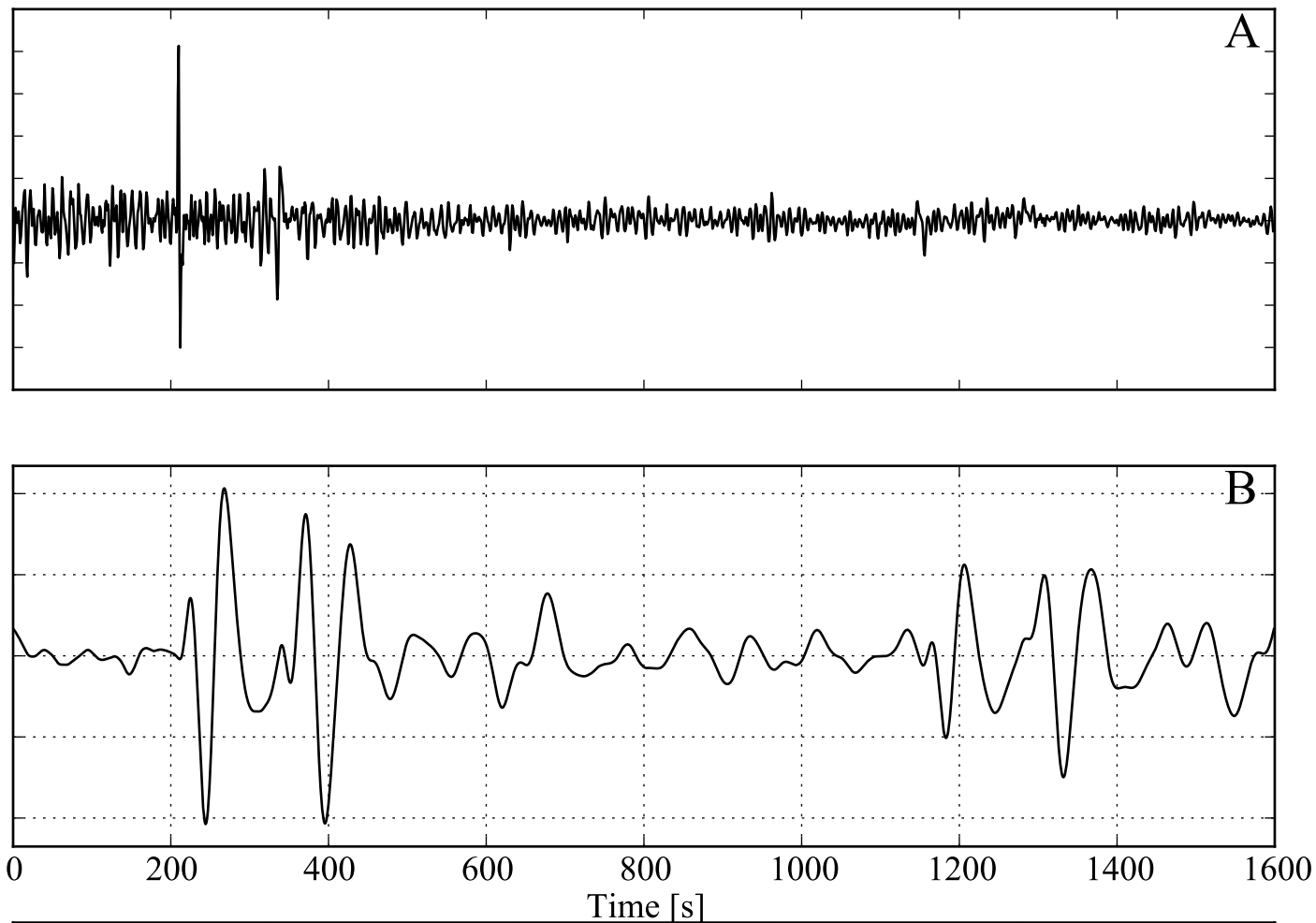






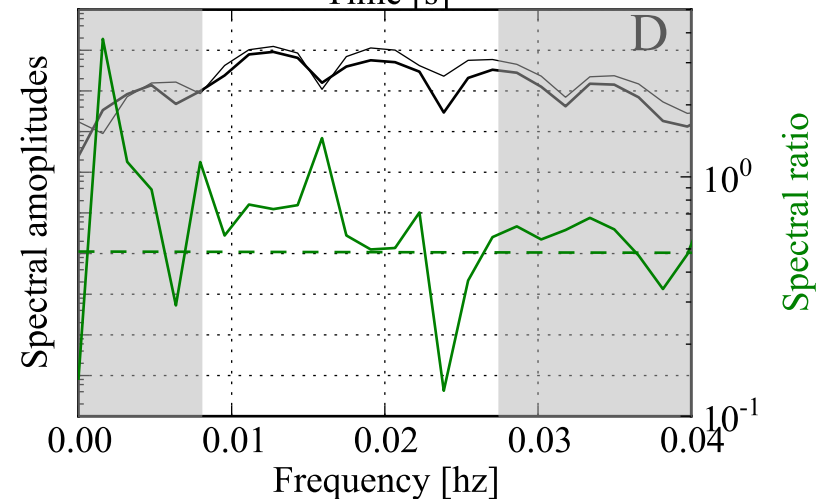


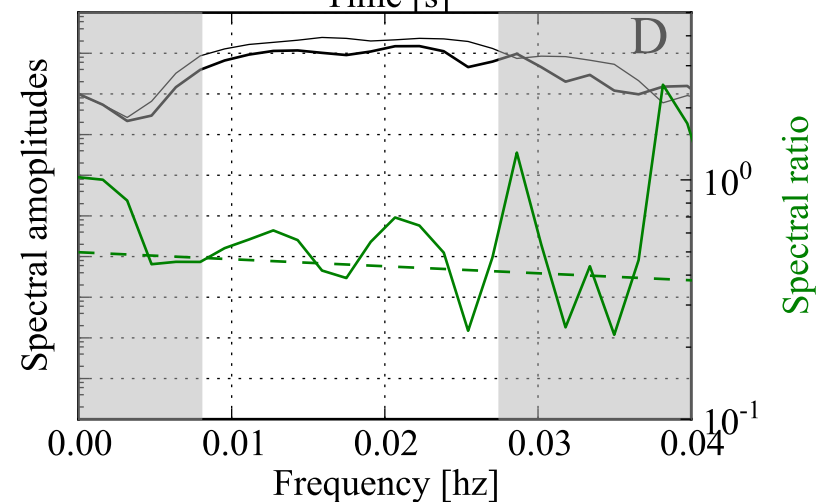
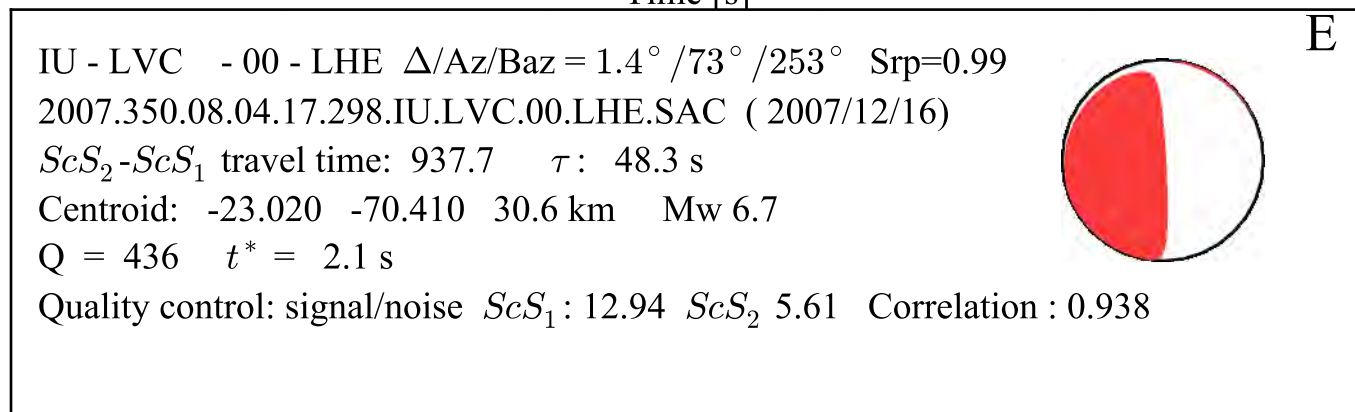
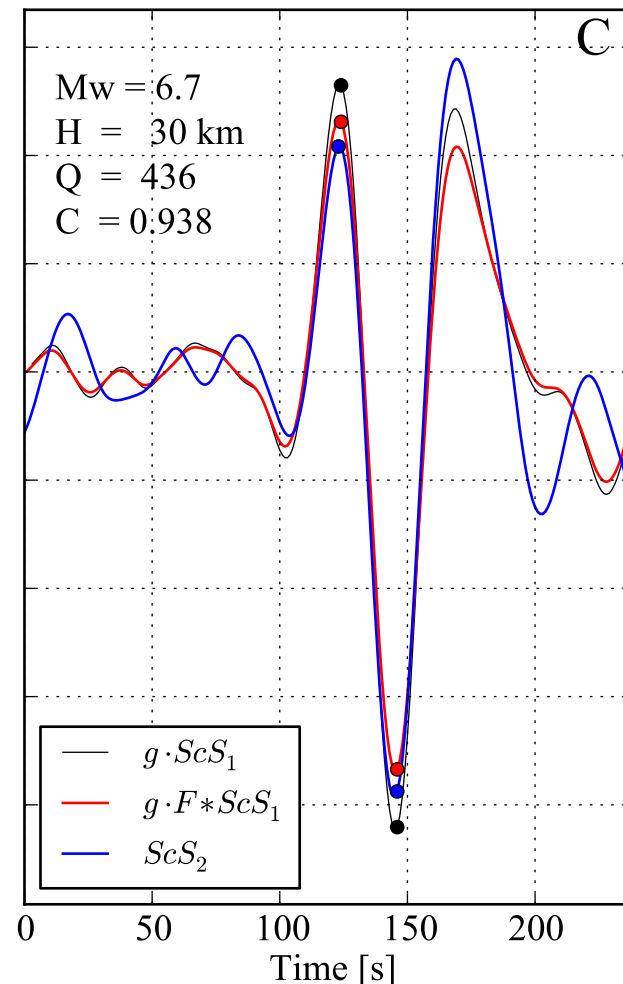
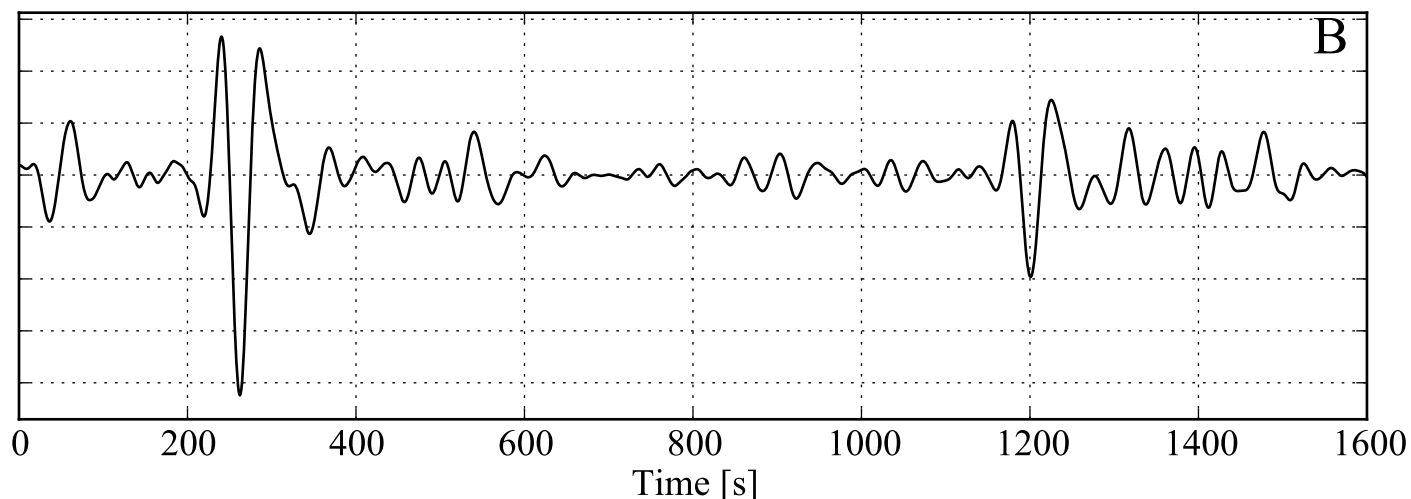
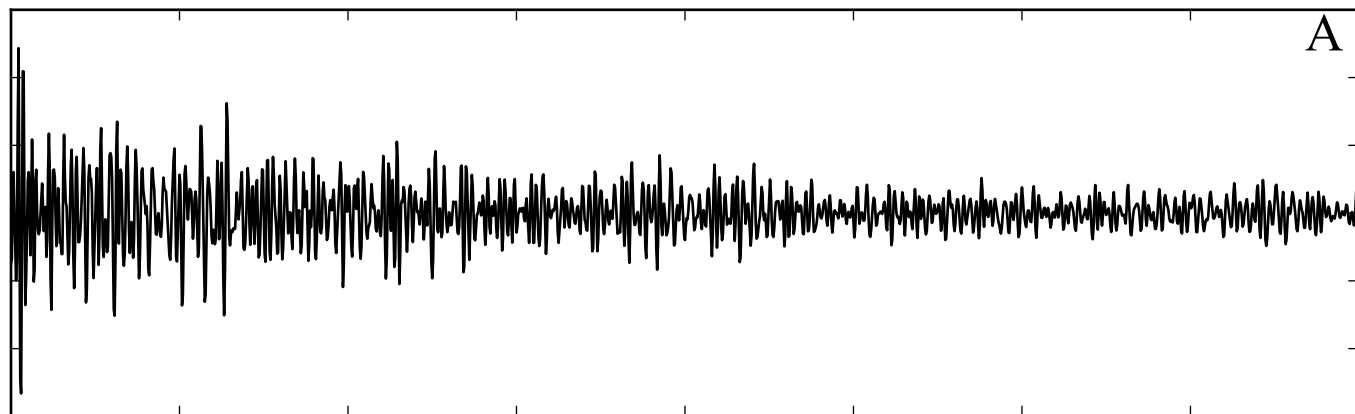


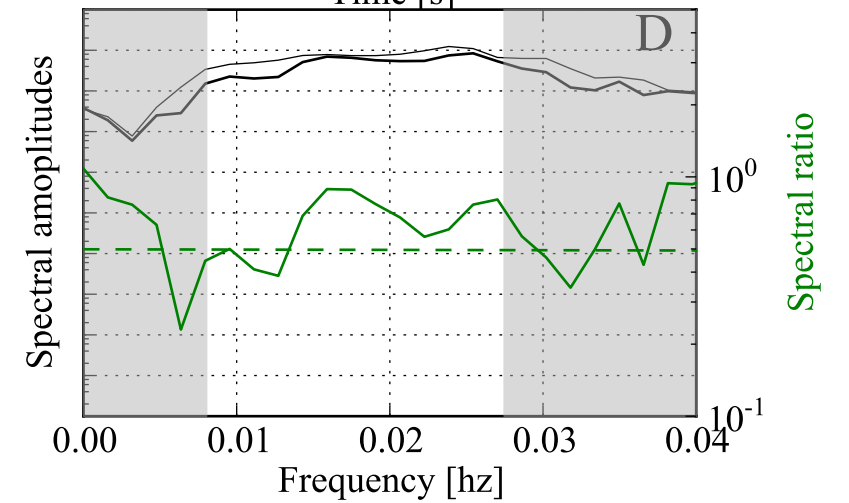
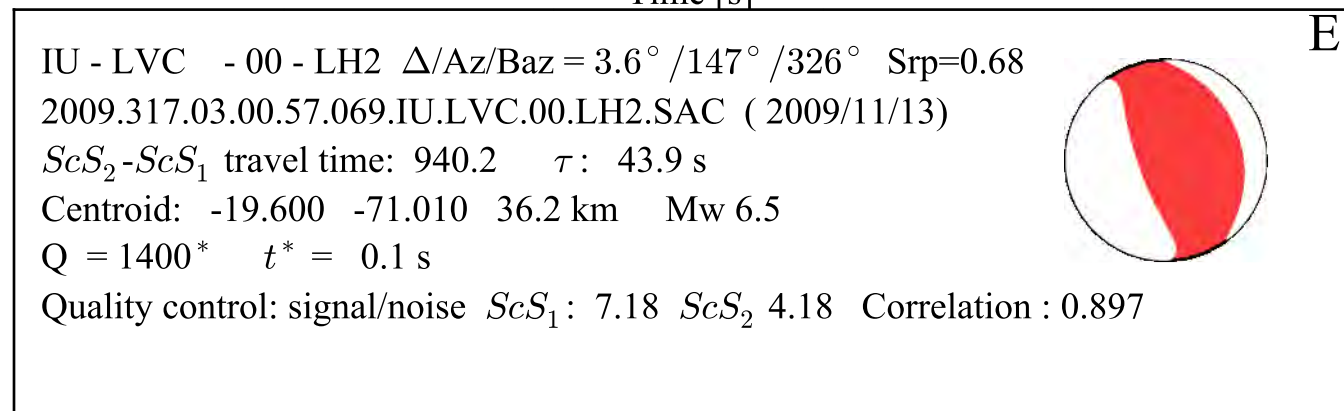
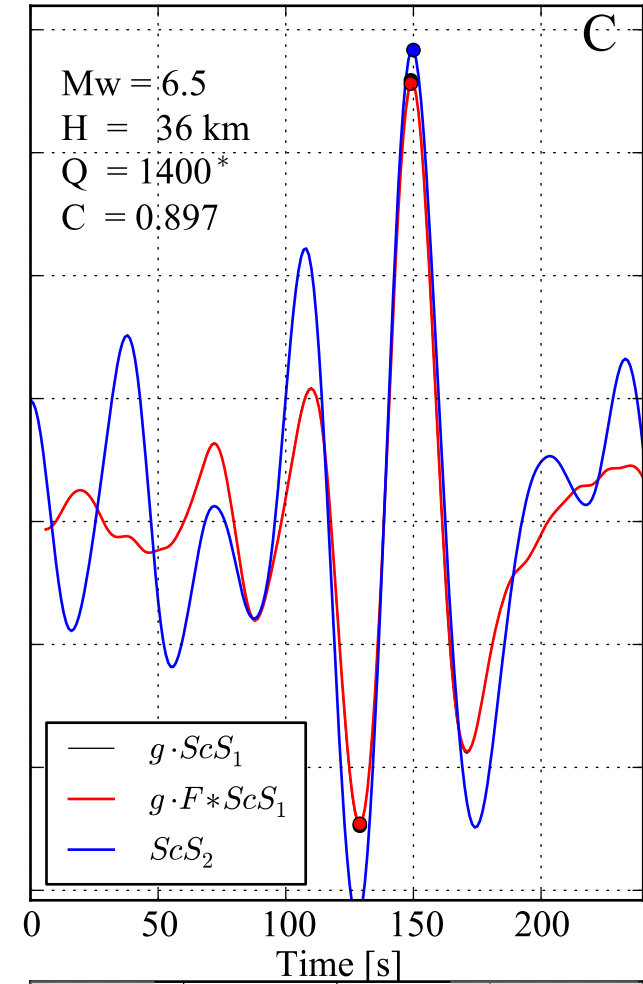
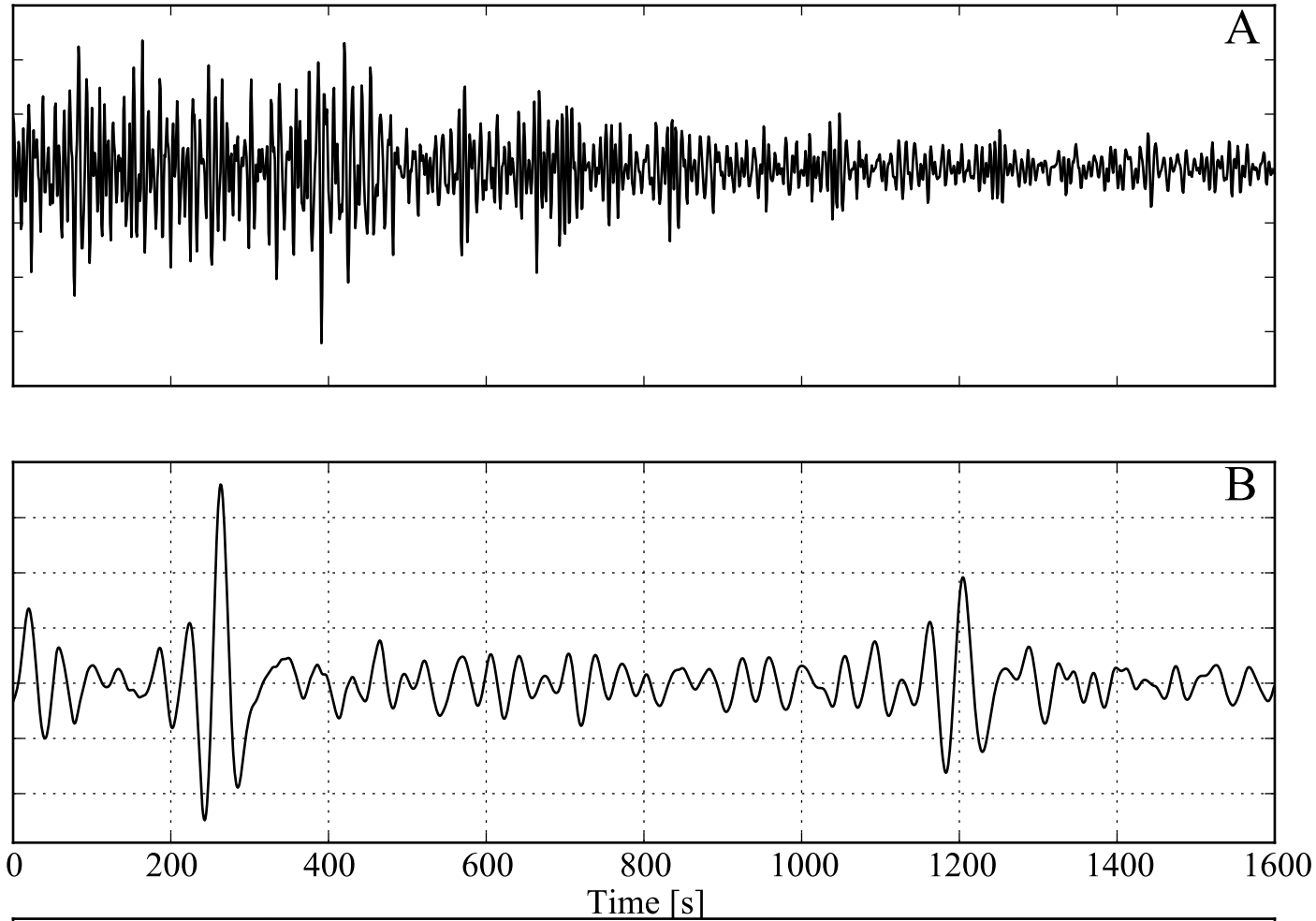


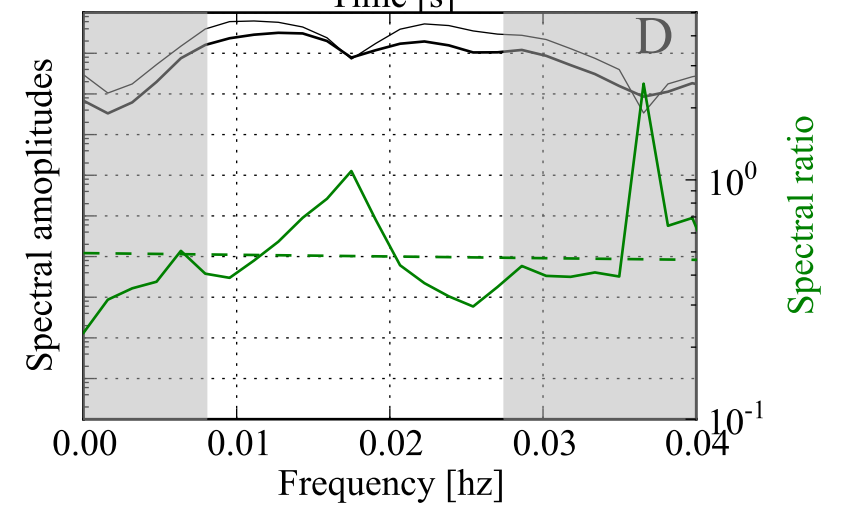
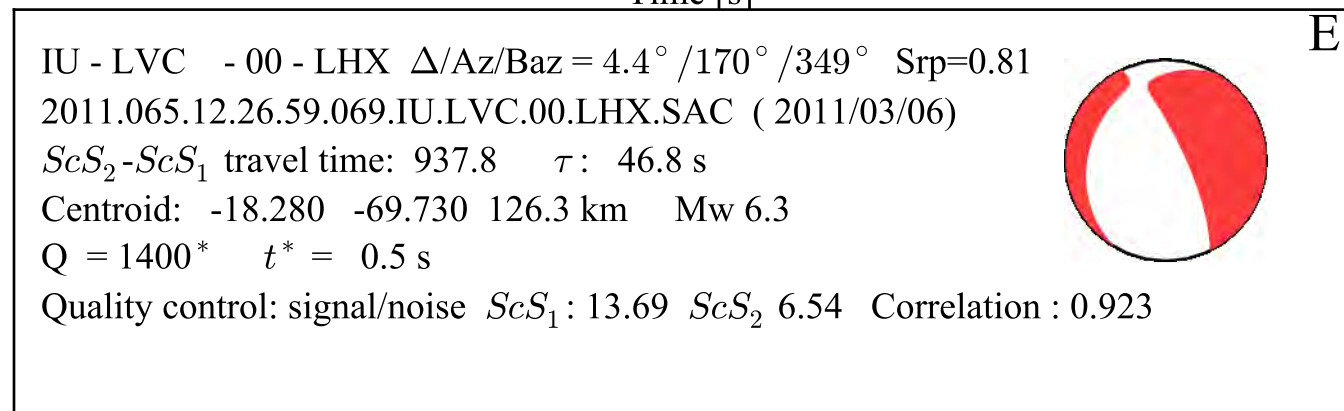
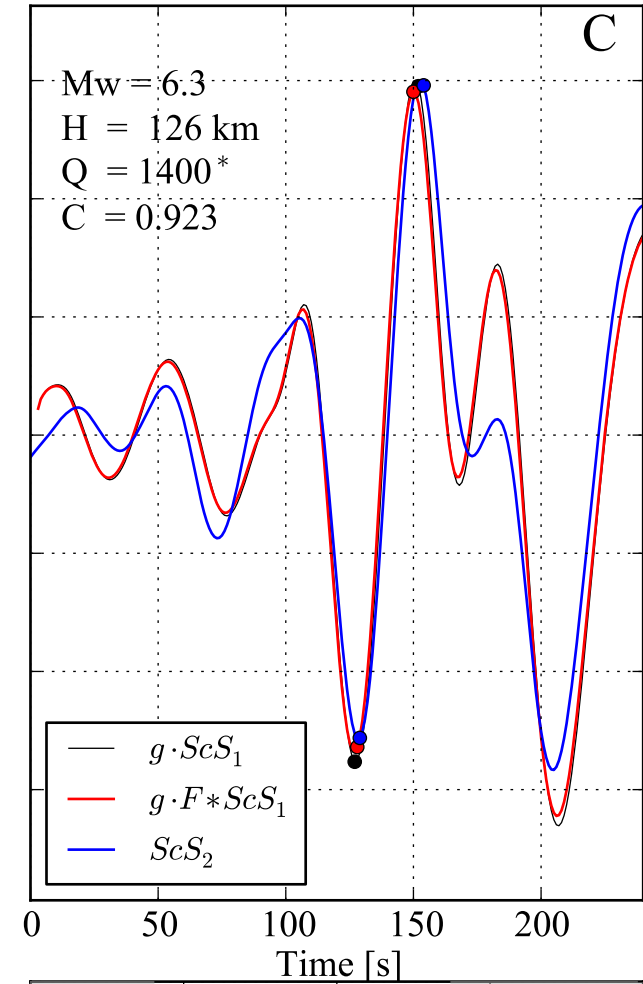
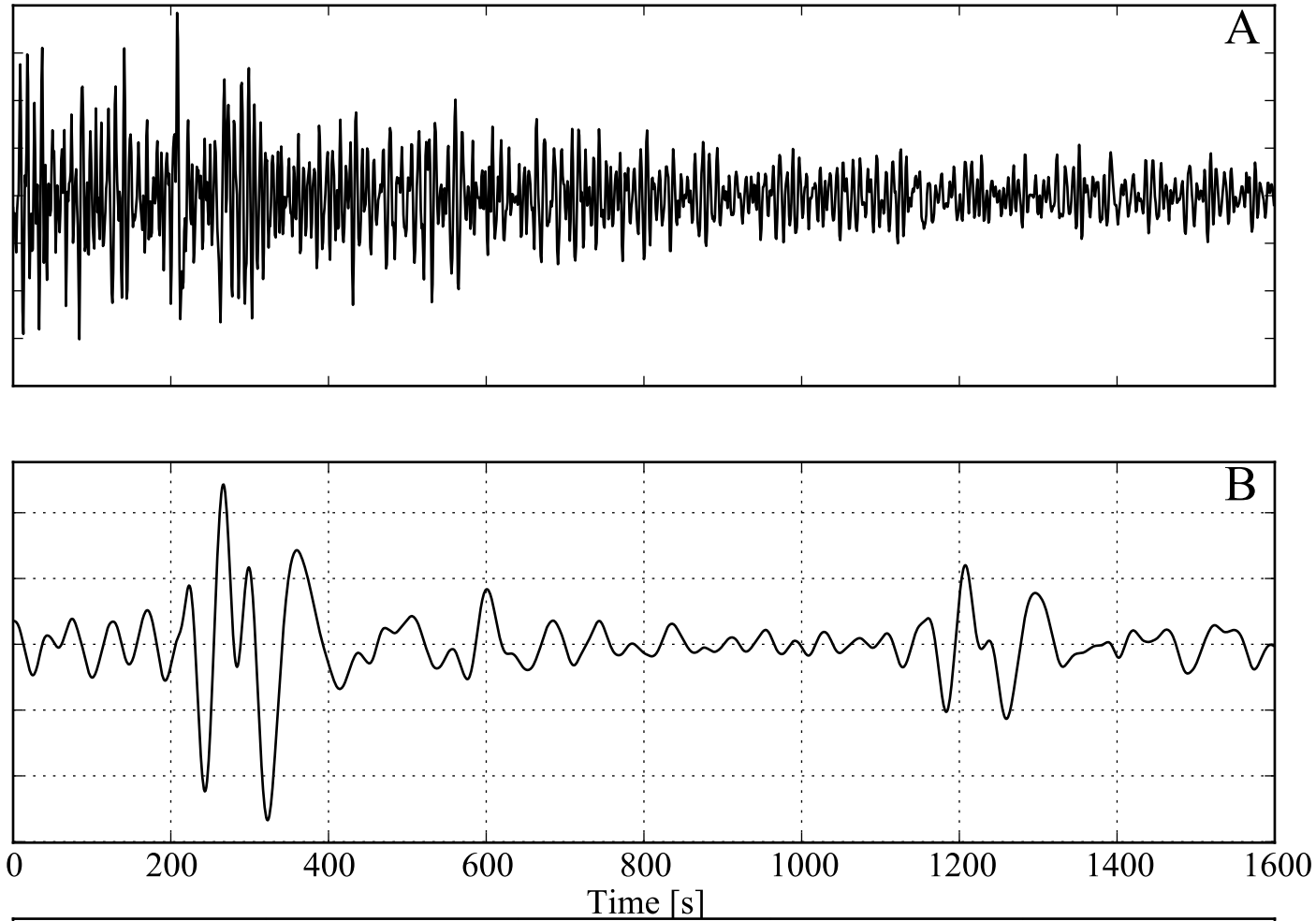
E

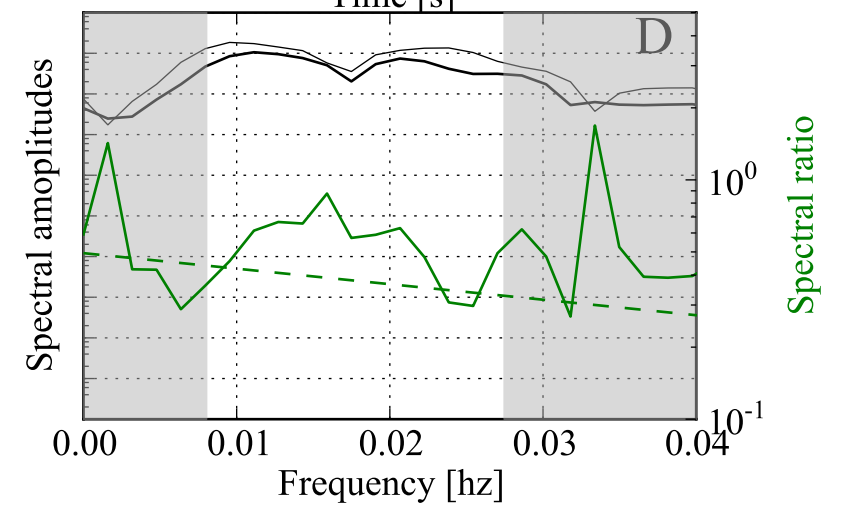
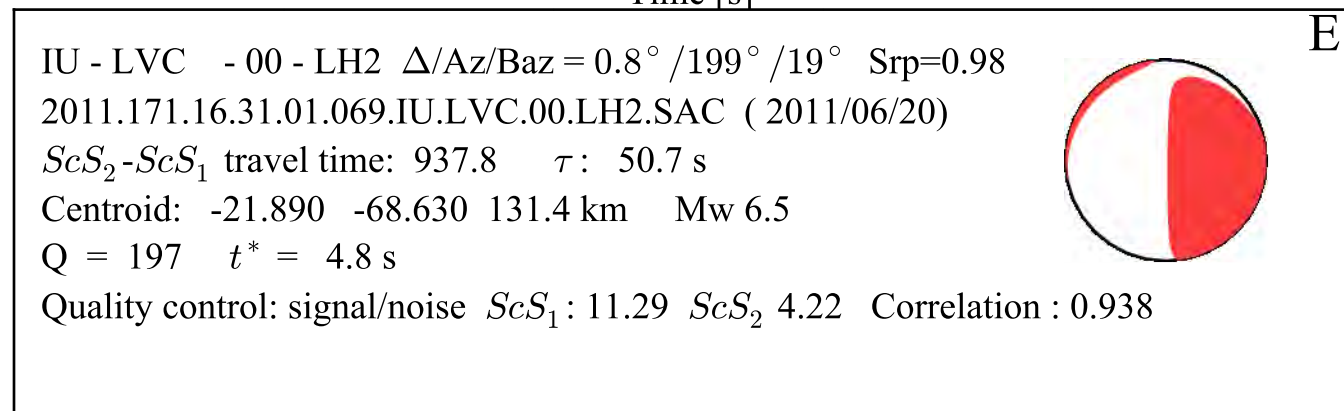
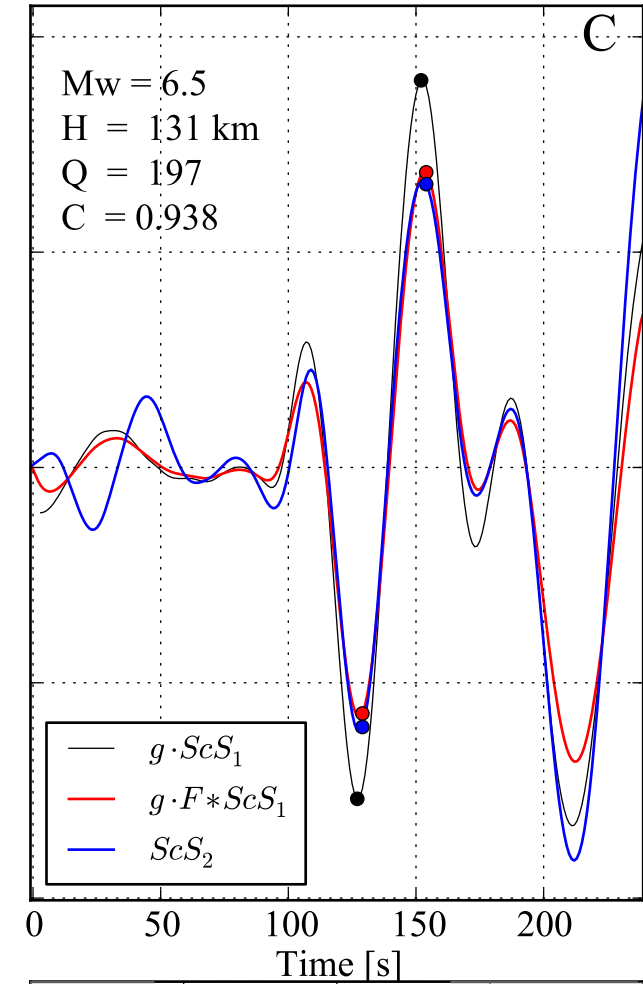
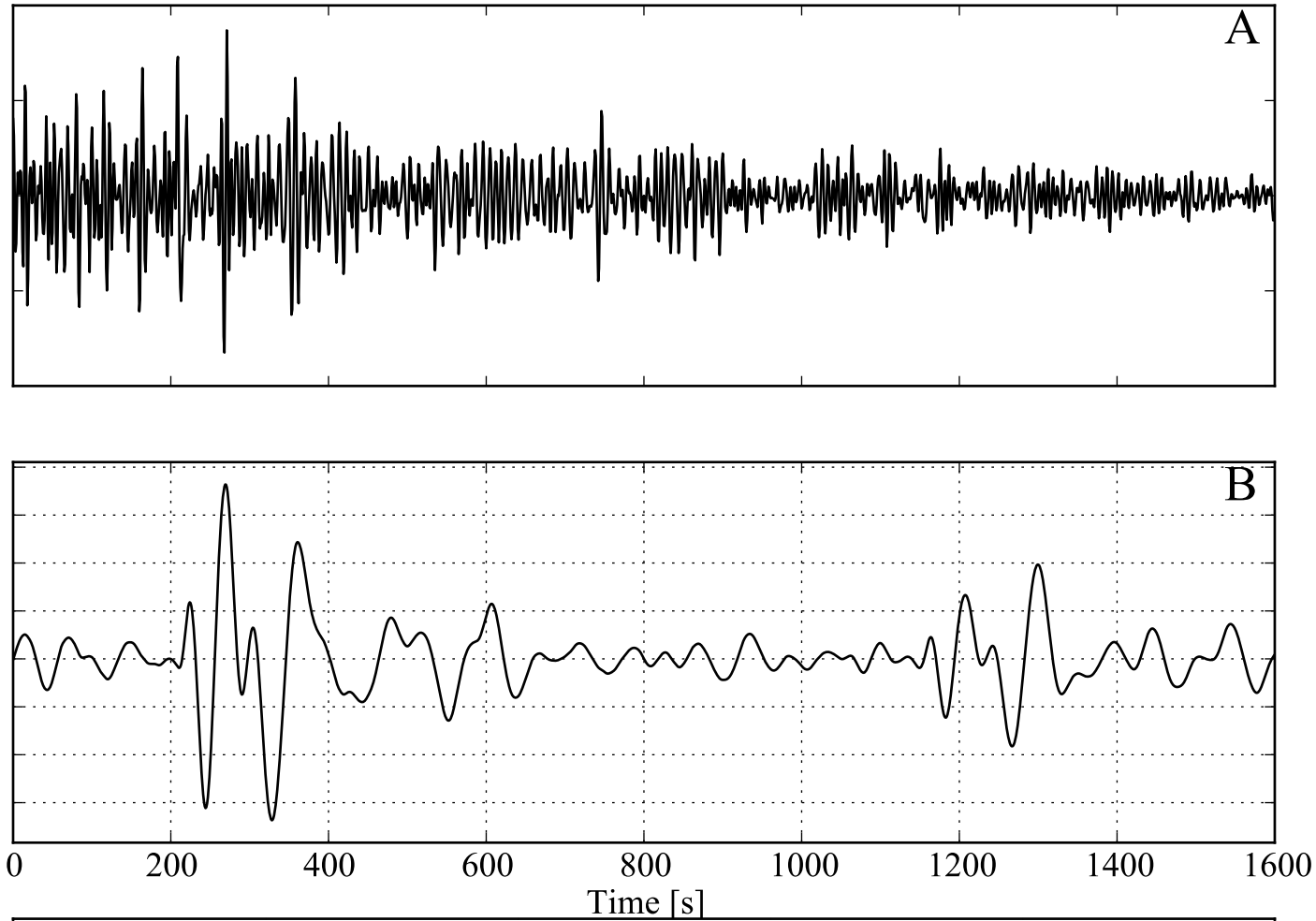
IU - LVC - 00 - LHE $\Delta/Az/Baz = 2.7^\circ / 263^\circ / 84^\circ$ $Srp=1.00$
 2007.202.15.29.52.298.IU.LVC.00.LHE.SAC (2007/07/21)
 $ScS_2 - ScS_1$ travel time: 937.5 τ : 52.0 s
 Centroid: -22.310 -66.000 280.2 km Mw 6.4
 Q = 1400* $t^* = 0.1$ s
 Quality control: signal/noise ScS_1 : 8.38 ScS_2 4.33 Correlation : 0.922

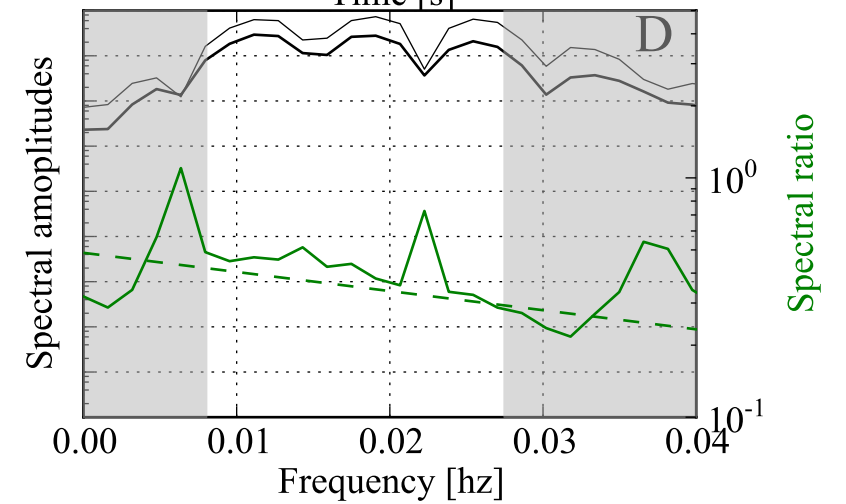
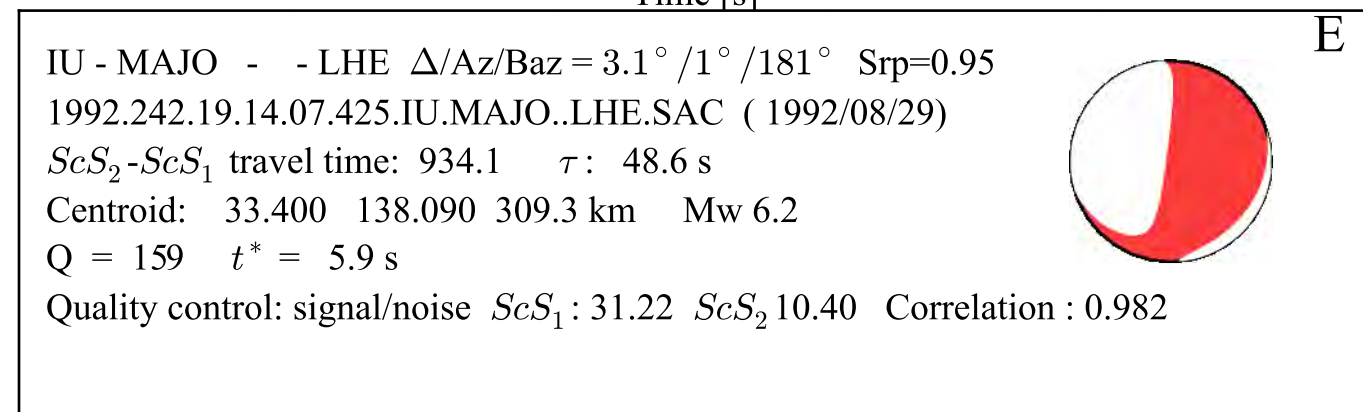
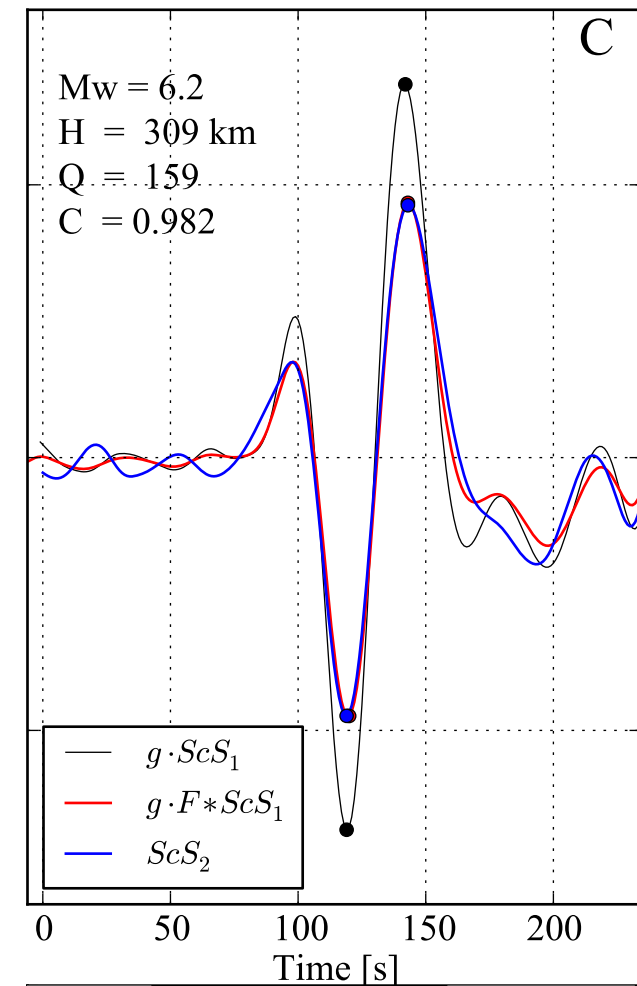
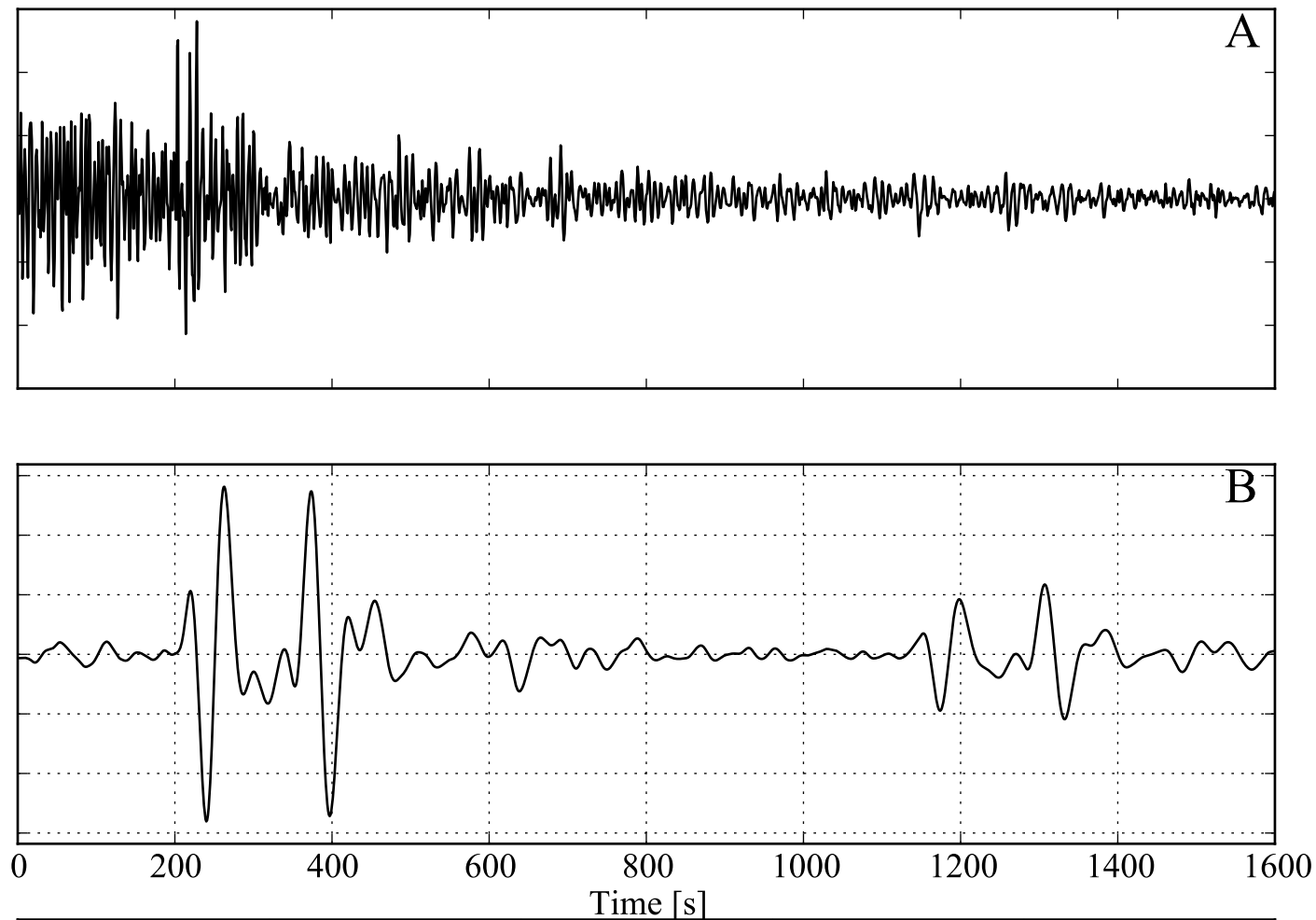


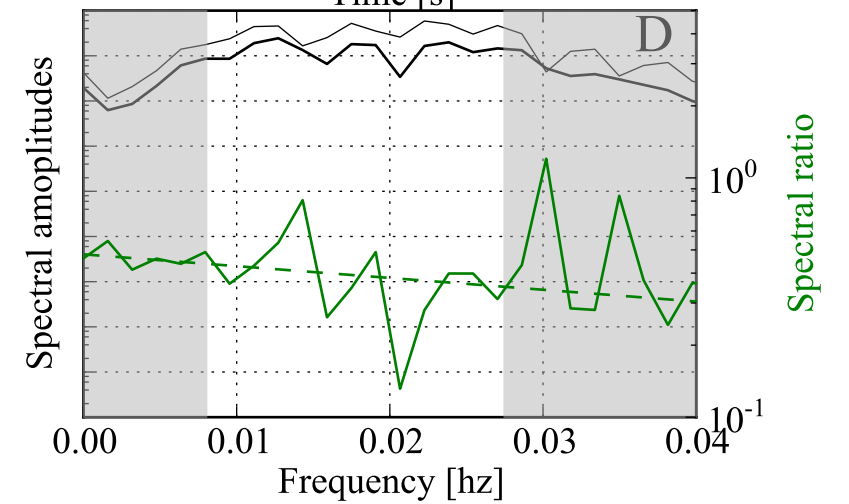
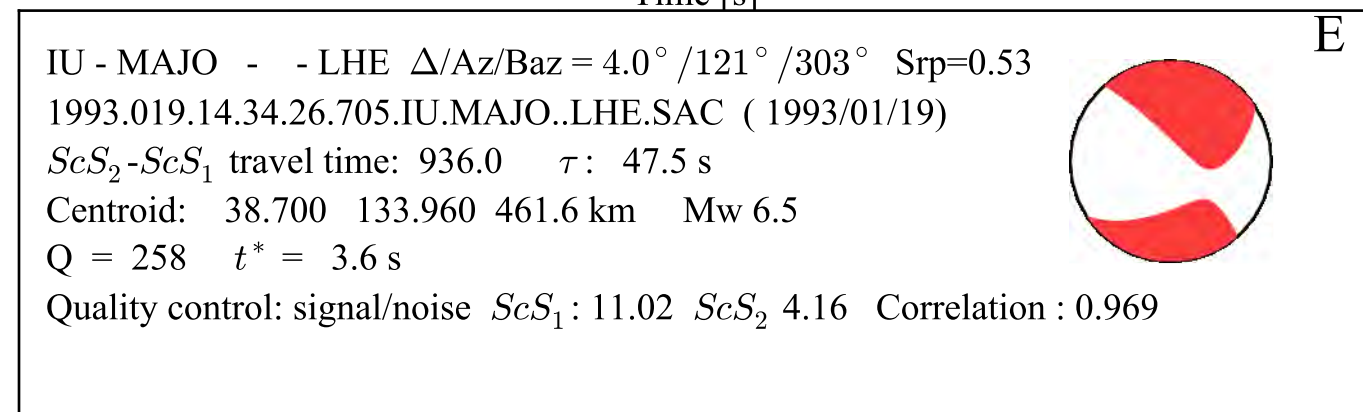
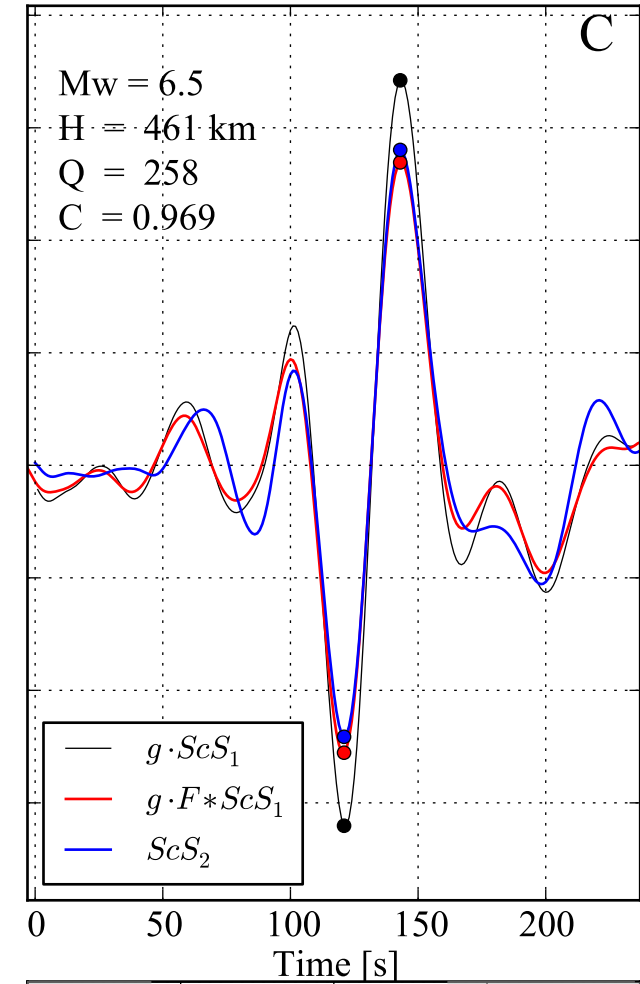
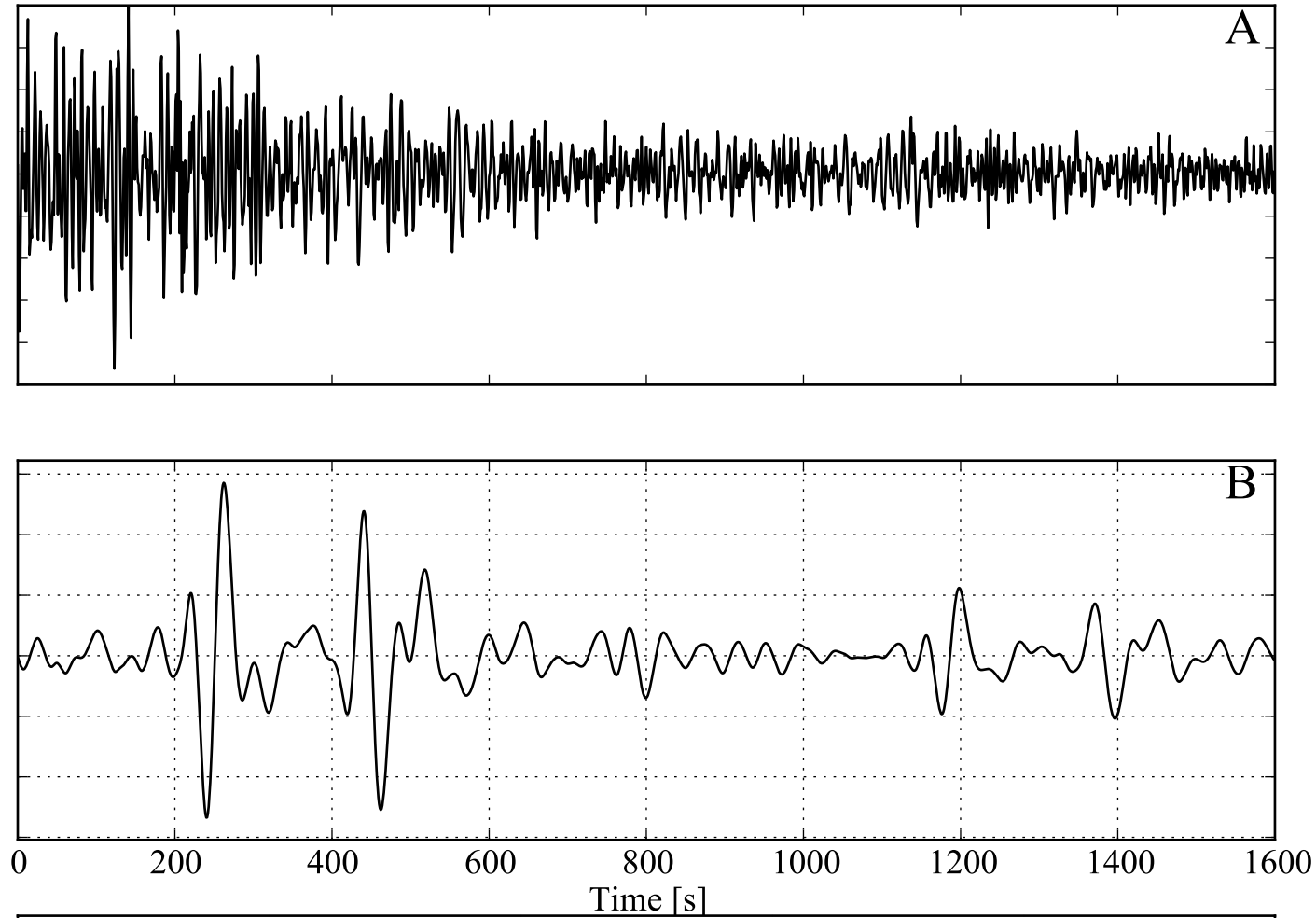


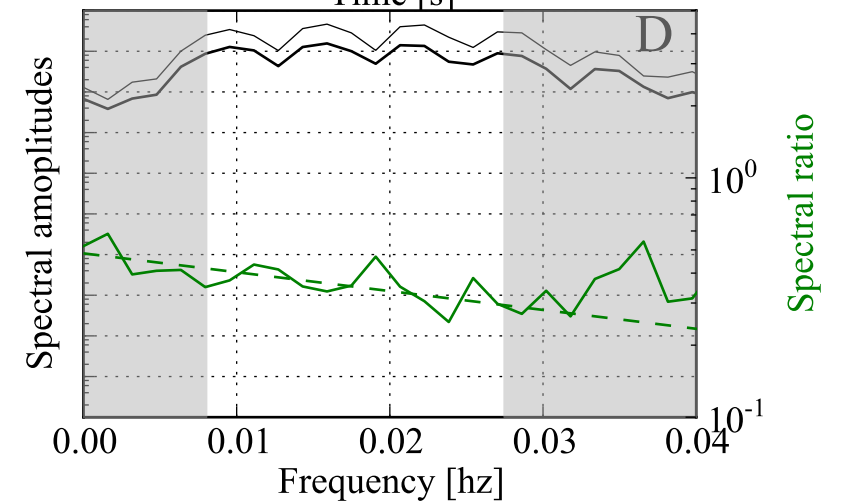
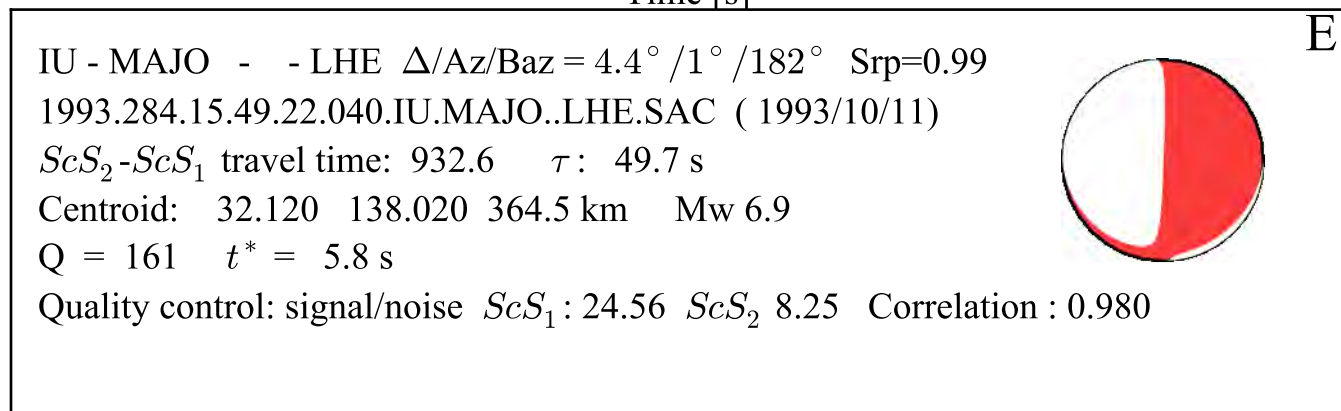
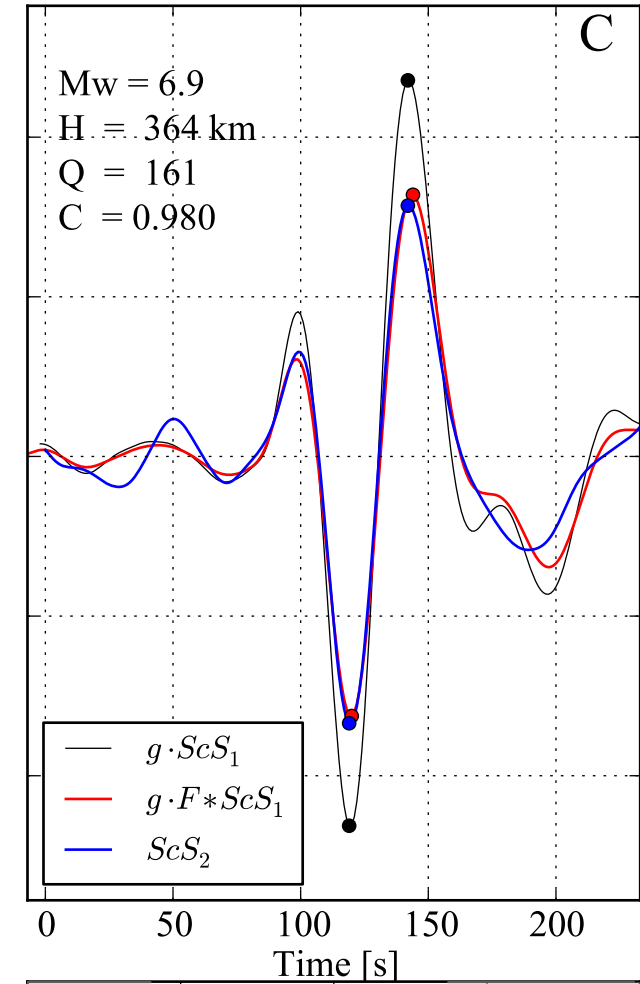
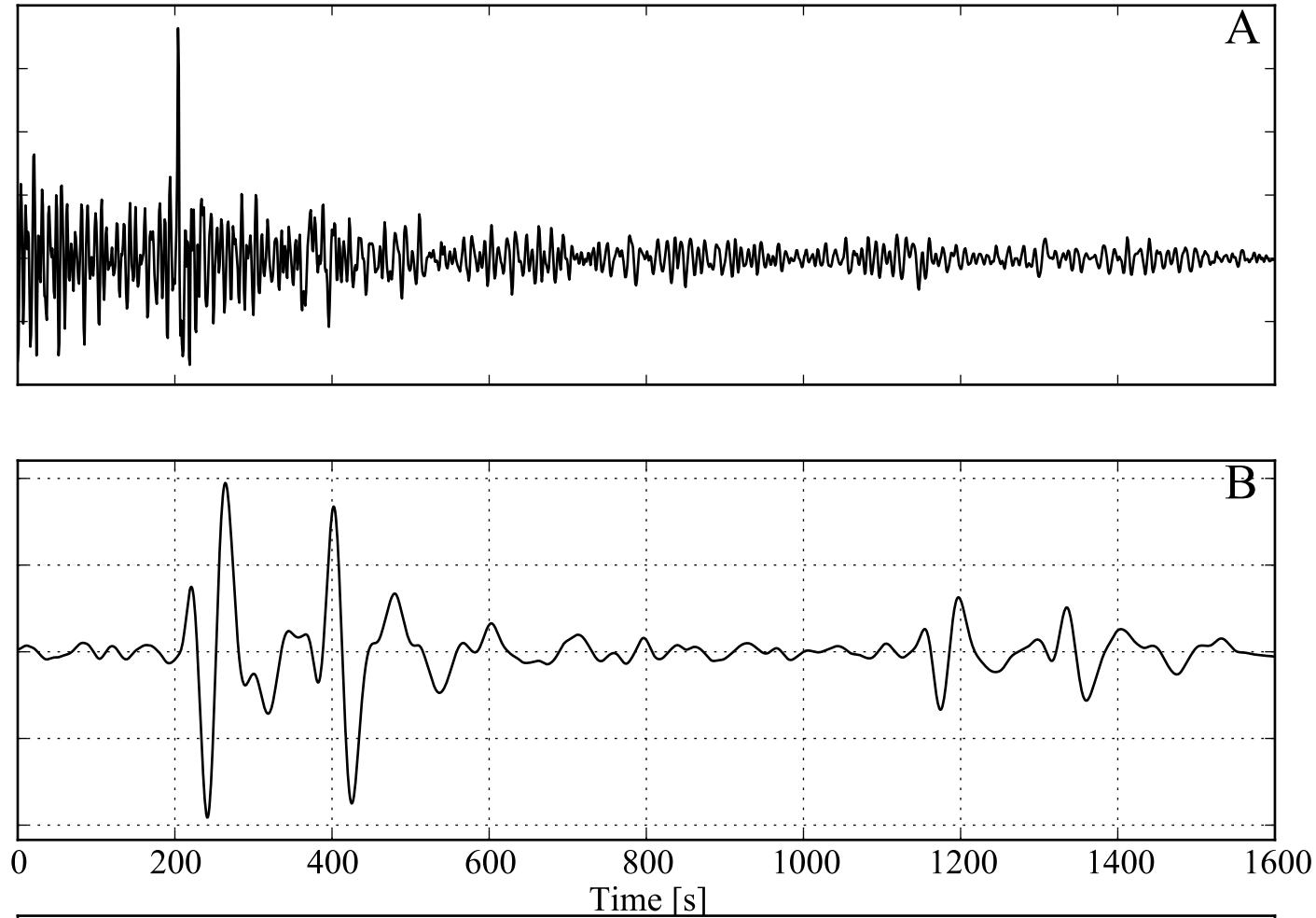


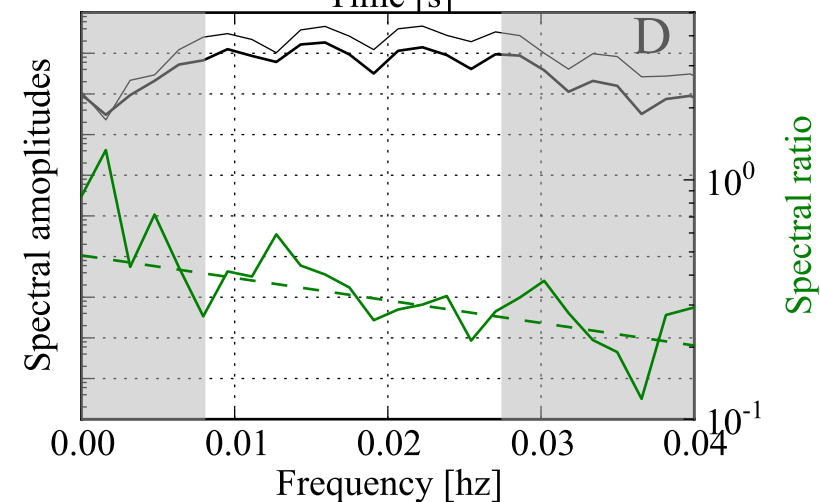
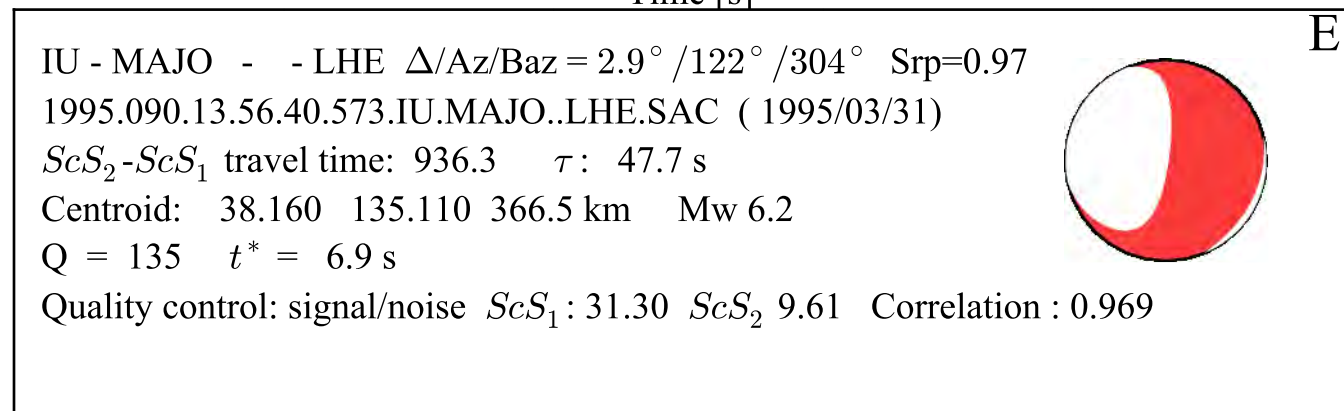
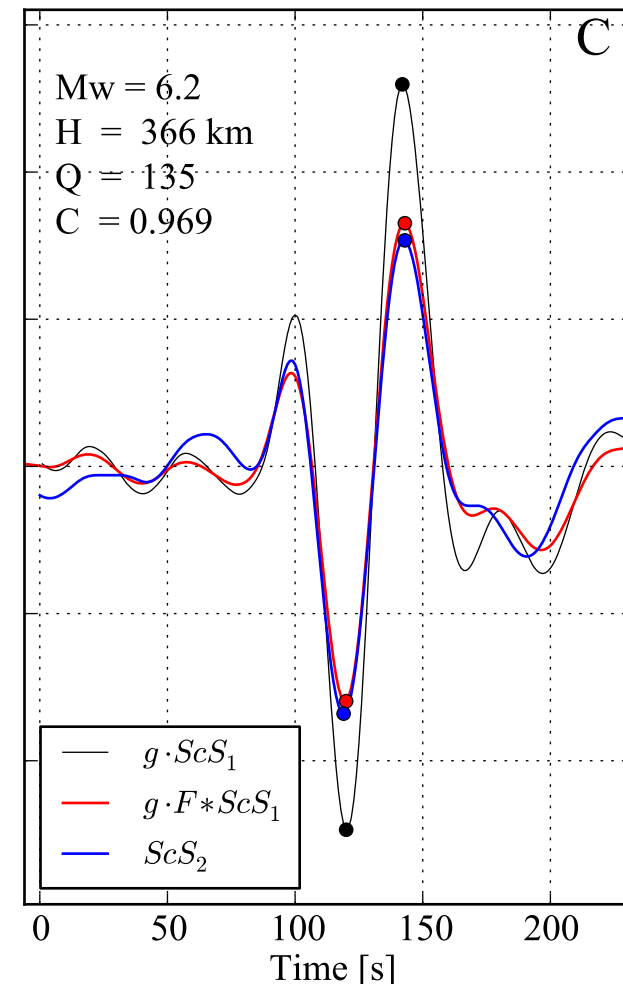
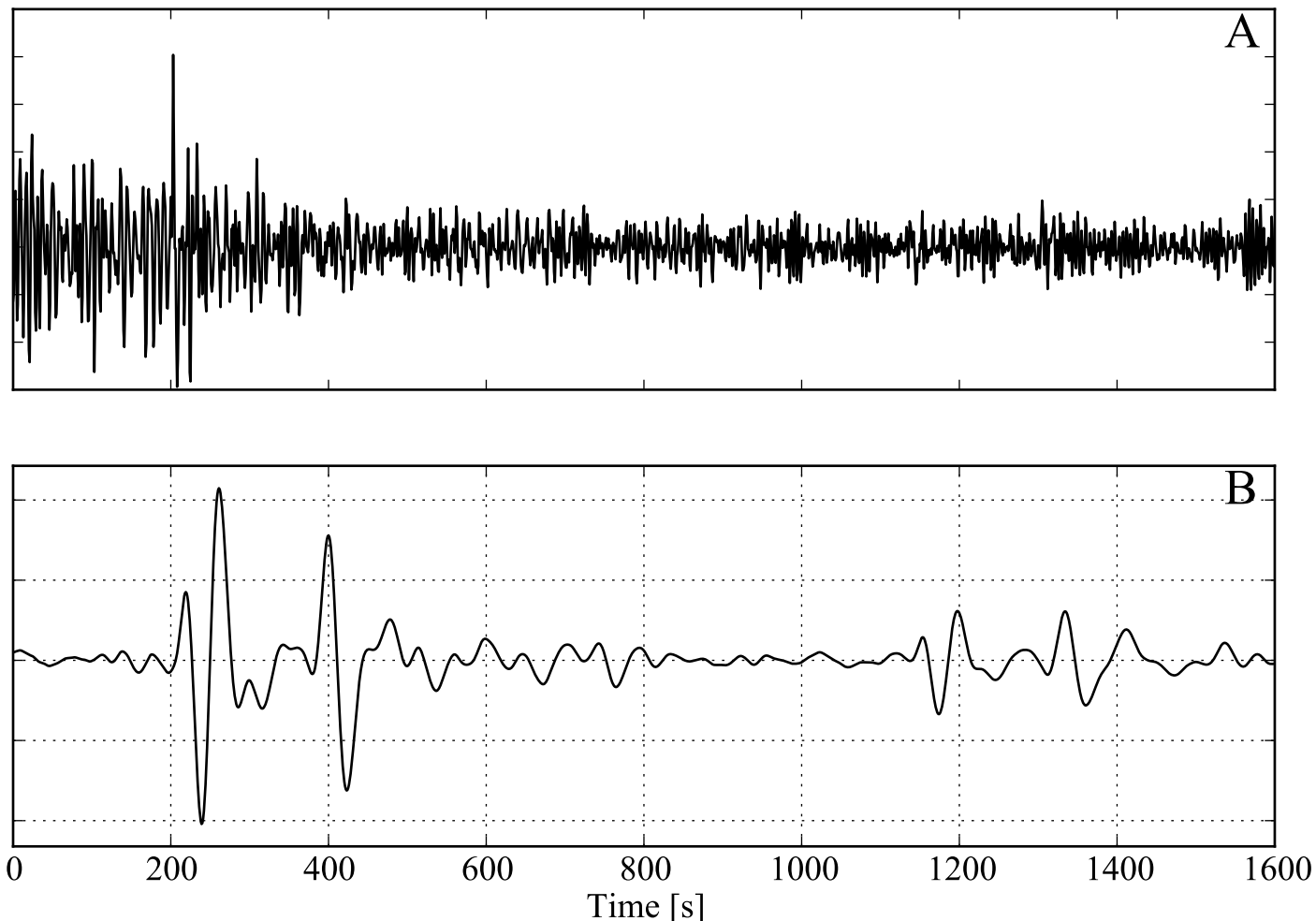


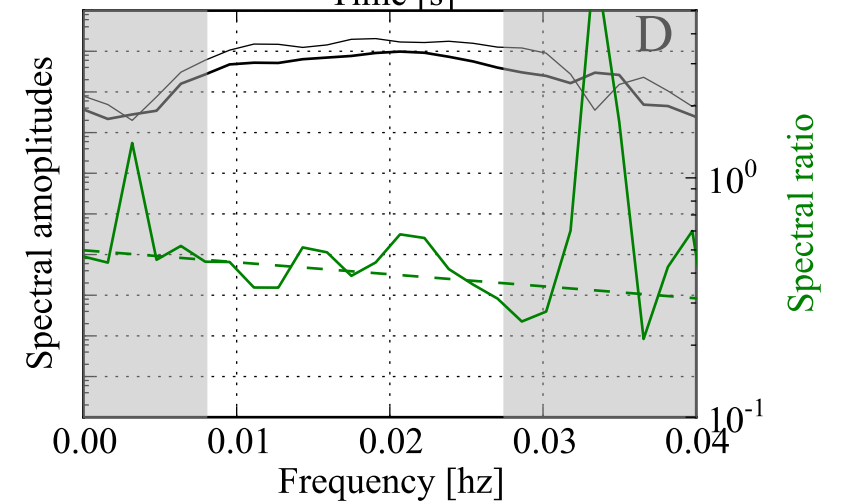
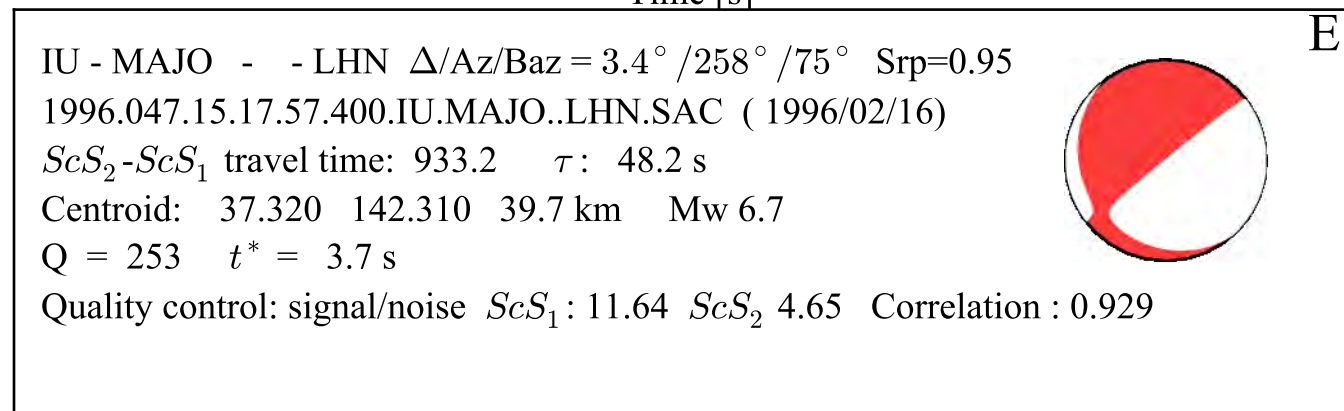
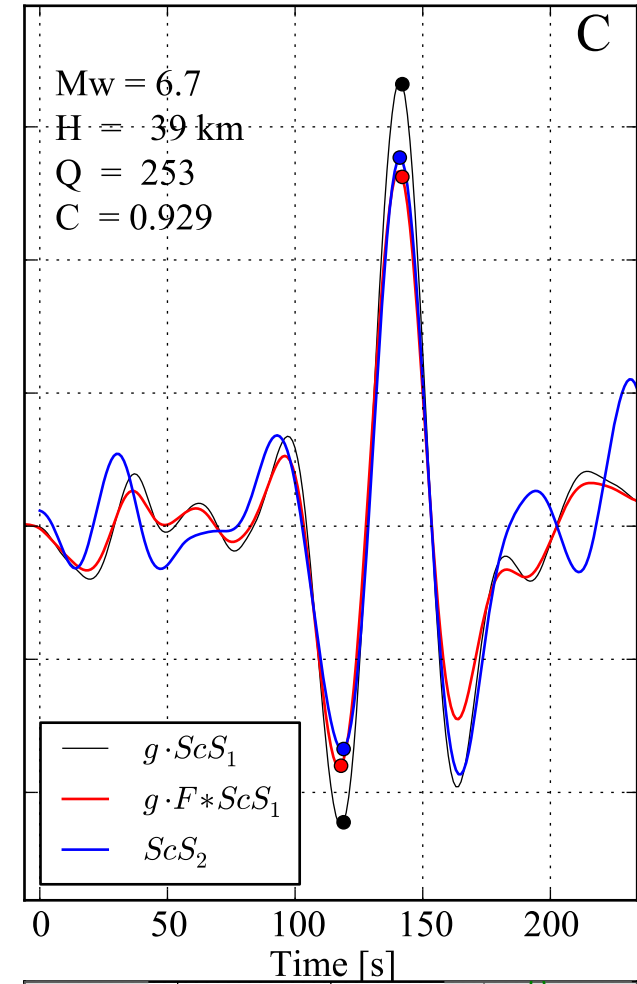
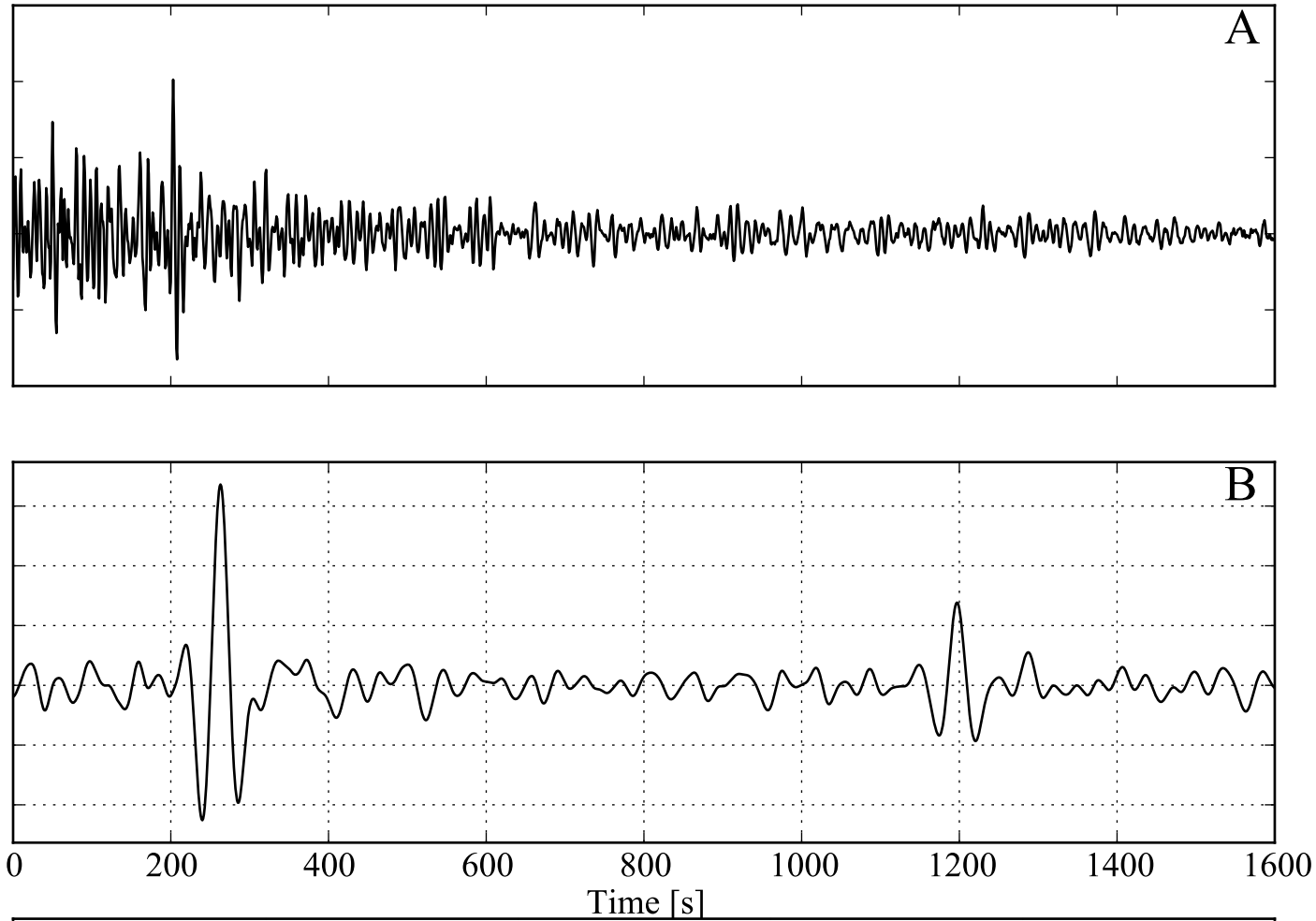


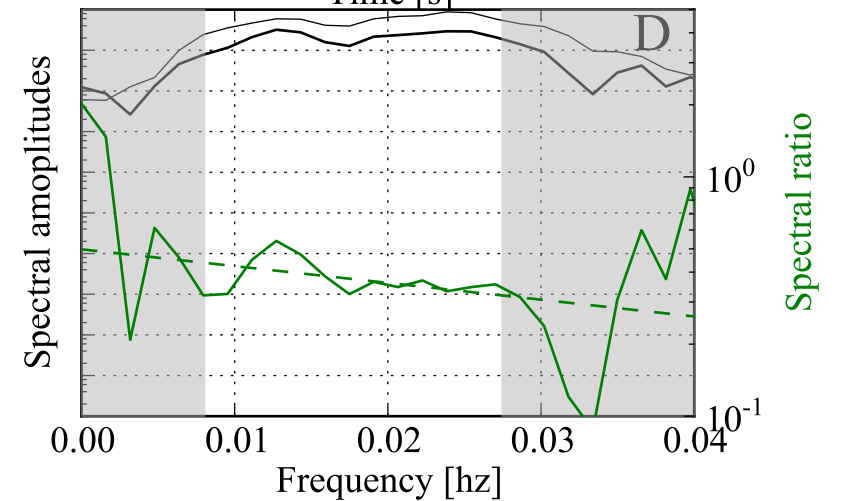
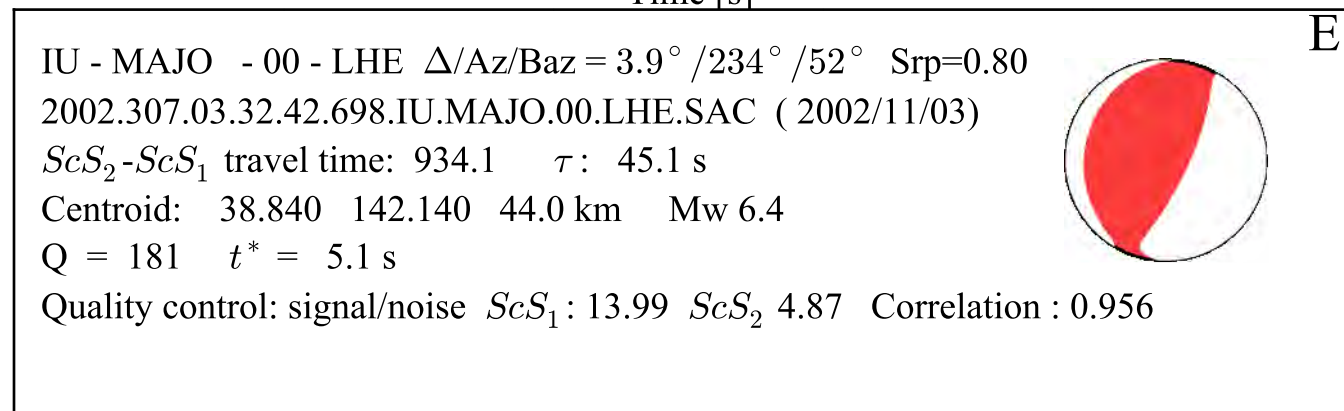
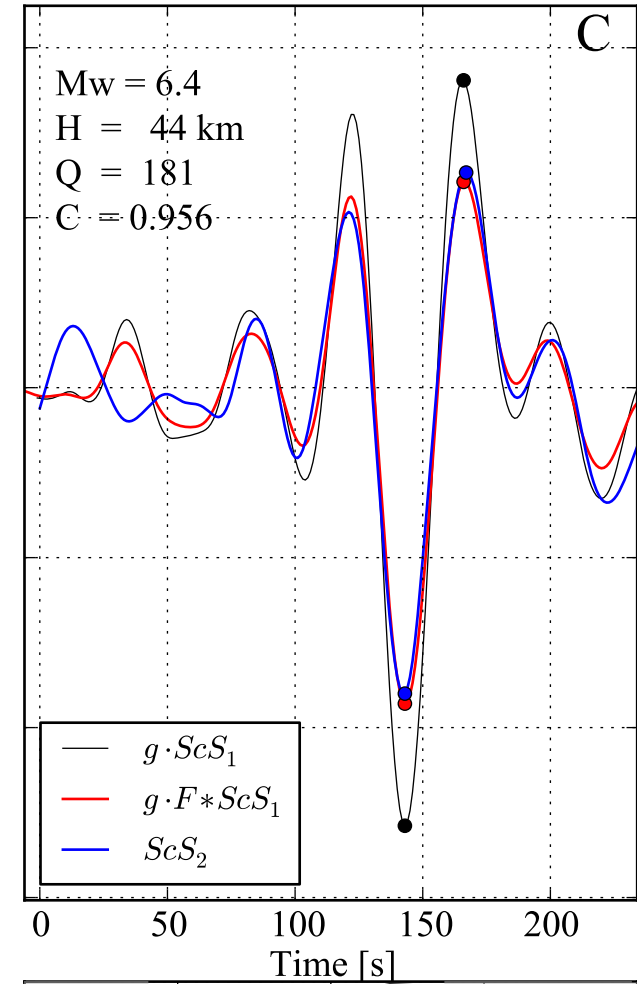
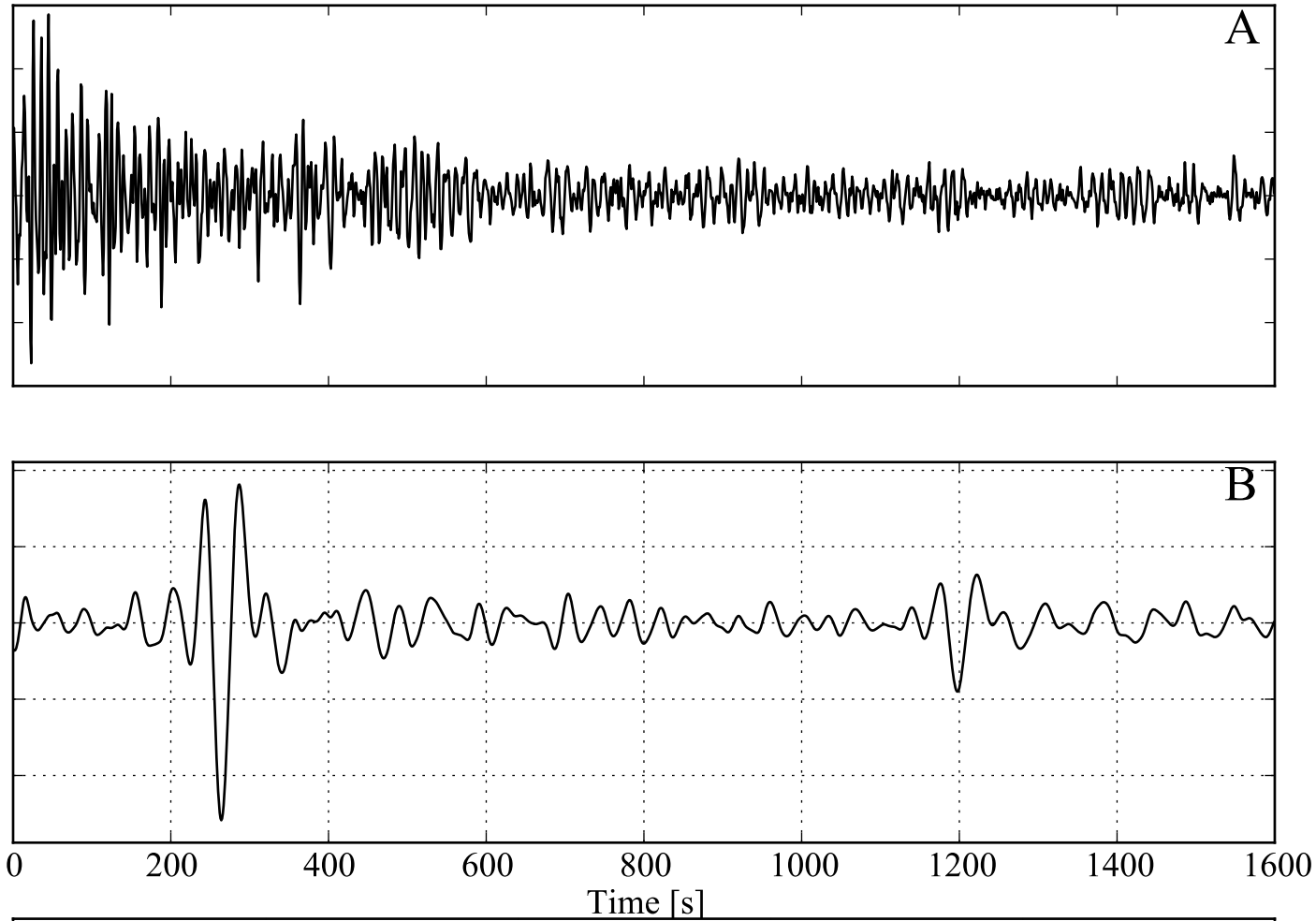


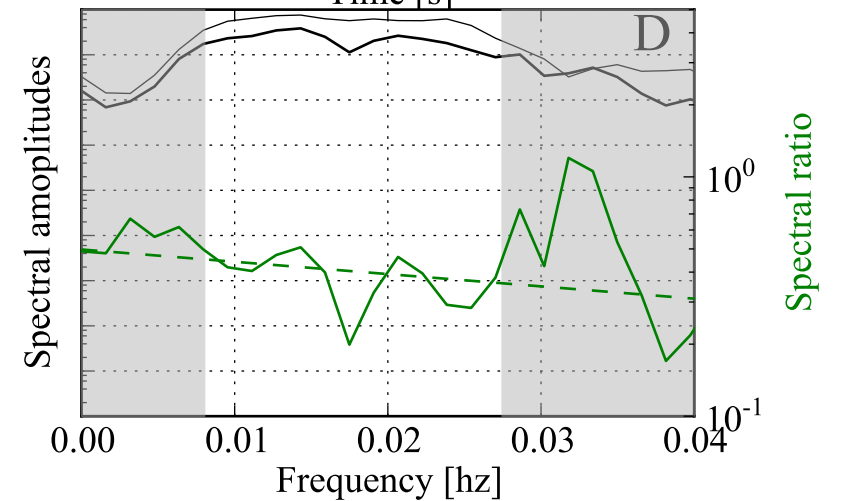
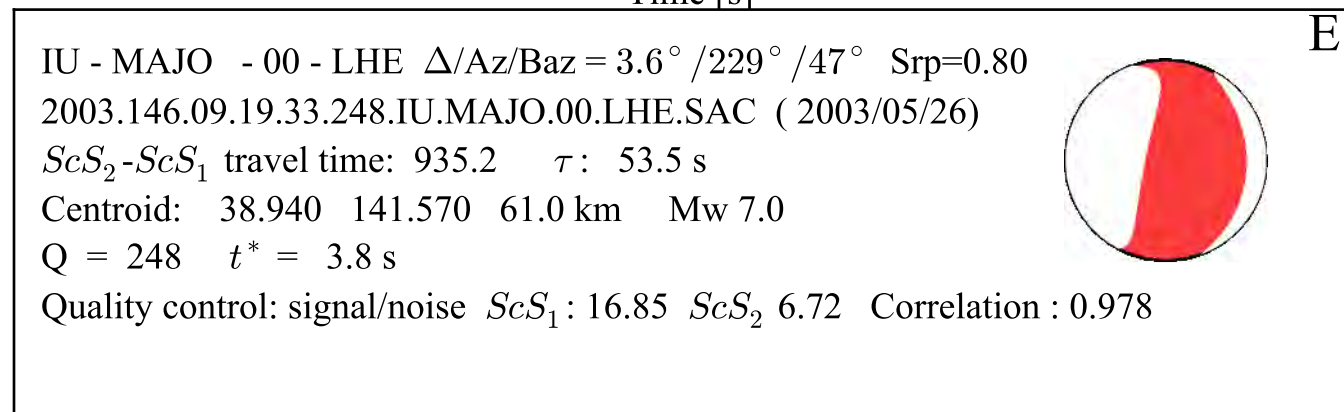
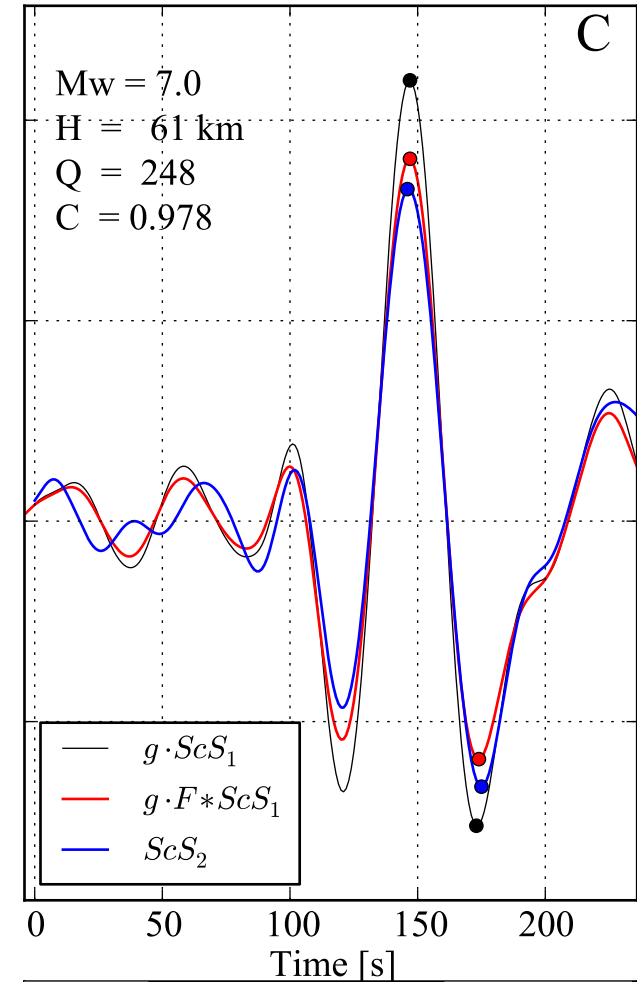
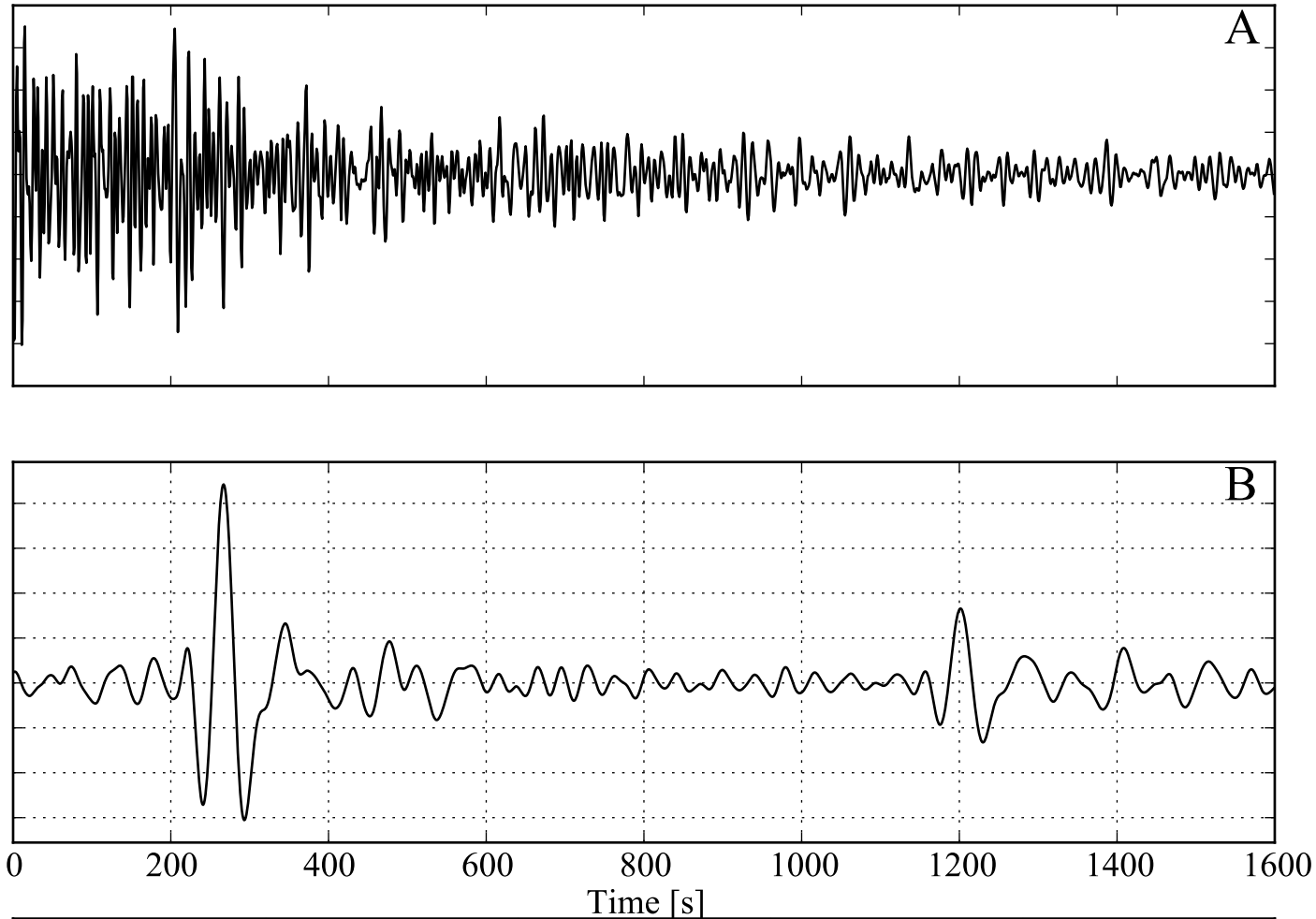


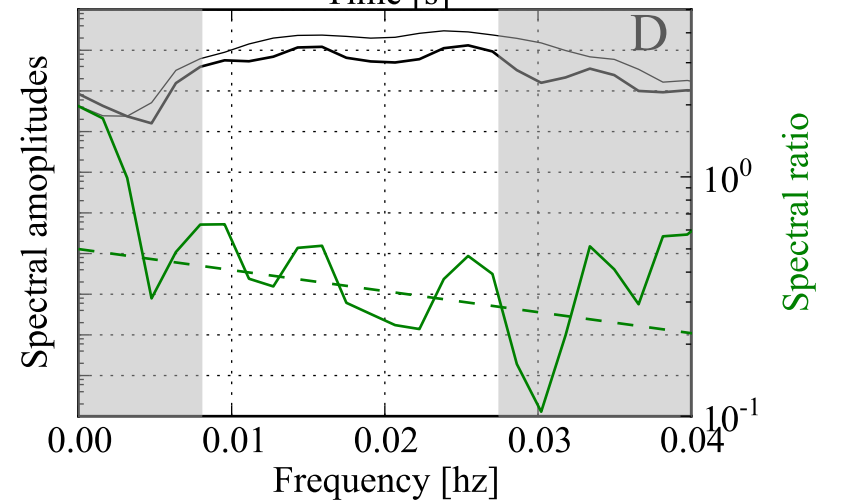
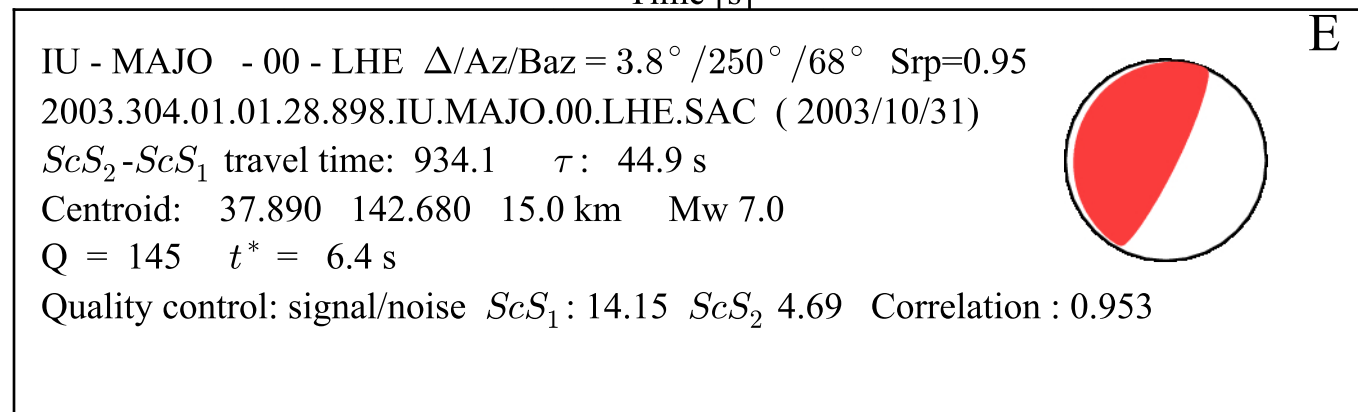
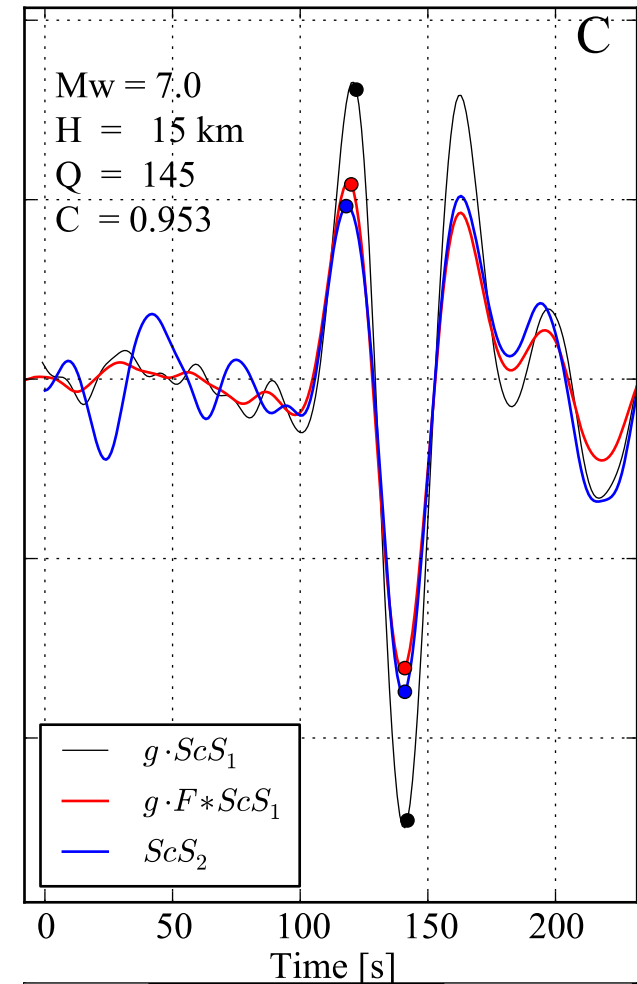
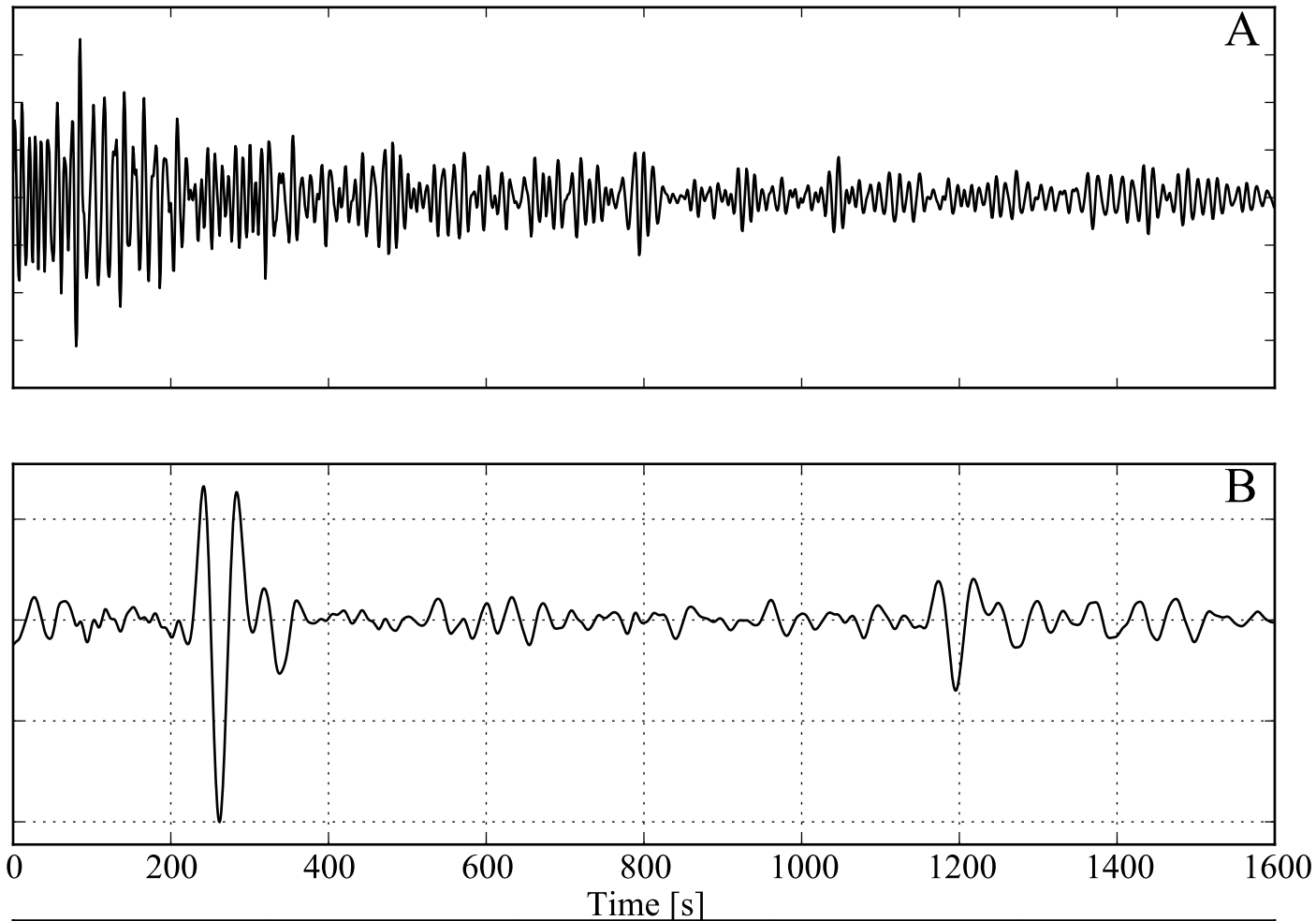


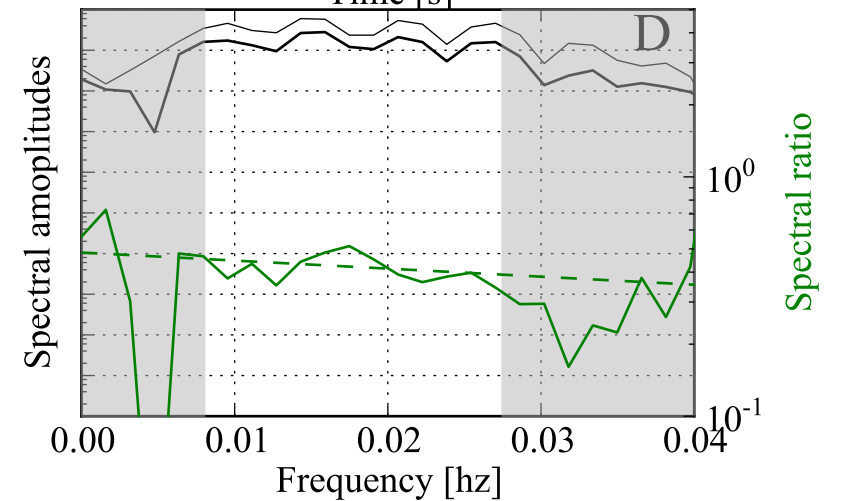
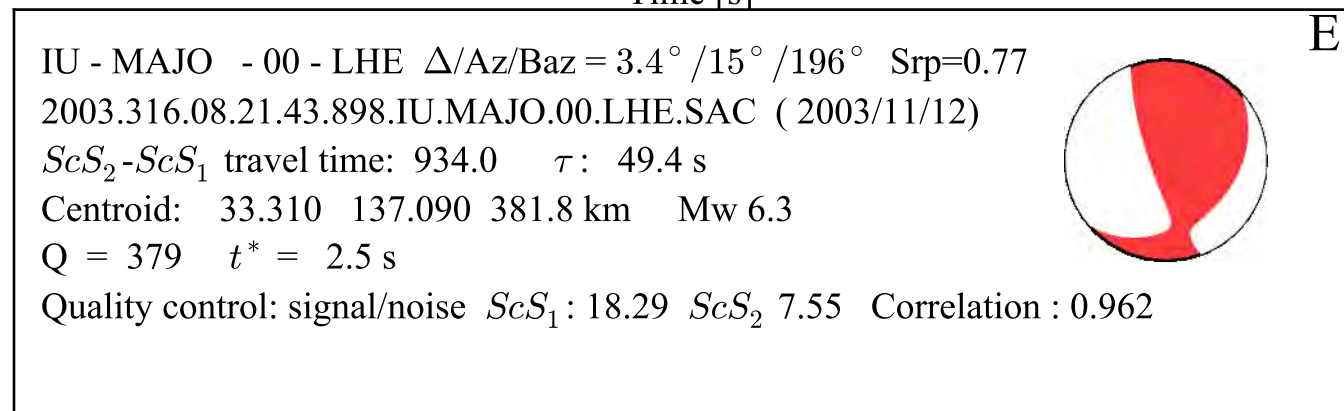
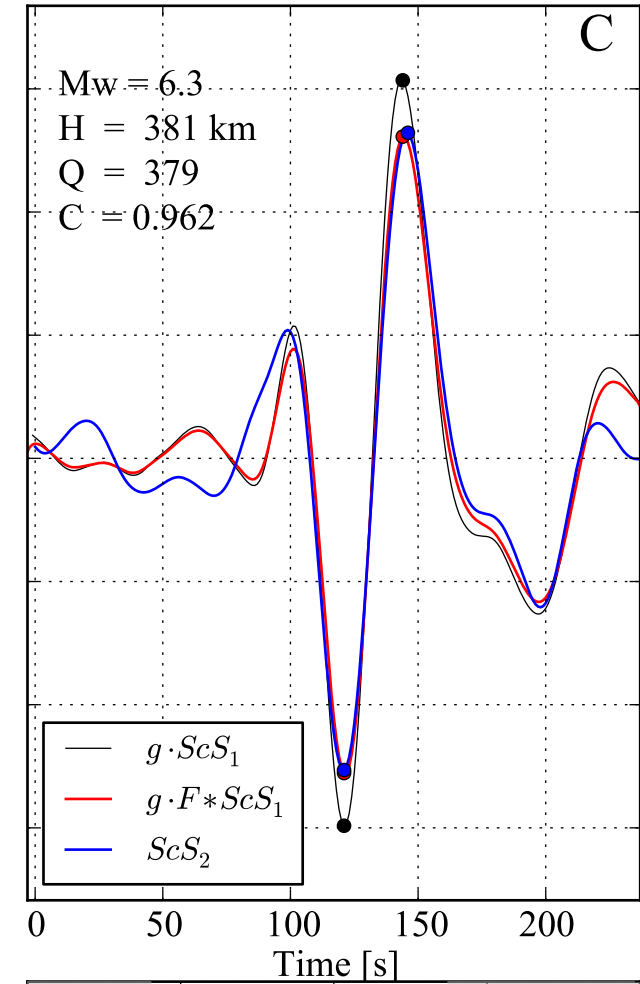
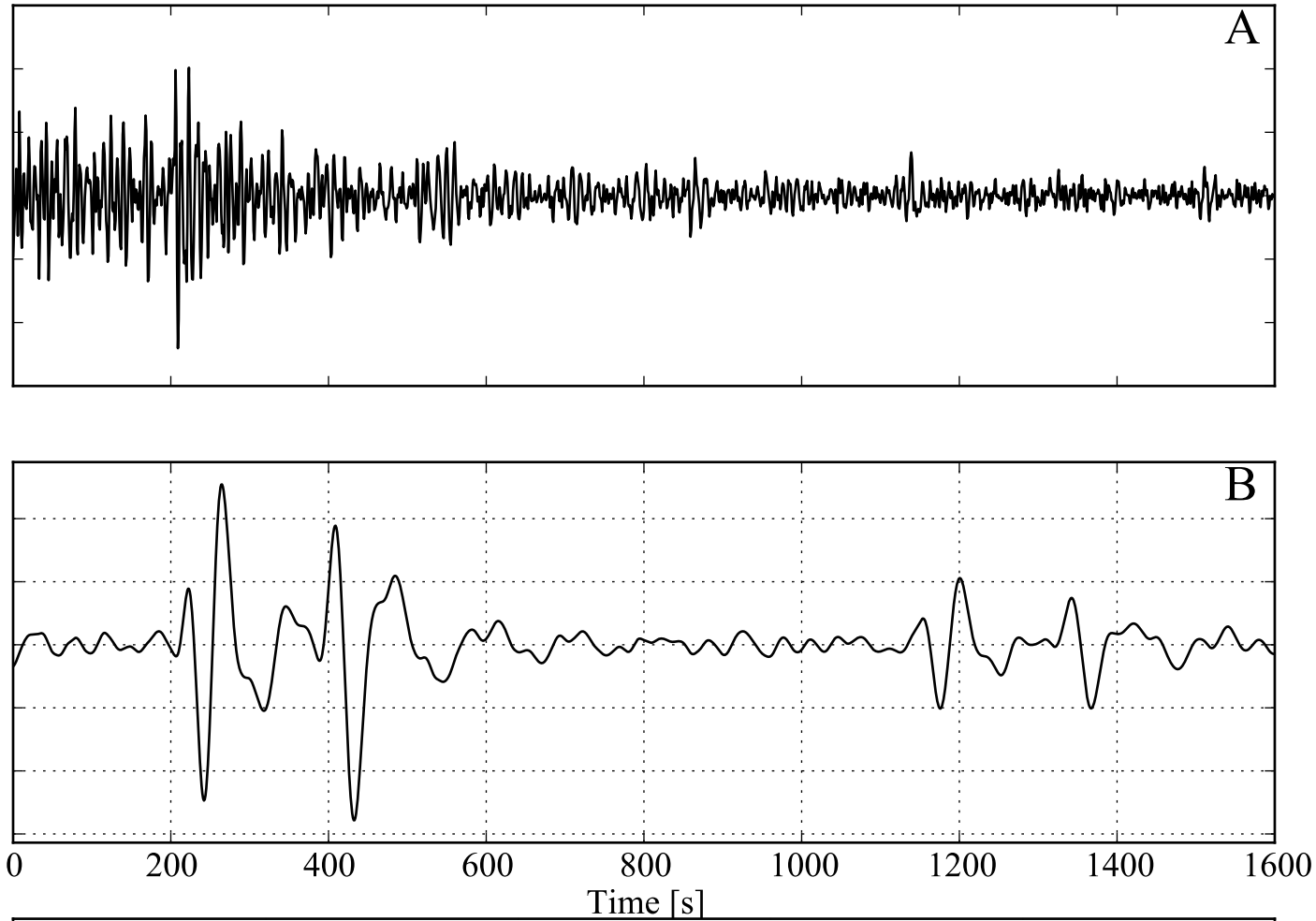


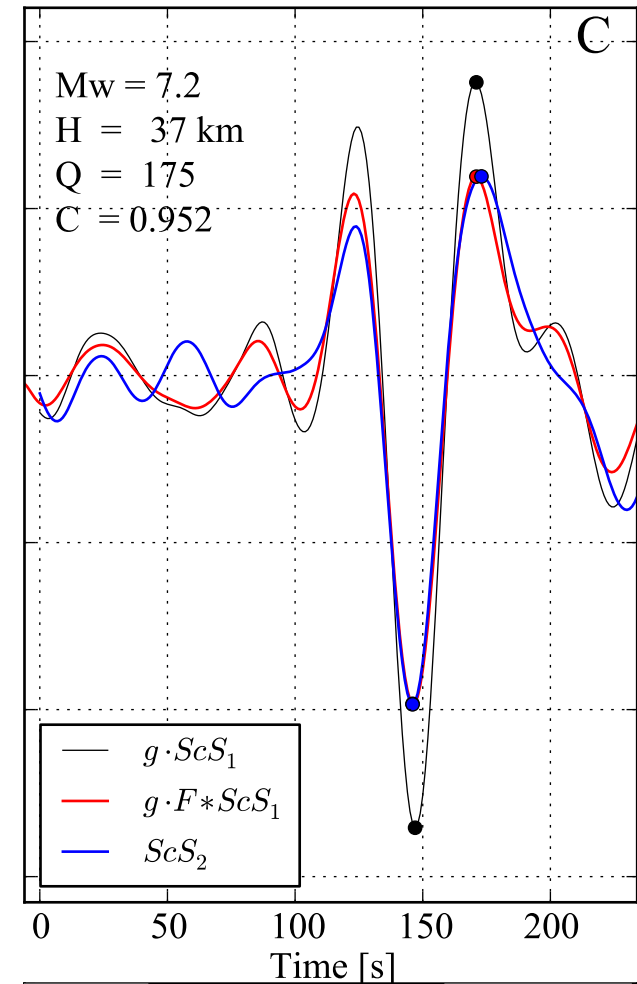
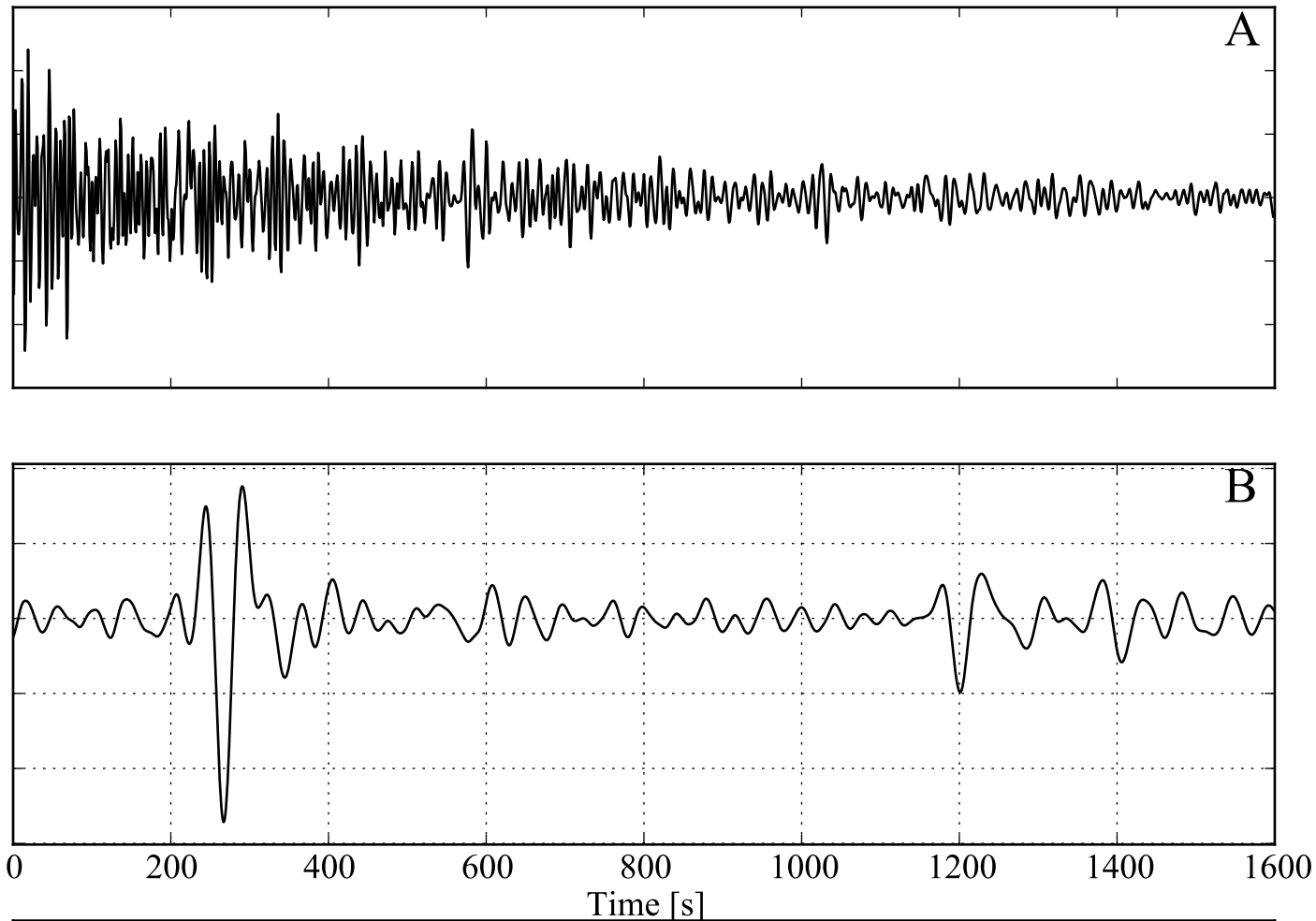






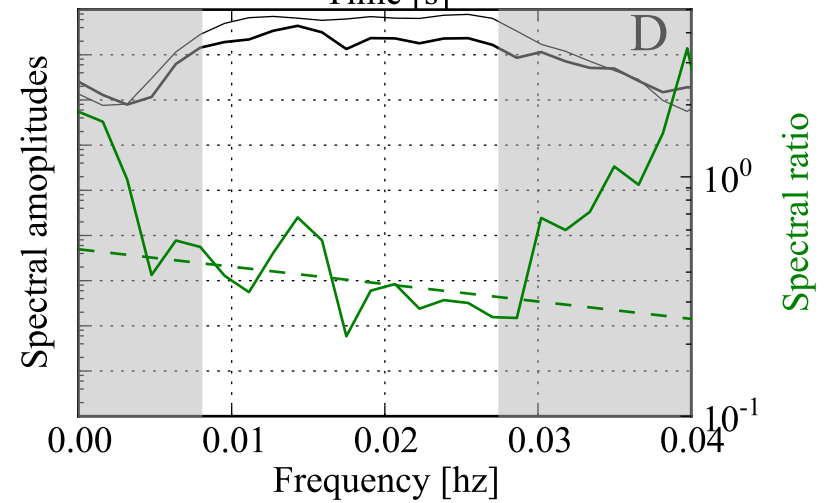


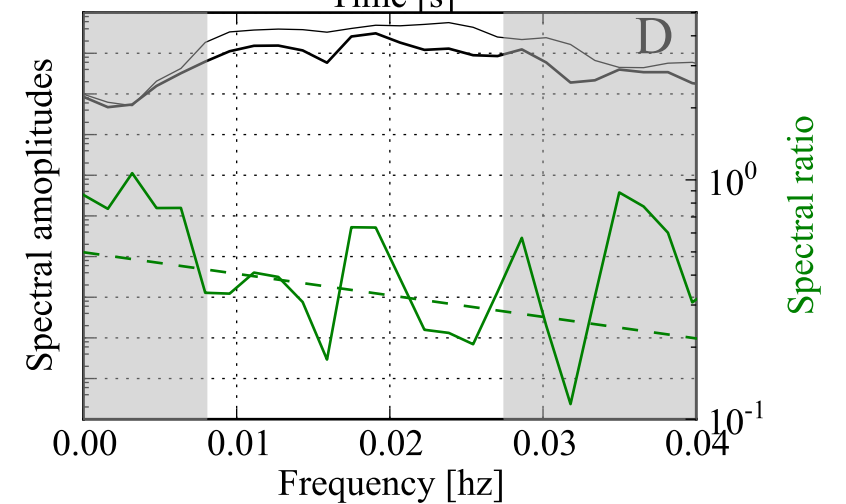
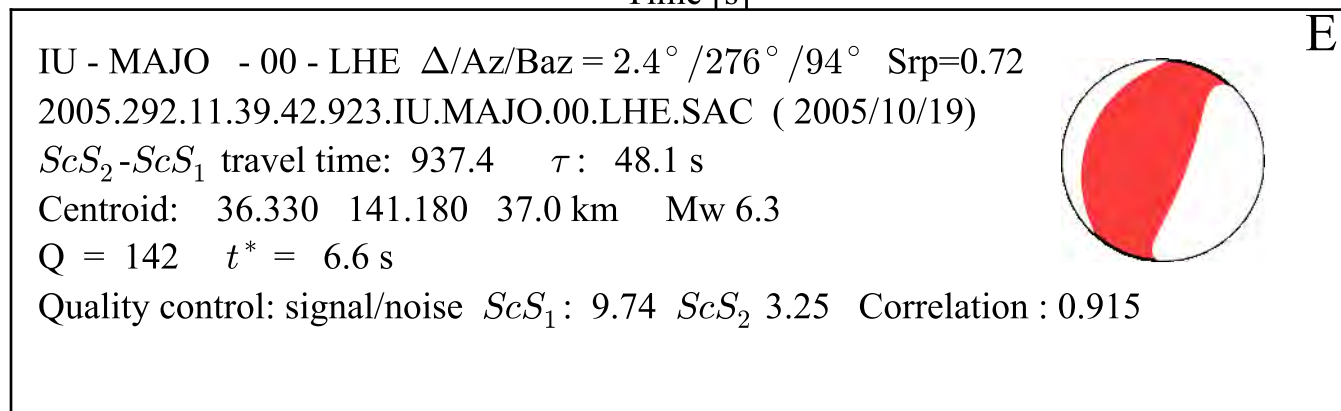
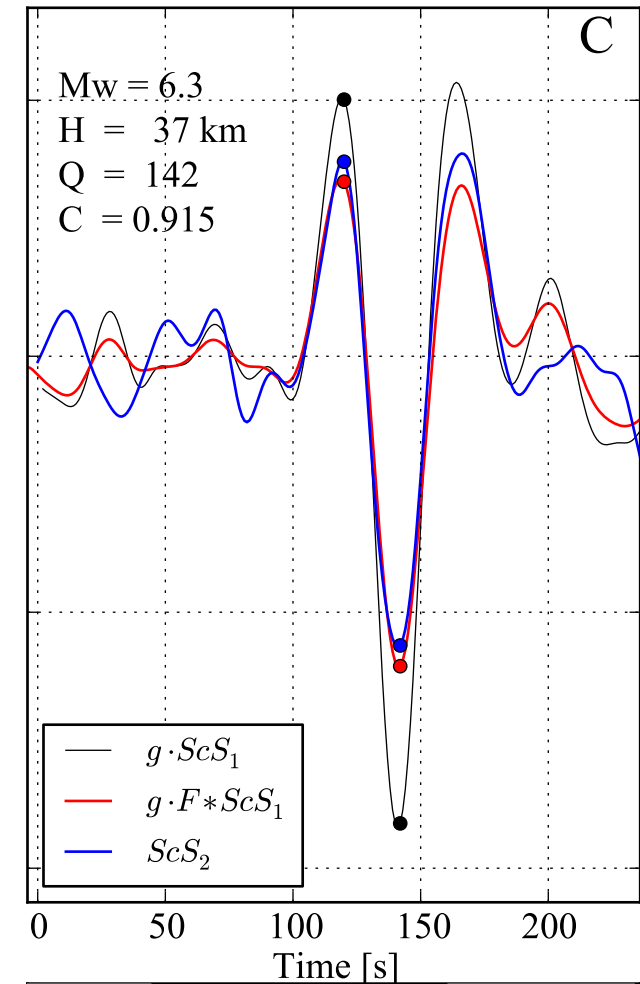
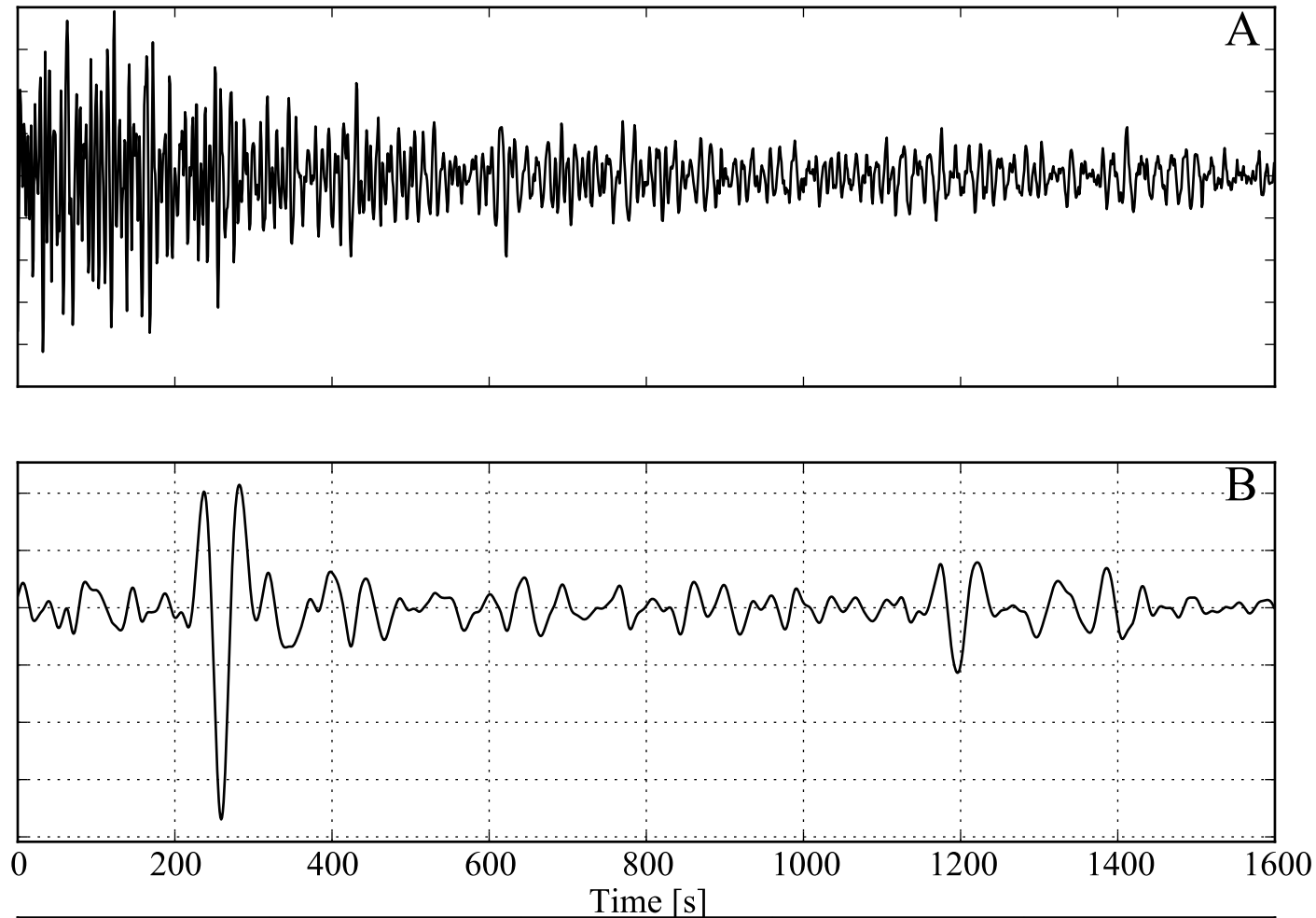


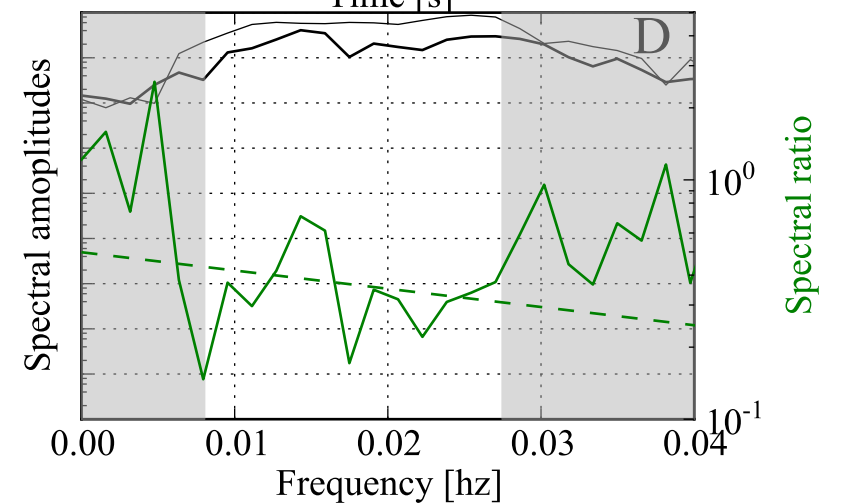
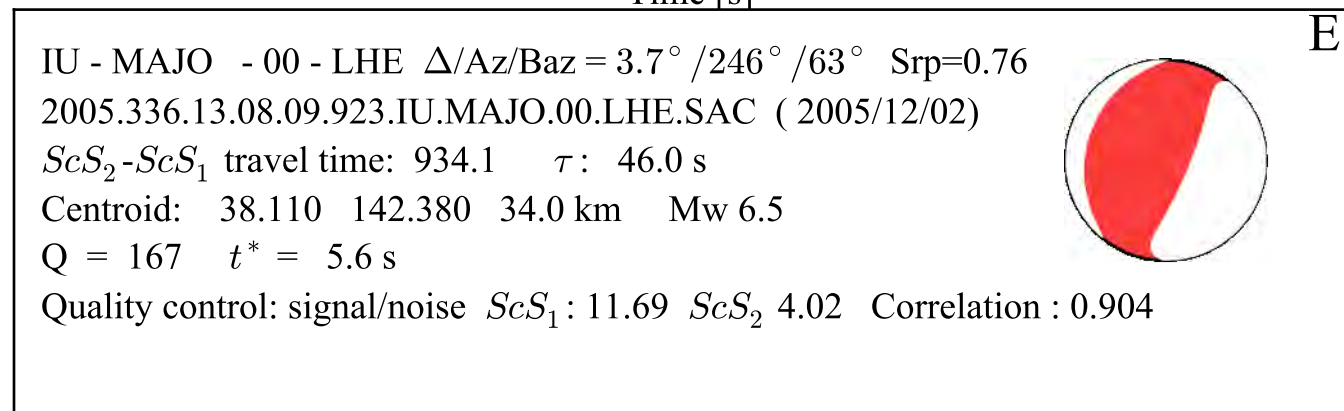
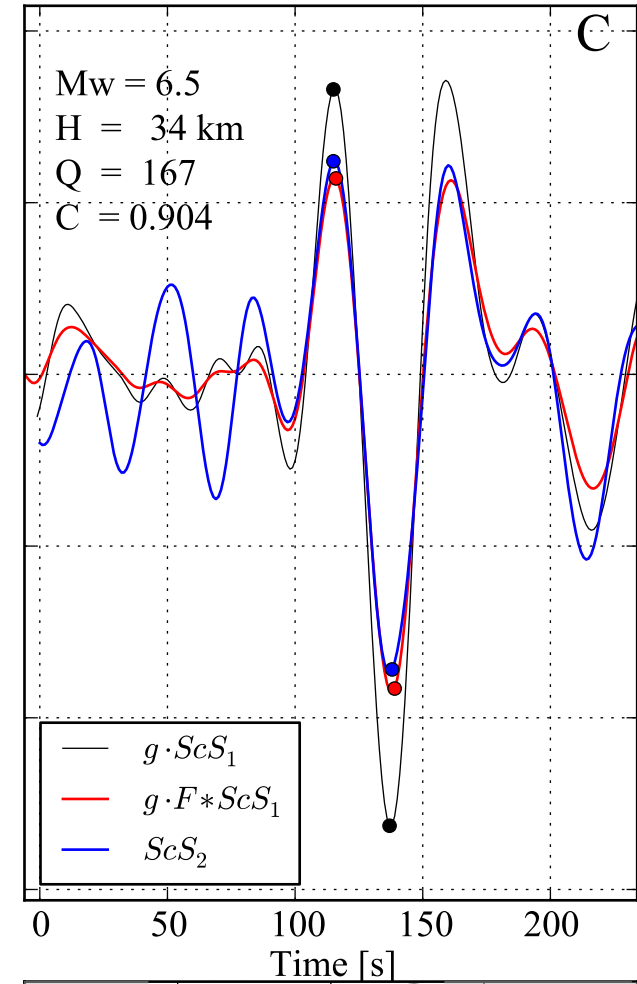
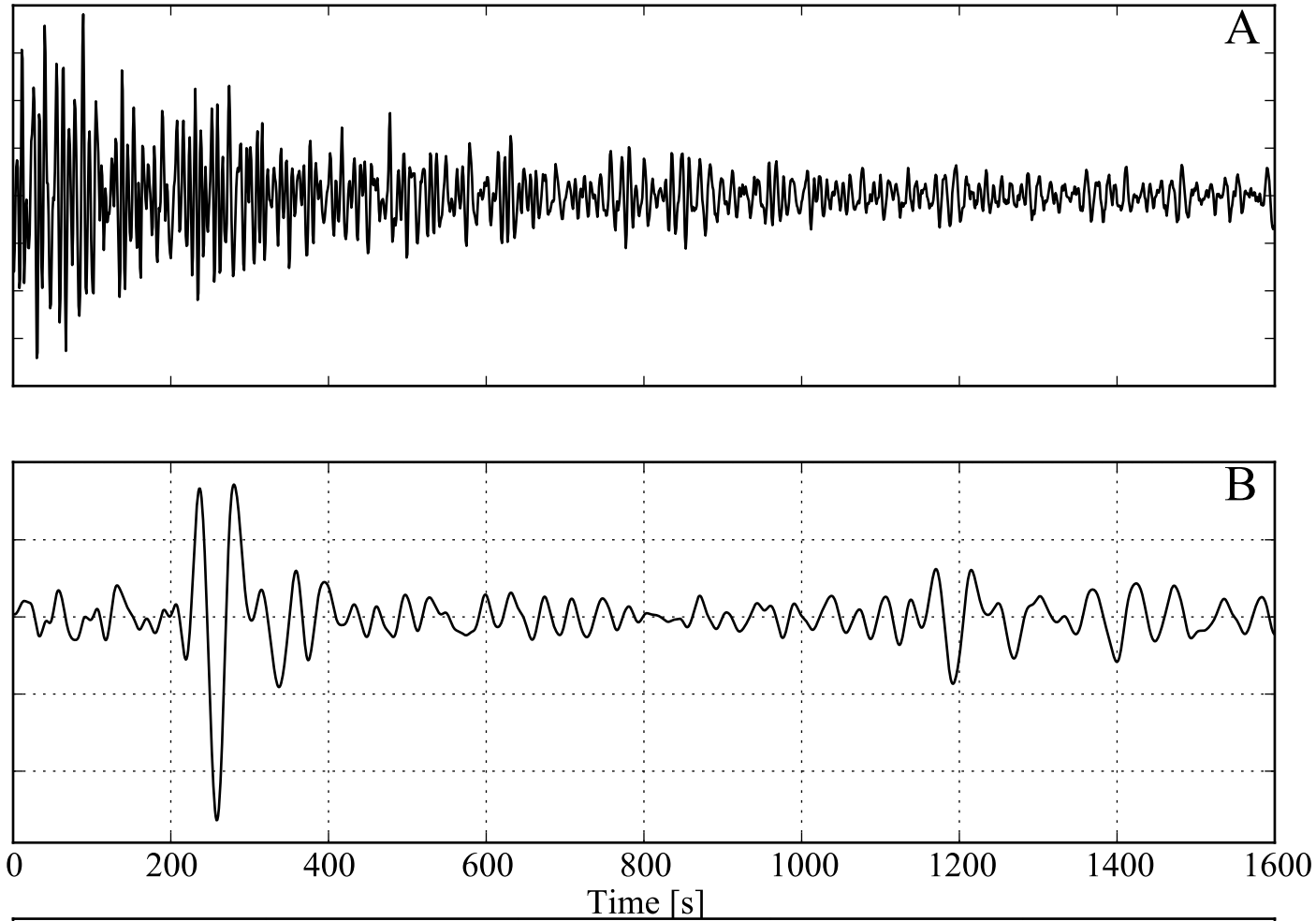


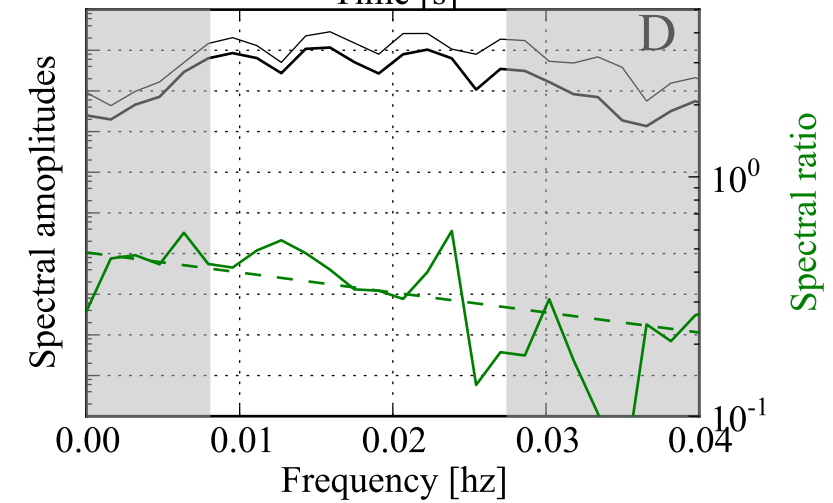
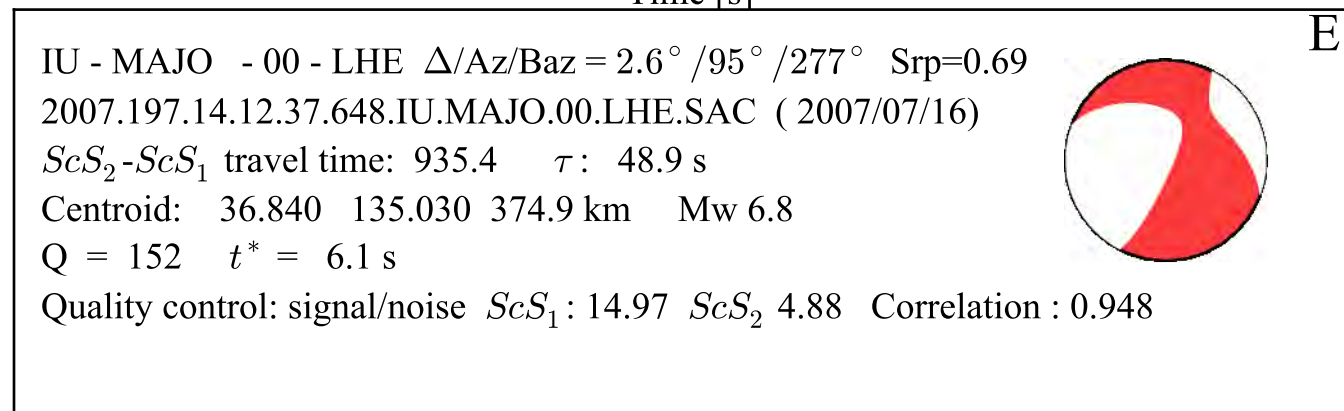
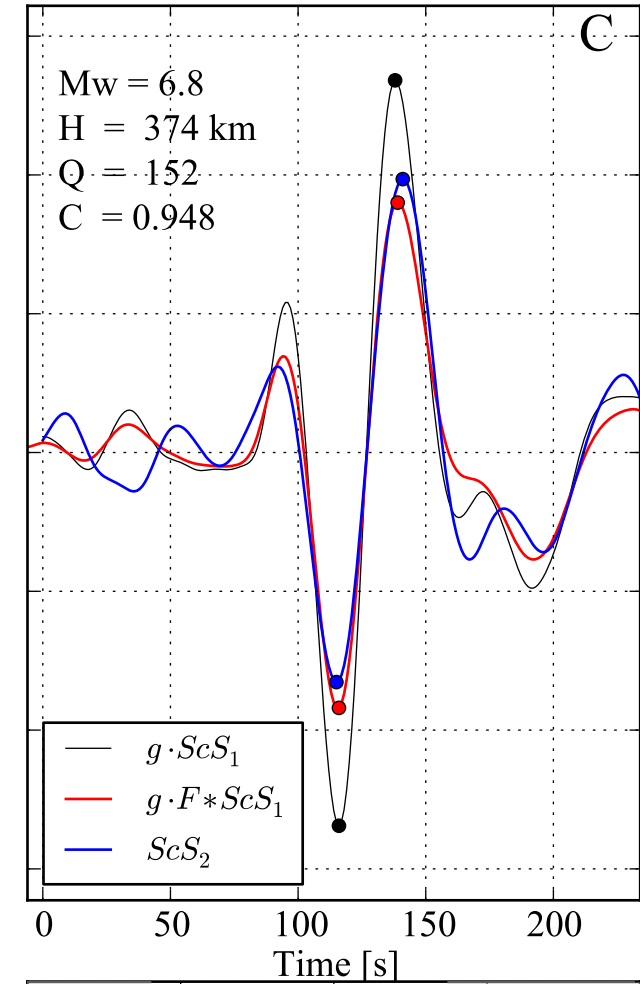
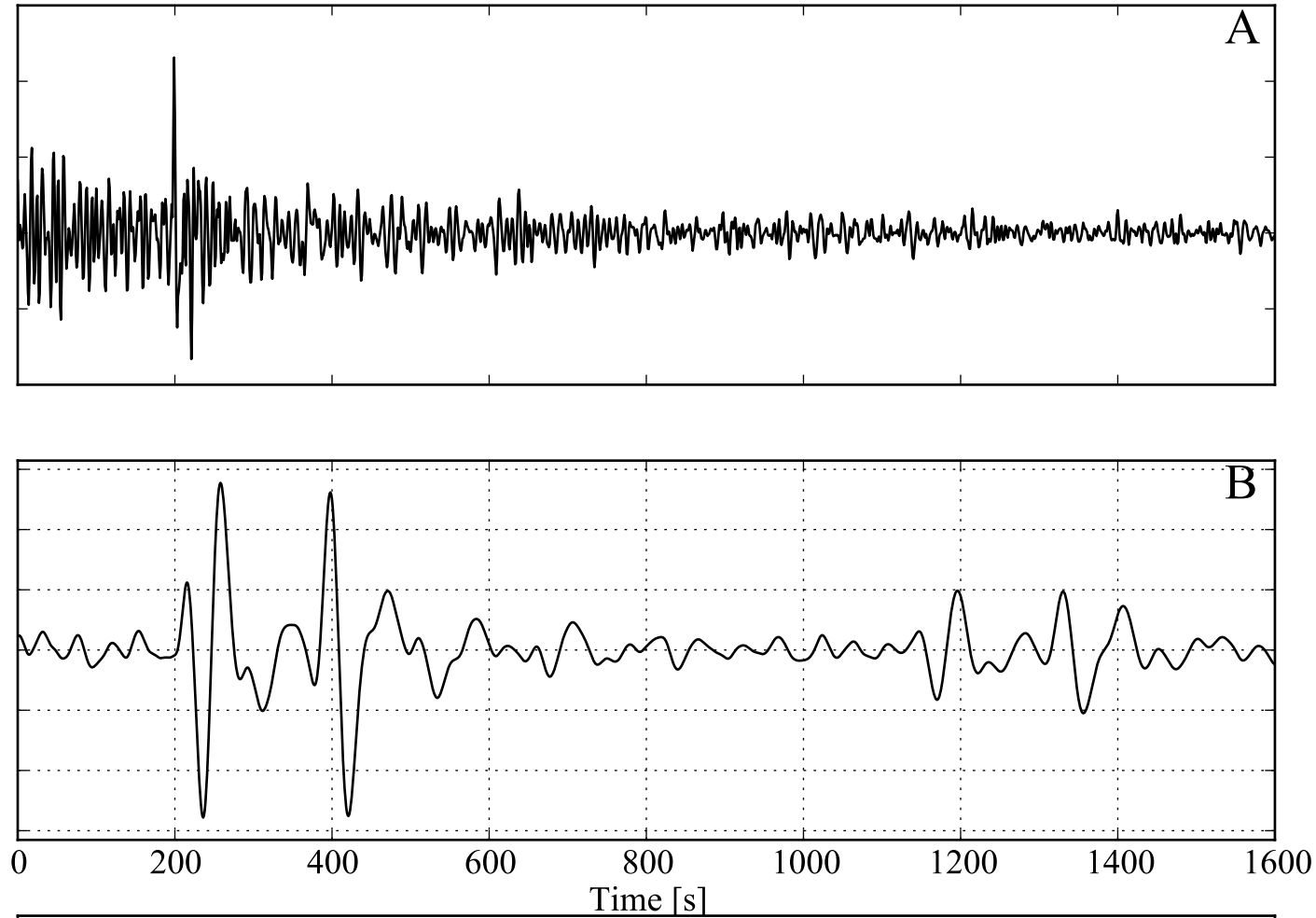
E

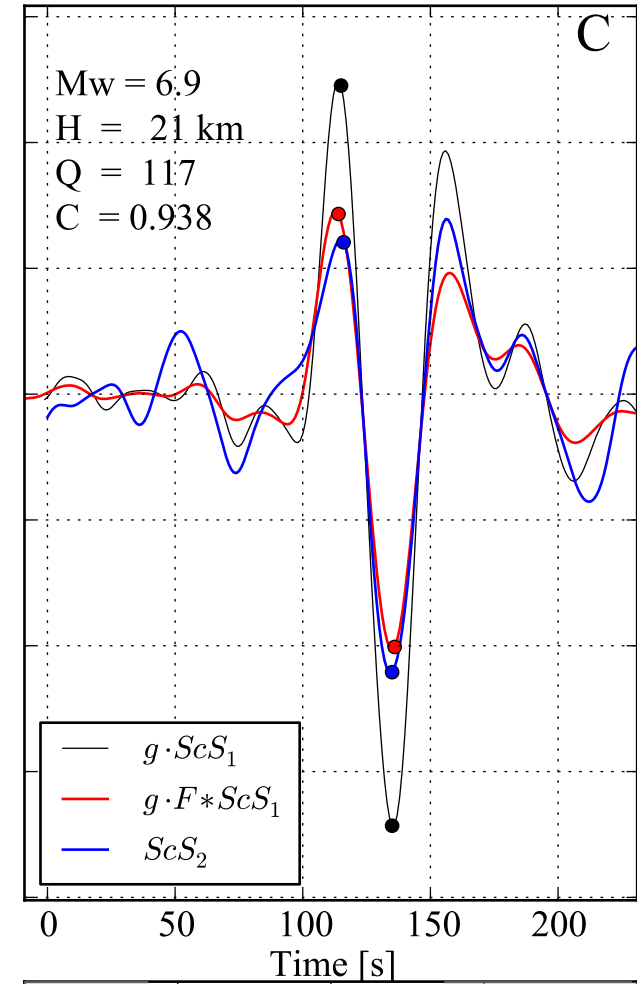
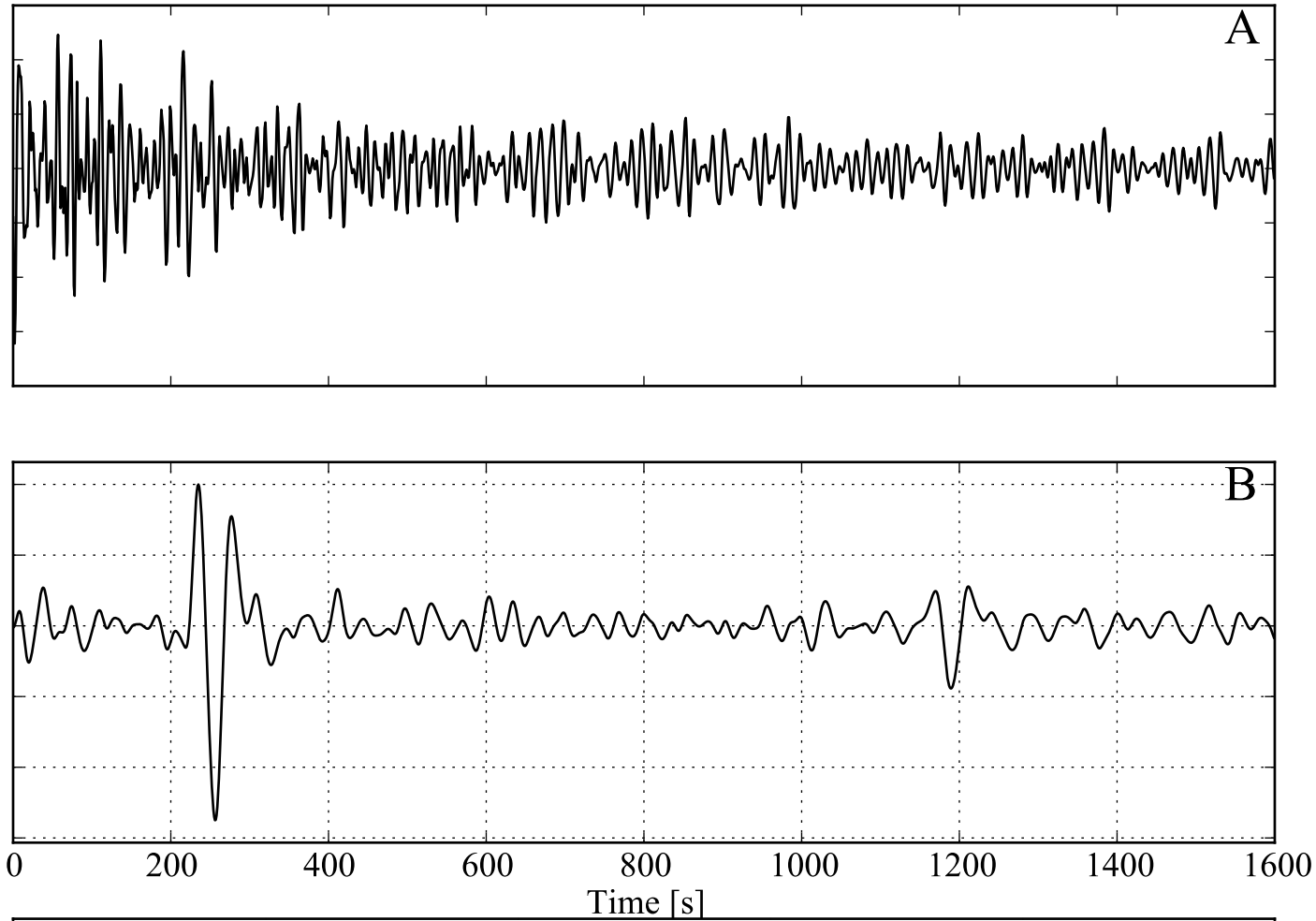
IU - MAJO - 00 - LHE $\Delta/Az/Baz = 3.5^\circ / 242^\circ / 59^\circ$ $Srp=0.85$
 2005.228.02.41.28.266.IU.MAJO.00.LHE.SAC (2005/08/16)
 ScS_2-ScS_1 travel time: 935.2 τ : 48.6 s
 Centroid: 38.240 142.050 37.0 km Mw 7.2
 Q = 175 $t^* = 5.3$ s
 Quality control: signal/noise ScS_1 : 13.37 ScS_2 4.72 Correlation : 0.952





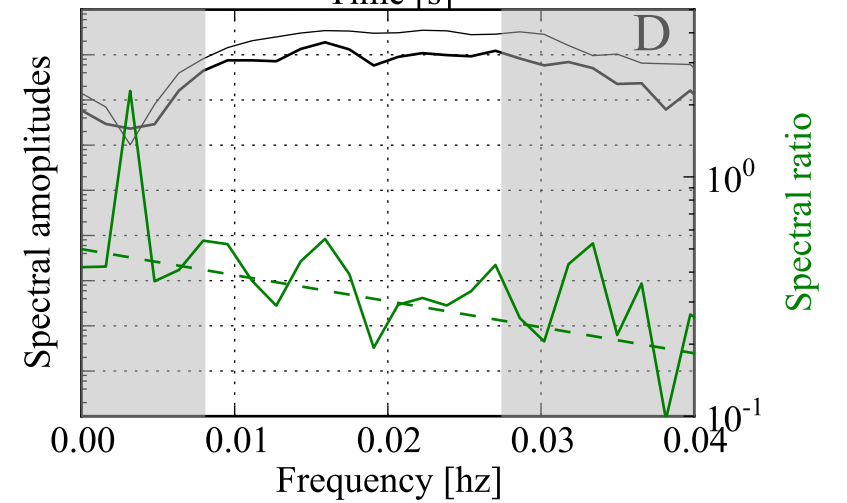


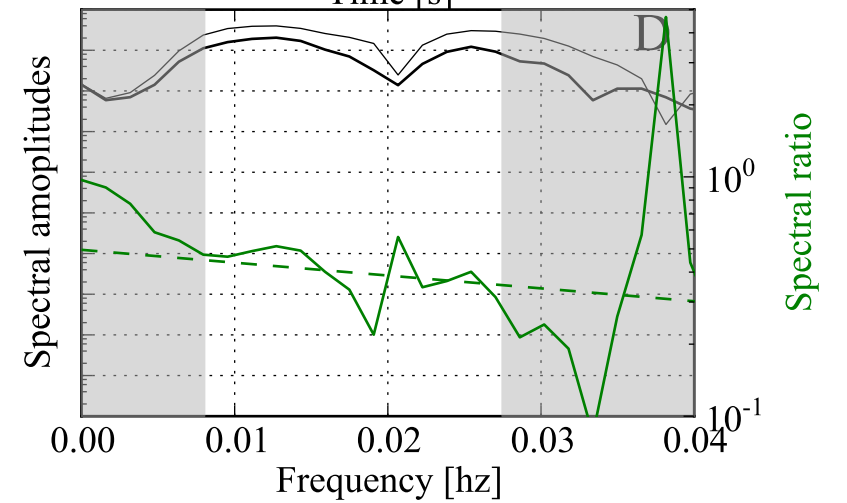
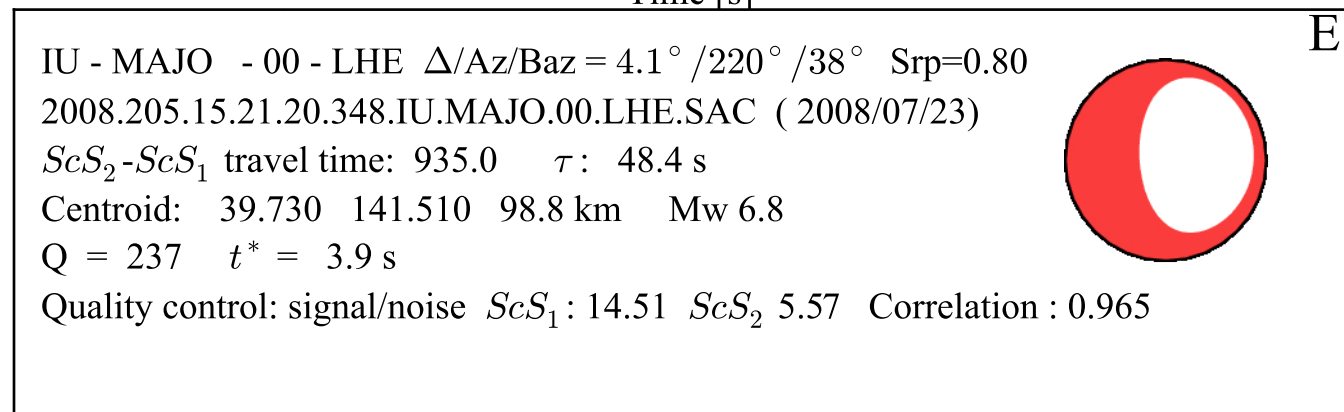
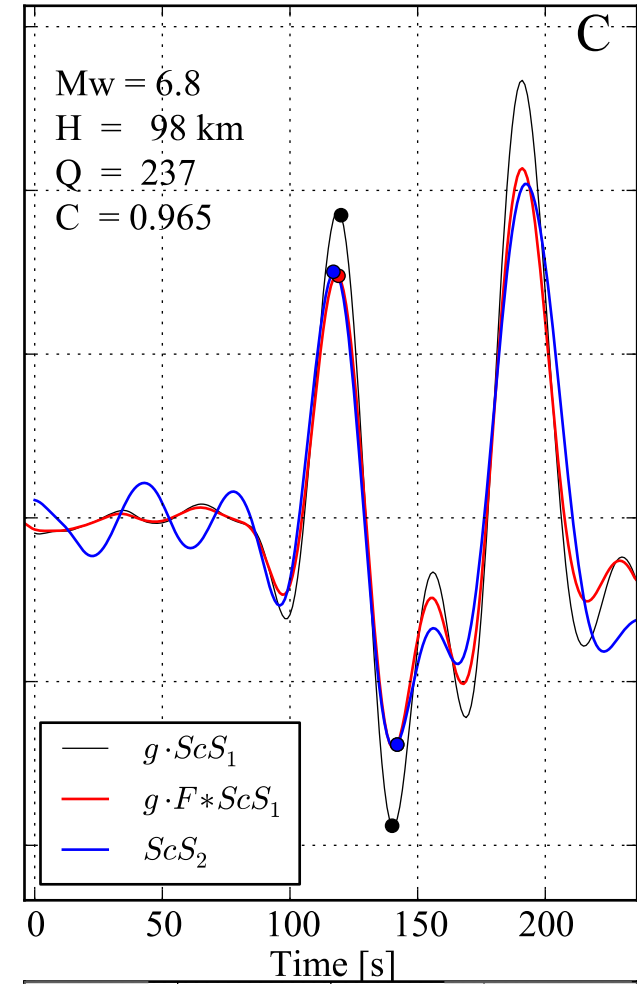
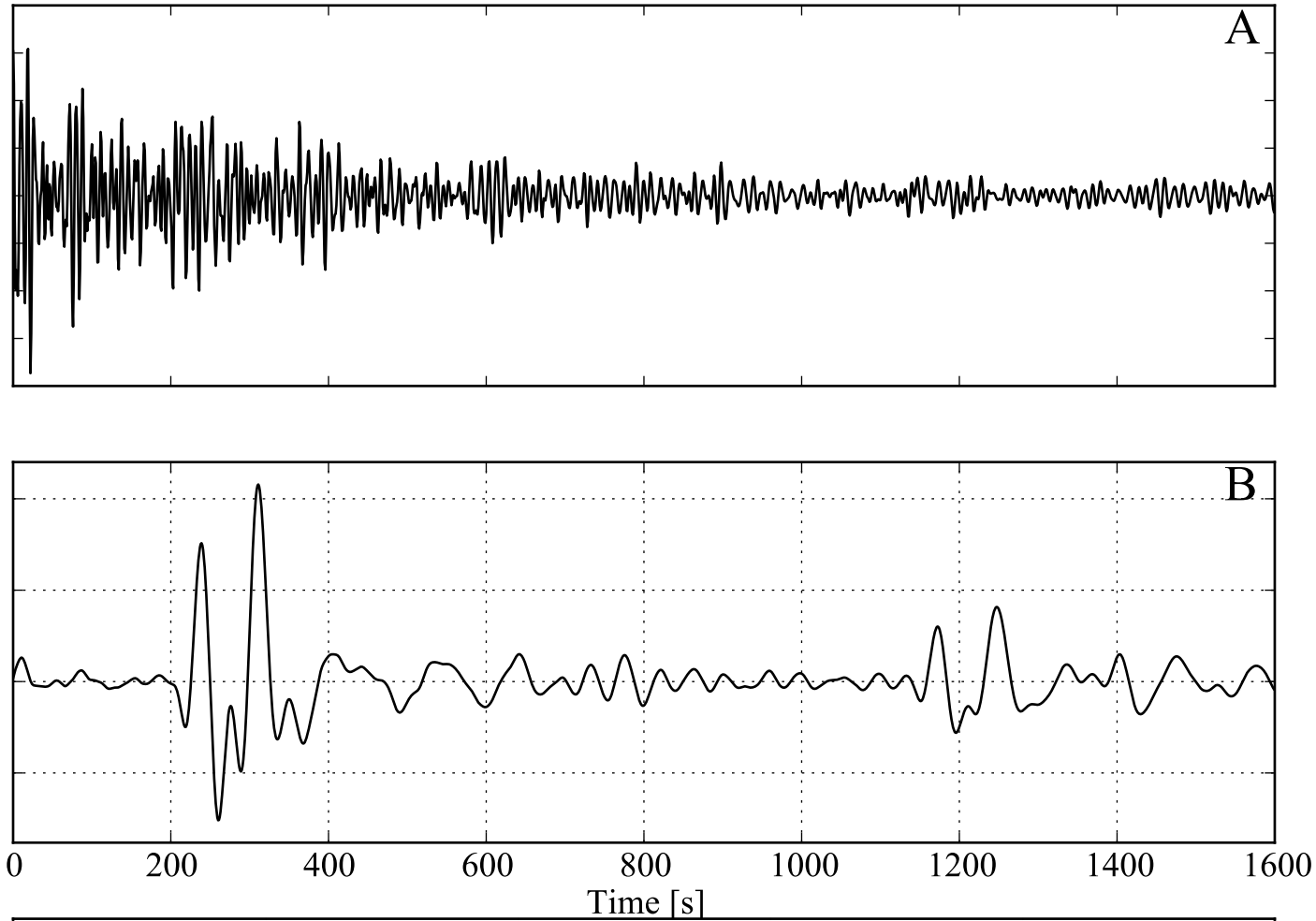


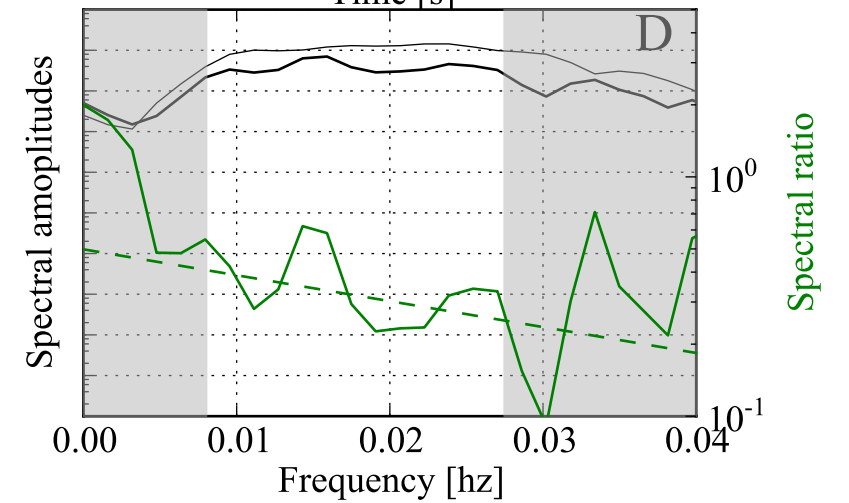
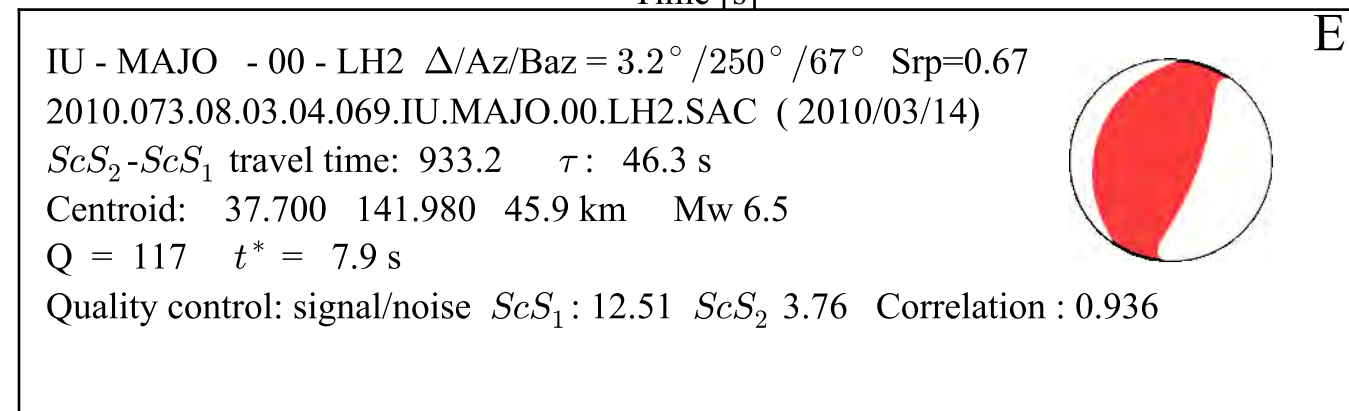
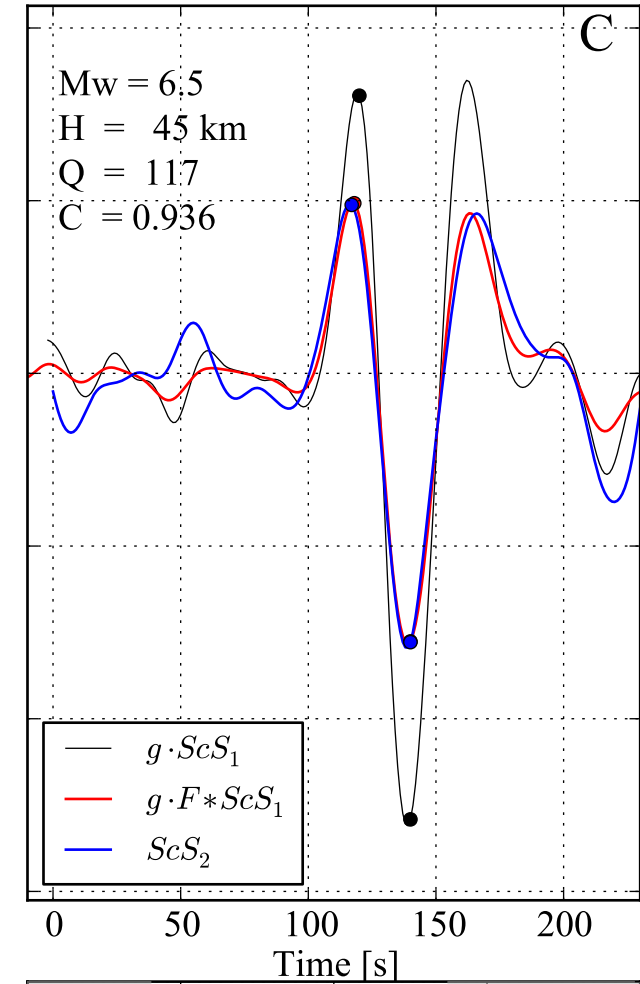
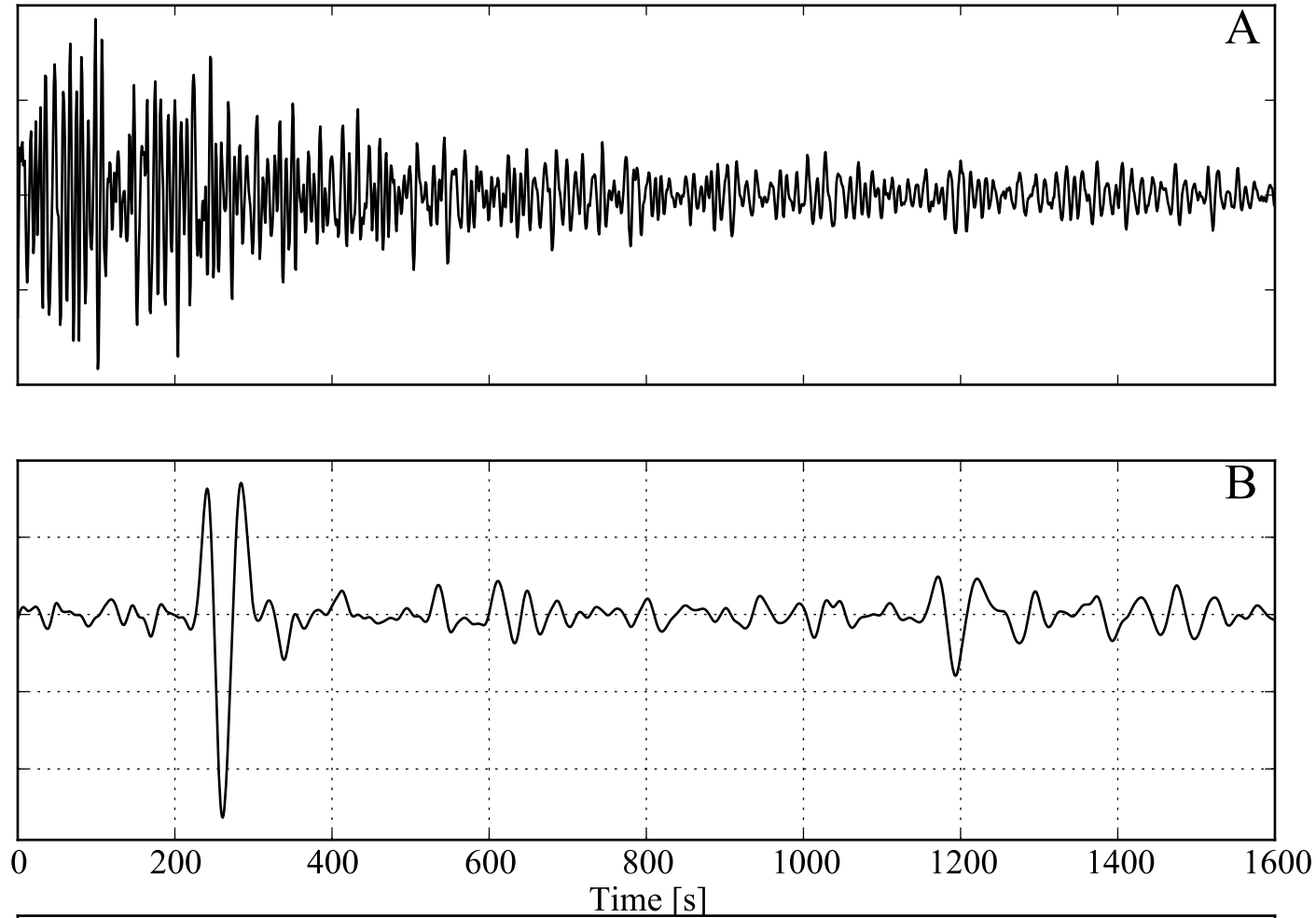


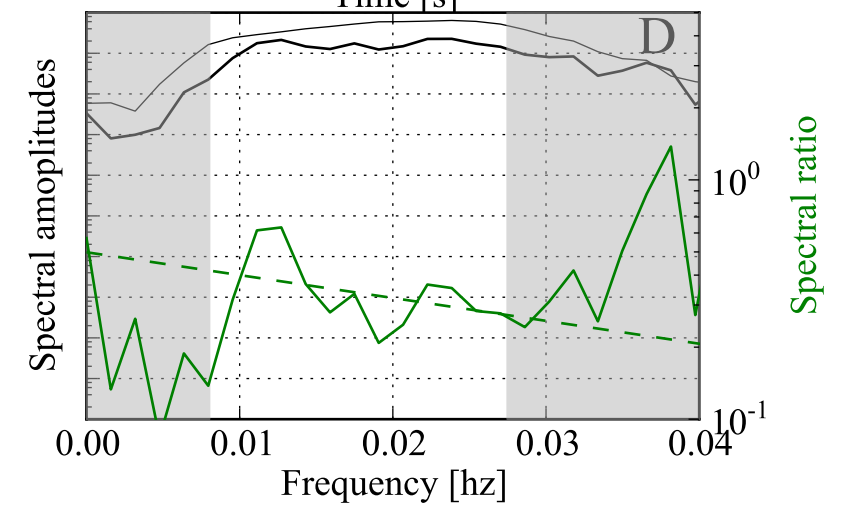
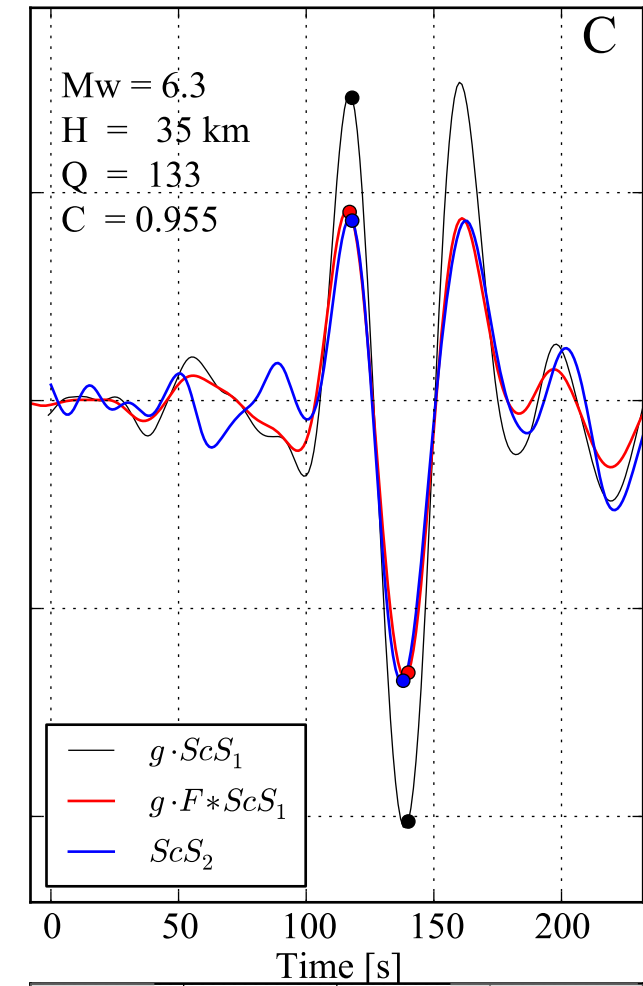
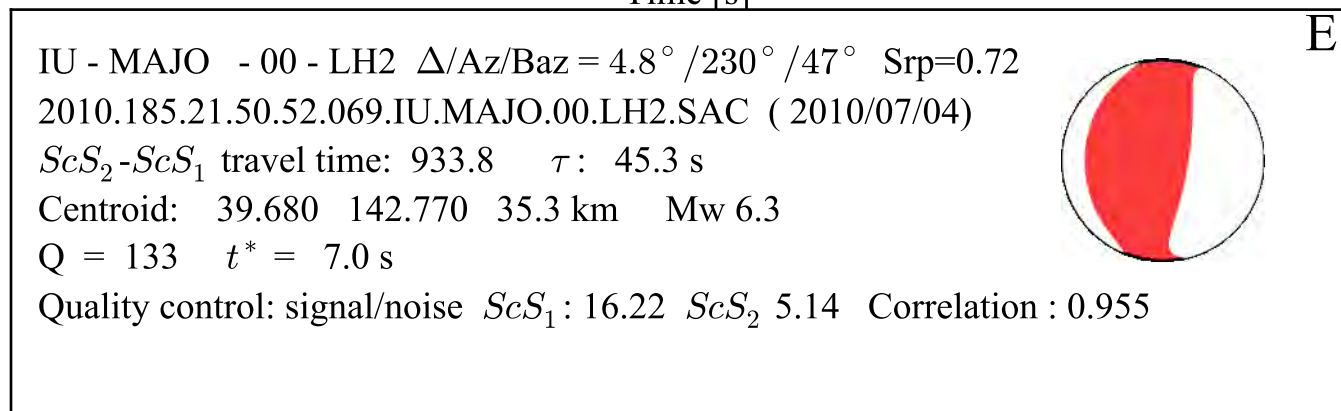
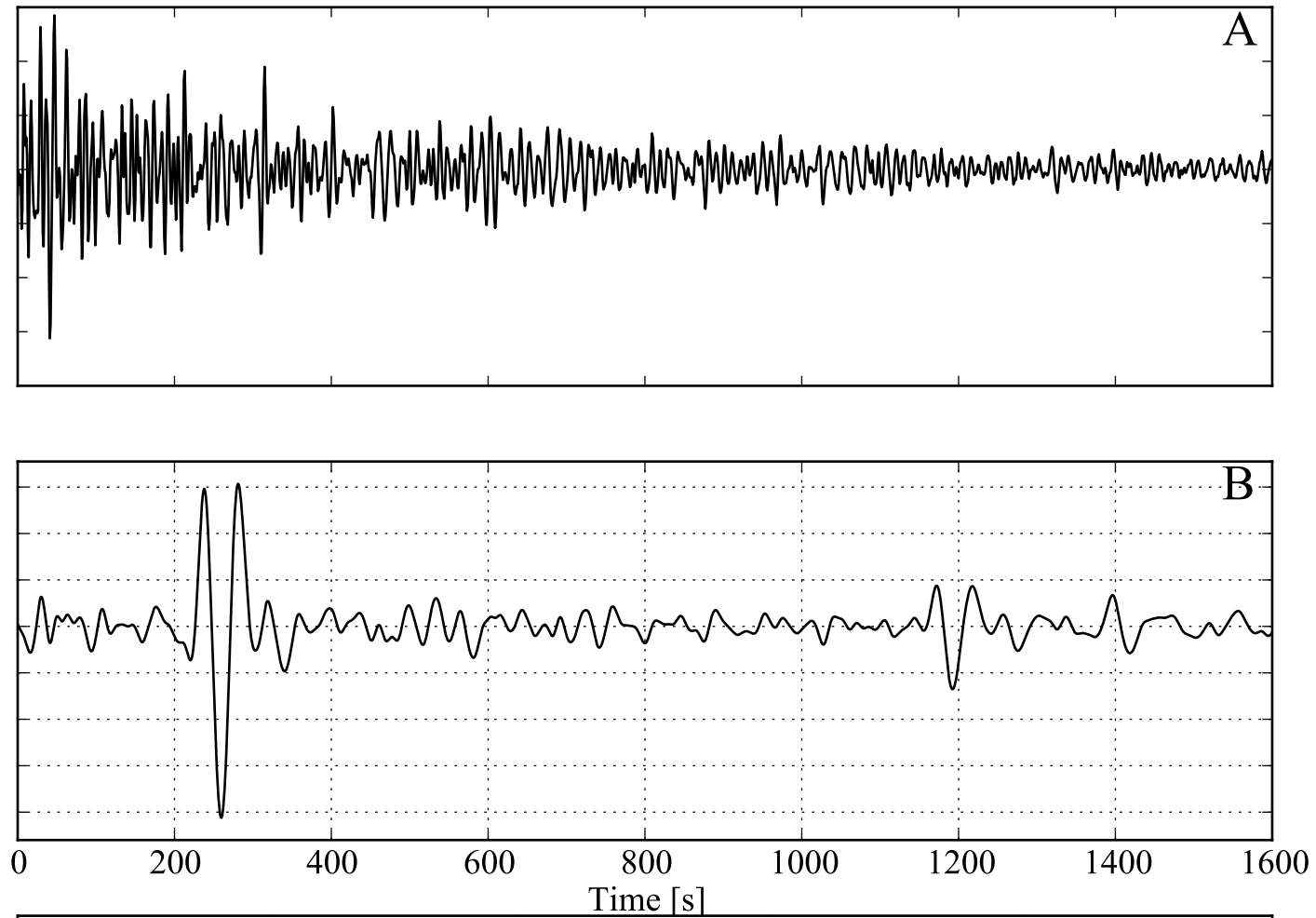
E

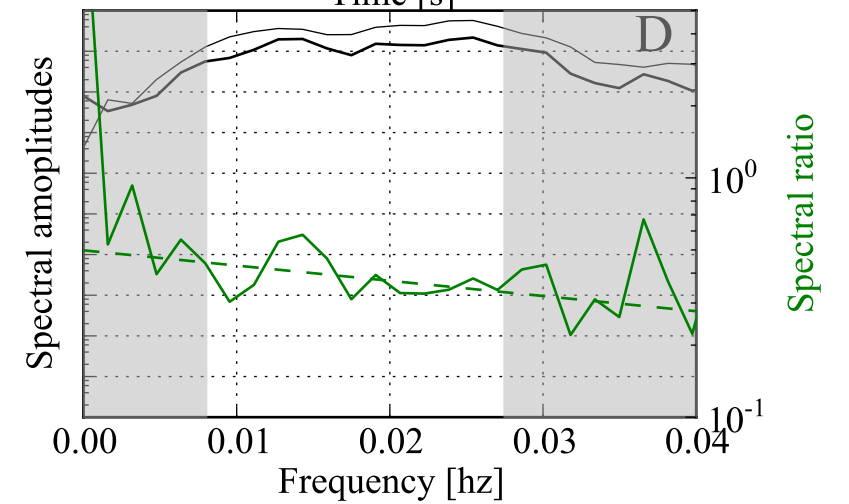
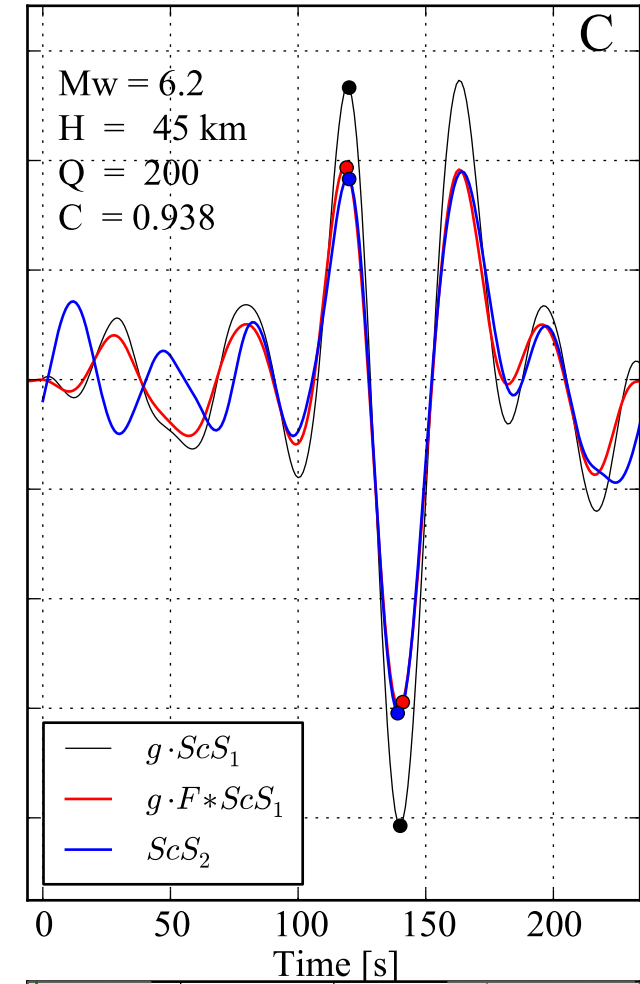
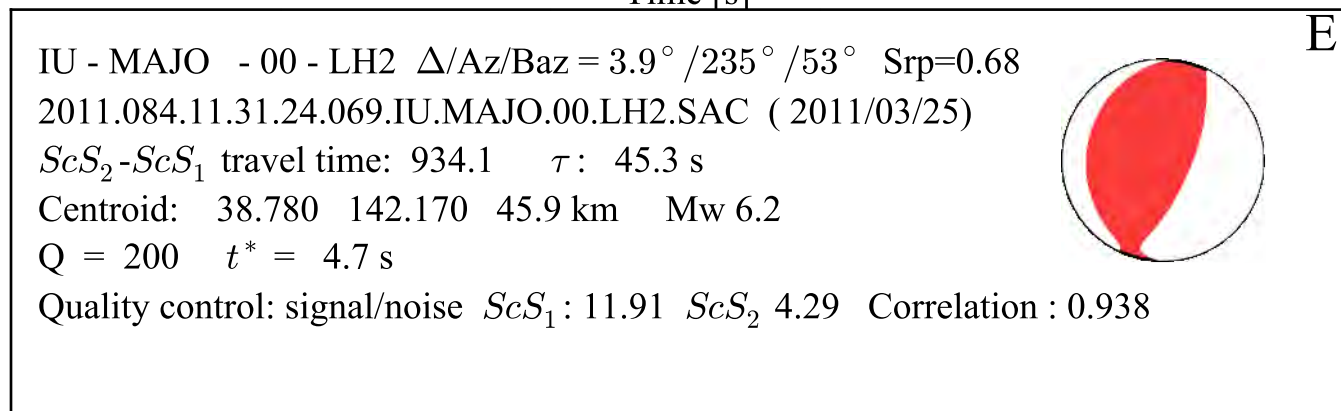
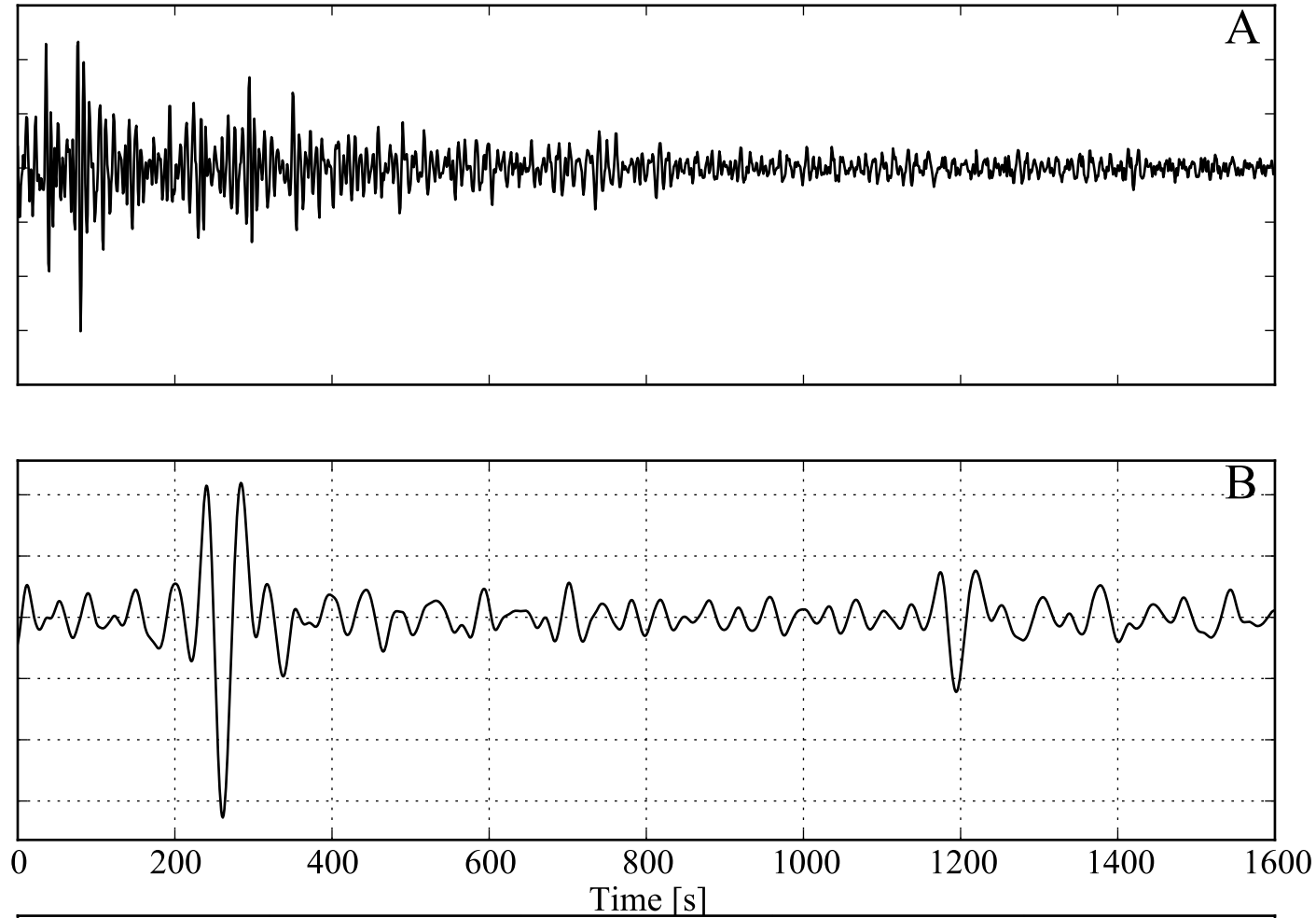
IU - MAJO - 00 - LHE $\Delta/Az/Baz = 3.5^\circ / 255^\circ / 73^\circ$ $Srp=0.85$
 2008.201.02.34.28.348.IU.MAJO.00.LHE.SAC (2008/07/19)
 ScS_2-ScS_1 travel time: 934.1 τ : 44.7 s
 Centroid: 37.470 142.420 21.8 km Mw 6.9
 Q = 117 $t^* = 8.0$ s
 Quality control: signal/noise ScS_1 : 13.11 ScS_2 3.80 Correlation : 0.938

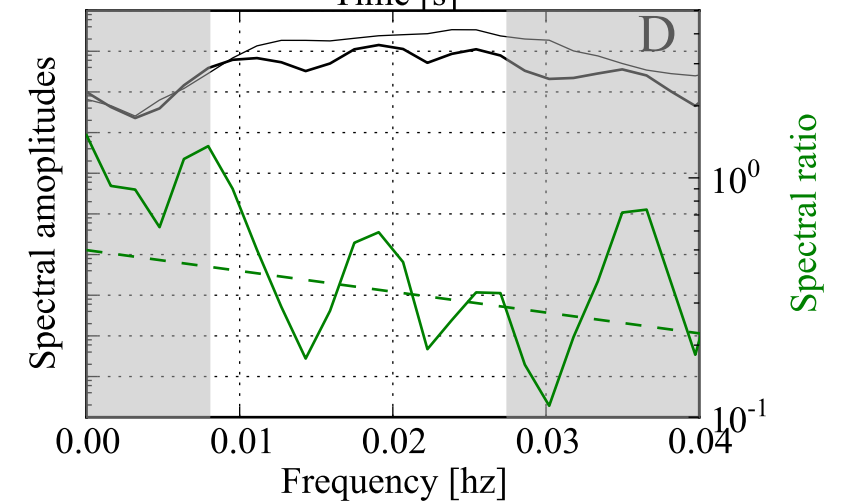
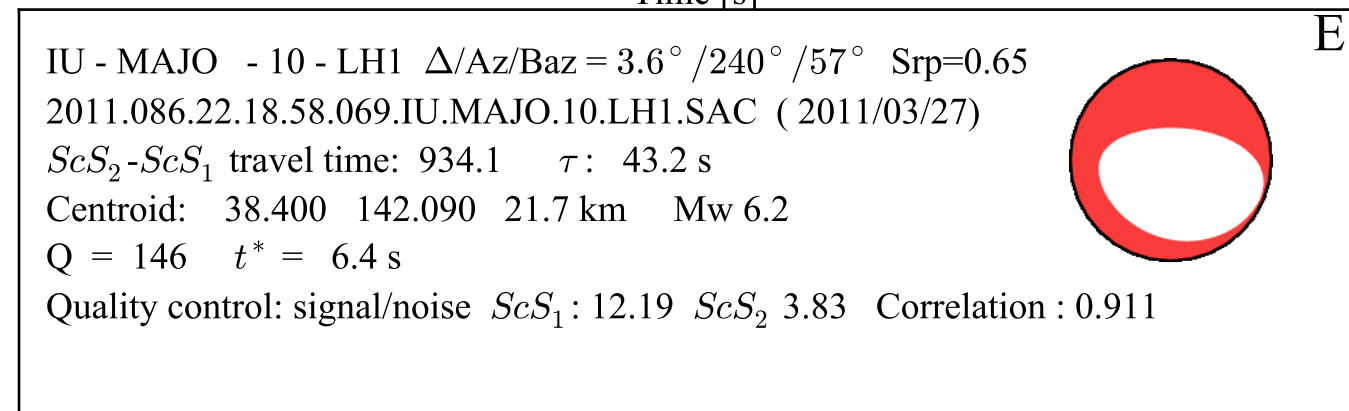
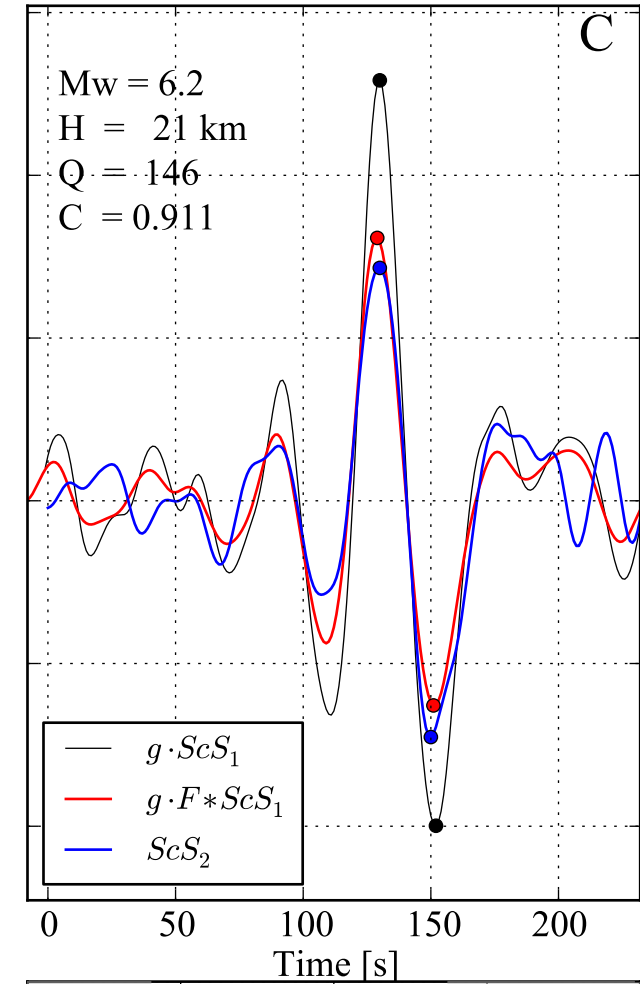
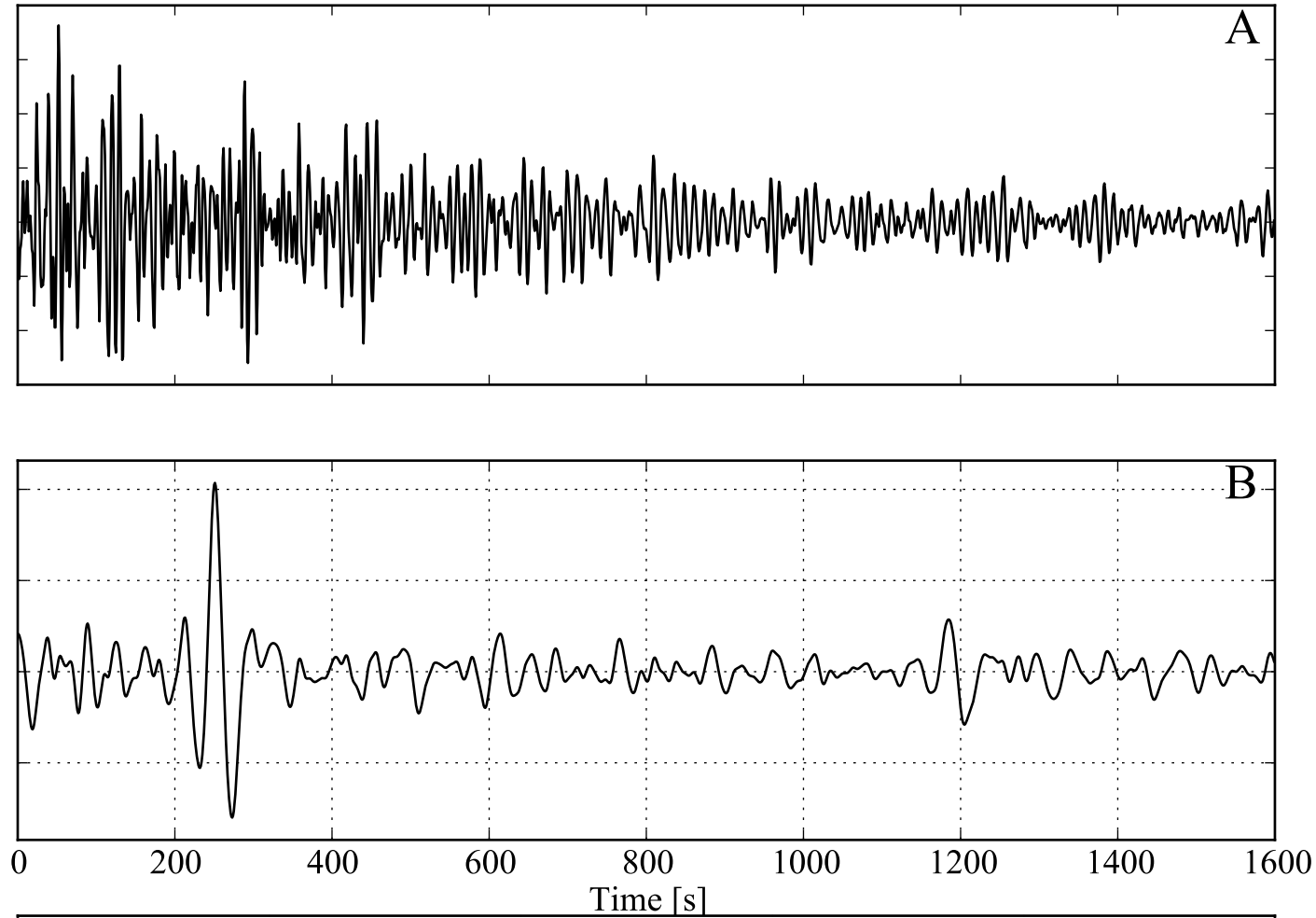


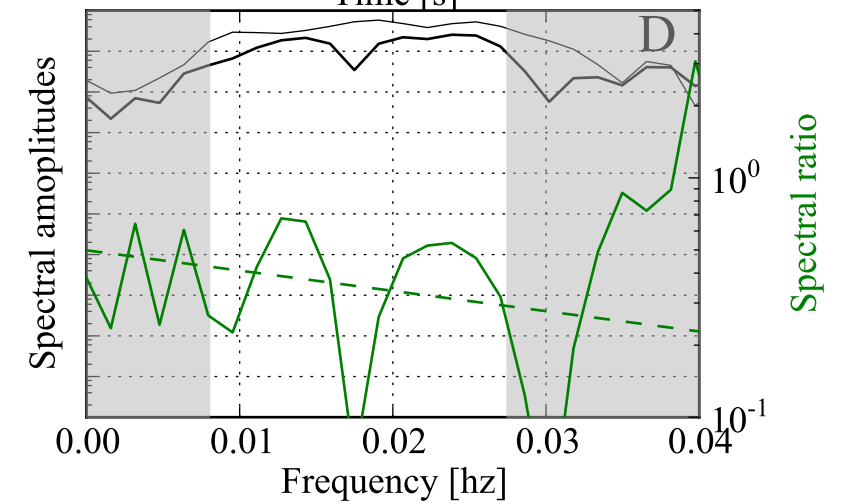
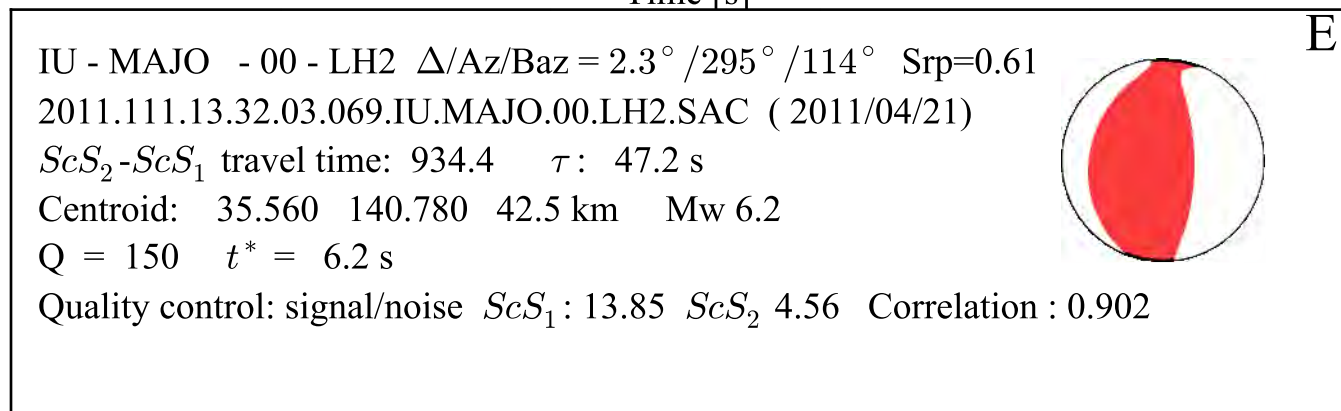
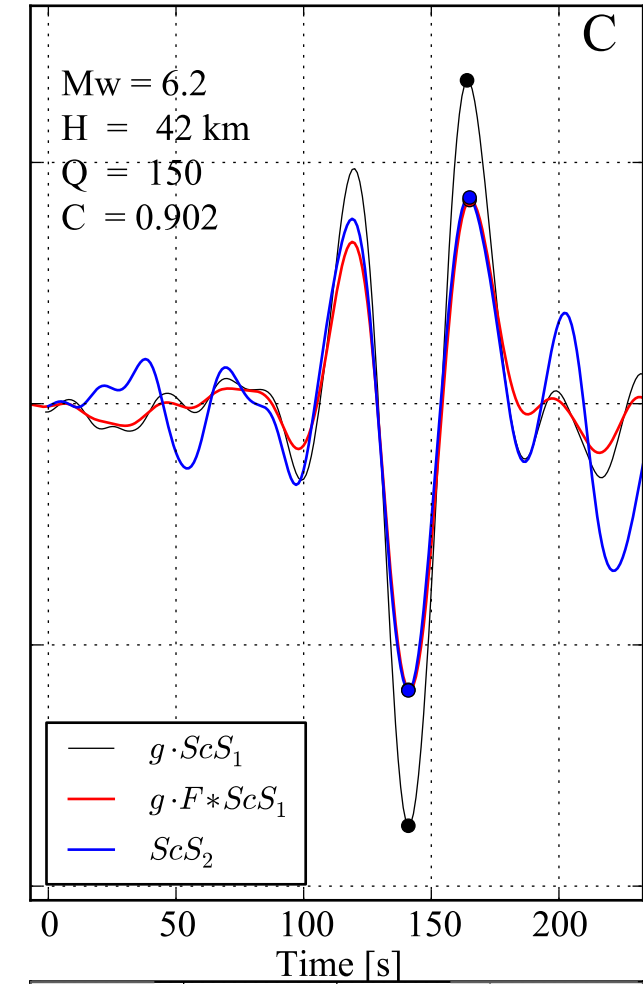
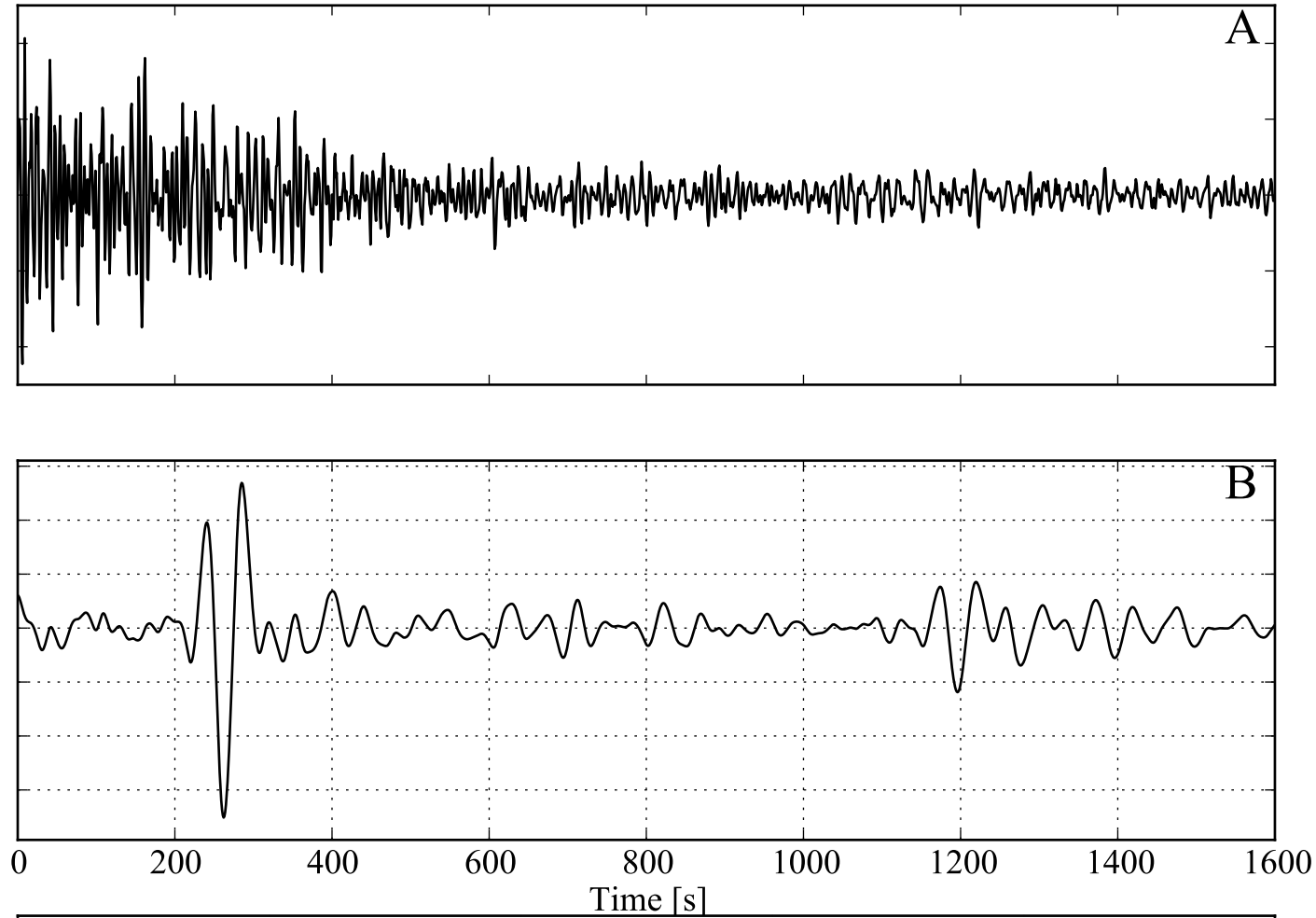


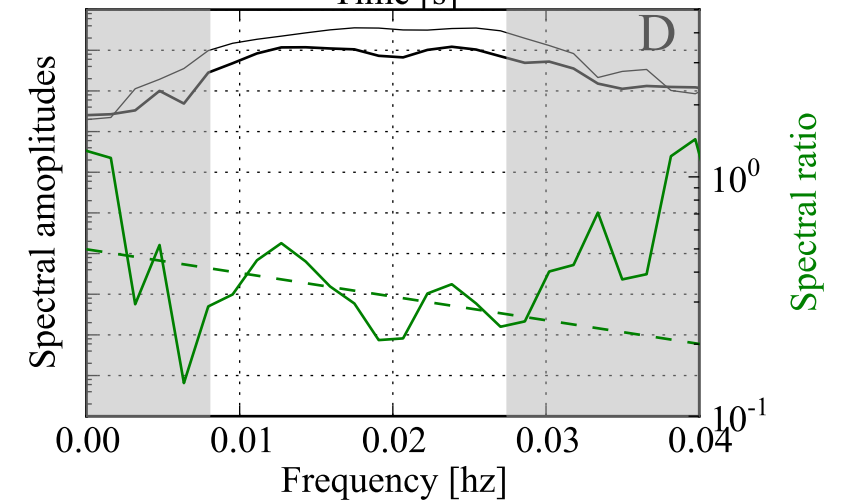
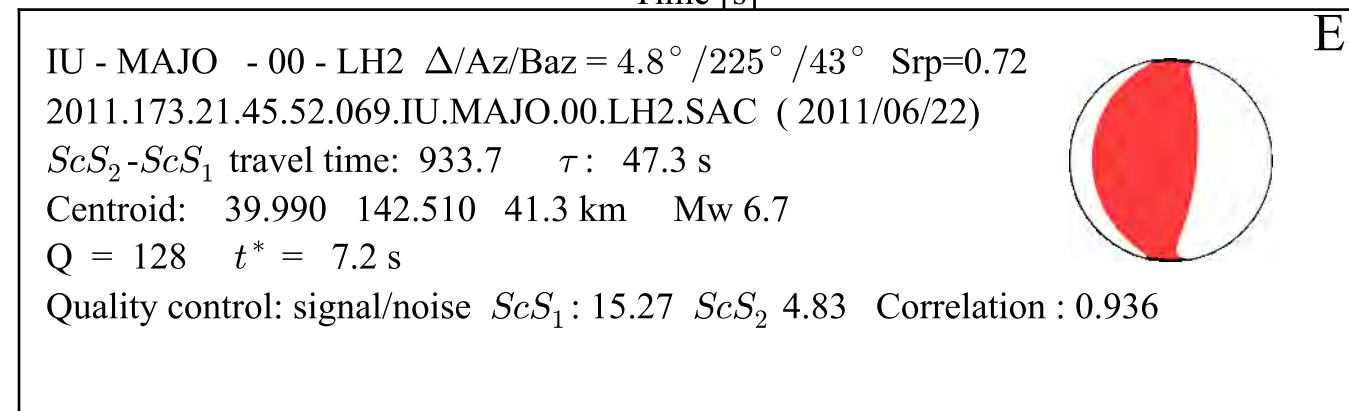
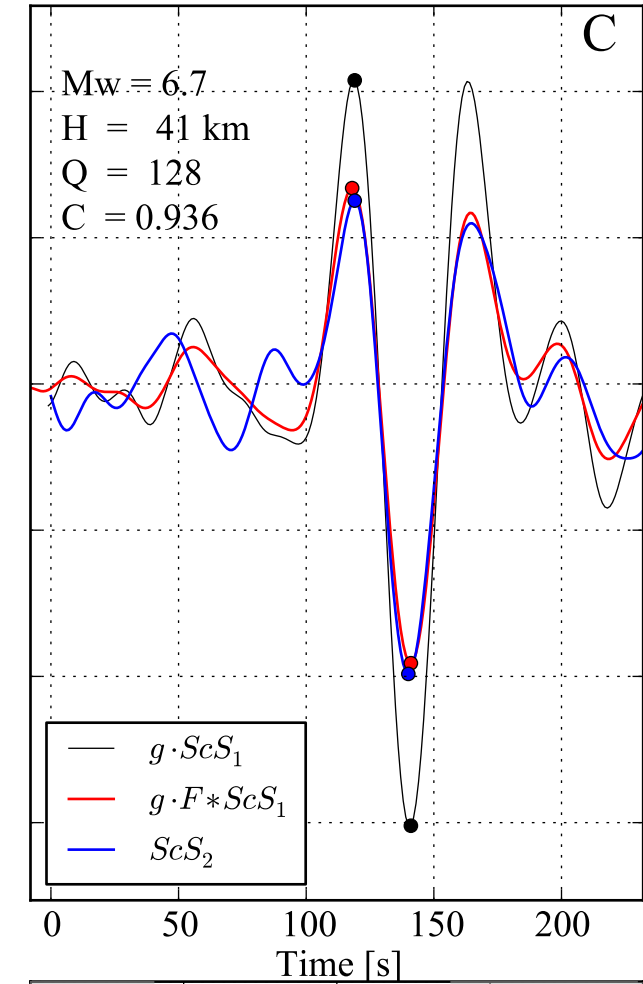
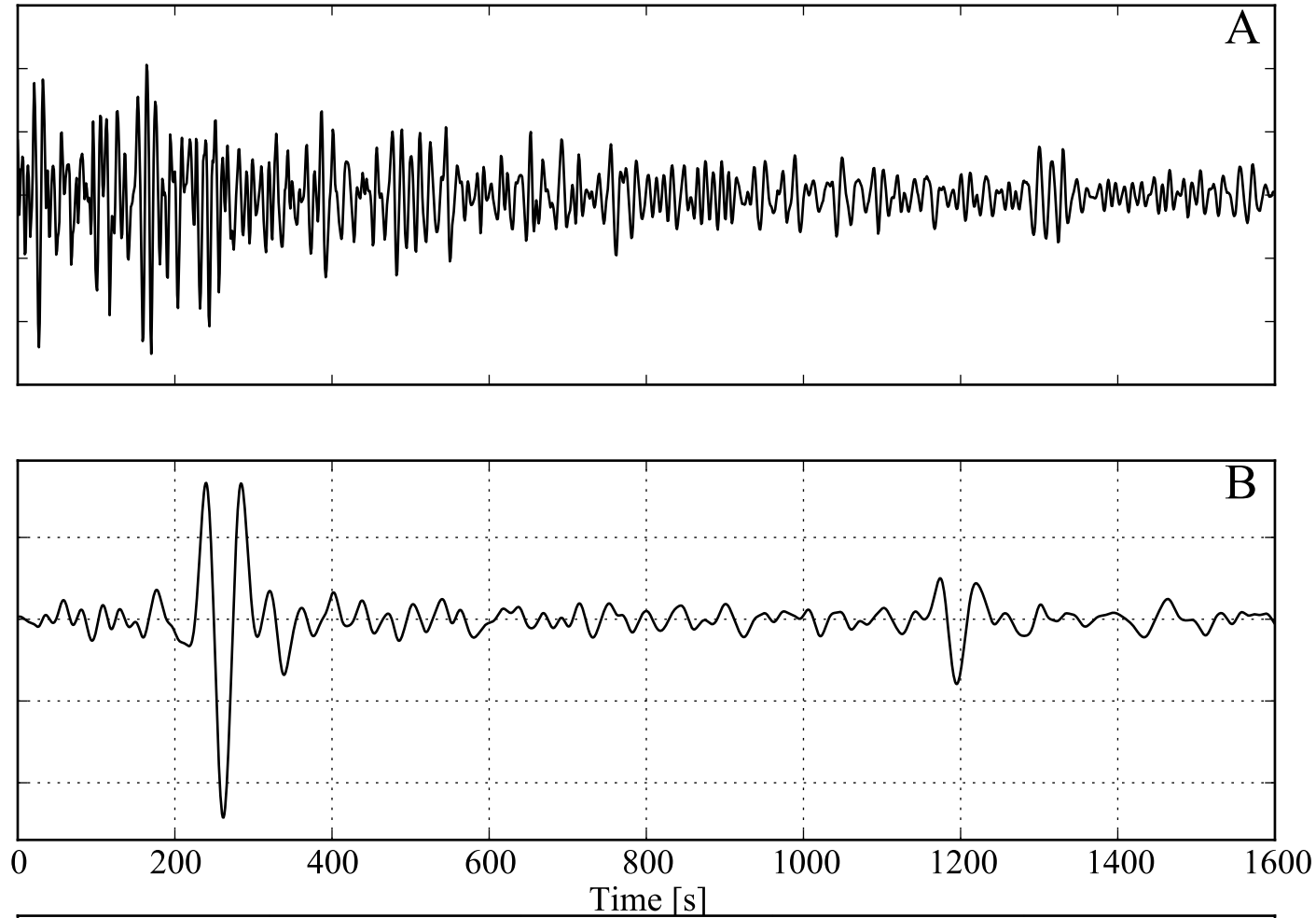


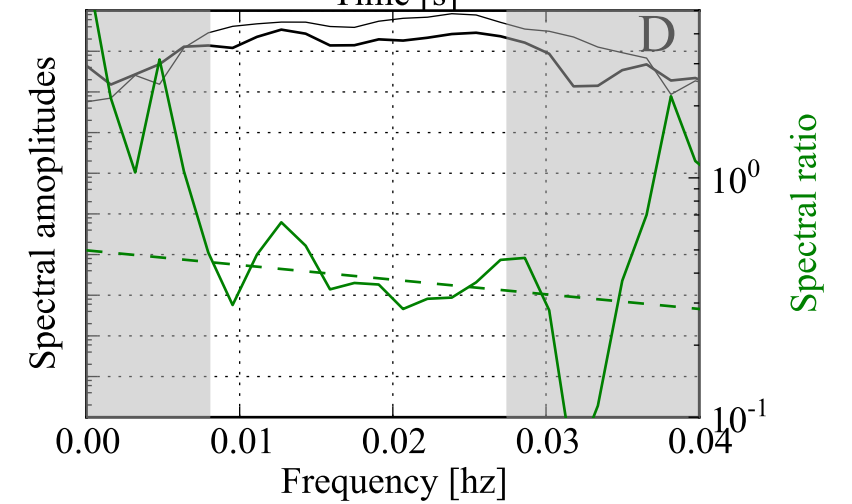
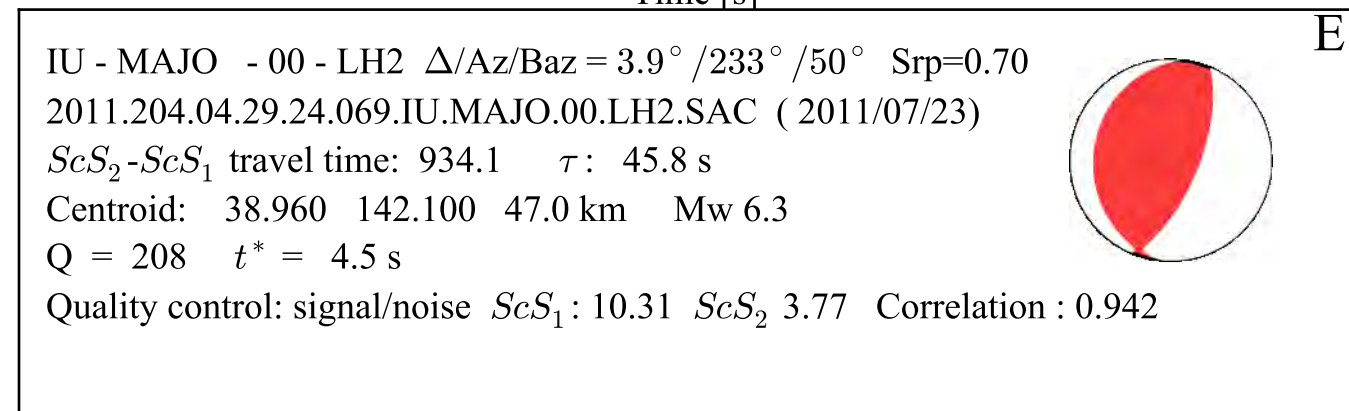
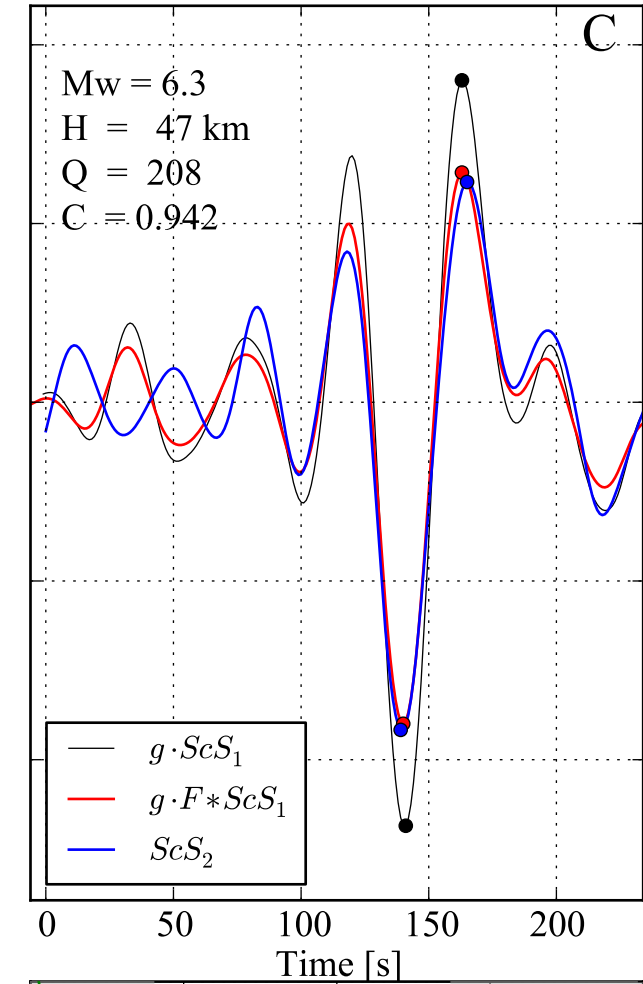
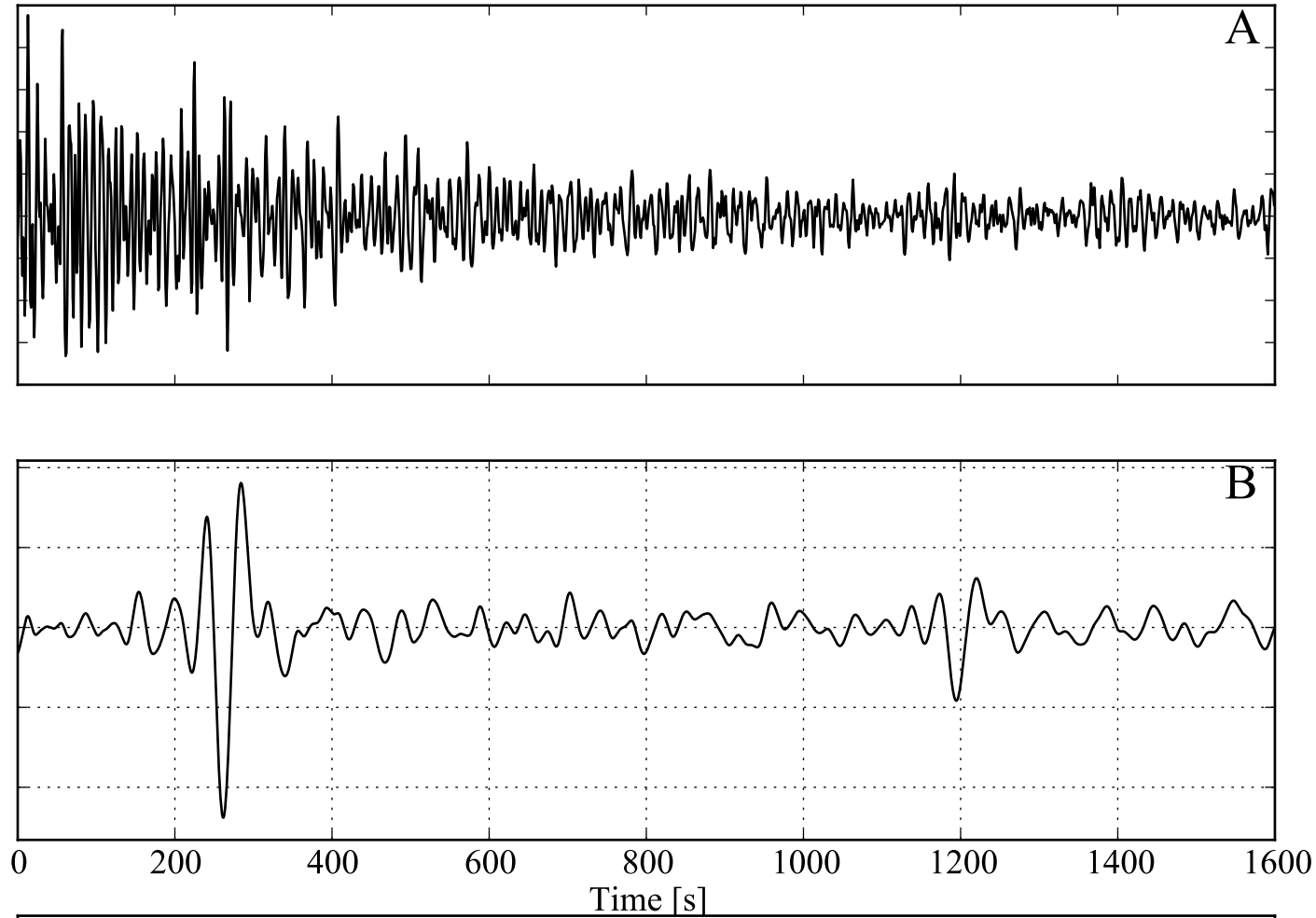


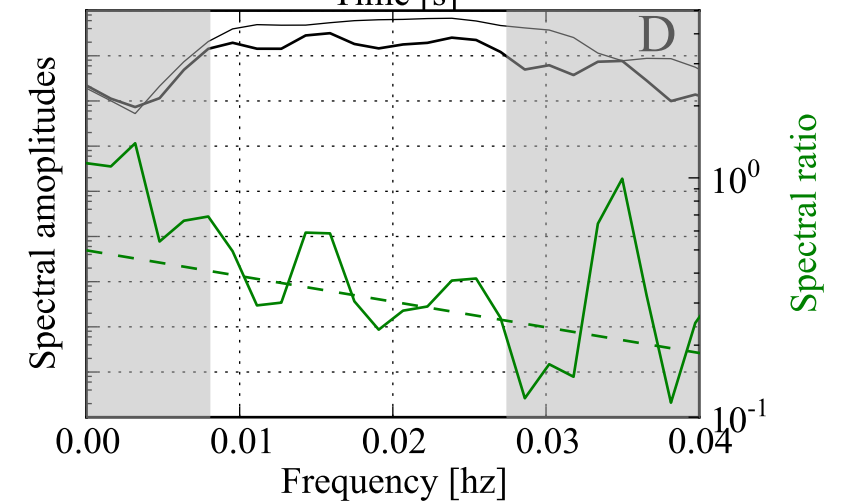
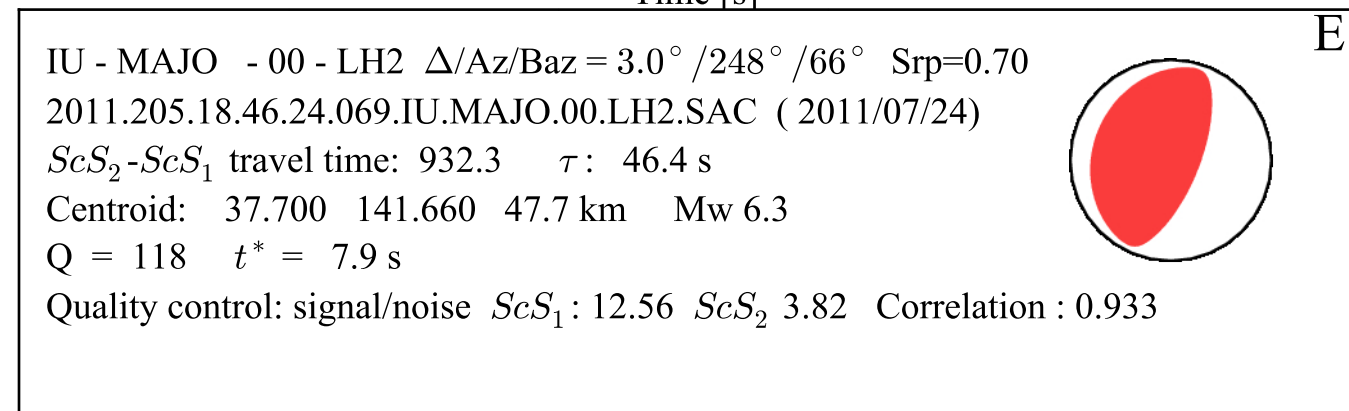
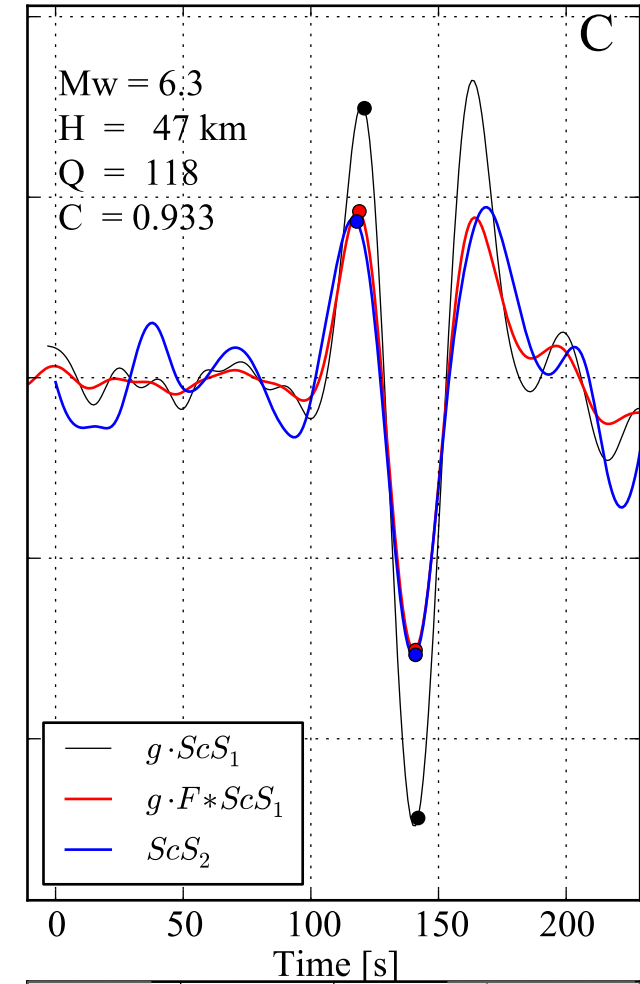
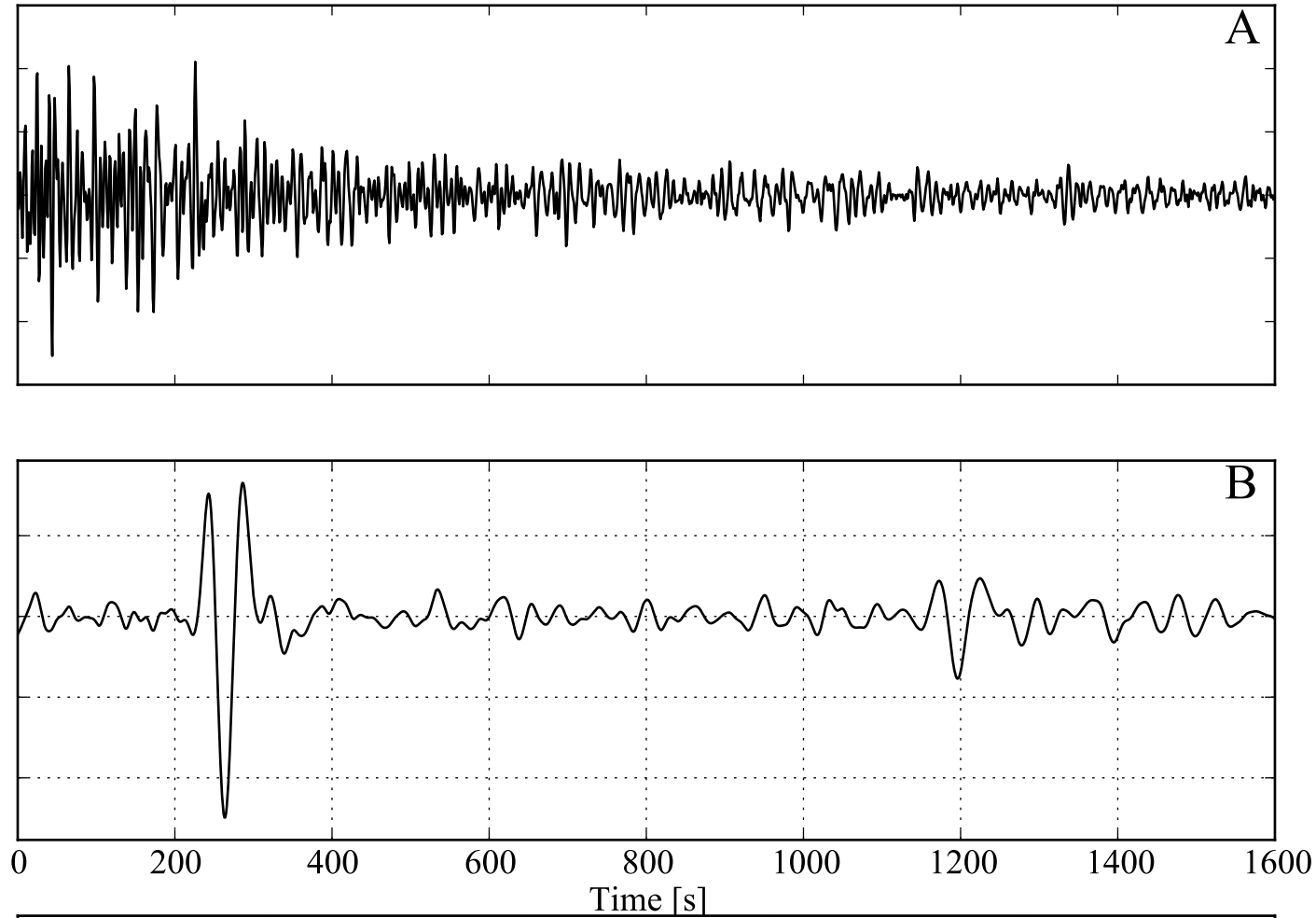


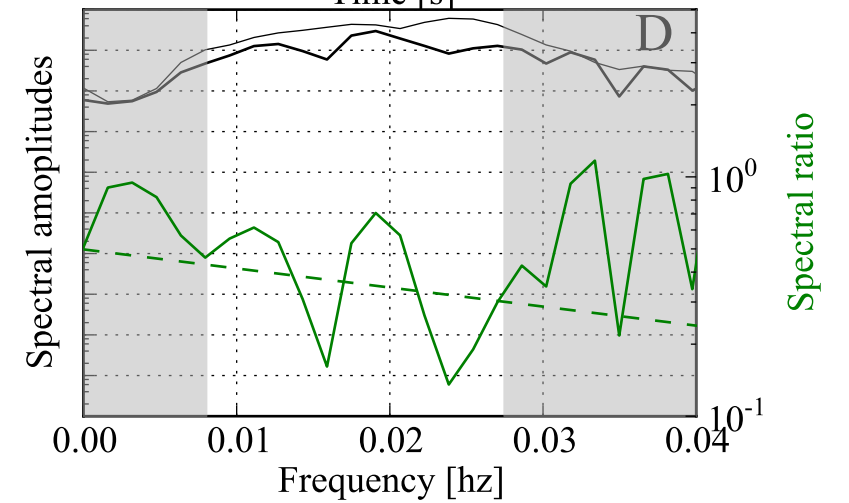
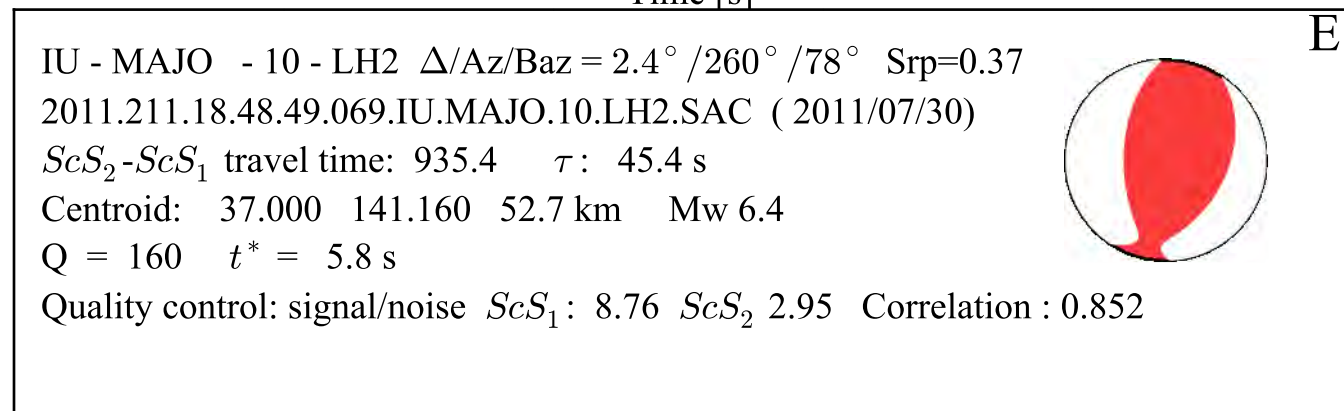
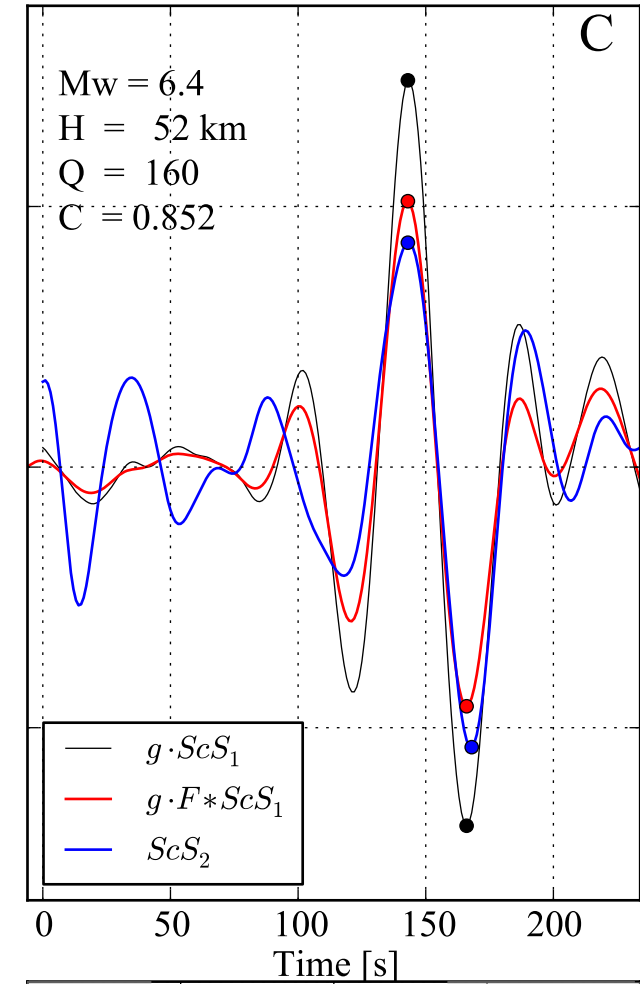
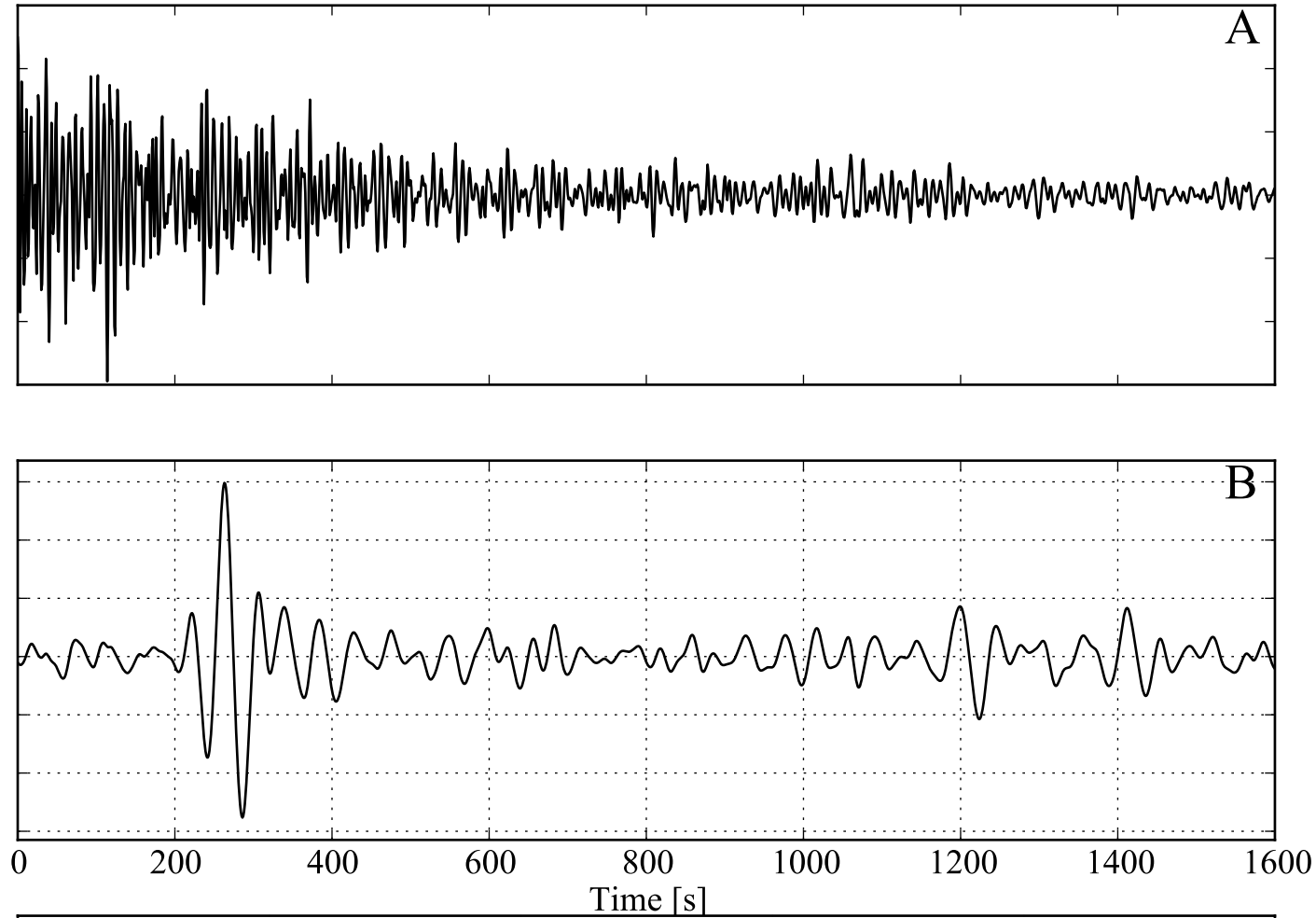


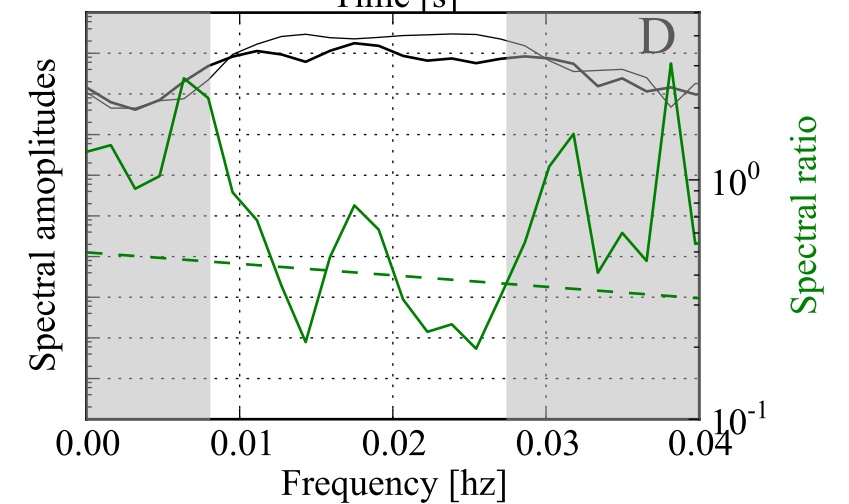
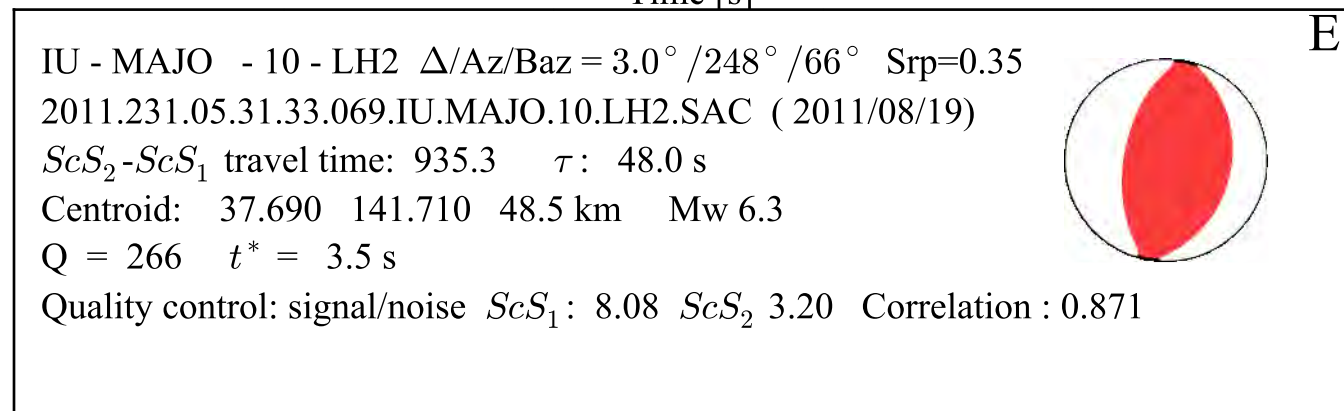
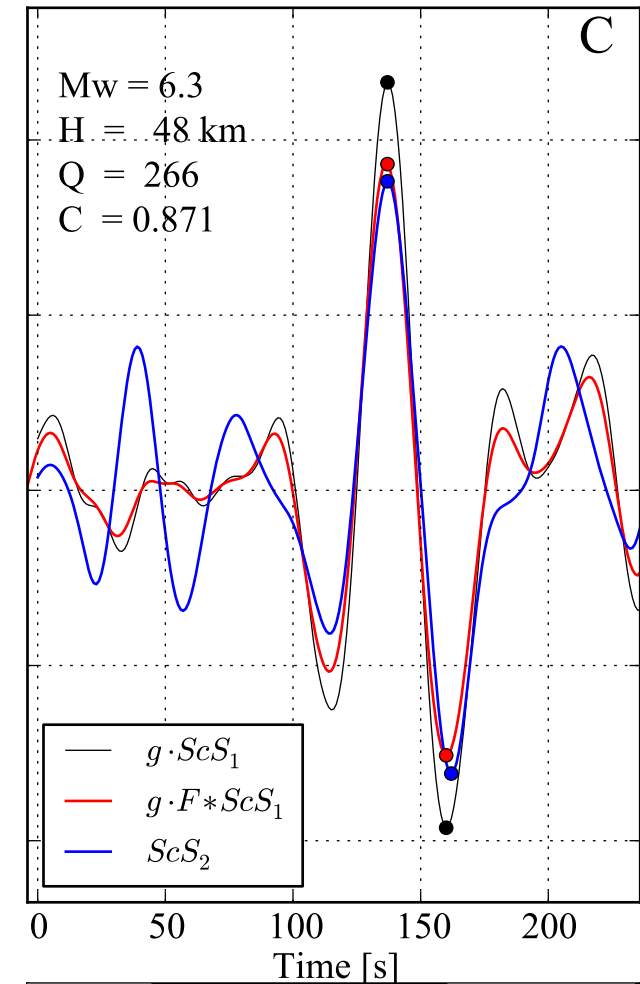
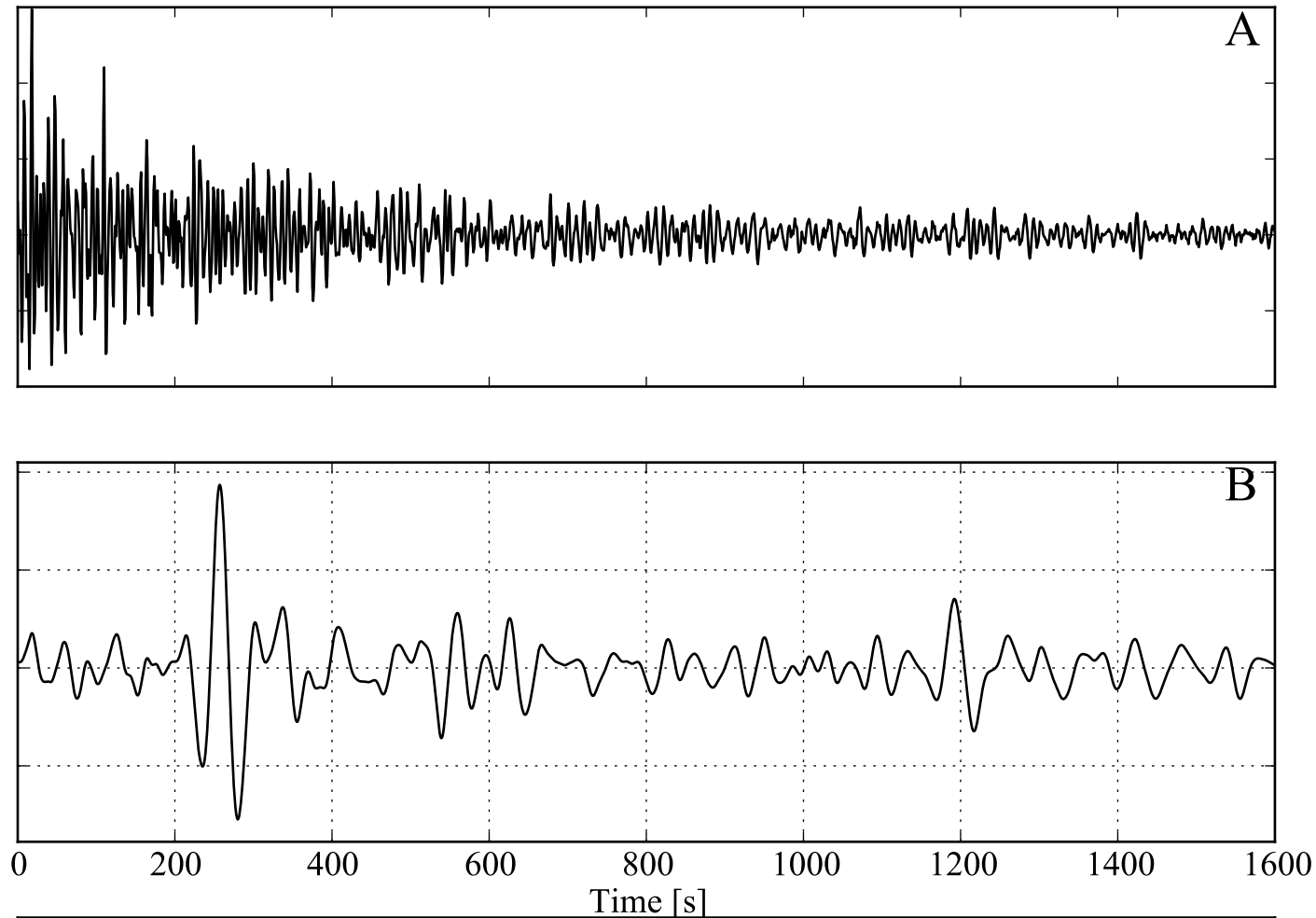


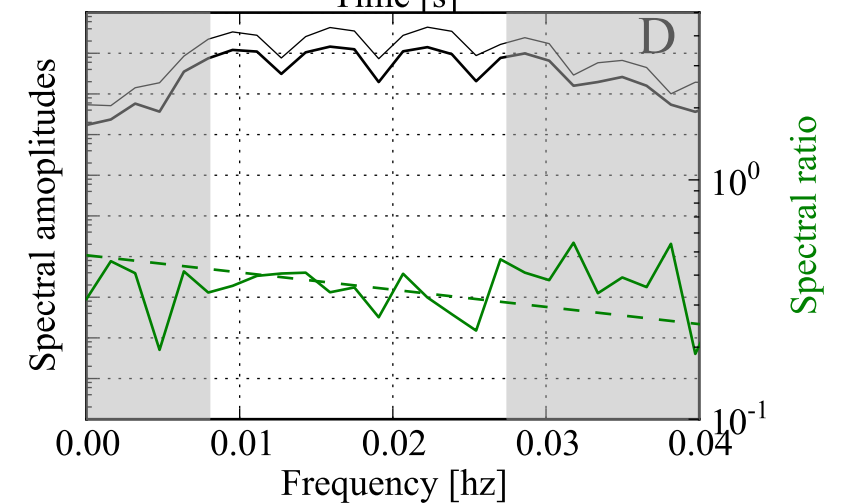
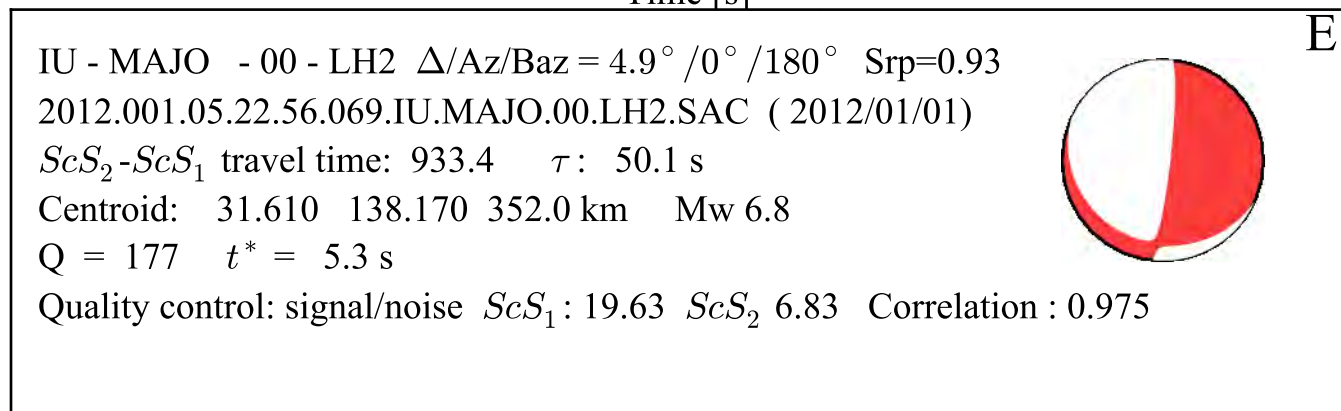
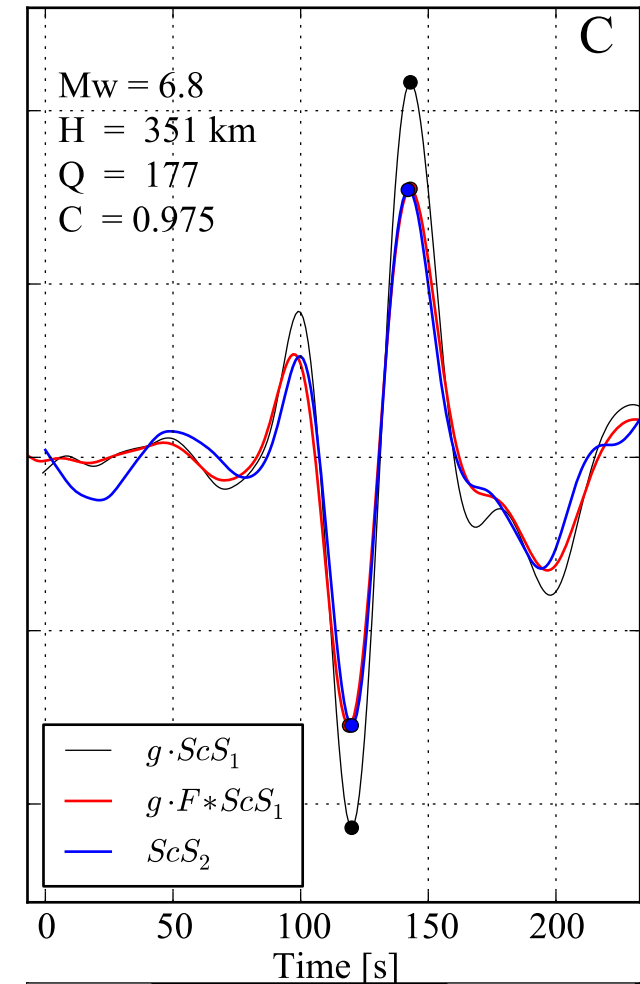
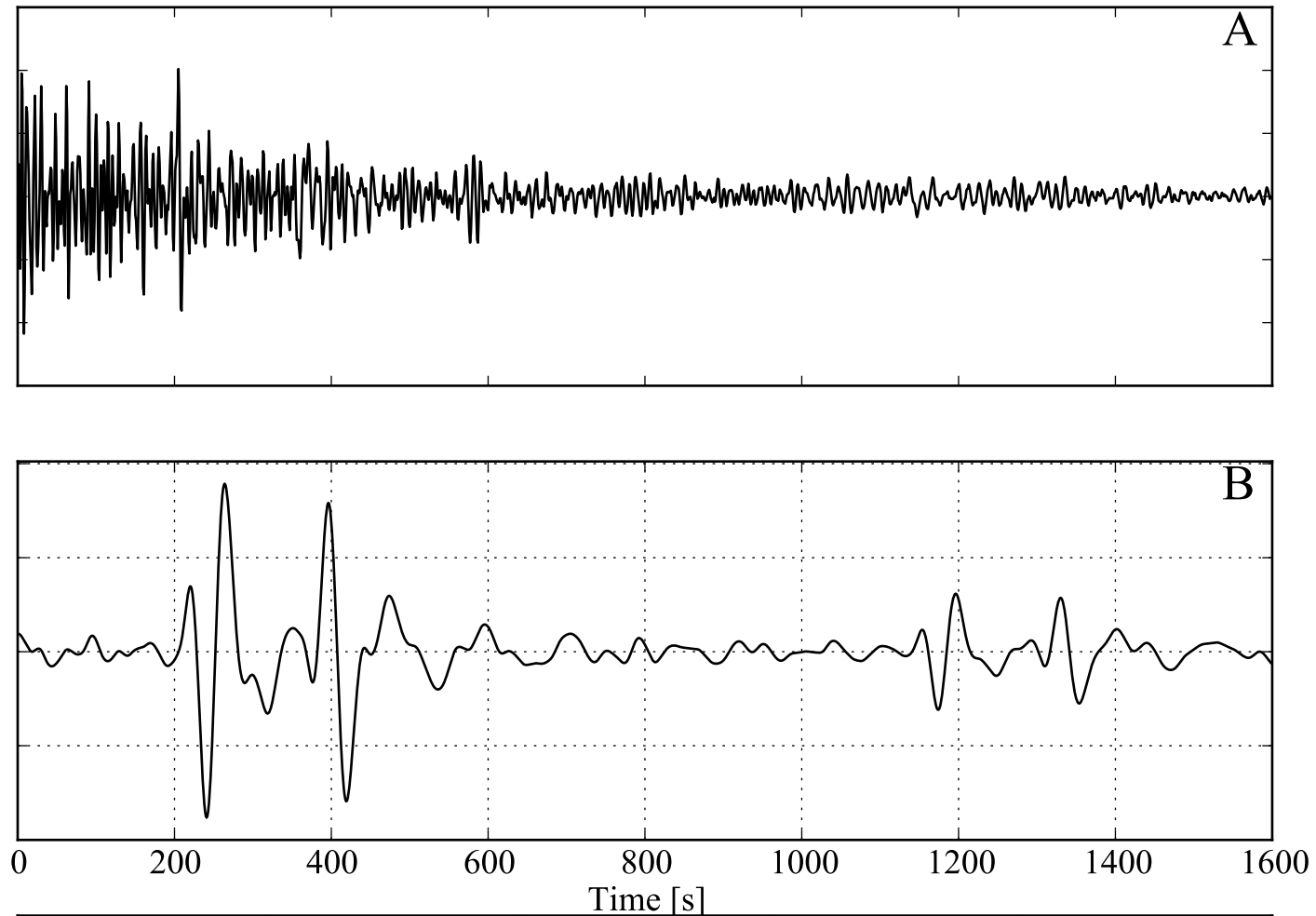


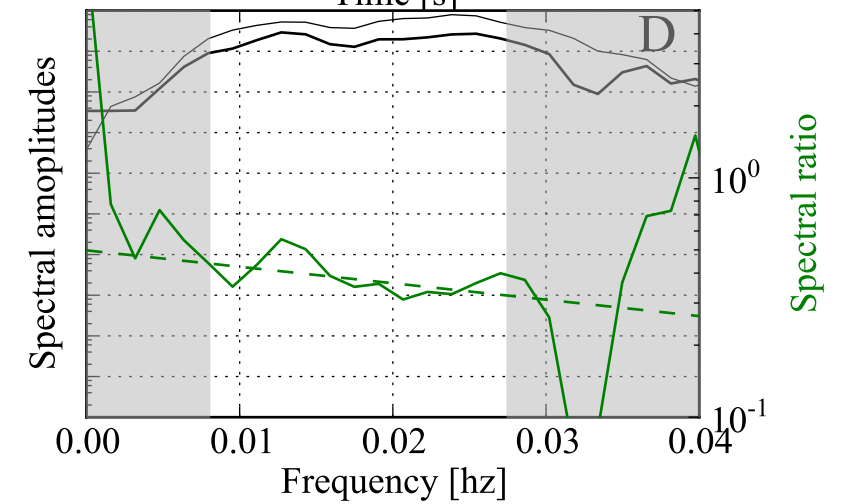
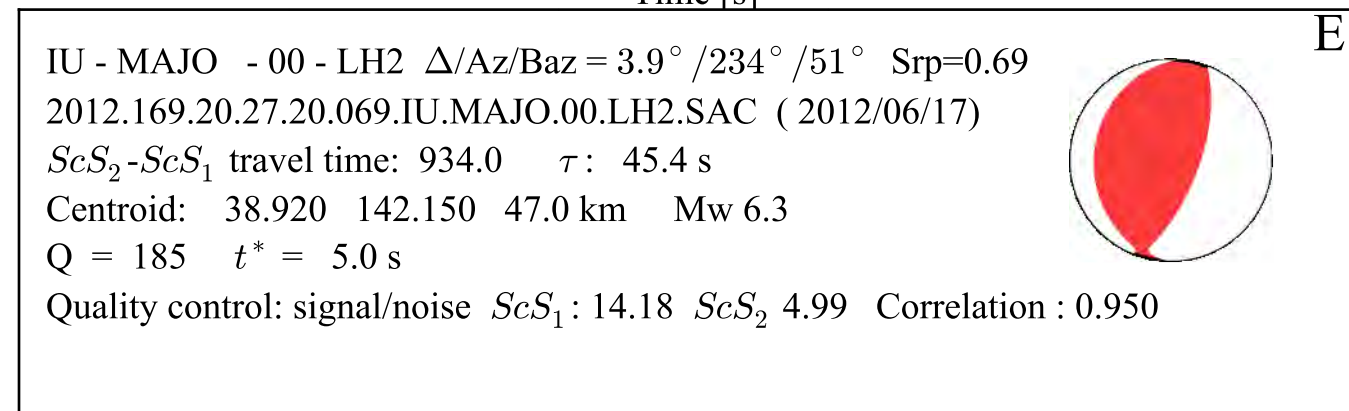
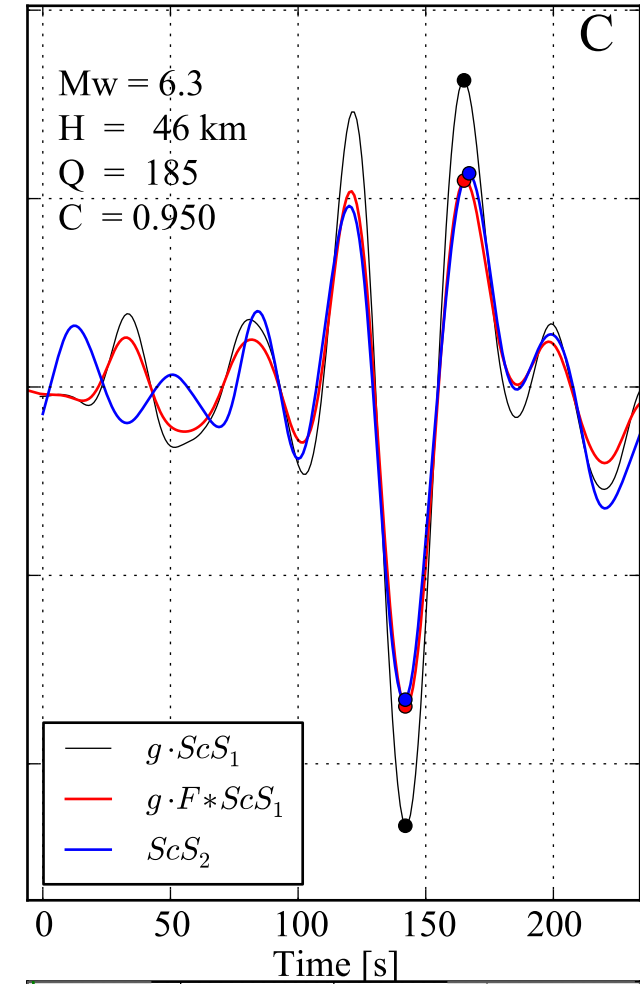
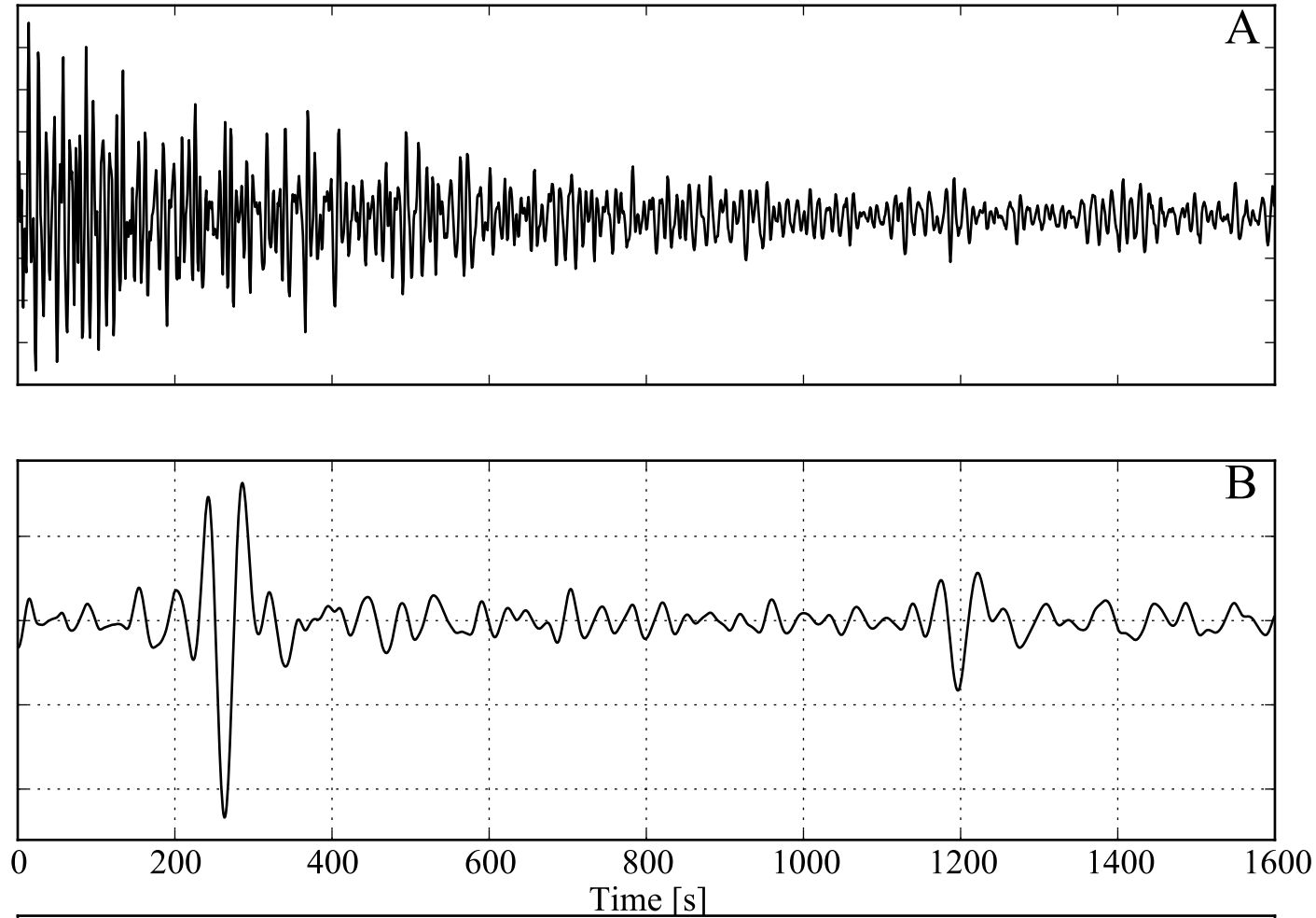


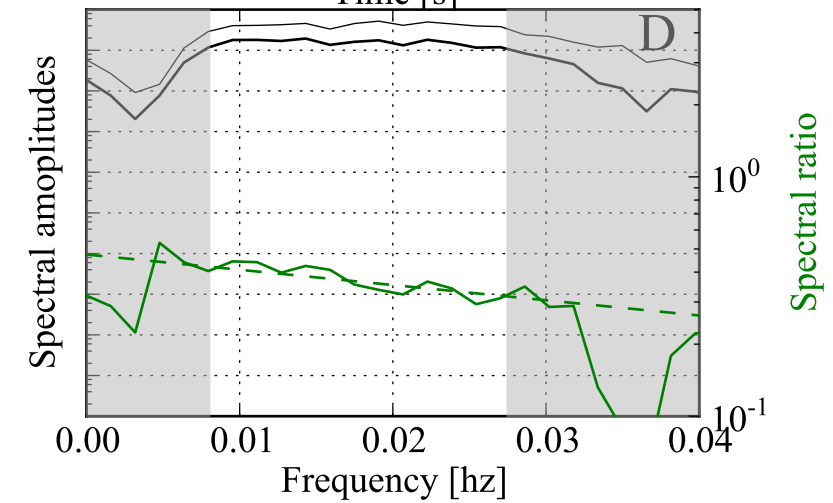
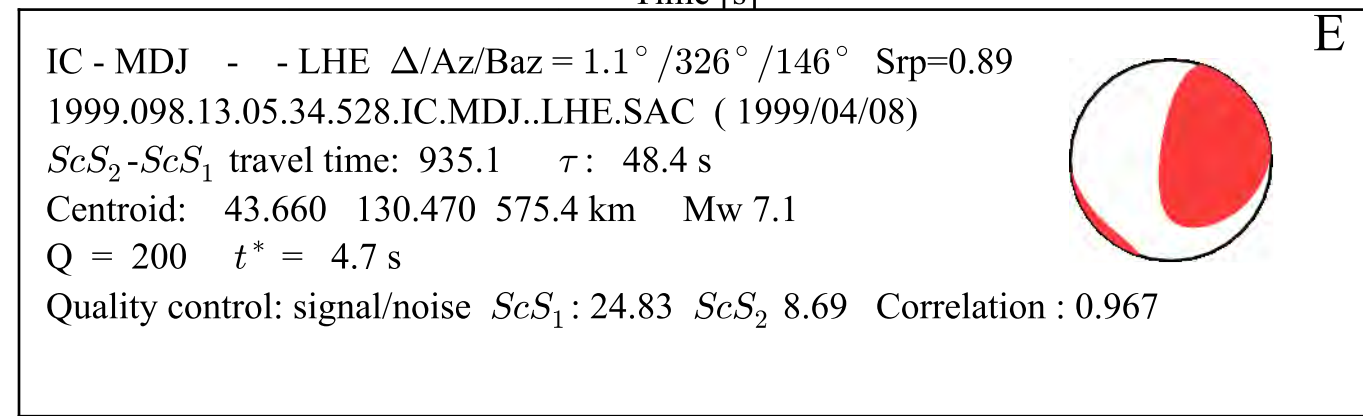
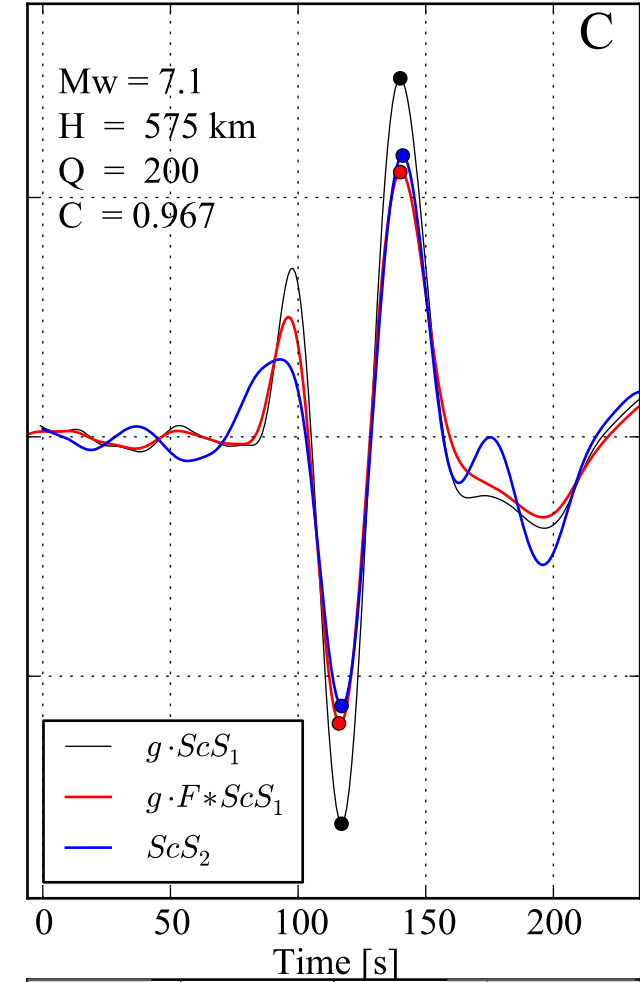
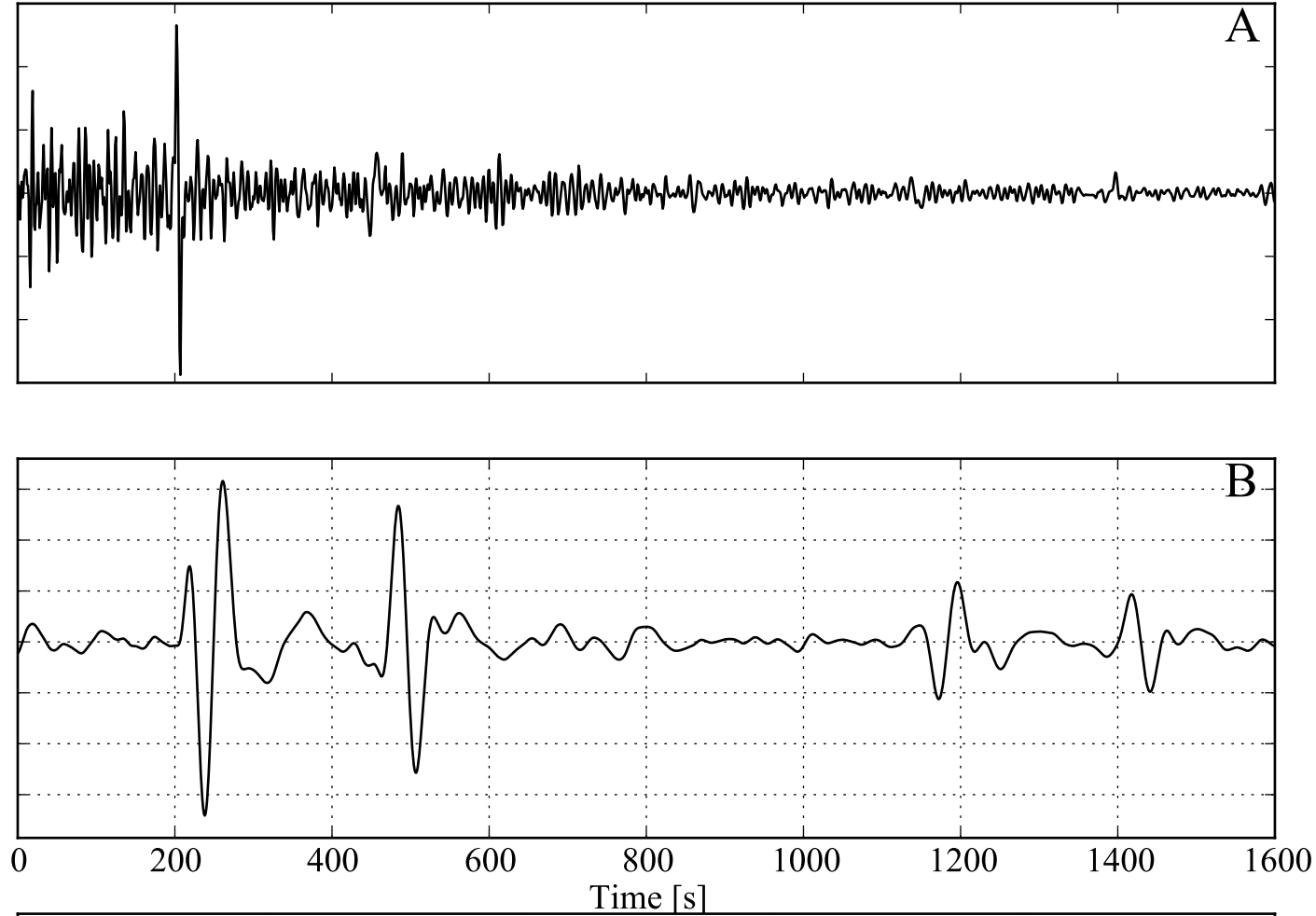


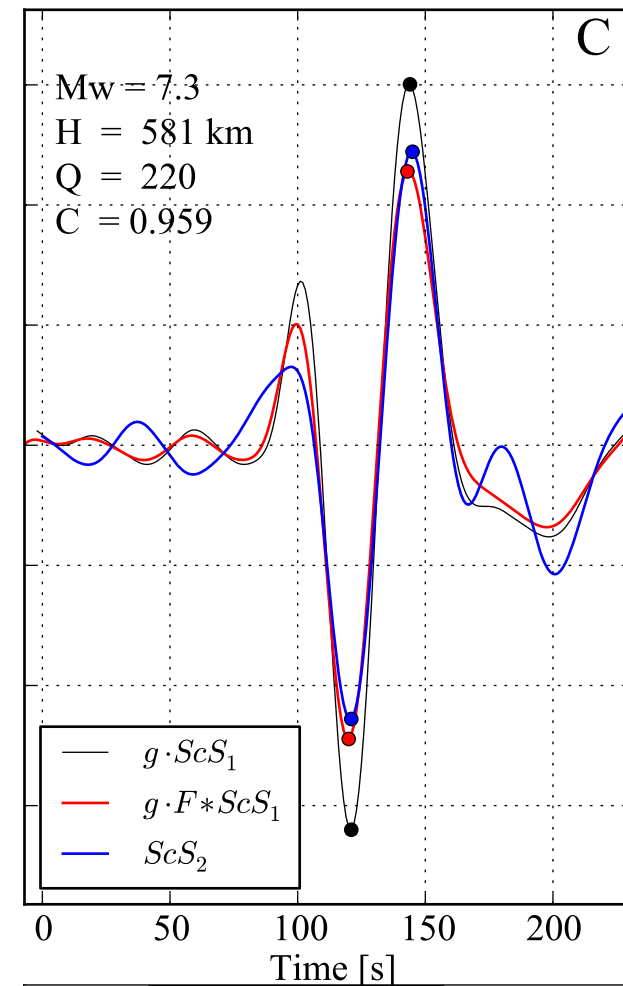
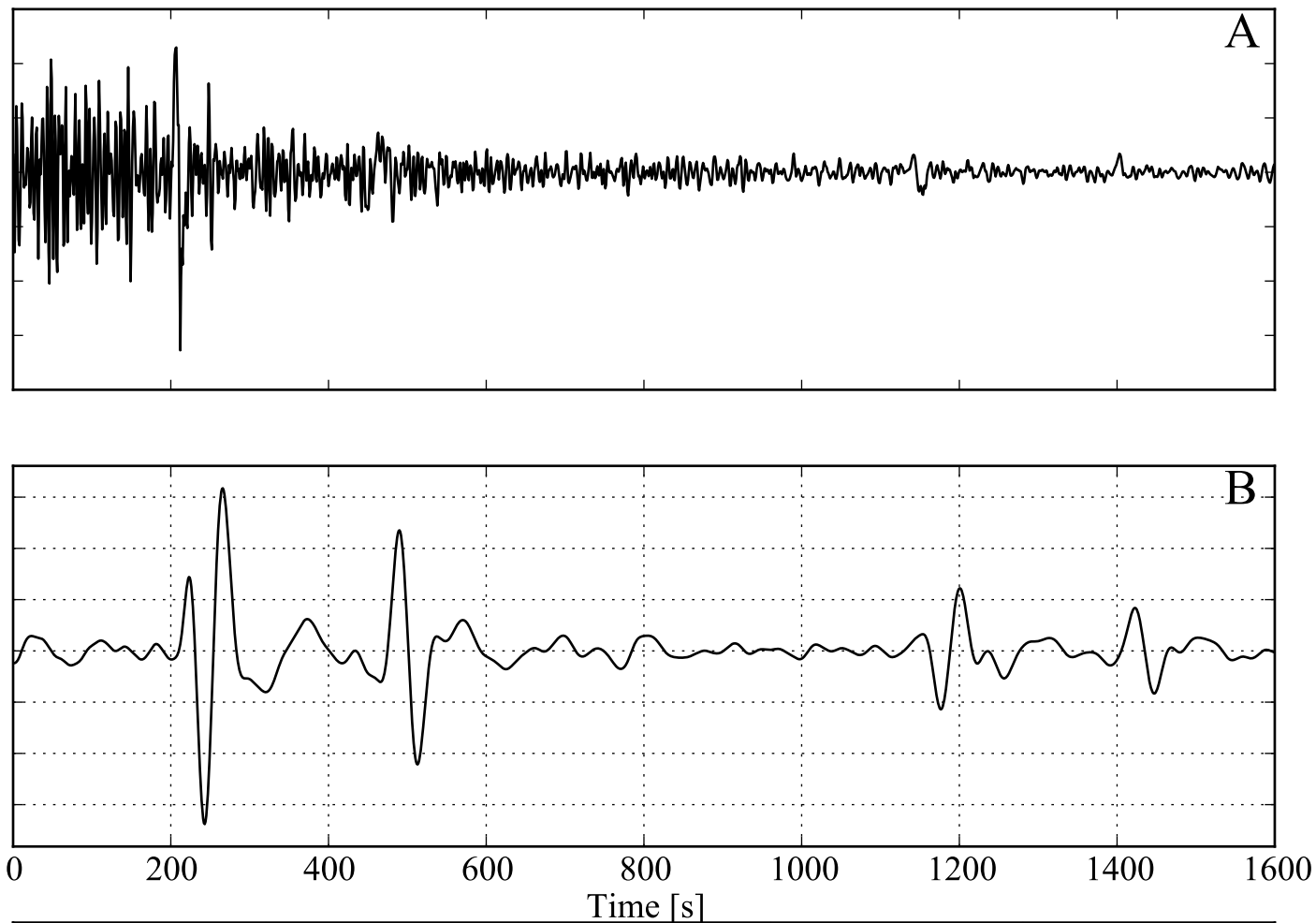




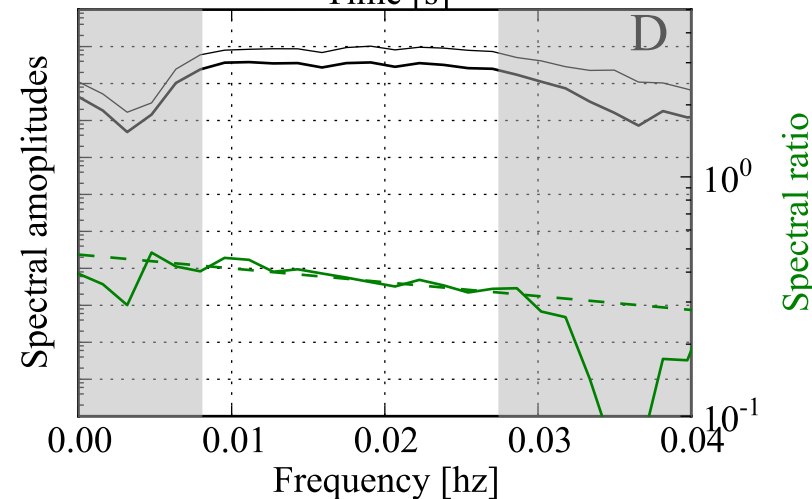


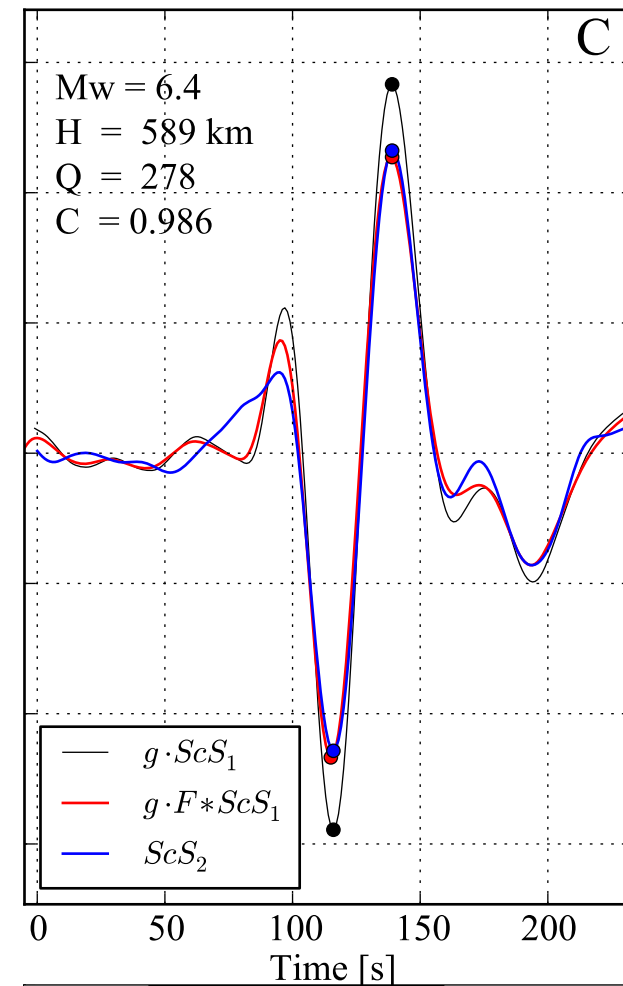
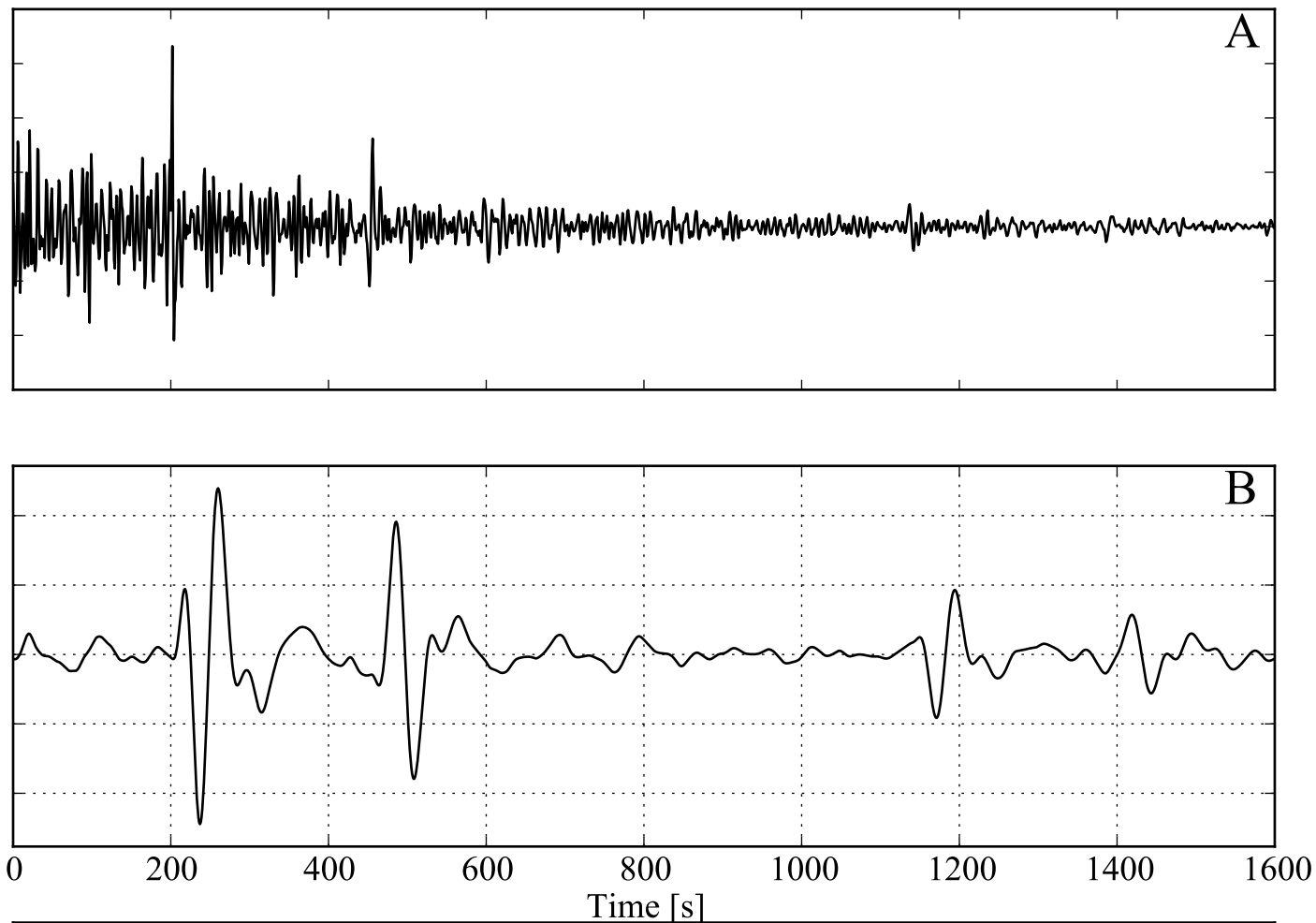







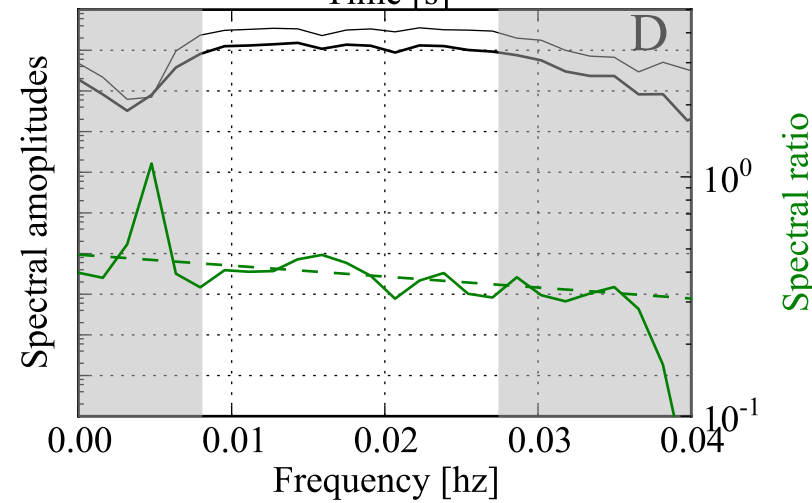
E
 IC - MDJ - 00 - LHE $\Delta/Az/Baz = 1.1^\circ / 325^\circ / 144^\circ$ $Srp=0.89$
 2002.179.17.14.30.098.IC.MDJ.00.LHE.SAC (2002/06/28)
 $ScS_2 - ScS_1$ travel time: 934.1 τ : 48.7 s
 Centroid: 43.740 130.450 581.5 km M_w 7.3
 $Q = 220$ $t^* = 4.2$ s
 Quality control: signal/noise ScS_1 : 23.25 ScS_2 8.38 Correlation : 0.959

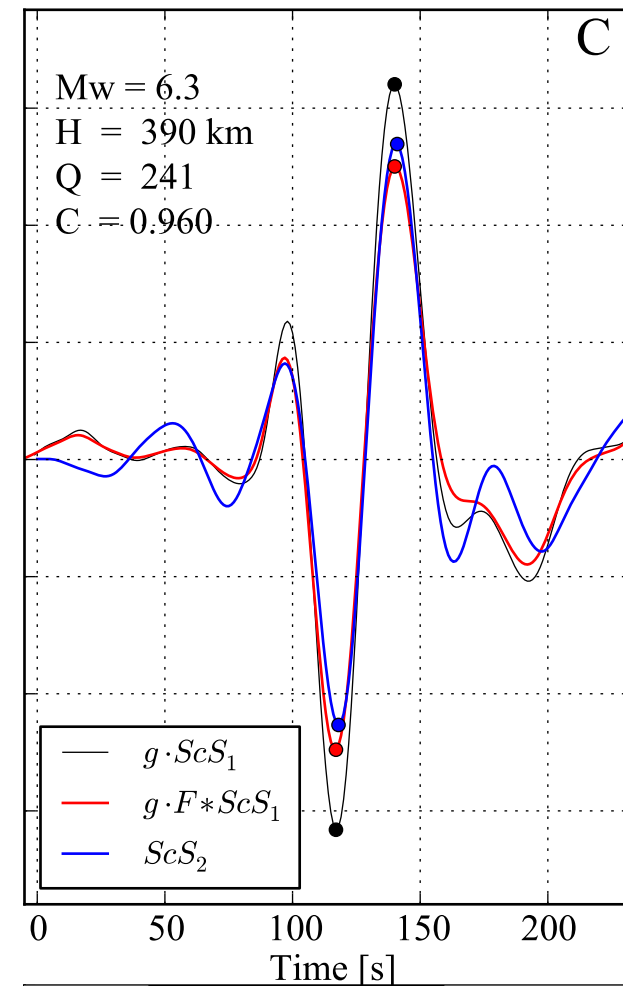
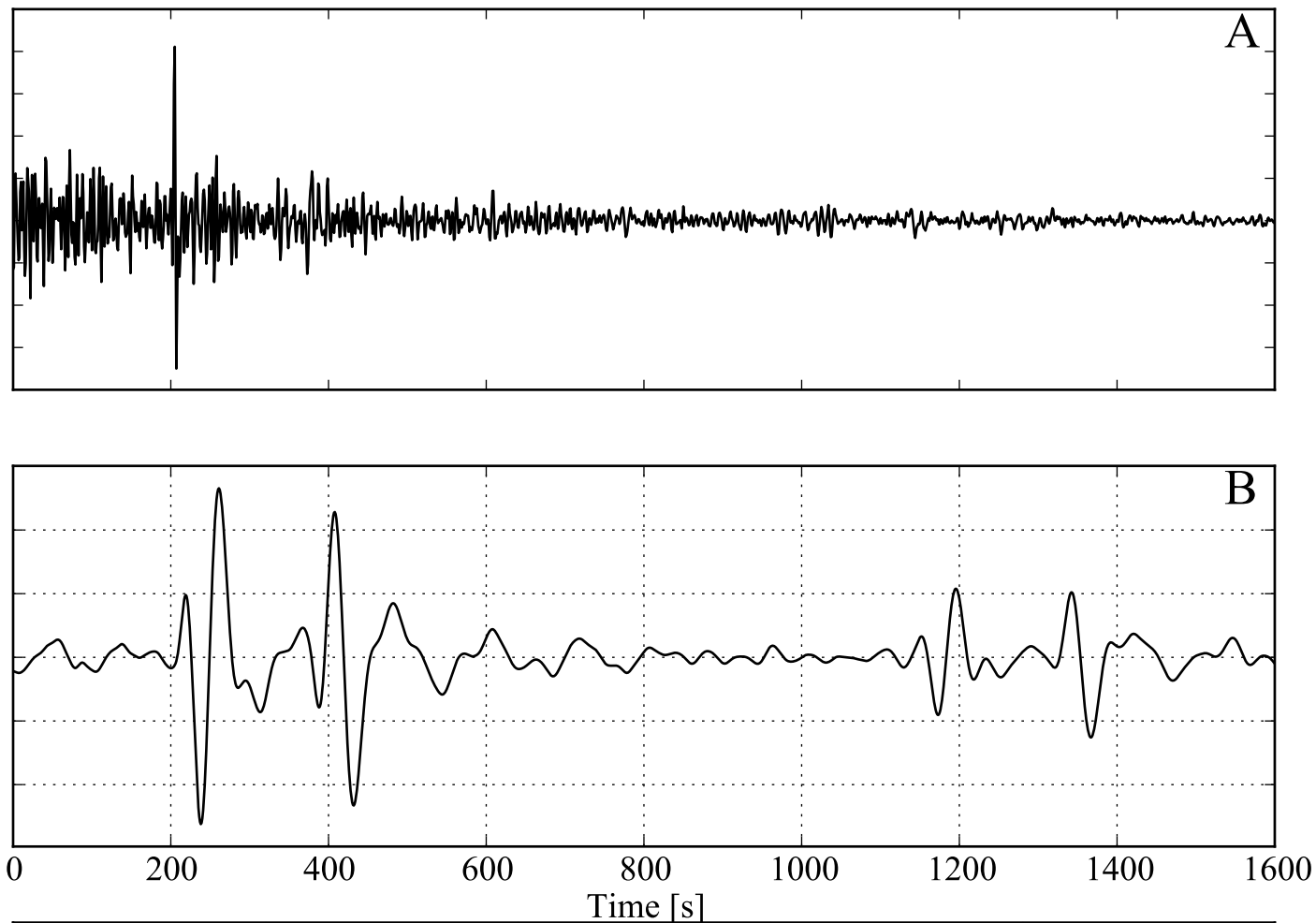




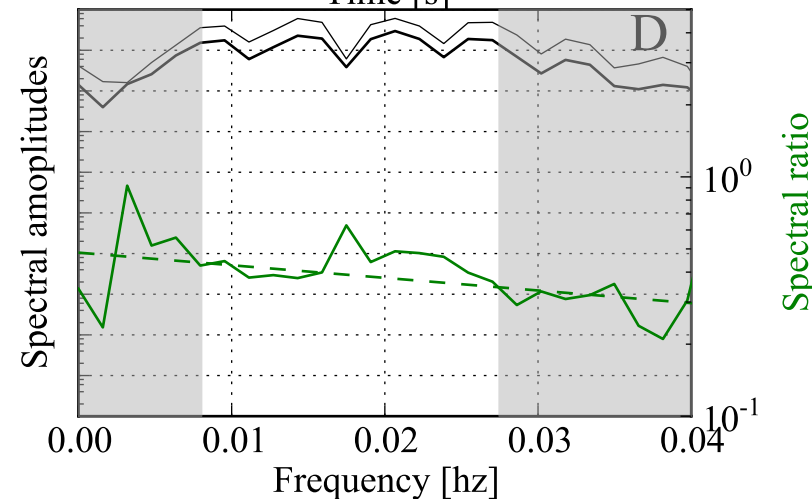
E

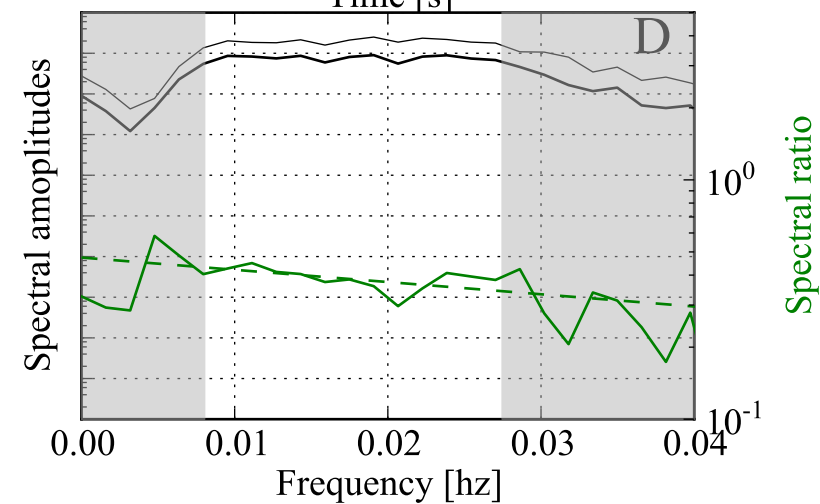
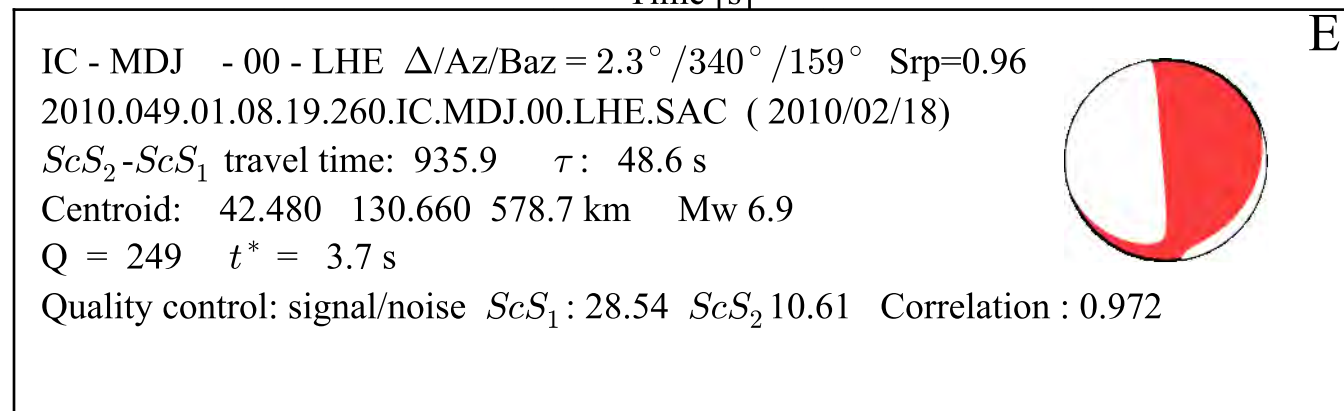
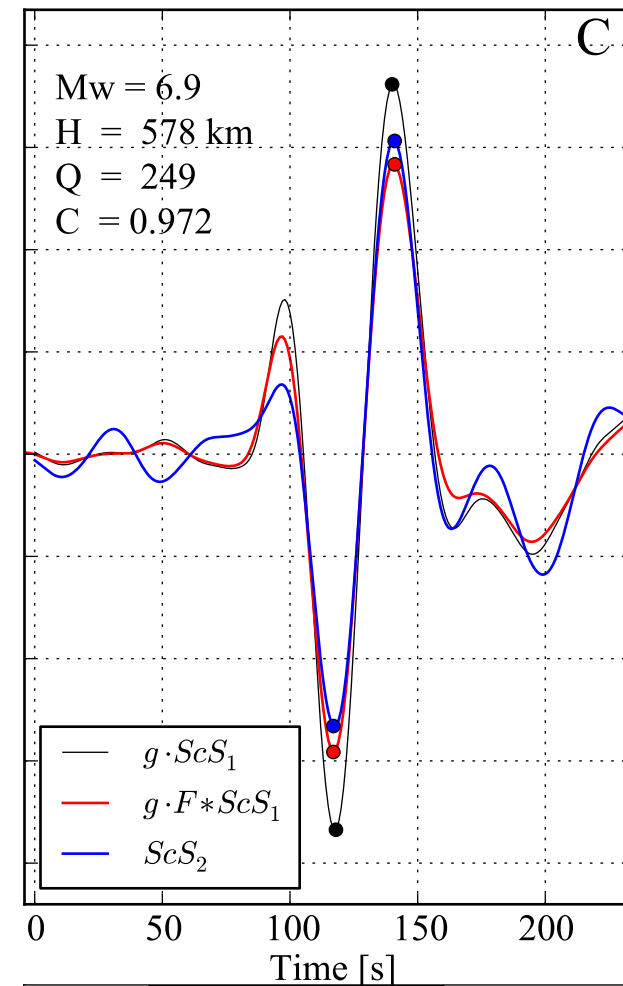
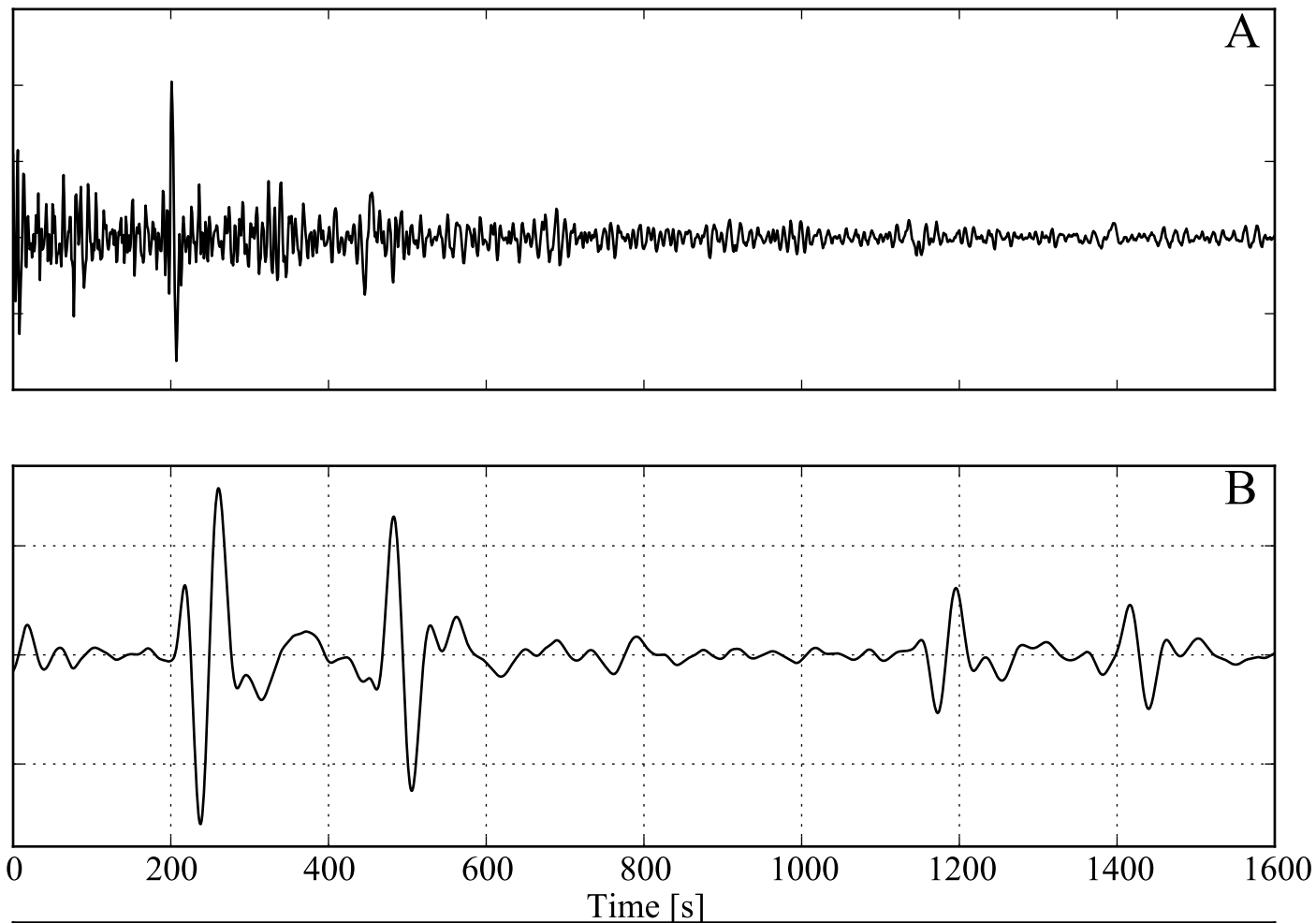
IC - MDJ - 00 - LHE $\Delta/Az/Baz = 0.4^\circ / 244^\circ / 64^\circ$ $Srp=0.93$
 2002.258.08.34.32.273.IC.MDJ.00.LHE.SAC (2002/09/15)
 ScS_2-ScS_1 travel time: 935.2 τ : 48.7 s
 Centroid: 44.770 130.040 589.4 km Mw 6.4
 $Q = 278$ $t^* = 3.4$ s
 Quality control: signal/noise ScS_1 : 25.97 ScS_2 9.89 Correlation : 0.986

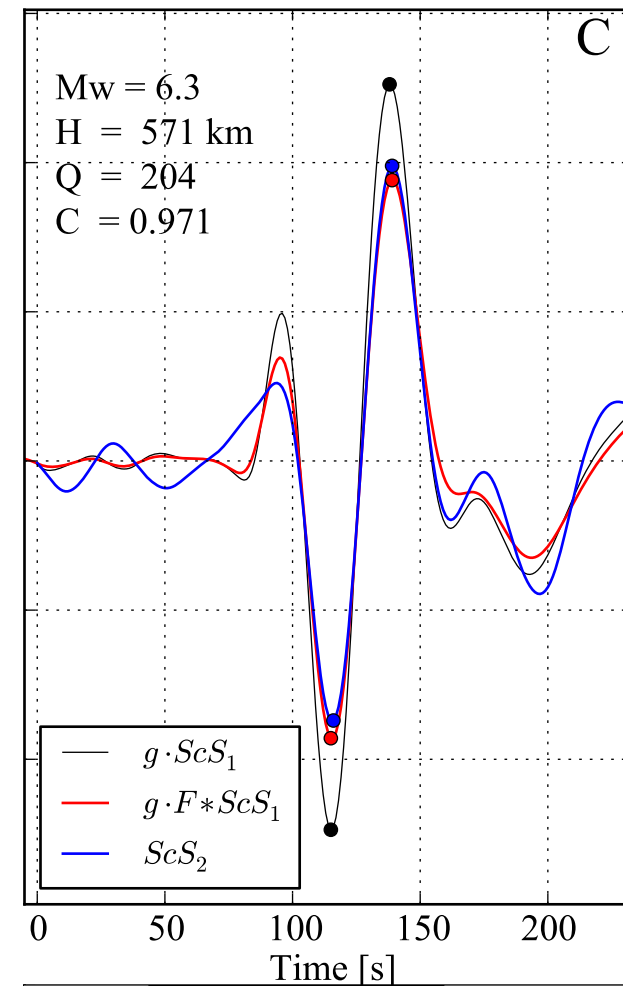
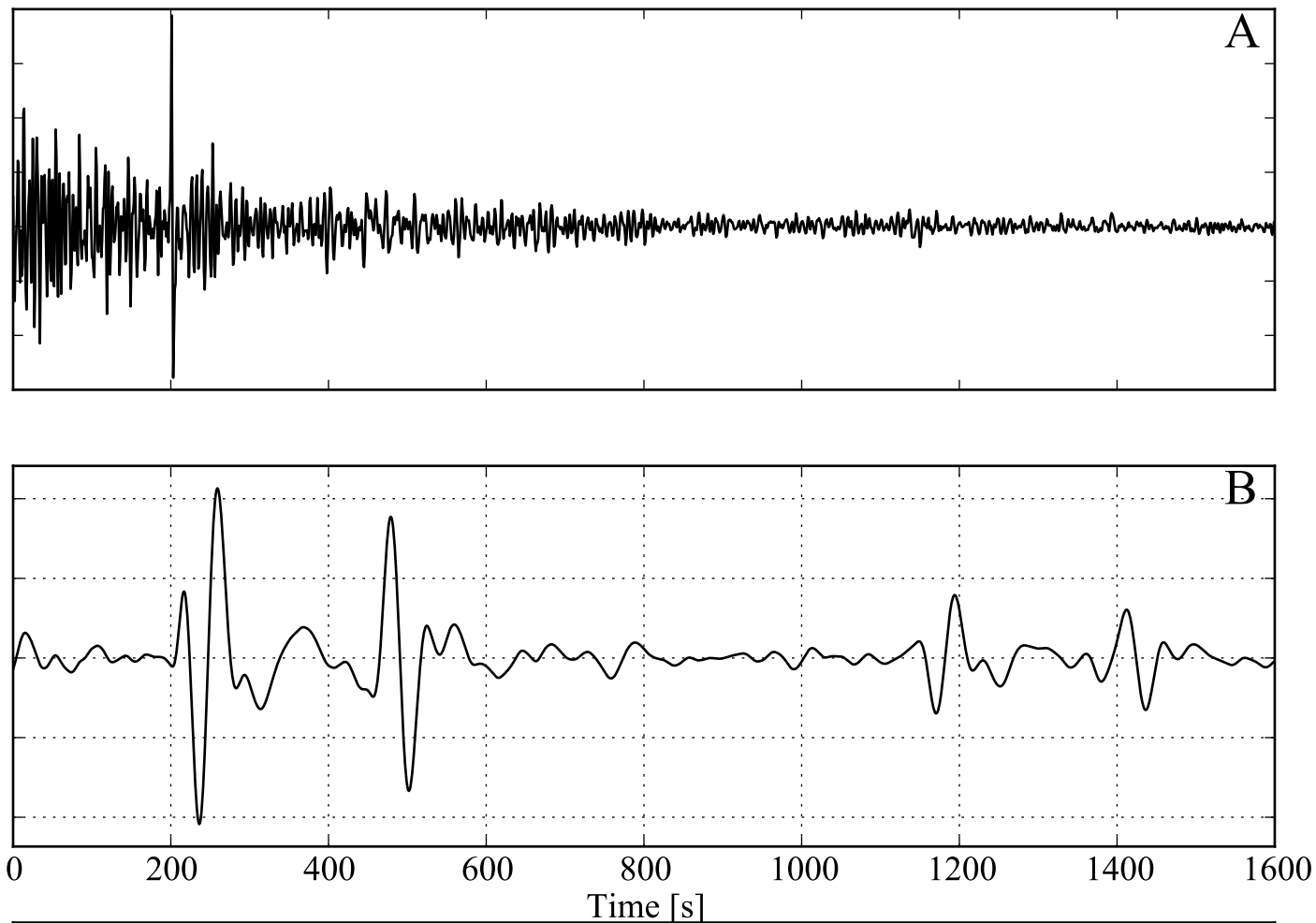





IC - MDJ - 00 - LHE $\Delta/Az/Baz = 4.6^\circ / 304^\circ / 120^\circ$ $Srp=0.90$
 2009.358.00.18.33.823.IC.MDJ.00.LHE.SAC (2009/12/24)
 $ScS_2 - ScS_1$ travel time: 934.1 τ : 48.7 s
 Centroid: 42.120 134.930 390.4 km M_w 6.3
 $Q = 241$ $t^* = 3.9$ s
 Quality control: signal/noise ScS_1 : 27.36 ScS_2 10.29 Correlation : 0.960

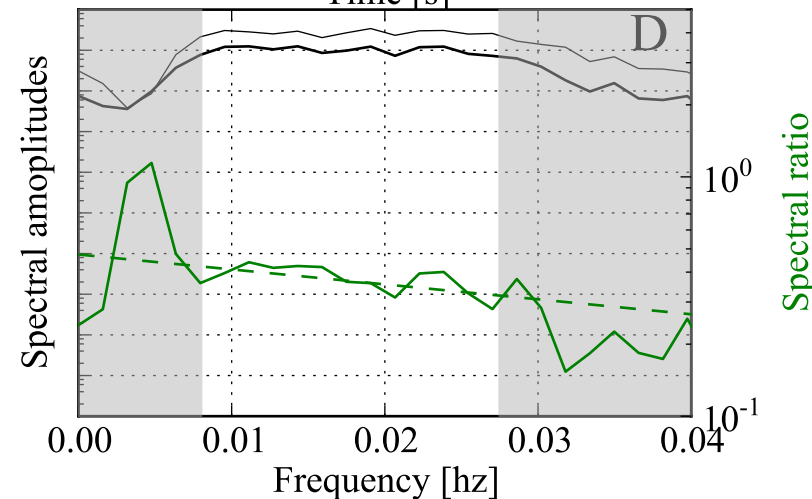


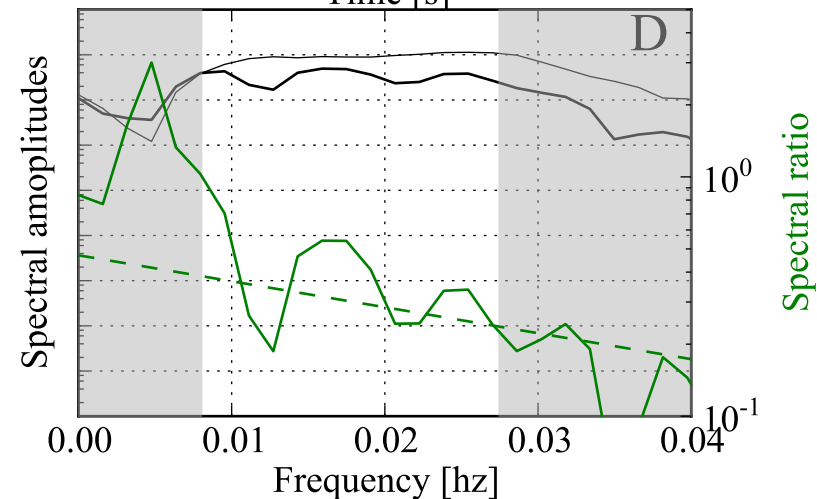
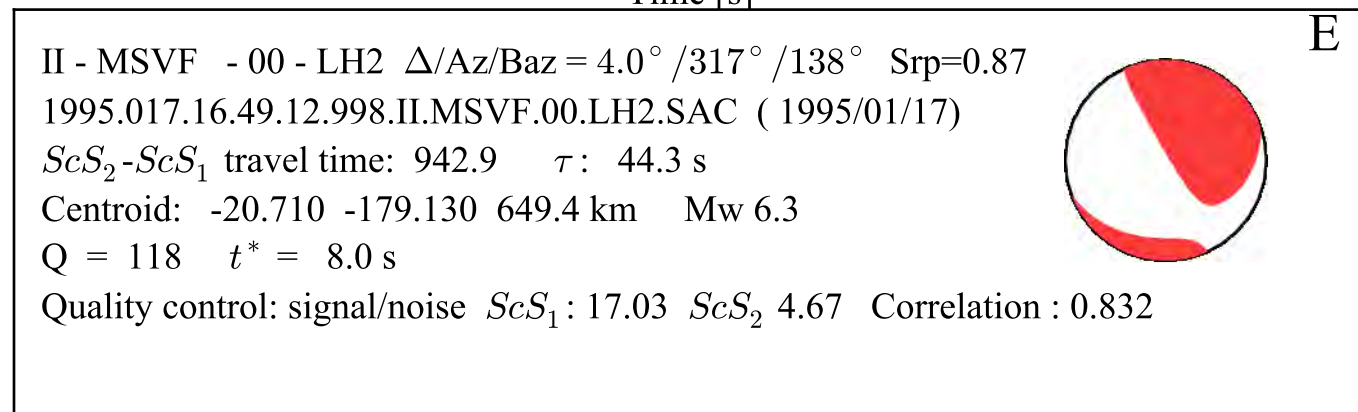
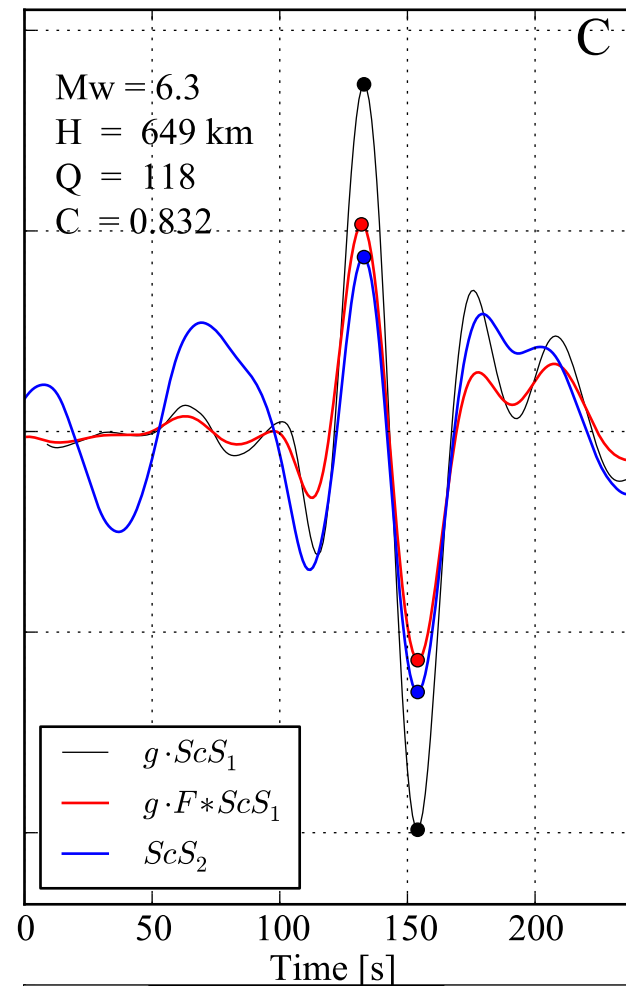
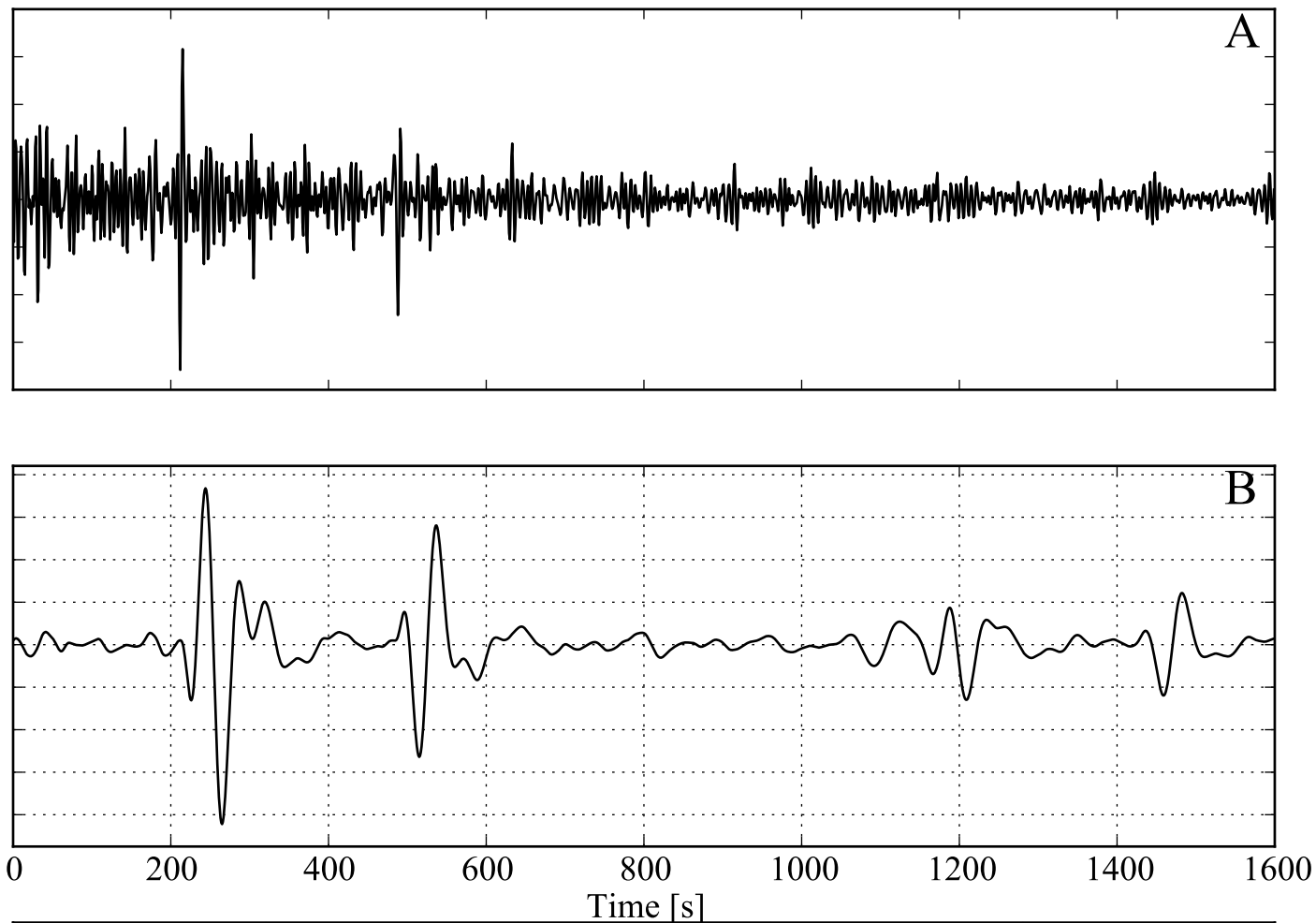


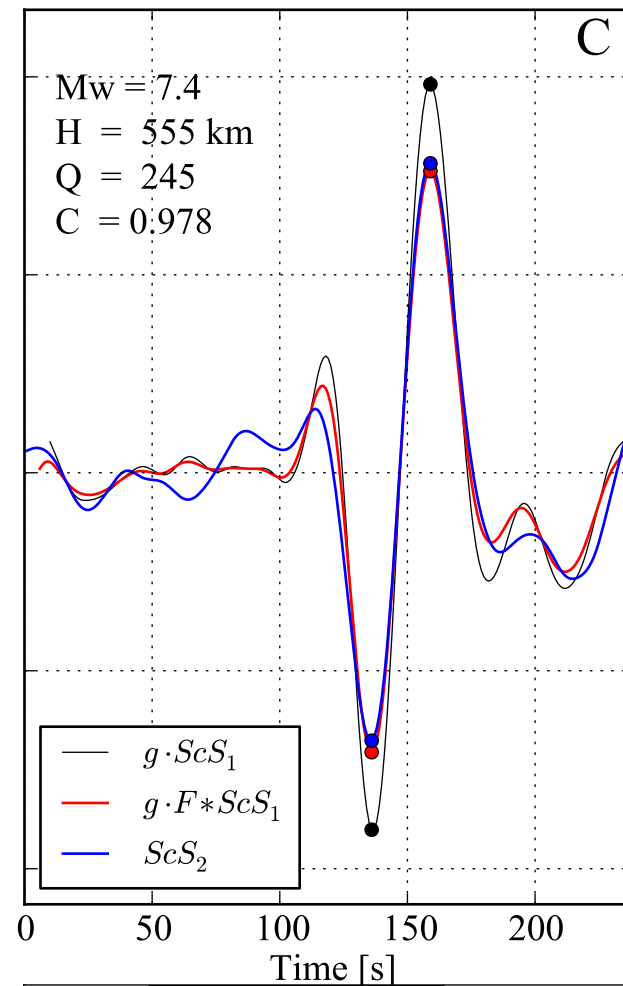
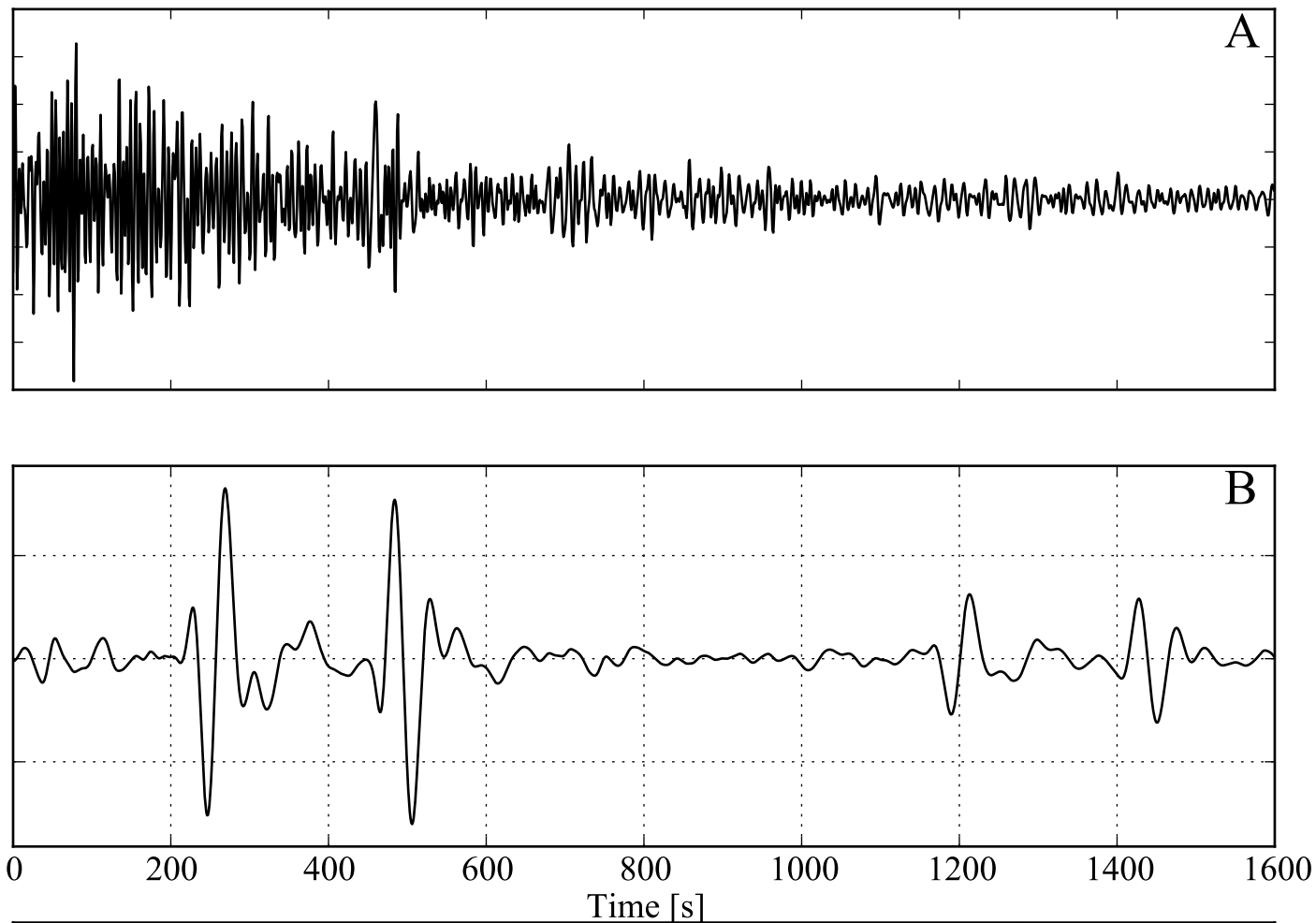


E

IC - MDJ - 00 - LHE $\Delta/Az/Baz = 2.1^\circ / 331^\circ / 150^\circ$ $Srp=0.97$
 2013.095.12.55.02.322.IC.MDJ.00.LHE.SAC (2013/04/05)
 ScS_2-ScS_1 travel time: 934.9 τ : 48.7 s
 Centroid: 42.770 131.020 571.9 km M_w 6.3
 $Q = 204$ $t^* = 4.6$ s
 Quality control: signal/noise ScS_1 : 27.86 ScS_2 9.83 Correlation : 0.971

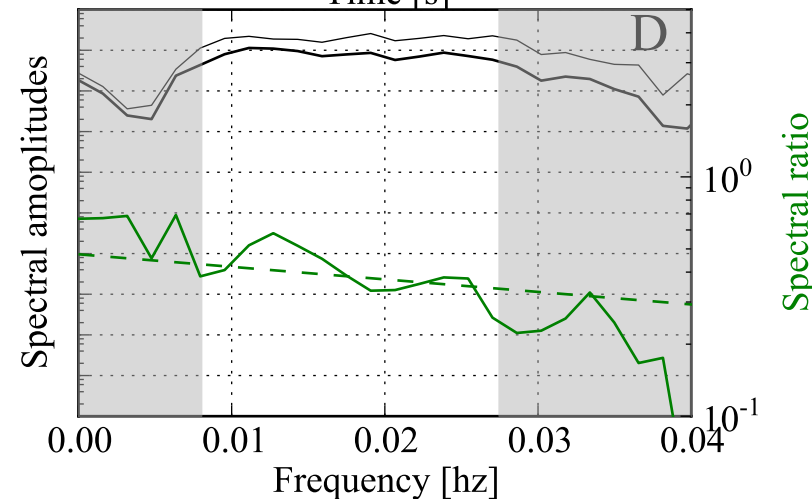


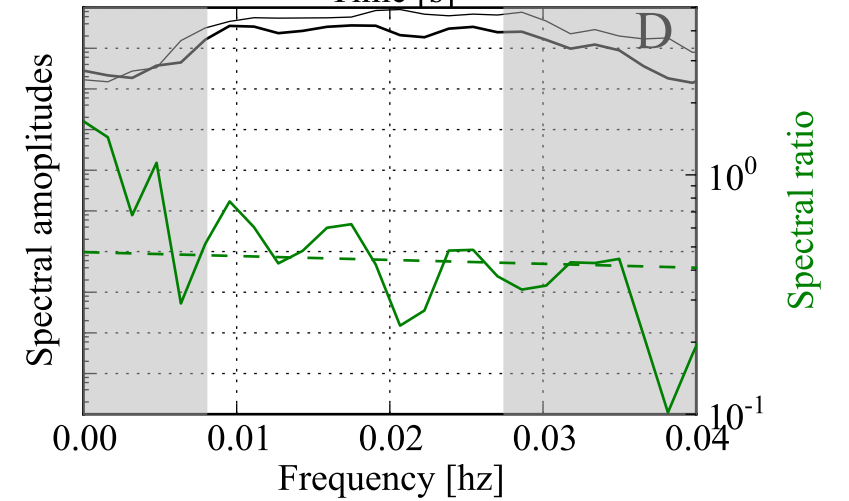
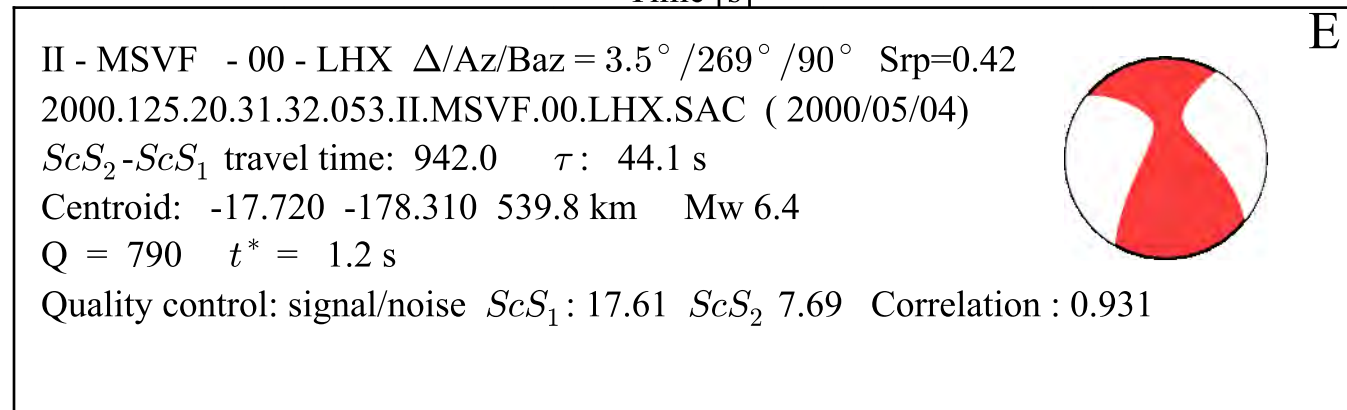
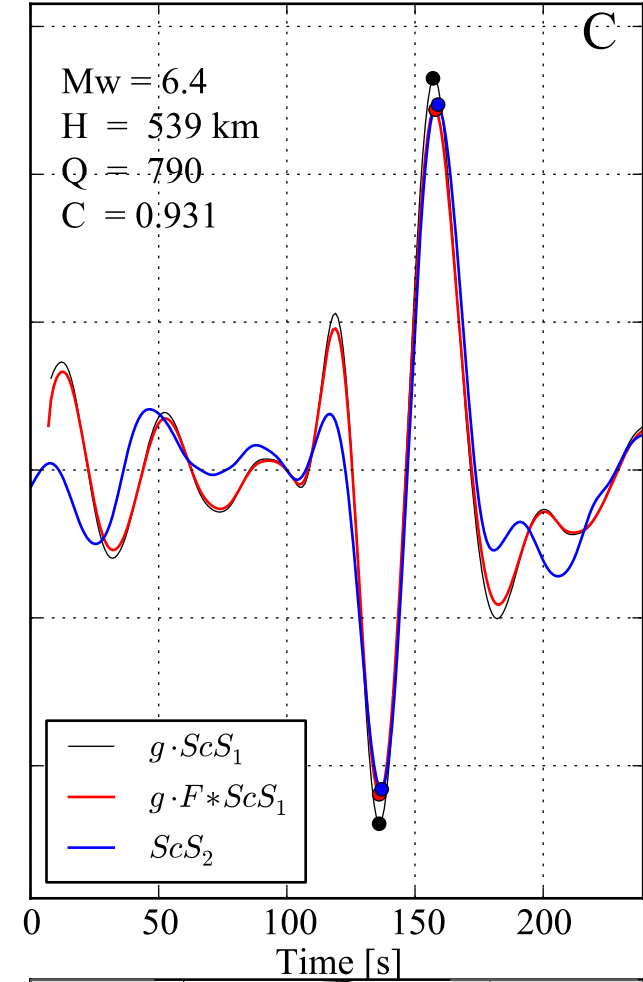
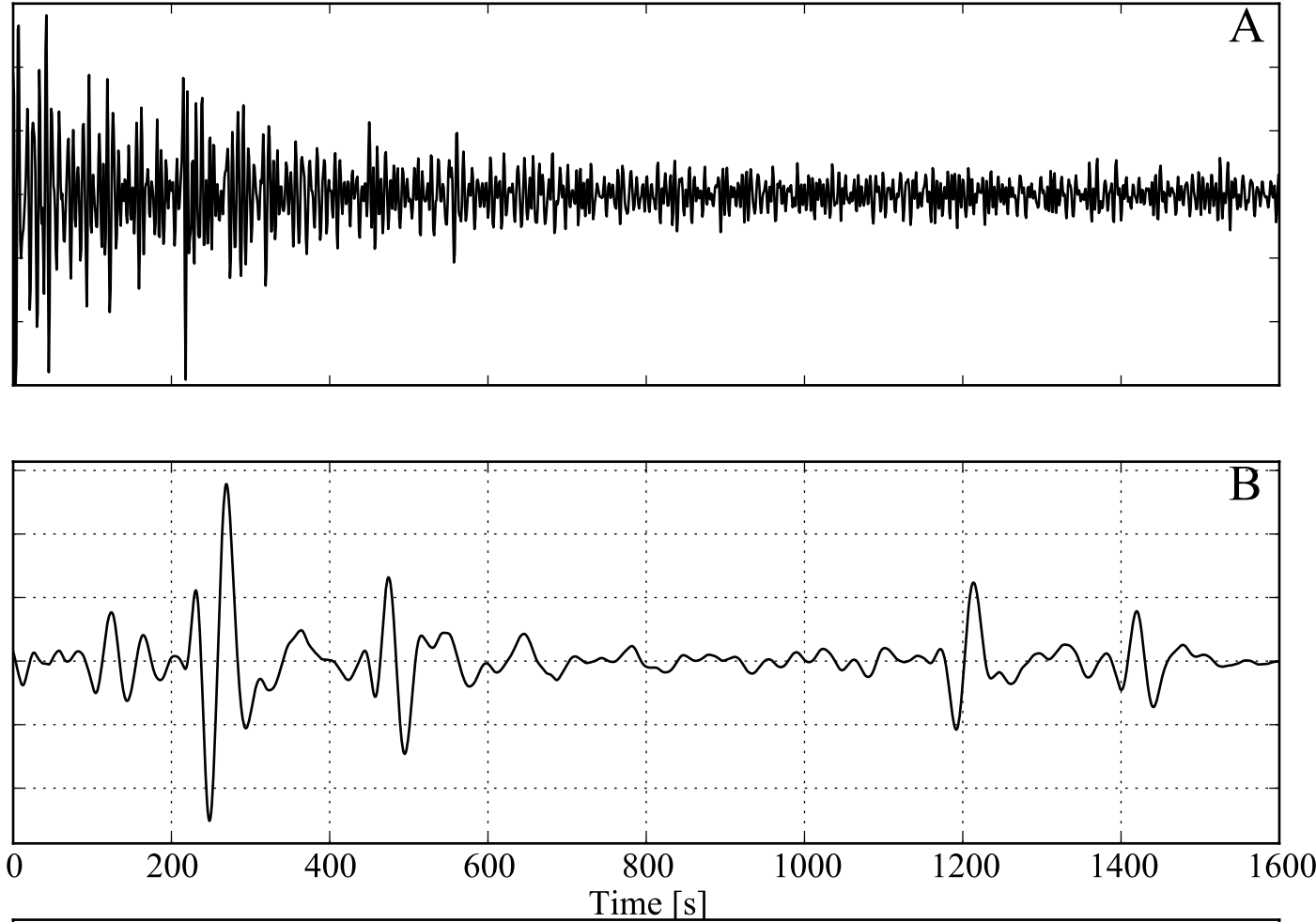


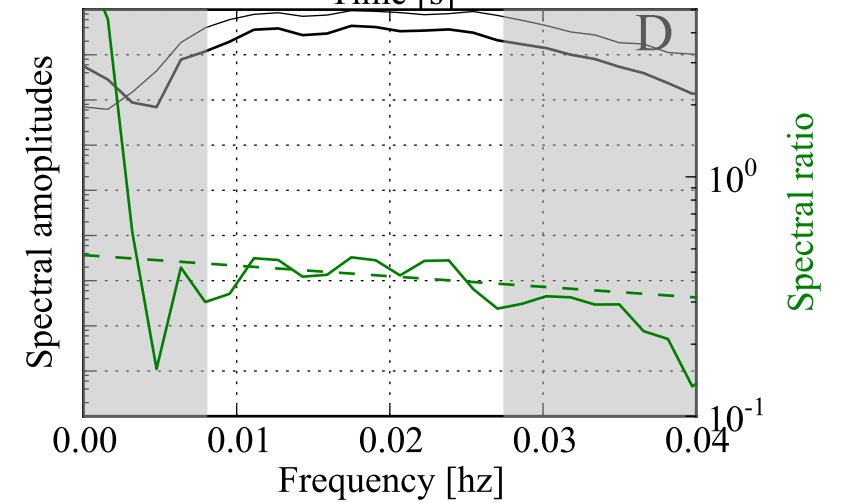
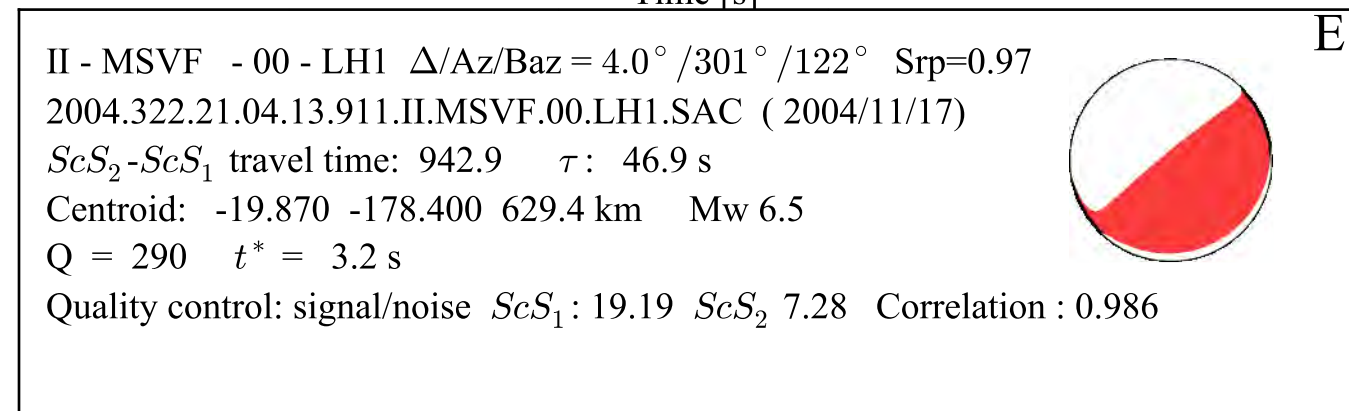
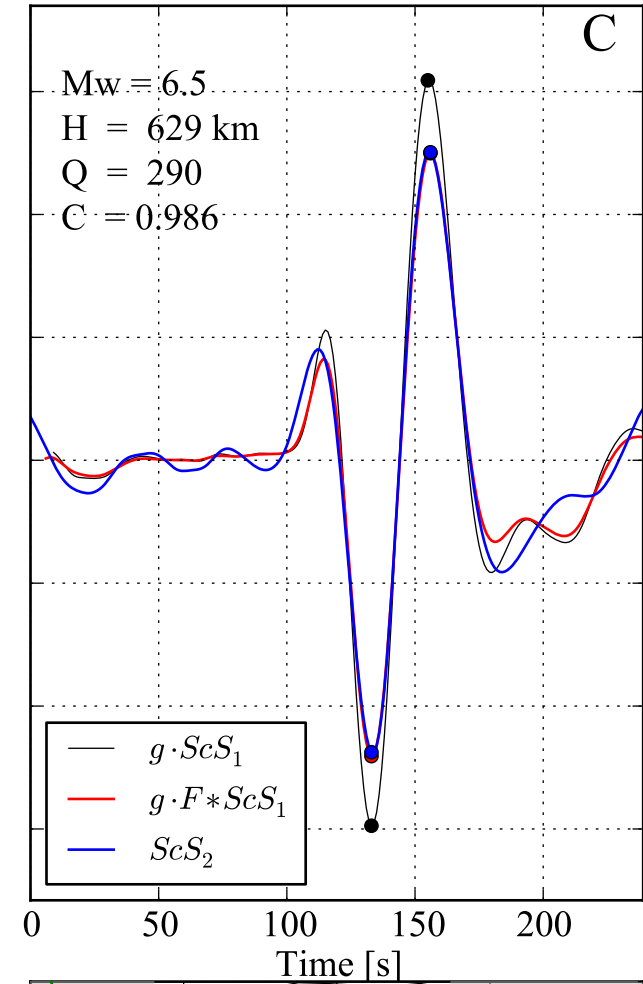
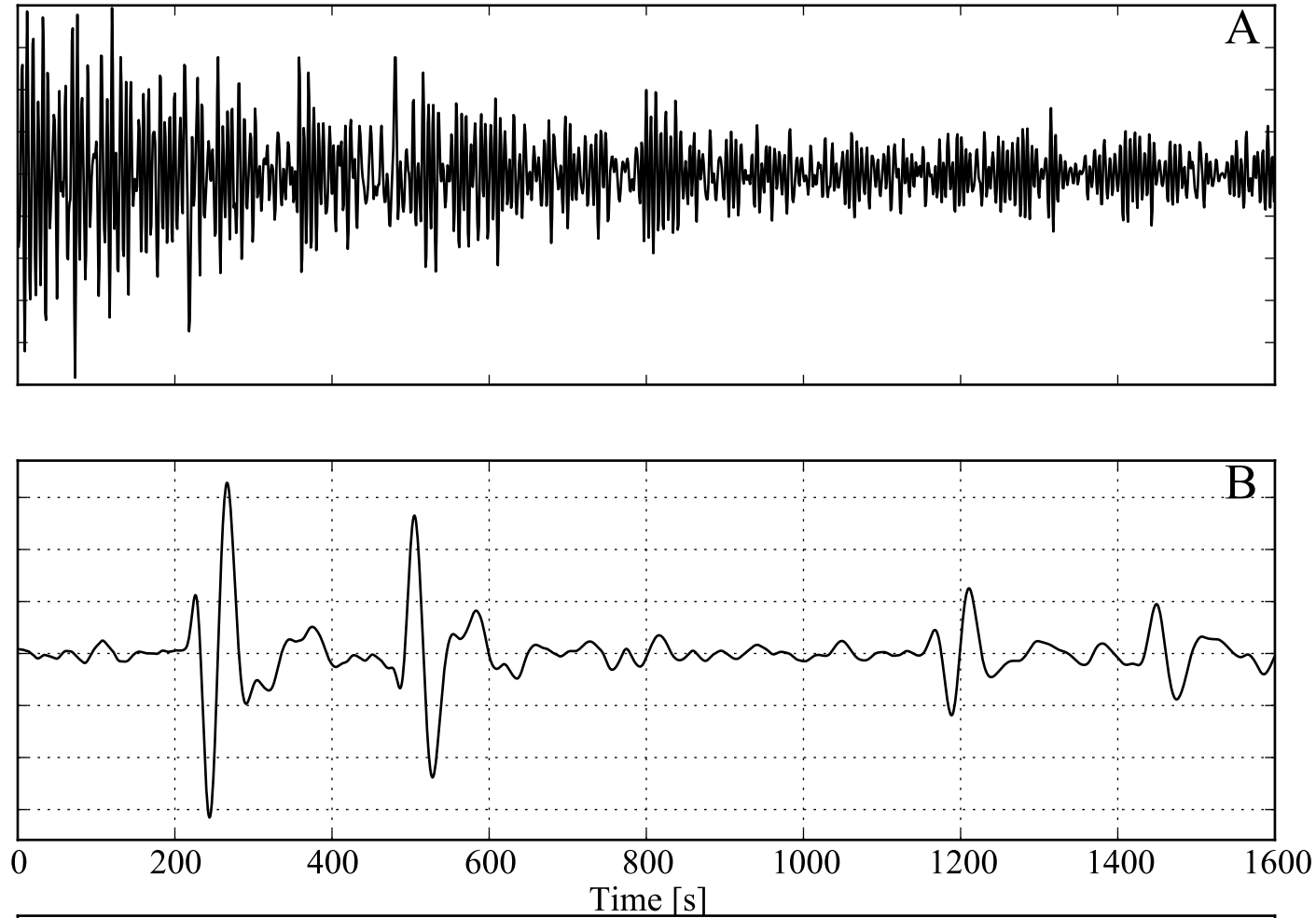


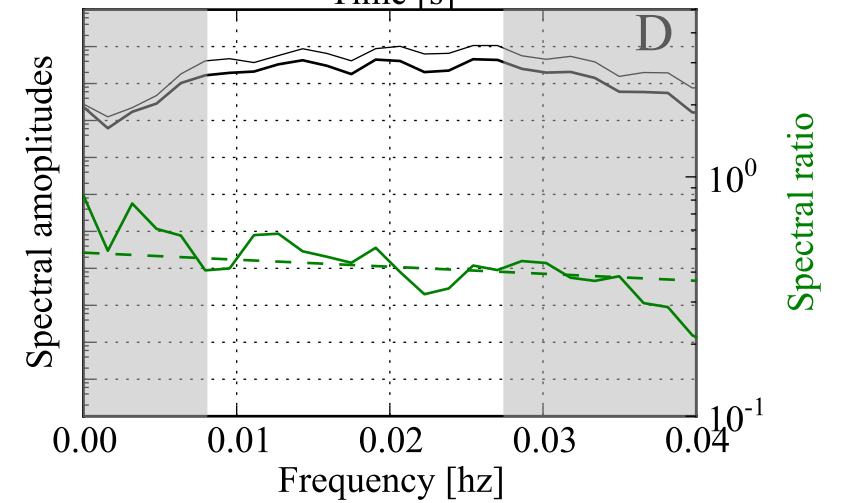
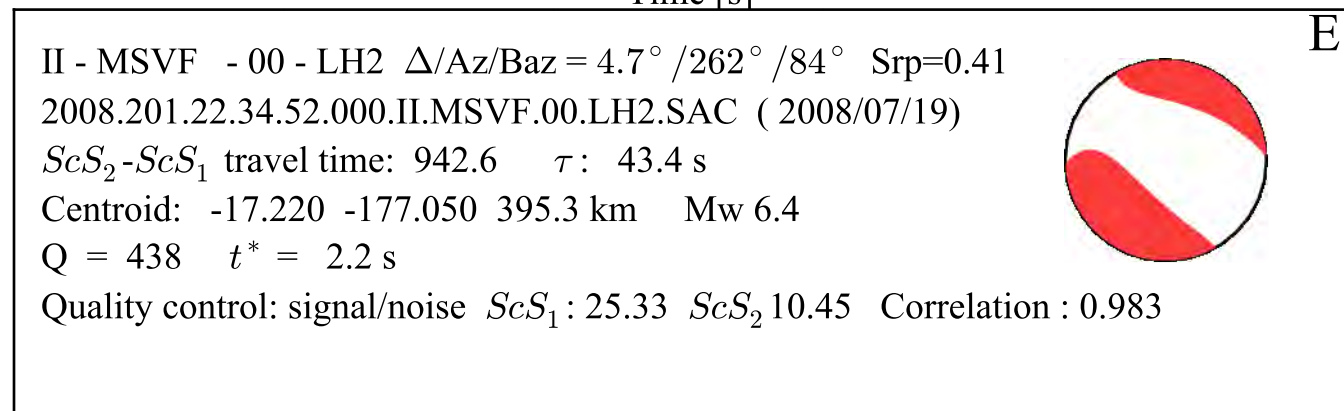
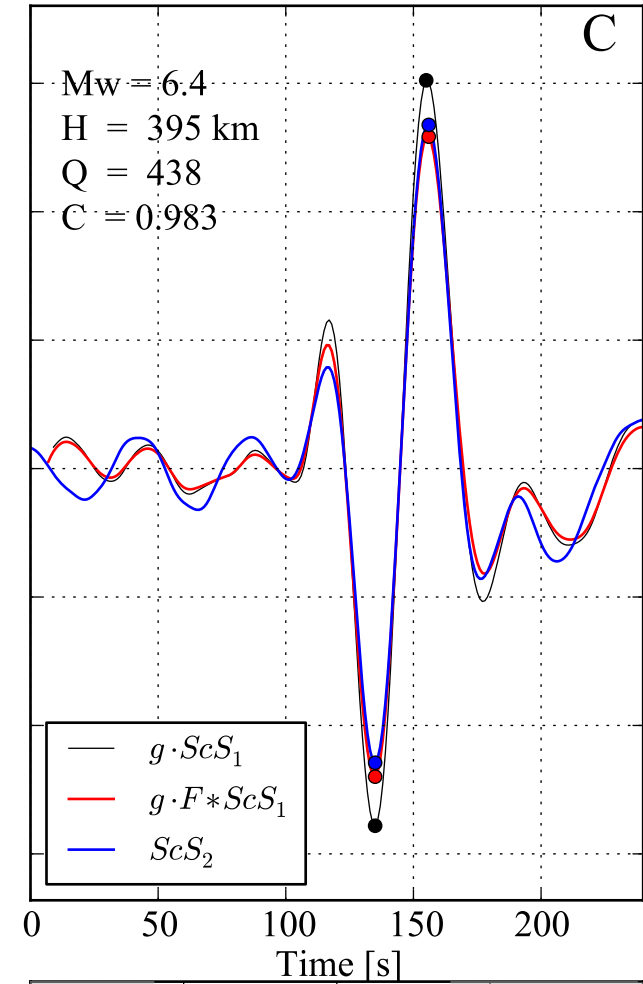
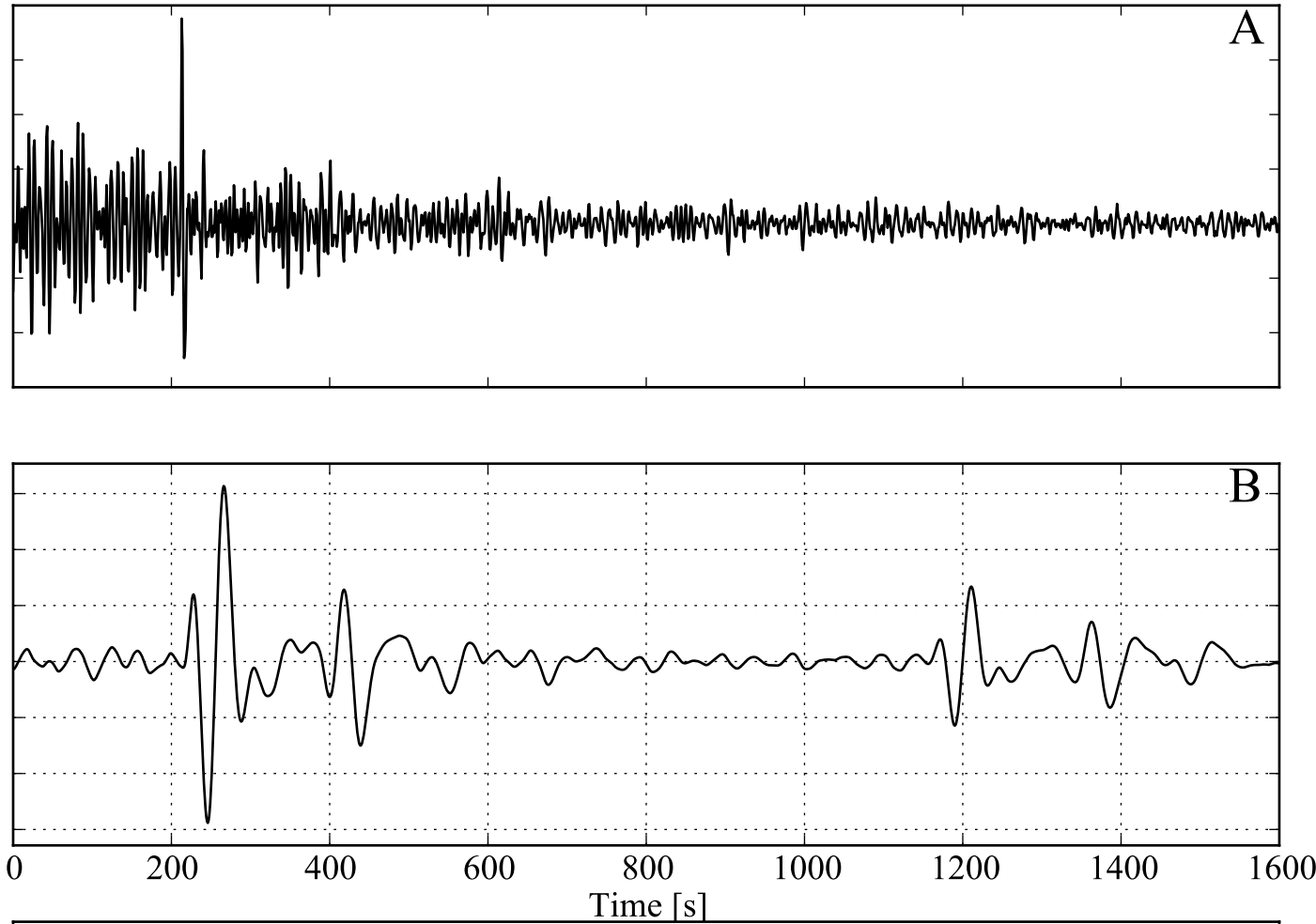
E

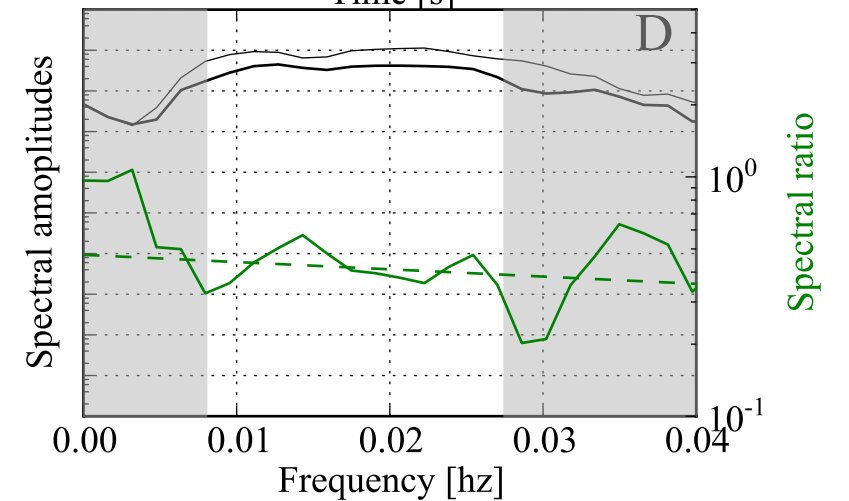
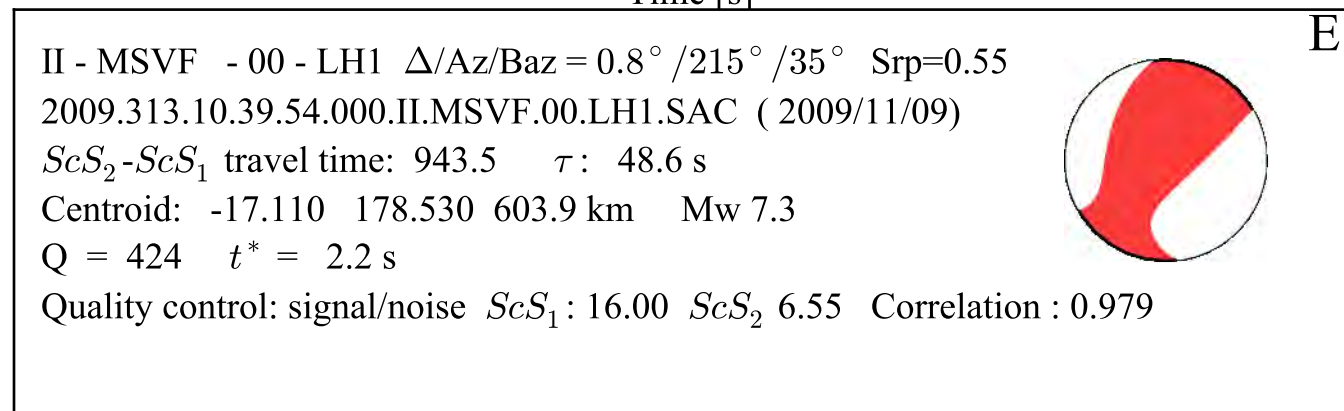
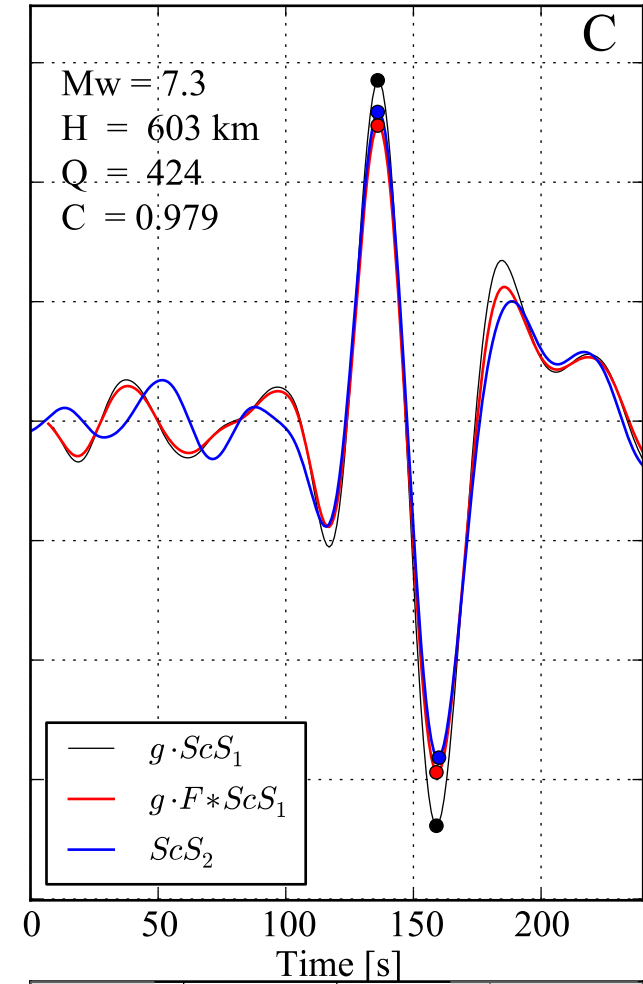
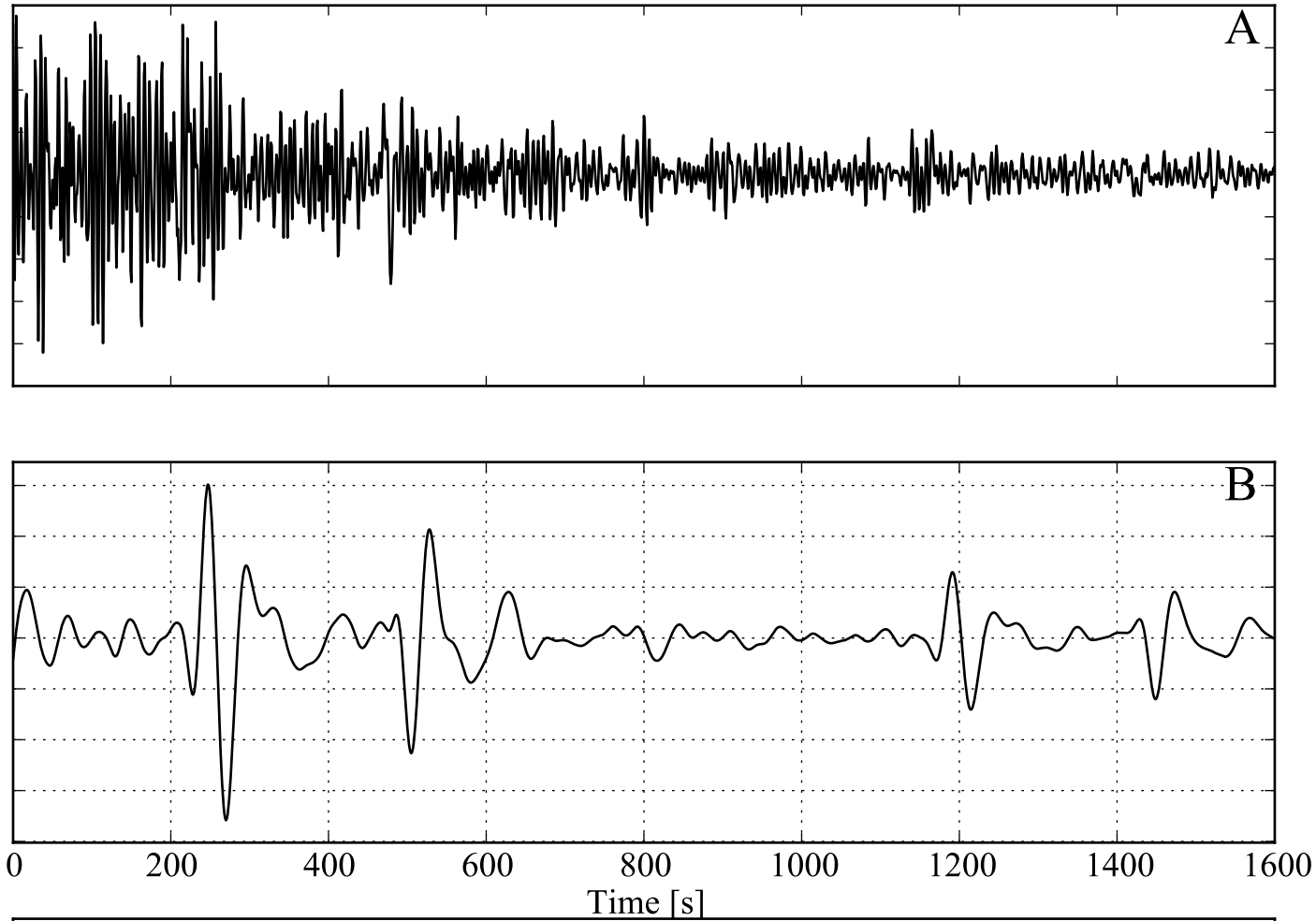
II - MSVF - 00 - LH1 $\Delta/Az/Baz = 4.6^\circ / 308^\circ / 130^\circ$ $Srp=0.77$
 1996.218.22.33.22.044.II.MSVF.00.LH1.SAC (1996/08/05)
 $ScS_2 - ScS_1$ travel time: 943.6 τ : 47.2 s
 Centroid: -20.720 -178.160 555.0 km Mw 7.4
 Q = 245 $t^* = 3.8$ s
 Quality control: signal/noise ScS_1 : 25.65 ScS_2 9.43 Correlation : 0.978

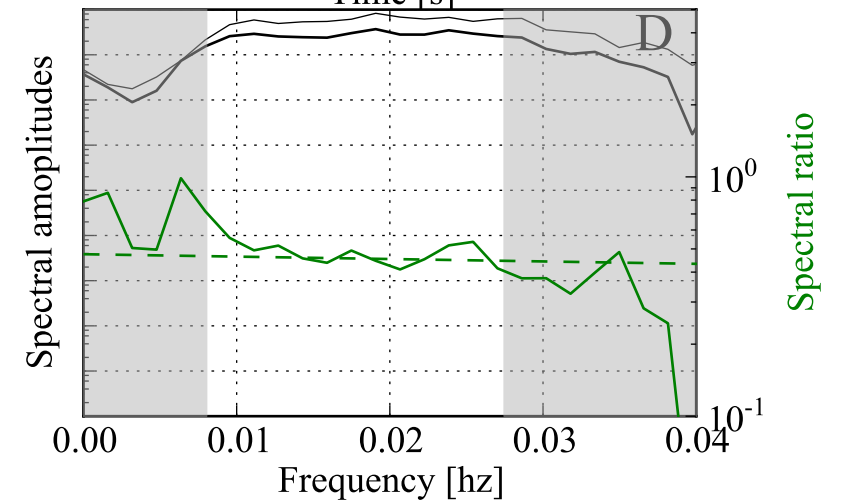
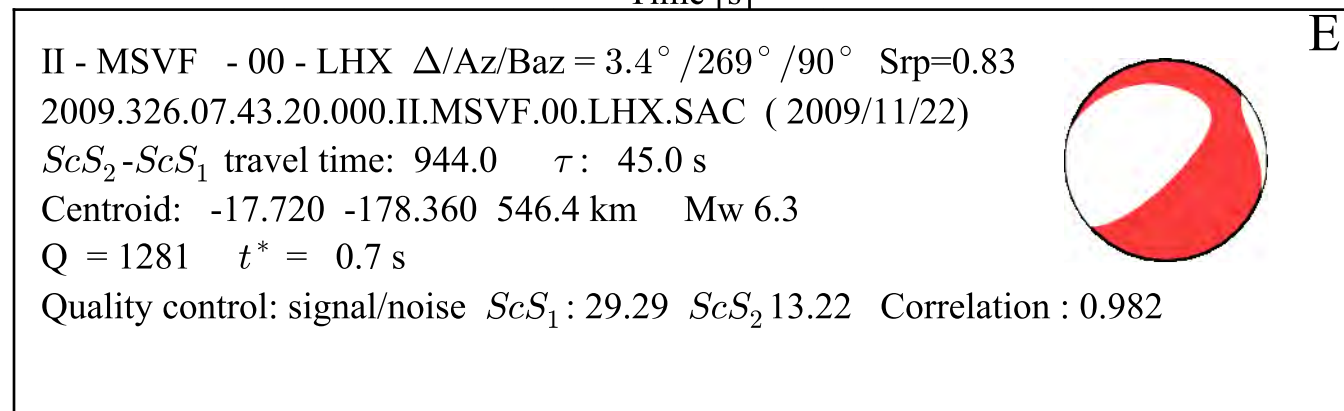
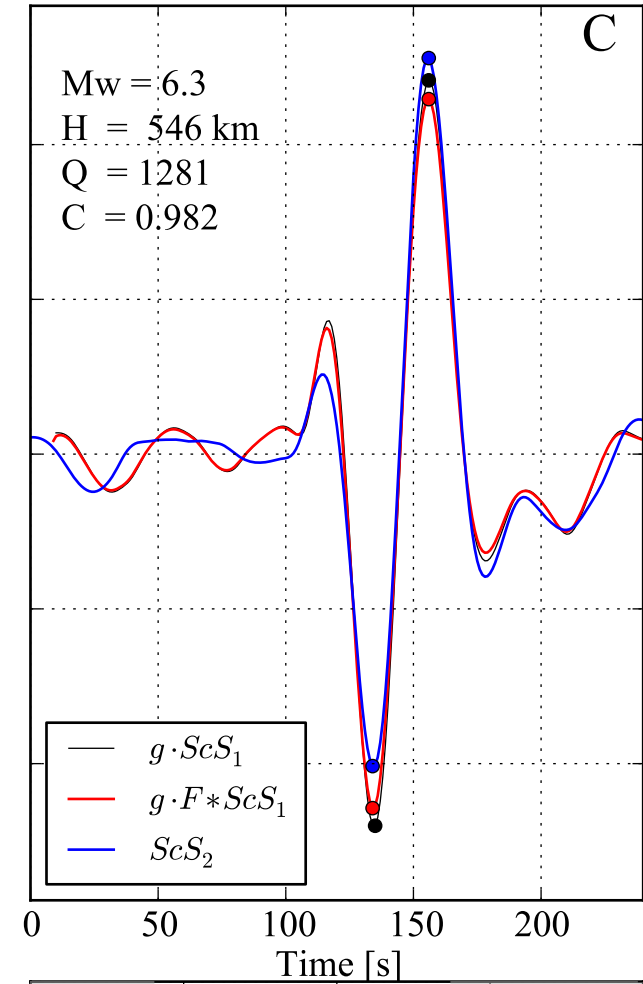
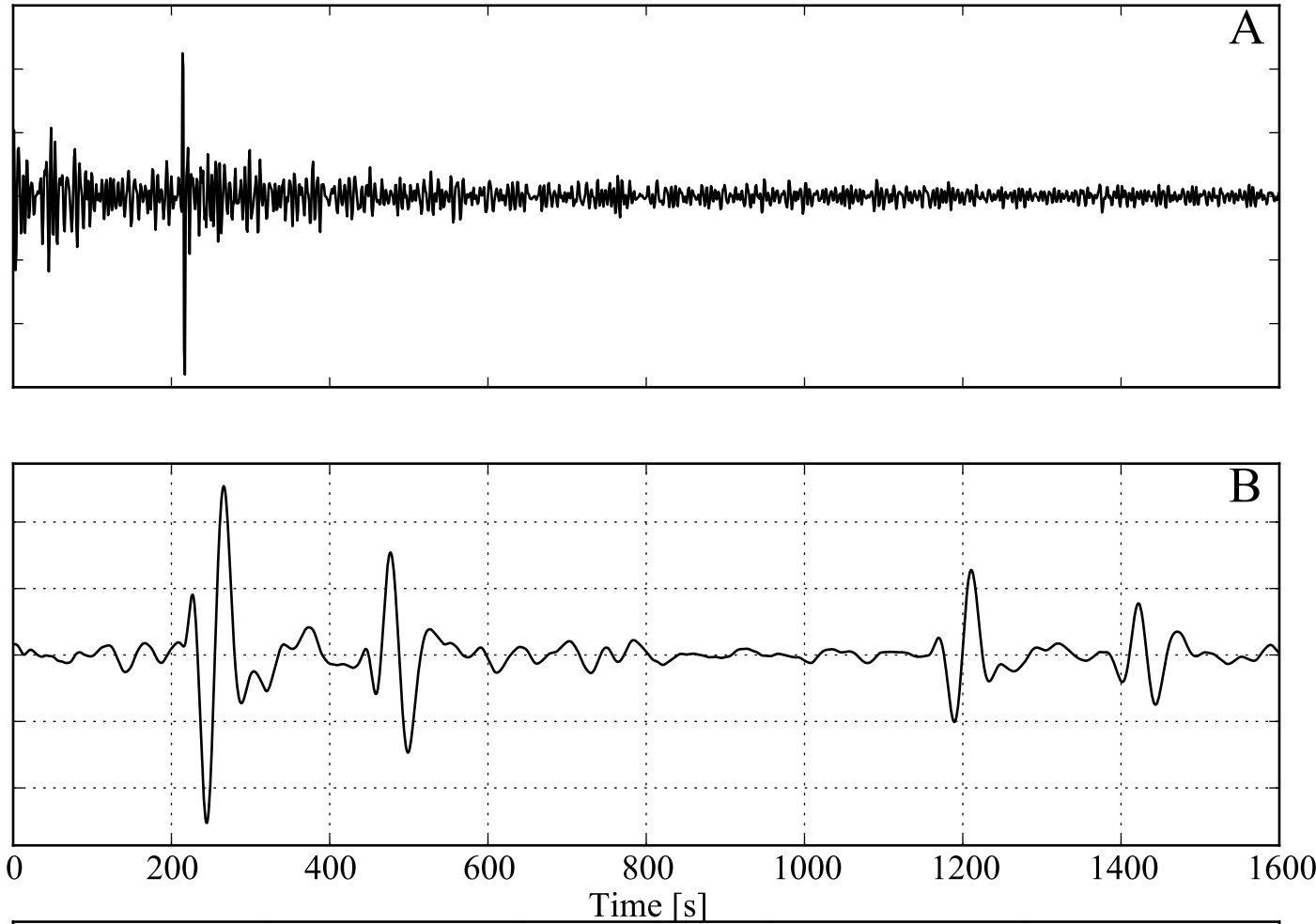


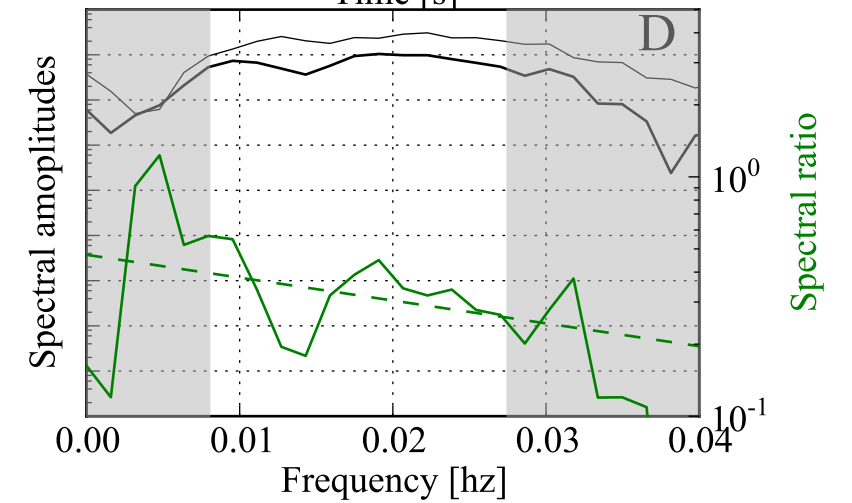
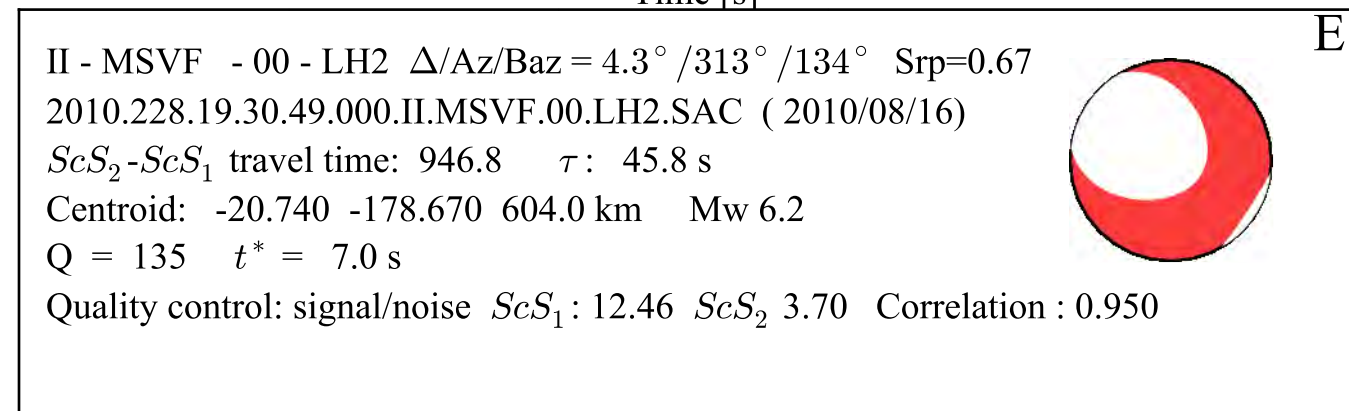
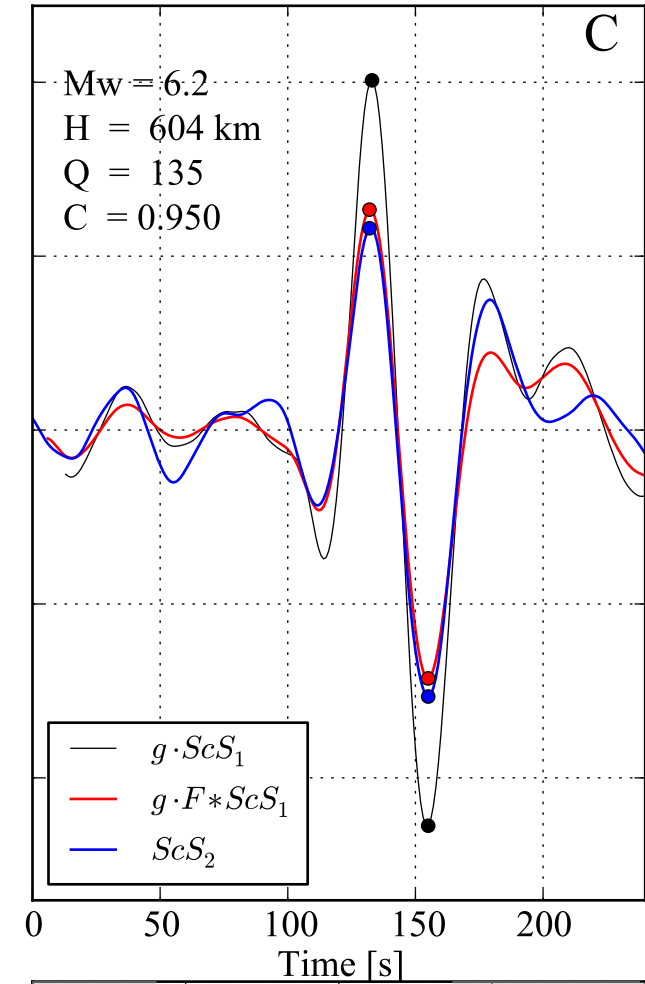
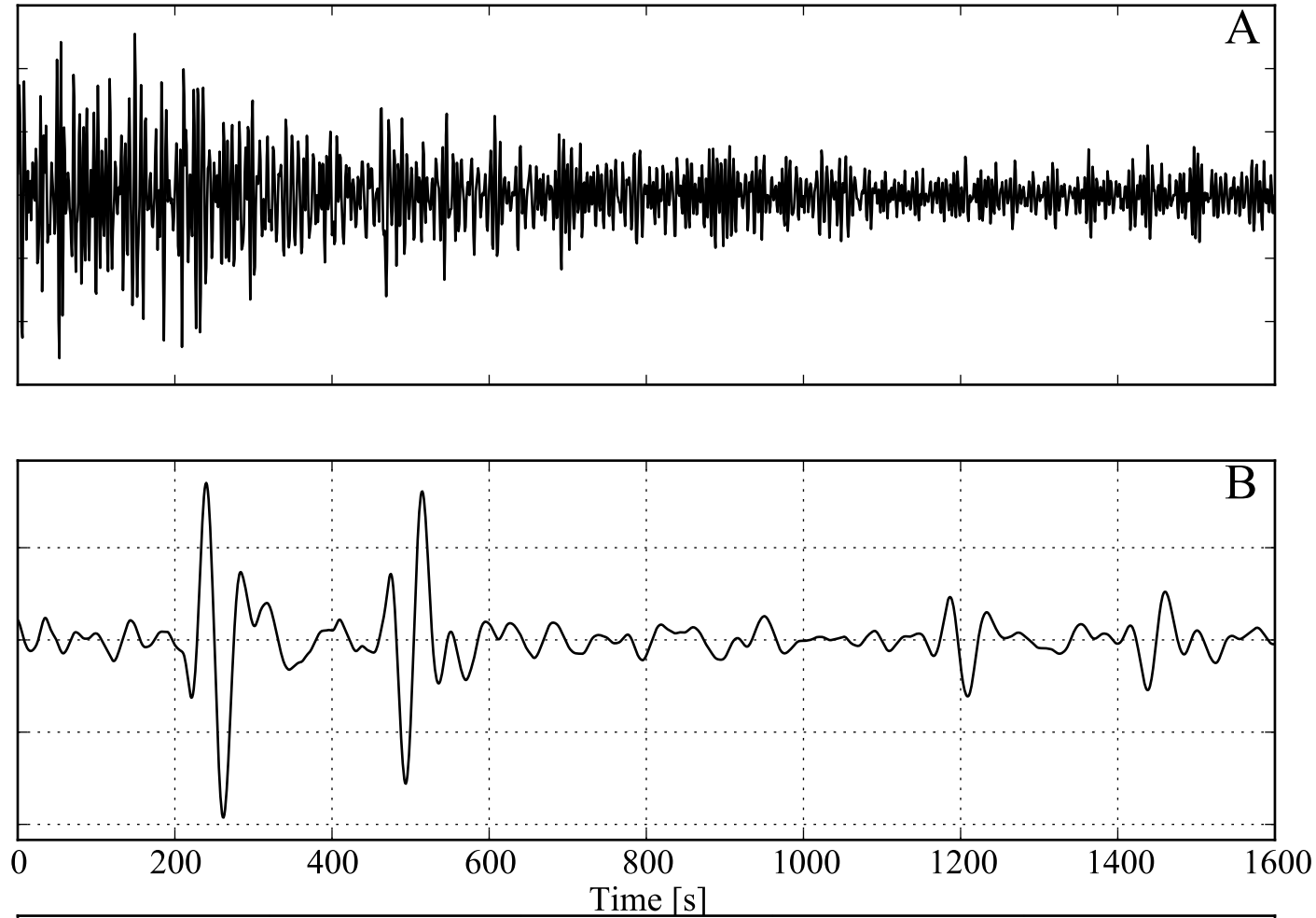


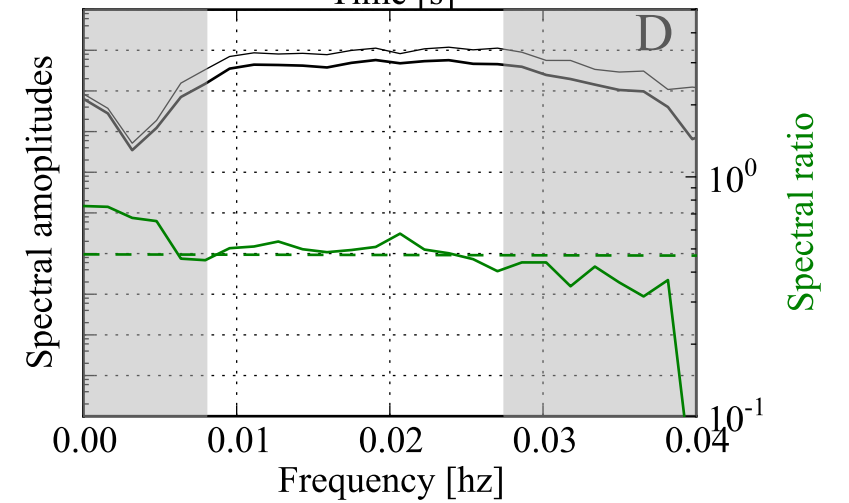
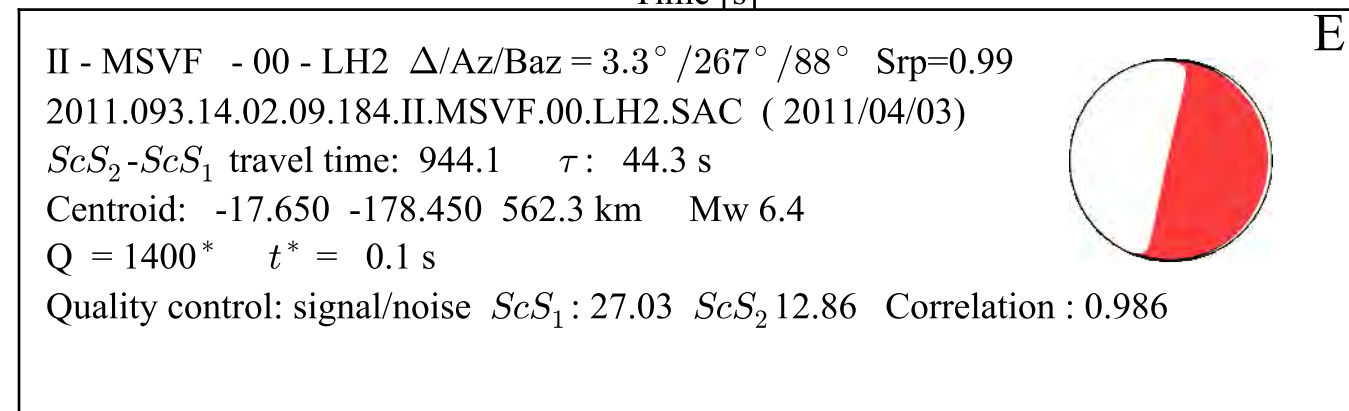
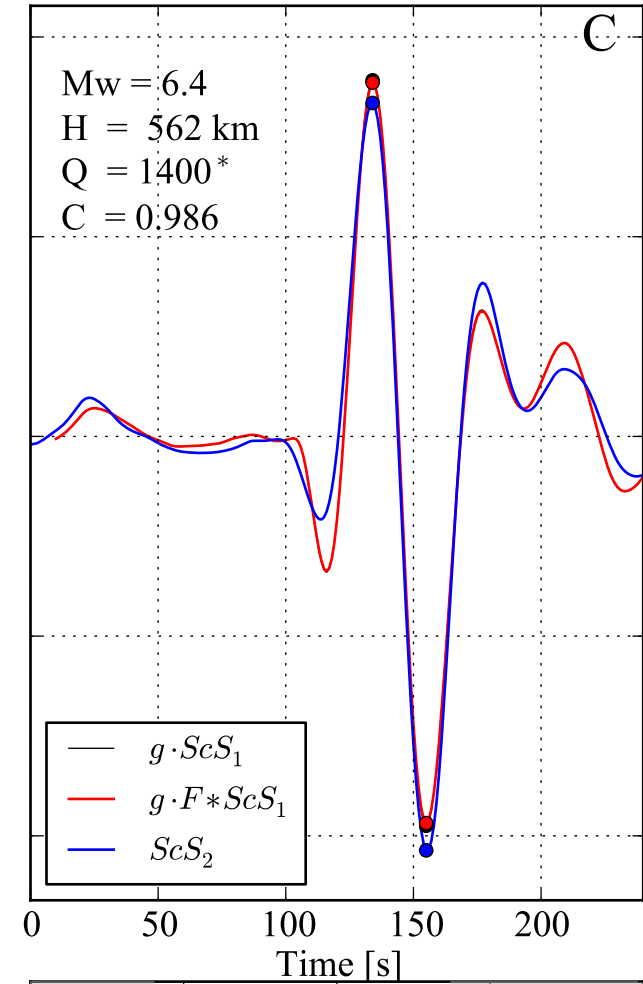
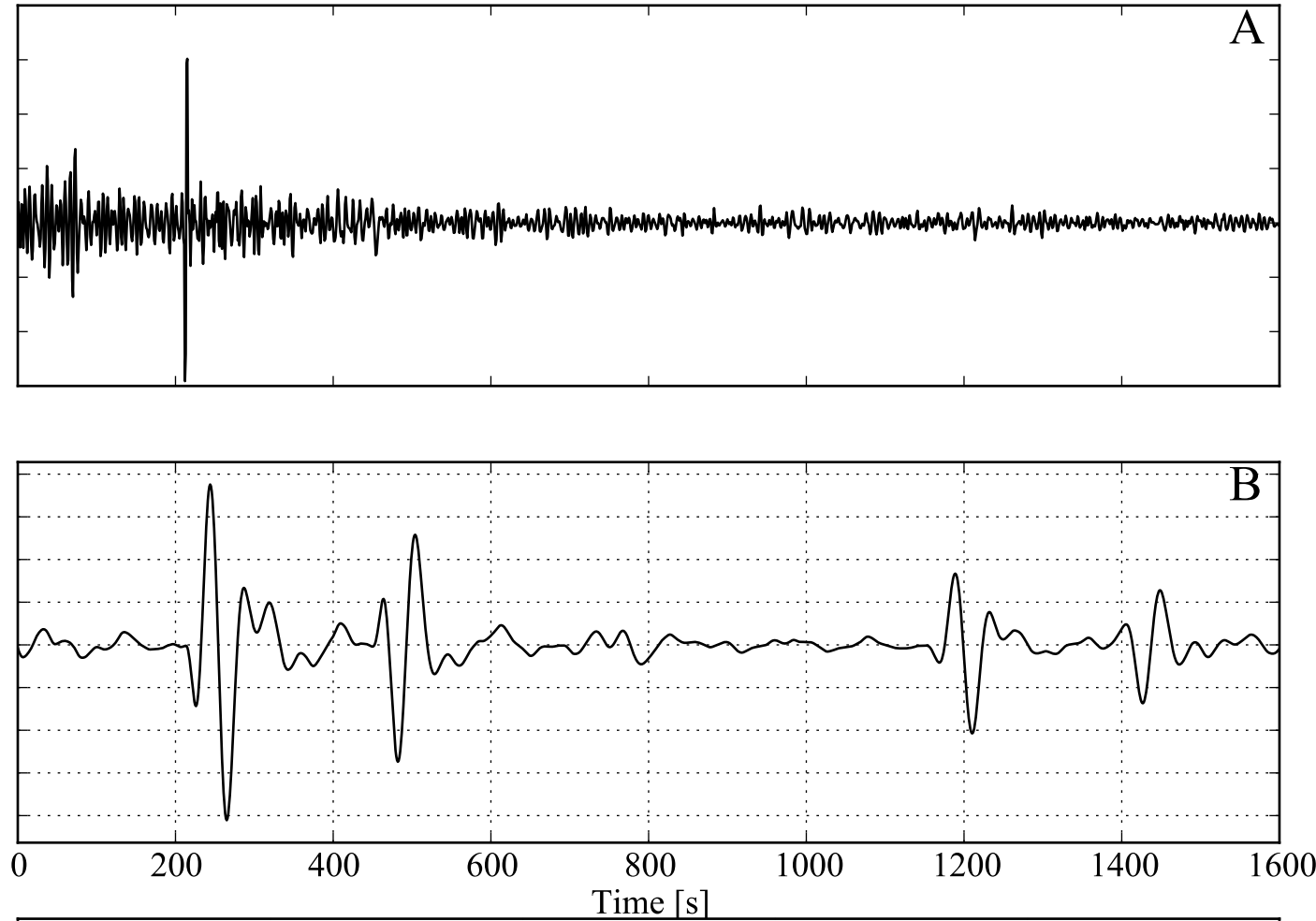


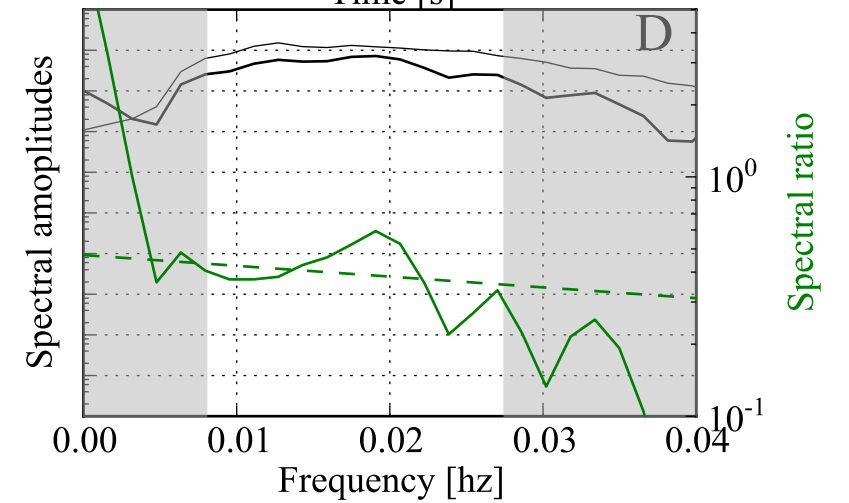
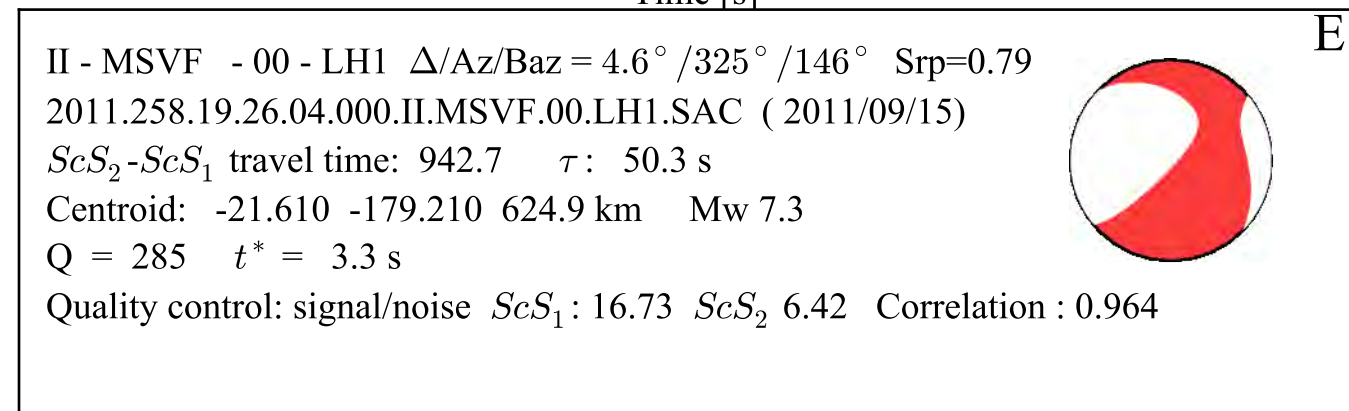
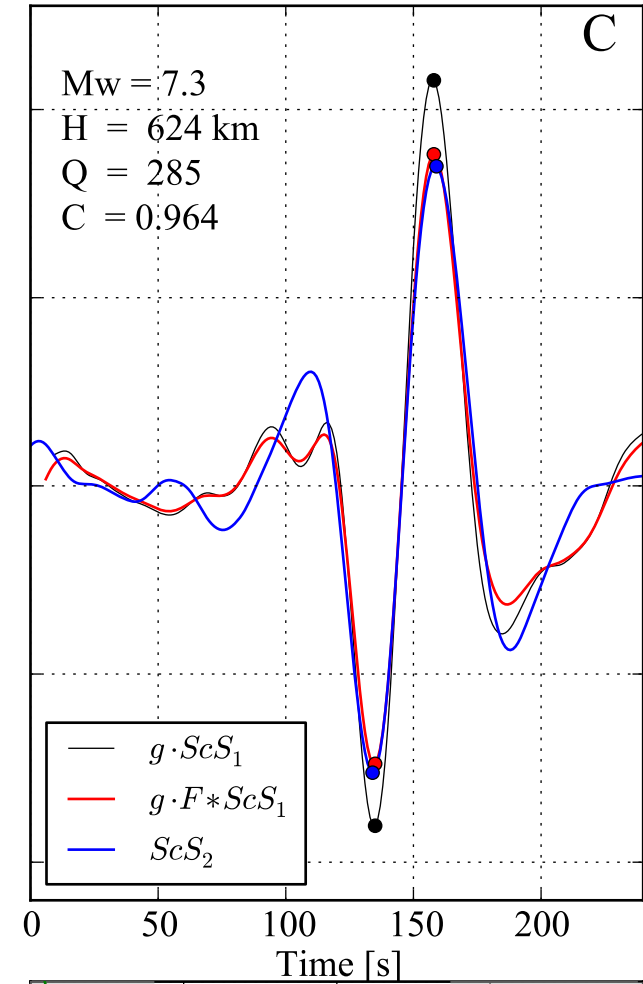
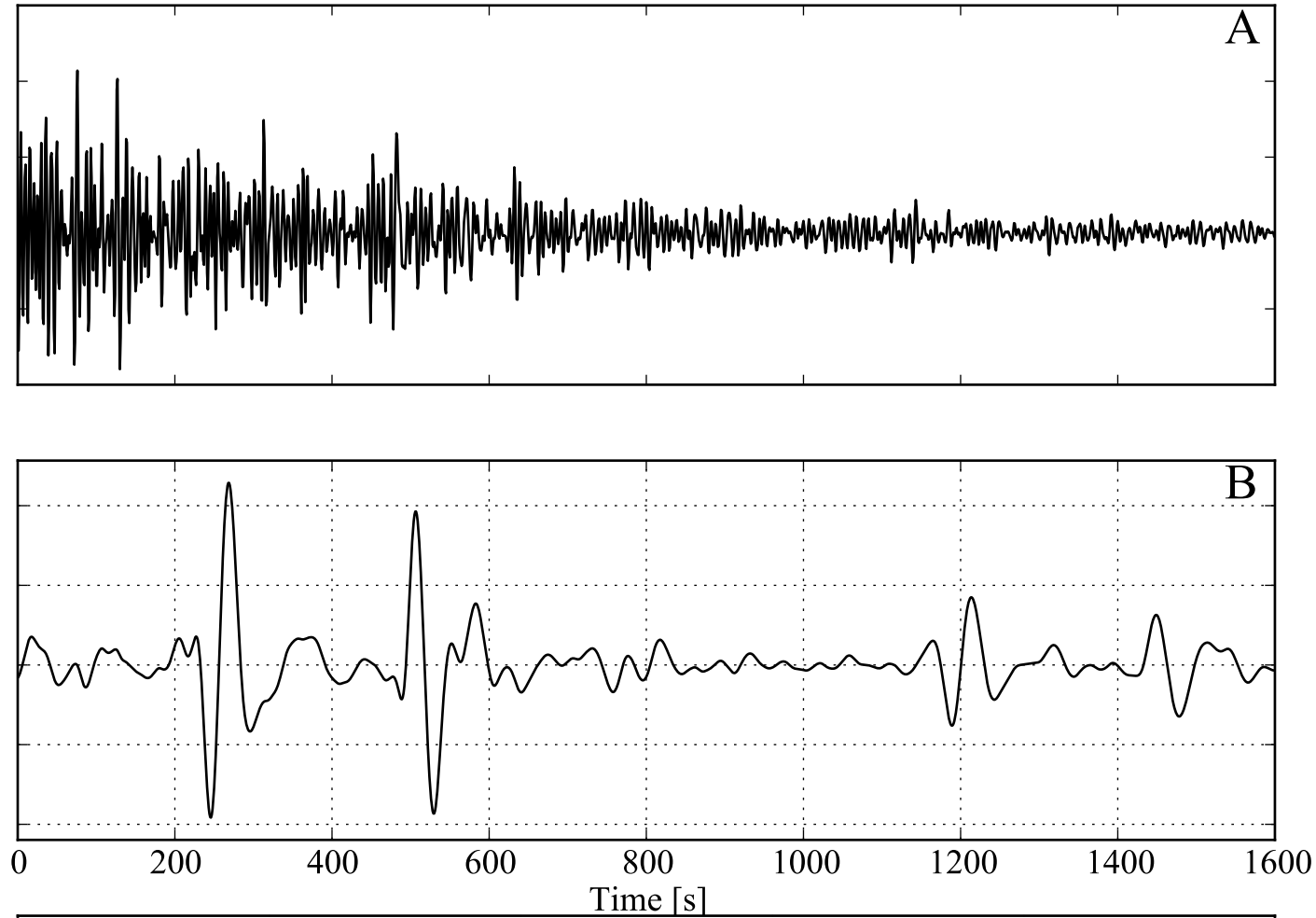


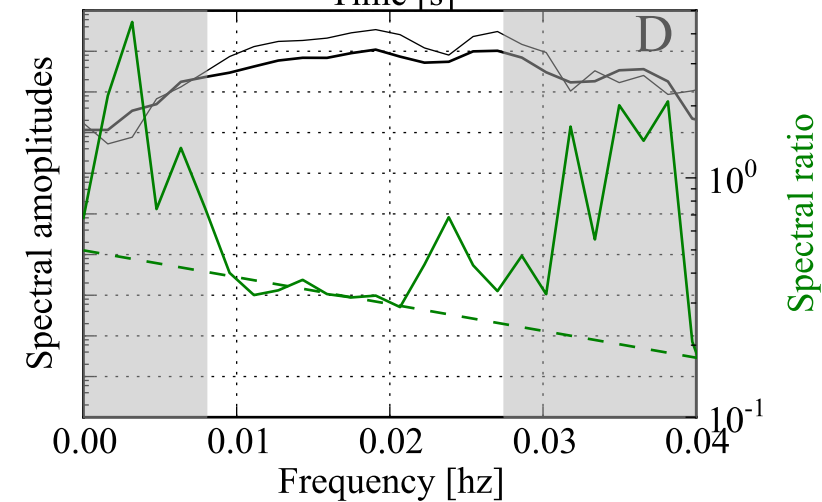
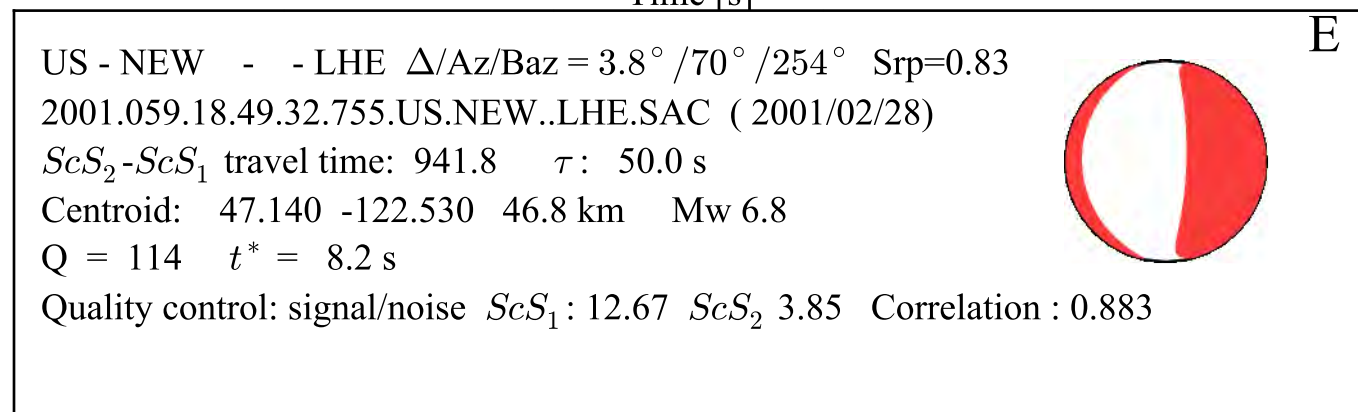
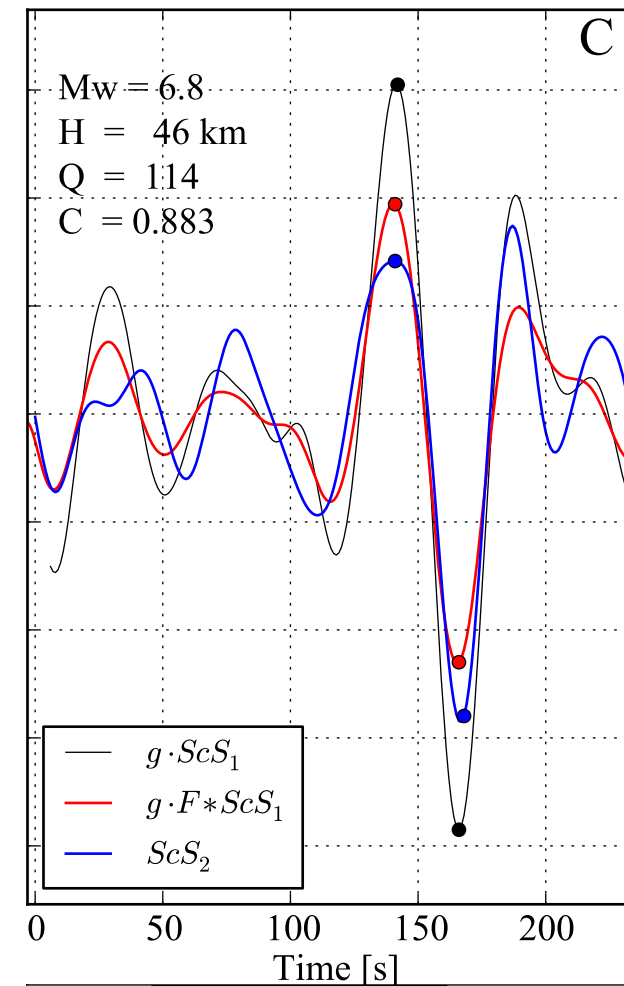
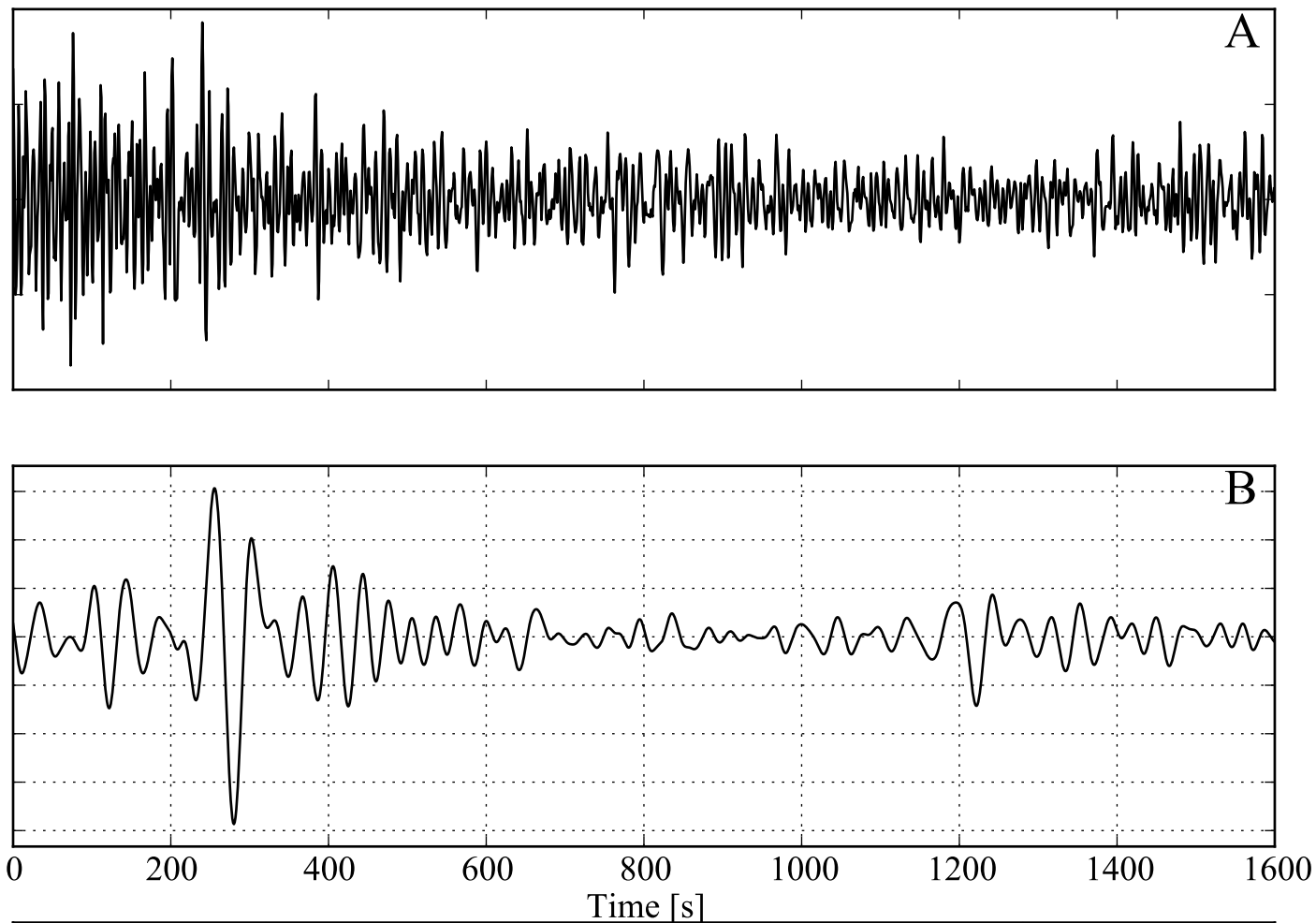


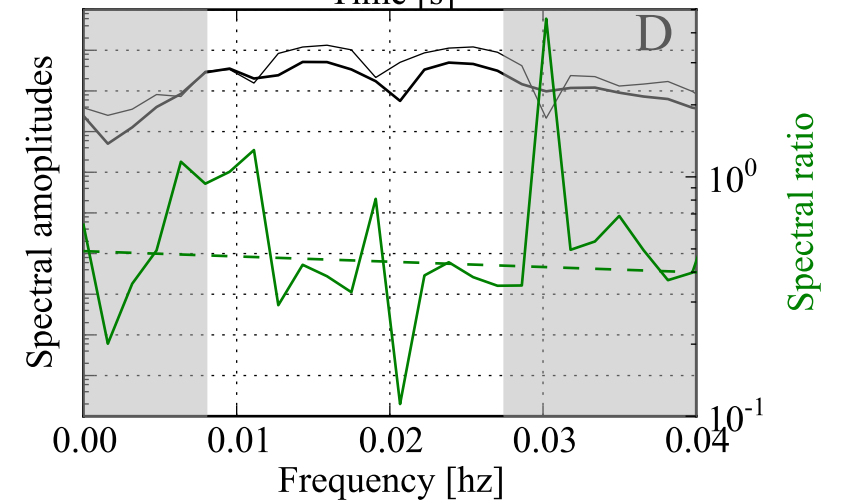
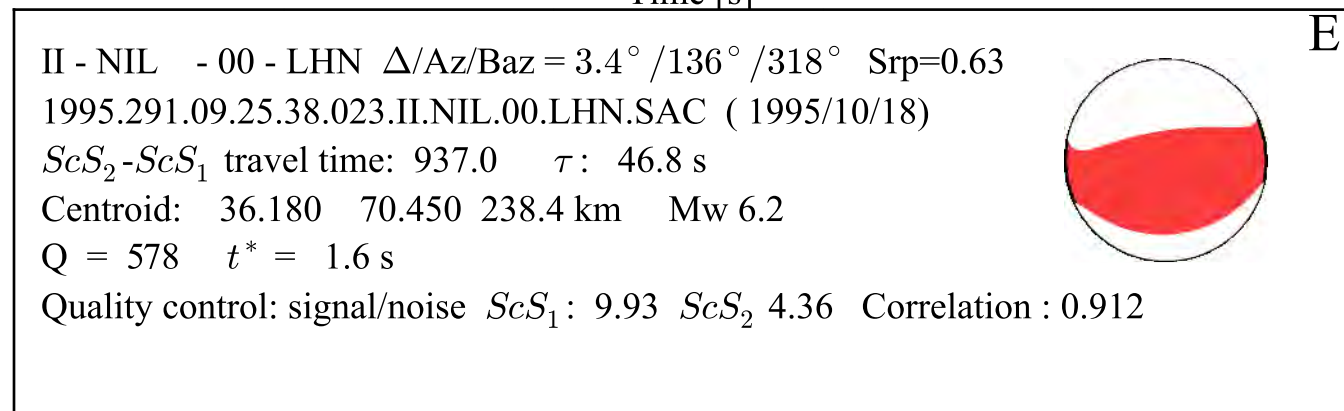
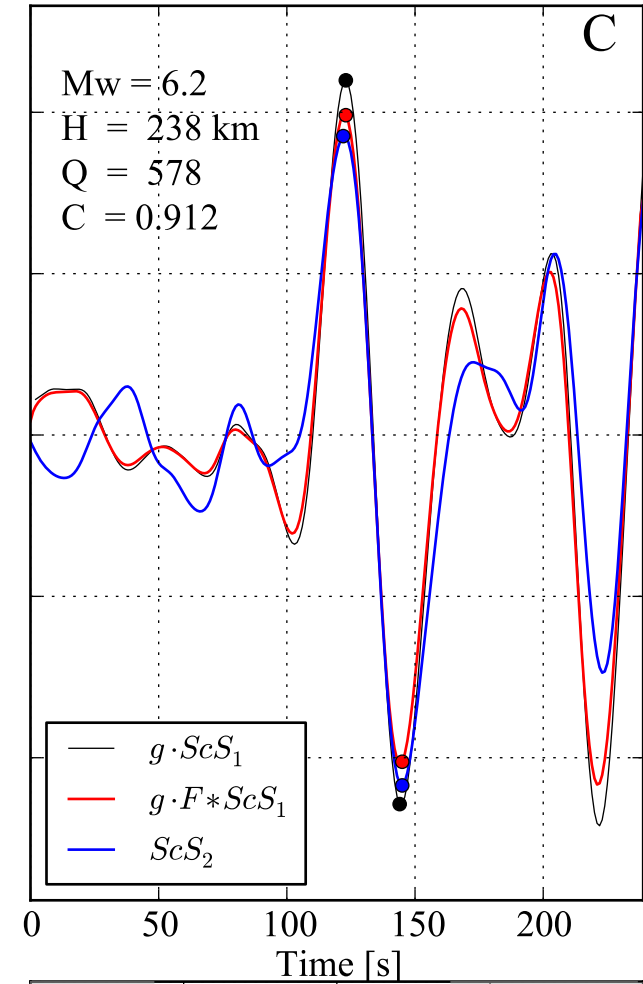
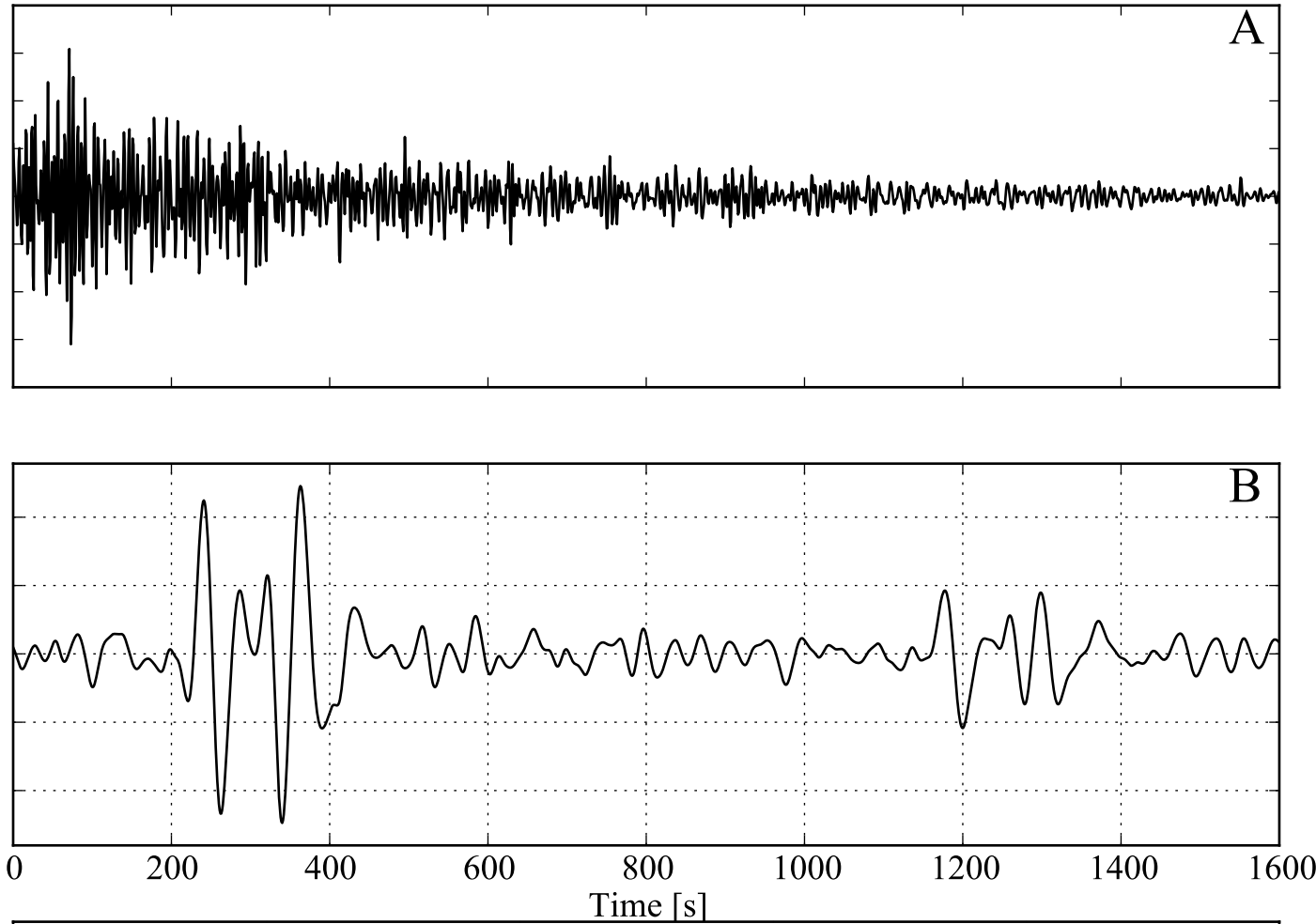


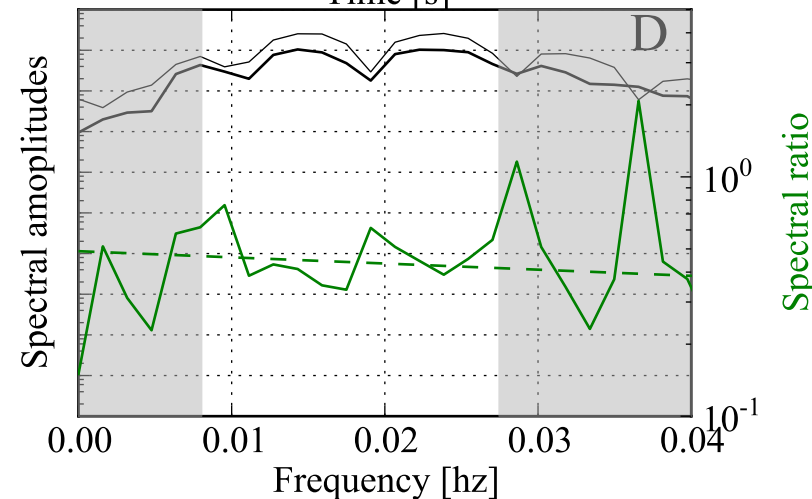
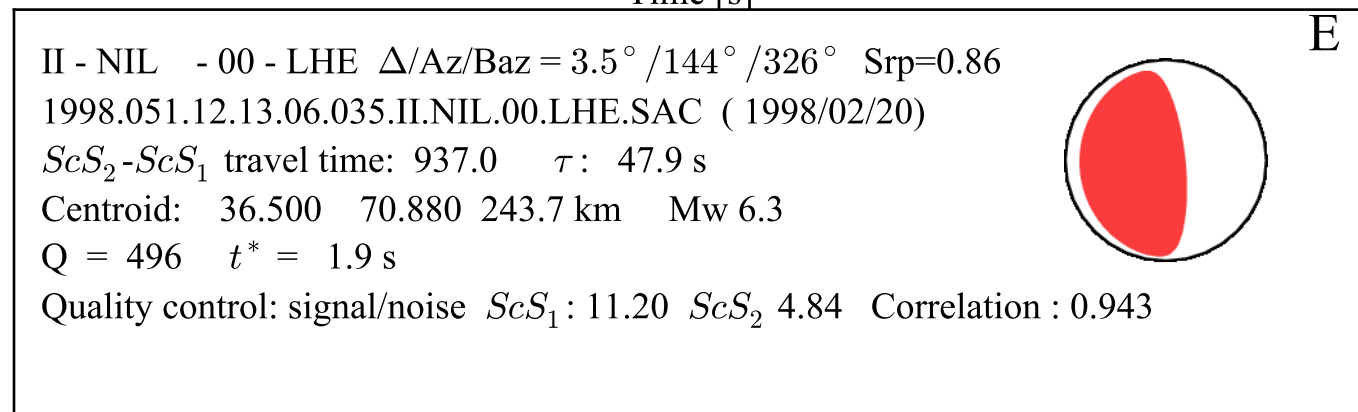
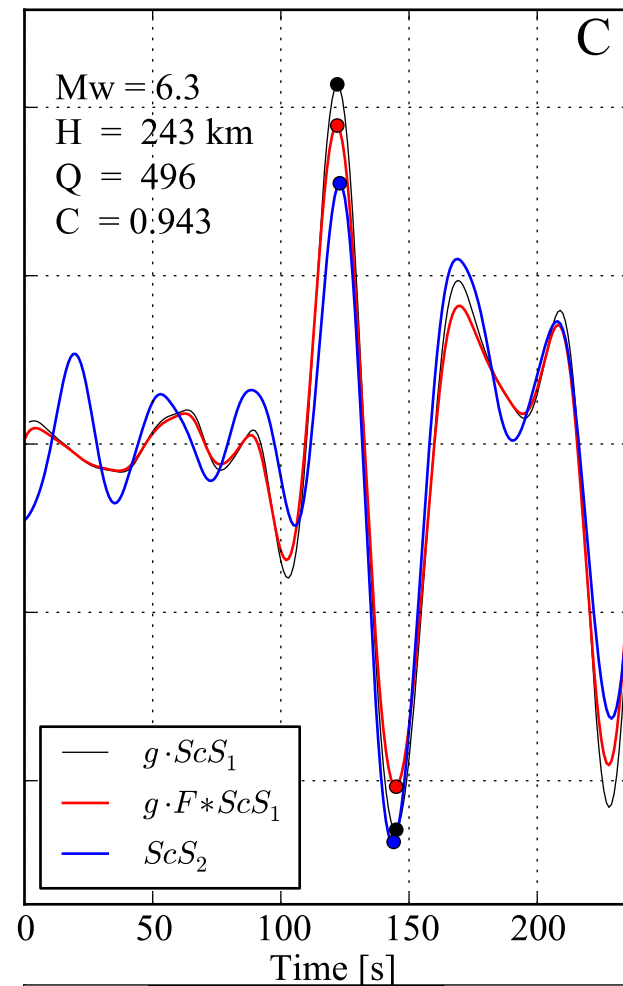
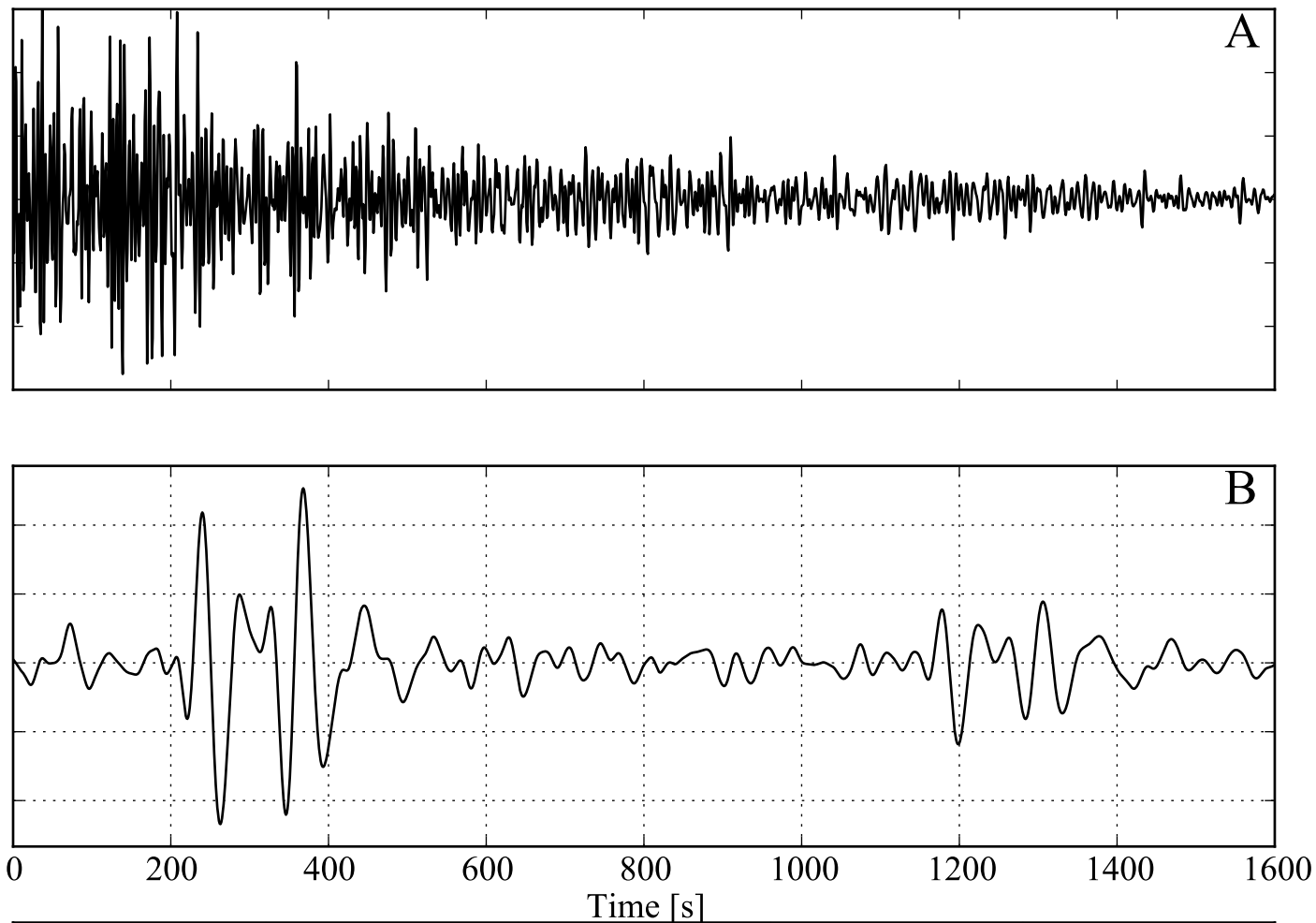


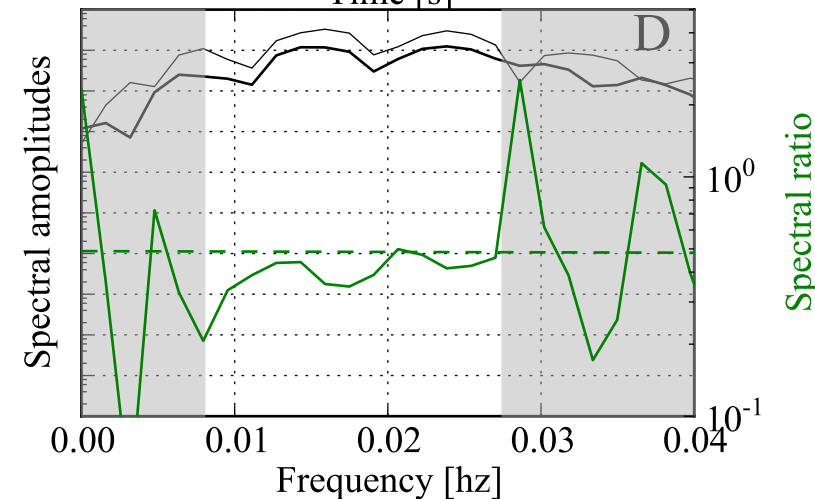
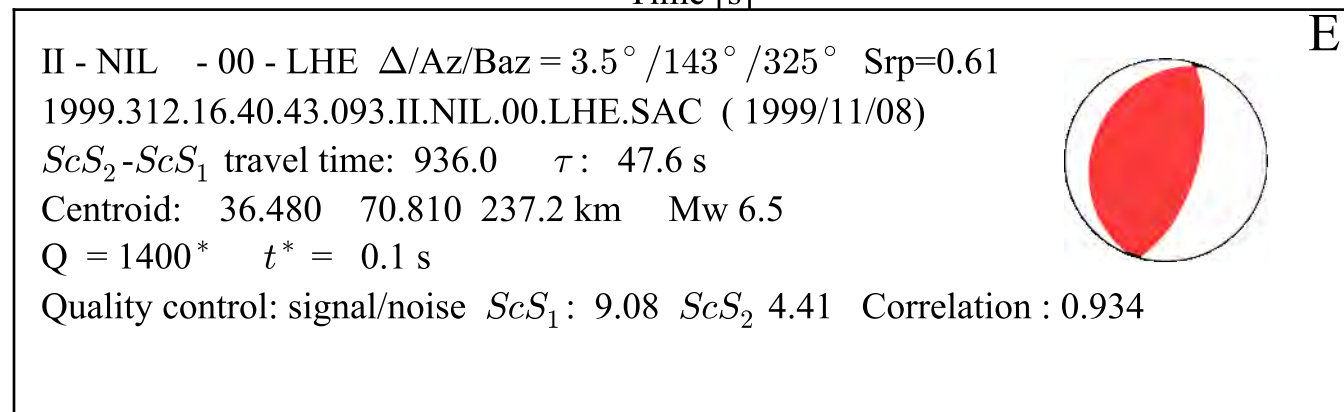
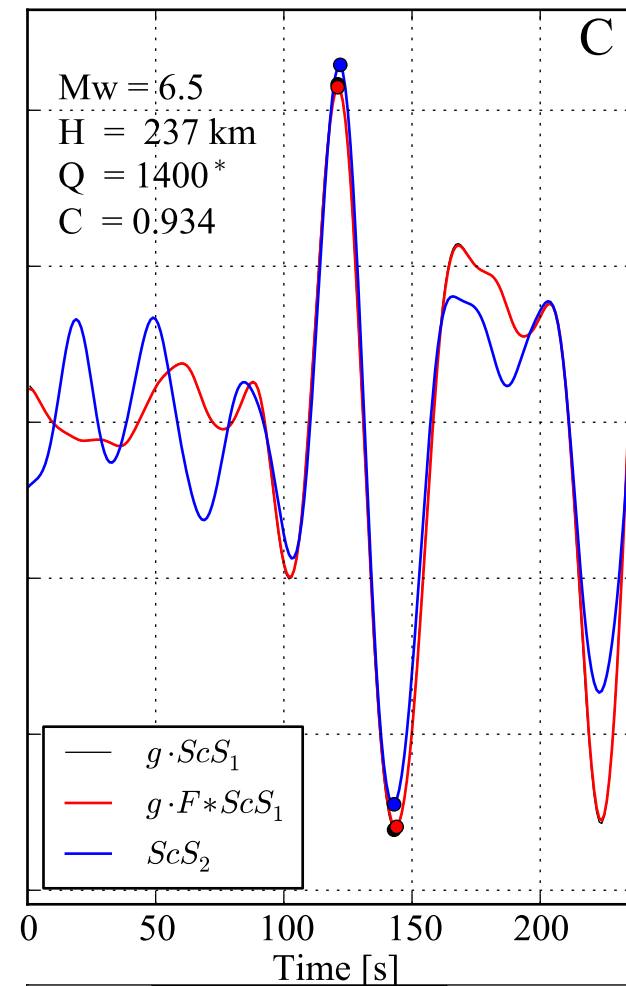
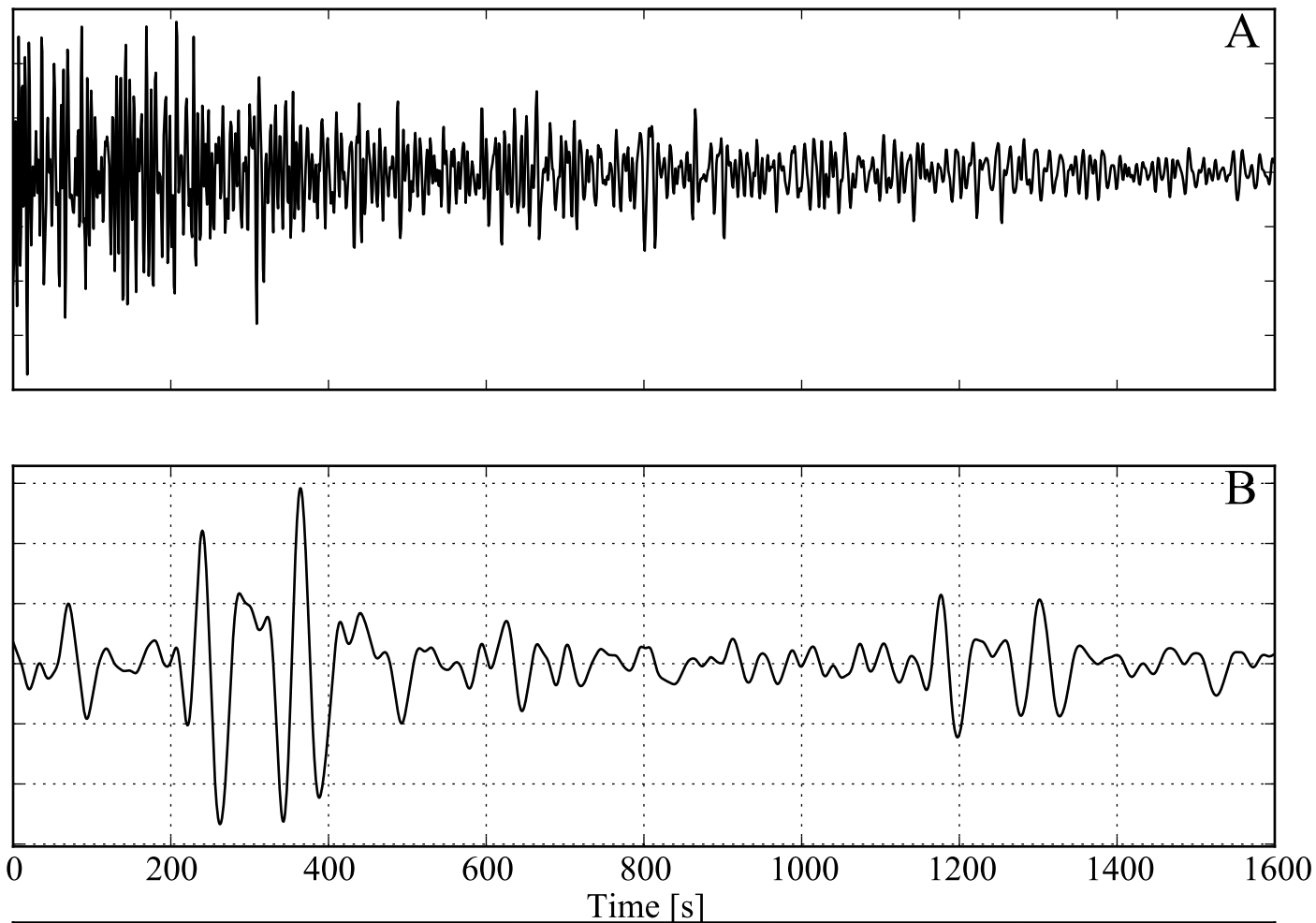


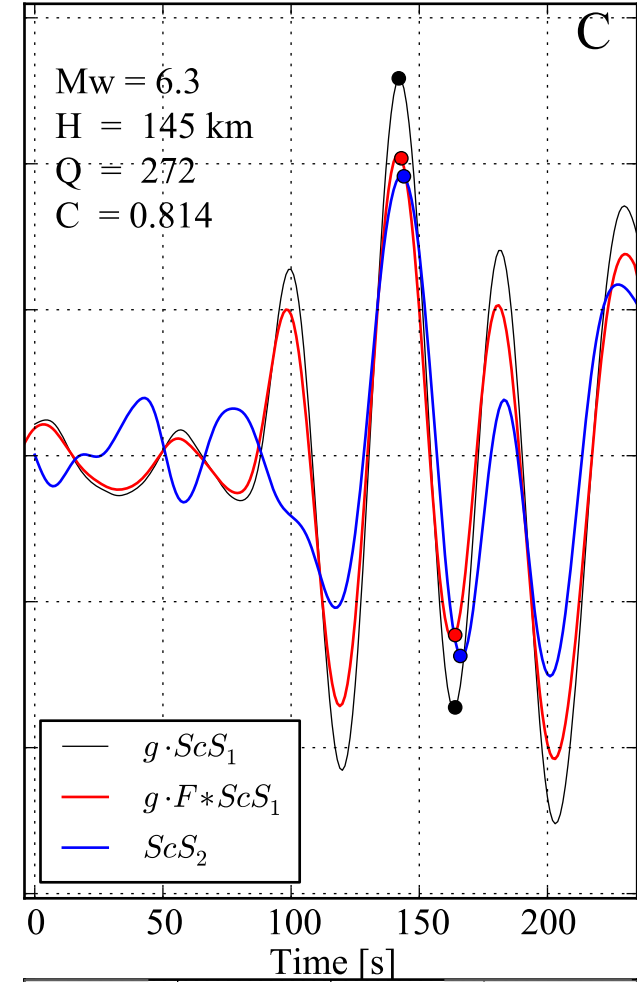
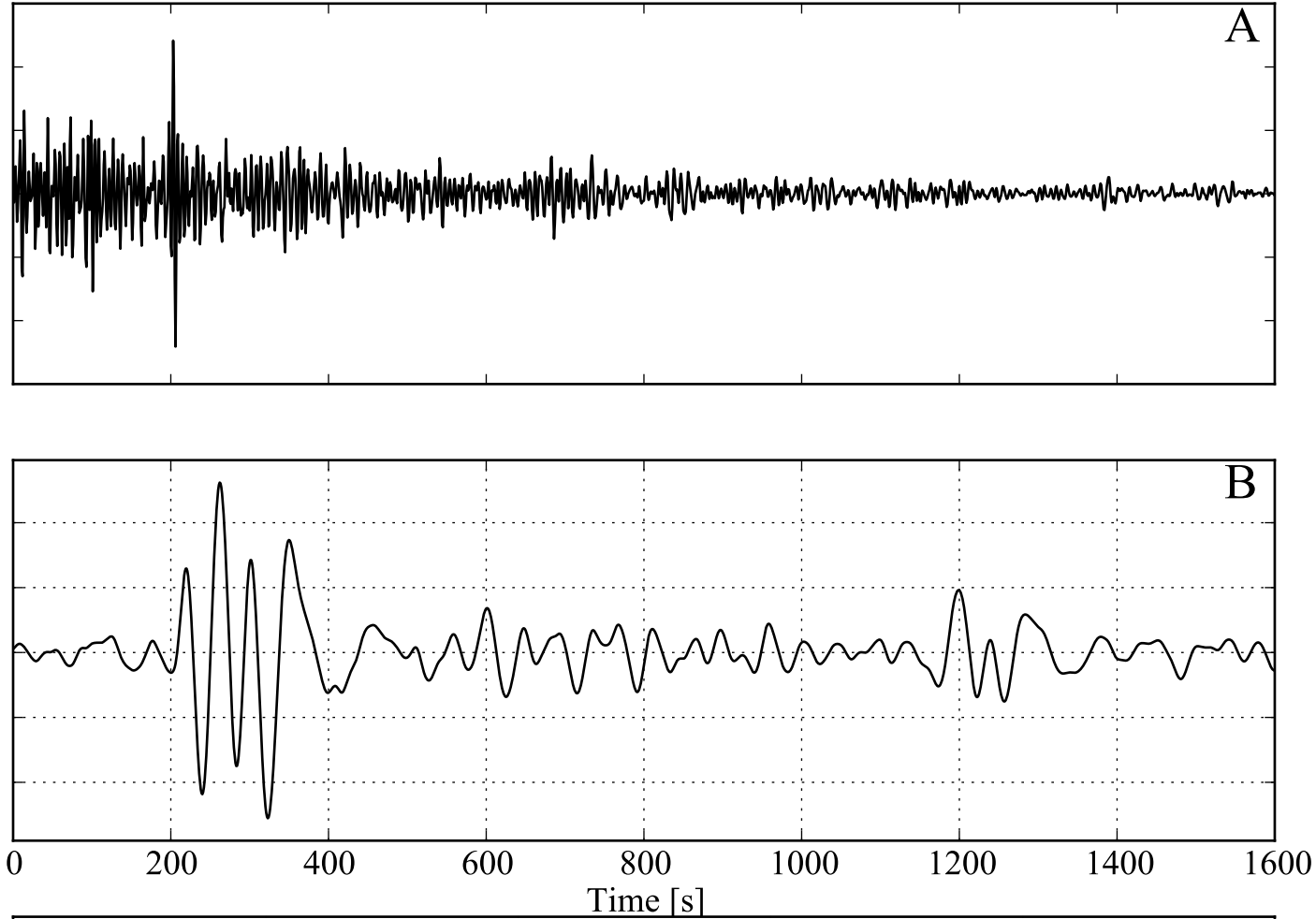






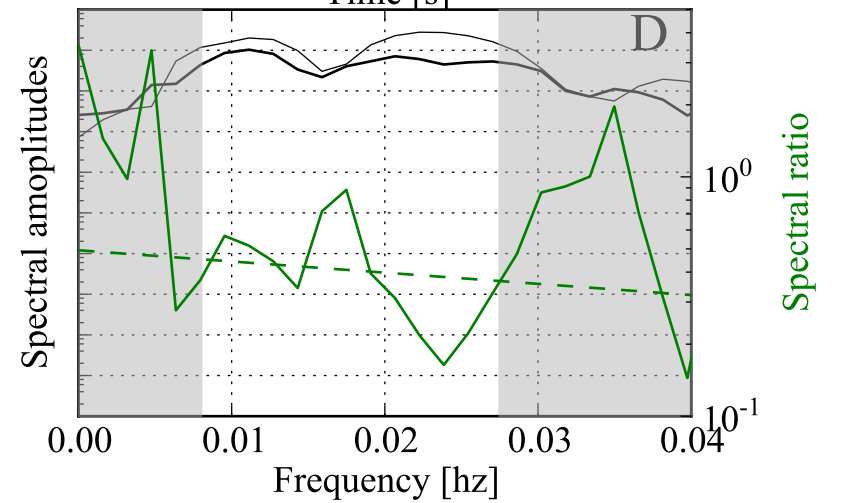


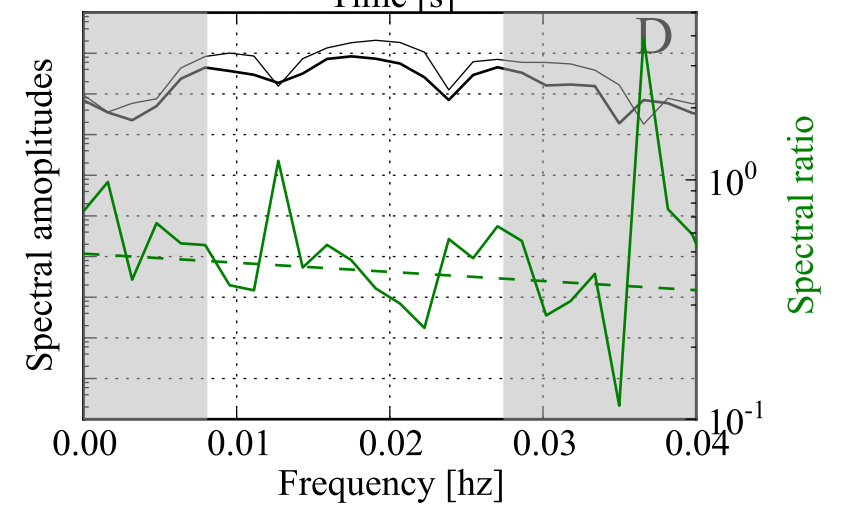
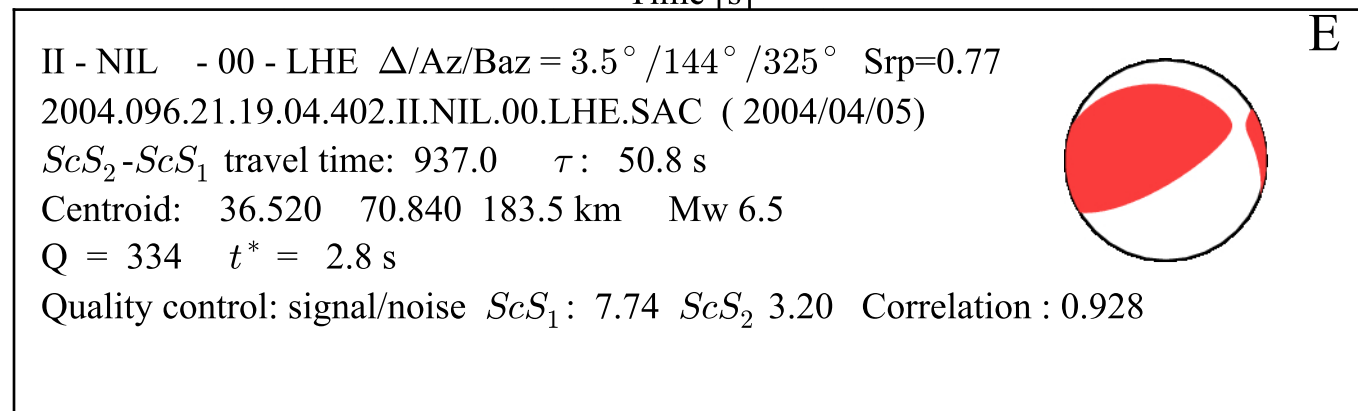
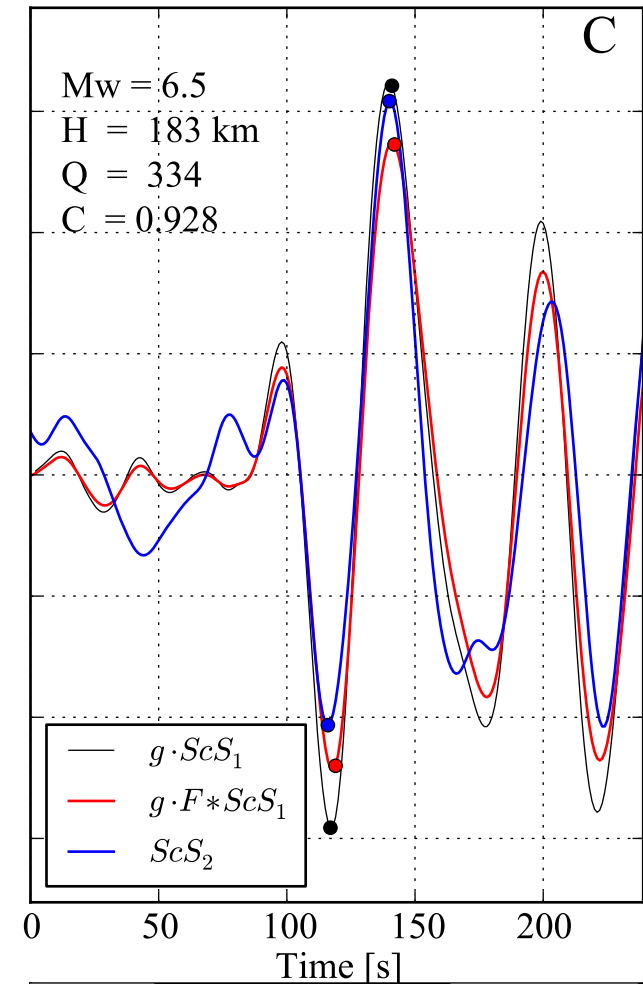
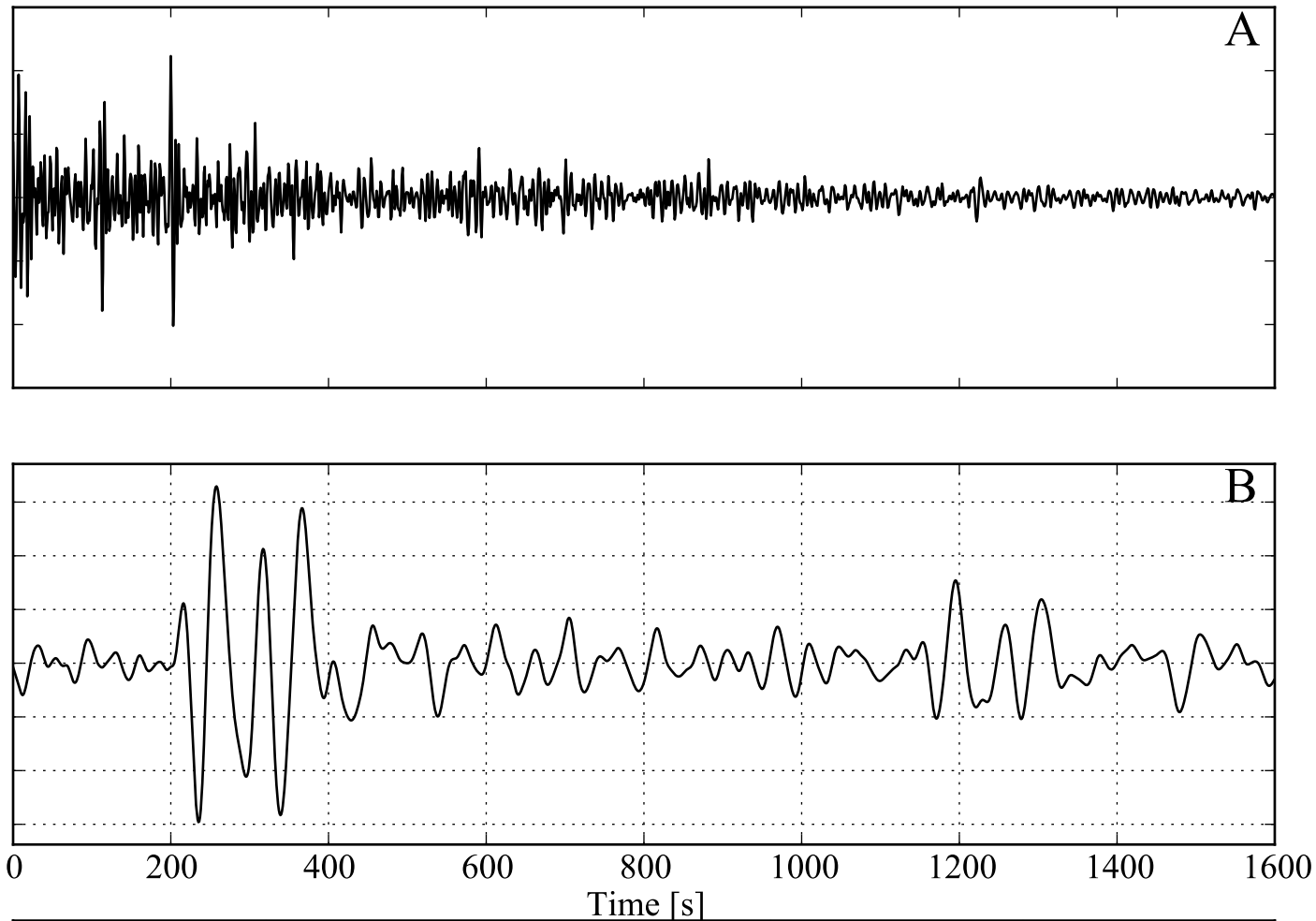


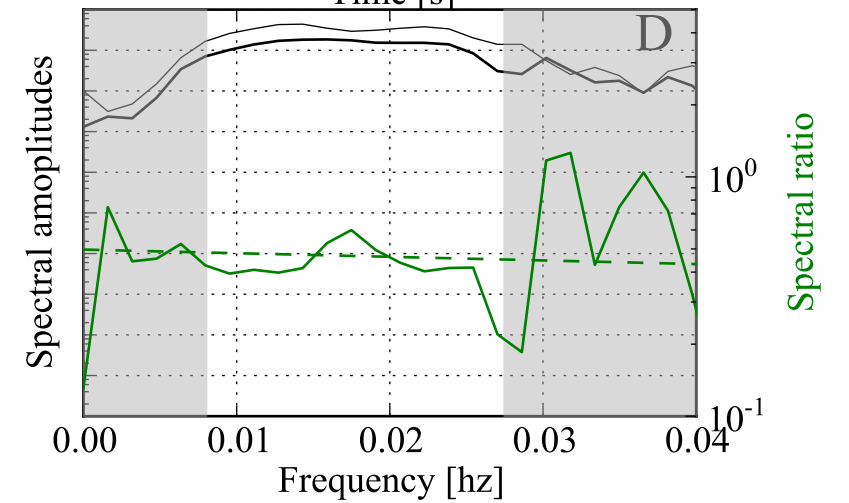
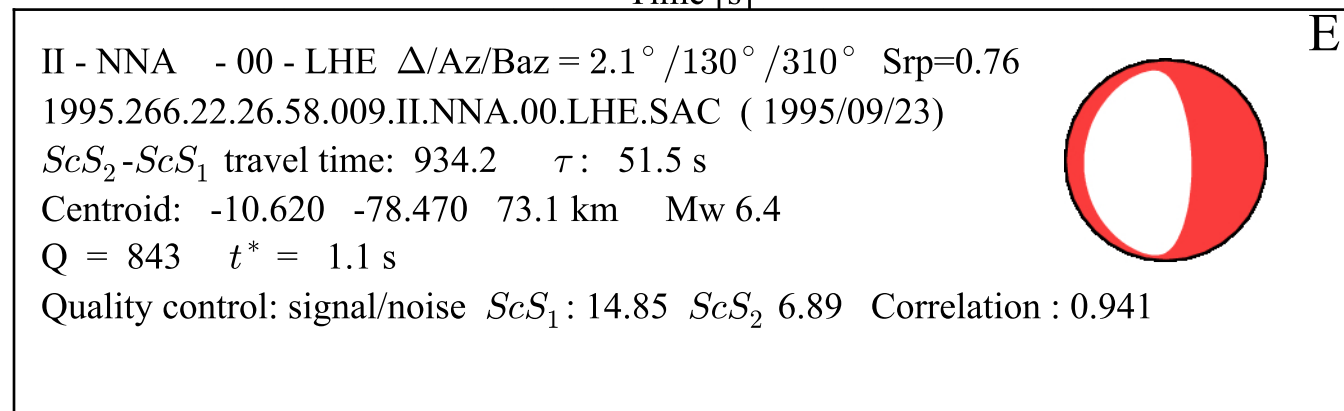
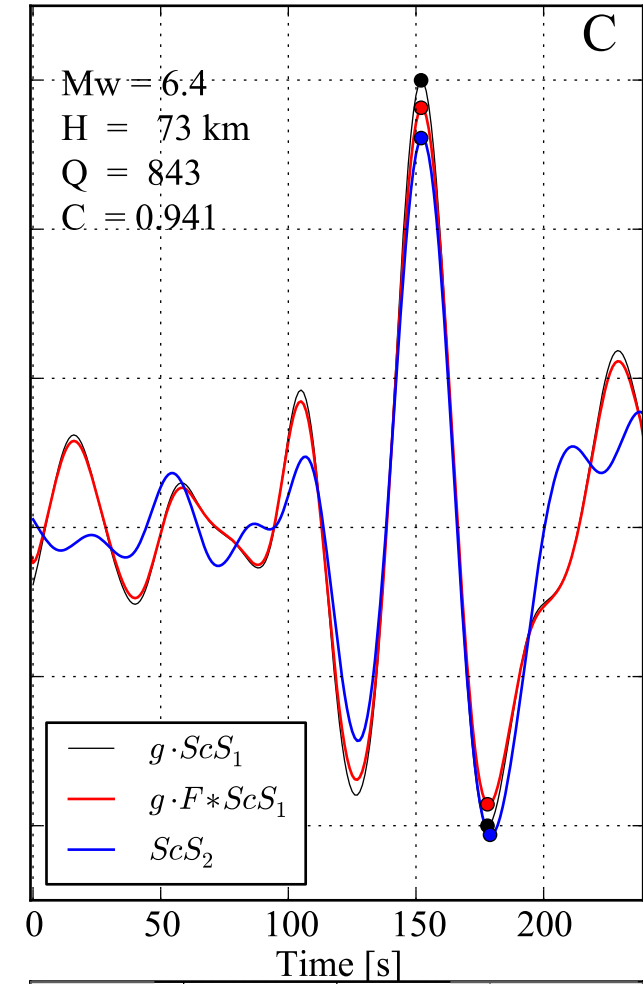
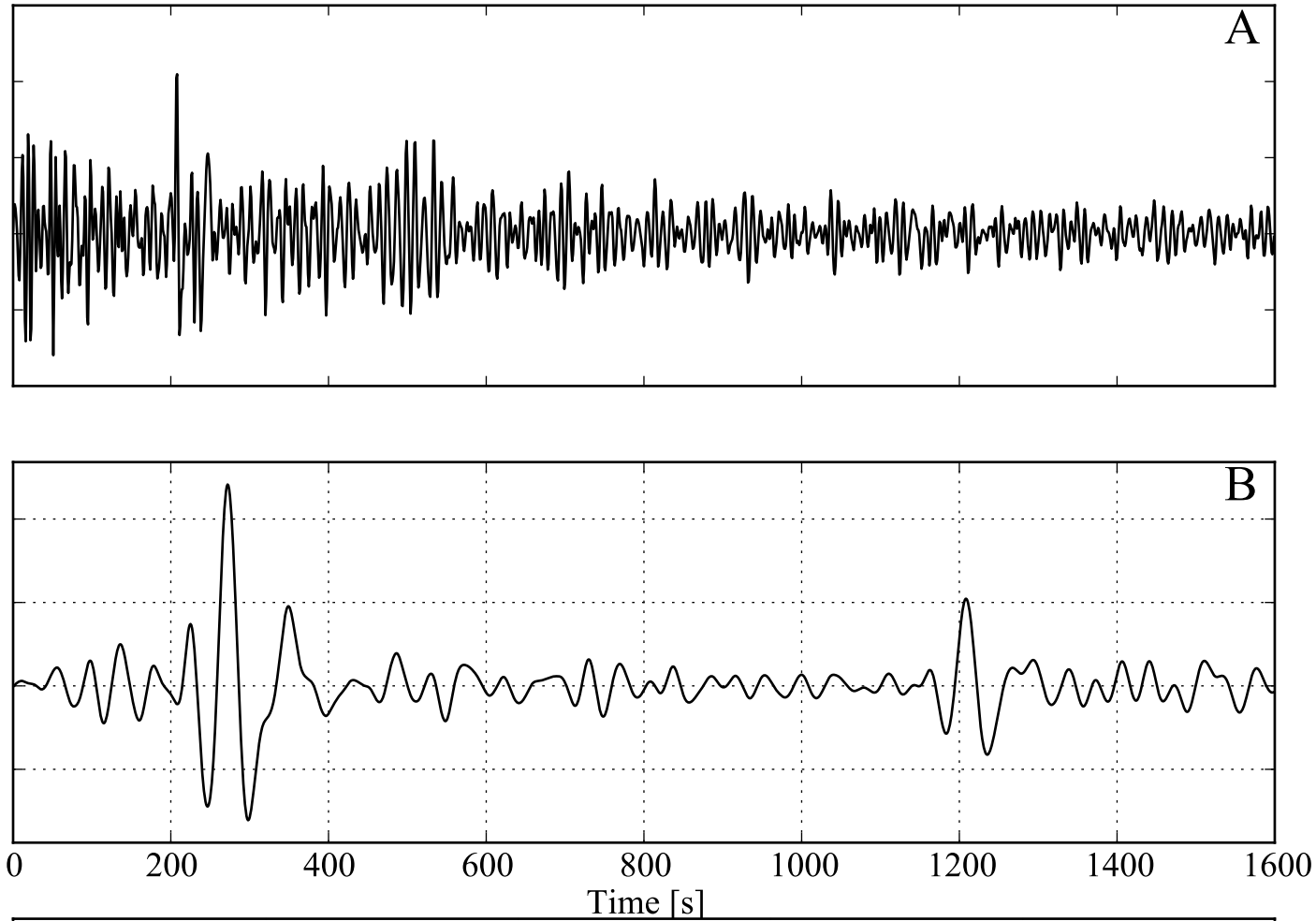


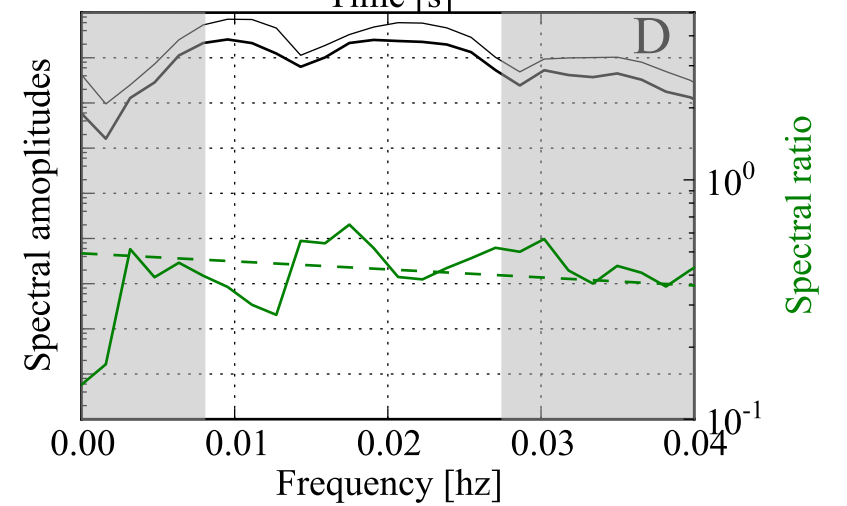
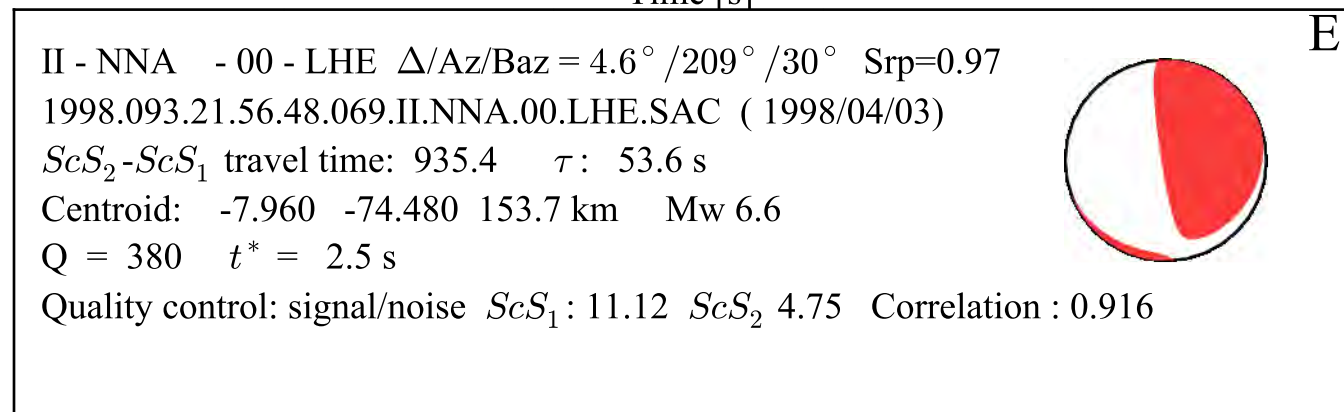
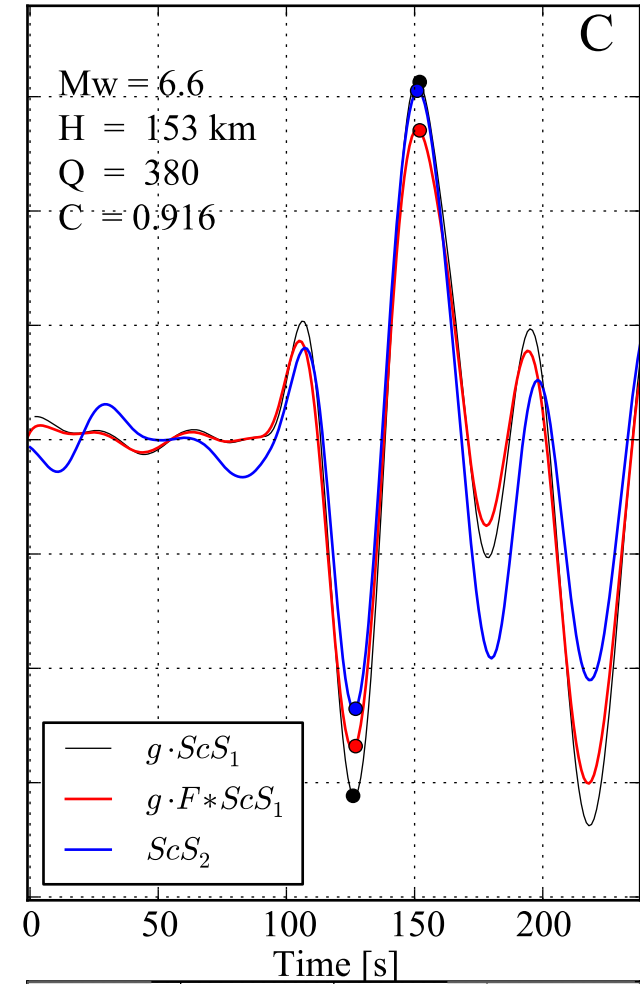
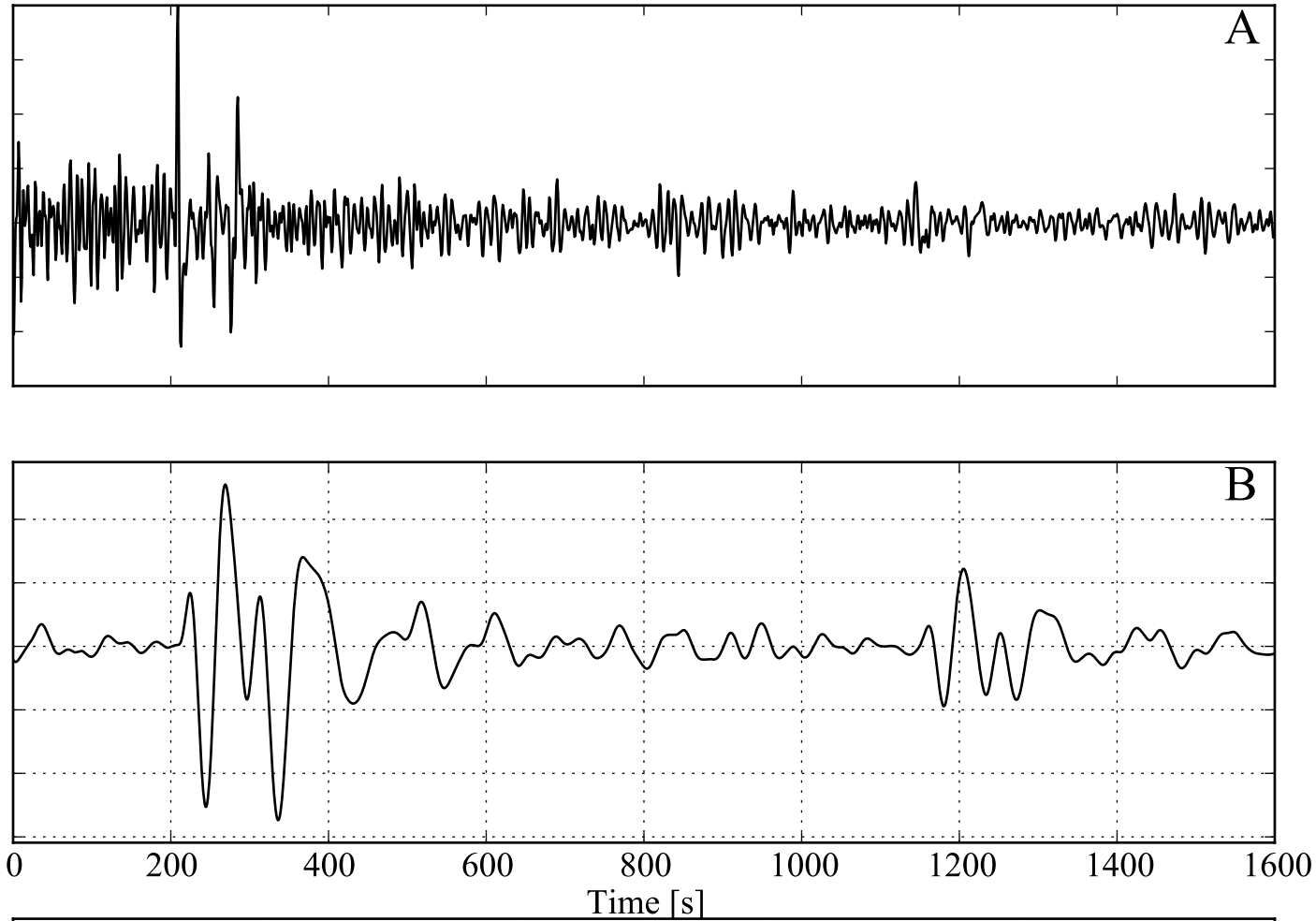
E

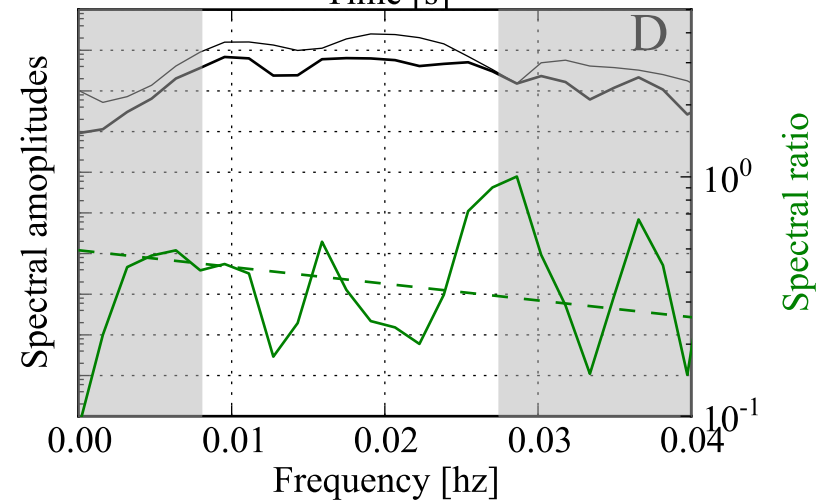
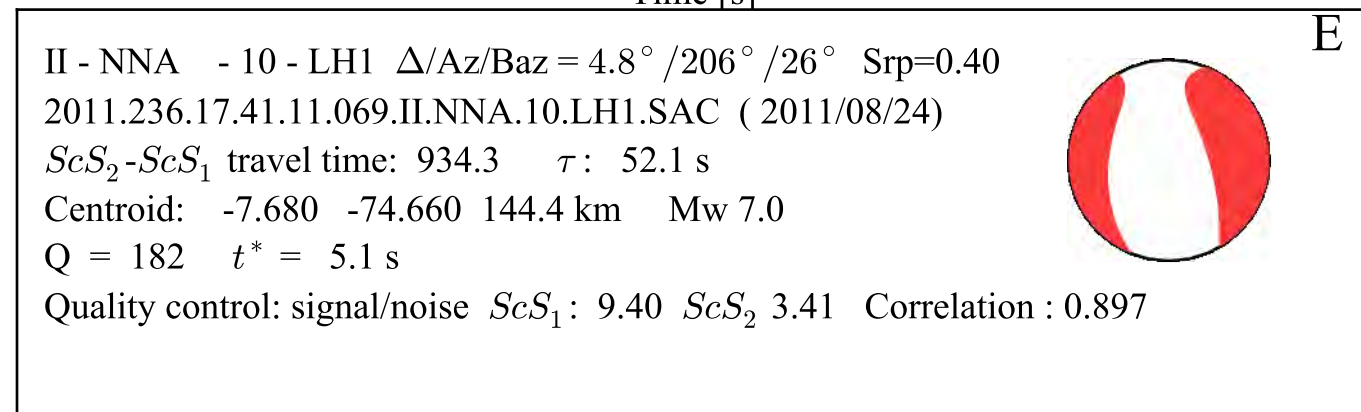
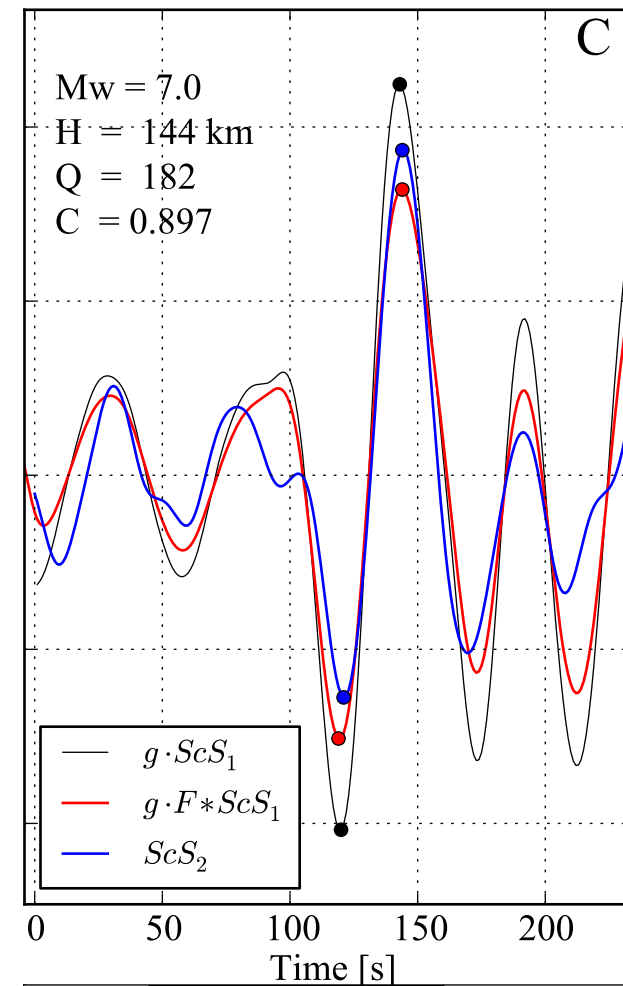
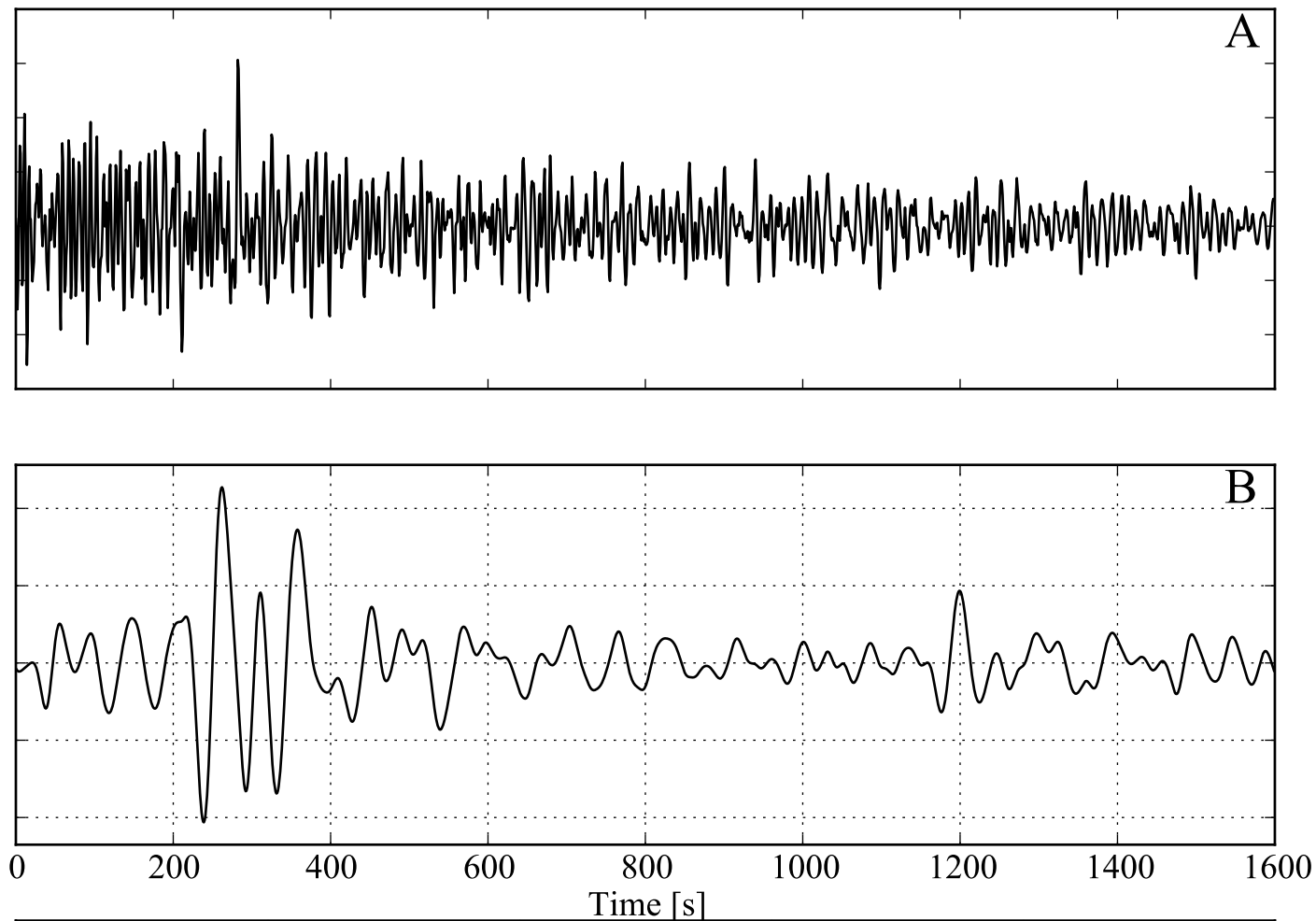
II - NIL - 00 - LHN $\Delta/Az/Baz = 3.3^\circ / 141^\circ / 322^\circ$ $Srp=0.84$
 2000.199.22.48.47.285.II.NIL.00.LHN.SAC (2000/07/17)
 ScS_2-ScS_1 travel time: 935.1 τ : 43.4 s
 Centroid: 36.240 70.820 145.5 km Mw 6.3
 $Q = 272$ $t^* = 3.4$ s
 Quality control: signal/noise ScS_1 : 8.58 ScS_2 3.23 Correlation : 0.814

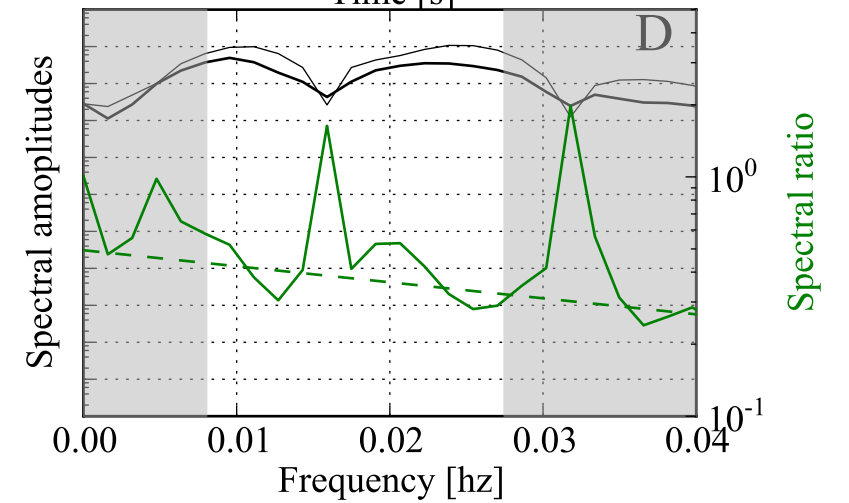
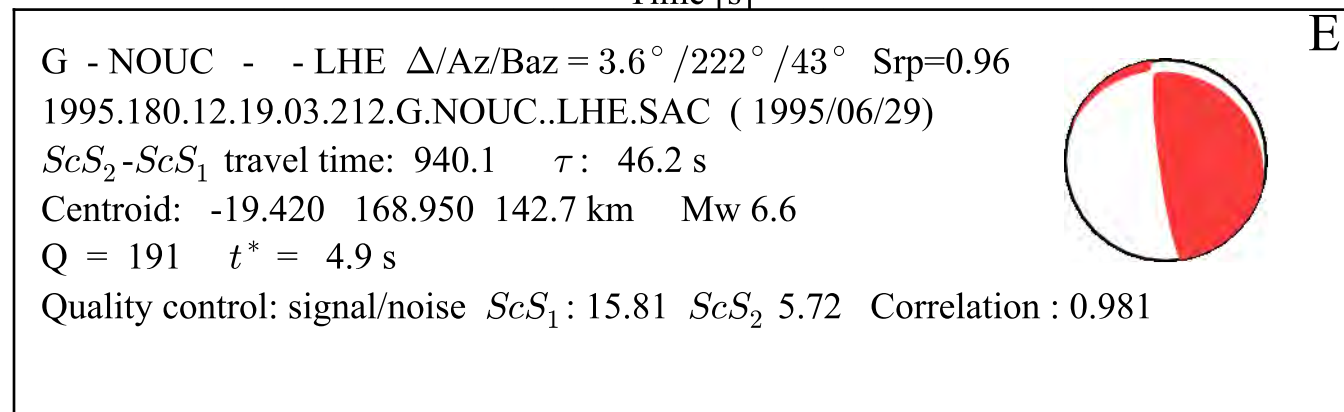
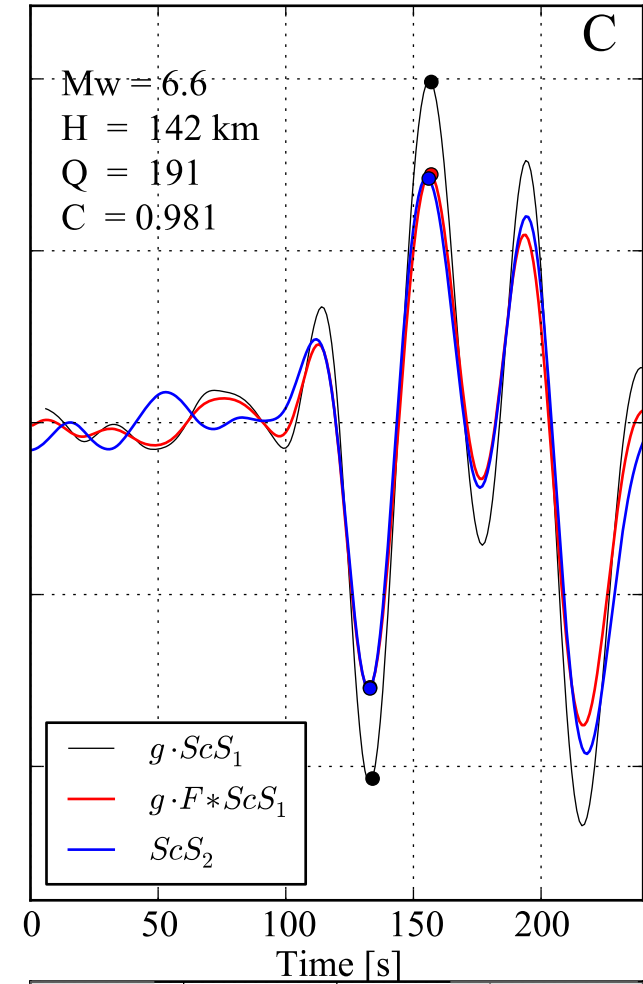
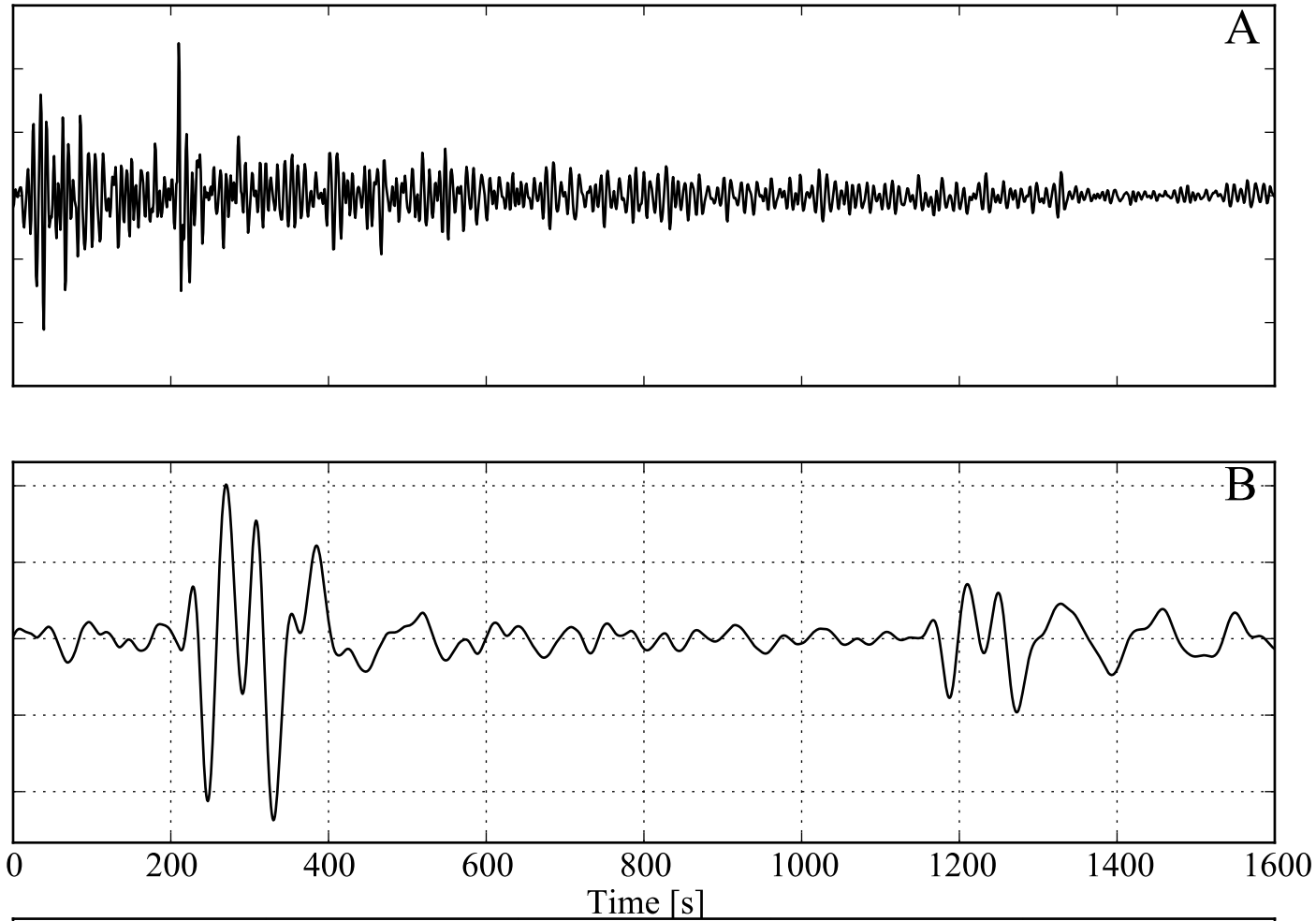


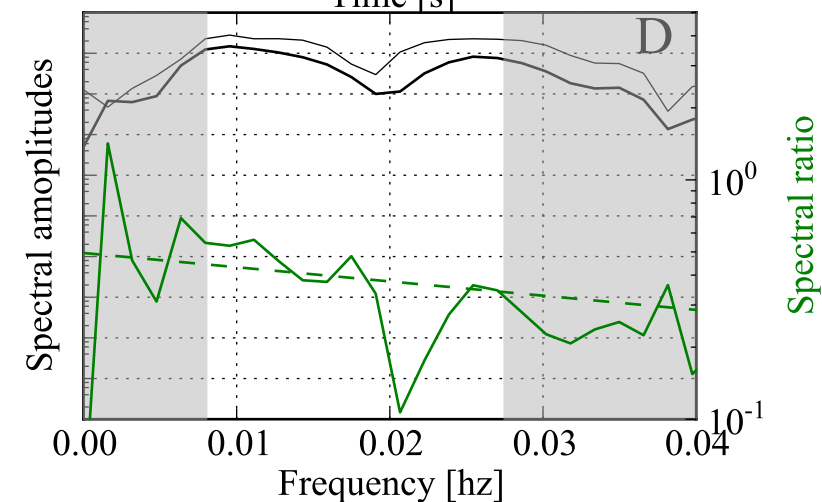
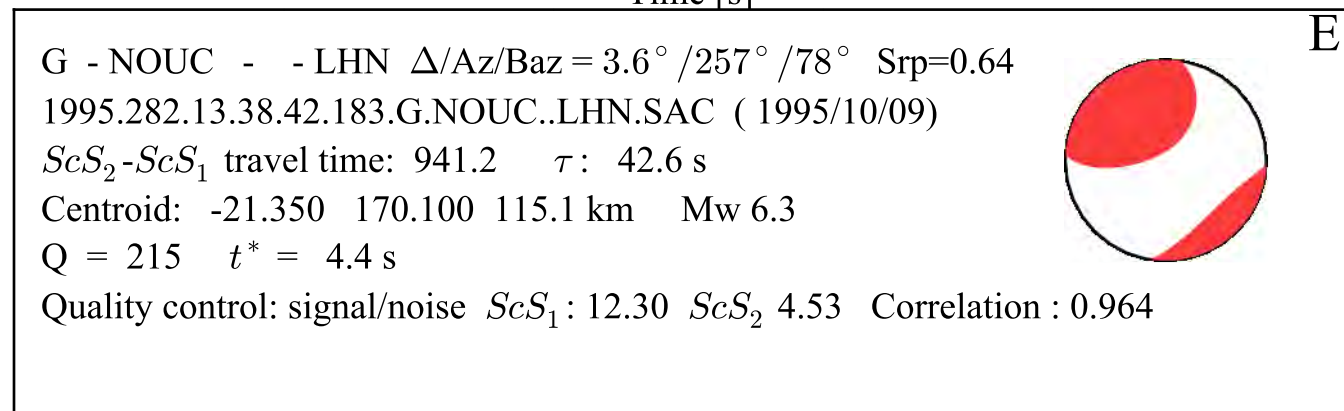
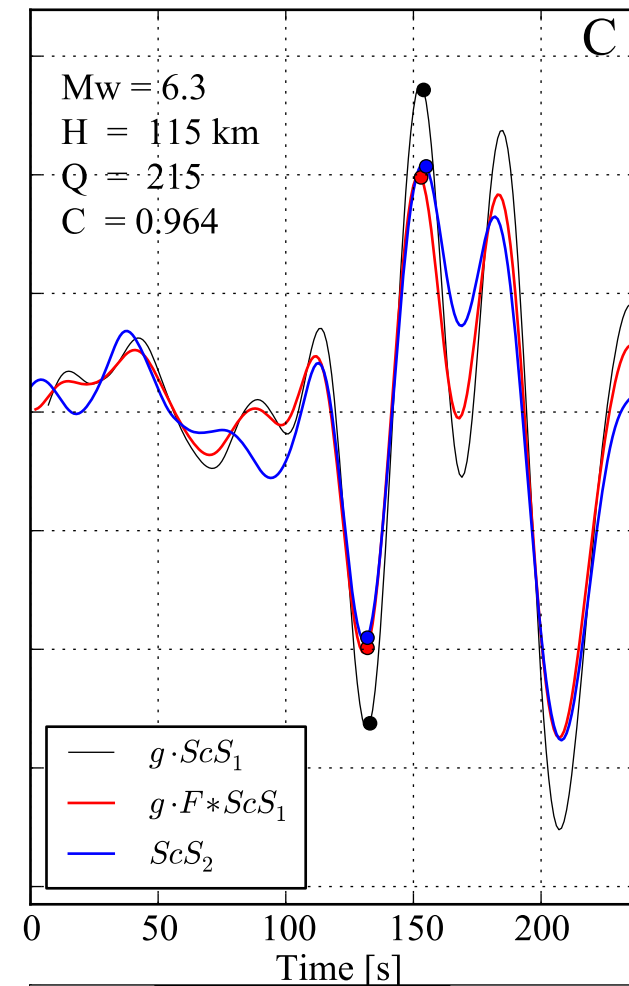
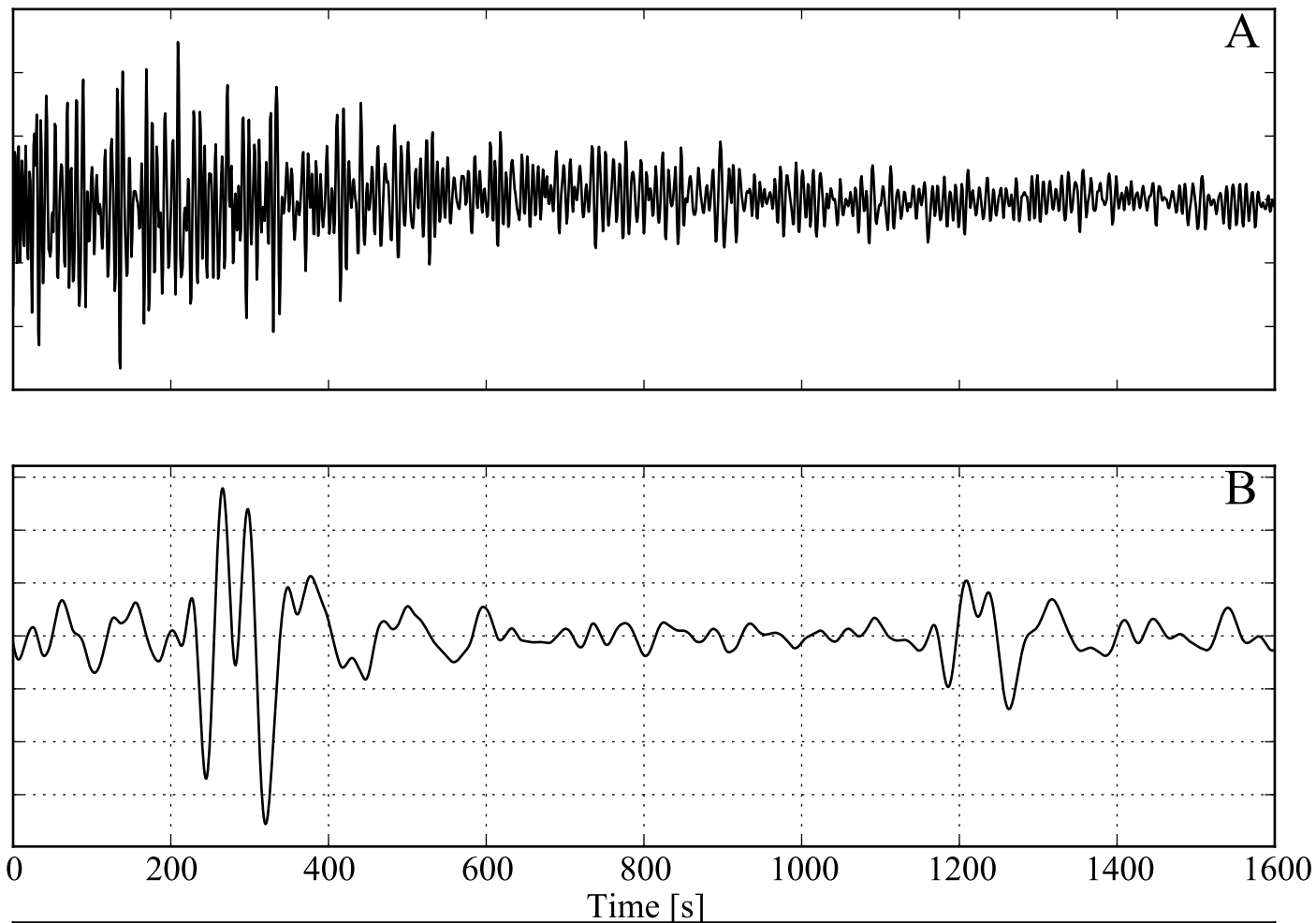


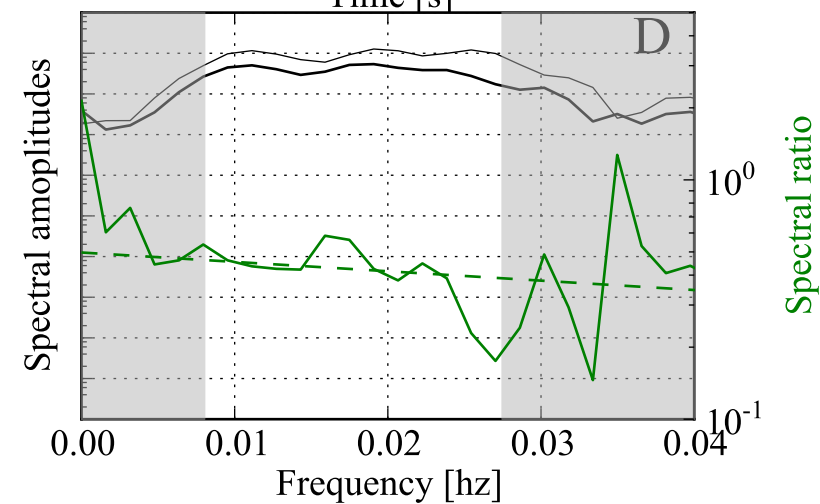
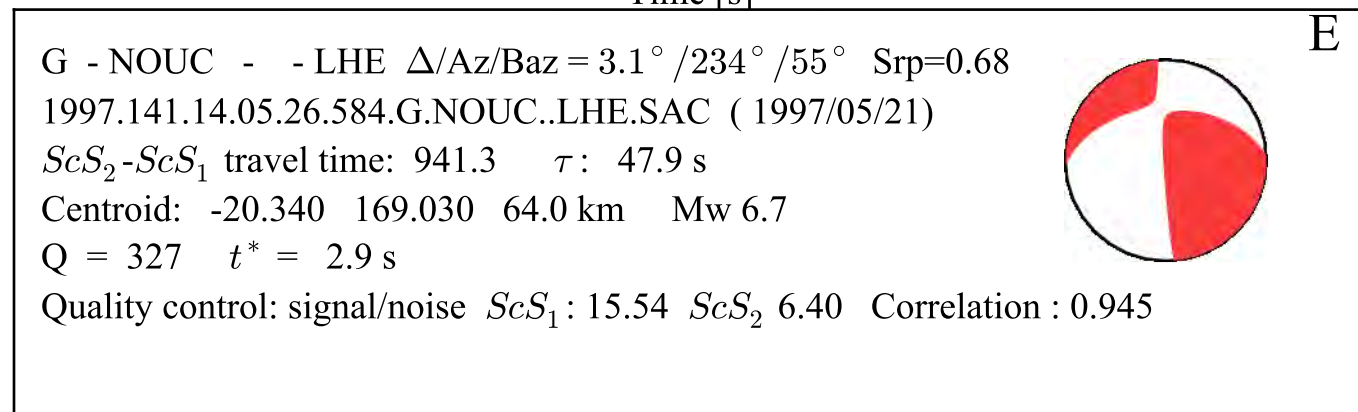
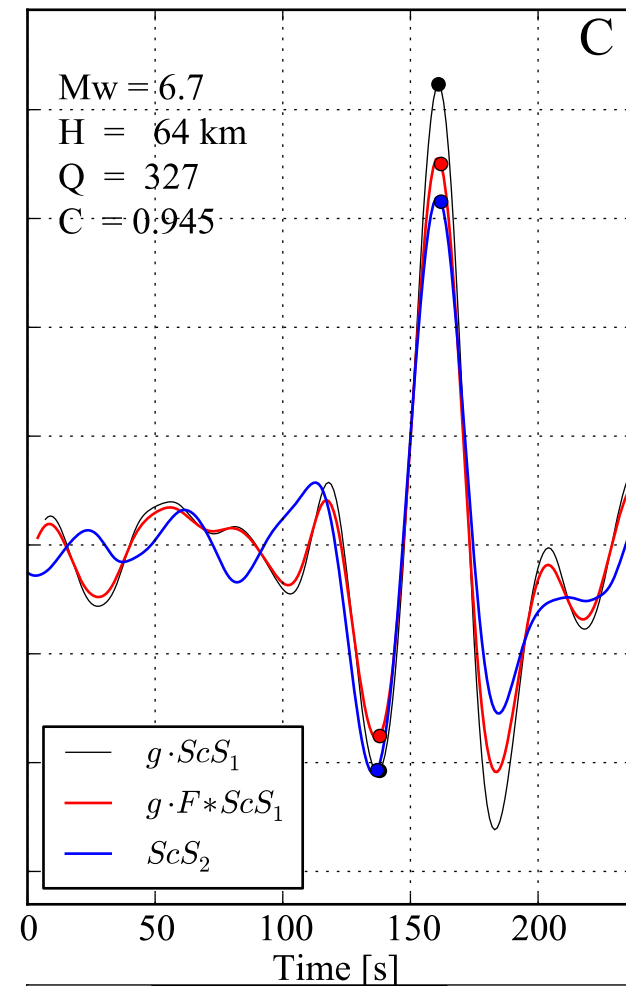
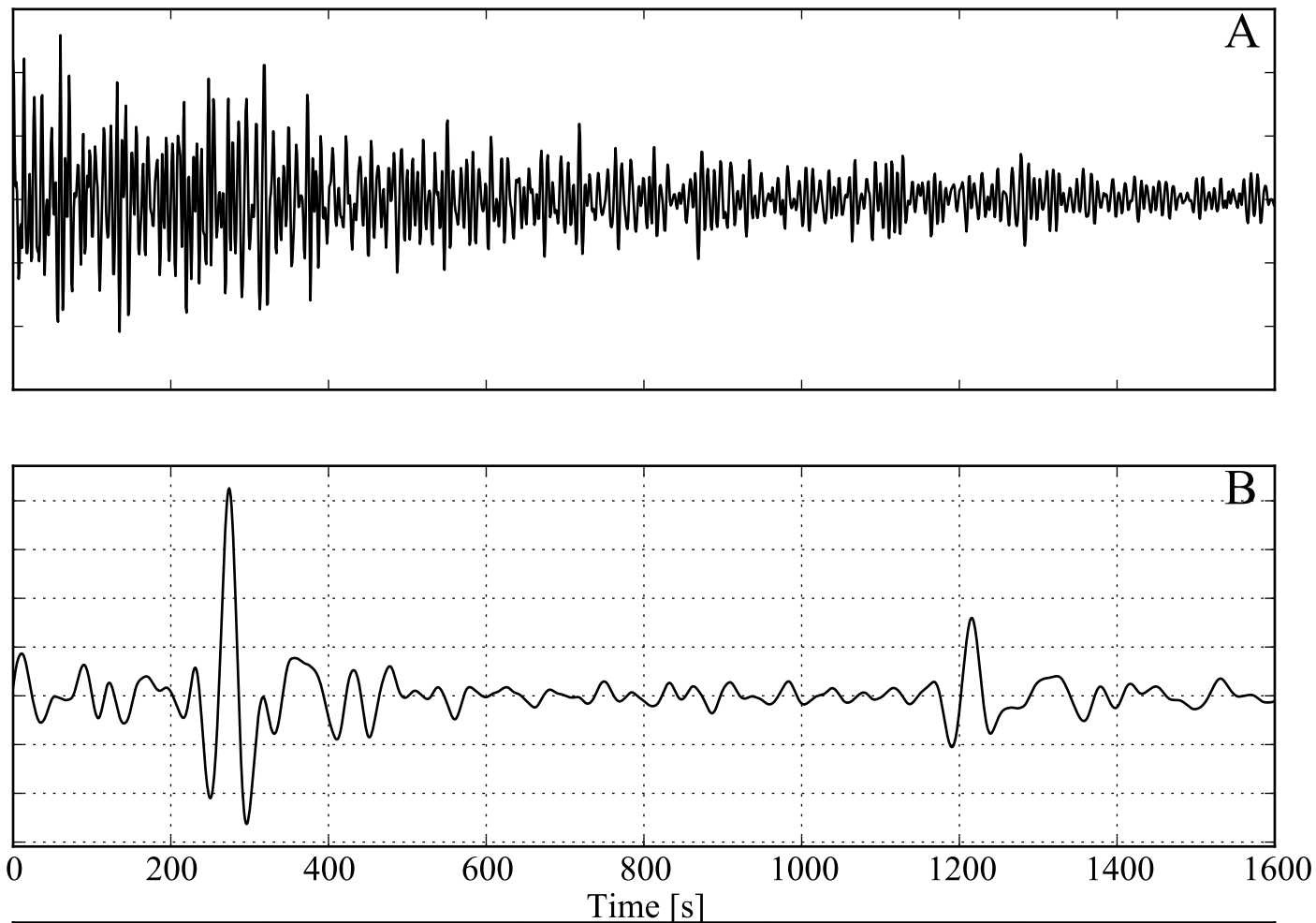


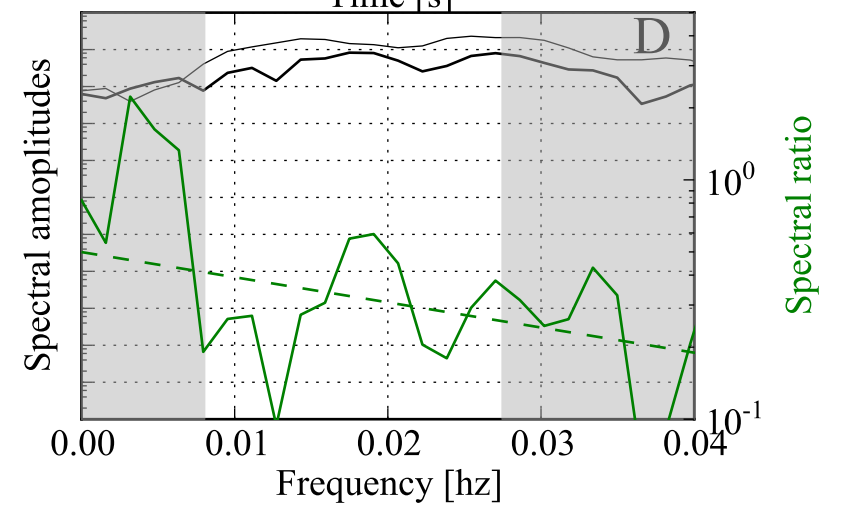
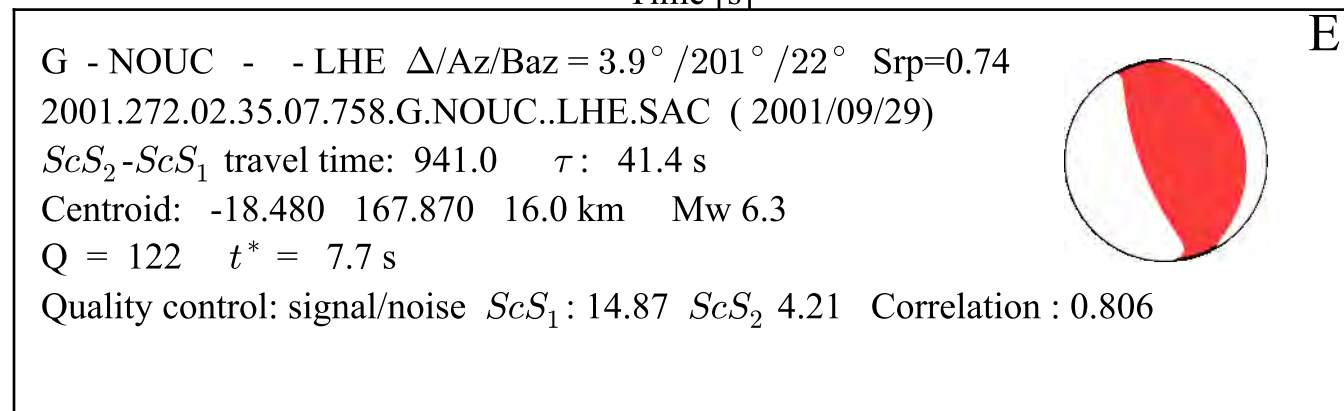
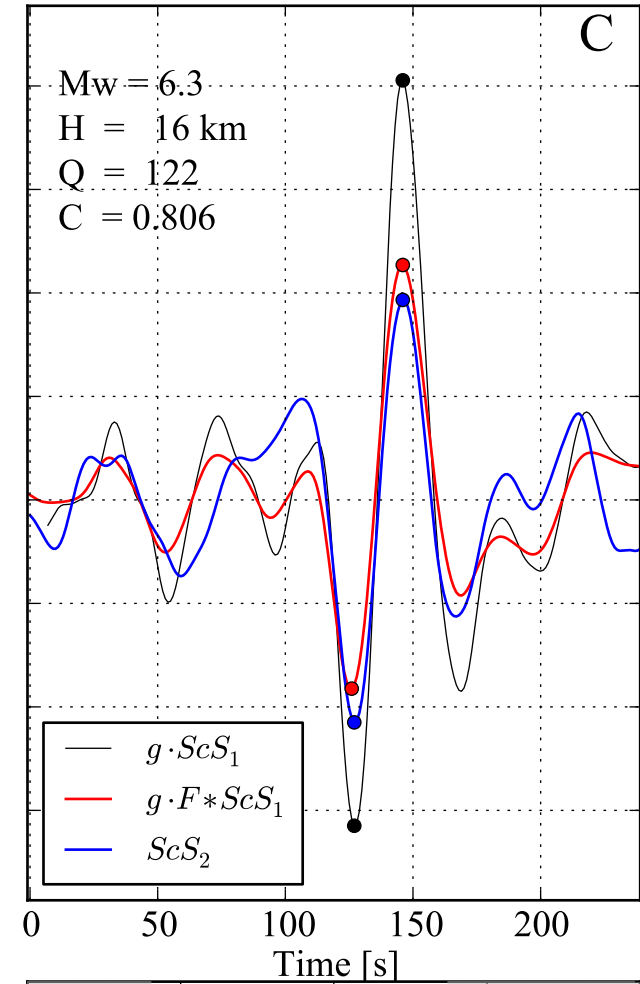
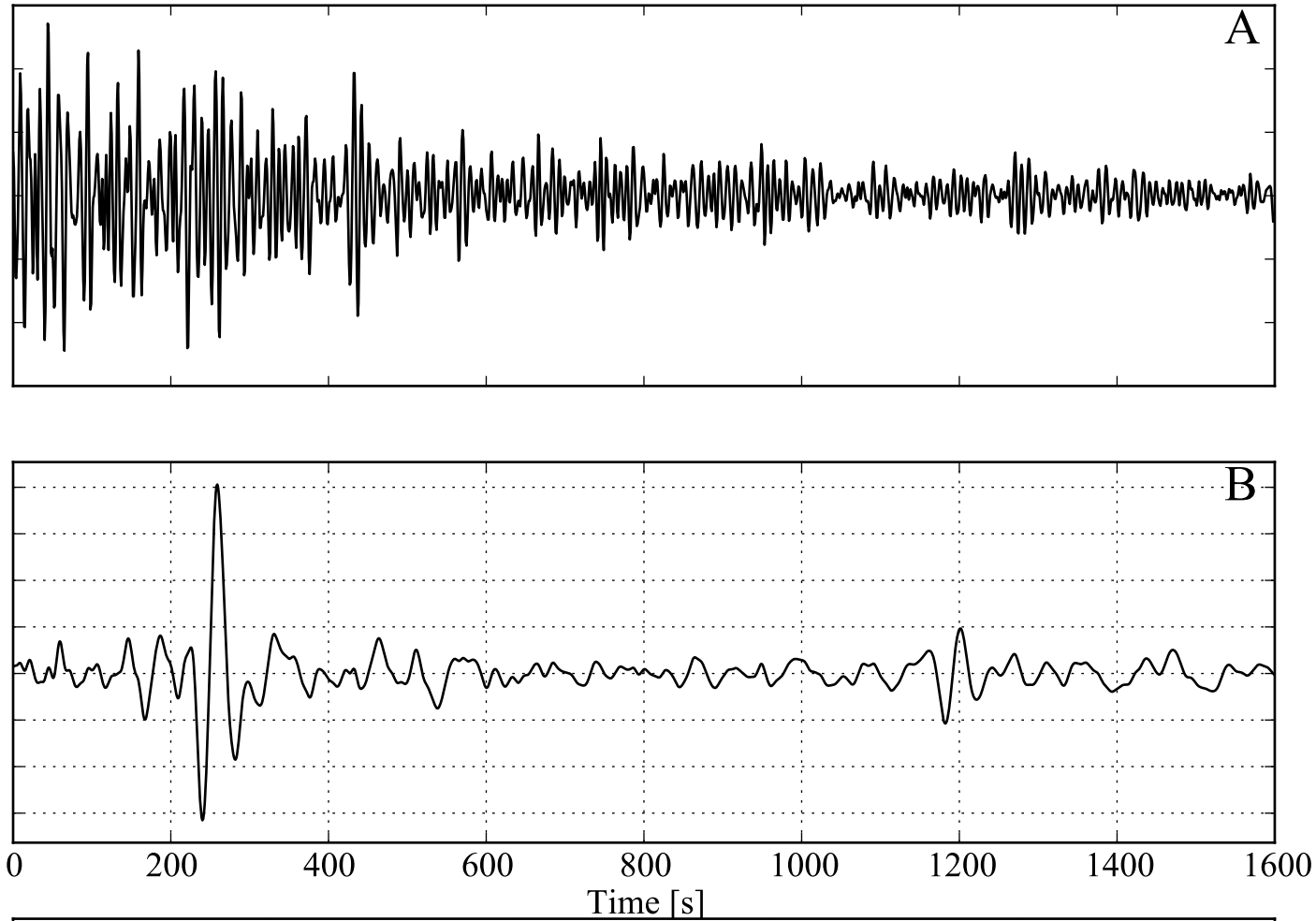


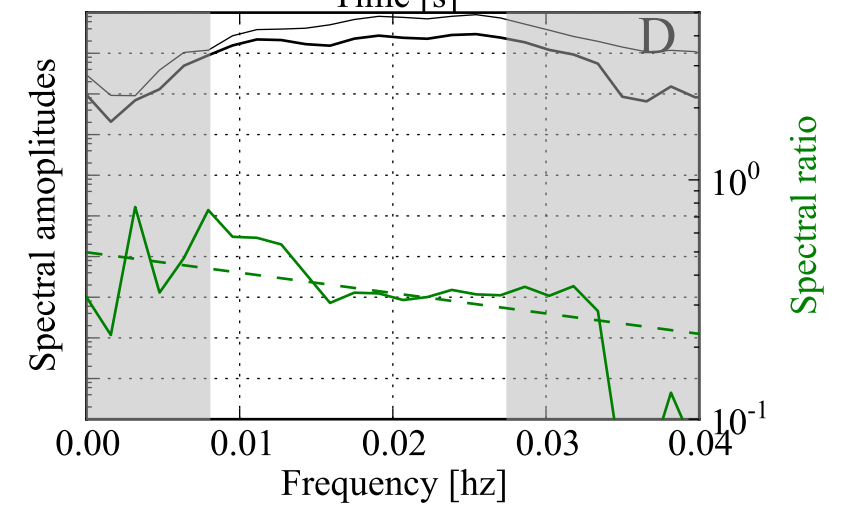
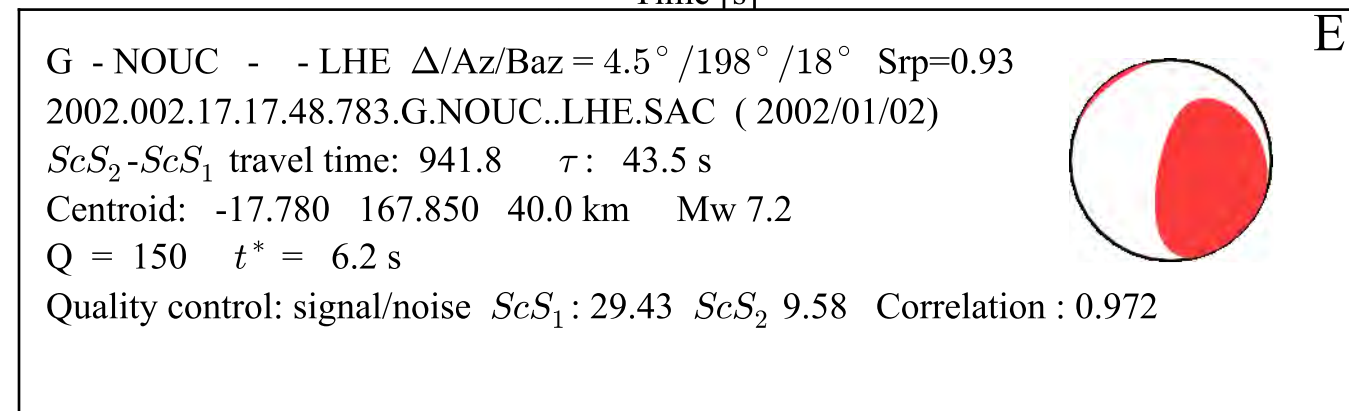
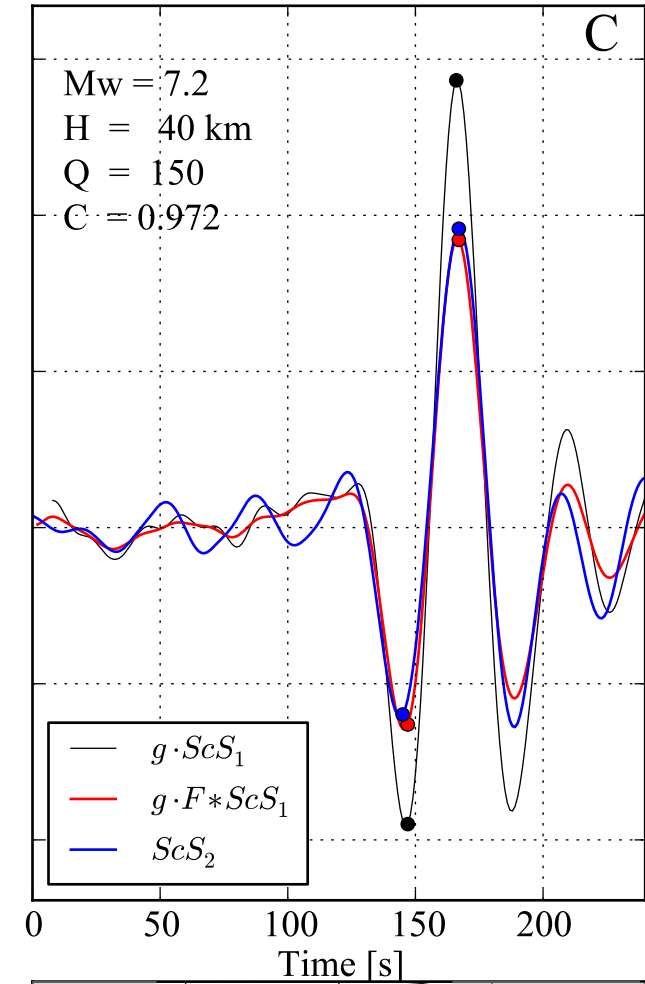
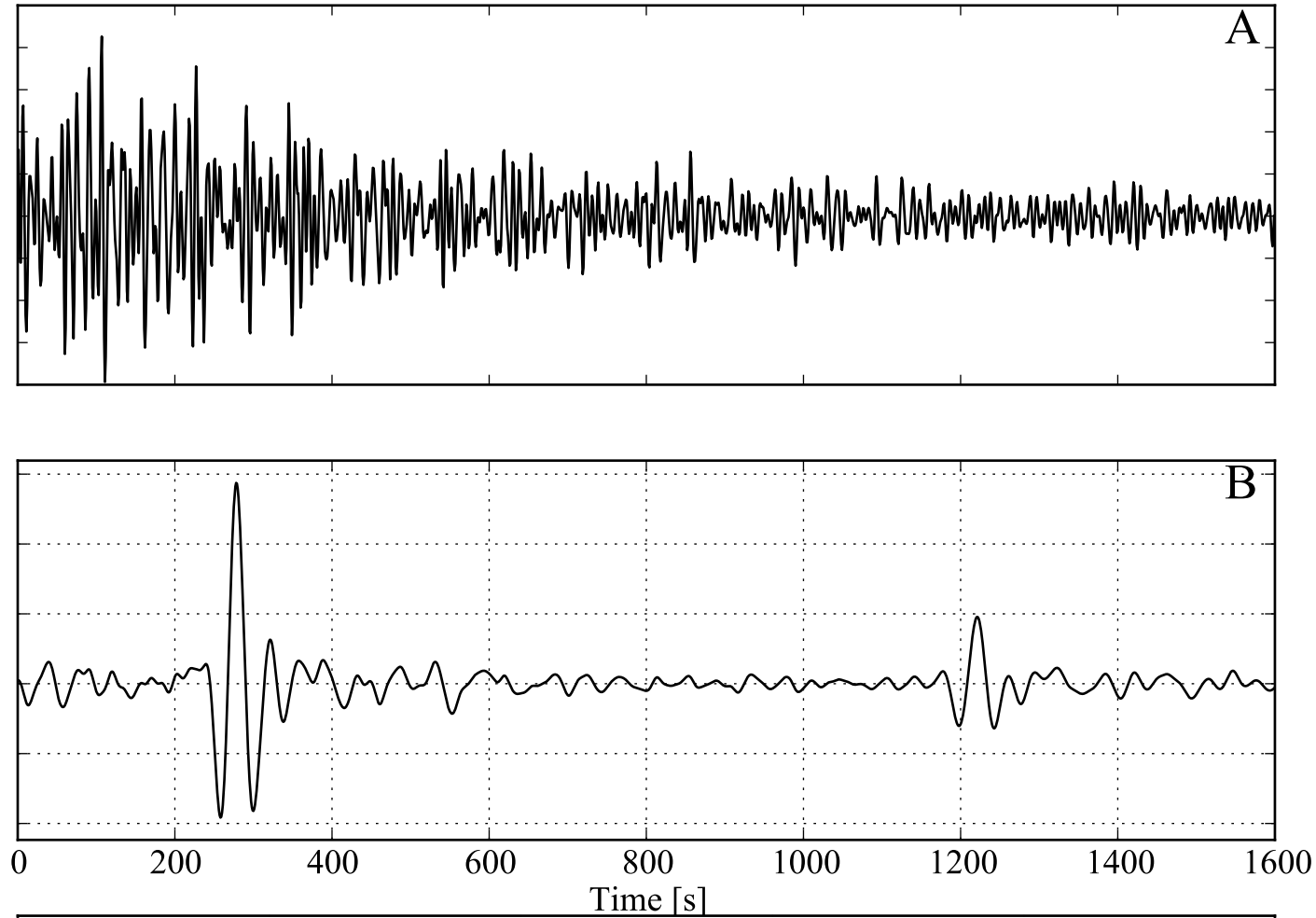


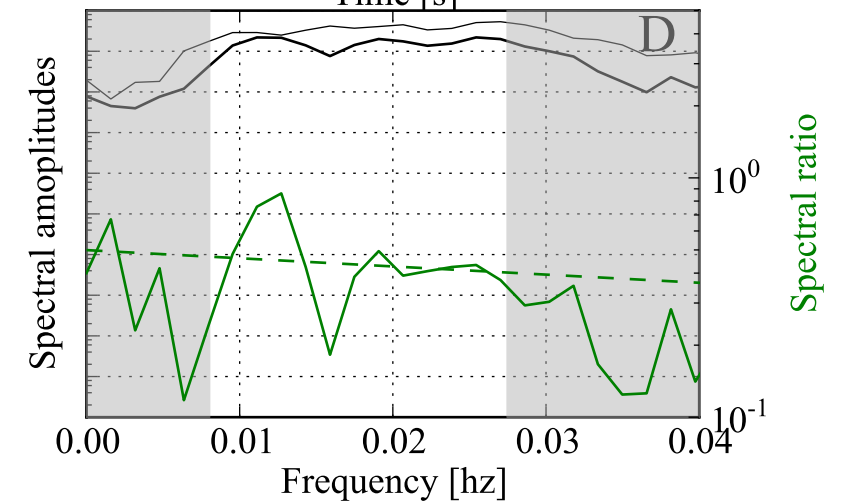
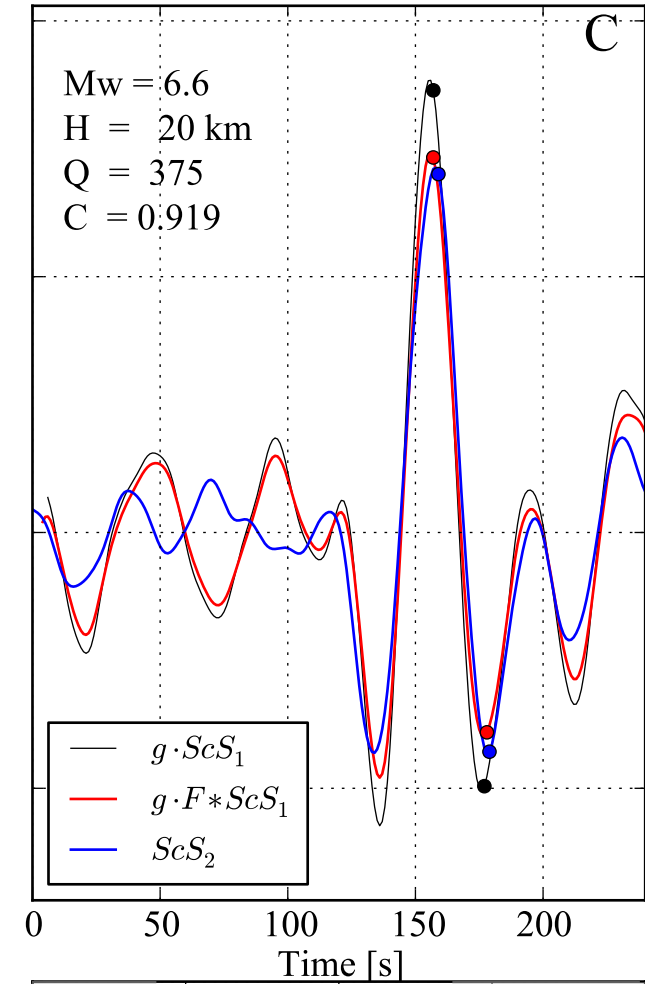
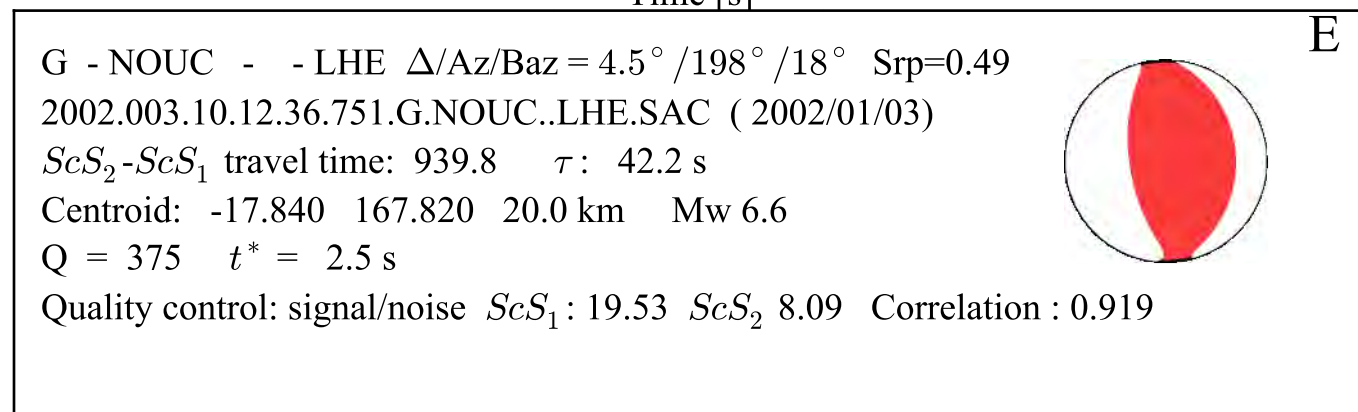
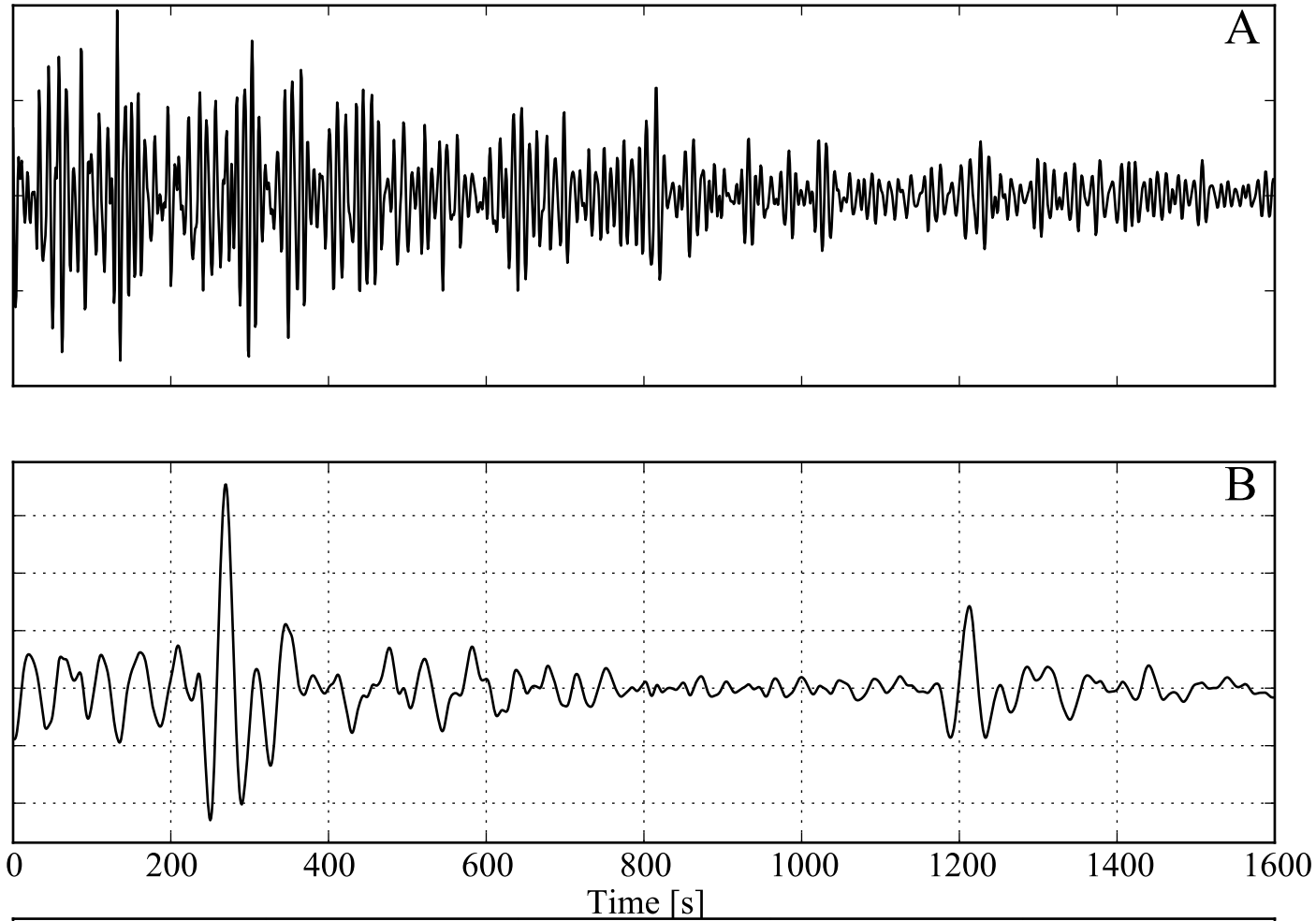


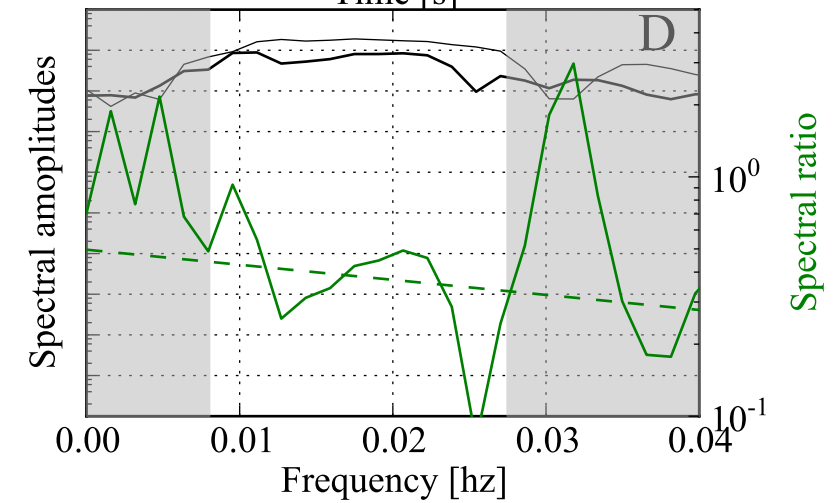
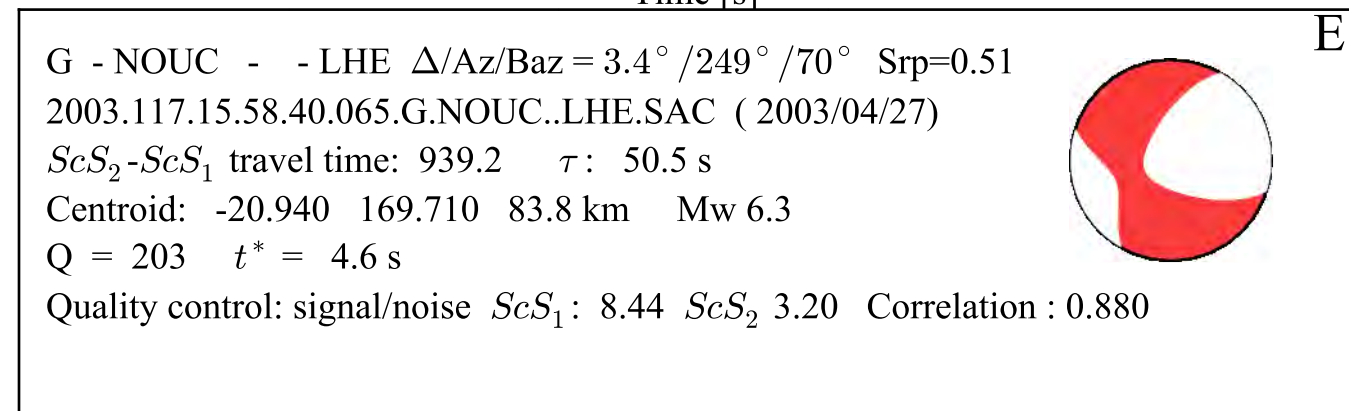
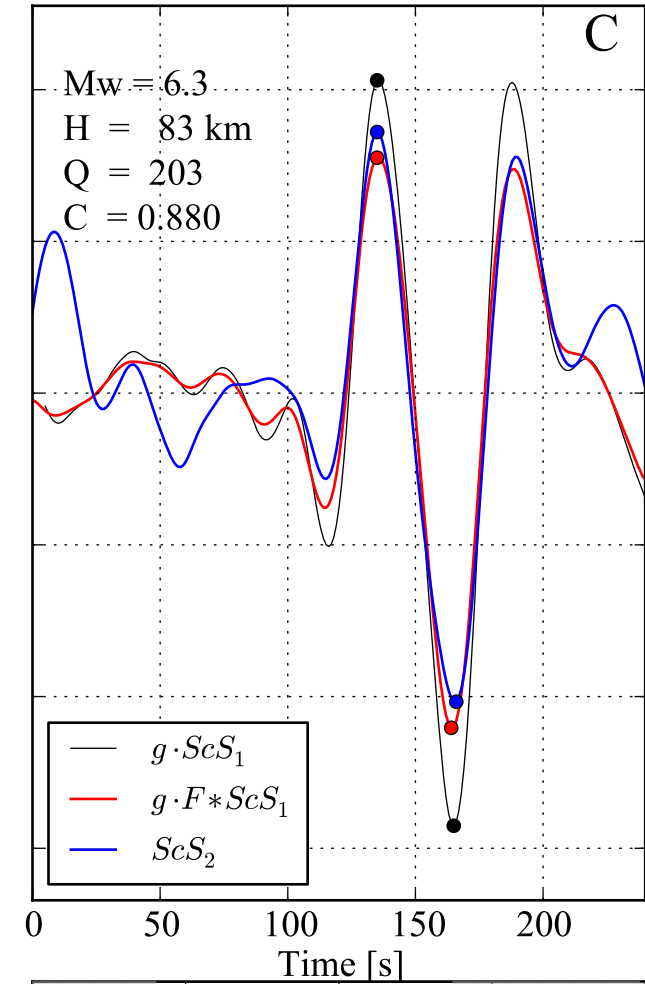
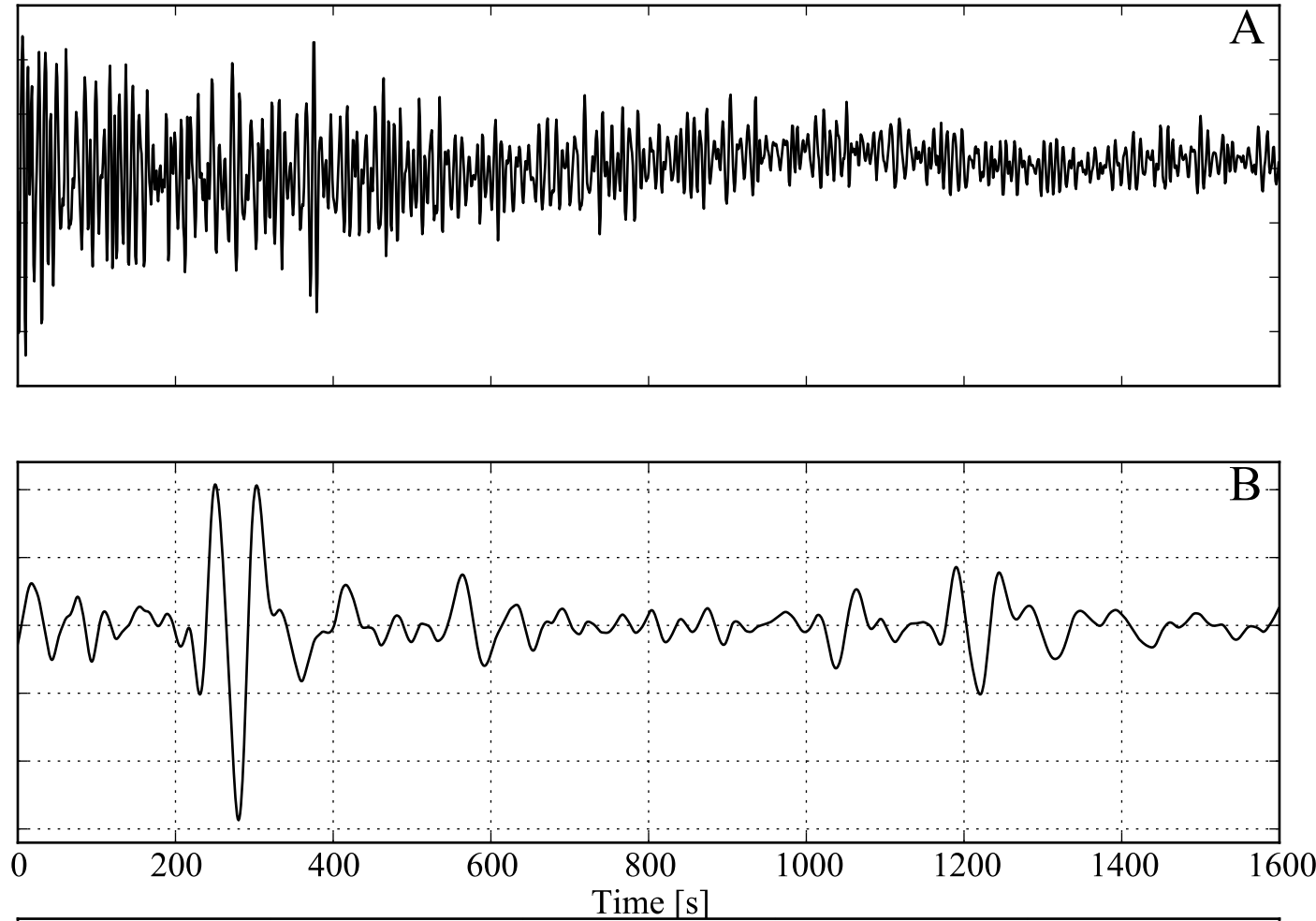


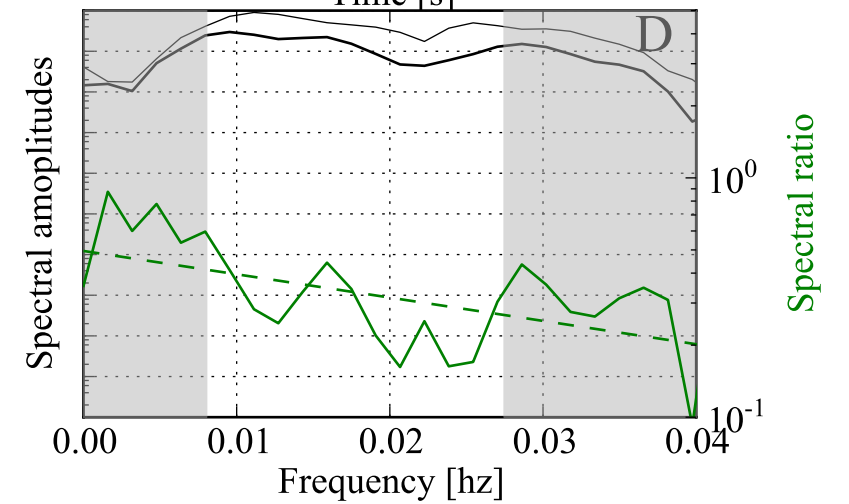
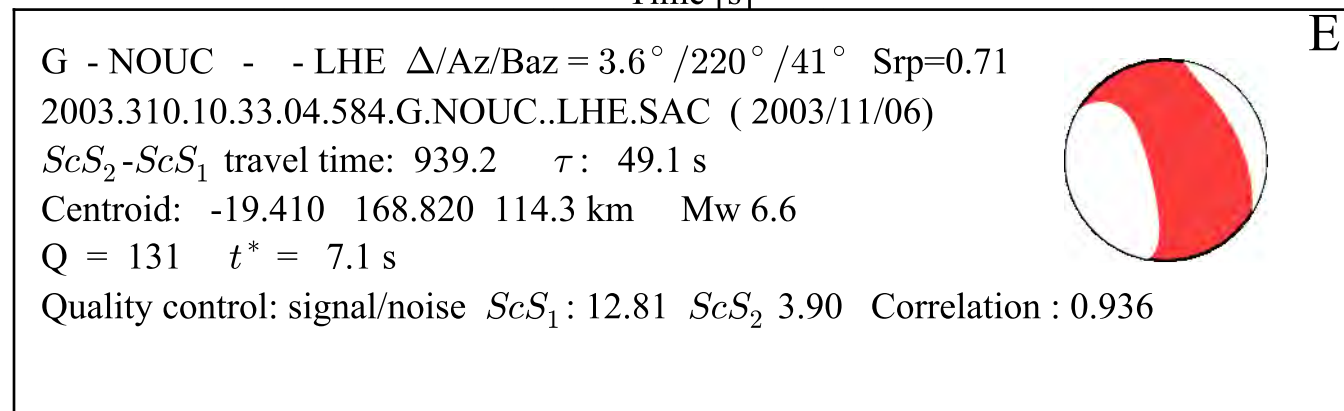
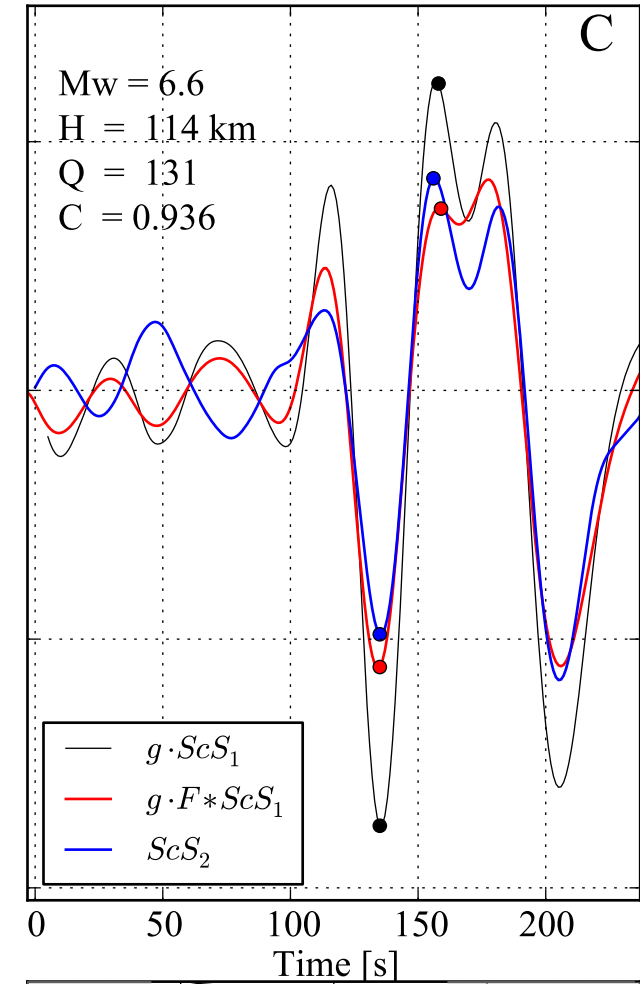
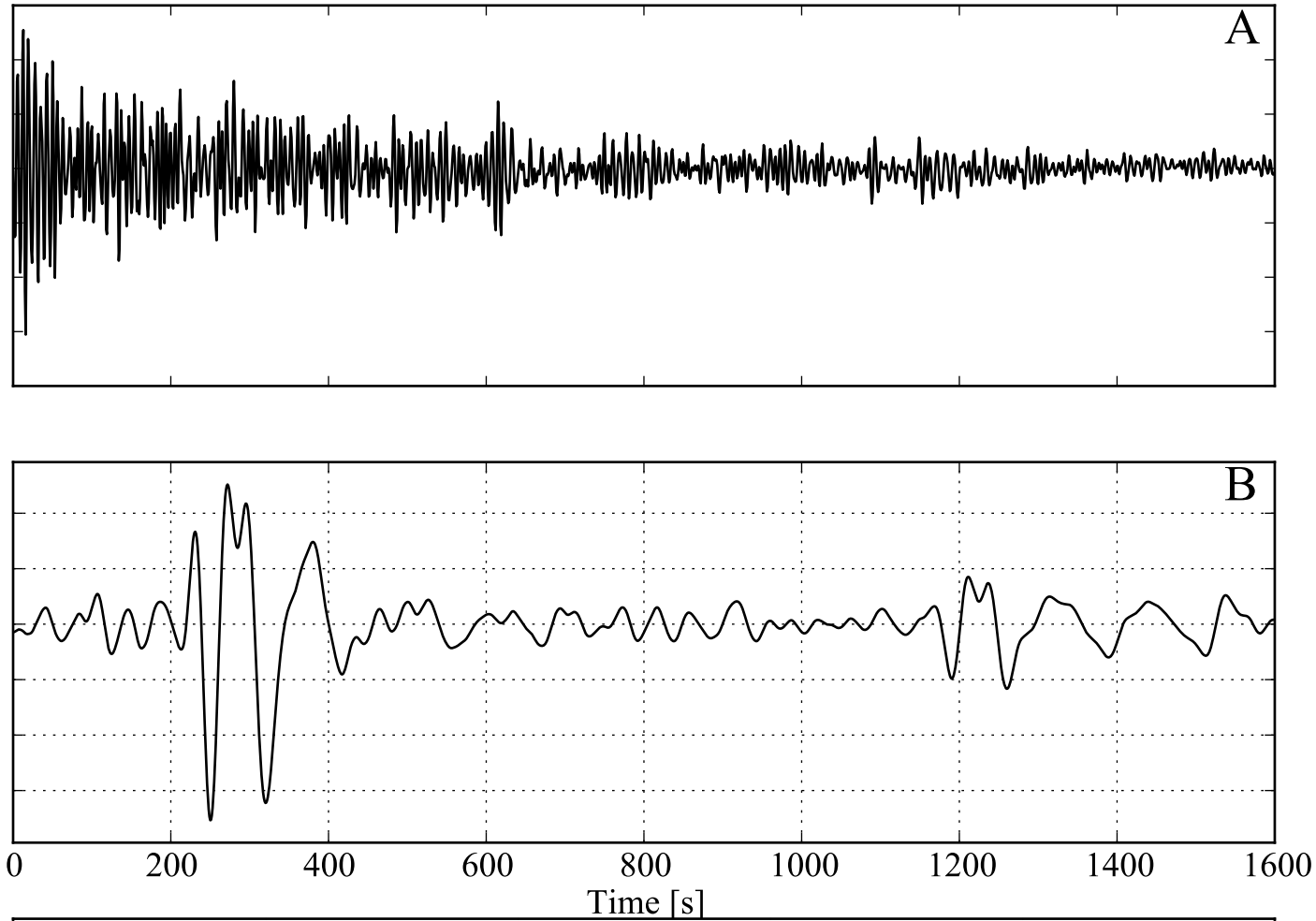


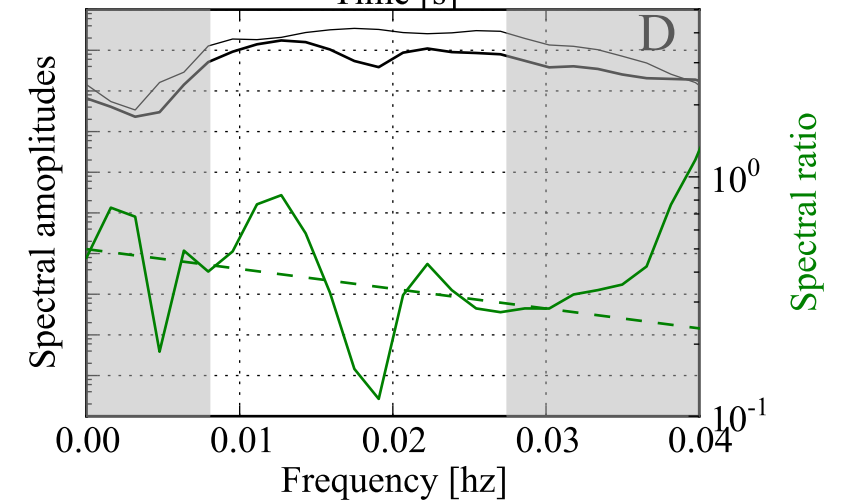
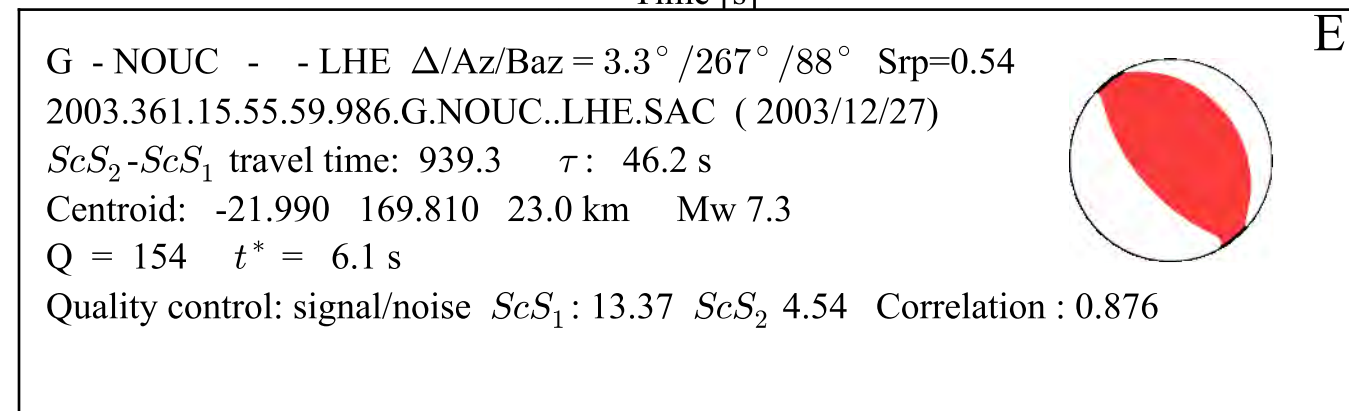
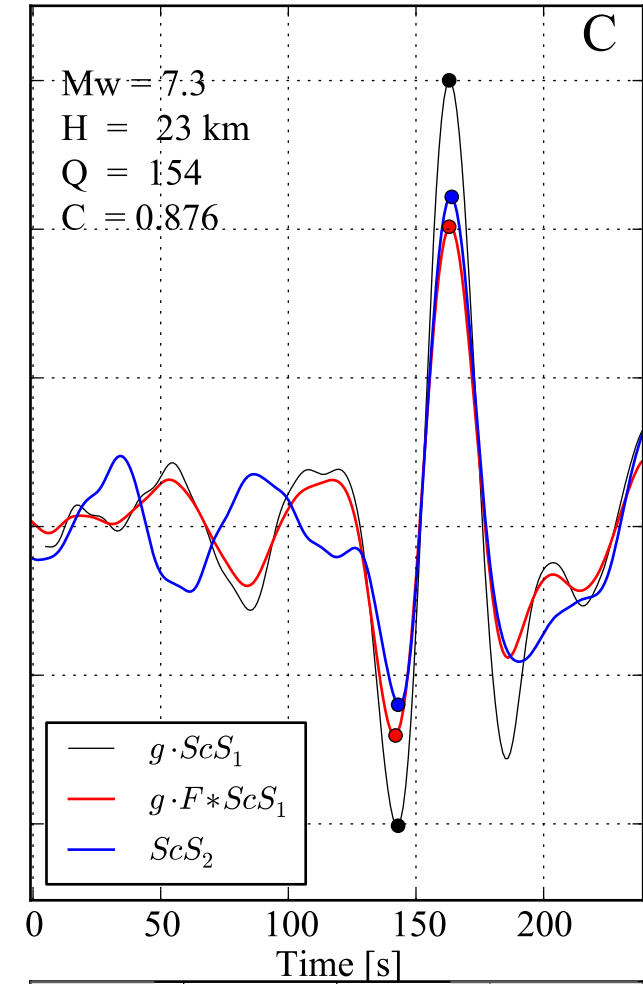
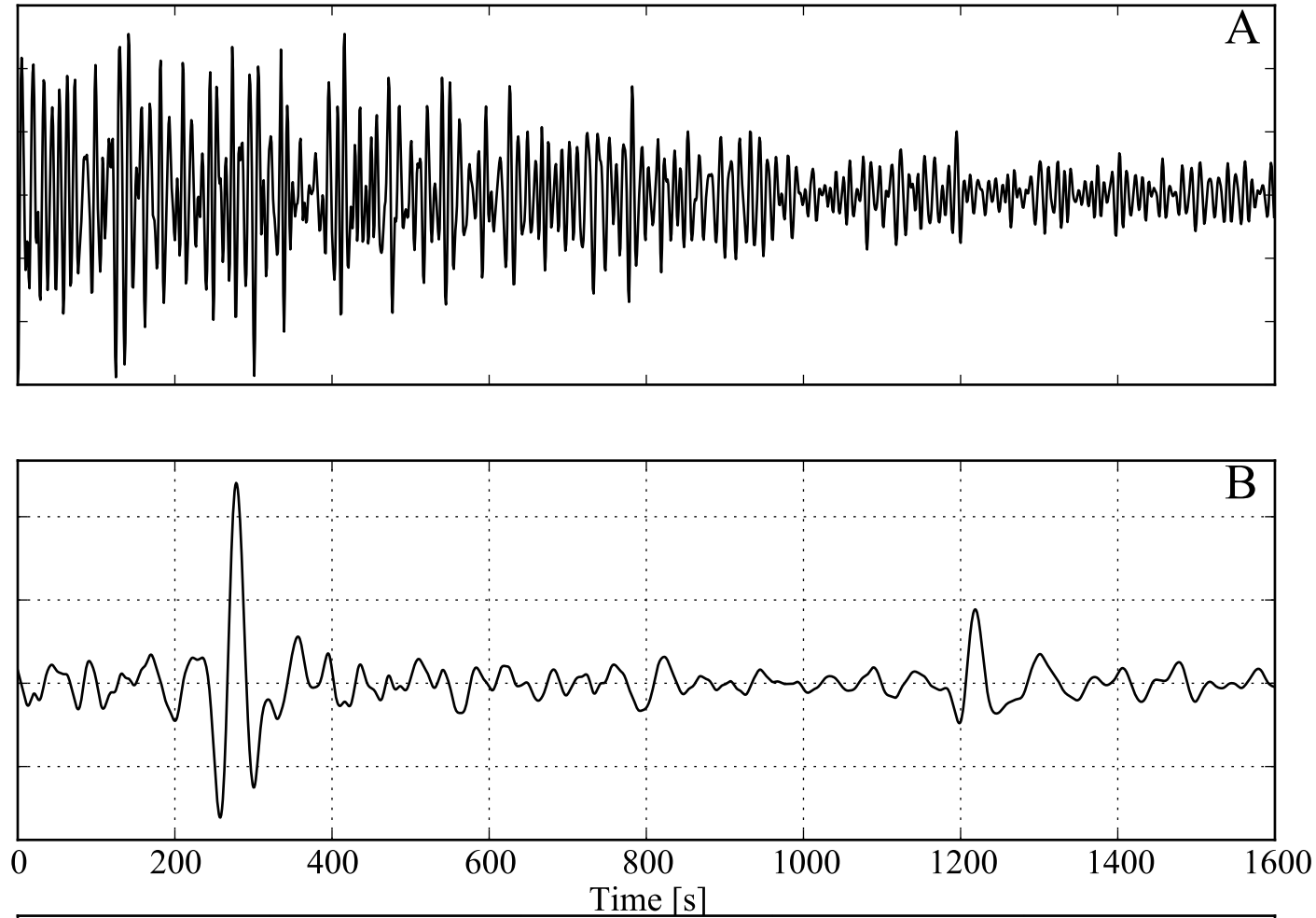


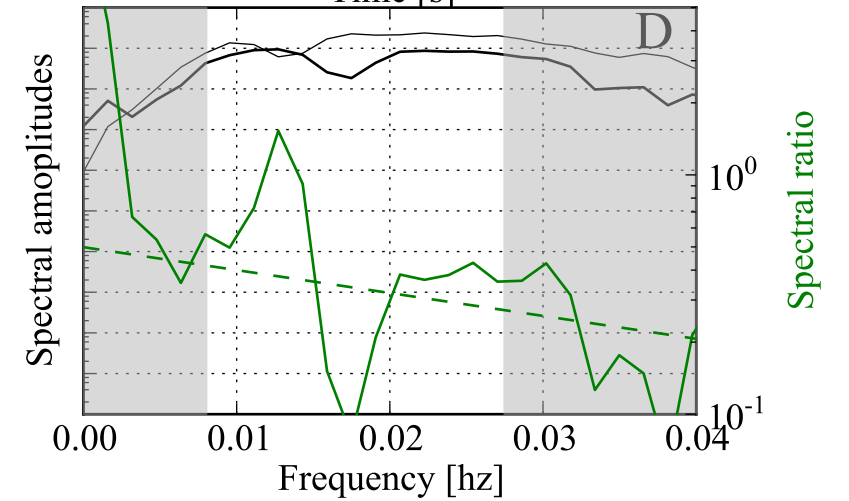
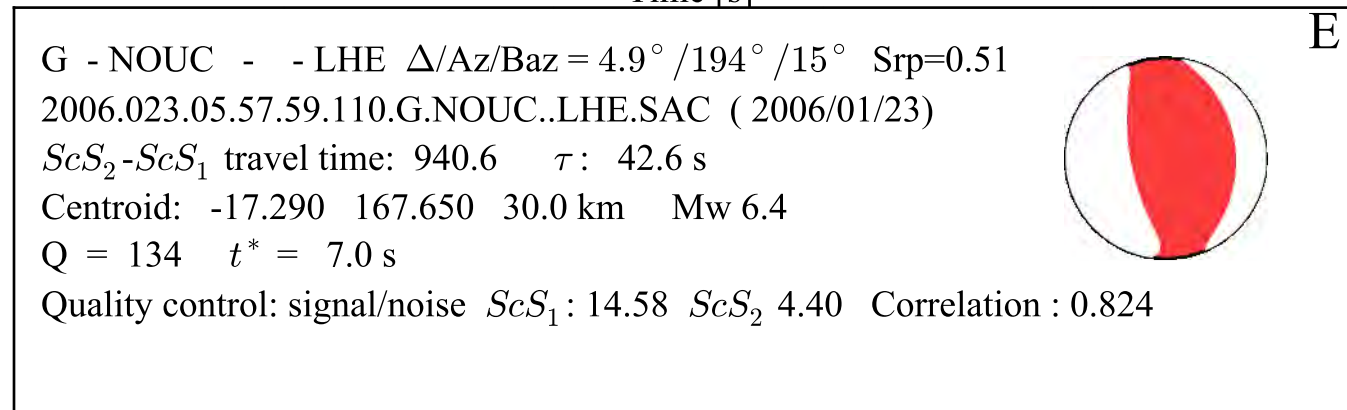
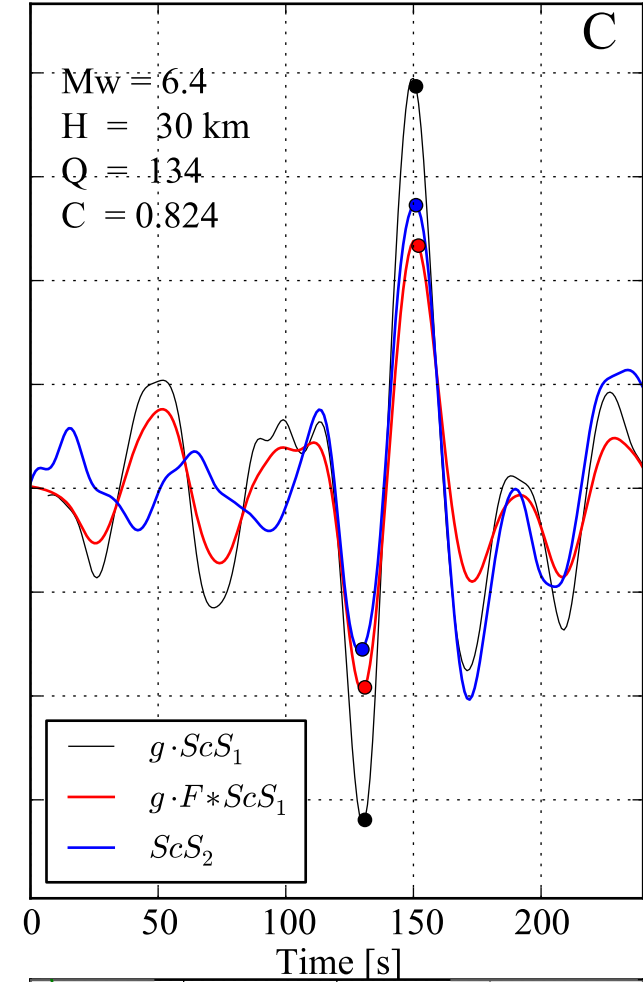
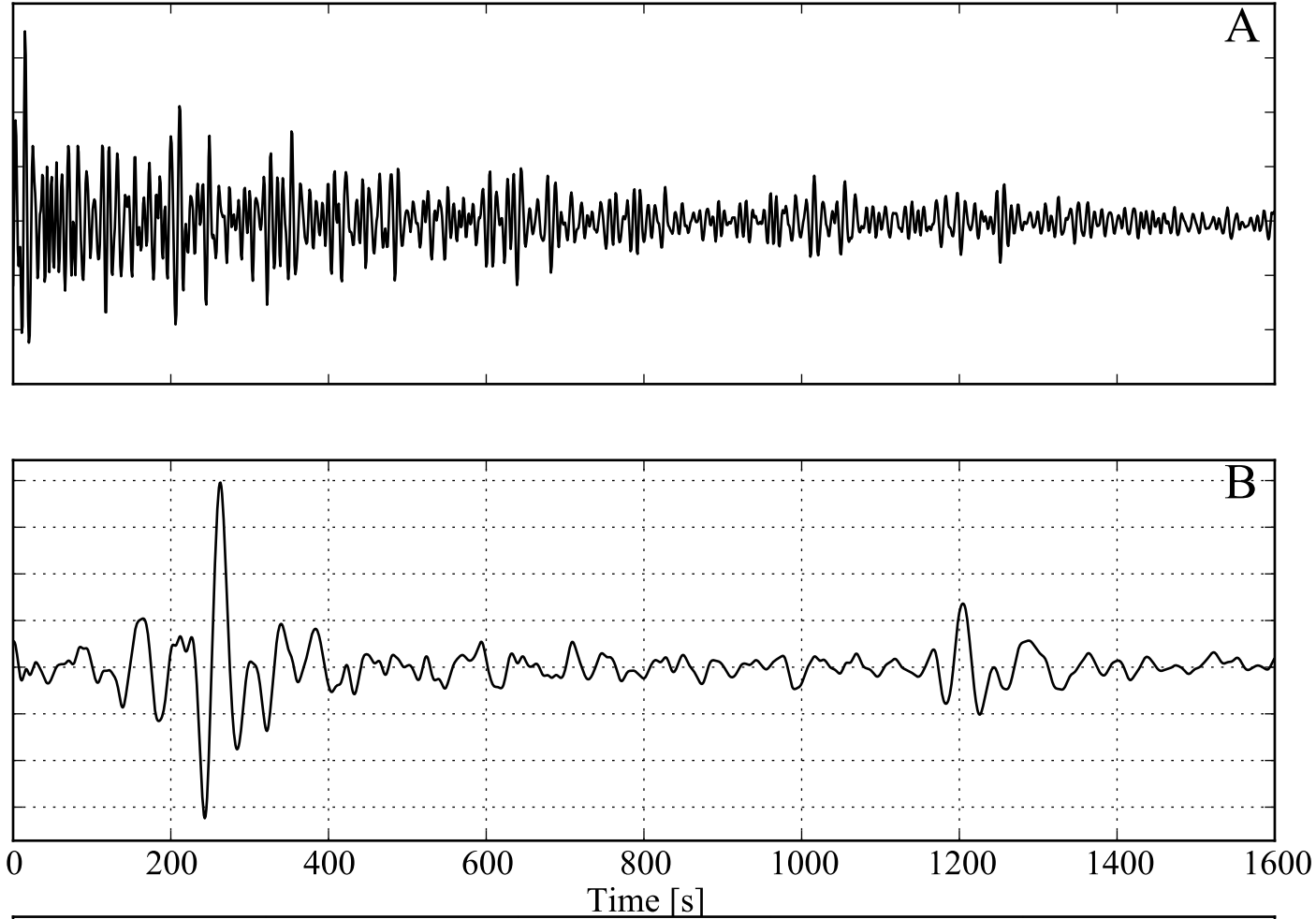


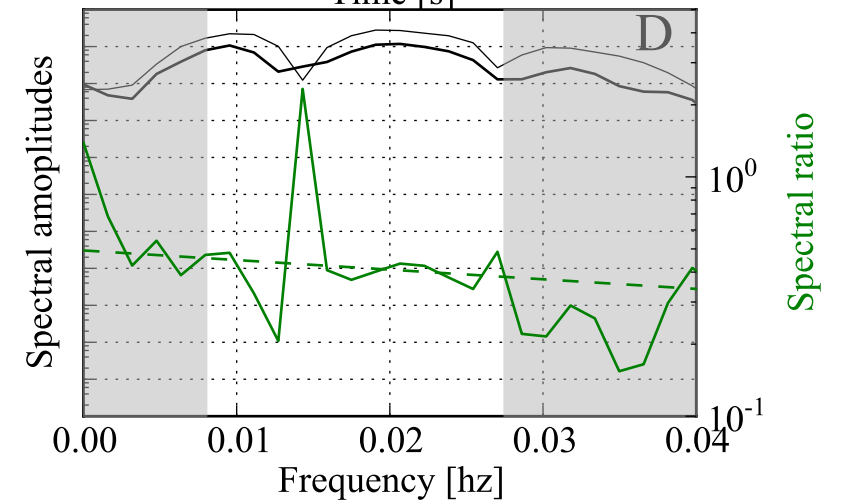
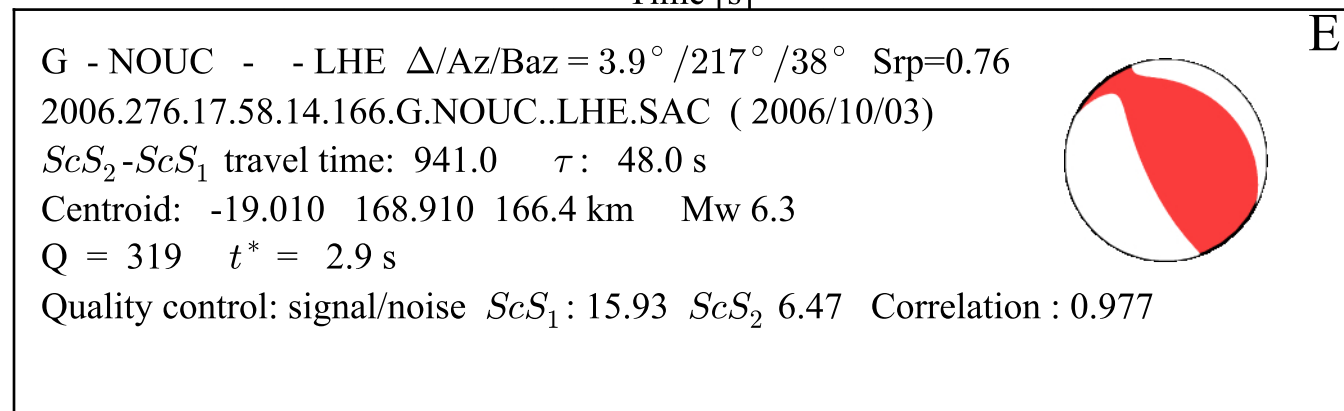
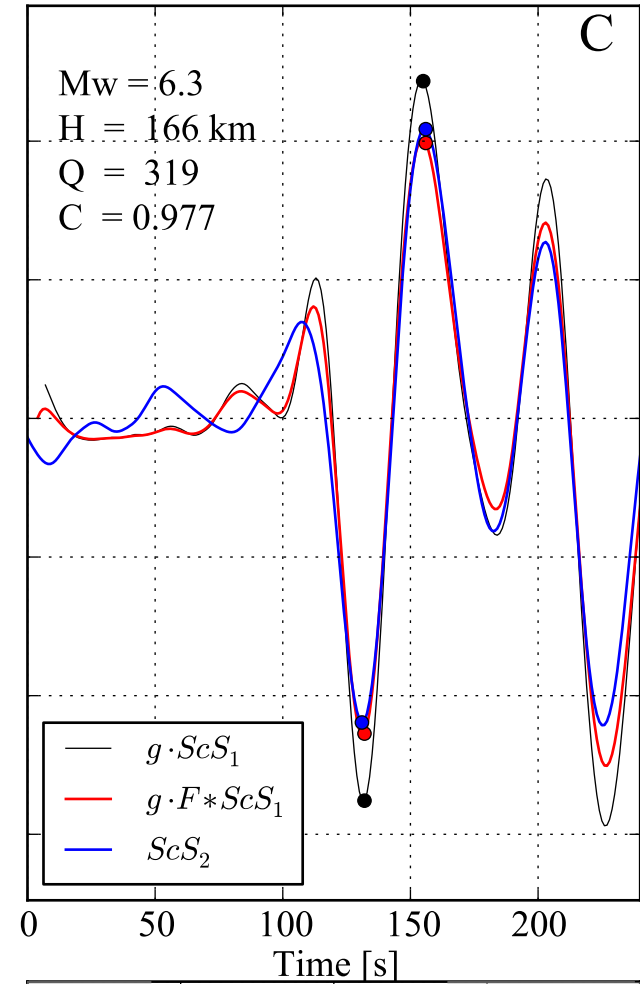
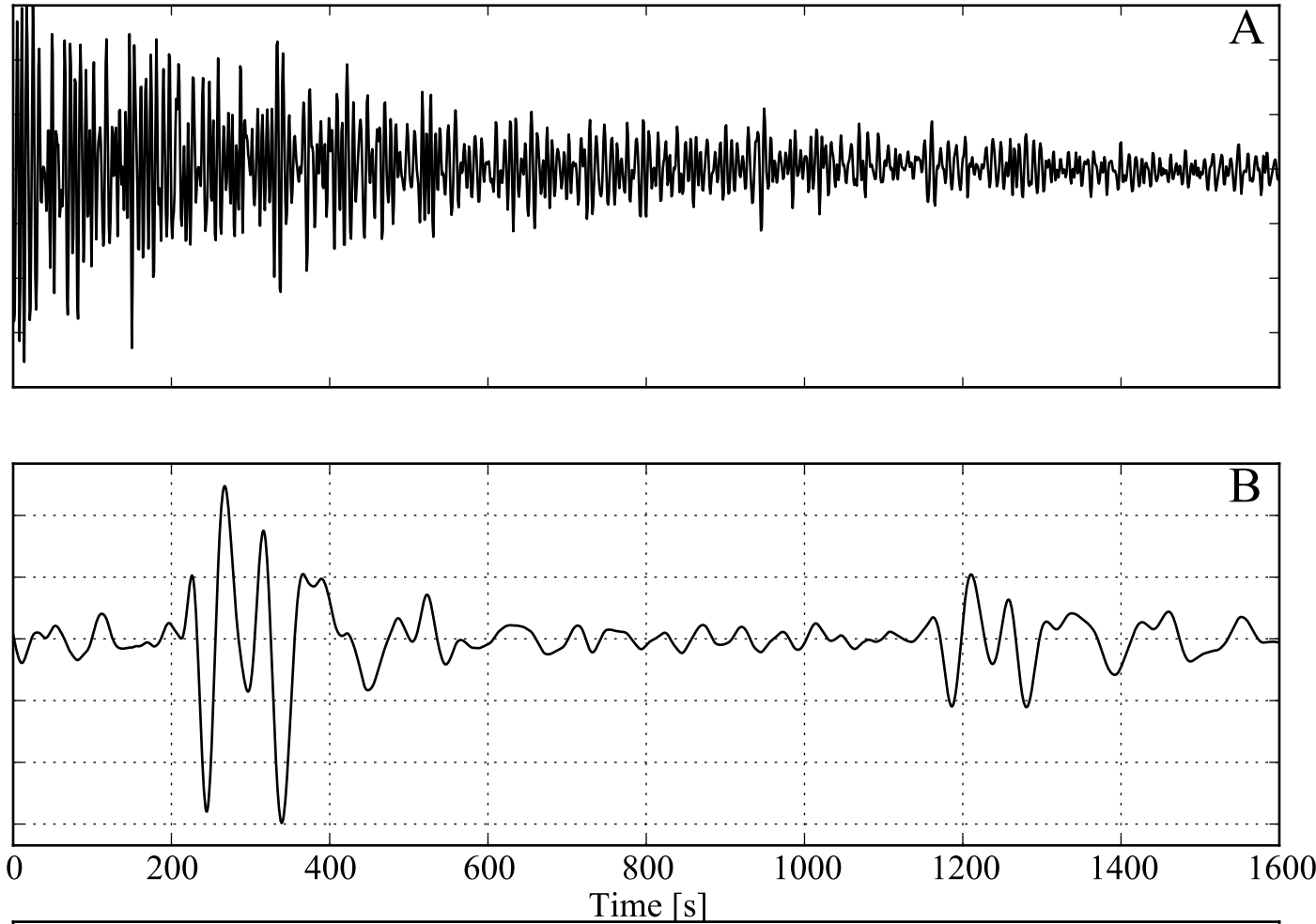


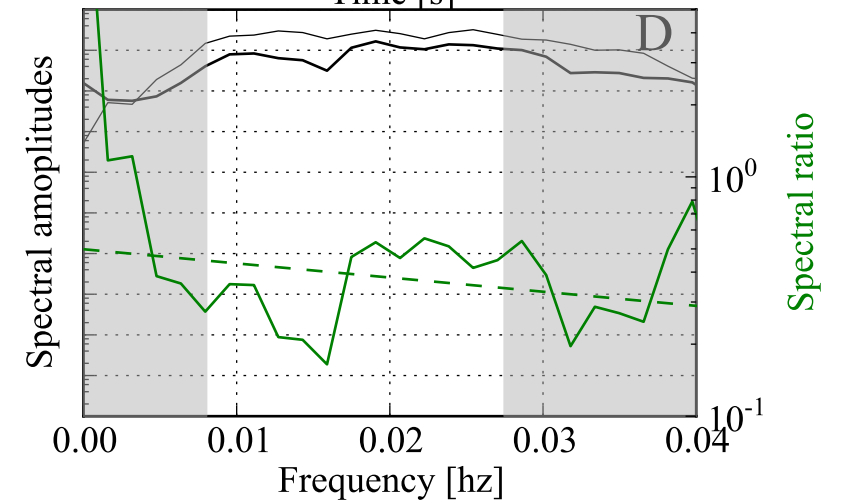
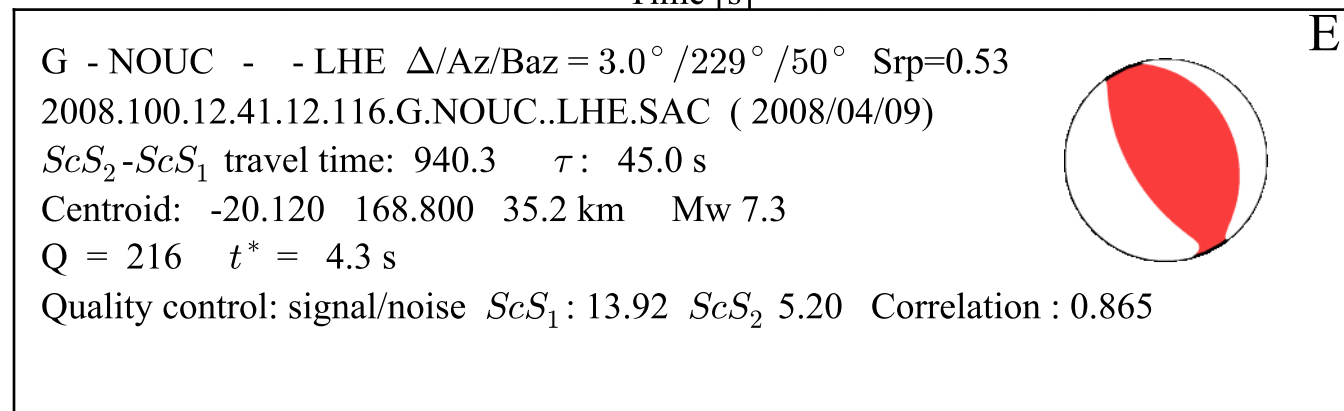
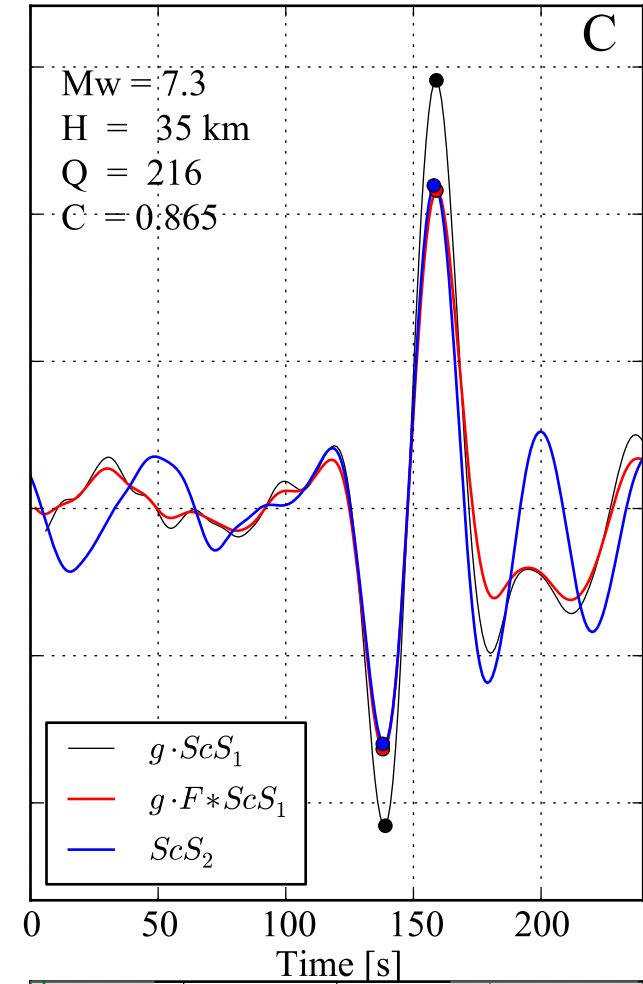
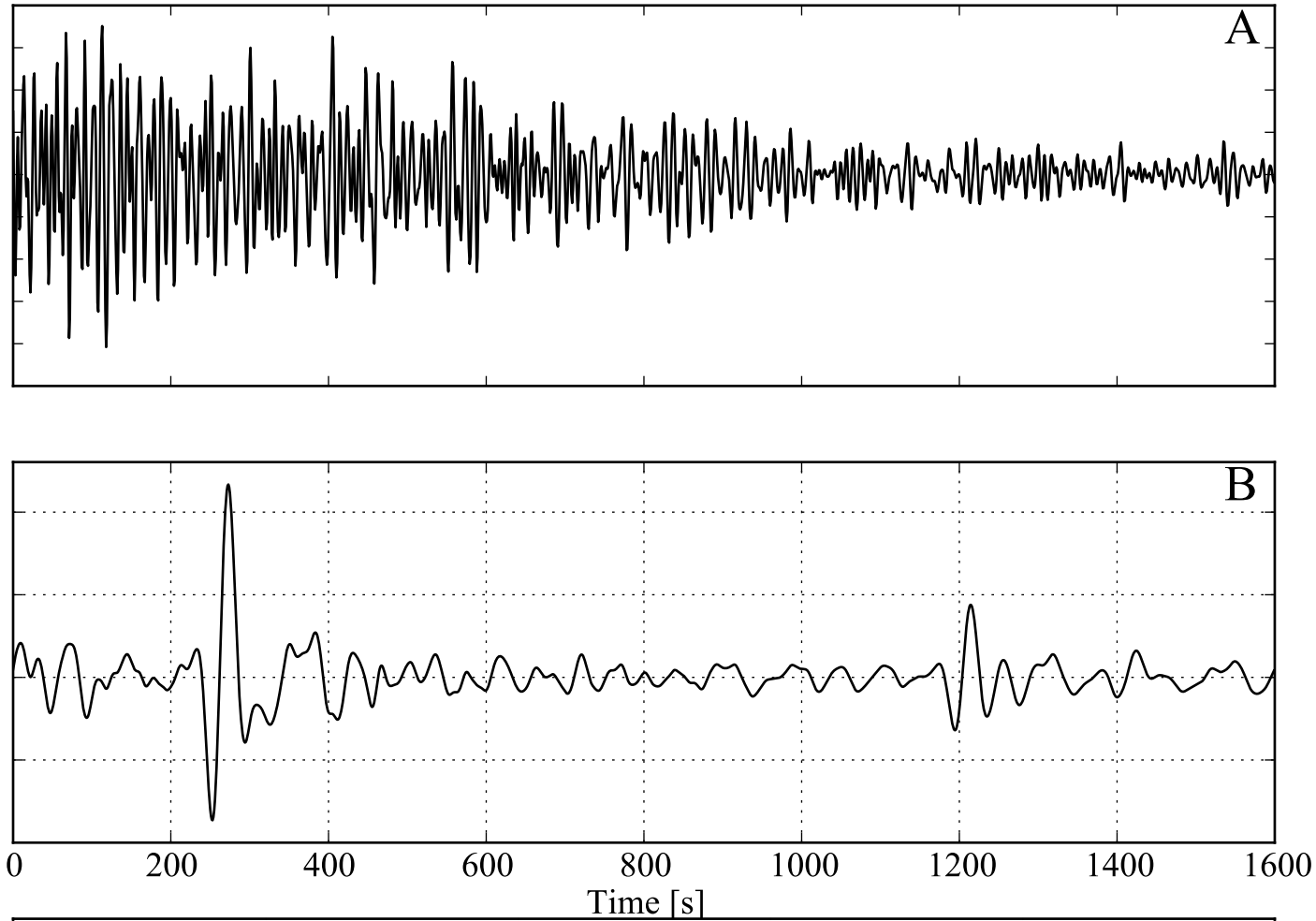


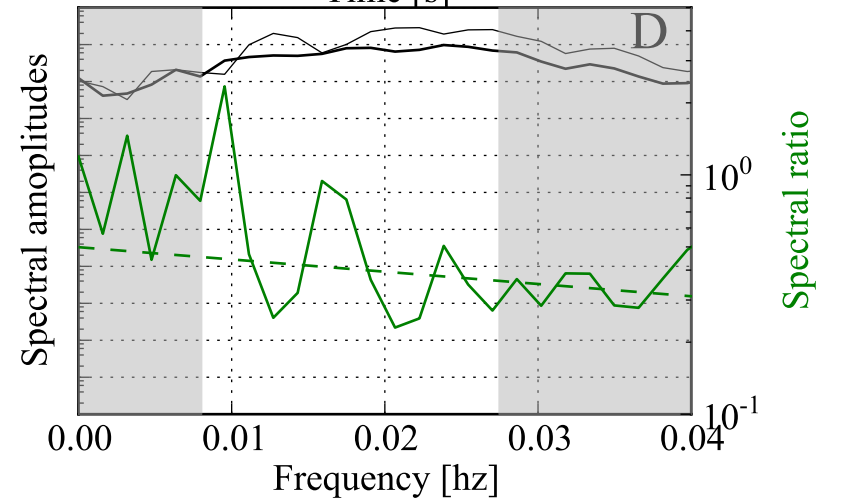
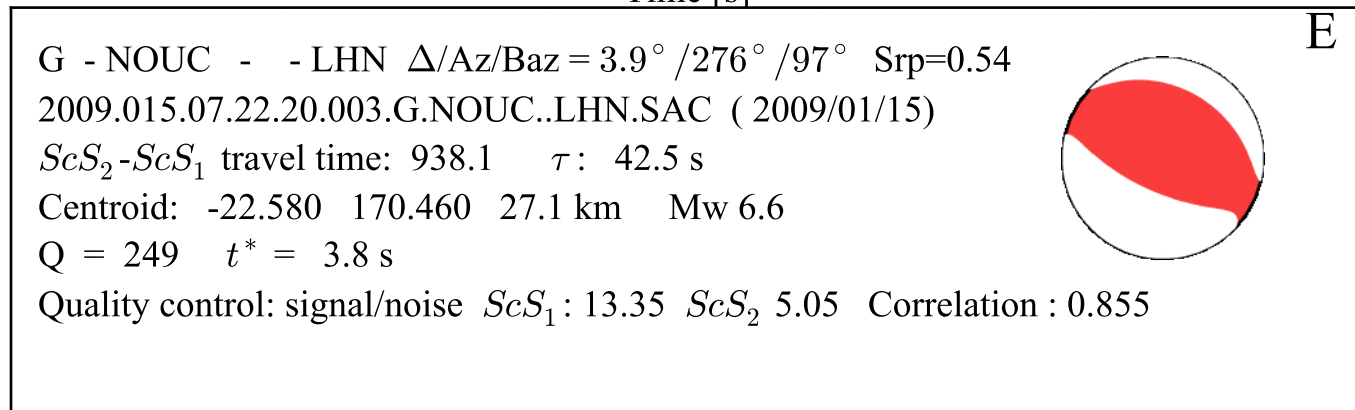
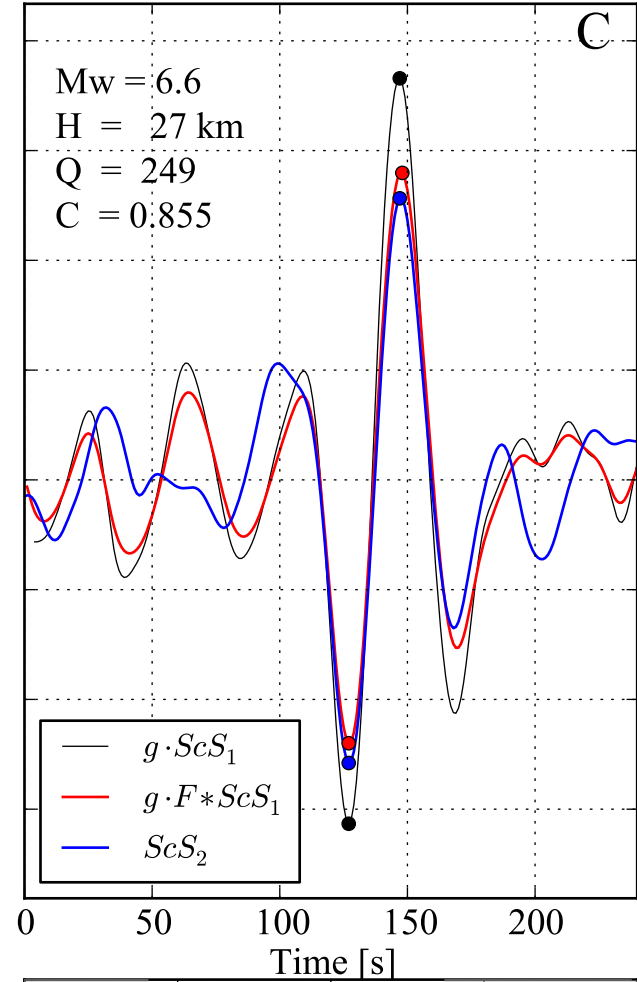
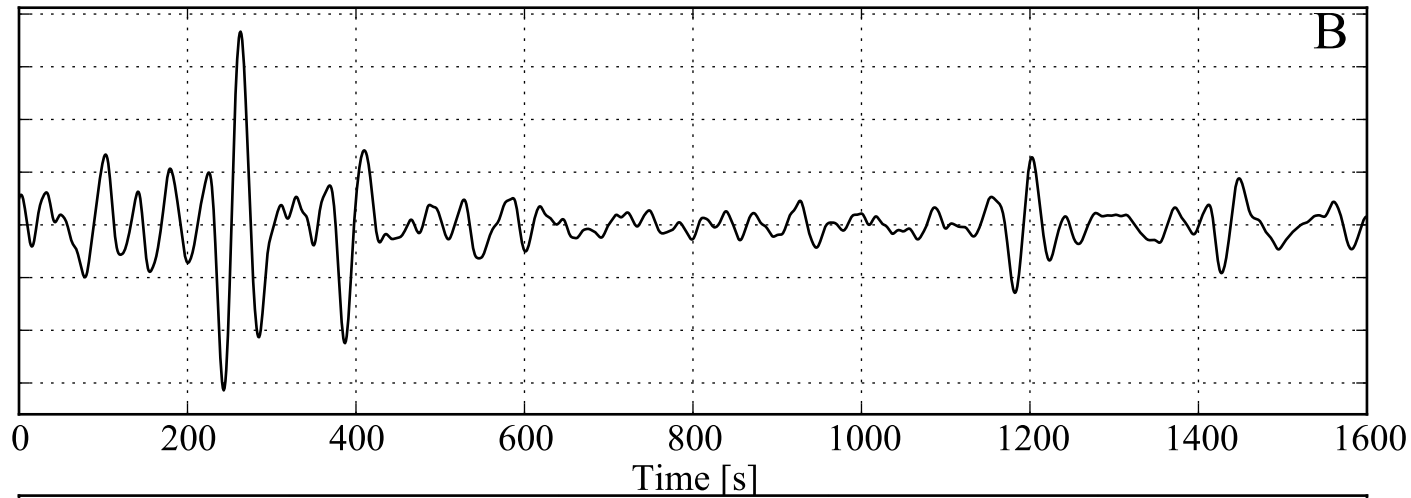
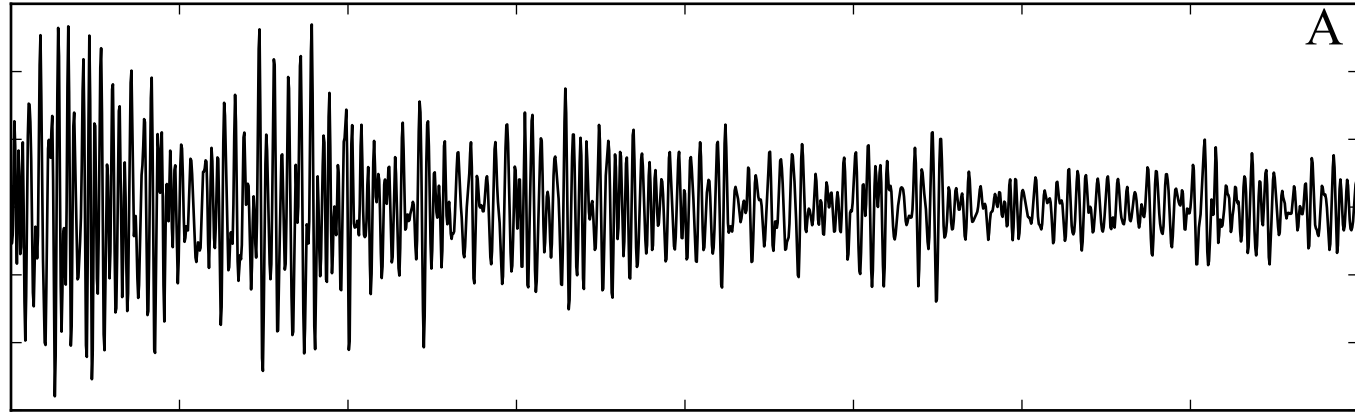


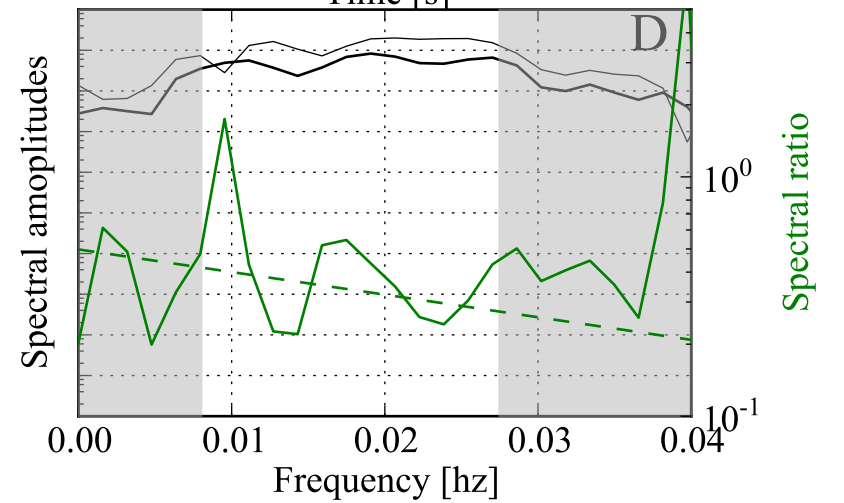
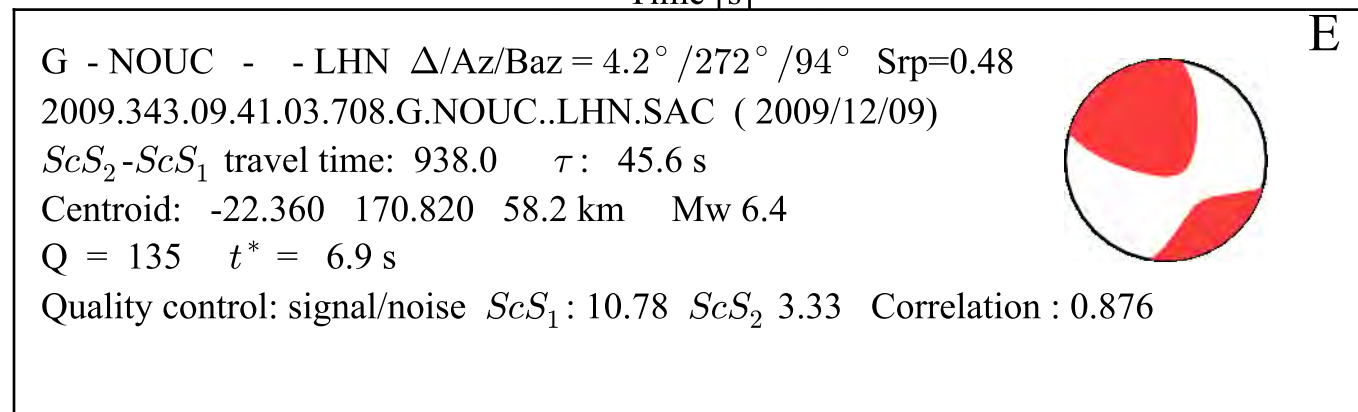
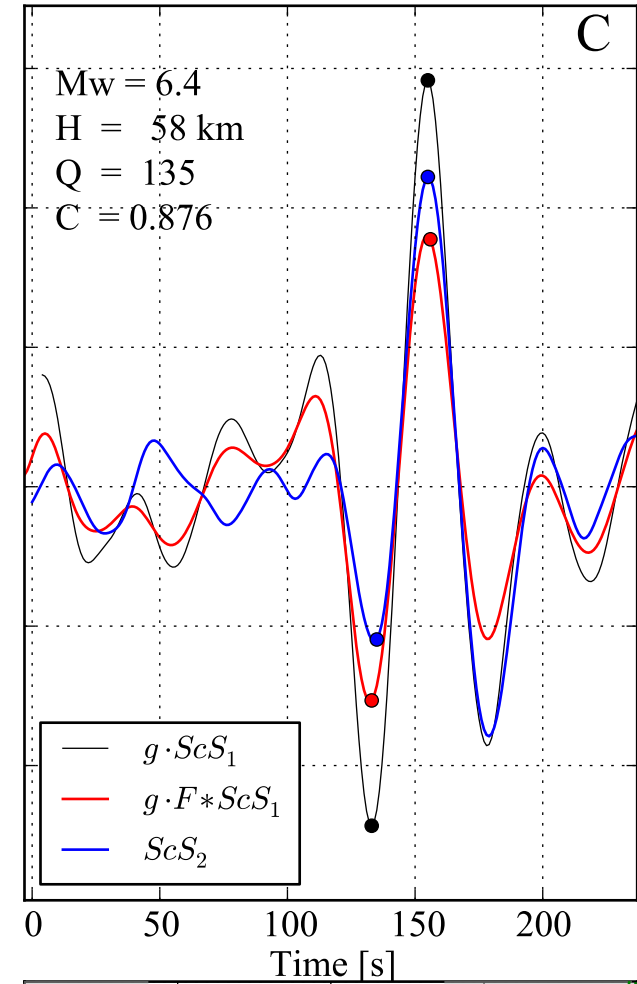
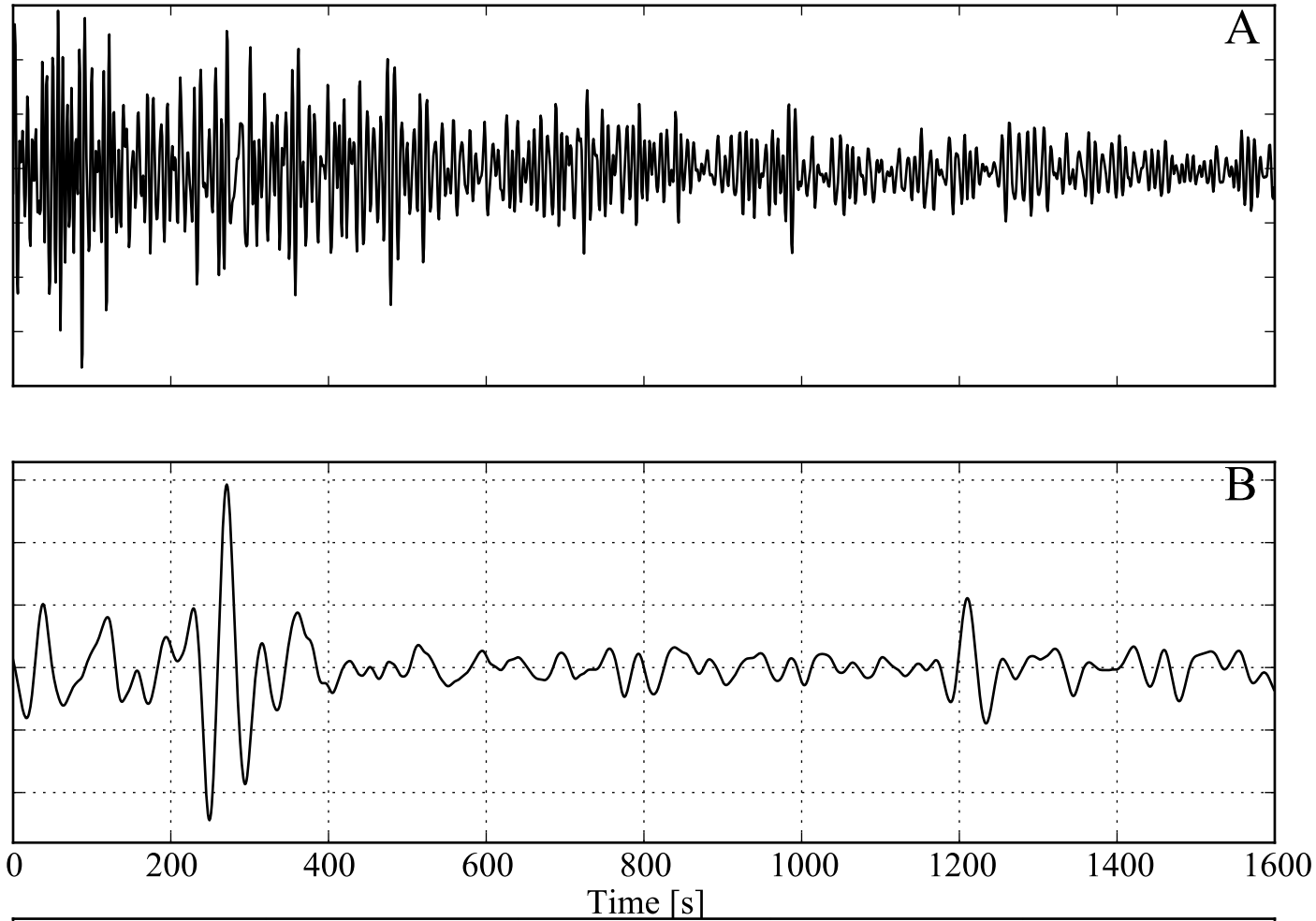


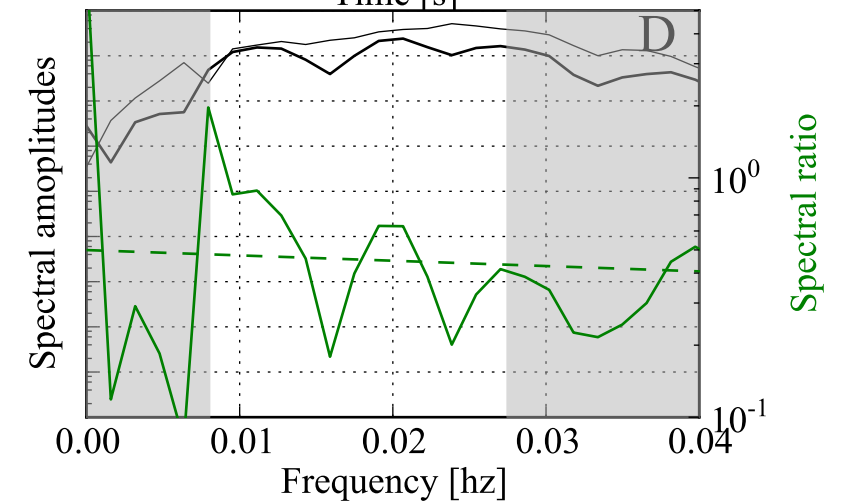
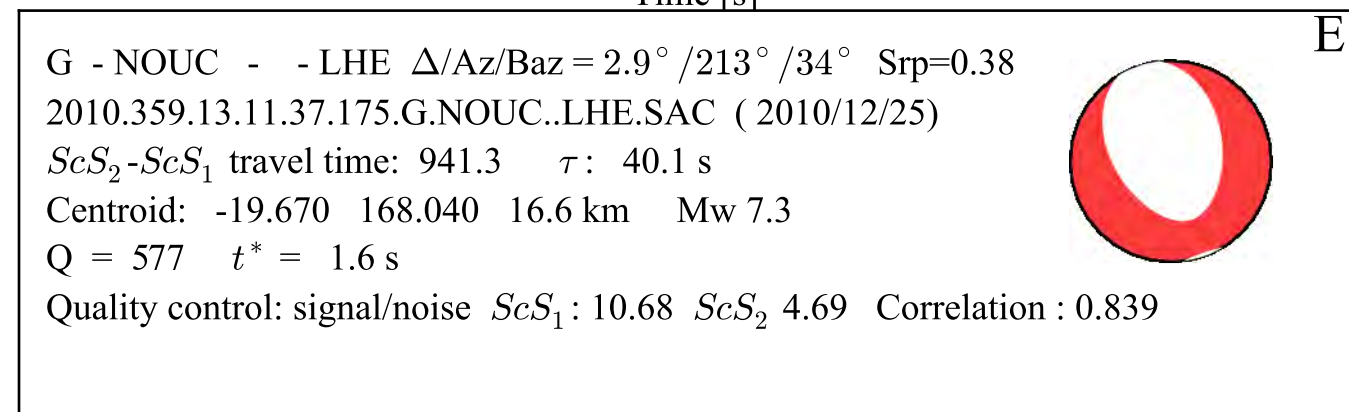
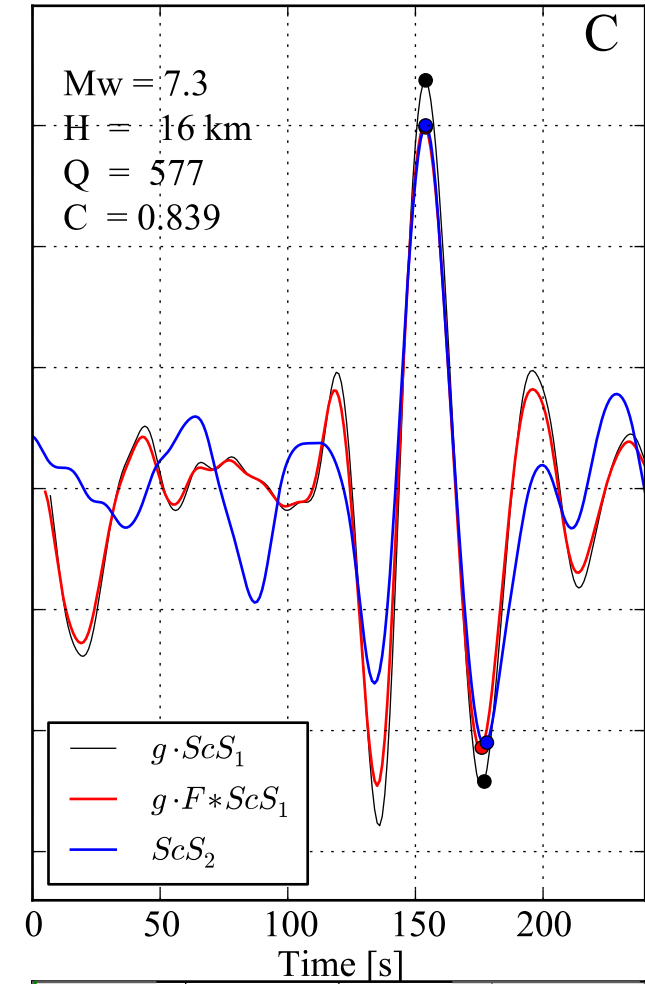
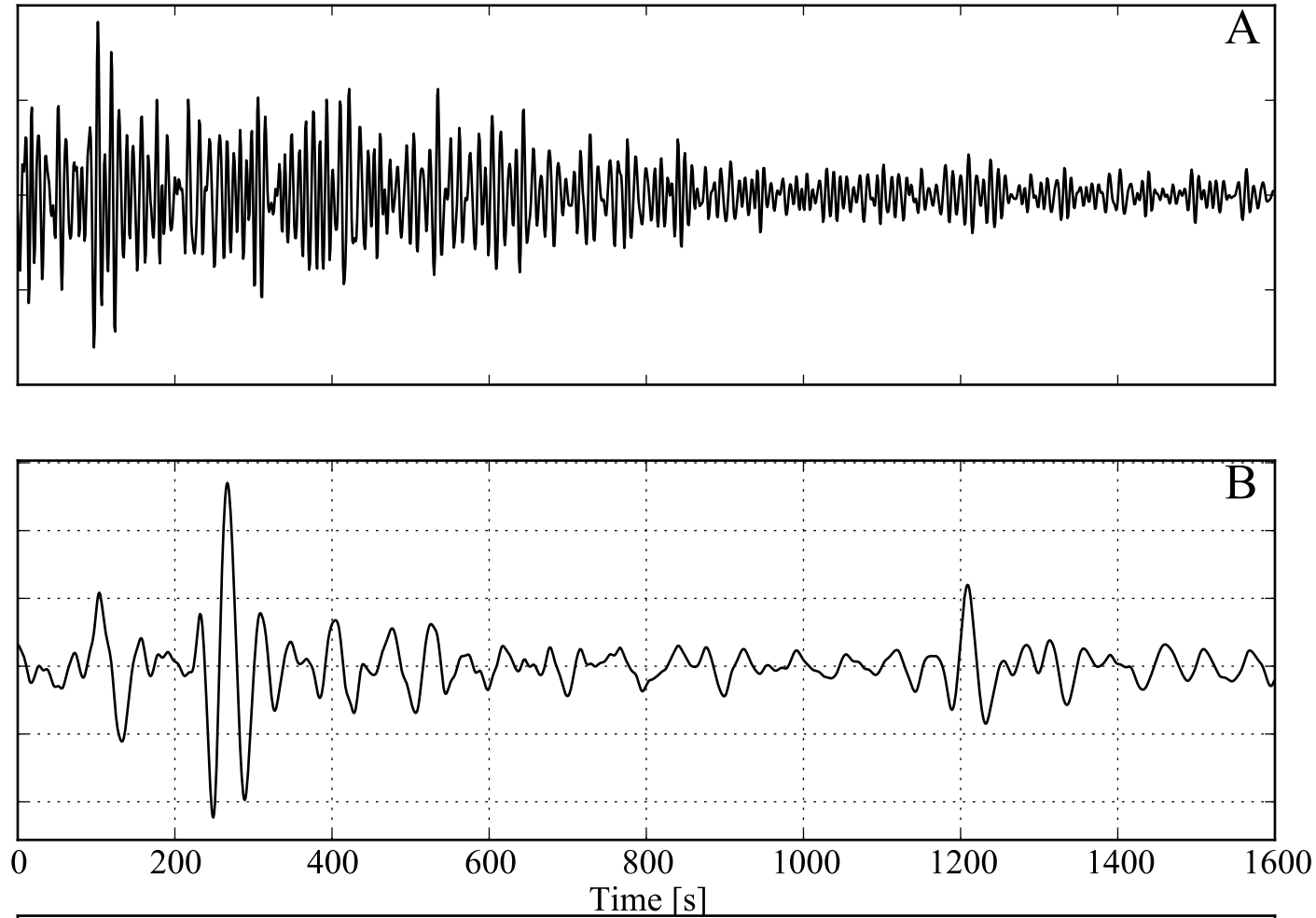


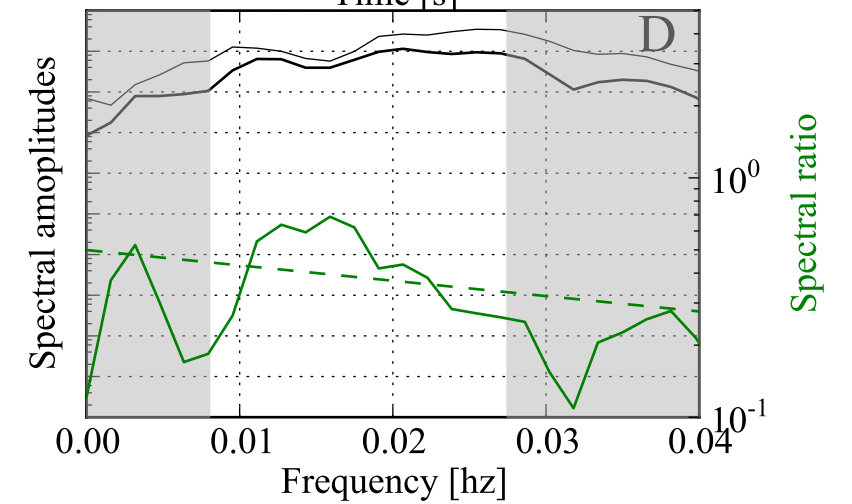
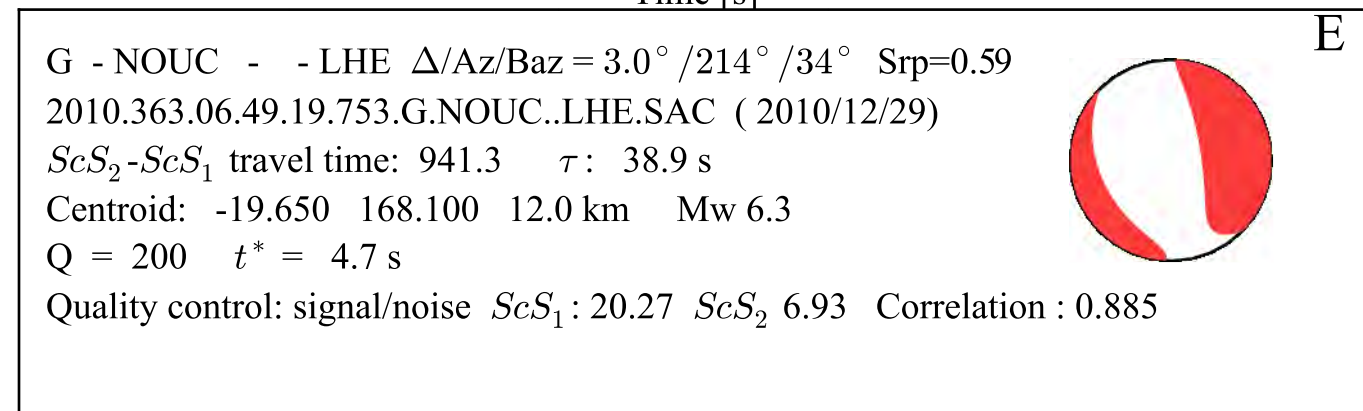
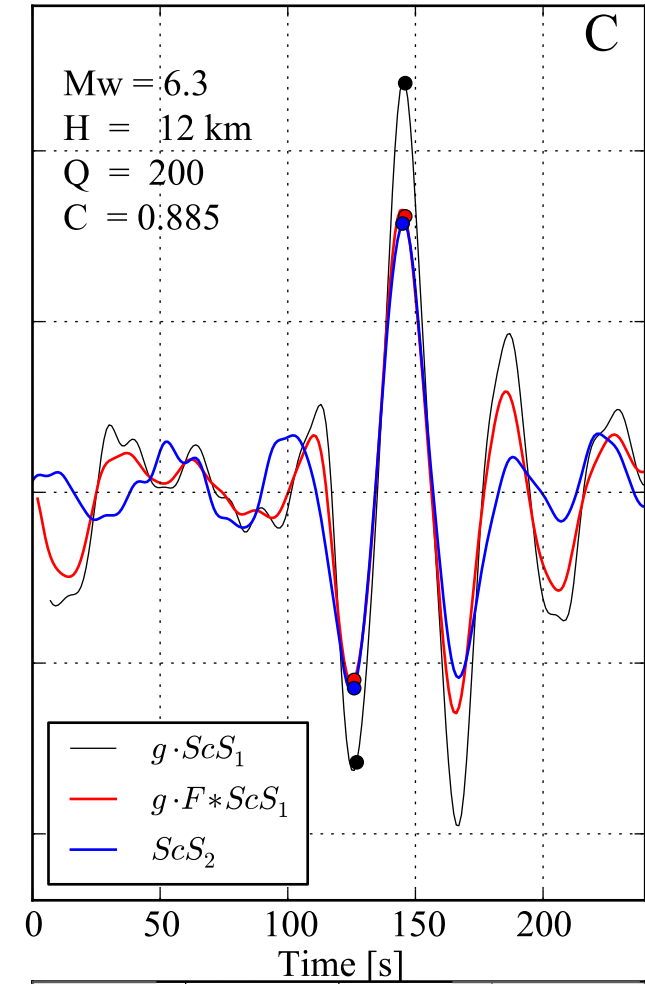
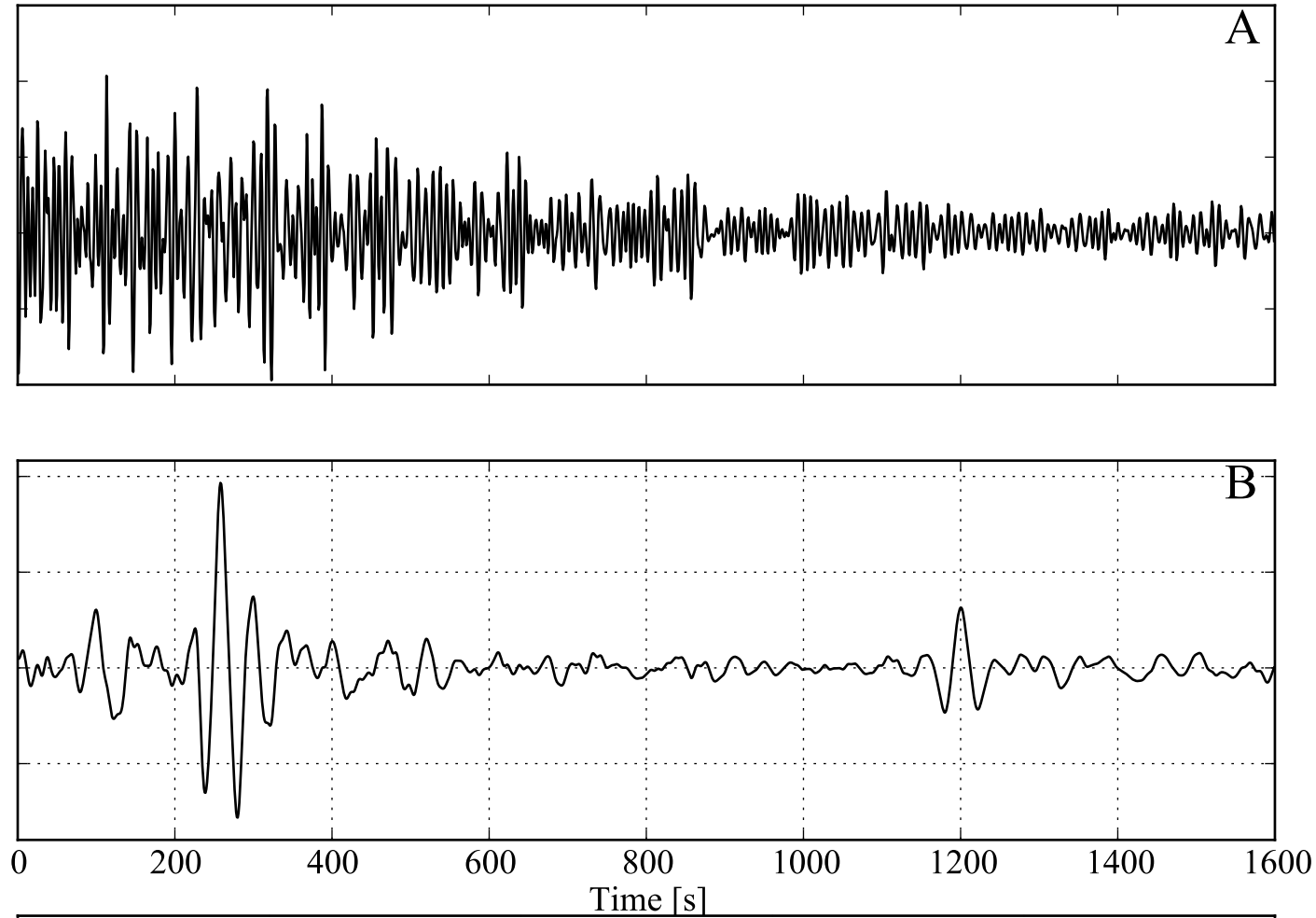


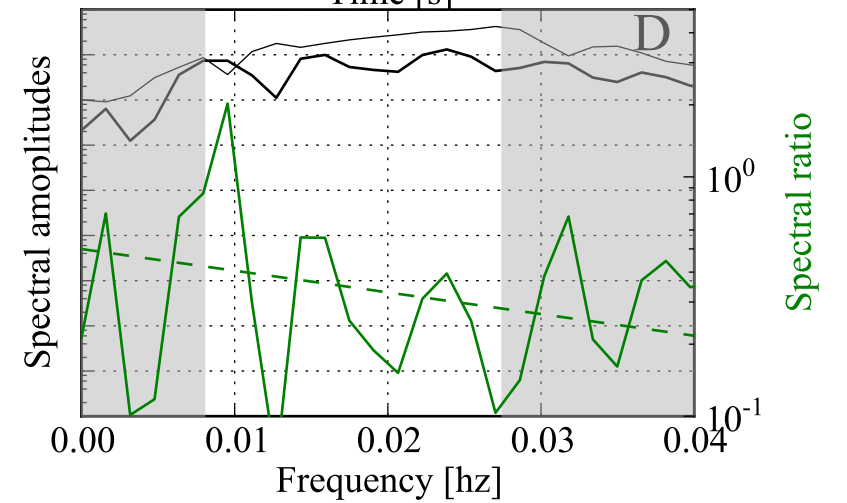
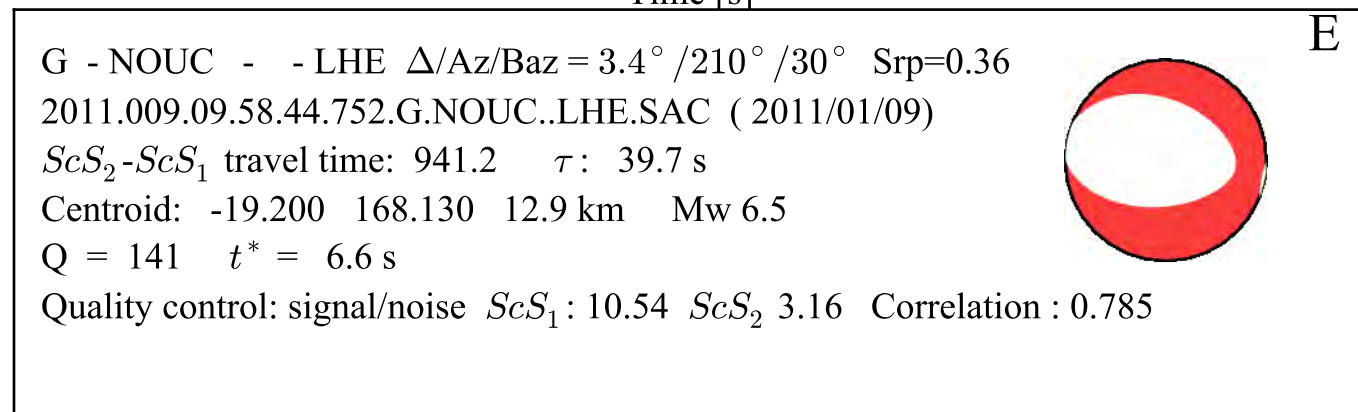
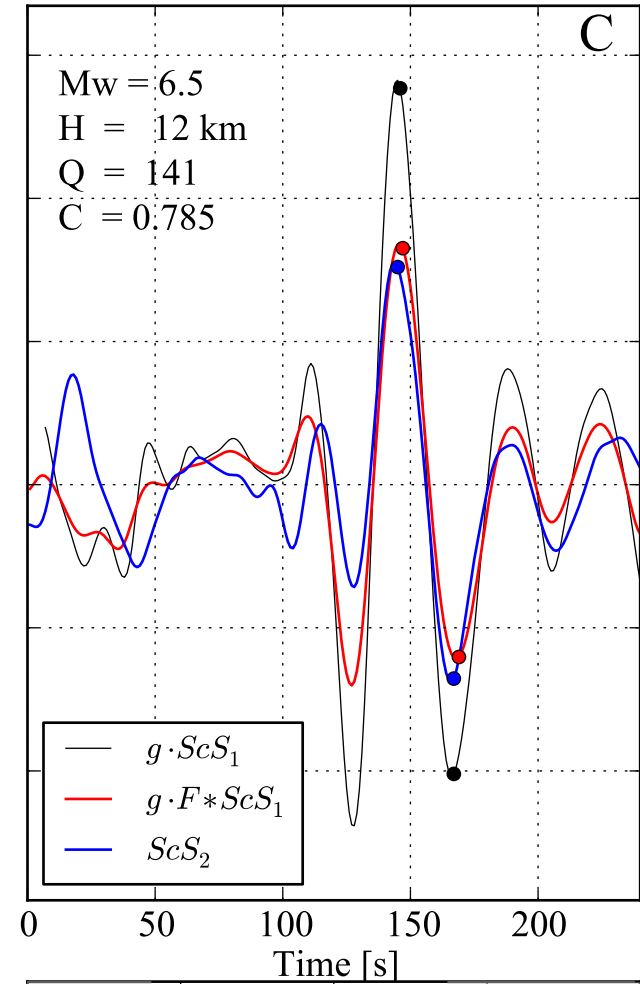
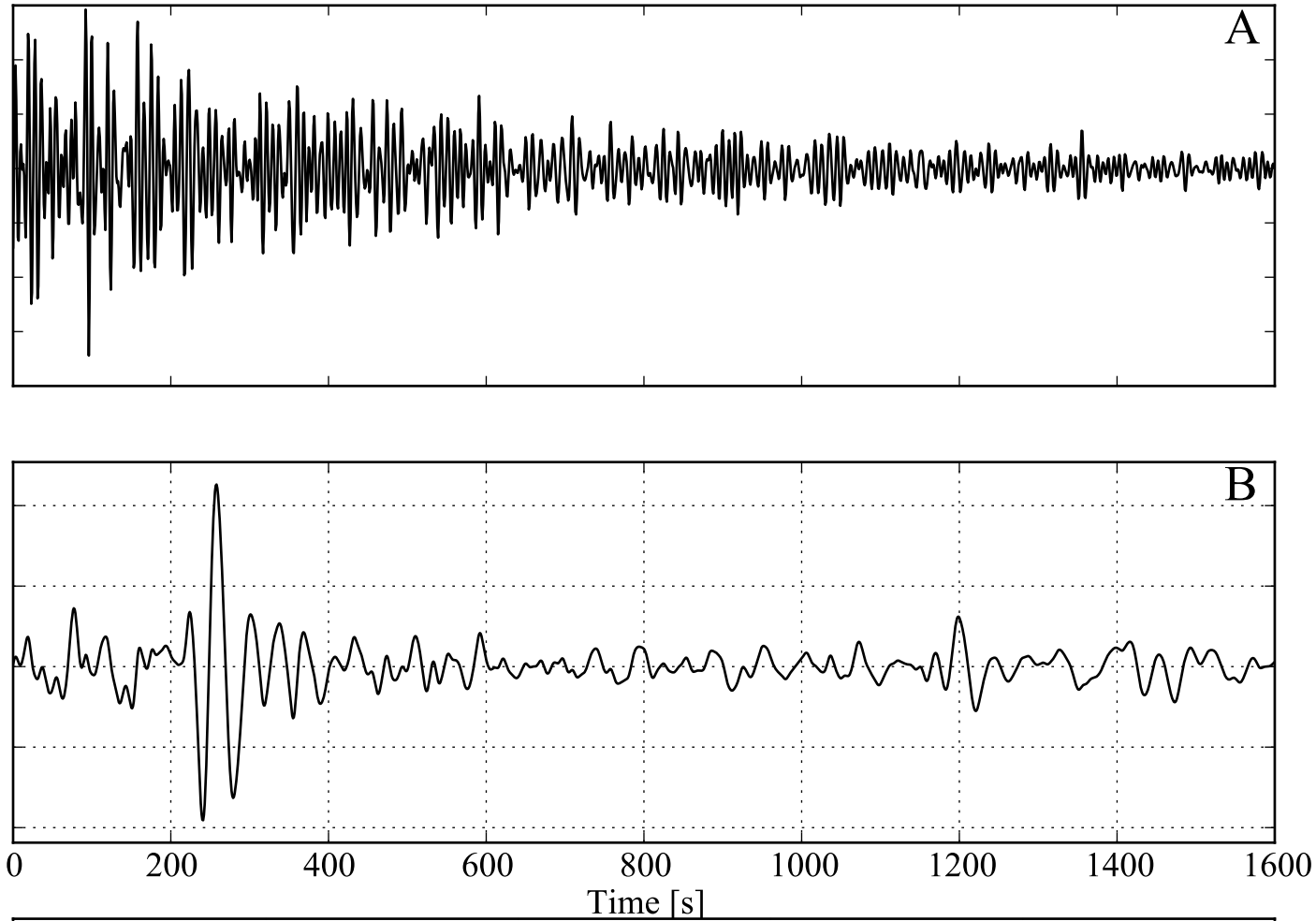


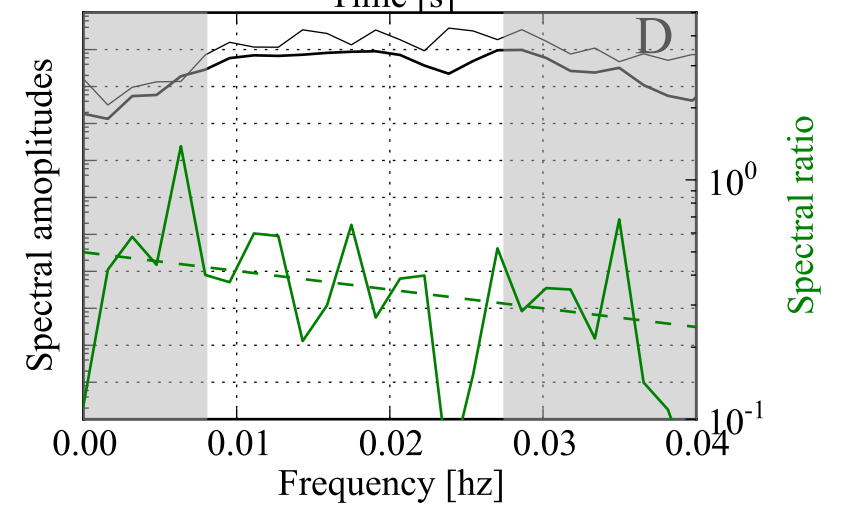
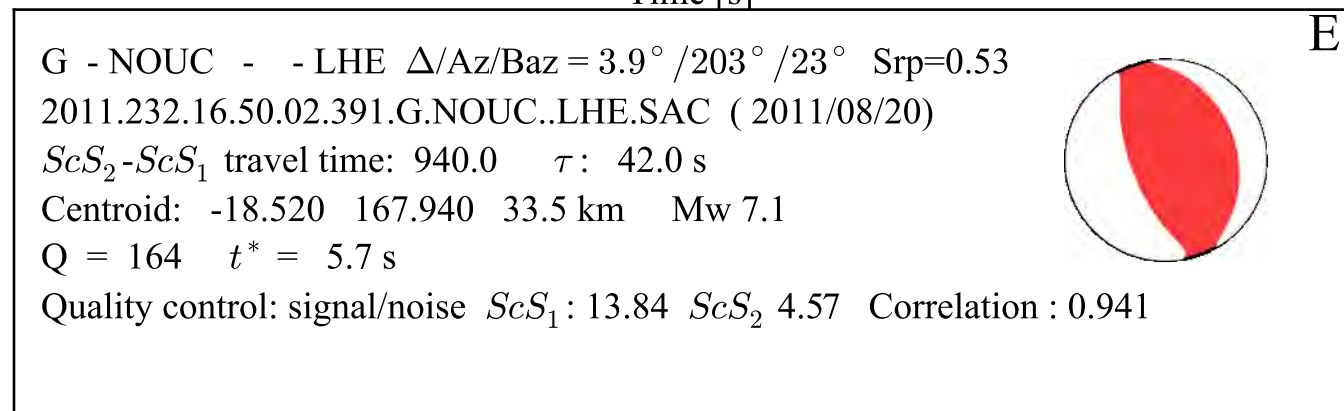
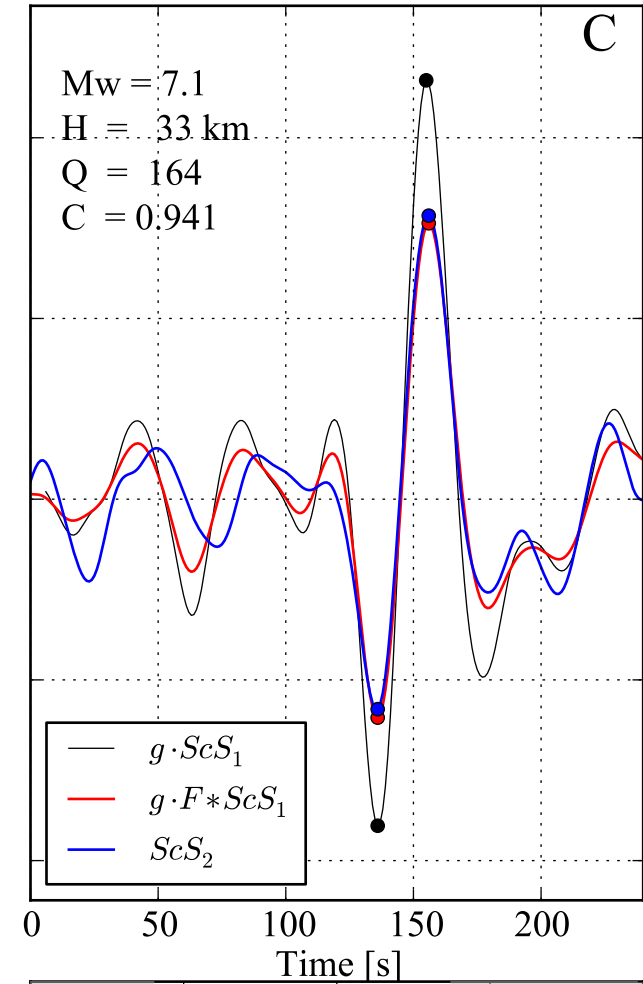
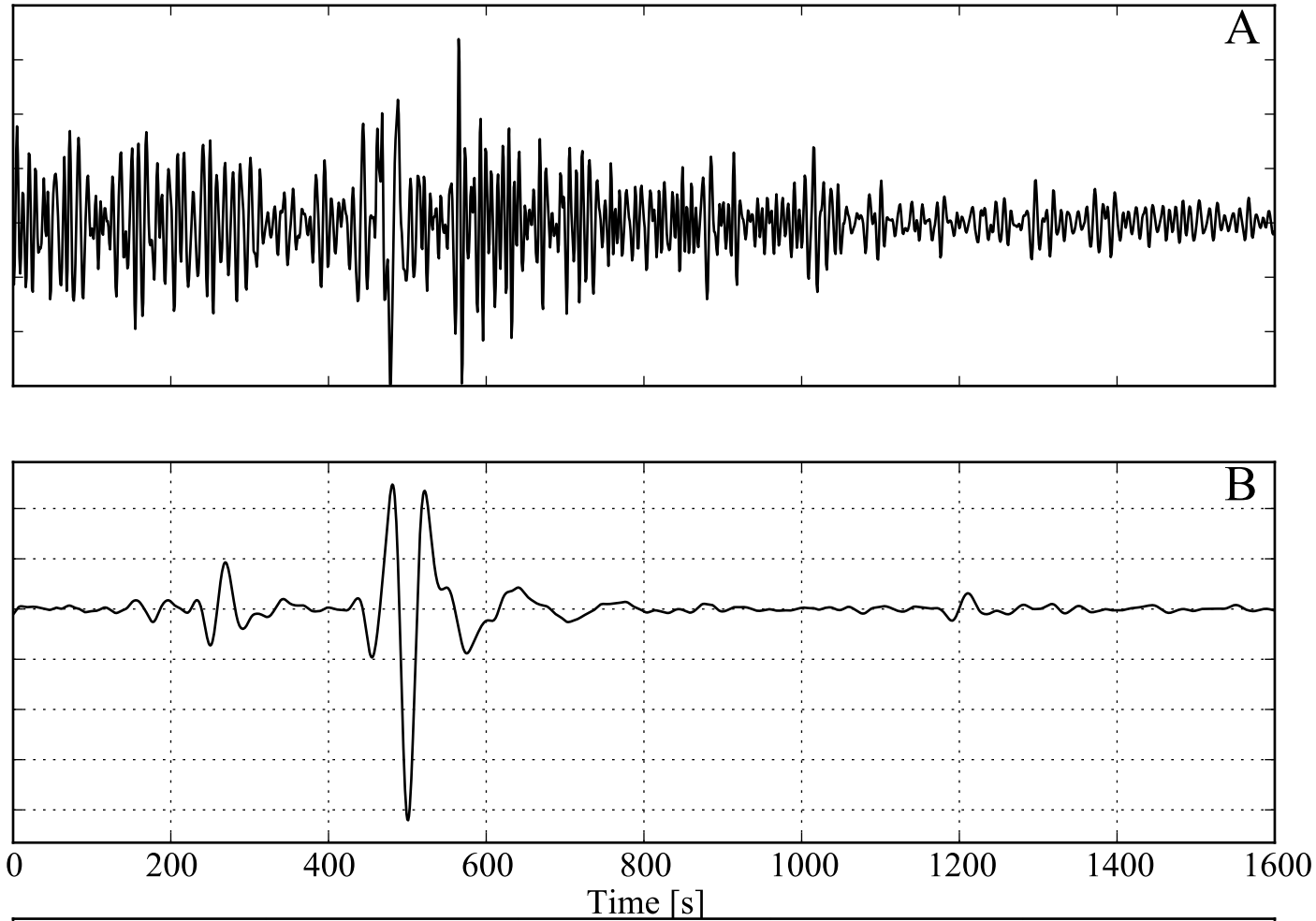


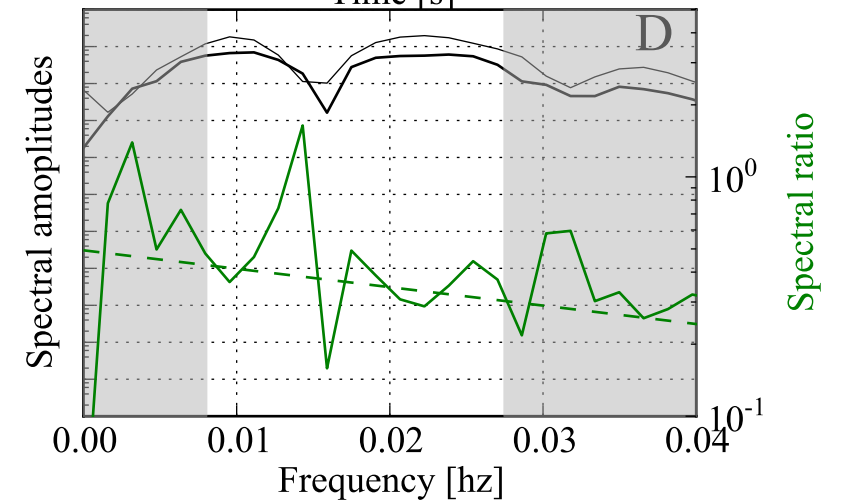
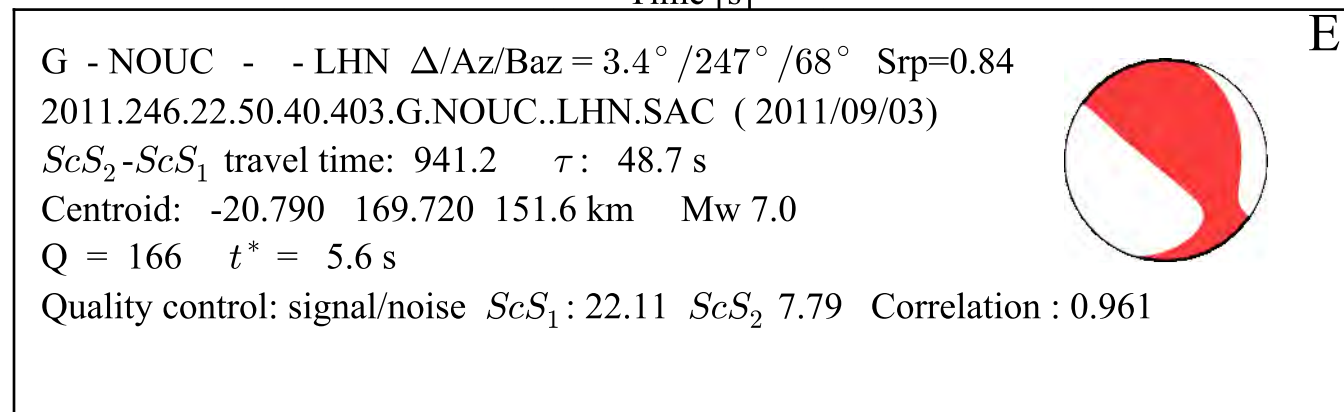
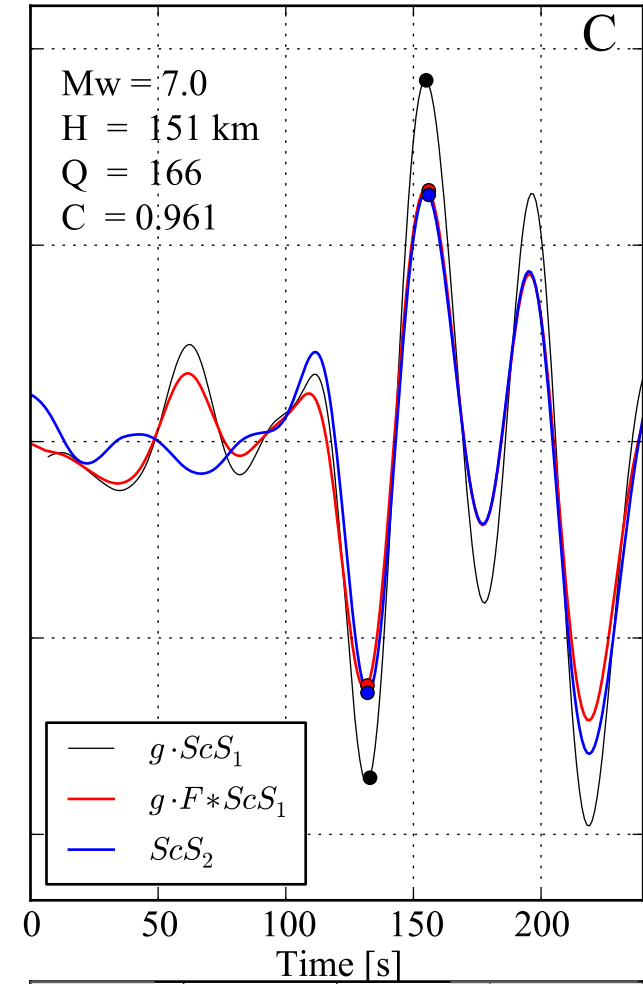
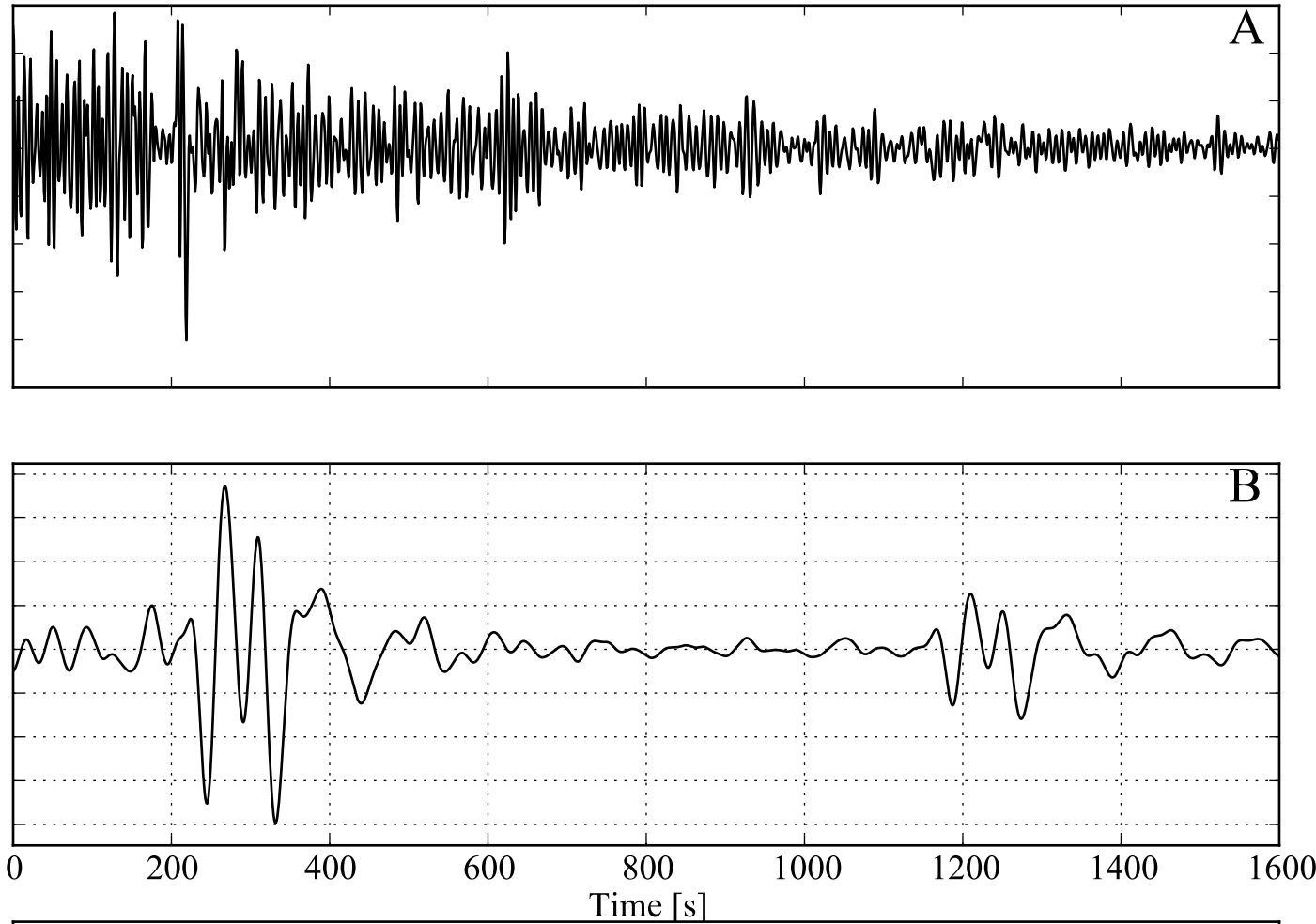


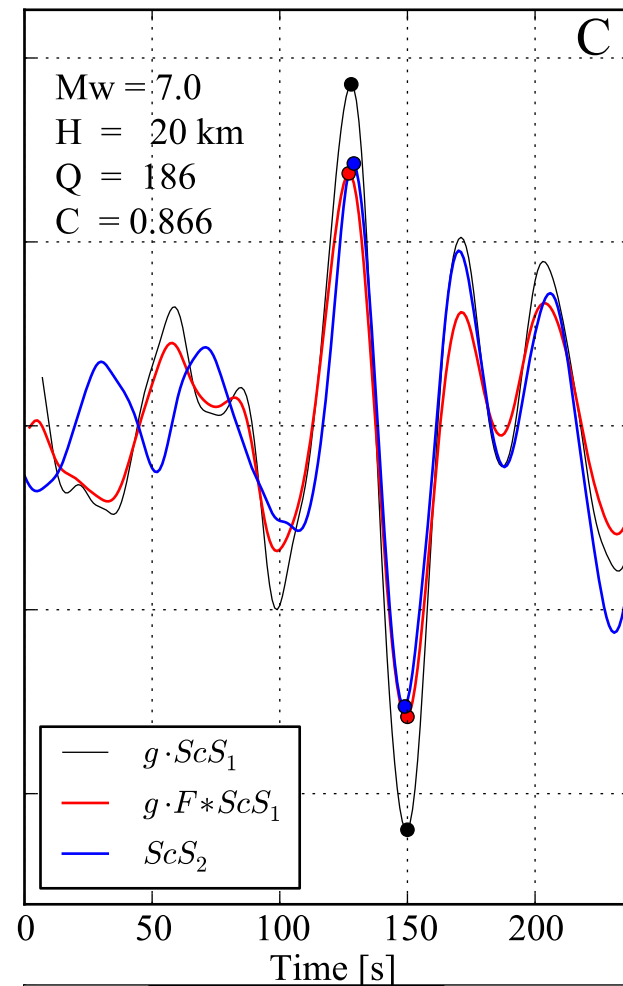
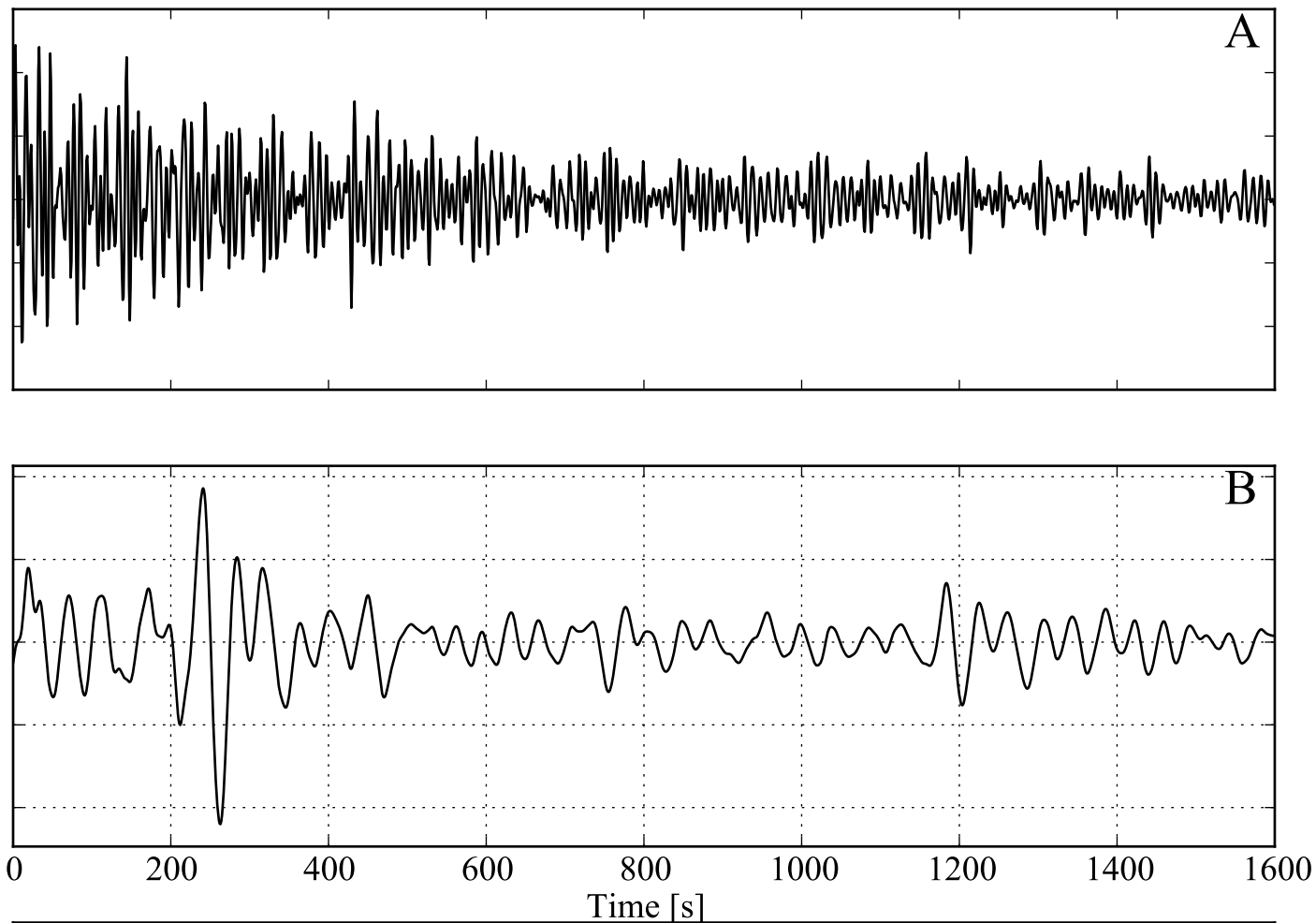







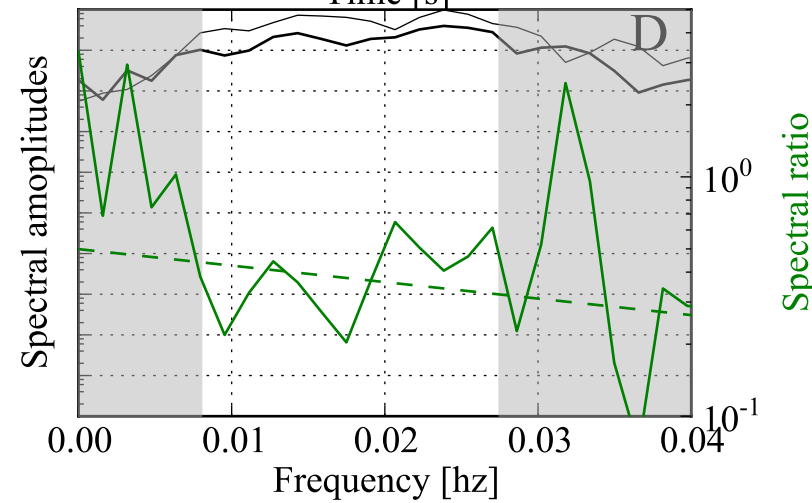


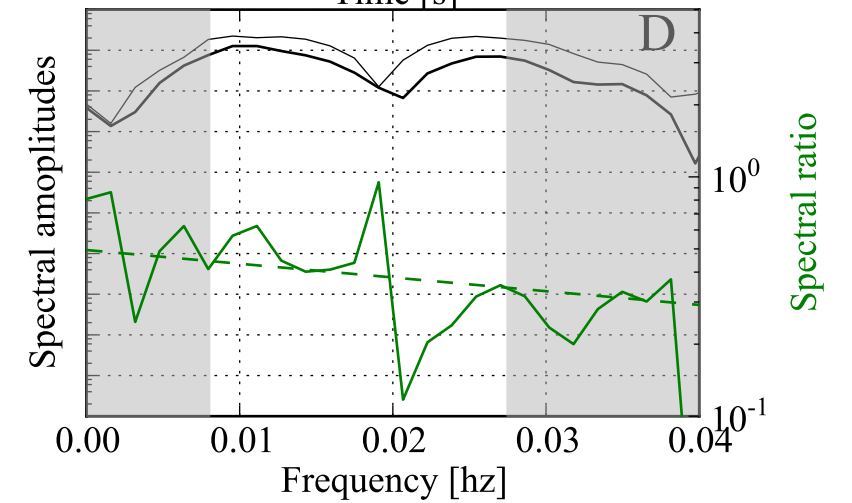
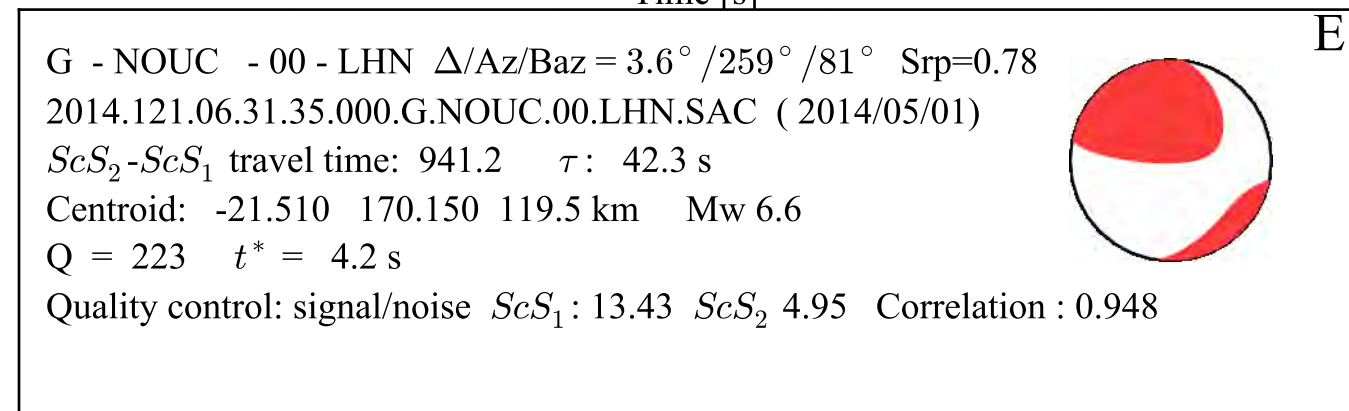
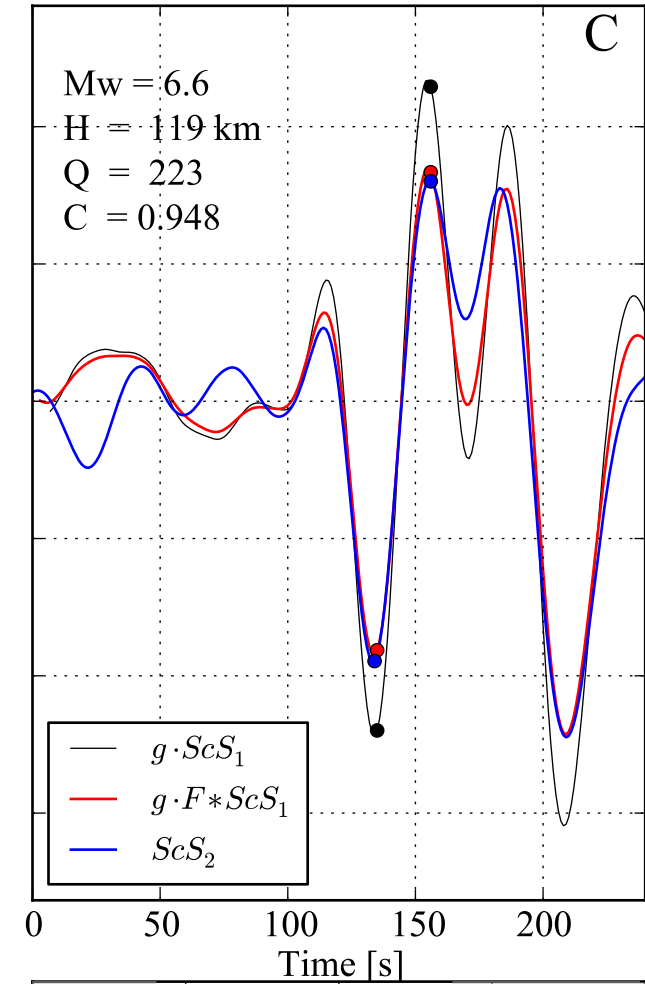
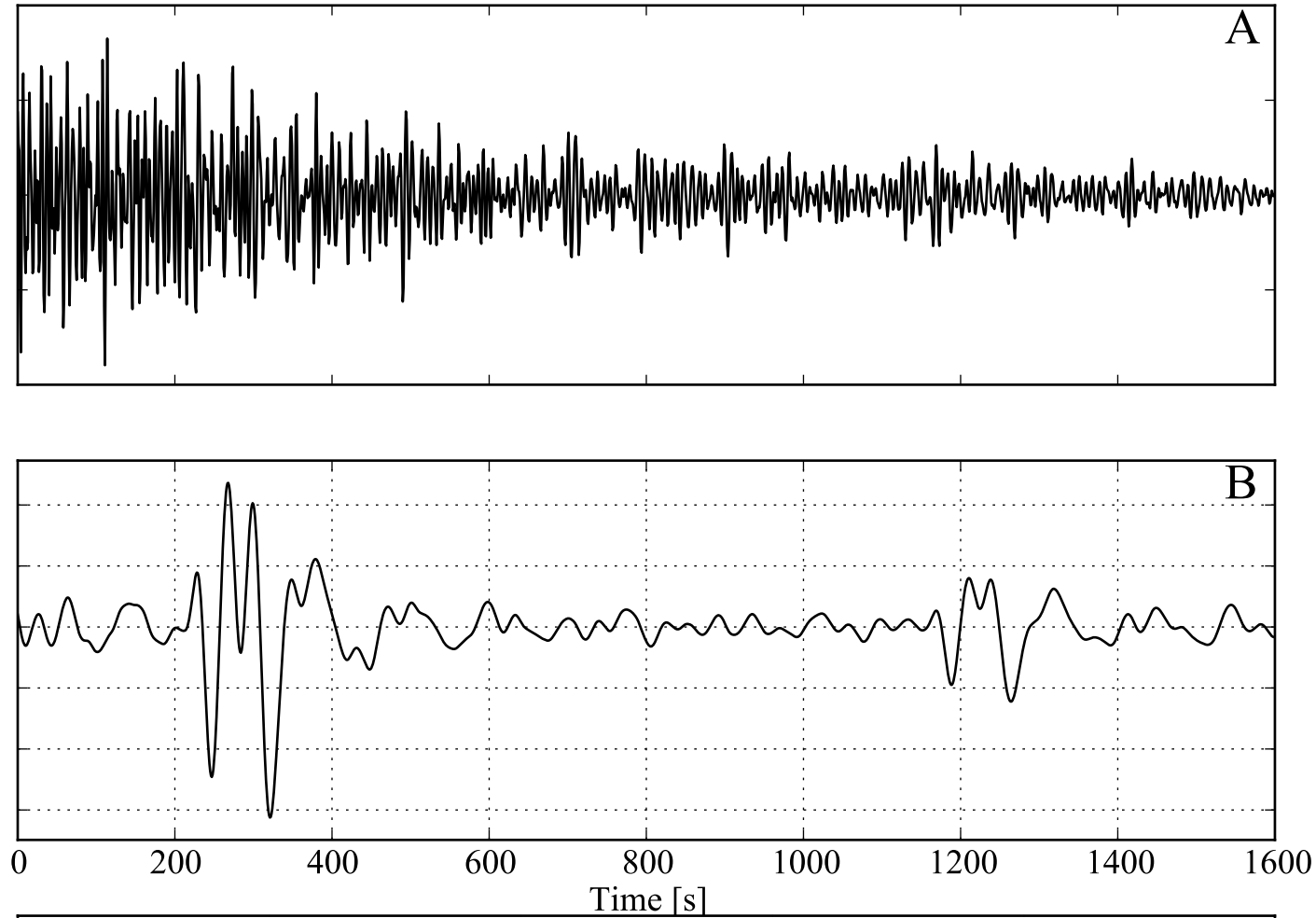


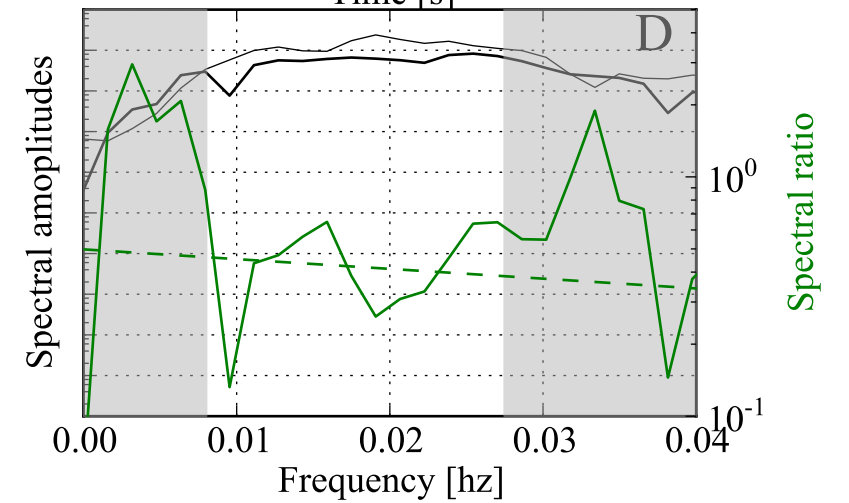
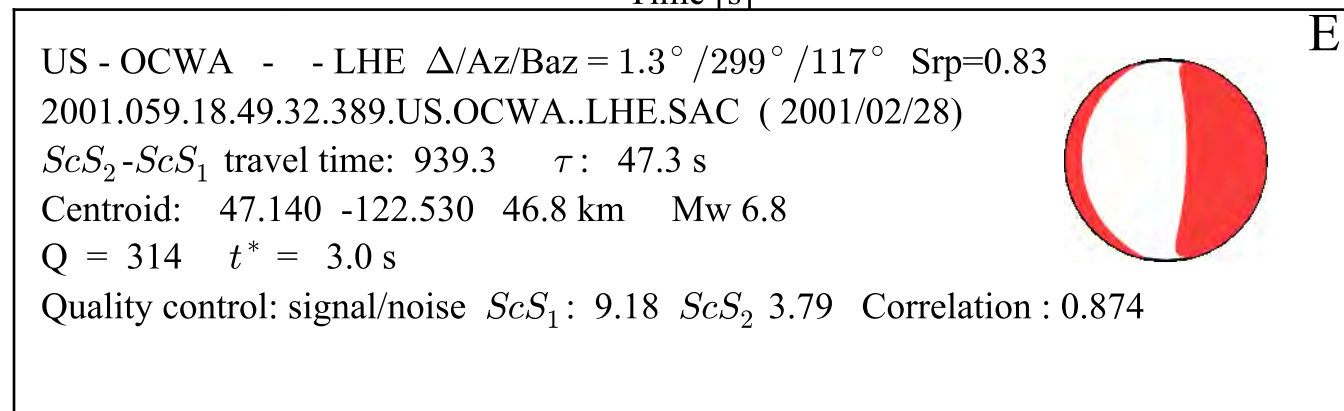
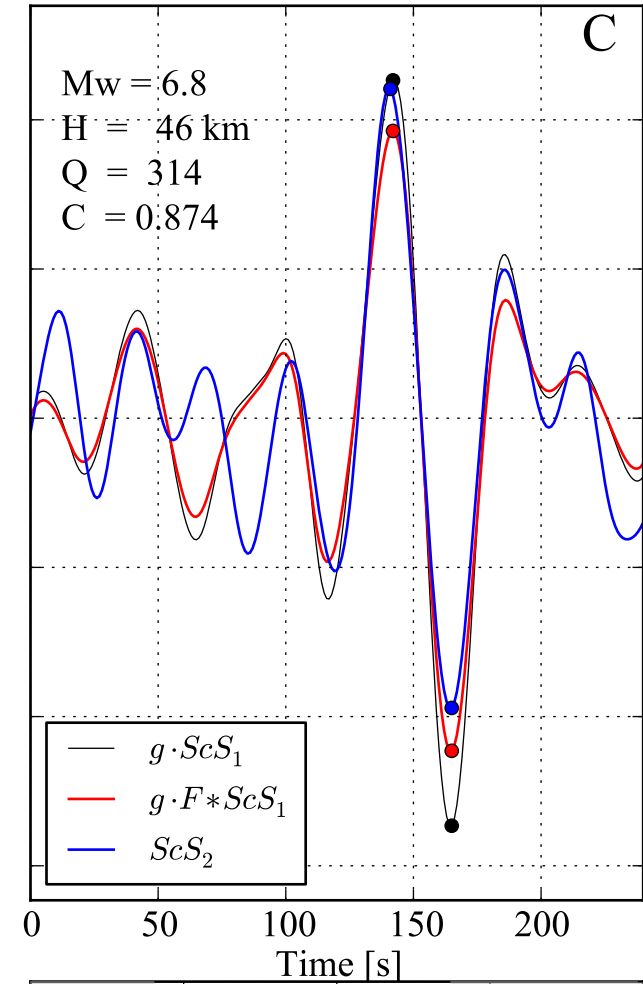
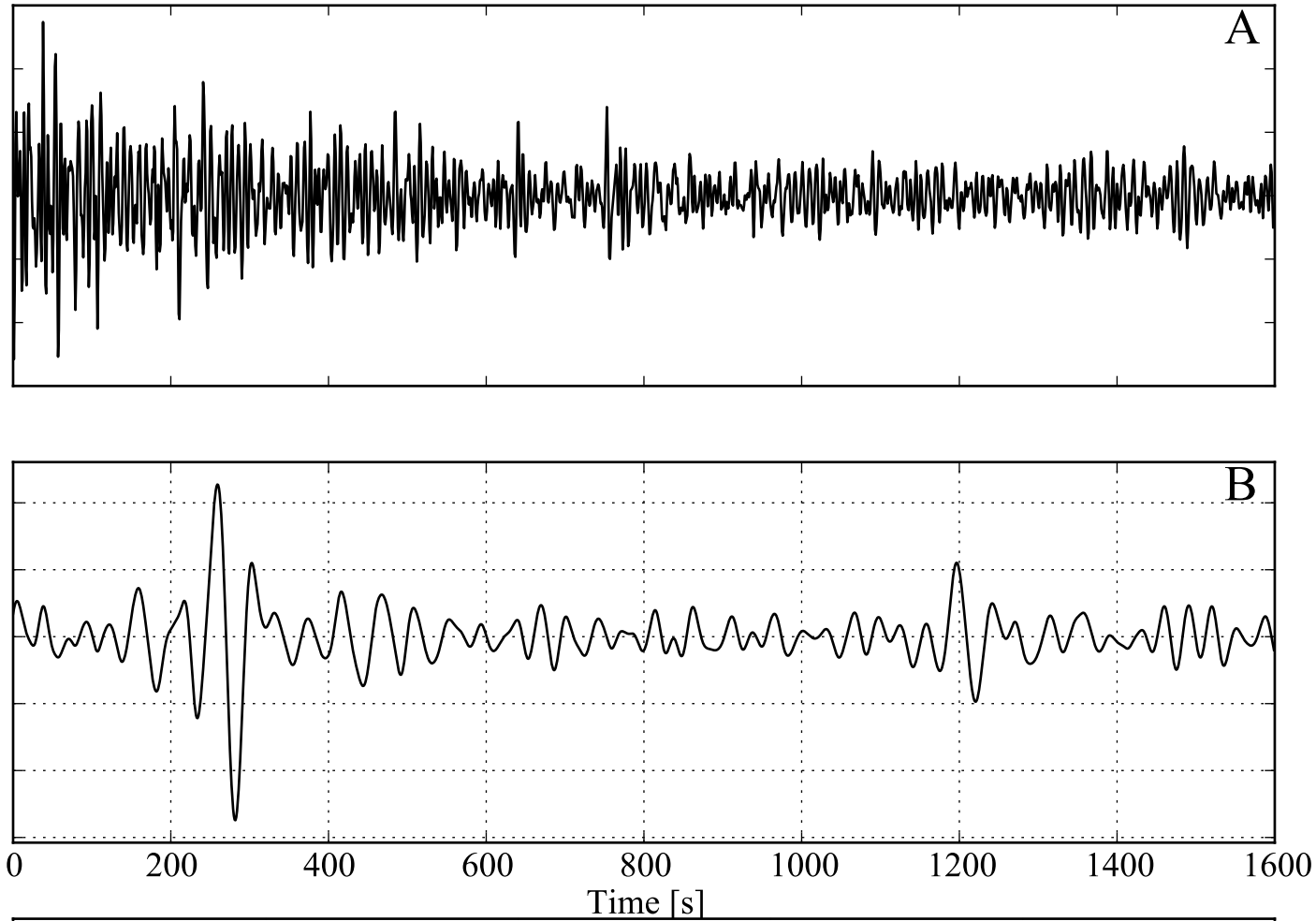


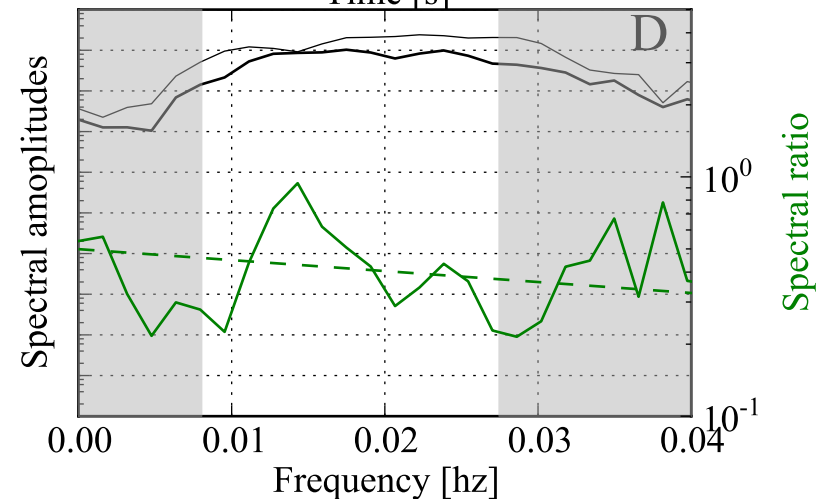
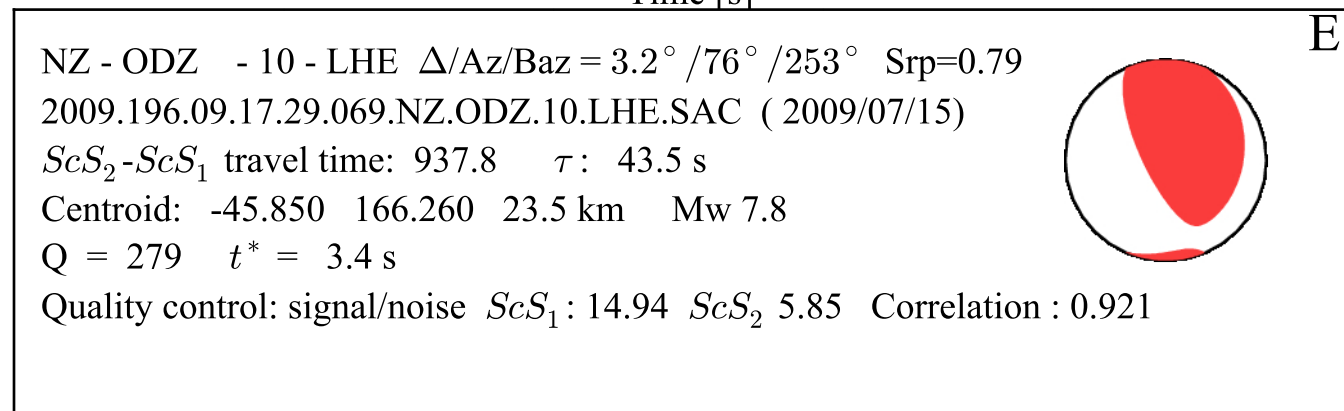
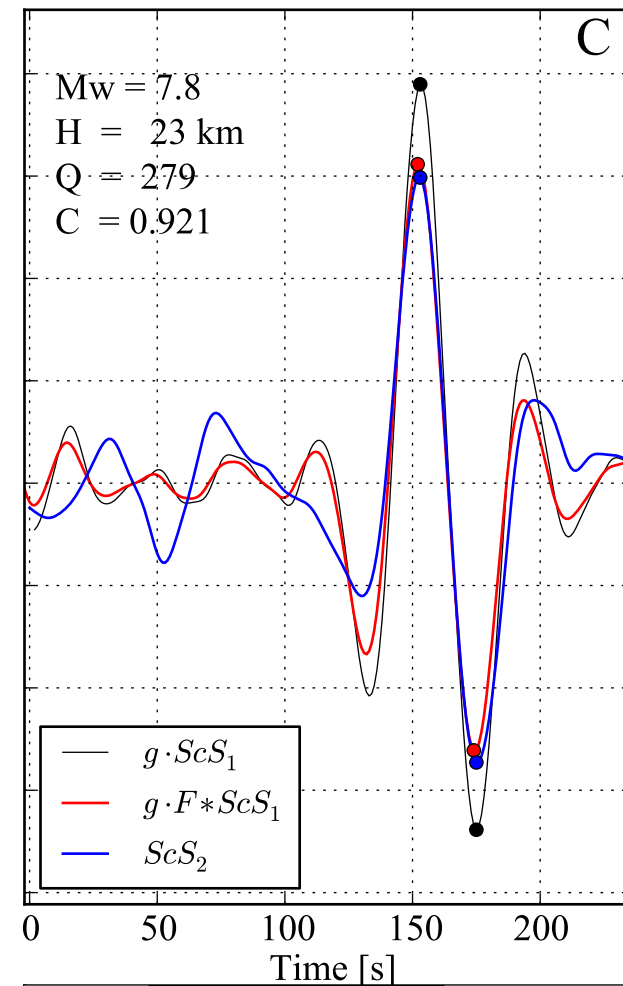
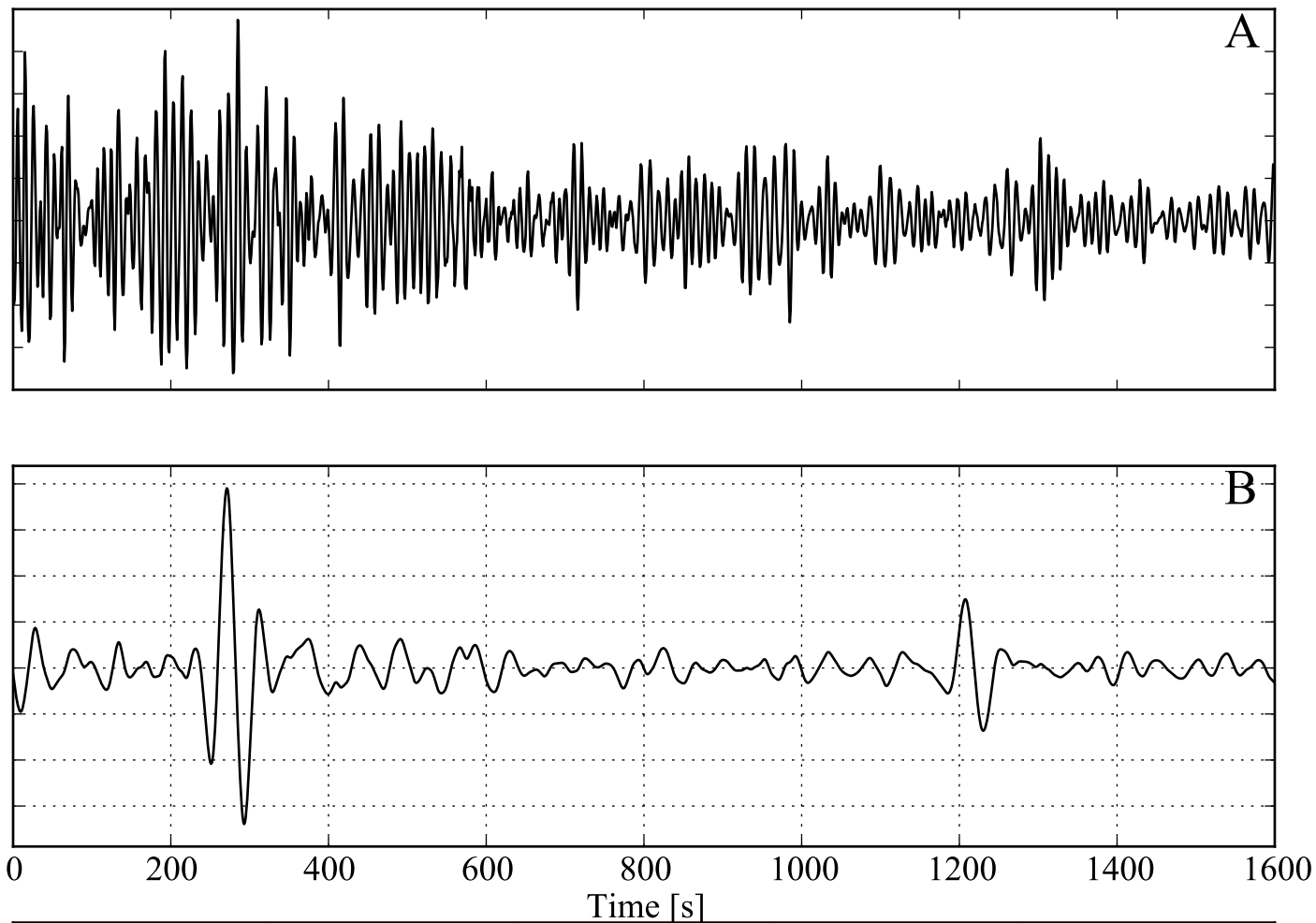
E

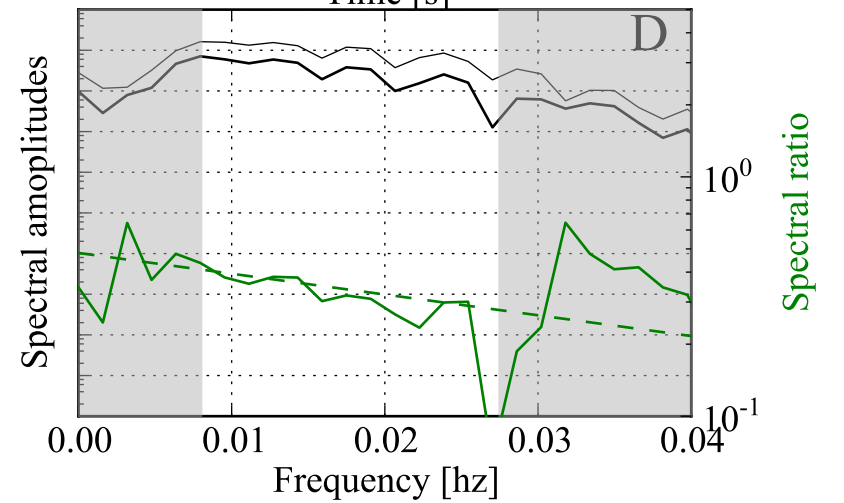
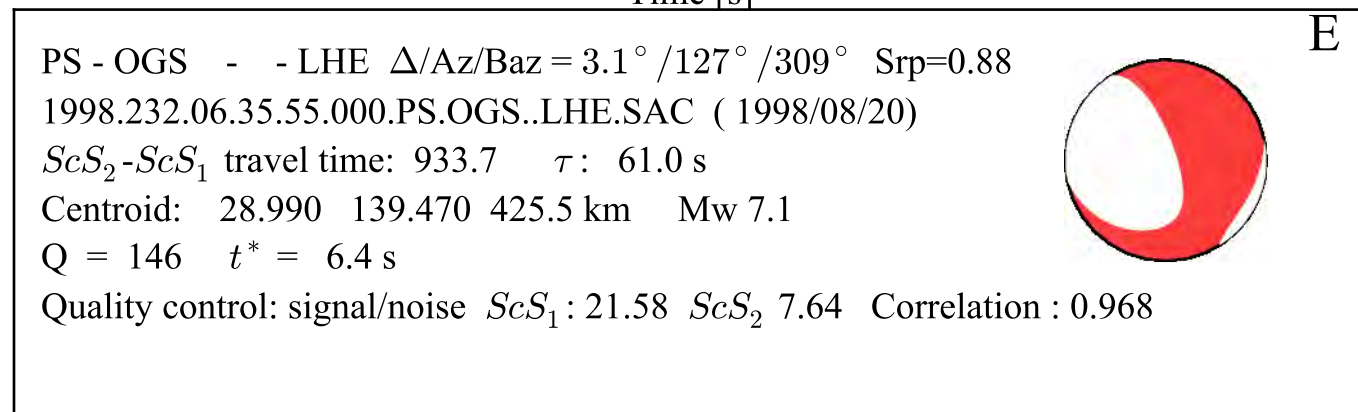
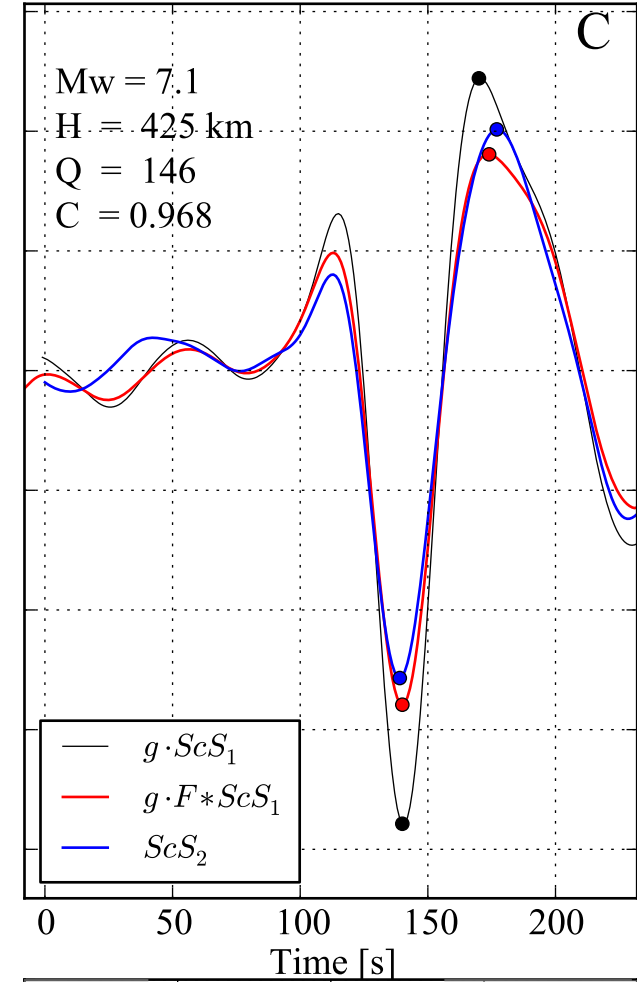
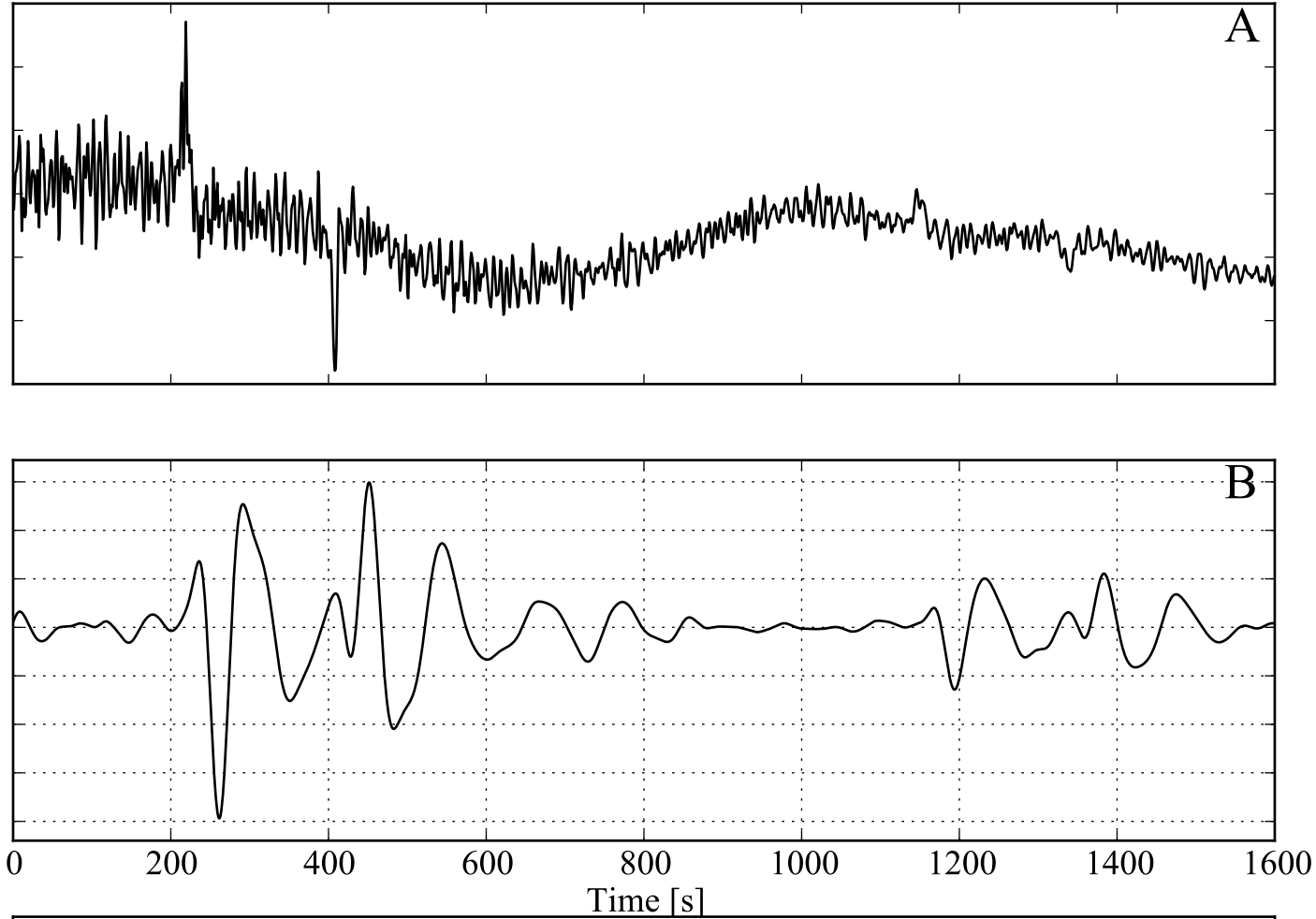
G - NOUC - - LHN $\Delta/Az/Baz = 4.5^\circ / 189^\circ / 9^\circ$ $Srp=0.28$
 2012.033.13.29.40.013.G.NOUC..LHN.SAC (2012/02/02)
 ScS_2-ScS_1 travel time: 940.8 τ : 46.4 s
 Centroid: -17.690 167.110 20.5 km Mw 7.0
 $Q = 186$ $t^* = 5.1$ s
 Quality control: signal/noise ScS_1 : 8.59 ScS_2 3.12 Correlation : 0.866

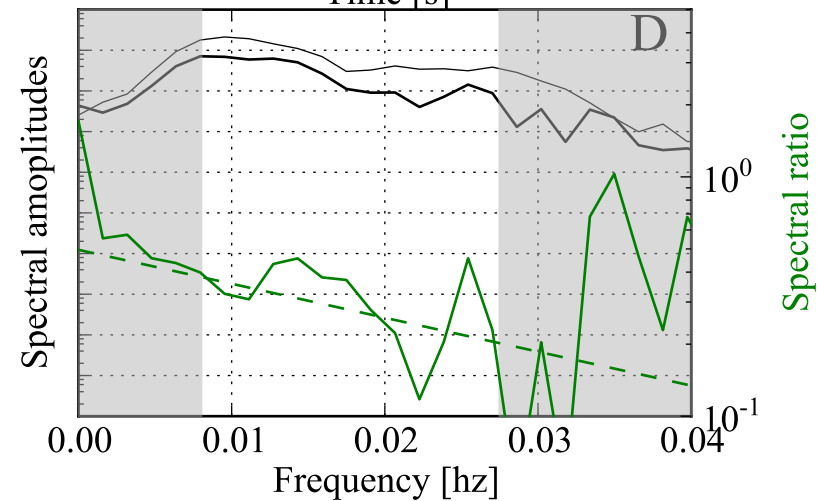
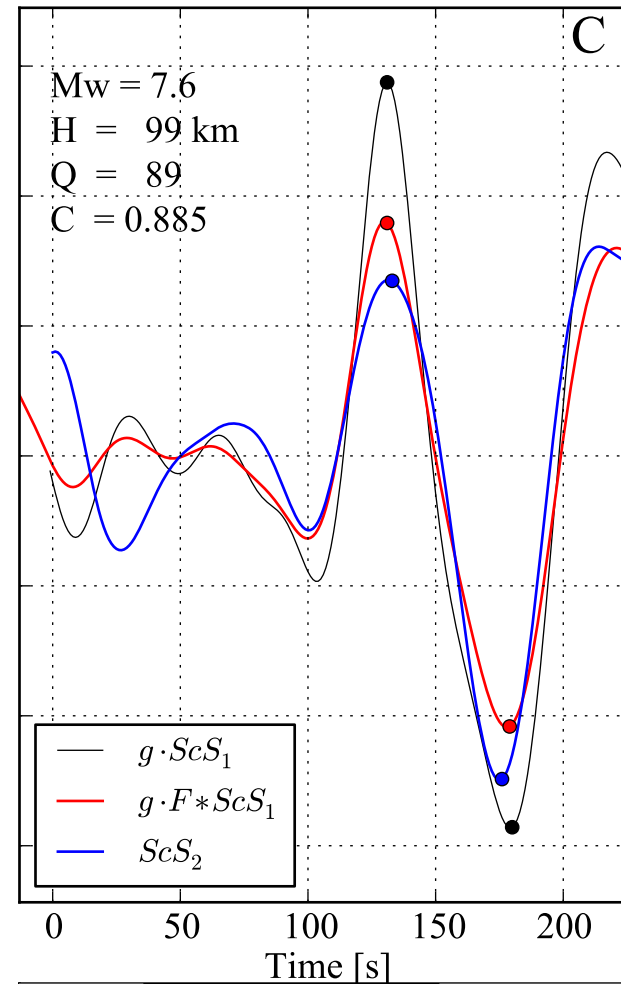
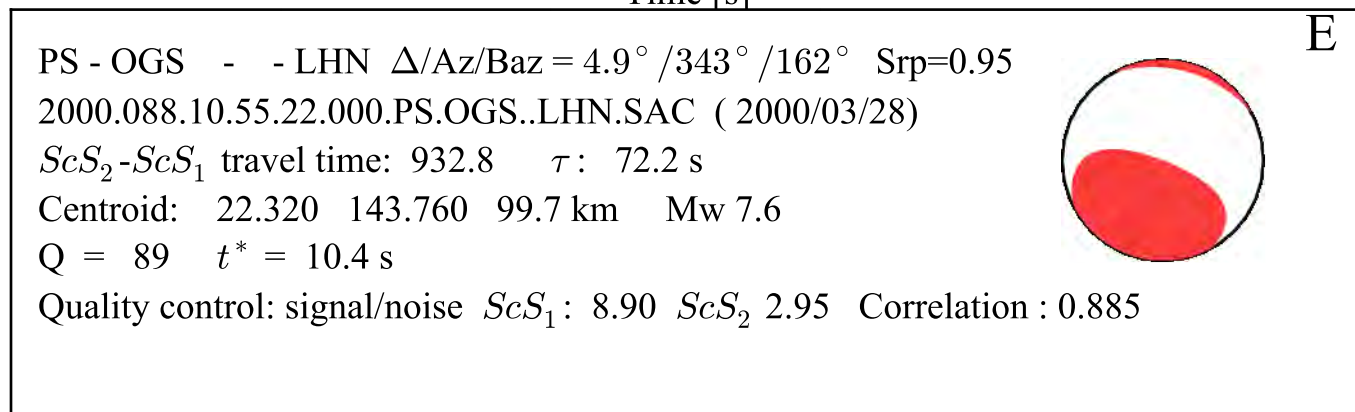
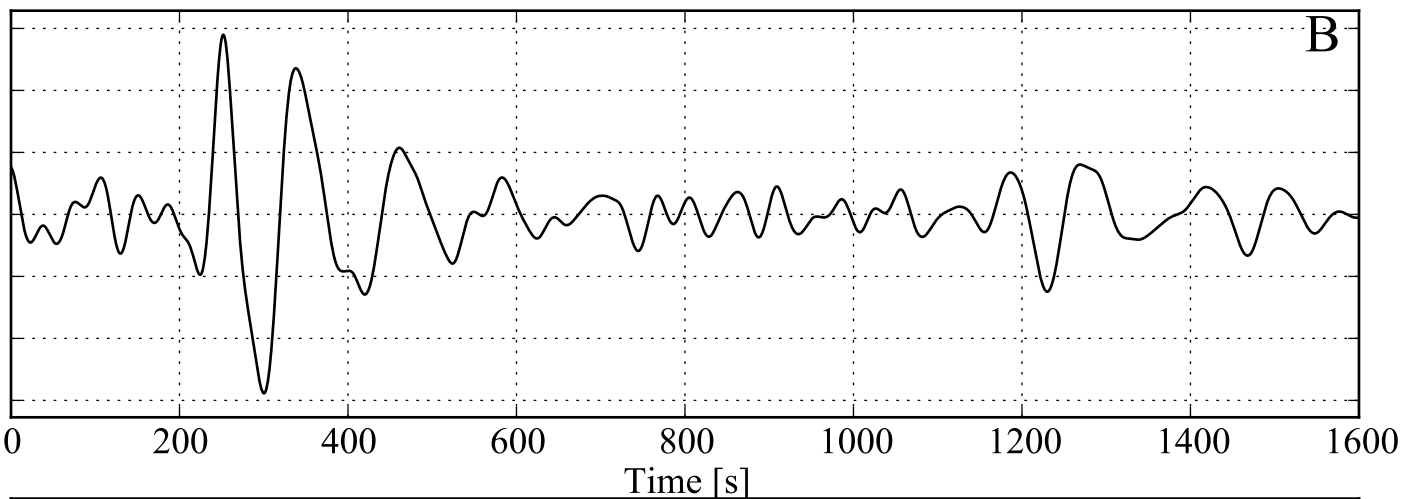
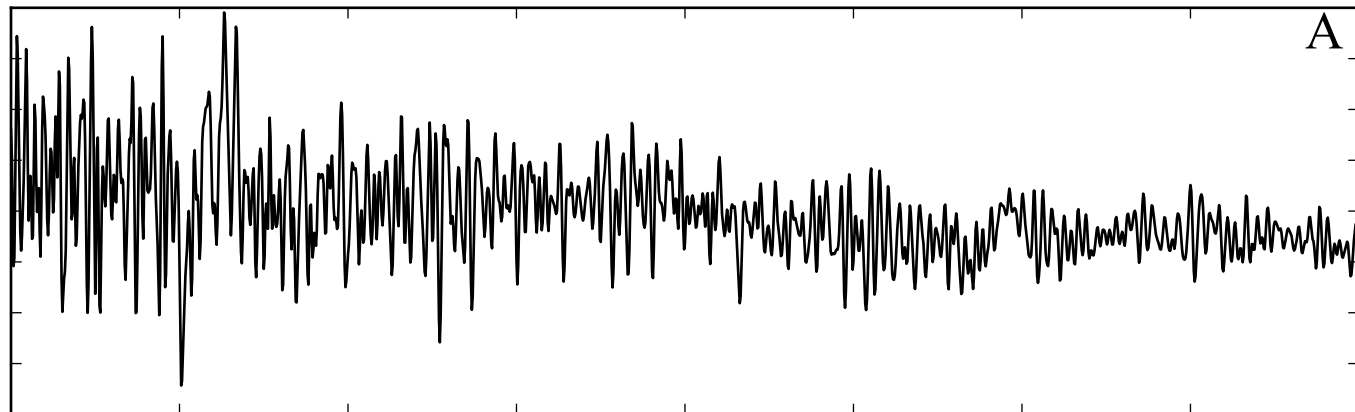



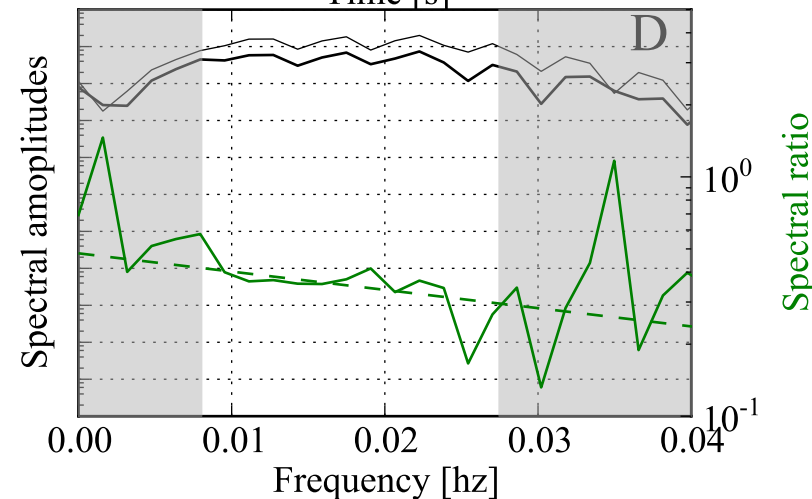
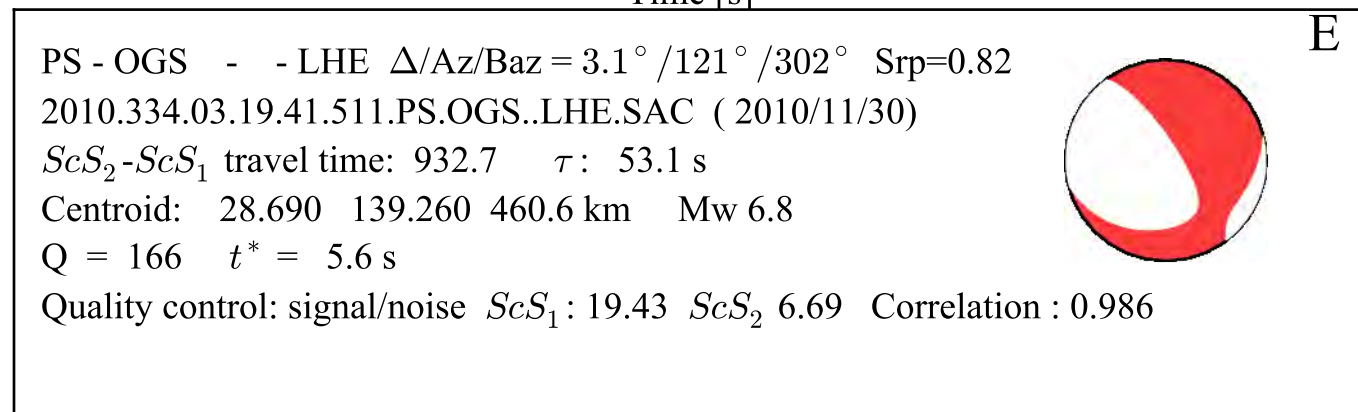
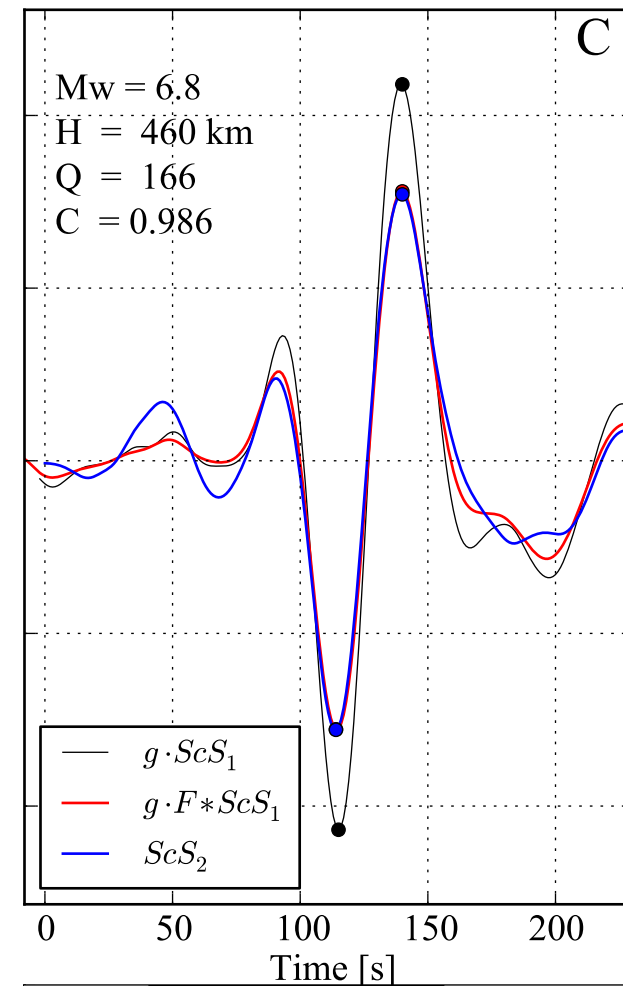
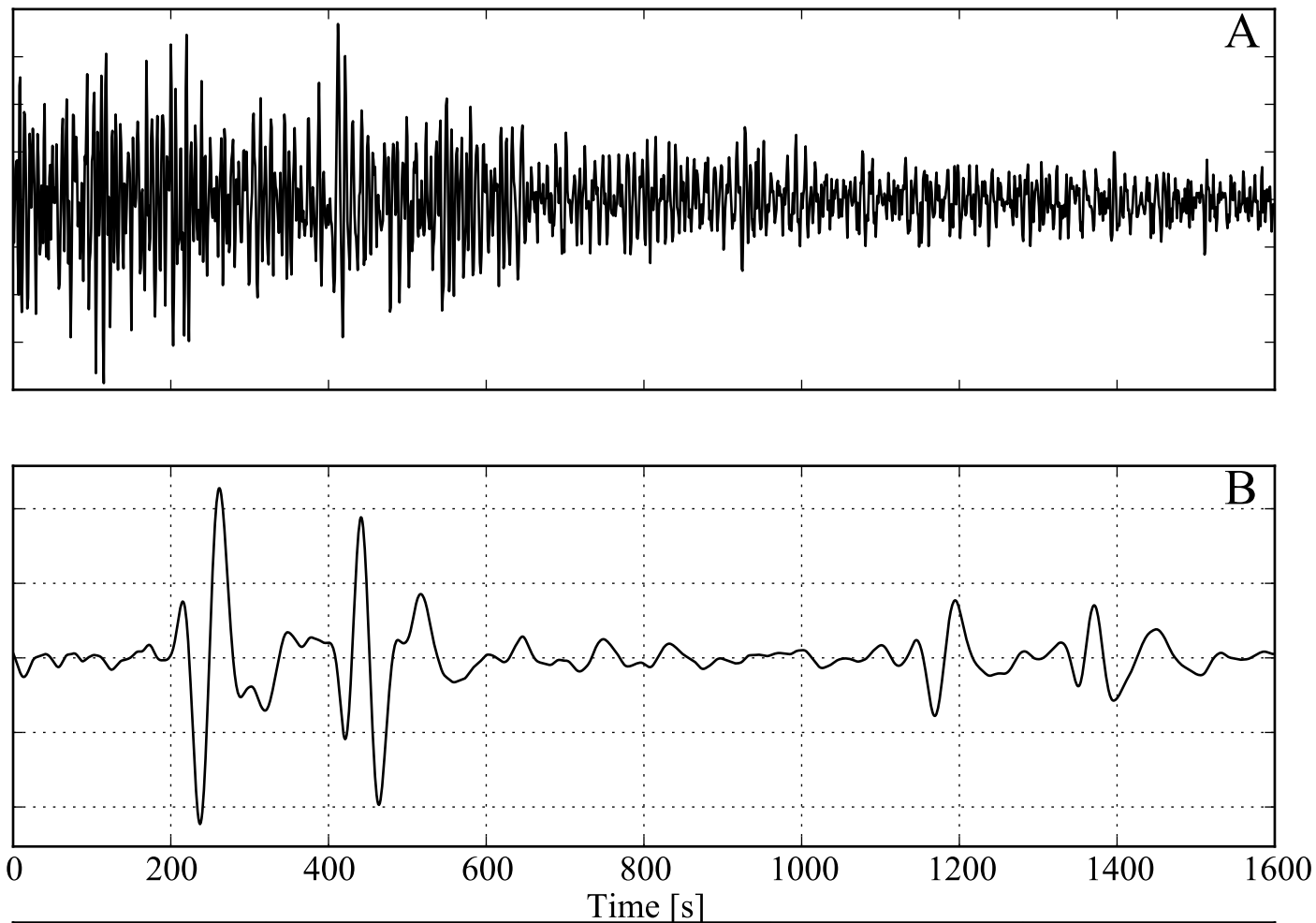


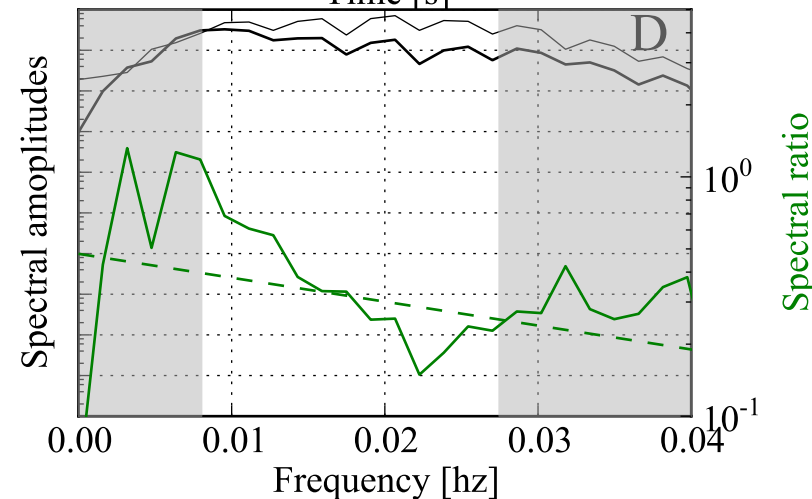
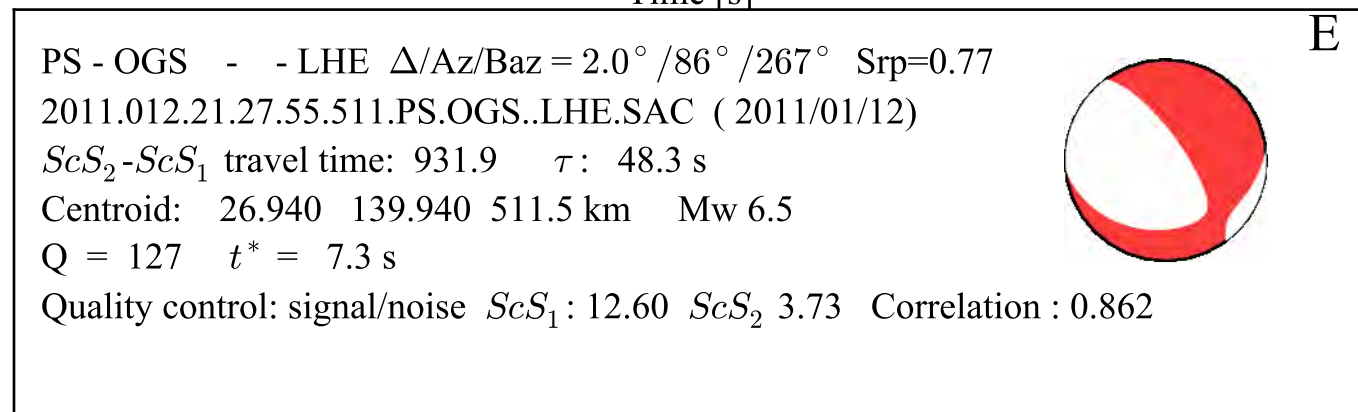
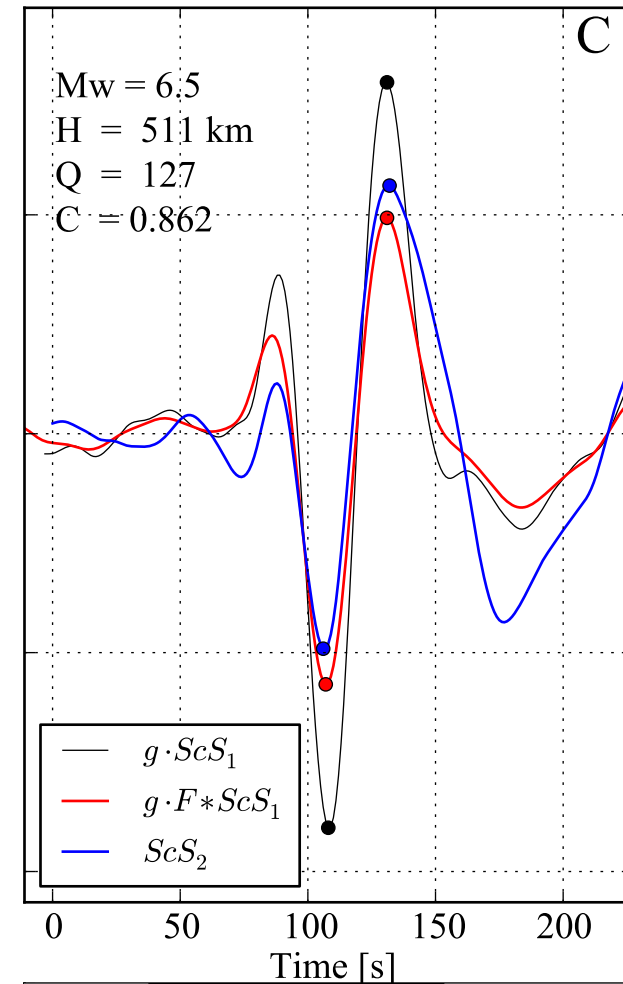
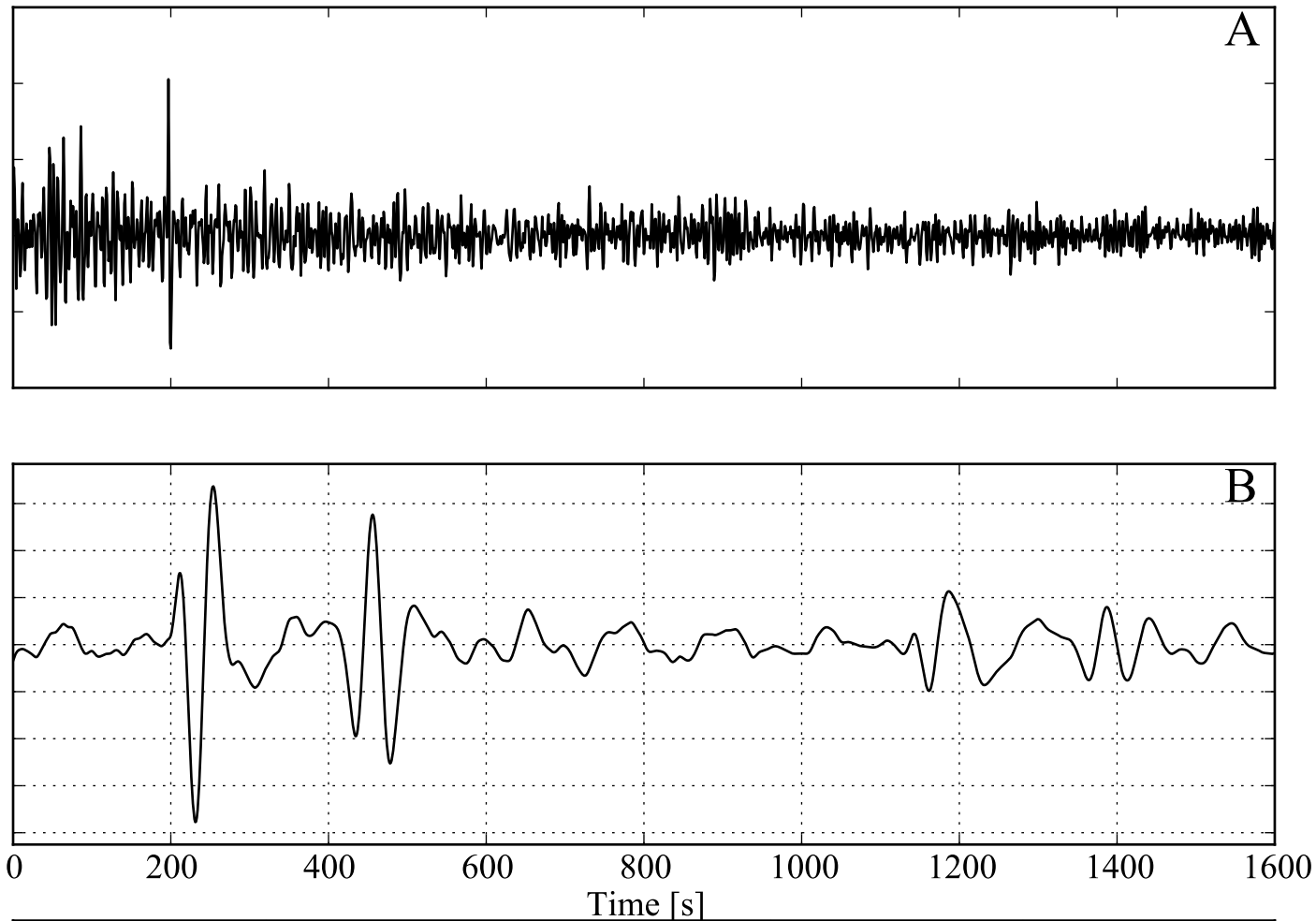


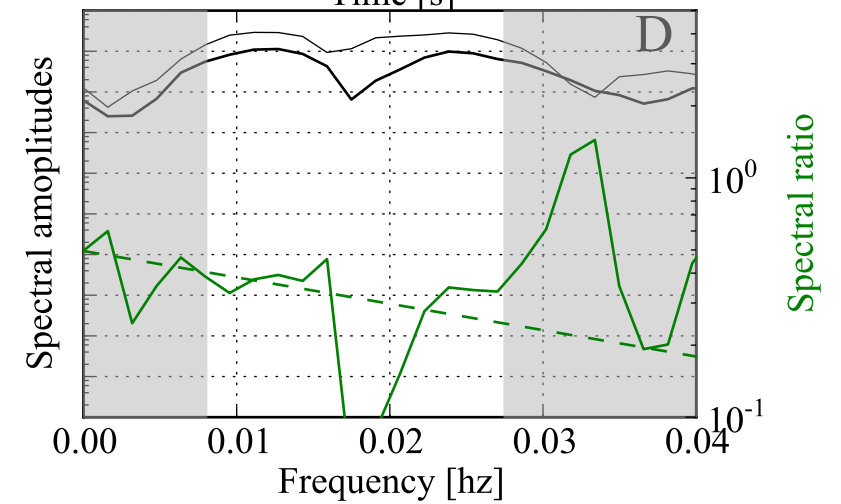
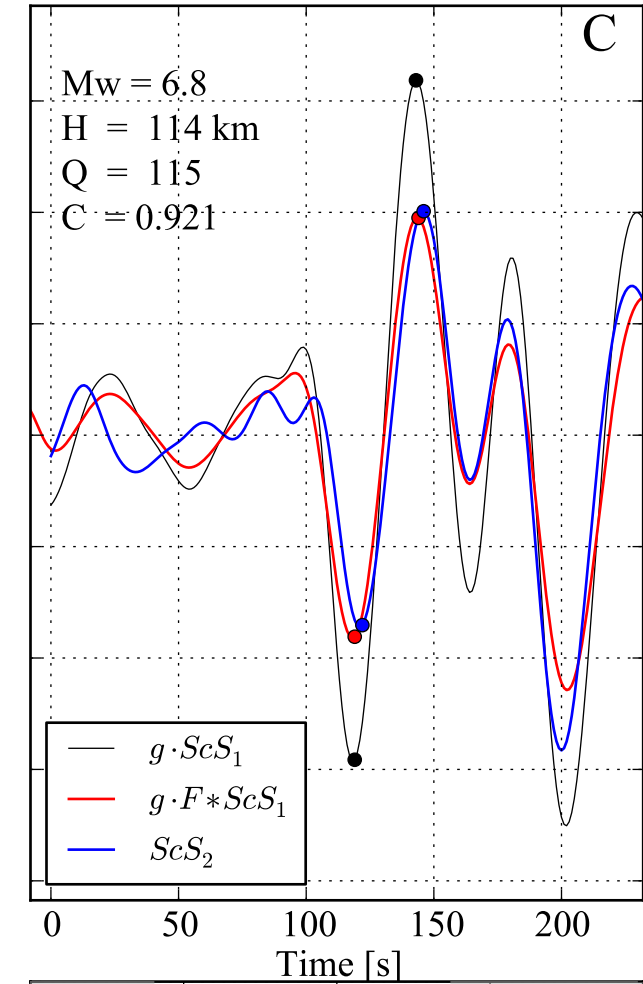
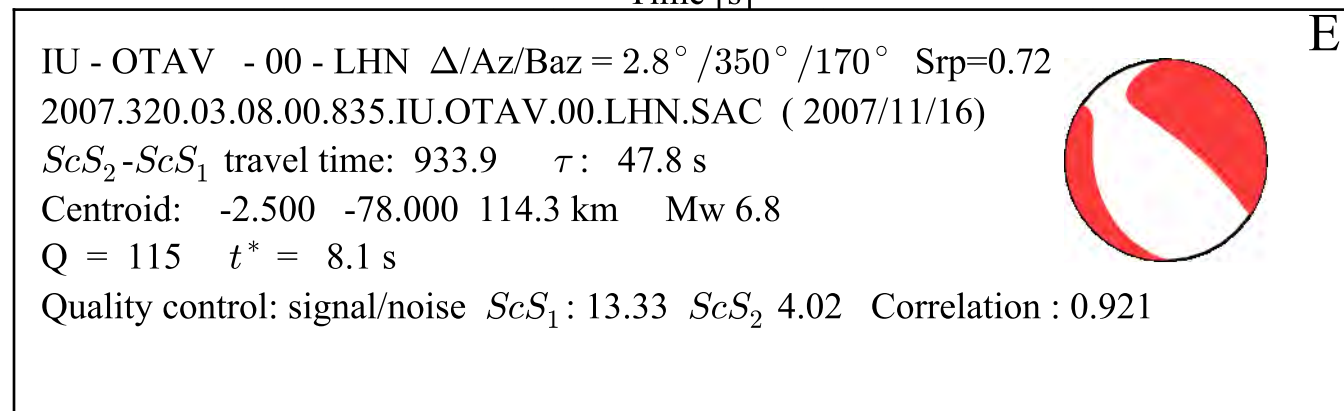
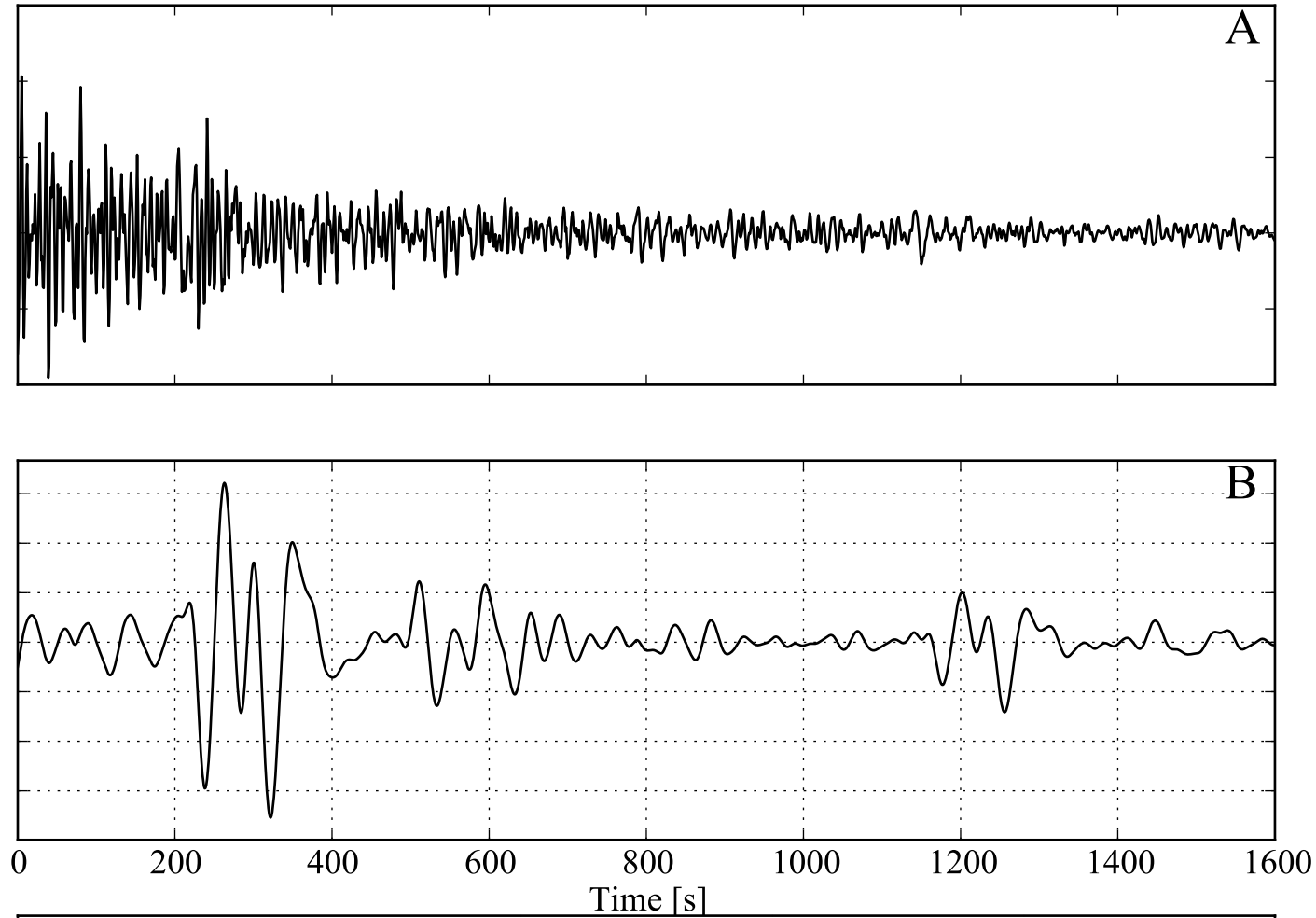


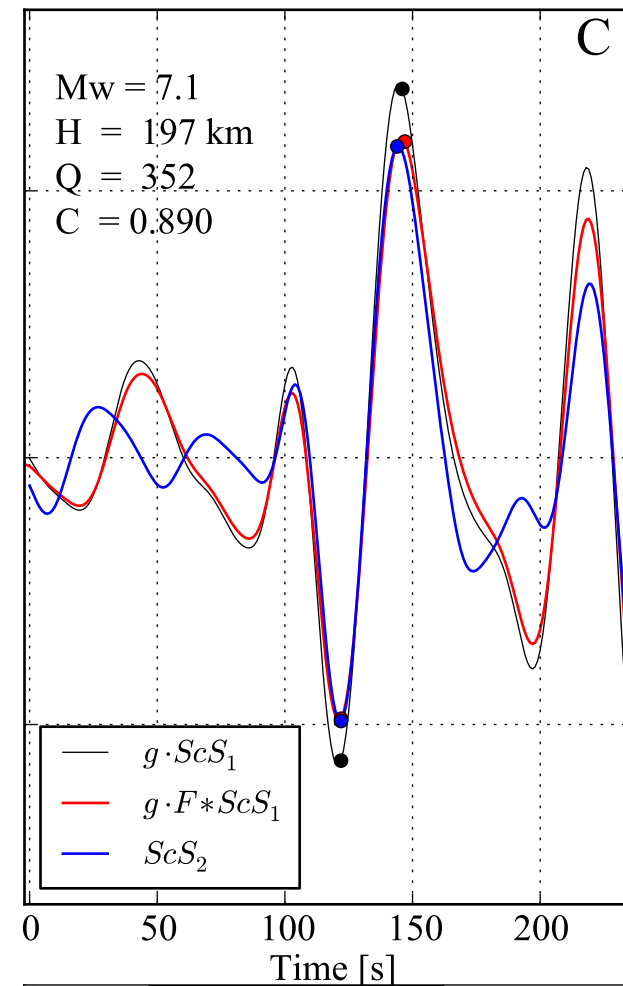
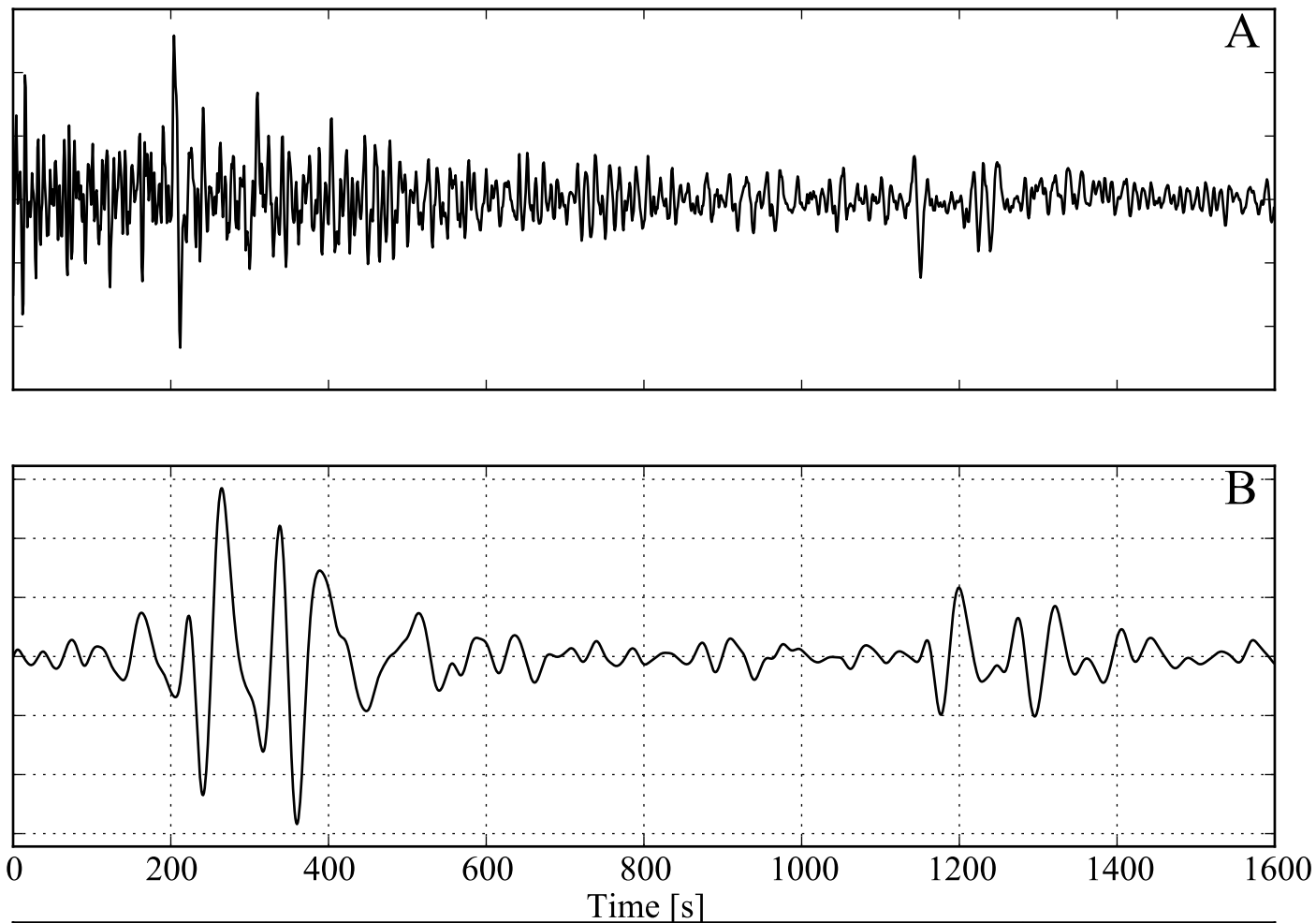





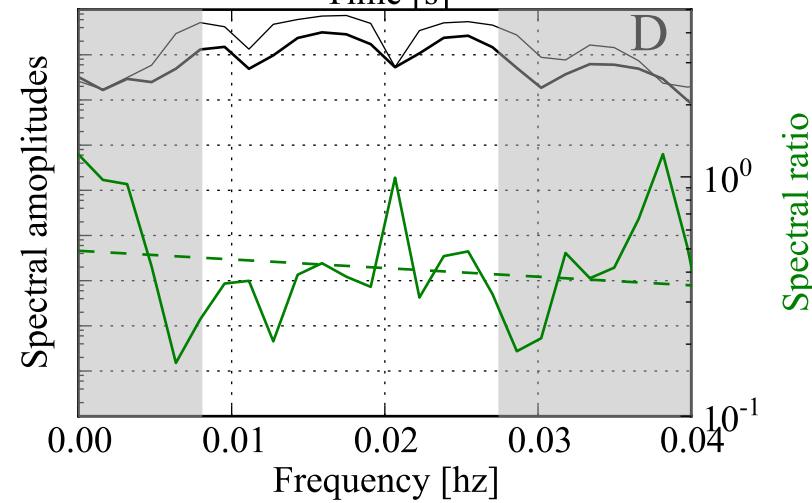


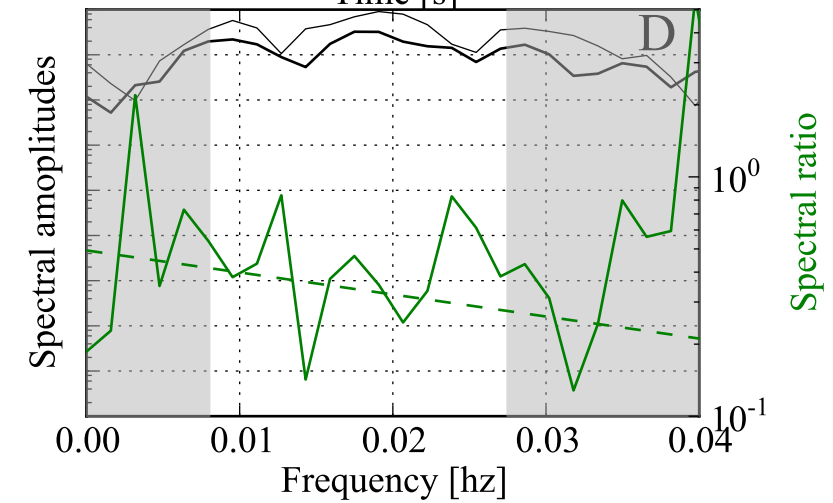
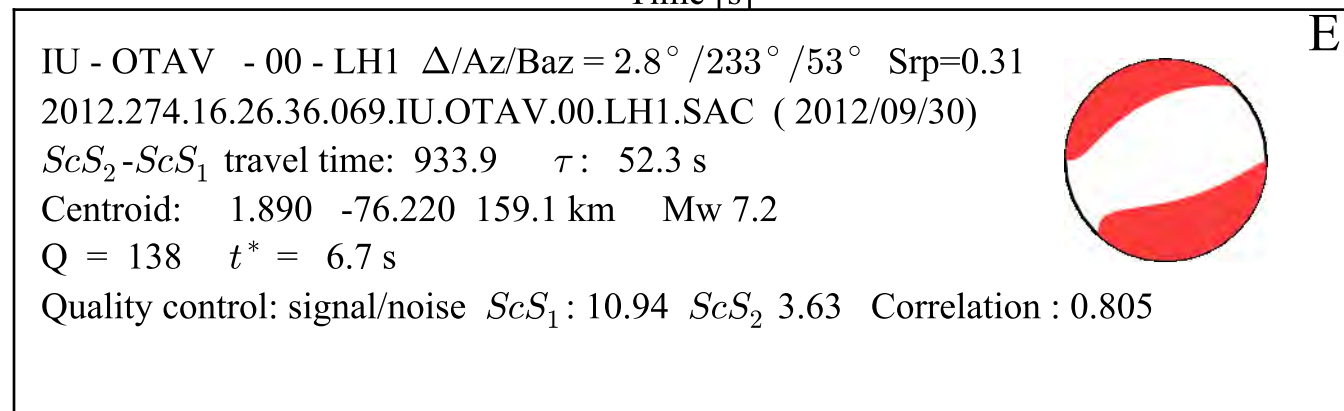
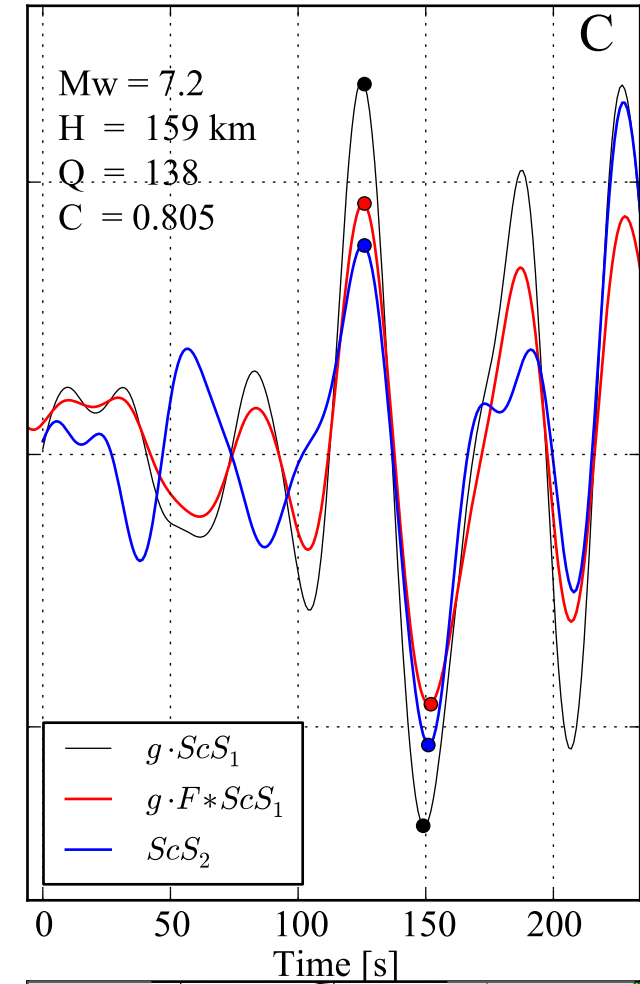
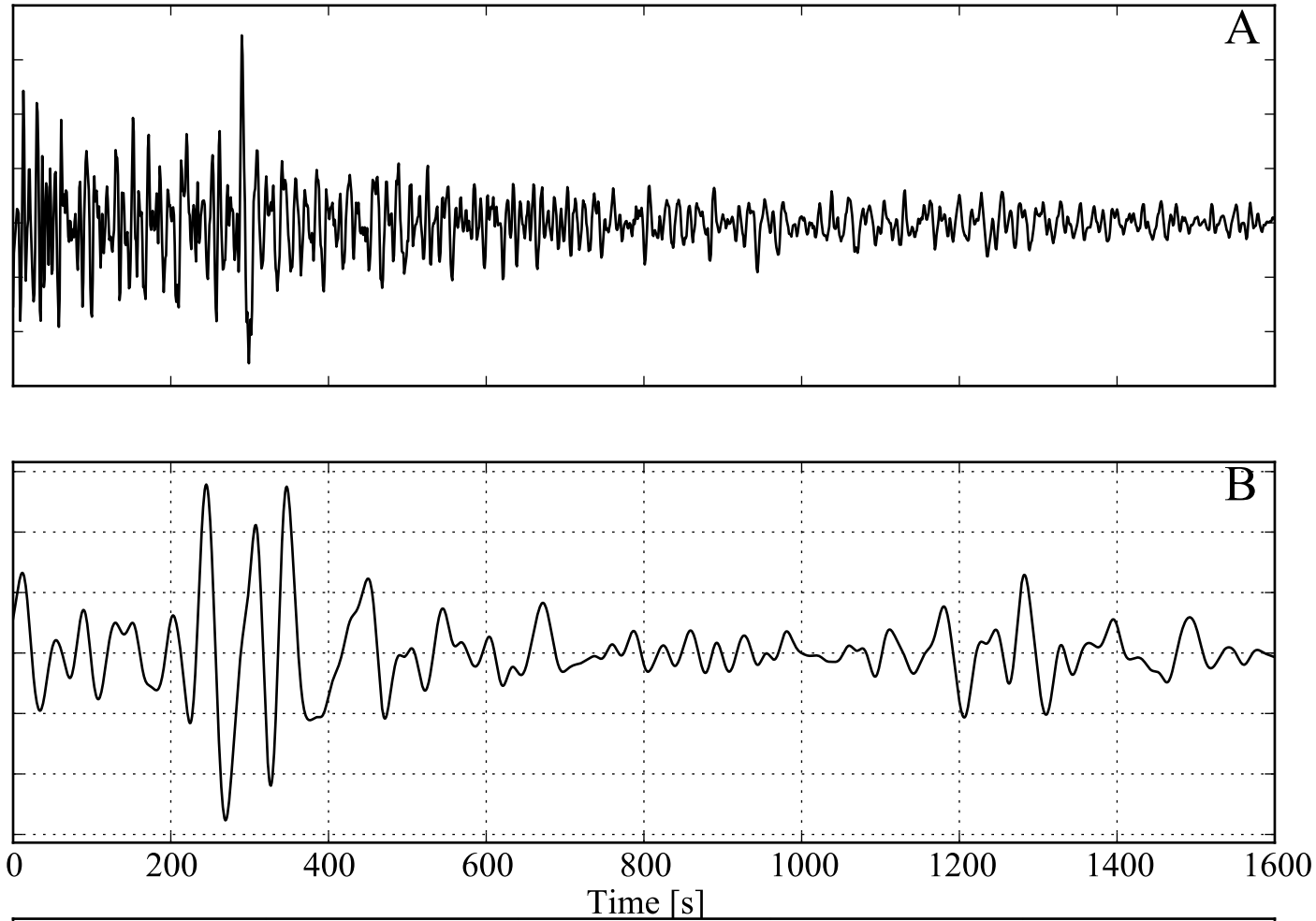


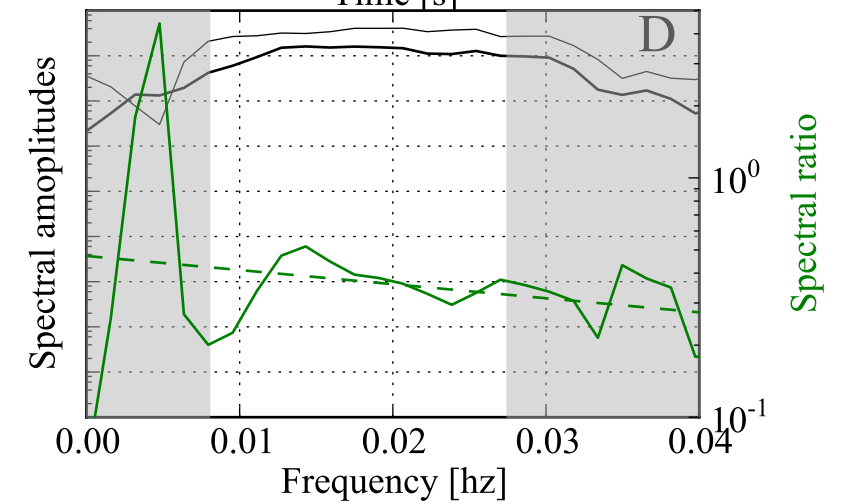
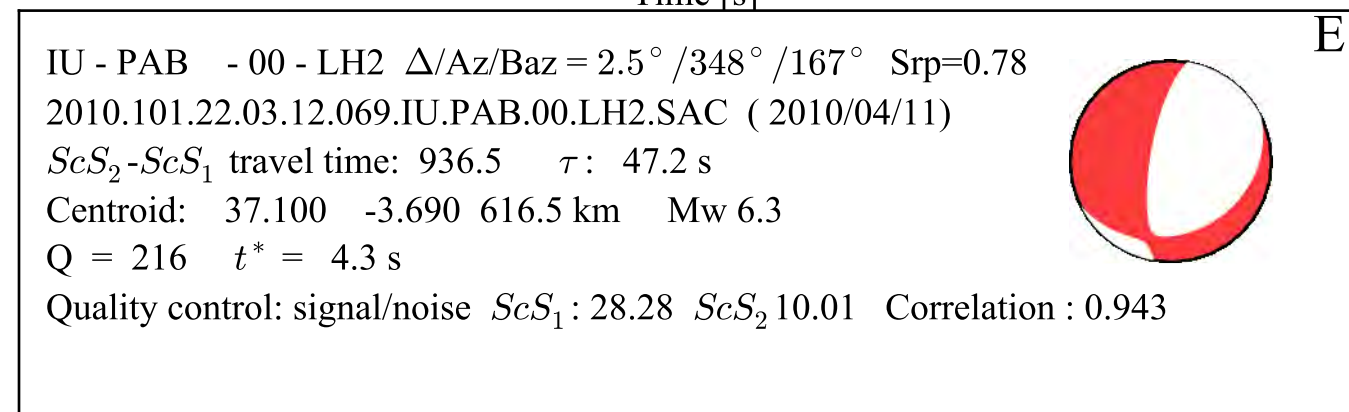
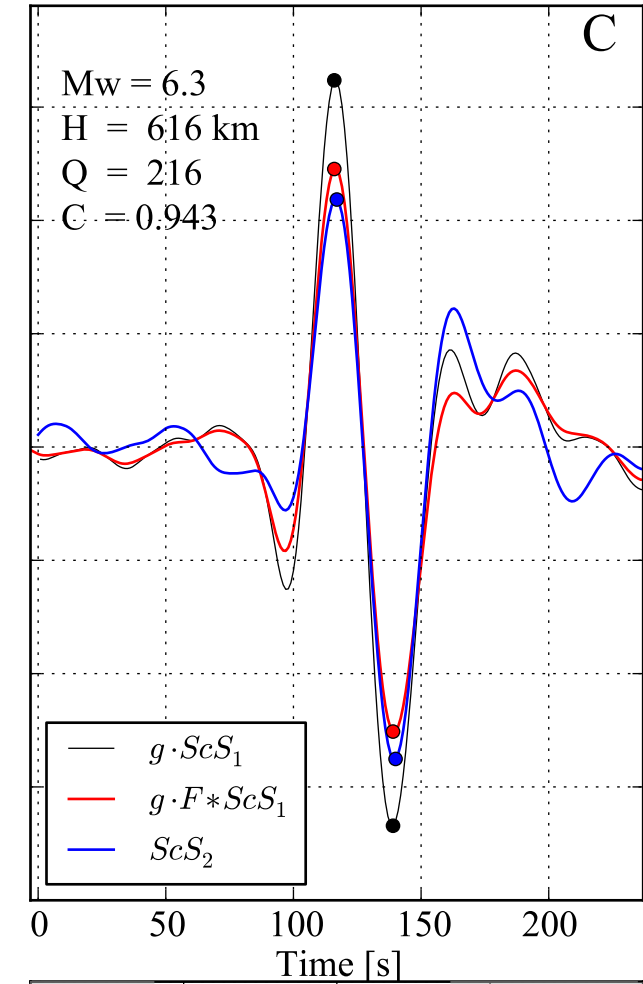
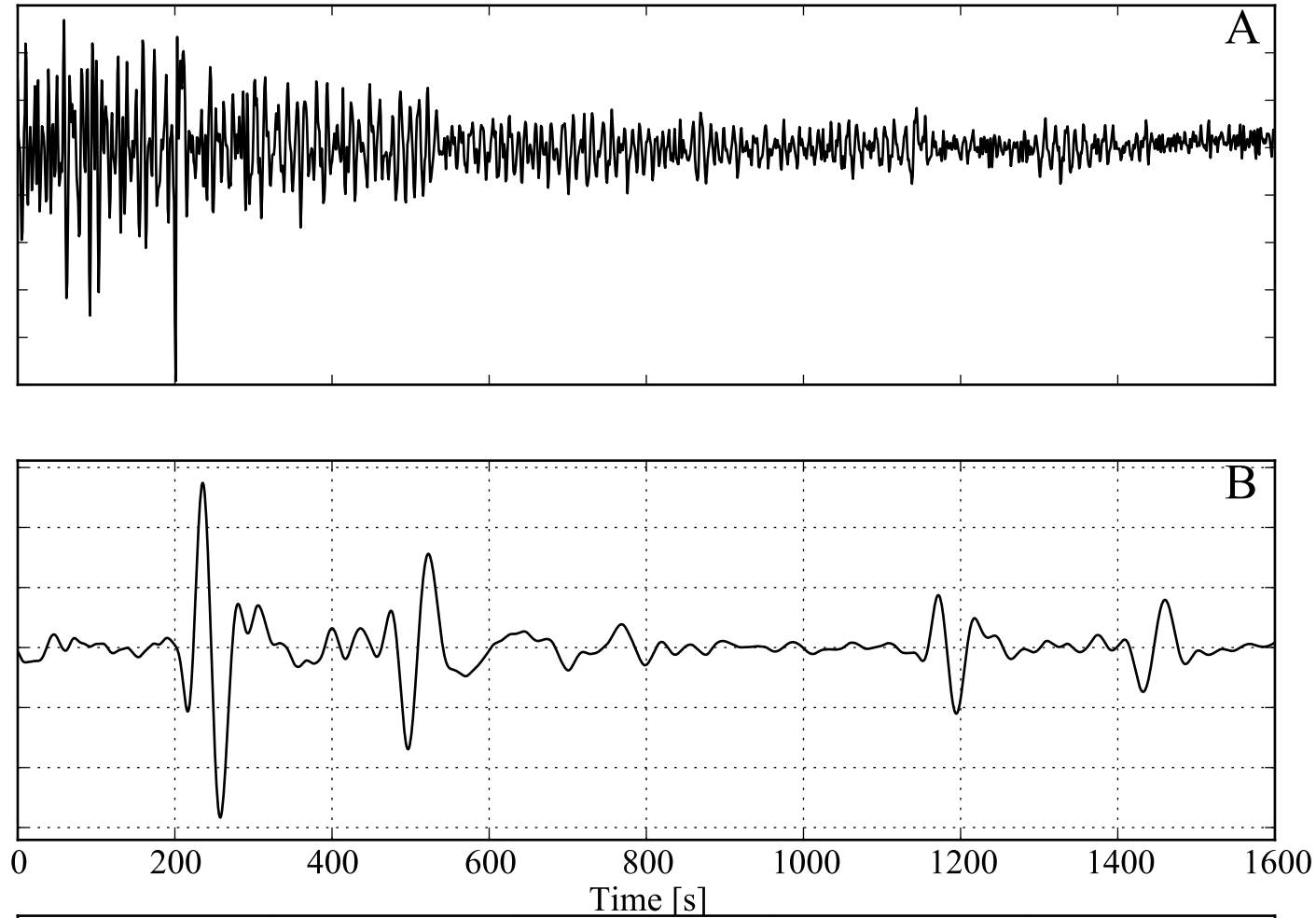


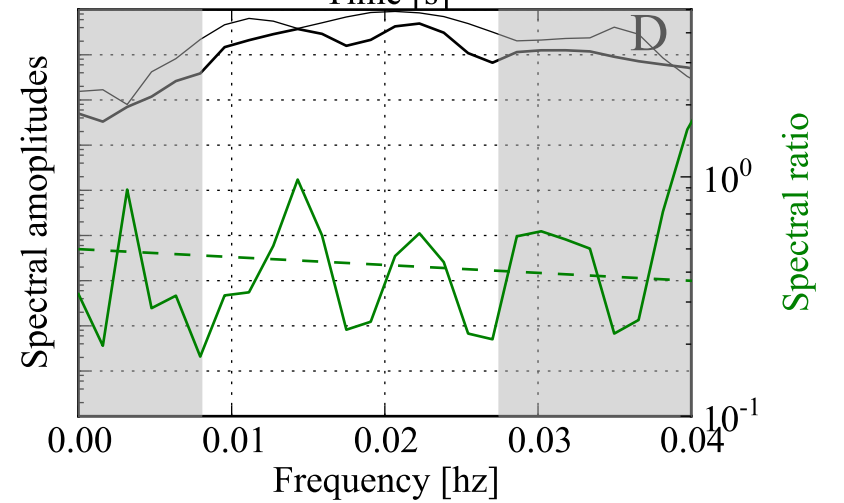
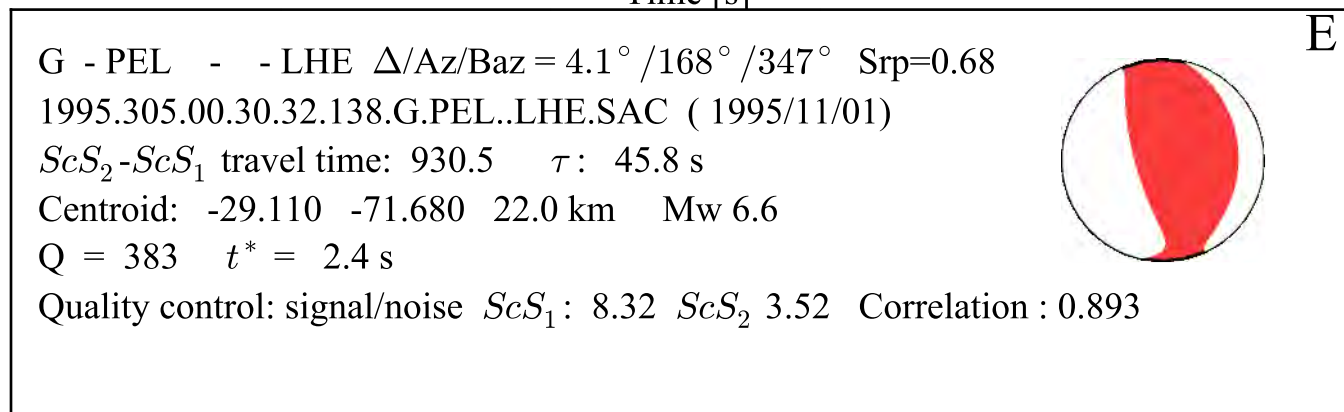
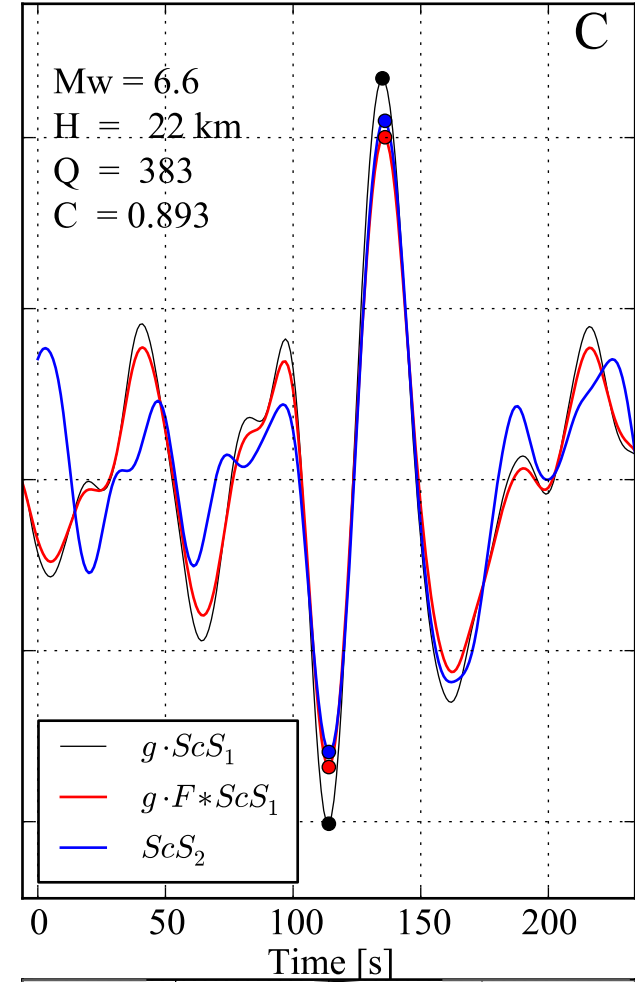
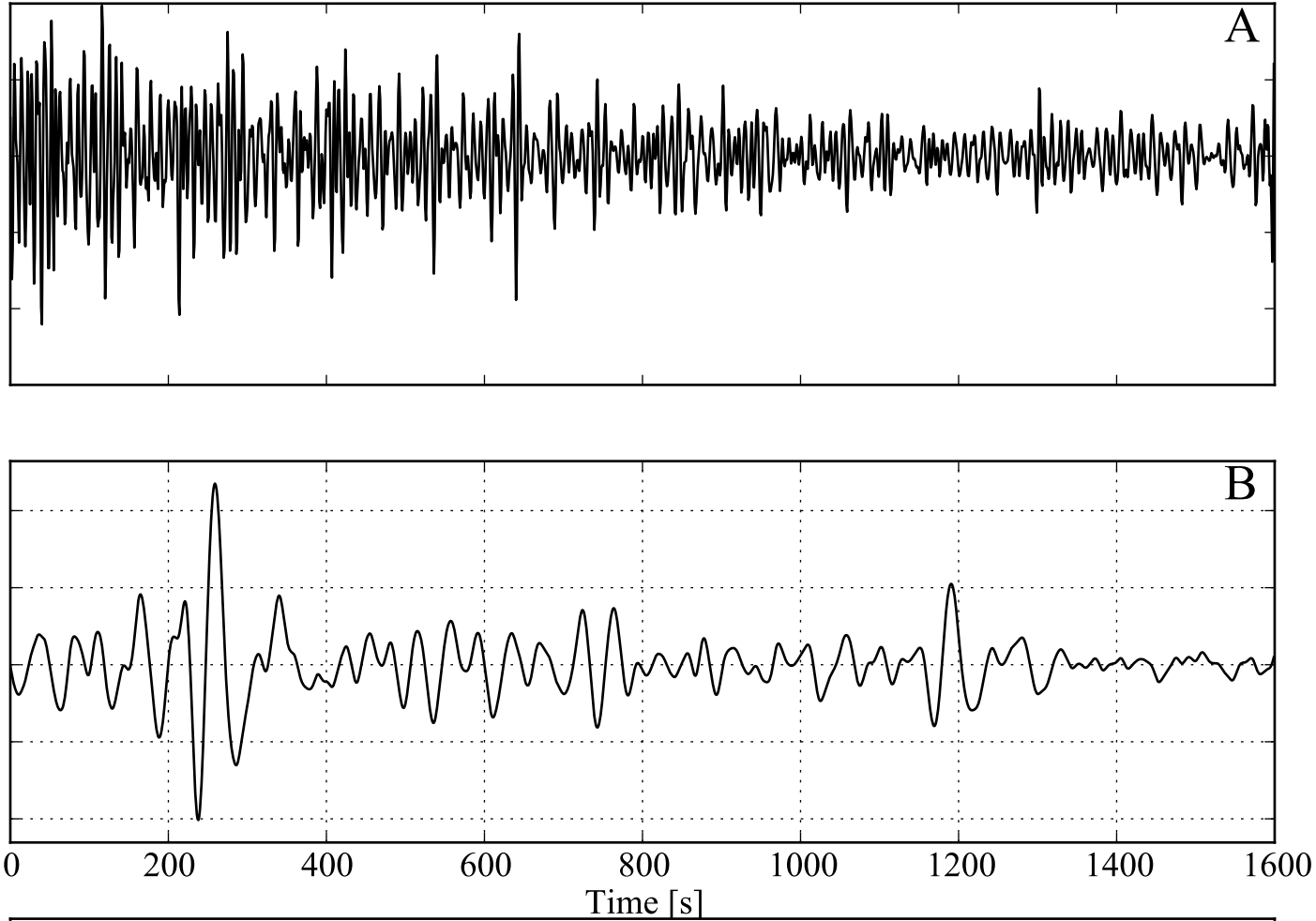


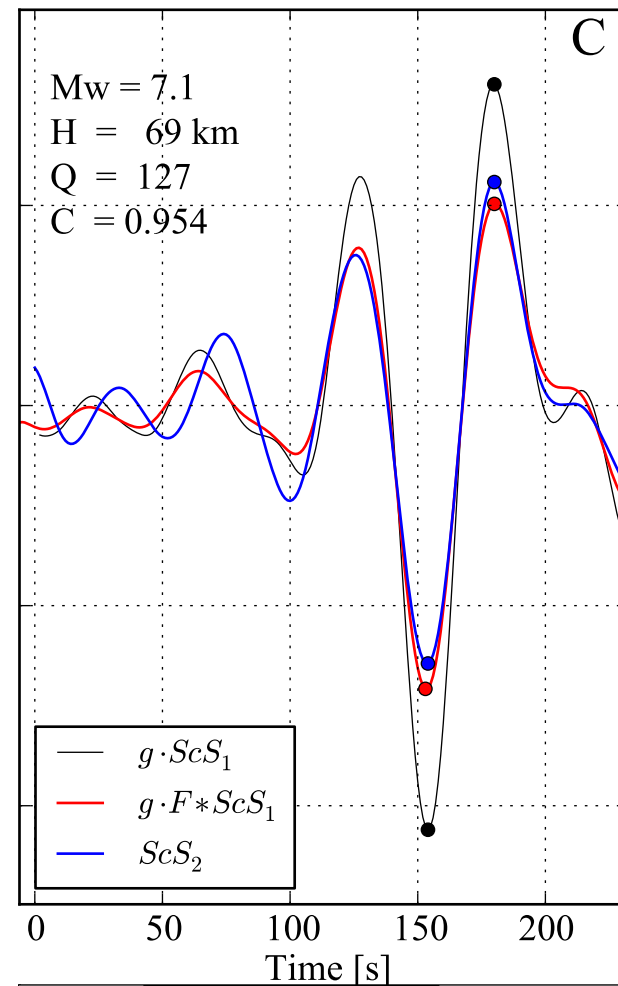
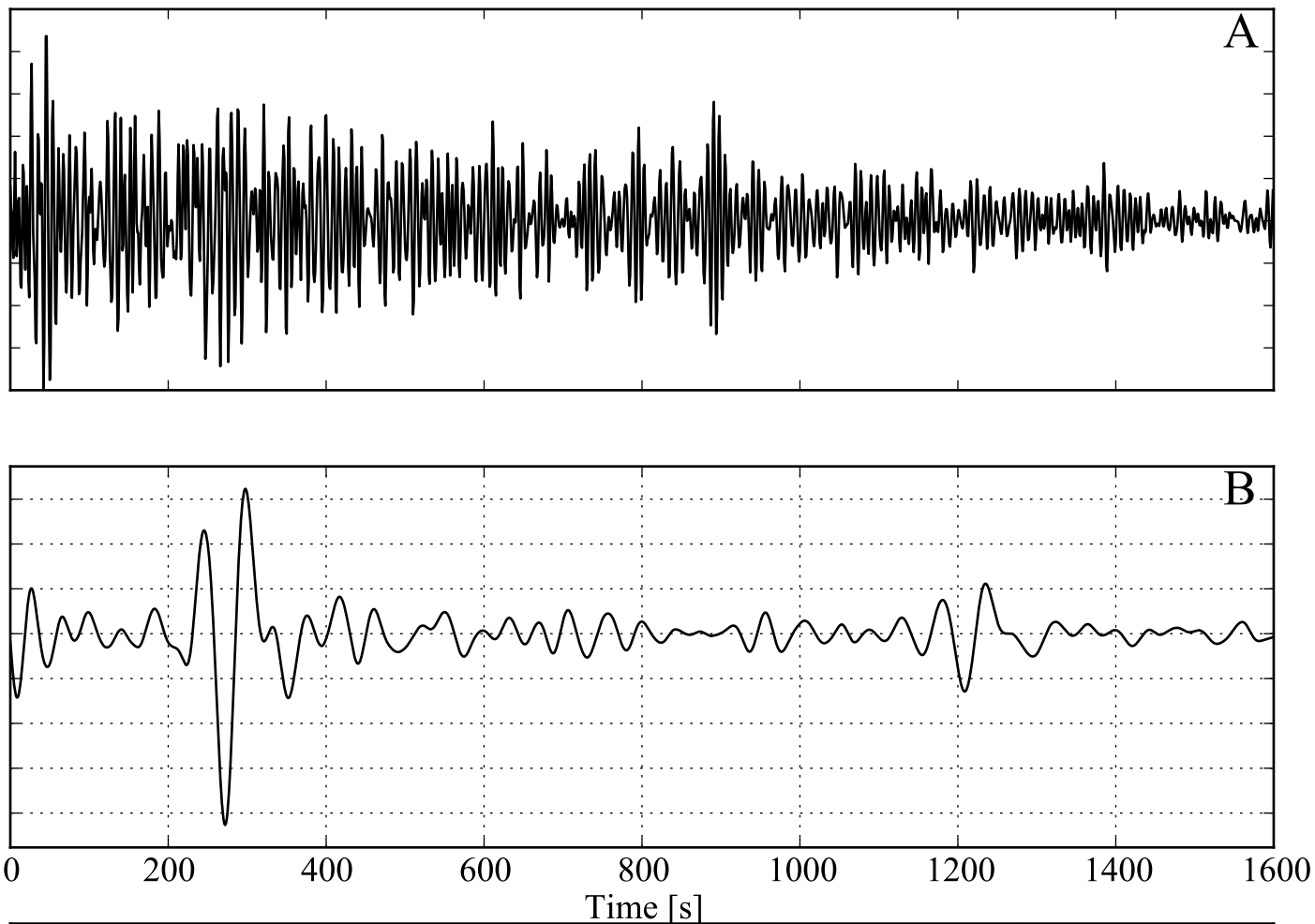
E
 IU - OTAV - 00 - LH1 $\Delta/Az/Baz = 2.0^\circ / 331^\circ / 151^\circ$ $Srp=0.77$
 2010.224.11.49.15.069.IU.OTAV.00.LH1.SAC (2010/08/12)
 $ScS_2 - ScS_1$ travel time: 934.0 τ : 53.3 s
 Centroid: -1.510 -77.510 197.8 km M_w 7.1
 $Q = 352$ $t^* = 2.6$ s
 Quality control: signal/noise ScS_1 : 12.60 ScS_2 5.29 Correlation : 0.890



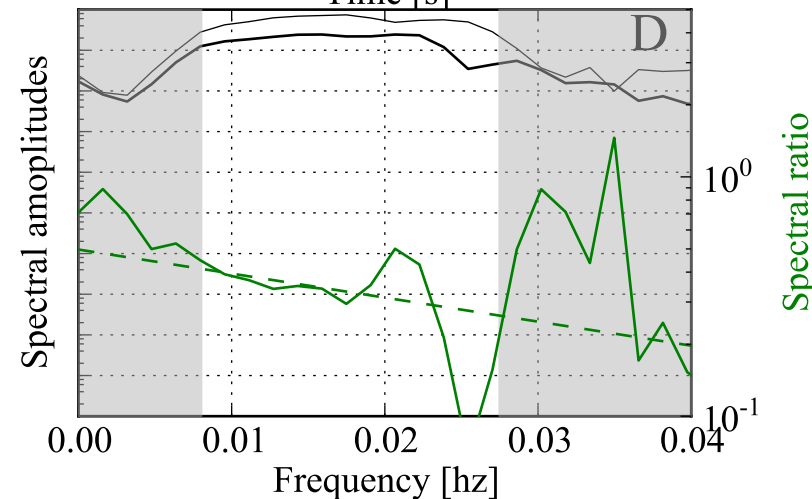


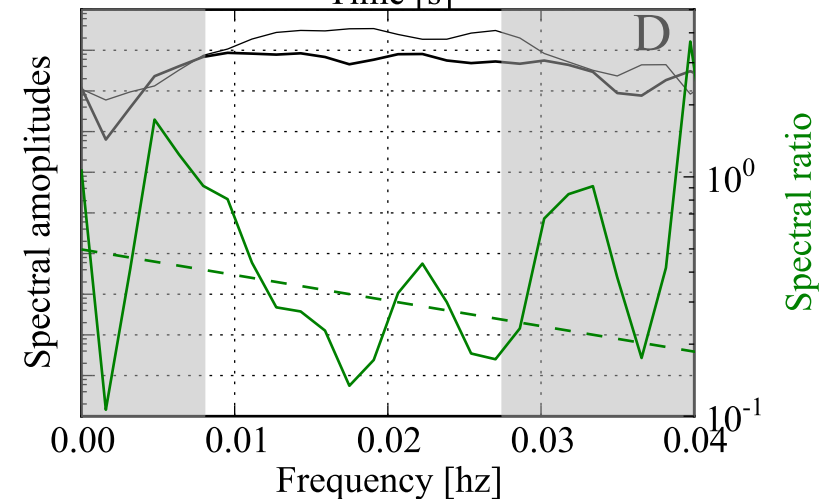
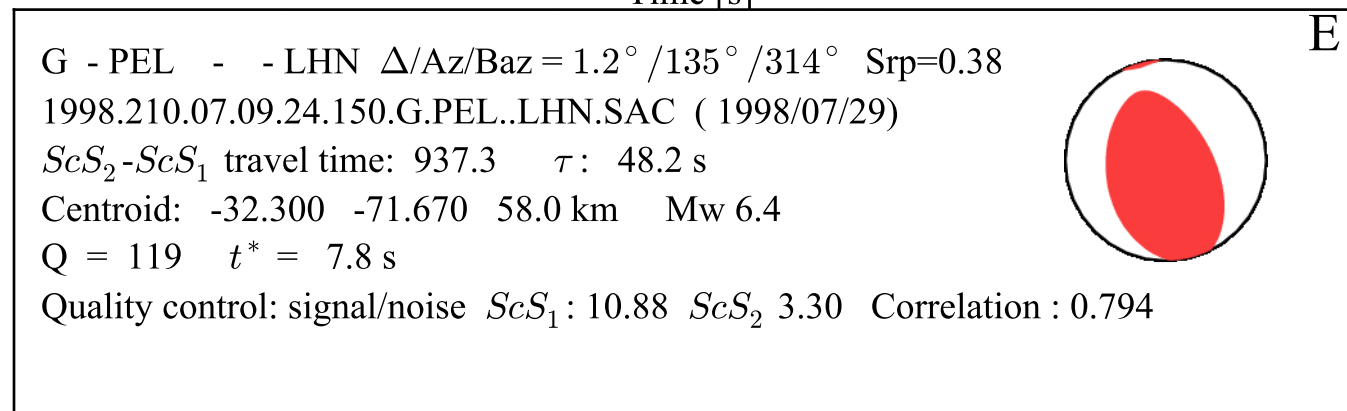
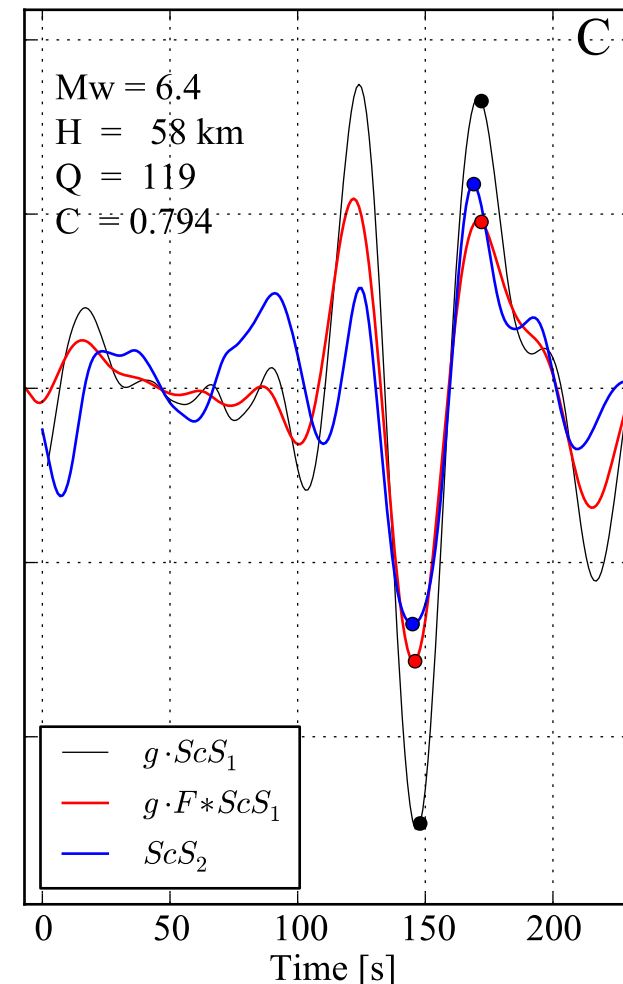
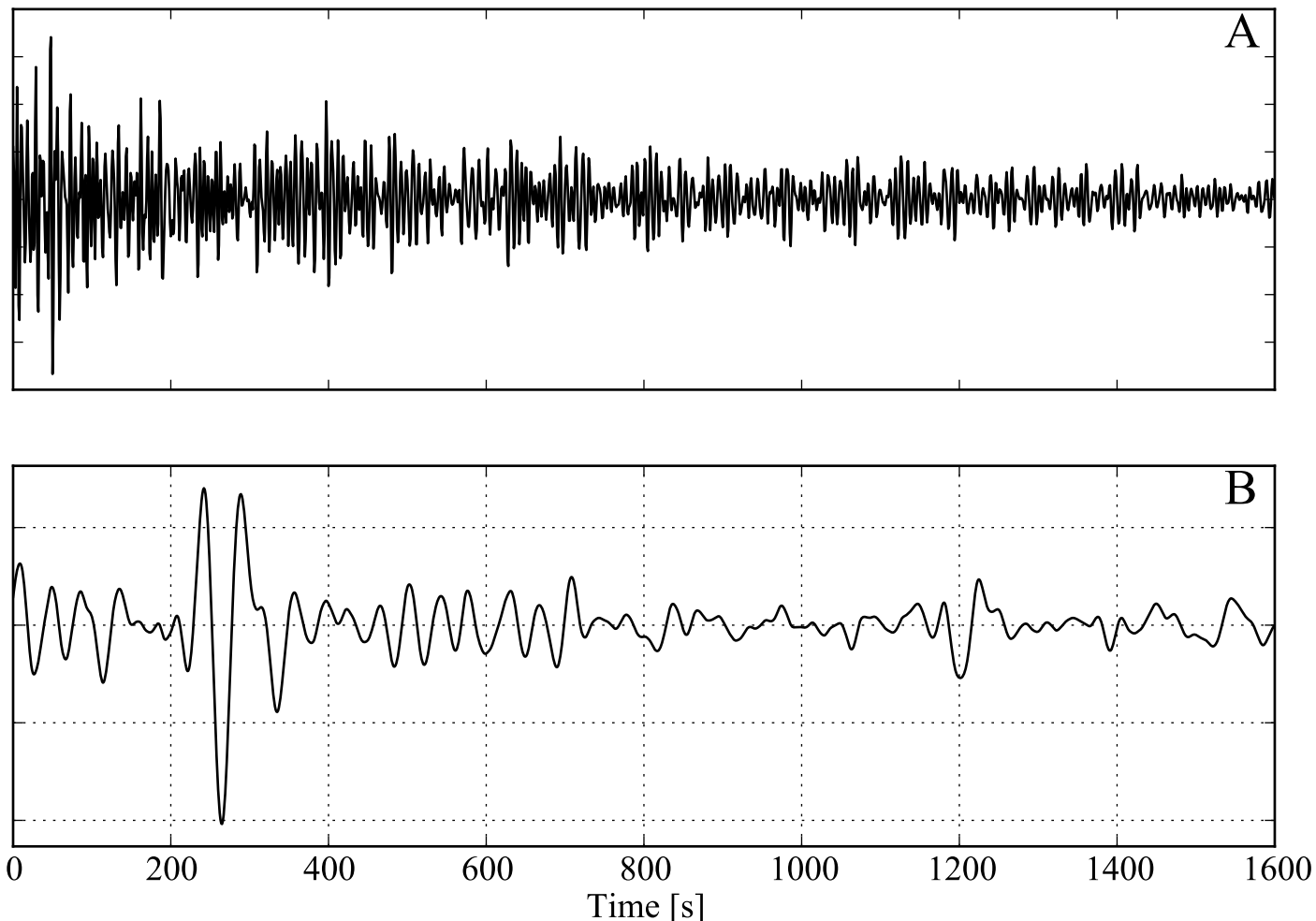


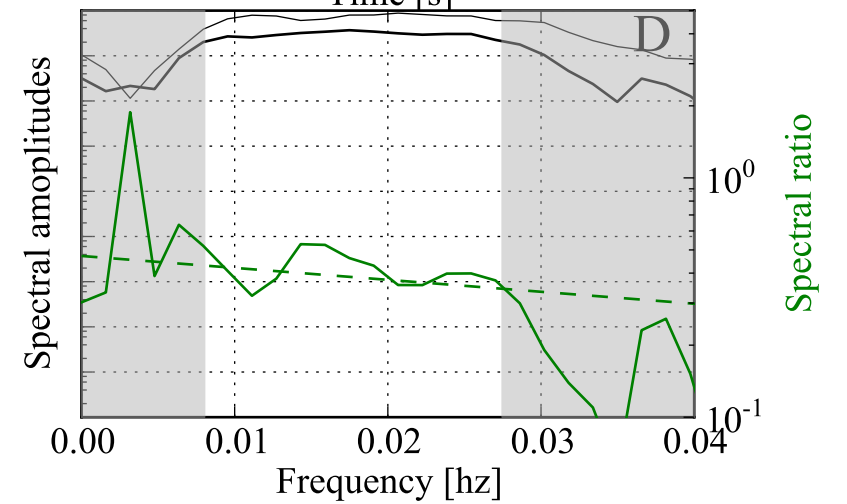
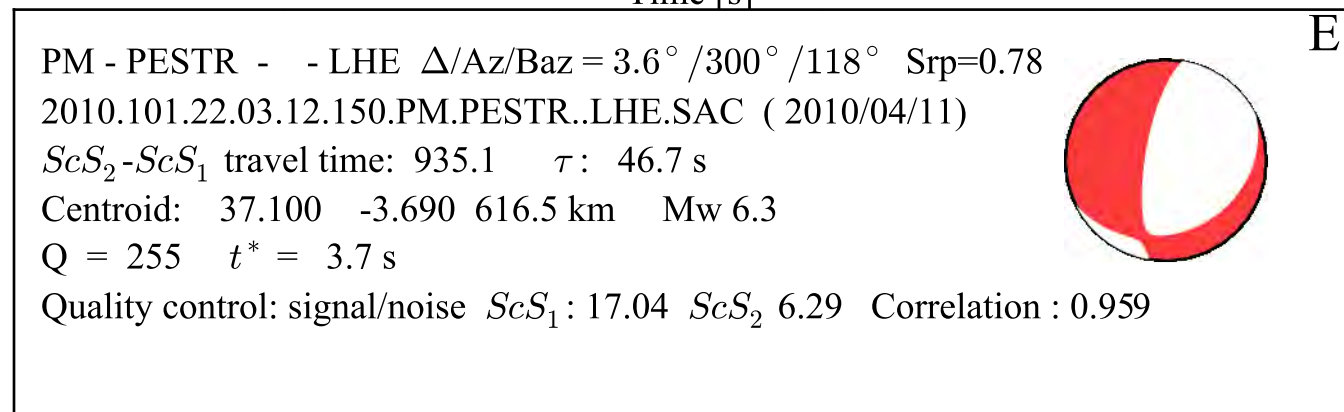
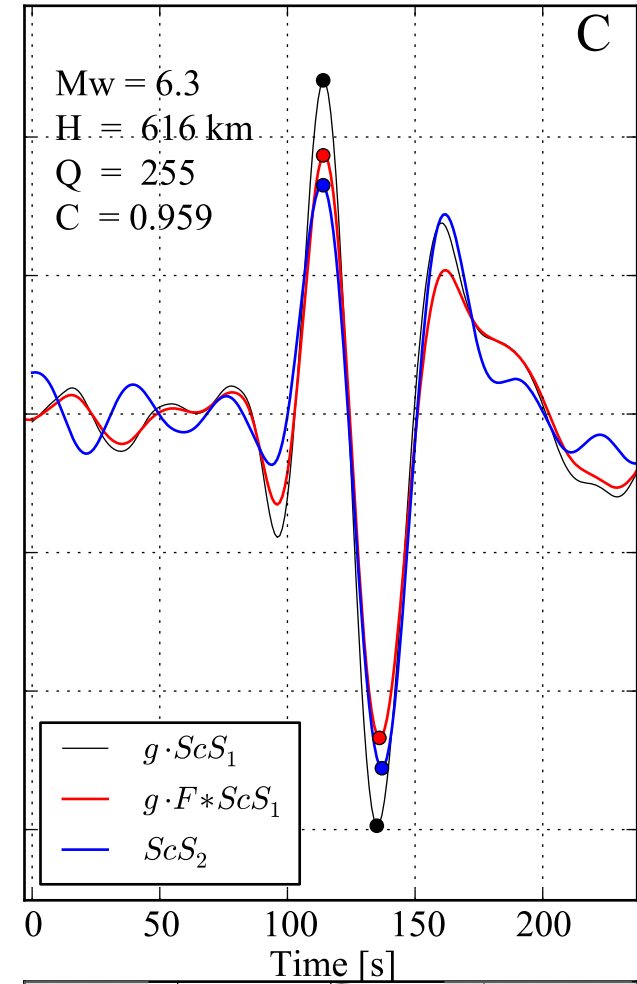
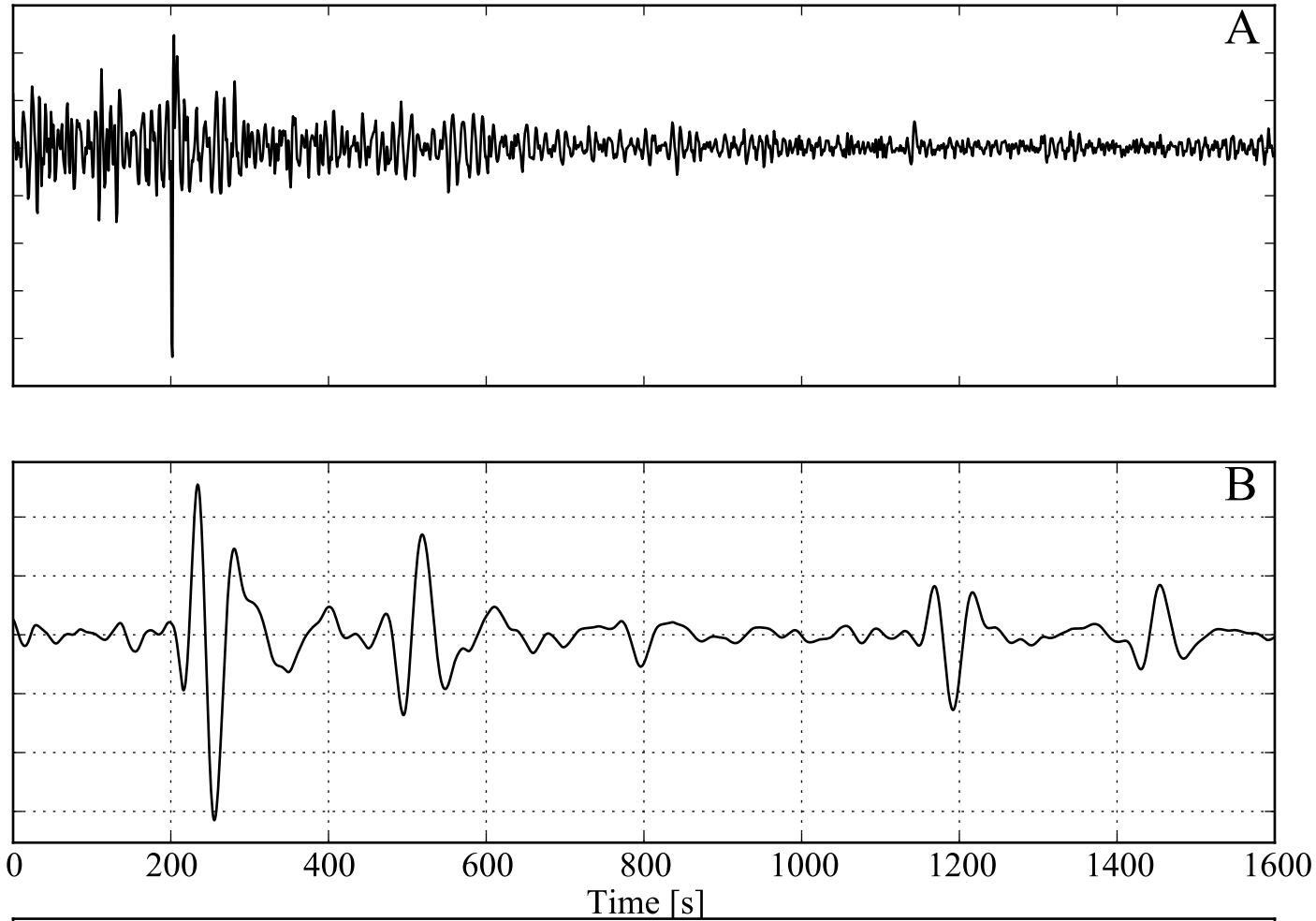


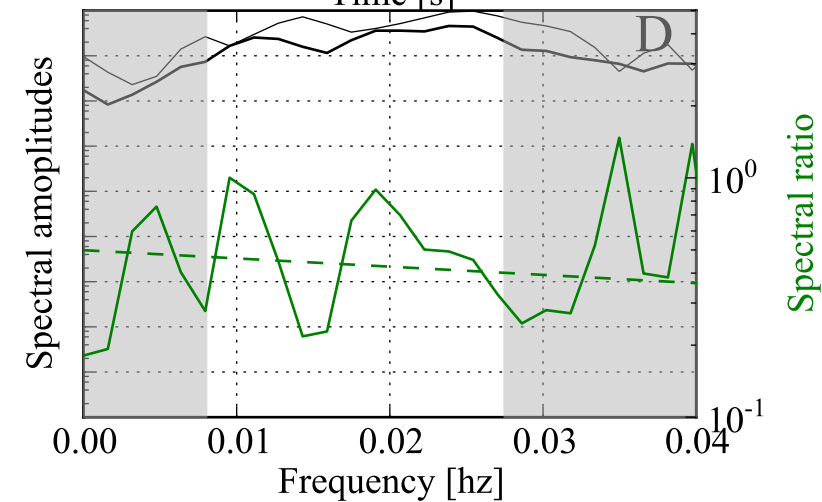
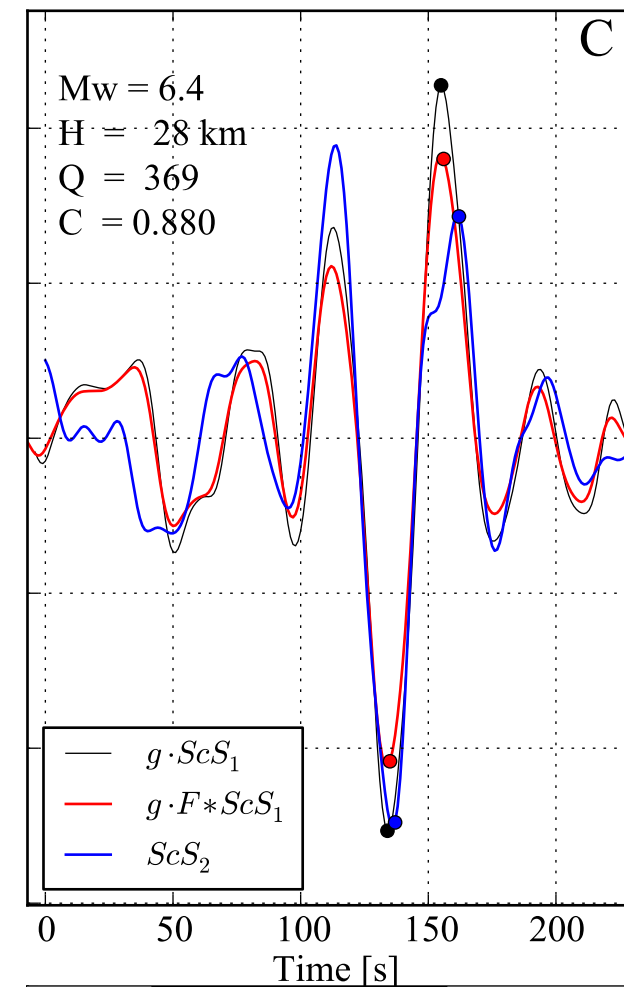
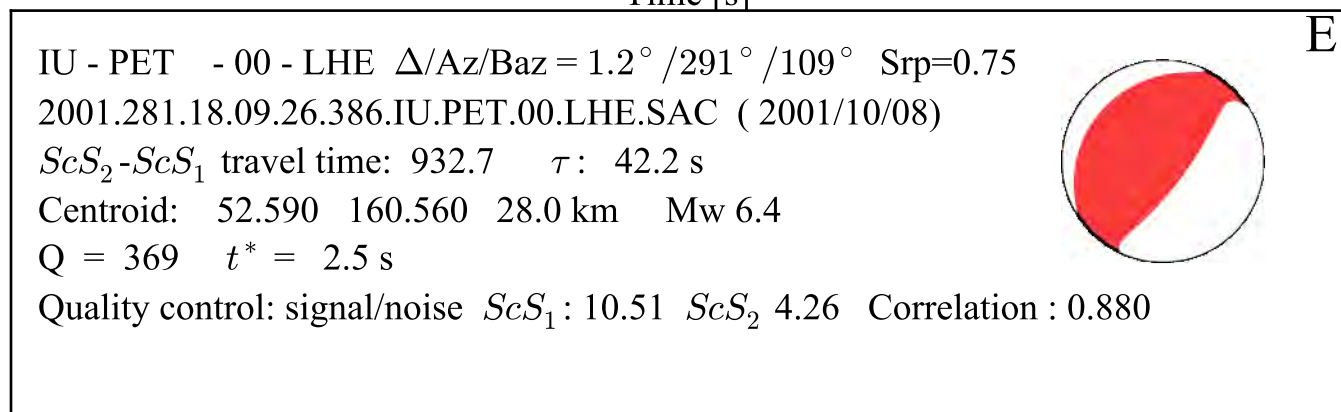
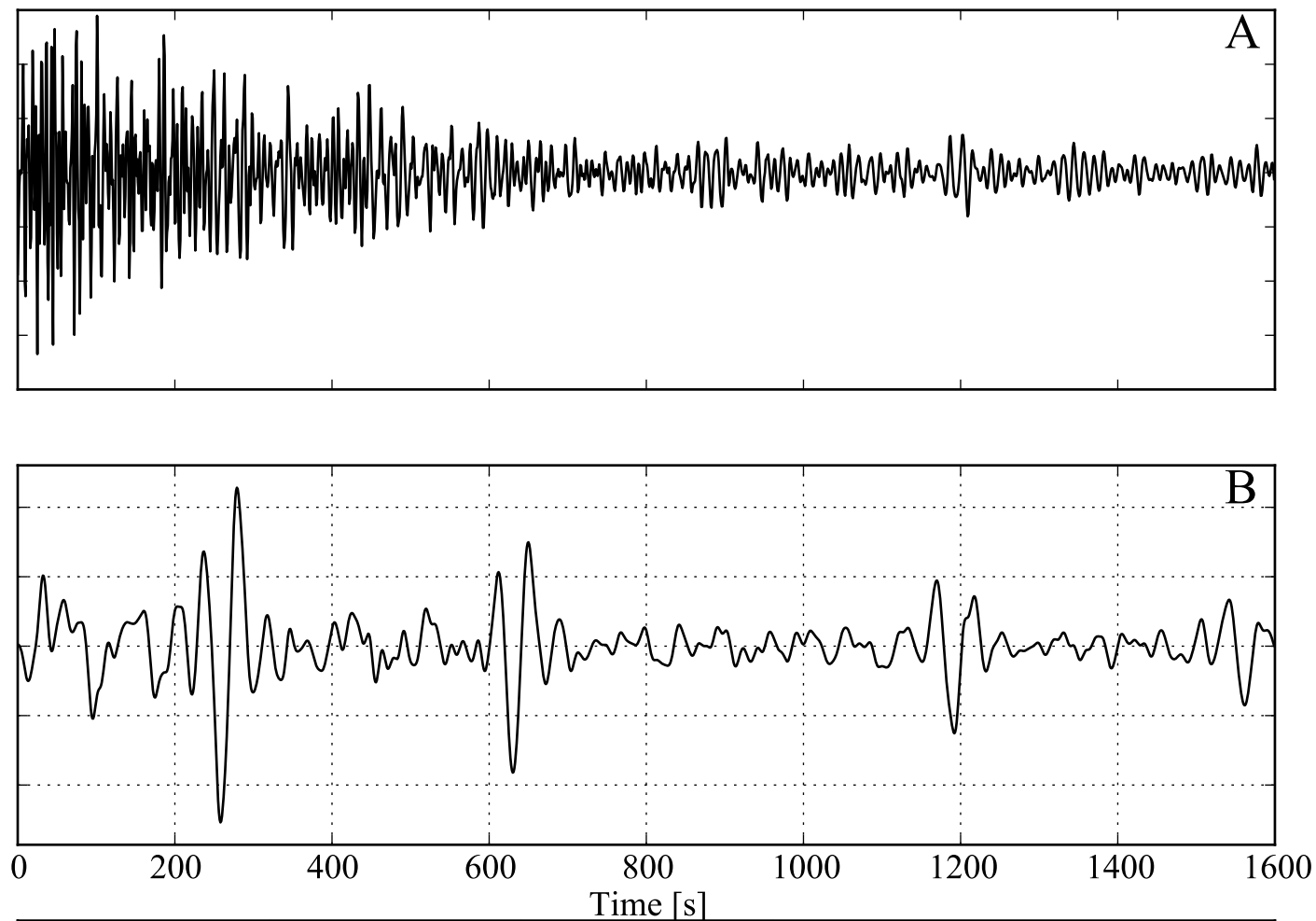
E

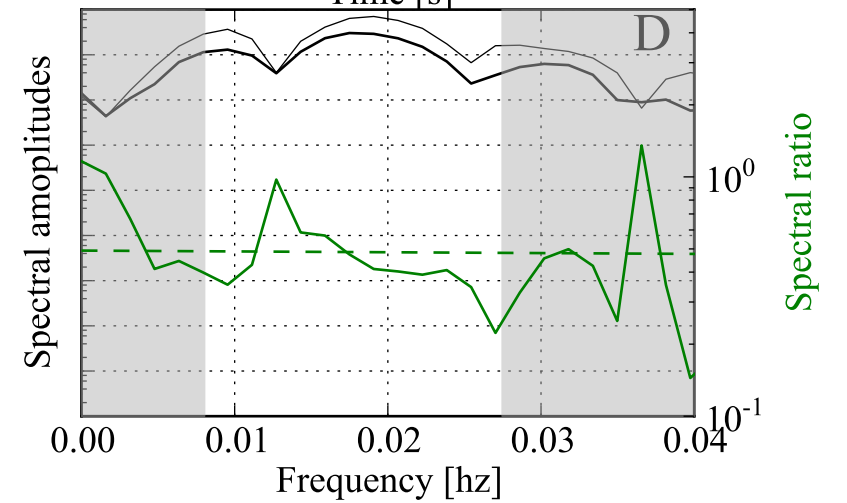
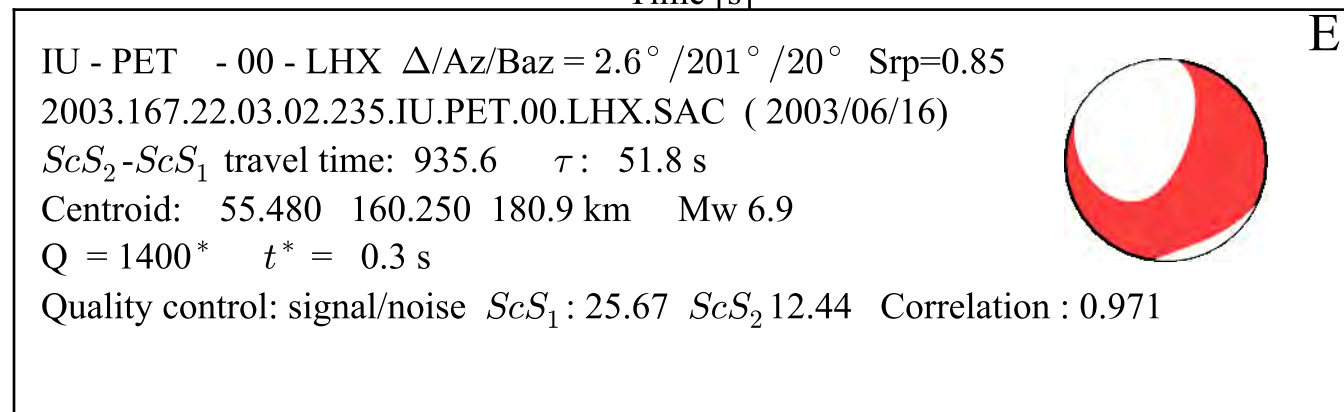
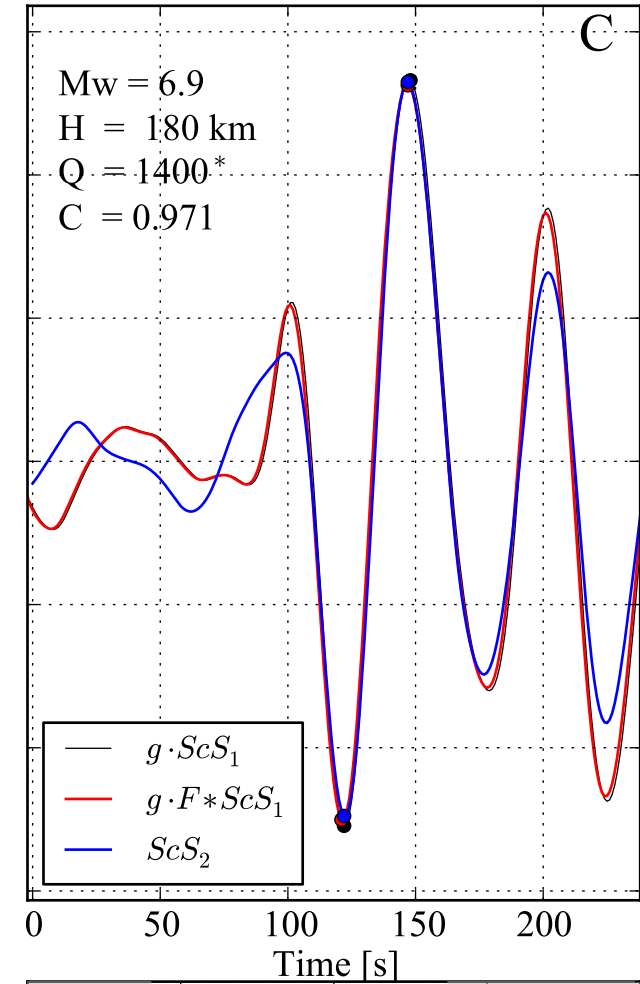
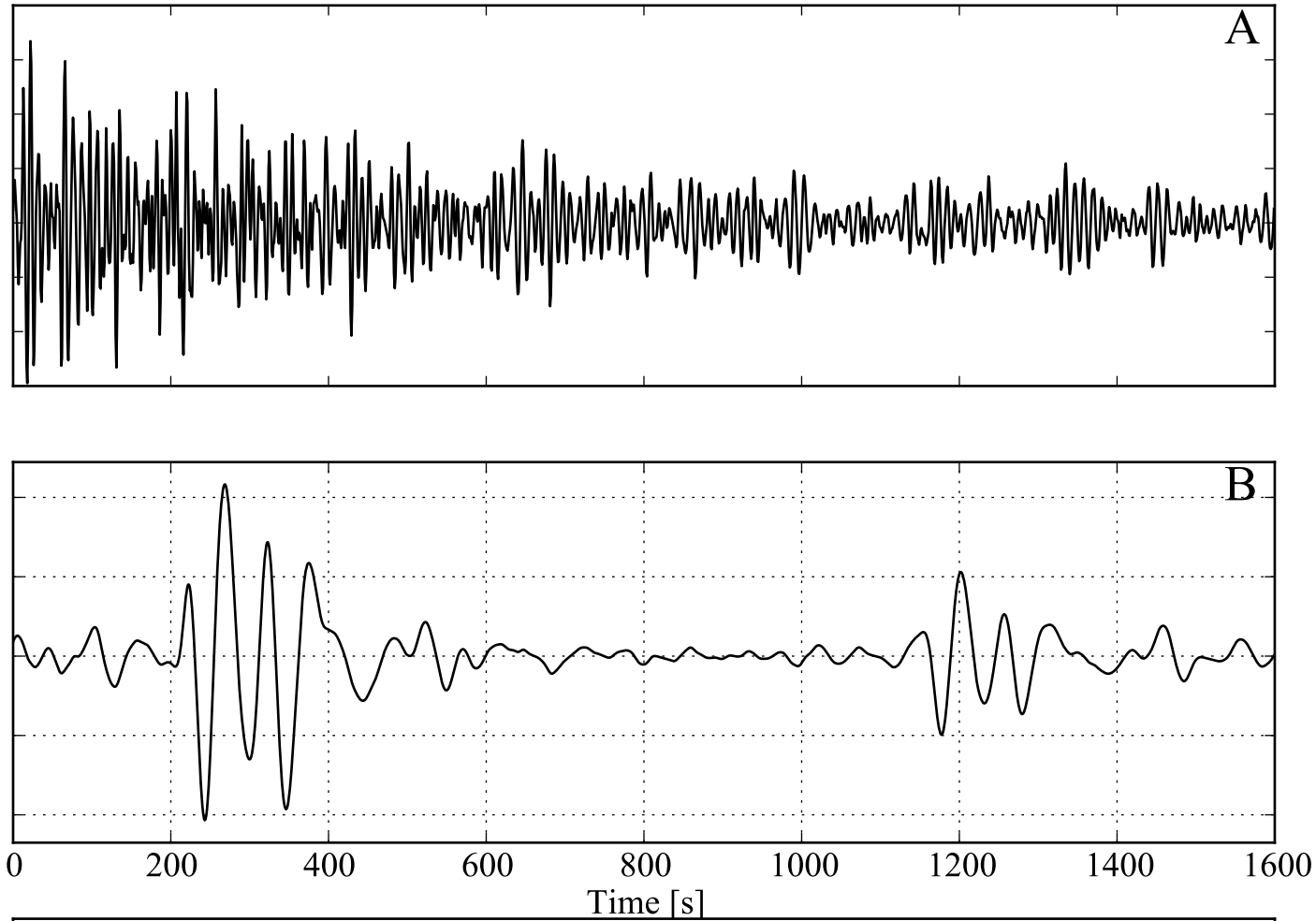
G - PEL - - LHE $\Delta/Az/Baz = 2.2^\circ / 163^\circ / 342^\circ$ $Srp=0.94$
 1997.288.00.58.33.131.G.PEL..LHE.SAC (1997/10/15)
 ScS_2-ScS_1 travel time: 937.1 τ : 52.9 s
 Centroid: -31.060 -71.420 69.8 km M_w 7.1
 $Q = 127$ $t^* = 7.4$ s
 Quality control: signal/noise ScS_1 : 14.78 ScS_2 4.74 Correlation : 0.954

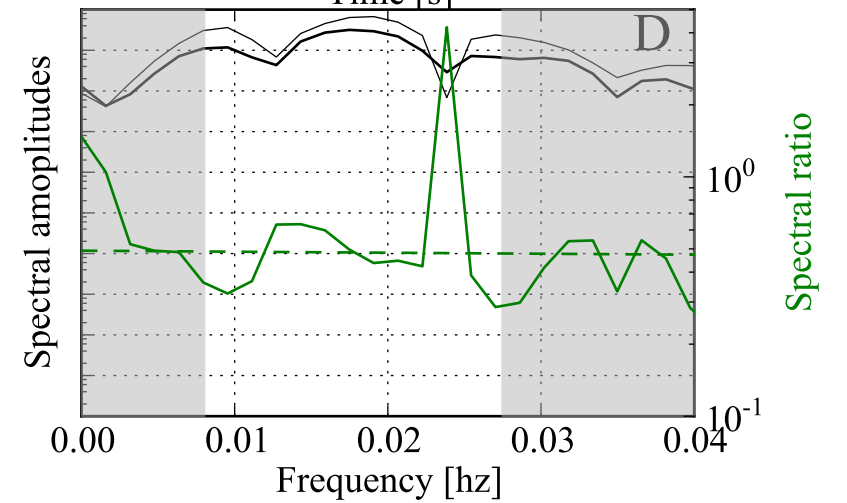
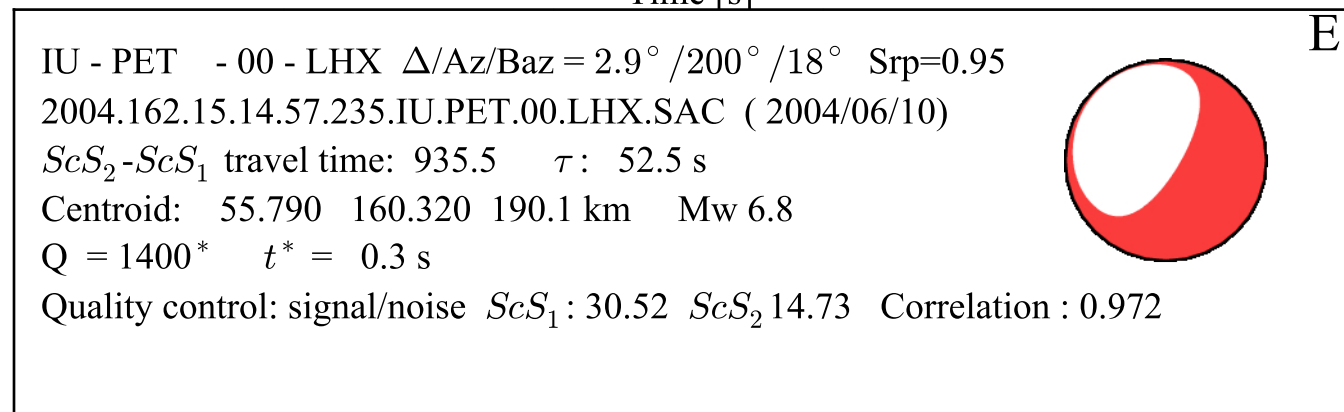
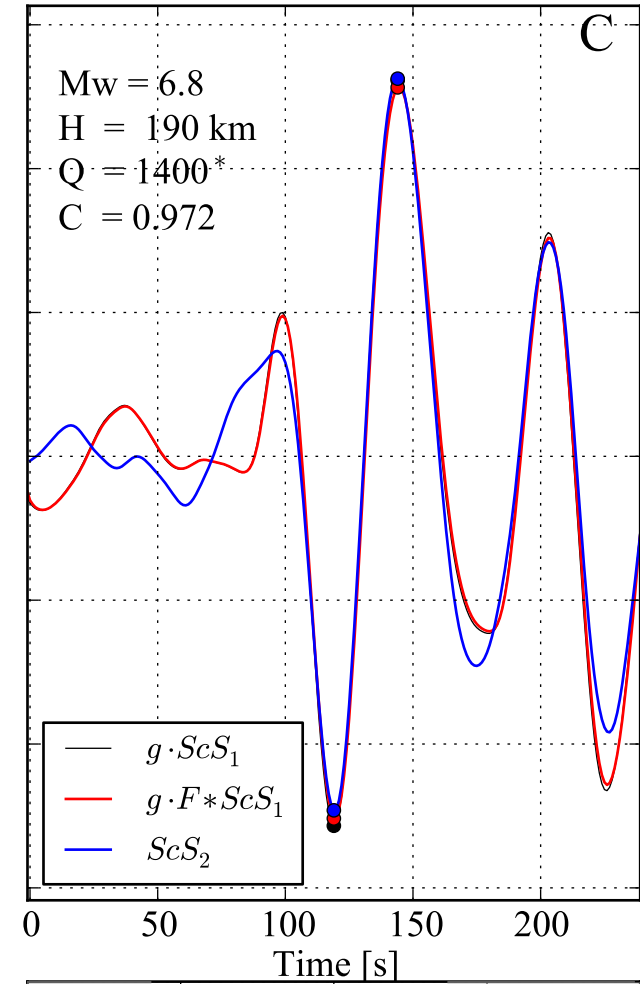
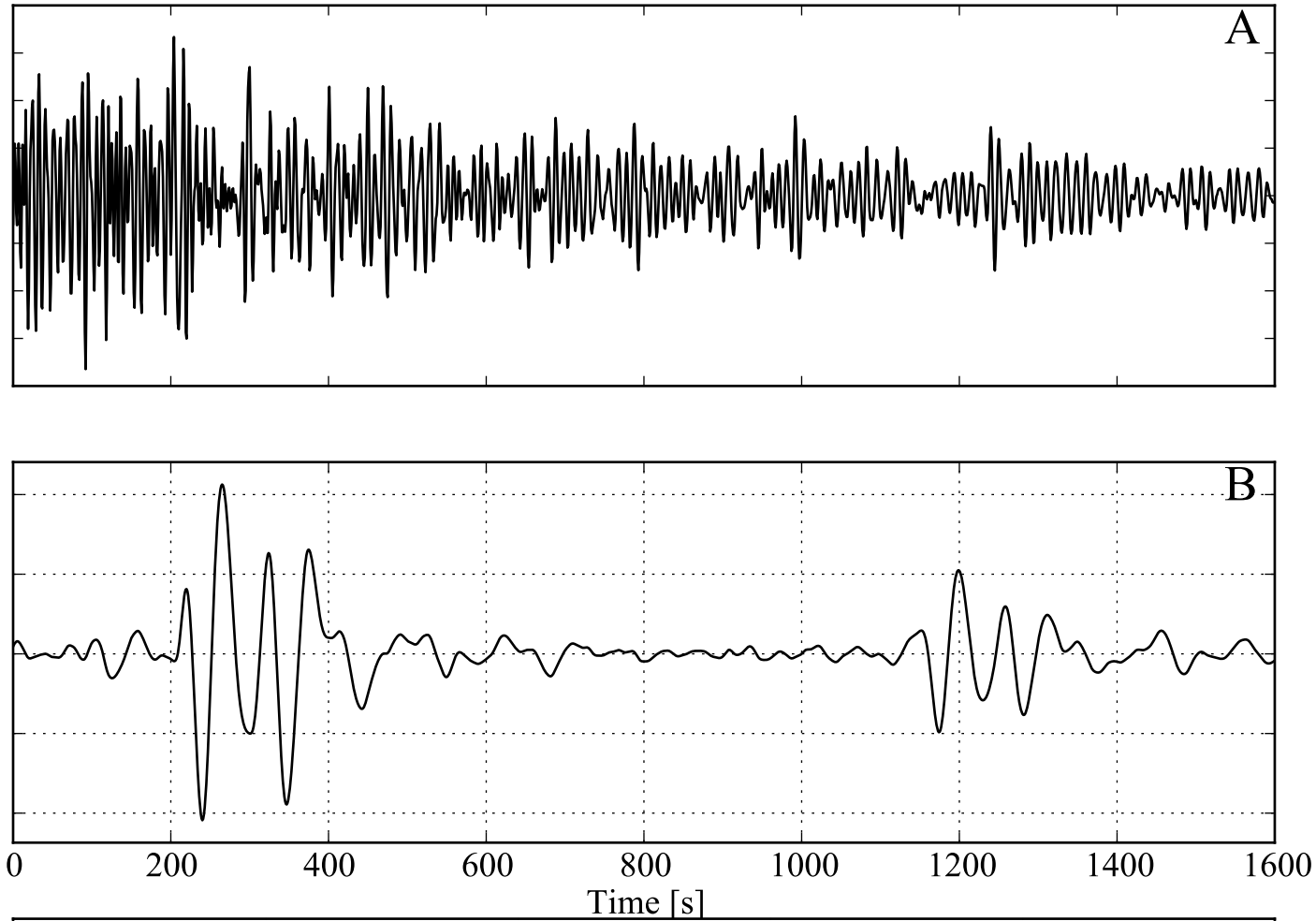


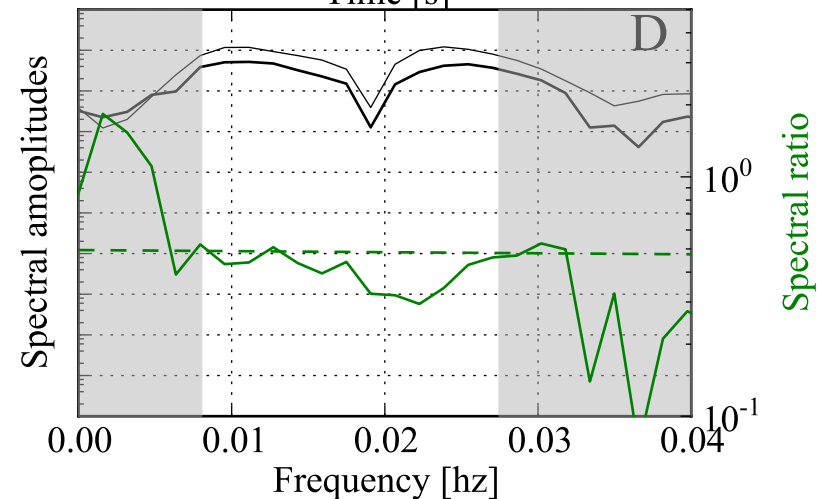
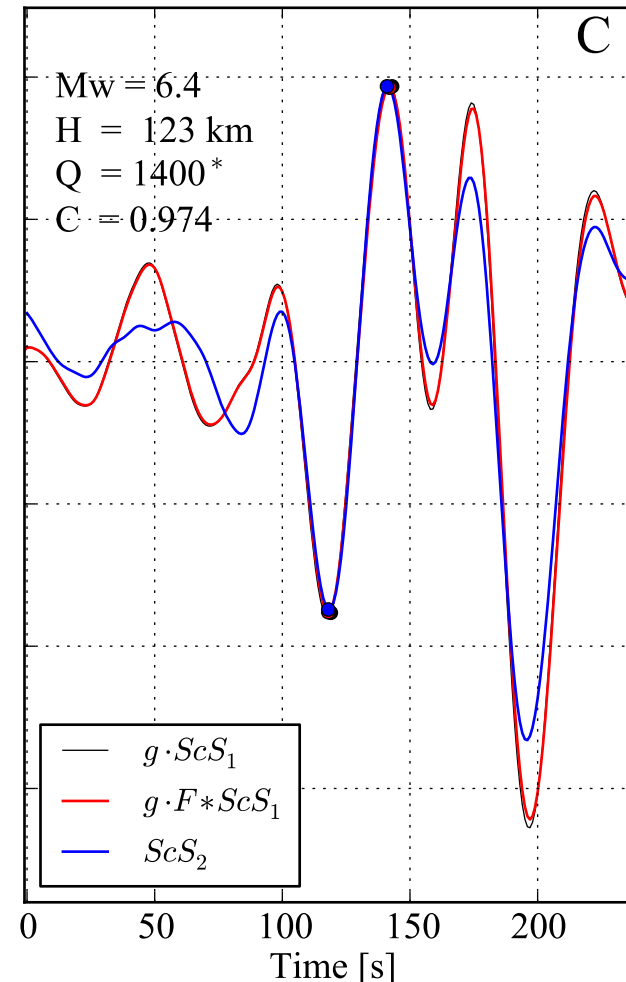
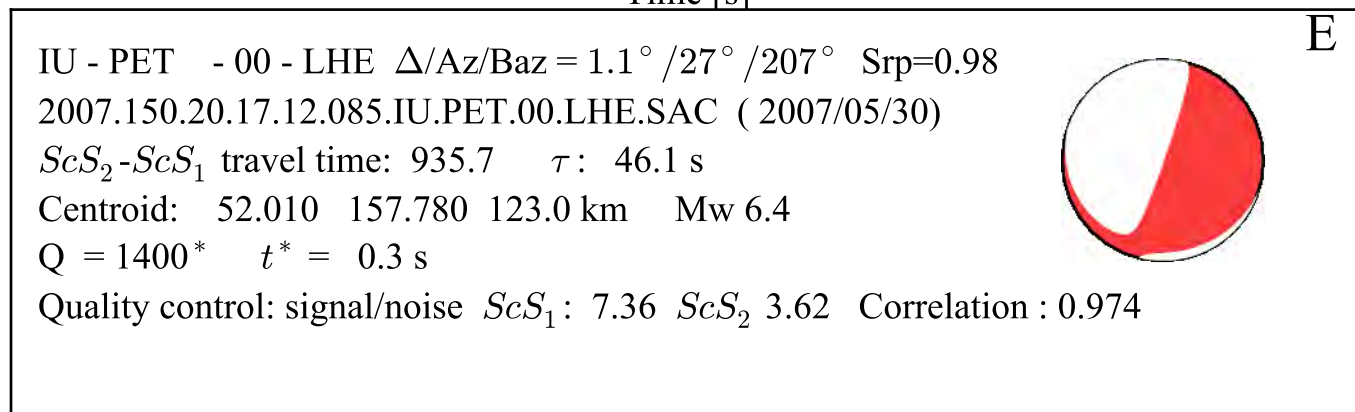
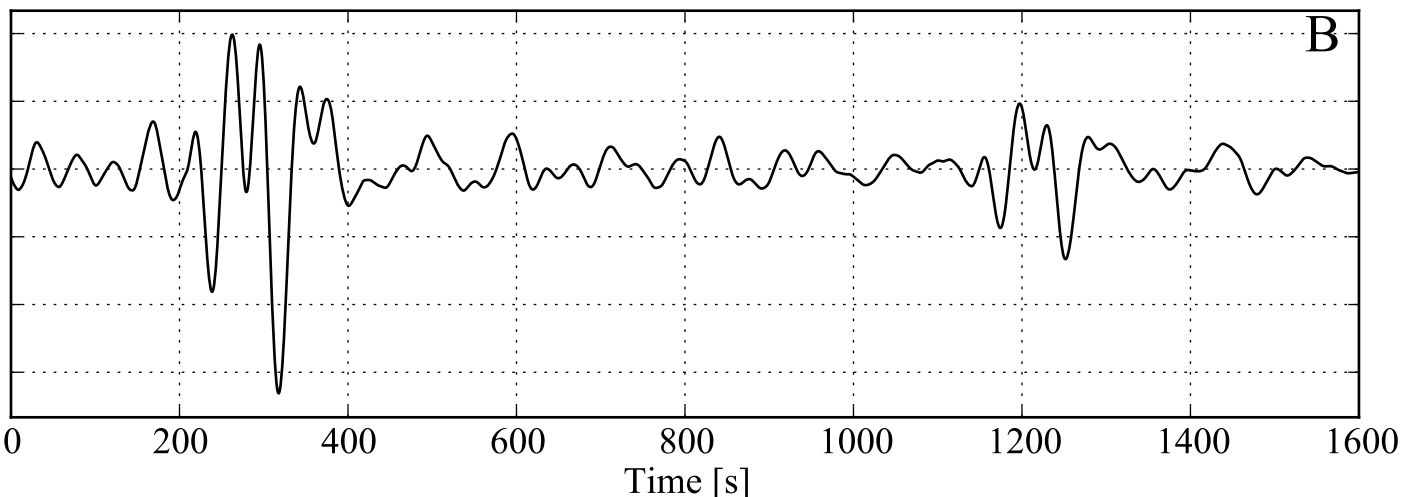
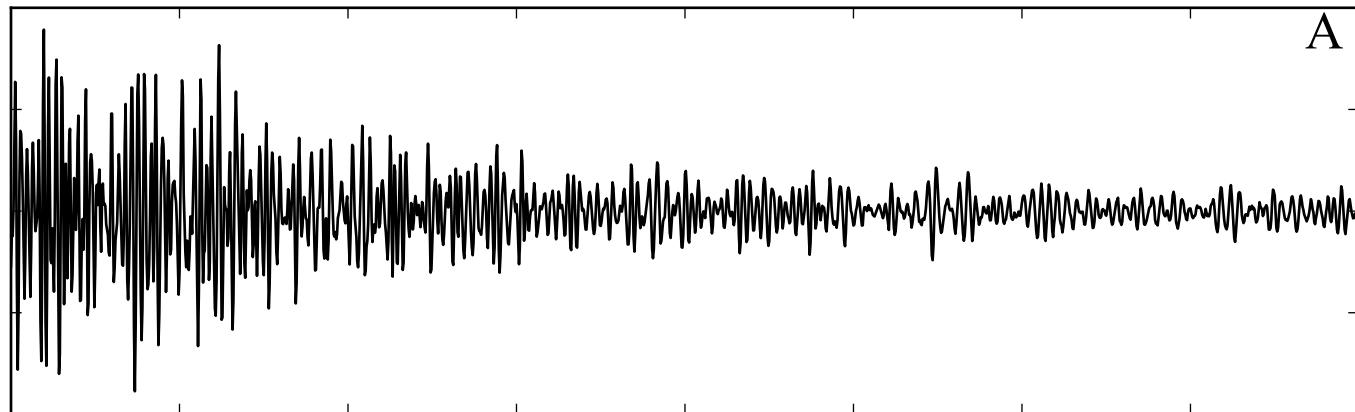


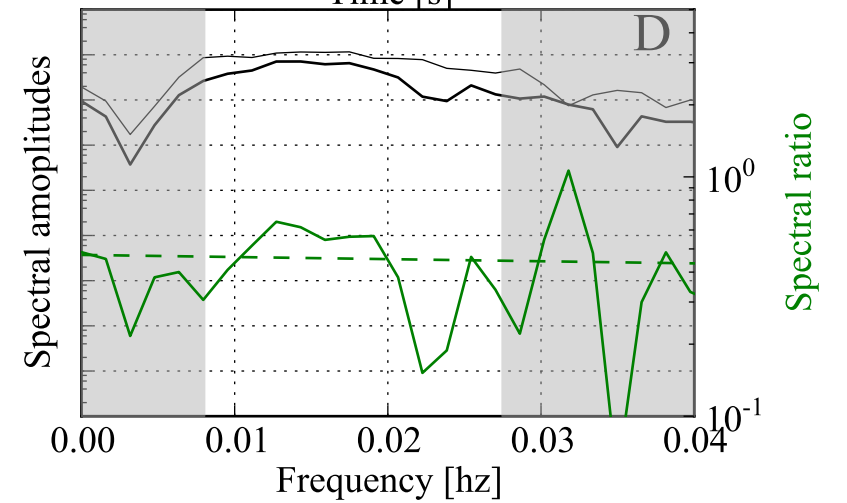
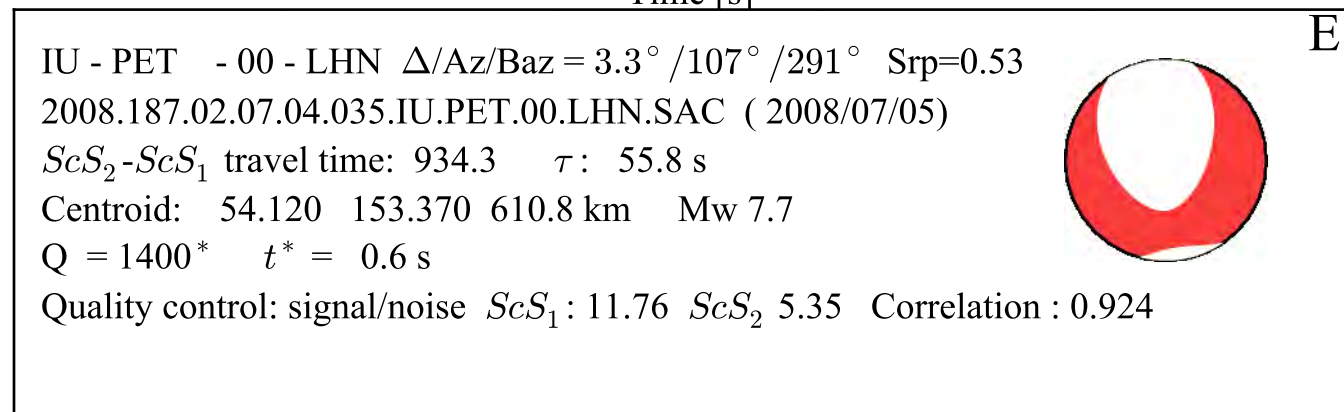
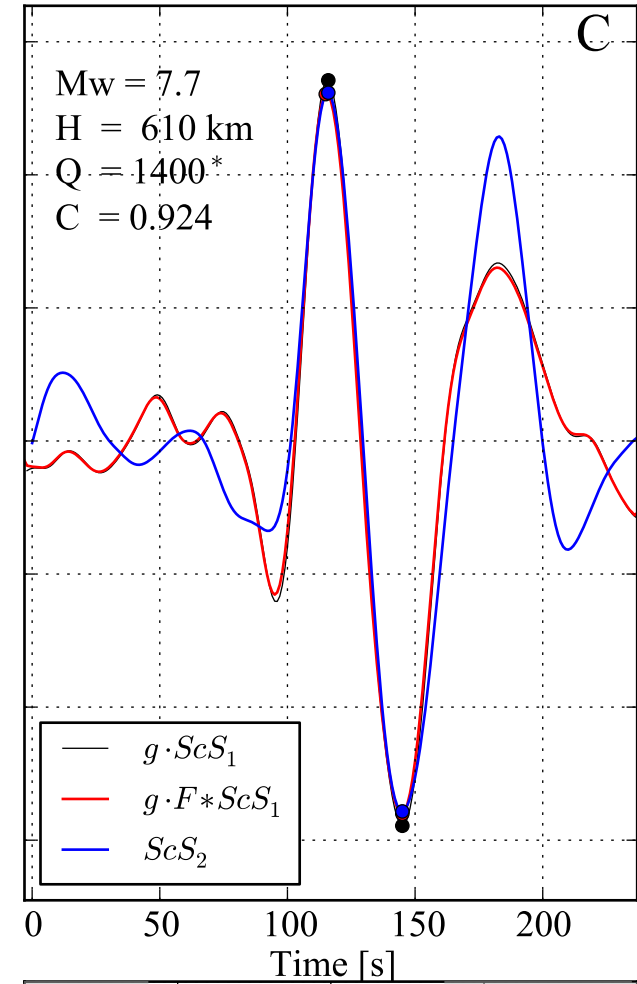
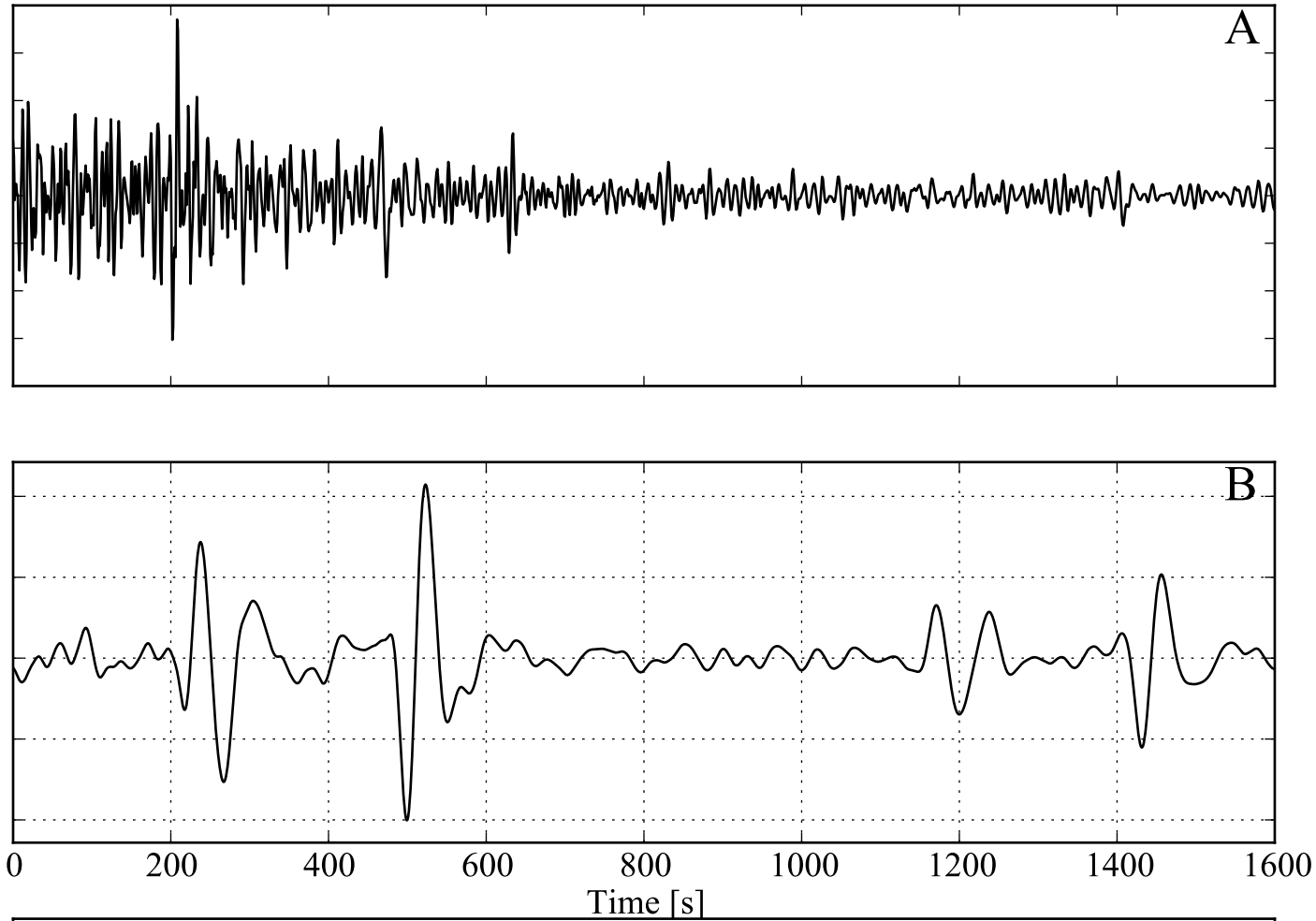


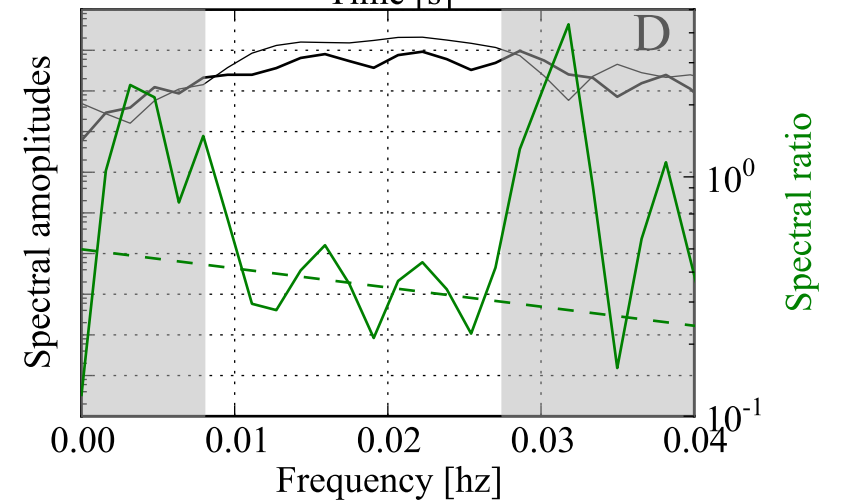
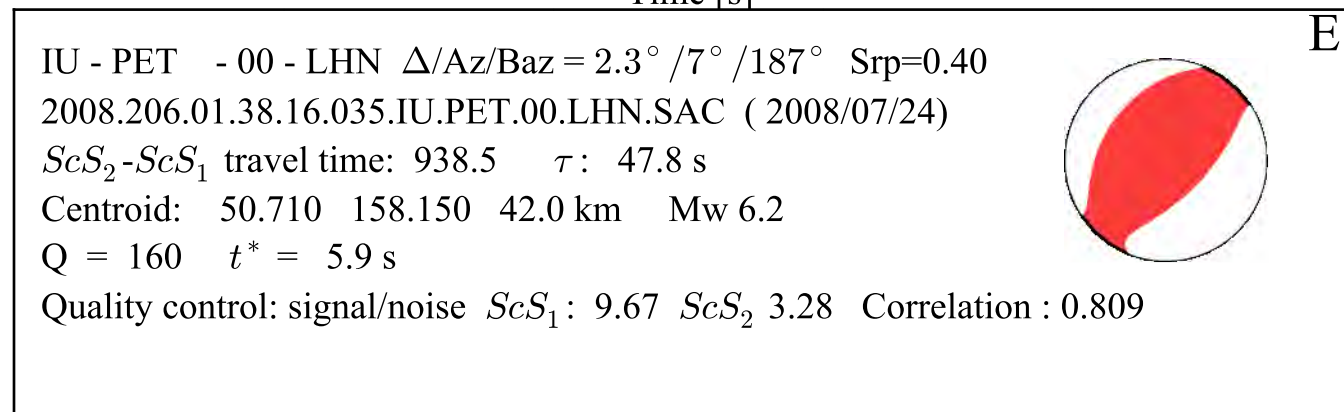
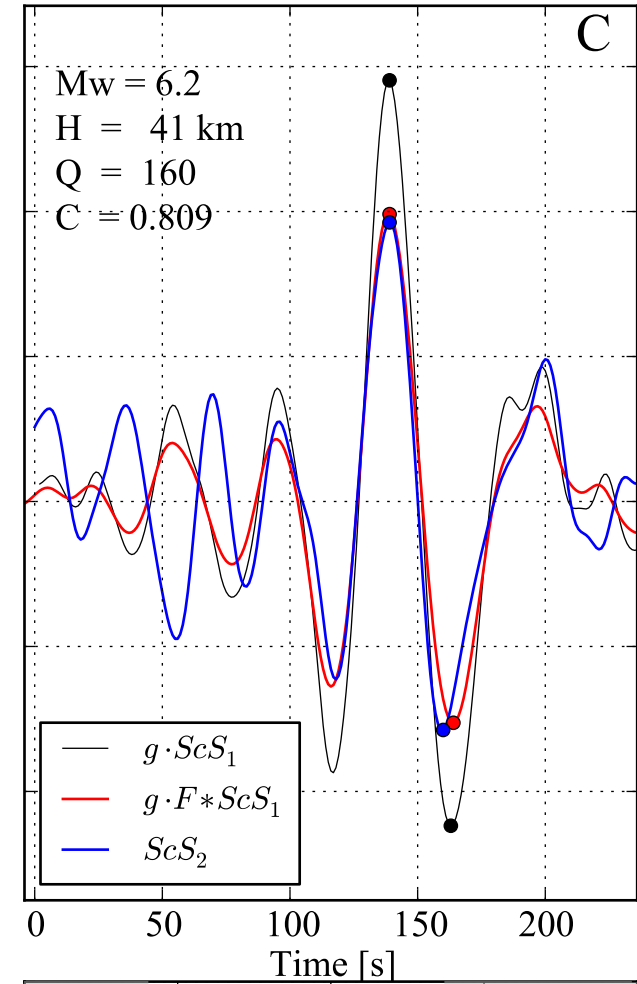
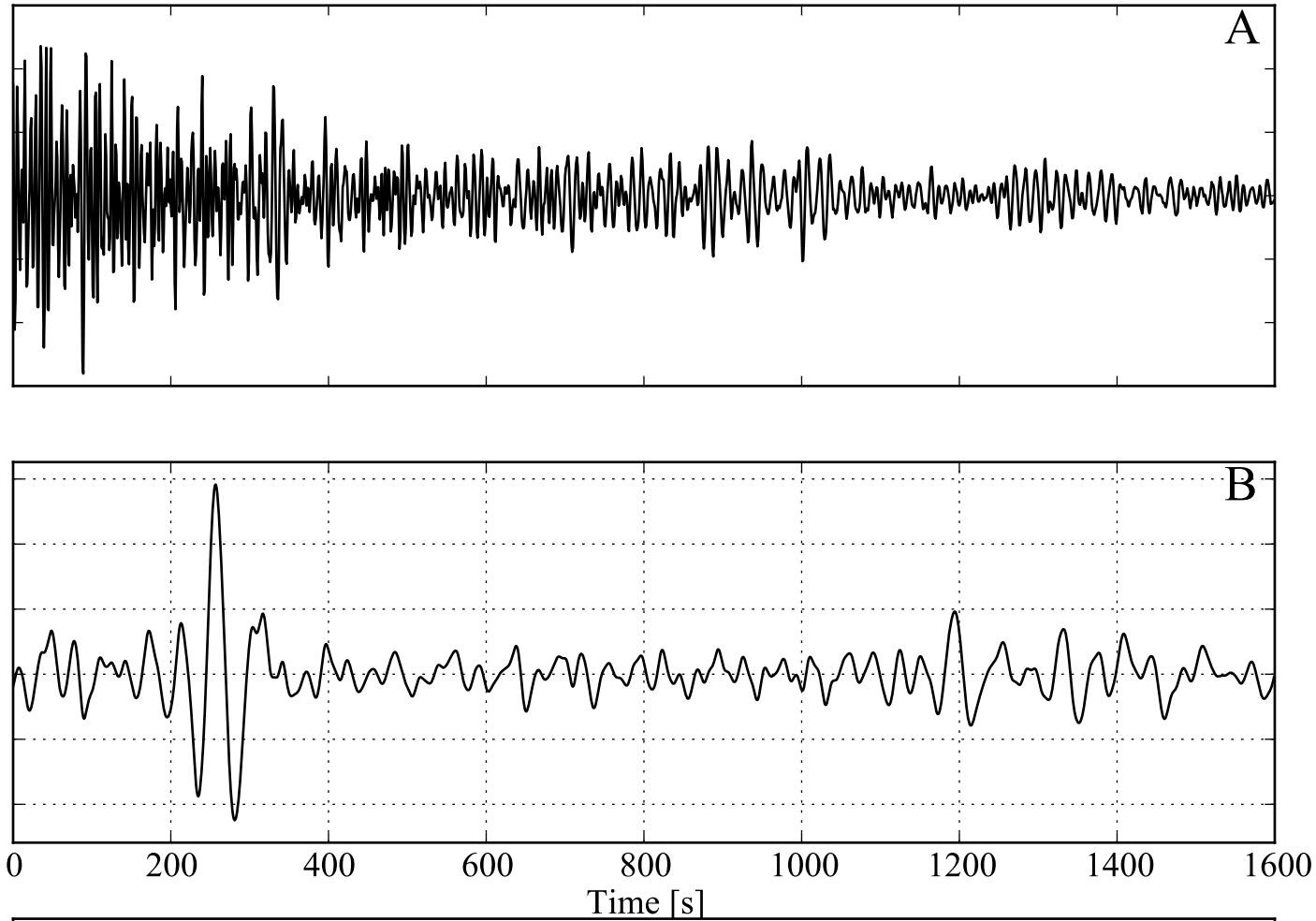


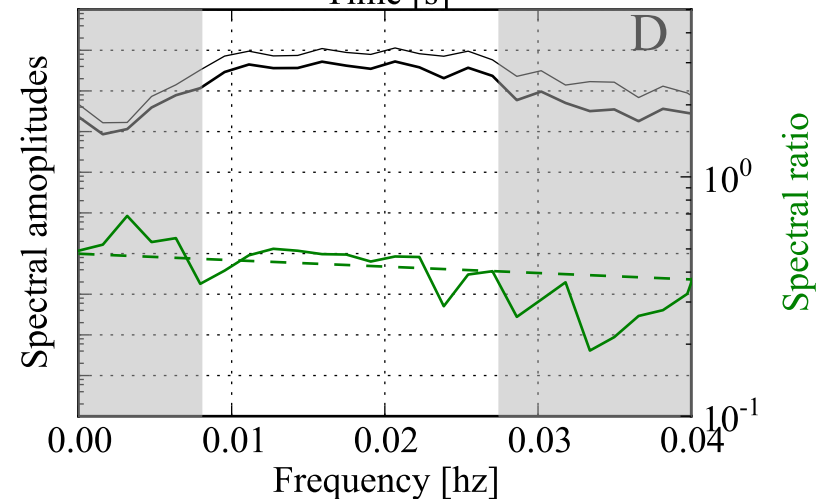
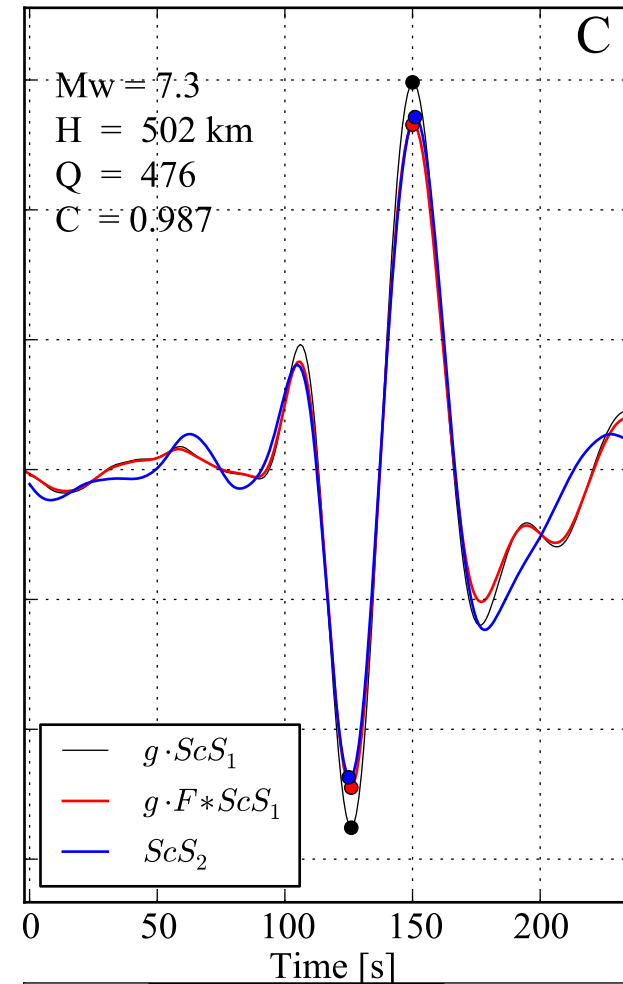
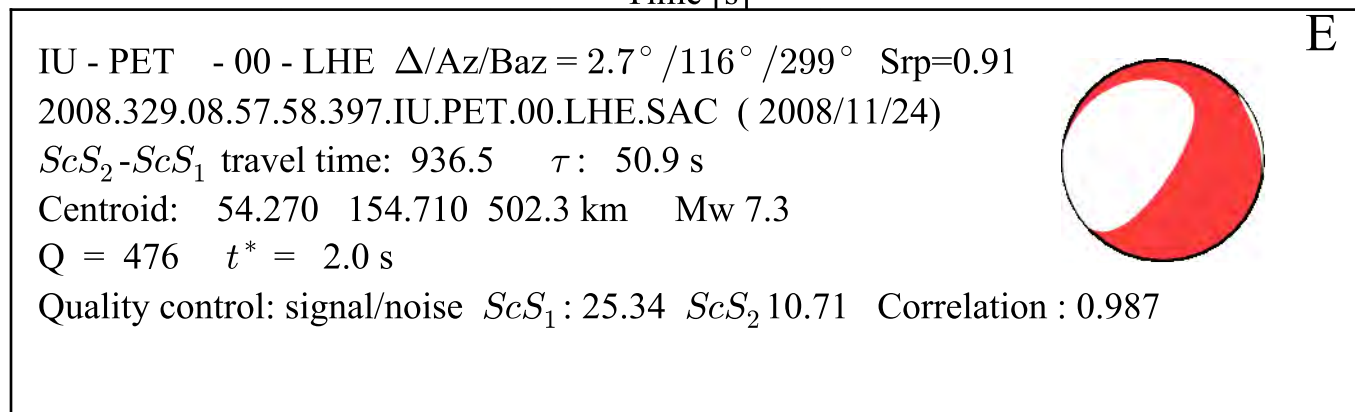
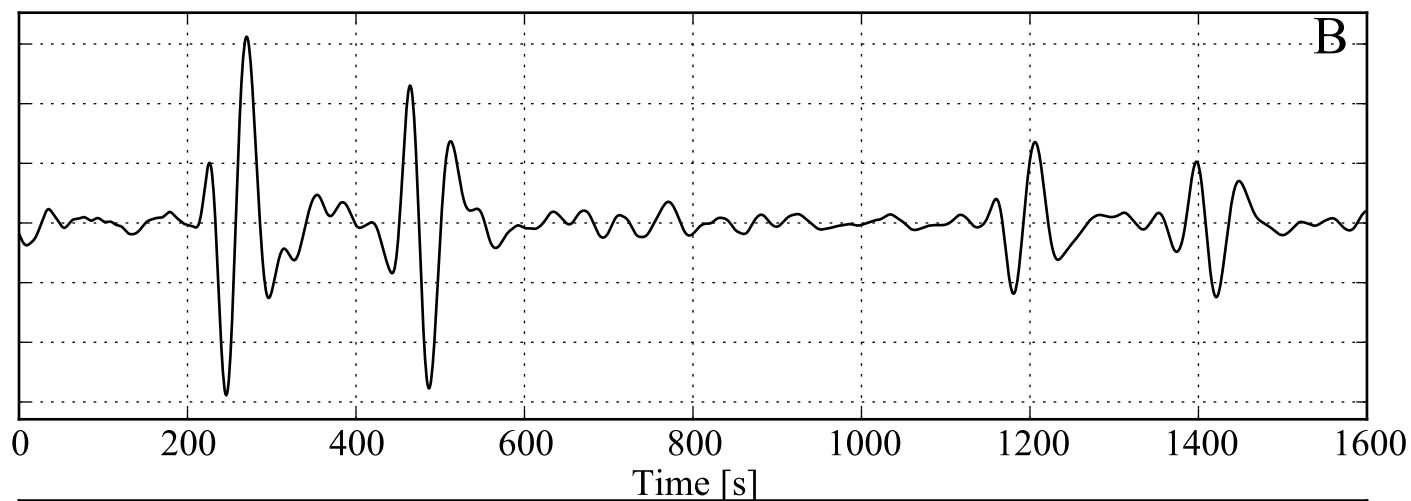
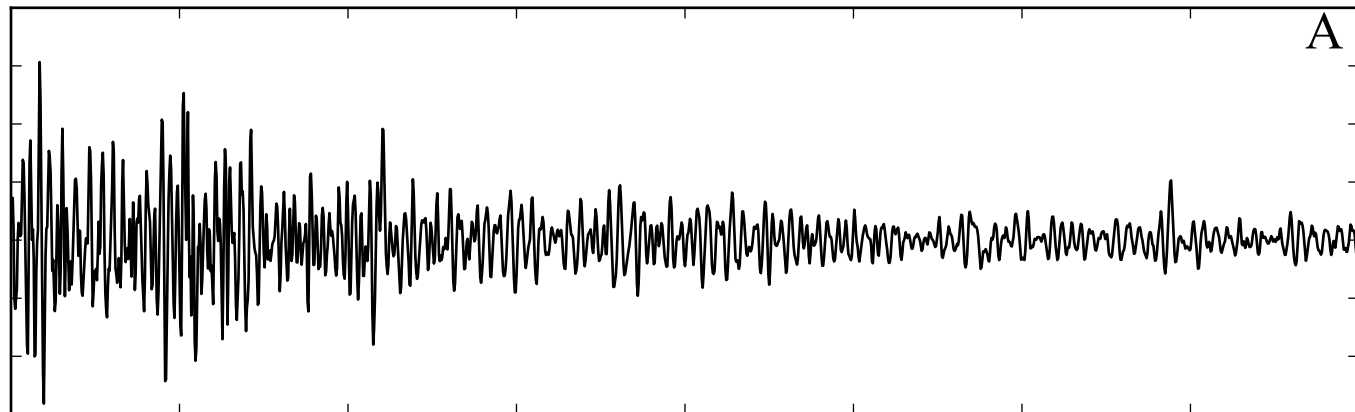


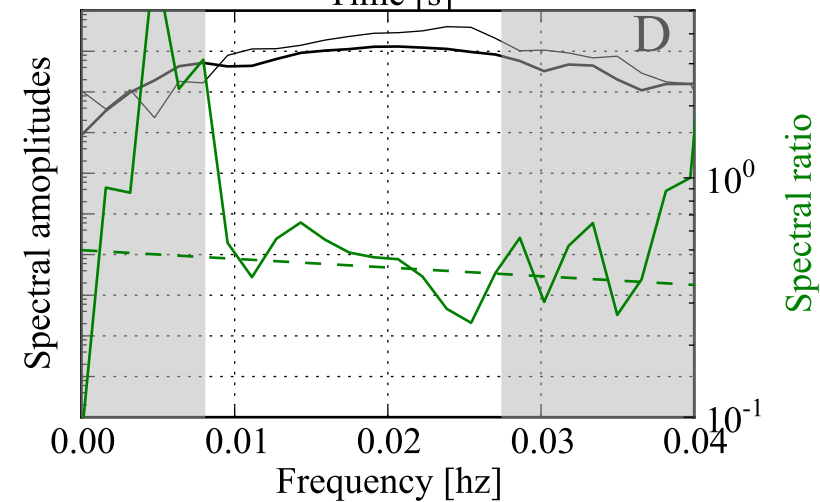
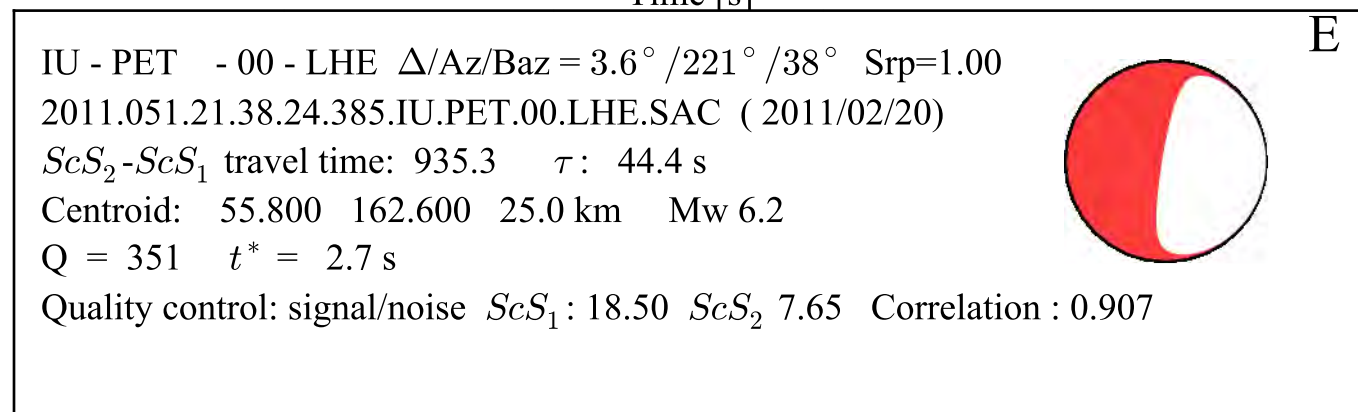
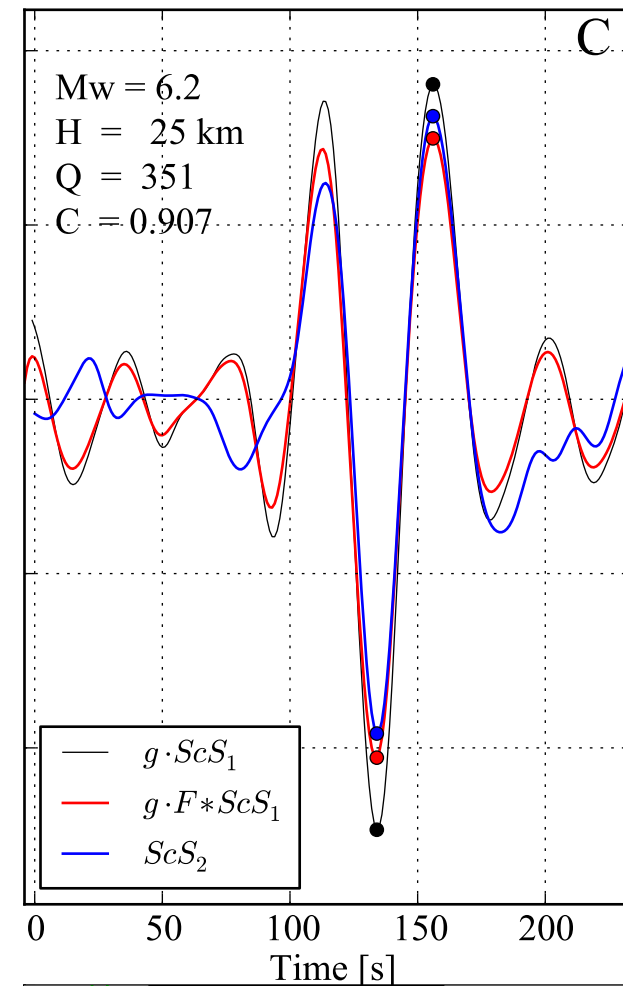
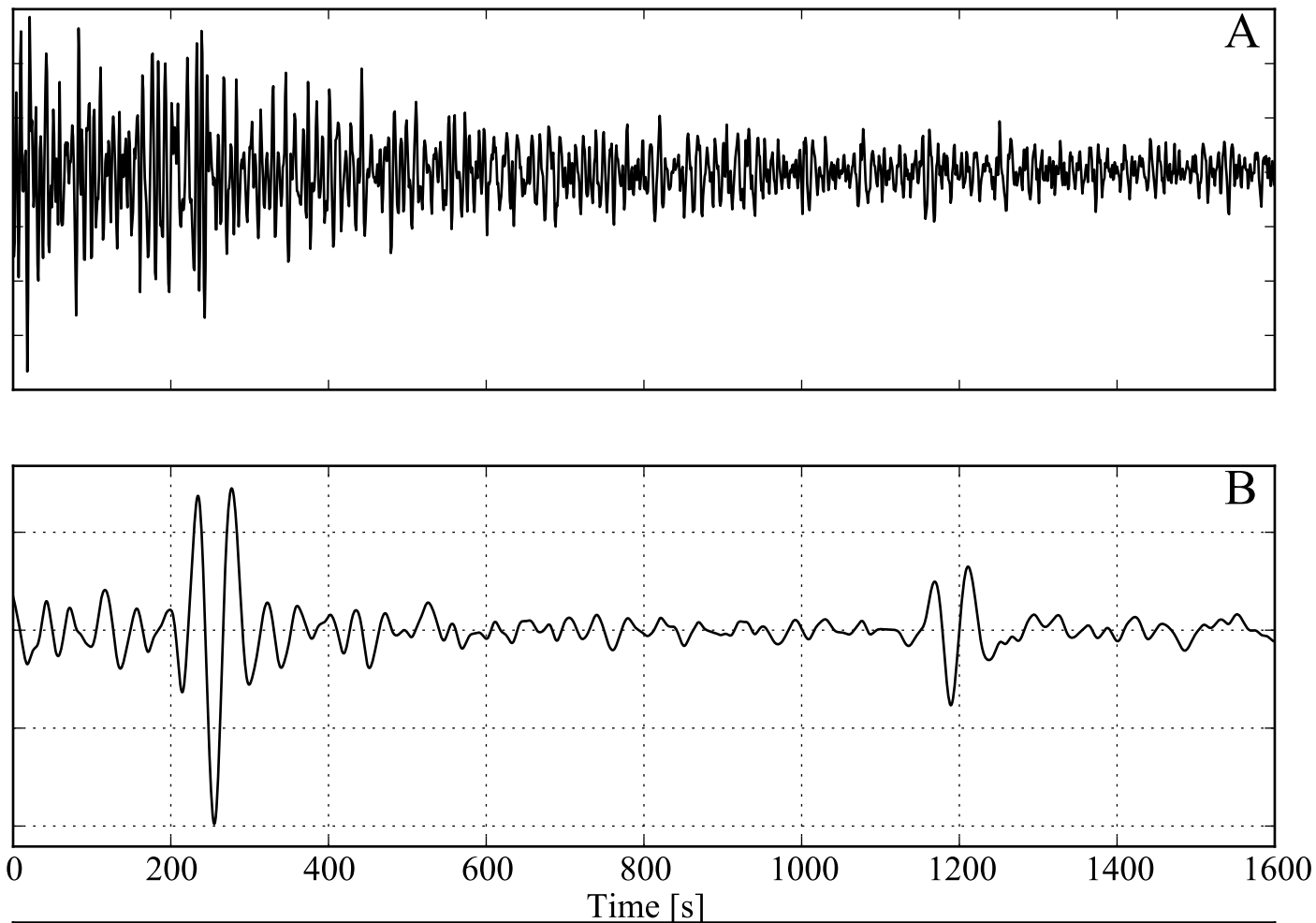


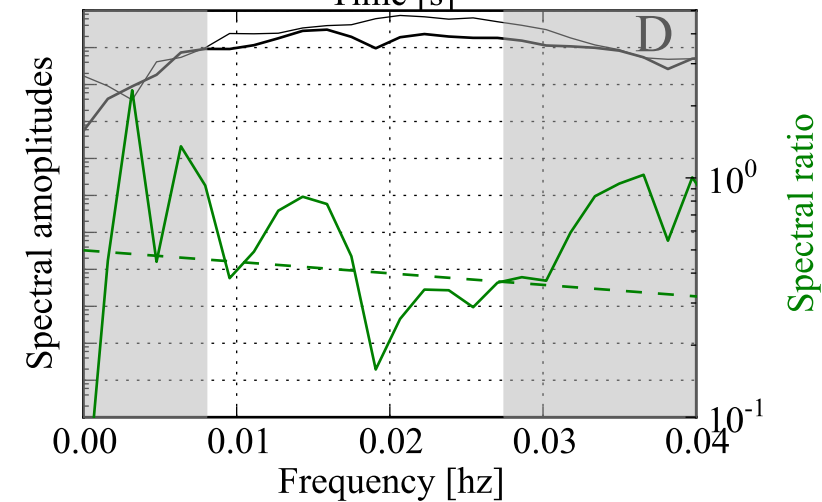
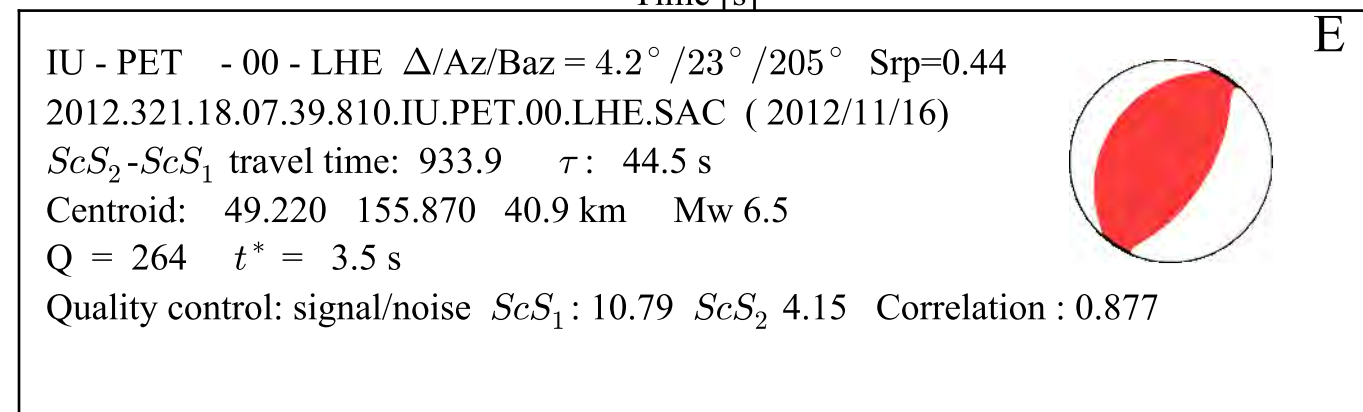
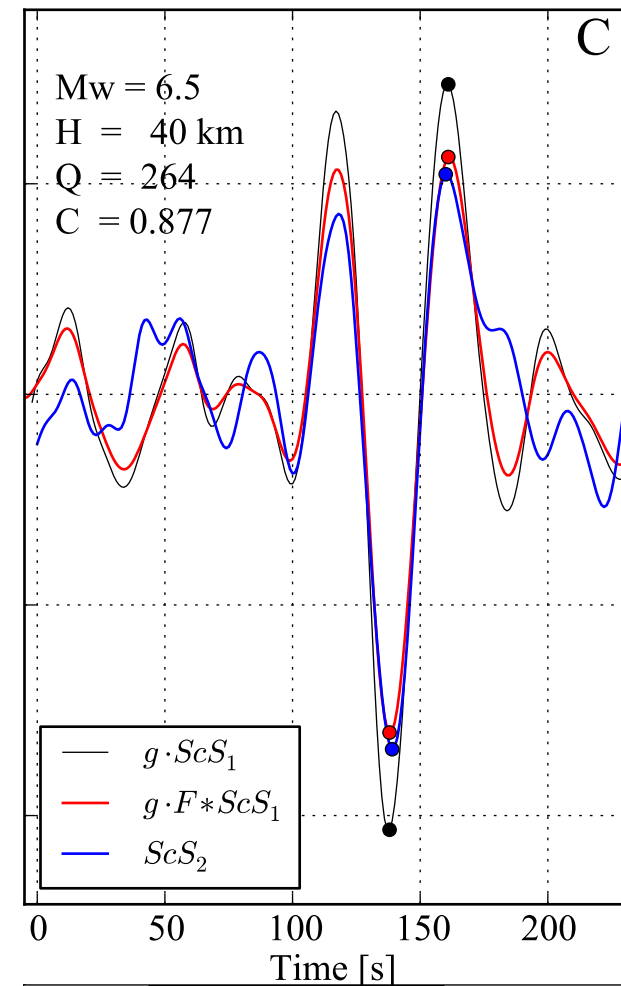
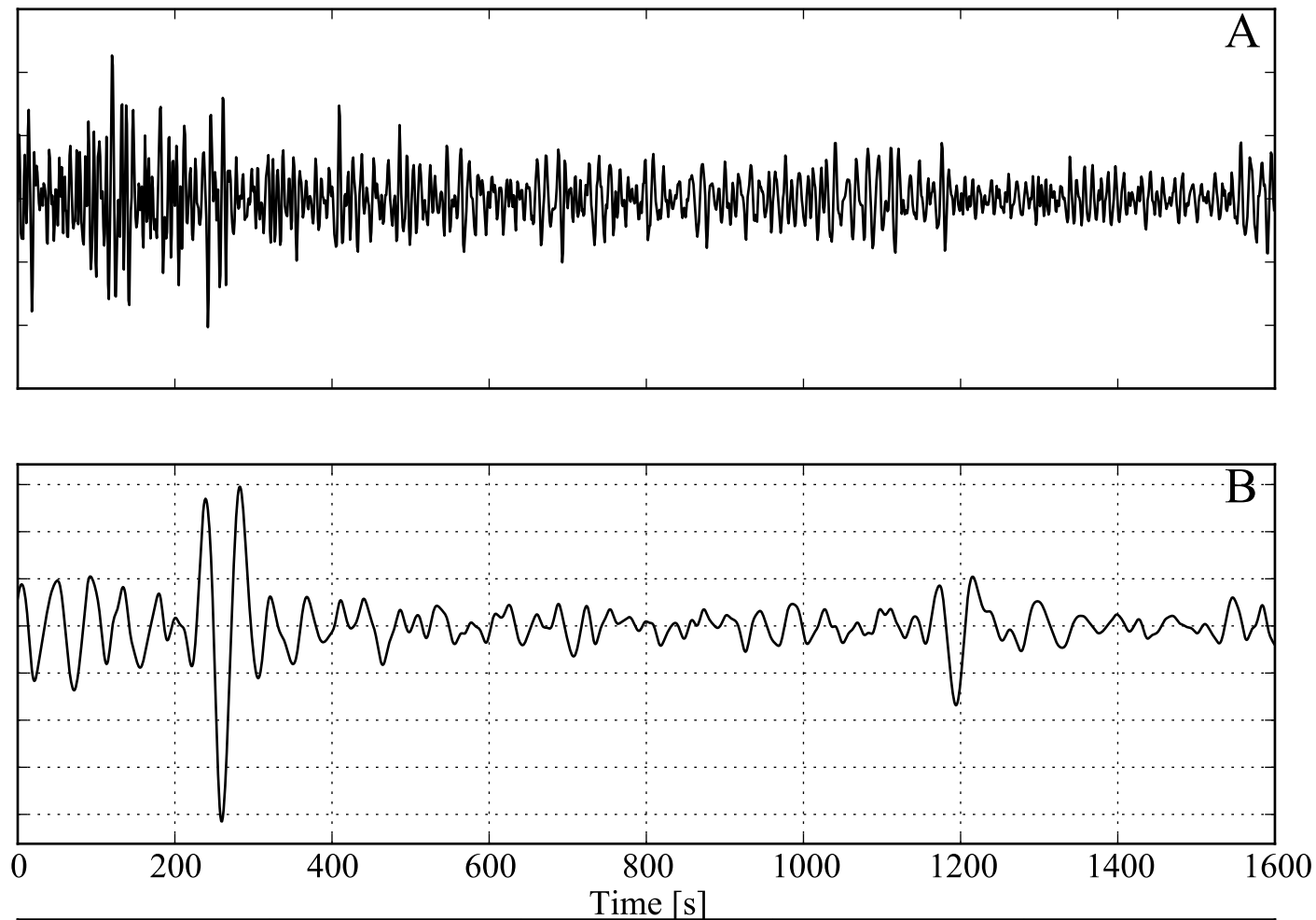


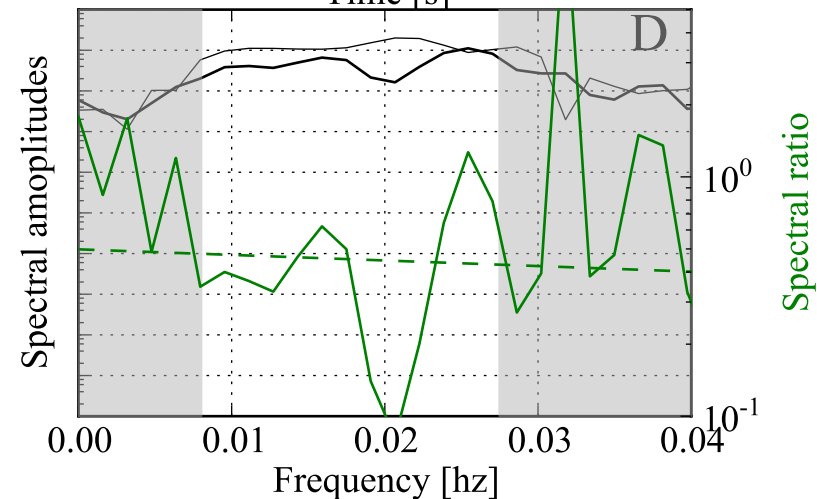
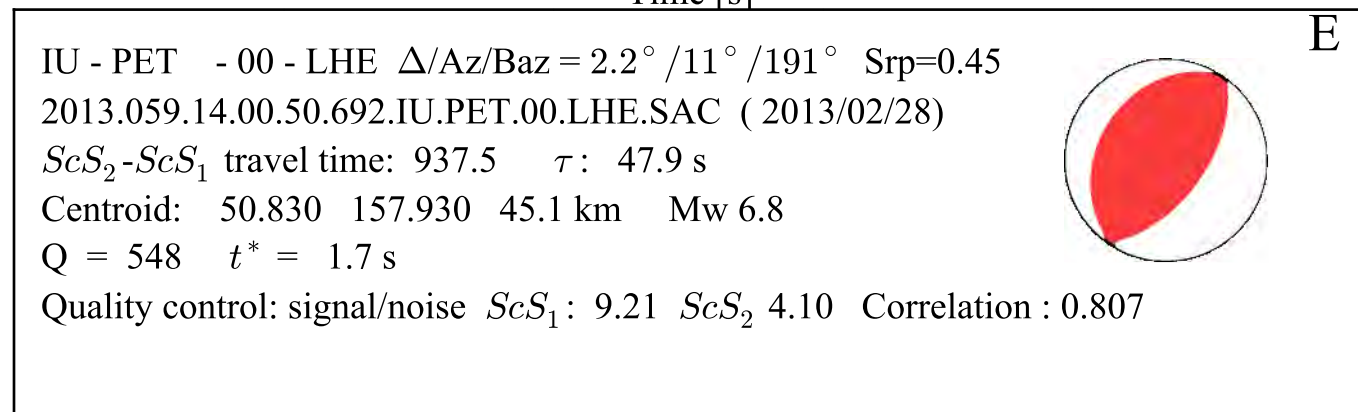
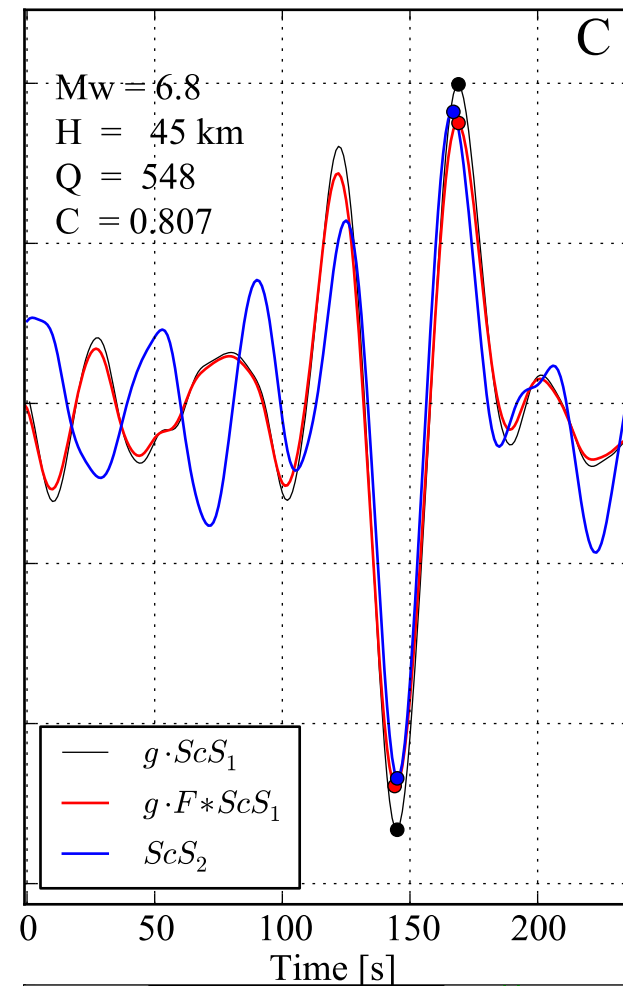
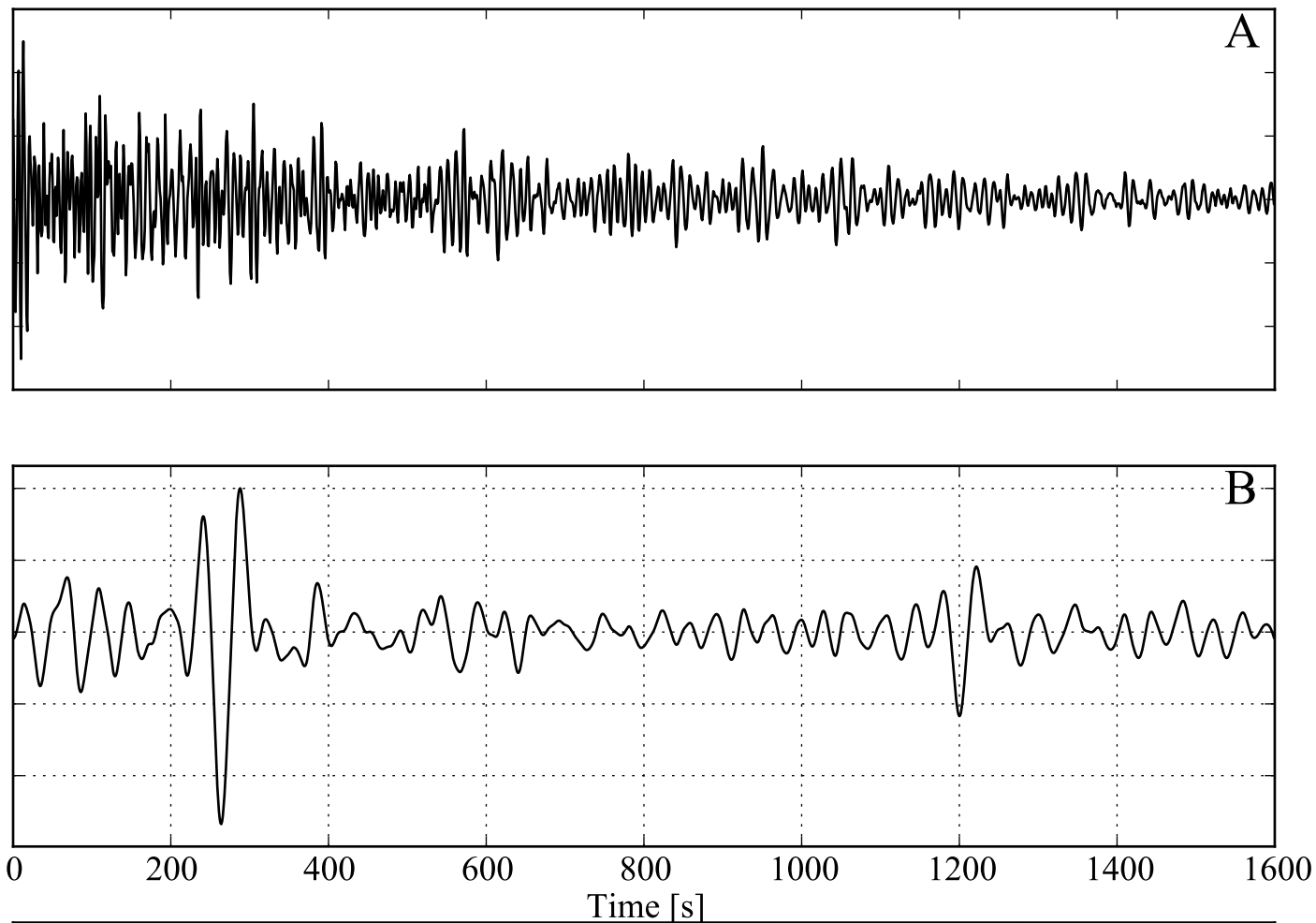


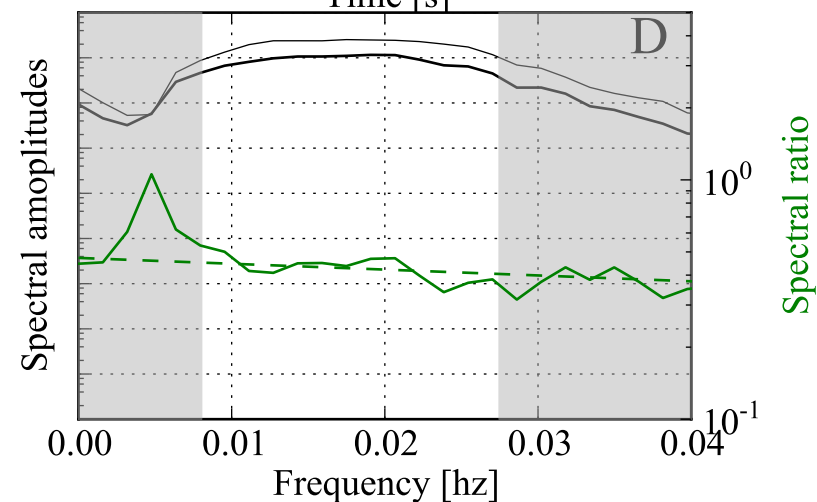
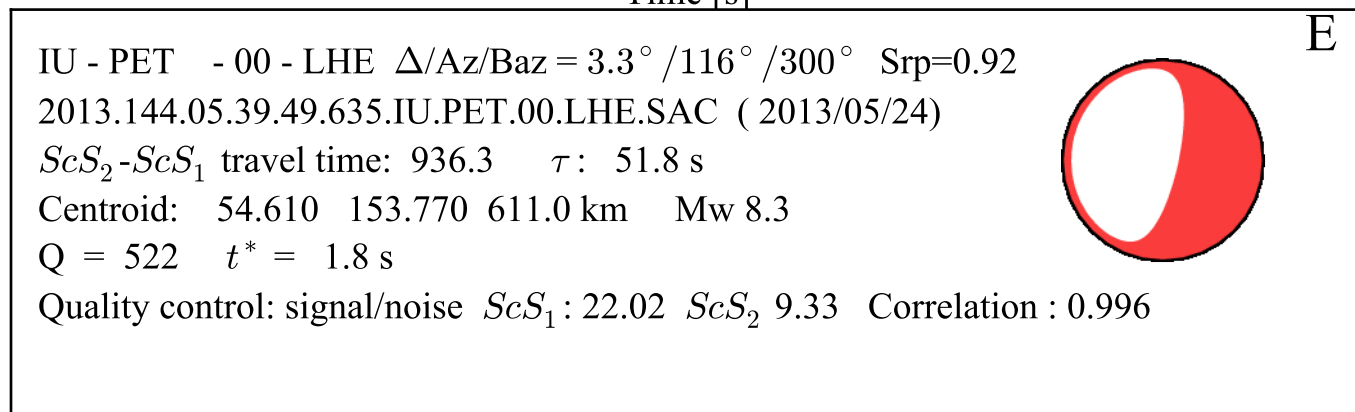
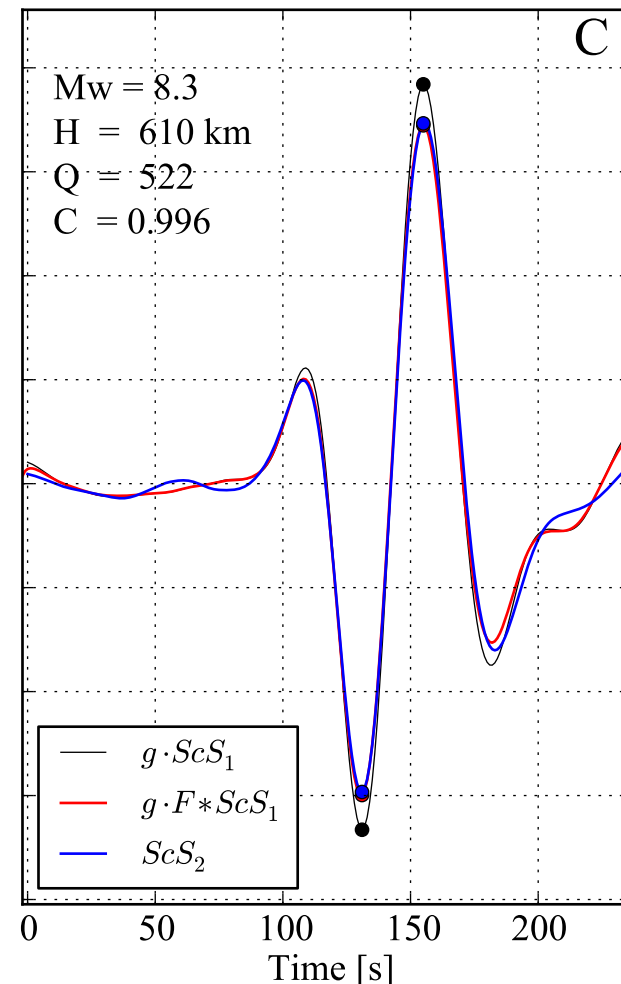
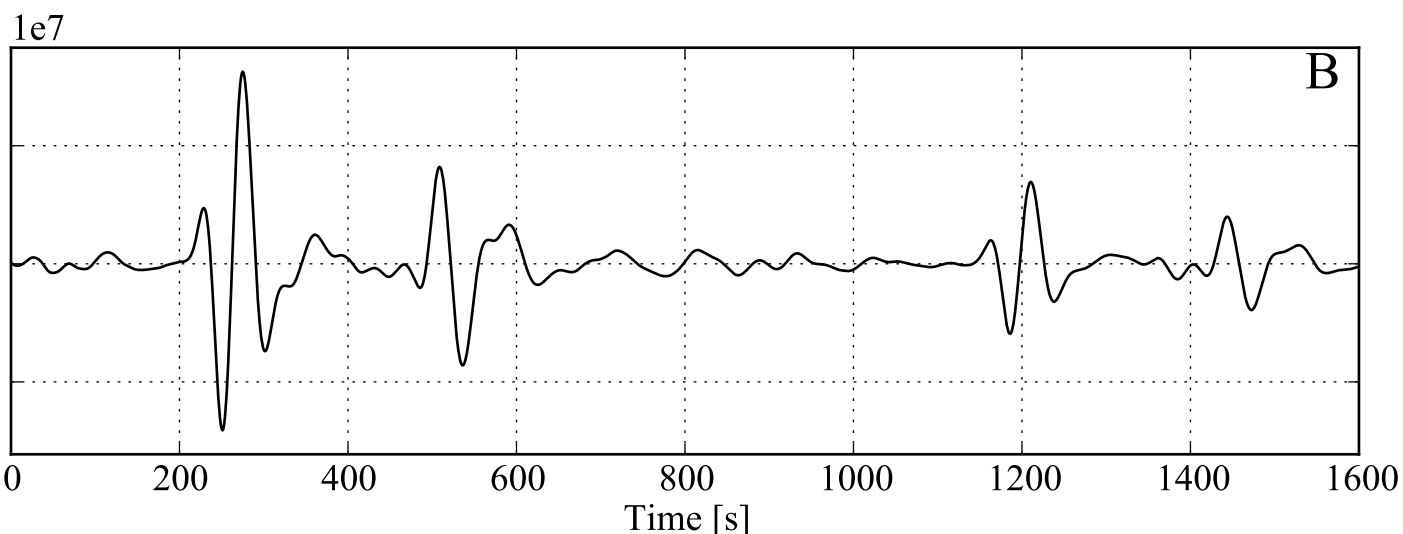
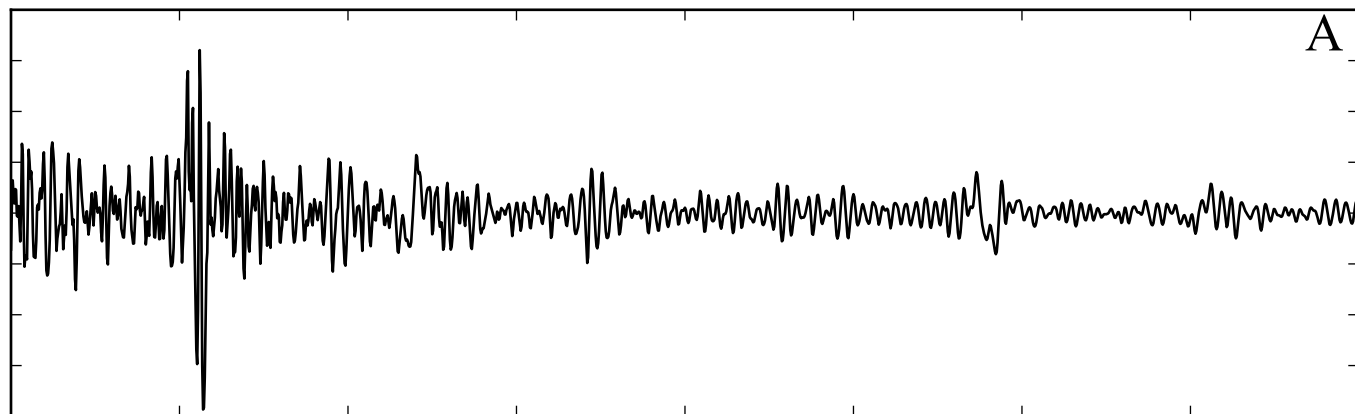


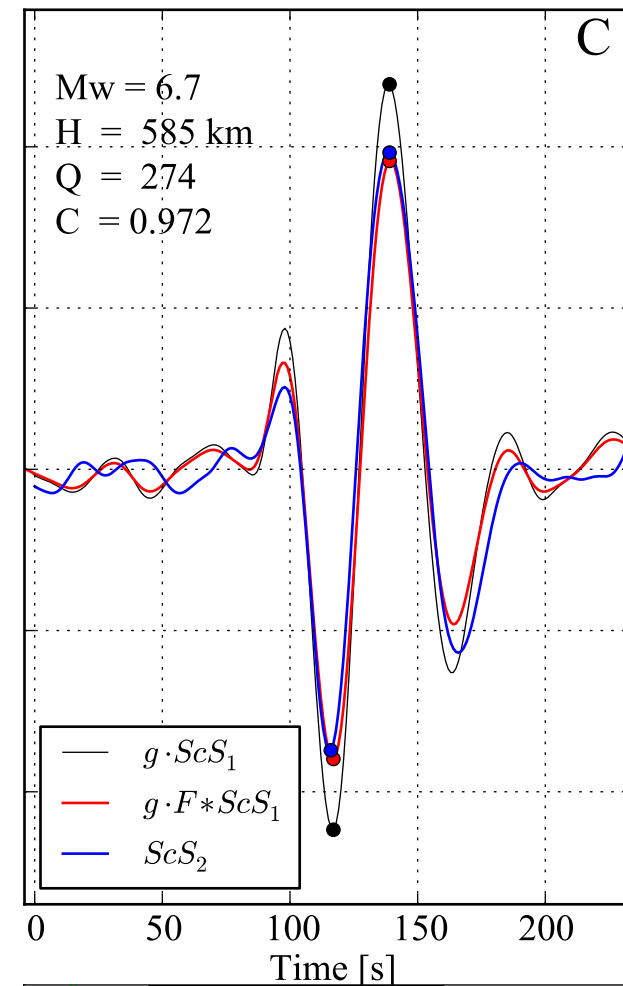
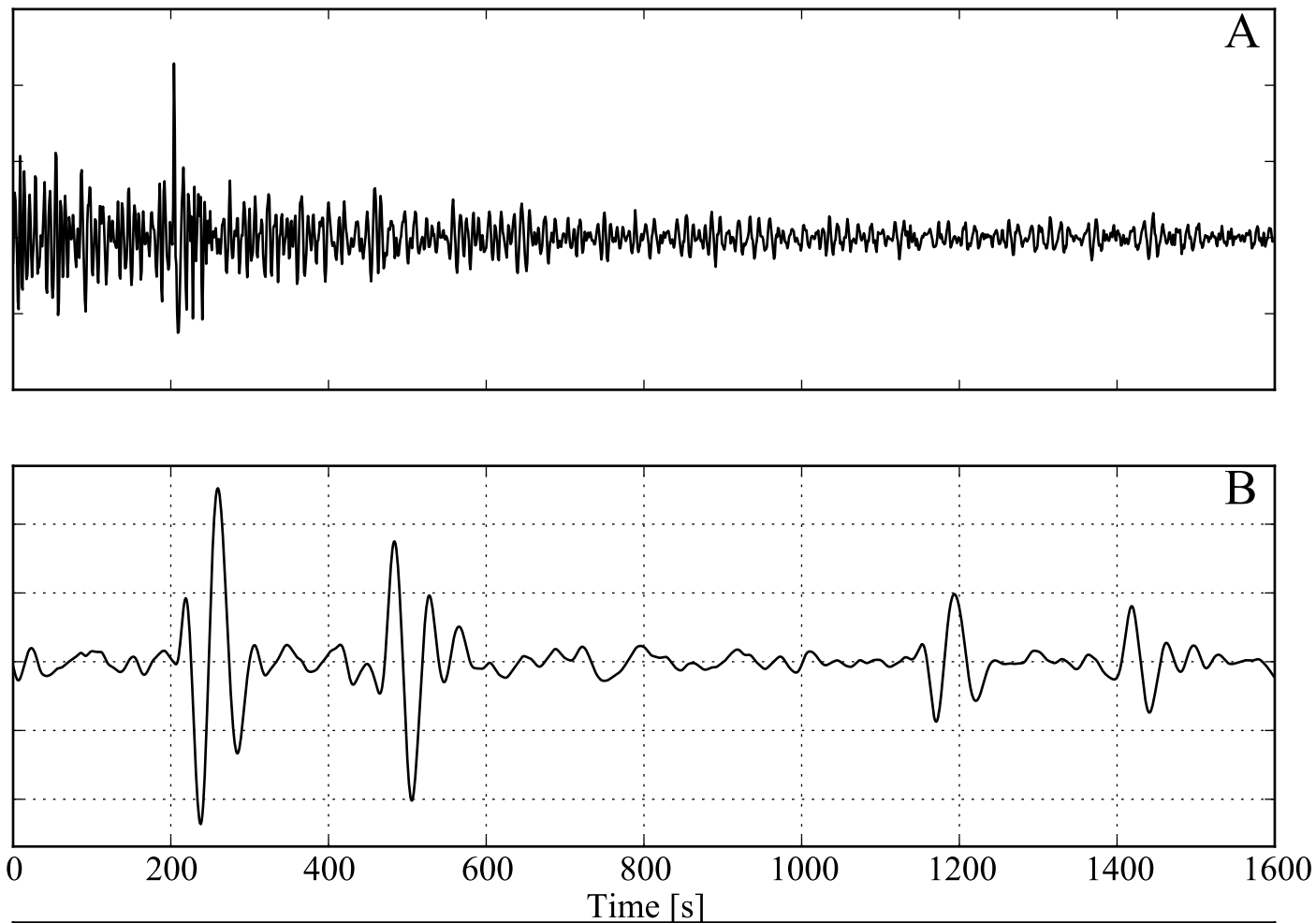






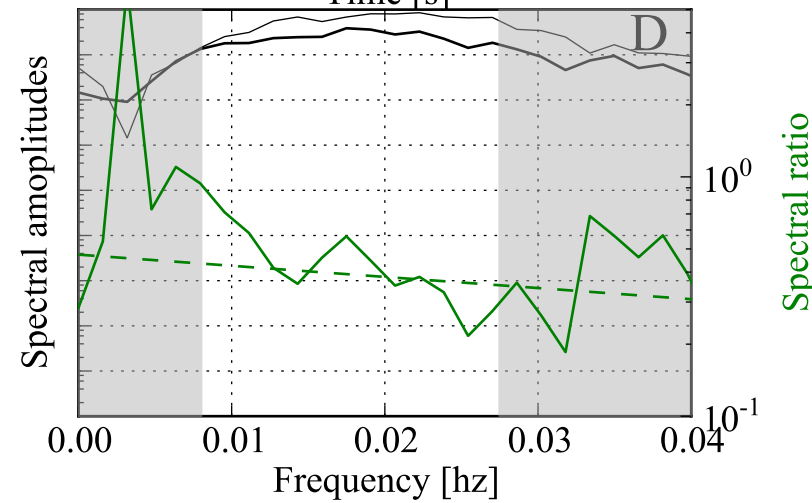


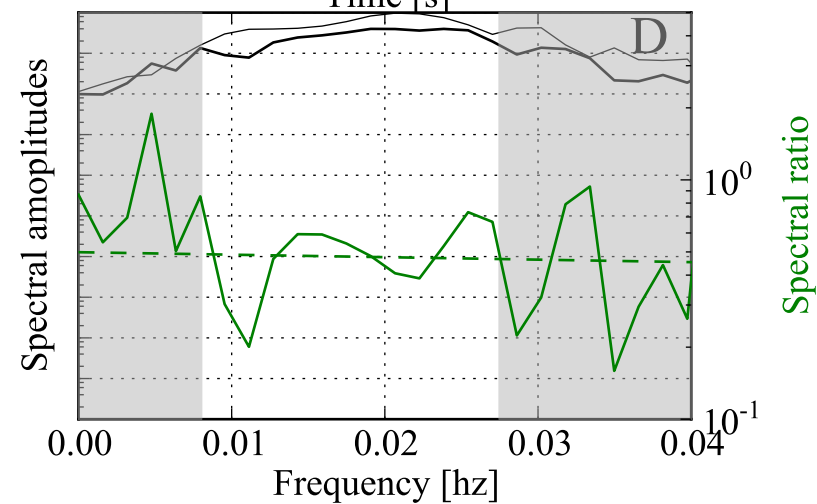
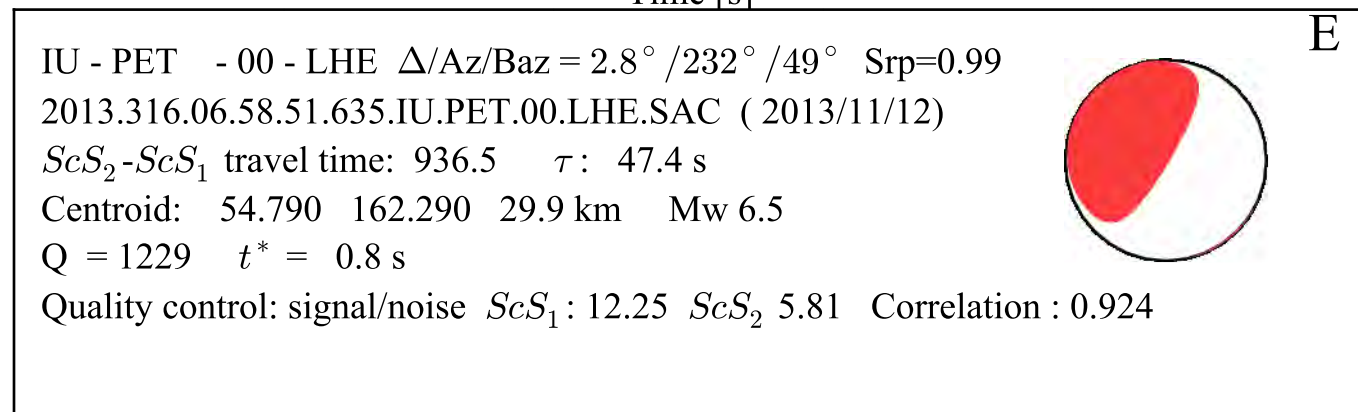
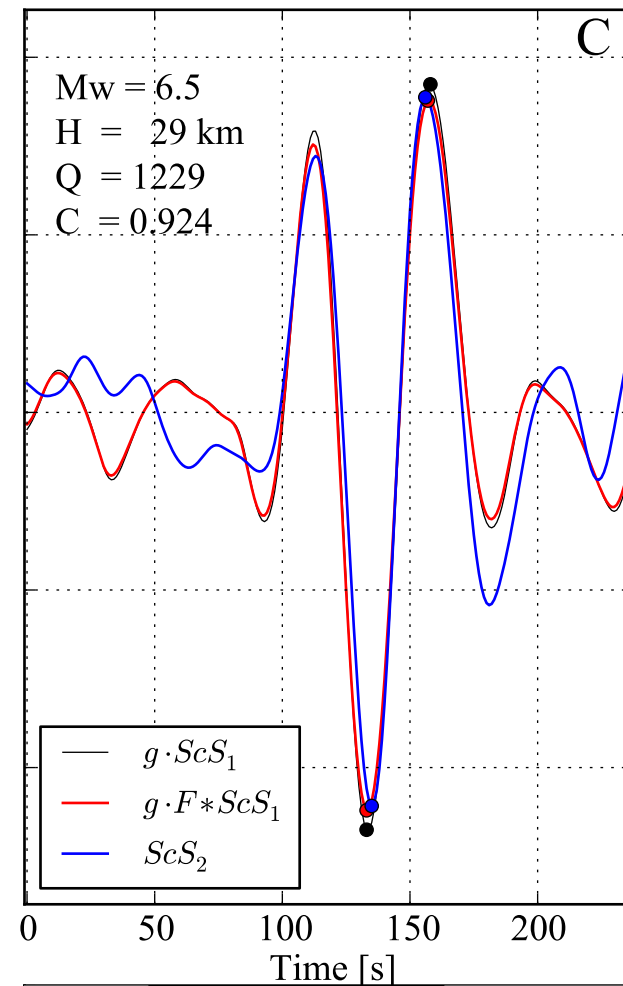
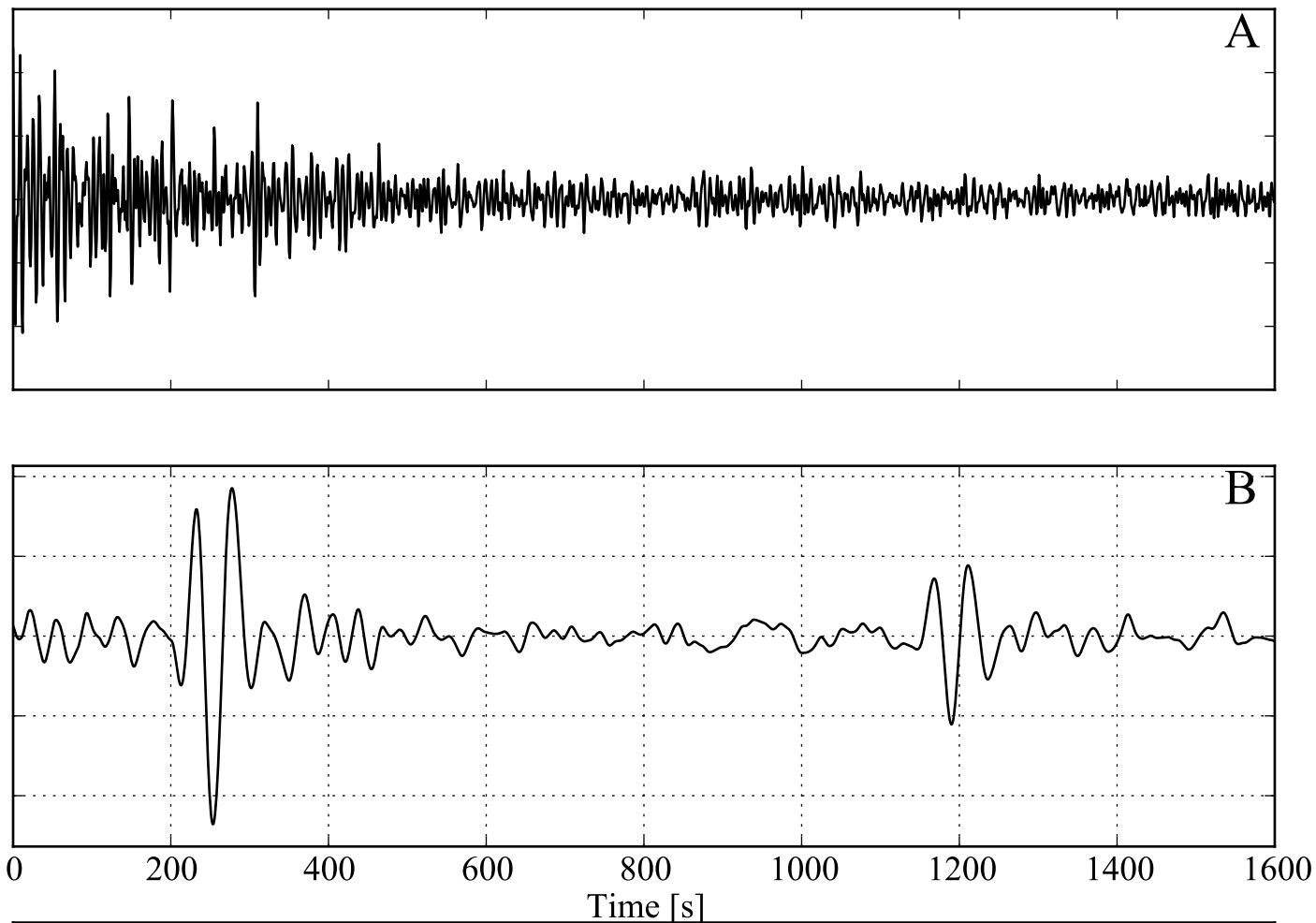


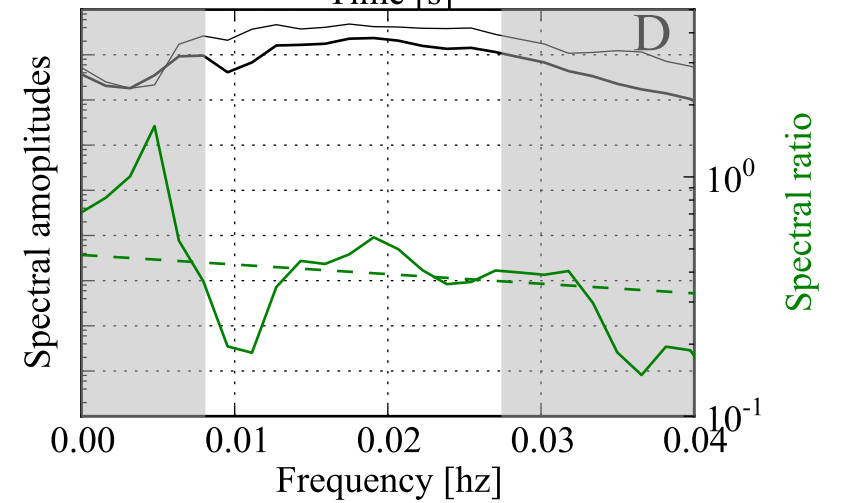
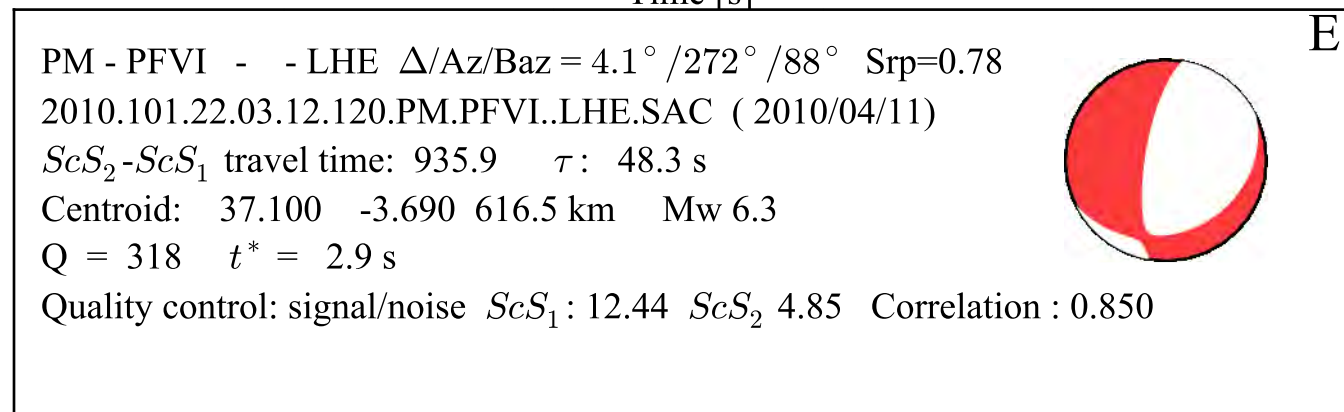
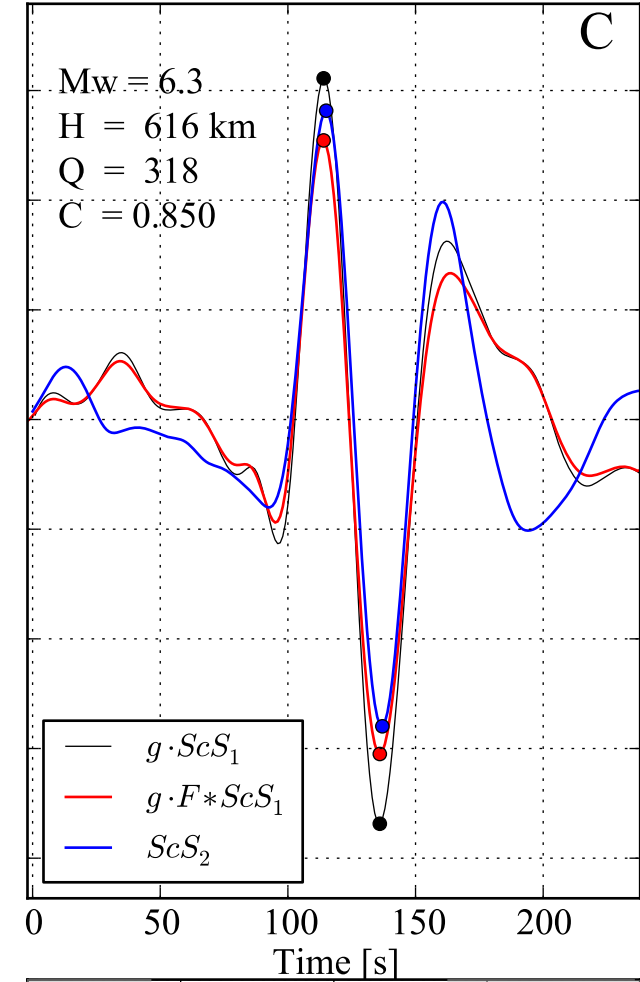
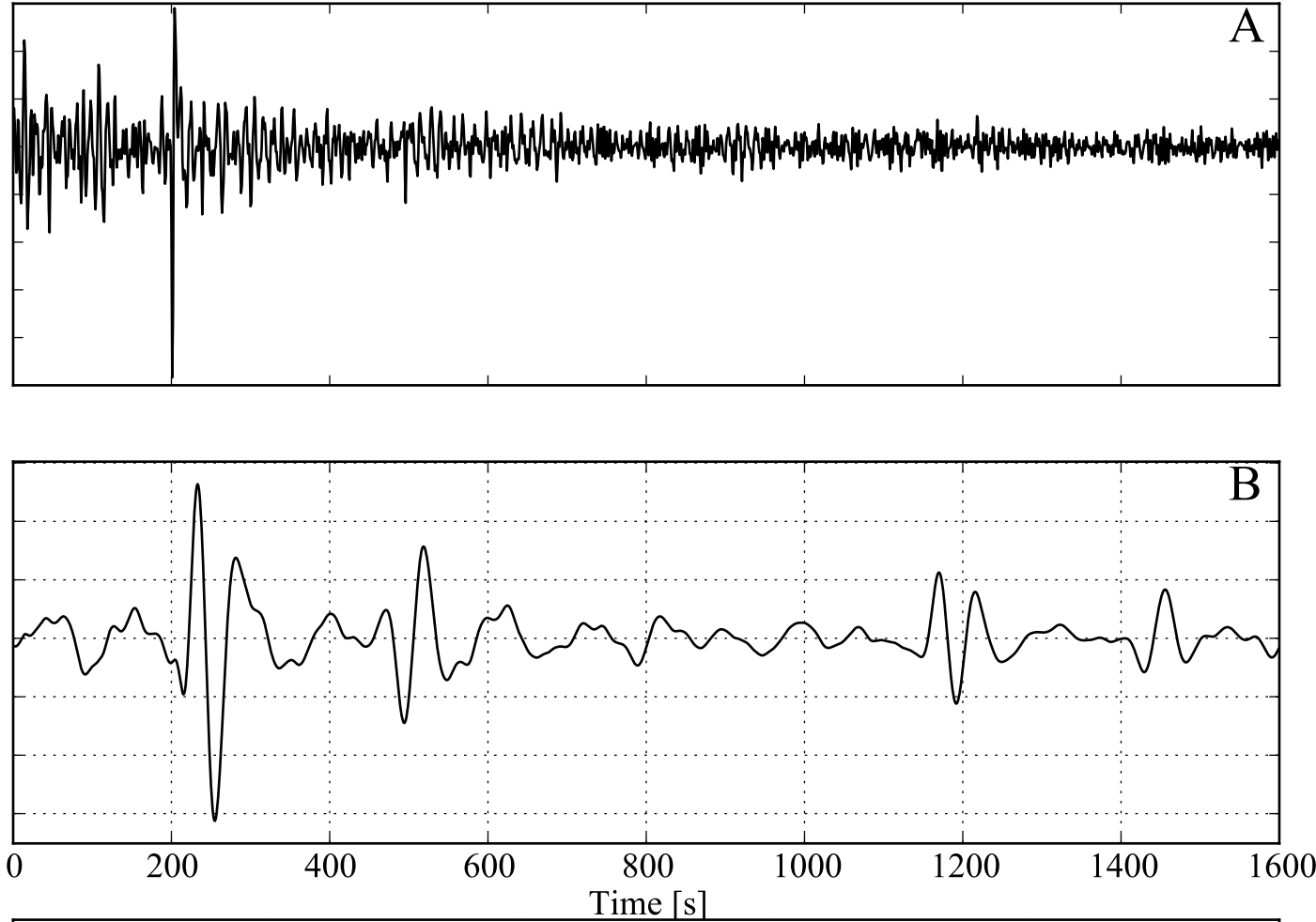


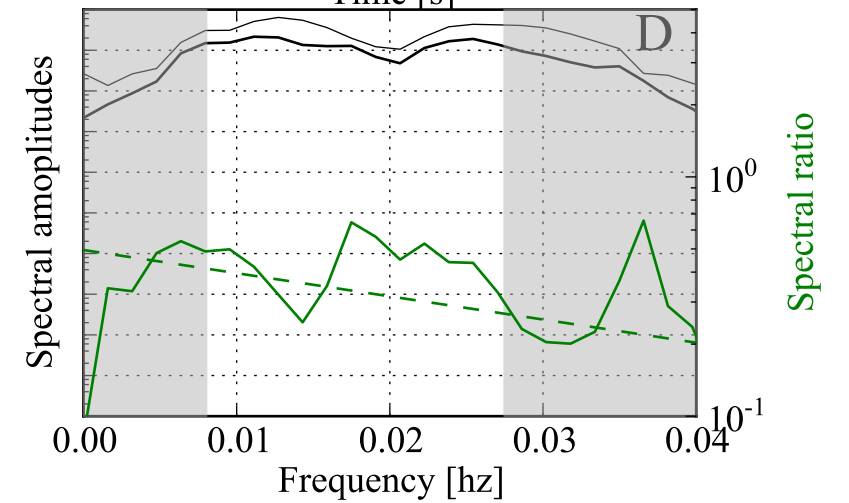
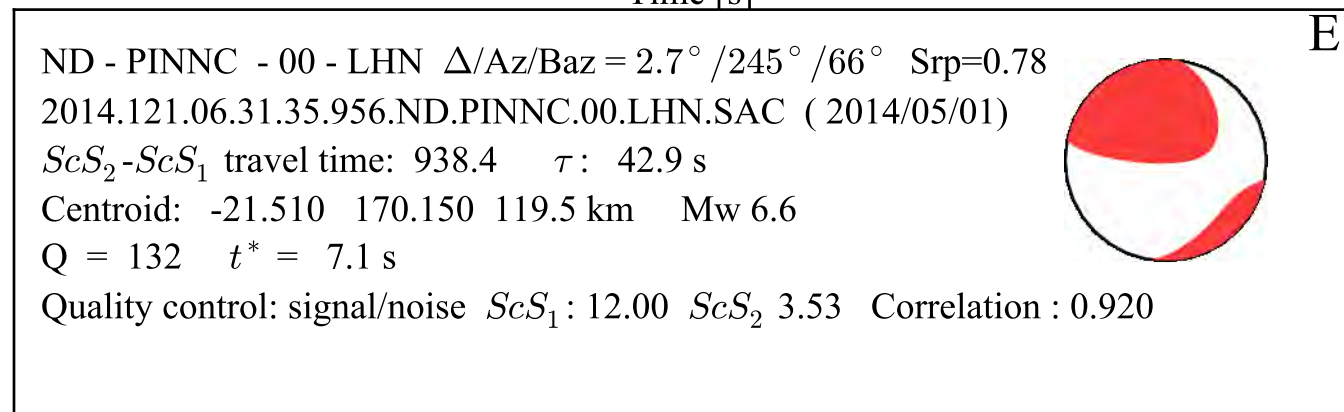
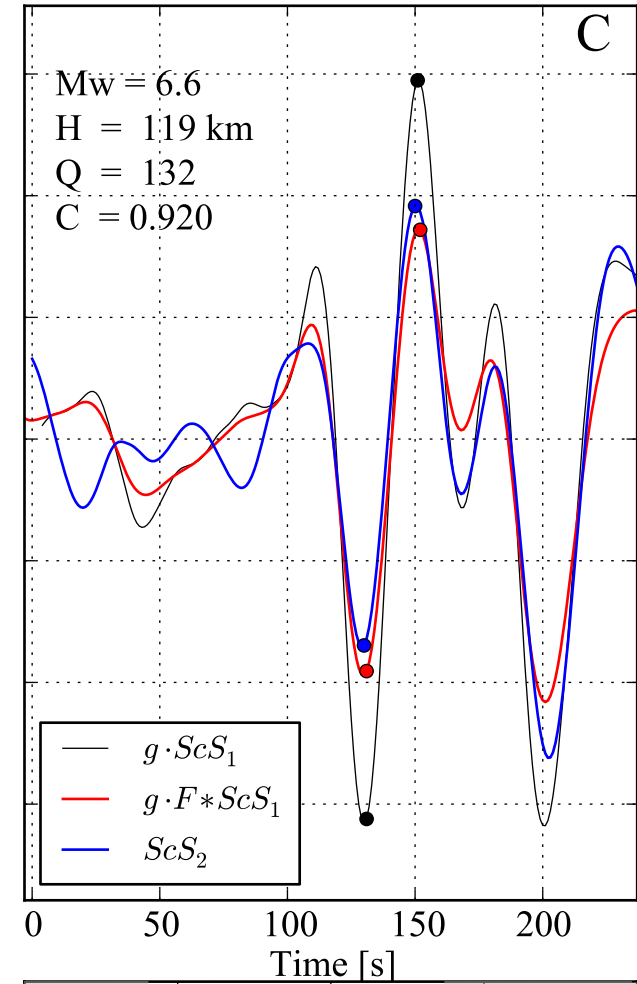
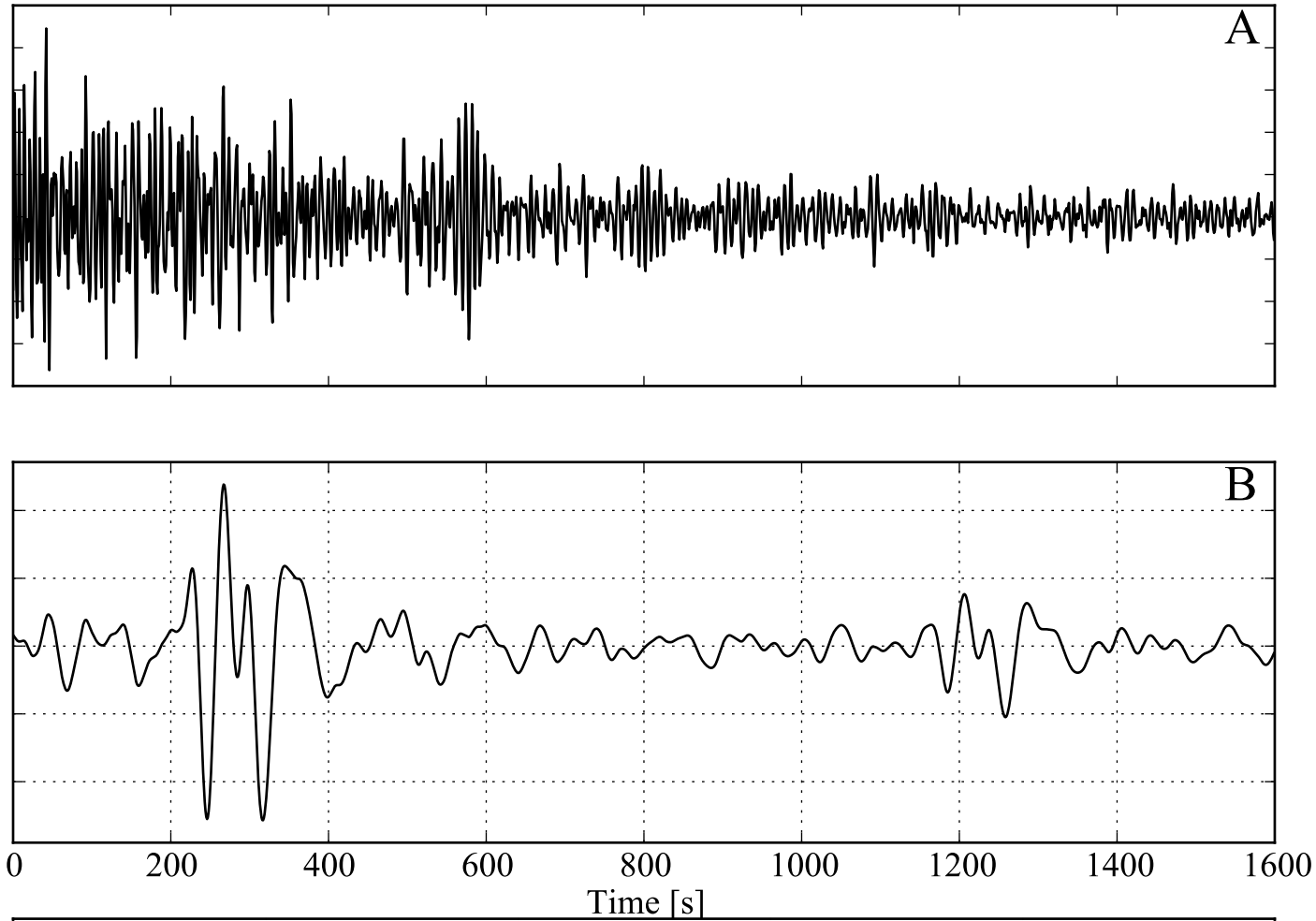
E

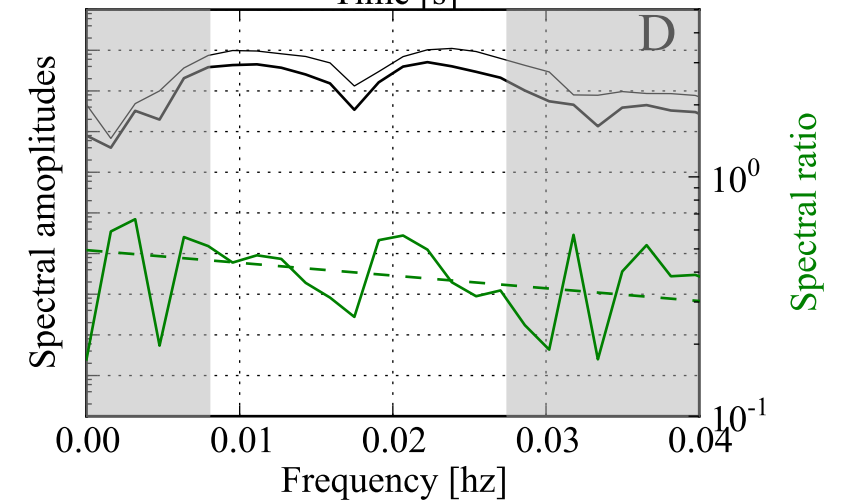
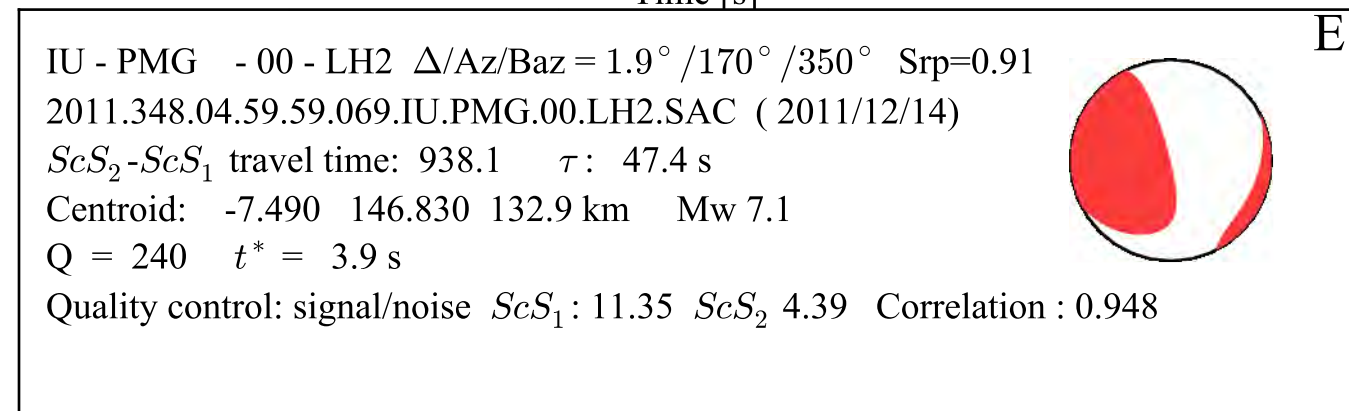
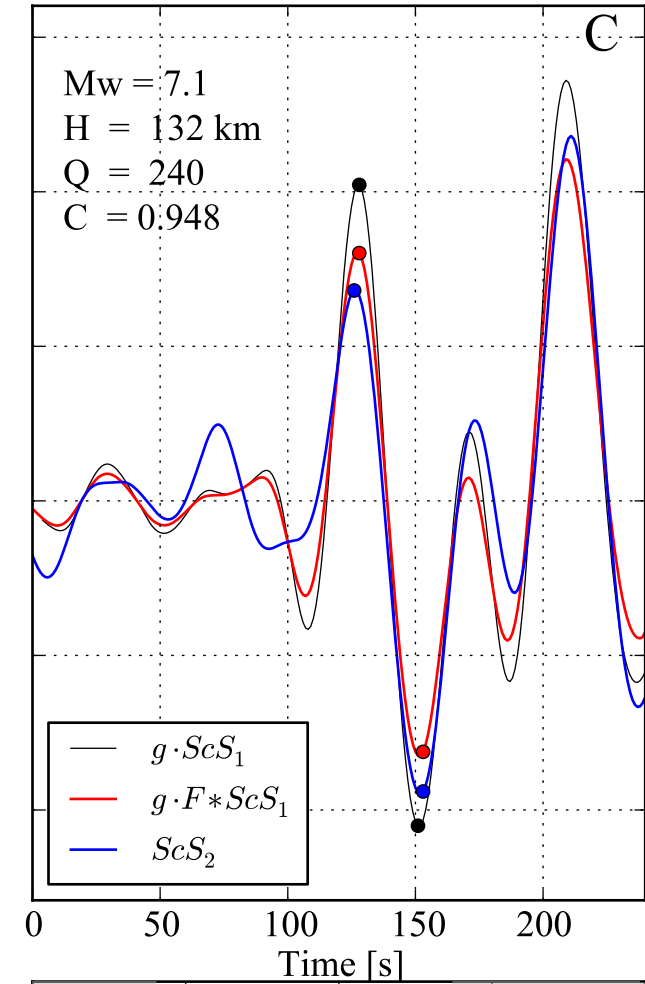
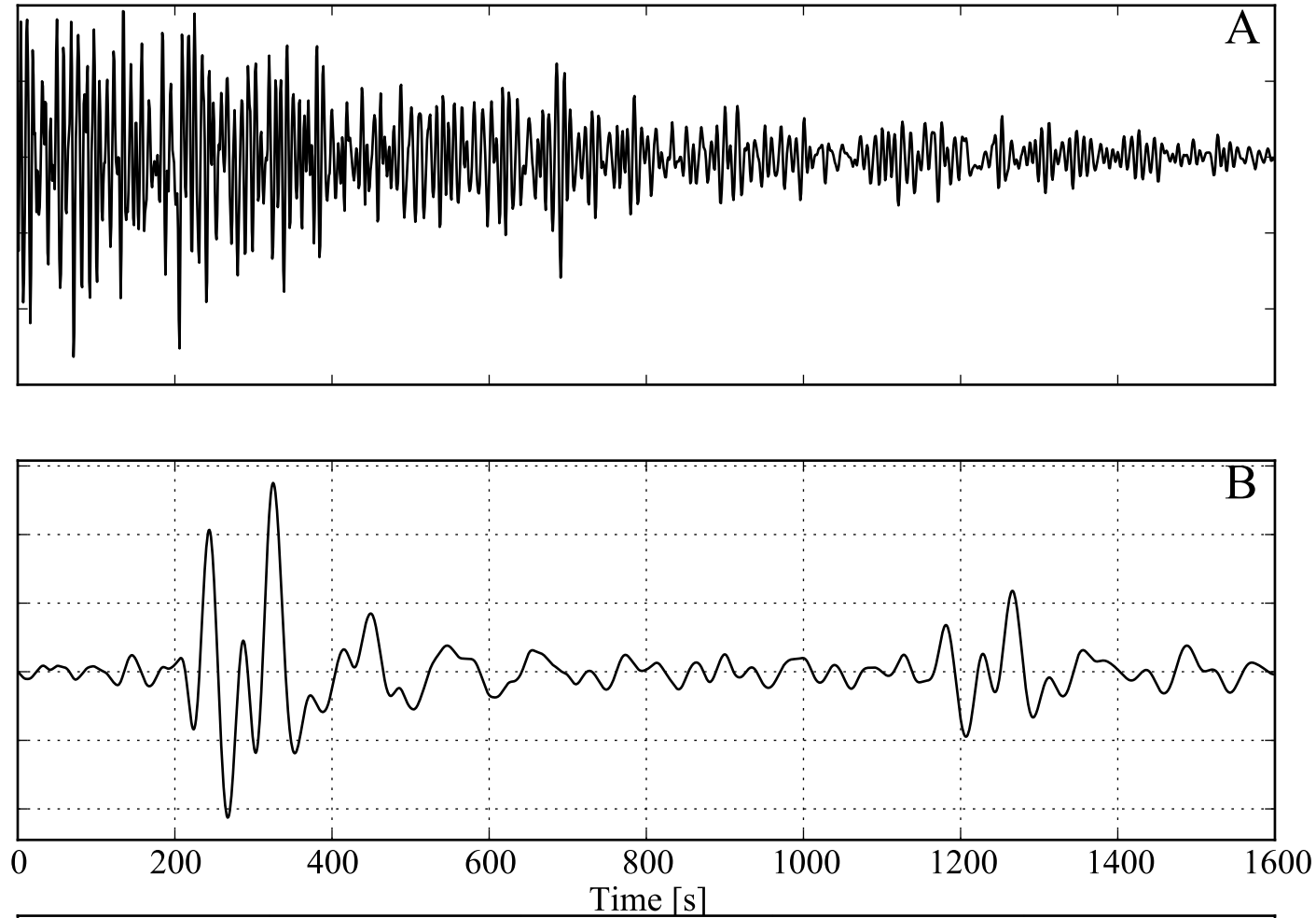
IU - PET - 00 - LHE $\Delta/Az/Baz = 3.5^\circ / 90^\circ / 275^\circ$ $Srp=0.64$
 2013.274.03.33.21.635.IU.PET.00.LHE.SAC (2013/10/01)
 $ScS_2 - ScS_1$ travel time: 935.2 τ : 46.4 s
 Centroid: 53.200 152.810 585.5 km Mw 6.7
 Q = 274 $t^* = 3.4$ s
 Quality control: signal/noise ScS_1 : 20.77 ScS_2 7.88 Correlation : 0.972

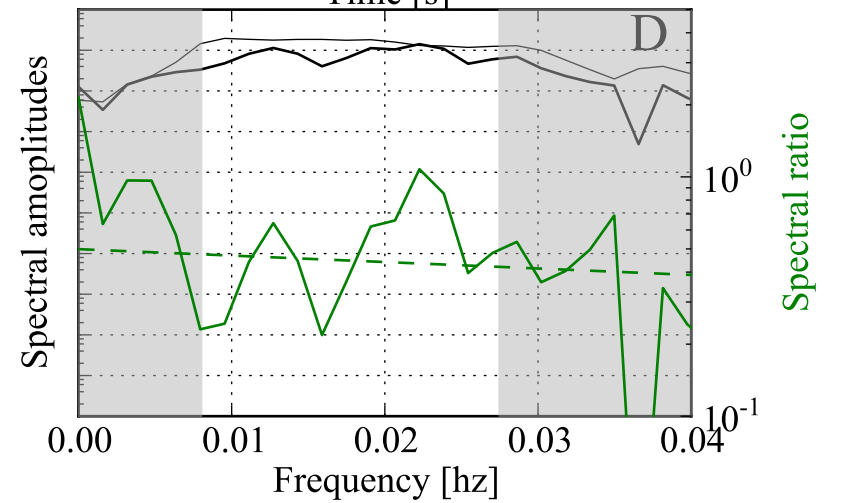
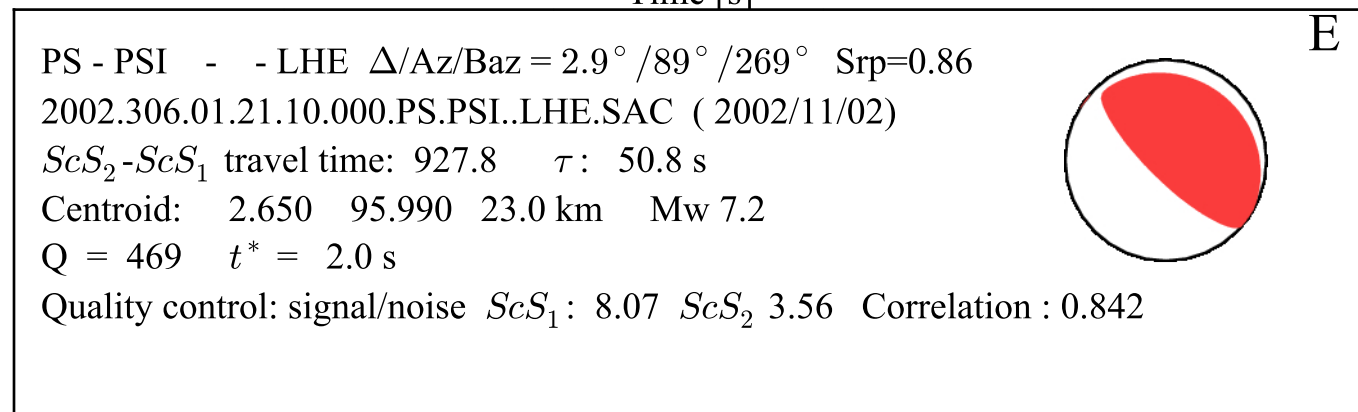
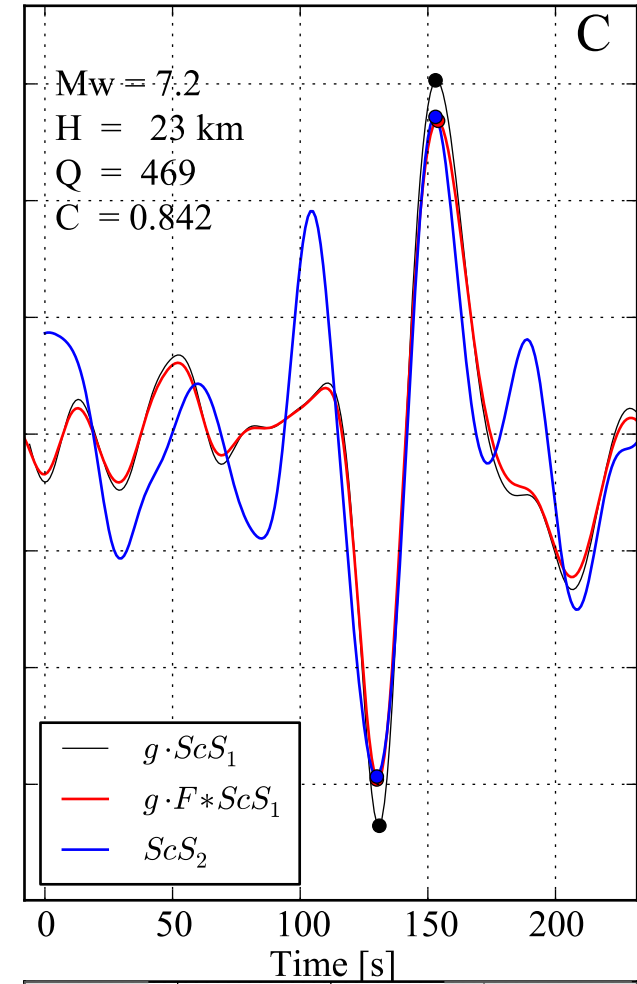
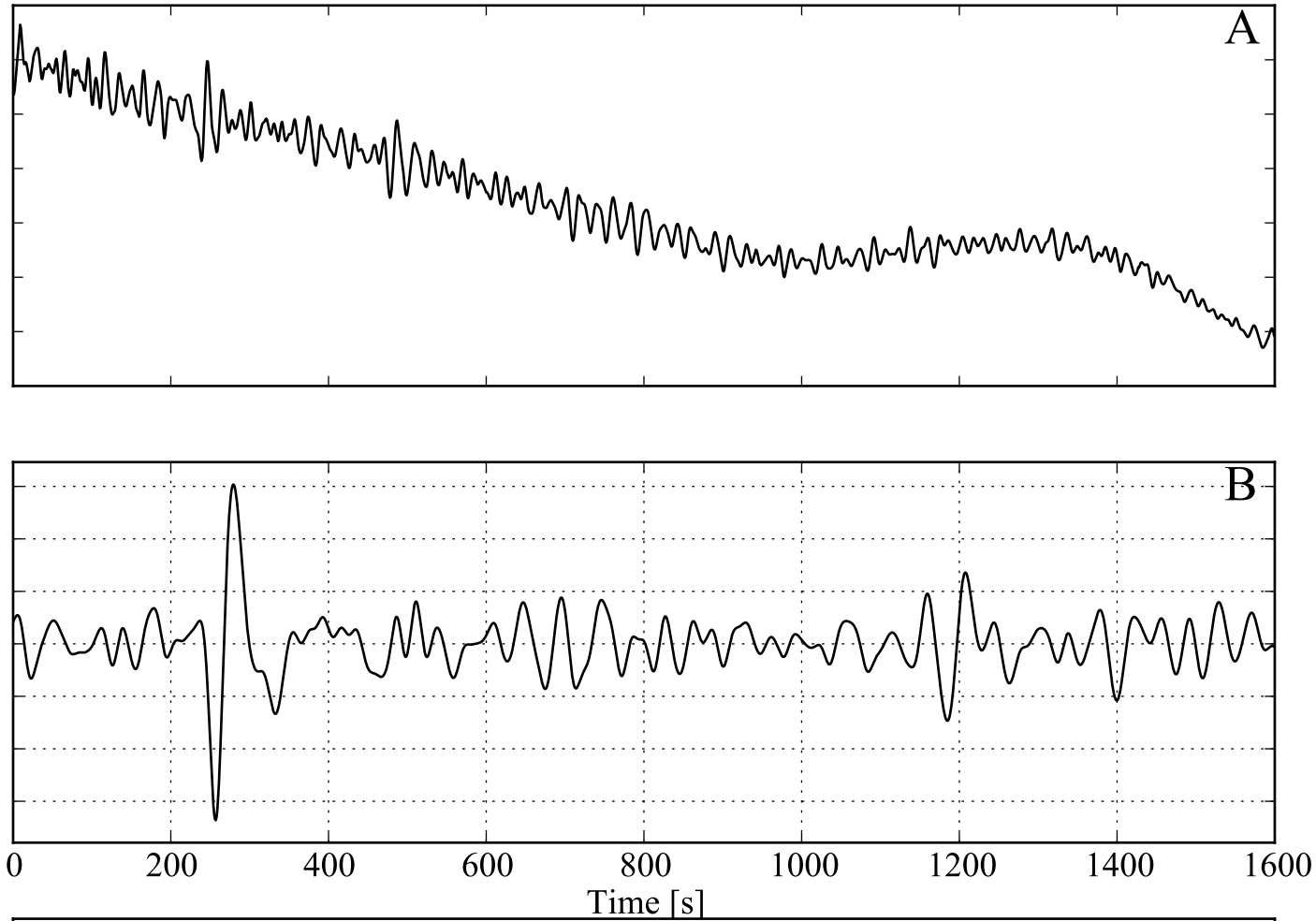


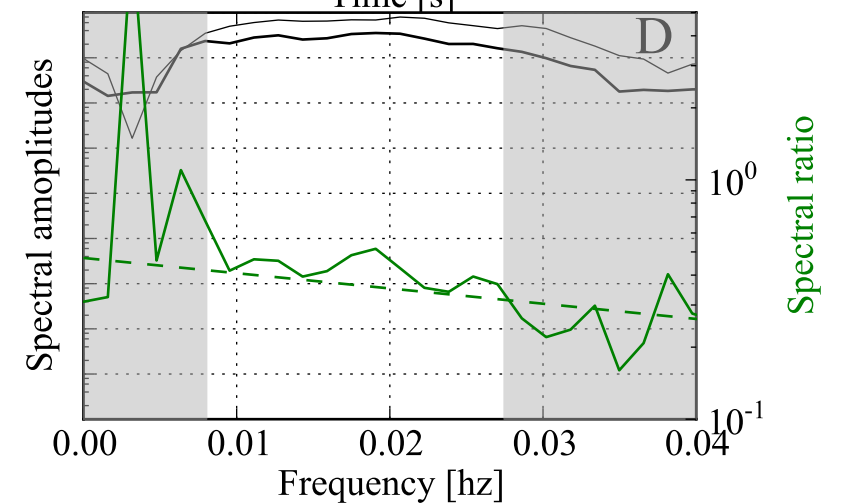
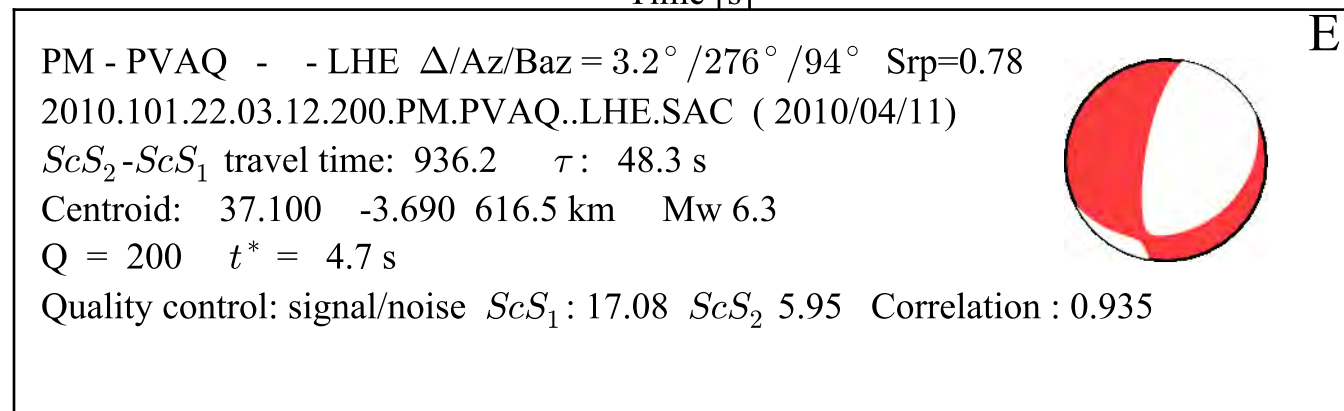
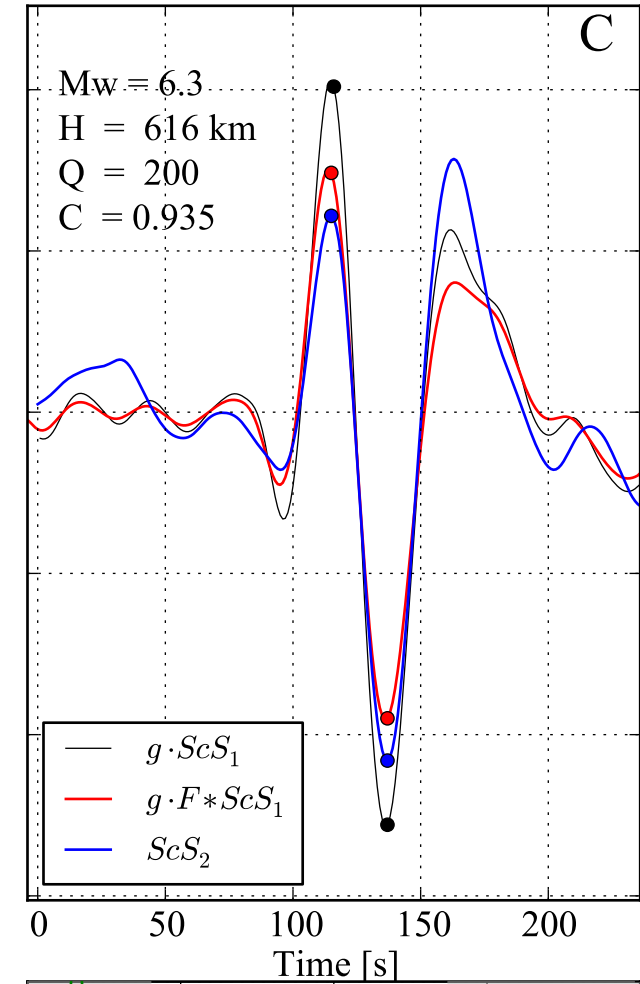
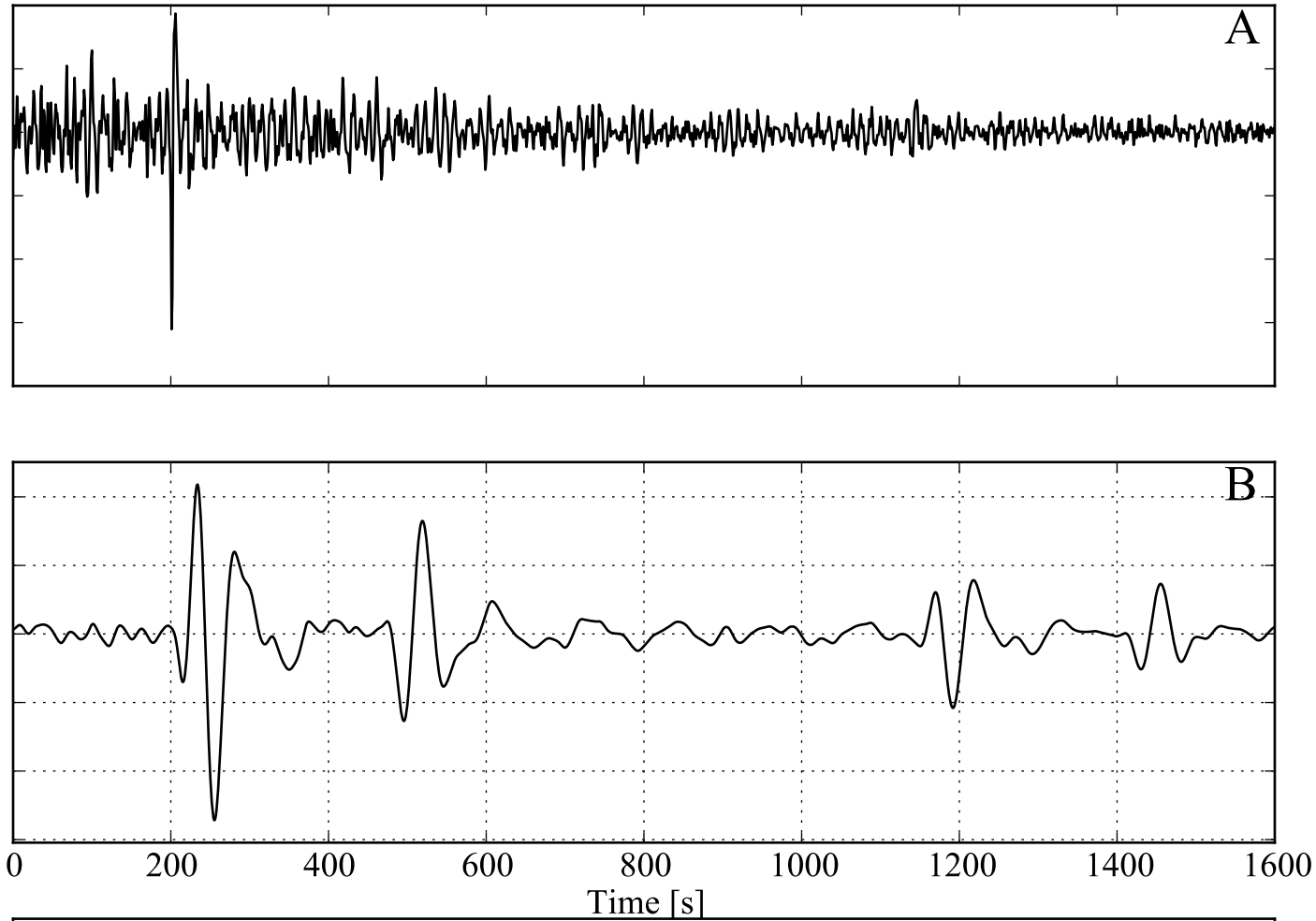


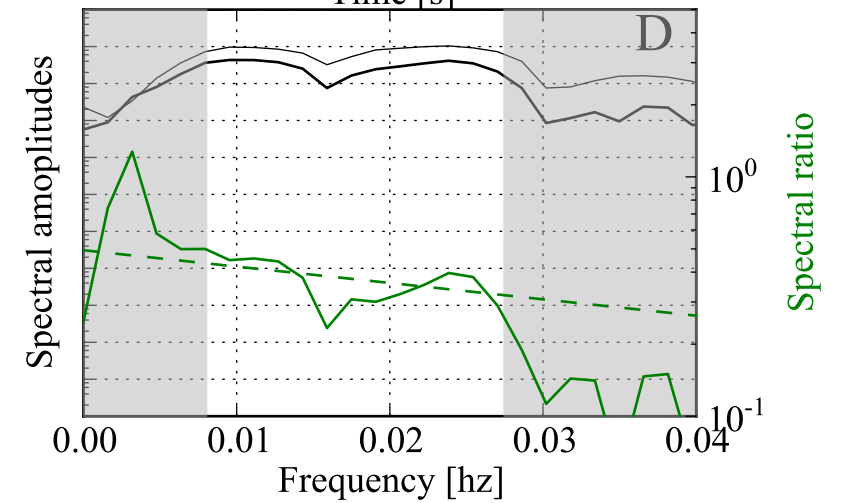
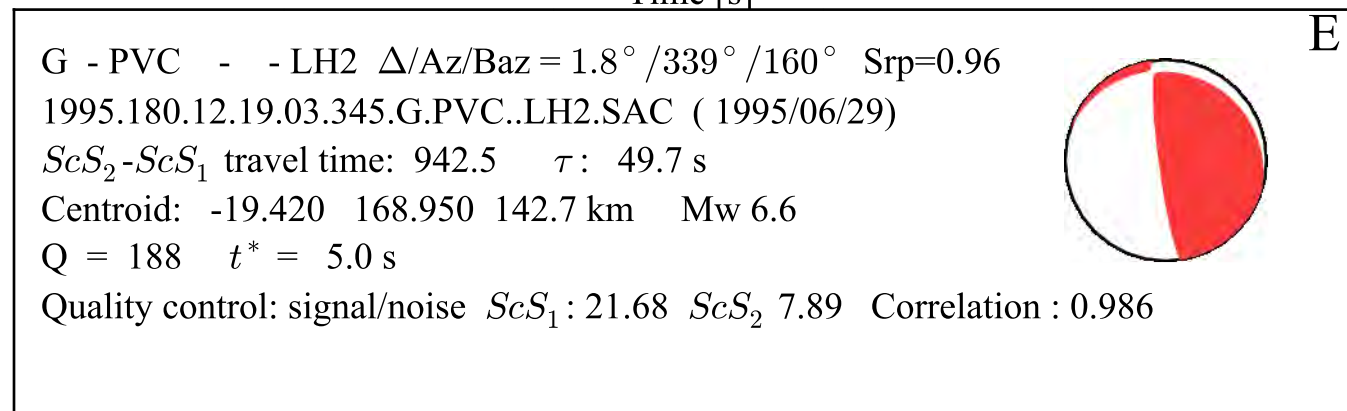
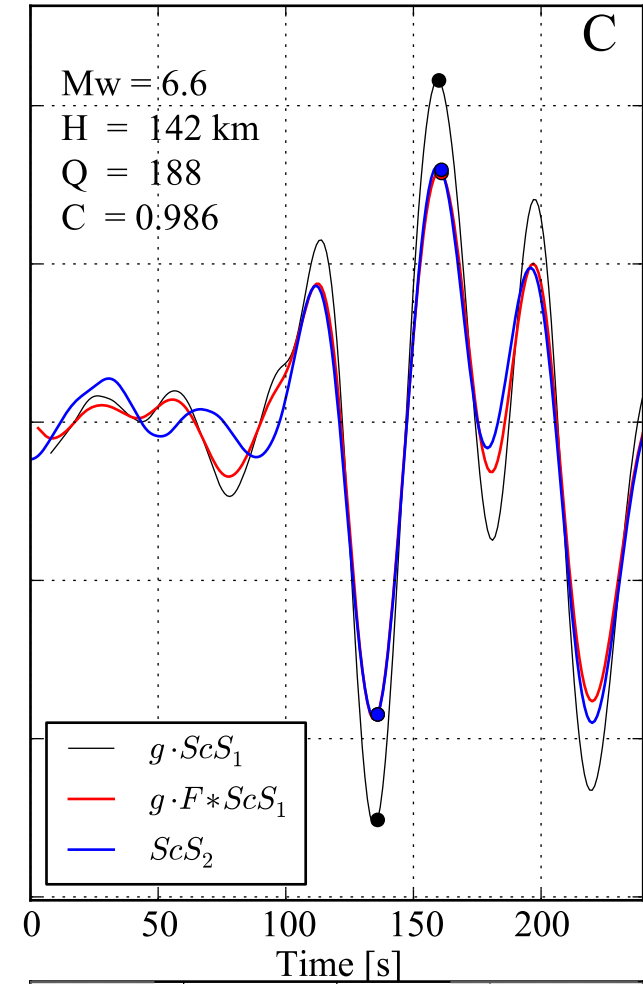
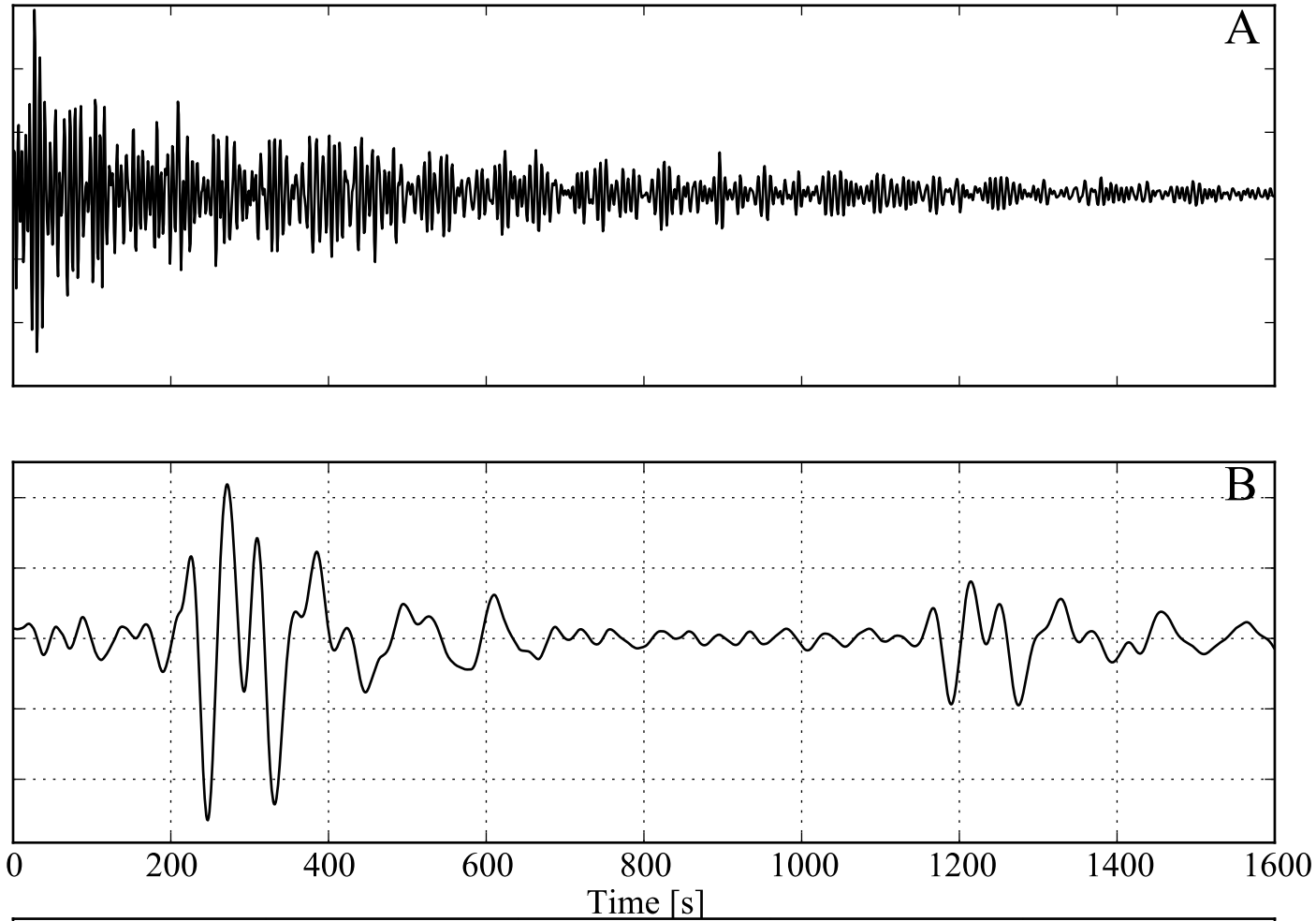


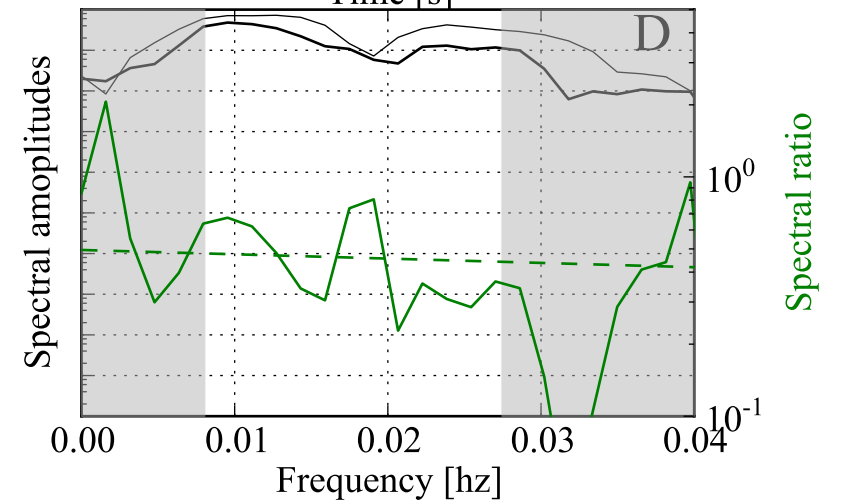
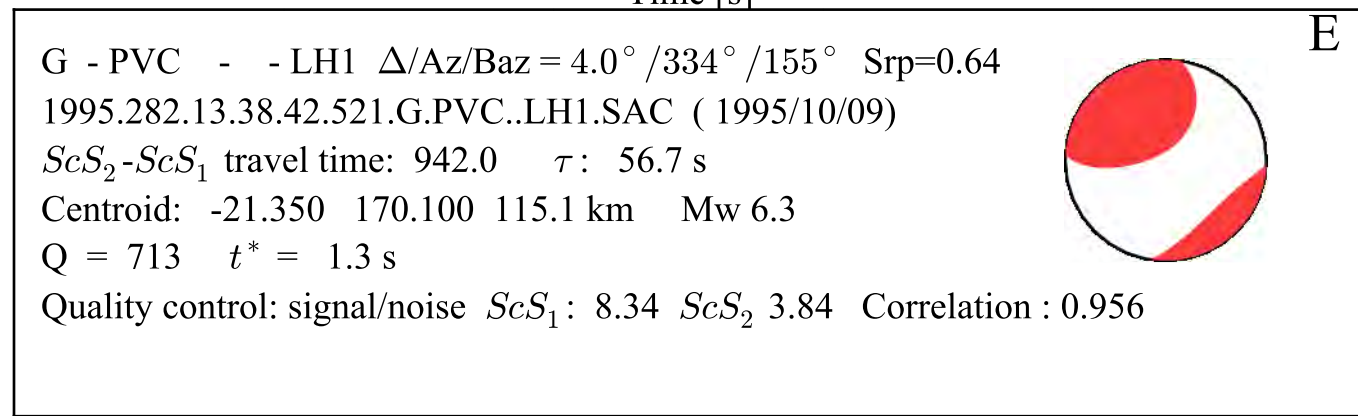
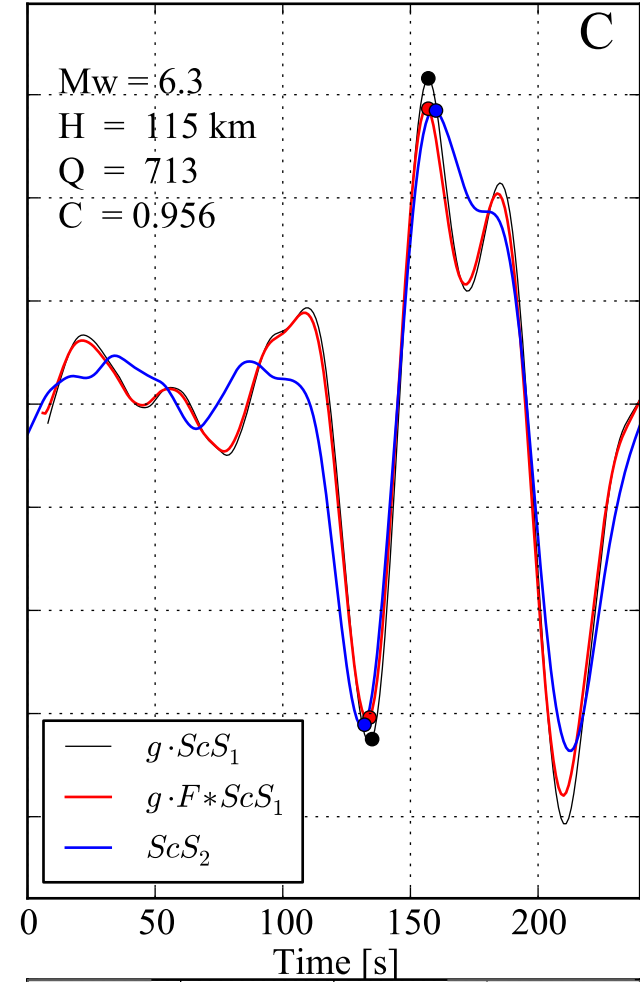
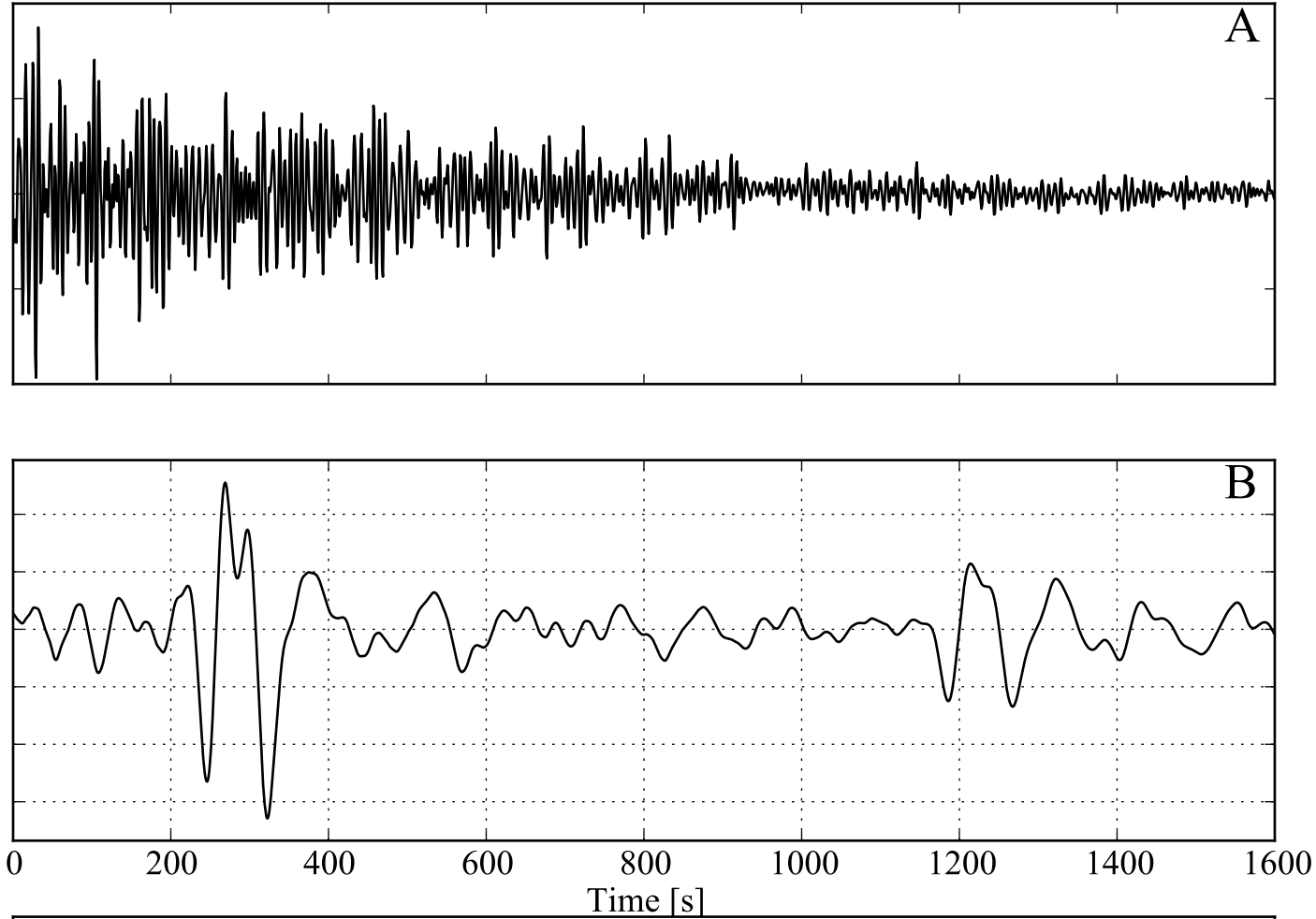


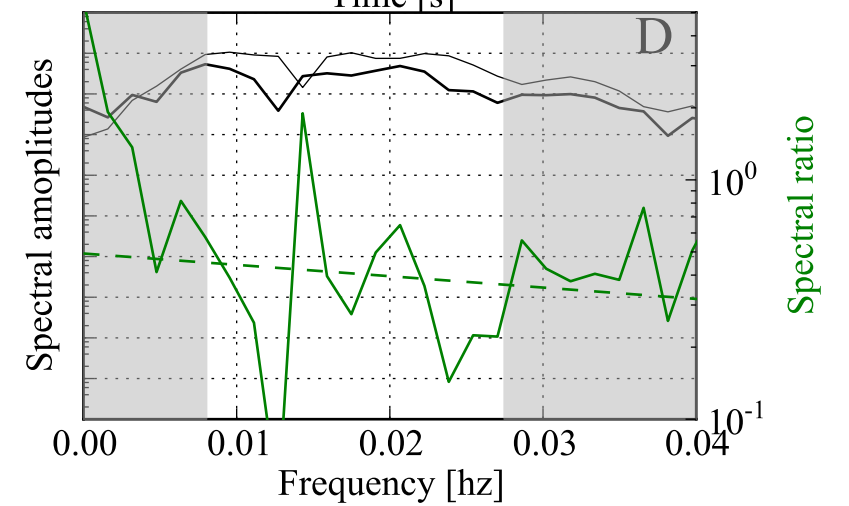
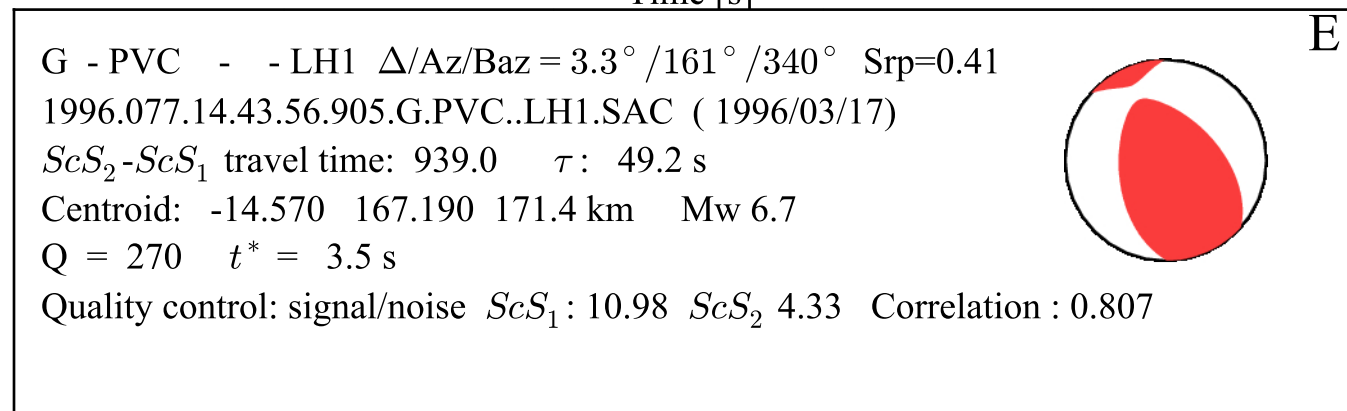
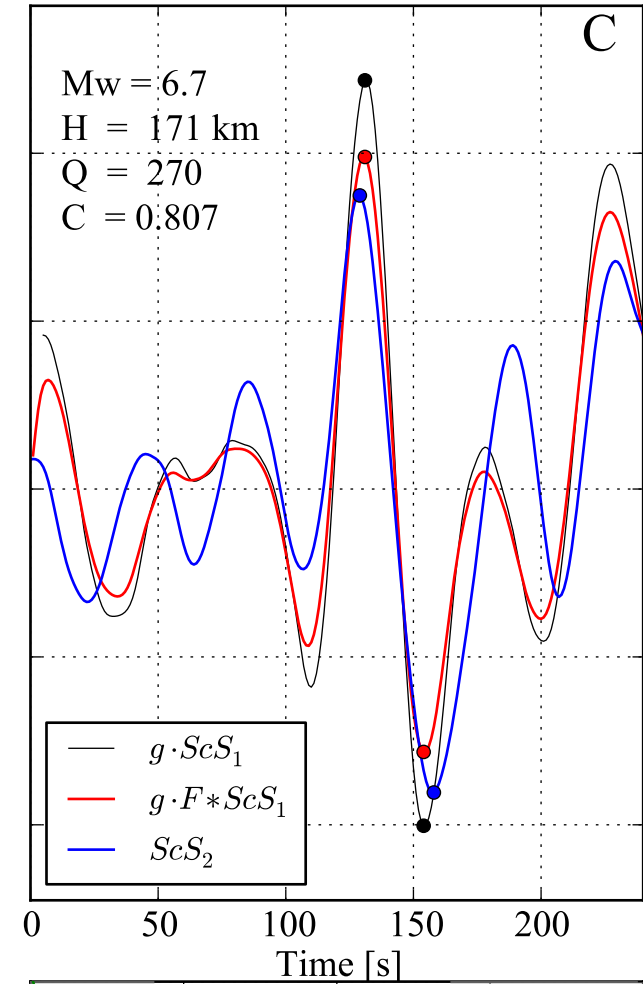
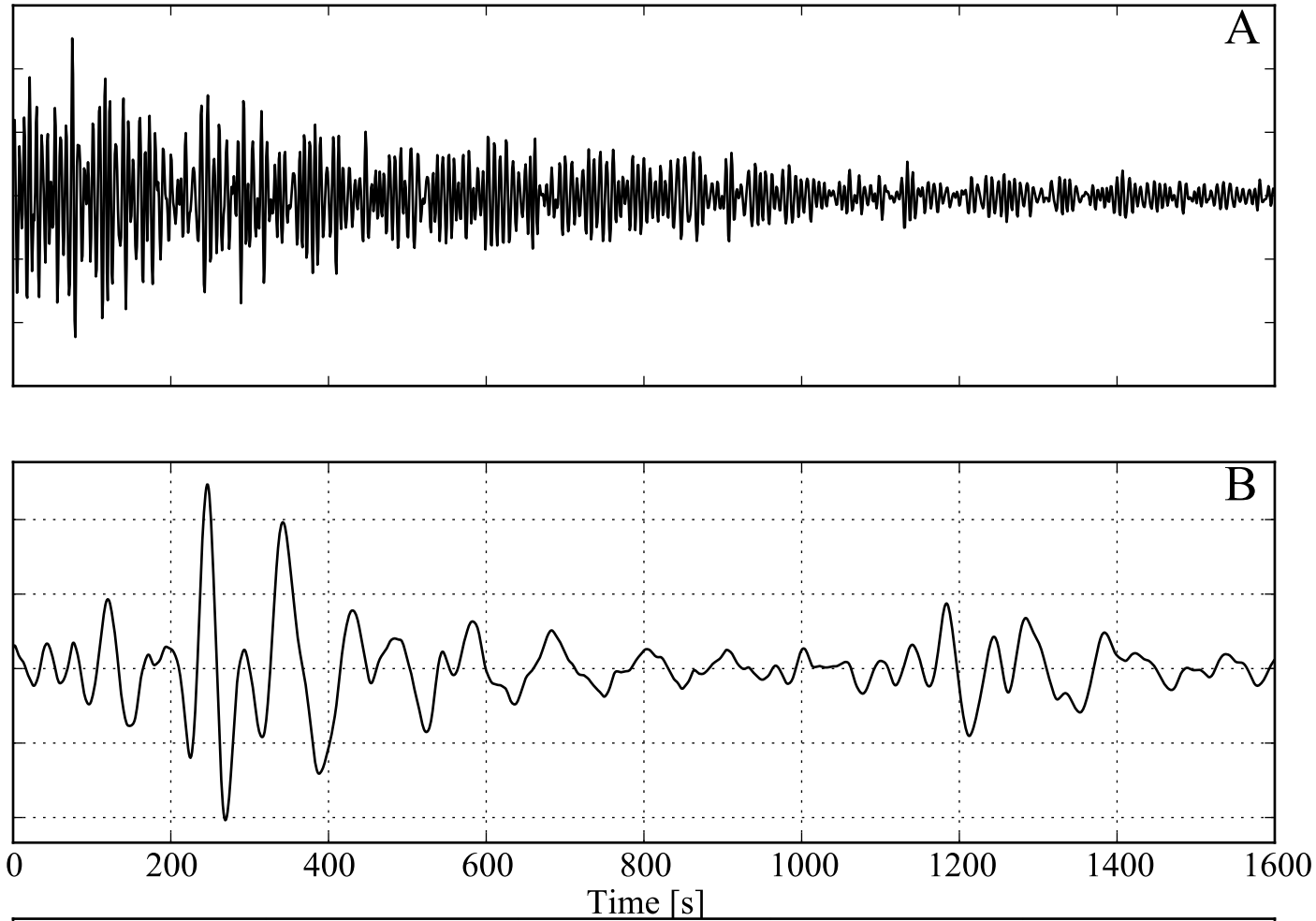


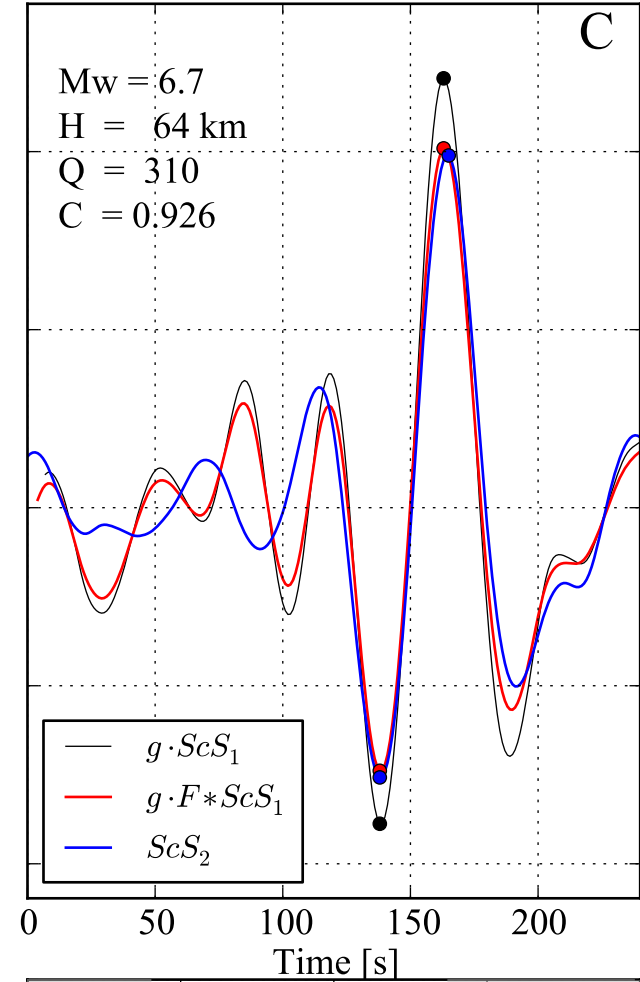
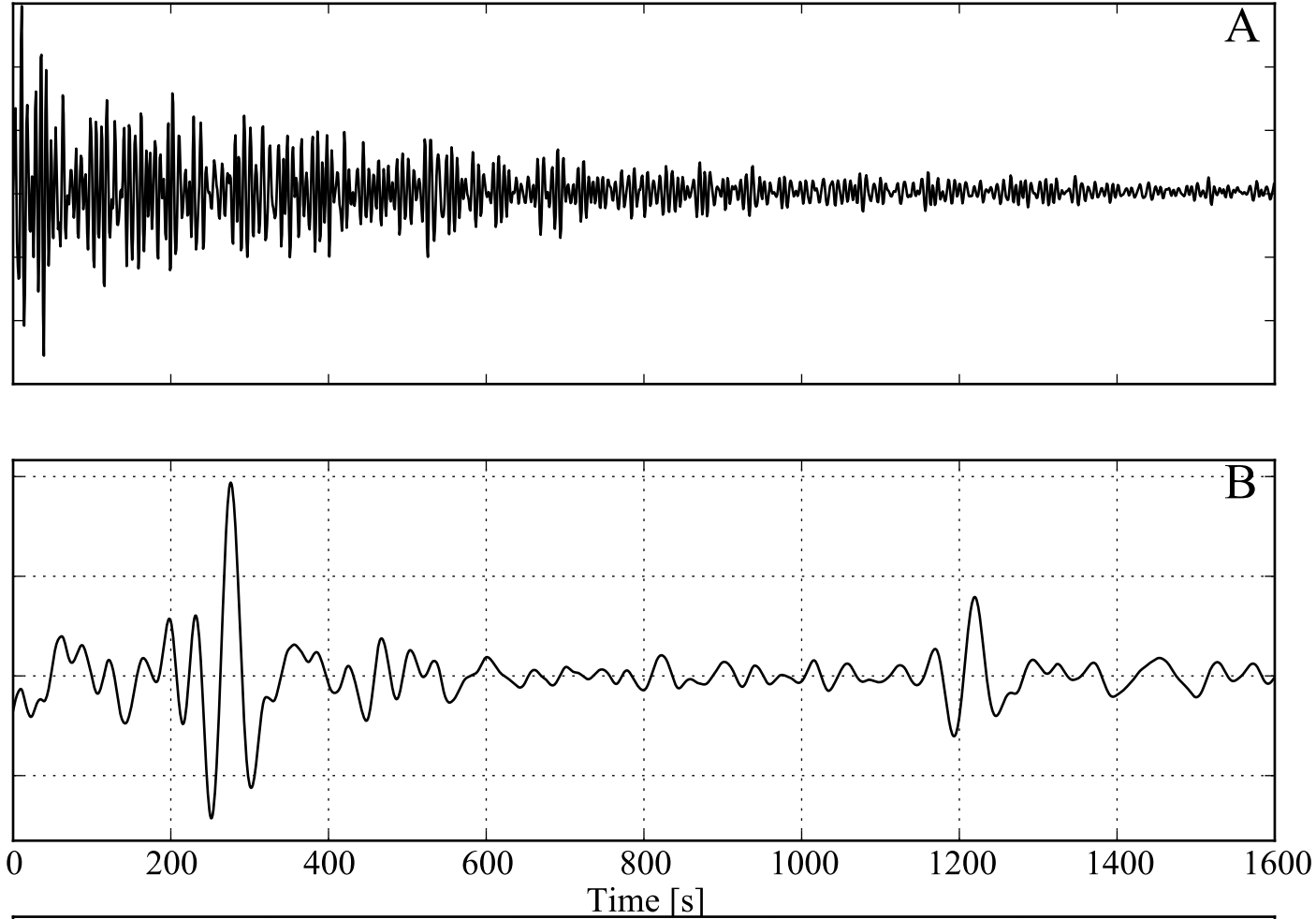







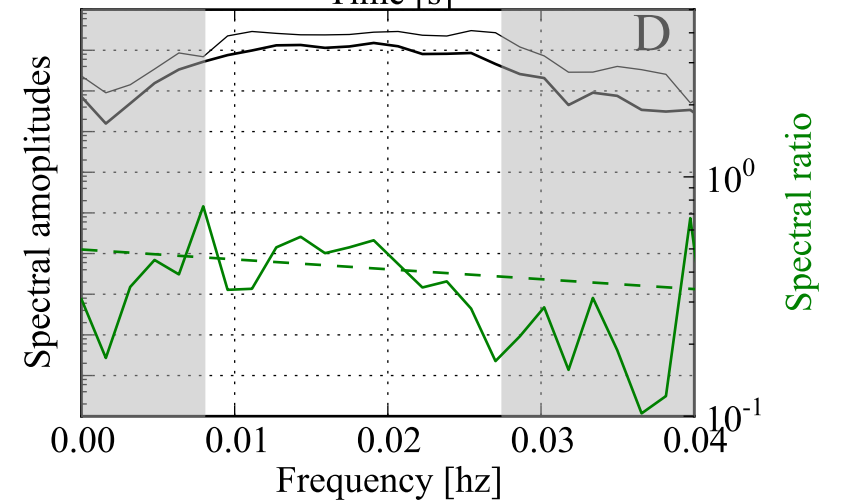


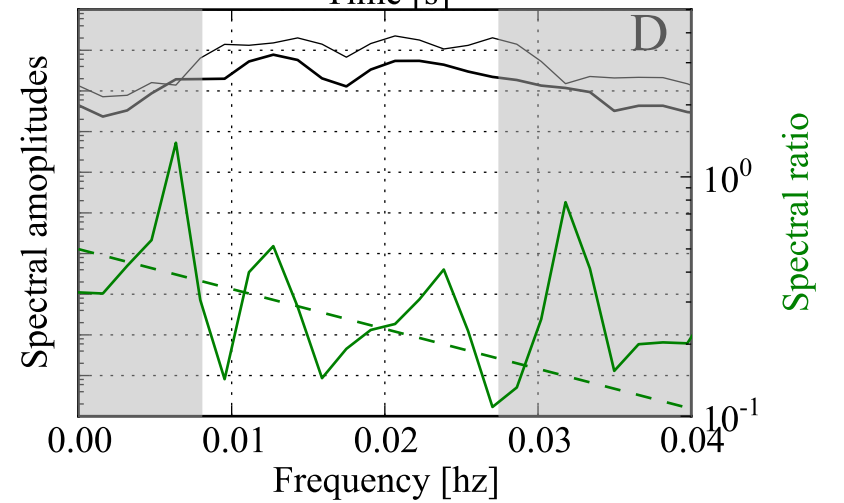
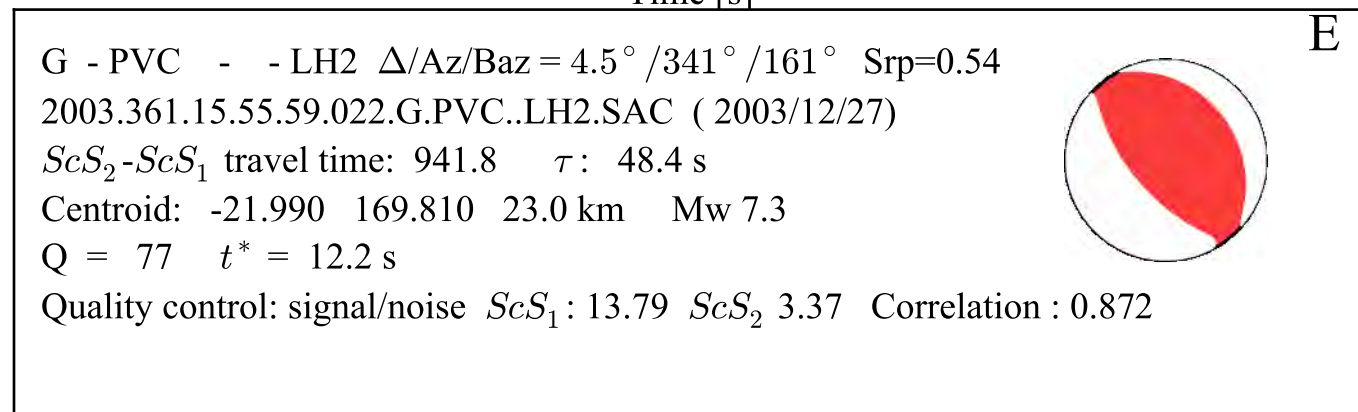
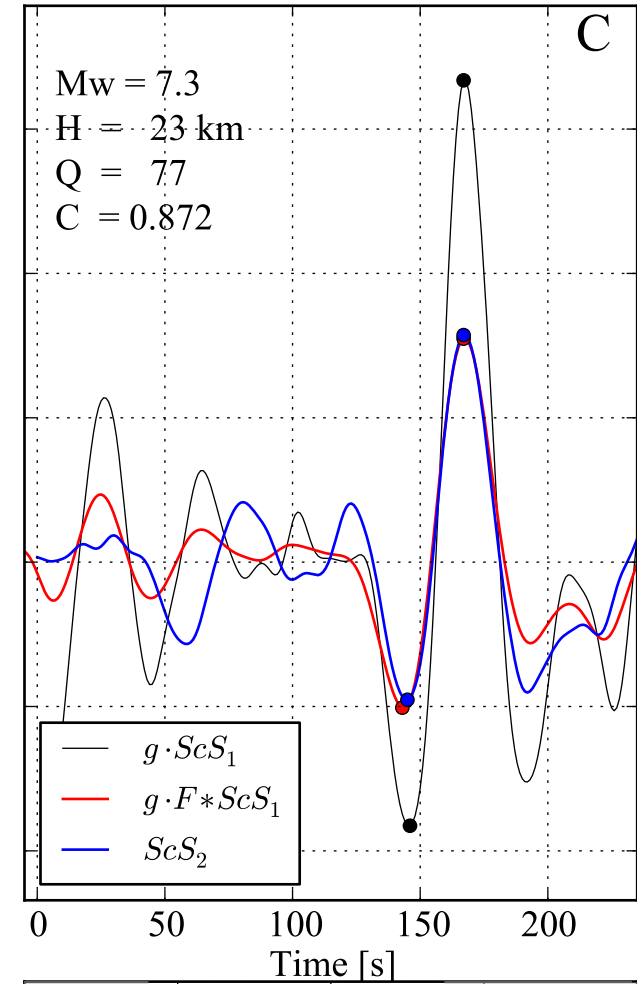
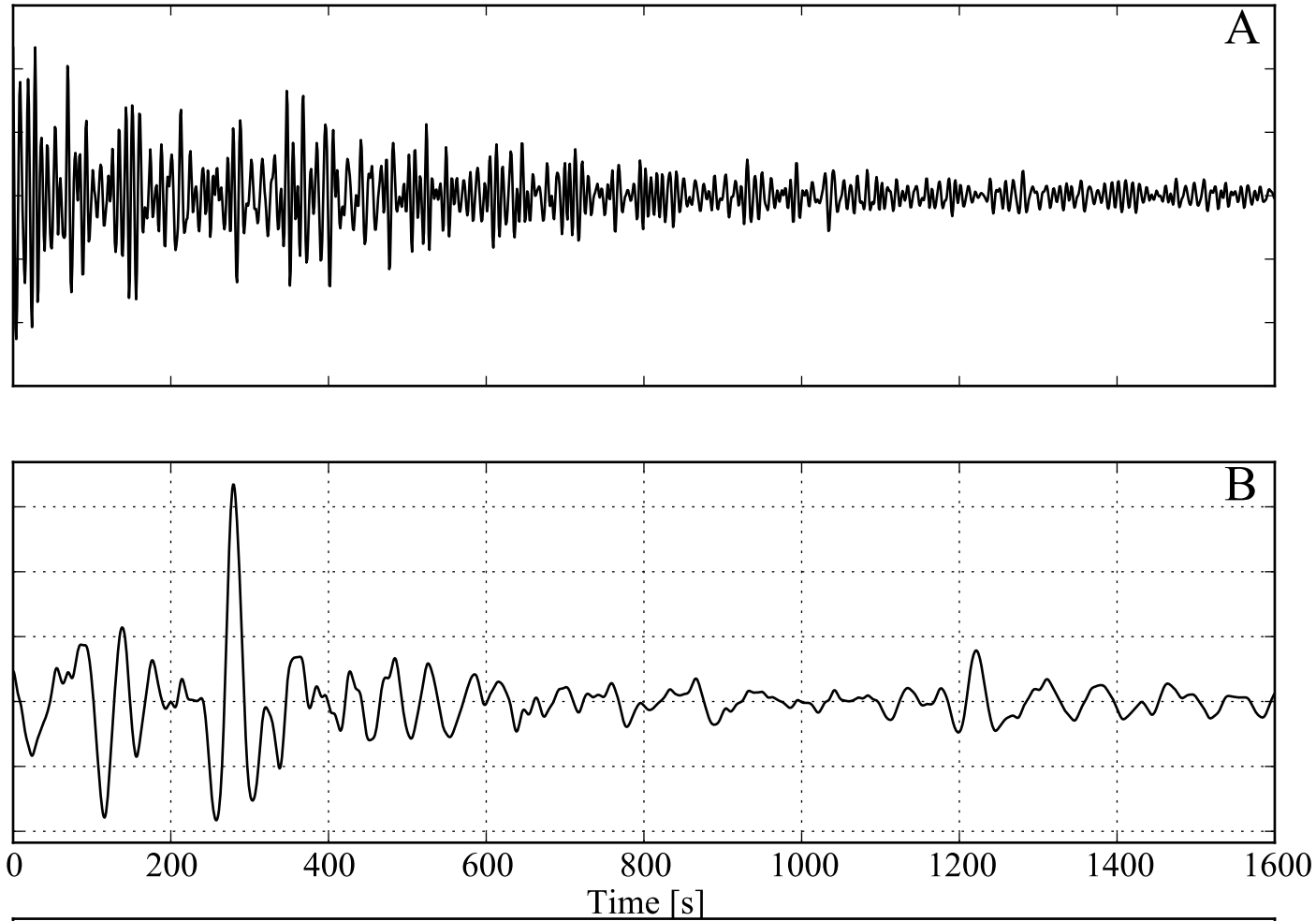


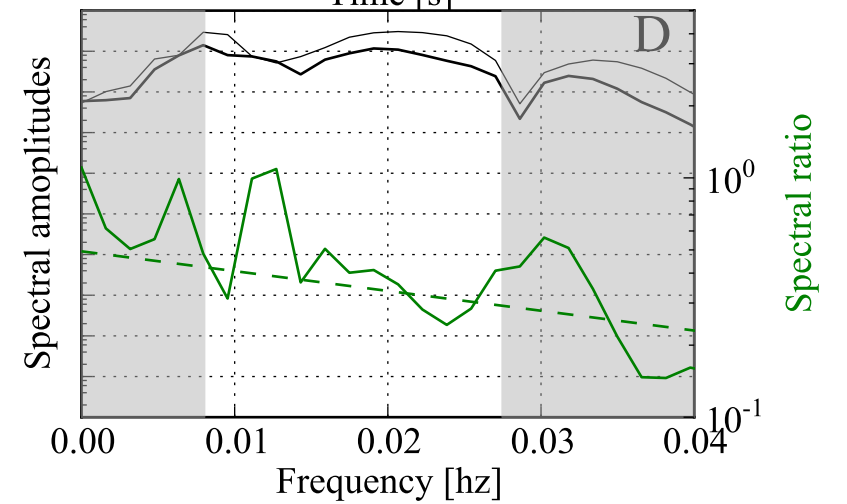
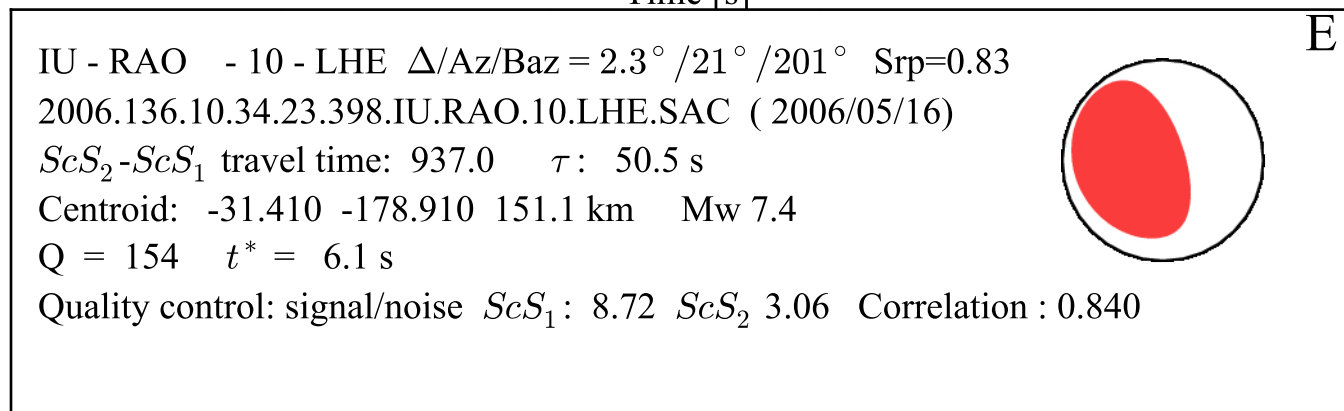
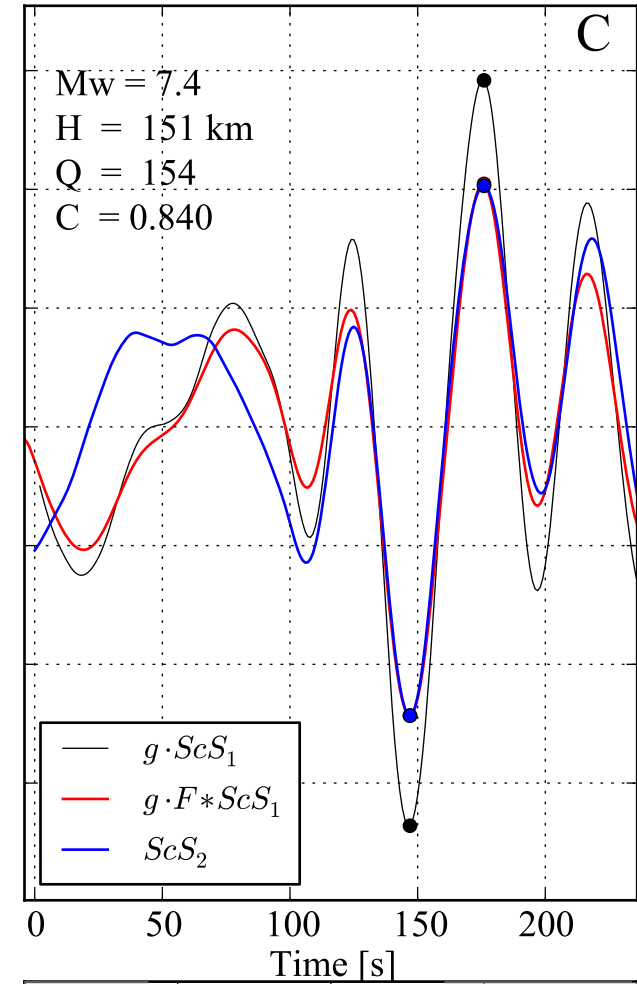
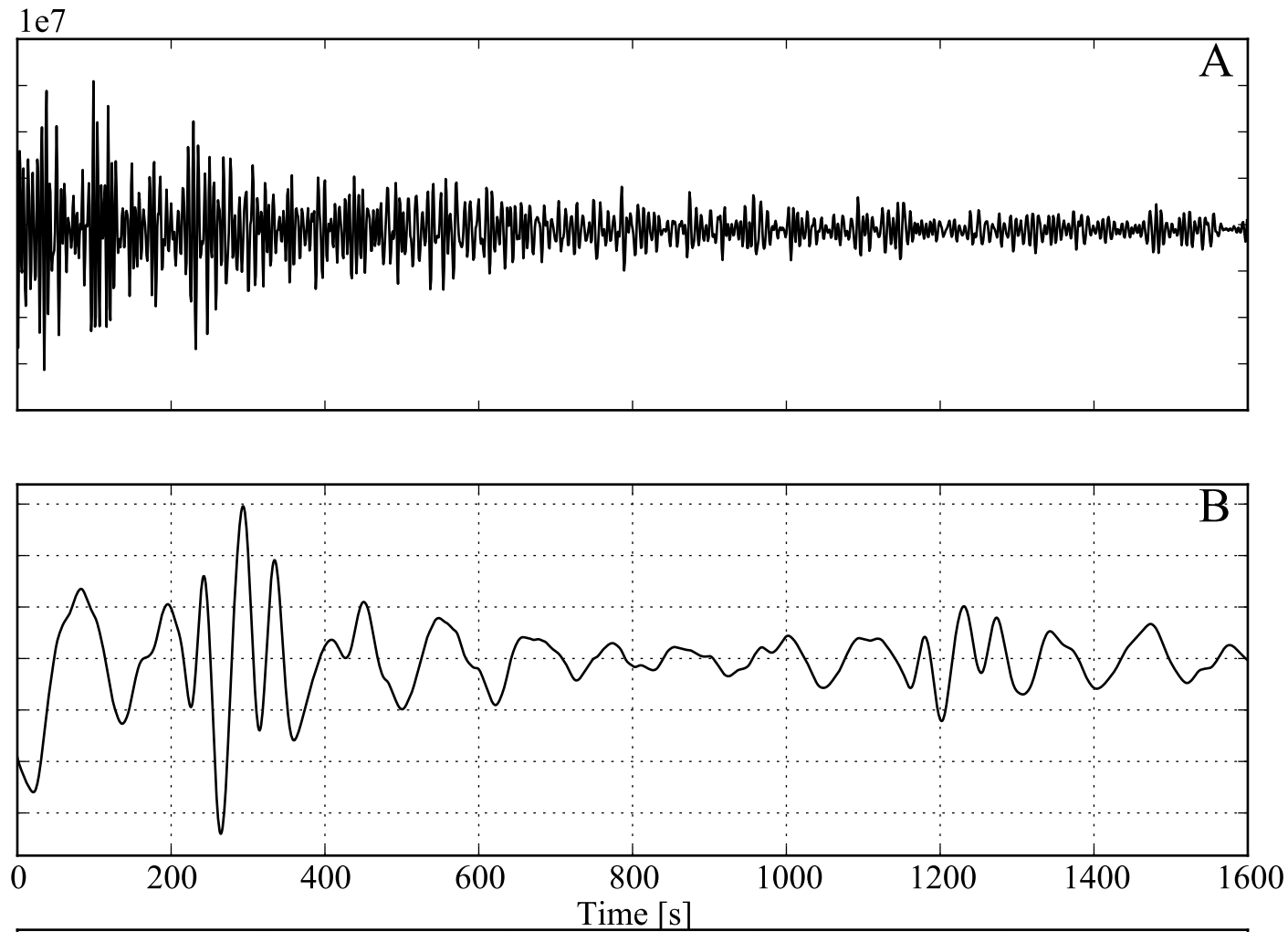


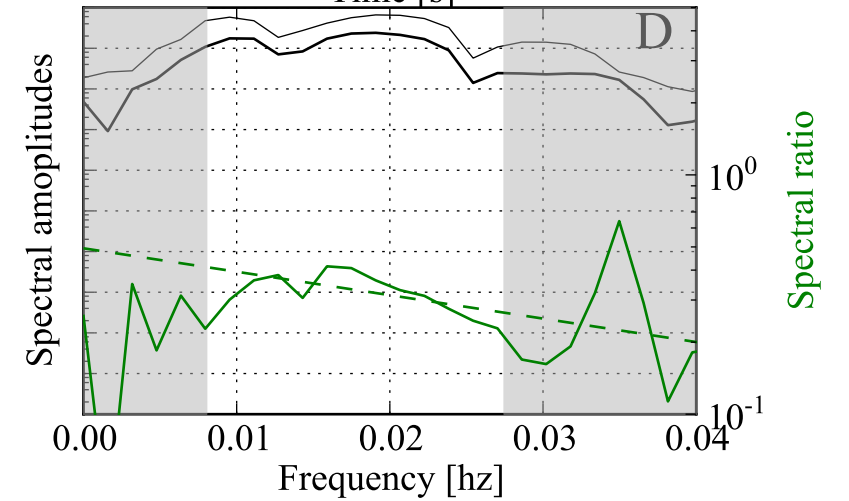
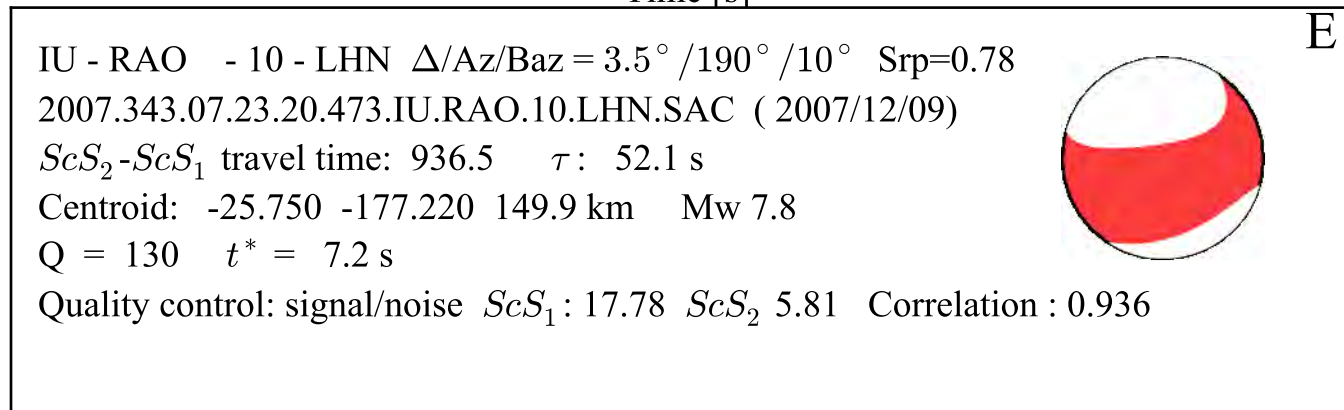
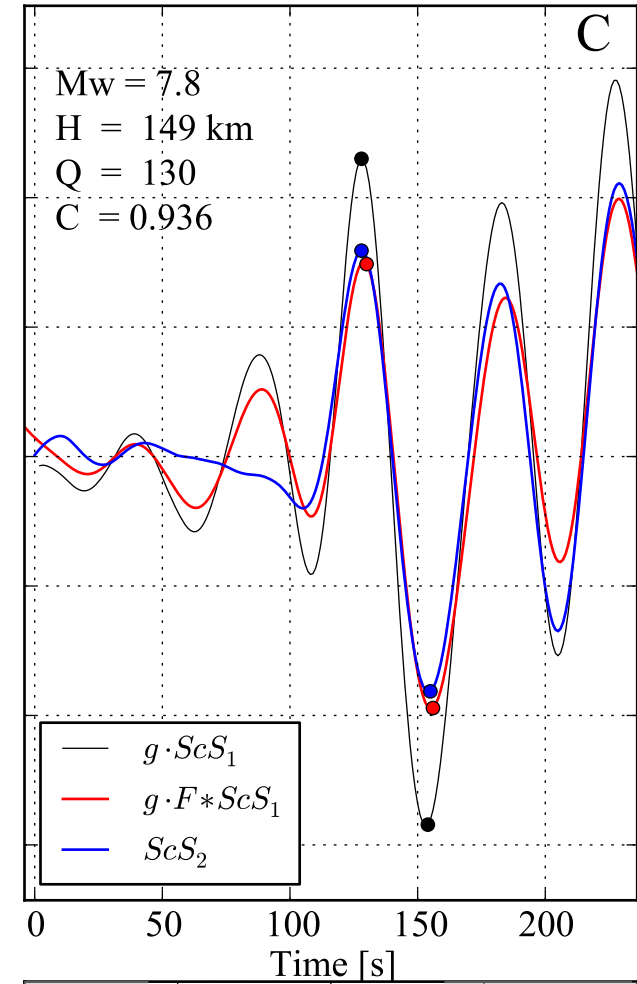
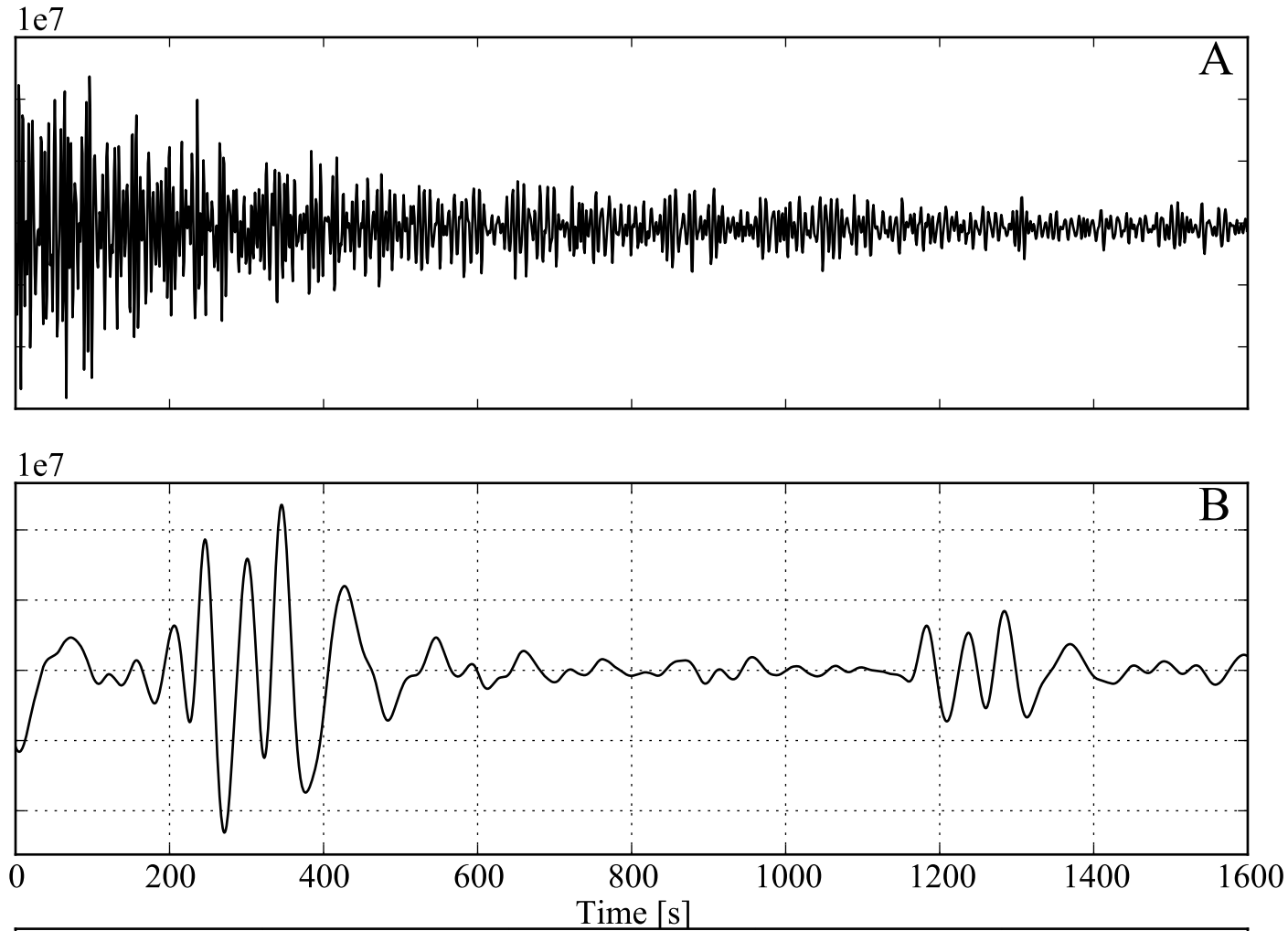
E

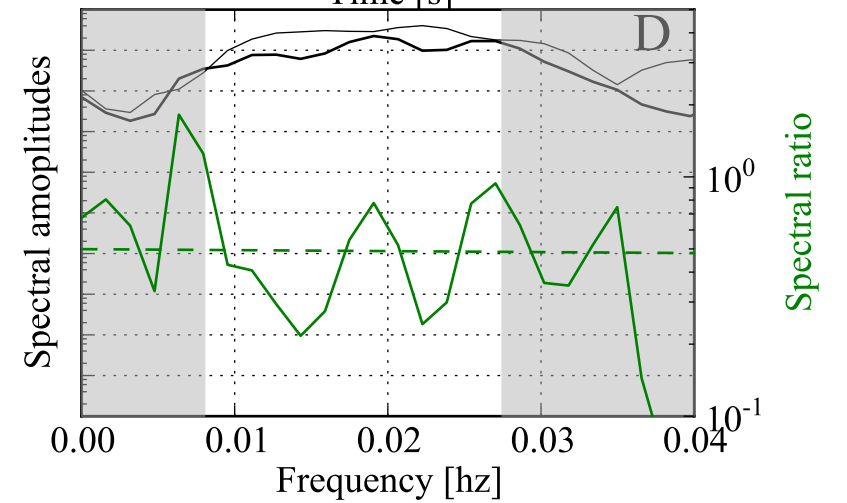
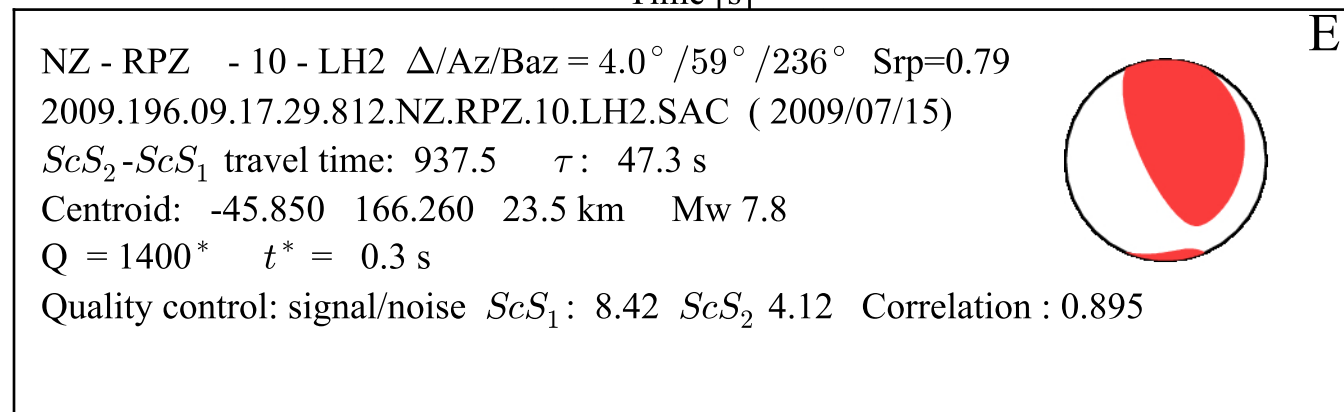
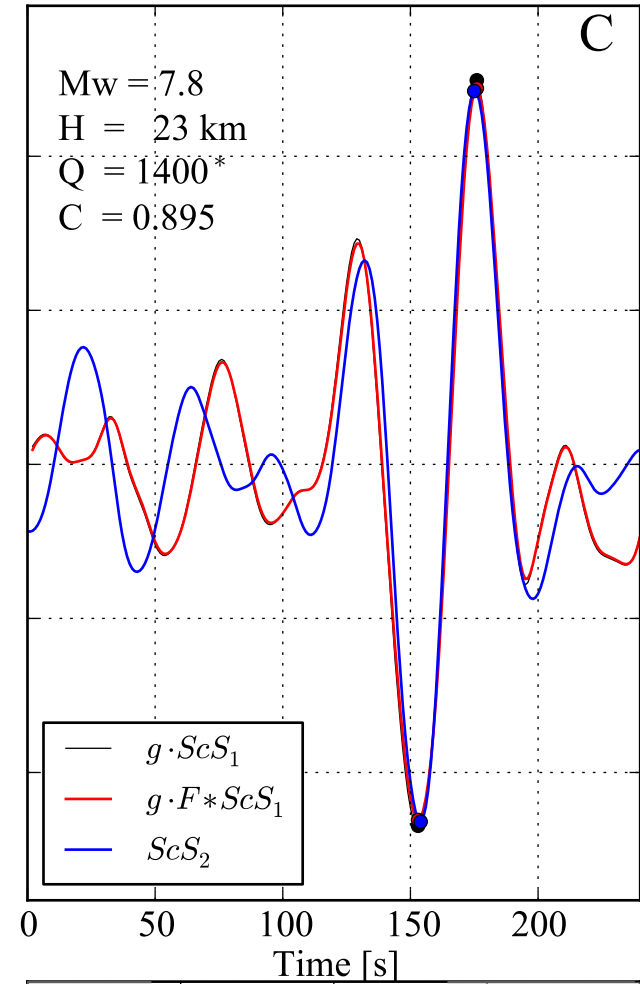
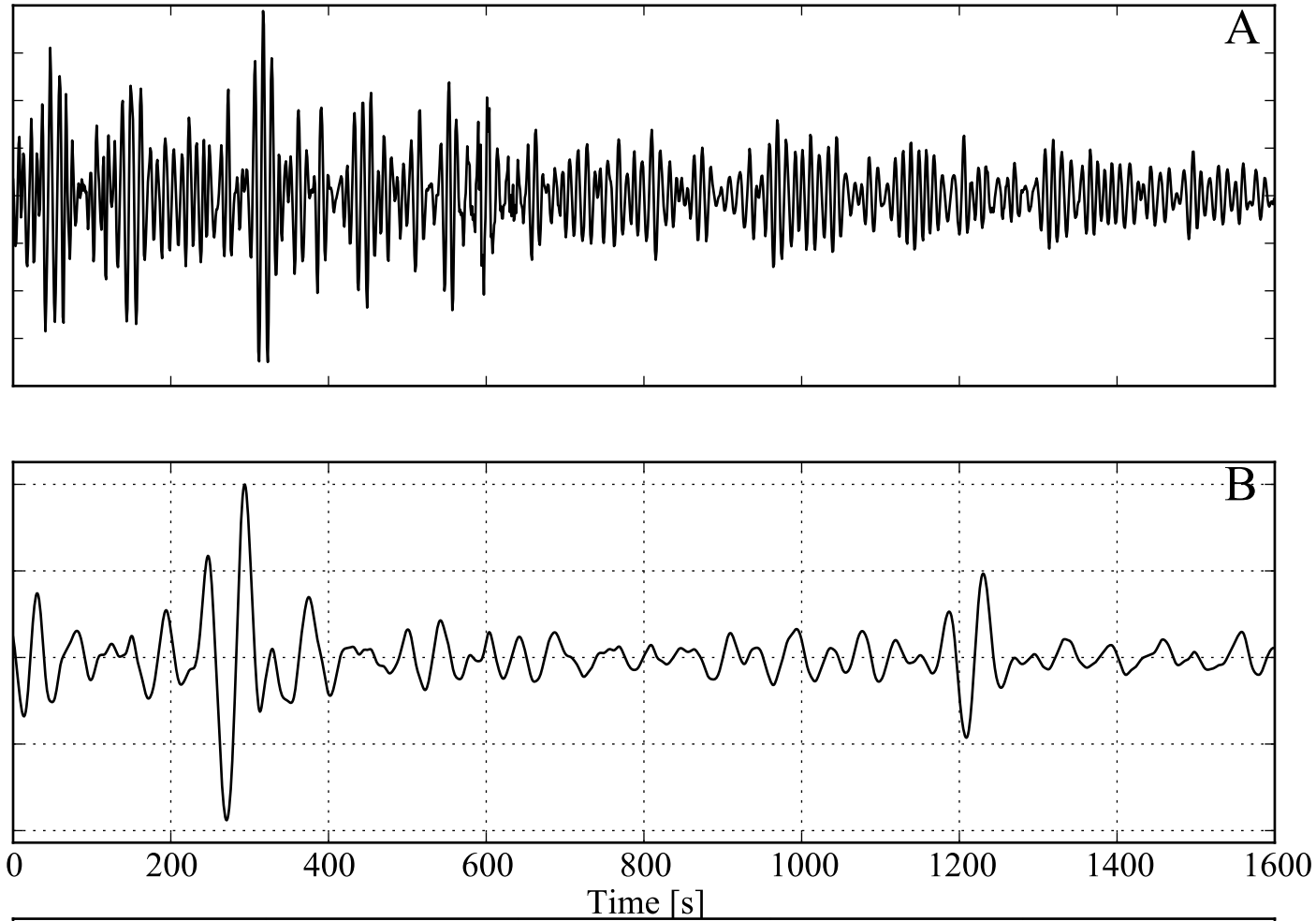
G - PVC - - LH2 $\Delta/Az/Baz = 2.7^\circ / 345^\circ / 165^\circ$ $Srp=0.68$
 1997.141.14.05.26.603.G.PVC..LH2.SAC (1997/05/21)
 $ScS_2 - ScS_1$ travel time: 941.3 τ : 48.7 s
 Centroid: -20.340 169.030 64.0 km Mw 6.7
 Q = 310 $t^* = 3.0$ s
 Quality control: signal/noise ScS_1 : 13.74 ScS_2 5.70 Correlation : 0.926

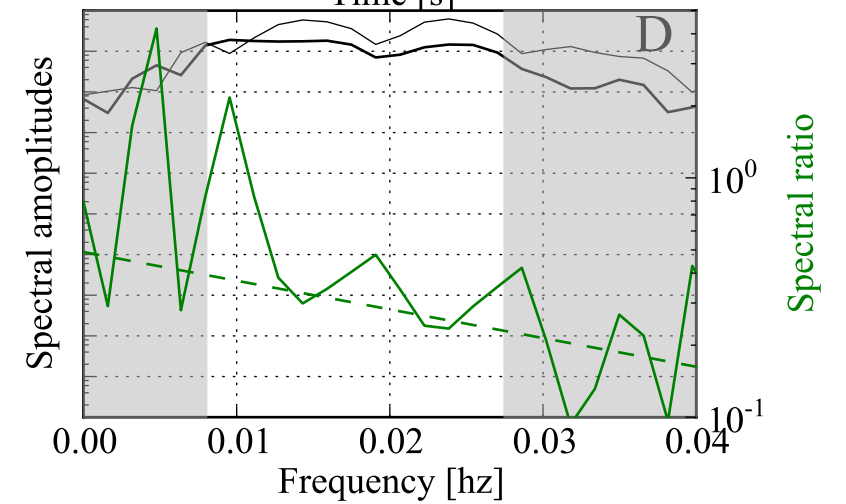
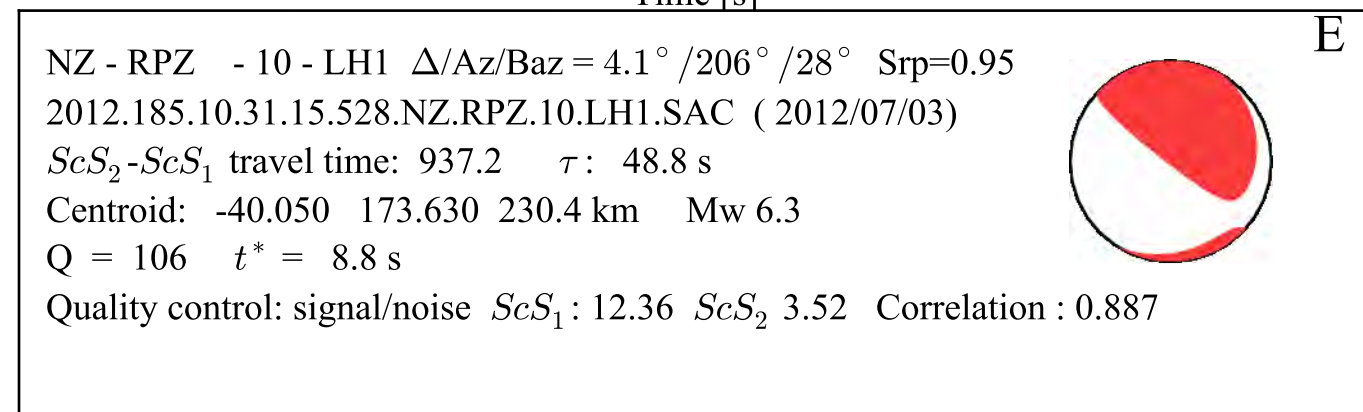
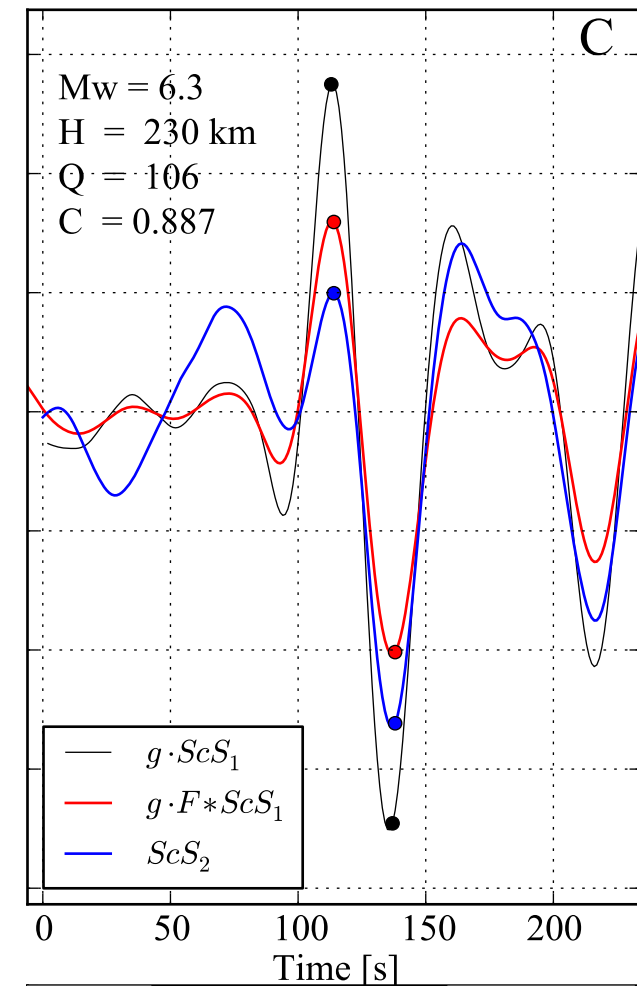
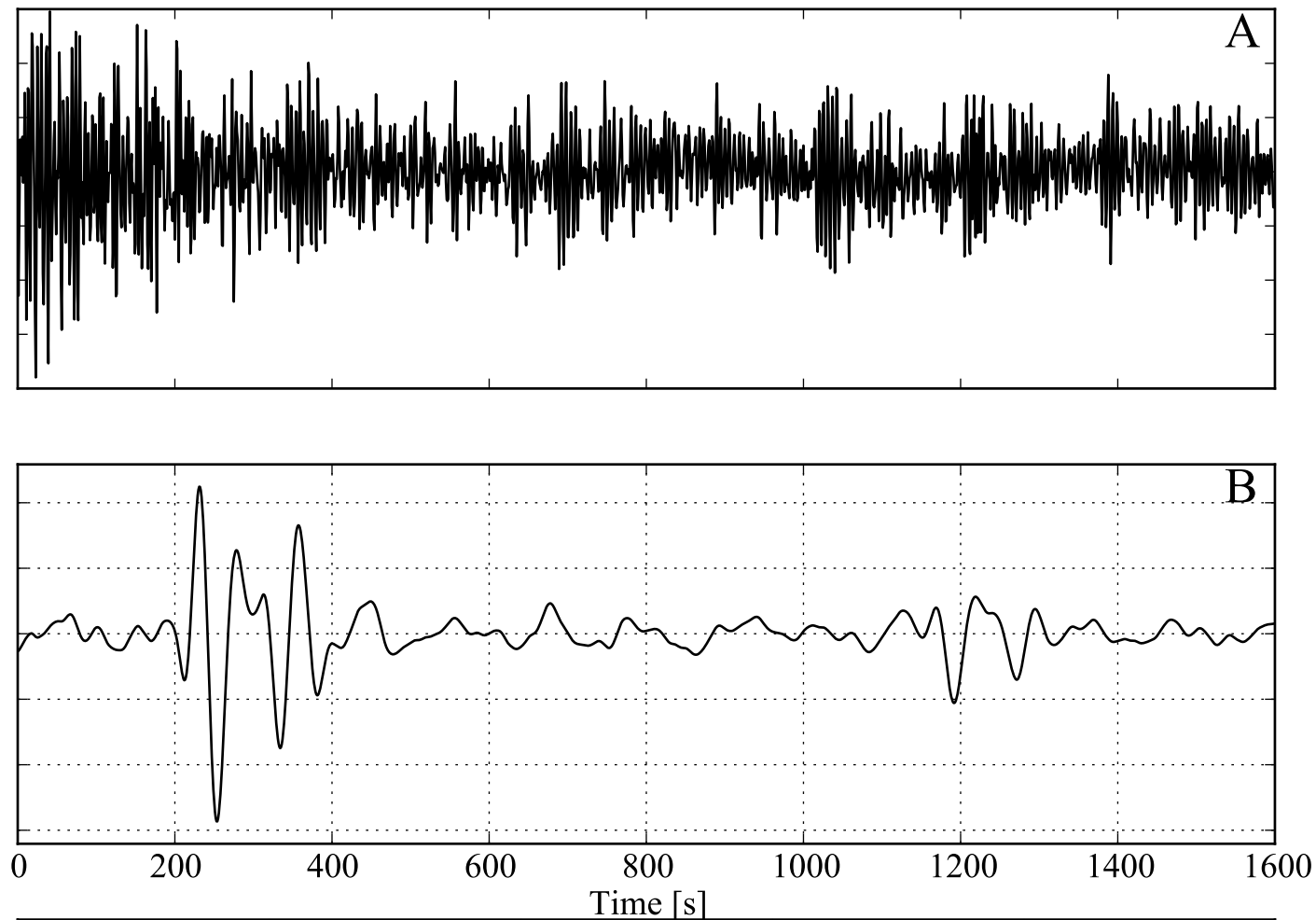



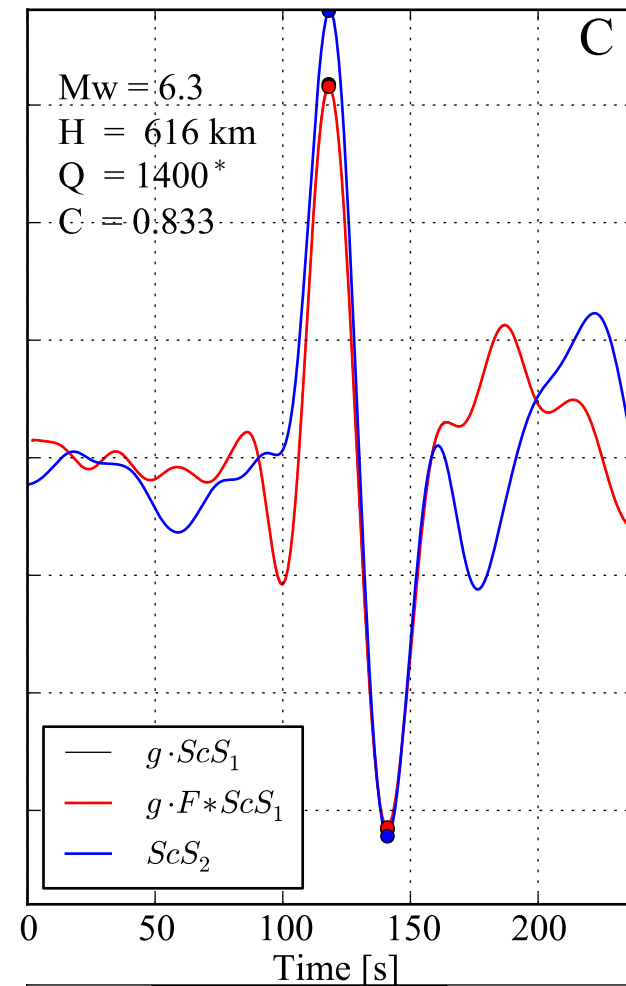
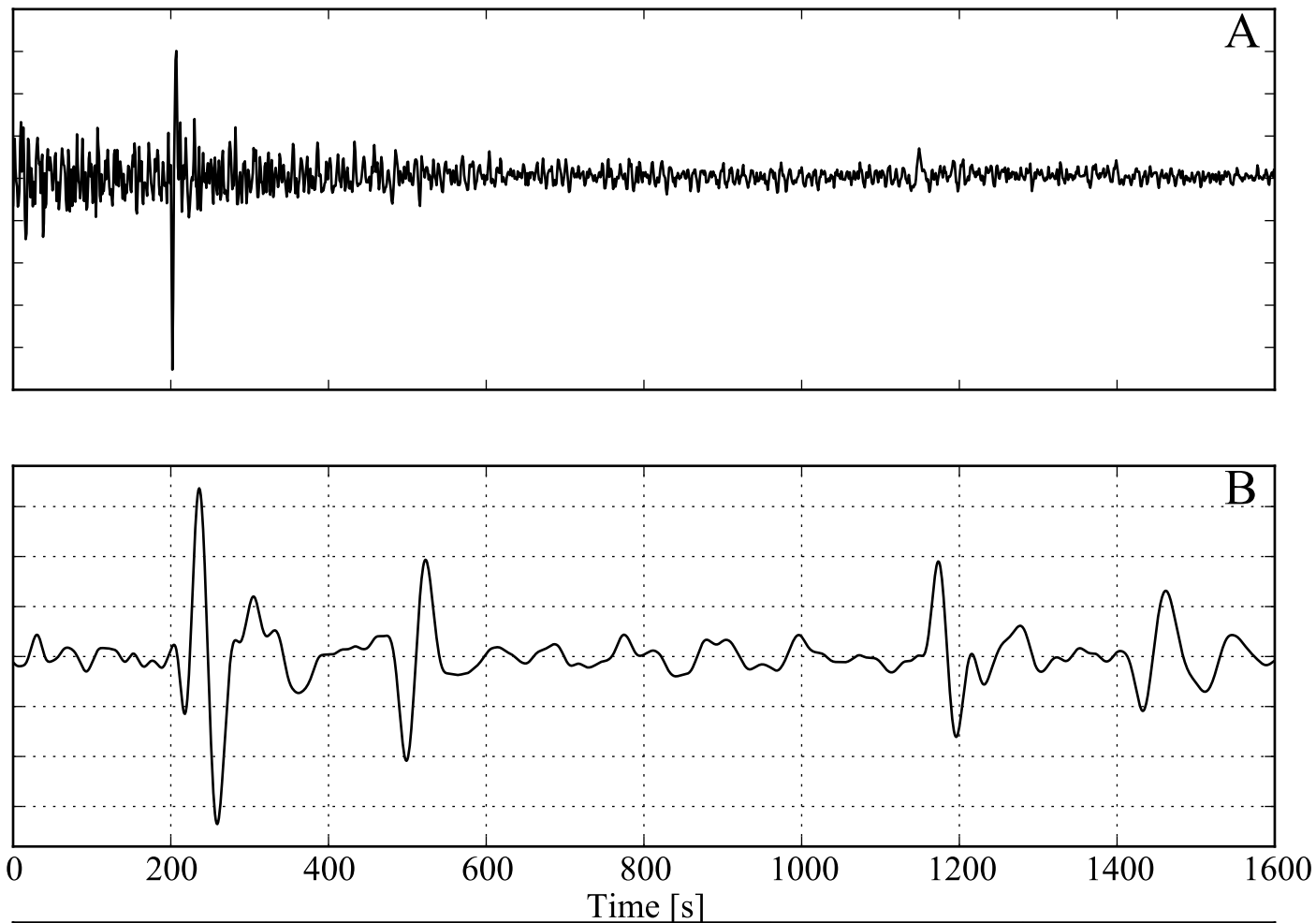







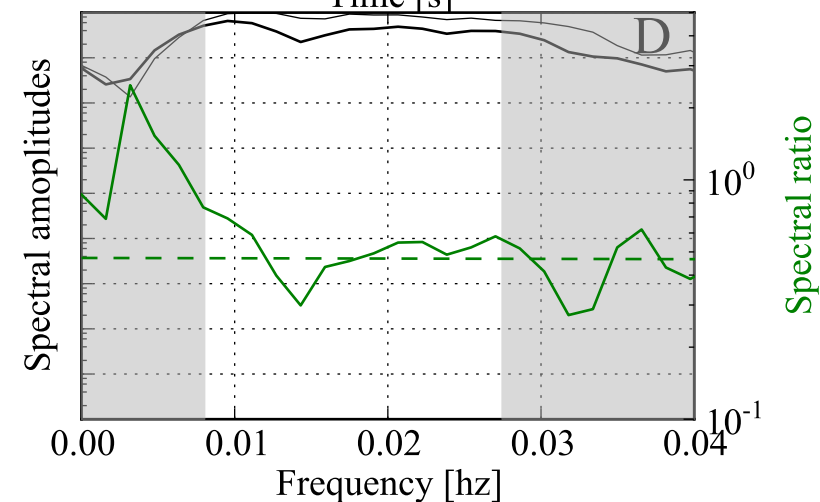


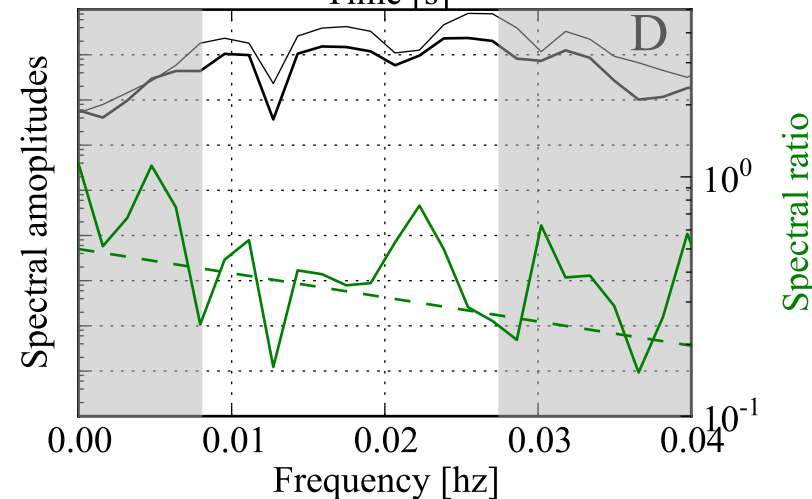
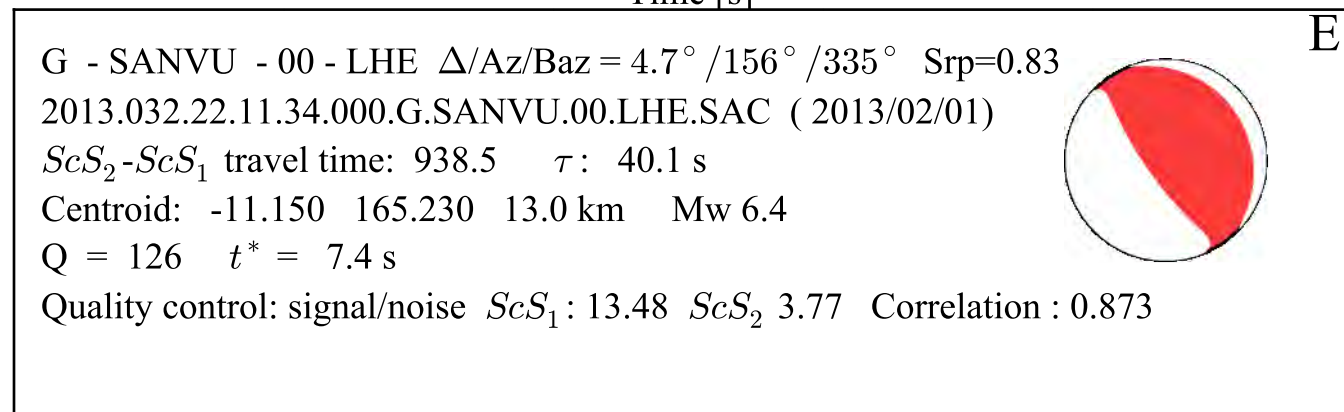
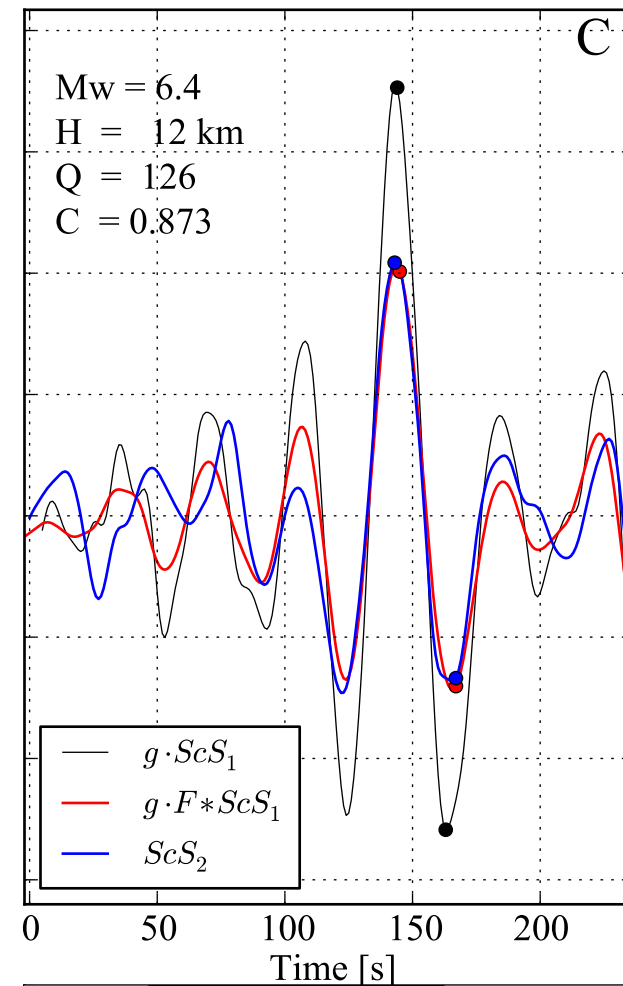
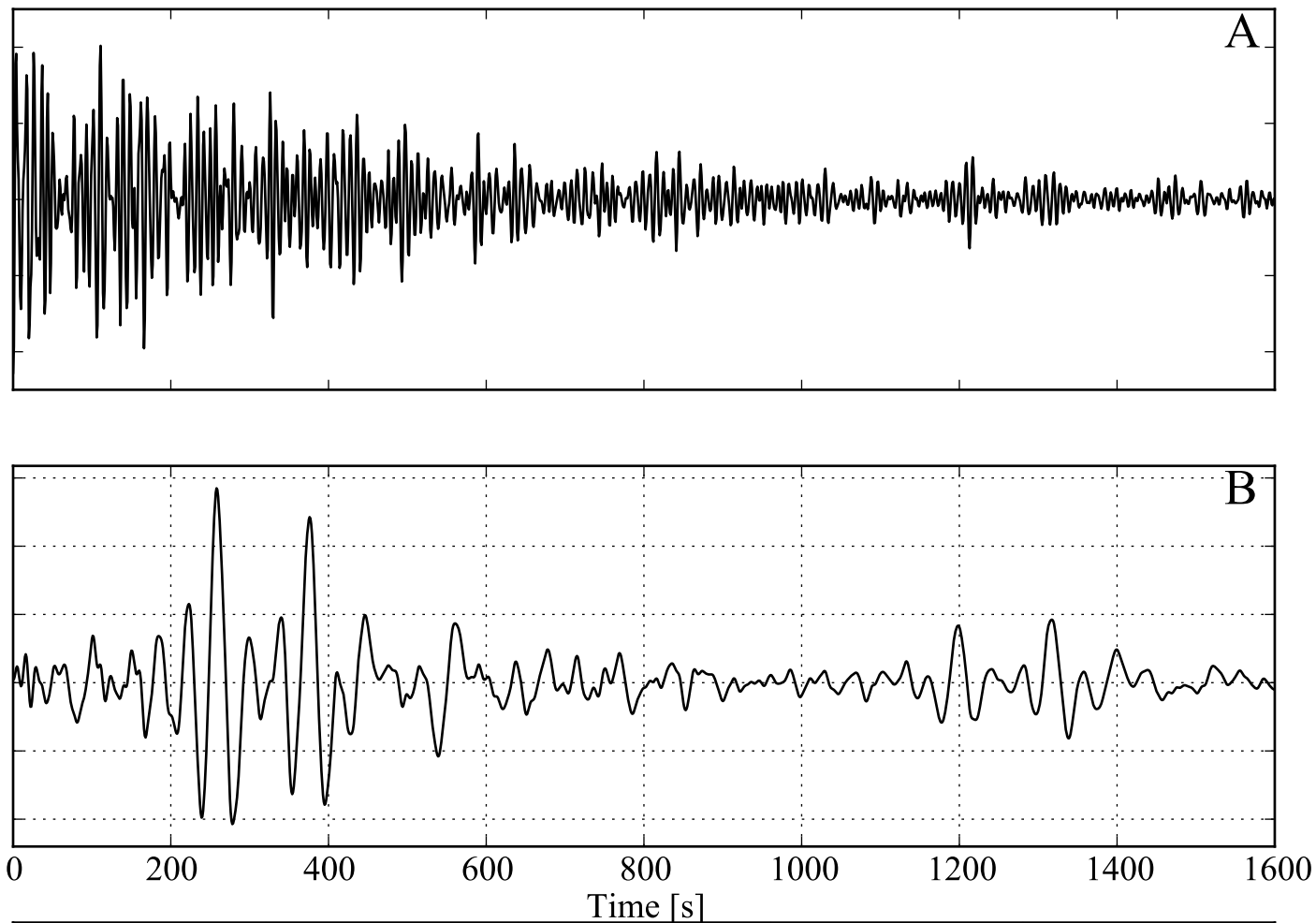


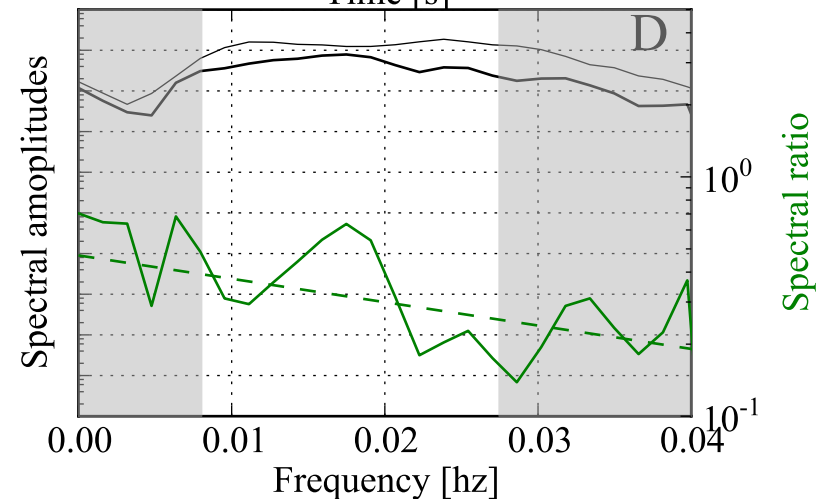
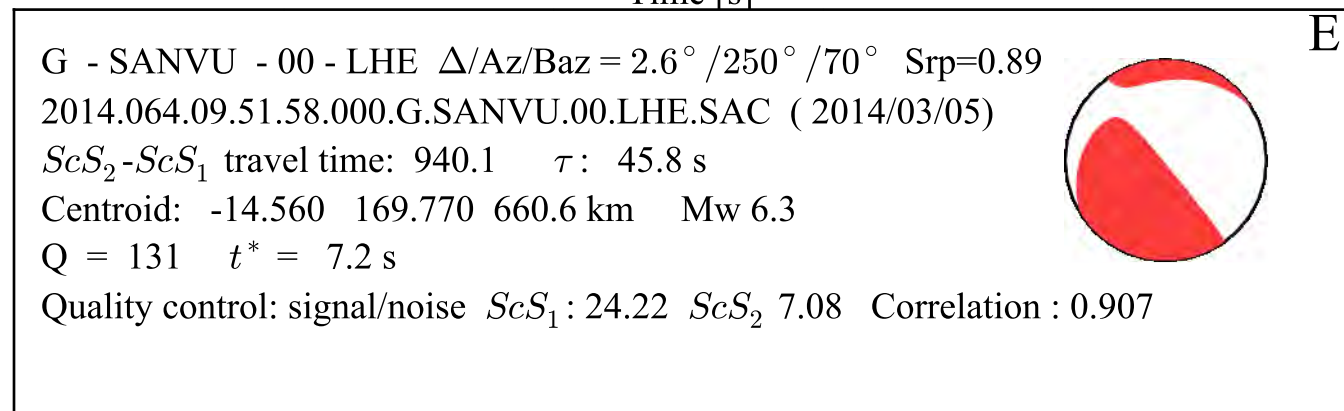
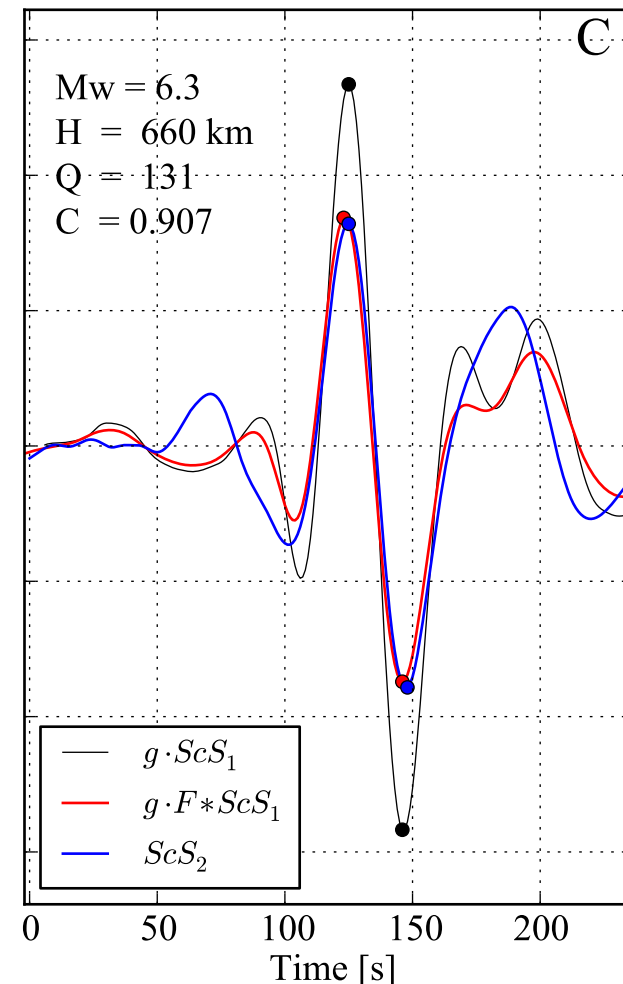
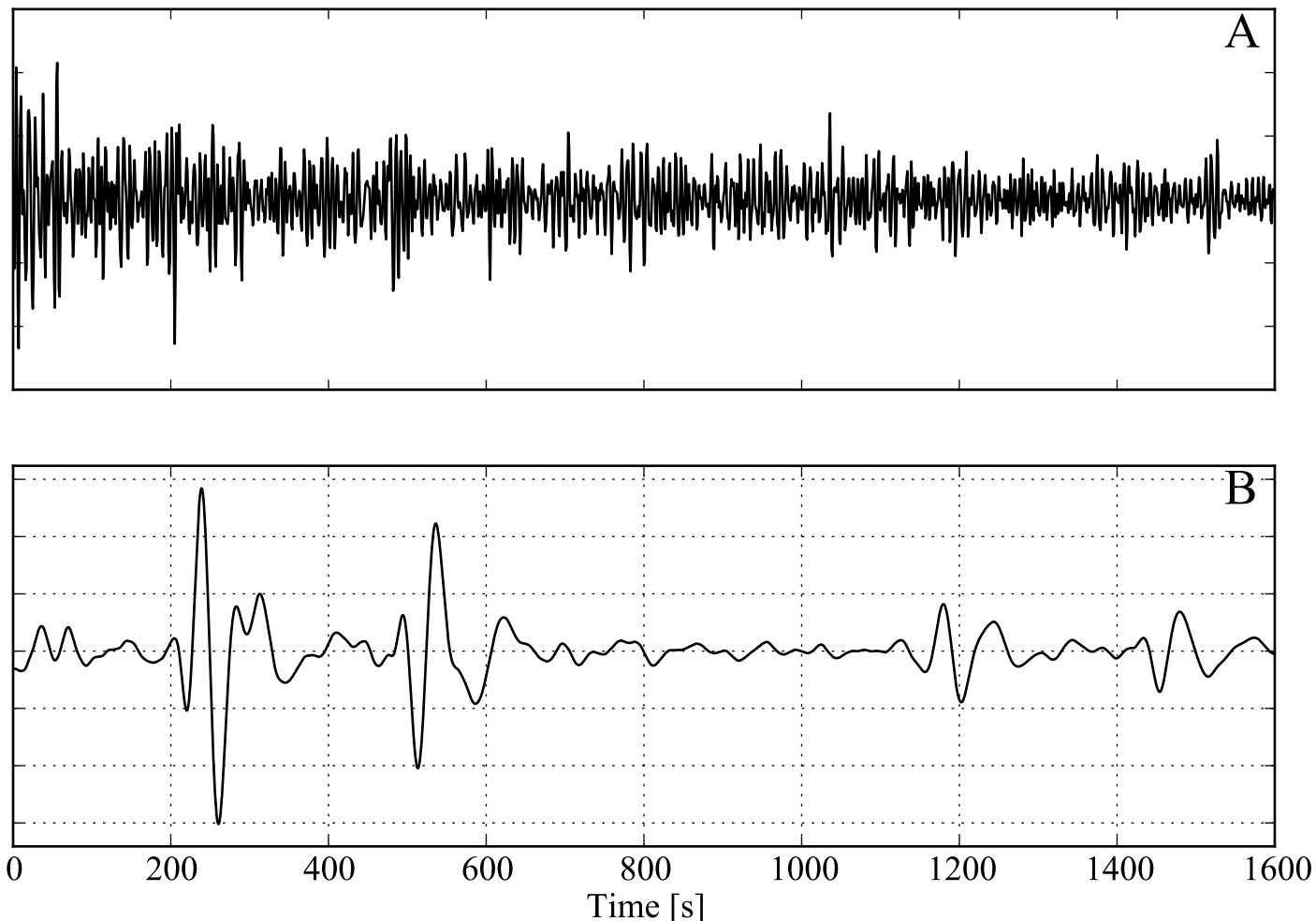


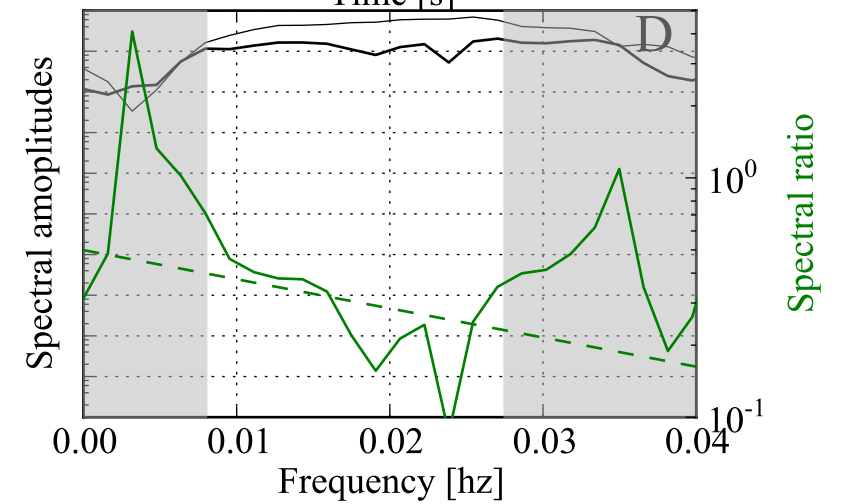
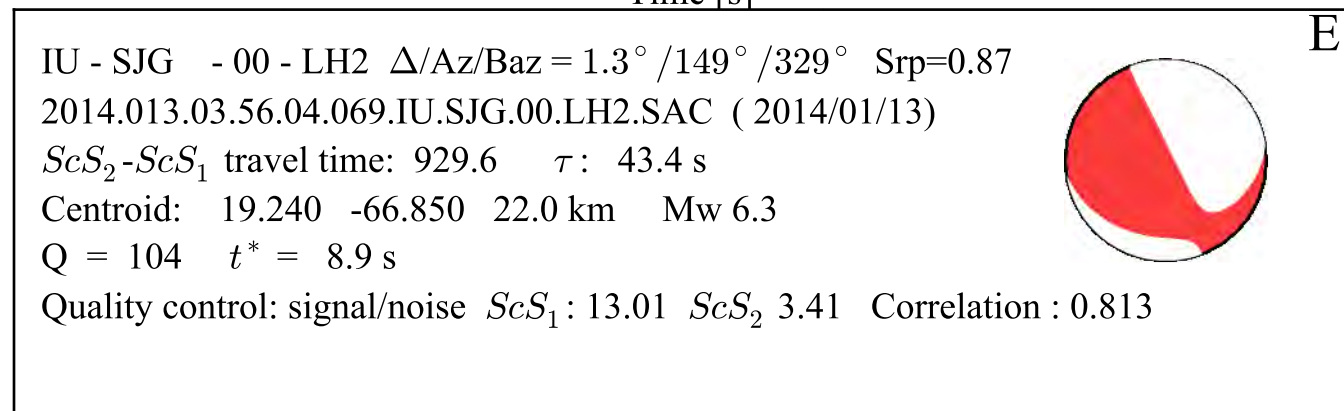
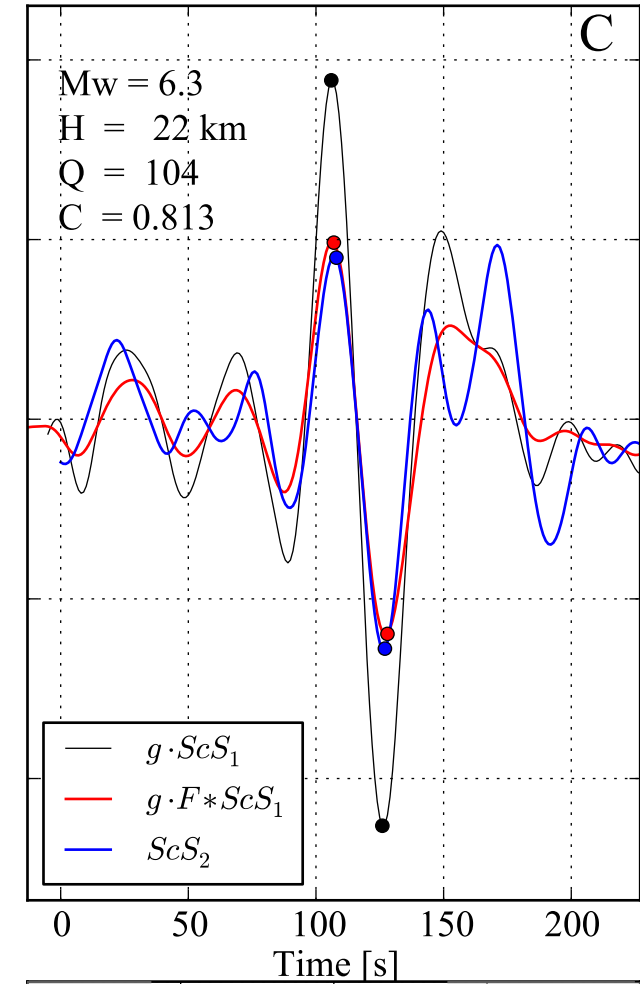
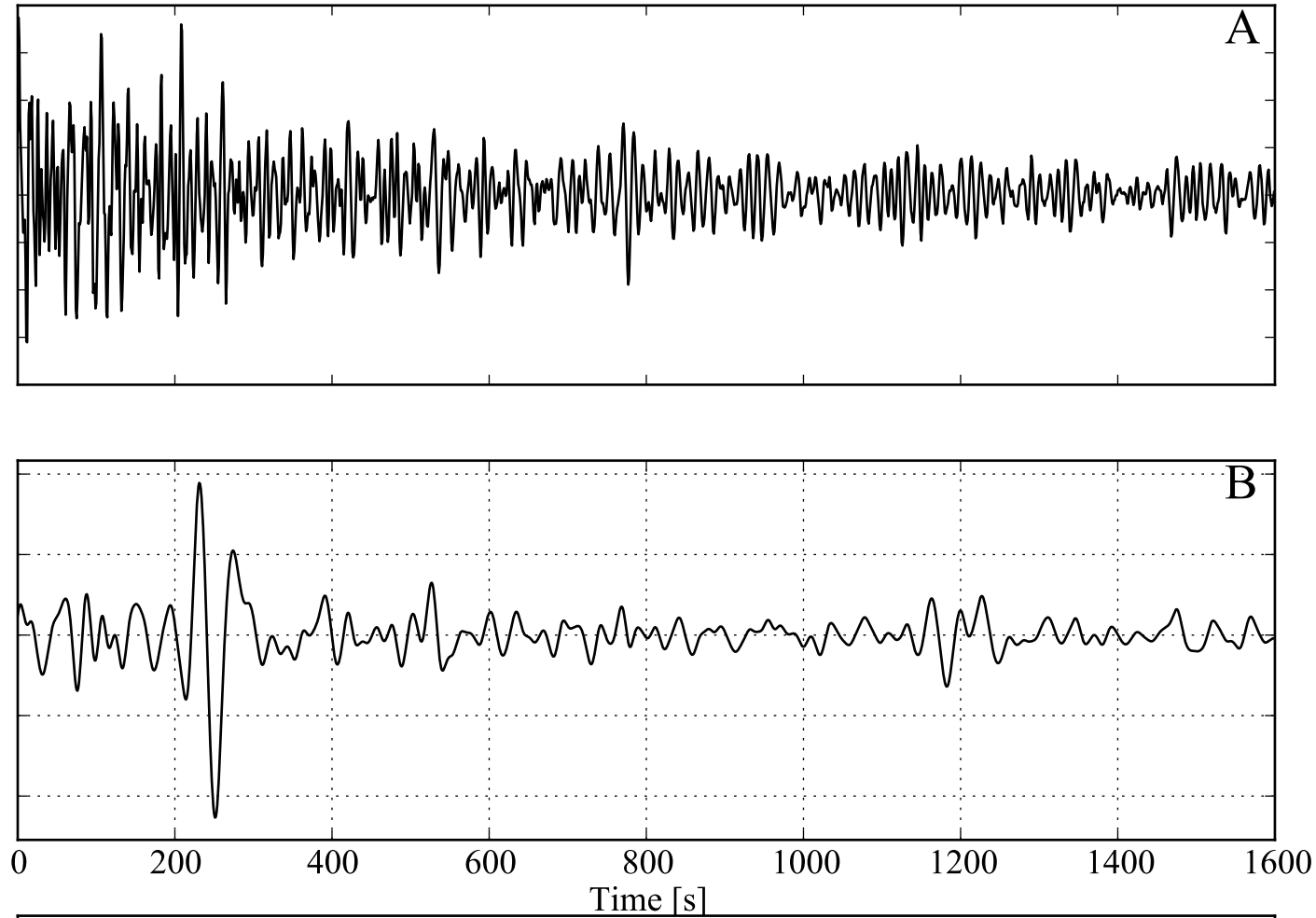
E

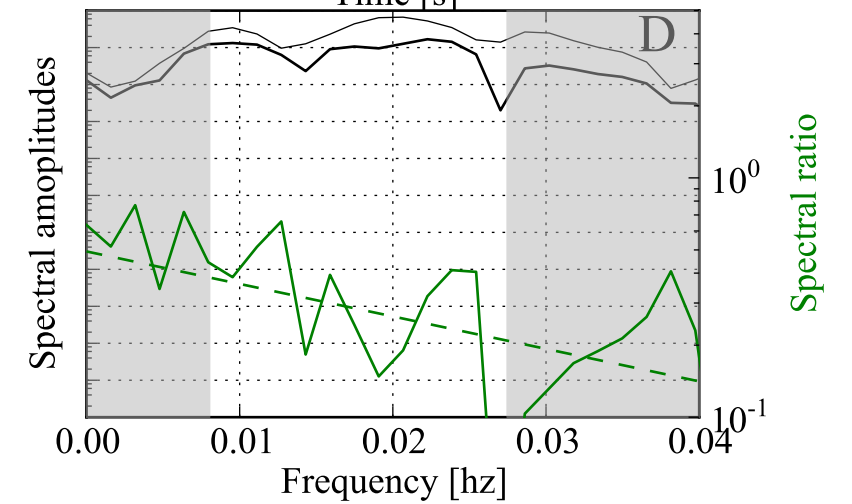
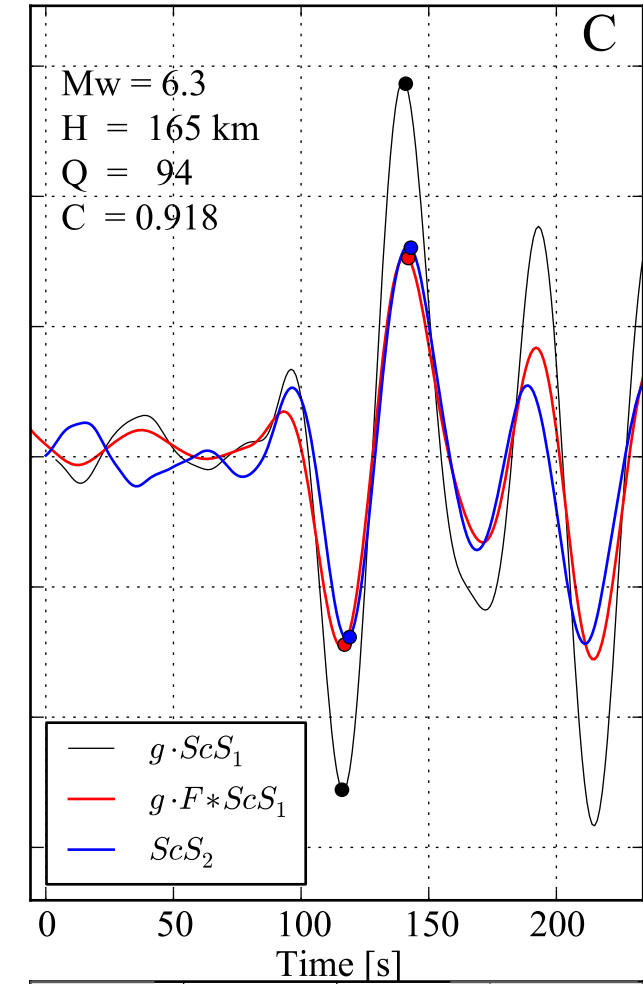
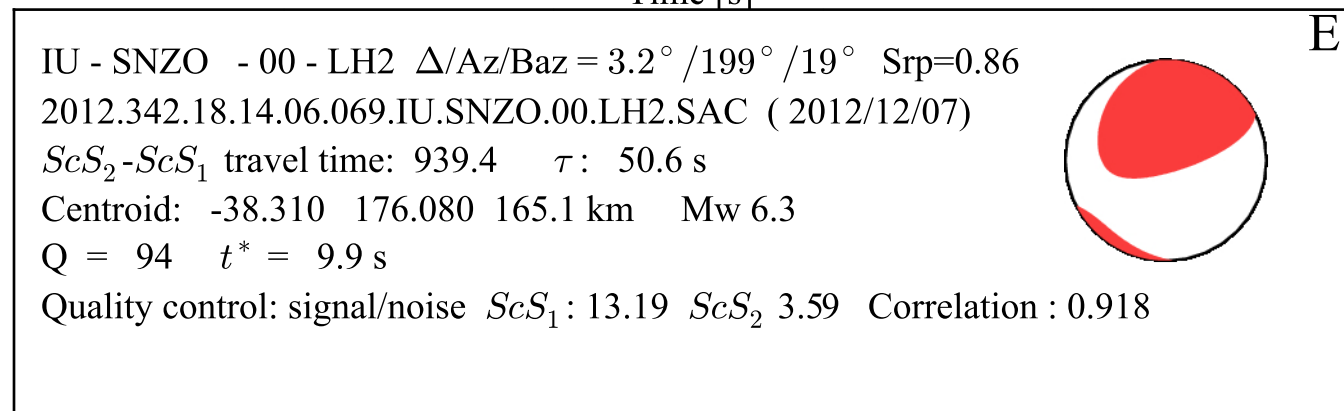
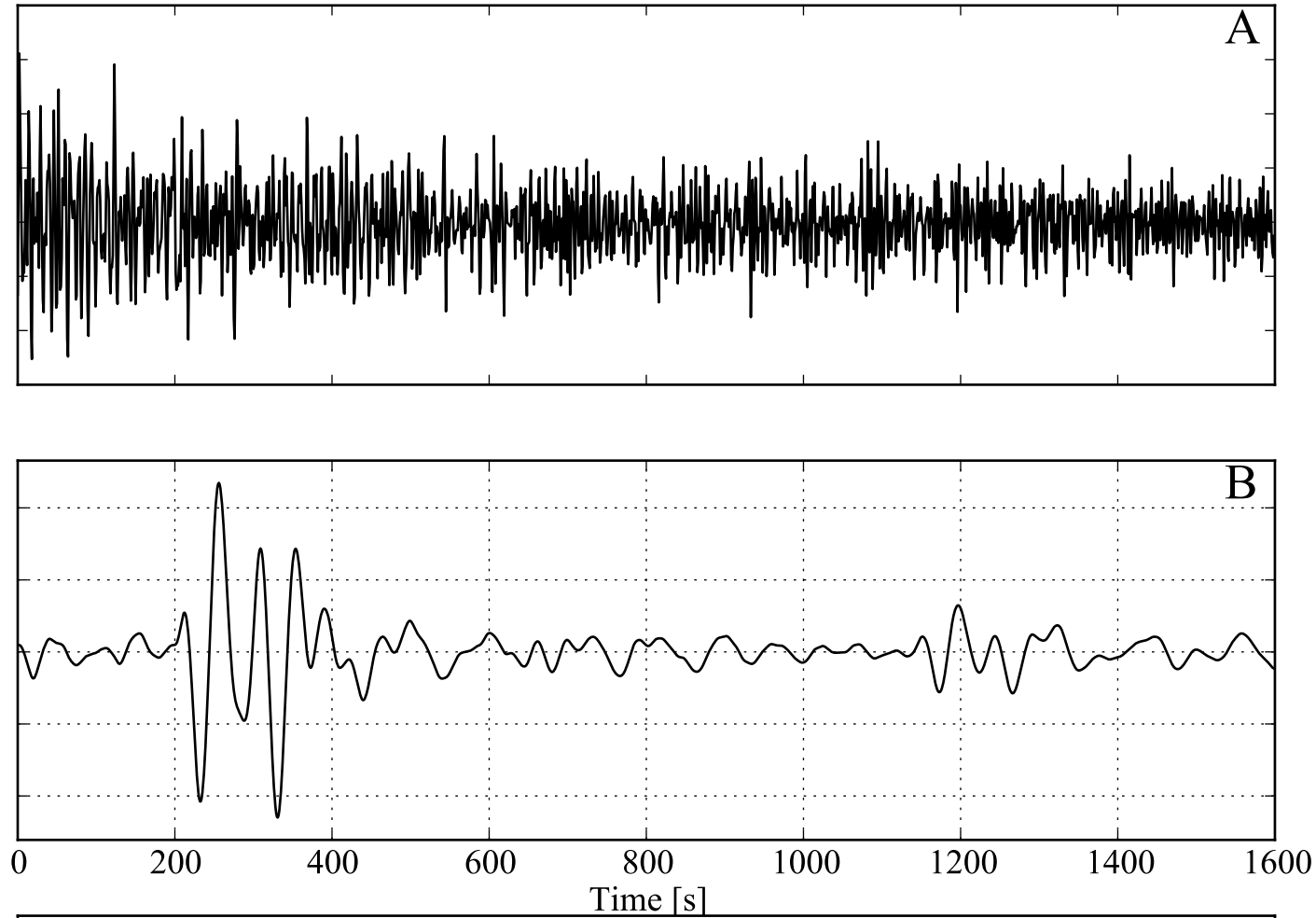
MN - RTC - - LHE $\Delta/Az/Baz = 4.0^\circ / 220^\circ / 38^\circ$ $Srp=0.78$
 2010.101.22.03.12.607.MN.RTC..LHE.SAC (2010/04/11)
 $ScS_2 - ScS_1$ travel time: 936.8 τ : 48.5 s
 Centroid: 37.100 -3.690 616.5 km Mw 6.3
 Q = 1400* $t^* = 0.1$ s
 Quality control: signal/noise ScS_1 : 11.06 ScS_2 5.78 Correlation : 0.833

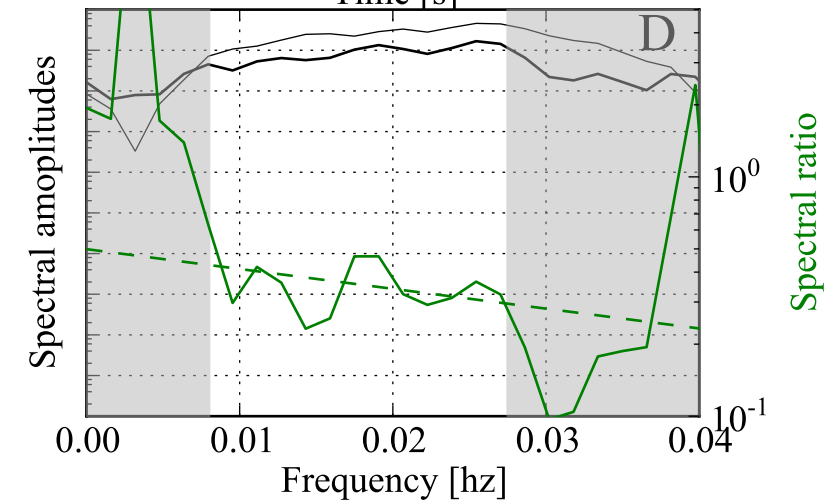
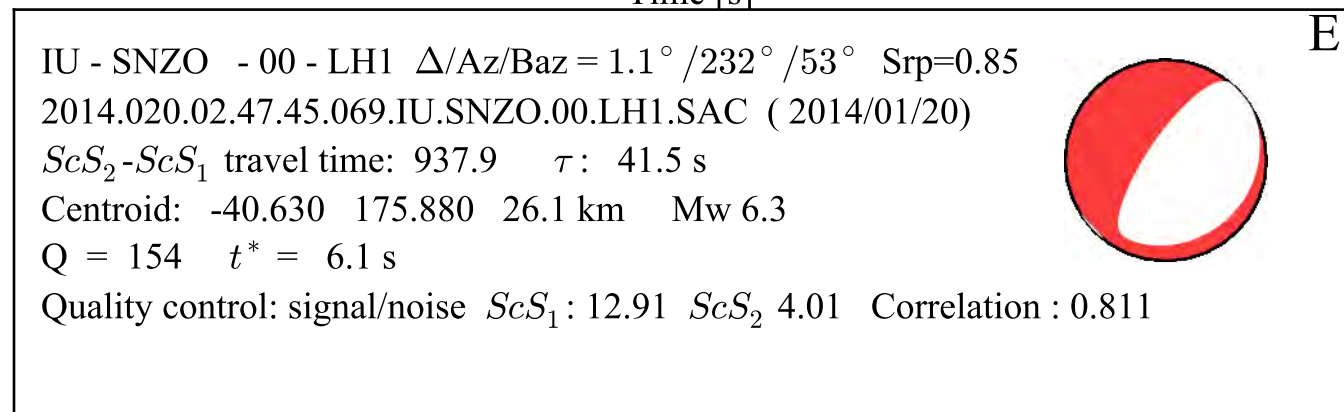
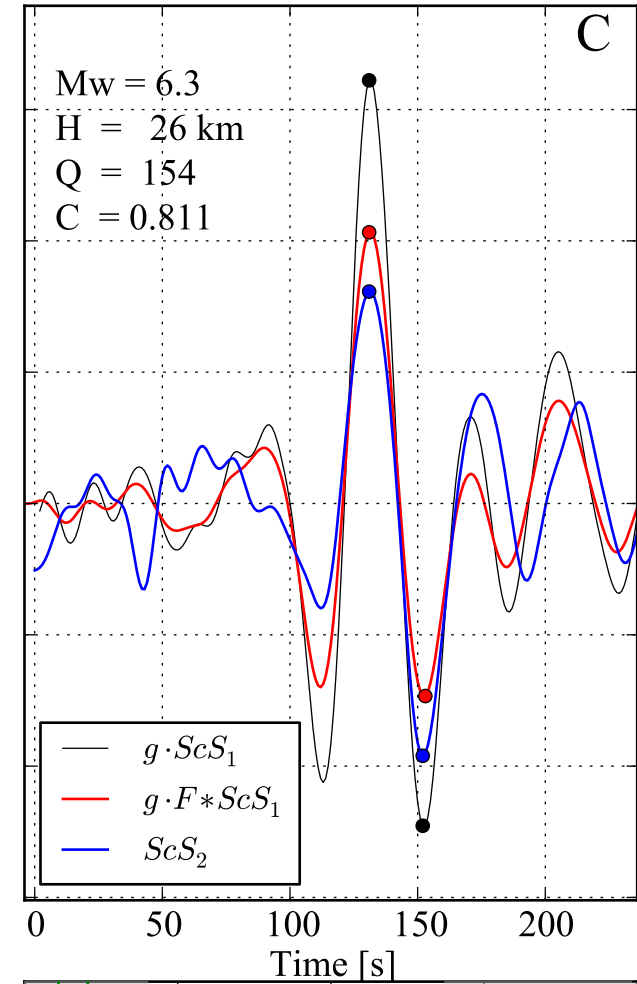
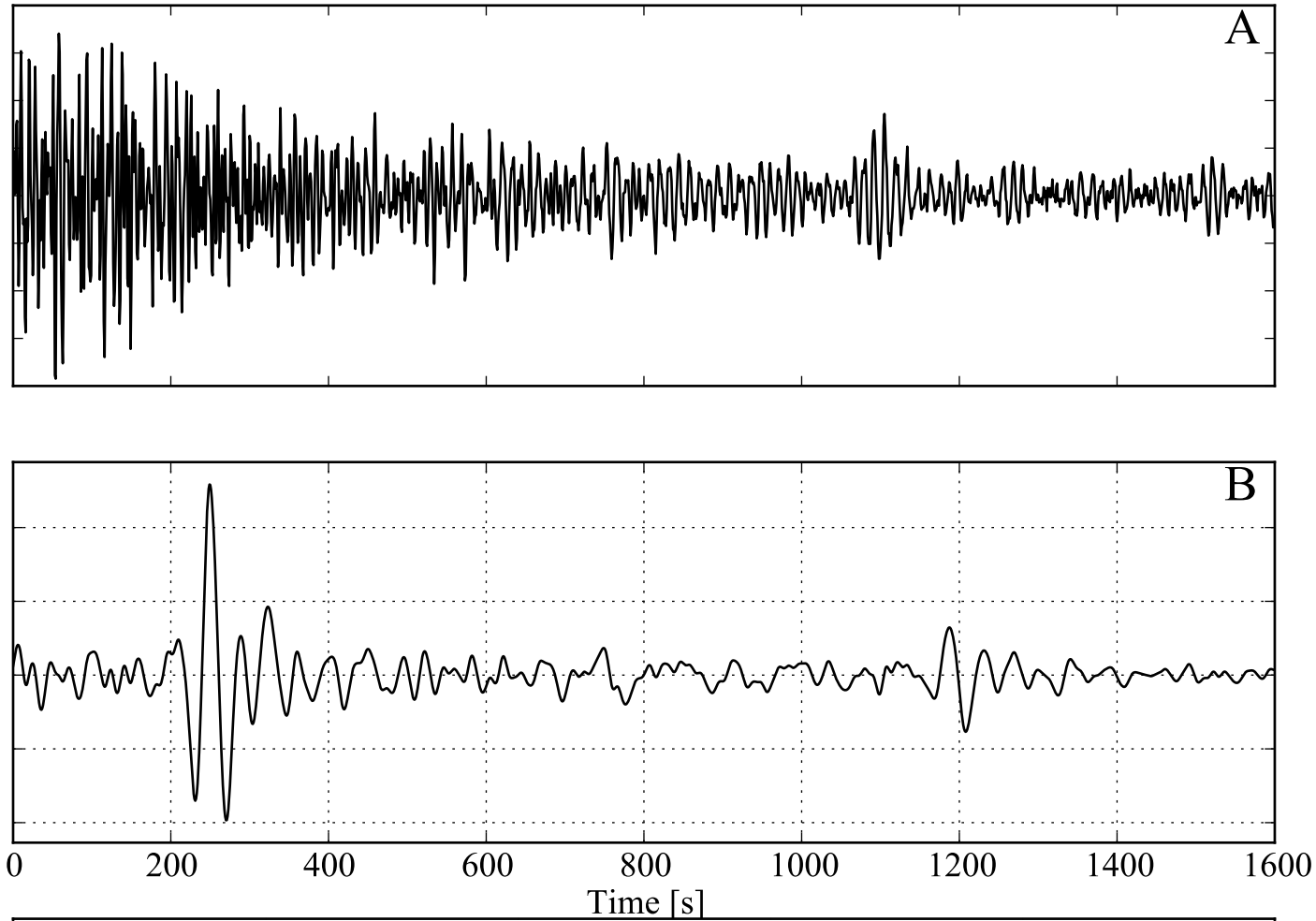



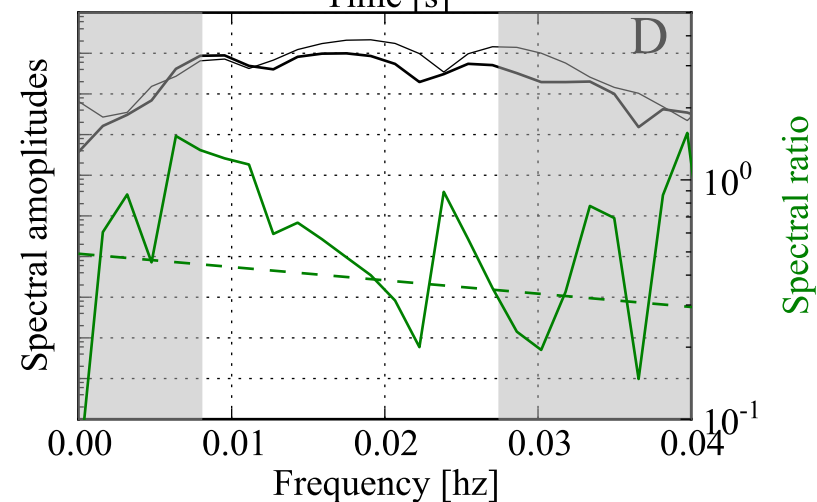
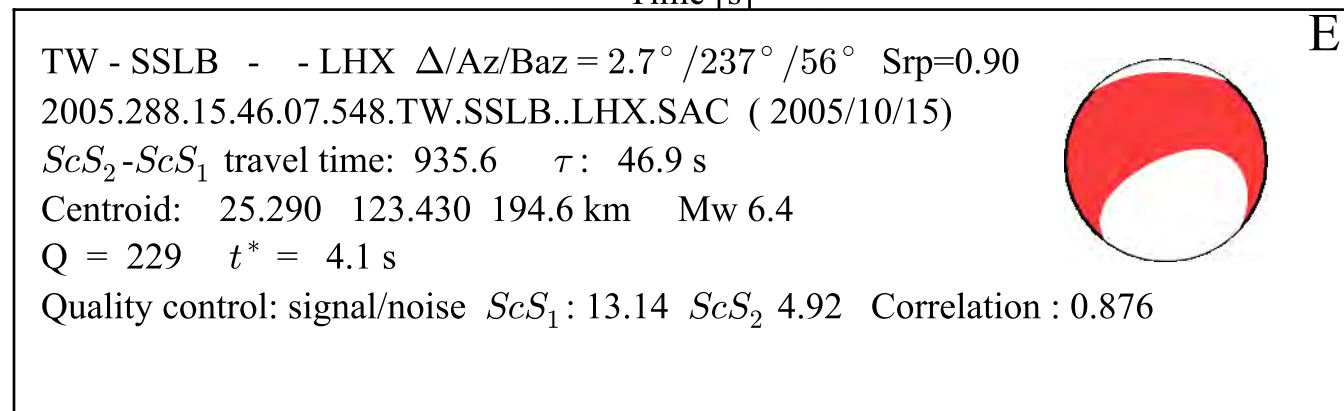
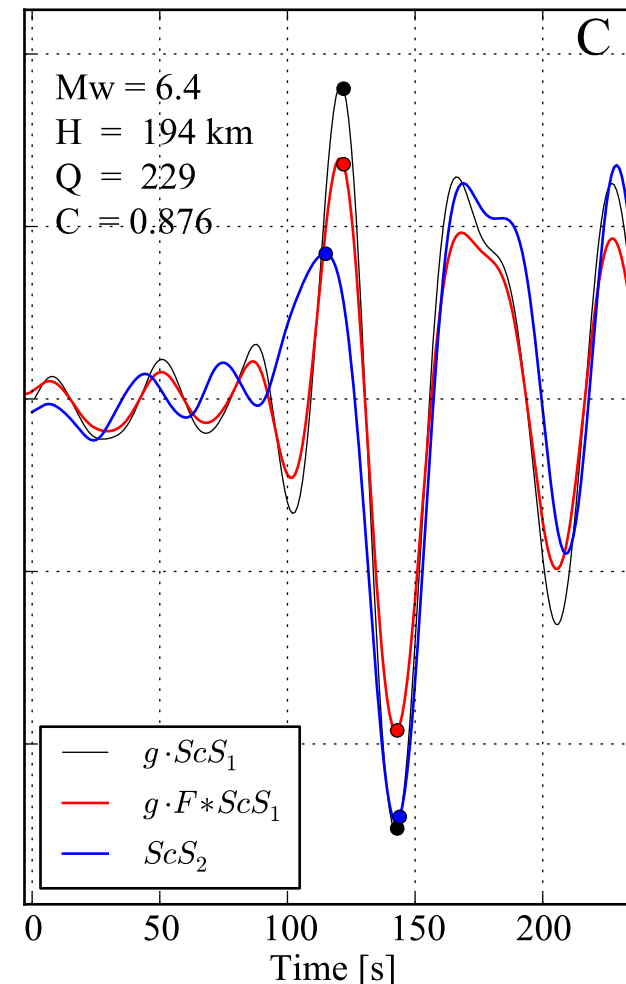
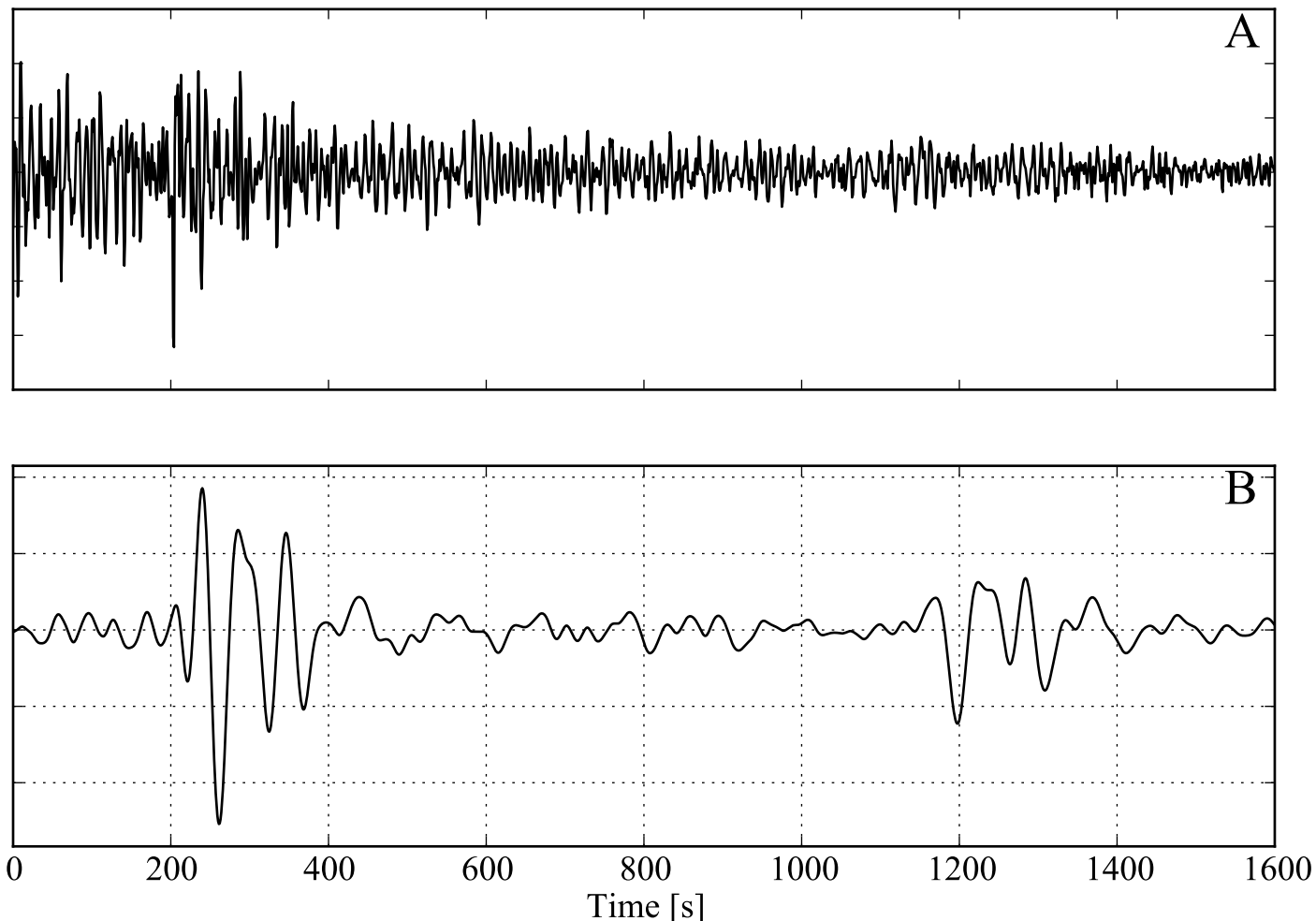


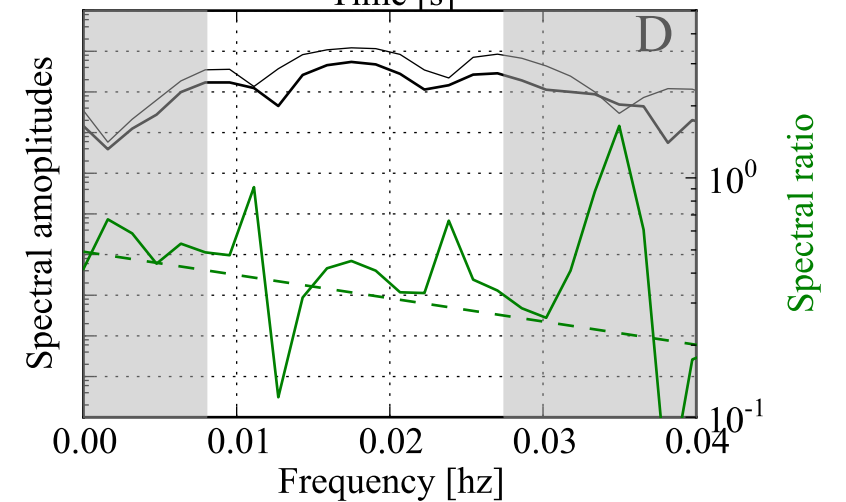
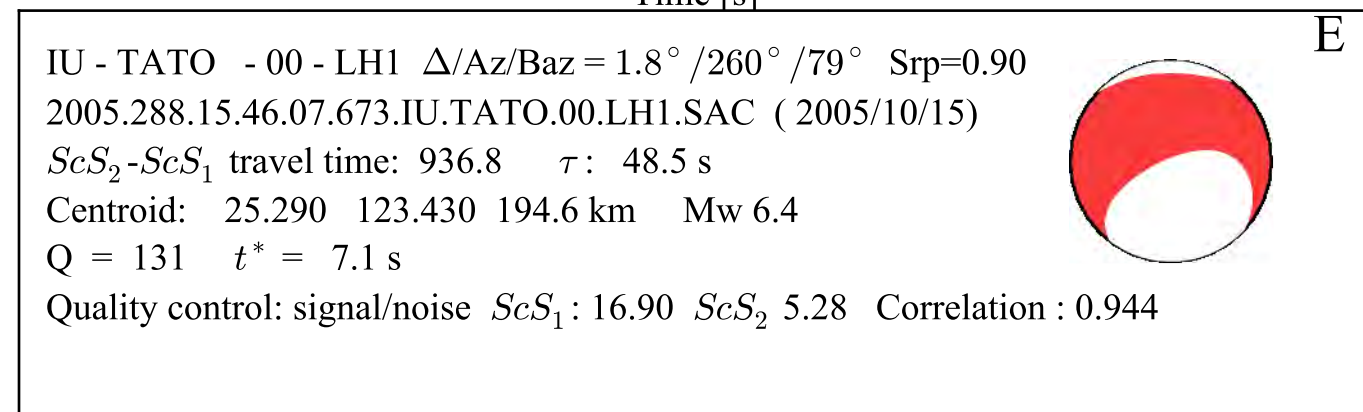
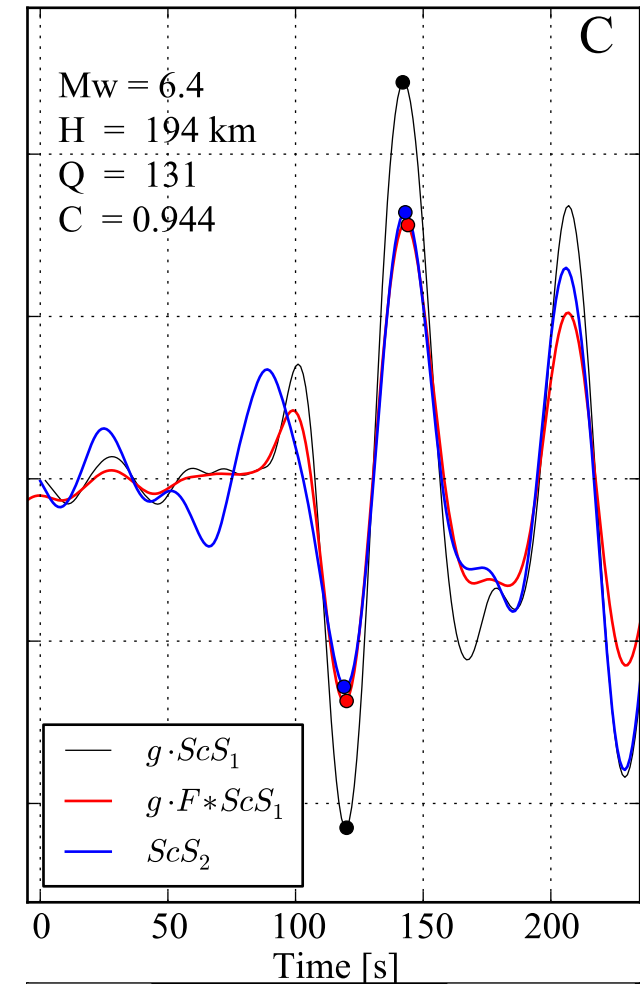
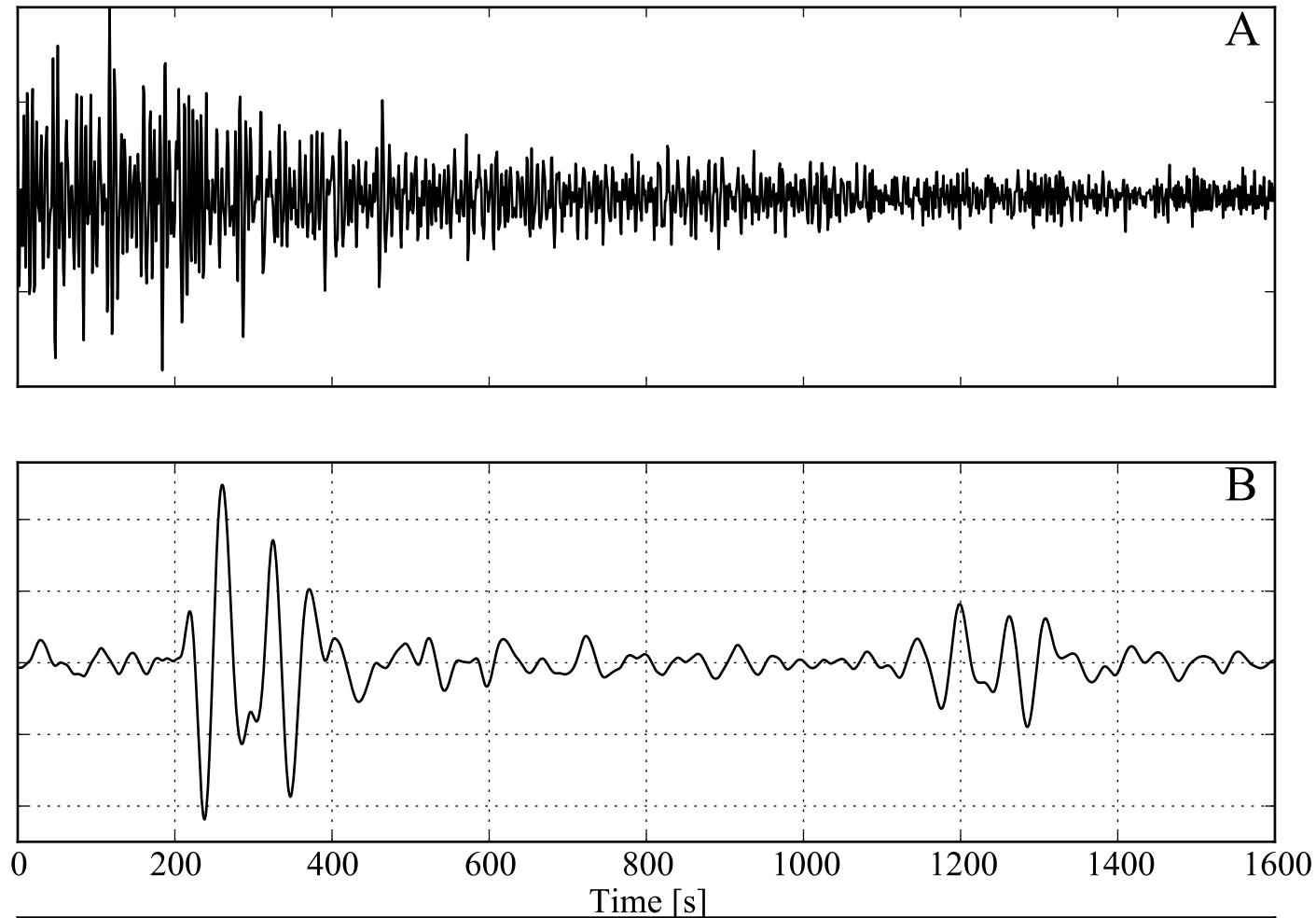


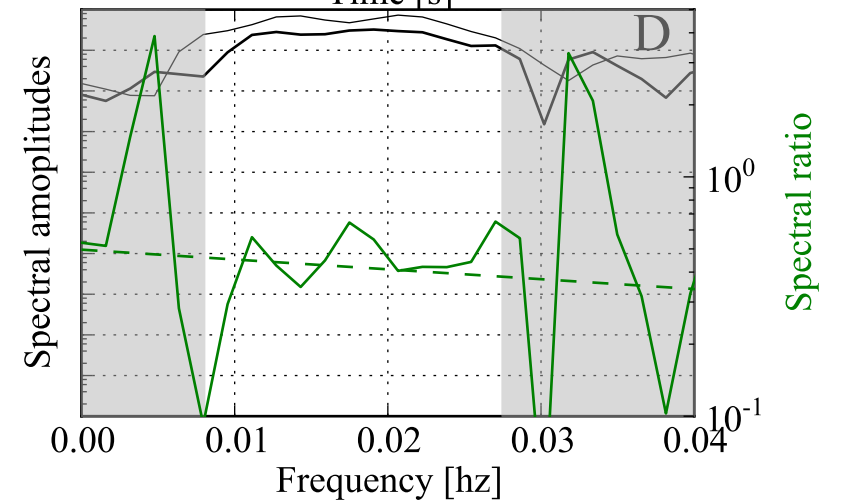
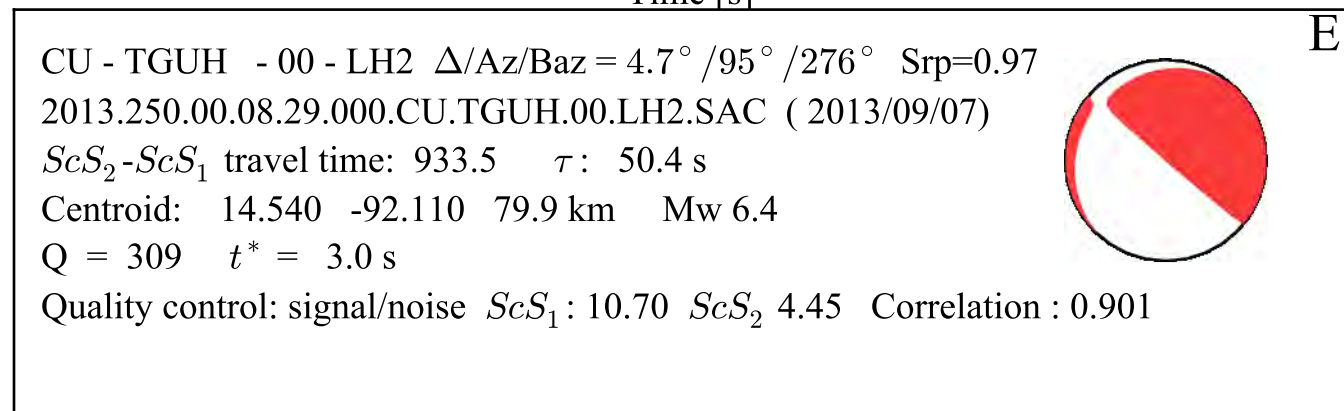
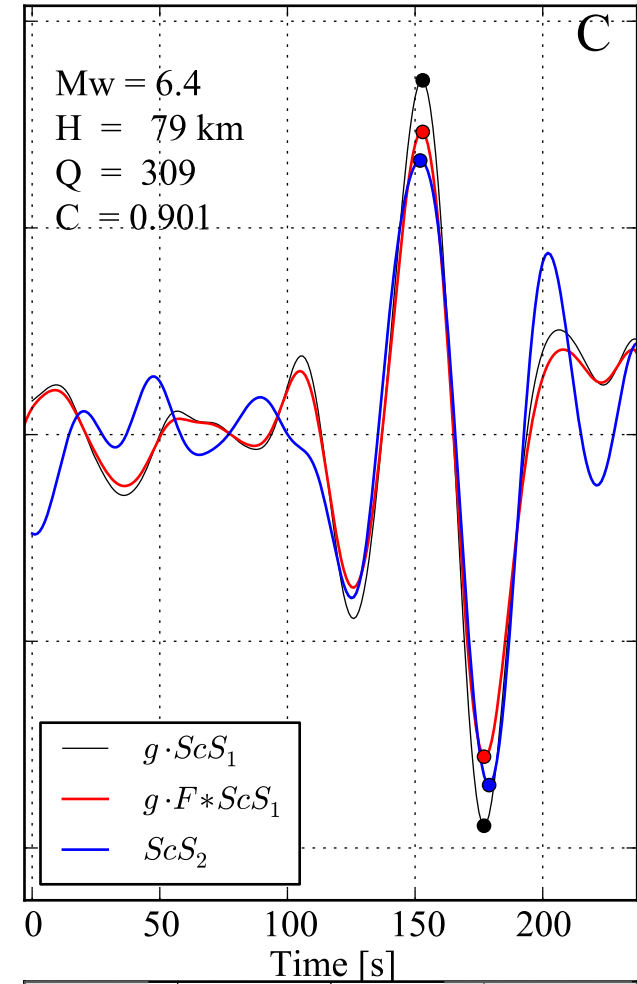
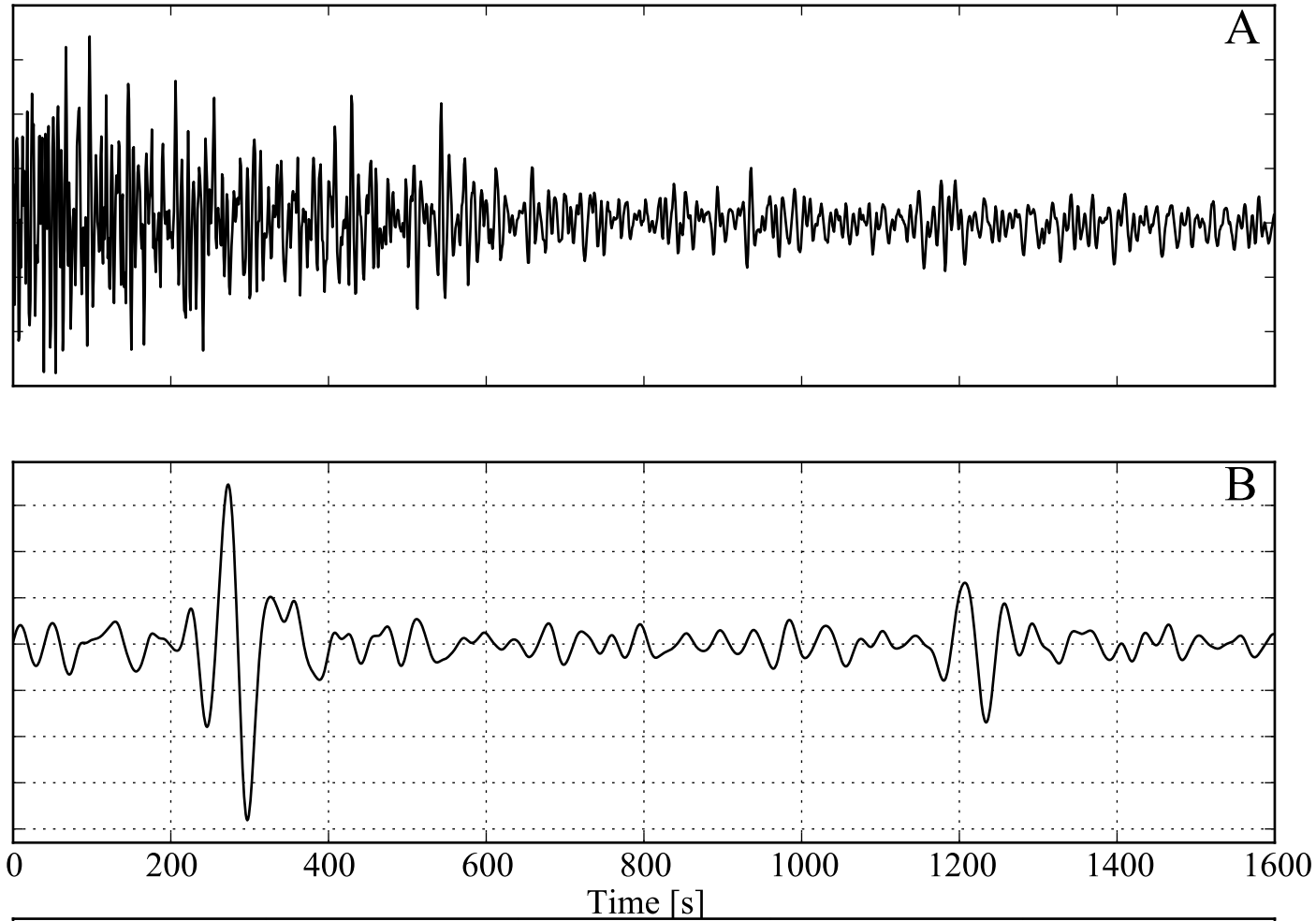


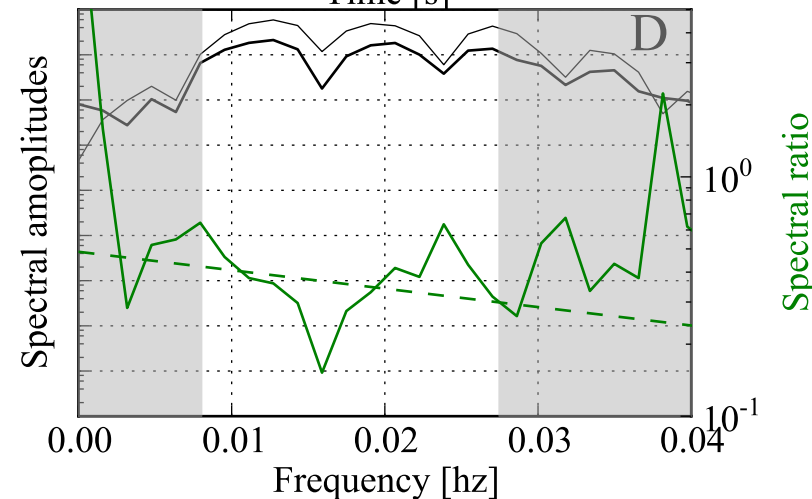
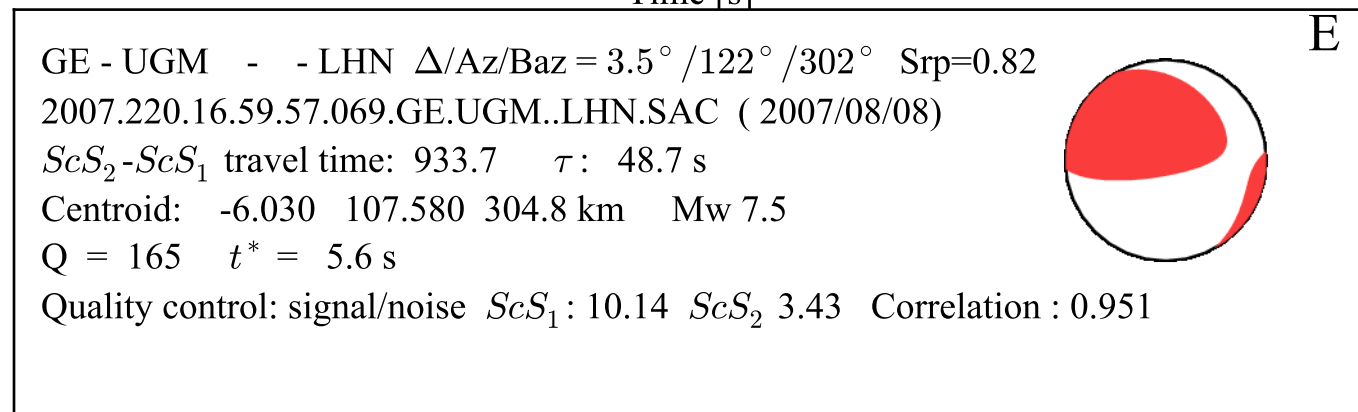
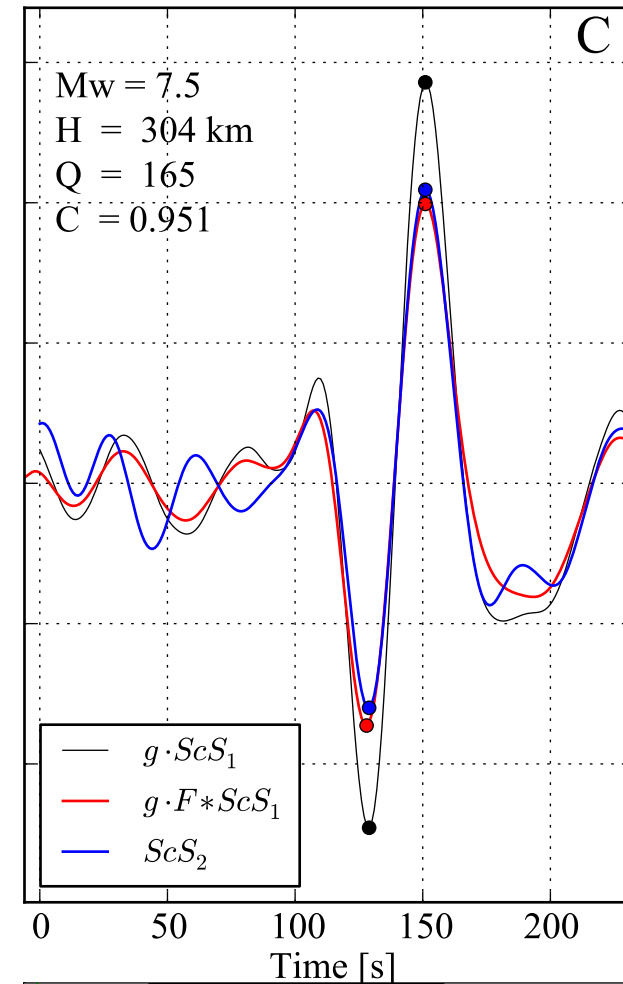
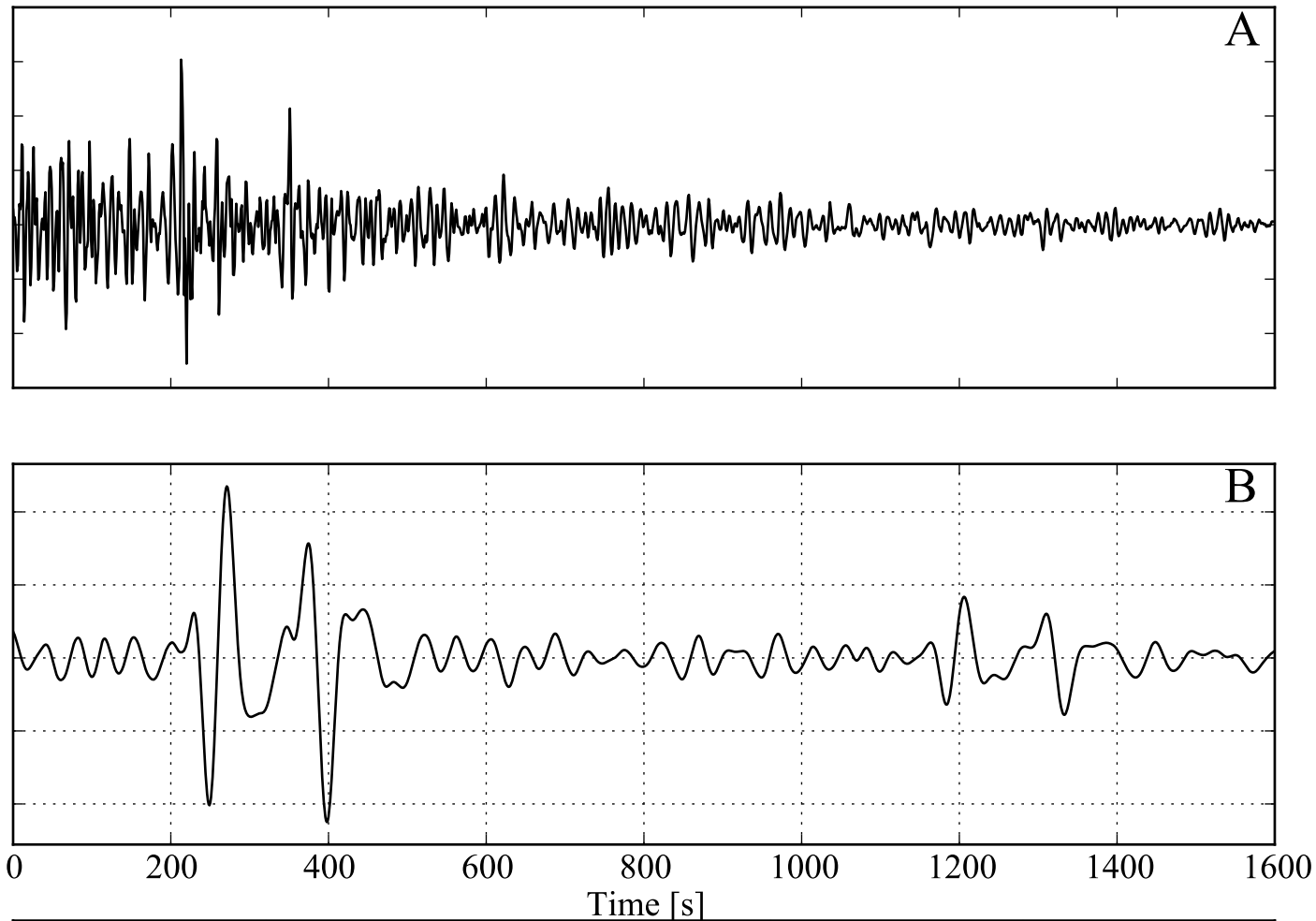


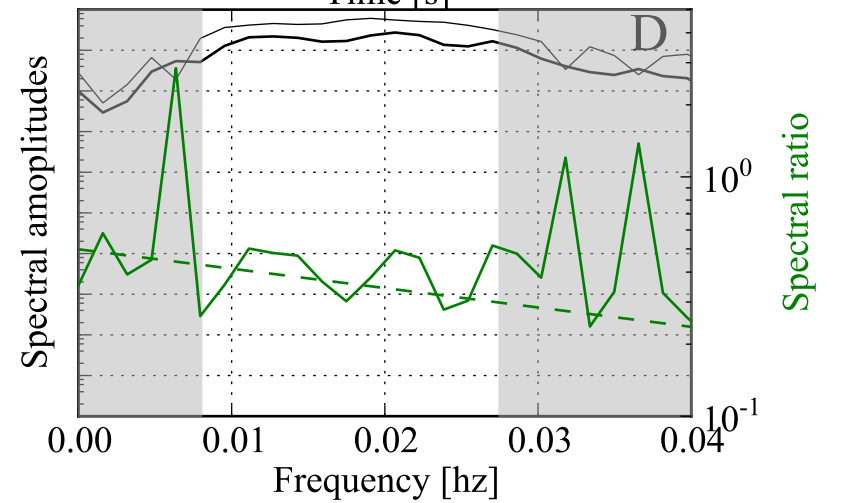
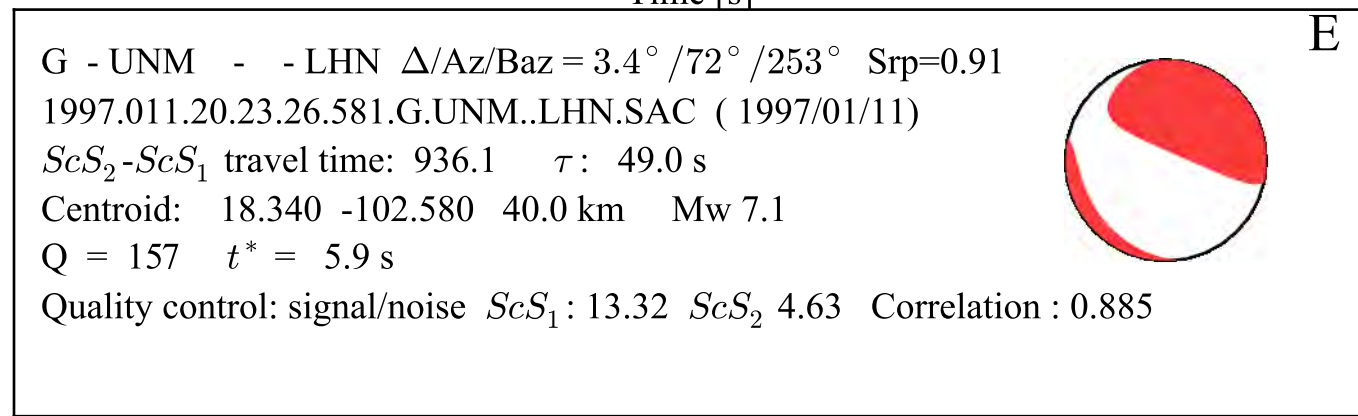
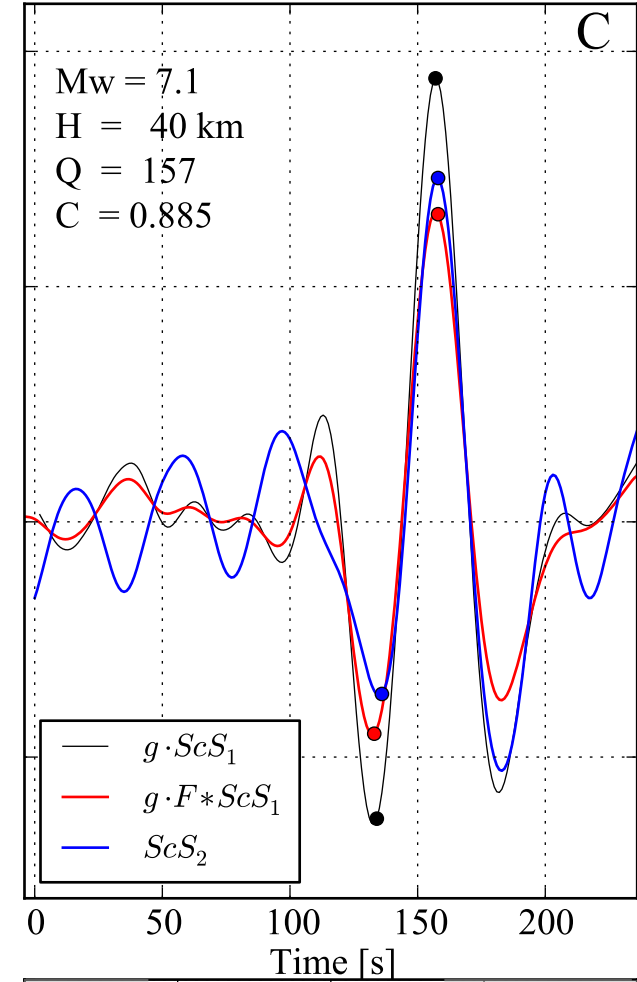
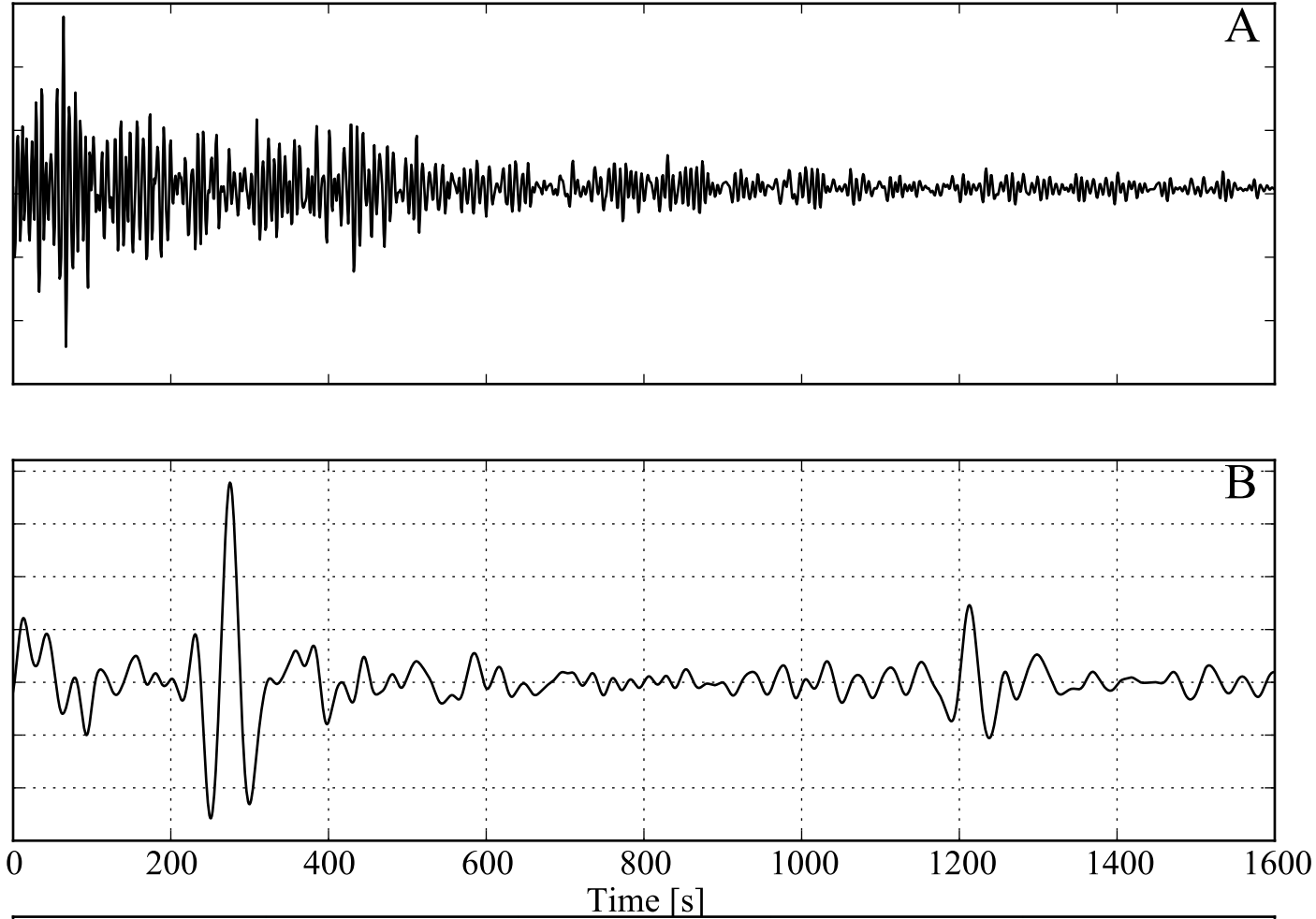


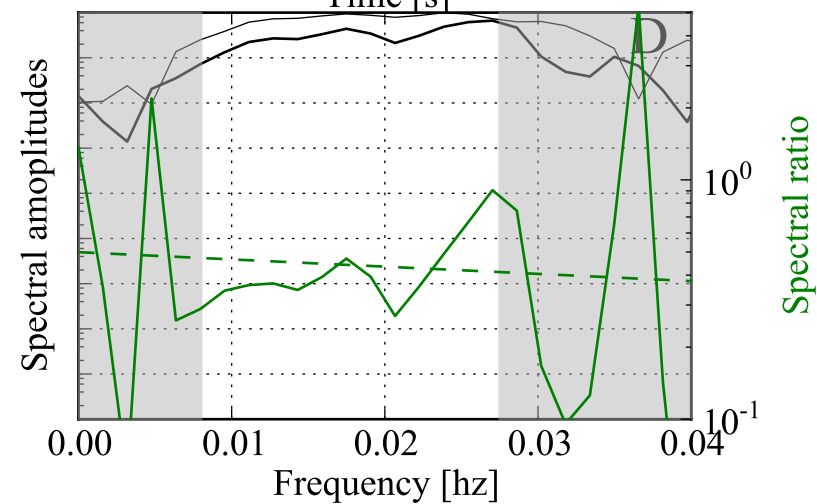
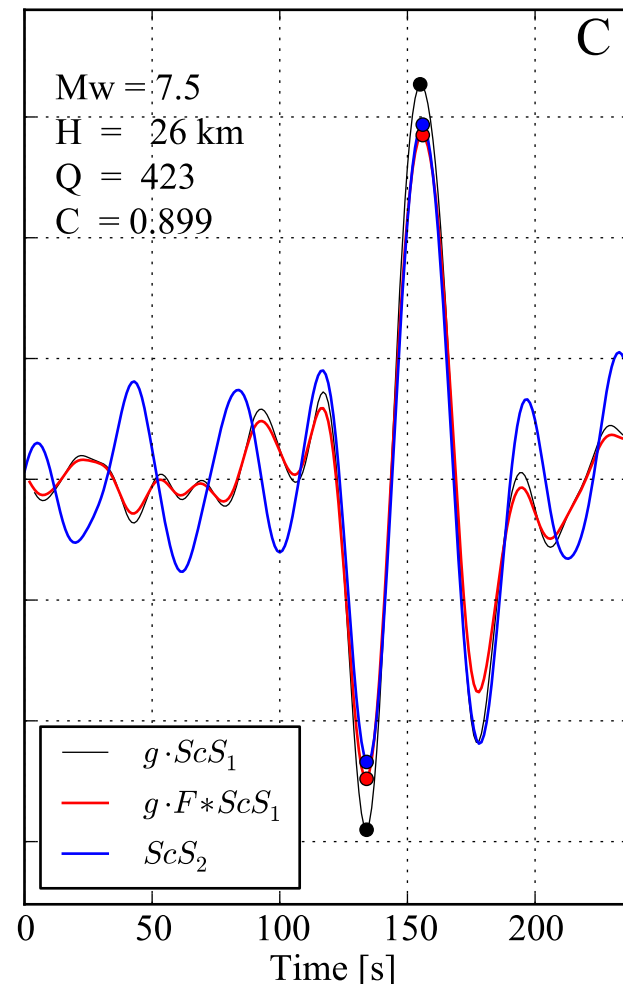
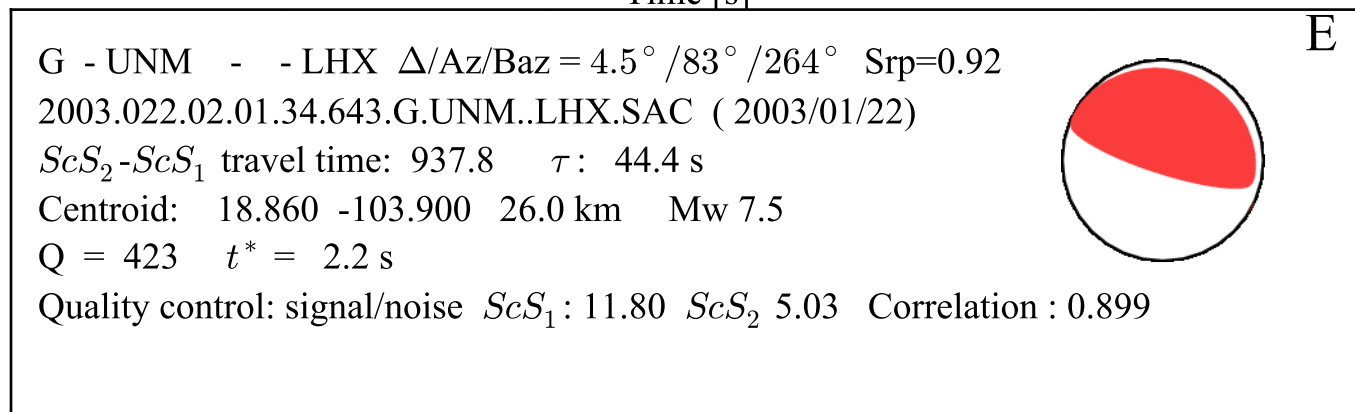
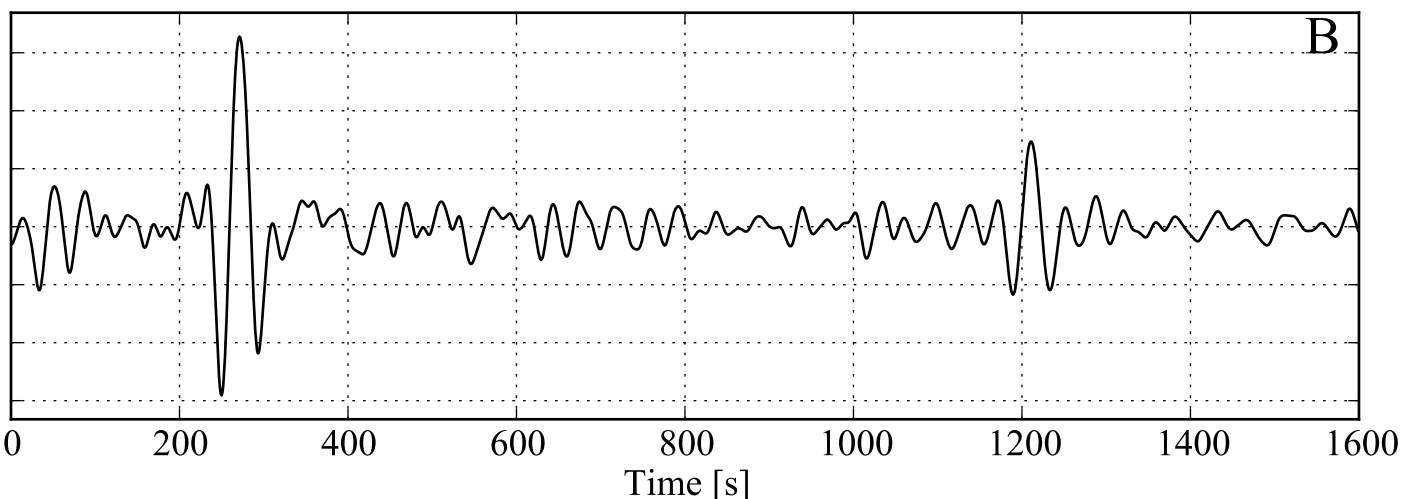
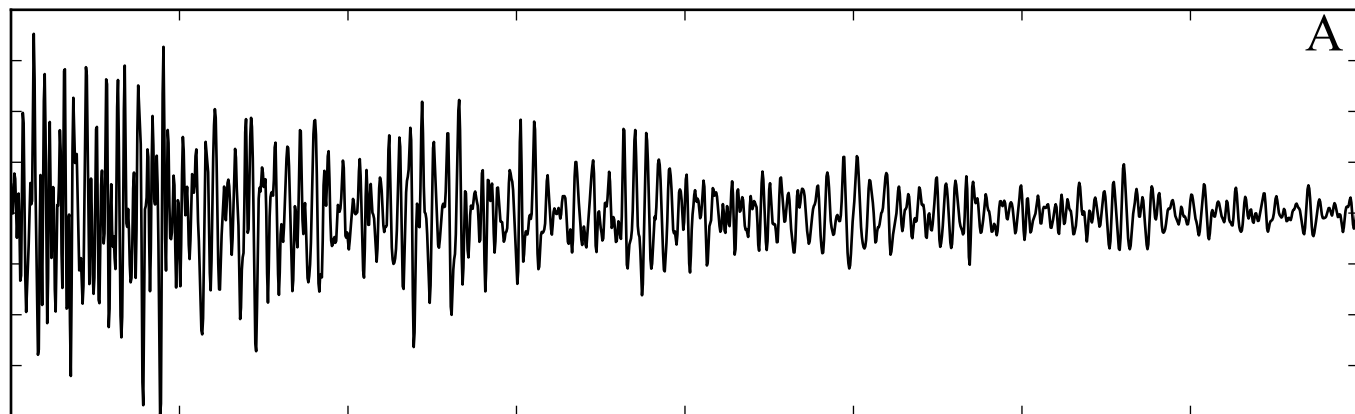


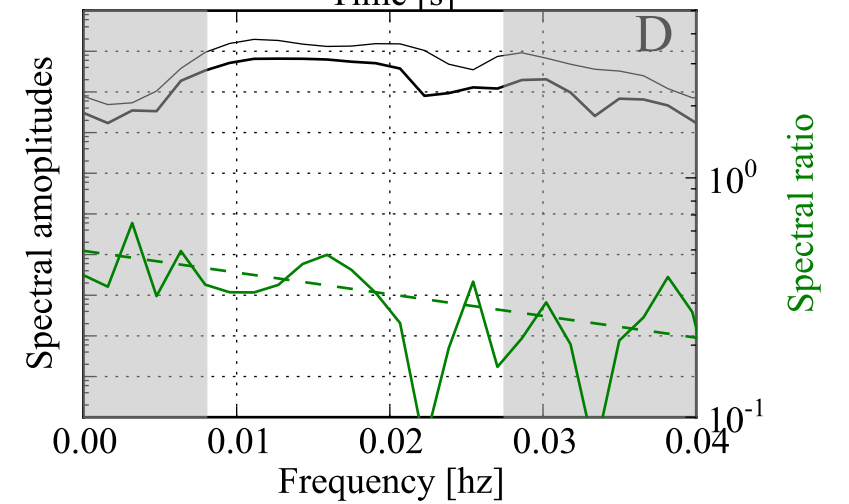
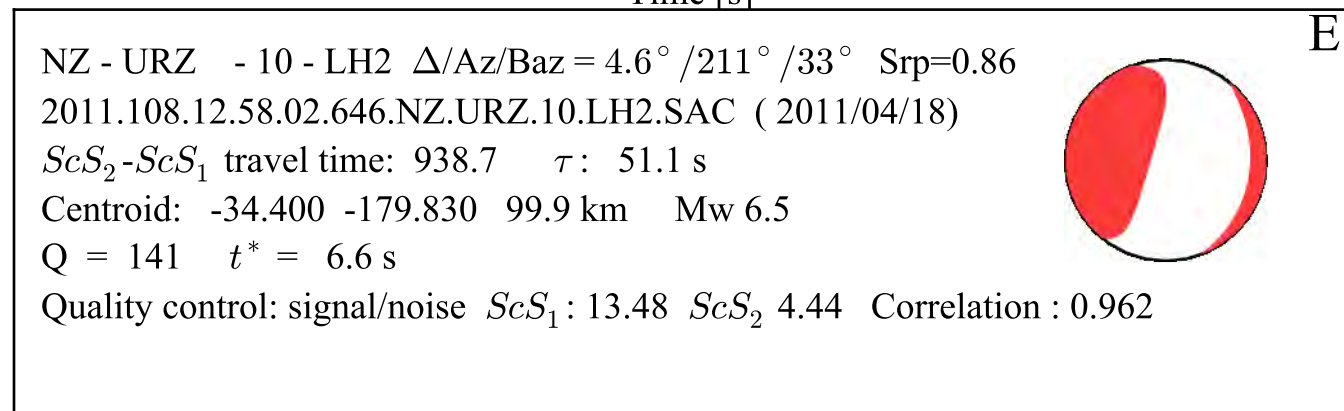
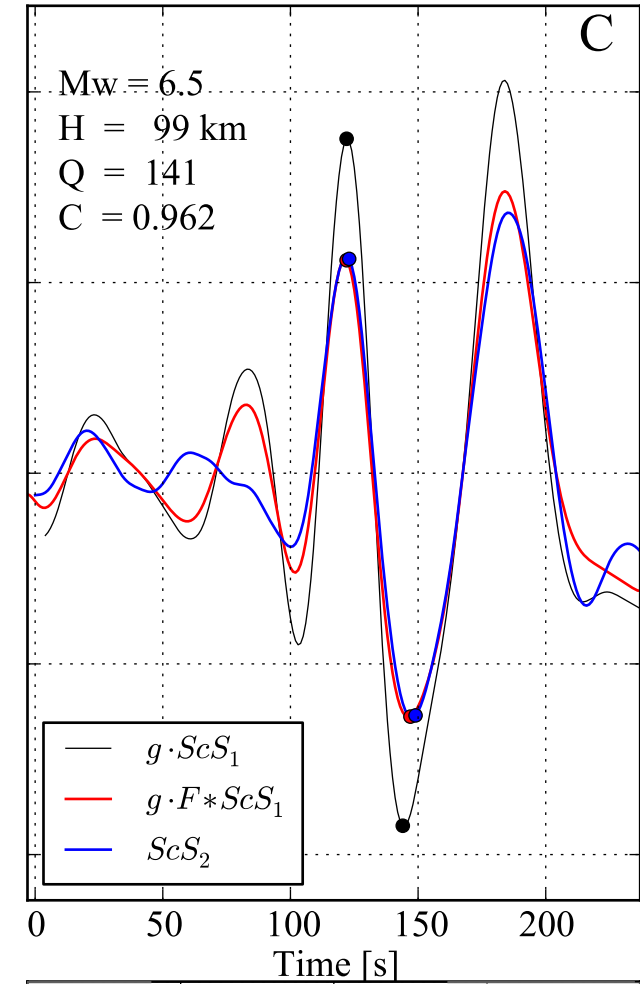
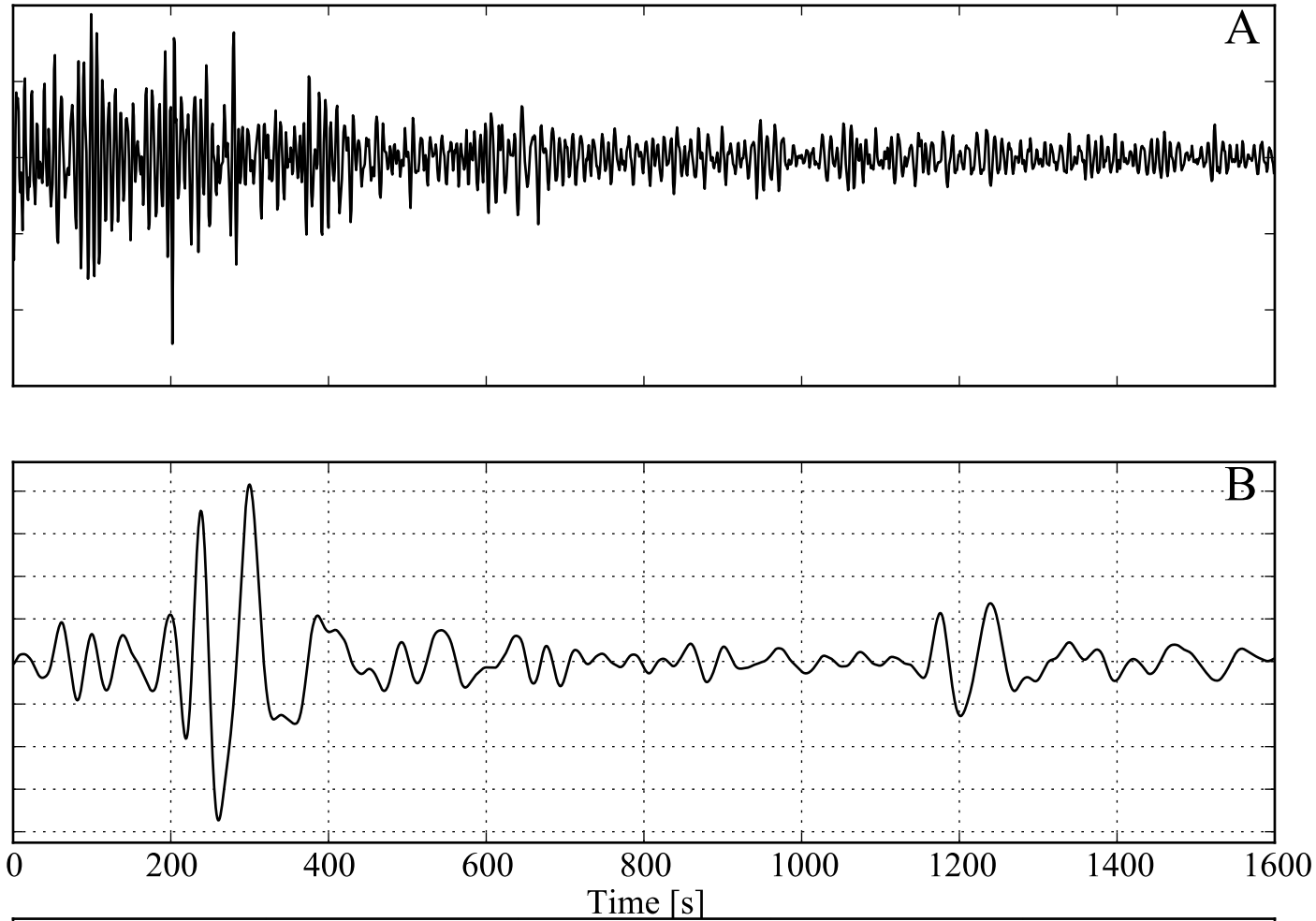


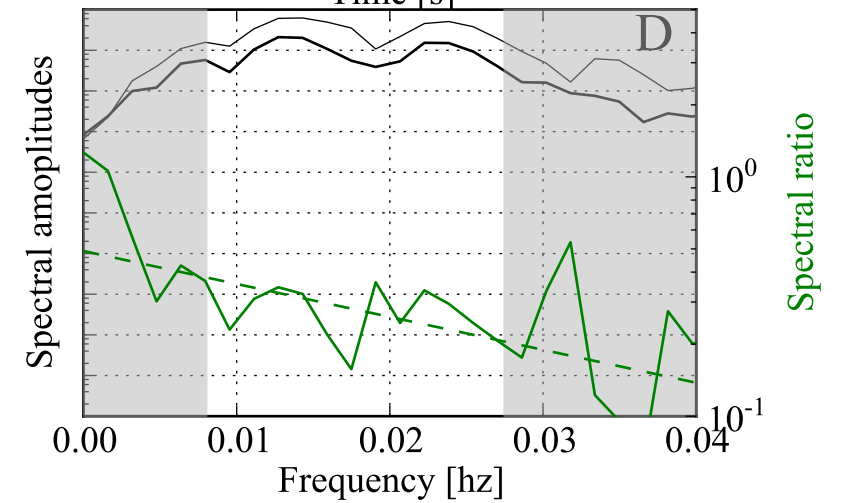
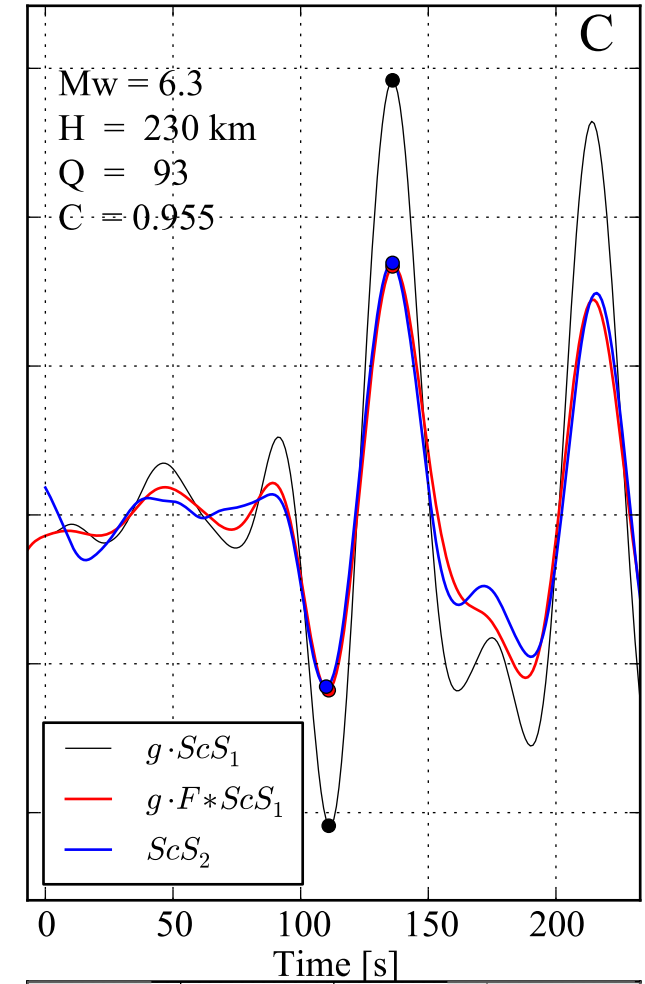
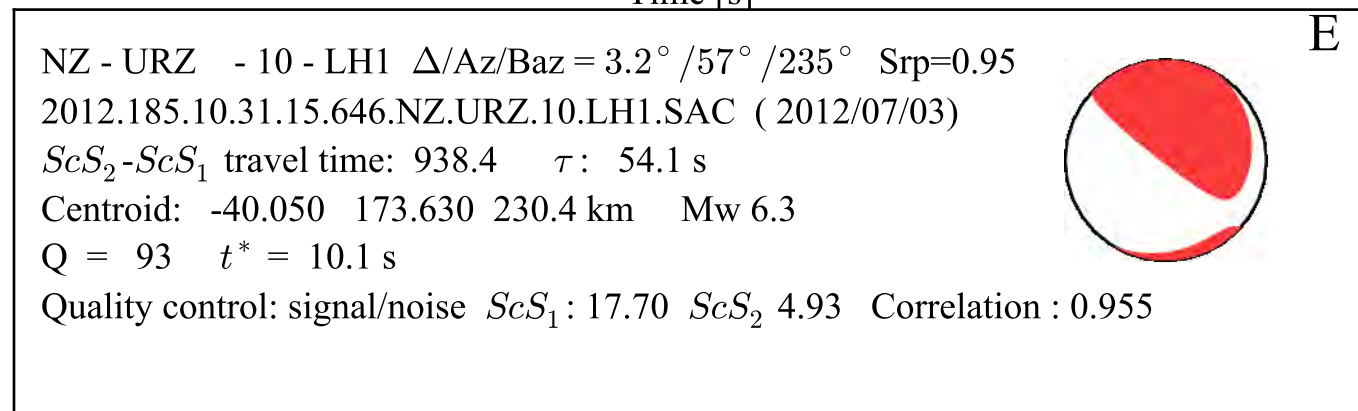
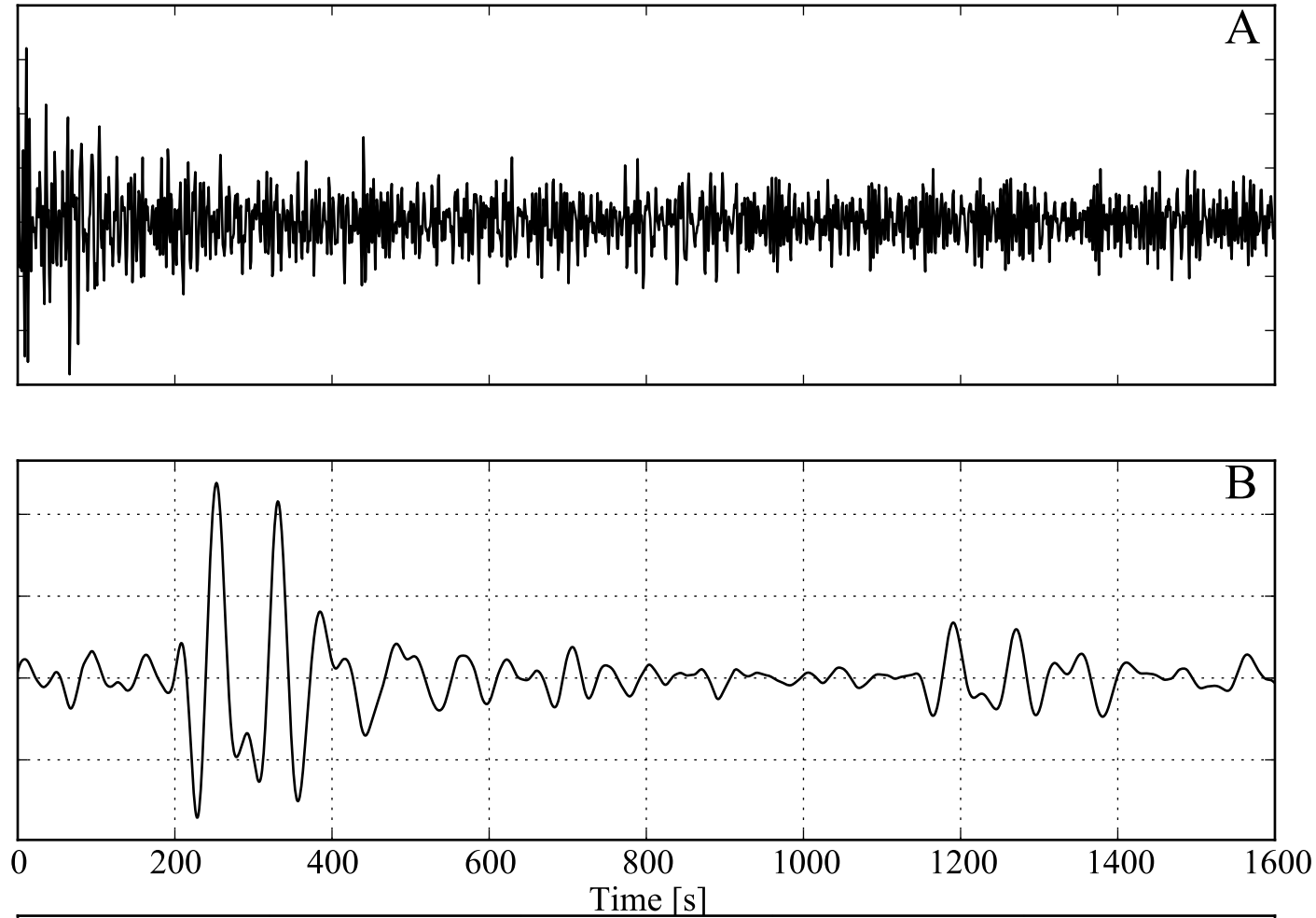


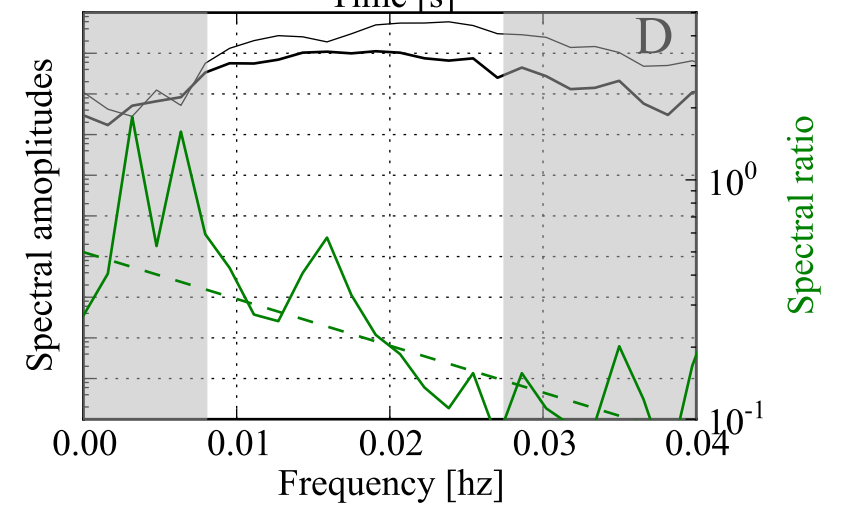
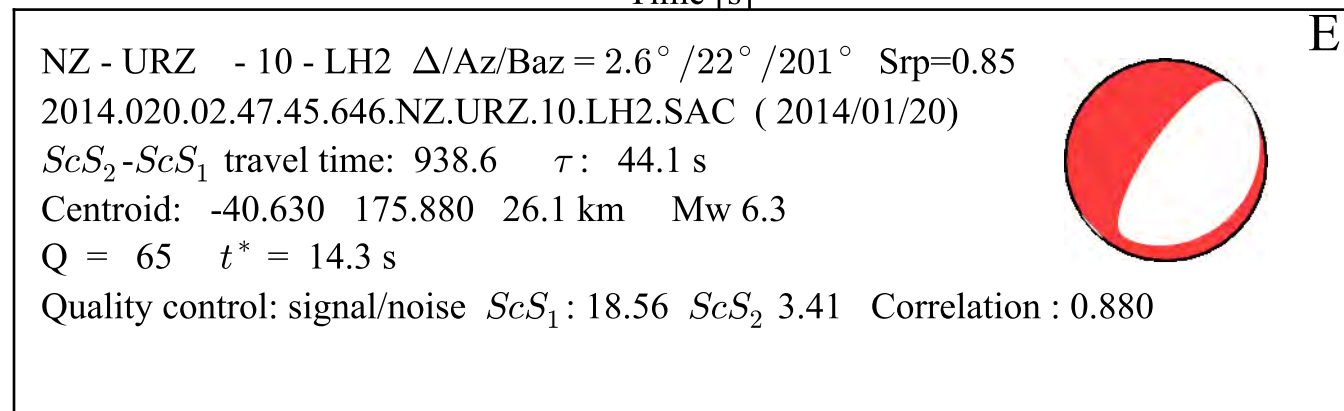
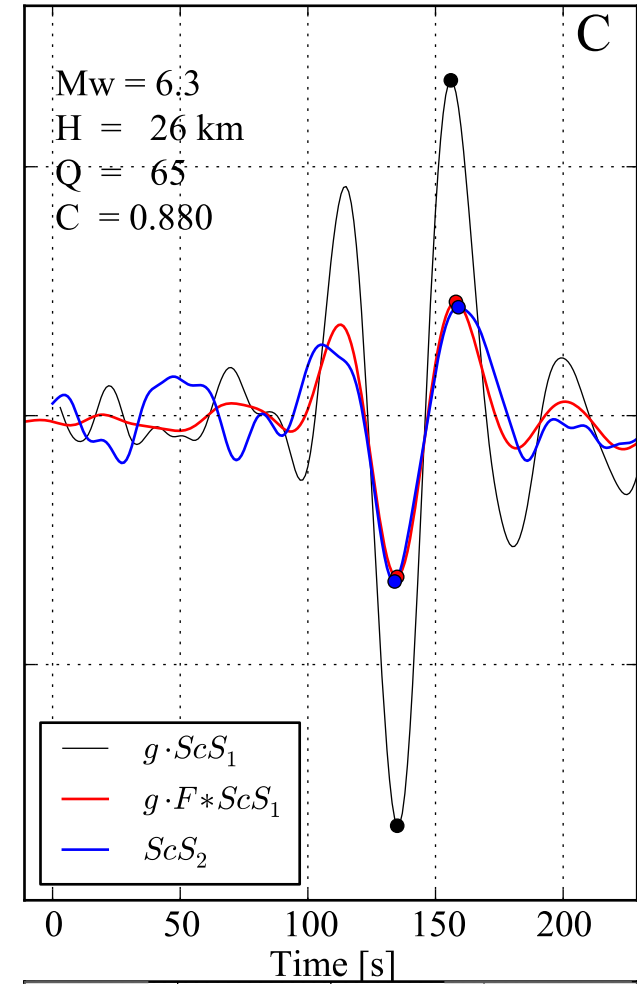
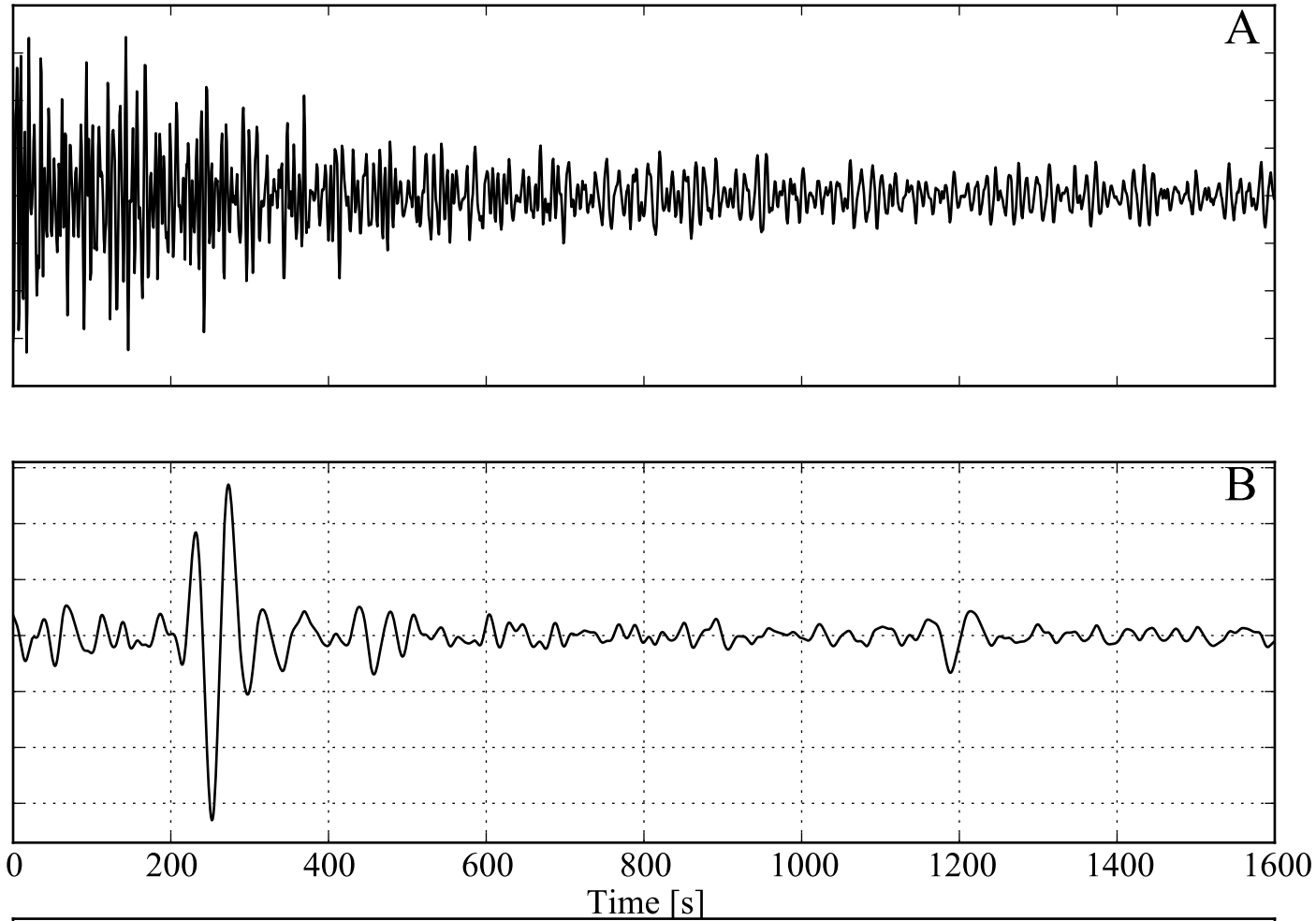


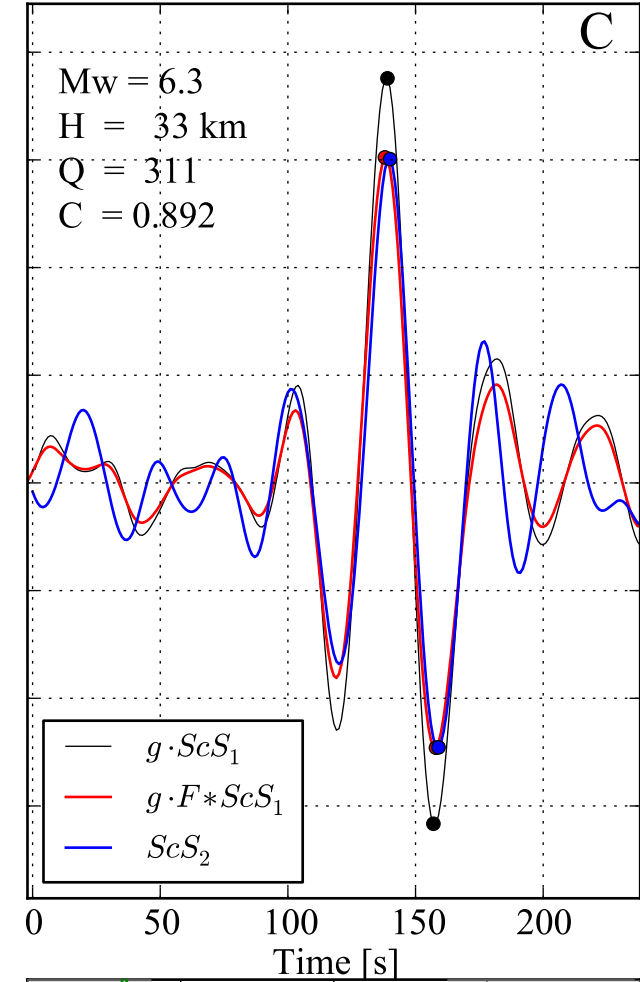
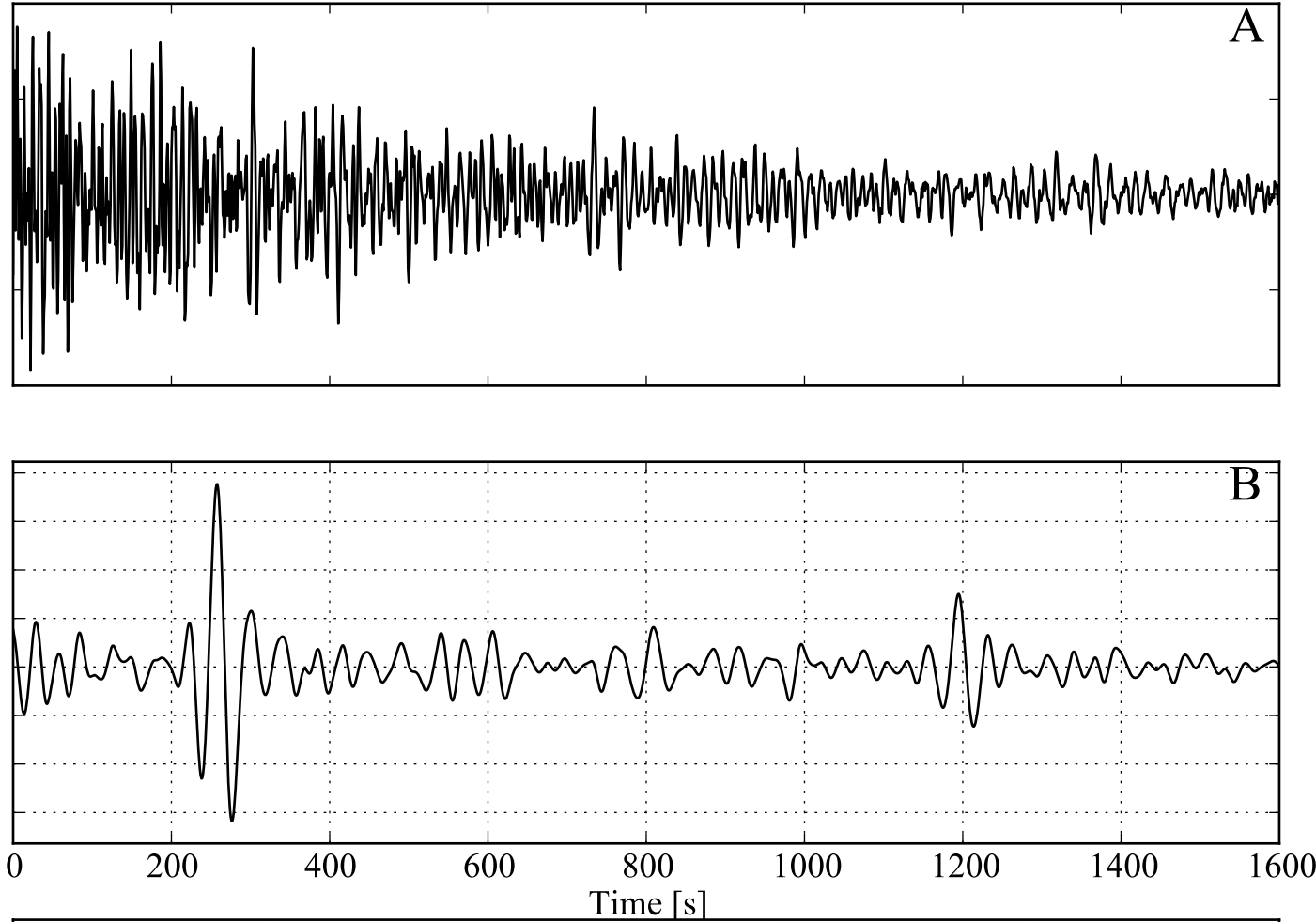






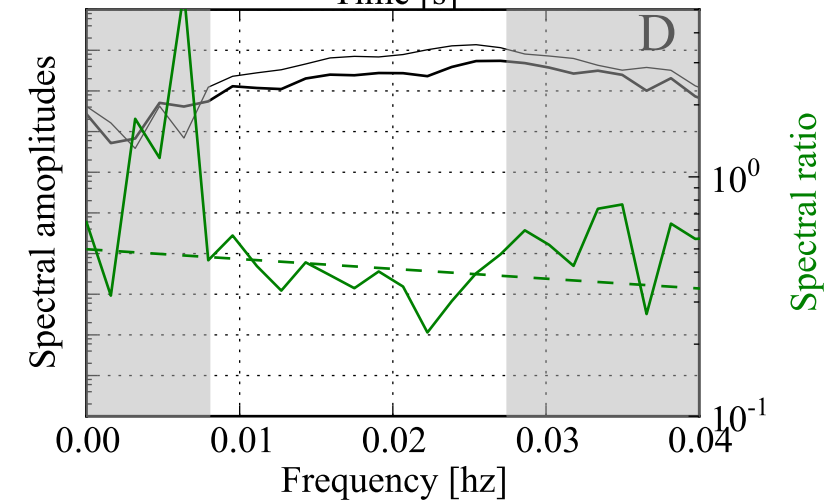


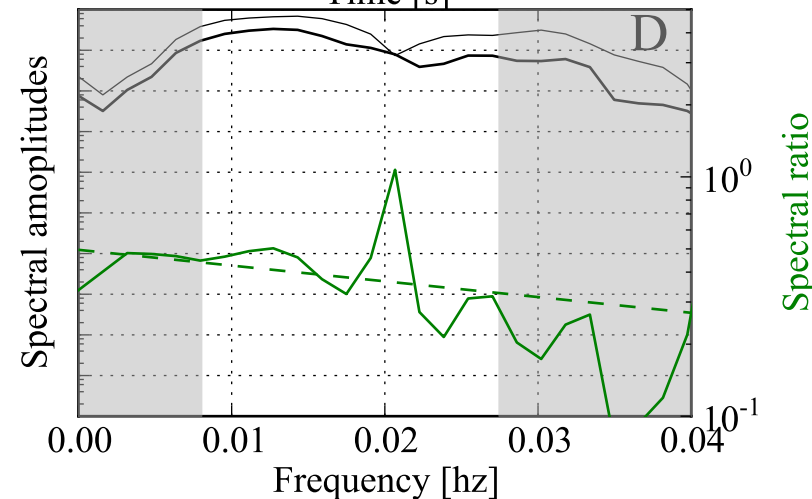
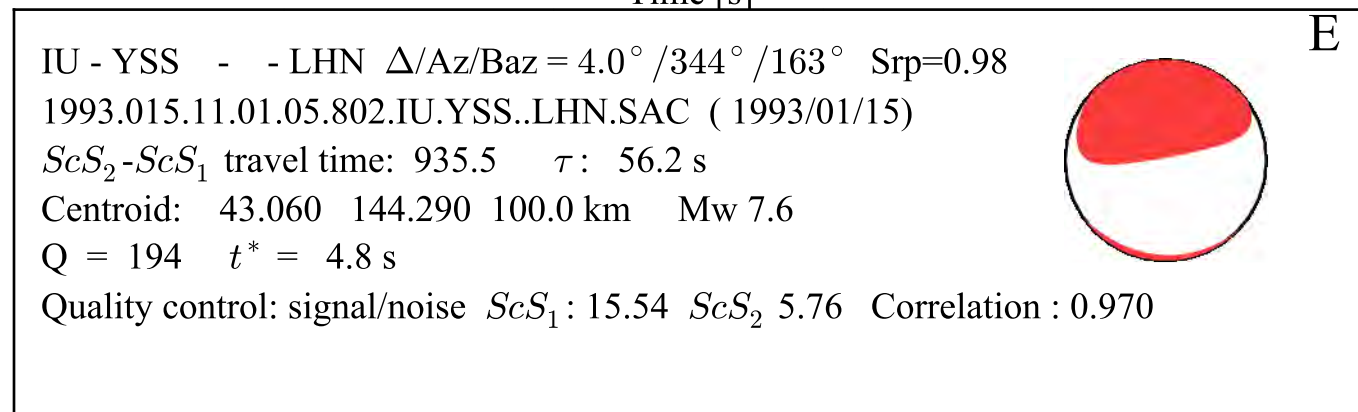
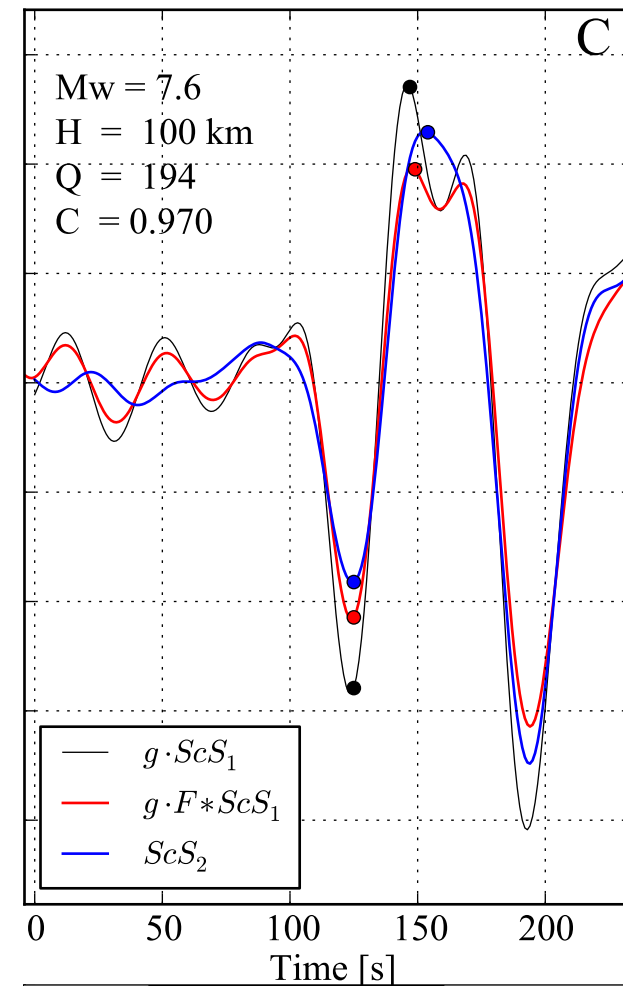
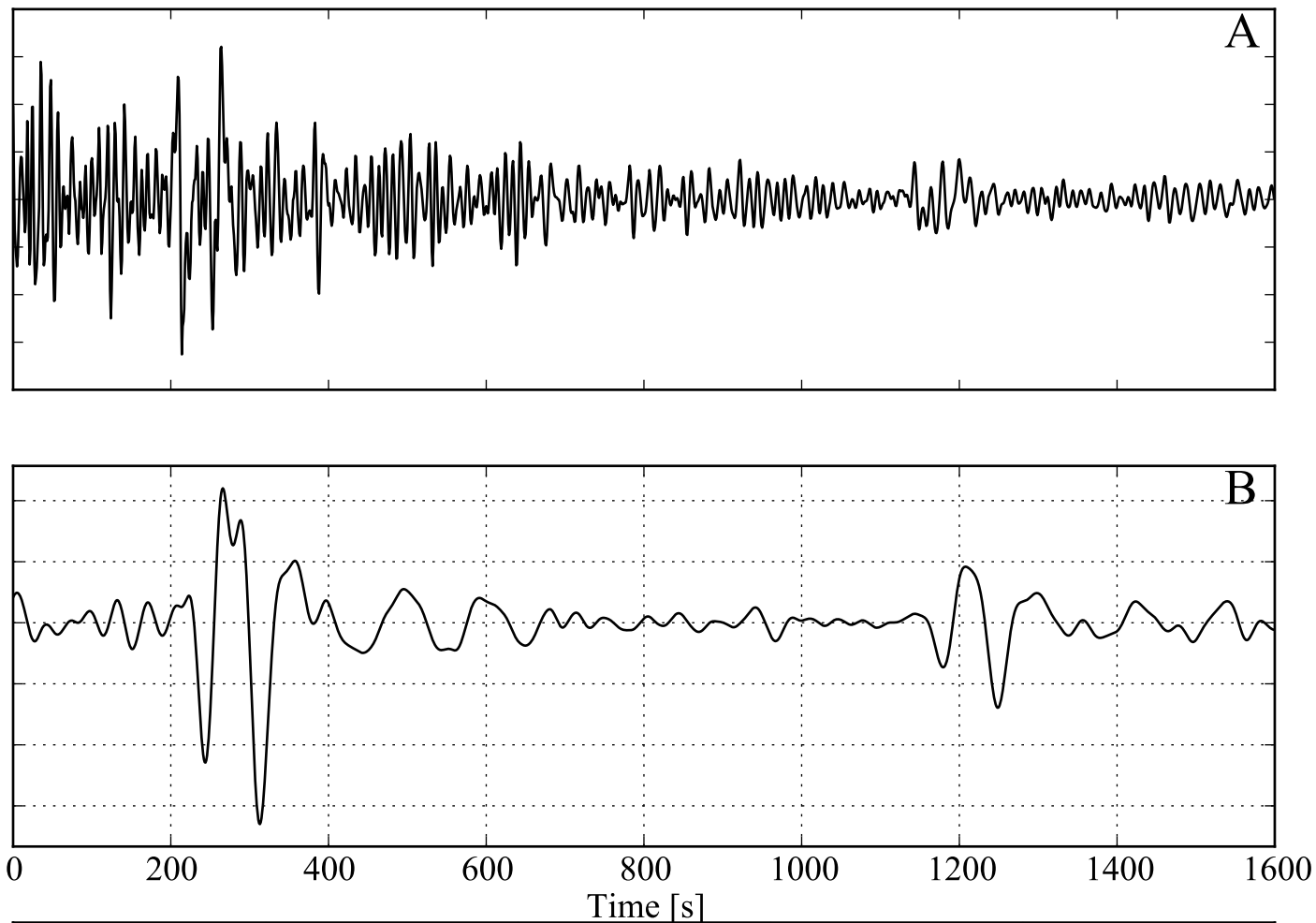


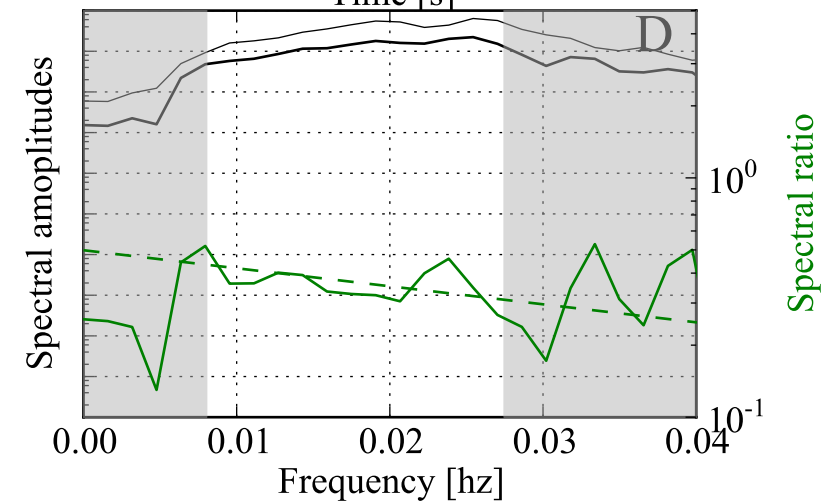
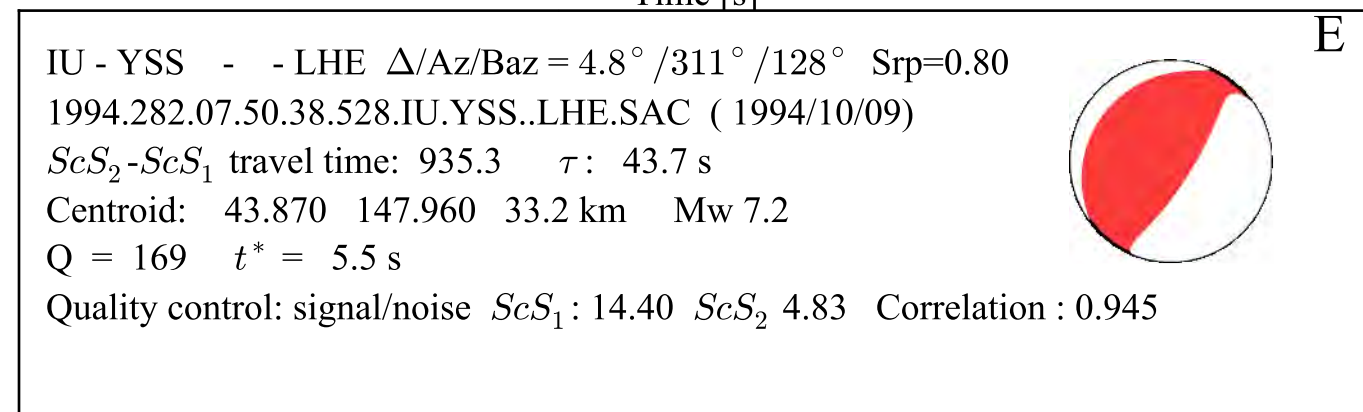
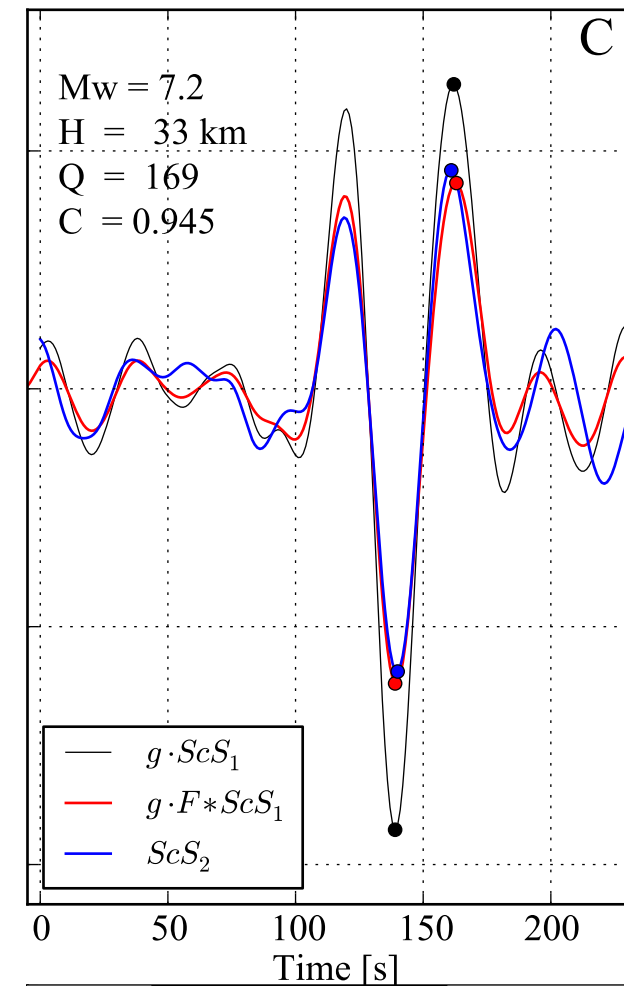
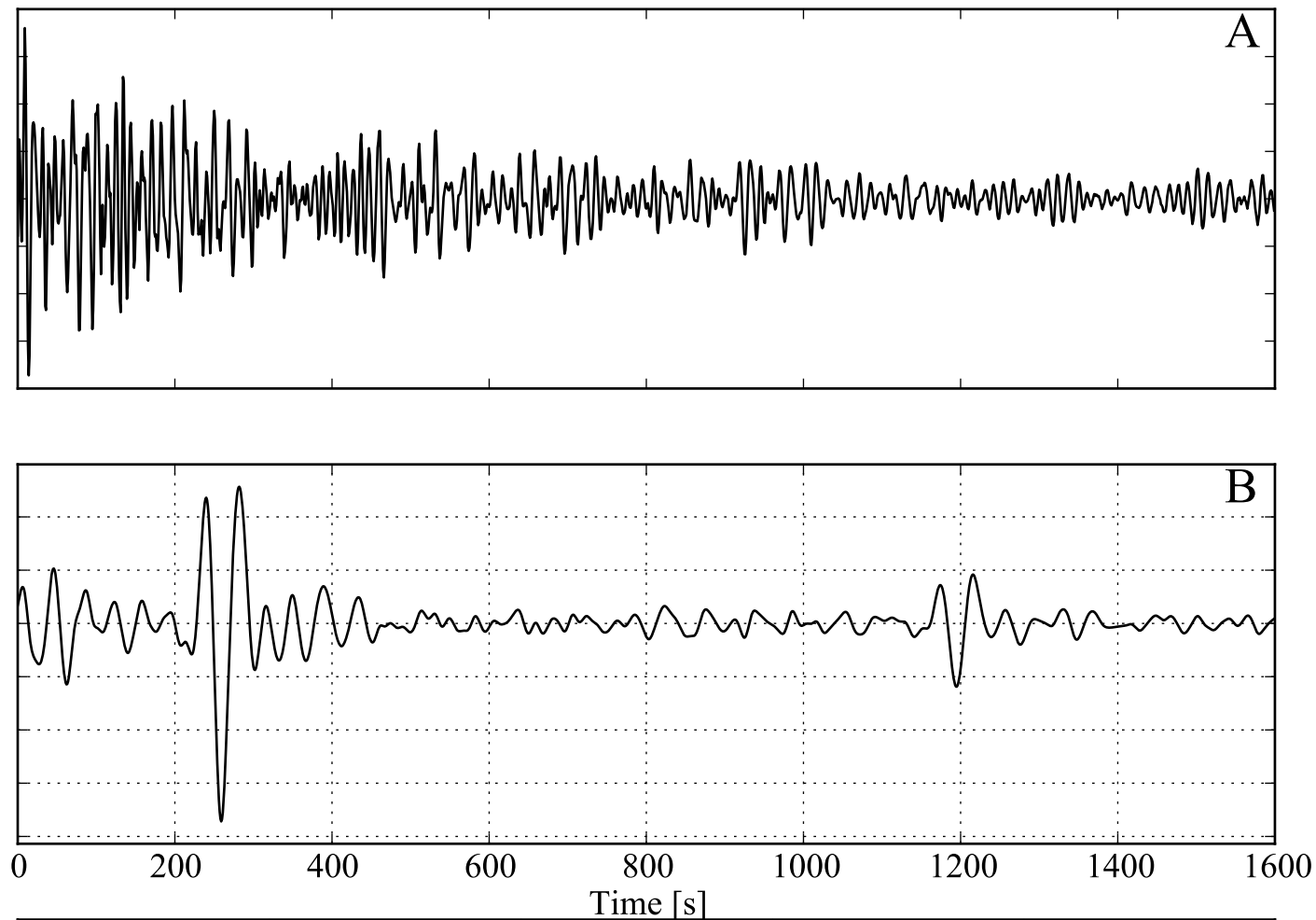


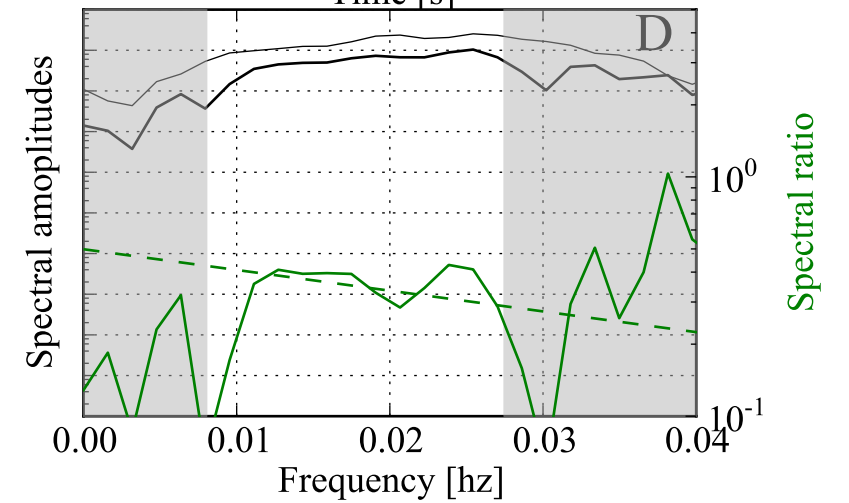
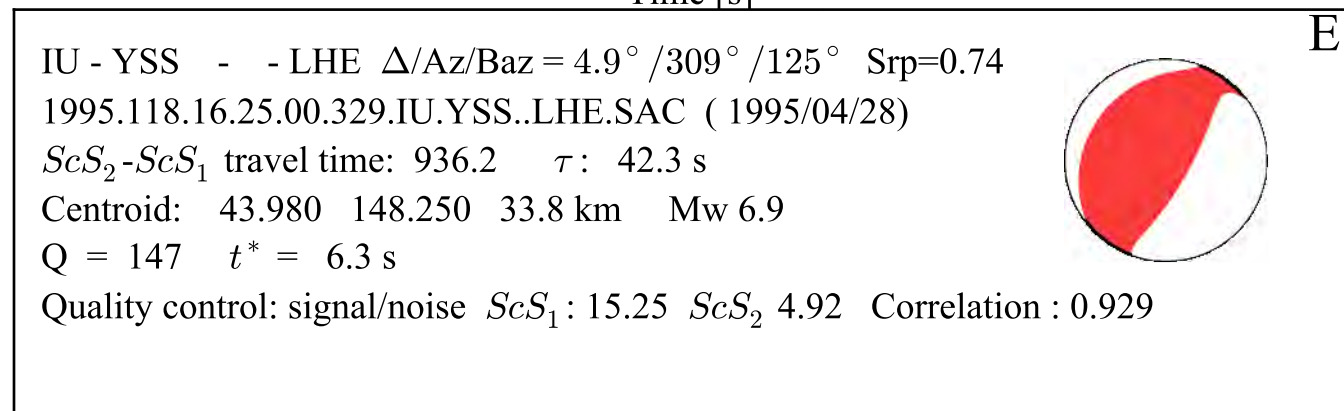
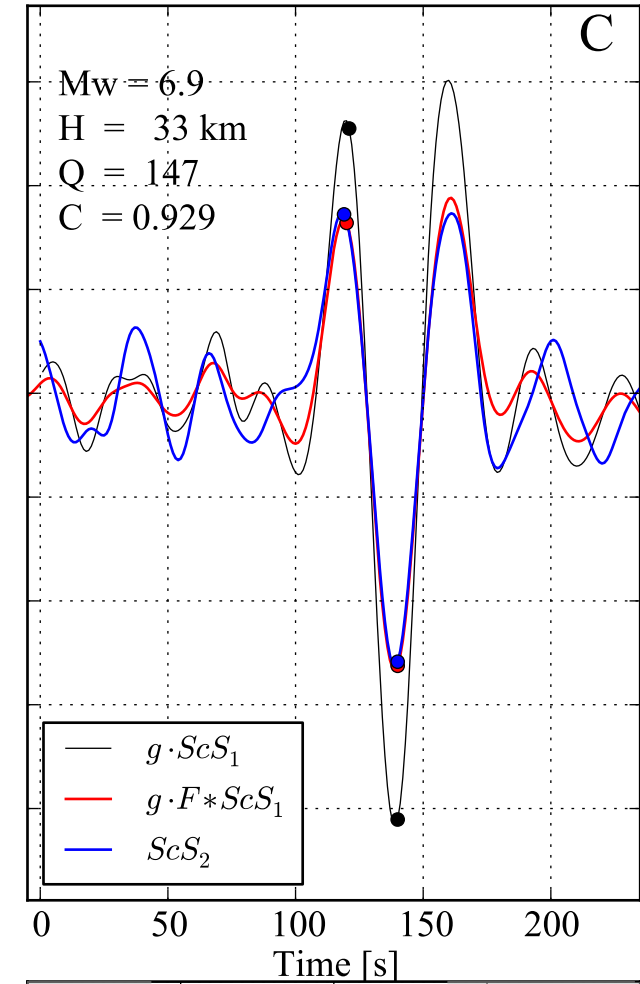
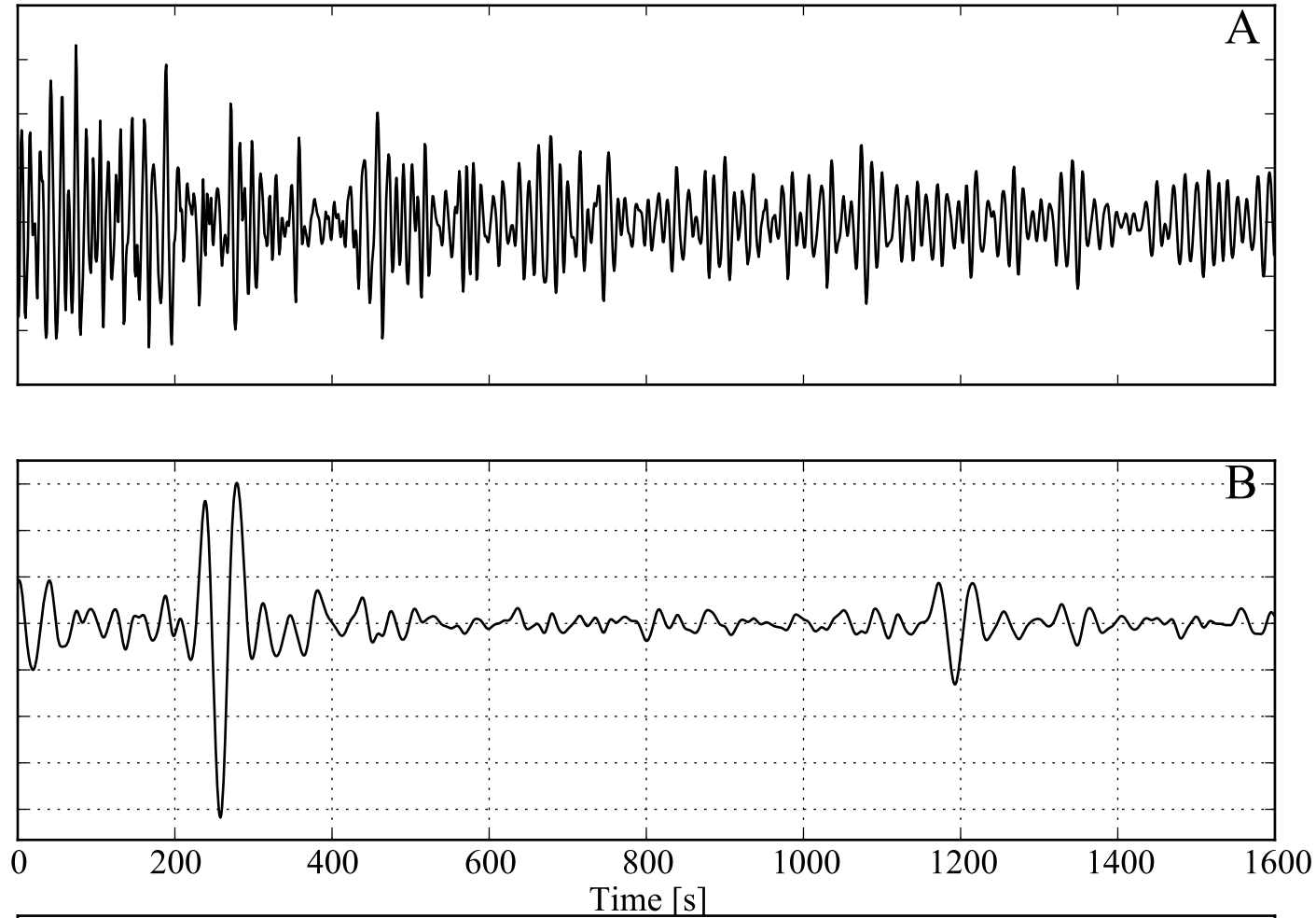
E

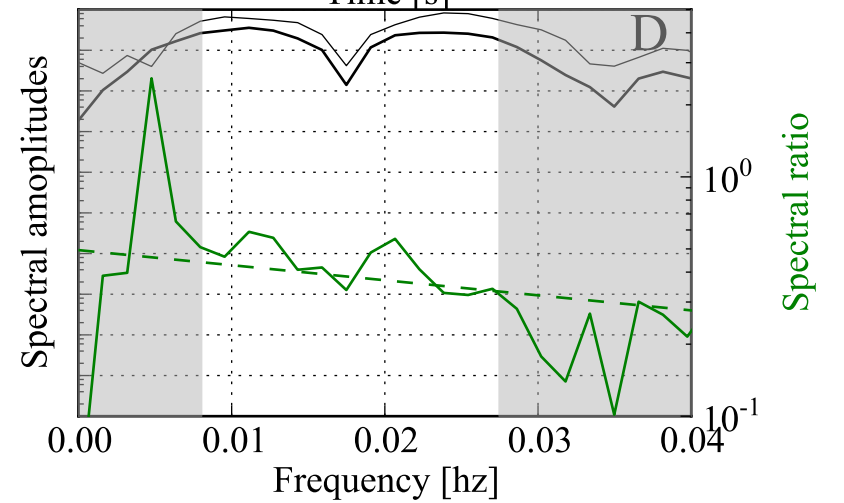
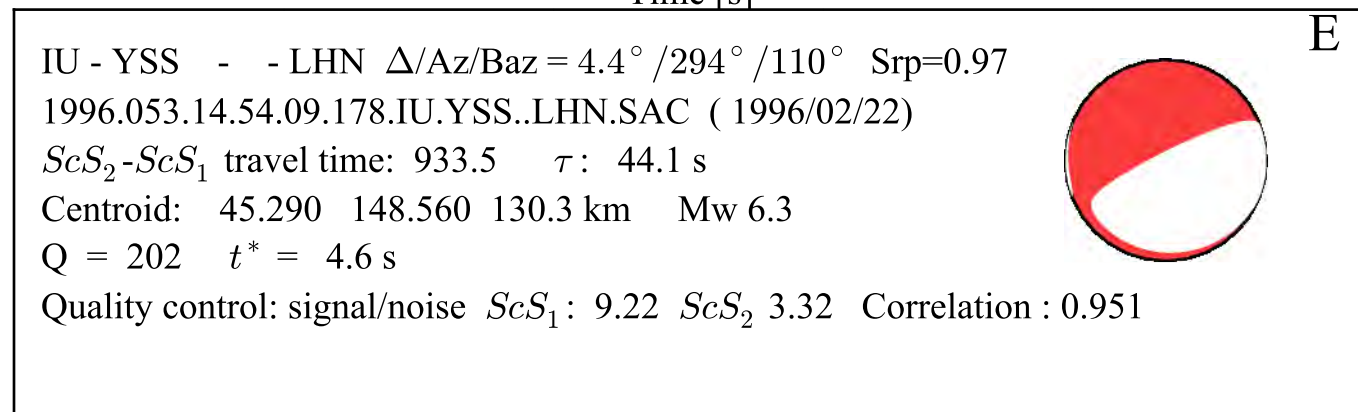
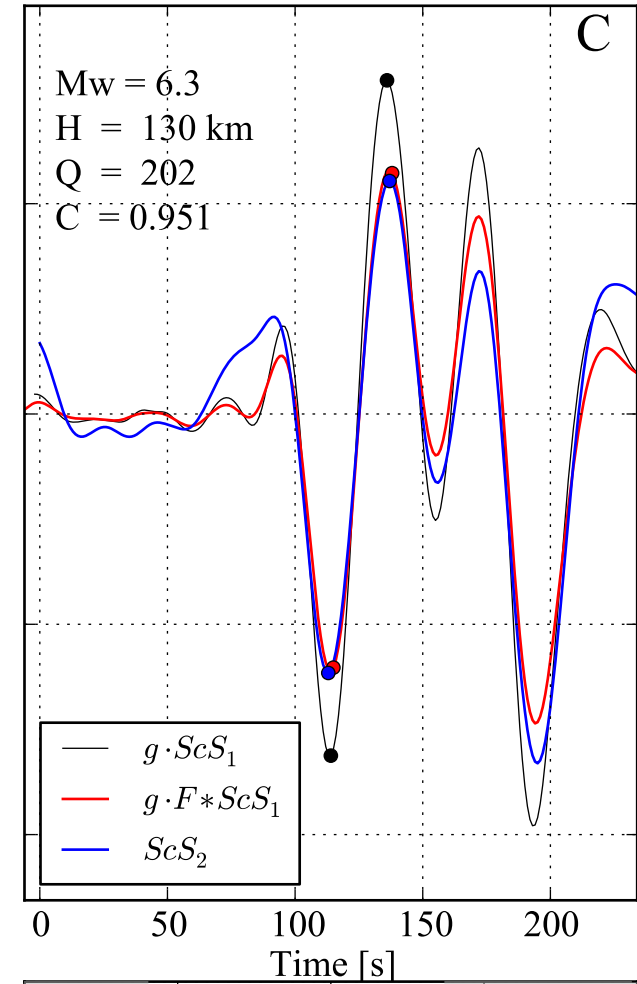
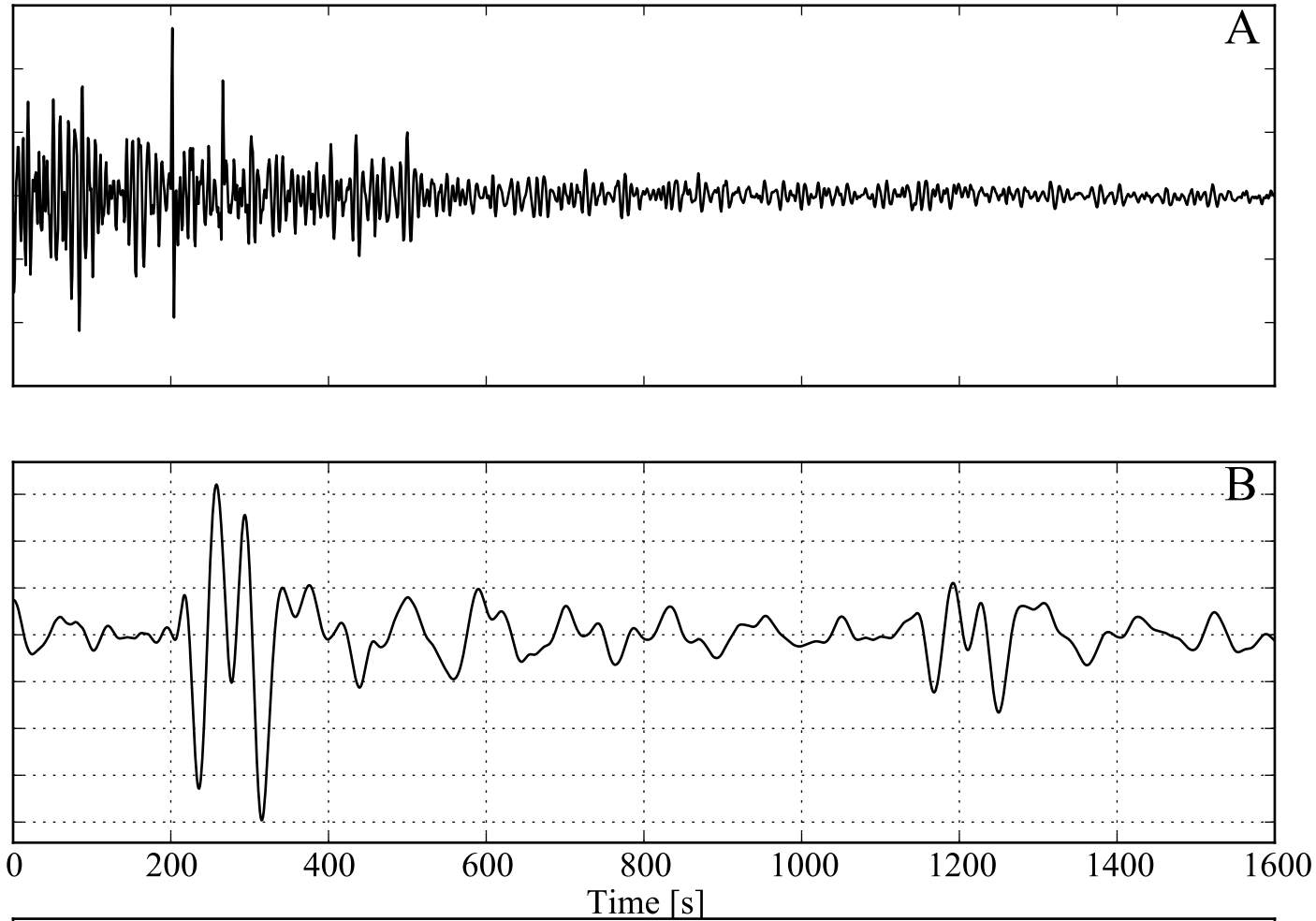
TW - YHNB - - LHN $\Delta/Az/Baz = 1.3^\circ / 310^\circ / 129^\circ$ $Srp=0.84$
 2004.313.15.50.01.069.TW.YHNB..LHN.SAC (2004/11/08)
 ScS_2-ScS_1 travel time: 935.8 τ : 39.9 s
 Centroid: 23.860 122.430 33.0 km Mw 6.3
 $Q = 311$ $t^* = 3.0$ s
 Quality control: signal/noise ScS_1 : 8.74 ScS_2 3.44 Correlation : 0.892

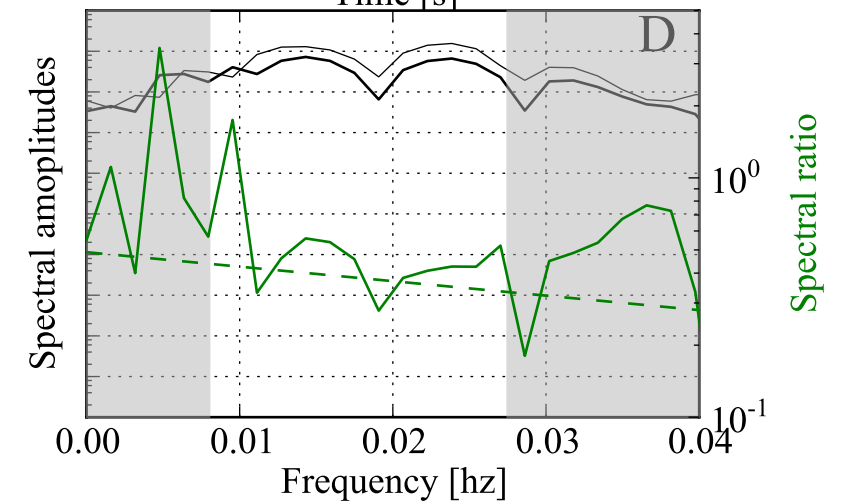
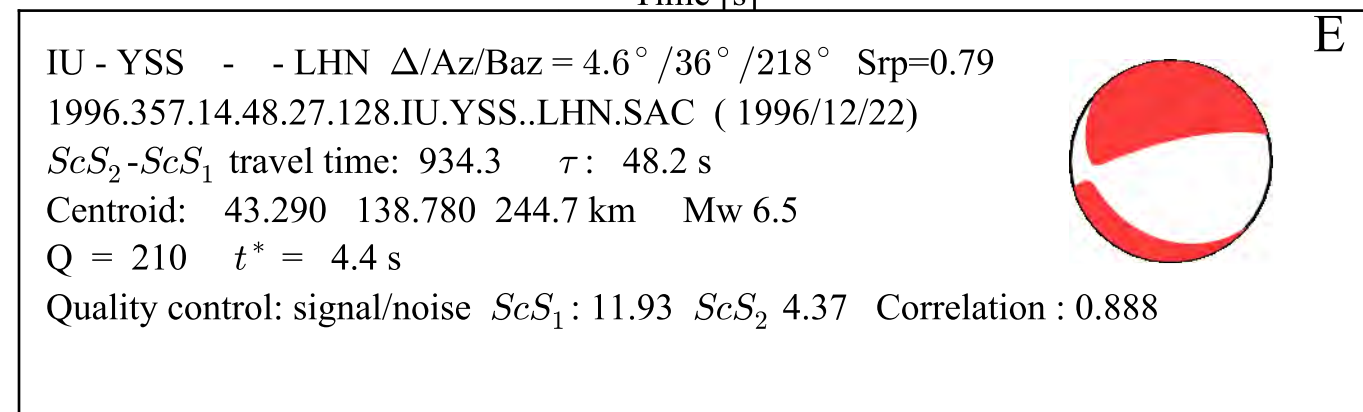
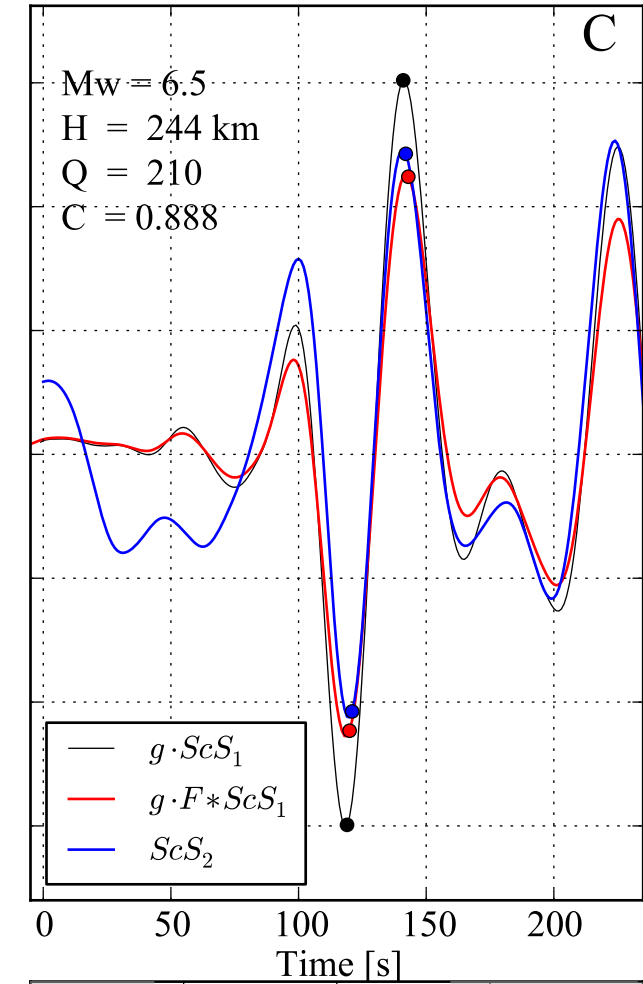
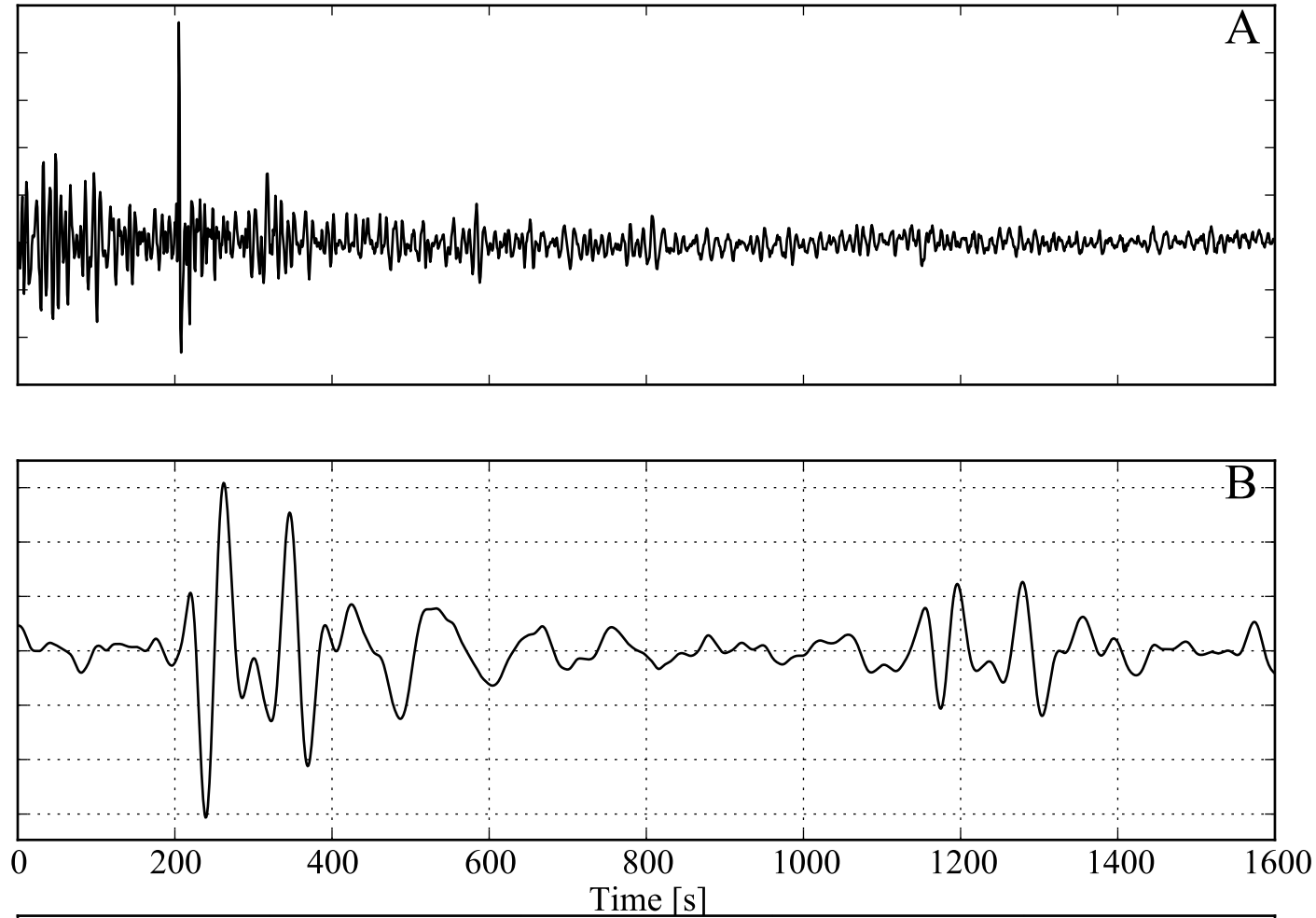


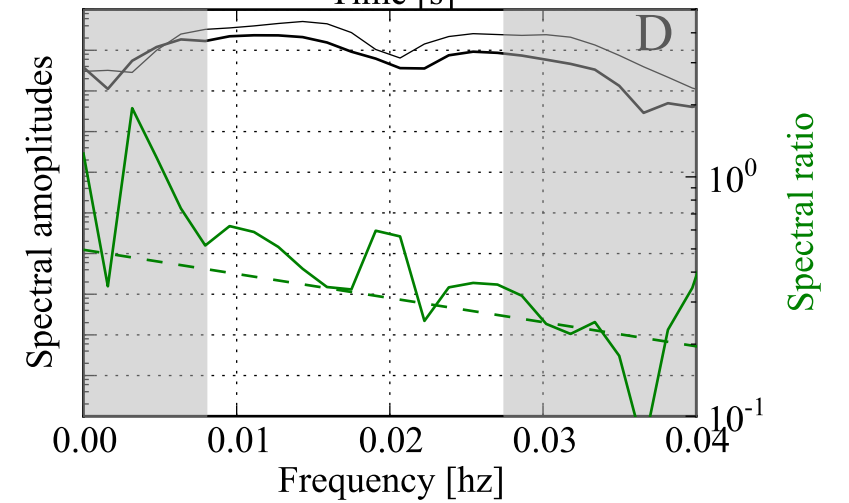
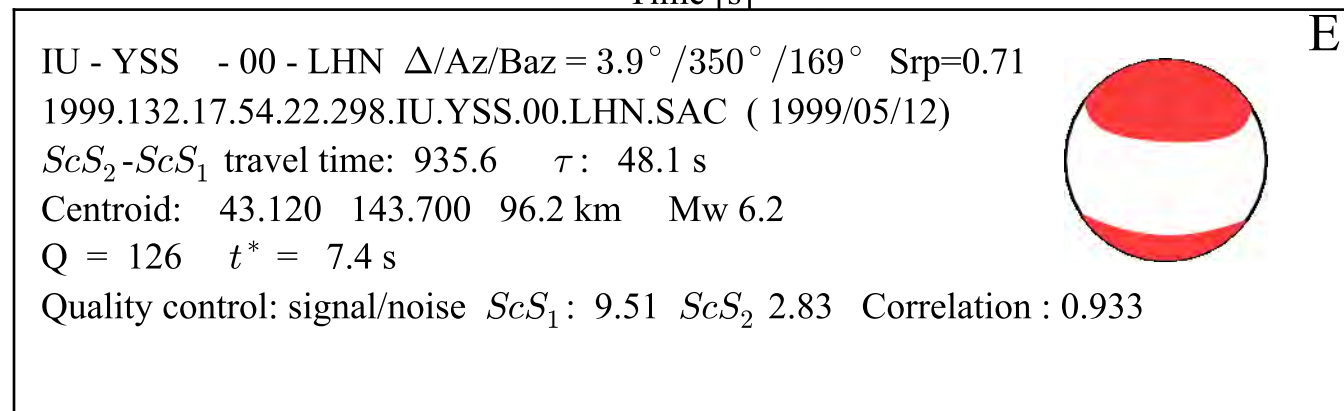
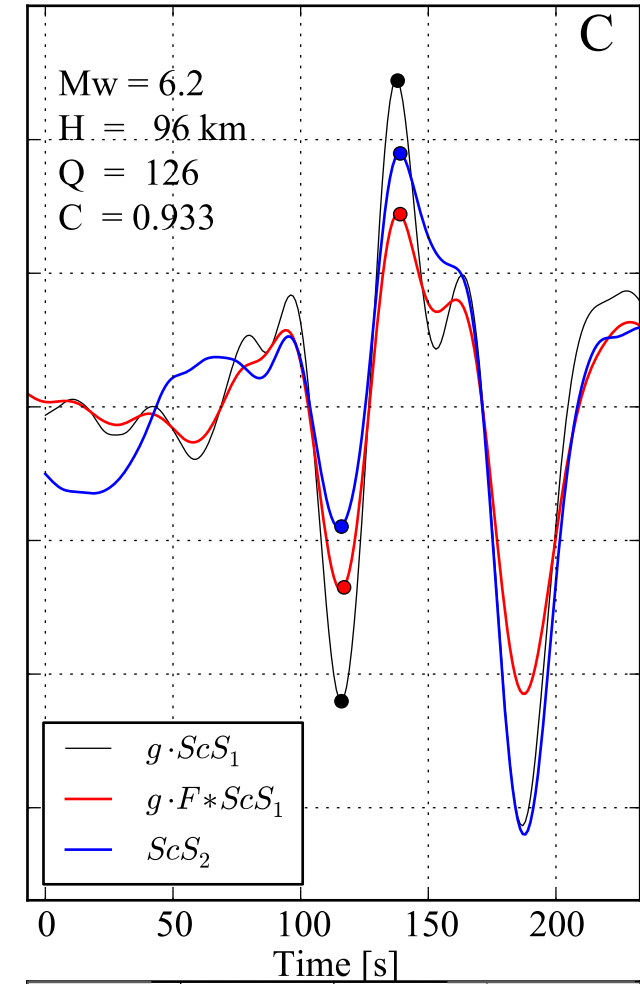
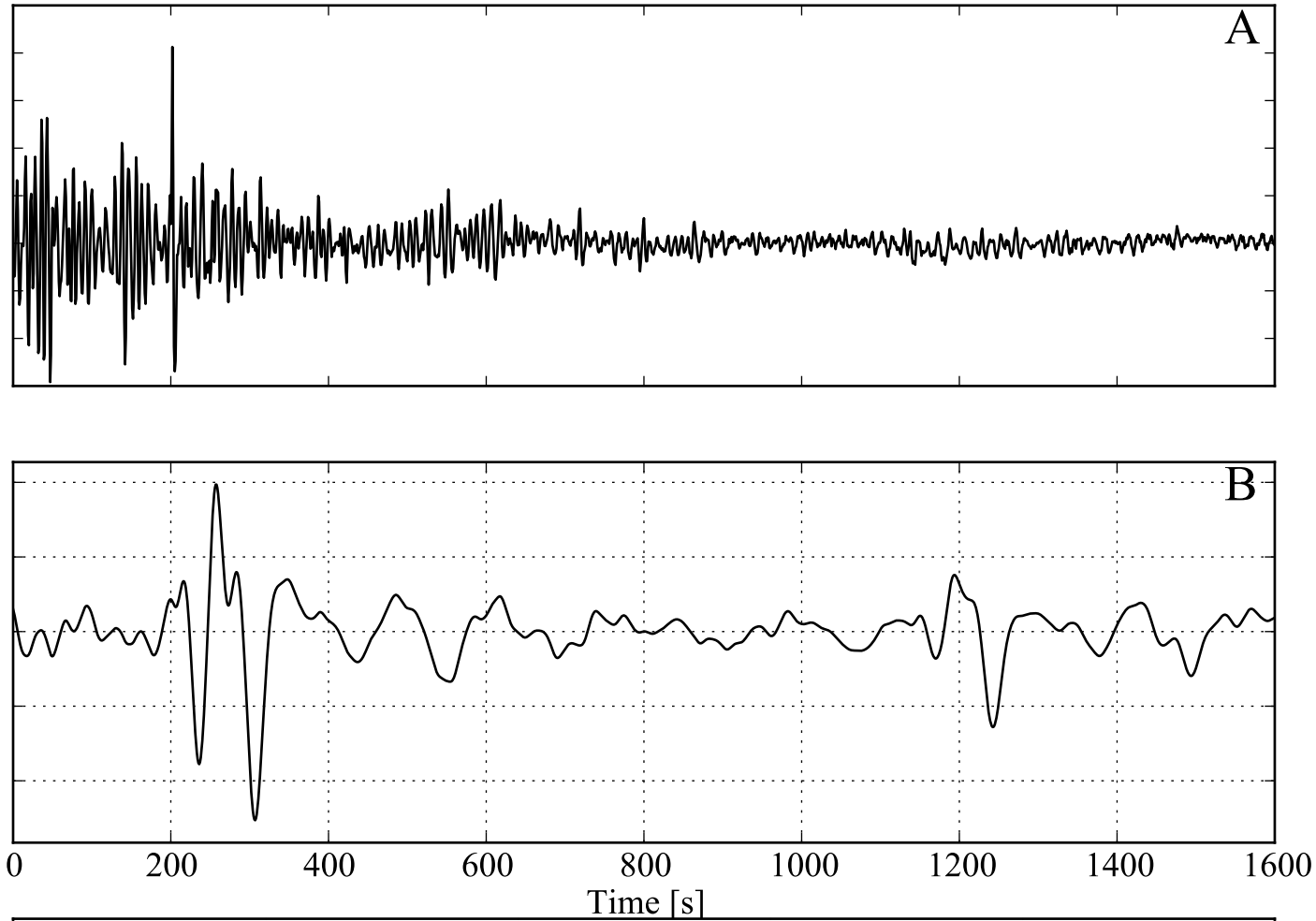


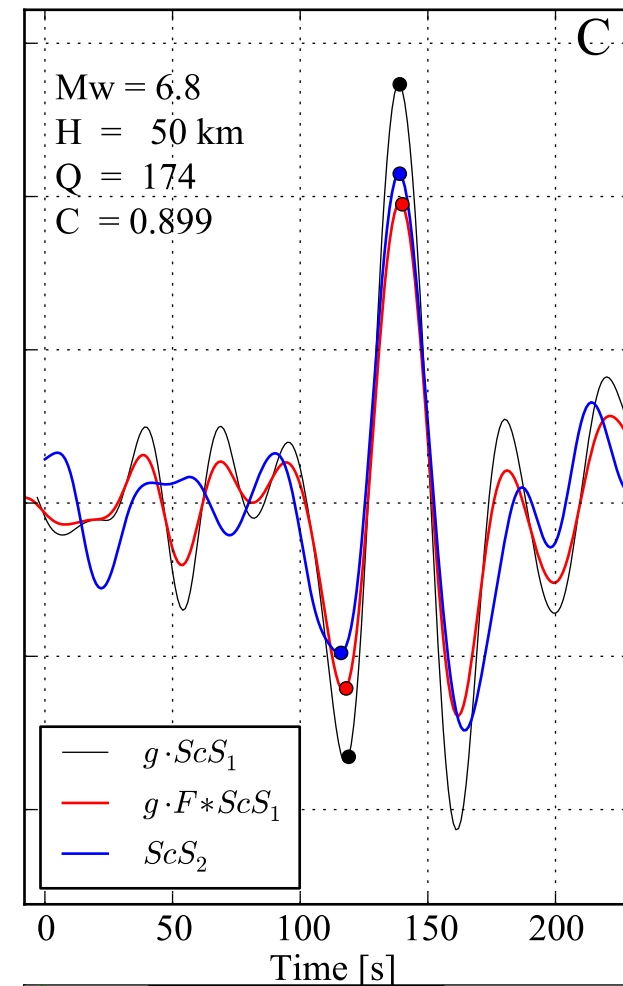
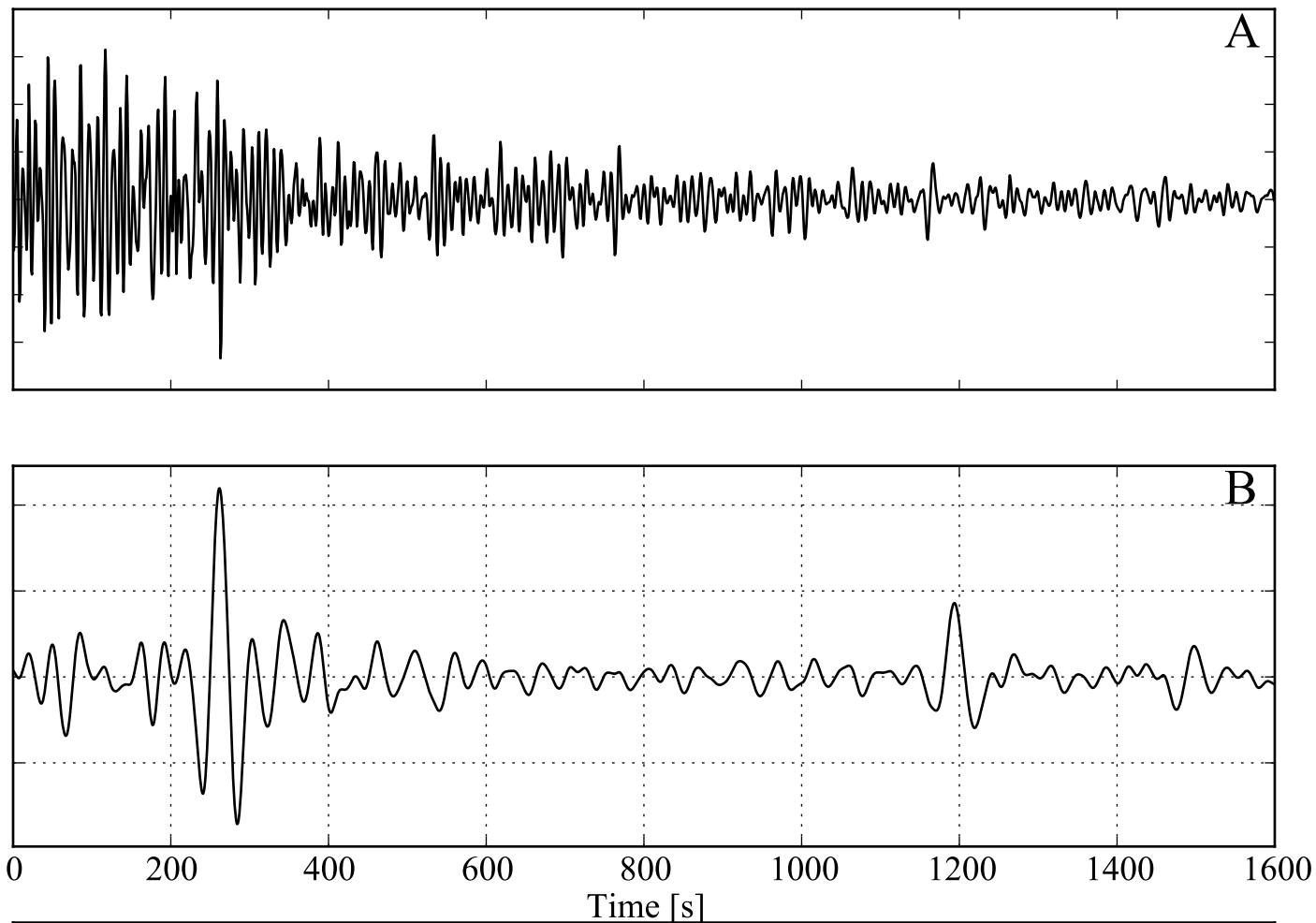












IU - YSS - 00 - LHN $\Delta/Az/Baz = 4.8^\circ / 324^\circ / 142^\circ$ Srp=0.75
 2000.028.14.16.07.948.IU.YSS.00.LHN.SAC (2000/01/28)
 $ScS_2 - ScS_1$ travel time: 932.2 τ : 46.0 s
 Centroid: 43.080 146.810 50.0 km Mw 6.8
 Q = 174 $t^* = 5.3$ s
 Quality control: signal/noise ScS_1 : 11.21 ScS_2 3.98 Correlation : 0.899

